Handbook of Engineering Hydrology

Modeling, Climate Change, and Variability

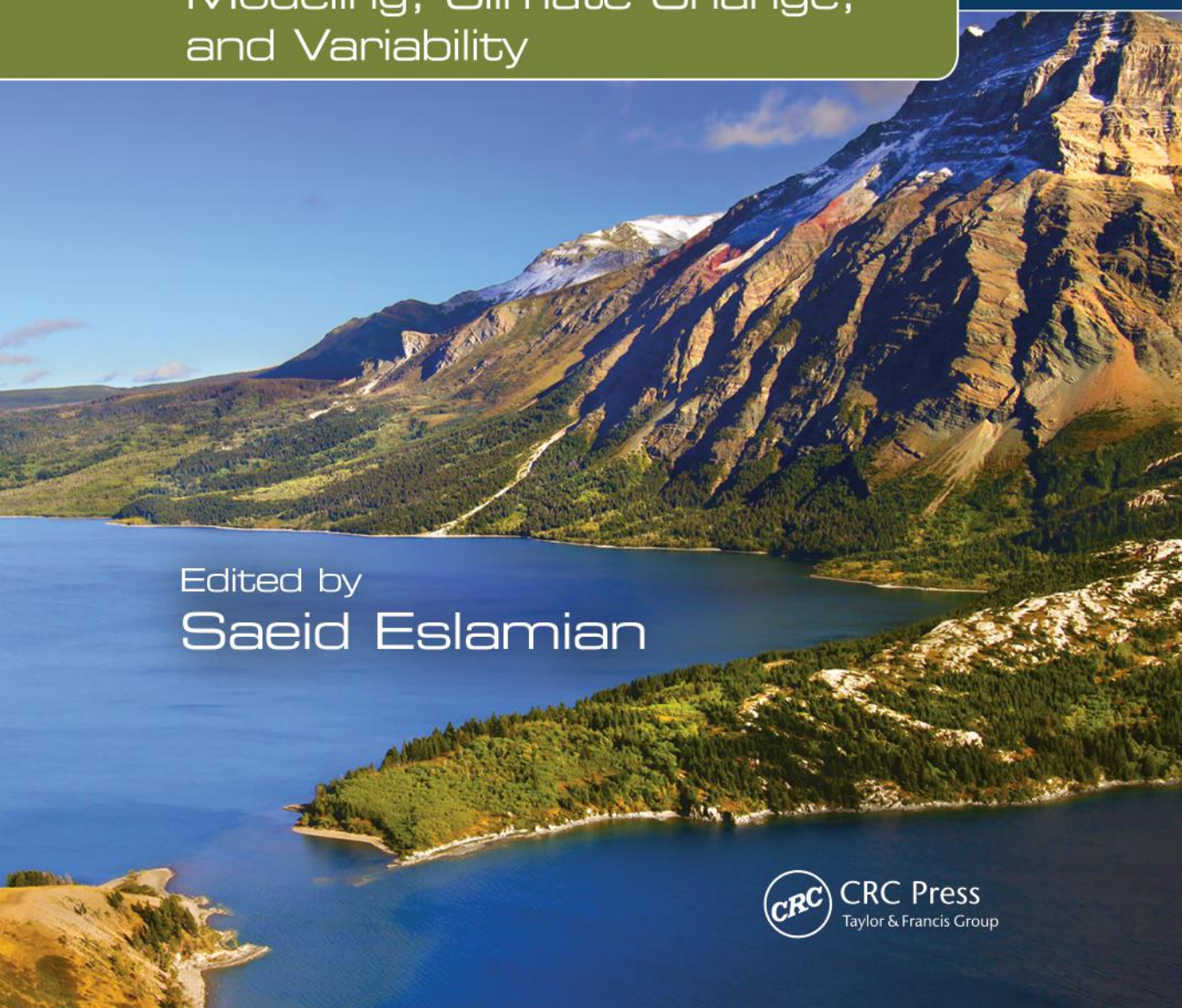

Edited by
Saeid Eslamian

CRC Press
Taylor & Francis Group

Handbook of Engineering Hydrology

Modeling, Climate Change, and Variability

Handbook of Engineering Hydrology

Handbook of Engineering Hydrology: Fundamentals and Applications, Book I

Handbook of Engineering Hydrology: Modeling, Climate Change, and Variability, Book II

Handbook of Engineering Hydrology: Environmental Hydrology and Water Management, Book III

Handbook of Engineering Hydrology

Modeling, Climate Change, and Variability

Edited by
Saeid Eslamian

CRC Press
Taylor & Francis Group
Boca Raton London New York

CRC Press is an imprint of the
Taylor & Francis Group, an **informa** business

CRC Press
Taylor & Francis Group
6000 Broken Sound Parkway NW, Suite 300
Boca Raton, FL 33487-2742

Version Date: 20140213

International Standard Book Number-13: 978-1-4665-5247-0 (eBook - PDF)

Contents

Preface

Hydrological and ecological connectivity is a matter of high concern. All terrestrial and coastal ecosystems are connected with water, which includes groundwater, and there is a growing understanding that "single ecosystems" (mountain forest, hill forest, mangrove forest, freshwater swamp, peat swamp, tidal mudflat, and coral reef) that are actually the result of an artificial perception and classification can, in the long term, only be managed by a holistic vision at the watershed level. It is essential to investigate ecosystem management at the watershed level, particularly in a changing climate.

In general, there are two important approaches:

1. Adaption to hydrological events such as climate change, drought, and flood
2. Qualitative and quantitative conservation of water, thereby optimizing water consumption

The *Handbook of Engineering Hydrology* aims to fill the two-decade gap since the publication of David Maidment's *Handbook of Hydrology* in 1993 by including updated material on hydrology science and engineering. It provides an extensive coverage of hydrological engineering, science, and technology and includes novel topics that were developed in the last two decades. This handbook is not a replacement for Maidment's work, but as mentioned, it focuses on innovation and provides updated information in the field of hydrology. Therefore, it could be considered as a complementary text to Maidment's work, providing practical guidelines to the reader. Further, this book covers different aspects of hydrology using a new approach, whereas Maidment's work dealt principally with classical components of hydrologic cycle, particularly surface and groundwater and the associated physical and chemical pollution.

The key benefits of the book are as follows: (a) it introduces various aspects of hydrological engineering, science, and technology for students pursuing different levels of studies; (b) it is an efficient tool helping practitioners to design water projects optimally; (c) it serves as a guide for policy makers to make appropriate decisions on the subject; (d) it is a robust reference book for researchers, both in universities and in research institutes; and (e) it provides up-to-date information in the field.

Engineers from disciplines such as civil engineering, environmental engineering, geological engineering, agricultural engineering, water resources engineering, natural resources, applied geography, environmental health and sanitation, etc., will find this handbook useful.

Further, courses such as engineering hydrology, groundwater hydrology, rangeland hydrology, arid zone hydrology, surface water hydrology, applied hydrology, general hydrology, water resources engineering, water resources management, water resources development, water resources systems and planning, multipurpose uses of water resources, environmental engineering, flood design, hydrometeorology, evapotranspiration, water quality, etc., can also use this handbook as part of their curriculum.

This set consists of 87 chapters divided into three books, with each book comprising 29 chapters. This handbook consists of three books as follows:

1. Book I: Fundamentals and Applications
2. Book II: Modeling, Climate Change, and Variability
3. Book III: Environmental Hydrology and Water Management

This book deals mainly with modeling, climate changes, and variability and can be classified in the following categories:

- *Climate changes*: Climate change and hydrological hazards, climate change and hydrological modeling, climate change and urban water systems, climate change impacts on hydrology and water resources, and climate change uncertainty, vulnerability, and adaption
- *Hydrologic changes and estimation*: Design rainfall estimation and changes, hydrological changes of mangrove ecosystems, impact of the development of vegetation on flow conditions and flood hazards, impacts of urbanization on runoff regime, discretization in urban watersheds
- *Mathematical modeling*: Artificial neural network–based modeling of hydrologic processes, flow and sediment transport modeling in rivers, hybrid hydrological modeling, hydrologic modeling: stochastic processes, time series analysis of hydrologic data
- *Risk and uncertainty*: Dam risk and uncertainty, drought indices for drought risk assessment in a changing climate, hydrologic prediction and uncertainty quantification, uncertainty and risk of the PMP and PMF
- *Spatial and regional analysis*: Geostatistics applications in hydrology, GIS applications in a changing climate, GIS-based upland erosion mapping, regional flood frequency analysis, regionalization of hydrological extreme events, remote sensing data and information for hydrological monitoring and modeling
- *Statistical analysis*: Application of copulas in hydrology, bankfull frequency of river, statistical parameters used for assessing hydrological regime, significance of statistical tests and persistence in hydrologic processes

About 200 authors from various departments and across more than 30 countries worldwide have contributed to this book, which includes authors from the United States comprising about one-third of the total number. The countries that the authors belong to have diverse climate and have encountered issues related to climate change and water deficit. The authors themselves cover a wide age group and are experts in their fields. This book could only be realized due to the participation of universities, institutions, industries, private companies, research centers, governmental commissions, and academies.

I thank several scientists for their encouragement in compiling this book: Prof. Richard McCuen from the University of Maryland, Prof. Majid Hassanizadeh from Utrecht University, Prof. Soroush Sorooshian from the University of California at Irvine, Profs. Jose Salas and Pierre Julien from Colorado State University, Prof. Colin Green from Middlesex University, Prof. Larry W. Mays from Arizona State University, Prof. Reza Khanbilvardi from the City College of New York, Prof. Maciej Zalewski from the University of Łodz´-Poland, and Prof. Philip B. Bedient from Rice University.

In addition, Research Professor Emeritus Richard H. French from Las Vegas Desert Research Institute, who has authored the book *Open Channel Hydraulics* (McGraw-Hill, 1985), has encouraged me a lot. I quote his kind words to end this preface:

> My initial reaction to your book is simply WOW!
>
> Your authors are all well known and respected and the list of subjects very comprehensive. It will be a wonderful book. Congratulations on this achievement.

Saeid Eslamian
Isfahan University of Technology
Isfahan, Iran

Editor

Saeid Eslamian is an associate professor of hydrology at Isfahan University of Technology, Iran, where he heads the Hydrology Research Group at the Department of Water Engineering. His research focuses mainly on statistical and environmental hydrology and climate change. In particular, he specializes in modeling and prediction of natural hazards including floods, droughts, storms, wind frequency, and groundwater drawdowns, as well as pollution in arid and semiarid zones, particularly in urban areas.

Prof. Eslamian was born in Isfahan, a large city located in the center of Iran. He received his BS in water engineering from Isfahan University of Technology in 1986. Later, he was offered a scholarship for a master's degree at Tarbiat Modares University, Tehran. He completed his studies in hydrology and water resources in 1989. In 1991, he was awarded a grant for pursuing his PhD in civil engineering at the University of New South Wales, Sydney, Australia. His supervisor was Professor David H. Pilgrim, who encouraged him to conduct research on regional flood frequency analysis using a new region of influence approach. Soon after his graduation in 1995, Eslamian returned to Iran and worked as an assistant professor at Isfahan University of Technology (IUT). In 2001, he was promoted to associate professor.

Eslamian was a visiting professor at Princeton University, Princeton, New Jersey, in 2006 and at the University of ETH Zurich, Switzerland in 2008. During this period, he developed multivariate L-moments for low flow and soil–moisture interaction.

Eslamian has contributed to more than 300 publications in books, research journals, and technical reports or papers in conferences. He is the founder and chief editor of the *International Journal of Hydrology Science and Technology* and the *Journal of Flood Engineering*. He also serves as an editorial board member and reviewer of about 30 Web of Science (ISI) journals. Recently, he has been appointed as the chief editor for a three-set book series Handbook of Engineering Hydrology by Taylor & Francis Group (CRC Press).

Prof. Eslamian has prepared course material on fluid mechanics, hydraulics, small dams, hydraulic structures, surface runoff hydrology, engineering hydrology, groundwater hydrology, water resource management, water resource planning and economics, meteorology, and climatology at the undergraduate level and material on evapotranspiration and water consumption, open channel hydraulics, water resources engineering, multipurpose operation of water resources, urban hydrology, advanced hydrology, arid zones hydrology, rangeland hydrology, groundwater management, water resources development, and hydrometeorology at the graduate level.

He has presented courses on transportation, Energy and Agriculture Ministry; and different university departments in governmental and private sectors: civil engineering, irrigation engineering, water engineering, soil sciences, natural resources, applied geography, and environmental health and sanitation.

Eslamian has undertaken national and international grants on "Studying the impact of global warming on the Kingdom of Jordan using GIS," "Study of the impact of different risk levels of climate change on Zayandehroud River Basin's climatic variables," "Feasibility of reclaimed water reuse for industrial uses in Isfahan Oil Refining Company," "Microclimate zoning of Isfahan city and investigation of microclimate effect on air temperature, relative humidity and reference crop evapotranspiration," "Feasibility of using constructed wetland for urban wastewater," "Multivariate linear moments for low flow analysis of the rivers in the north-eastern USA," and "Assessment of potential contaminant of landfill on Isfahan water resources." He has received two ASCE and EWRI awards from the United States in 2009 and 2010, respectively, as well as an outstanding researcher award from Iran in 2013. Persian being his native language, Prof. Eslamian is also fluent in English and is professionally familiar with French and Arabic.

Contributors

Jazuri Abdullah
Department of Civil and Environmental Engineering
Colorado State University
Fort Collins, Colorado

Iván Rivas Acosta
Hydrology Department
Mexican Institute of Water Technology
Jiutepec, Mexico

Pradeep Adhikari
Department of Geography and Environmental Sustainability
University of Oklahoma
Norman, Oklahoma

Carmen Agouridis
Department of Biosystems and Agricultural Engineering
University of Kentucky
Lexington, Kentucky

Hussam Al-Bilbisi
Faculty of Art
University of Jordan
Amman, Jordan

Rezaul K. Chowdhury
Department of Civil and Environmental Engineering
United Arab Emirates University
Al Ain, United Arab Emirates

Emery A. Coppola Jr.
NOAH LLC
Lawrenceville, New Jersey

Caleb M. DeChant
Department of Civil and Environmental Engineering,
Portland State University
Portland, Oregon

Hamze Dokohaki
Department of Water Engineering
Isfahan University of Technology
Isfahan, Iran

Tayel El-Hasan
Faculty of Science
Mutah University
Al-Karak, Jordan

Saeid Eslamian
Department of Water Engineering
Isfahan University of Technology
Isfahan, Iran

Masoomeh Fakhri
Department of Hydraulic and Sanitary Engineering
Chamran University
Ahvaz, Iran

Iman Fazeli Farsani
Department of Soil Science
Shahrekord University
Shahrekord, Iran

Mohammad Reza Farzaneh
Department of Water Engineering
Tarbiat Modares University
Tehran, Iran

Brian A. Fuchs
National Drought Mitigation Center
University of Nebraska-Lincoln
Lincoln, Nebraska

Emna Gargouri-Ellouze
Laboratory of Hydraulic and Environmental Modeling
Tunis El Manar University
Tunis, Tunisia

Germán Gavilán
University of California, Merced
Merced, California

Albrecht Gnauck
Department of Ecosystems and Environmental Informatics
Brandenburg University of Technology at Cottbus
Cottbus, Germany

Ehsan Goodarzi
Department of Civil and Environmental Engineering
Georgia Institute of Technology
Atlanta, Georgia

Khaled Haddad
School of Computing Engineering and Mathematics
University of Western Sydney
Sydney, New South Wales, Australia

James S. Halgren
Riverside Technology Inc.
Fort Collins, Colorado

Khaled H. Hamed
Faculty of Engineering
Irrigation and Hydraulics Department
Cairo University
Giza, Egypt

Michael J. Hayes
National Drought Mitigation Center
University of Nebraska-Lincoln
Lincoln, Nebraska

Yang Hong
School of Civil Engineering and Environmental Science
University of Oklahoma
and
Advanced Radar Research Center
National Weather Center
Norman, Oklahoma

Shafi Noor Islam
Department of Ecosystems and Environmental Informatics
Brandenburg University of Technology at Cottbus
Cottbus, Germany

Pierre Y. Julien
Department of Civil Engineering
Colorado State University
Fort Collins, Colorado

Tomasz Kałuża
Department of Hydraulic and Sanitary Engineering
Poznan University of Life Sciences
Poznan, Poland

Reza Khanbilvardi
Cooperative Remote Sensing Science and Technology Center
National Oceanic and Atmospheric Administration
The City College of New York
New York, New York

Nir Krakauer
Cooperative Remote Sensing Science and Technology Center
National Oceanic and Atmospheric Administration
The City College of New York
New York, New York

Tarendra Lakhankar
Cooperative Remote Sensing Science and Technology Center
National Oceanic and Atmospheric Administration
The City College of New York
New York, New York

Lu Liu
Pacific Northwest National Laboratory
Joint Global Change Research Institute
College Park, Maryland
and
School of Civil Engineering and Environmental Science
University of Oklahoma
Norman, Oklahoma

Jansen Luis
Tenaga Nasional Berhad
Kuala Lumpur, Malaysia

Gregoire Mariethoz
School of Civil and Environmental Engineering
University of New South Wales
Sydney, New South Wales, Australia

Ole Mark
DHI
Horsholm, Denmark

Mohammed Matouq
Faculty of Engineering Technology
Al-Balqa Applied University
Amman, Jordan

Seyed Jalal E. Mirnezami
Department of Water Engineering
Tarbiat Modares University
Tehran, Iran

Hamid Moradkhani
Department of Civil and Environmental Engineering
Portland State University
Portland, Oregon

Never Mujere
Department of Geography and Environmental Science
University of Zimbabwe
Harare, Zimbabwe

Rouzbeh Nazari
Cooperative Remote Sensing Science and Technology Center
National Oceanic and Atmospheric Administration
The City College of New York
New York, New York

Birgit Paludan
Greve Solrød Water Utility
Roskilde, Denmark

Al Powell
Center for Satellite Applications and Research
Satellite and Information Service (NESDIS)
National Oceanic and Atmospheric Administration
Camp Springs, Maryland

Lei Qiao
School of Civil Engineering and Environmental Science
University of Oklahoma
and
Advanced Radar Research Center
National Weather Center
Norman, Oklahoma

Ataur Rahman
School of Computing Engineering and Mathematics
University of Western Sydney
Sydney, New South Wales, Australia

Fernando R. Salas
Department of Environmental and Water Resources Engineering
The University of Texas at Austin
Austin, Texas

Jose D. Salas
Department of Civil and Environmental Engineering
Colorado State University
Fort Collins, Colorado

Rina Schumer
Division of Hydrologic Sciences
Desert Research Institute
Reno, Nevada

Lariyah M. Sidek
Department of Civil Engineering
Universiti Tenaga Nasional
Kajang, Malaysia

Óli Grétar Blöndal Sveinsson
Landsvirkjun
Reykjavík, Iceland

Mark D. Svoboda
National Drought Mitigation Center
University of Nebraska-Lincoln
Lincoln, Nebraska

Anna Szidarovszky
Zonge International Inc.
Tucson, Arizona

Ferenc Szidarovszky
NOAH LLC
Lawrenceville, New Jersey

Pejman Tahmasebi
Department of Energy Resources Engineering
Stanford University
Stanford, California

Soo Huey Teh
Institute for Sustainability and Peace
United Nations University
Tokyo, Japan

Mehdi Vafakhah
Department of Watershed Management
Tarbiat Modares University
Tehran, Iran

Hans-Jürgen Voigt
Department of Environmental Geology
Brandenburg University of Technology at Cottbus
Cottbus, Germany

Donald A. Wilhite
School of Natural Resources
University of Nebraska-Lincoln
Lincoln, Nebraska

1

Applications of Copulas in Hydrology: Geomorphological Instantaneous Unit Hydrograph and Intensity Index of Infiltration Frequency

Emna Gargouri-Ellouze
Tunis El Manar University

Saeid Eslamian
Isfahan University of Technology

AUTHORS

Emna Gargouri-Ellouze received a PhD in hydraulic engineering from the University of El Manar I, Tunisia in 2011; completed the Civil Competitive Examination for posts on the teaching staff of Lycées and Universities in 1998; the certificate of the specialized higher education option civil engineering from High School of Sciences and Technics of Tunis in 1996; and the Bachelor of hydraulic engineering from the National School of Engineers of Tunis in 1990.

Dr. Emna Gargouri-Ellouze serves as an associate professor at the National School of Engineers of Tunis and as a research associate at the Hydraulic Environmental Modeling Laboratory. Her main research topic

is the predetermination of the runoff of ungauged basins using statistical tools. Copulas are currently her research domain.

She is the vice-president of ICSH-IAHS (International Commission of Statistical Hydrology of International Association of Hydrological Sciences), which coordinates, optimizes, and concentrates resources for statisticians who would like to understand hydrological applications, for hydrologists who need to use a statistical tool and would like to easily understand what is the right approach, and for statistical hydrologists to easily stay updated on recent developments in their research field.

She is a member of American Geophysical Union (AGU), International Association of Hydrological Sciences, and Réseau National des Systèmes Complexes (RNSC).

Saeid Eslamian received a PhD from the University of New South Wales, Australia, under Professor David Pilgrim. He was a visiting professor in Princeton University, Princeton, New Jersey, and ETH Zurich, Switzerland. He is currently an associate professor of Hydrology in Isfahan University of Technology. He is the founder and chief editor of the *Journal of Flood Engineering* and the *International Journal of Hydrology Science and Technology*. He has to his credit more than 200 publications mainly in statistical and environmental hydrology and hydrometeorology.

PREFACE

Hydrological observations, experiments, and practices show that hydrological events are described through various characteristics that are generally correlated. Taking into account this aspect, it is necessary when modeling hydrological events to consider their characteristics jointly. One often uses families of multivariate distributions that are extensions of univariate ones. However, these distributions suffer from several limitations and constraints. Copulas models offer to overtake these difficulties. For this reason, the attraction of the mathematical simplicity of copulas models has interested researchers since the 2000s.

The use of copulas in hydrology is rapidly growing. Copulas offer the opportunity to treat one of the main researched objectives by hydrologists: the determination of the statistic quantities such as joined probabilities, conditioned probabilities, and return periods of events. We first present in this article the notion of multivariate return period and also multivariate quantile. We also present two hydrological applications to explain the approach of copulas and how to model with them. At the end of the text, we give relevant appendixes for the goodness of fit of copulas, which remains an open issue.

1.1 Introduction

Hydrological observations, experiments, and practices show that hydrological events are described through various characteristics, which are generally correlated. Taking into account this aspect, it is necessary when modeling hydrological events to consider their characteristics jointly. Indeed, in the past few years, bivariate and multivariate modeling has received increased attention. Among the proposed models, one has the frequency analysis procedures. They are commonly used as tools for the analysis of hydrological events. These procedures join the magnitude of events to their frequency of occurrence.

One often uses families of multivariate distributions that are extensions of univariate ones such as multivariate normal distribution or its extensions: multivariate lognormal distribution, Student t distribution and Fishers F distribution or multivariate logistic Gumbel (see Reference 27), multivariate gamma distributions (e.g., [24], see Reference 32), multivariate exponential distribution [31], and multivariate generalized Pareto distributions [25]. However, these distributions suffer from several

limitations and constraints, such as that the marginal distributions may belong to the same probability family [22,27]. Thus, to avoid these limitations, copulas models are used [12]. Copulas allow the description of the dependence structure between random variables without information on the marginal distributions and also the description of the multivariate distributions with any kind of marginal distributions [2]. It is worth noting that copulas are not the only models that fulfill these requirements, as underlined recently by Ashkar et al. [1] "These other models were ignored, or overlooked, because it was wrongly assumed that they do not allow for sufficient flexibility in the choice of marginal distributions for the two variables being modeled." These authors compared copulas to three bivariate distributions (Downton's bivariate exponential distribution, bivariate Fisher distribution, and bivariate Pearson Type 2 distribution) and showed that these distributions have their own dependence structures, and need to be given the same level of consideration in hydrology as copula. In 1997, Kelly and Krzysztofowicz [18] presented the flexibility of Méta-Gaussian distribution. However, the attraction of the mathematical simplicity of copulas models has kindled the interest of researchers since the 2000s.

The use of copulas in hydrology, as well as in other geophysical and environmental sciences, is rapidly growing. The addressed fields mainly are flood frequency analysis, drought frequency analysis, rainfall frequency analysis, design rainfall, design floods, regional analysis, analysis under climate change, hydrological extremes, uncertainty modeling, geostatistical models, remote sensing observations, and others fields (see http://www.stahy.org/Activities/STAHYReferences/).

Copulas offer the opportunity to treat one of the main researched objectives by hydrologists: the determination of the statistic quantities such as joined probabilities, conditioned probabilities, and return periods of events. For example, extreme floods or droughts, which are essentially natural hazards, occur "infrequently." In most cases, excessive or scarce precipitation is the main cause of these catastrophic events. Indeed, the severity of these phenomena is the consequence of different behaviors of the same cause: too small precipitation for a long time (drought) or too large precipitation for a short time (floods) and also too large precipitation for a long time (floods). An event could thus be defined as unsafe if either precipitation or time exceeds the given threshold or precipitation and time are larger than the prescribed values.

1.2 Notion of Multivariate Return Period and Multivariate Quantile

The concept of return period is proposed to characterize the frequency of occurrence of a phenomenon. This is probably in a pedagogical concern that statisticians wanted to translate the probability of an event, especially mysterious concept known in return period, assumed more understandable for managers and public [14]. Consequently, it is more convenient to talk about the risk (or probability) of the occurrence of an event rather than its return period. In the same context, Chebana and Ouarda in 2009 [4] specified the concept of multivariate quantile, which is the value of the variable leading to the risk. This concept was initially established by Salvadori in 2004 [26], for univariate case and then was generalized to multivariate case.

Here, we focus on the bivariate case that could be extended for multivariate case. In the bivariate case, we assume that X and Y are two random variables with joint distribution F_{XY}, marginal distributions F_X and F_Y, respectively, and copula C, which is implicitly defined through the functional identity:

$$F_{XY}(x,y) = C\left(F_X(x), F_Y(y)\right) \tag{1.1}$$

Since copulas are invariant under strictly increasing transformations of X and Y, thanks to probability integral transformation, one can deal with the pair of RVs (U, V) given by [23]

$$\begin{cases} U = F_X(x) \\ V = F_Y(y) \end{cases} \tag{1.2}$$

Let consider a sequence of E_1, E_2, … of independent events. Each event E_i is characterized by the joint behavior of a pair of RVs $(U,V) \sim C_{U,V}$, which can be expressed in terms of univariate marginal events. Using the (inclusive) OR operator "∪" and the AND operator "∩," it is possible to combine the marginal events in several ways. Eight combinations are possible.

The latter authors proposed to retain only the following events $E_{u,v}$, which are the main of interest in hydrology.

$$E_{u,v}^{\cup} = \{U > u\} \cup \{V > v\} \quad \text{and} \quad E_{u,v}^{\cap} = \{U > u\} \cap \{V > v\} \tag{1.3}$$

In addition, [26] proposed the expression of the isolines of bivariate return period and [4] expressed the isolines of bivariate quantiles, for a couple of Archimedean copulas.

For the case of $E_{u,v}^{\cup}$:

$$p_{u,L_t(u)}^{\cup} = 1 - C\left(u, L_t(u)\right) = 1 - t, \quad t \le u \le 1 \tag{1.4}$$

For the case of $E_{u,v}^{\cap}$:

$$p_{u,L_t(u)}^{\cap} = -u + L_{1-t}(1-u) + C\left(u, 1 - L_{1-t}(1-u)\right) = 1 - t, \quad 0 \le u \le t \tag{1.5}$$

with

$$p_{u,v}^{\cup} = \boldsymbol{P}(U > u \cup V > v) \quad \text{and} \quad p_{u,v}^{\cap} = \boldsymbol{P}(U > u \cap V > v) \tag{1.6}$$

$p_{u,v}^{\cup}$ and $p_{u,v}^{\cap}$ are joint probabilities and L_t the level curve:

$$L_t = \left\{(u,v) \epsilon\ [0,1]^2 : C(u,v) = t\right\}, \quad 0 < t \le 1 \tag{1.7}$$

Relevant findings presented by Chebana and Ouarda in 2009 [4] showed that for the univariate analysis, each variable needs to be treated separately, which implicitly involves several events, and consequently several risk levels to associate. On the contrary, for multivariate analysis, for a given joint event, "one" risk level is associated. The univariate analysis can only provide the bounds of each variable without any information about the shape of the relation between the variables. In addition, the univariate estimation does not take into account the dependence structure between variables and should be used cautiously [4]. Another convenient, some events cannot be expressed in the univariate context. These issues are solved by the use of multivariate analysis. However, they moderate their comments: "the performances of univariate and bivariate procedures are evaluated on the basis of different criteria. The main differences between univariate and bivariate estimations are conceptual."

In the following sections, two applications of copulas are presented.

1.3 Application 1: Runoff Estimation for an Ungauged Catchment Using GIUH

GIUH (Geomorphological Instantaneous Unit Hydrograph) is till now still largely used as a tool of flood discharges predetermination in catchments, and particularly in ungauged ones [7,16,19,20,28].

GIUH is a very attractive model due to the parsimony of necessary inputs and the simplicity of its application. It is an effective rainfall-runoff model [21]; however, it presents the disadvantage of the prior knowledge of effective rainfall [3], which is particularly complicated to determine for ungauged basins.

The effective rainfall is determined by index infiltration method (φ-index) that represents the average value of infiltration capacity through the duration of effective rainfall.

In the perspective of the applicability of the GIUH to ungauged basins, Gargouri-Ellouze and Bargaoui [10] (1) relaxed the prior knowledge of effective rainfall since runoff volumes and hydrographs are unavailable, introduced uncertainties in its amount and temporal structure; and (2) investigated and exploited the dependence between φ-index and rainfall characteristics in order to derive hydrograph's components.

They generated hydrographs with Monte Carlo simulations, then analyzed the dispersion of their characteristics (peak discharges, peak times, base times, and the volumes), after they studied the coupling between φ-index and rainfall characteristics (rainfall depth, maximum intensity, average intensity, and rainfall duration) and reconstituted the observed hydrographs, finally compared the different methods of φ-index estimation and their impact on GIUH's outputs.

The studied site is a small catchment: Saddine 1, near Makthar (Tunisia) in a mountainous zone, monitored by the DGACTA* from 1992 to 2000, within the framework of the HYDROMED† project. This catchment is controlled by a headwater dam and its area is equal to 3.84 km^2.

They used a sample of hydrological events (hyetographs and runoff volumes, see Table 1.1) that covers a large value range of total depth rainfall (P), rainfall duration (D), rainfall maximum intensity (I_{max}), rainfall average intensity (I_{moy}), runoff volumes (V), peak discharges (Q_p), time to peak (t_p), base time (t_b), and φ-index (φ).

TABLE 1.1 Characteristics of Studied Events

Event	P (mm)	D (min)	I_{max} (mm/h)	I_{moy} (mm/h)	V (m^3)	Q_p (m^3/s)	t_p (min)	t_b (min)	φ (mm/h)
20/5/92	106	116	260.0	55	30,059	34.70	25	60	166.0
24/5/92	36	299	36.0	7	1,509	0.60	25	85	26.2
14/9/93	26	27	84.0	58	10,657	3.00	60	120	58.0
31/7/94	35.5	42	120.0	51	20,843	19.80	30	60	73.0
8/1/95	12	138	10.0	5	400	0.10	60	190	9.0
8/6/95	14	28	58.8	30	1,768	0.04	—	—	53.0
24/6/95	11.5	13	101.0	53	3,980	0.60	50	470	87.8
24/8/95	12.5	12	102.0	63	41,940	26.70	20	95	5.5
4/9/95	39.5	13	324.0	182	67,200	85.60	15	29	162.0
4/9/95bis*	8.5	30	30.6	17	15,164	2.10	50	200	10.6
16/9/95	7.5	14	56.0	32	16,055	0.10	60	—	13.1
7/2/96	8	73	31.2	7	3,152	0.40	5	360	21.3
15/8/96	39.5	44	115.0	54	1,476	2.00	10	—	103.2
9/9/96	12	74	56.6	10	15,573	10.40	25	35	13.1
9/9/96bis*	13	53	28.8	15	15,030	0.10	40	—	13.1
18/8/97	10.5	26	68.4	24	6,308	2.60	45	225	48.4
21/9/97	17.5	21	118.8	50	26,393	22.30	25	85	38.8
4/11/97	5.5	16	32.4	20	383	0.20	95	240	31.2
6/12/97	10.5	243	4.8	3	2,306	0.20	135	305	3.8
5/8/99	27	36	99.6	45	35,093	7.90	60	390	47.3

Note: P, rainfall depth; D, rainfall duration; I_{max}, rainfall maximum intensity; I_{moy}, rainfall average intensity; V, runoff volume; Q_p, peak discharge; t_p, time to peak; t_b, base time; φ, infiltration index. 4/9/95 event occurred at 16h50 and 4/9/95bis* occurred at 23h45. 9/9/96 occurred at 5h15 and 9/9/96 occurred at 14h55.

* DGACTA: Direction Générale des Aménagements et Conservation des Terres Agricoles.

† HYDROMED: Programme de recherche sur les lacs collinaires dans les zones semi-arides du pourtour méditerranéen.

TABLE 1.2 Variable Distribution and Their Characteristics

Variable X	Distribution	Mean μ	Standard Deviation Σ	Parameter Position X_0	p-Value
I_{max} (mm/h)	Exponential	46.5	42.6	3.9	0.94
φ-index (mm/h)	Exponential	32.4	29.2	3.2	0.30
D (min)	Exponential	77.9	67.3	10.6	0.09
I_{moy} (mm/h)	Lognormal	2.6	0.97	—	0.30
P (mm)	Exponential	13.3	9.00	4.3	0.19

TABLE 1.3 Kendall's τ Values and Their $z^\star$ Statistics

Couple	Sample Size	τ	$z^\star$	H_0
(φ, I_{max})	51	0.72	0.19	Rejection
(φ, I_{moy})	51	0.57	0.19	Rejection
(φ, D)	51	−0.42	0.19	Rejection
(φ, P)	51	0.18	0.19	Acceptance

Note: I_{max}, maximum rainfall intensity; I_{moy}, average rainfall intensity; D, rainfall duration; P, rainfall depth; τ, Kendall's τ; $z^\star$, test statistic; H_0, null hypothesis.

The marginal distributions of variables: I_{max}, φ-index, D, I_{moy}, and P are fitted using (HYFRAN*). The parameters are estimated by the maximum-likelihood method, and the goodness-of-fit is achieved with the chi-square test. Table 1.2 recapitulates the main characteristics of the variable distributions.

To measure the association between φ-index and rainfall characteristics, the rank correlation coefficient Kendall's tau (τ) [17] is used for the characterization of dependence. Table 1.3 deals with τ's values and their corresponding statistics for the different couples (φ, I_{max}), (φ, I_{moy}), (φ, D), and (φ, P). The analysis of Table 1.3 shows that H_0† independence hypothesis is rejected for the first three couples and accepted in the latter. Consequently, φ depends on I_{max}, which confirms the previous works of Gargouri-Ellouze and Bargaoui in 2009 [9]; in addition, φ depends on I_{moy}, which implicitly depends on event duration. Indeed, the correlation between φ and D gives a τ's value equal to −0.41 ($z^\star = 4.20$), that is the more the duration increases the more φ decreases. As a conclusion, the maximum intensity plays the most significant role, followed by average intensity and finally by duration, but the rainfall depth seems to have no importance. Therefore, in this chapter, we only focus and exploit the following relationships: (φ, I_{max}), (φ, I_{moy}), and (φ, D).

1.3.1 Modeling with Copulas

For the modeling of the joint cumulative distribution function of pairs (I_{max}, φ), (φ, I_{moy}), and (φ, D), Archimedean copulas with one parameter (a) are used. For the goodness-of-fit of copulas, the methodology of Gargouri-Ellouze and Chebchoub in 2008 [8] is adopted: we select among three models (Gumbel, Frank and Clayton, see Appendix 1.A.1 for details) by comparing the empirical versions of the functions K, J, M, L, and R ([29,30], see Appendix 1.A.2 for details) and the theoretical versions and also

* Software developed by INRS-ETE, Chaire en hydrologie statistique (HYDRO-QUÉBEC/ALCAN/CRSNG).

† A test of independence can be adopted for Kendall's τ, since under the null-hypothesis H_0, this statistic is close to Normal distribution with zero mean and variance $2(2n+5)/[9n(n-1)]$ (n size of sample). As a result H_0 would be rejected at an approximate level α if $|\tau| > z_{\alpha/2}\sqrt{\left[2(2n+5)\right] / \left[9n(n-1)\right]}$. For α = 5%, $z_{\alpha/2} = 1.96$. Let $z^\star$ represent the quantity $z_{\alpha/2}\sqrt{\left[2(2n+5)\right] / \left[9n(n-1)\right]}$.

by using bivariate χ^2 test as proposed by Hürlimann in 2004 [15] (see Appendix 1.A.3). Consequently, for each couple, one copula is estimated according to Kendall's τ.

Based on this methodology, Gumbel copula is adopted for (φ, I_{max}) and (φ, I_{moy}) with a parameter a respectively of $a_{Imax} = 4.8$ and $a_{Imoy} = 3$ and Frank copula is adopted for (φ, D) with a parameter $a_D = -4.4$. Thus, φ-index can be generated conditioned to I_{max}, I_{moy}, and D.

Figure 1.1a–c shows the simulated and observed values for each studied couples. Note that the observed values are reconstituted for the pairs φ-index conditioned to I_{max} and I_{moy}, even those used for the validation. However, it is not the case for φ-index conditioned to D (Figure 1.1c), several values are not reconstituted. This may be due to the weakness of the relationship between φ-index and D ($\tau = -0.42$) and the choice of the copula model. Other types of copulas that model negative correlations should be tested. Therefore, the authors suggested prospecting only the couples (I_{max}, φ)

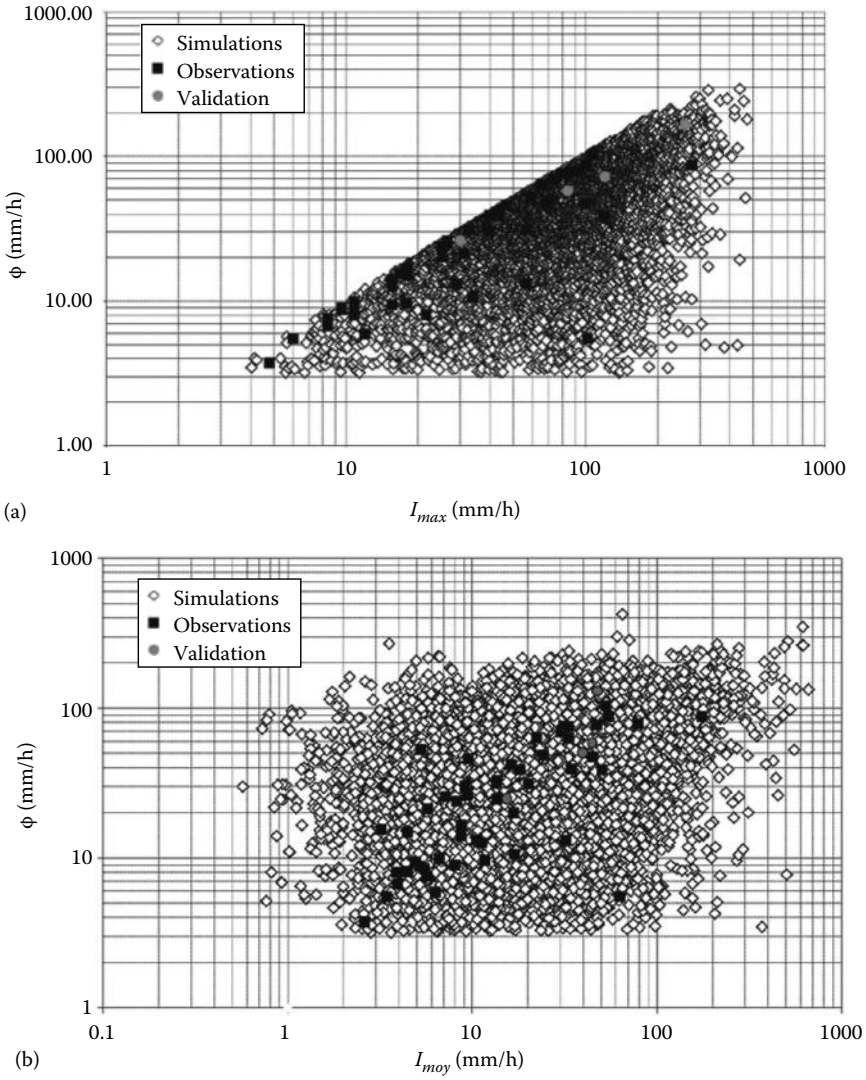

FIGURE 1.1 (a) φ-index conditioned to I_{max}. (b) φ-index conditioned to I_{moy}.

(*continued*)

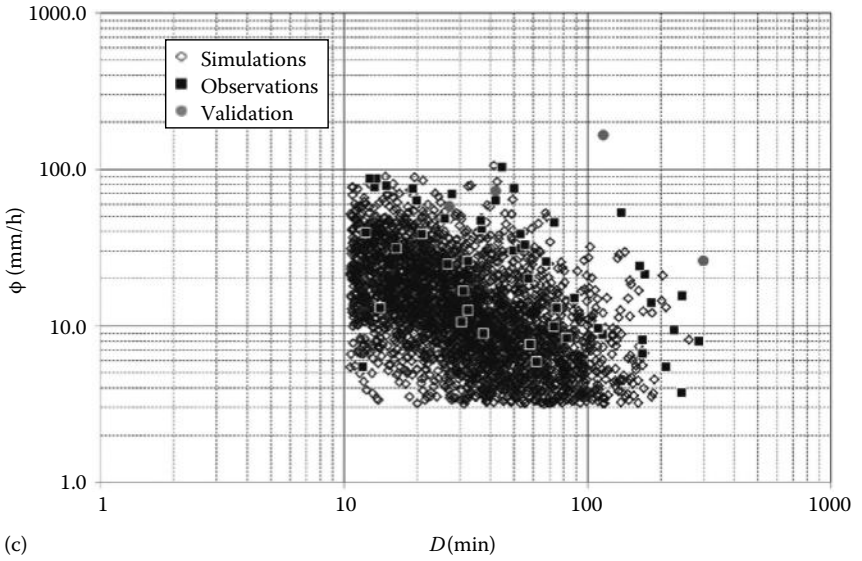

FIGURE 1.1 (continued) (c) φ-index conditioned to *D*.

and (I_{moy}, φ). It is worth noting that during the simulation of couples (φ, I_{max}) φ is rejected when φ is greater than I_{max} (unfeasible case).

In order to understand and exploit these correlations, Figure 1.2a and b represents the isolines of simulated couples (I_{max}, φ) and (I_{moy}, φ). These isolines correspond to *Intensity–φ-index–Frequency* curves. They give for each fixed intensity (maximum or average) the distribution of φ-index. We notice that for the high values of intensities (maximum or average) φ-index becomes constant.

1.3.2 Stochastic Generation of Simulated Hydrographs

The effective rainfall is considered intensities as a vector of model parameter. The vector components are estimated from the knowledge of φ-index for each event. Each rainy event is separately considered without presuming its occurrence probability. The generation process of hydrographs is as follows:

- Data insertion: geomorphological parameters and rainfall hyetograph with constant time increment for all simulations.
- Draw the different values of φ-index in a distribution conditioned to rainfall characteristic $F(\varphi|I_o)$, using Monte Carlo Simulations.
- For each φ-index value, the different components of effective rainfall are calculated.
- Simulation of different hydrographs for each estimated effective rainfall vector.
- Statistical analysis of simulated hydrographs.

The methodology proposed earlier is simultaneously applied to effective rainfall intensities deduced from the couples (φ, I_{max}) and (φ, I_{moy}). For each event E_i, the authors used MCS by drawing φ conditioned to I_{max} or I_{moy}. They thus obtained a distribution $F(\varphi|I_o)$, knowing that during the simulations of $(\phi|I_{moy})$, φ is rejected if it is greater than event I_{max}. Then, the vectors of effective rainfall intensities are estimated corresponding to each distribution. This procedure is repeated for all events.

1.3.3 Results and Discussions

The obtained hydrographs from the two φ distributions give statistically the same results: dispersion and variability for all studied characteristics (V, Q_p, t_p, and t_b). Even if the mode of the variation

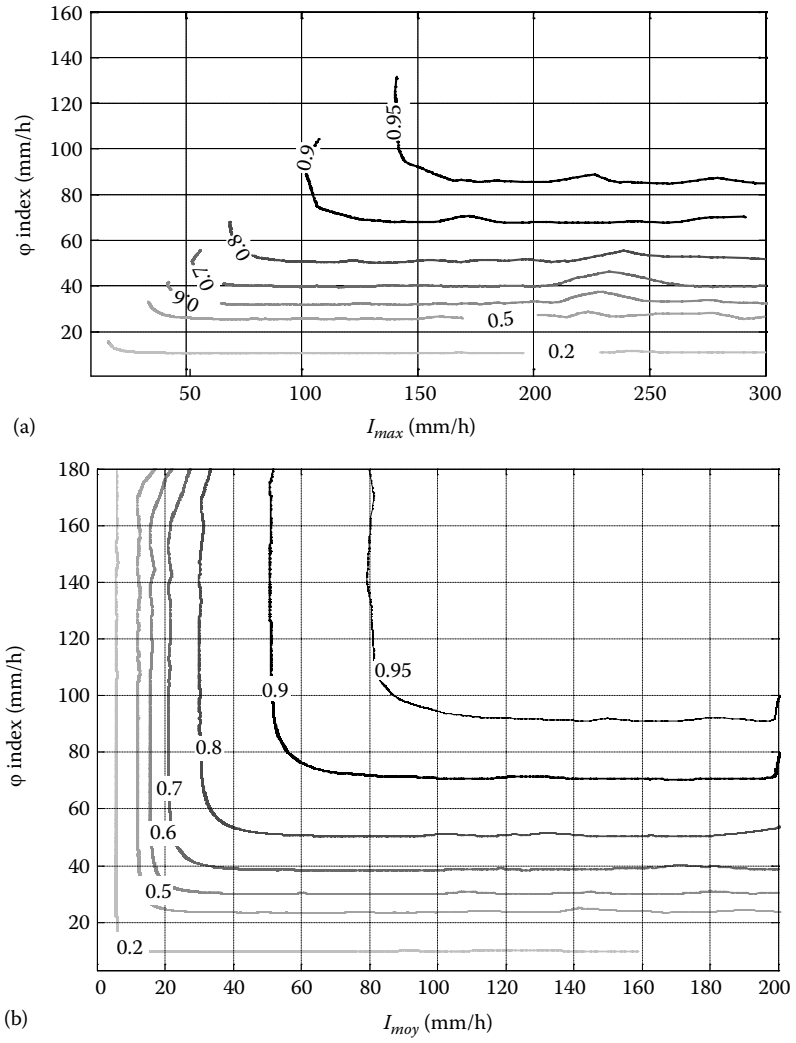

FIGURE 1.2 (a) Maximum intensity–φ-index–frequency. (b) Average intensity–φ-index–frequency.

coefficients for t_p and t_b is of 0.40, which is not relevant for the water management knowing that the time scale is of 5 min. Besides for V and Q_p derived distribution, 40% of events are not restituted either for volume or for peak discharge or for both. Consequently, the duration that is implicitly in the I_{moy} term does not improve the results, unlike what we expect. This is predictable if we examine Kendall's τ, it is more important (0.72) for the couple (φ, I_{max}). Thus, the hypothesis of φ to I_{max} conditioning is justified, and the results suggest that the formation of runoff in this catchment may be governed by rainfall kinetic energy.

In conclusion, in order to apply the GIUH to ungauged basins, MCS are achieved for generating hydrographs. The dispersion of their characteristics (volume, peak discharge, time to peak, and base time) is analyzed, and allowed selecting the design hydrograph. The effective rainfall input of GIUH model is considered here as unknown and is estimated with infiltration index method (φ-index). Three main correlations are detected and tested between this index and the characteristic rainfall intensities: maximum intensity, average intensity, and duration. They are modeled with Archimedean copulas. Consequently, assuming distributions, the effective rainfall hyetographs are generated. It appears that

- The conditioning of φ-index to D disables the reconstitution of the observed values. At this step of this research, no conclusions can be drawn. Other types of copulas that model negative correlations have to be tested.
- The resulting hydrographs from the two φ-Intensities distributions give statistically the same results: dispersion and variability for all studied characteristics (V, Q_p, t_p, and t_b).
- The effective rainfall hyetographs derived from the two φ-Intensities distributions allowed reconstituting observed hydrographs; unlike the case of which deals with rainfall duration (I_{moy} is the ratio between rainfall depth and duration). The average intensity does not seem to improve the results.
- The encouraging results derived from distribution allow supporting the hypothesis of the conditioning of φ to I_{max}. Moreover, they suggest that kinetic rainfall energy may control runoff.
- Other investigations may be possible between φ and other variables such as antecedent rainfall or kinetic rainfall energy.

1.4 Application 2: Intensity–Index of Infiltration Frequency: (2I2F)

The discharge prediction in ungauged basins constitutes a very important stage in the conception of road drainage works, stream crossing, flood protection, water resource and water quality management, and generally in the definition of soil occupation and regional development schemas.

Effective rainfall constitutes the climatological inputs of discharge prediction in models based on Unit Hydrograph methodology. It derives from infiltration process that represents an important part of streamflow process. One of the approximation infiltration process models is the Horton process supposing that runoff is generated by rainfall intensities that are greater than the soil infiltration capacity. The index infiltration method (φ-index) represents the average value of infiltration capacity f through the duration (D_R) of rainfall (Equation 1.8). This method is still largely used for estimating effective rainfall and deducing flood volume for specific rainfall events.

$$\varphi = \frac{1}{D_R} \int f(t) \mathrm{d}t \tag{1.8}$$

However, the applicability of the φ-index method reveals particularly complicated for ungauged basins due to the large degree of spatial heterogeneity of soil basin and rainfall. For this reason, the regionalization is suggested as a solution to provide the estimation of variables in ungauged basins.

Basing on the works of Ellouze-Gargouri and Kebaili-Bargaoui in 2006 [5], the authors [9] focused only on modeling the relationship between φ-index and maximum rainfall intensity (I_{max}).

They began by modeling the correlation between φ-index and I_{max}, for 22 catchments (areas between 1 and 10 km^2) in Tunisia (from 35°N to 37°N, from 8°E to 11°E), in a semi-arid climate zone (average annual rainfall between 280 and 500 mm) [9]. Then, they regionalized the copula parameter based on physiographic and geographical catchment characteristics to explain the inter-sites variability.

1.4.1 Bivariate Modeling of Infiltration Index and Rainfall Intensity

The series (I_{max}, φ) of 22 catchments are considered separately. The detection of the nature of dependence between these variables is achieved with K-plot (see Appendix 1.A.4).

Figure 1.3 shows the different K-plots for each catchment. This reveals that the dependence between I_{max} and φ exists, for all of the catchments, which is positive and very important. Indeed, the points fall near the curve K_0. The degree of this dependence is measured by Kendall's τ, which is reported in Table 1.4 as well as their test statistic z^*. It shows that the hypothesis of independence between I_{max} and φ is rejected for the all of the catchments and that the correlation is very high. Indeed, the values range from 0.47 to 0.91.

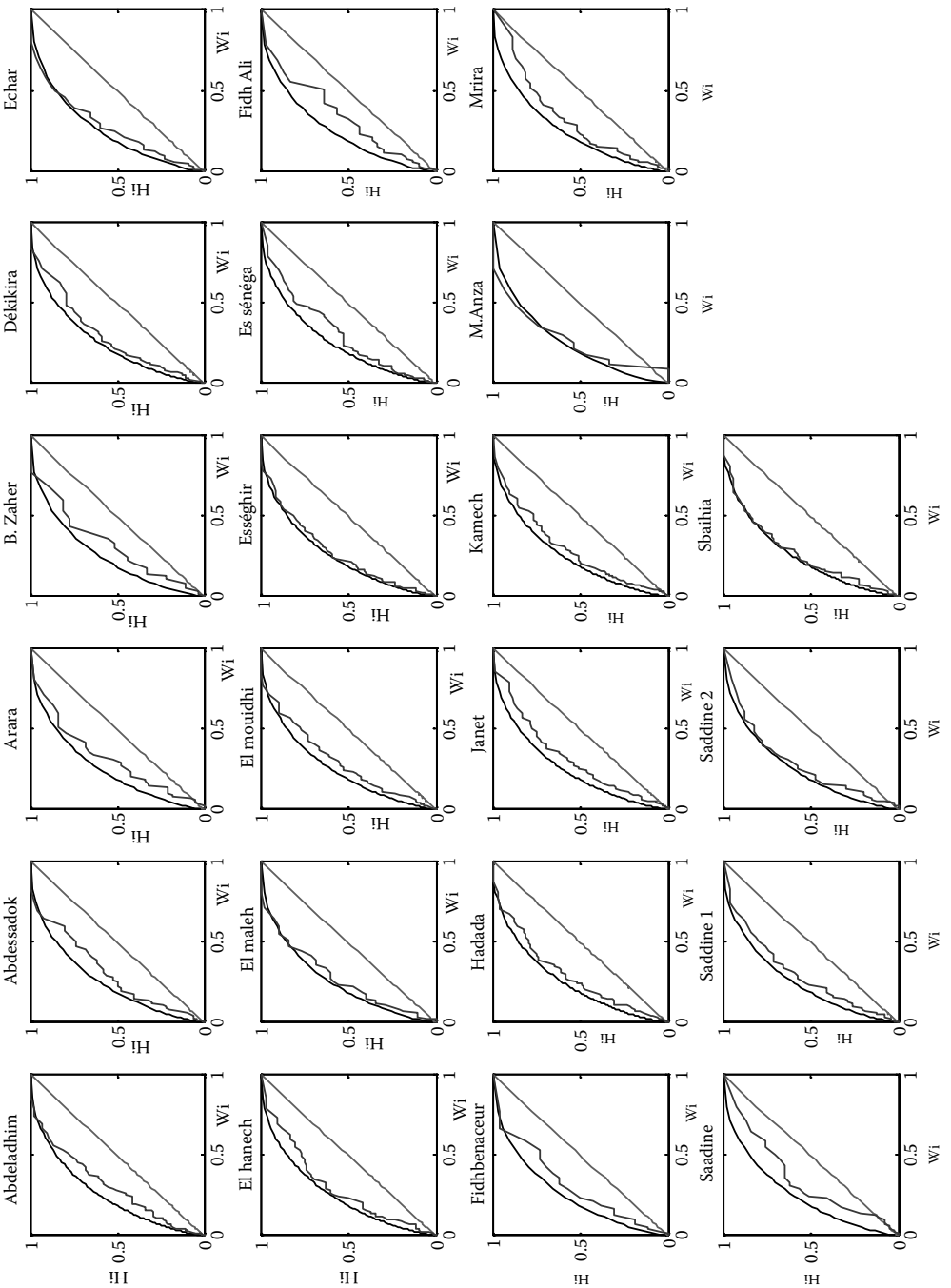

FIGURE 1.3 K-plots for the different catchments.

TABLE 1.4 Independence Test Results H_0 for (I_{max}, φ).

Designation	Basin	Sample Size	T	z^*	H_0	a
14	Abdeladhim	74	0.68	8.58	Rejected	3.13
10	Abdessadok	57	0.68	7.50	Rejected	3.16
15	Arara	39	0.58	5.24	Rejected	2.41
22	BrahimZaher	29	0.60	4.59	Rejected	2.52
11	Dékikira	62	0.77	8.81	Rejected	4.30
13	Echar	37	0.80	7.00	Rejected	5.08
9	El hanech	73	0.76	9.48	Rejected	4.12
20	El Maleh	39	0.81	7.27	Rejected	5.29
16	El mouidhi	67	0.72	8.64	Rejected	3.60
19	Es séghir	70	0.88	10.74	Rejected	8.14
12	Es sénéga	76	0.72	9.23	Rejected	3.60
4	Fidh Ali	32	0.53	4.28	Rejected	2.14
3	Fidhbenaceur	28	0.66	5.04	Rejected	3.08
7	Hadada	69	0.73	8.91	Rejected	3.75
8	Janet	73	0.64	8.06	Rejected	2.81
21	Kamech	91	0.75	10.53	Rejected	4.00
5	MrichetAnza	16	0.78	4.23	Rejected	4.61
26	Mrira	54	0.67	7.11	Rejected	3.00
18	Saadine	38	0.47	4.19	Rejected	1.90
1	Saddine 1	51	0.73	7.55	Rejected	3.68
2	Saddine 2	44	0.76	7.28	Rejected	4.18
17	Sbaihia	97	0.86	12.44	Rejected	7.00

Note: τ, Kendall's τ; z^*, test statistic; H_0, null hypothesis; a, copula parameter.

Hence to model the previous correlations, the methodology used is as indicated in the previous application. Gumbel copula could be selected for the whole basins, with a local parameter a_i varying from 1.9 to 11.1.

1.4.2 Regionalization of Copula Parameter

To regionalize the model parameter a_i through sites ($i = 1, m$; m number of observed sites), the $\tau^{(l)}$ ($l = 1, k$; k number of physiographic and geographical characteristics $Q_i^{(l)}$) were calculated for each couple ($a_i, Q_i^{(l)}$). The $\tau^{(l)}$ allow the analysis of whether the correlations between catchment characteristics and model parameter exist. Moreover, $\tau^{(l)}$ indicate the representativeness of characteristic. The higher degree of dependence is, the more representative the characteristic is. Consequently $\tau^{(l)}$ makes it possible to sort the characteristics relatively to their explanatory capacity in copula parameter.

The delimitation of catchments into regions according to each representative characteristic is achieved with the maximization of Kendall's τ by subregion. Let consider the sorted representative characteristic set $Q_i^{(l)}$ according to the sign of $\tau^{(l)}$, and the copula parameter set a_i, then seek for the subset ($Q_p^{(l)}$, a_p) ($p = 1, m$; m number of observed sites) that maximize the $\tau_p^{(l)}$. This subset of p catchments corresponds to the desired region. The considered physiographic characteristics are area, perimeter, maximum altitude, minimum altitude, specific height (difference between maximum altitude and minimum altitude), global slope index, equivalent rectangle length, equivalent rectangle width, Gravellus index, the percentage of pasture land, the percentage of forest cover, the percentage of cereal culture area, the percentage of arboriculture area and the percentage of area affected by antierosive practices. The former percentage is calculated on the basis of the area controlled by antierosive practices. In addition, geographical characteristics North latitude and East longitude are considered.

1.4.3 Results of Regionalization

The regionalization leads to the formation of four main groups of copula parameters: the first region (*R*1) is the catchments situated in North with a percentage of less than 20% of antierosive practices and without forest cover, the second region (*R*2) is constituted of South-Western catchments with a percentage of less than 20% of antierosive practices and without forest cover, the region (*R*3) includes the catchments with forest cover and the last region (*R*4) encloses the catchments with a nonweak percentage of anti-erosive practices. The results show that the catchments in a same region are not necessary geographically contiguous. Indeed, the delineation is hydro-physiographical and not geographical ones.

To illustrate the impact of the regionalization on the joint distribution of (I_{max}, φ), one may propose to generate, for fixed catchments belonging to a given region, couples (I_{max}, φ), obeying to the regional copula parameter. To this end the case of Kamech catchment is presented, which belongs to *R*1. The considered samples of (I_{max}, φ) are constituted of 91 independent events over a period of 11 years from 1994 to 2004 for Kamech. The fitted marginal distribution of I_{max} is Lognormal distribution with $\mu_{Imax} = 3.30$ and $\sigma_{Imax} = 0.83$ and the one of φ is Gamma distribution with $\mu_{\varphi} = 27.2$ mm/h and $\sigma_{\varphi} = 24.2$ mm/h.

In order to simulate couples (I_{max}, φ), the methodology of generation proposed by [6] is adopted. One deals with the couple ($F_{Imax}(I_{max})$, $F_{\varphi}(\varphi)$) and not with the couple (I_{max}, φ). Thus, one uses the random vector ($U = F_{Imax}(I_{max})$, $V = F_{\varphi}(\varphi)$), which has uniform marginals on [0, 1]. Consequently in order to simulate the couples (*U*, *V*), one has to use the conditional distribution of *V* knowing *U*. However, the conditional distribution of Gumbel copula is not reversible, [6] proposed to

a. Simulate independently *s* and *q* in uniform through the interval [0, 1]
b. Determinate $t = K^{-1}(q)$ with $K(t) = t(1 - \ln(t)/a)$
c. Determinate $u = \phi^{-1}(s\phi(t))$ and $v = \phi^{-1}((1 - s)\phi(t))$, φ is the Gumbel copula generator
d. Determinate $F^{-1}_{\mathrm{Im}ax}(u)$ and $F^{-1}_{\varphi}(v)$ according to I_{max} and φ distributions

The number of generated couples is equal to 10,000. Should be it is that observed values concern independent rainfall events, and any conclusion does not be drawn for simulated ones. Figure 1.4 shows the isolines of simulated couples (I_{max}, φ) with regional Gumbel copula and those of observed ones. These isolines correspond to I_{max}–φ–*frequency* curves (*2I2F*) and provide for a fixed frequency, the diverse possible couples of (I_{max}, φ). One notes that for the small probabilities of nonexceedance, the simulated and observed values

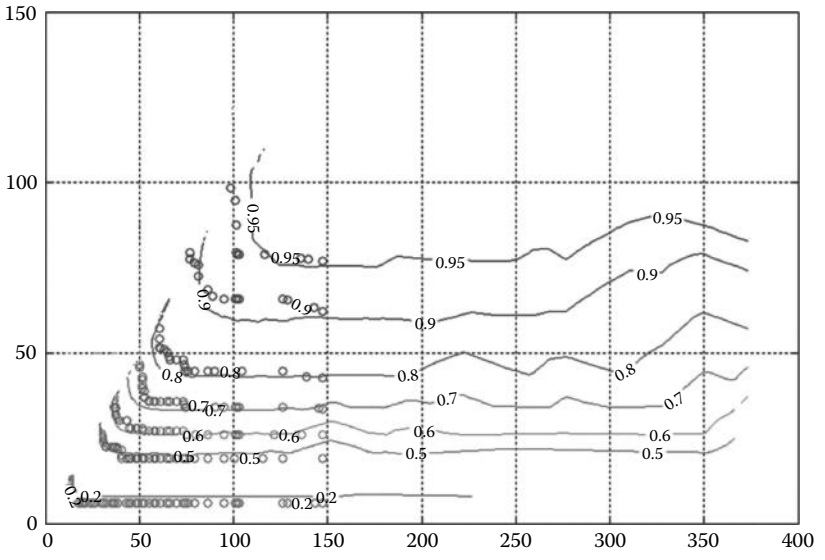

FIGURE 1.4 Isolines 2I2F of Kamech catchment.

are close. On the other hand, starting from the frequency 0.90, the copula of Gumbel overestimates the quantiles. Thus, the event of 12 October 1995 (I_{max} = 148 mm/h, φ = 34 mm/h) has been reconstituted with the same joint frequency of 0.7 (simulated and observed). Should be it is that this event represents one of main observed flood volumes with a frequency of 0.99, and I_{max} frequency equal to 97.3% and the one of φ equal to 71%. As a result, the determination of φ-index allows calculating runoff volumes, which represent an important stake in water resource management. Indeed, runoff volume intervenes in the estimation of sediment transport, filling or draw-off of reservoirs. However, the event (I_{max}, φ) frequency may not be sufficiently informative concerning the occurrence of flood volume.

1.5 Summary and Conclusions

Copulas are mathematical objects that fully capture the dependence structure among random variables and hence offer great flexibility in building multivariate stochastic models. Since their introduction in hydrology in the 2000s, copulas have gained considerable popularity in several fields of hydrological sciences such as flood frequency analysis; drought frequency analysis; rainfall frequency analysis; design rainfall; design floods; regional analysis; analysis under climate change; hydrological extremes; uncertainty modeling; geostatistical models; remote sensing observations.

Copulas offered the opportunity to determinate multivariate statistic quantities such as joined probabilities, conditioned probabilities, and return periods of events that were unsolvable by classical multivariate distributions. A monthly updated database of recent references on copula can be found in www.STAHY.org.

In this chapter, two applications were presented: the first is the estimation of runoff for an ungauged catchment using geomorphological instantaneous unit hydrograph and the second is the modeling of the correlation of infiltration and rainfall intensities. The main conclusions that can be drawn are

- The conditioning of infiltration-index to rainfall duration disables the reconstitution of observed hydrograph. We suggest testing other types of copulas which model negative correlations.
- The effective rainfall hyetographs derived from two φ-Intensities distributions (maximum intensity and average intensity) allowed reconstituting observed hydrographs; unlike the case of which deals with rainfall duration. We note that the average intensity does not seem to improve the results.
- The encouraging results derived from distribution allow supporting the hypothesis of the conditioning of infiltration index to maximum intensity and suggest that kinetic rainfall energy may control runoff.
- Particular isolines *2I2F* (Intensity-Index of Infiltration Frequency) were proposed. They can be used in design effective rainfall or design flood.
- Other investigations may be possible between Infiltration index and other variables such as antecedent rainfall or kinetic rainfall energy.

1.A Appendix

1.A.1 Archimedean Copulas, Their Generator, and Relation between Copula Parameter and Kendall's Tau

Several references published copula models. One famous reference: [23] who presented among these models, the Archimedean ones and particularly those of one parameter. Table 1.5 shows the copula generators and the relation between the copula parameter and Kendall's τ.

1.A.2 Functions of Goodness-of-Fit

K(z) function is the distribution function of the copula $C(U, V)$. Reference 13 showed that this distribution function is related to the generator ϕ of an Archimedean copula through the expression of $K(z)$:

TABLE 1.5 Archimedean Copulas, Their Generator, and Relation between Copula Parameter and Kendall's τ

One-Parameter Archimedean Copulas	Generator	Relation between Copula Parameter a and Kendall's τ
Frank	$\phi(t) = -\ln\left(\frac{e^{-at}-1}{e^{-a}-1}\right) \quad a \neq 0$	$\tau(a) = 1 - \frac{4}{a} + \frac{4}{a^2}\int_0^a \frac{t}{e^t - 1}\mathrm{d}t$
Gumbel	$\phi(t) = (-\ln(t))^a \; a > 0$	$\tau(a) = 1 - 1/a$
Clayton	$\phi(t) = a(t^{-1/a-1}) \; a > 0$	$\tau(a) = 1/(2\,a+1)$

$$K(z) = \frac{z - \phi(z)}{\phi'(z)} \tag{1.9}$$

An empirical $K(z)$ can be calculated for any z as the proportion of empirical values of $C(u, v)$ that is less than z:

$$K_{emp}(z) = \frac{\{\text{number of } z_i \leq z\}}{n} \tag{1.10}$$

$J(z)$ function or cumulative: Tau is related to a copula through the expression

$$\tau = -1 + 4\int_0^1\int_0^1 C(u,v)c(u,v)\,\mathrm{d}u\mathrm{d}v \tag{1.11}$$

$J(z)$ function is expressed by

$$J(z) = -1 + 4\frac{\left(\int_0^z\int_0^z C(u,v)c(u,v)\,\mathrm{d}u\mathrm{d}v\right)}{C(z,z)^2} \tag{1.12}$$

The full double integral is a probability weighted average of $C(u, v)$. To compare this, the partial integral has to be divided by the weights, thus the first power of $C(z,z)$ is the denominator. This quotient gives the average value of $C(u, v)$, which increases as a function of z. The second $C(z, z)$ divisor expresses this average relative to $C(z, z)$. It should be that $J(1) = \tau$.

An empirical cumulative τ can also be calculated, expressed by

$$J(z) = \frac{-1 + 4I(z)}{C(z,z)^2} \tag{1.13}$$

where $I(z)$ is defined by $I(z) = 1/n\sum_{i=1}^{n} z_i \times \mathbf{I}\{u_i < zetv_i < z\}$, with $\mathbf{I}$ is the indicator function.

M(z) function is the cumulative conditional mean defined by

$$M(z) = E(V|U < z) = \frac{\int_{u=0}^{z}\int_{v=0}^{1} v \cdot c(u,v)\,\mathrm{d}u\mathrm{d}v}{z} \tag{1.14}$$

Verifying $M(1) = 1/2$.

Let $D(z)=\sum_{i=1}^{n}\mathbf{I}\{u_i<z\}$ and $N(z)=\sum_{i=1}^{n}v_i\mathbf{I}\{u_i<z\}$, the empirical version of $M(z)$ is expressed by

$$M(z)=\frac{N(z)}{D(z)} \tag{1.15}$$

With $D(1)=n$ and $N(1)=n/2$.

L(z) and R(z) functions are *Left* and *Right* tail concentration functions. The two functions $L(z)$ and $R(z)$ are

$$L(z)=\frac{P(U<z,V<z)}{z}=\frac{C(z,z)}{z} \tag{1.16}$$

$$R(z)=\frac{P(U>z,V>z)}{1-z}=\frac{1-2z+C(z,z)}{1-z} \tag{1.17}$$

[17] defined lower tail dependence parameter for $L(0)=\lambda_{\min}=\lim_{u\to 0}P(Y\le F_Y^{-1}(u)|X\le F_X^{-1}(u))=\lim_{z\to 0}L(z)$ (left tail), and upper tail dependence parameter for $R(1)=\lambda_{\max}=\lim_{u\to 1}P(Y>F_Y^{-1}(u)|X>F_X^{-1}(u))=\lim_{z\to 1}R(z)$ (right tail).

L function is analyzed for $z\in[0,1/2]$ and R function for all $z\in[1/2,1]$.

1.A.3 Goodness-of-Fit: Bivariate χ^2

Let (X, Y) be a sample of size n.

The X_i and Y_i are regrouped into six classes, respectively $(v_0; v_1]$; $(v_1; v_2]$; …; $(v_5; v_6]$, and $(w_0; w_1]$; $(w_1; w_2]$; …; $(w_5; w_6]$, where the boundaries v_i's (w_i) are chosen such that the number of observations λ_1, λ_2 …, λ_6 respectively η_1, η_2, …, η_6, in the corresponding classes are as symmetrically distributed as possible. We thus obtain 36 two-dimensional intervals $(v_{i-1}; v_i]\ x\ (w_{i-1}; v_i]$, $i, j=1\ldots6$. Then, we regroup these intervals in k larger rectangular interval classes, such that an expected frequency of at least 1% in each class and a 5% expected frequency in 80% of the classes. The fitted number of observations $f_{i,j}$ in each 36 two-dimensional intervals $(v_{i-1}; v_i]\ x\ (w_{i-1}; v_i]$, is given by

$$f_{i,j}=n\Big[\big(F(v_i),F(w_j)\big)-\big(F(v_{i-1}),F(w_j)\big)-\big(F(v_i),F(w_{j-1})\big)+\big(F(v_{i-1}),F(w_{j-1})\big)\Big]$$
$$i,j=1\ldots6,\qquad F(x,y)=C\big(F_X(x),F_Y(y)\big) \tag{1.18}$$

Let $z_{i,j}$ be the number of observations in the 36 two-dimensional intervals. Through summation of z_{ij}'s respectively $f_{i;j}$'s, one obtains the number of observations O_k, respectively, the expected number of observations E_k, in each rectangular interval class k. The bivariate chi-square statistic is then defined by

$$\chi^2=\sum_{k=1}^{m}\frac{\big(O_k-E_k\big)^2}{E_k} \tag{1.19}$$

1.A.4 Kendall's Plots

For a bivariate sample (X, Y) of size n, one defines for a given pair (X_i, Y_i) a random variable $H(i)$:

$$H(i)=\frac{1}{n-1}\#\big\{j\ne i: X_j\le X_i, Y_j\le Y_i\big\}\text{ for each } i:\ 1\le i\le n \tag{1.20}$$

Let the quantity $W_{i:}n$ represent the expectation of the ith order statistic associated to the random variable H of size n from the distribution K_0, under the null hypothesis of independence. By definition, it is expressed by

$$W_{i:n} = n\binom{n-1}{i-1}\int_0^1 w k_0(w)\{K_0(w)\}^{i-1}\{1-K_0(w)\}^{n-i}\,\mathrm{d}w \tag{1.21}$$

[11] proposes to take as H distribution, the asymptotic null distribution K_0, defined by

$$K_0(w) = \Pr(UV \le w) = \int_0^1 \Pr(U \le w/v)\mathrm{d}v = \int_0^w 1\mathrm{d}v + \int_w^1 w/v\,\mathrm{d}v = w - w\log w;\ \text{with } w \in [0,1] \tag{1.22}$$

k_0 is the density corresponding to K_0 (U and V are independent uniform random variables on the interval [0,1]).

After sorting $H(i)$ to get $H(1) < H(2) \ldots < H(n)$, one plots the pairs ($W_{i:}n$, $H(i)$), for each $i \in [1,n]$. The interpretation of the graph ($W_{i:}n$; $H(i)$): K-plot allows to detect the dependence: the greater departure from the 45° reference line, the greater the dependence. For negative dependence, the points fall on the horizontal axis. Similarly, for a positive dependence, the points fall on the curve $K_0(w)$. The denomination Kendall plot comes from the relation between the $H(i)$ and the Kendall's τ [11]. They demonstrate that an estimation of Kendall's τ can be calculated as follows:

$$\hat{\tau} = -1 + 4\frac{1}{n}\sum_{i=1}^{i=n} H(i) \tag{1.23}$$

References

1. Ashkar, F. and Aucoin, F., 2011. A broader look at bivariate distributions applicable in hydrology. *Journal of Hydrology* 405: 451–461.
2. Bárdossy, A., 2006. Copula-based geostatistical models for groundwater quality parameters. *Water Resources Research* 42: W11416, doi: 10.1029/2005WR004754, 12pp.
3. Bárdossy, A., Mascellani, G., and Franchini, M., 2006. Fuzzy unit hydrograph. *Water Resources Research* 42: W02401, doi: 10.1029/2004WR003751, 10pp.
4. Chebana, F. and Ouardaa, T.B.M.J., 2009. Multivariate quantiles in hydrological frequency analysis. *Environmetrics* 22: 63–78.
5. Ellouze-Gargouri, E. and Kebaili-Bargaoui, Z., 2006. Prédétermination des débits maximaux de crue par simulation Monte-Carlo de la pluie nette. *Revue des Sciences de l'Eau* 19(4): 327–345.
6. Embrechts, P., Lindskog, F., and McNeil, A.J., 2003. Modelling dependence with copulas and applications to risk management. In: *Handbook of Heavy Tailed Distributions in Finance*, ed. S. Rachev, pp. 329–384. Elsevier Sciences, New York.
7. Fleurant, C., Kartiwa, B., and Roland, B., 2006. Analytical model for a geomorphological instantaneous unit hydrograph. *Hydrological Processes* 20(18): 3879–3895.
8. Gargouri-Ellouze, E. and Chebchoub, A., 2008. Depth–duration–frequency with copulas. *Hydrological Sciences Journal* 53(4): 802–817.
9. Gargouri-Ellouze, E. and Bargaoui, Z., 2009. Investigation with Kendall plots of infiltration index–maximum rainfall intensity relationship for regionalization. *Journal of Physics Chemistry and Earth*, 34(10–12), 642–653. doi:10.1016/j.pce.2009.02, 12pp.
10. Gargouri-Ellouze, E. and Bargaoui, Z., 2012. Runoff estimation for an ungauged catchment using geomorphological instantaneous unit hydrograph (GIUH) and copulas. *Water Resources Management* (26): 1615–1638. doi: 10.1007/s11269-012-9975-6, 24pp.

11. Genest, C. and Boies, J.C., 2003. Detecting dependence with Kendall plots. *American Statistician* 57: 275–284.
12. Genest, C. and Favre, A.C., 2007. Everything you always wanted to know about copula modeling but were afraid to ask. *Journal of Hydrological Engineering ASCE* 12: 347–368.
13. Genest, C. and Rivest, L., 1993. Statistical inference procedures for bivariate Archimedean copulas. *Journal of American Statistics Association* 88: 1034–1043.
14. Hubert, P., 2000. *Glossaire International d'Hydrologie* (1992) http://hydrologie.org/glu/frdic/dictemps.htm.
15. Hürlimann, W., 2004. Fitting bivariate cumulative returns with copulas. *Comparative Statistical Data Analysis* 45: 355–372.
16. Jain, V. and Sinha, R. 2003. Derivation of unit hydrograph from GIUH analysis for a Himalayan river. *Water Resources Management* 17(5): 355–376(22).
17. Joe, H. 1997. *Multivariate Models and Dependence Concepts. Monographs on Statistics and Applied Probability*. Chapman & Hall, London, U.K.
18. Kelly, K.S. and Krzysztofowicz, R., 1997. A bivariate meta-Gaussian density for use in hydrology. *Stochastic Hydrology and Hydraulics* 11: 17–31.
19. Kumar, R., Chatterjee, C., Singh, R.D., Lohani, A.K., and Kumar, S., 2007. Runoff estimation for an ungauged catchment using geomorphological instantaneous unit hydrograph (GIUH) models. *Hydrological Processes* 21(14): 1829–1840.
20. Kumar, R., Chatterjee, C., Lohani, A.K., Kumar, S., and Singh, R.D., 2002. Sensitivity analysis of the GIUH based Clark model for a catchment. *Water Resources Management* 16(4): 263–278.
21. Kurothe, R.S., Goel, N.K., and Mathur, B.S., 1997. Derived flood frequency distribution for negatively correlated rainfall intensity and duration. *Water Resources Research* 30(9): 2103–2107.
22. Meylan, P., Favre, A.-C., and Musy, A., 2008. *Hydrologie Fréquentielle: Une Science Prédictive*. PPUR Presses Polytechniques, Switzerland, 173pp.
23. Nelsen, R.B., 1999. *An Introduction to Copulas*. Springer, New York.
24. Prékopa, A. and Szántai, T., 1978. A new multivariate gamma distribution and its fitting to empirical streamflow data. *Water Resources Research* 14(1): 19–24.
25. Rootzén, H. and Tajvidi, N., 2006. Multivariate generalized Pareto distributions. *Bernoulli* 12(5): 917–930.
26. Salvadori, G., 2004. Bivariate return periods via 2-copulas. *Statistical Methodology* 1: 129–144.
27. Salvadori, G. and De Michele, C., 2010. Multivariate multiparameter extreme value models and return periods: A copula approach. *Water Resources Research* 46: W10501, doi:10.1029/2009WR009040, 11pp.
28. Sarangi, A., Madramootoo, C., Enright, P., and Prasher, S., 2007. Evaluation of three unit hydrograph models to predict the surface runoff from a Canadian watershed. *Water Resources Management* 21(7): 1127–1143.
29. Venter, G., 2002. Tails of copulas. *Proceedings of the Casualty Actuarial Society* 89: 68–113.
30. Venter, G., 2003. Quantifying correlated reinsurance exposures with copulas. *Casualty Actuarial Society Forum* Spring: 215–229.
31. Yue, S., 2001. Applicability of the Nagao–Kadoya bivariate exponential distribution for modeling two correlated exponentially distributed variates. *Stochastic Environmental Research and Risk Assessment* 15(3): 244–260.
32. Yue, S., Ouarda, T.B.M.J., and Bobée, B., 2001. A review of bivariate gamma distributions for hydrological application. *Journal of Hydrology* 246: 1–18.

2

Artificial Neural Network–Based Modeling of Hydrologic Processes

Emery A. Coppola Jr.
NOAH LLC

Anna Szidarovszky
Zonge International Inc.

Ferenc Szidarovszky
NOAH LLC

AUTHORS

Emery A. Coppola Jr. is president and cofounder of NOAH LLC, a firm that specializes in the application of artificial neural network (ANN), optimization, and other advanced techniques to hydrologic modeling and water resources management. Dr. Coppola received a BS in geology and oceanography from the University of Miami (Florida), an MS in geological engineering from Drexel University, and a PhD in hydrology from the University of Arizona. Dr. Coppola has consulted internationally on water resources evaluation and sustainability projects and has conducted research funded by the US Geological Survey, the US Environmental Protection Agency, the National Science Foundation, and the European Science Foundation. He has peer review publications on topics that include ANNs, fuzzy logic, optimization, multiobjective analysis, and conflict resolution. One of the most experienced hydrologists in the United States for applying ANNs to water resources management problems, Dr. Coppola has served as project manager on ANN modeling projects that include groundwater resources, water distribution systems, and surface water systems.

Anna Szidarovszky, employed by Zonge International, Inc., as a geophysical data processor, received her BS in math education and MS in mining, geological, and geophysical engineering from the University of Arizona. She has a diverse practical and theoretical background in ANNs and has applied them to complex problems as well as developed computer source code for their implementation. During her graduate work for the Strategic Environmental Research and Development Program, Ms. Szidarovszky developed an ANN system for identifying unexploded ordinances. The methodology she implemented included an advanced statistical procedure for minimizing false classifications. She has published her work in peer review journals and has been an invited speaker to annual international geophysical conferences.

Ferenc Szidarovszky, vice-president, cofounder, and director of Operations Research for NOAH LLC, received his PhD in mathematics from Eotvos University of Sciences of Budapest, Hungary, and a second PhD in economics from the Budapest University of Economic Sciences. He is also a recipient of two higher scientific degrees given by the Hungarian Academy of Sciences: candidate in mathematics and doctor of engineering sciences. In Hungary, he held faculty positions with the Eotvos University of Sciences, University of Horticulture and Food Industry as well as with the Budapest University of Economic Sciences. Dr. Szidarovszky moved to the United States in 1987 and, until his retirement in 2011, was a full professor with the Systems and Industrial Engineering Department at the University of Arizona and subsequently received a joint appointment with the Department of Hydrology and Water Resources. He has been involved in many projects investigating theoretical issues and applications in mathematics, economics, and natural resources management. Dr. Szidarovszky is the author of nine textbooks and monographs in the United States, including a recent one in water resources systems analysis. He is also the author of over 300 research publications in leading journals and has given many presentations in conferences around the world. He was recognized with the prestigious award (1998) "Dr. Habil in Engineering," Budapest Technical University.

PREFACE

In the late 1990s and early 2000s, when we and our colleagues began applying artificial neural networks (ANNs) to hydrologic problems, there was relatively little interest in the field. Most researchers were not familiar with ANN technology, and those who had a minimal understanding often expressed an aversion to a "less than elegant black-box approach." It was often difficult to convince peer reviewers that ANN-related modeling research had technical merit or that the findings were universally transferable and constituted a significant contribution to hydrology. Over the last 10 years, with a seemingly exponential increase in publications demonstrating the power of the ANN technology, this view has changed dramatically. Now, researchers and practitioners alike are using ANNs in larger numbers for addressing a wide variety of serious and complex hydrologic processes and problems.

As will be presented in this chapter, ANNs have certain inherent advantages over traditional physical-based models that often make them better suited for particular types of hydrologic modeling. Their flexibility and adaptability to a range of hydrologic process modeling and prediction applications and the ease of coupling ANNs directly with real-time data streams and optimization significantly increase their power and value. There is no doubt that they will become a basic modeling and management tool for hydrologic problems that continue to grow worldwide as human populations, economic activities, and climate changes impose new stresses and changes.

The purpose of this chapter is to

- Justify the use of ANN modeling for modeling complex hydrologic processes
- Contrast ANNs with more traditional physics-based modeling approaches like numerical models
- Provide an introductory overview of the invention and development of ANNs, along with their theoretical underpinning
- Provide general guidelines for developing and testing ANN models
- Use case studies to illustrate development and use of ANN modeling on representative hydrologic modeling applications

It is our hope that this chapter will not only introduce readers to the proven power of the ANN technology but its potential for new and novel applications in hydrologic modeling. In closing, we wish to acknowledge the contributions of several collaborators on previous work, some of which is presented in this chapter, particularly Dr. Mary Poulton of the University of Arizona and Mr. Emmanuel Charles of the US Geological Survey. They shared a vision of applying ANN technology to complex hydrologic problems and were among its earliest advocates as a standard modeling and prediction tool in hydrology.

2.1 Introduction

Clean water is rapidly becoming an increasingly scarce resource in many regions of the world; so much so, that in some places, it is now traded on water markets, similar to traditional commodities like oil and natural gas. While some may argue that a market-based system will incentivize more efficient use of this essential and irreplaceable resource, increasing worldwide demand, improper practices that diminish water quality, wasteful and inefficient water management practices, and climate change will continue to reduce the availability of clean water. Today, 1.2 billion people, approximately 20% of the world population, live in water-scarce areas. It is estimated that by the year 2025, 1.8 billion people will be living in regions with absolute water scarcity, and two-thirds of the world's population could be living under stressed conditions. Water resource problems that have become more serious in recent years include

aquifer overdraft (i.e., mining) of groundwater systems, saltwater intrusion and/or upcoming into coastal aquifers, algal blooms of surface water systems, and extreme low flow and flooding events on rivers.

In an effort to more effectively monitor and manage water, there has been a rapid proliferation of data acquisition of critical hydrologic and water management variables. A relatively recent technology adaptation in water management has been supervisory control and data acquisition (SCADA) systems. SCADA systems consist of instrumentation sensors and relay that measure, transmit, and store hydrologic and operational data at virtually any time frequency of interest (e.g., second, minute, and hour). As their name implies, SCADA systems extend beyond simple data collection and storage, in that data can be transmitted for display and analysis in real time, with human decision control variables like pumping rates adjusted to achieve operational and management objectives.

Data visualization tools like geographic information systems (GIS) have been used with much success to spatially depict and analyze data. Still, data monitoring and SCADA systems have largely been underutilized, where all too often, little to no effort is dedicated to analyzing or extracting useful information from these continuous data streams in real time to facilitate effective management decisions; in short, a "data-rich but information-poor" culture pervades much of the industry.

Given this confluence of increasingly serious water problems, the increasing proliferation of large and continuous data streams, and the need for real-time decision-making capability, there is a premium for a fast and accurate data-processing tool. Artificial neural networks (ANNs), a form of artificial intelligence modeled after the human brain, are a class of "data-driven" models that "learn" system behavior of interest from data. Due to their mathematical structure, ANNs are capable of providing extremely accurate predictions at specific target locations (e.g., groundwater monitoring wells, surface water stations) in real time using easily measurable variables like water levels, water extraction rates, and weather conditions. They have been used in a variety of hydrologic and water management applications, including groundwater level prediction, water treatment processes, streamflow prediction, algal bloom forecasting, and water demand.

In this chapter, the underlying theoretical and structural underpinnings of the ANN technology, its advantages and disadvantages relative to other methodologies, example applications, and its integration with optimization for promoting improved decision-making capability will be presented.

2.2 Differences between Physical-Based Models and ANN

Before presenting the underlying historical and theoretical underpinnings of ANNs, it is useful from a pedagogical perspective to first contrast this technology with more traditional physics-based modeling approaches. Physical-based models like analytical and numerical models are based upon the governing physics of the problem of interest. For example, the numerical groundwater flow model, MODFLOW, developed by the US Geological Survey (USGS), and used worldwide, uses the principles of mass conservation and momentum as the basis of its underlying numerical equations. The physics of flow is approximated by MODFLOW using Darcy's law, which assumes a porous media with laminar flow conditions. While the model can be used to represent a variety of hydrogeological environments, the accuracy of its solution is constrained by how close its underlying physical assumptions (e.g., Darcian flow) represent reality, the accuracy of its estimated input parameter values, boundary conditions, and for transient simulations, its initial conditions. Real-world groundwater systems exhibit significant spatial (i.e., heterogeneity), temporal (i.e., nonstationary), and even directional (i.e., anisotropy) variability, with parameter values like hydraulic conductivity exhibiting orders of magnitude variation directionally, even within very short distances and, in the unsaturated zone, temporally. Representing this real-world variability in a numerical model is infeasible, and often an average or typical representation of the system with the model is sought. Consequently, while these models are often effective at simulating and predicting general trends over space and time, their ability to accurately predict state variables like water levels at specific locations (e.g., monitoring well) in real time is limited.

In contrast, ANNs as an empirical-based model are not bound by simplifying physical and mathematical assumptions. In addition, they do not require inputs of difficult to estimate and/or characterize

parameter values like hydraulic conductivity. Instead, they learn directly from easily measurable variables, like water levels, pumping rates, and precipitation values. This underscores one of the major advantages of ANN models; they often use variables that are often more "transparent" (i.e., more directly measureable and quantifiable) than parameters used in traditional physics-based models.

While the historical data set used for developing the ANN model should ideally span the expected system behavior of interest for optimal performance, data sets approaching this range are often available or can be generated over time (e.g., variable pumping rates). Unlike physics-based models, a disadvantage to the ANN approach occurs if the system fundamentally changes, for example, installation of a new production well. Under these circumstances, a new ANN model would have to be developed with data that includes the effect of the changes on the system. However, based upon the literature, ANN models often do not require data sets that span relatively long historical periods to accurately model hydrologic systems for their typical range of behavior. This is attributable to the well-behaved nature of most hydrologic systems; that is, while system behavior may be highly nonlinear, it is typically not contradictory or inconsistent, whereby a small change in a particular input variable does not produce inconsistent results (e.g., more precipitation does not diminish groundwater levels).

Another powerful advantage that ANN models have is that, unlike numerical models, they can be initialized to real-time conditions, which is invaluable for accurate real-time prediction and management capability. The parameter and boundary conditions values of numerical models are calibrated to an assumed (often average) initial condition, and deviation from this initial condition can produce an imbalance in the calibrated model, producing highly erroneous solutions. This ability to initialize the ANN models to real-time conditions increases prediction accuracy over shorter time periods at location specific points. At the same time, as presented later in this chapter in the saltwater upconing case study, ANN models have proven capable of accurately predicting over extended time periods that span years.

A further advantage of the ANN model is their simple mathematical structure, which enables computation of solutions in seconds or less. Unlike numerical models, which consist of a system of numerical equations that must be solved simultaneously using complex numerical techniques like iterative matrix manipulations, the ANN equations are solved with simple mathematical operations. Because of this computational efficiency, ANN models are often used as "meta-models" or surrogate models for numerical models, where an ANN is trained from and used in lieu of a companion numerical model to exploit its superior computational speed while providing the same simulation or prediction capability. Their condensed nature also lends them to more efficient and effective integration with formal optimization.

While the use of ANN models in hydrologic problems are becoming more common, the methodology is still less accepted than more traditional physics-based models. Some of this aversion is due to a combination of a reluctance to use "black-box" models that do not explicitly represent the underlying physics as well as a general lack of familiarity with the ANN methodology. There is also an aversion because there is no mathematically strict rationale for determining the structure of an ANN model, although general heuristic guidelines are offered in the literature.

The reality is that no modeling approach is universally better or more applicable than another for all problems. ANN models offer relative advantages and disadvantages versus their counterpart physics-based models. For many types of problems, however, they provide not only an acceptable but superior alternative and should continue to receive increasing attention in the hydrologic field, particularly with the increasing proliferation of continuous data streams like SCADA.

2.3 Historical Overview of ANN Development

ANNs were first developed not in an effort to perform complex modeling and estimation for engineering and science applications but rather to understand brain operation and human learning. Humans and indeed animals can process complex signals from which they extract information and make informed

decisions. Over time, "reinforcement learning" enables humans and animals to extract relationships that arise not through complicated mathematical models but from repeated experiences.

The first mathematically functioning ANN can be famously traced back to McCulloch and Pitts [11]. McCulloch was interested in understanding learning in the brain, and Pitts was a first-rate mathematician who assisted McCulloch in developing the first mathematical model for learning, which consisted of nodes, representing brain neurons, connected by mathematical functions, representing the synaptic connections with weights, which were adjusted during "learning." Not only was their work revolutionary, their model actually serves today as the basis for the multilayered perceptron, which is the most commonly used ANN.

A number of important theoretical breakthroughs emerged over the 1940s, 1950s, and 1960s, including Hebb [8], who described the interrelations between the neurons during learning; Von Neuman [18], the father of the modern computer, who discussed the role of memory and the way how biological networks can form memories by strengthening synaptic connections in creating physical changes in the brain; the first neurocomputer by Minsky in 1951, demonstrating that Hebbian learning could be implemented by a machine [12]; and Rosenblatt and Wightman, who developed the Mark I perceptron neurocomputer [15], which was able to produce interesting and complex behaviors, recognize patterns, and make associations. Widrow and Hoff [20] developed a similar computer (called ADALINE and later the MADALINE), which had binary inputs and outputs (–1 and 1), and as in the perceptron a linear combination of the inputs was computed, where the weights were updated based on the value of this linear combination. Time-varying data were introduced into the McCulloch–Pitts neuron by Caianiello [3]. The very special and simple learning algorithms posed a very strong limitation on the complexity of problems that could be solved by these neural computers.

In 1969, Minsky and Papert [12] published the book *Perceptron*, which exposed limitations of certain ANNs for solving select problems. This publication reduced the level of interest and research in ANNs until the 1980s. The limitations and perceived drawbacks were eliminated by the introduction of a then new back-propagation learning algorithm [12,16,19]. As a result, research and applications in ANNs exploded in the 1980s and 1990s in fields spanning most disciplines in engineering and science, with even significant applications in business.

2.4 Kolmogorov's Theorem

Like many breakthroughs in applied science, astute scientists found an apparent relation between two different fields of study that connected the applied with the theoretical. In the case of ANNs, Hecht-Nielsen [9] noticed a connection between neural networks and a purely theoretical result posited by the father of modern probability theory A.N. Kolmogorov. Kolmogorov elegantly solved a major mathematical puzzle of the famous mathematician Hilbert, who in 1900 formulated 23 major unsolved mathematical problems as challenges for the twentieth century. Kolmogorov proved that any arbitrary continuous function on an n-dimensional cube can be exactly represented as a composition of additions and single-variable functions. The resulting theorem is considered as the theoretical foundation of ANN modeling and is an extremely important mathematical proof that attests to the powerful nonlinear modeling capability of ANN.

2.5 General ANN Structure

In the structure of neural networks, there are three kinds of neurons: input, output, and hidden neurons. The structure of a three-layer perceptron is shown in Figure 2.1, where m is the number of inputs, n is the number of outputs, and p is the number of nodes in the hidden layer.

We note that the structure shows that every node in the hidden layer is connected to all nodes in the input and output layers. The bias unit (B) assumes unit input values and its role is to speed up the learning process. Note that it is connected to all hidden nodes as well as to all outputs. Multilayer perceptrons have a similar structure. Each node receives several inputs, which depend on the location of this node in the hierarchy. Its inputs can be original inputs or hidden variables. It also generates an output that is

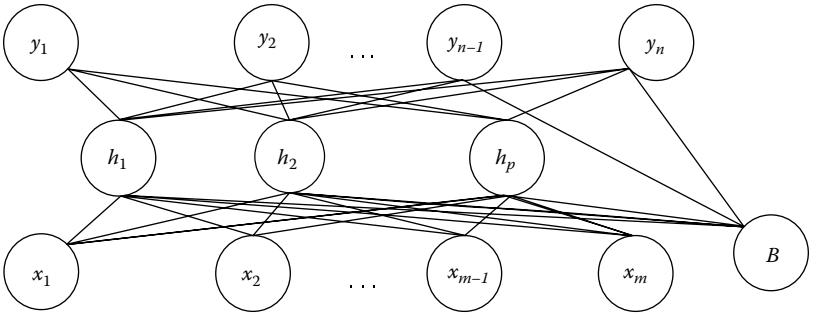

FIGURE 2.1 Three-layer perceptron structure.

directed toward to the nodes of the next hidden layer or to the output variables of the system. For notational convenience, let x_i, …, x_n denote the inputs and y denotes the output of a perceptron. The value received by the perceptron is a linear combination of its inputs:

$$Sum = \sum_i w_i x_i + w \tag{2.1}$$

where
the coefficients w_i are the multipliers of the inputs
w is the coefficient of the bias unit (with unit input value)

The output is then obtained from *Sum* via an activation function

$$v = f(Sum) \tag{2.2}$$

In practical applications, f is selected either the sigmoid

$$f(Sum) = \frac{1}{1+e^{-Sum}} \tag{2.3}$$

or the hyperbolic tangent function

$$\overline{f}(Sum) = \frac{e^{Sum} - e^{-Sum}}{e^{Sum} + e^{-Sum}} \tag{2.4}$$

The graphs of these functions are shown in Figure 2.2, and it is easy to show that

$$\frac{1}{2}\left(1+\overline{f}(Sum)\right) = \frac{1}{2}\left(1+\frac{e^{Sum}-e^{-Sum}}{e^{Sum}+e^{-Sum}}\right) = \frac{e^{Sum}}{e^{Sum}+e^{-Sum}} = \frac{1}{1+e^{-2Sum}} = f(2Sum) \tag{2.5}$$

Observe that f transforms *Sum* into the unit interval (0,1) and $\overline{f}$ transforms it into (–1,1) and that the two most popular activation functions are basically the same, they are linear transformations of each other. With given weights the first hidden variables can be computed from the inputs by using Equations 2.2 and 2.3, and then the second hidden variables can be obtained, and so on in the case of multiple hidden layers, and finally all outputs can be calculated. That is, with given set of weight values w_{ij}, the output y_k can be directly and very easily obtained for any input selection x_1, …, x_m.

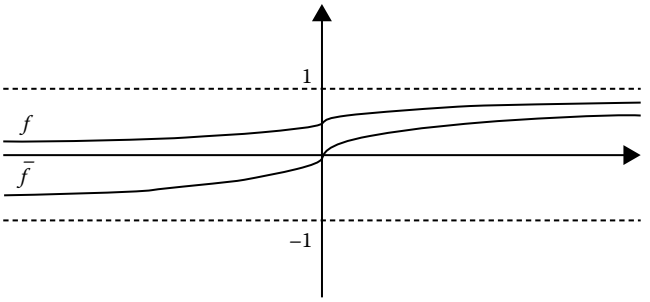

FIGURE 2.2 Graph of the sigmoid and hyperbolic tangent activation functions.

This recursive procedure is a function $\underline{y} = \underline{F}(\underline{x}, \underline{w})$, where $\underline{x}$ is an input vector, $\underline{w}$ is the vector having all connection weights, and $\underline{y}$ is the output vector. Learning algorithms are used to identify the optimal connection weight values. Training and validation are the two stages of any learning process. First, about half of the data are used to determine the connection weights, and then the second half of the data are used to check the accuracy of the obtained input–output relation $\underline{F}$. There are various references that discuss the popular learning algorithms for ANNs, and good summaries may be found, for example, in Poulton [14] Lingireddy and Brion [10], and Parker [13].

The training of an ANN requires the solution of an optimization problem, in which the unknown weights w_{ij} are the unknowns and the objective function is the mean squared error between the computed and actually observed output values. The most popular back-propagation method is the application of the gradient optimization method for this specially structured problem.

2.6 Development of a Particular ANN Model

2.6.1 Variable Selection

A very basic overview of the types of variables used for developing an ANN model is presented here. In accordance with systems theory, variables for systems may be classified into three general types: state variables, input variables, and output variables. State variables represent some fundamental inherent measure of the system's state or condition; examples include water levels and water quality concentrations. A state variable typically evolves over time and also often exhibits spatial variations.

State variables are often used as both input and output variables in an ANN model, with the set of inputs representing the state(s) of a previous time step(s) and the output variables often representing the state(s) for a future time step. Another typical group of input variables for ANN models are control variables, often called decision variables, which are variables over which humans have control; examples include extraction rates of a production well, the chemical dosing rate in a water treatment plant, and the storage release rates from a dam. Another group of input variables are random variables and, as the name implies, are variables that exhibit statistical randomness, over which there is no control; weather variables such as precipitation or temperature are classic examples. While the future value of these variables can be estimated using statistical methods, there is no way to control their outcome. The ANN outputs are the variables of most concern for the modeler, for example, the computed future water levels, salinity concentrations, algae counts, or even objective function values like economic costs, which may evolve over time in response to some combination of prior state(s), human controls, and random variables.

A critical first step in developing a robust and accurate ANN model is identifying the critical input or predictor variables necessary for predicting the system states of interest. One frequent criticism of ANN models is that they are "black boxes" that do not explicitly account for the physics of the system of interest. While this is true, in order to develop a robust model capable of accurately predicting system behavior of interest, a strong conceptual if not theoretical understanding of the system is necessary. Without

this understanding, the modeler will have difficulty in identifying the important input variables, related temporal and spatial issues that are important for proper data characterization and preprocessing, as well as characterizing the conditions under which the model will perform well, versus conditions where the model may not achieve desired performance.

Often, there is a temptation to "throw" as many variables into the model as possible, with the belief that the ANN model will identify the critical variables and minimize the relative predictive importance of the irrelevant variables accordingly. While this may be partially true, with limited data sets, more input variables result in a more complex or higher dimension error surface, which can compromise learning. The "principle of parsimony" is a general modeling edict that holds for all modeling in general; the complexity of the model should be reduced to the extent possible without compromising its ability to represent the fundamental properties of the system of interest. The goal of the modeler should be to develop an ANN that utilizes the critical input variables and can generalize system behavior, thereby consistently providing sufficiently accurate predictions. There is often a temptation for modelers to strive to achieve the lowest possible prediction error during validation or testing. Although not intuitively obvious, as discussed later in this chapter, achieving the lowest validation error does not necessarily ensure that the ANN (or other competing) model will be best for providing accurate predictions over a range of conditions.

For very complicated systems like algal blooms, where there are many possible input variables, a number of techniques may be used to identify an appropriate set of input variables. Principal component analysis is often used to identify strongly correlated variables to reduce the number of inputs for the ANN model. Another common modeling approach is the use of a special type of ANN called self-organizing maps (SOM) or Kohonen networks, which can be used to classify systems into different classes and identify the relevant variables for each. For example, Bae et al. [2] used SOM to classify 720 sampling sites on the basis of 27 environmental variables into seven clusters, with significant differences of environmental conditions among these clusters.

Another method is to use the ANN model to help identify relevant variables through trial and error and a sensitivity analysis. The ANN model can be used to generate sensitivity ratios that quantify how the training and validation errors change with and without inclusion of each of the candidate input variables. A more detailed overview of this may be found in Coppola et al. [5].

Yet another way to reduce the number of input variables, and therefore the dimensionality of the modeling problem, is to eliminate or combine highly correlated variables. For example, evapotranspiration is highly dependent on temperature. However, spatial and temporal variability of evapotranspiration across a study area is a function of differences in land use, type of vegetation, surface slopes, etc., and may produce significant variations in correlation between evapotranspiration and temperature. In cases where there is little variation in correlation between the two variables, a single variable (e.g., temperature) may be used in lieu of the two variables. In areas where there is significant variation between the two variables, a single lumped value that is the additive or average of the two variables may suffice. For cases where there is a significant difference in the magnitude of the values, normalization should be used to offset these differences. Lastly, time lags for select input or predictor variables may significantly improve ANN forecasting accuracy, particularly where a "memory" in the system affects and/or is correlated with future system outcomes that the ANN model is predicting.

2.6.2 Determining the Number of Hidden Nodes

Identifying the "optimal" number of hidden nodes is problem dependent, and a certain amount of trial and error is necessary. From Kolmogorov's theorem, Hecht-Nielsen [9] derived that the upper bound of the required number of hidden nodes is one greater than twice the number of input nodes. The number of hidden nodes must be capable of two simultaneous objectives; providing sufficient representation of the task but sufficiently low to achieve generalization in order to avoid over-fitting. If the data do not contain much information, or contain a high degree of noise, a fewer number of hidden nodes than the theoretical limit is advisable in order to prevent over-fitting. In some cases, a "fan-in" approach may

be desirable, where a fewer number of hidden nodes is used related to the number of input nodes. This "fan-in" structure reduces the dimensionality of the data set, promoting generalization. Therefore, in many cases, the optimum number of hidden nodes may be significantly less than the theoretical limit.

2.6.3 Training Patterns for ANN Learning

As "data-driven" models, robust ANN development is fundamentally dependent upon the quantity and quality of the data used to train the models. As discussed by Coppola et al. [4], "appropriate training set size for an ANN depends upon a number of factors, including its dimension (i.e., number of connection weights), the required ANN accuracy, the probability distribution of behavior, the level of noise in the system, and the complexity of the system." Complexity within the context of ANN modeling refers to a system where small changes in model input values produce large and even contradictory changes in model output values. A system that does not exhibit this type of complexity may then be referred to as a "well-behaved" system.

There is no theoretical derivation for determining the number of necessary training patterns for a given ANN model development problem. However, some researchers suggest that the minimum number of training data required for robust ANN model development is

$$\text{Minimum number of required training samples} = [(1.5 \times m) + (1.5 \times n)] \times c \tag{2.6}$$

where

m is the number of input nodes
n is the number of output nodes
c is some constant, typically ranging between 4 and 10

Note that the previous equation does not account for the number of hidden nodes in the ANN. It can be stated that, in general, more connection weights, partly a function of hidden nodes, necessitate more training samples. Therefore, c can be expected to increase with a higher number of hidden nodes for a particular modeling problem. Similarly, c will increase with more complex and/or nonlinear behavior.

Ideally the training samples should span the range of measured or expected behavior. Therefore, it is not simply a matter of using a sufficient number of training samples but the degree to which they statistically represent the problem behavior of interest over its full range.

2.6.4 Over-Fitting Data

As discussed earlier, over-fitting of data should be avoided in ANN modeling and, fortunately, can be avoided by following basic protocol. Often, ANN modelers are excessively intent on reducing or minimizing training error to the maximum extent possible. Typically, a researcher will compare two competing models, and even when the relative error difference is almost insignificant, the researcher or modeler will select the model with the lowest error as the de facto superior one.

While low training and validation errors are obviously desirable, it does not ensure that one has developed a robust ANN (or other) model that is capable of generalizing system behavior over a wide range of conditions or that a particular model is necessarily superior to a competing or comparison model with a larger error. To help demonstrate this important concept, Figure 2.3 illustrates an over-fitting example, where the parabola represents the exact function for the system behavior, and the measurements have some random errors.

A function perfectly fit to the measurements produces an error of 0 between the measured and fitted values; however, the fitted function does not show the basic properties of the true function, monotonicity and convexity, by producing a varying wavy function.

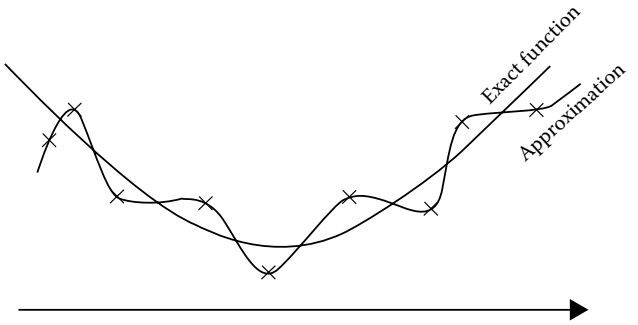

FIGURE 2.3 Consequence of over-fit.

The knowledge of the behavior of the data as well as their accuracy can be used to determine the needed accuracy of the ANN fit. One does not want to fit a function with a smaller error than the errors of the data; when this occurs, one is fitting random errors, rather than the tendency of the function, which is the objective.

2.7 ANN Applications with Case Studies

In order to demonstrate the utility of ANN models, several case studies from the literature are briefly overviewed in the following. These case studies are by no means an exhaustive survey of the literature but demonstrate the basic operational principles and applications of ANNs as discussed earlier.

2.7.1 ANN Applications to Predicting Groundwater Levels

Accurately predicting groundwater levels has numerous important benefits, including protection against aquifer overdraft, streamflow depletion, wetlands dewatering, water quality degradation (e.g., saltwater intrusion), among others. Traditionally, numerical groundwater flow models are used for modeling and predicting groundwater levels in response to variable weather and pumping stresses. ANN models have fairly recently been proven to have the capability of accurately modeling complex groundwater systems, providing highly accurate predictions over small and large spatial scales, over short- and long-term prediction horizons, using a number of different types of input or predictor variables. This section will briefly summarize two case studies where ANN models have been developed for predicting groundwater levels in complex real-world groundwater systems.

2.7.2 Case Study for Predicting Groundwater Levels in Tampa Bay, United States

The city of Tampa Bay, located along the southwestern Florida coast, has undergone tremendous population growth over the past several decades. Consequently, the groundwater system used to meet much of the area's water demand has suffered excessive water level declines. The area resides above a complex hydrogeological system, with a sedimentary unconfined aquifer overlying a low-permeability clay layer, below which lies a semi-confined and more complex limestone aquifer, which is characterized by complex karst features in places.

The Northwest Hillsborough Wellfield consists of seven high-capacity production wells, which pump from the lower limestone aquifer. Numerous monitoring wells were installed in the vicinity of the wellfield to monitor groundwater level changes in response to pumping, with some wells screened within the upper sedimentary unconfined aquifer and others in the deeper limestone aquifer.

An ANN model was developed to predict groundwater levels at monitoring wells over forecast periods (i.e., stress period) ranging from 3 to 24 days. The ANN inputs consisted of initial water levels for 12 monitoring wells; pumping extractions of individual extraction wells over the stress period length; precipitation; temperature; dew point; wind speed, as measured at the Tampa Bay Airport; and stress period length. The ANN outputs consisted of the water levels at the 12 monitoring wells at the end of the stress period. ANN predictive capability was compared both against measured groundwater levels and reforecasts (i.e., back prediction using information pertaining to that period) of groundwater levels by a coupled numerical surface water/groundwater flow model developed and operated by the water utility that manages the wellfield using a validation data set consisting of 10 consecutive weeks of weekly data, which was not used during ANN model development.

For the 120 validation predictions (i.e., 12 monitoring wells over 10 stress periods), the ANN model not only achieved a significantly lower validation error than the numerical model, 0.16 m versus 0.85 m, respectively, but also accurately reproduced the general behavior, accurately capturing increasing and decreasing water level periods in response to variable weather and pumping conditions in both the unconfined sedimentary aquifer and deeper semi-confined limestone aquifer. A sensitivity analysis with the ANN models demonstrated that precipitation events are the most significant factor on short-term water level changes in the shallow unconfined aquifer, while pumping rates of the production wells are the most significant factors on short-term water level changes in the semi-confined aquifer. The interested reader is referred to Coppola et al. [4] for a more in-depth presentation of this work.

2.7.3 Case Study for Predicting Groundwater Levels in Minqin Oasis, China

In the Tampa Bay Water modeling problem presented earlier, there was explicit information for the seven input pumping variables. In many areas where there is a high number of pumping wells (e.g., hundreds or more), as in a large agricultural area, this information will not be available. Often, when explicit information regarding an important variable is missing, a surrogate variable(s) may be used. The case study presented by Feng et al. [7] presents such an example when applying ANN modeling to a regional groundwater modeling problem.

The Minqin Oasis, situated in northwest China near Mongolia, is an area encompassing 160,000 km^2 and is surrounded by the Bandanjilin and Tenggeli Deserts. Over decades spanning from the 1950s to the present, high groundwater pumping in the region augments surface water diverted from the Hongyashan Reservoir, located at the lowest reach of the Shiyang River. This combination of high groundwater pumping and high surface water use has reduced both groundwater storage and recharge, resulting in extreme groundwater level declines throughout the region. The researchers developed ANN models trained and validated with historical data, which were then used to predict average groundwater level declines within the oasis under different land use conditions.

With more than 9000 irrigation wells in the area, even if actual pumping data existed, which does not, it would be impractical to explicitly represent each well. Instead, historical annual irrigation groundwater pumping for the region was estimated by accounting for the irrigation area and types of crops, from which water demand was calculated. The ANN model used seven input variables for predicting the average basin groundwater levels 1 month into the future: initial groundwater level, monthly total precipitation, monthly total water surface evaporation, monthly total surface water reservoir inflow, population, monthly synthesis irrigation ratio, and irrigation. As pointed out by the authors, agriculture irrigation always exceeded surface water inflow into the reservoir. Irrigation demand is obviously a function of agricultural factors, which are represented by the two ANN input prediction variables: monthly total surface water evaporation and the monthly synthesis irrigation ratio. Some quantity of groundwater pumping is attributable to potable consumption for the resident population. Therefore, using the two agricultural factors in combination with population represents the total water demand for the region, and in conjunction with surface water inflow, it was used as surrogate variables to represent total groundwater pumping in the region for discrete monthly stress periods.

Two different subregions of the study area, Xiqu, more distant from the reservoir, and Xinhe, more proximate to the reservoir, were modeled by separate ANN models using the same seven input variables. In both cases, the ANN models achieved high prediction accuracy during validation, with an average root mean squared error of 0.37 m or less for the two validation cases. In addition, during validation, both models accurately reproduced the seasonal and overall annual trends of groundwater level changes, achieving a relative validation error with respect to the average monthly range of groundwater level fluctuations of around 8.8% on average for the two study areas. The models were then used to project groundwater level declines under various potential irrigation demands over 1-year periods using monthly time steps and to identify scenarios that would reduce and/or eliminate continued overdraft of the groundwater systems.

Sensitivity analyses results obtained with both models were consistent with the hydrogeological system. Surface water inflow into the reservoir was only the fourth most important predictor variable for the Xiqu region, while it was the most important predictor variable for the Xinhe region, which is significantly closer to the reservoir, and therefore has more access to and uses more surface water for irrigation. This higher surface water use has two important effects on groundwater levels in the Xinhe region: first, it reduces demand for groundwater extractions, and second, it artificially increases areal recharge from irrigation. In addition, leakage through the unlined reservoir bottom acts as an additional source of groundwater recharge to the region.

In summary, highly accurate ANN prediction models were developed using seven input variables for accurately predicting monthly average groundwater level changes within two large regional study areas and performing a sensitivity analysis that enhanced system understanding. Because explicit groundwater extraction pumping information was not available for this large irrigation area, the researchers used surrogate variables indicative of irrigation and potable use as surrogate variables for this critical governing variable. This work demonstrates how ANN models can implicitly represent important causal variables with correlative variables that capture the important physical components of the system, achieving high prediction capability.

2.7.4 ANN Applications to Predicting Water Quality

Predicting water quality in both man-made and natural systems is an extremely important and common objective, with numerous applications in the literature using ANN, including saltwater intrusion and upconing, algal blooms, nitrate loading, and water treatment, among just some of the examples. Many mechanistic models are limited in accurately predicting complex chemical processes, for example, the onset, duration, and intensity of algal blooms in surface water systems. In this section, an ANN water quality modeling application addressing groundwater upconing problem for a community well located in Provincetown, Massachusetts, with an extended 46-month simulation is presented.

2.7.5 Case Study for Predicting Saltwater Upconing in Provincetown, United States

Provincetown, Massachusetts, situated on a peninsula between the Cape Cod Bay and the Atlantic Ocean, is a popular resort that experiences significantly higher water use during summer. A production well was installed in the middle of the peninsula in 1987 to help meet water demand for the community. Over time, increases in salinity concentrations in the aquifer were measured in a monitoring well located near the production well. The salinity concentrations in the aquifer, as measured in the monitoring well, generally decrease during lower demand periods but increase during higher pumping periods.

In order to predict variable salinity concentrations (i.e., conductivity) in the monitoring well in response to variable pumping and weather conditions, ANN models were developed to predict conductivity levels 30, 60, and 90 days ahead. The ANN model inputs consisted of initial conductivity value, measured at the beginning of the prediction period in the monitoring well; total pumping extraction

over the prediction period; total precipitation over the prediction period; and average air temperature. The ANN models in general achieved excellent predictive accuracy, accurately reproducing variable conductivity levels in the monitoring well over time. Although significantly higher conductivity changes occurred over the longest 90-day prediction period, higher accuracy was achieved, as total pumping extraction becomes more closely correlated with conductivity levels over longer periods. A sensitivity analysis also revealed that weather variables in general become more important as predictors of conductivity levels in the aquifer with longer prediction horizons.

A final ANN model was used to perform an extended 46 month simulation period using monthly time steps. The model accurately simulated variable conductivity levels in the monitoring well over the extended period, reproducing the higher and lower conductivity periods. This performance demonstrates that ANN models can be used for providing extended simulations over multiple time steps that span years into the future. A more detailed overview of this research may be found in Coppola et al. [5].

2.7.6 ANN Application to Formal Management Optimization

Formal optimization can be performed to identify the optimal values for human control or decision variables that minimize a negative objective (e.g., operating costs) and/or maximize a positive objective (e.g., water supply) while satisfying both management objectives (e.g., minimum required water levels) and the physics of the problem (e.g., conservation of mass). Optimization has been used extensively in water resources planning and management, ranging from groundwater extraction policies that minimize environmental impacts while maximizing water supply to surface water extractions that maximize storage while minimizing flooding. Traditionally, physical-based models (e.g., numerical) have been used as the basis for performing the optimization. The reader is referred to Ahlfeld and Mulligan [1] for a more detailed overview of the method. However, ANN models developed for the physical system of interest can serve as a more efficient and even accurate surrogate for traditional physical-based models in performing optimization.

2.7.7 Case Study for Optimizing Wellfield Pumping in Toms River, United States

An ANN model developed from a physics-based numerical groundwater flow model was used to perform formal optimization of a public supply wellfield [6]. The public supply wellfield, located in Toms River, New Jersey, is at risk to a groundwater contamination plume originating from a highly contaminated site. A detailed five-layered numerical groundwater flow model, consisting of over 77,000 active cells, was developed by the New Jersey Geological Survey to simulate the groundwater system and resulting capture zones generated by the individual pumping wells under variable pumping and natural recharge conditions. The objective of the optimization analysis was to balance the two conflicting objectives of maximizing pumping supply while minimizing wellfield vulnerability to contamination from the plume.

Using simulation sets generated by the numerical groundwater flow model, the ANN model was trained to accurately predict in response to variable pumping and recharge rates groundwater levels (i.e., head) one month ahead at select model cell locations situated between the capture wells used to contain the plume and nearby community supply wells. From the predicted water levels, hydraulic head differences along the downgradient plume boundary were computed, which was used to estimate the level vulnerability of the supply production wells to the groundwater contamination plume under different pumping and recharge rates.

The inputs to the ANN model consisted of initial water levels at 32 cell locations at the beginning of the monthly stress period, the pumping rates for each of the four production wells over the monthly stress period, and the monthly areal recharge rate. The output variables consisted of the final water levels at the 32 cell locations at the end of the monthly stress period. A different ANN model was developed for each month, and in all cases, the ANN models achieved excellent prediction results, with a mean

absolute error of just 0.03 m in predicted water levels for a system that experienced an average monthly change of 0.70 m. The 12-monthly ANN models were linked and demonstrated to maintain high predictive capability for one year prediction horizons.

The ANN model equations were directly embedded within the optimization formulation, from which the corresponding Pareto frontier was generated. Using the Pareto frontier, various distance-based methods were used to select the best trade-off point in accordance with the priorities and preferences of the decision makers. The solutions obtained by the ANN-optimization model compared favorably with the results validated with MODFLOW. In short, the ANN-optimization model was able to achieve high accuracy while attaining orders of magnitude higher computational efficiency than a corresponding numerical model approach. In addition, the ANN model could be used independent of optimization efficiently performing thousands of simulations that would otherwise be infeasible with the corresponding numerical groundwater flow model.

2.8 Summary and Conclusions

ANN models are a powerful alternative to more traditional physical-based models, having been applied with success to a number of different hydrologic areas, including groundwater and surface water resources, process control of water treatment systems, water demand forecasting, and unsaturated flow. They have accurately predicted future system states that include water levels, flow rates, and water quality in response to various factors, including weather and human controls. ANNs offer a number of other advantages, such as the nonnecessity of including often difficult to estimate physical model parameter values, superior computational efficiency and speed, and their ability to provide insights into physical systems.

One of the more frequent criticisms of the empirically based ANN is their "black-box" approach, where the fundamental governing physics are not embedded within their equations. However, because hydrologic systems all too often lack the necessary spatial and/or temporal characterization of physical parameters necessary for developing and calibrating an accurate physical-based model, this "black-box" approach that relies on more easily measureable variables that conform with the physical rules is often a distinct advantage. In effect, the physics of the system is captured implicitly via the data. At the same time, it is important that modelers have a solid conceptual if not theoretical understanding of the system of interest. Modelers must be careful in using the necessary input variables for modeling the system of interest over its expected range. In addition, a solid system understanding is vital for not only promoting development of a robust ANN model but understanding its limitations under different conditions.

One of the major advantages posed by ANN models that has received far too little attention is that, unlike numerical models, ANNs can be directly integrated with real-time data streams for initialization of its input variables to real-time conditions. This real-time initialization capability not only increases predictive accuracy but allows the ANN models to provide forecasts in real time that reflect existing system (e.g., weather) conditions. In addition, this real-time initialization allows the ANN models to attain location specific accuracy at discrete locations (e.g., monitoring wells) that are otherwise not possible with a traditional-based model.

Undoubtedly, there are many additional innovations and advancements that remain to be realized with ANN technology. For example, ANN models have also been demonstrated both in theory and simulations to have the potential of improving numerical model simulations by constraining their set of equations to discrete future values predicted independently by the ANN models [17]. ANN models can also easily be combined with interpolation equations and/or physics-based equations to expand the domain of prediction capability. ANN models can be efficiently combined with formal optimization, helping to overcome some of the traditional problems associated when performing optimization with physics-based equations. As an extension to this, ANN models that can achieve a higher level of accuracy in predicting real-time responses in the natural system will produce more accurate optimal solutions.

As water resources are increasingly stressed and depleted, the need for more accurate modeling will only increase. That ANN models can be continuously updated by real-time data streams, can be combined with other modeling techniques for increasing the domain of predictions and achieving superior real-time prediction capability, as well as can serve as segments in optimization models, all of these will ensure that they will continue to be used to address some of the most pressing water problems confronting humans in the twenty-first century.

References

1. Ahlfeld, D.P. and Mulligan, A.E. 2000. *Optimal Management of Flow in Groundwater Systems*. San Diego, CA: Academic Press.
2. Bae, M., Kwon, Y., Hwang, S., Chon, T., Yang, H., Kwak, I., Park, J., Ham, S., and Park, Y. 2011. Relationships between three stream assemblages and their environmental factors in multiple spatial scales. *International Journal of Limnology* 47: S91–S105.
3. Caianiello, E. 1961. Outline of a theory of thought-processes and thinking machines. *Journal of Theoretical Biology* 2: 204–235.
4. Coppola, E., Szidarovszky, F., Poulton, M., and Charles, E. 2003. Artificial neural network approach for predicting transient water levels in a multilayered groundwater system under variable state, pumping, and climate conditions. *Journal of Hydrologic Engineering* 8(6): 348–359.
5. Coppola, E., McLane, C., Poulton, M., Szidarovszky, F., and Magelky, R. 2005. Predicting conductance due to upconing using neural networks. *Journal of Ground Water* 43(6): 827–836.
6. Coppola, E., Szidarovszky, F., Davis, D., Spayd, S., Poulton, M., and Roman, E. 2007. Multiobjective analysis of a public wellfield using artificial neural networks. *Journal of Ground Water* 45(1): 53–61.
7. Feng, S., Kang, S., Huo, Z., Chen, S., and Mao, X. 2008. Neural networks to simulate regional groundwater levels affected by human activities. *Journal of Ground Water* 46(1): 80–90.
8. Hebb, D.O. 1949. *The Organization of Behavior*. New York: Wiley.
9. Hecht-Nielsen, R. 1990. *Neurocomputing*. Reading, MA: Addison-Wesley.
10. Lingireddy, S. and Brion, G., eds. 2005. *Artificial Neural Networks in Water Supply Engineering*. Reston, VA: American Society of Civil Engineers.
11. McCulloch, W.S. and Pitts, W. 1943. A logical calculus of the ideas immanent in nervous activity. *Bulletin of Mathematical Biophysics* 5: 115–133.
12. Minsky, M.L. and Papert, S.A. 1969. *Perceptrons*. Cambridge, MA: MIT Press.
13. Parker, D. 1985. Learning-logic: Technical Report TR-47, Center for Computational Research in Economics and Management Science, MIT, Cambridge, MA (April).
14. Poulton, M.M. 2001. *Computational Neural Networks for Geophysical Data Processing*. Amsterdam, the Netherlands: Pergamon.
15. Rosenblatt, F. 1958. The perceptron: A probabilistic model for information storage and organization in the brain. *Psychological Review* 65: 386–408.
16. Rumelhart, D. and McClelland, J. 1986. *Parallel Distributed Processing. Explorations in the Microstructure of Cognition*. Cambridge, MA: MIT Press.
17. Szidarovszky, F., Coppola, E., Long, J., Hall, A., and Poulton, M. 2007. A hybrid artificial neural network-numerical model for ground water problems. *Journal of Ground Water* 45(5): 590–600.
18. Von Neuman, J. 1958. *The Computer and the Brain*. New Haven, CT: Yale University Press.
19. Werbos, P. 1974. Beyond regression: New tools for prediction and analysis in the behavioral sciences. PhD dissertation, Applied Math, Harvard University, Cambridge, MA.
20. Widrow, B. and Hoff, M. 1960. Adaptive switching circuits. *IRE WESCON Convention Record* 4: 96–104.

3

Bankfull Frequency in Rivers

Carmen Agouridis
University of Kentucky

AUTHOR

Carmen Agouridis is an assistant professor in the Biosystems and Agricultural Engineering Department at the University of Kentucky. A licensed professional engineer in Kentucky and West Virginia, Dr. Agouridis has expertise in stream restoration and assessment, riparian zone management, hydrology and water quality of surface waters, and low-impact development. She is the recipient of over $5 million in grants, has authored a number of publications related to streams and riparian management, and is the director of the Stream and Watershed Science Graduate Certificate at the University of Kentucky. Having received training in Rosgen Levels I–IV along with courses at the North Carolina Stream Restoration Institute and various conference workshops, she teaches Introduction to Stream Restoration, which is a senior- and graduate-level course at the University of Kentucky.

PREFACE

Bankfull discharge is often used as a surrogate for channel-forming or dominant discharge—the morphologically significant discharge that shapes the river. Because of this, understanding the magnitude and frequency of bankfull discharge is important for river management and restoration. While an average return period of 1.5 years is often cited for bankfull discharge, this event can occur at intervals of less than one year to more than a decade. Determining bankfull discharge magnitude and frequency requires the ability to identify bankfull elevation in the field, transform this elevation into a discharge, and then compute the frequency of the resultant discharge.

3.1 Introduction

Bankfull discharge represents the maximum flow that a river can convey without overflowing its banks [5,19,42,77]. This discharge is considered morphologically significant as it represents the separation between river formation processes and floodplain processes [19,42,57]. Bankfull discharge is considered deterministic and as such is frequently used to estimate the channel-forming or dominant discharge of alluvial rivers [19,27,66]. Channel-forming discharge is a theoretical discharge that if maintained for an indefinite period of time (i.e., held constant) would produce the same river morphology as that of the long-term hydrograph [2,19,66,69]. Bates and Jackson [9] define channel-forming discharge as the "discharge of a natural channel which determines the characteristics and principal dimensions of the channel." The concept of channel-forming discharge is applicable to stable rivers [19].

As channel-forming discharge is theoretical, it is not measured directly; rather it is indirectly estimated using bankfull discharge although effective discharge, the discharge that transports the maximum annual sediment load, is sometimes used [1,5,11,19,25,26,62,78,79]. Soar and Thorne [69] describe effective discharge as the "integration of sediment transport with flow-duration." As seen in Figure 3.1 with curves (i) and (ii), frequent but small discharges transport small amount of the sediment, and infrequent but large discharges transport large amount of sediment. However, when considering the effectiveness of a given discharge, as seen in curve (iii), it is the intermediate discharges that transport the greatest fraction of the average annual sediment load [5,56,69].

Computing effective discharge requires the use of long-term discharge and sediment data, of which obtainment of the latter can be especially challenging. Few monitoring stations collect sediment data, and of those that do, it is the suspended fraction that is sampled. Juracek and Fitzpatrick [36] note that very few US Geological Survey (USGS) gage sites have bed load transport curves. The type of sediment data required to compute effective discharge depends on the river of interest. For rivers dominated by suspended load, effective discharge had been calculated using just this fraction [56]. For gravel-bed rivers, effective discharge has been computed using only bed load data although the bed load transport rates were calculated instead of measured given the difficulty in collecting bed load data [5,60]. In cases

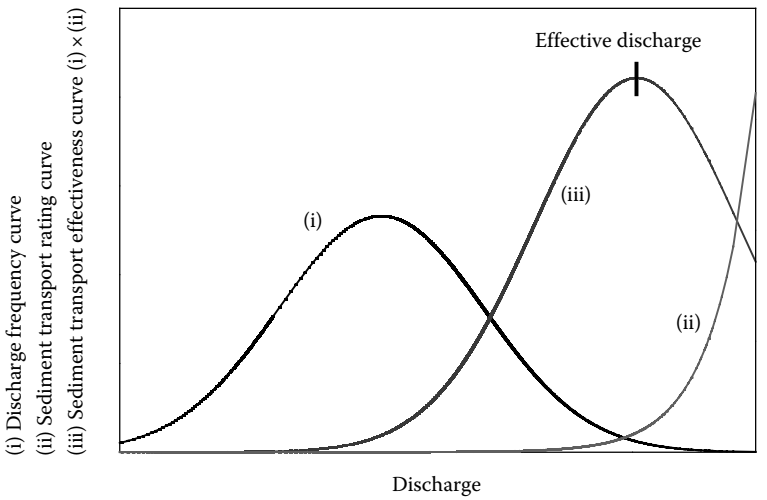

FIGURE 3.1 Effective discharge curve (iii) developed from discharge frequency curve (i) and sediment transport rating curve (ii). (Adapted from Soar, P.J. and Thorne, C.R., *Channel Restoration Design for Meandering Rivers*, ERDC/CHL CR-01, U.S. Army Corps of Engineers, Coastal and Hydraulics Laboratory, U.S. Army Engineer Research and Development Center (ERDC), Vicksburg, MS, 2001.)

where rivers have a significant bed and suspended loads, the total bed material load is recommended [5,6,69]. Details regarding the procedure for calculating effective discharge are provided in Biedenharn et al. [11] and Soar and Thorne [69].

As determining bankfull discharge is less data intensive than computing effective discharge, and since it can be determined on both gaged and ungaged rivers, bankfull discharge is more commonly used by scientists, engineers, planners, and other environmental professionals than effective discharge. Estimations of bankfull discharge magnitude and frequency are particularly important in river restoration projects, which have increased dramatically in the United States [10,70], as bankfull discharge is a critical design parameter [2,14,68,74].

Williams [77] noted the frequency of bankfull discharge is not common across rivers. While the one–two year recurrence interval is often cited as the mean frequency of bankfull discharge [15,22,41], Williams [77] found it could vary widely from 0.25 to 32 years. Table 3.1 contains a summary of bankfull discharge return periods throughout the United States and in some locations in Europe, Caribbean, Australia, and Middle East.

3.2 Identifying Bankfull

Computation of bankfull discharge first requires locating bankfull elevation. Identification of bankfull elevation is done in the field [31,64] though limited efforts have examined techniques for remotely determining bankfull characteristics [12,13]. Identifying bankfull elevation requires practice with the degree of uncertainty in identifying bankfull elevation decreasing with increasing experience [31]. The degree of difficulty in identifying bankfull stage is also related to the stability state of the river and its location in the watershed. Bankfull elevation is often difficult to identify in unstable rivers [35], which are the very rivers for which restoration efforts are focused. Identifying bankfull elevation is more challenging with rivers without well-developed floodplains such as those in more mountainous regions [64].

3.2.1 Field Indicators

Identification of bankfull elevation is best done through the use of multiple indicators, if possible. These indicators should identify a consistent bankfull elevation throughout the project reach [37,64]. For unstable rivers or those without well-developed floodplains, the presence of reliable bankfull indications will likely be limited. Regional curves, which are curves relating drainage area to the bankfull characteristics of width; mean depth; cross-sectional area; and discharge are useful in helping to identify and validate bankfull elevation (Figure 3.2) [14,22,37,48].

Bankfull indicators vary in importance and reliability in identifying bankfull elevation. Bankfull indicators commonly used, listed in order of importance, include [14,37,48,64,72]

a. Flat depositional surfaces immediately adjacent to the river (Figure 3.3)
b. Top of the highest depositional feature such as point bars and central bars (Figure 3.4)
c. Prominent changes or breaks in the slope of a bank
d. Erosion or scour features
e. Vegetation

The use of vegetation is not recommended in the eastern portion of the United States as it is common for vegetation to grow below bankfull elevation. In the western portion of the United States, bankfull elevation has been successfully identified using vegetation.

In some instances, the flat depositional surfaces *immediately* adjacent to the river are inner berm features. The inner berm is developed and maintained by discharges that are smaller and more frequent than the bankfull discharge. This feature is more common in rivers that are or have adjusted to changing

TABLE 3.1 Bankfull Discharge Return Periods for the United States, Europe, Caribbean, Australia, and Middle East

Under Study Location	Bankfull Discharge Return Period (Years)		Source
	Range	Average	
Eastern United States			
New York (regions 1 and 2)	1.01–3.8	2.1	[55]
New York (region 3)	1.2–3.4	2.1	[51]
New York (regions 4 and 4a)	1.2–2.7	1.5	[52]
New York (region 5)	1.1–3.4	1.6	[74]
New York (region 6)	1.01–2.4	1.5	[53]
New York (region 7)	1.1–3.6	2.1	[54]
Pennsylvania and Maryland	1.01–2.3	1.4	[16]
Piedmont of Pennsylvania and Maryland	1.01–1.5	1.3	[17]
Piedmont of Pennsylvania and Maryland	1.2–1.5	1.4	[75]
Allegheny Plateau and Valley and Ridge of Maryland	1.1–1.8	1.5	[44]
Coastal Plains of Maryland	1.0–1.4	1.2	[45]
Piedmont of Maryland	1.3–1.8	1.5	[46]
Coastal Plains of Virginia and Maryland	<1.01–2.1	1.4	[39]
Piedmont of Virginia	1.0–4.3	1.8	[43]
Valley and Ridge of Maryland, Virginia, and West Virginia	<1.1–2.3	1.4	[37]
Piedmont of North Carolina (rural)	1.01–1.8	1.4	[29]
Mountains of North Carolina	1.1–1.9	1.5	[30]
Coastal Plains of North Carolina	1.0–1.3	1.1	[21]
Coastal Plains of North Carolina	0.1–0.3[a]	0.2[a]	[71]
Piedmont of North Carolina (urban)	1.01–1.8	1.4	[23]
Florida	1.0–1.4	1.1	[48]
Bluegrass region of Kentucky	<1.01–1.2	1.1	[14]
Eastern Coal Fields of Kentucky	<1.01–1.5	1.1	[73]
Ohio	<1.01–1.4	1.1	[62]
Ohio	1.01–9.7	1.7	[67]
Michigan	1.0–1.8	1.3	[49]
Michigan	1.1–10	3.4	[63]
Western United States			
Western United States	1.01–32	14.0	[77]
Oklahoma	1.01–3.7	1.4	[24]
Montana	1.0–4.4	1.9	[40]
Arizona and New Mexico	1.1–1.8	1.4	[50]
Colorado	1.3–1.8	1.5	[80]
Colorado	0.7–0.9[a]	0.8[a]	[66]
Yampa River Basin of Colorado and Wyoming	1.01–4	—	[5]
Pacific Northwest	1.01–3.1	1.4	[15]
Europe			
Belgium	1.1–5.3	2.1	[59]
Cumberland Basin in New South Wales	4–10	—	[60]
Caribbean			
Puerto Rico	0.1–0.2[a]	0.1[a]	[61]
Australia			
Northern Territory	1.8–7.6	4.1	[65]
Middle East			
Fars Province, Iran	—	1.1	[3]

Note: Reported values are based on annual series unless otherwise noted.

[a] Partial-duration series.

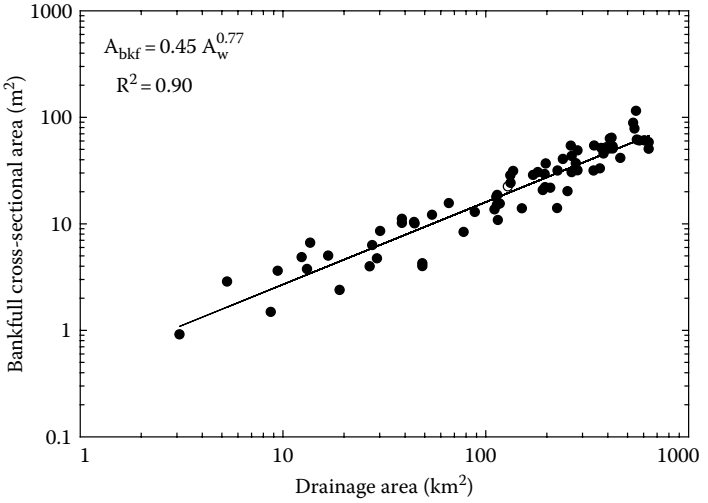

FIGURE 3.2 Regional curve comparing drainage area (A_w) to bankfull cross-sectional area (A_{bkf}) for the Valley and Ridge physiographic province. (Developed using data from McCandless, T.L., *Maryland Stream Survey: Bankfull Discharge and Channel Characteristics of Streams in the Allegheny Plateau and the Valley and Ridge Hydrologic Regions*, U.S. Fish and Wildlife Service CBFO-S03-01, Annapolis, MD, 2003; Chaplin, J.J., Development of regional curves relating bankfull-channel geometry and discharge to drainage area for streams in Pennsylvania and selected areas of Maryland, U.S. Geological Survey Scientific Investigations Report 2005-5147, Reston, VA, 2005; Keaton, J.N. et al., Development and analysis of regional curves for streams in the non-urban valley and ridge physiographic province, Maryland, Virginia, and West Virginia, U.S. Geological Survey Scientific Investigations Report 2005-0576, Reston, VA, 2005.)

FIGURE 3.3 Flat depositional surfaces immediately adjacent to the channel, as noted by the arrows, are good indicators of bankfull elevation. (Photo courtesy of Greg Jennings, North Carolina State University, Raleigh, NC.)

FIGURE 3.4 The top of the point bar, as noted by the arrow, is a good indicator of bankfull elevation. (Photo courtesy of Carmen Agouridis, University of Kentucky, Lexington, KY.)

watershed conditions such as urbanization [20,23]. Identifying the inner berm elevation as bankfull elevation would result in an incorrect bankfull discharge [14].

3.2.2 Minimum Width-to-Depth Ratio

Finding the elevation at which the width-to-depth ratio is at a minimum is a means of aiding in the identification of bankfull elevation, particularly in uniform reaches of the channel [14,19,38,77] (Table 3.2). In uniform reaches, the width of the channel changes slowly in relation to the channel depth until bankfull elevation is reached. As bankfull represents the breakpoint between in-channel and floodplain processes, width increases substantially in comparison to the mean depth (Figure 3.5).

3.3 Determining Bankfull Discharge

The procedure for computing bankfull discharge varies depending on whether or not the site of interest is gaged and the length of the discharge record. In both instances of gaged and ungaged sites, bankfull elevation must be identified in the field.

3.3.1 Gaged Sites

The USGS presently collects discharge and water level data at over 25,000 locations within the United States. Records are also available for over 11,000 additional decommissioned sites. A number of other countries operate monitoring programs similar to the USGS (e.g., Water Survey of Canada, Environment Agency of the United Kingdom). Many times, other entities such as universities and state and local governments also collect discharge data. However, such data are generally acquired for short periods of time meaning the data record may be of insufficient length for bankfull frequency analysis. A data record of at least 10 years is recommended for bankfull frequency analysis.

Fluctuations in budgets and population densities in addition to changing monitoring needs (e.g., total maximum daily loads) means that the gage network evolves. While some monitoring stations are decommissioned, new sites are initiated or activated. Discharge data from these inactive and active

TABLE 3.2 Minimum Width-to-Depth Ratio Method Is a Useful Aid for Identifying Bankfull Elevation

Elevation (m)	Width (m)	Mean Depth (m)	W/D
1.90	0.94	0.04	23.50
1.95	0.99	0.09	11.00
2.00	1.05	0.13	8.08
2.05	1.13	0.17	6.65
2.10	1.23	0.20	6.15
2.15	1.37	0.23	5.96
2.20	1.47	0.26	5.65
2.25	1.56	0.30	5.20
2.30	1.63	0.33	4.94
2.35	1.70	0.37	4.59
2.40	2.40	0.30	8.00
2.45	2.96	0.29	10.21
2.50	3.26	0.31	10.52
2.55	3.74	0.32	11.69
2.60	4.21	0.33	12.76
2.65	4.69	0.34	13.79
2.70	5.06	0.37	13.68
2.75	5.67	0.38	14.92
2.80	6.40	0.38	16.84
2.85	6.75	0.41	16.46
2.90	6.95	0.45	15.44

Note: Data correspond to Figure 3.5.

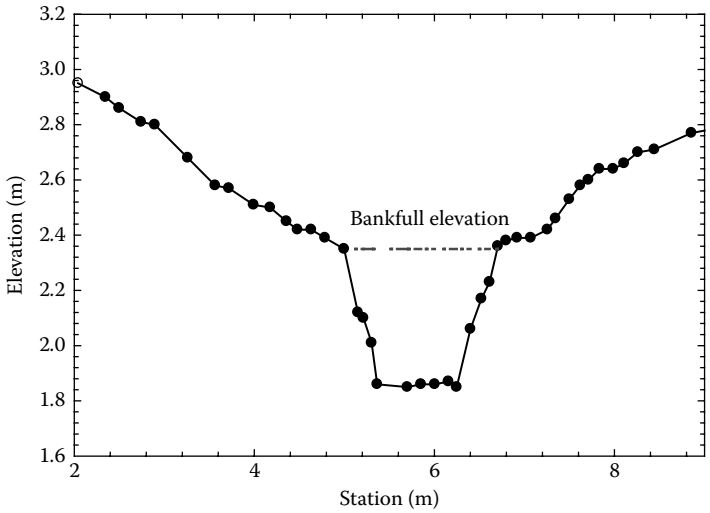

FIGURE 3.5 Channel width is fairly uniform until bankfull elevation where it increases at a much greater rate than depth. Note the flat depositional surfaces located on both banks of the channel.

(a) (b)

FIGURE 3.6 USGS hydrologic monitoring station comprised of (a) equipment housing unit with real-time data-transmittal capabilities and (b) staff gage for visually assessing water level (units are in feet). (Photo courtesy of Carmen Agouridis, University of Kentucky, Lexington, KY.)

gaged sites are useful in bankfull frequency analysis provided bankfull elevation can be identified, and for inactive sites, an undisturbed staff gage is present (Figure 3.6).

3.3.1.1 Active Gages: Real-Time Data

If the active gage site is equipped to transmit data in real time (e.g., at 15–60 min intervals), it is likely that a staff gage is absent. To determine the stage at which bankfull elevation occurs, complete the following steps [14]:

a. Identify bankfull elevation.
b. Measure the elevation difference between bankfull elevation and water surface elevation. Be sure to note the exact date and time of the measurements.
c. Access the Internet and find the stage that corresponds to the exact date and time of the measurements.
d. Add the elevation difference, recorded in Step b, to the stage in Step c to get the water level or stage at bankfull.
e. Use the most current discharge rating curve for the gaged site to determine bankfull discharge. For the USGS, discharge rating curves for active gages are available at the ratings depot.

3.3.1.2 Active Gages: Nonreal-Time Data

In cases where the data are not collected and transmitted in real time, a staff gage should be present. The staff gage is used to reference both water surface and bankfull stages. For active gages with only a staff gage present, complete the following steps [14,72]:

a. Identify bankfull elevation.
b. Measure the elevation difference between bankfull elevation and water surface elevation.
c. Read the water surface elevation on the staff gage.
d. Add the elevation difference, recorded in Step b, to the staff gage reading in Step c to get the water level or stage at bankfull.
e. Use the most current discharge rating curve for the gaged site to determine bankfull discharge. For the USGS, discharge rating curves for active gages are available at the ratings depot.

3.3.1.3 Inactive Gages

Determining bankfull discharge at inactive gages is the same for active gages without real-time capabilities (i.e., only a staff gage is present). The only difference is that discharge rating curves are not maintained for inactive sites. In the United States, one may either contact the USGS to obtain the last developed discharge rating curve or one may develop a stage-discharge rating curve using historic streamflow data [47]. Care should be exercised in using inactive gaged sites as the characteristics of the site (e.g., percent impervious area) may have changed considerably since the data were collected. If this were the case, treat the site as an ungaged site.

3.3.2 Ungaged Sites

While bankfull frequency cannot be determined at ungaged sites, information regarding bankfull discharge is useful. At ungaged sites, bankfull discharge must be estimated using hydraulic equations for open channel flow. In the United States, Manning's equation is commonly used (3.1) [21,23,31,48]:

$$Q = \frac{1}{n} AR^{2/3} S^{1/2} \tag{3.1}$$

where

Q represents the bankfull discharge ($m^3\ s^{-1}$)
n is the Manning's coefficient
A is the bankfull cross-sectional area (m^2)
R is the hydraulic radius (m)
S is the slope ($m\ m^{-1}$)

With Manning's equation, cross-sectional surveys are required to compute the bankfull channel dimensions width, cross-sectional area, and mean depth; a longitudinal survey is needed to compute bankfull slope; and a Manning's roughness coefficient is selected. Numerous references are available for assisting in the selection of a Manning's roughness coefficient [7,8,18,28,32,34]. A comparison of Manning's n values and bankfull discharge estimates from ungaged sites to those from similar gaged sites is recommended for purposes of validation [23,48]. In cases where detailed river and floodplain surveys are available, bankfull discharge can be estimated using United States Army Corps of Engineers program Hydraulic Engineering Center River Analysis System (HEC-RAS).

3.4 Computing Bankfull Frequency

Once bankfull discharge is known, the next step is to compute the frequency at which it occurs. Recall that the frequency with which bankfull occurs can only be computed for gaged sites. Computing the frequency of bankfull is helpful in validating whether or not bankfull elevation was correctly identified. While the frequency with which bankfull discharge occurs has been shown to vary considerably by Williams [77], the variation in a physiographic region is typically relatively small (Table 3.1). Within a physiographic region, bankfull return period values that are notably lower or higher than those found in the area require further examination. Other bankfull characteristics such as width, cross-sectional area, and mean depth should be compared to an appropriate regional curve to ensure an inner berm feature (bankfull return period too small) is not mistakenly identified as bankfull elevation or that channel incision does not mistakenly result in the identification of the top of the lowest bank as bankfull elevation (bankfull return period too large).

The Interagency Advisory Committee on Water Data (IACWD) published guidelines on the determination of flood flow frequency—*Guidelines for Determining Flood Flow Frequency, Bulletin 17B of the*

TABLE 3.3 Software Programs Utilizing Flood Flow Frequency Computations Using *Bulletin 17B* Guidelines

Software Program	Developer	Domain	Website
HEC-SSP	US Army Corps of Engineers	Public	http://www.hec.usace.army.mil/software/hec-ssp/
Peak FQ	US Geological Survey	Public	http://water.usgs.gov/software/PeakFQ/
RIVERMorph	RIVERMorph, LLC	Private	http://www.rivermorph.com/

Source: IACWD (Interagency Advisory Committee on Water Data), *Guidelines for Determining Flood Flow Frequency-Bulletin 17B of the Hydrology Subcommittee*, U.S. Geological Survey Office of Water Data Coordination, Reston, VA, 1982.

Hydrology Subcommittee [33]. Commonly known as *Bulletin 17B*, this document serves as the standard for determining the frequency of bankfull discharges. The guidelines are applicable for stream gage records for at least 10 years in length, unregulated or at least not appreciably altered flows, and fairly consistent watershed conditions for the period of record studied [76]. A number of free and commercially available software programs are available for computing flood flow frequencies using the *Bulletin 17B* guidelines (Table 3.3).

3.4.1 Example

Determine the bankfull frequency for USGS gage station 01613900 Hogue Creek near Hayfield, Virginia, United States. Discharge data were collected starting in 1961. A cross-sectional view of a riffle surveyed at the site is shown in Figure 3.7. Keaton et al. [37] contains a detailed description of the site. All elevations are in reference to the staff gage datum.

3.4.2 Solution

The solution consists of three parts: identifying bankfull elevation, determining bankfull discharge, and computing the return period or frequency of the bankfull discharge:

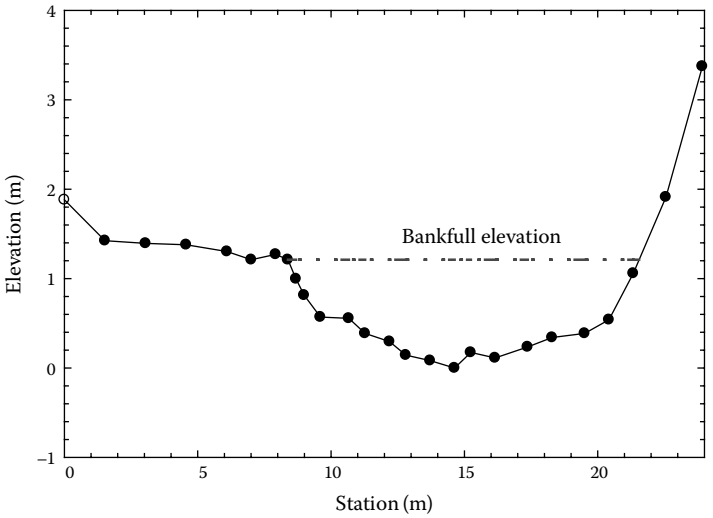

FIGURE 3.7 Riffle cross section at USGS gage station 01613900 Hogue Creek near Hayfield, Virginia, United States. Bankfull elevation, as shown by the dotted line, occurs at a flat depositional surface immediately adjacent to the channel.

a. Bankfull is identified as the flat depositional surface adjacent to the channel, as shown with the dotted line in Figure 3.7. Bankfull occurs at an elevation of 1.21 m at station 8.38 m. The minimum width-to-depth ratio is used to verify bankfull elevation, as shown in Table 3.4. At an elevation of 1.21 m, the width-to-depth ratio is about 16.0.
b. The stage-discharge ratings table for the gage station is used to identify bankfull discharge. Table 3.5 contains a portion of the ratings table. At an elevation of 1.21 m, the corresponding discharge is 17.8 $m^3 s^{-1}$.

TABLE 3.4 Width-to-Depth (W/D) Ratios for Riffle Cross Section at USGS Gage Station 01613900 Hogue Creek near Hayfield, Virginia, United States

Elevation (m)	Width (m)	Mean Depth (m)	W/D
0.05	0.75	0.03	25.00
0.10	1.58	0.05	31.60
0.15	3.42	0.06	57.00
0.20	4.49	0.09	49.89
0.25	5.16	0.12	43.00
0.30	5.77	0.16	36.06
0.35	6.85	0.18	38.06
0.40	8.33	0.19	43.84
0.45	8.82	0.23	38.35
0.50	9.32	0.27	34.52
0.55	9.77	0.30	32.57
0.60	11.00	0.32	34.38
0.65	11.22	0.36	31.17
0.70	11.43	0.40	28.58
0.75	11.65	0.45	25.89
0.80	11.86	0.49	24.20
0.85	12.04	0.53	22.72
0.90	12.21	0.57	21.42
0.95	12.38	0.62	19.97
1.00	12.54	0.66	19.00
1.05	12.71	0.70	18.16
1.10	12.86	0.74	17.38
1.15	13.00	0.78	16.67
1.20	13.15	0.82	16.04
1.25	14.55	0.79	18.42
1.30	15.59	0.79	19.73
1.35	16.62	0.79	21.04
1.40	19.29	0.72	26.79
1.45	20.48	0.73	28.05
1.50	20.72	0.77	26.91
1.55	20.96	0.81	25.88
1.60	21.19	0.85	24.93
1.65	21.43	0.89	24.08
1.70	21.67	0.93	23.30
1.75	21.90	0.97	22.58
1.80	22.14	1.01	21.92
1.85	22.38	1.05	21.31

TABLE 3.5 Portion of the Stage-Discharge Rating Table for USGS Gage Station 01613900 Hogue Creek near Hayfield, Virginia, United States

Stage (m)	Q ($m^3 s^{-1}$)
1.189	17.1
1.192	17.2
1.195	17.3
1.198	17.4
1.201	17.5
1.204	17.6
1.207	17.7
1.210	17.8
1.213	17.9
1.216	18.0
1.219	18.1

c. The bankfull return period or frequency is computed using the publically available software program Hydrologic Engineering Center Statistical Software Package (HEC-SSP). Table 3.6 contains the annual peak flow data used in the analysis. Note that the peak streamflow for water year 2009 was not used because the gage height was not the maximum for the year.

The bankfull return period is 1.5 years meaning the event occurs twice every 3 years.

3.5 Summary and Conclusions

Knowledge of the magnitude and frequency of bankfull discharge in rivers has important implications for river management and restoration. Changes or modifications to the flow regime of a river such as in the case of irrigation, dams/impoundments, urbanization, or even climate change can alter the frequency with which the floodplain is inundated (i.e., bankfull discharge producing events occur) meaning the geomorphic and ecological functions of the riverine system will change as well [58]. Bankfull events not only shape the channel but these and larger discharges influence riparian ecosystems through sediment, nutrient, and woody debris deposits onto the floodplains. Such deposits influence nutrient cycling in riparian soils and hence hyporheic and instream water quality [4].

Efforts to manage and restore rivers must carefully consider bankfull discharge magnitude and frequency. While many studies report bankfull return periods between 1 and 2 years, others report values on the order of months to decades. Selecting a specified return interval (e.g., 1.5 years) for a restoration design without carefully evaluating the expected bankfull return period for a physiographic region can result in large errors in estimating channel-forming discharge [19]. If the specified return period is much lower than the actual bankfull return period, then the channel will be undersized (i.e., bankfull discharge is actually larger than what is modeled) and will likely erode. Contrarily, if the specified return period is much larger than the actual bankfull return period, then the channel will be too large (i.e., bankfull discharge is actually smaller than what is modeled) and will likely aggrade [14]. The interaction between the channel and its floodplain is critical. As such, successful management strategies and restoration efforts will seek to maintain, or if needed, reestablish this connection.

TABLE 3.6 Annual Peak Flow Data for USGS Gage Station 01613900 Hogue Creek near Hayfield, Virginia, United States

Water Year[a]	Date	Q ($m^3 s^{-1}$)	H (m)
1961	April 13, 1961	14.22	1.32
1962	March 21, 1962	22.09	1.53
1963	March 19, 1963	20.39	1.61
1964	November 7, 1963	11.10	1.27
1965	March 5, 1965	20.87	1.62
1966	September 21, 1966	27.86	1.79
1967	March 7, 1967	31.43	1.87
1968	March 17, 1968	14.50	1.42
1969	July 27, 1969	1.16	0.60
1970	July 9, 1970	55.22	2.26
1971	November 13, 1970	51.25	2.19
1972	June 22, 1972	78.15	2.70
1973	December 8, 1972	10.93	1.17
1974	December 26, 1973	11.67	1.21
1975	March 19, 1975	30.30	1.85
1976	January 1, 1976	31.43	1.88
1977	October 9, 1976	53.24	2.34
1978	August 6, 1978	75.89	2.61
1979	February 25, 1979	30.02	1.60
1980	October 2, 1979	31.15	1.61
1981	April 13, 1981	3.62	0.62
1982	June 13, 1982	39.08	1.84
1983	April 24, 1983	22.09	1.34
1984	February 14, 1984	51.25	2.32
1985	November 28, 1984	28.60	1.76
1986	November 4, 1985	20.08	1.49
1987	April 17, 1987	25.37	1.66
1988	May 6, 1988	28.88	1.76
1989	March 6, 1989	10.70	1.12
1990	July 13, 1990	4.87	0.78
1991	October 23, 1990	34.26	1.91
1992	July 25, 1992	21.41	1.53
1993	March 4, 1993	65.70	2.22
1994	November 28, 1993	33.13	1.60
1995	June 27, 1995	21.18	1.30
1996	September 6, 1996	115.82	2.96
1997	December 2, 1996	13.05	1.06
1998	November 7, 1997	29.45	1.51
1999	March 17, 1999	4.56	0.69
2000	August 6, 2000	30.58	1.54
2001	June 22, 2001	82.40	2.49
2002	May 2, 2002	5.15	0.72
2003	January 1, 2003	22.20	1.33
2004	September 28, 2004	67.68	2.25
2005	March 28, 2005	12.01	1.02
2006	November 29, 2005	25.66	1.42
2007	April 15, 2007	19.43	1.26
2008	April 20, 2008	21.29	1.31
2009	May 4, 2009	14.61	1.11
2010	March 13, 2010	37.66	1.70

[a] A water year encompasses the period from October 1 to September 30.

References

1. Afzalimehr H., M. Abdolhosseini, and V. Singh. 2010. Hydraulic geometry relations for stable channel design. *Journal of Hydraulic Engineering* 15: 859–864.
2. Agouridis C.T., R.R. Brockman, S.R. Workman, L.E. Ormsbee, and A.W. Fogle. 2011. Bankfull hydraulic geometry relationships for the Inner and Outer Bluegrass Regions of Kentucky. *Water* 3: 923–948.
3. Alireza K. and S.H. Nabavi. 2007. Dominant discharge in the Kor River, upstream of Doroodzan Dam, Fars Province, Iran. *Trends in Applied Sciences Research* 2: 158–164.
4. Andrews D.A., C.D. Barton, R.K. Kolka, C.C. Rhoades, and A.J. Dattilo. 2011. Soil and water characteristics in restored canebrake and forest riparian zones. *Journal of the American Water Resources Association* 47: 772–784.
5. Andrews E.D. 1980. Effective and bankfull discharge of streams in the Yampa River Basin, Colorado and Wyoming. *Journal of Hydrology* 46: 311–330.
6. Annable W.K., V.G. Lounder, and C.C. Watson. 2011. Estimating channel-forming discharge in urban watercourses. *River Research and Applications* 27: 738–753.
7. Arcement G.J. and V.R. Schneider. 1989. Guide for selecting Manning's roughness coefficients for natural channels and flood plains. Washington, DC: U.S. Geological Survey Water-Supply Paper 2339.
8. Barnes H.H. 1967. Roughness characteristics of natural channels. Washington, DC: U.S. Geological Survey Water-Supply Paper 1849.
9. Bates R.L. and J.A. Jackson. 1987. *Glossary of Geology*. Alexandria, VA: American Geosciences Institute.
10. Bernhardt E.S., M.A. Palmer, J.D. Allan, G. Alexander, K. Barnas, S. Brooks, J. Carr et al. 2005. Synthesizing U.S. river restoration efforts. *Science* 308: 636–637.
11. Biedenharn D.S., C.R. Thorne, P.J. Soar, R.D. Hey, and C.C. Watson. 2001. Effective discharge calculation guide. *International Journal of Sediment Research* 16: 445–459.
12. Bjerklie D.M. 2007. Estimating the bankfull velocity and discharge for rivers using remotely sensed river morphology information. *Journal of Hydrology* 341: 144–155.
13. Bjerklie D.M., D. Moller, L.C. Smith, and S.L. Dingman. 2005. Estimating discharge in rivers using remotely sensed hydraulic information. *Journal of Hydrology* 309: 191–209.
14. Brockman R.R., C.T. Agouridis, S.R. Workman, L.E. Ormsbee, and A.W. Fogle. 2012. Bankfull regional curves for the Inner and Outer Bluegrass Regions of Kentucky. *Journal of the American Water Resources Association* 48: 391–406.
15. Castro J.M. and P.L. Jackson. 2001. Bankfull discharge recurrence intervals and regional hydraulic relationships: Patterns in the Pacific Northwest. *Journal of the American Water Resources Association* 37: 1249–1262.
16. Chaplin J.J. 2005. Development of regional curves relating bankfull-channel geometry and discharge to drainage area for streams in Pennsylvania and selected areas of Maryland. Reston, VA: U.S. Geological Survey Scientific Investigations Report 2005-5147.
17. Cinotto P.J. 2003. Development of regional curves of bankfull-channel geometry and discharge for streams in the non-urban, Piedmont physiographic province, Pennsylvania and Maryland. New Cumberland, PA: U.S. Geological Survey Water-Resources Investigations Report 03-4014.
18. Coon W.F. 1995. Estimates of roughness coefficients for selected natural stream channels with vegetated banks in New York. Ithaca, NY: U.S. Geological Survey Open-File Report 93-161.
19. Copeland R.R., D.S. Biedenharn, and J.C. Fischenich. 2000. *Channel-Forming Discharge*. Washington, DC: U.S. Army Corps of Engineers.
20. DCR (Department of Conservation and Recreation). 2004. *The Virginia Stream Restoration and Stabilization Best Management Practices Guide*. Richmond, VA: DCR.
21. Doll B.A., A.D. Dobbins, J. Spooner, D.R. Clinton, and D.A. Bidelspach. 2003. Hydraulic geometry relationships for rural North Carolina coastal plain streams. Report to NC Division of Water Quality for 319 Grant Project No. EW20011. Raleigh, NC: North Carolina Stream Restoration Institute.

22. Doll B.A., G.L. Grabow, K.R. Hall, J. Halley, W.A. Harman, G.D. Jennings, and D.E. Wise. 2003. *Stream Restoration: A Natural Channel Design Handbook*. Raleigh, NC: North Carolina Stream Restoration Institute, North Carolina State University.
23. Doll B.A., D.E. Wise-Frederick, C.M. Buckner, S.D. Wilkerson, W.A. Harman, R.E. Smith, and J. Spooner. 2002. Hydraulic geometry relationships for urban streams throughout the Piedmont of North Carolina. *Journal of the American Water Resources Association* 38: 641–651.
24. Duntell R.C. 2000. *Development of Bankfull Discharge and Channel Geometry Relationships for Natural Channel Design in Oklahoma Using a Fluvial Geomorphic Approach*. Norman, OK: University of Oklahoma.
25. Emmett W.W. and M.G. Wolman. 2001. Effective discharge and gravel-bed rivers. *Earth Surface Processes and Landforms* 26: 1369–1380.
26. Ferro V. and P. Porto. 2012. Identifying a dominant discharge for natural rivers in southern Italy. *Geomorphology* 139–140: 313–321.
27. FISRWG (Federal Interagency Stream Restoration Working Group). 1998. Stream corridor restoration: Principles, processes, and practices. By the Federal Interagency Stream Restoration Working Group (FISRWG) (15 Federal agencies of the US gov't). GPO Item No. 0120-A; SuDocs No. A 57.6/2:EN3/PT.653.
28. Gillen D.F. 1996. Determination of roughness coefficients for streams in west-central Florida. Tampa, FL: U.S. Geological Survey Open-File Report 96-226.
29. Harman W.A., G.D. Jennings, J.M. Patterson, D.R. Clinton, L.O. Slate, A.G. Jessup, J.R. Everhart, and R.E. Smith. 1999. Bankfull hydraulic geometry relationships for North Carolina streams. Presented at *AWRA Wildland Hydrology Symposium*, Bozeman, MT.
30. Harman W.A., D.E. Wise, M.A. Walker, R. Morris, M.A. Cantrell, M. Clemmons, G.D. Jennings, D.R. Clinton, and J.M. Patterson. 2000. Bankfull regional curves for North Carolina mountain streams. Presented at *AWRA Conference: Water Resources in Extreme Environments*, Anchorage, AK.
31. Harrelson C.C., C. Rawlins, and J. Potyondy. 1984. Stream channel reference sites: An illustrated guide to field techniques. Fort Collins, CO: USDA Forest Service Rocky Mountain Forest and Range Experiment Station General Technical Report RM245.
32. Hicks D.M. and P.D. Mason. 1991. *Roughness Characteristics of New Zealand Rivers*. Christchurch, New Zealand: National Institute of Water and Atmospheric Research Ltd.
33. IACWD (Interagency Advisory Committee on Water Data). 1982. *Guidelines for Determining Flood Flow Frequency-Bulletin 17B of the Hydrology Subcommittee*. Reston, VA: U.S. Geological Survey Office of Water Data Coordination.
34. Jarrett R.D. 1985. Determination of roughness coefficients for streams in Colorado. Lakewood, CO: U.S. Geological Survey Water-Resources Investigations Report 85-4004.
35. Johnson P.A. and T.M. Heil. 1996. Uncertainty in estimating bankfull conditions. *Journal of the American Water Resources Association* 32: 1283–1291.
36. Juracek K.E. and F.A. Fitzpatrick. 2009. Geomorphic applications of stream-gage information. *River Research and Applications* 25: 329–347.
37. Keaton J.N., T. Messinger, and E.J. Doheny. 2005. Development and analysis of regional curves for streams in the non-urban valley and ridge physiographic province, Maryland, Virginia, and West Virginia. Reston, VA: U.S. Geological Survey Scientific Investigations Report 2005-0576.
38. Knighton D. 1998. *Fluvial Forms and Processes*. London, U.K.: Hodder Education.
39. Krstolic J.L. and J.J. Chaplin. 2007. Bankfull regional curves for streams in the non-urban, non-tidal Coastal Plain physiographic province, Virginia and Maryland. Reston, VA: U.S. Geological Survey Scientific Investigations Report 2007-5162.
40. Lawlor S.M. 2004. Determination of channel-morphology characteristics, bankfull discharge, and various design-peak discharges in western Montana. Reston, VA: U.S. Geological Survey Scientific Investigations Report 2004-5263.
41. Leopold L.B. 1994. *A View of the River*. Cambridge, MA: Harvard University Press.

42. Leopold L.B., M.G. Wolman, and J.P. Miller. 1964. *Fluvial Processes in Geomorphology*. New York: Dover Publications, Inc.
43. Lotspeich R.R. 2009. Regional curves of bankfull channel geometry for non-urban streams in the Piedmont physiographic province, Virginia. Reston, VA: U.S. Geological Survey Scientific Investigations Report 2009-5206.
44. McCandless T.L. 2003. Maryland stream survey: Bankfull discharge and channel characteristics of streams in the Allegheny Plateau and the Valley and Ridge hydrologic regions. Annapolis, MD: U.S. Fish and Wildlife Service CBFO-S03-01.
45. McCandless T.L. 2003. Maryland stream survey: Bankfull discharge and channel characteristics of streams in the Coastal Plain hydrologic region. Annapolis, MD: U.S. Fish and Wildlife Service CBFO-S03-02.
46. McCandless T.L. and R.A. Everett. 2002. Maryland stream survey: Bankfull discharge and channel characteristics of streams in the Piedmont hydrologic region. Annapolis, MD: U.S. Fish and Wildlife Service CBFO-S02-01.
47. McCuen R.H. 2004. *Hydrologic Analysis and Design*. Upper Saddle River, NJ: Prentice Hall.
48. Metcalf C.K., S.D. Wilkerson, and W.A. Harman. 2009. Bankfull regional curves for North and Northwest Florida streams. *Journal of the American Water Resources Association* 45: 1260–1272.
49. Mistak J.L. and D.A. Stille. 2008. Regional hydraulic geometry curve for the Upper Menominee River. Ann Arbor, MI: Michigan Department of Natural Resources Fisheries Division, Technical Report 2008-1.
50. Moody T., M. Wirtanen, and S.N. Yard. 2003. *Regional Relationships for Bankfull Stage in Natural Channels of the Arid Southwest*. Flagstaff, AZ: Natural Channel Design, Inc.
51. Mulvihill C.I. and B.P. Baldigo. 2007. Regionalized equations for bankfull-discharge and channel characteristics of stream in New York state-hydrologic region 3 east of the Hudson River. Reston, VA: U.S. Geological Survey Scientific Investigations Report 2007-5227.
52. Mulvihill C.I., B.P. Baldigo, S.J. Miller, D. DeKoskie, and J. DuBois. 2009. Bankfull discharge and channel characteristics of stream in New York state. Reston, VA: U.S. Geological Survey Scientific Investigations Report 2009-5144.
53. Mulvihill C.I., A.G. Ernst, and B.P. Baldigo. 2005. Regionalized equations for bankfull discharge and channel characteristics of streams in New York state: Hydrologic region 6 in the southern tier of New York. Reston, VA: U.S. Geological Survey Scientific Investigations Report 2005-5100.
54. Mulvihill C.I., A.G. Ernst, and B.P. Baldigo. 2006. Regionalized equations for bankfull-discharge and channel characteristics of streams in New York state: Hydrologic region 7 in western New York. Reston, VA: U.S. Geological Survey Scientific Investigations Report 2006-5075.
55. Mulvihill C.I., A. Filopowicz, A. Coleman, and B.P. Baldigo. 2007. Regionalized equations for bankfull discharge and channel characteristics of streams in New York state—Hydrologic regions 1 and 2 in the Adirondack region of northern New York. Reston, VA: U.S. Geological Survey Scientific Investigations Report 2007-5189.
56. Nash D.B. 1994. Effective sediment-transporting discharge from magnitude-frequency analysis. *Journal of Geology* 102: 79–95.
57. Navratil O., M.B. Albert, E. Herouin, and J.M. Gresillon. 2006. Determination of bankfull discharge magnitude and frequency: Comparison of methods on 16 gravel-bed river reaches. *Earth Surface Processes and Landforms* 31: 1345–1363.
58. Page K., A. Read, P. Frazier, and N. Mount. 2005. The effect of altered flow regime on the frequency and duration of bankfull discharge: Murrumbidgee River, Australia. *River Research and Applications* 21: 567–578.
59. Petit F. and A. Pauquet. 1997. Bankfull discharge recurrence interval in gravel-bed rivers. *Earth Surface Processes and Landforms* 22: 685–693.
60. Pickup G. and R.F. Warner. 1976. Effects of hydrologic regime on magnitude and frequency of dominant discharge. *Journal of Hydrology* 29: 51–75.

61. Pike A.S. and F.N. Scatena. 2012. Riparian indicators of flow frequency in a tropical montane stream network. *Journal of Hydrology* 382: 72–87.
62. Powell G.E., D. Mecklenberg, and A. Ward. 2006. Evaluating channel-forming discharges: A study of large rivers in Ohio. *Transactions of the ASABE* 49: 35–46.
63. Rachol C.M. and K. Boley-Morse. 2009. Estimated bankfull discharge for selected Michigan rivers and regional hydraulic geometry curves for estimating bankfull characteristics in southern Michigan rivers. Reston, VA: U.S. Geological Survey Scientific Investigations Report 2009-5133.
64. Rosgen D.L. 1996. *Applied River Morphology*. Pagosa Springs, CO: Wildland Hydrology.
65. Rustomji P. 2009. *A Statistical Analysis of Flood Hydrology and Bankfull Discharge for the Daly River catchment, Northern Territory, Australia*. Clayton South, Victoria, Australia: CISRO, Water for a Healthy Country National Research Flagship.
66. Segura C. and J. Pitlick. 2010. Scaling frequency of channel-forming flows in snowmelt-dominated streams. *Water Resources Research* 46: W06524.
67. Sherwood J.M. and C.A. Huitger. 2005. Bankfull characteristics of Ohio streams and their relation to peak streamflows. Reston, VA: U.S. Geological Survey Scientific Investigations Report 2005-5153.
68. Shields F.D., R.R. Copeland, P.C. Klingeman, M.W. Doyle, and A. Simon. 2003. Design for stream restoration. *Journal of Hydraulic Engineering* 129: 575–584.
69. Soar P.J. and C.R. Thorne. 2001. *Channel Restoration Design for Meandering Rivers*. ERDC/CHL CR-01. Vicksburg, MS: U.S. Army Corps of Engineers, Coastal and Hydraulics Laboratory, U.S. Army Engineer Research and Development Center (ERDC).
70. Sudduth E.B., J.L. Meyer, and E.S. Bernhardt. 2007. Stream restoration practices in the southeastern United States. *Restoration Ecology* 15: 573–583.
71. Sweet W.V. and J.W. Geratz. 2003. Bankfull hydraulic geometry relationships and recurrence intervals for North Carolina's coastal plain. *Journal of the American Water Resources Association* 39: 861–871.
72. U.S. Department of Agriculture, Forest Service. 2005. Guide to identification of bankfull stage in the northeastern United States. Fort Collins, CO: Rocky Mountain Research Station, General Technical Report RMRS-GTR-133-CD.
73. Vesely W.S., A.C. Parola, and C. Hansen. 2008. Geomorphic characteristics of streams in the eastern Kentucky coal field physiographic region of Kentucky. Final Report for Section 319(h) Nonpoint Source Implementation Program Cooperative Agreement #C9994861-01. Frankfort, KY: University of Louisville Stream Institute for the Kentucky Division of Water.
74. Westergard B.E., C.I. Mulvihill, A.G. Ernst, and B.P. Baldigo. 2004. Regionalized equations for bankfull-discharge and channel characteristics of streams in New York state: Hydrologic region 5 in central New York. Reston, VA: U.S. Geological Survey Scientific Investigations Report 2004-5247.
75. White K.E. 2001. Regional curve development and selection of a reference reach in the non-urban, lowland sections of the Piedmont physiographic province, Pennsylvania and Maryland. New Cumberland, PA: U.S. Geological Survey Water-Resources Investigations Report 01-4146.
76. Wilkerson G.V. 2008. Improved bankfull discharge prediction using 2-year recurrence-period discharge. *Journal of the American Water Resources Association* 44: 243–58.
77. Williams G.P. 1978. Bankfull discharge of rivers. *Water Resources Research* 14: 1141–1154.
78. Wolman M.G. 1967. A cycle of sedimentation and erosion in urban river channels. *Geografiska Annaler* 49A: 385–395.
79. Wolman M.G. and J.P. Miller. 1960. Magnitude and frequency of geomorphic processes. *Journal of Geology* 68: 54–74.
80. Yochum S.E. 2003. *Regional Bankfull Characteristics for the Lower Willow Creek Stream Restoration*. Lakewood, CO: U.S. Department of Agriculture, Natural Resources Conservation Service Northern Plains Engineering Team.

4

Climate Change and Hydrological Hazards

Yang Hong
University of Oklahoma and National Weather Center

Lu Liu
University of Oklahoma and Joint Global Change Research Institute

Lei Qiao
University of Oklahoma and National Weather Center

Pradeep Adhikari
University of Oklahoma

AUTHORS

Yang Hong is currently professor of hydrometeorology–climatology and remote sensing in the School of Civil Engineering and Environmental Sciences and the School of Meteorology at the University of Oklahoma. Previously, he was a research scientist at NASA's Goddard Space Flight Center and postdoc researcher at University of California, Irvine. He currently directs the Hydrometeorology and Remote Sensing Lab at the National Weather Center (http://hydro.ou.edu).

Lu Liu is a postmaster research associate at the Joint Global Change Research Institute (JGCRI), a collaboration between the University of Maryland and the Pacific Northwest National Laboratory (PNNL). Her research interests generally include the development of global hydrological models, assessment of climate change impacts on global and regional hydrological regimes, and implementation of global and regional sectoral water demand models from an integrated assessment framework. Lu received both her BS and MS in environmental science at the University of Oklahoma.

Lei Qiao is a postdoctoral research fellow in the School of Civil Engineering and Environmental Sciences at the University of Oklahoma. He was graduated from Saint Louis University in 2012, with PhD studies focusing on climate change and its effects on terrestrial hydrological systems.

Pradeep Adhikari is a PhD student at the Department of Geography and Environmental Sustainability, University of Oklahoma. His research focuses on climate change and its impact on land and water resources.

PREFACE

According to the Intergovernmental Panel on Climate Change (IPCC) report, the global temperature rise has increased the evaporation rate and moisture-holding capacity in the atmosphere, which in turn alters the hydrological cycle, changes precipitation patterns, and thus streamflow extremes and soil water content. Due to continuous accumulation of atmospheric greenhouse gases and aerosols, climate predictions consistently warn of increases in global temperature for the current century, which could potentially result in more severe extreme weather impact such as drought and floods.

This chapter reviews the climate change and its impacts on regional hydrological systems under different climate scenarios. The case studies in the southern United States demonstrate the seasonal and spatial variability of hydrological response to the changing climate.

4.1 Introduction

Climate is the average weather in a place over a long period of time. Climate influences the Earth through changing temperature, precipitation, snowmelt, and a host of other natural phenomenon, and it is also in turn influenced by the variability on Earth [16]. Regional climate, which is characterized by local atmospheric variability and regional atmosphere–surface interaction, is a combined product of global climate forcing and also of regional atmosphere–land surface feedbacks. Given the assessment of regional climate, the linkage between climate and water resources management could be localized, which allows more relevant and localized practices [17]. As is known that the frequency and areal extent of local extreme weather is of great importance to regional social and economic systems, regional climate therefore plays a significant role in policy making and business management [13,17].

Global climate models (GCMs) have been developed over decades to study the global climate as a whole. Since the early generation of climate models that were not capable of fully characterizing the Earth's climate, GCMs nowadays are capable of capturing global climate characteristics temporally and spatially. The complexity of the Earth's climate is demonstrated using a variety of dynamic, chemical, and biological equations that form the computationally intensive GCMs [30]. GCM outputs usually have coarse resolutions and perform poorly at smaller scales, therefore inappropriate for regional impact assessment [22]. To solve the problem, downscaling techniques were applied to subset global climate data to the specific study region. The two primary downscaling methods commonly used are dynamic and statistical downscaling [11,38]. Dynamic downscaling techniques considers regional surface features by applying regional climate models (RCM) to the GCM outputs and as a result performs better at capturing local processes and feedbacks. However, it is relatively expensive to operate [21]. Statistical downscaling, however, finds the statistical relationship between large-scale climate features and local climate and simply applies the relationship to downscale the GCM outputs. Therefore, it is computationally less intensive but less physically relevant and dependent on the quality of the observational data [22].

Uncertainties are normally expected in climate simulations and projections produced by GCMs. There is no doubt that the Earth is a complicated natural system including tremendous processes and feedbacks between different components. Many of the processes are yet not fully understood by human. Therefore, it is unlikely to include these unknown uncertainties in the models until better understanding has been achieved. Therefore, the predictions made by the GCMs are largely dependent on the extent to which current models understand the natural processes. In addition, many of the uncertainties in the predictions of future climate are not even due to lack of understanding of the natural processes. Instead, future human behavior is the most unpredictable component in climate modeling. For example, technology innovations that limit the amount of greenhouses gases, regulations that change the amount of

pollutants, and how the population will be growing in the future all remain somewhat unknown [14]. Each of these is able to make a significant difference to the future climate that is beyond predictability.

4.2 Climate Change Impacts

Global climate change has profound effects on society's physical systems and human activities [14]. The Global Climate Change Impacts in the US Report compiled by the US Global Change Research Program claims that "Climate changes are already affecting water, energy, transportation, agriculture, ecosystems, and health" and additionally finds that the "global temperature has increased over the past 50 years." Many studies have been carried out to assess the climate change impacts on water, agriculture, health, and other aspects of life [29,31,34]. In this chapter, a case study will be used as an example to show the climate change processes over the southern United States.

4.2.1 Case Study: Climate Change Projection over the Southern United States

The area of focus for the case study is the six-state region of responsibility for the Southern Climate Impacts Planning Program (SCIPP) (http://www.southernclimate.org/)—Oklahoma, Texas, Arkansas, Louisiana, Tennessee, and Mississippi—hereafter referred to as the SCIPP region (Figure 4.1). SCIPP is a southern US-focused climate hazards preparedness program that aims to bridge the gap between climate science and local-level climate hazard planning processes.

The average temperature for the period of 1950–1999 was 17.4°C in SCIPP. Climate in the SCIPP region is characterized by maximum temperature in July (~27.3°C) and minimum temperature in

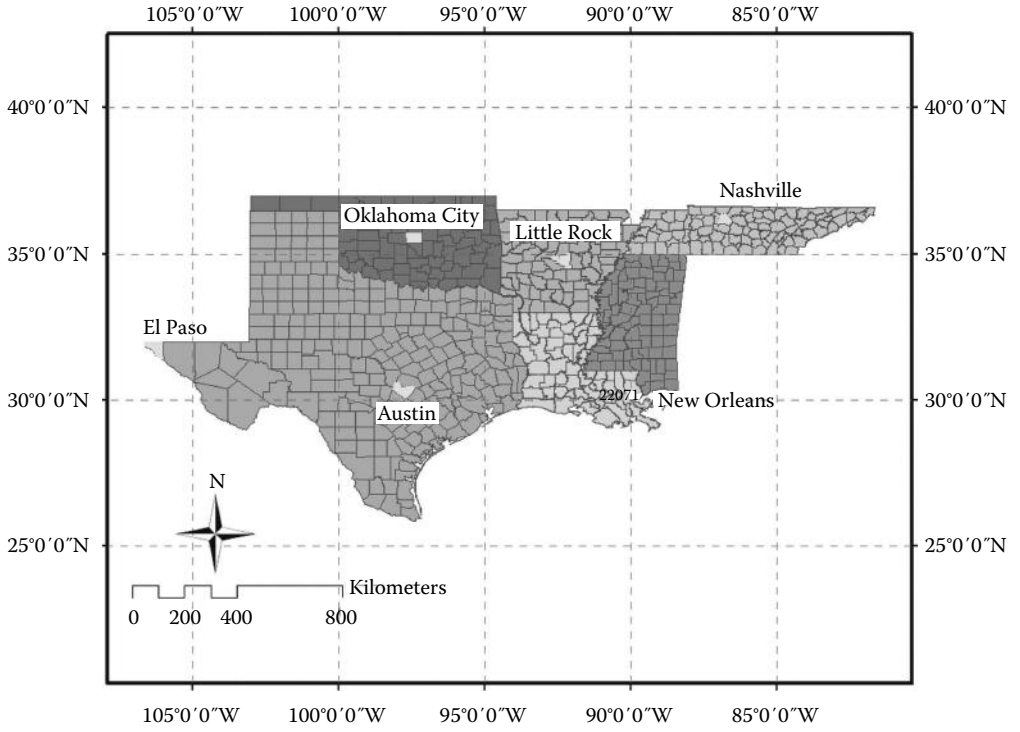

FIGURE 4.1 SCIPP region. (From Liu, L. et al., *Theor. Appl. Climatol.*, 109, 345, 2012.)

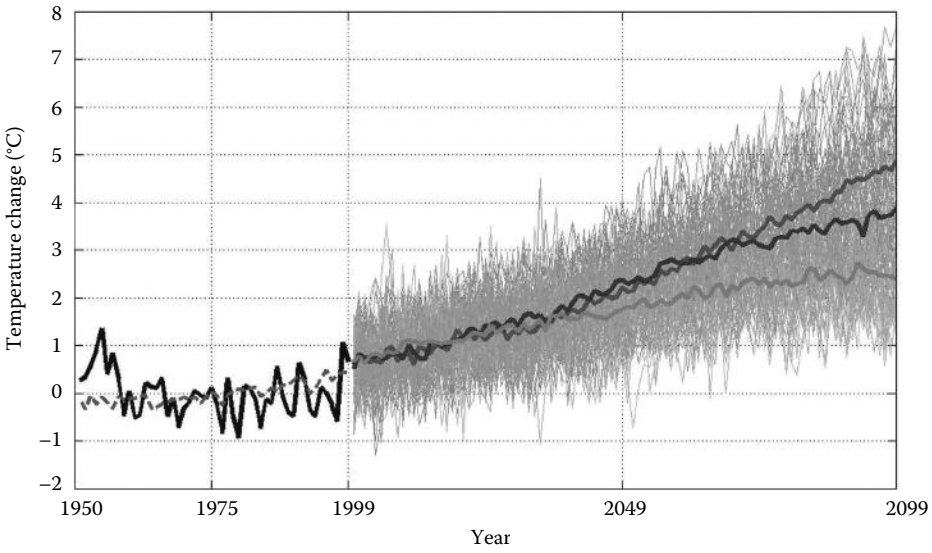

FIGURE 4.2 Surface temperature anomaly relative to 1950–1999 mean over SCIPP from 2000–2099. Light background is the 16 GCMs' temperature projection for all scenarios. Bold lines are the ensemble means for the A2, A1B, and B1 scenarios (top to bottom). (From Liu, L. et al., *Theor. Appl. Climatol.*, 109, 345, 2012.)

January (~3°C). The historical temperature distribution across the SCIPP region is characterized by an increasing trend from north to south, with the Gulf Coast region warmer than the northern portion of SCIPP. The 1950–1975 period exhibited an overall cooling trend, while warming was predominant during 1976–2000 (Figure 4.2). Studies have found out that the influence on climate from increasing greenhouse gas emissions has been the strongest during the past 50 years [16].

As defined in the IPCC Special Report on Emissions Scenarios, scenario A2 is a higher CO_2 emission path and describes a populated world where technological change and economic growth are more fragmented and slower. Scenario A1B is a middle emission path known as business-as-usual and describes a balanced world where people do not rely too heavily on any particular energy source. Scenario B1 is a lower emission path where clean and sustainable technology is highly emphasized. Sixteen GCM projections indicate an increase in temperatures across SCIPP ranging between 2.3°C and 4.8°C by the end of the twenty-first century depending on the emission scenario (Figure 4.2).

The second half of the twenty-first century is projected to be warmer than the first half century as a whole by an average of 2.2°C, 1.8°C, and 1°C as projected by A2, A1B, and B1 scenarios. The most significant changes in temperature are projected to occur in the summer and fall seasons. A warming signal is also present during the spring and winter but is less significant relative to the summer and fall (Figure 4.3a). The monthly future temperature changes projected by A1B are broken down into every two decades in Figure 4.3b. The changes are phenomenal during the last two decades of the century with over 4°C of warming being projected to occur for half of the year. Figure 4.4 provides a spatial representation of future temperature conditions based on the ensemble GCMs. More significant warming is projected is the second half century than the first half. Warming is projected to be more significant across the northwestern portions of SCIPP, with less substantial warming near the Gulf Coast. One significant concern regarding the projected increase in surface temperatures is the potential influence on temperature-related hazards such as drought [6]. Warmer summer conditions could potentially contribute to more droughts, though that would be highly dependent on future precipitation conditions.

In conclusion, projected temperature for the twenty-first century is highly dependent on the emission scenario with the A2 scenario exhibiting the highest relative increases in temperature, particularly

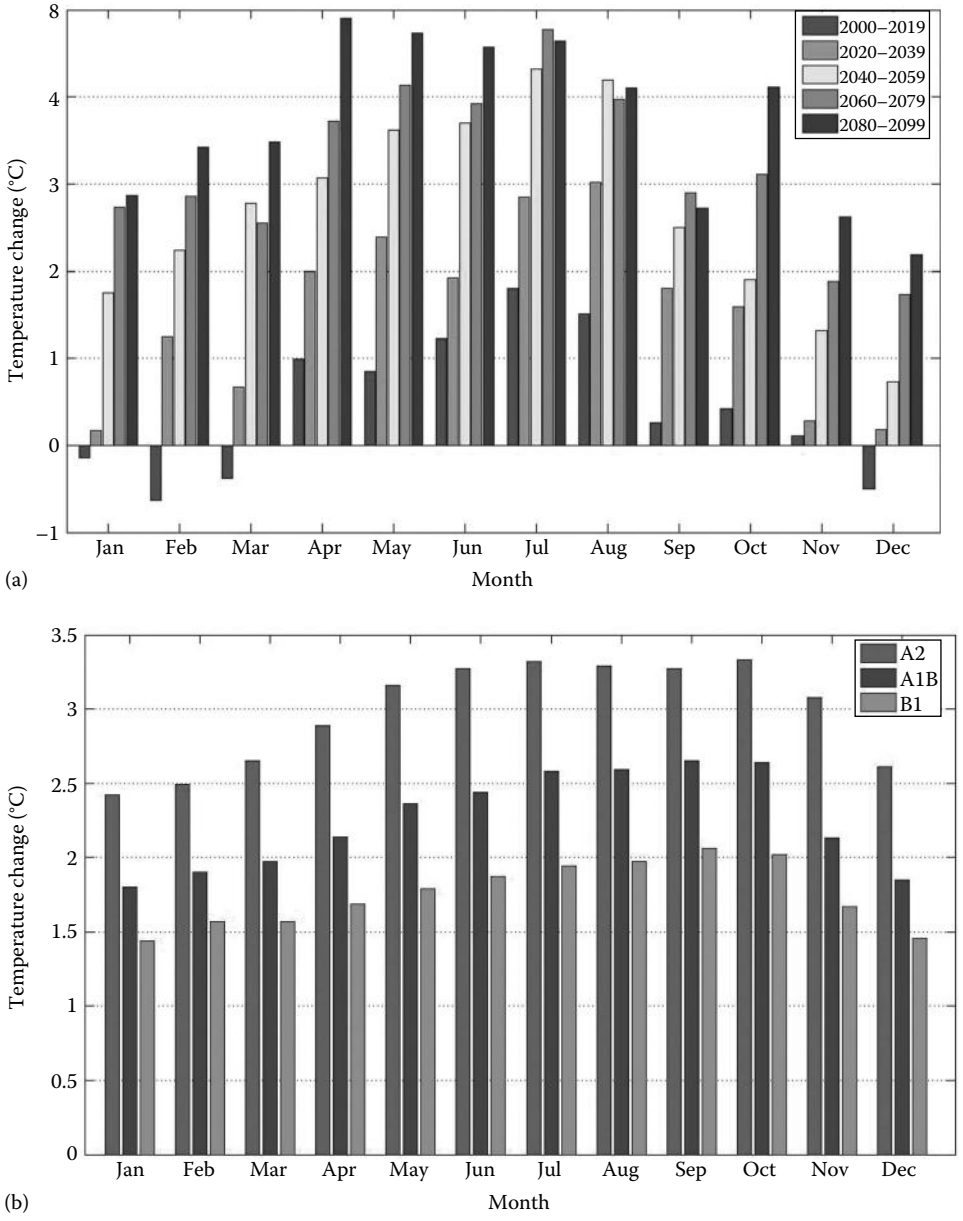

FIGURE 4.3 (a) Projected monthly ensemble temperature change relative to 1950–1999 monthly mean for the period of 2000–2099 based on different scenarios. (b) Projected A1B monthly ensemble temperature change for each two-decade period. (From Liu, L. et al., *Theor. Appl. Climatol.*, 109, 345, 2012.)

for the summer and fall months. The changes in monthly temperature are crucial to numerous sectors, including agriculture, water resources, and energy. A change in climate induces various biological effects that can result in impacts on crop production and supply, which could further impact systems and lead to more economic and social issues [25].

The SCIPP region has a very diverse precipitation pattern. The historical average annual precipitation across the SCIPP region has been 955.7 mm (38.2 in.) the past 50 years and has slightly increased over time. Western portions of the region experience arid conditions and less than 254 mm

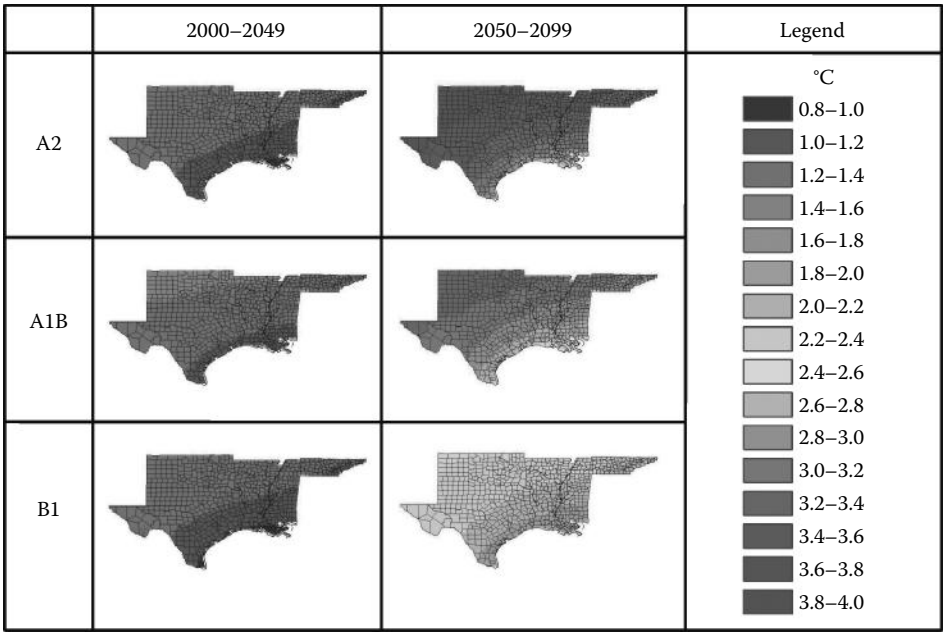

FIGURE 4.4 Projected ensemble temperature change distribution for each state within the SCIPP region for the period 2000–2049 and 2050–2099 relative to 1950–1999 mean. (From Liu, L. et al., *Theor. Appl. Climatol.*, 109, 345, 2012.)

of precipitation per year on average, while southeastern portions of the region (southern Louisiana and Mississippi) receive significantly greater amounts of precipitation of greater than 1524 mm/year on average. One major feature contributing to this disparity in rainfall is the presence of the Gulf of Mexico, which provides a significant amount of the moisture to the region, particularly to the locations closer to the coast.

The results found that future precipitation conditions do not show significant trend overall (Figure 4.5). However, projected precipitation under B1 scenario is tested to have more increase compared to that of A1B and A2. Future increases are projected in the northeastern portions of SCIPP, with Tennessee having the most significant increase of precipitation. Southwestern portions of SCIPP are projected to have a drier future, with A2 producing 0.35% less rainfall during 2050–2099 than the historical mean (Figure 4.5), although change is not considered statistically significant. Precipitation is projected to increase in southwest Texas and eastern Tennessee during the summer, with a shift toward the Gulf Coast during the fall. Winter is projected to be wetter in the northeast and drier in the south (Figure 4.6). Seasonal precipitation variation differed according to the different scenarios; however, common characteristics were found. The spring season, which provides a substantial portion of the annual precipitation total to the region, is projected to be drier [19].

Rainfall is projected to increase nearly 7% in December relative to 1950–1999 mean according to the A1B scenario (Figure 4.7). However, 7% of increase is not incredibly significant in this case. The three states exhibiting the most noticeable change are Tennessee, Texas, and Louisiana. The state of Tennessee is expected to have 10–30 mm of precipitation increase in the winter months from 2050 to 2099. Texas is projected to be drier for most months except for several months during the fall (September and November). Louisiana exhibits tremendous changes throughout the year, with rainfall increases during February and rainfall decreases during January and April (Figure 4.8).

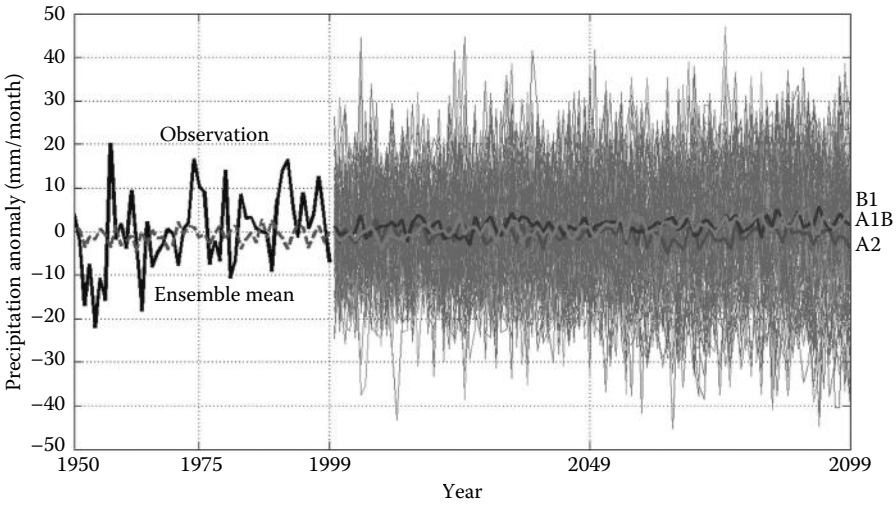

FIGURE 4.5 Precipitation anomaly over SCIPP from 2000 to 2099. The 16 GCM precipitation projections for the A2, A1B, and B1 scenarios are shown in the background. Bold lines are the ensemble means for the corresponding scenario. (From Liu, L. et al., *Theor. Appl. Climatol.*, 109, 345, 2012.)

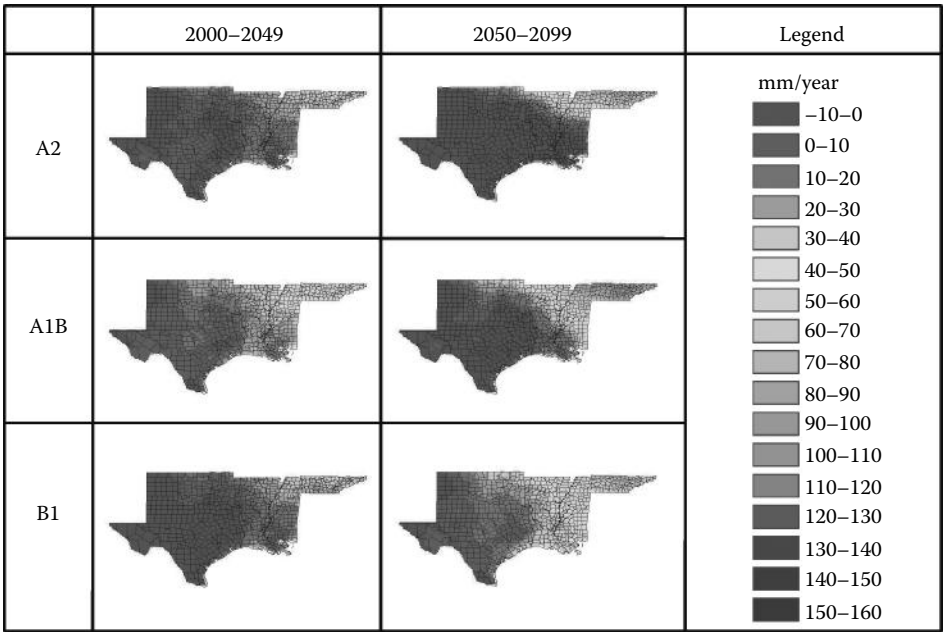

FIGURE 4.6 Projected ensemble precipitation change for each state within the SCIPP region for the period 2000–2049 and 2050–2099. (From Liu, L. et al., *Theor. Appl. Climatol.*, 109, 345, 2012.)

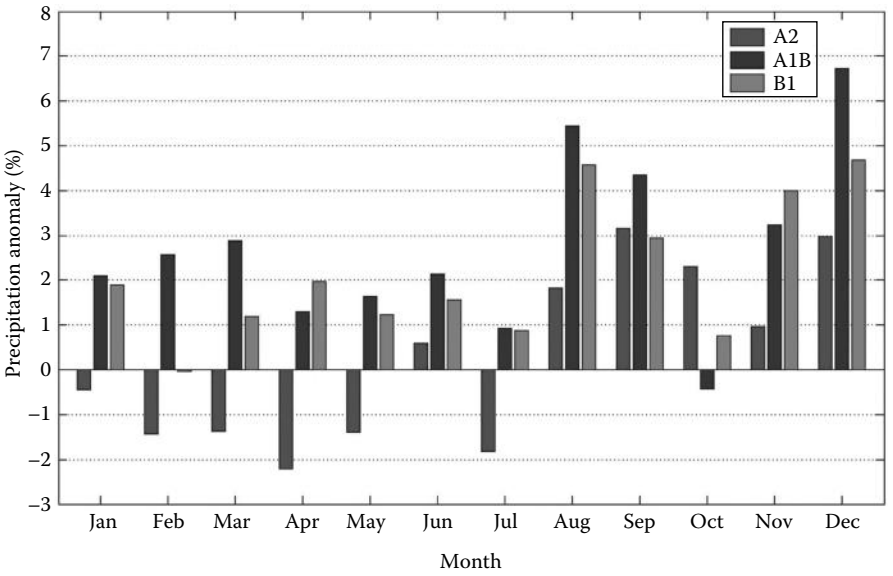

FIGURE 4.7 Projected monthly ensemble precipitation change for the period of 2000–2099 based on different scenarios relative to 1950–1999 mean. (From Liu, L. et al., *Theor. Appl. Climatol.*, 109, 345, 2012.)

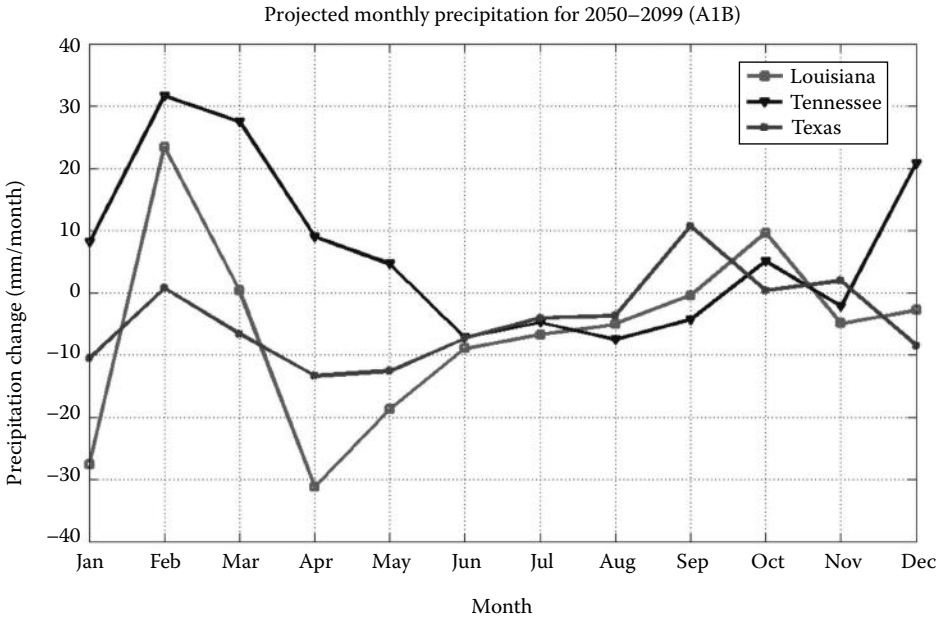

FIGURE 4.8 Projected monthly precipitation change for 2050–2099 under A1B scenario relative to 1950–1999 mean over the three states with the most noticeable change. (From Liu, L. et al., *Theor. Appl. Climatol.*, 109, 345, 2012.)

4.3 Hydrological Hazards Related to Climate Change

4.3.1 Droughts

Drought is usually defined on the basis of the degree of dryness and the duration of the dry period [27]. Scientifically speaking, it is considered to be a deficiency of precipitation over an extended period of time, which might result in a water shortage for some activity, group, or environmental sector [18]. Scientists have developed four classifications to describe different kinds of drought, which are meteorological drought, agricultural drought, hydrological drought, and socioeconomic drought [39].

Meteorological drought is simply the departure from normal conditions of meteorological variables that induces drying of the surface. It is region-specific because the atmospheric conditions of different areas have high local variability in space and time [24]. Agricultural drought occurs when the soil moisture fails to provide enough nourishment to the plants. It indicates whether the water quantity in soil can meet the demand of plants at various growing stages. Hydrological drought, which is initially caused by rainfall deficits, is normally associated with reservoirs or lake levels within a basin [34]. It is important to note that the hydrological responses normally are latent to precipitation deficiencies in a basin. Therefore, not all meteorological droughts will immediately trigger a hydrological drought because reservoir levels remain fairly constant over a short period of time. Socioeconomic drought is different from the aforementioned types of droughts because it is a measure of the gap between supply and demand. If the water supply cannot meet the demand of water consumption such as hydroelectric power, food production, and fishery activities, a socioeconomic drought will occur due to the demand–supply unbalance [24].

4.3.1.1 Drought Quantification

Drought is difficult to be quantified due to its dependence on different geographic regions, needs, and disciplinary perspectives [23,33]. Various drought indices have been developed over the past few decades to assimilate thousands of bits of data on rainfall, snowpack, streamflow, and other water supply indicators into a comprehensible big picture. These drought indices were developed for different purposes. In this chapter, we introduce three different kinds of drought indices, Standardized Precipitation Index (SPI) [23], Palmer Drought Severity Index (PDSI) [27], and Standardized Runoff Index (SRI) [39].

SPI is a meteorological drought index. As mentioned previously, meteorological drought is mainly caused by a deficiency of precipitation. A long-term precipitation record is needed in order to calculate SPI. After the statistical fitting and transformation of the long-term precipitation data, region-specific deviations are mostly minimized. SPI is a probability-based index, so the heaviness or lowness of a precipitation event in the SPI is relative to the rainfall characteristics of that area. SPI has a very straightforward classification of different drought severities (Table 4.1).

Although SPI is fairly easy to calculate compared to the other indices [2], it is very effective in providing early drought warning and drought damage control. However, the disadvantage of SPI is that it only considers one climate variable, precipitation, and not incorporating evapotranspiration (ET) or soil moisture, which is essential parameter in hydrological process. Therefore, comprehensive indices that involve more complex natural hydrological process are also developed to address droughts.

TABLE 4.1 SPI Classification

2.0+	Extremely wet
1.5–1.99	Very wet
1.0–1.49	Moderately wet
−0.99 to 0.99	Near normal
−1.0 to −1.49	Moderately dry
−1.5 to −1.99	Severely dry
−2 and less	Extremely dry

TABLE 4.2 PDSI Classification

Palmer Classifications	
4.0 or more	Extremely wet
3.0–3.99	Very wet
2.0–2.99	Moderately wet
1.0–1.99	Slightly wet
0.5–0.99	Incipient wet spell
0.49 to −0.49	Near normal
−0.5 to −0.99	Incipient dry spell
−1.0 to −1.99	Mild drought
−2.0 to −2.99	Moderate drought
−3.0 to −3.99	Severe drought
−4.0 or less	Extreme drought

The PDSI is an indicator of hydrometeorological drought that has been used for the last 45 years. Instead of taking only precipitation into account, PDSI also accounts for temperature that has a huge impact on ET and soil moisture. This index provides a more comprehensive method to assess the impacts of climate change on drought since it requires more climate variables as input [2,12,27].

PDSI has different classification from that of SPI (Table 4.2).

The SRI appeared in Vasiliades et al. [39] as Water Balance Derived Drought Index. Input for this index is monthly streamflow data. Vasiliades et al. [39] fitted monthly streamflow data into to Pearson type III distribution and transformed it using Box–Cox transformation [5] to remove skewness.

The transformed streamflow values are then standardized to translate into a runoff index known as Z_{WBI}. SRI has the same classification with that of SPI; therefore, the region-specific deviation is minimized. SRI is fairly new compared to SPI and PDSI, so the fundamental idea of using SRI is to examine drought from a hydrological perspective and compare it with the traditional drought indices, namely, SPI and PDSI.

4.3.1.2 Drought History in the Southern United States

Historical records documented that Oklahoma, which is within southern Unites States, experienced six major droughts since the twentieth century: 1909–1918, 1931–1941, 1950–1956, 2001–2002, 2005–2006, and 2010–2011. While the drought of the 1930s is historically associated with the Dust Bowl of the Great Plains, statistics show that the drought of the 1950s was more severe for Oklahoma as indicated by record low drought indices values [3]. However, socioeconomic impacts were less severe as Oklahoma's population learned to cope with the Dust Bowl and put into place agricultural and water management practices that mitigated many of the worst impacts of the Dust Bowl. The drought history in the southern United States reveals that the southern United States is a drought-prone region. This raises the concern of how the future is going to be in terms of drought and whether climate change plays a role in affecting the drought condition. In this part, a case study will be talked about to show how the drought in the southern United States is projected under a changing climate.

4.3.1.3 Case Study: Blue River Basin, OK

The Blue River Basin (Figure 4.9) is particularly important to the State of Oklahoma and local surrounding communities. Historically, several Native American tribal communities have used the river as their important water source. Recently, however, there have been increasingly competing demands from surrounding industrial and metropolitan areas located in Oklahoma and Texas. The Blue River Basin is also a drought-prone region. It is very essential to study the future drought in this basin given the already-stressed water conflict in the region.

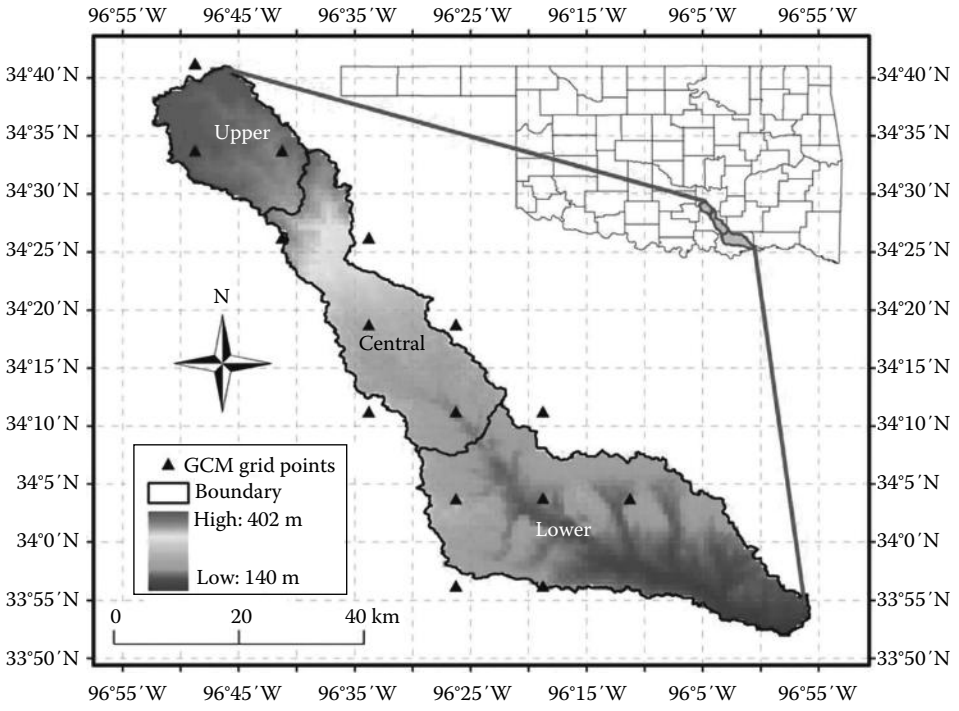

FIGURE 4.9 The Blue River Basin. (From Liu, L. et al., *Water Resour. Manage.*, 26(10), 2761, 2012.)

The three drought indices mentioned previously are first validated against the historical records. Results show that the three indices all capture the historical droughts with SPI and SRI showing better agreement with the records [20].

In terms of the drought projection, the three drought indices give similar but somewhat different drought projects in the Blue River Basin (Figure 4.10). SPI indicates one minor drought in the early 2020s, and the frequency and intensity of drought appear to increase substantially after 2050. PDSI and SRI show similar results and many more droughts are projected after 2050. More drought events are displayed on the PDSI panel than on the SRI panel, and severe droughts on PDSI are projected to be more severe (PDSI < −5) than those on SRI, except for the early 2080s.

The Blue River Basin is projected to be nearly constantly under wet conditions before 2050 for both PDSI and SRI, with a slight decreasing trend of wetness from 2011 to 2050. It is not surprising to see that both PDSI and SRI demonstrate more severe and frequent drought after 2050, although the magnitude and timing of droughts are not exactly the same. Based on the projections from Thornthwaite monthly water balance model, which is a hydrological model that gives future changes of hydrological variables, the Blue River Basin is expected to have an increasing trend of ET and decreasing trend in total runoff under A1B scenario. Actual ET is expected to increase by up to 8% on average, and runoff is projected to decrease by more than 10% by the end of the twenty-first century (Figure 4.11). Accordingly, more water is going out as ET and less water will be available for surface runoff.

In conclusion, three types of drought indices (SPI, PDSI, and SRI) capture the major droughts documented in history. The results projected by the drought indices under the business-as-usual A1B scenario suggest that more drought events might occur in the second half of the twenty-first century. This could be caused by the fact that the precipitation predicted by the GCM GISS-ER shows a descending trend, while the temperature is slowly but constantly increasing after 2010. Moreover, the ET projected by the Thornthwaite monthly water balance model also has a significant increasing trend under such a

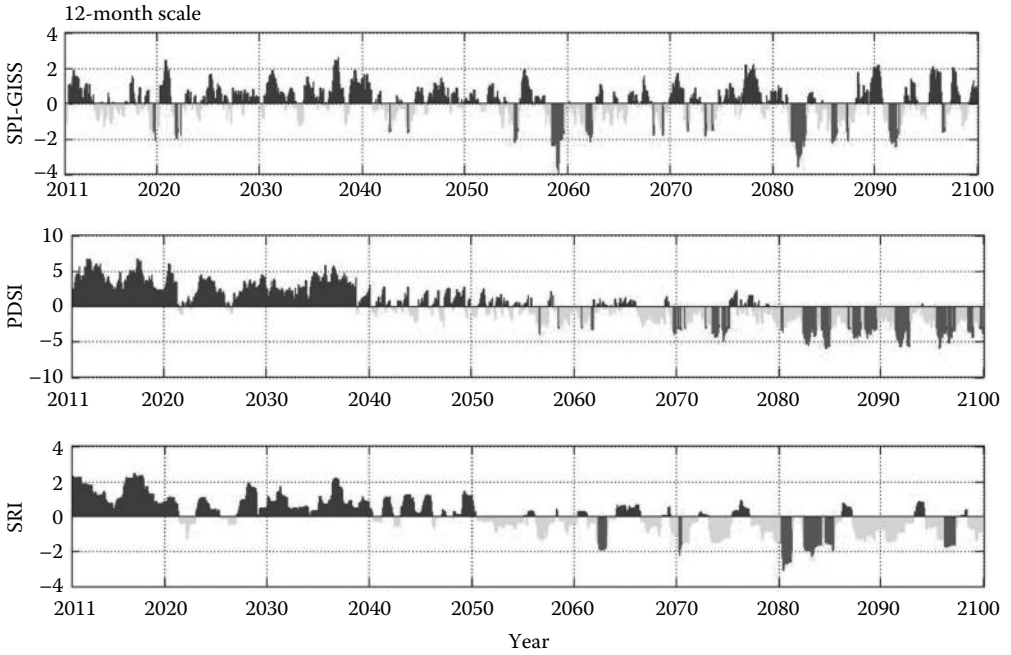

FIGURE 4.10 Projected time series variation of SPI, PDSI, and SRI. (From Liu, L. et al., *Water Resour. Manage.*, 26(10), 2761, 2012.)

warming climate. Therefore, it is very likely that future drought in the Blue River Basin will be more severe and intense compared to the 1950–1999 period, especially for the second half of the twenty-first century.

4.3.2 Floods

4.3.2.1 Flood Definition

Floods are an overflow or inundation that comes from a river or other body of water and often threaten lives and properties. Floods can happen when the flow capacities of river channels, streams, or coastal areas are exceeded due to heavy, intense, or continuous rainfall or when the absorptive capacity of the soils is exceeded. This causes water in a river channel to overflow its banks onto adjoining land area, known as a floodplain. Floodplains are highly prone to flood. In addition, places like coasts and deltas, areas immediately below dams, inland shorelines, and alluvial fans are also vulnerable to floods [36].

Flooding creates a significant threat to life and property. Communities located near riverbanks or coastal zones are most vulnerable to flood, but many historic cities and towns have been built in such areas because of the conveniences of transportation, commerce, and recreation. Occasionally, flood hazard and flood risk are used interchangeably. Generally, flooding creates images of destruction and catastrophe. However, floods also play an important role in the functioning of ecosystems, analogous to wildfire. Floodwaters sometimes are beneficial because they increase soil fertility by depositing nutrients from upstream and recharging ground water. Many aquatic species depend on normal flooding to wash debris into the water, which they subsequently use for shelter and food. Periodic floods also transport eroded soil and other materials that are essential for delta areas and coastal marshes to persist over time and sustain the wetland ecosystems. Freshwater floods in particular play an important role in maintaining ecosystems in river corridors and are a key factor in maintaining floodplain biodiversity [4]. Many ecosystems develop with regular flooding as one of the key components to their existence. Similarly, it has been found that flooding was the key to the well-being and prosperity of ancient communities along the Nile, the Tigris Euphrates, the Yellow, and the Ganges Rivers.

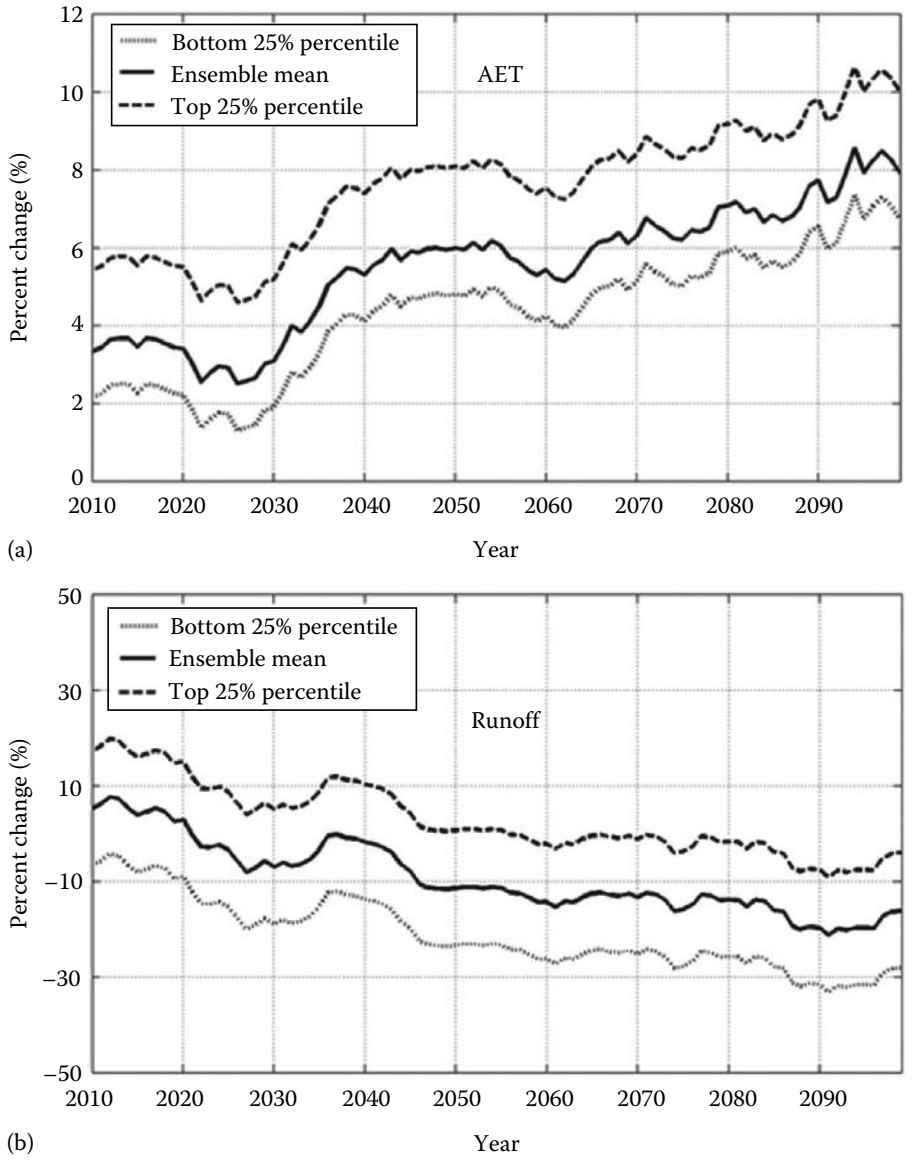

FIGURE 4.11 (a) 10-year moving average of projected AET change as percentage of 1950–1999 mean. (b) 10-year moving average of projected runoff change as percentage of 1950–1999 mean. (From Liu, L. et al., *Water Resour. Manage.*, 26(10), 2761, 2012.)

4.3.2.2 Global Flood Database

A number of flood databases exist. The Emergency Disasters Database (EM-DAT) is a publicly accessible international database with information on natural and technological disasters including floods. The United Nations Office for the Coordination of Humanitarian Affairs (OCHA) through its portal ReliefWeb provides current disaster information on humanitarian emergencies and disasters relief works (ReliefWeb, http://www.reliefweb.int/). It does not intend to provide a comprehensive database of disaster events but can serve as a valuable resource to verify current events and obtain additional disaster details for rapid response and humanitarian support. The Dartmouth Flood Observatory (DFO) compiled the

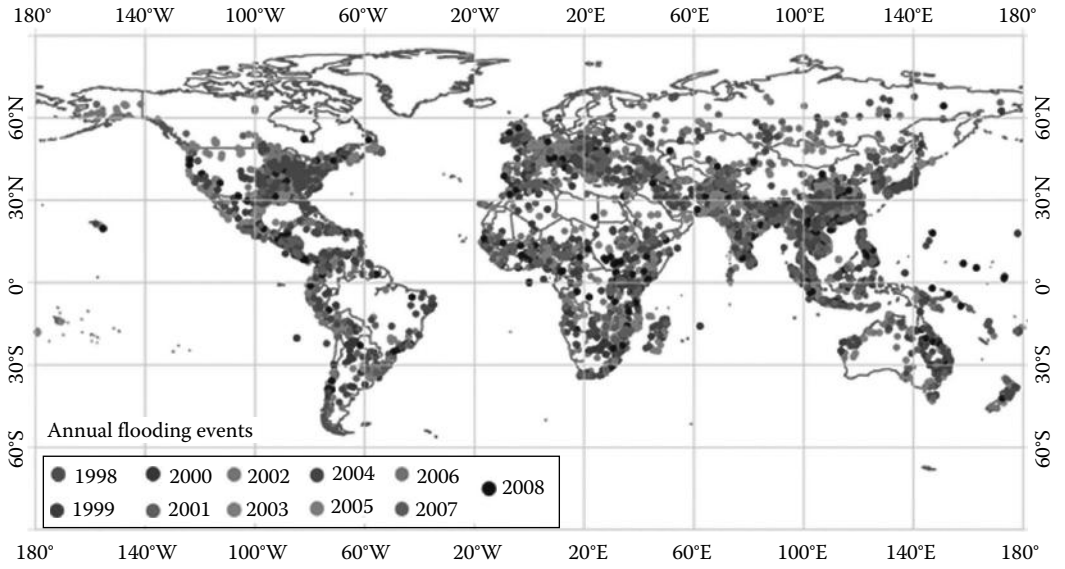

FIGURE 4.12 Global flooding events 1998–2008. (From Adhikari, P. et al., *Nat. Hazards*, 55, 405, 2010.)

Global Archive of Large Flood Events, which covers events from 1985 to the present in a simple Microsoft Excel spreadsheet format (DFO, http://www.dartmouth.edu/~floods/). This database also includes links to high-quality maps for selected events since 2006, showing the entire affected region. The database is exclusively dedicated for flood hazards. It has about 3400 events recorded for 1985–2008 (Figure 4.12). The global flood inventory (GFI) has compiled global flood data for 1998–2008 from publicly available online resources, irrespective of their scale of impacts so as to have a comprehensive flood database. It has geo-referenced locations of all the flooding events for a period of 11 years. The GFI has record of approximately 2700 events in total for the period, which is about 250 per annum [1]. The discrepancies in the database discussed previously are mainly due to the inherited biases as a result of the scope of the database. The entry criteria, sources of data, and definition of specific hazard terms differ among the databases.

It is obvious that analyses based on different database entries might result in contradicting conclusions. It is important to note that some databases are impact-based, making them potentially biased toward reporting more events in populated areas, whereas others are compiled from publicly available resources. The latter are prone to undermine the number of actual flooding events because only those floods that have significant effects on the community, local government, or national government are recorded. Therefore, a very careful interpretation of flood data is necessary before reaching conclusions regarding the number of events or their impacts to the people and the community. Based on the GFI, it is found that the United States has recorded the highest number of flood events followed by China and India for the period 1998–2008. In addition, the GFI shows a seasonal pattern in flooding, with the number of events increasing in May and peaking in the months of July to August (Figure 4.13). In terms of the spatial distribution of flooding, GFI is also able to show the percentage of reported flooding events for each region, sorted by year. Asia and Africa continuously recorded the highest percentage of events throughout the globe, followed by Southeast Asia, Central America, and the Caribbean [1].

4.3.2.3 Future Flood Risk under Changing Climate

Of the major flood-inducing factors, climate change and the alternation of extreme weather, which directly impact water availability and variability, play the primary role in water-related issues and are of more concern worldwide. According to the Intergovernmental Panel on Climate Change (IPCC) report [14], the global temperature rise has increased the evaporation rate and moisture-holding capacity in

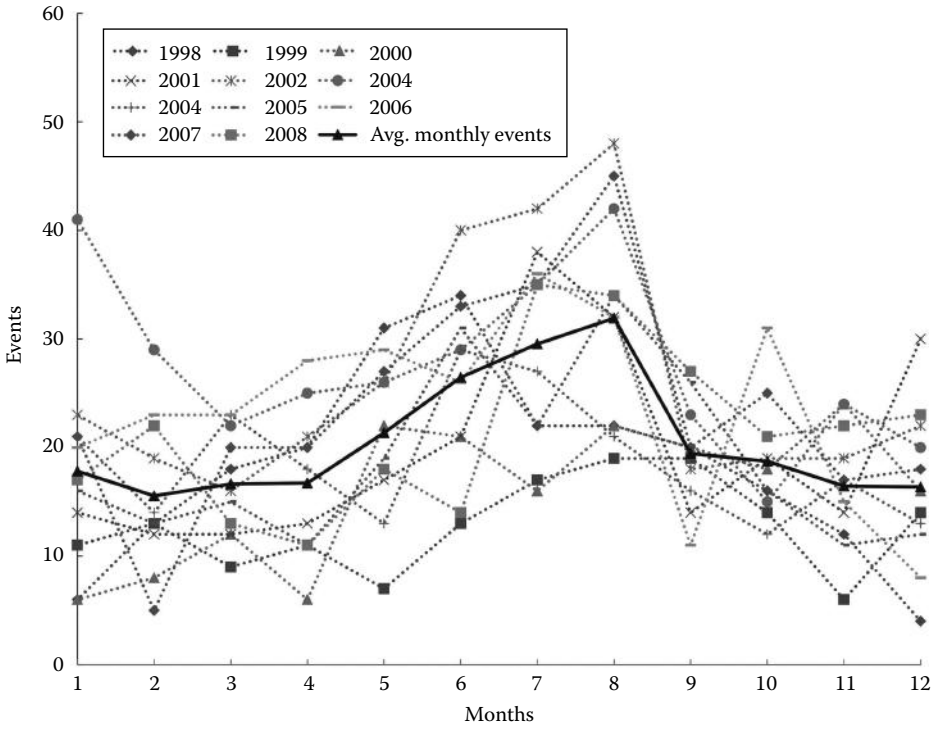

FIGURE 4.13 Seasonal variation flood events for each year of the GFI record. (From Adhikari, P. et al., *Nat. Hazards*, 55, 405, 2010.)

the atmosphere, which in turn alters the hydrological cycle, changes precipitation, and thus streamflow and soil water content. Due to continuous accumulation of atmospheric greenhouse gases and aerosols, climate predictions consistently warn of increases in global temperature for the current century, which could potentially result in more severe extreme weather impact such as floods. Although the predicted climate change impacts remain significant uncertainty, many regions across different continents are projected toward worse flooding expectation.

The upper Mississippi River Basin and the lower Missouri River Basin (LoMRB) would be more likely to have intensified precipitation and flooding. With a regional climate simulation model, Pan et al. [28] predicted a warming hole in 2040s over the central United States and suggested that 21% more precipitation and 51% more streamflow would happen in the upper Mississippi River Basin. A similar increase of streamflow for this region was also presented by Jha et al. [15] through integrated simulations combining an RCM and the soil and water assessment tool (SWAT). Stone et al. [37] compared simulations with a coarse-resolution GCM and a fine-resolution RCM and found, although the two types of resolution models disagree on the magnitude of the effects, water yield would increase in the LoMRB. Qiao [32] used the newly available North American Regional Climate Change Assessment Program (NARCCAP) climate data to study the hydrological variability for the region, and his study showed that, following the seasonal variability of precipitation, various water fluxes would increase and expected precipitation tends to increase in intensity triggering faster water accumulation to form floods. In other regions like the United Kingdom, Osborn et al. [26] showed an upward trend in rainfall and related increase in magnitude for high streamflow since 1960s. By using statistical rainfall models and high-resolution RCMs, a 20% increase in peak flow over the next 50 years was suggested in the United Kingdom [35]. Some studies [8,9] indicated longer wet and dry durations in Iran under different statistical downscaling of GCM projections. However, uncertainties arising from different sources in climate change studies are

significant, imposing grand challenging on climate change adaptation, mitigation, and preparation with manageable solutions [7,10,34].

4.4 Summary and Conclusions

This chapter reviews the climate change and its impacts on regional hydrological systems such as drought and flood effects under different climate scenarios. The case studies in the southern United States demonstrate the seasonal and spatial variability of hydrological response to the changing climate. General conclusions related to the cases are as follows:

- The projected temperature for the twenty-first century is highly dependent on the emission scenario with the A2 scenario exhibiting the highest relative increases in temperature, particularly for the summer and fall months.
- The SCIPP region has diverse precipitation change pattern in both time and spatial scales. The projected precipitations under B1 scenario have more increase compared to that of A1B and A2. Increases are projected for the northeastern portions of SCIPP, while the southwestern portions of SCIPP have a drier future, with A2 producing 0.35% less rainfall during 2050–2099 than the historical mean. Winter is projected to be wetter in the northeast and drier in the south. The spring season, which provides a substantial portion of the annual precipitation total to the region, is projected to be drier.
- The study for the Blue River Basin in Oklahoma shows that the three types of drought indices (SPI, PDSI, and SRI) can capture the major droughts documented in history. The projections by the drought indices under the business-as-usual A1B scenario suggest that more drought events might occur in the second half of the twenty-first century. This could be caused by a descending trend of precipitation predicted by the GCM GISS-ER and a significant increasing trend of ET under a warming after 2010.
- Common consensus that climate change would cause wet region wetter and dry region drier. The warming climate increase water vapor contents in atmosphere, which could result in more intense rainfall and potentially more flood events for the wet regions such as central and eastern United States, western Europe, and Southeast Asia.

References

1. Adhikari, P., Hong, Y., Douglas, K.R., Kirschbaum, D.B., Gourley, J., Adler, R., and Brakenridge, G.R., 2010, A digitized global flood inventory (1998–2008): Compilations and preliminary results. *Natural Hazards* 55: 405–422.
2. Alley, W.M., 1984, The Palmer Drought Severity Index: Limitations and assumptions. *Journal of Climate and Applied Meteorology* 23(7): 1100–1109.
3. Arndt, D.S., 2002, The Oklahoma Drought of 2001–2002. Oklahoma Event Summary. Oklahoma Climatological Survey. Published September 24, 2002.
4. Associated Program on Flood Management (APFM), 2006, Environmental aspects of integrated flood management, APFM Technical Document No. 3, Flood Management Policy Series, World Meteorological Organization. pp. 174–178.
5. Box, G.E.P. and Cox, D.R., 1964, An analysis of transformations. *Journal of the Royal Statistical Society B* 26: 211–234.
6. Edwards, D.C. and McKee, T.B., 1997, Characteristics of 20th century drought in the United States at multiple timescales. Climatology Report Number 97-2. Colorado State University, Fort Collins, CO.
7. Eslamian, S.S., Gilroy, K.L., and McCuen, R.H., 2011, Climate change detection and modeling in hydrology, Chapter 5. In *Climate Change Research and Technology for Adaptation and Mitigation*. J. Blanco and H. Kheradmand, eds., InTech, Rijeka, Croatia, pp. 87–100.

8. Fakhri, M., Farzaneh, M.R., Eslamian, S., and Khordadi, M.J., 2012, Uncertainty assessment of downscaled rainfall: Impact of climate change on the probability of flood. *Journal of Flood Engineering* 3(1): 19–28.
9. Fakhri, M., Farzaneh, M.R., Eslamian, S.S., and Khordadi, M.J., 2012, Confidence interval assessment to estimate dry and wet spells under climate change in ShahrekordStation, Iran, ASCE. *Journal of Hydrologic Engineering* 18(7): 911–918.
10. Farzaneh, M.R., Eslamian, S.S., Samadi, Z., and Akbarpour, A., 2012, An appropriate general circulation model (GCM) to investigate climate change impact. *International Journal of Hydrology Science and Technology* 2(1): 34–47.
11. Giorgi, F., Christensen, J., Hulme, M., von Storch, H., Whetton, P., Jones, R., Mearns, L., Fu, C., Arritt, R., Bates, B., Benestad, R., Boer, G., Buishand, A., Castro, M., Chen, D., Cramer, W., Crane, R., Crossly, J., Dehn, M., Dethloff, K., Dippner, J., Emori, S., Francisco, R., Fyfe, J., Gerstengarbe, F., Gutowski, W., Gyalistras, D., Hanssen-Bauer, I., Hantel, M., Hassell, D., Heimann, D., Jack, C., Jacobeit, J., Kato, H., Katz, R., Kauker, F., Knutson, T., Lal, M., Landsea, C., Laprise, R., Leung, L., Lynch, A., May, W., McGregor, J., Miller, N., Murphy, J., Ribalaygua, J., Rinke, A., Rummukainen, M., Semazzi, F., Walsh, K., Werner, P., Widmann, M., Wilby, R., Wild, M. and Xue, Y., 2001, Regional Climate Information-Evaluation and Projections, Climate Change 2001: The Scientific Basis. Contribution of Working Group to the Third Assessment Report of the Intergouvernmental Panel on Climate Change [Houghton, J.T. et al. (eds)]. Cambridge University Press, p. 881.
12. Guttman, N.B., 1998, Comparing the palmer drought index and the standardized precipitation index. *Journal of the American Water Resources Association* 34(1): 113–121.
13. Hellmuth, M.E., Moorhead, A., Thomson, M.C., and Williams, J., eds., 2007, *Climate Risk Management in Africa: Learning from Practice*. International Research Institute for Climate and Society (IRI), Columbia University, New York.
14. IPCC, 2007, Climate Change 2007: Synthesis Report. *Contribution of Working Groups I, II and III to the Fourth Assessment Report of the Intergovernmental Panel on Climate Change*. Core Writing Team, R.K. Pachauri and A. Reisinger, Geneva, Switzerland, 104pp.
15. Jha, M., Pan, Z., Takle, E.S., and Gu, R., 2004, Impacts of climate change on streamflow in the Upper Mississippi River Basin: A regional climate model perspective. *Journal of Geophysical Research* 109(D9): D09105.
16. Karl, T.R., Melillo, J.M., and Peterson, T.C., 2009, *Global Climate Change Impacts in the United States*. Cambridge University Press, New York.
17. Karl, T.R. and Trenberth, K.E., 2003, Modern global climate change. *Science* 302: 1719–1723.
18. Landsberg, H.E., 1982, Climatic aspects of drought. *Bulletin of the American Meteorological Society* 63: 593–596.
19. Liu, L., Hong, Y., Hocker, J., Shafer, M., Carter, L., Gourley, J., Bednarczyk, C., Yong, B., and Adhikari, P., 2012, Analyzing projected changes and trends of temperature and precipitation in the southern USA from 16 downscaled global climate models. *Theoretical and Applied Climatology* 109: 345–360. doi: 10.1007/s00704-011-0567-9.
20. Liu, L., Hong, Y., Hocker, J.E., Shafer, M.A., and Bednarczyk, C.N., 2012, Hydro-climatological drought analyses and projection using meteorological and hydrological drought indices: A case study in Blue River Basin, Oklahoma. *Water Resources Management* 26(10): 2761–2779. doi: 10.1007/S11269-012-0044-y.
21. Lo, J.C.-F., Yang, Z.-L., and Pielke, R.A., Sr., 2008, Assessment of three dynamical climate downscaling methods using the Weather Research and Forecasting (WRF) model. *Journal of Geophysical Research* 113(D9), D09112; Maurer, E.P., Brekke, L., Pruitt, T., and Duffy, P.B., 2007, Fine-resolution climate projections enhance regional climate change impact studies. *Eos Transactions American Geophysical Union* 88(47): 504.
22. McKee, T.B., Doesken, N.J., and Kleist, J., 1993, The relationship of drought frequency and duration to time scales. Preprints. *Proceedings of the 8th Conference on Applied Climatology*, Anaheim, CA, p. 6.

23. Hayes, M., 2006, Comparison of major drought indices: introduction, National Drought Mitigation Center. Access date: 9/23/2013. http://drought.unl.edu/Planning/Monitoring/ComparisonofIndicesIntro.aspx.
24. Nelson, G.C. and Institute, I.F.P.R., 2009, *Climate Change: Impact on Agriculture and Costs of Adaptation*. International Food Policy Research Institute, Washington, DC.
25. Osborn, T.J., Hulme, M., Jones, P.D., and Basnett, T.A., 2000, Observed trends in the daily intensity of United Kingdom precipitation. *International Journal of Climatology* 20: 347–364.
26. Palmer, W.C., 1965, Meteorological drought. Research Paper No. 45. U.S. Weather Bureau, Washington, DC.
27. Pan, Z., Arritt, R.W., Takle, E.S., Gutowski, W.J., Anderson, C.J., and Segal, M., 2004, Altered hydrologic feedback in a warming climate introduces a " warming hole". *Geophysical Research Letters* 31(17): L17109, 17101–17104.
28. Patz, J.A., Campbell-Lendrum, D., Holloway, T., and Foley, J.A., 2005, Impact of regional climate change on human health. *Nature* 438(7066): 310–317.
29. Phillips, N.A., 1956, The general circulation of the atmosphere: A numerical experiment. *Quarterly Journal of the Royal Meteorological Society* 82(352): 123–164.
30. Piao, S., Ciais, P., Huang, Y., Shen, Z., Peng, S., Li, J., Zhou, L. et al., 2010, The impacts of climate change on water resources and agriculture in China. *Nature* 467(7311): 43–51.
31. Qiao, L., 2012, Climate change impacts on the hydrological system of the Lower Missouri River Basin. PhD thesis, Saint Louis University, St. Louis, MO, 105pp.
32. Rajabi, A., Sedghi, H., Eslamian, S.S., and Musavi, H., 2010, Comparison of Lars-WG and SDSM downscaling models in Kermanshah (Iran). *Ecology, Environment and Conservation* 16(4): 1–7.
33. Rathore, M.S., 2005, *State Level Analysis of Drought Policies and Impacts in Rajasthan, India*. International Water Management Institute, Colombo, Sri Lanka.
34. Reynard, N., Crooks, S., Wilby, R.L., and Kay, A., 2004, Climate change and flood frequency in the UK, *Proceedings of the Defra National Conference*, University of York, York, U.K.
35. Smith, K. and Petley, D.N., 2008, *Environmental Hazards, Assessing Risk and Reducing Disaster*, 5th ed. Routledge, London, U.K.
36. Stone, M.C., Hotchkiss, R.H., and Mearns, L.O., 2003, Water yield responses to high and low spatial resolution climate change scenarios in the Missouri River Basin. *Geophysical Research Letters* 30(4), 1186.
37. Wilby, R.L. and Wigley, T.M.L., 1997, Downscaling general circulation model output: A review of methods and limitations. *Progress in Physical Geography* 21(4): 530–548.
38. Wilhite, D.A. and Glantz, M.H., 1985, Understanding: the drought phenomenon: The role of definitions. *Water International* 10(3): 111–120.
39. Vasiliades, L., Loukas, A., and Liberis, N., 2011, A water balance derived drought index for Pinios River basin, Greece. *Water Resources Management* 25(4): 1087–1101.

5

Climate Change and Hydrologic Modeling

Rezaul K. Chowdhury
United Arab Emirates University

Saeid Eslamian
Isfahan University of Technology

AUTHORS

Rezaul K. Chowdhury has been recognized for his innovative and industry-oriented research activities in water resources management. He is an assistant professor of Water Resources at the United Arab Emirates University. Previously, Dr. Chowdhury was a research fellow of Water Engineering at the University of South Australia and was a scientist of Integrated Water Systems Planning and Management at the Commonwealth Scientific and Industrial Research Organization (CSIRO) in Australia. Dr. Chowdhury started his career as a lecturer of Civil and Environmental at the ShahJalal University of Science and Technology in Bangladesh. He has published more than 40 research articles in leading international journals and conferences. He is an active reviewer of several high impact factor journals. Dr. Chowdhury is involved in supervising postgraduate research students.

Saeid Eslamian received his PhD from the University of New South Wales, Australia, with Professor David Pilgrim. He was a visiting professor in Princeton University, Princeton, NJ, and ETH Zurich, Switzerland. He is currently an associate professor of Hydrology in Isfahan University of Technology. He is the founder and chief editor of *Journal of Flood Engineering* and *International Journal of Hydrology Science and Technology*. He has published more than 200 publications mainly in statistical and environmental hydrology and hydrometeorology.

PREFACE

Climate changes due to increased concentration of greenhouse gases (GHGs) have obvious effects on the regional landscape systems, water cycles, and particularly catchment hydrology. Changes in hydrologic cycle will affect almost every aspects of socioeconomic life, from agricultural production and energy consumption to flood control, municipal and industrial water supply, conservation of natural resources, and ecohydrological management. Some parts of the world may experience increases in precipitation and some may experience decreases. The timing and frequencies of storm events may alter in some areas, and some regions may experience the increased potential for evapotranspiration. Because of close interactions between water, socioeconomic activities, and cultural practices, climate change impact on regional water availability is considered one of the most important impacts of future climatic changes on society. Therefore, a reliable estimation of stream flows is required for water resources planning, design, and management in a changing climate. A fundamental problem is the fact that the spatial and time scales of global climate models (GCMs) and hydrological models are extensively different. As a result, downscaling of climate model outputs is essential. Assessment of uncertainty in the simulated outputs of climate downscaling technique and in the predicted stream flows is also necessary before their application to climate change impact studies. Selection of climate predictors in downscaling studies and selection of an appropriate hydrologic model are critical issues in climate change impact studies. This chapter provides the details of climate models, their downscaling techniques, selection of appropriate hydrologic models, and uncertainty analysis, and delineates recommendations for climate change impact studies on water resources.

5.1 Introduction

Increased concentration of GHGs in the atmosphere is scientifically acknowledged to alter the radiative balance in the stratosphere, causing increases in temperature. This phenomenon is generally known as global warming. Alternation of radiative balance and increased temperature in the atmosphere will change precipitation patterns and other climatic variables [39]. Because of close interactions between water, socioeconomic activities, and cultural practices, climate change impact on regional water availability is considered one of the most important impacts on the society of future climatic changes. Global climate change is considered to impose significant alterations on regional landscape systems, regional water cycles, and particularly catchment hydrology [55]. Changes in hydrological regimes will affect almost every aspect of socioeconomic life, from agricultural production and energy consumption to flood control, municipal and industrial water supply, conservation of natural resources, and ecohydrological management. Anticipated increased flow volumes will require larger reservoir spillways and drainage waterways for flood management, whereas decreased flow volumes will need increased capacity of flood storage for the security of water supply schemes. Therefore, it is necessary to understand how climate change and climate variability could affect regional water availability.

Reliable estimation of stream flows from catchments is required for water resources planning, design, and management. Stream flow characteristics such as high-flow, medium-flow, and low-flow conditions; flow duration relationships; and spatial and temporal variability of stream flows and their probability distributions are important decision parameters for water and agricultural management. Numerous hydrologic models are being used by hydrologists and water professionals for the reliable estimation of stream flows from catchments. General techniques of stream flow estimation involve

- Calibration and validation of an appropriate hydrologic model using observed rainfall, runoff, and catchment data

- Generation of runoff data using calibrated model parameters by feeding long-term rainfall, evaporation, and temperature data into the hydrologic model
- Analyses of simulated stream flow time series

Quality assurance in hydrologic modeling through a series of principles and actions in model development, implementation, and applications is collectively known as the best-practice modeling [11]. In the changing climate, calibrated hydrologic models are used for stream flow projections into future by using projected rainfall and other climatic variables. GCMs and regional climate models (RCMs) are used for the projection of climatic variables. Because of their coarse spatial resolution, downscaling of projection is required. Also, large uncertainties are observed in the projected magnitude, variability, and patterns of climatic variables. Therefore, it is generally considered that reliable projection of rainfall and other water-related variables is not possible using the most sophisticated GCMs/RCMs though these data are the best available source of climate projections used as driving inputs into calibrated hydrological models, transferring future climate projections into hydrological quantities at the landscape or catchment scale. The interactions between climate and hydrological modeling in water resources decision systems are shown in Figure 5.1.

For the development of climate change adaptation strategies, several climate models' outcomes covering a wide spectrum of possible projections are currently available. The uncertainties involved in these climate projections as well as in subsequent hydrologic modeling tools are currently a limiting factor for the formulation of a meaningful adaptation strategy into practice [47,57]. Hydrologic models used for operational purposes (such as flood forecasting or reservoir management) are generally exposed to more or less sophisticated calibration and validation procedures [10,24,62]. While reliable results can be obtained from these models under current flow conditions, they are not appropriate enough in a changing climate. This is because of nonstationary properties of climate projections [20]. Moreover, high data demand, wide parameter space, complex process descriptions, and complicated handling are also considered as difficulties to these models. Selection of appropriate hydrologic model is a critical decision for climate change impact assessment on water resources. The level of complexity of a given hydrological model may limit its application in some cases, characterized by spatial and temporal resolutions and by predominant hydrological decision variable (e.g., stream flow at the catchment outlets or soil moisture

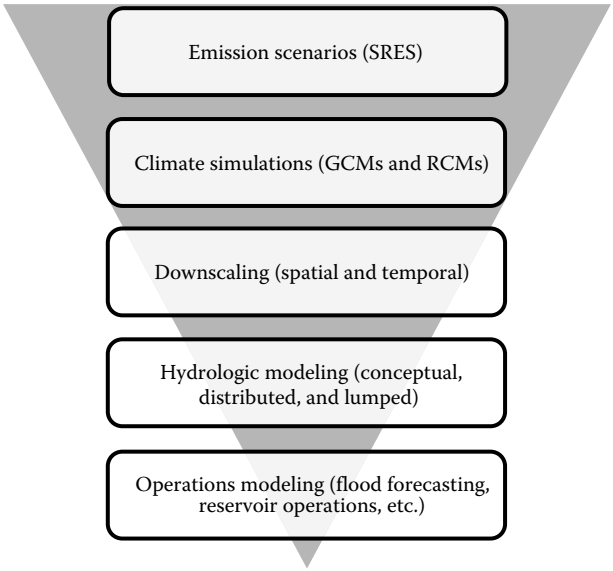

FIGURE 5.1 Interactions between climate and hydrologic modeling in water resources management.

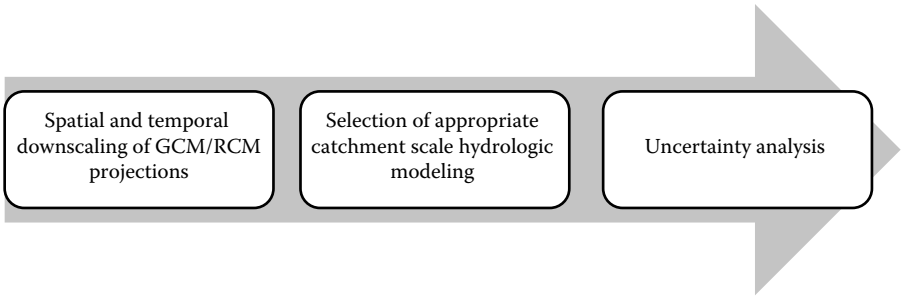

FIGURE 5.2 Three major challenges in climate change impact analyses on water resources.

content at field scale). Currently, there are three major challenges in climate change impact analyses on water resources, which are provided in Figure 5.2. The arrow sign in Figure 5.2 indicates propagation of uncertainty.

5.2 Emission Scenario

Climate changes due to increased concentration of GHGs have obvious effects on the hydrological cycle. Some parts of the world may experience increases in precipitation and some may experience decreases. The timing of rainy seasons may change in some areas, and some areas may experience the increased potential for evapotranspiration. Therefore, projection of GHGs is the first concern for any climate change impact assessment, as indicated in Figure 5.1. The IPCC Special Report on Emissions Scenarios (SRES) [42] describes different possible GHG projections, and their different scenarios are being widely used in climate change impact studies. The starting point for each projection of future emissions was considered as a "storyline," describing the way world population, economics, and political structure may evolve over the next few decades. The storylines were grouped into four scenario families, which led to the construction of six SRES scenarios.

The *A1* scenario family considers rapid economic growth with global population, which will peak in mid-century and decline thereafter, and the rapid introduction of new and more efficient technologies. Major underlying themes are convergence among regions, capacity building, and increased cultural and social interactions, with a substantial reduction in regional differences in per capita income. On the basis of sources of energy for this rapid growth, there are three variants in A1 scenario family: *A1FI* (fossil intensive), *A1T* (nonfossil fuels), and *A1B* (balance across all sources). The *B1* scenario family considers same population growth as *A1*, but development takes a much more environmentally sustainable pathway with global-scale cooperation and regulation. Clean and efficient technologies are considered to be introduced. The *A2* scenario family is based on heterogeneous market-led world and less rapid economic growth but more population growth than A1. Economic growth is considered to be regionally oriented, which will promote regionally diverse income growth and technological development. The *B2* scenario considers population increases at a lower rate than A2 but at a higher rate than A1 and B1. The development is considered to follow environmentally, economically, and socially sustainable regionally oriented pathways.

Figure 5.3 shows the carbon emissions associated with each scenario, together with global temperature change relative to the temperature in 1990 [43]. For a given GCM, there is little difference in the pattern of runoff changes from different emissions scenarios [3]. By 2080s, magnitudes of runoff vary; highest and lowest changes are because of the A1FI and B1 scenarios, respectively. Two extreme emissions scenarios are the A1FI (highest carbon emissions) and B1 (lowest carbon emissions) scenarios. In some cases, A1B scenario is used as an average scenario in climate change impact assessment.

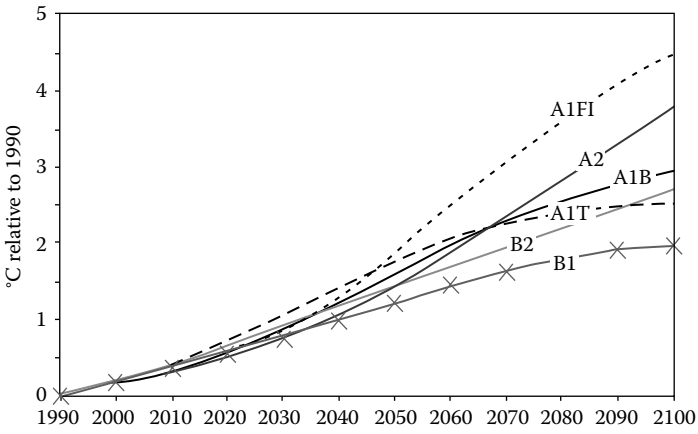

FIGURE 5.3 Carbon emissions together with temperature change associated with each SRES emission scenario. (From IPCC [Intergovernmental Panel on Climate Change], Climate change 2001: The science of climate change, Report of working group 1 to the third assessment report of IPCC, Cambridge University Press, Cambridge, U.K., 2001.)

5.3 Global Climate Models

The GCMs were initially developed to simulate average synoptic-scale (104–106 km^2 spatial scale) atmospheric circulation patterns for specified external forcing conditions [60]. Since then, several atmospheric GCMs were conceptually designed to simulate average large-scale atmospheric circulation (e.g., [38]). For about last two decades, GCMs are applied to simulate climatic sensitivity to increased concentration of GHGs to predict future climatic change. GCMs are developed based on well-established physical principles and are demonstrated to reproduce observed features of recent climate and past climate changes [61]. It is acknowledged that the atmosphere–ocean general circulation models (AOGCMs) provide credible quantitative estimates of climate scenarios at the continental and larger scales. Confidence levels are high for some climate variables (e.g., temperature) and low for some others (e.g., precipitation). GCMs are still under ongoing improvements to their resolution, computational methods and parameterizations, and additional processes. Figure 5.4 shows their development progress since mid-1970s. Different modeling components were developed first separately and then coupled with the comprehensive climate models [43]. As development progresses, performances of climate models are improved. Some reported improvements on AOGCMs are [61]

- Most AOGCMs are no longer using flux adjustments, and thereby uncertainty associated with the use of flux adjustments has been decreased.
- Improvement has been occurred in the simulation of important modes of climate variability, for example, the El Niño–Southern Oscillation.
- Ability to simulate extreme events (hot and cold spells) has improved, but the frequency and the amount of precipitation in extreme events are underestimated.
- Improvement has occurred in the simulation of extratropical cyclones.

The GCM data can be obtained from the Program for Climate Model Diagnosis and Intercomparison (PCMDI) (http://www-pcmdi.llnl.gov). These GCMs were used in the production of the IPCC fourth assessment report (2007). The GCMs are BCCR-BCM 2.0 (Bjerknes Centre for Climate Research, Norway); BCC-CM1 (Beijing Climate Center, China); CCCMA-CGCM 3.1(T47) and CCCMA-CGCM 3.1(T63) (Canadian Centre for Climate Modeling and Analysis, Canada); CNRM-CM3 (Météo-France/Centre National de Recherches Météorologiques, France); CSIRO-Mk3.0 and CSIRO-Mk3.5

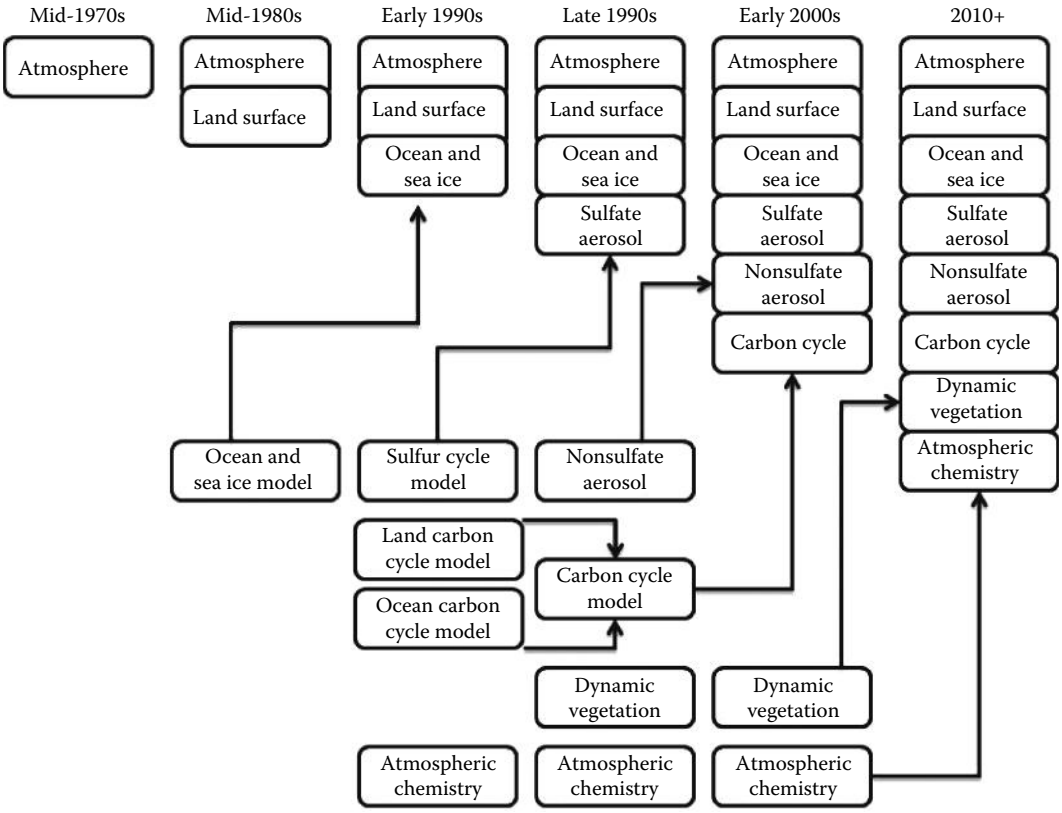

FIGURE 5.4 Development of climate models (different components are first developed separately and then coupled into comprehensive climate models). (From IPCC [Intergovernmental Panel on Climate Change], Climate change 2001: The science of climate change, Report of working group 1 to the third assessment report of IPCC, Cambridge University Press, Cambridge, U.K., 2001.)

(Commonwealth Scientific and Industrial Research Organisation, Australia); Max Planck-ECHAM5/MPI-OM (Max Planck Institute for Meteorology, Germany); MIUB/KMA-ECHO-G (Meteorological Institute of the University of Bonn, Germany, and Meteorological Research Institute of the Korea Meteorological Administration, Korea); LASG/IAP-FGOALS-G1.0 (National Key Laboratory of Numerical Modeling for Atmospheric Sciences and Geophysical Fluid Dynamics (LASG)/Institute of Atmospheric Physics, China); GFDL-CM2.0 and GFDL-CM2.1 (National Oceanic and Atmospheric Administration/Geophysical Fluid Dynamics Laboratory, United States); GISS-AOM, GISS-EH, and GISS-ER (National Aeronautics and Space Administration/Goddard Institute for Space Studies, United States); INM-CM3.0 (Institute for Numerical Mathematics, Russia); IPSL-CM4 (Institut Pierre Simon Laplace, France); CCR-MIROC-H and CCR-MIROC-M (Center for Climate System Research, University of Tokyo and National Institute for Environmental Studies and Frontier Research Center for Global Change, Japan); MRI-CGCM2.3.2 (Meteorological Research Institute, Japan); UKMO-HadCM3 and UKMO-HadGEM1 (Hadley Centre for Climate Prediction and Research/Met Office, United Kingdom); and NCAR-CCSM3 and NCAR-PCM1 (National Center for Atmospheric Research, United States). Details of these GCMs are available at the PCMDI website. For example, details on the CSIRO-Mk3.5 are available at http://www-pcmdi.llnl.gov/ipcc/model_documentation/CSIRO-Mk3.5.htm

Researchers throughout the world analyzed climate impact assessment in various conditions. Some used a selected GCM and emission scenario, and some others used various conditions due to differences in GCMs and emission scenarios. A key point in the review of these GCMs is the lack of a fixed trend

in projection outputs due to different GCMs, and even in some studies, different models had completely reversed the results [26]. A performance comparison study between four GCMs (CSIRO, CGCM2, CCSR, and HadCM3) in the projection of rainfalls at Shahrekord climate station was conducted in Iran, and it was observed that HadCM3 performed well [26]. Though GCMs operate on large spatial scale and their temporal resolution corresponds to monthly averages at best, the reality is that GCMs are the only available tool for detailed modeling of future climate evolution. The ensembles of models represent a new resource for studying the range of plausible climate responses to a given forcing. Such ensembles can be generated either by collecting results from a range of models from different modeling centers (known as *multimodel ensembles*) or by generating multiple model versions within a particular model structure, by varying internal model parameters within plausible ranges (known as *perturbed physics ensembles*).

5.4 Hydrologic Models

Hydrological models are required to understand catchment hydrological responses to climate change. Nowadays, several hydrologic models are available. These can be categorized based on their modeling approaches as (a) simple empirical methods (e.g., curve number); (b) large-scale energy–water balance equations (e.g., Budyko curve); (c) conceptual rainfall–runoff models (e.g., Sacramento); (d) landscape daily hydrological models (e.g., WaterDyn model); and (e) fully distributed hydrologic models (e.g., Système Hydrologique Européen—SHE model, TOPOG model). Selection of an appropriate model is generally based on an understanding of the objectives and characteristics of the system to be modeled. According to [79], the following factors should be considered prior to the selection of a hydrologic model:

- Modeling objectives—hydrological forecasting, climate change impact assessment, human influences on hydrological regime, etc.
- System to be modeled—small catchment, large river basin, river reach or reservoir, etc.
- Hydrological elements to be modeled—floods, daily discharges, monthly or annual discharge, water quality, etc.
- Climate and physiographic characteristics of the system to be modeled—catchment in arid, semi-arid, or tropical conditions, etc.
- Data availability in terms of type (sub-daily, daily, monthly, seasonal, or annual data), length (length in years for model calibration and validation), and quality (percentage of missing data, homogeneity, consistency of data), etc.
- Model simplicity—number of model parameters to be optimized and ease of model application for practical purposes.

Selection of appropriate hydrologic model is a critical issue in climate change impact assessment. The choice of a hydrologic model for a particular case study depends on many factors: purpose of study, model, and data availability have been the dominant ones [59,82]. For the regional scale assessment of water resources management, *monthly rainfall–runoff models* are generally useful for identifying hydrologic consequences of changes in temperature, precipitation, and other climatic variables [5,34,56,80,81]. For detailed assessments of surface flow, *conceptual lumped-parameter models* are useful. One of the more frequently used models in this group is the Sacramento Soil Moisture Accounting Model [13]. This model has been used by many researchers in the United States for studying the impact of climate change [22,35,53,58,66]. The HBV model [9] is widely used in Nordic countries as a tool to assess the climate change effects [65,73]. The SIMHYD model (a conceptual lumped model) has been used in several Australian studies on climate change impact assessment. Several other models having a similar structure to the earlier-mentioned two models, but with different process conceptualizations, have been used to assess the effect of climate change on many regions of the globe [51]. Effects of variations of climatic parameters (precipitation, temperature, relative humidity, wind speed, and sunshine

duration) on potential evapotranspiration estimation in arid and semiarid Iran regions were previously investigated using the Penman–Monteith Potential Evapotranspiration model [25]. Temperature and relative humidity were found most sensitive in the model. For simulation of spatial patterns of hydrologic response within a basin, *process-based distributed-parameter models* are required [8,64,69]. For estimating changes in the average annual runoff for different climate change scenarios, simple empirical and regression models were used previously. Examples include those models used in the United States [63] and in the United Kingdom [4].

The models that are complex in terms of structure and input requirements could be expected to provide adequate results for a wide range of applications; the more simple models that have smaller range of applications can give adequate results at greatly reduced cost, provided that the objective function is suitable. The distinction between simple and physically based distributed-parameter models is not only one of lesser or greater sophistication, but also intimately bound up with the purposes for which such models are to be used. Therefore, choosing a suitable model is equivalent to distinguishing the situation between when simple models can be used and when complex model must be used.

5.5 Spatial and Temporal Resolutions of Climate Models

GCMs are the primary tools to study and estimate the nature of climate change. Based on the physical laws for the atmospheric composition and behavior, they attempt to provide a calculable model of the earth's climate system, including internal and external forcing as well as feedback in the climate system. The size of the climate system (atmosphere, oceans, land) and the time range of climate experiments (several decades to thousands of years) place a significant constraint on the design of the GCMs. This leads to spatial and temporal coarseness. Hydrological models are frequently concerned with small subcatchment (even hillslope)-scale processes, occurring on spatial scales much smaller than those resolved in GCMs. While GCMs predict the climate using a three-dimensional grid that generally has a horizontal resolution within 250–600 km, 10–20 vertical layers in the atmosphere, and sometime 30 layers in the oceans. Operation on such large spatial scales prevents explicit modeling of such climate-modifying local geographic factors as topography and land/water distribution or vegetation type. Moreover, although GCMs use short time steps, commonly 10–30 min, cascading through 10 or more atmospheric layers and then providing information for a range of climatic variables (e.g., temperature, rainfall), most verifications of the models have been based on long-term mean simulations for base cases similar to present conditions, and the most reliable temporal scale to date remains seasonal [67].

Hydrological models, on the other hand, typically use a time step of one day (even subdaily), commonly cascading rainfall through two to three soil layers to produce output on hydrological variables. The ability of GCMs to predict spatial and temporal distributions of climatic variables declines from global to regional to local catchment scales, and from annual to monthly to daily amounts. However, the hydrological importance of climate predictions increases from global to local scales and from annual to daily amounts. Therefore, downscaling of the GCM climate projection is necessary. Two types of spatial downscaling are generally adopted, dynamic and statistical downscaling methods.

5.5.1 Dynamic Downscaling

The goal of dynamic downscaling, that is, to extract local-scale information from large-scale GCM data, is achieved by nesting a high-resolution limited area climate model to a GCM or by developing RCMs. It fits output from GCMs into regional meteorological models. Rather than using equations to bring global-scale projections down to a regional level, dynamic downscaling involves using numerical meteorological modeling to reflect how global patterns affect local weather conditions. RCMs can attain horizontal resolution on the order of tens of kilometers, over selected areas of interest. They have been

applied with relative success to numerous regions [30–33,44,45]. Compared with GCMs, the resolution of these RCMs is much closer to that of landscape-scale hydrologic models and makes coupling of RCMs and hydrologic models potentially suitable for evaluating the effects of hydrologic systems. The main shortcomings of the dynamic modeling include that RCMs still require considerable computing resources and are as expensive to run as a global GCM, that these models still cannot meet the needs of spatially explicit models of ecosystems or hydrological systems, and that there will remain the need to downscale the results from such models to individual sites or localities for impact studies [76]. The amount of computations involved in dynamical downscaling makes it significantly difficult to produce decades-long simulations with different GCMs or multiple emissions scenarios. As a result, most research aimed at producing regional projections involves statistical downscaling.

5.5.2 Statistical Downscaling

Statistical downscaling establishes a connection between large-scale climate variables (predictors) and local-scale or station-scale climate variables (predictands) through a statistical model [49,74]. Instead of maintaining a dynamic climate model at the higher resolution of a region, this approach applies the information from GCMs to the region by using a series of equations to relate variations in global climate to variations in local climate. Regression models (linear regression and artificial neural network [ANN]), weather typing schemes (analogue method, fuzzy classification, and Monte Carlo method), and weather generators (Markov chain, stochastic model, and spell length model) are the main types of statistical downscaling methods [78]. The underlying assumption of statistical downscaling methods is that the predictor–predictand relation is assumed to be stationary and will remain the same in future with changed climate. Selection of domain for predictors and predictands is one of the challenges in statistical downscaling methods. According to [23], a general equation for the downscaling methods can be expressed as $R = F(X)$, where R represents the local climate variable known as predictand, X is the set of GCM-produced large-scale climate variable (predictor), and F is the stochastic or deterministic function that establishes relation between the predictand (R) and predictors (X). Predictands are the local climate variables such as rainfall and temperature. Predictors are the large-scale circulation and atmospheric variables that have direct influence on the local climate variables. Sea-level pressure, relative humidity, air temperature, specific humidity, geopotential height, sea surface temperature, etc., are the most commonly used predictors in spatial downscaling. Statistical downscaling requires less computational effort than dynamic downscaling. Therefore, the method is more popular. Advantages of statistical modeling include the opportunity to use "ensemble" GCM results. An ensemble of numerous GCMs is better than a single model, since ensemble values, which average results from many models, tend to match overall observations better than the results from any individual model. With statistical downscaling, the ensemble average for a region can be applied using equations that relate the larger-scale observations to regional climate parameters.

Statistical downscaling methods can be classified based on either the use of techniques or the choice of predictor variables. The commonly used predictor sets can include both atmospheric variables such as geopotential heights and/or surface patterns such as sea-level pressure [6,46,77]. The method often involves "bias correction," the correction of factors inaccurately modeled by GCMs. If GCMs overestimate precipitation, for instance, on the order of a millimeter a day, or an inch a month, a downscaling method can correct that bias before modeling future rainfall. It plays an important role in translating global climate change scenarios to more regional impact assessment [74,76].

The nonhomogeneous hidden Markov model has been used in spatial downscaling of rainfalls [7,16,17,29,41]. The statistical downscaling model has also been widely used in downscaling climate projections [18,40,48,75]. The generalized linear model-based downscaling models are also popular in downscaling climate projections [1,15,21,83–85].

5.5.3 Predictor Selection in Statistical Downscaling

The National Centre for Environmental Prediction (NCEP/NCAR) reanalysis dataset (available at http://www.esrl.noaa.gov/psd) is widely used in downscaling works. The dataset represents the state of earth's atmosphere, which is the combined result of the numerical weather prediction model and observed data from 1948 to present. These data are continuously updated and generated on a $2.5° \times 2.5°$ spatial resolution grid covering the whole globe. Sea-level pressure, specific humidity, relative humidity, geopotential height, surface temperatures, etc., are the few variables available in the NCEP/NCAR reanalysis data. Reanalysis data are significantly used in several climate change studies all over the world [16,19,27–29,70–72].

Selection of climate predictors in downscaling studies is an important issue. Choice of predictors could vary from region to region depending on the characteristics of the large-scale atmospheric circulation [2]. Poor selection of predictors will produce poor simulation results. In stochastic methods, predictor selection generally depends on the correlation coefficient between the atmospheric predictors and local (station) rainfalls. The Spearman correlation coefficient was used by [27]. The ANN was used in previous studies [14]. In some cases, application of atmospheric circulation predictors in spatial downscaling is not sufficient enough for better prediction of rainfall. Some other predictors used in downscaling techniques are specific humidity, total rainfall, mean temperature, relative humidity, etc. [19,27,29,52,72].

Selection of predictor domain varies in terms of spatial extent and obviously a critical parameter for the quality of downscaling performance. The large-scale circulation pattern of the single GCM grid covered by the selected point stations may not capture the local processes; these may result from the effects of neighboring location. In some cases, maximum correlation between precipitation and mean sea-level pressure occurred away from the grid box [50]. Considering and averaging the values of predictors from several GCM grid points around the downscaling point location have the advantage of capturing spatial variation of predictor variables [28]. Few studies have recommended considering continental scale predictor domain while using slowly varying atmospheric circulation variables [78]. In [36], they selected 26 exogenous atmospheric variables from the grid point that cover the climate station and from the surrounding eight grid points; suitable predictors were selected from each grid by partial correlation method at the 5% significance level. Finally, four grids were selected out of nine on the basis of variance, and the predictors from each selected four grids were further selected based on the partial correlation.

5.6 Uncertainty Analysis

Assessment of uncertainty in the simulated outputs of downscaling technique is necessary before their application to climate change impact studies [12]. Sources of uncertainty in downscaling are the concept of the downscaling method, data used in the model such as predictor and its domain, GCMs outputs, and predictant database. Uncertainty in downscaled precipitation was found very high, and the simulated precipitation variable was found inappropriate to reproduce the extreme events accurately in many studies [48,68]. Because of climate variability and uncertainty in computational methods, it is generally recommended to express the climate change projection in terms of probability. Probabilistic projections of climate change based on the multimodel ensemble are comparatively a new idea in uncertainty quantification. The Bayesian method has also been applied to multimodel ensembles to quantify the uncertainty for climate changes [37,54].

Uncertainties are also involved in hydrologic modeling. Sources of uncertainty in hydrologic modeling are

- Model input data including parameters, constants, and driving data set
- Model assumptions and simplifications
- The science underlying the model
- Stochastic uncertainty also known as variability
- Code uncertainty such as numerical approximations and undetected software bugs

Major uncertainties come from input data sets. Uncertainties are associated with measured rainfall data, potential evapotranspiration data, and stream flow data (associated with rating curve development). Spatial variability of rainfall in a catchment is generally ignored in lumped hydrologic models. A single raingauge in a catchment may not be representative of all rainfall events in a catchment. Nowadays, spatial gridded climate data are available, and uncertainties may be associated in the interpolation of raingauge data. Models are simplified representation of actual hydrological processes in a catchment. The assumptions and simplifications considered in a model are sources of uncertainty and are known as structural uncertainty in hydrologic modeling. Sensitivity analysis is also a commonly applied tool for quantitative estimation of parameter uncertainty in hydrologic modeling.

5.7 Summary and Conclusions

A review of studies identified four major limitations in assessing climate change impacts on hydrology. These are related to (a) capacity of GCMs, (b) limitation of downscaling techniques, (c) selection of hydrological modeling tools, and (d) uncertainty involved in both climate and hydrologic modeling. A fundamental problem is the fact that the spatial and time scales of GCMs and hydrological models are extensively different. Major challenges in climate and hydrologic modeling and in climate change impact assessment on water resources are provided in the following text. Recommendations are also provided. A general recommendation is to adopt collaborative studies between climate modelers and hydrologists in this field, which could be potentially useful to minimize this limitation.

Improved methodologies are required for the development of climate change scenarios. Removing uncertainties in current scenarios is dependent on improvements in both GCMs and downscaling techniques. Scenarios must provide the spatial and temporal resolutions required by assessment models, and they must incorporate the simulated changes in mean and variability of climate variables. Collection of reliable data at a range of spatial and temporal scales is critical to improving our understanding of hydrologic processes and in testing and validating the downscaling techniques and hydrological models that are being developed. Utilization and comparison of the existing databases from GCM and RCM are required for the estimation of their respective intrinsic variability and their contribution to the overall uncertainty related to climate change projections. An appropriate approach for the assessment of uncertainty in climate prediction scenario as well as in downscaling procedures and hydrological impact modeling is also significantly important. Uncertainty measures could provide an estimate of confidence limits on model results and would be of value in the application of these results in risk and policy analyses. Development and application of ensembles of hydrologic models can be followed for an improved understanding of the impact of the complexity of process descriptions on simulated hydrological variables and predictive power, evaluation of intrinsic variability, and uncertainties in hydrologic modeling.

It is recommended that improvement is required in the scaling procedures for the utilization of RCM results in regional watershed management and evaluation and improvement of transferability of existing bias correction methods between station measurements and RCM outputs for future climate conditions. The challenge in hydrological modeling is to determine required hydrological model complexity needed for climate change impact studies with specific consideration of the available data for parameterization and of the required accuracy to develop specific adaptation options. After the projection of climate, downscaled and incorporated into a calibrated hydrologic model, it is necessary to develop, compare, and evaluate watershed adaptation options and climate change impacts (to address water quantity and quality challenges, changing land-use patterns, dam management, irrigation needs, etc.).

References

1. Abaurrea, J. and Asín, J. 2005. Forecasting local daily precipitation patterns in a climate change scenario, *Climate Research* 28:183–197.

2. Anandhi, A., Srinivas, V., Kumar, D.N., and Nanjundiah, R.S. 2009. Role of predictors in downscaling surface temperature to river basin in India for IPCC SRES scenarios using support vector machine, *International Journal of Climatology* 29(4):583–603.
3. Arnell, N.W. 2003. Effects of IPCC SRES emissions scenarios on river runoff: A global perspective, *Hydrology and Earth System Sciences* 7(5):619–641.
4. Arnell, N.W. and Reynard, N.S. 1989. Estimating the impacts of climatic change on river flows: Some examples from Britain, *Proceedings of the Conference on Climate and Water*, Helsinki, Finland, Vol. 1, pp. 413–425.
5. Arnell, N.W. 1992. Factors controlling the effects of climate change on river flow regimes in a humid temperate environment, *Journal of Hydrology* 132:321–342.
6. Bardossy, A. and Plate, E.J. 1992. Space-time model for daily rainfall using atmospheric circulation patterns, *Water Resources Research* 28:1247–1260.
7. Bates, B.C., Charles, S.P., and Hughes, J.P. 1998. Stochastic downscaling of numerical climate model simulations, *Environmental Modelling and Software* 13(3):325–331.
8. Bathurst, J.C. and O'Connell, P.E. 1992. Future of distributed parameter modeling: The Systeme Hydrologique Europeen, *Hydrological Processes* 6:265–277.
9. Bergström, S. 1976. Development and Application of a Conceptual Runoff Model for Scandinavian Catchments, Department of Water Resources Engineering, Lund Institute of Technology/Bulletin Series A-52, Swedish Meteorological and Hydrological Institute, Norrköping, Sweden.
10. Beven, K.J. and Freer, J. 2001. Equifinality, data assimilation and uncertainty estimation in mechanistic modeling of complex environmental systems using the GLUE methodology, *Journal of Hydrology* 249:11–29.
11. Black, D., Wallbrink, P., Jordan, P., Waters, D., Carroll, C., and Blackmore, J. 2011. *Guidelines for Water Management Modeling: Towards Best-Practice Model Application*, eWater Cooperative Research Centre, Canberra, Australian Capital Territory, Australia, ISBN 978-1-921543-46-3.
12. Blöschl, G. and Montanari, A. 2010. Climate change impacts—Throwing the dice? *Hydrological Processes* 24(3):374–381.
13. Burnash, R.J.C., Ferral, R.L., and McGuire, R.A. 1973. *A Generalized Streamflow Simulation System, Conceptual Modeling for Digital Computer*, U.S. Department of Commerce, National Weather Service and State of California, Department of Water Resources, Sacramento, CA.
14. Cavazos, T. and Hewitson, B.C. 2005. Performance of NCEP-NCAR reanalysis variables in statistical downscaling of daily precipitation, *Climate Research* 28(16):95–107.
15. Chandler, R.E. and Wheater, H.S. 2002. Analysis of rainfall variability using generalized linear models: A case study from the west of Ireland, *Water Resources Research* 38(10):1192, doi: 10.1029/2001WR000906.
16. Charles, S.P., Bates, B.C., Smith, I.N., and Hughes, J.P. 2004. Statistical downscaling of daily precipitation from observed and modelled atmospheric fields, *Hydrological Processes* 18(8):1373–1394.
17. Charles, S.P., Bates, B.C., Whetton, P.H., and Hughes, J.P. 1999. Validation of downscaling models for changed climate conditions: Case study of southwestern Australia, *Climate Research* 12(1):1–14.
18. Chen, H., Xu, C.Y., and Guo, S. 2012. Comparison and evaluation of multiple GCMs, statistical downscaling and hydrological models in the study of climate change impacts on runoff, *Journal of Hydrology* 434:36–45.
19. Chiew, F.H.S., Kirono, D.G.C., Kent, D.M., Frost, A.J., Charles, S.P., Timbal, B., Nguyen, K.C., and Fu, G. 2010. Comparison of runoff modelled using rainfall from different downscaling methods for historical and future climates, *Journal of Hydrology* 387(1):10–23.
20. Chowdhury, R.K. and Beecham, S. 2011. Stormwater drainage design under climate change and variability conditions, *Proceedings of 34th IAHR World Water Congress and Hydrology and Water Resources Symposium* Brisbane, Queensland, Australia, June 2011.
21. Coe, R. and Stern, R.D. 1982. Fitting models to daily rainfall data, *Journal of Applied Meteorology* 21(7):1024–1031.

22. Cooley, K.R. 1990. Effects of CO_2-induced climatic changes on snowpack and streamflow, *Hydrological Sciences Journal* 35:511–522.
23. Dibike, Y.B. and Coulibaly, P. 2005. Hydrologic impact of climate change in the Saguenay watershed: Comparison of downscaling methods and hydrologic models, *Journal of Hydrology* 307(1–4):145–163.
24. Duan, Q.Y., Gupta, V.K., and Sorooshian, S. 1993. Shuffled complex evolution approach for effective and efficient for global minimization, *Journal of Optimization Theory and Applications* 76:501–521.
25. Eslamian, S., Khordadi, M.J., and Abedi-Koupai, J. 2011. Effects of variations in climatic parameters on evapotranspiration in the arid and semi-arid regions, *Global and Planetary Change* 78:188–194.
26. Farzaneh, M.R., Eslamian, S., Samadi, S.Z., and Akbarpour, A. 2012. An appropriate general circulation model (GCM) to investigate climate change impact, *International Journal of Hydrology Science and Technology* 2(1):34–47.
27. Fealy, R. and Sweeney, J. 2007. Statistical downscaling of precipitation for a selection of sites in Ireland employing a generalised linear modelling approach, *International Journal of Climatology* 27(15):2083–2094.
28. Frost, A.J. 2007. *Australian Application of a Statistical Downscaling Technique for Multi-Site Daily Rainfall: GLIMCLIM*, Modeling and Simulation Society of Australia and New Zealand, Waikato, New Zealand, pp. 553–559.
29. Frost, A.J., Charles, S.P., Timbal, B., Chiew, F.H.S., Mehrotra, R., Nguyen, K.C., Chandler, R.E., McGregor, J.L., Fu, G., Kirono, D.G.C., Fernandez, E., and Kent, D.M. 2011. A comparison of multi-site daily rainfall downscaling techniques under Australian conditions, *Journal of Hydrology* 408(1):1–18.
30. Giorgi, F. and Mearns, L.O. 1991. Approaches to the simulation of regional climate change: A review, *Reviews of Geophysics* 29:191–216.
31. Giorgi, F., Brodeur, C.S., and Bates, G.T. 1994. Regional climate change scenarios over the United States produced with a nested regional climate model, *Journal of Climate* 7:375–399.
32. Giorgi, F., Marinucci, M.R., and Visconti, G. 1990. Use of a limited-area model nested in a general circulation model for regional climate simulation over Europe, *Journal of Geophysical Research* 95:18413–18431.
33. Giorgi, F. 1990. Simulation of regional climate using a limited area model nested in a general circulation model, *Journal of Climate* 3:941–963.
34. Gleick, P.H. 1986. Methods for evaluating the regional hydrologic impacts of global climatic changes, *Journal of Hydrology* 88:97–116.
35. Gleick, P.H. 1987. The development and testing of a water balance model for climate impact assessment: Modelling the Sacramento basin, *Water Resources Research* 23:1049–1061.
36. Guo, J., Chen, H., Xu, C.Y., Guo, S., and Jiali, G. 2012. Prediction of variability of precipitation in the Yangtze River Basin under the climate change conditions based on automated statistical downscaling, *Stochastic Environmental Research and Risk Assessment* 26(2):157–176.
37. Hashmi, M.Z., Shamseldin, A.Y., and Melville, B.W. 2012. Statistically downscaled probabilistic multi-model ensemble projections of precipitation change in a watershed, *Hydrological Processes* 27:1021–1032.
38. Holton, J.R. 1992. *An Introduction to Dynamic Meteorology*, 3rd ed., Academic Press, San Diego, CA.
39. Houghton, J.T., Jenkins, G.J., and Ephraums, J.J. (eds.) 1990. *Climate Change. The IPCC Assessment*, Cambridge University Press, Cambridge, U.K.
40. Huang, J., Zhang, J., Zhang, Z., Xu, C.Y., Wang, B., and Yao, J. 2011. Estimation of future precipitation change in the Yangtze River basin by using statistical downscaling method, *Stochastic Environmental Research and Risk Assessment* 25(6):781–792.
41. Hughes, J.P., Guttorp, P., and Charles, S.P. 1999. A non-homogeneous hidden Markov model for precipitation occurrence, *Journal of the Royal Statistical Society: Series C (Applied Statistics)* 48(1):15–30.
42. IPCC (Intergovernmental Panel on Climate Change). 2000. Special report on emissions scenarios, Cambridge University Press, Cambridge, U.K.

43. IPCC (Intergovernmental Panel on Climate Change). 2001. Climate change 2001: The science of climate change, Report of working group 1 to the third assessment report of IPCC, Cambridge University Press, Cambridge, U.K.
44. Jenkins, G.S. and Barron, E.J. 1997. General circulation model and coupled regional climate model simulations over the eastern United States: GENESIS and RegCM2 simulations, *Global and Planetary Change* 15:3–32.
45. Jones, R.G., Murphy, J.M., and Noguer, M. 1995. Simulation of climate change over Europe using a nested regional climate model. I. Assessment of control climate, including sensitivity to location of lateral boundaries, *Quarterly Journal of Royal Meteorological Society* 121:1413–1450.
46. Karl, T.R., Wang, W.C., Schlesinger, M.E., Knight, R.W., and Portman, D. 1990. A method of relating general circulation model simulated climate to observed local climate. Part I: Seasonal statistics, *Journal of Climate* 3:1053–1079.
47. Khalili, M., Leconte, R., and Brissette, F. 2006. On the use of multi-site generated meteorological input data for realistic hydrological modeling in the context of climate change impact studies, *IEEE EIC Climate Change Technology Conference*, Ottawa, Ontario, Canada, Vol. 10(12), pp. 1–7.
48. Khan, M.S., Coulibaly, P., and Dibike, Y. 2006. Uncertainty analysis of statistical downscaling methods, *Journal of Hydrology* 319(1):357–382.
49. Kim, J.W., Chang, J.T., Baker, N.L., Wilks, D.S., and Gates, W.L.P. 1984. The statistical problem of climate inversion: Determination of the relationship between local and large-scale climate, *Monthly Weather Review* 112:2069–2077.
50. Lambert, S.J. and Boer, G.J. 2001. CMIP1 evaluation and intercomparison of coupled climate models, *Climate Dynamics* 17(2):83–106.
51. Leavesley, G.H. 1994. Modelling the effects of climate change on water resources—A review, *Climatic Change* 28:159–177.
52. Leith, N. 2005. Using generalised linear models to simulate daily rainfall under scenarios of climate change, Technical Report, University College London, London, U.K., available at http://www.ucl.ac.uk/statistics/research/Rainfall/FD2113_rpt2.pdf, accessed on 18 May 2012.
53. Lettenmaier, D.P. and Gan, T.Y. 1990. Hydrologic sensitivity of the Sacramento-San Joaquin River Basin, California, to global warming, *Water Resources Research* 26:69–86.
54. Lopez, A., Tebaldi, C., New, M., Stainforth, D., Allen, M., and Kettleborough, J. 2006. Two approaches to quantifying uncertainty in global temperature changes, *Journal of Climate* 19:4785–4796.
55. Ludwig, R., Mauser, W., Niemeyer, S., Colgan, A., Stolz, R., Escher-Vetter, H., Kuhn, M. et al. 2003. Webbased modelling of energy, water and matter fluxes to support decision making in mesoscale catchments—The integrative perspective of GLOWA-Danube, *Physics and Chemistry of the Earth* 28:621–634.
56. Mimikou, M., Kouvopoulos, Y., Cavadias, G., and Vayianos, N. 1991. Regional hydrological effects of climate change, *Journal of Hydrology* 123:119–146.
57. Minville, M., Brissette, F., and Leconte, R. 2008. Uncertainty of the impact of climate change on the hydrology of a northern watershed, *Journal of Hydrology* 358(1–2):70–83.
58. Nash, L. and Gleick, P. 1991. Sensitivity of streamflow in the Colorado basin to climatic changes, *Journal of Hydrology* 125:119–146.
59. Ng, H.Y.F. and Marsalek, J. 1992. Sensitivity of streamflow simulation to changes in climatic inputs, *Nordic Hydrology* 23:257–272.
60. Phillips, N.A. 1956. The general circulation of atmosphere: A numerical experiment, *Quarterly Journal of the Royal Meteorological Society* 82:123–164.
61. Randall, D.A., Wood, R.A., Bony, S., Colman, R., Fichefet, T., Fyfe, J., Kattsov, V. et al. 2007. Climate models and their evaluation, in: *Climate Change 2007: The Physical Science Basis*, Contribution of Working Group I to the Fourth Assessment Report of the Intergovernmental Panel on Climate Change, S. Solomon, D. Qin, M. Manning, Z. Chen, M. Marquis, K.B. Averyt, M. Tignor, and H.L. Miller (eds.), Cambridge University Press, Cambridge, U.K. pp. 591–662.

62. Refsgaard, J.C. 2001. Towards a formal approach to calibration and validation of models using spatial data, in: *Spatial Patterns in Catchment Hydrology: Observations and Modeling*, R. Grayson and G. Blöschl (eds.), Cambridge University Press, New York, pp. 329–354.
63. Revelle, R.R. and Waggoner, P.E. 1983. Effect of carbon dioxide-induced climatic change on water supplies in the western United States, in: *Changing Climate*, National Academy of Sciences, National Academy Press, Washington, DC.
64. Running, S.W. and Nemani, R.R. 1991. Regional hydrologic carbon balance responses of forests resulting from potential climate change, *Climatic Change* 19:349–368.
65. Saelthun, N.R. 1996. The 'Nordic' HBV model—Version developed for the project climate change and energy production, NVE Publication No. 7, Norwegian Water Resources and Energy Administration, Oslo, Norway.
66. Schaake, J.C. 1990. From climate to flow, in: *Climatic Change and U.S. Water Resources*, P.E. Waggoner (ed.), John Wiley & Sons, New York, pp. 177–206.
67. Schulze, R.E. 1997. Impacts of global climate change in a hydrologically vulnerable region: Challenges to South African hydrologists, *Progress in Physical Geography* 21:113.
68. Souvignet, M. and Heinrich, J. 2011. Statistical downscaling in the arid central Andes: Uncertainty analysis of multi-model simulated temperature and precipitation, *Theoretical and Applied Climatology* 106:229–244.
69. Thomsen, R. 1990. Effect of climate variability and change in groundwater in Europe, *Nordic Hydrology* 21:185–194.
70. Timbal, B. 2004. Southwest Australia past and future rainfall trends, *Climate Research* 26(3):233–249.
71. Timbal, B. and Jones, D.A. 2008. Future projections of winter rainfall in southeast Australia using a statistical downscaling technique, *Climatic Change* 86(1):165–187.
72. Timbal, B., Fernandez, E., and Li, Z. 2009. Generalization of a statistical downscaling model to provide local climate change projections for Australia, *Environmental Modelling and Software* 24(3):341–358.
73. Vehviläinen, B. and Lohvansuu, J. 1991. The effects of climate change on discharges and snow cover in Finland, *Hydrological Sciences Journal* 36:109–121.
74. von Storch, H., Zorita, E., and Cubash, U. 1993. Downscaling of global climate change estimates to regional scales: An application to Iberian rainfall in wintertime, *Journal of Climate* 6:1161–1171.
75. Wetterhall, F., Halldin, S., and Xu, C.Y. 2007. Seasonality properties of four statistical-downscaling methods in central Sweden, *Theoretical and Applied Climatology* 87(1):123–137.
76. Wilby, R.L. and Wigley, T.M.L. 1997. Downscaling general circulation model output: A review of methods and limitations, *Progress in Physical Geography* 21:530–548.
77. Wilby, R.L. 1995. Simulation of precipitation by weather pattern and frontal analysis, *Journal of Hydrology* 173:91–109.
78. Wilby, R., Charles, S., Zorita, E., Timbal, B., Whetton, P., and Mearns, L. 2004. Guidelines for use of climate scenarios developed from statistical downscaling methods, available from the DDC of IPCC TGCIA (http://www.narccap.ucar.edu/doc/tgica-guidance-2004.pdf). Accessed on 9 May 2012.
79. WMO (World Meteorological Organization). 2008. *Guide to Hydrological Practices, Vol. I: Hydrology-from Measurement to Hydrological Information*, WMO No. 168, 6th ed., World Meteorological Organization, Geneva, Switzerland, ISBN 978-92-63-10168-6.
80. Xu, C.Y. and Singh, V.P. 1998. A review on monthly water balance models for water resources investigations, *Water Resources Management* 12:31–50.
81. Xu, C.Y. and Halldin, S. 1997. The effect of climate change on river flow and snow cover in the NOPEX area simulated by a simple water balance model, *Nordic Hydrology* 28:273–282.
82. Xu, C.Y. 1999. From GCMs to river flow: A review of downscaling methods and hydrologic modeling approaches, *Progress in Physical Geography* 23(2):229–249.

83. Yan, Z., Bate, S., Chandler, R.E., Isham, V., and Wheater, H. 2002. An analysis of daily maximum wind speed in northwestern Europe using generalized linear models, *Journal of Climate* 15(15):2073–2088.
84. Yan, Z., Bate, S., Chandler, R., Isham, V., and Wheater, H. 2006. Changes in extreme wind speeds in NW Europe simulated by generalized linear models, *Theoretical and Applied Climatology* 83(1):121–137.
85. Yang, C., Chandler, R.E., Isham, V.S., and Wheater, H.S. 2005. Spatial-temporal rainfall simulation using generalized linear models, *Water Resources Research* 41:W11415, doi: 10.1029/2004WR003739.

6

Climate Change and Urban Water Systems

Ole Mark
DHI

Birgit Paludan
Hydraulics Greve
Solrød Water Utility

AUTHORS

Ole Mark is a worldwide, well-recognized, high-level expert in the modeling of all urban waters, that is, urban hydrology, storm water management, flood forecasting, climate change, and real-time decision support. He has written for more than 100 publications, and he is one of the main authors of the *Climate Cook Book,* which gives recipes for consistent analyses of climate change impacts on urban drainage and sewer systems with a focus on flood risk management. Ole Mark is a visiting professor at Exeter University and ICEWE, Myanmar. He has experience in research and teaching from Asian Institute of Technology, Thailand; IHE Delft, the Netherlands; and other European universities, and has conducted many training courses. At DHI, he is the head of Research & Development and has the responsibility for managing DHI's research contract, Performance Contract with the Ministry of Science.

Birgit Paludan is a pioneer in climate change adaptation in Denmark. For the last 10 years, Birgit has developed and implemented several climate change adaptation plans, including methods for prioritizing

adaptation and flood risk management. Birgit Paludan is one of the main authors of the *Climate Cook Book*, which gives recipes for consistent analyses of climate change impacts on urban drainage. She works for the official Danish government "Task Force on Climate Change Adaptation," which brings knowledge and inspiration to the Danish municipalities on adaptation to the changing climate.

PREFACE

Future climate changes may have significant impacts on the urban water cycle. One of the main threats is increased flooding in the cities, which may be very extensive and cause serious flood damages. This chapter outlines how climate changes may have an impact on the urban drainage systems. The impact on the urban drainage system is discussed in terms of changes in performance of the urban water systems. The main principles for analyses of the impact on the urban water systems are presented, and strategies for adapting urban water systems to climate change are outlined and discussed. Finally, adaptation principles and measures are outlined for the urban water systems.

6.1 Introduction

It is in the interest of society to provide protection for the population and to protect infrastructure against flooding and to protect the aquatic environments against polluted sewer overflows in a timely and cost-efficient way [8]. Climate changes (precipitation, increase in temperature, and mean sea level) may have significant impact on the urban water cycle [5]. Hence, it is important to identify and quantify the impact on the main urban water systems, such as sewer systems, wastewater treatment plants, storm water overflows, and combined sewer overflows, to receiving waters, such as rivers, lakes, estuaries, and the sea.

In the past, infrastructure, located facilities, buildings, or new urban areas were designed based on the assumption that the future was like the past. Parameters were measured in nature, and they were used as design basis, for infrastructure, which should last for many years (100+) into the future. Today, we are in a situation where we know that it is insufficient to make decisions that have consequences far into the future—without taking into account the changes that we already know will happen in nature due to climate change. A climate adaptation strategy for urban water systems shall therefore be based on the protection of the society on the basis of the knowledge we already have and optimize both existing and new infrastructure based on the knowledge we currently have about the movements of climate change.

6.2 Principles for Adapting Urban Water Systems to Climate Change

The aim of any climate adaptation strategy should be to adapt the society in such a way that

1. The negative social consequences of climate change (including economic, technical, social, and other effects) are minimized to a deliberately chosen level.
2. It creates confidence among the public that the consequences of climate change are identified and taken care of, and that the citizens' views are heard.
3. Climate change adaptation of the society becomes an integral part of the planning processes.

These three objectives must be achieved through *conscious and informed choices* about how we deal with the consequences of climate change. This requires that we have mapped both the possible effects of

climate change and the associated uncertainty estimates. The *conscious and informed choice* on climate adaptation consists of the following equal elements:

1. Assessments of the effects of climate change and thus the usefulness of climate change adaptation measures are subject to uncertainties. In many situations, the uncertainties will not have a significant impact on the choice of adaptation measures. In this context, it is important to acknowledge uncertainties and use that knowledge constructively, that is, the uncertainties must not be used as an excuse for inaction. On the other hand, you cannot select solutions without considering the actions that are most robust against uncertainties. This is an important point that a deliberate and documented choice (which may also be doing nothing) must be taken—on the basis of acknowledged uncertainties.
2. Climate changes may have serious impact on the living conditions for many urban citizens in connection with the urban water systems, for example, in terms of increased urban flooding or a reduced supply safety for water. Hence, stakeholder involvement is essential—both in relation to the identification of problems and when it comes to assessment of possible climate change adaptation measures. This provides the opportunity to involve all relevant information, and, not least, to achieve a high degree of common understanding of the problems and character. Many climate change adaptations require change in the behavior of citizens and changing social environment, which in turn requires stakeholder involvement to anchor the decisions and behavior of citizens.
3. Selection of climate change adaptation measures can have effects that are positive for one sector and negative for another, and perhaps unknown to a third sector. Cross-sectoral assessments are therefore essential to ensure socially sound and sustainable solutions. Cross-sectoral solutions often require priorities between different sectoral interests (stakeholders), which illustrate the need for stakeholder involvement.
4. Handling of the extreme events due to climate change. Extreme events will always occur with strength, which exceed the design; even after design, the standards have been updated based on the latest climate change projections. This is, for example, the case for urban flooding. The deliberate handling of extreme events consists of an analysis of the respective risk and damage from extreme weather events held up against the costs to manage them. The results of such analyses provide valuable information for the long-term social planning, for example, when drawing up plans for where new infrastructure can be built and where existing infrastructure and buildings have to be moved from vulnerable areas. In addition to these primary economic analyses, there is also a need for outlining the general ethical and social consequences as the society can accept. Finally, the need comes for emergency plans for handling of extreme weather situations as they arise in the future and even today.

The core of the *conscious and informed choice* is that all relevant effects of climate change are identified (including uncertainties) and that there is a documented choice of what you choose to do. A *conscious and informed choice* of action can also be not to do anything today, but to wait for more knowledge in the field. Climate change adaptation (as described in points 1–4) must be integrated into the existing plan—planning processes in the society. That is, climate adaptation of society becomes part of the continuous and rolling planning cycle within the authorities.

6.3 Predicted Climate Changes Impacting on the Urban Setting

6.3.1 Future Rain

In some places, the annual rainfall may change so that the easily available water resources for the drinking water supply will be reduced. The rainy season may shift a bit, and more extreme rain events may occur, especially during summer. In the Northern Hemisphere, in many places it is expected that the precipitation will increase during winter; the accumulated precipitation will be reduced during summer,

but with an increase in single extreme rainfall events. The question now is which changes will occur and how quickly will they come? Both issues are important to consider in planning the augmentations of urban drainage systems. In some cases, there is a need for estimates of future precipitation in the rest of this century, while in other cases, estimates of future precipitation is required only for a shorter time scale. It depends entirely on the actual problem, not least on the potential to continuously adapt the system to increased load and to judge the consequences of an error estimate in the prediction. New local rainfall for design can today be estimated using statistical downscaling from GCM climate projections. At present, the local design storm found by means of this method indicated an increase in design rainfall in the order of 20%–50% for urban drainage and storm water systems.

6.3.2 Future Water Levels in Marine Waters

In the future, the mean sea level along the coasts will increase due to climate-related sea-level rise. In addition to this, new climate-related extreme wind fields will lead to backwater or increases in nearshore sea level. Changing sea levels will affect the hydraulic conditions at the outlets in drainage systems, which discharge by gravity to the sea [4]. More specifically, the mean sea level is expected to rise by 50–150 cm during this century. Additionally, a wind contribution by storm surges of up to 50–100 cm in maximum sea water levels is expected around the world. The impact of the new extreme water levels for coastal municipalities should be calculated as sea-level rise plus backwater from new climate-related extreme wind fields. Output from these oceanographic calculations will be extreme water levels for relevant return periods including a measure of duration (i.e., day maximum or similar). This information can be used to estimate the required pumping in a given urban drainage system and whether inflow from the sea through rivers may occur.

6.3.3 Future Water Levels in Lakes and Rivers

Rivers have large differences in water flow patterns. Some creeks have a relatively constant water flow with small differences between winter and summer flows. They can have a little sensitivity to extreme rainfall events, while other streams and rivers have large differences between winter and summer flows, and they can have a strong response to extreme rainfall events. This type of urban stream/river may have a tendency to dry out in summer. In the future, it is expected that rivers will also be affected by climatic changes. Sea-level rise will affect rivers and reduce the drainage capacity, and in situations of extreme water levels, the impact is increased. Since the rivers often act as boundary condition to the urban drainage system, it is recommended to describe the river hydraulics together with the urban drainage network.

6.3.4 Future Water Levels/Pressures in Groundwater

Any changes in the groundwater conditions are interesting from an urban drainage point of view. If the groundwater table changes, it might impact the infiltration to the urban drainage system, the secondary groundwater zone that has an impact on the runoff on terrain to storm water and combined systems as well as rivers. When heavier rainfall events occur, the surface runoff from permeable areas to the urban drainage systems will increase. The expected increase in precipitation events with high intensity may have local impact on the groundwater conditions. Especially in areas with coarse sandy sediments, a rapid rise in groundwater table may occur under very intense rainfall with potential infiltration into sewers, basements, and other underground structures. At the same time, there may be disturbances in the dewatering plant pumping from the upper aquifers. The projected sea-level rise in coastal areas would cause a rise in groundwater potentials. The risk of intrusion of saline water into coastal groundwater wells will increase, and the drainage of coastal catchment areas will be disturbed or altered. In many cases, the sea-level rise will have only very local impact on groundwater conditions. However, it

may have significant impact on runoff conditions in coastal rivers, where gradients are small, especially combined with the anticipated increased intensity of rainfall.

6.4 Changes in Performance of the Urban Water Systems

6.4.1 Urban Flooding

Drainage systems are designed to be full flowing for a certain return period of rainfall, for example, 5, 10, or 25 years, depending on the location of the drainage system (e.g., rural, suburban, and financial district) [12]. Hence, if nothing is done to the urban drainage systems, their performance will certainly drop in locations exposed to more frequent or extreme rain events. Consequently, city areas will be flooded with an increase in flood damages [13]. Several studies suggest that the economic consequences by failing to change the city's design for the drainage systems are very large; the studies state that it pays off to extend the capacity of new pipes being built today, so they correspond to the last climate projections.

6.4.2 Overflows to Receiving Waters

Drainage systems are designed to relieve (send rainwater mixed with water) to recipients (e.g., lakes, rivers, and estuaries) in case that the drainage system is overloaded. This design practice has changed over the years, and now it is more common to use objectives, which are determined on the basis of the vulnerability of individual recipients to water. Increase in annual precipitation may increase sewer overflows, but no general statement can be made, and local analyses (e.g., by urban drainage modeling) are required to estimate an impact from the future rainfall on overflows.

6.4.3 Changes in Inflow to Wastewater Treatment Plants

If the precipitation is increased during winter, biological wastewater treatment plants located in cold areas may have a readied efficiency as cold weather and water slow down the biological activity and reduce the efficiency of the wastewater treatment plant. Conversely, the generally higher temperatures in winter will reduce the need for preventing slippery roads by means of chemical and salt, and this will reduce the load of these substances on the wastewater treatment plant and the aquatic environment.

6.5 Adaptation of Urban Water Systems

Climate change adaptation in urban areas is described in this section by applying risk assessments in practical solutions in order to achieve desired standards of services in preparation and layout of contingency plans [3].

6.5.1 Risk Analysis: Damage Assessment Using a Risk Analysis

Assessing the risk of damages in an urban drainage catchment can be undertaken at different levels, from broad qualitative analysis to quantitative analysis. Other impacts may be taken into account in the analysis. Besides the influence of extreme rainfall, there are also risks in the general operation of drainage systems.

A complete risk analysis of the system can be undertaken by systematically examining how the drainage system operates under different conditions during both extreme rain events and periods with disruptions in the service by weighting the various disruptions by their importance. A simpler risk analysis focused on extreme flooding is also possible. Analyses at both levels are very useful tools that can be used in prioritizing the maintenance, and operational actions should be continuously made to upgrade the drainage system.

Traditionally, damage caused by surcharged water on terrain is divided into three categories:

1. Direct damage—typically, damage caused by standing or flowing water
2. Indirect damages—for example, traffic accidents due to aquaplaning, traffic disruptions, administrative costs, labor costs, loss of production, etc.
3. Social costs—negative long-term effects of a more economical nature, such as reducing the value of property in areas subject to flooding and slower economic growth

A big advantage of a risk analysis is that all causes of flooding are assessed and weighted. Hence, optimizing the time and avoiding disproportionate spending of time on some measures, while others, perhaps more important, are overlooked. As an example, a pump failure of a pumping station due to obstruction or power failure during a moderate rain event could result in flooding comparable to the flood caused by an extreme rainfall event. One method to find the cost related to flooding in urban areas is to collect information on documented flood incidents by the insurance companies as, for example, made in Norway [6] or Brazil [10]. An internationally recognized technique to quantify the damage is the use of "flood damage curves," describing the extent of the damage as a function of land use and water level, refer to [10]. Currently, such "flood damage curves" do not exist for any areas in Denmark. The following issues should be included in an assessment of damage related to flooding [11]:

1. To prevent that the population is brought into contact with a mixture of sewage and rainwater due to overloading of the drainage systems
2. The vital community functions, such as electricity supply, water supply, heat supply, communication points, and access to hospitals, are not out of operation due to flooding
3. The number of affected basements and buildings is minimized
4. The number of flooded electrical power cabinets and other equipment is minimized
5. The impact from flooding on traffic is minimized

6.5.2 Risk Analysis: Definition of Risk Concept

Risk is the combination of the probability of an adverse event (e.g., failure of wastewater treatment plant/pump station, basement flooding, releases of hazardous substances, errors in management/SCADA) and the magnitude of the consequences (e.g., damage to facilities, personal injury, odor, traffic delays, fish kills) and severity (is it the release of 1 or 100 L, is it the hospital that gets flooded, how many are injured). *Mathematically expressed as risk = probability times consequence.*

A plan for managing risk includes the following seven steps:

1. Identify the risks (e.g., what can go wrong?)
2. Assess the likelihood and consequences of these risks
3. Determine the risk mitigation options
4. Assess the economic, environmental, public relations and operational costs and benefits of the options
5. Prioritize the mitigation option
6. Identify the decision makers
7. Develop the implementation plan

The steps in a risk analysis are illustrated in Figure 6.1.

The first step is data collection, where knowledge of the drainage system is obtained. This is followed by a coarse risk analysis during which a screening of infrastructure is undertaken by experts and special

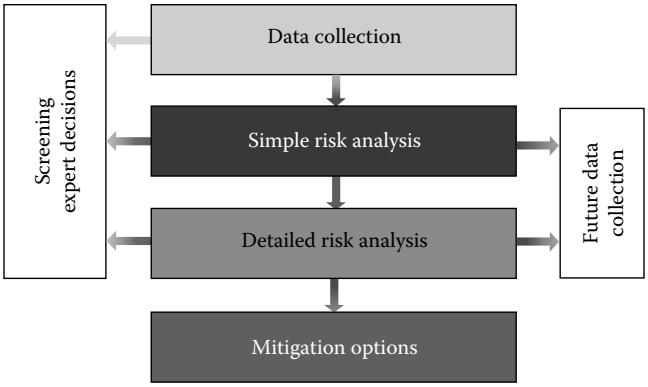

FIGURE 6.1 Risk analysis process.

risk tools. After the coarse risk analysis, there are two options: either to prepare a detailed risk analysis with a focus on selected areas from the coarse risk analysis or to go directly on to identify mitigation measures. If it is decided to proceed with the detailed risk analysis, it is possible to quantify different priority risk mitigation measures. In order to prioritize the selected sites, it is necessary to establish three matrices:

1. A frequency matrix
2. A consequence matrix
3. A risk matrix

The frequency matrix consists of seven intervals named F1–F7. F1 is an event that statistically occurs less frequently than once every 10,000 years. F7 is an event that statistically occurs 10–100 times a year. The frequency ranges are constructed according to a logarithmic scale. Because of the logarithmic scale, it is not important to know the frequencies of adverse events accurately. It is important to know the magnitude of a given event to be used. The frequency matrix is shown in Table 6.1.

A logarithmic scale is used between the individual impact categories in the matrix to make it possible to compare the impact groups. "Negligible," for instance, indicates an economic value of 10,000–100,000 DKK, while "marginal" indicates a value between 100,000 and 1 million DKK. The economic scale used in the consequence matrix is not arbitrary. Each figure is estimated from available sources and practical guidance numbers. The consequence matrix can describe the different impact categories ranging from no/negligible impact to the disastrous impact described in both qualitative and quantitative terms. The accumulated risk matrix is shown in Figure 6.2.

TABLE 6.1 Frequency Matrix

Frequency Interval	Classification	Frequency per Year
Daily to monthly	F7	10–100
Monthly to year	F6	1–10
1–10 year	F5	0.1–1
10–100 year	F4	0.01–0.1
100–1,000 year	F3	0.001–0.01
1,000–10,000 year	F2	0.0001–0.001
<10,000 year	F1	0.00001–0.0001

Source: DANVA, *Urban Climate Change* (Original title: En kogebog for analyser af klimaændringers effekter på oversvømmelser i byer), 2011.

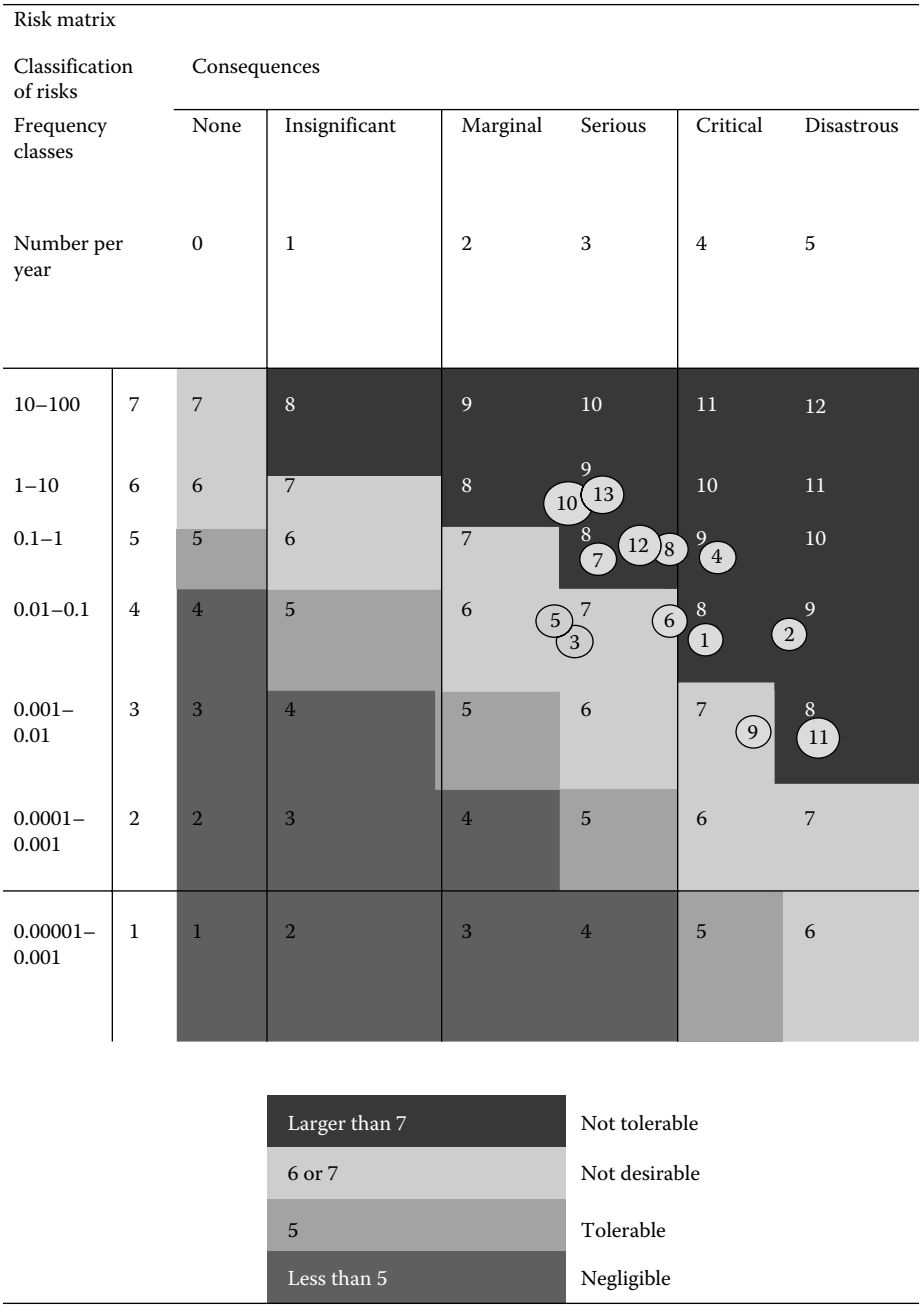

FIGURE 6.2 Risk matrix. In the matrix are examples of selected sites in sewers placed in relation to the assessed frequencies and consequences. (From DANVA, *Urban Climate Change* [Original title: En kogebog for analyser af klimaændringers effekter på oversvømmelser i byer].)

Four scales of gray are used in the risk matrix to indicate whether the calculated risk level for a given event is tolerable or not. A risk level above six or seven shall lead to implementation of defined actions to reduce risk levels. According to Figure 6.2, identified mitigation measures must be implemented for the two events classified in the nontolerable region indicated by circle nos 4 and 13 in Figure 6.2.

All items located in the light gray area should be evaluated based on a cost–benefit analysis that can determine what and how much is required to reduce the level of risk and whether an investment should be made here and now, or only when the impact occurs. An analysis provides the basis for assessing the risk level for the entire drainage system and to assess this level relative to the acceptance threshold defined in the risk matrix. For incidents above the acceptance threshold, risk mitigation measures must be identified and implemented. For incidents that lie in the acceptance area, an identification of optional mitigation measures must be undertaken and assessed through a cost–benefit analysis.

6.5.3 Risk of Flooding from Extreme Rainfall

A risk analysis of flooding from extreme rainfall alone can be based on flood maps [7]. The simulation results of rain with high return periods may be plotted using GIS themes or aerial photos in order to identify problematic areas. Each area must be assessed as to whether flooding is a problem and whether there may be damages. The assessment shall be based on the following considerations:

- If a park or football field is flooded for a given return period, is it acceptable? Is the inundation from a separate or combined system? How long does it take before the area can be used again and is cleanup required?
- What flood levels will affect basements, first floor, electrical cabinets, parked cars, etc.?
- How much does the number of different damages increase caused by climate change? Is there a risk of more damages related to urban development and what is the flood impact from planned upgrades of drainage system? Can damages caused by flooding be exported to other locations?
- What is the level of uncertainty in the model results? How well is the model calibrated, and has a safety factor been included? Is it reasonable to interpret the results directly, or should a safety factor be applied to the results?

6.5.3.1 Compilation of Damages

The cost of flood damage varies depending on what is damaged, if the damaged items have been completely or partly written off, replacement cost, etc. Moreover, the cost depends on whether the flooding was caused by rainwater and sewage, and where the flooding occurred. It is therefore very difficult to generalize the damage costs. A general list that accurately describes the cost of flooding of electrical cabinets, basements, houses, etc., cannot be developed. It is therefore recommended to first determine the number of damages by type and then to cost the damage.

To quantify the loss by flooding, it is desirable to have a geographical overview of what values might be flooded. Typically, municipalities have records of where the buildings are located, and housing registration contains information about the location of basements. The basis for the comparison is established by combining the building theme and the house registration data. Public buildings will often have a higher value than a single dwelling, so it may be appropriate to categorize the public institutions in terms of use, that is, as kindergarten or a nursing home.

Streets convey rainfall water into the drains. However, when the capacity of the drainage system is exceeded, the water may surcharge to the roads. The roads are then used to convey the excess water during the rainfall event [9]. In these situations, it is important to know estimates of water depths, water velocities, and where the water flows. Roads are usually designed to drain storm water quickly and efficiently. However, when there are significant amounts of water on roads, it might conflict with the original design of the road. If an analysis shows that a road under future climate conditions will be flooded more frequently, it should be discussed and resolved with the road authorities. The road construction

may be adapted. In connection with the damage assessment of roads, it is pertinent to examine the criteria for the operation: How much water on the road is allowed by the authorities before the road must be closed? And to investigate the road quality, so it can be determined how much water it takes to destroy the foundation of the road and how long the road can be flooded before damage occurs.

6.5.3.2 Valuation

The following parameters can be used for valuation of flooding:

- Housing
- Crèches
- Kindergartens
- Nursing homes and sheltered housing
- Water distribution. Flooding of the building of the water treatment plant causing possible contamination of clean water
- Water wells, flooding may lead to contamination of the bore field
- Petrol stations where there may be a risk of water flowing into the tanks, so that the petrol runs out (service stations with newsstand sales, auto service, etc.)
- Areas of storage of oil and hazardous waste near recipients
- Companies with oil and petrol separators connected to the sewage system and storm water system. Oil/gasoline may either surcharge inside a building or outside (it will run approximately 50–100 L from each separator)
- Especially for wastewater systems:
  - Avoid overflows from sewage pumping stations
  - Avoid swimming pools becoming contaminated with sewage

It is important that people with the greatest knowledge of the area being examined are consulted to determine appropriate values for the various categories provided earlier. In some cases, the GIS staff has a good overview of the information available. The boundaries of what can be illustrated and calculated from GIS primarily depend on what information is available. The following are a few examples for inspiration.

Figure 6.3 shows a theme with houses inundated by various return periods. The GIS layer of simulated floods is linked to the GIS layer of houses taking into account the foundation level. In Figure 6.4, the electricity cabinets are illustrated with floods exceeding 40 cm, by which flooded electricity cabinets can be identified and counted.

Figures 6.5 and 6.6 show the specific buildings plotted together with the extent of the flooding and flood depth. In this example, schools, kindergartens, and service stations are shown. This type of GIS illustration shows how and where health or environmental issues may arise.

For valuation of a new road foundation, the following should be noted:

- Cost varies according to thickness, etc.
- Most expensive is asphalt-layered roads. In this situation, it will be necessary to remove and deposit the asphalt before construction of new foundation, followed by a new asphalt pavement.
- In parts of the foundation, there will be cables, and costs associated with coping and any repairs due to damage caused by replacement of the foundation are impossible to estimate. Worst case = much more expensive than road foundation and asphalt replacement.

6.5.4 Priority Adapting to Floods under a Changing Climate

As it appears, the risk analysis can be used as a basis for prioritizing actions to prevent floods and to adapt to climate change, but in many cases, it will not be necessary to implement the full risk analysis to get started. Analyses of climate adaptation can be achieved at many different levels. These methods

FIGURE 6.3 Example of GIS theme of the houses flooded at different return periods. (From DANVA, *Urban Climate Change* [Original title: En kogebog for analyser af klimaændringers effekter på oversvømmelser i byer], 2011.)

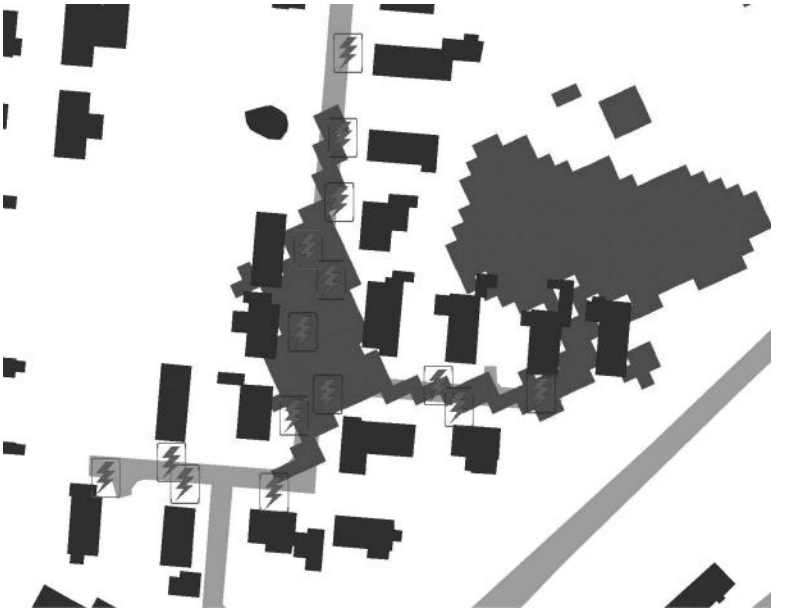

FIGURE 6.4 Example of GIS theme of electrical cabinets damaged. Placement of electrical cabinets is pictured together with water levels above 40 cm. (From DANVA, *Urban Climate Change* [Original title: En kogebog for analyser af klimaændringers effekter på oversvømmelser i byer], 2011.)

FIGURE 6.5 Example of GIS theme showing specific buildings. Flood propagation is pictured together with the location of schools and kindergartens and gas stations. (From DANVA, *Urban Climate Change* [Original title: En kogebog for analyser af klimaændringers effekter på oversvømmelser i byer], 2011.)

FIGURE 6.6 Example of GIS theme showing specific buildings. Flood levels are pictured together with the location of schools, kindergartens, and gas stations. (From DANVA, *Urban Climate Change* [Original title: En kogebog for analyser af klimaændringers effekter på oversvømmelser i byer], 2011.)

can be used for different degrees of priority: establishing a basis for getting started, where models shall be established, prioritizing measurement programs, prioritization of specific climate adaptation in the form of installations, priority for emergency action, etc. In relation to the specific climate adaptation, it will be necessary to implement according to priorities of both the economy and technical measures, which are highly political decisions, but the political decisions must obviously be made on a sound technical basis. Priorities not only can be carried out based on assessments of risks of flooding, but can also be implemented based on economic assessments: Where do you get the greatest reduction in flood risk or most climate change adaptation for the money? Prioritization of climate change adaptation can be based on the climate-meter. Among others, it will be possible to prioritize where to undertake registration of the pipe network if it is not available in a digital form. The digitization can be undertaken based on the relatively simple depression map method combined with a simple hydraulic mode.

6.6 Options for Adapting the Urban Drainage System

The expected higher rainfall in the cities should be either discharged or stored in order to avoid flooding. Possibly, part of the water can infiltrate locally before it enters the urban drainage system. A wide range of technical options exist to solve this. The drainage system can be built out with additional or larger pipes, and ponds for storing can be constructed. In the following examples, various augmentation options are given. Main groups of options are

- Active reduction of inflow of rainwater to the drainage system, that is, through increased infiltration of rainwater
- Temporary controlled storage of rainwater, that is, using wetlands
- Augmentations in the drainage system that increases capacity, that is, larger pipes, basins, etc.

6.6.1 Physical Measures on Drainage System

Addressing the increased rainfall from our urban areas in order to meet the standard of services and reduce the flooding can be done in a variety of ways. There are three types of solutions: to avoid the increased volume of water discharged to the drainage system, increasing the discharge or the storage capacity of the drainage system, or possibly a combination of these. Reduction of inflow to the drainage system can usually be achieved only by establishing local infiltration of water. Drainage of storm water can be done through open channels or closed pipes to the recipient, to larger infiltration units, or with any wastewater to treatment plants.

Storage systems can be either traditional basins like concrete boxes or pipe basins, or it can be lakes and ponds. Beyond the physical conditions in the catchment, treatment plant capacity, and conditions in the receiving waters, it is crucial whether the drainage system is a combined system or a separate system. In a separate storm water system, it is usually much easier to find diversion options for a local recipient than it is for overflow originating from a combined system. Figure 6.7 shows an overview of possible ways of regulating storm water into a drainage system.

The following describes some of the most common approaches expected to be used for augmenting existing drainage systems, so that they can meet performance requirements during the future increased load. The municipality should be aware that actions often lead to a need for revision of both wastewater and discharge or infiltration permits, for example, if overflow volumes or local infiltration is increased/established.

6.6.2 Infiltration of Storm Water

Where it is geologically and hydrologically possible, infiltration of storm water can be established at each property, or complete infiltration solutions can be made for small urban areas. Storm water from

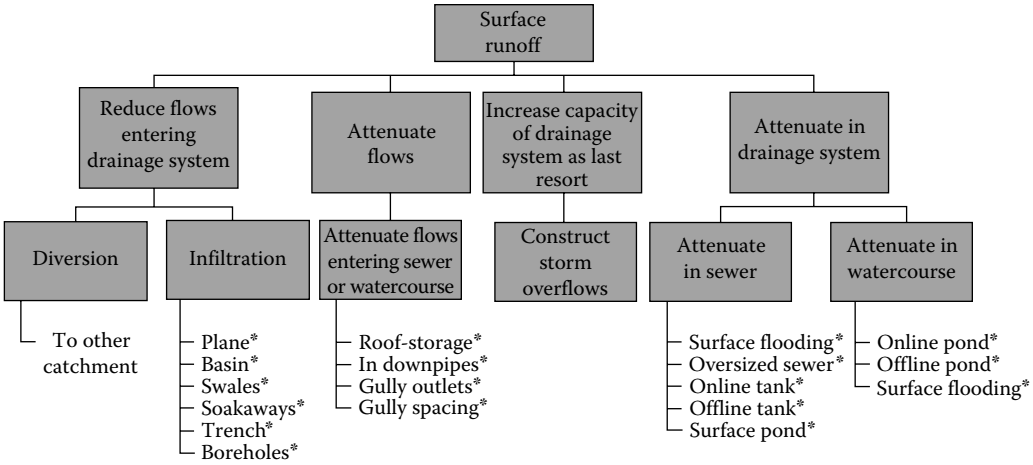

*Options for use on the development site. (From Parkinson, J. and Mark, O., *Urban Stormwater Management in Developing Countries,* The International Water Association (IWA) Publishing, London, UK., 2005, 222 pp.)

FIGURE 6.7 Schematic overview of possible ways of regulating runoff.

roads, sites, car parks, etc., may in some cases be infiltrated, but in those cases, it must be determined whether the infiltration may pose a threat to groundwater quality. Infiltration is basically the best environmental approach for discharging unpolluted rainwater, as it largely corresponds to the natural way and results in only limited interventions in the natural water cycle. Drainage structures should be designed so that there is emergency overflow from infiltration facilities to the public storm water system. This reduces the risk of flooding, and the size of the infiltration facilities required is limited. However, this has the unfortunate consequence that during heavy rain, the fascines can be filled up, resulting in a quite instantaneous and uneven flow back to the drainage system, which must therefore be designed to cope with these peaks in the flow.

The capacity of fascines may typically be of a size equivalent to 20–30 mm of rain, but there is no assurance that fascines are empty at the beginning of rainfall events. For this reason, it is not certain during an extreme rainfall event that flooding is reduced significantly. However, fascines can reduce the yearly runoff volume considerably and increase groundwater recharge.

6.6.3 Combination of Infiltration and Storing

As mentioned, infiltration systems for storm water usually have a limited capacity, requiring water to be stored during periods of major inflows. The optimal combination of storage size and infiltration capacity can be calculated or estimated based on the knowledge of soil infiltration capacity, flow conditions, etc.

6.6.4 Separation of Combined Systems

Many of the most appropriate measures to address the increased rainfall are ill-suited for combined systems. The mixture of sewage and storm water is so polluted that the water must be treated with caution. Human contact with the water poses a risk of disease, and there are aesthetic problems at outlets. Functional requirements are therefore much more stringent to the combined systems than to storm water systems. It is natural to consider changing the old combined systems to separate systems, especially if the spare capacity of the combined system is limited requiring major built-outs. In practice, this involves so many problems that only a few places exist where it is implemented. It is very expensive and very difficult to build a completely new drainage system, which also requires that the pipes located at each parcel are converted to a separate system.

Separating the combined system is carried out in smaller communities and new built-outs, but rarely in the old city centers where the need is often the greatest. Therefore, there is a need for other solutions to address at these sites. There is currently a "standard" solution for these city problems.

6.6.5 Increasing Pipe Sizes

If the conceptual layout of a drainage system cannot be changed, it can be chosen to simply increase the dimension of all the pipes in the system, so the capacity will meet the requirements in the standard of services. Alternatively, an additional pipeline can be added along the existing pipeline. Prior to this augmentation, the drainage system should be carefully analyzed in order to make only the necessary substitutions, and it should be considered to increase existing dimension on some stretches and whether there are alternative pipeline options, which can reduce costs for expansion.

6.6.6 Trunk Mains

The increased runoff flow from a catchment can be conveyed through larger pipes or stored in basins. Due to lack of space, it may be difficult to expand the sewage system, and an option could be to build tunnels conveying the water from strategically well-placed nodes in a catchment area to the recipient or main trunk line. The tunnels can also act as extra storage capacity. The technical and economic feasibility of using such solutions have been considerably improved in recent years. It should be noted that the increased water flow can be critical for the rehabilitation method that can be used, and thus for the expense.

6.6.6.1 Overflow

In combined systems, overflow or spillways are often installed to prevent the water level in the drainage system from exceeding a certain level that protects areas from flooding as well as ensures that only the designed volumes of water are conveyed through the system. Overflow discharges across a weir to basin, outlet pipe, or recipient. To ensure the same hydraulic functionality at the overflow structure during higher inflow and constant outflow, it will be required to increase the width of the weir crest or lower the weir crest level. The latter will, however, have the unfortunate consequence that the number of overflow increases.

To ensure the best hydraulic function of an overflow structure, that is, ensuring that most water flows through the structure without an increase in the backwater, the weir structure can be equipped with movable weir, dynamically controlled crest level, or a moveable flap. This can also maximize the basin effect in the upstream drainage system. In addition to the hydraulically justified augmentations, treatment measures are also installed at overflow structures, normally, automatically cleaned strainers or grids, but in some cases, more extensive treatment measures, that is, removal of nutrients and sanitation. The development will certainly lead to such cleaning being more and more prevalent, providing increased and better cleaning methods for use by local treatment. If the discharged water is sufficiently cleaned, the cleaning can compensate for the increased overflow volumes, so that the impact on the recipient is reduced despite the increased overflow.

6.6.6.2 Basins

At many locations where it is chosen to reduce the hydraulic capacity in an outgoing pipe, basins are built that can act as buffer in the drainage system. Basins are often constructed with an overflow ensuring only overflows to the recipient at a chosen frequency. The basins can be designed both to store the extreme peaks of the runoff, so flooding is avoided or reduced, and also to reduce the overflow to the recipient. In combined systems, the stored water is conveyed to the water treatment plants in the normal way after a rainfall event. In separate systems, basins are usually used to not only smooth runoff flow, but also add some treatment of the water before it is discharged into the recipient.

Sizing of basins in combined systems can be made from the discharge capacity of the basin and selected return period of overflow. There are formulas in Guide 26 to determine the required volume of the basins, but it is recommended that updated rain series are used and in addition the effect of climate change incorporated. A subsequent calculation is undertaken with historical rain to verify the function of the basin.

Basins in separate storm water systems can often be engaged in recreational areas and therefore have other functions than just smoothing the runoff. In this case, the size of the basins may be determined by the permissible water level variation, that is, of requirements to retention time limits. The retention time may not be too short because it gives too little withdrawal of substance, and it must not be too long as it can cause excessive algae growth in the basin/pond. This type of basins may also be recommended because they are often very flexible to increased inflows, partly because overflows due to the location do not cause major damage.

6.6.6.3 Local Storage

Wherever there is a possibility, it will be a good idea to store rainwater in extreme situations. It should therefore be considered to place basins in as many small watersheds as possible, that is, in the drainage of minor roads, parking lots, etc. Perhaps at some locations the storm water inlets can be made so large that they can act as smaller basins during extreme rainfall by reducing the outgoing pipe capacity. Developments such as these can be performed when there is still rehabilitation undertaken and can thus assist in compensating for extreme rainfall beyond the level of service.

It could be considered at the planning stage that newly paved areas can serve multiple purposes, so that planned activities in this area are not harmed by water depths of approximately 5–10 cm in the area during extreme rainfall in a short period.

6.6.6.4 Control and Regulation of Drainage System

Drainage systems are dimensioned to handle a design rainfall and thereby meet performance requirements. Since rainfall often falls unevenly across a catchment basin and the capacity of the pipeline system is often varied, there may be a good opportunity to improve the use of a drainage system by introducing dynamic control of certain elements in the system, for example, the outflow from the basins. This can contribute to both reduced flooding and, in combined systems, reduced overflow to recipients. For drainage systems with multiple basins, pumping stations, etc., it is strongly recommended to investigate the potential for dynamic control. As part of augmentations in the system, it may be appropriate to examine whether control can allow for more appropriate solutions to problems such as the storage basins or large pipe basins can be better placed in the system.

6.6.6.5 Use of the Road System

Normally, runoff from the roads is conveyed to the drainage system to avoid water or aquaplaning on the road. In some cases, it may be considered to exploit the road profile to convey water away during extreme rainfall. If the terrain is suitable and a model can be assessed in terms of how the system will operate, it may be an excellent way to get the water transported from critical areas to suitable recipients or storage options. The method can be recommended to be used only to separate storm water systems and in situations where the design rainfall has been exceeded (i.e., in emergency situations).

6.6.7 Augmentation on Private Property

6.6.7.1 Physical Measures

It may be useful to encourage owners to collect and divert rainwater on their own land in order to avoid that the water is collected and hence requiring large drainage capacity. Additionally, less effect on the water circulation in the area is achieved by infiltrating the water locally. However, it requires

that groundwater, soil, and terrain conditions fulfill certain conditions so that it is possible to divert the water locally, without introducing local problems and damages.

If a parcel with a relatively small impervious area of 150 m^2 is considered, this corresponds to the landowner being able to store and dispose 7.5 m^3 of rainwater in a five-year rainfall event (rainfall equivalent to 50 mm), if there is no connection of storm water to sewer. This amount equates to 30 standard rain barrels or a pond in the grounds of 5×5 m and 30 cm deep. If more water falls, the owner needs to have a management plan in place for handling this extra amount of water volume locally to prevent flooding on his own or other people's parcels.

Managing storm water on their own land without drainage to the combined drainage system may therefore be recommended primarily for environmental reasons and in order to recharge groundwater. When looking at the hydraulic balance, these constructions are not the solution, but a complement to climate adaptation.

It is recommended not to base an adaptation solely on efforts by private landowners for many reasons. The fact alone that it is not possible to control when landowners are ready to disconnect their storm water system is reason enough not to rely on this method from a hydraulic standpoint.

6.6.7.2 Infiltration of Rainwater

This refers to the diversion of rainwater into fascines on the site. Infiltration requires adequate soil conditions. Fascines are often designed in a size equal to 20–30 mm of rainfall, but no certainty exists that the complete capacity is available when the rainfall starts. If, for example, grass armor stone or similar surfaces are used in parking spaces, etc., a large part of rainfall is infiltrated on site depending on the soil type. But in case of intense rainfall, water will run on the surface and be discharged to the drainage system.

6.6.7.3 Rainwater Barrels

By collecting rainwater in rain barrels, a reduction in the discharge to the drainage system is obtained, and water consumption is reduced in cases where the water replaces the standard drinking water supply used, for example, for garden watering. The volume that can be collected is often very limited, 200–500 L is often seen, and this is only a modest proportion of the volume of extreme rain on a roof. Rainwater barrels can be full at the start of the rainfall and therefore not reduce runoff at all.

6.6.7.4 Reuse of Rainwater

Use of rainwater in homes as a substitute for water supply has only been implemented in a few places, but has the same advantages as rain barrels and the further advantage that consumption—as opposed to irrigation—is more evenly distributed over time. A major drawback is also here that the storage capacity is limited, and therefore there is no guarantee that systems can store water during critical situations.

In many places, a rainwater tank of approximately 3–5 m^3 is used, and it is estimated that a tank like this will be able to store a large part of the annual precipitation to be used in the dwelling for toilet flushing and washing machines. In connection with extreme rainfall, an overflow is required to divert water, since a 5-year storm event alone requires in the order of 7.5–10 m^3 for a single-family house.

6.6.7.5 Green Roofs

Techniques have been developed for using the so-called green roofs, where a grid of growth layers in which plants can grow are laid out on the roofs of buildings. The aim is to store the water fallen on the roof in the growing layer where it is absorbed by plants. However, the storage ability of the growth layer is limited, only 6–10 mm, so the storage effect during extreme rainfall is limited. Even so, on an annual basis, a quite good effect can be achieved in terms of reduced inflow to drainage systems.

As shown in the mentioned examples of actions on private land, it is hard to find solutions for the public, which are as safe and easy as discharging to the public drainage system, and it is hard to find solutions that can handle the very critical periods of extreme rainfall.

6.6.7.6 Private Prevention of Basement Flooding

If a landowner needs to guard the basement against flooding from sewers, nonreturn or check valves can be installed so that water cannot flow backward into the basement. If the basement drainage system is connected to a pump, wet well pumping to drainage system, then even higher security is gained toward basement flooding. This also ensures that the private installations can be used regardless of the water level in the public drainage system.

6.6.7.7 Drainage of Road Space

In most places, drainage of road space works very effectively. This is also the target from the road authority's side, since water on the roadway constitutes a danger to traffic, and water in the road paving and road base layer may damage the road. Drainage of especially smaller roads and streets, however, could perhaps be made so that the water in a lesser degree was led directly to the drainage system, but first had to pass through some kind of retention system such as infiltration devices. There is also scope for increased use of semipermeable pavements, through which part of the water from the road could infiltrate.

6.6.8 Flood Emergency Preparedness

Municipalities shall determine the desired standards of services that they will offer citizens. This has to be done under conditions that are more extreme than the defined desired standards of service, which cannot prevent floods. However, it is possible to minimize damage and inconvenience by increasing emergency preparedness. The level of flood emergency preparedness needs to be balanced by the financial effort (see Section: 6.5.2).

Preparedness involves a wide range of activities and assessments that can protect assets and people from damage caused by water. The contingency plans should of course contain important phone numbers and other important administrative information, but in this report, only the hydraulic aspects of preparedness will be discussed.

Preparedness can be divided into before, during, and after because the state of emergency must be investigated and planned *before* it occurs, actions may be required *during* the emergency situation, and there will be an evaluation *after* the event where the experience will be evaluated and possibly incorporated into new updated contingency plans (Figure 6.8).

In the following sections, the flood preparedness components are elaborated.

6.6.8.1 Before the Rainfall Event

6.6.8.1.1 Establishment of Contingency Plans if Necessary for Climate Change Adaptation

All municipalities should, as a part of the overall civilian preparedness, have a contingency plan in place. There is currently no requirement for the municipalities to develop a specific plan for the operation of urban drainage systems and wastewater treatment plants. Some municipalities have, however, made such plans that accommodate a number of issues that are critical to the operation of the urban drainage system, for example, power failures, flood damages in exposed locations, and staff/contractor preparedness for emergencies that could maintain a minimum service level.

Contingency plans are those that are used by municipalities to respond to overloads to urban drainage system and water surcharges to terrain, and they include the following:

- Actual physical measures to reduce the effects of an extreme rainfall situation and resulting floods such as earth embankments and walls designed to hold water back in predefined depressions.
- Preparedness for emergency ad hoc efforts, that is, placement of sandbags and use of mobile pumps.
- Information/alerts both internally within the municipality's operations and externally.
- Preparatory work must be undertaken where all details related to physical measures, acute ad hoc efforts, information, and alerts are reviewed.

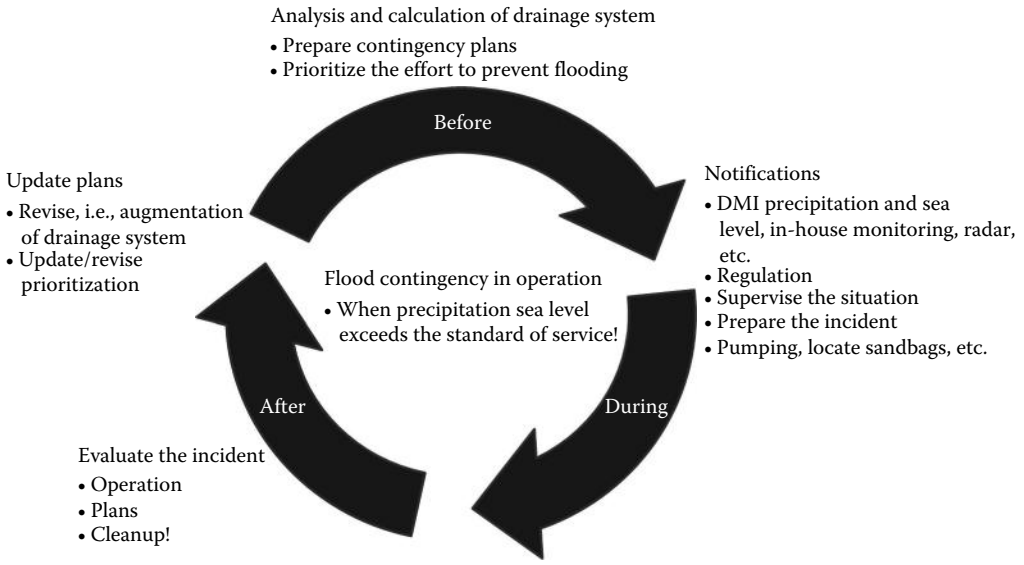

FIGURE 6.8 Illustration of the flood preparedness cycle.

6.6.8.1.2 Priority for Contingency Plans

Contingency plans should be available to all urban and possibly rural areas where it is estimated that flooding may cause significant either human health related or costly damages. Once contingency plans have been established for a large area, for example, a municipality or a region, priorities for all catchment areas in the region should be set. This must be done before a critical situation occurs, because there might not be sufficient personnel and equipment available to implement the effort in all catchments at once. A prioritized contingency plan would be a good decision support tool for incident management team. The hierarchy of plans can be implemented using the same principles as the prioritization of climate change adaptation.

6.6.8.1.3 Structural Responses to Flooding

In relation to obtaining a climate change service level for a catchment area, analysis and detailed projects will uncover the critical issues within the area. The solutions that exist could to some degree be expanded without significant additional costs. It may also be required to be able to protect vulnerable housing areas using banks of earth or terrain regulated through embankments or excavation so that water can be conveyed to less critical areas.

Examples of permanent measures include embankment at Godsparken in Greve, Denmark, to prevent a river from flowing into an urban area, and a gutter near the Sports Park in Odense, which convey the water onto the running path to avoid damage to floors in buildings. The embankment at Godsparken is not expensive in construction and ensures not only against extreme long-term rainfall, but also against extreme water levels in the ocean (Figure 6.9).

6.6.8.1.4 Mobile Preparedness Actions

Besides the stationary emergency response, there is a wide range of possibilities for mobile emergency measures, for example, mobile pumps, sandbags, and shutters. Partly through terrain analysis, calculations, and experiences, a strategy can be created in advance for how surface water is conveyed in an emergency situation, and the necessary dimensions for pumps and mobile walls can be assessed. It is essential that the number and precise location of such sandbags are known and that everything is available in stock and ready before the situation arises (Figures 6.10 and 6.11).

FIGURE 6.9 Establishment of embankment at Godsparken in Greve. (From DANVA, *Urban Climate Change* [Original title: En kogebog for analyser af klimaændringers effekter på oversvømmelser i byer], 2011.)

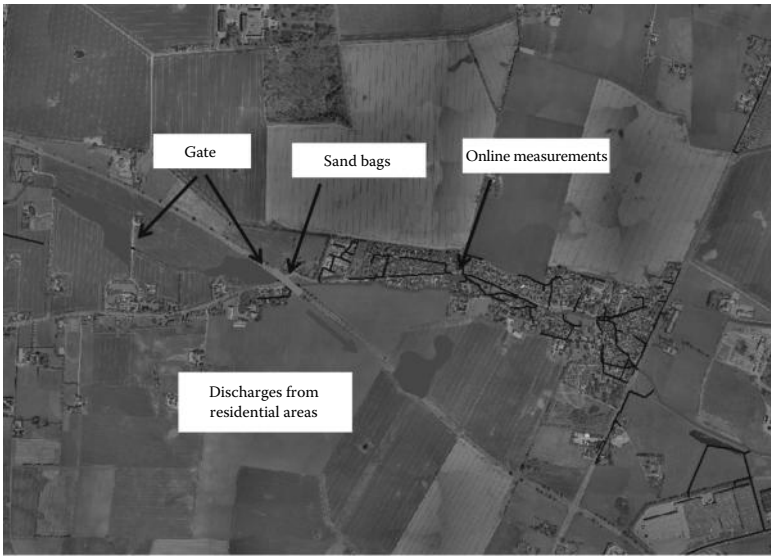

FIGURE 6.10 Sample proposals for mobile emergency response in combination with online measurement. (From DANVA, *Urban Climate Change* [Original title: En kogebog for analyser af klimaændringers effekter på oversvømmelser i byer], 2011.)

6.6.8.1.5 Warning

It is essential that the municipality and wastewater utilities are warned about possible adverse events that should be acted upon. Meanwhile, it is also appropriate that citizens are warned that flooding is expected and advised to secure personal belongings.

A number of meteorological institutes forecast heavy rainfall events today, but the risk of subsequent floods in cities is often based on experience. This is inadequate because local conditions in the urban

FIGURE 6.11 Mobile pump used at Greve Gymnasium during extreme rainfall in Greve on July 5, 2010. (From DANVA, *Urban Climate Change* [Original title: En kogebog for analyser af klimaændringers effekter på oversvømmelser i byer], 2011.)

drainage systems determine if flooding occurs or not. Alerts are currently used in selected locations abroad to reduce costs associated with flooding. Can the urban drainage system, for instance, be partially emptied until rain arrives, or traffic radio can be used to warn people to stay away from urban areas at risk of flooding? [1].

Some floods are acceptable if people are informed in a timely and appropriate manner about how to behave. However, this requires that the municipality is in possession of an appropriate action and contingency plan that can be executed when an extreme rainfall is warned. If an analysis shows that there will be flooding in an area under future climate change conditions that are not acceptable, then it will take some time from the analysis is performed until new infrastructure is built. In this period, a warning is useful.

When the warning comes into force, it is important that the wastewater utility has a communication channel set up through which information to the citizens about the measures affecting them can be communicated. Before the emergency situation occurs, citizens must be aware of how to seek information: website, radio, or similar.

It is appropriate to have a contingency plan based on a warning of heavy rainfall for viaducts or similar flood-prone sites. Using the warning, such sites can be isolated before the flood is so high that people are at risk if attempting to walk or drive through the water. Whether the warning will be appropriate and economically viable must be assessed on a case-by-case basis.

Responses to the flooding may depend on

- Existing storage basins, canals, streams, rivers, and lakes that can be drained before the emergency situation arises, ensuring an optimum volume available in the systems
- How soon operational staff can be warned so they are ready to implement contingency plans
- Existing grates, outlets, nonreturn valves, etc., are reviewed to ensure that they are fully operational before the rainfall occurs

6.6.8.1.6 Control and Supervision

Control can be implemented in urban drainage systems if there is additional storage available or long transport times present. A control strategy could be developed when there is a sufficient understanding

of how the urban drainage system functions are available. The computer modeling may be useful to provide an overview of where it is appropriate to control the water, for example, by implementing gates or pumps. The analysis may have identified a critical area where it may be useful to store water upstream by flooding less critical areas. By applying online meters at strategic locations in the urban drainage system, gates or pumps can be controlled by set points and be in operation at the right time. Additional storage can be created by emptying existing ponds, canals, rivers, and lakes before the situation arises.

6.6.8.2 During the Rainfall Event

During the extreme rainfall and the time just after (depending on rainfall character), the urban drainage systems are monitored and the contingency plans are initiated when required.

6.6.8.3 Capture of Evidence and Experience

To ensure that the entire organization will be wiser from the experience gained during the incident, it is very important to conduct a detailed documentation of the incident. The documentation should include at least the log of adjustments and operation actions in urban drainage system (who has done, what, and when) and preferably include notes of why and on what basis the action was implemented. Observations in the field are very valuable (preferably with pictures) when experience should be used in further analysis and possible in updating the contingency plans.

After a flood event, very detailed knowledge of what exactly happened during the incident is required.

6.6.8.4 After the Rainfall Event

After the floods, a cleanup of both the urban drainage systems and the terrain is required. It must be ensured that facilities have not have damaged and that the function and capacity have not been reduced by trapped items.

6.6.8.5 Updating Contingency Plans

Thorough documentation and experience of the flooding incident may be used to evaluate whether the contingency plans need to be updated. This includes evaluation of the prioritization of the plans, whether the hydraulic model requires recalibration after the incident, as well as finding solutions to the challenges or ensuring that service levels are met.

6.6.8.6 Operating Experience

It is valuable to compare experiences with expectations and conclude if flooding is caused by operational problems or lack of capacity in the urban drainage systems.

6.7 Case Study

The method described earlier was used in Greve, Denmark, to enable politicians to decide whether to adapt to climate change or not and to what extent. The method was applied to the most vulnerable area in the municipality, and the cost was calculated. In Greve Municipality, it is politically decided that the entire drainage system in the city shall be upgraded to a maximum flooding frequency of once every 10 year. Based on experiences from the flooding in 2002 and 2007 (see Figure 6.12) and a vulnerability map prepared using a GIS model, the municipality is divided into 42 urban areas and the climate adaptation is prioritized over the next 12–15 years.

Prioritization is carried out by the motto: those areas that have been hit the hardest will be adapted first, an approach that is politically accepted. The hydraulic models will be developed and improved through measurement campaigns and experiences. If these models show that there is reason to prioritize differently from that is done here, reprioritization will be made and presented to the political system. Economic issues may similarly prove it necessary to reprioritize, for example, if a relatively simple and inexpensive measure will have significant positive impact on climate adaptation.

FIGURE 6.12 Flooding, Greve 2002—before adaptation to climate changes. (From DANVA, *Urban Climate Change* [Original title: En kogebog for analyser af klimaændringers effekter på oversvømmelser i byer], 2011.)

For the prioritization, the following data are used:

- Lessons from the floods in July 2007, which is reported directly from citizens or landowners
- The digitization of storm water system
- The digital terrain model for Greve Municipality, which is used to calculate the depth of surface depressions
- GIS themes of buildings in the municipality and the theme of business and public buildings

Figure 6.13 shows the prioritizing Greve. If only a few previous flooding experiences exist in a city, terrain models or/and hydraulic modeling can be used to prioritize which areas to work on first.

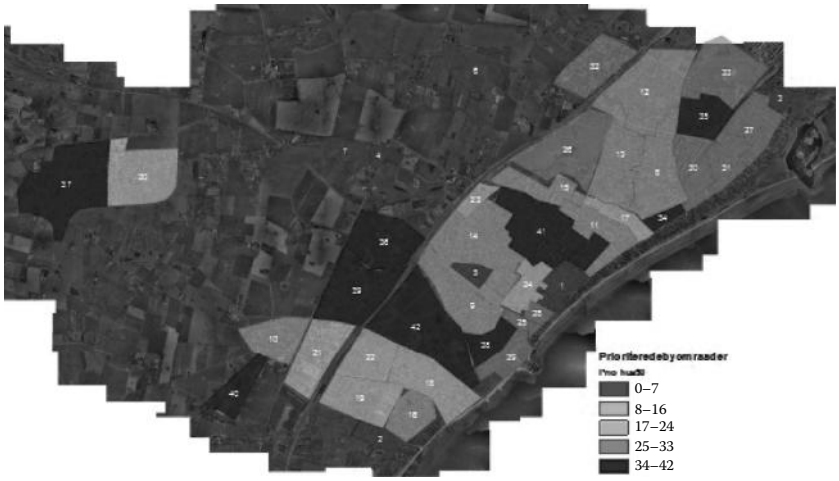

FIGURE 6.13 The prioritized city areas of Greve, Denmark. (From DANVA, *Urban Climate Change* [Original title: En kogebog for analyser af klimaændringers effekter på oversvømmelser i byer], 2011.)

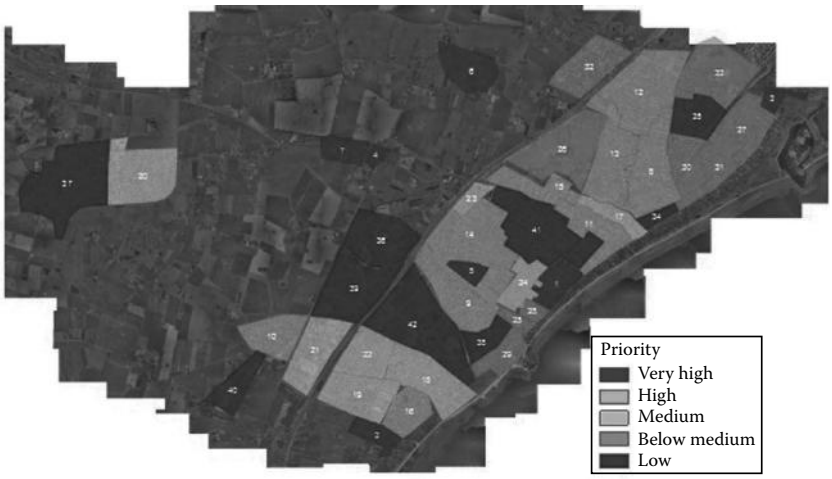

FIGURE 6.14 Extreme rainfall. (a) Without activating an emergency plan. (b) With an emergency plan activated. (From DANVA, *Urban Climate Change* [Original title: En kogebog for analyser af klimaændringers effekter på oversvømmelser i byer], 2011.)

In Greve, a model of the total storm water system (including streams) has been developed. To simulate flow on the terrain, the digital terrain model has been used to locate depressions in the city areas. This model, called "the strategic hydraulic model of Greve," has been used to quality-assure the prioritization.

Detailed emergency plans are in the process of being prepared for all areas to minimize the material damage and health risk in case of extreme rainfall. An example is shown in Figure 6.14.

6.8 Summary and Conclusions

Increased frequency and intensity of flooding events, combined with trends in growing urban population in most countries, have led to the need for increased and internationally coordinated efforts to enhance technologies and policies for dealing with floods. On the top of today's flood problems come the impacts from climate change, which in many places will aggravate the situation.

Estimates of impacts from climate changes are proposed to be carried out by the use of flood modeling, and based on the flood maps, transparent and informed decisions must be made—taking the uncertainty into account. After the flood impact assessment, the problems should be prioritized, for example, by the use of risk assessment tools. Based on the findings, the municipalities must develop a plan for timely management and mitigation of the impacts from climate changes. The plan should contain descriptions of how and when climate changes are analyzed and managed for:

1. Planning and design of new sewer systems
2. Existing sewers where maintenance and reconstruction are already planned
3. Existing sewers where no maintenance and reconstruction are scheduled today

Case studies on the mitigation of the climate change impacts have been carried out in a number of places around the world, for example, for catchment areas in Sweden and Denmark [9].

The development of flood mitigation strategies for sewer systems under the impact of climate changes has resulted in sets of guidelines for municipalities [2]. It is believed that such sets of guidelines will provide the municipalities with a timely and cost-efficient strategy for coping with climate changes and their impacts on sewer system.

References

1. Chumchean, S., Einfalt, T., Vibulsirikul, P., and Mark, O. 2005. To prevent floods in Bangkok: An operational radar and RTC application—Rainfall forecasting. *10th International Conference on Urban Drainage*, Copenhagen, Denmark.
2. DANVA. 2011. *Urban Climate Change* (Original title: En kogebog for analyser af klimaændringers effekter på oversvømmelser i byer).
3. Djordjevic, S., Butler, D., Gourbesville, P., Mark, O., and Pasche, E. 2011. New policies to deal with climate change and other drivers impacting on resilience to flooding in urban areas: The CORFU approach. *Environmental Science and Policy* 14: 864–873.
4. Domingo, N.D.F., Sunyer, M.A., Hansen, F., Madsen, H., Mark, O., and Paludan, B. 2010. Modelling of sea level rise and subsequent urban flooding due to climate changes. *Conference: SimHydro: Hydraulic Modeling and Uncertainty*, Nice, France.
5. IPCC. 2007. Rapports from FN's International Climate Panel. ipcc.ch/publications_and_data/ar4/syr/en/contents.html. Accessed on February, 2007.
6. König, A., Sægrov, S., Schilling, W. 2002. Damage Assessment for Urban Flooding, 9th International Conference on Urban Drainage, Portland, Oregon, USA.
7. Mark, O. and Djordjević, S. 2006. While waiting for the next flood in your city.… *7th International Conference on Hydroinformatics*, Nice, France.
8. Mark, O., Svensson, G., König, A., and Linde, J.J. 2008. Analyses and adaptation of climate change impacts on urban drainage systems. *11th International Conference on Urban Drainage*, Edinburgh, U.K.
9. Mark, O., Weesakul, S., Apirumanekul, C., Boonya Aroonnet, S., and Djordjević, S. 2004. Potential and limitations of 1-D modelling of urban flooding. *Journal of Hydrology* 299: 284–299.
10. Nascimento, N., Baptista, M., Silva, A., and Machado, M.L. 2005. Flood damage curves: Methodological development for the Brazilian context. *10th International Conference on Urban Drainage*, Copenhagen, Denmark.
11. Paludan, B., Brink-Kjær, A., Nielsen, N.H., Linde, J.J., Jensen, L.N., and Mark, O. 2010. Climate change management in drainage systems—A "Climate Cookbook" for adapting to climate changes. *Novatech*, Lyon, France.
12. Parkinson, J. and Mark, O. 2005. *Urban Stormwater Management in Developing Countries*, The International Water Association (IWA) Publishing, London, U.K., 222pp.
13. Speight, L. 2006. *Analysis of the Causes of Flood Risk in Urban Areas*, The University of Newcastle upon Tyne, Newcastle upon Tyne, U.K.

7

Climate Change Impacts on Hydrology and Water Resources

Never Mujere
University of Zimbabwe

Saeid Eslamian
Isfahan University of Technology

AUTHORS

Never Mujere holds a master of philosophy degree in geography from the University of Zimbabwe (UZ). Currently, he is a physical geography lecturer in the UZ's Department of Geography and Environmental Science. He is the founder of a local nongovernmental organization, Environmental Management Trust (EMT). His areas of research interests are water resources and environmental issues. He has authored two books, contributed to some chapters of four books, published seven papers in referred journals, and presented papers at international workshops.

Saeid Eslamian received his PhD from the University of New South Wales, Australia, with Professor David Pilgrim. He was a visiting professor in Princeton University, United States, and ETH Zurich, Switzerland. He is currently an associate professor of hydrology in Isfahan University of Technology. He is the founder and chief editor of *Journal of Flood Engineering* and *International Journal of Hydrology Science and Technology*. He has published more than 200 publications mainly in statistical and environmental hydrology and hydrometeorology.

PREFACE

Global climate change characterized by rising global temperature and precipitation is projected to have significant major impacts on freshwater systems by intensifying the hydrological cycle. The potential effects of climate change on hydrology (focusing on cycling of water) and water resources (focusing on human and environmental use of water) are receiving great academic attention. It is important to emphasize that climate change is just one of many pressures facing the hydrological system and water resources. Changing land-use and land-management practices are altering the hydrological system, often leading to deterioration in the resource base. Changing and competing water demands are generally increasing pressure on available resources. This chapter analyzes the potential effects of climate change on the hydrology and water resources in the Nyanyadzi River catchment in eastern Zimbabwe. The impacts of climate change on the hydrological and water resource systems of the catchment were analyzed using Commonwealth Scientific and Industrial Research Organization (CSIRO) model projections for two SRES emission scenarios compared to the 1961–1990 baseline climate data. Modeling results showed significant reductions of river flows by 2020, 2050, and 2080. Changes in river hydrology will reduce reliability and amount of irrigation water supply and its reliability, thus negatively affecting irrigation development in the catchment.

7.1 Introduction

Global climate change is one of the most complex and challenging environmental challenges facing the world today. It is a global issue of concern, which has received the increased attention in recent years. The subject has been debated across various scales with an emphasis on national and international acceptance, adaptation, and, subsequently, mitigation. It is a critical and urgent challenge where the top-down technical consideration needs to be met with a bottom-up community-based approach to better inform policy and practice at higher levels. Global efforts designed to tackle climate change–related problems at national, regional, and international levels include the Montreal Protocol in 1987 to reduce the production and consumption of ozone-depleting substances; United Nations Framework Convention on Climate Change (UNFCCC) of 1992 encouraged industrialized countries to stabilize greenhouse gas (GHG) emissions; and Kyoto protocol in 1997, which compelled industrialized countries to reducing GHG emissions [16]. However, lack of compliance to the agreements is a major challenge. The World Meteorological Organization (WMO) and the United Nations Environment Programme established the Inter-governmental Panel on Climate Change (IPCC) in 1988 with the assigned role of assessing the scientific, technical, and socioeconomic information relevant for understanding the risk of human-induced climate change [19].

Research evidence has also shown that global mean surface air temperature over the twenty-first century is expected to rise by 0.6°C over the twentieth-century average of 14°C. A net increase in mean global air temperature of 0.74°C has been reported by the IPCC from 1906 to 2008. Several models have predicted increases in mean global temperatures of 1°C–5°C over the next 100 years [15]. On the other hand, globally averaged precipitation is projected to increase in the twenty-first century by 1.1 mm over the twentieth-century average of 2.4 mm [6,11].

The Second Assessment Report of the IPCC warned that global warming would lead to increases in both floods and droughts [6]. Global climate change characterized by rising global temperature and precipitation is projected to have significant major impacts on freshwater systems by intensifying the hydrological cycle. Changes in seasonal and annual temperatures, precipitation patterns, and amounts will drive important hydrological processes, resulting in extreme weather conditions.

This chapter analyzes the effects of climate change on hydrology and water resources. It first summarizes the evidence of climate change (Section 7.1), before assessing its general effects on hydrology,

water resources, and water resources management. Section 7.2 gives definitions of the terms climate, climate change, and climate variability while Section 7.3 examines the causes of climate change. The implications of climate change on hydrology are reviewed in Section 7.4 with Section 7.5 focusing on climate change–water resource management nexus. The issue of climate change risk management is explored in Section 7.6. A case study approach has been adopted in Section 7.7, where the Nyanyadzi River catchment has been introduced. Sections 7.8 and 7.9 explain the issues of climate change scenarios and baselines. The potential hydrological impacts of climate change are presented in Section 7.10. The final Section 7.11 gives a discussion on summary and conclusions.

7.2 Climate Change and Variability

7.2.1 Climate

Climate is a periodic–stochastic process whose realizations are states of atmosphere (weather) and can be described by a set of quantifiable attributes [12]. The WMO defines climate as the average weather, that is, the statistical description in terms of the mean and variability of surface variables such as temperature, precipitation, and wind over a period of time ranging from months to thousands or millions of years. The classical period of time is 30 years [10].

The climate system is a complex interactive system consisting of the atmosphere, land surface, snow and ice, oceans and other bodies of water, and living things. The atmospheric component of the climate system characterizes climate. It evolves in time under the influence of its own internal dynamics and due to changes in external factors that affect climate (called forcings). External forcings include natural phenomena such as volcanic eruptions and solar variations, as well as human-induced changes in atmospheric composition. Solar radiation powers the climate system. There are three fundamental ways to change the radiation balance of the Earth: (1) by changing the incoming solar radiation (e.g., by changes in Earth's orbit or in the Sun itself); (2) by changing the fraction of solar radiation that is reflected (albedo), for example, by changes in cloud cover, atmospheric particles, or vegetation; and (3) by altering the long-wave radiation from Earth back toward space (e.g., by changing GHG concentrations). Climate, in turn, responds directly to such changes, as well as indirectly through a variety of feedback mechanisms [10,11].

7.2.2 Climate Variability

Climate variability refers to deviations of climatic statistics over a given period of time (e.g., a month, season, or year) from the long-term statistics relating to the corresponding calendar period. The term also denotes variations in the mean state and other statistics (e.g., standard deviations and the occurrence of extremes) of climate on temporal and spatial scales beyond that of individual weather events, including the fluctuations associated with El Niño (dry) or La Niña (wet) events [10]. Variability may be due to natural internal processes within the climate system (internal variability) or to variations in natural or anthropogenic external forcing (external variability).

7.2.3 Climate Change

Climate change refers to a statistically significant variation in either the mean state of the climate or its variability, persisting for an extended period (typically decades or longer), and may be due to natural internal processes or external forcings or to persistent anthropogenic changes in the composition of the atmosphere or in land use. The UNFCCC defines climate change as a change of climate, which is attributed directly or indirectly to human activity that alters the composition of the global atmosphere and which is in addition to natural climate variability observed over comparable time periods [12]. Note that the definition of climate change used in the UNFCCC is more restricted, as it includes only

those changes that are attributable directly or indirectly to human activity. According to the IPCC, climate change refers as any change in climate over time, whether due to natural variability or as a result of human activity [9,10]. Thus, the IPCC makes a distinction between climate change attributable to human activities altering the atmospheric composition and climate variability attributable to natural causes.

From the two definitions, it is vital to note that climate change is any change in climate over time, whether due to natural variability or as a result of human activity. The climate of a place or region is changed if over an extended period there is a statistically significant change in measurements of either the mean state or the variability of the climate for that place or region. While weather and climate are closely related, as such, climate change and weather are intertwined. Observations can show that there have been changes in weather, and it is the statistics of changes in weather over time that identifies climate change.

7.3 Causes of Climate Change

The definitions of climate change highlighted in Section 7.2 have shown that changes in climate may be due to natural processes or persistent anthropogenic changes in atmosphere and land use. Climate change is caused by GHGs, which enhance the greenhouse properties of the earth's atmosphere. These gases allow solar radiation from the sun to travel through the atmosphere but prevent the reflected heat from escaping back into space. This green house effect causes global warming as a result of rising earth temperatures.

The climate of the earth changes continually on a range of timescales due to internal and external factors. Internal factors are natural and arise from complex interactions within the climate system. In general, internal variability on short timescales (days to weeks—what we know as weather) is generated by atmospheric instability. Variability on longer timescales (intraseasonal, interannual, and decadal to centennial) can be enhanced by complex interactions between not only the atmosphere and other components of the climate system, mostly the oceans, but also the terrestrial biosphere and the cryosphere.

Natural external factors include the earth's rotations that produce diurnal and seasonal cycles, variations in the amount of radiant energy emitted by the sun (e.g., sunspot cycles have a period of about 11 years), volcanic eruptions, and changes in the Earth's orbital parameters (e.g., due to Milankovitch cycles, which have a dominant period of 100,000 years). Substantial global warming at the end of ice ages over the past half million years was triggered by changes in the Earth's orbit and subsequently enhanced by natural increases in GHGs [8].

Humans are also responsible for external factors such as [11,15].

- Changes in atmospheric composition (e.g., in concentrations of stratospheric ozone and GHGs: carbon dioxide, methane, nitrous oxide, chlorofluorocarbons, and tropospheric ozone)
- Release of atmospheric particulates (e.g., sulfate aerosols and black carbon)
- Modification of the terrestrial ecosystems (e.g., by land clearance and agricultural practices)

7.4 Climate Change and Hydrological Cycle

Climate and hydrology are inextricably linked. Although the hydrological system influences climate change, climate change also affects the hydrological system with changes in surface temperature, precipitation patterns, and evapotranspiration rate. Water vapor is a key component in GHG [1,17]. Changes in temperature and precipitation patterns as a consequence of the increase in concentrations of GHGs affect the hydrological process, availability of water resources, and water use for agriculture, population, mining industry, aquatic life, and hydropower.

According to the IPCC, a notable reduction of the water resources service is projected where the runoff decrease, and also the projection of water stress for 2050s indicates an increase in the range of

62%–76% of the global land areas. The twenty-first-century simulations with climate models indicate an increase in the global evaporation, water vapor, and precipitation [9]. The hydrological impacts of climate change, including changes in temperature, precipitation, and sea-level rise, are expected to have varying consequences for the availability and management of freshwater resources around the world. Changes in river runoff, for example, will affect the yields of rivers and reservoirs and navigation and have an impact on the energy sector, finally affecting the recharging of groundwater [3].

The main components of hydrology cycle are the precipitation, evaporation, runoff, groundwater, and soil moisture. They are all linked with changes in atmospheric temperature and radiation balance. This section gives a review of the potential effects of climate change on these components of the water balance and their variability over time.

7.4.1 Precipitation

Precipitation is the main driver of variability in the water balance over space and time. Changes in precipitation have very important implications for hydrology and water resources. Variations in precipitation over daily, seasonal, annual, and decadal timescales influence hydrological variability over time in a catchment. Flood frequency is affected by changes in the year-to-year variability in precipitation and by changes in short-term rainfall properties (such as storm rainfall intensity). The frequency of low flows or drought flows is affected primarily by changes in the seasonal distribution of precipitation, year-to-year variability, and the occurrence of prolonged droughts. The spatial change in amount, intensity, and frequency of the precipitation will affect the magnitude and frequency of stream flows; consequently, it increases the intensity of floods and droughts, with substantial impacts on the water resources at local and regional levels.

Climate models are revealing that at the global scale, precipitation will generally increase over the tropical Pacific and high latitudes by 10%–20%. Increase in annual precipitation of more than 20% will occur in high latitudes such as in northern part of central Asia, Eastern Africa, and the Equatorial Pacific Ocean. However, in the subtropics, mean precipitation is expected to decrease in the same range of 10%–20%. For instance, the mean annual precipitation will decrease by up to 20% in the Caribbean regions, subtropical western coasts, Mexico, Central America, Southern United States, and over the Mediterranean [11,12].

Decrease and increase in precipitation will increase the risks of droughts and flooding respectively due to the increase in the intensity and variability of the precipitation in the twenty-first century. Dry periods are projected for mid-continental zones in summer (subtropics, low, and midlatitudes), with marked risk of droughts in these regions. Likewise, extreme rainfall is projected to increase in tropical and high-latitude regions that experiment increases of the mean precipitation [11].

7.4.2 Evapotranspiration

The rate of evaporation from the land surface is driven essentially by meteorological controls, mediated by the characteristics of vegetation and soils, and constrained by the amount of water available. The primary meteorological controls on evaporation are the amount of energy available (characterized by net radiation), the moisture content of the air (humidity is a function of water vapor content and air temperature), and the rate of movement of air across the surface (a function of wind speed). Increasing temperature generally results in an increase in potential evaporation, largely because the water-holding capacity of air is increased. Changes in other meteorological controls may exaggerate or offset the rise in temperature, and it is possible that increased water vapor content and lower net radiation could lead to lower evaporative demands. The relative importance of different meteorological controls, however, varies geographically. In dry regions, for example, potential evaporation is driven by energy and is not constrained by atmospheric moisture contents, so changes in humidity are relatively unimportant.

Annual evaporation increases over most oceans as surface temperature increases. At the global scale, mean evaporation changes, but it is different at local scale due to changes at the atmospheric transport of water vapor [8]. In humid regions, however, atmospheric moisture content is a major limitation to evaporation, so changes in humidity have a very large effect on the rate of evaporation. Evapotranspiration is projected to increase almost everywhere as the water-holding capacity of the atmosphere increases with increasing temperatures [3]. An increase in the rate of evaporation will also affect water supply and contribute to the salinization of irrigated agricultural lands.

7.4.3 Soil Moisture

The amount of water stored in the soil influences the rate of actual evaporation, groundwater recharge, and generation of runoff. Spatial and temporal changes in soil moisture depend on precipitation and evaporation, which may be affected by changes in the land use and land cover. Local effects of climate change on soil moisture vary with the degree of climate change and soil characteristics. The water-holding capacity of soil affects possible changes in soil moisture deficits. Hence, soils with low water-holding capacity are highly sensitivity to climate changes. Climate changes also affect soil characteristics, perhaps through changes in waterlogging or cracking, which in turn affect soil moisture storage properties. Infiltration capacity and water-holding capacity of many soils are influenced by the frequency and intensity of freezing [3]. In limestone terrains, infiltration and water-holding capacity of soils are greater with increased frost activity, and increased temperatures could lead to increased surface or shallow runoff.

Climate change projections indicate that the annual mean soil moisture content will increase by 15% in some regions like East Africa and central Asia, where precipitation is expected to increase, while it will decrease in subtropical and the Mediterranean zone. Climate models show that a rise in GHG concentrations is associated with reduced soil moisture in Northern Hemisphere midlatitude summers. This is the result of higher winter and spring evaporation, caused by higher temperatures and reduced snow cover, and lower rainfall inputs during summer.

7.4.4 Groundwater

Groundwater is the major source of water across much of the world, particularly in arid and semiarid regions. Groundwater recharge has a direct influence on the base flow of rivers, when the water table depth and groundwater decrease; the base flow is reduced fundamentally in dry seasons. Climate change affects the groundwater recharge. Some research results indicate that the groundwater recharge decreased by more than 70% for the South West Africa and Northeastern Brazil. In addition, the Near East, Western United States, northern China, and Siberia are zones where the groundwater recharge is estimated to increase by more than 30% by the 2050s; consequently, the water table will increase, and it will affect agriculture areas located in the lower basins by soil salinization [11].

7.4.5 Runoff

Climate change increases water resources stresses in some parts of the world. Runoff is expected to decrease around the Mediterranean, in some parts of Europe, central and southern America, and southern Africa. In high-latitude rivers and other water-stressed parts of the world, particularly in southern and eastern Asia, climate change increases runoff, but this may not be very beneficial in practice because the increases tend to come during the wet season and the extra water may not be available during the dry season [2]. Changes in stream flows in rivers depend fundamentally on the change in the volume and time precipitation, and some cases of the snow melting.

Runoff depending on changes in precipitation is noted to decrease in Central America and Europe. Risks of droughts are projected for subtropical, low and midlatitudes, and floods for tropical and high

latitudes. Some results from GCMs reveal that climate change will affect directly on the water resources systems, indicating that in the next 50 years the water stress on land areas will increase.

7.5 Climate Change Impacts on Water Resources Management

Global water demand is increasing due to population growth, and regionally, substantial changes in irrigation water demand are expected as a result of climate change [11]. Climate change affects the management and operation of existing water infrastructure such as irrigation systems [12]. This situation is even more complicated if the characteristics and policies of water resources management systems are not adequate to mitigate these changes. Irrigation methods and water management practices also will be affected [18]. The main water resources for agriculture come from base flows in rivers (for dry periods), which will be affected due to the changes in the recharge of groundwater (effect on aquifers in long term).

7.6 Managing Predicted Climate Change Risks

The reality, however, is that climate change is already occurring. There are two ways to manage the risks posed by climate change: mitigation and adaptation. Mitigation of GHGs aims to slow or reverse the pace of climate change. It implies the human measures, structural and nonstructural, undertaken to limit the adverse impacts of climate change by reducing the levels of GHGs in the atmosphere [4]. This is accomplished through the development of appropriate technology for reducing emissions and/or capturing them at their source. Examples of mitigation measures include energy efficiency, promotion of renewable energy sources, and carbon trading.

Adaptation refers to all climate change responses that may be used to reduce vulnerability to climate change impacts. It is achieved through actions designed to take advantage of new opportunities that may arise as a result of climate change [19]. Therefore, adaptation describes a set of responses to actual and potential impacts of climate change in order to moderate the harm or take advantage of the opportunities that climate change may bring.

This section has generally reviewed the possible effects of climate change on the water resource base in a global context. It highlighted the two approaches toward climate change risk reduction: mitigation and adaptation. In the following sections, an assessment is done on the likely hydrological effects of climate change in the Nyanyadzi River catchment is Zimbabwe.

7.7 Nyanyadzi River Catchment Water Resources System

As was discussed in the preceding sections, the potential effect of climate change on the precipitation and runoff would affect directly the water resources availability in region. Water for agriculture, population, etc., depends on the hydrological cycle. This section focuses on Nyanyadzi River catchment as a case study. Population in the catchment stands at 19,366.

Nyanyadzi River (Figure 7.1) flows westward from its source in the eastern highlands of Chimanimani District at an altitude of 1500 m and high annual rainfall of 1200 mm on fertile soils. The river and its main tributaries, the Shinja, Biriwiri, and Makwe streams, cover a catchment area of 458 km^2 [13]. On its way westward, it flows through farmlands before it enters the Odzi River at an altitude of 530 m where vegetation is sparse, soils are less fertile, annual rainfall is less than 400 mm, and temperatures are more than 21°C/annum.

The catchment is characterized by a moderate climate. Rainfall is highly seasonal and unevenly distributed spatially, with about 95% occurring between October and April, typically concentrated in a number of isolated rain days and in isolated locations. It also varies significantly from year to year. Annual rainfall is 635 mm/year, mean annual temperature is 15°C, and potential or pan evaporation rate is 2000 mm/year. Flooding and droughts are major water-related impacts of climate change in the catchment [5,14].

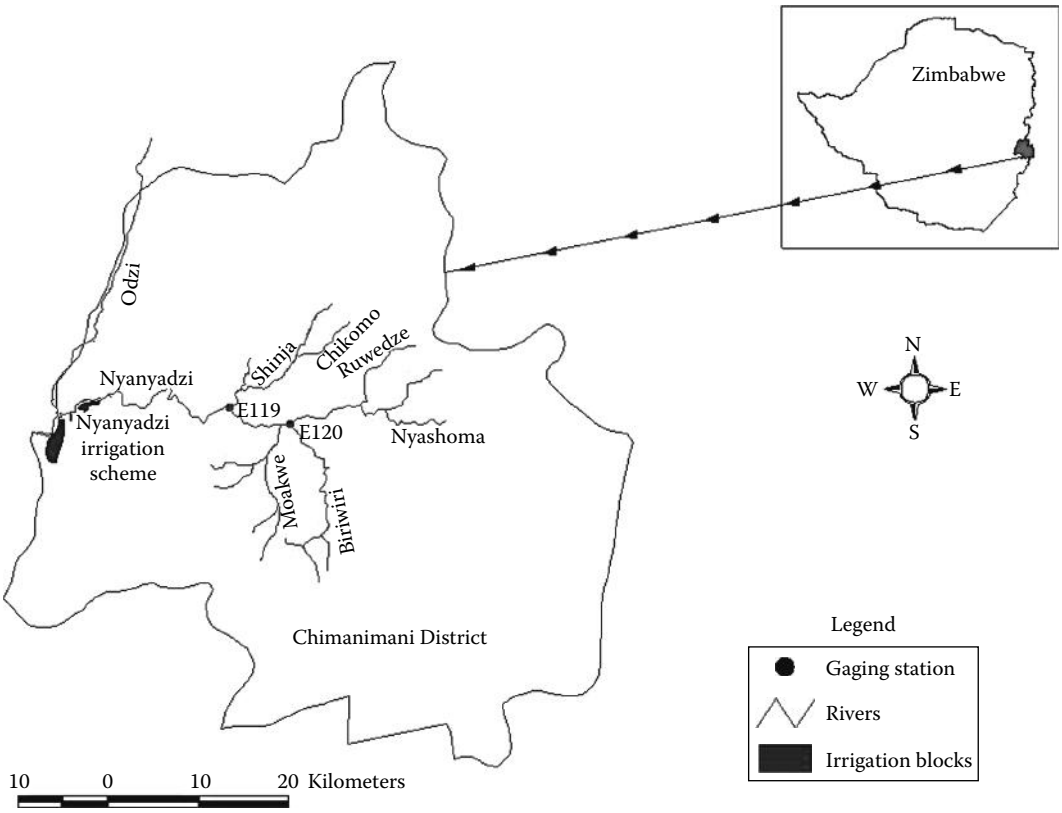

FIGURE 7.1 Nyanyadzi River catchment in Chimanimani District.

Before Nyanyadzi River enters the Odzi River, a 414 ha smallholder Nyanyadzi irrigation scheme taps away water by means of a permanent weir. The scheme was established by the government in 1934 and has been government managed ever since. About 578 plot holders occupy the scheme. Cropping pattern comprises beans, tomatoes, vegetables, maize, and wheat [13].

7.8 Climate Change Scenarios

The impacts of climate change on hydrology are usually estimated by defining scenarios for changes in climate inputs. A scenario is an internally consistent set of climatological relationships and assumptions of radiative forcing, and plausible outline of a possible future state of the world or description of its future development [19]. Climate scenarios often make use of climate projections by manipulating model outputs and combining them with observed climate data. The IPCC Special Report on Emissions Scenarios (SRES) storylines, which form the basis of many studies of projected climate change on water resources, consider a range of plausible changes in population and economic activity over the twenty-first century [7].

In this analysis, the CSIRO model version 3.5 and two GHG emission scenarios, namely, the A2a (worst case) and B2a (reduced emissions), from the scenario family in the IPCC SRES were used. The scenarios assume less globalization or cooperation and global population to increase until 2100, reaching 10.4 billion (B2) and 15 billion (A2) by the end of the century. The scenario A family represents a business as usual future world with growth-focused policy objectives, while the B family represents ecofriendly policies resulting in reduced emissions. The two scenarios are more geopolitically divided, representing regional-oriented growth [8,19].

7.9 Baseline Climate and Hydrological Data

In climate change impacts assessment, a period of 30 years of observed meteorological data is used to define a current climate baseline. The WMO and IPCC define and recommend that the 1961–1990 period is the 30-year normal period for use as a baseline period in climate change impact studies [19]. Such a long period of continuous record of historical climate data is widely used for creating a baseline and is likely to contain wet, dry, warm, and cool periods. It also contains significant temperature and precipitation global trends and a more extensive network of observing stations to record more variables than earlier periods. It represents climate before significant changes attributable to human activity were detected. The period 1961–1990 was chosen as the baseline because it is the current WMO normal period and is recommended by IPCC as a historical period for climate change impact and adaptation assessment [9–11]. Three points in time, 2020, 2050, and 2080, were used in the analysis.

The average monthly temperature, rainfall, and evapotranspiration for the 1961–1990 baseline period are 22.5°C, 870.8 mm, and 122.5 mm, respectively. Table 7.1 shows climate data for the baseline meteorological years. A meteorological year in Zimbabwe starts from July 1 and ends on June 30 of the following year.

The mean monthly runoff for the baseline period is 3168×10^3 m^3. On average, the highest rainfall was received in February while September received the lowest. Table 7.2 shows river flow data for the 1961–1990 water hydrological years. A hydrological year in Zimbabwe starts from October 1 and ends on September 30 of the following year.

7.10 Projected Hydroclimatological Changes

7.10.1 Temperature Changes

The mean monthly temperature is expected to increase by 1.5°C (i.e., 6.7%) under the two climate change scenarios from 2020 to 2080. The A2a scenario will realize the highest increase of 2.9°C (12.8%) in 2080 and the lowest figure of 0.5°C (2.2%) in 2020. January is expected to experience the lowest temperature increase of 0.8°C (3.7%) while June will experience the highest, 2.1°C (14.8%). Figure 7.2 shows the predicted changes in monthly temperature for the two climate change scenarios.

TABLE 7.1 Baseline Climate Data for the Nyanyadzi River Catchment from 1961 to 1990

Month	T (°C)	P (mm)	ET (mm)
July	14.1	7.3	72
August	16.1	9.3	102
September	19.0	11.0	141
October	21.6	35.0	178
November	21.7	96.3	159
December	21.7	174.7	151
January	21.6	178.0	153
February	21.1	164.0	126
March	20.7	104.0	134
April	19.3	41.3	106
May	16.7	16.3	83
June	14.2	12.7	65
Average	22.5	870.8	122.5

TABLE 7.2 Baseline Hydrological Data for the Nyanyadzi River Catchment (1961–1990)

Month	Runoff (10^3 m^3)
October	1166.7
November	1733.9
December	4108.8
January	5054.6
February	7960.4
March	8614.6
April	4655.9
May	3146.4
June	2195.0
July	1826.4
August	1321.6
September	1037.4
Average	3169.2

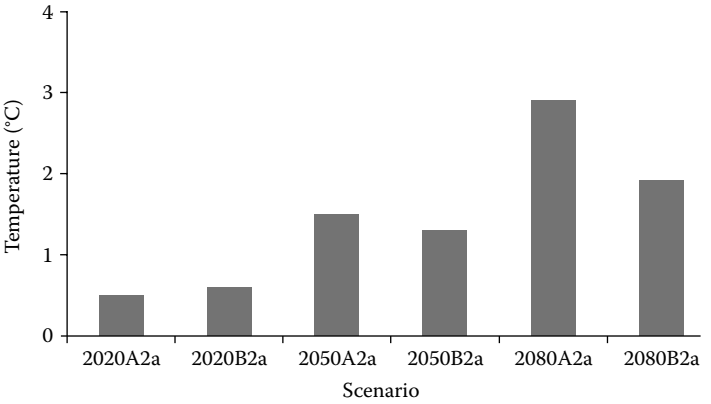

FIGURE 7.2 Changes of mean monthly temperature relative to 1961–1990 baseline.

7.10.2 Precipitation Changes

The mean monthly precipitation is expected to increase by 7.2 mm (10.2%) with climate change. Highest precipitation increase of 8.4 mm (11.9%) is expected under the 2080B2a scenario while the 2080A2 predicts the lowest increase of 1.6 mm (2.3%). April is expected to have the highest increase of 8.2 mm (19.9%). However, July, August, September, and November will have a decrease in precipitation with October having the highest decrease of 11.2 mm (32%). Figure 7.3 shows the predicted changes of rainfall in two climate change scenarios: A2a and B2a in the 2020, 2050, and 2080 periods.

7.10.3 Changes in Potential Evapotranspiration

A linear relationship was established between mean monthly temperature and potential evapotranspiration (PET) using baseline data. Thus, PET data for the 2020, 2050, and 2080 periods were estimated projecting CSIRO temperature data. With climate change, mean monthly PET is projected to increase by 14.9 mm (12.2%) for both scenarios and all time points, 2020, 2050, and 2080. Between the two

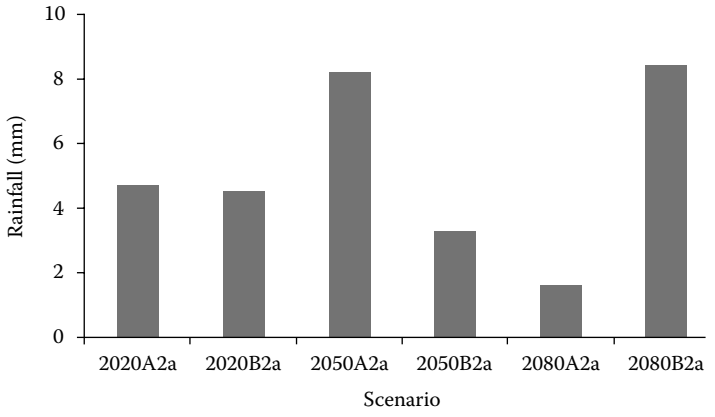

FIGURE 7.3 Changes of mean monthly rainfall relative to 1961–1990 baseline.

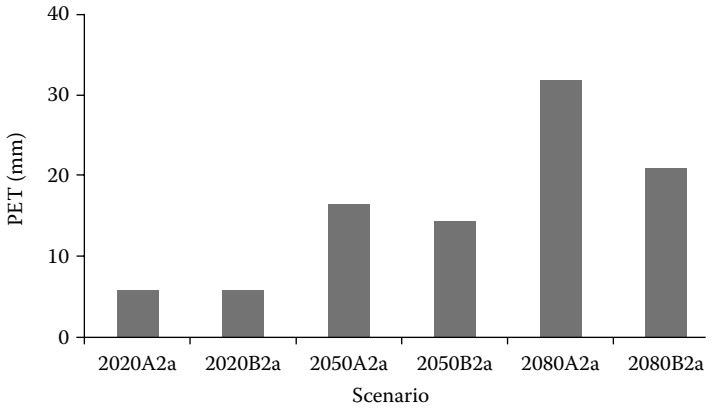

FIGURE 7.4 Changes of mean monthly potential evapotranspiration relative to 1961–1990 baseline.

scenarios, A2a predicts a higher increase of 31.8 mm (26%) in 2080 primarily because of the severest warming effects brought about by the 2080A2a (see Section 7.10.1) and therefore raise in PET most rapidly. The lowest mean monthly increase of 5.7 mm (4.7%) is expected under the 2020A2a scenario. June will experience the highest increase of 41.4%, while October is expected to have a largest decrease of 3.9% from the baseline. Figure 7.4 shows mean monthly PET changes under the two climate change scenarios.

7.10.4 River Flow Changes

Predicted changes in rainfall under the CSIRO model were used to estimate runoff using the established rainfall–runoff relationship from baseline data. A linear relationship was established between rainfall and runoff using the baseline data. Thus, runoff data for the 2020, 2050, and 2080 periods were estimated from the established relationship using projected rainfall data from the CSIRO model. With climate change, runoff was predicted to decrease for both scenarios. On average, monthly runoff will decrease by 550×10^3 m^3 representing a change of 15.4% change. Highest change of 608.3×10^3 m^3 is expected under the 2080A2a while the lowest of 13.9% or 496.6×10^3 m^3 is expected under the 2080B2a. From February to September, runoff is expected to decrease with September experiencing the largest decline of 87.5%. However, the months October to January are expected to have an increase in runoff, with

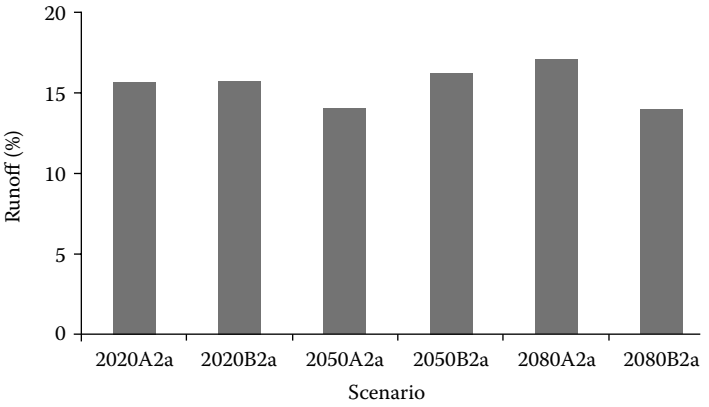

FIGURE 7.5 Percentage changes in runoff relative to the 1961–1990 baseline.

October experiencing the highest increase of 85.3%. Figure 7.5 shows the predicted changes in runoff for the two climate change scenarios, A2a and B2a, for the 2020, 2050, and 2080 periods.

7.10.5 Changes in Water Resources Availability

The major water uses are for irrigation, domestic, and the environmental requirements. Irrigation requires 1026.4 m^3/month, while the environment flow requirements are 10% of the mean annual flow [13]. With the projected climate change, the availability of water resources availability will decrease by about 15.4%. This has adverse implications on irrigation water supply, environmental water requirements, domestic water use, watering animals, and other uses. Table 7.3 shows the changes in water resources availability under climate change impacts.

7.11 Summary and Conclusions

Global warming, due to the enhanced greenhouse effect, is likely to have significant effects on the hydrological cycle. The hydrological cycle will be intensified, with more evaporation and more precipitation, but the extra precipitation will be unequally distributed around the globe. Some parts of the world may experience significant reductions in precipitation, or major alterations in the timing of wet and dry seasons.

Assessing the implications of climate change on hydrology is essential for planning future water resources activities on a regional scale. This chapter analyzed the potential effects of climate change on the hydrology and water resources in general and the Nyanyadzi River catchment in eastern Zimbabwe in particular. The impacts of climate change on the hydrology of the Nyanyadzi River catchment were examined using the CSIRO climate model projections, two SRES emission scenarios (A2a and B2a), three points in time (2020, 2050, and 2080), and the 1961–1990 baseline climate data. Both scenarios predict increases in mean monthly temperature, rainfall, and evapotranspiration.

TABLE 7.3 Changes in Monthly Water Resources Availability (10^3 m^3) for Different Uses

Scenario	Baseline	2020A2a	2020B2a	2050A2a	2050B2a	2080A2a	2080B2a
Runoff	3169.2	2612.8	2609.7	2669.4	2589.6	2560.9	2672.6
Environment	316.9	261.3	261.0	266.9	259.0	256.1	267.3
Irrigation	1026.4	1026.4	1026.4	1026.4	1026.4	1026.4	1026.4
Others	1852.8	1325.1	1322.3	1376.0	1304.2	1278.4	1378.9

Significant reductions of runoff are expected for all time periods under the two climate change scenarios. Changes in river flows the availability of water use in the catchment. Thus, sound water management strategies need to be put in place.

References

1. Arnell, N.W. 1999. Climate change and global water resources. *Global Environmental Change* 9: 531–549.
2. Arnell, N.W. 2004. Climate change and global water resources: SRES emission and socio-economic scenarios. *Global Environmental Change* 14: 31–52.
3. Arnell, N. and Liu, C. 2001. Hydrology and water resources, Chapter 4. In: Mc Carthy, J.J., Canziani, O.F., Leary, N.A., Dokken, D.J., and White, K.S. (eds.), *Climate Change 2001: Impacts, Adaptation and Vulnerability*. Contribution of Working Group II to the third assessment report of the Intergovernmental Panel on climate change. Cambridge University Press, Cambridge, U.K., pp. 192–233.
4. Beck, L. and Bernauer, T. 2011. How will combined changes in water demand and climate affect water availability in the Zambezi River basin? *Global Environmental Change* 21: 1061–1072.
5. Bolding, A., Manzungu, E., and van der Zaag, P. 1996. Farmer initiated irrigation furrows: Observations from the Eastern Highlands. In: Manzungu, E. and van der Zaag, P. (eds.), *The Practice of Smallholder Irrigation: Case Studies from Zimbabwe*. University of Zimbabwe Publications, Harare, Zimbabwe, pp. 191–218.
6. IPCC. 1995. *Climate Change 1995: Impacts, Adaptations and Mitigation of Climate Change* Contribution of Working Group II to the third assessment report of the Intergovernmental Panel on Climate Change. Cambridge University Press, Cambridge, U.K.
7. IPCC. 2000. Emissions scenarios 2000: Special report of the Intergovernmental Panel on Climate Change. Cambridge University Press, Cambridge, U.K.
8. IPCC. 2001. *Climate Change 2001: The Scientific Basis*. Contribution of Working Group I to the third assessment report of the Intergovernmental Panel on Climate Change. Cambridge University Press, Cambridge, U.K.
9. IPCC. 2007. *Climate Change 2007: Impacts Adaptation and Vulnerability*. Contribution of Working Group II to the fourth assessment report of the Intergovernmental Panel on Climate Change. Cambridge University Press, Cambridge, U.K.
10. IPCC. 2007. *Climate Change 2007: The Physical Science Basis*. Contribution of Working Group I to the fourth assessment report of the Intergovernmental Panel on Climate Change. Cambridge University Press, Cambridge, U.K.
11. IPCC. 2012. *Managing the Risks of Extreme Events and Disasters to Advance Climate Change Adaptation*. Cambridge University Press, Cambridge, U.K.
12. Kaczmarek, Z., Napiórkowski, J., and Strzepek, K. 1996. Climate change impacts on the water supply system in the Warta River catchment, Poland. *International Journal of Water Resources Development* 12: 165–180.
13. Mujere, N. 2011. *River Flow Variations and Crop Yields at Nyanyadzi Irrigation Scheme*. Lambert Academic Publishing, Saarbrücken, Germany.
14. Neff, R., Chang, H., Knight, C.G., Najjar, R.G., Yarnal, B., and Walker, H.A. 2000. Impact of climate variation and change on Mid-Atlantic Region hydrology and water resources. *Climate Research* 14: 207–218.
15. Pitchford, J.L., Wu, C., Lin, L., Petty, J.T., Thomas, R., Veselka, W.E., Welsch, D., Zegre, N., and Anderson, J.T. 2012. Climate change effects on hydrology and ecology of wetlands in the Mid-Atlantic Highlands. *Wetlands* 31:21–33.
16. UN. 1992. *United Nations Framework Convention on Climate Change*. UN, New York.

17. UNESCO. 2011. The impact of global change on water resources: The response of UNESCO's International Hydrological Programme. UNESCO, Paris, France.
18. WaterAid. 2007. Climate change and water resources. WaterAid, London, U.K.
19. WMO/IPCC/UNEP. 2000. IPCC special report on emission scenarios: Summary for policy markers. IPCC, England, U.K.

8

Climate Change: Uncertainty, Impact, and Adaptation

Mohammad Reza Farzaneh
Tarbiat Modares University

Saeid Eslamian
Isfahan University of Technology

Seyed Jalal E. Mirnezami
Tarbiat Modares University

AUTHORS

Mohammad Reza Farzaneh was born in Iran in March 1986. He is currently a PhD student of Water Resources in Tarbiat Modarres University, Tehran, Iran. His scientific experiences include being author and coauthor for two international handbooks, adviser for six master theses, more than 40 under-review and published papers in conferences and journals; collaboration in national and international projects such as study of climate change impact on African water resources; teaching climate change, GIS, hydrology, and water resources; and registration of four inventions.

Saeid Eslamian received his PhD from the University of New South Wales, Australia, with Professor David Pilgrim. He was a visiting professor in Princeton University, USA, and ETH Zurich, Switzerland. He is currently an associate professor of hydrology in Isfahan University of Technology. He is founder and chief editor of *Journal of Flood Engineering* and *International Journal of Hydrology Science and Technology*. He has published more than 200 publications mainly in statistical and environmental hydrology and hydrometeorology.

Seyed Jalal E. Mirnezami was born in July 1987 in Iran. He received his BS degree in 2009 in agricultural-water engineering from University of Tehran, Iran. Jalal studied water resources engineering in the same university and received his MSc in 2011. During this period, he studied modeling water resources and created a model for optimizing allocation of water in river basins. Following a desire to work on

sustainable development and IWRM implications in water conflict through adaptive management, he is now a PhD student at Tarbiat Modares University, Iran.

PREFACE

Climate change is one of the most important topics that has lots of different consequences on several environmental phenomena such as water resources. In this chapter, some basic concepts of climate change, the Atmosphere-Ocean General Circulation Models (AOGCM), emission scenarios, and down scaling methods are presented. After that, the consequences of climate change and adaption are reviewed. Finally, a case study on the evaluation of climate change effects on water resources and preparation for adaption is presented.

8.1 Introduction

In recent decades, special increase in greenhouse gases has led to the disturbance of climatic equilibrium of the Earth, which is referred to as the "climate change" phenomenon [9,14]. Research disclosed that this phenomenon may have negative effects on water resources, agriculture, environment, sanitation, industry, and economy. Because of this, climate change has been considered to be important and the ways to face with the associated dangers and even the protection of water resources, agriculture, and environmental resources against its hazards have become a common issue around the world. Considering scarcity as a victim of climate change, assessing its variation in coming years will contribute to a great extent to overcome problems such as droughts, flash floods, evaporation alteration, etc. The main purpose of this chapter is to introduce IPCC, climatic, and non-climatic scenarios and their roles in the Atmosphere-Ocean General Circulation Models (AOGCM) simulations. Also, some international databases will be introduced in order to receive these models outputs. Downscaling and quality improvement processes would be also explained as alternatives to convert large-scale outputs into regional data that can be useful for further computations. Preparing useful data is not the end but it is a starting point for climate change studies. The three main so-called main parts will remain that should be passed one after another, which are impact assessment, adaptation to climate change, and uncertainty analysis, and would be explained in this chapter.

8.2 Climate Change Concept

Atmosphere, cryosphere, biosphere, and hydrosphere form the main parts of Earth's climate. Earth's atmosphere encompasses various gases, which lead, to absorption, diffusion, and reflection of different wavelengths and control of atmosphere temperature. Greenhouse gases, carbon dioxide (CO_2), methane (CH_4), nitrogen dioxide (N_2O), and halo carbons (CFC), have a great effect on atmosphere surface temperature, due to absorption. Sun light, which is mostly of short length wave, can pass through these gases and reach Earth, but after its reflectance in infrared form because of land surface heat, these gases act as barriers against them due to infrared long length wave; in other words, when wavelengths become longer the greenhouse gases form a barrier and absorb the wave, so they become hotter and the surface temperature of Earth increases. Cryosphere encompasses the ice around the ground surface and therefore plays the main role in the reflection (albedo) of received waves into Earth. Biosphere, through evapotranspiration of plants and sun light reflection, is one of the main producers and consumers of carbon dioxide, which lead to the great effects on climate system energy. Seas, lakes, rivers, and oceans, which constitute hydrosphere have serious impacts on atmosphere carbon dioxide absorption because of huge heat inertia present in them.

Multiple factors may lead to disturbance of governing situation on various parts of Earth and therefore disturbance of these parts too. The proposed factors can be categorized into two main branches, the first stem, from the internal actions of the climate parts and the second forms from external factors such as sun radiation, volcanic activities, and irregular increase in greenhouse gases. The changes that are shaped from internal activities of climate system are called internal climate variability, for example, El-Nino phenomenon is one of this category's members. Sun radiation and volcanic activities are the external factors, which may cause change in climate. After volcanic activities and aerosol occur in the air, light reflection occurs and prevents light transmission to the lower layers of atmosphere. Another classification is based on the source of these factors, and branches into of natural and artificial climate variability. Only greenhouse gases increase is artificial in the mentioned factors. Research discloses that after industrial evolution in the mid-eighteenth century, a serious increase in greenhouse gas concentration has happened, especially carbon dioxide, which could be related to the prevalence of fossil fuel consumption and spread of industries. Changes in greenhouse gas concentration, causes climate changes, because the more greenhouse gases, the more absorbed heat would occur [3].

8.3 Scenarios in Future Periods

As mentioned before, any change in greenhouse gas concentration will lead to a disturbance of equilibrium in the climate system Earth. But how much of these gases are produced by human beings and consequently what is likely to happen, is not determined yet. Therefore, the scenarios have been introduced in an uncertain manner. These are divided into climatic and nonclimatic scenarios, which will be discussed in the following sections.

8.3.1 Nonclimatic Scenarios

Economic activities and consequently the growth of industries and factories and also change in land use are the main reasons for the increase in greenhouse gases. Thus, the socioeconomic situation of future periods is necessary to be analyzed. In general, a nonclimatic scenario encompasses socioeconomic situation and greenhouse gas emission rates, which are so-called emission scenarios.

Intergovernmental Panel on Climate Change (IPCC) is responsible for identifying all aspects of climate change phenomenon and disseminated the first series of emission scenarios in 1992, namely, IS92 (IPCC scenario) (IS92a-IS92f). Through these scenarios, the greenhouse gas content will increase at a constant rate until 2100. In 1996, a newer series of emission scenarios disseminated by the name of SRES (Special Report on Emission Scenarios) in order to update the previous version and as a substitute for IS92. Generally, 40 various SRES subscenarios are produced, which encompass a wide range of population growth rates in future, and also economic and technological factors affecting greenhouse gas emission and suspended dust. Each of these scenarios is categorized in to one of four groups: A1, A2, B1, and B2. The main feature of this category is depicted in Figure 8.1.

In the scenario family of A1, the world is assumed to have a fast economic growth, increasing population growth till the mid-twenty-first century and then a decrease, and also introduction of newer and better technologies. There is more focus on economic issues than on environmental, and aspects seem to be more global and not be local. Considering three kinds of technologies used in the twenty-first century, three branches can be identified for this family, which are different approaches in technological advancement, respectively, intensification of fossil fuel consumption (A1FI), non-fossil fuel consumption (A1T), and finally both fossil and non-fossil fuel consumption.

The main subject of scenario family of A2 is promotion of local population forces with regard to family values and traditions, rapid growth of population, and less dependency on fast economic growth.

Population growth in B1 scenario is similar to A1, but the focus is on the usage of clean energies and a global aspect emphasis is placed on sustainable economy and environment.

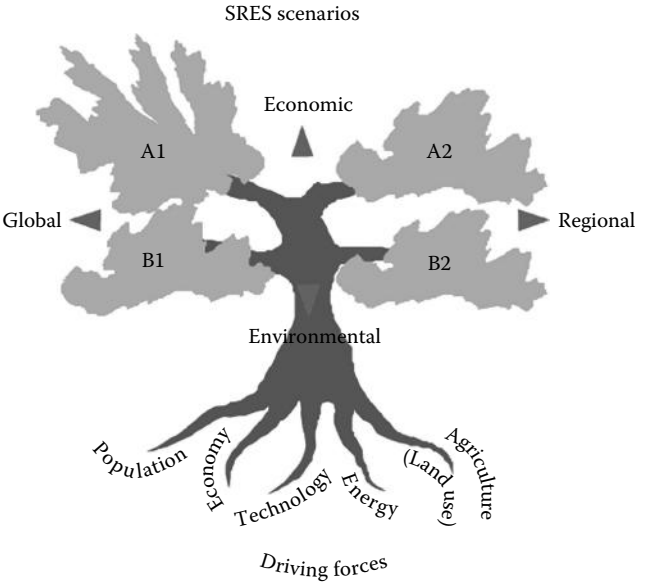

FIGURE 8.1 SRES scenarios.

In B2 family, there is more emphasis on local solutions to economic, social, and environmental development. This is formed in a heterogeneous world that despite having more variety in technologies the rate of alteration in technologies is lower. Main focus is on society innovation in finding local solutions instead of global ones.

Scenario A1FI is the first in producing radiation forces till 2100, and B1 is the least, thus A1FI would have more impact in comparison to B1. The ranking of scenarios on their radiation force generation basis in descending order is A1FI, A2, A1B, B2, A1T, and B1 [17].

8.3.2 Climatic Scenarios

Now it is a common belief for most scientists that greenhouse gases concentration would increase in future and consequently the average surface temperature of Earth would increase too. But the change in climatic variables in regional scale is not explicitly definable. Thus, the alternative to pass this problem is to define possible future climatic scenarios, but we should not forget that a climatic scenario is not a weather prediction [10].

Few approaches are available now to generate climatic scenarios for future periods but the most elementary one is synthetic scenario generation. In this way, climatic variables are arbitrarily increased or decreased [21,25]. For instance, we can decrease rainfalls or increase temperatures to a defined percentage. Despite its easiness, there is no physical basis at the background and therefore the outputs are not acceptable sometimes.

Another approach to achieving this target is the extension of available data trend for future. For this, using statistical methods that present a trend can be extended for future simulation periods [26]. The main weakness in this approach is considering and using experienced trends in previous periods. Research has demonstrated that observatory trends in regional statistical periods might be a part of a long-term internal change cycle in a regional climate system [11,27]. Thus, an extension of a trend for future periods may not imply climate change for that variable in the proposed region.

At present, the most reliable tool for generation of climatic scenarios is three-dimensional coupled AOGCM models [13,16,24]. Although there are some simple models that can imitate the AOGCM models, which will be described in summary in the following sections.

There are two points that should be considered during scenario selection. At first, the climatic variables needed for further simulation in impact assessment models should be defined and checked with the scenarios because there is no single scenario that contains all climatic variables. Second, it is recommended to use as much scenarios that are available and possible, but if you have limitations in time and scenario selection, do not forget to choose scenarios with extreme changes in their variables like temperature and precipitation for the intended region.

8.4 AOGCM Models

The AOGCM models are based on mathematical relations and are solved in a 3D network for the entire Earth's surface. Main processes of the climate system (atmosphere, ocean, Earth surface, membrane ice, and biosphere) are solved in various sub-models separately. Then, all atmosphere and ocean sub-models are coupled and form the AOGCM Model. In sub-models momentum displacement, heat and moisture will be simulated in a large scale too. The horizontal resolution of these models in dry areas is generally about 250 km and this value changes to 1 km in vertical direction. But the resolution differs in oceans and for horizontal and vertical directions; they are respectively 125–250 km and 200–400 m. Despite minimum time scale to solve these relations is 30 min, there are many other physical processes related to the clouds and oceans, which occur in less time intervals and cannot be explicitly solved. In such cases, their average impacts are considered using physical relations of large-scale variables in the model, which is called parameterization. It should be noted that the AOGCM models have been advanced to a great extent in recent decades due to computer technology improvements [10].

AOGCM models imply two kinds of climatic variables simulations. In the first, greenhouse gases concentration is set to the observed values of year the 1860 as a constant quantity. This type of simulations, which is called control run, executes simulations for a 1000-year period. Obviously, due to constant values of external factors like greenhouse emissions and sun radiation, only internal climatic factors play the main role and the outputs will depict the impacts of internal forces on the internal variability of climate system. Assuming no change for external factors in the future, this simulation would imply natural climate variability.

To assess past Earth's climate, in the other type, the observed data of greenhouse emissions, sun radiation fluctuations, and produced aerosols from volcanic activities till 2000 are inserted as input time series into the model in monthly scale. A comparison between these model outputs and observed mean annual and seasonal temperature and precipitation data and also atmospheric phenomena like ENSO, Monsoon, El-Nino, NAO, and exceptional occurrence of extreme temperature and precipitation has proven the validity of these simulations [2,12,19,23]. But this simulation is for the past period; for simulation of future periods, it is needed to introduce conditions of greenhouse emissions in the future to the AOGCM model. Therefore, emission scenarios (which are generally defined till 2100) are converted into concentrations and finally radiation forces using other models and then inserted into the AOGCM model. Finally, a time series of climatic variables would be produced for the future period till 2100.

8.5 Introduction of the AOGCM Databases

One of the limitations related to the project that is associated with change in the climate is accessing toward the output of the AOGCM models. Sensitivity has been decreased during the time and increase of databases related to climate meaningfully. Despite the widespread development of such databases, an attempt is made here to point out the popular databases briefly.

8.5.1 IPCC

The Intergovernmental Panel on Climate Change (IPCC) which was instituted in 1988 by the World Meteorological Organization and United Nation Environmental Program is responsible for the identification of

various aspects of climate change. IPCC released the first series of emission scenarios in 1992, namely IS92. Through scenarios, greenhouse gas measure is increasing with a constant rate up to 2100. In 1996, the new series of emission scenarios called the SRES was released, which contains 40 subscenarios. In 1998, a committee was set up to gather the AOGCM output scenarios, namely Data Distribution Center.

8.5.2 CCCSN

Canadian Climate Change Scenarios Network (CCCSN) was established in 2005 with support from Environment Canada, the Climate Change Adaptation Fund, and University of Regina, but since January 2012 it is only being supported by Environment Canada. CCCSN conducts climate change impact and adaptation, and also research in climate change. This database presents various downscaling software and a lot of information about major and minor concepts of climate change. But the main support of this site is providing the AOGCM model's outputs for researchers (Table 8.1).

8.5.3 PCMDI

In 1989, Program for Climate Model Diagnosis and Intercomparison (PCMDI) was established at the Lawrence Livermore National Laboratory to develop improved methods and tools for comparison of GCMs simulations. In this website, the AOGCM outputs for twentieth, twenty-first, and twenty-second centuries is prepared. Future data of twenty-first and twenty-second centuries will be calculated based on the IPCC request for various scenarios. The scientific initiatives are other interesting part of this website.

8.5.4 CRU

The Climatic Research Unit (CRU) has gathered various datasets about climate change phenomenon. CRU database includes two types of data. The first is with 2° resolution and the latter is with 0.5° resolution. Also, two sets of data are available on this website. The first set called HadCRUT3 is the surface land temperature on a 0.5×0.5 grid from the year 1850 for 4349 weather stations around the world [4]. The next set is the rainfall data on a $2.5° \times 3.75°$ grid [8]. Although the rainfall data are in a larger cell size, it also has some gaps in the northern part of North America, middle east Asia, and Africa. In spite of this, this database is a popular and user-friendly one.

8.5.5 TYN

The Tyndall Centre (TYN) is composed of many advisory and management teams in order to enhance a global qualified source for climate change research. It seeks to be a reliable source for long-term strategic climatic policies around the globe.

TABLE 8.1 AOGCM Databases

ID	Sign	Name	Website
1	IPCC	Intergovernmental Panel on Climate Change	IPCC.ch
2	CCCSN	Canadian Climate Change Scenarios Network	www.cccsn.ec.gc.ca
3	PCMDI	Program for Climate Model Diagnosis and Intercomparison	www.pcmdi.llnl.gov/publications/index.php
4	CRU	Climatic Research Unit	www.cru.uea.ac.uk
5	TYN	Tyndall Centre for Climate Change Research	www.tyndall.ac.uk

8.6 Downscaling

The process of downscaling will be done in their large computational cell accuracy after receiving the output of the AOGCM models. There are different methods for downscaling climate impact under the effect of climate change, both dynamic and statistical methods. These methods are explained briefly by Fowler et al. [7].

Dynamic methods are executed using the numerical models. In these methods, the resolution is higher, but they are much more expensive and harder than statistical ones. The main approach in statistical methods is relating some predictants with predictors. The predictants are downscaled parameters and the predictors are the outputs of the AOGCM models that are calculated in large-scale computational size. Generally, the statistical methods are more popular than dynamic ones, because setting up numerical models needs too much time and expense. Statistical methods are sorted in three main branches, namely, weather classification, weather generator, and regression models. In each of these methods, the predictors and predictants are related using various formulations and mechanisms. Here, because of limitations we do not explain each one separately, but you may refer to multiple scientific sources to find out more about them.

8.7 Climate Change Uncertainty

An important point in the studies of climate change is uncertainty. Because of different sources of uncertainty in different processes related to climate change, considering this issue causes a mistake in the final output. The most important steps in uncertainty is recognizing its different sources. In this part, main sources have been presented:

- AOGCM simulation's uncertainty in regional level
  - Assessment of climatic variables in regional level shows different simulation results of the same climatic variables because of short-scale event parameterization.
- Downscaling uncertainty
  - Multiple ways are devise for downscaling, which have both special benefits and defections. Each of these approaches results in different outputs, so their outputs are uncertain.
- Greenhouse gas emissions scenarios uncertainty
  - Talking about future is definitely uncertain, because using a specific measure for greenhouse gas emission in the further, especially for such a long period (100 years), is not deterministic.
- The uncertainty related to the sensitivity of the different AOGCM models to the same radiation force
  - Different models convert the radiation into heat using various formulations, thus a source of uncertainty is the sensitivity of the models in converting the radiation into heat. Based on IPCC reports, the amount of increase in the temperature of the atmosphere is estimated to be 2°C–5.1°C based on the various AOGCM models outputs.
- Uncertainty in conversion of greenhouse gases to atmospheric concentrations and radial force
  - In order to present various emission scenarios to the AOGCM models, it is needed to firstly convert the amount of the gas into the atmospheric concentration and then calculate the radiation force. Since there exists a lack of knowledge about these processes, the AOGCM model outputs would be accompanies with related uncertainty.

8.8 Impact Assessment

Climate change has a great effect on the various aspects of nature, thus the main objective in climate change is the identification and assessment of possible future conditions in the nature. For this, many researches have been implemented in order to analyze climate change impact on hydrological cycle, water balance in river basin, and extreme events like droughts and floods.

Most researches have been focused on hydrological cycle, and realizing this can help so much in the evaluation of various water aspects in nature, because the components of hydrological cycle form the situation of the basin. But floods are less focused as the purpose for climate change studies, because the outputs of GCM models are usually monthly, which is not enough to study floods. Although the available data from the models are not seemingly useful for climate change impact on floods, we can find various studies in this field.

Precipitation as the basic component in hydrological cycle is under direct effect of climate change, thus it should be clearly studied for impact assessment. A decrease in precipitation consequently results in ground and surface water recharge decrease and also lower soil moisture. It should be noted that not only water resources are under the great effect of climate change, but also it changes water consumption ratio greatly. Agricultural demand as the largest part in water demands in this century is mostly affected by climatic variables. Plant growth period, transpiration, and irrigation demand are under direct relation with precipitation, temperature, and radiation. Limitations formed by climate change may result in stresses on economic, social, and environmental aspects of a region, thus impact assessment can obviously contribute to a great extent to better management of a region in order to lessen bad situations. In other words, the climate change impact assessment helps in identifying probable future issues and even threats to human and nature; thus, it can be executed in a general or specified condition.

Inputs for impact assessment studies are scenarios, which might be generated from artificial assumptions in change of climatic variables, or even outputs of the GCM models. The main processors are simulators, which help us in the assessment of scenarios utilities, but obviously the type and precision of these models depend heavily on the available data and requested precision. In this area, economic, social, and environmental simulation models can be used.

The most important point in climate change impact assessment problems is misunderstanding in climate change stimuli's. Change in hydrological cycle components, water balance, or increase in occurrence of extreme events cannot be interpreted only by greenhouse gases irregular emission, and it might be shaped from land use or water management strategy alteration. For instance, drought is heavily affected by water management strategies and it should not be evaluated only as a result of climate change. In addition, the climate change effect is much weaker than those of economic and technological changes.

8.9 Adaptation

As discussed before, the main objective in the climate change problem is its impact assessment and finally searching for the way out of unwanted future conditions that are likely to happen. On this basis, in the present section, adaptation as an anticipatory method for preparing to overcome probable future issues of climate change would be explained specifically. Another approach, which acts in a reactive manner, is mitigation. In other words, adaptation and mitigation are two different methods that can be used future situations; the first is an anticipatory and the second is a reactive one, and adaptation makes the system prepared to overcome the present situation in order to lessen the burden in the future.

Various definitions could be found in the give references, which are given below

1. Adaptation to climate change is a process that stakeholder groups try to decrease unwilling health and welfare issues and to increase advantages from it [5].
2. Adaptation is any course of action that is implemented in order to adapt with harmful predictions of climate change and improve its disadvantages [22].
3. Burton et al. [5] defines adaptation as responses to climate change in order to decrease vulnerability.
4. Adaptation is a response to climate change for maintaining possibility of life, with maximizing benefits and minimizing damages [20].

It is shown that adaptation is any response and reaction to future changes, which can be implemented to remove damages or improvement of willing outputs of climate change. Due to multiple trade-offs,

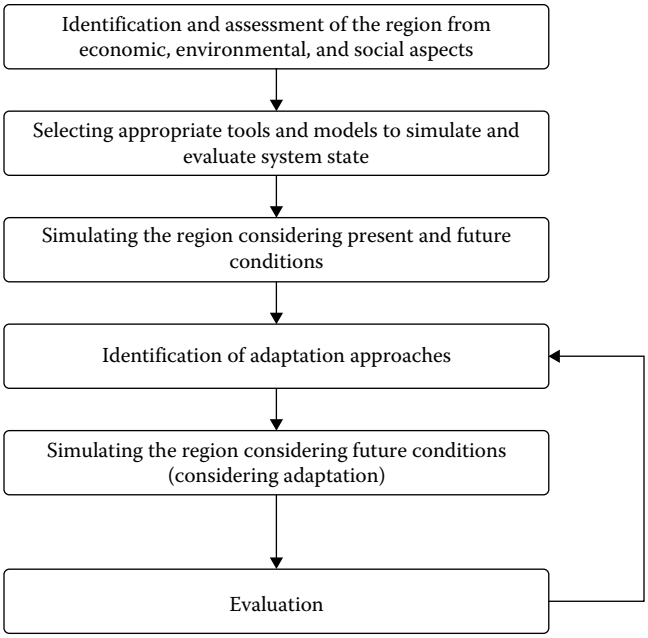

FIGURE 8.2 Adaptation flowchart diagram.

adaptation is a hard activity, but through participation of various stakeholders it becomes much easier and better. Stakeholders in climate change problem may vary from public to governors and their participation would contribute very much to problem solving and adaptation (Figure 8.2).

System and its boundary are the first things that should be evaluated, in such way that it could be concluded that adaptation is done for what. System characteristics are other significant things in this stage that needed to be analyzed. The most important characteristics are sensitivity, vulnerability and adaptability. Vulnerability refers to the amount of exposure of a system (nature or human being) to danger by climate change outputs. Adaptability can be defined as the potential of a system to encounter possible damages and finally sensitivity is the rate of response of the system to the variability of climate variables.

This is the first step, and now it is needed to select appropriate tools or models for assessment. This step depends mostly on the requested precision and also on available data, thus it might vary from a simple model to some complicated models in various aspects such as economic, environmental, and social.

Simulation of the present state of the model can help a lot in identifying the current situation of the system, the potentials, and facilities to incorporate adaptation. Now it could be considered as the reference for other simulations, and comparisons between this simulation and the others would help to understand what the impacts of various scenarios are and the performance of various management strategies could be assessed more descriptively.

Now it is the time for doing the major part of the adaptation process, which is the identification and selection of adaptation approaches, which remove the negative effects of climate change in the future. No specific approach exists that fit, to all cases, thus, considering various aspects of each case and the availability of potentials we can select an approach for the adaptation. Sometimes, it might be needed to innovate new approaches for the specific case and solve the problem with the least availabilities. But, in general, most adaptive approaches are made through modification of current measures. The more awareness about the case and its realities, the more appropriate approaches would be presented. Structural and nonstructural potentials of the system are of great significance and should be studied

carefully before any approach is selected of created. Many studies have been conducted in this area, but here a classification presented by Feenstra et al. [6] is given

1. Bear losses
   Considered as a base action for comparing various adaptation methods. In the case of fronting to climate change, no action is done, only tolerating bad situations is selected as an approach to battle with undesirable climate change impacts.
2. Share losses
   This is another kind of the former method, and through multiple functions, the impact of climate change is spread over greater society, instead of its acceptance only by the most vulnerable part in the society.
3. Modify the threat
   Modifying the threat includes actions that reduce future threat, like reducing greenhouse gas emission into the atmosphere. Unlikely in some classifications this method is called mitigation and is placed in another class than adaptation methods.
4. Prevent effects
   In this class, expected effects are prevented by doing some actions, like using more fertilizers in agricultural sites that would receive less rainfall, and preventing the sites from loss in biomass production.
5. Change use
   If conditions do not support any more for some special uses, changing the usage would help a lot in adaptation to climate change. For example, usage of less water consumer plants is a change use action.
6. Change location
   In addition to usage change, changing location would also help in the reduction of undesirable aspects of climate change.
7. Research
   Research can play the main role in adaptation is considered as a single class of adaptation measures. Getting familiar to new technologies and latest researches would have a great effect on adaptation.
8. Educate, inform, and encourage behavioral change
   Higher education and knowledge will serve as the last class in adaptation actions. Unfortunately this type of adaptation is forgotten in most researches and projects, but it should be noted that higher knowledge would result in behavioral change, which can contribute too much to the adaptation process.

Selection of these approaches needs a case-based study. Some other useful adaptation measures can be found in Mathews [15]. Based on his paper, seven major steps can be imagined in order to reduce global carbon dioxide emissions by 70% by 2050. These steps are

1. A global carbon pricing regime
   An effective and market-driven system to reduce carbon emissions by introducing taxes.
2. Global satellite monitoring of greenhouse gas emission
   To control the product of greenhouse gas emissions to ensure that countries are adopting emission rules regulated for them.
3. Compensating developing countries for preserving rainforest
   Conserving rainforests in developing countries as solution to promote carbon dioxide sinks.
4. Creation of a global market for responsible biofuels
   As a way to set conditions for developing biofuel usage instead of fossil fuel use.
5. Creation and furtherance of markets for renewable electricity.
   Providing better situations for creation of electricity energy generation from renewable energy sources like solar and wind energy.

6. A global moratorium on building new coal-fired power stations
   An initiative at global level to preventing construction of more coal-fired power stations.
7. Creation of global incentives for developing countries that are moving to adopt nonfossil-fuel industrial pathways.

Encouraging developing countries by adopting various international acts to use fossil fuels lesser after selection of adaptation approach, its performance in reduction of negative effects should be assessed. The only alternative is simulation of the proposed conditions in the form of a scenario using various models.

Evaluation is the last step and affects directly on the final result of adaptation. Any mistake may cause misleading approaches that change the climate system destination into a dangerous position. Iteration is a common method in finding best management practices. In this way, various adaptation approaches would be assessed using simulation models. Evaluation and finally selection of best approaches can be implemented by sensitivity analysis, scenario analysis, and multicriteria analysis. Using these methods, some ranked approaches will be generated that are the most suitable ones for the executive managers. Ranking processes encompass evaluation of different aspects of each scenario and adaptation action, thus, in addition to availability of a set of suitable practices, learning process would also occur.

It is worthy to note that the described structure is so general and at execution time it may change in various aspects, but rationally it forms the main path to climate change adaptation goal. For more details, refer to the proposed adaptation approach in *Climate Change in Contrasting River Basins* [1]. In this book, an innovative approach called "Adaptation Methodology for River Basins" is introduced for various river basins around the world. Based on this methodology, four main aspects, namely, agricultural water, drinking water, industrial water, and ecological water are considered and these are related with the physical states of river basin water resources system using various indices.

8.10 Case Study

For more illustration, a case study is presented here. North Behesht-abad, Iran, is chosen as the case study (Figure 8.3).

In this study, the aim is to assess climate change impact on future runoff considering various uncertainty sources for near future period (2040–2069). Therefore, the output data of HADCM3 model for scenario A2 are extracted from the IPCC database. As mentioned before, in order to use these data in hydrologic models, we need to downscale the outputs to achieve higher resolution. Here, statistical regression method is applied using the SDSM model. The first step is preparing observation data, measured predictors of NCEP, and simulated predictors of A2 scenario from HADCM3 model. Large-scale data can be downloaded from the CCCSN database for the selected region and after downscaling, verification, and validation will respectively be done.

As shown in Figures 8.4 through 8.6, assessment of average, variance, dry and wet periods of boot strapped rainfall data demonstrates appropriate accuracy of the model in the calculation of rainfall properties in the region. Variance uncertainty range in first months of the year is greater and the greatest values are recorded in the dry periods of warm months in the year because of low precipitation and increase in dry periods. The mentioned range increases in wet periods in the cold months of the year, which is for precipitation increase in such months. Comparison of setup and assessment periods of the model implies high capability of the model in estimating rainfall parameter in future periods. But in minimum and maximum temperature, considering Figure 8.4, most of the variation in observation data is placed in the uncertainty of the model estimation, which demonstrates enough accuracy of downscaling process. Only in minimum temperature data it is observed that the value estimated by the model is partially greater than the observed values, which implies greater fluctuations of downscaled parameters in comparison with measured ones. Also, comparison between setup and assessment periods of the model shows its capability in the estimation of minimum and maximum temperature values in future period.

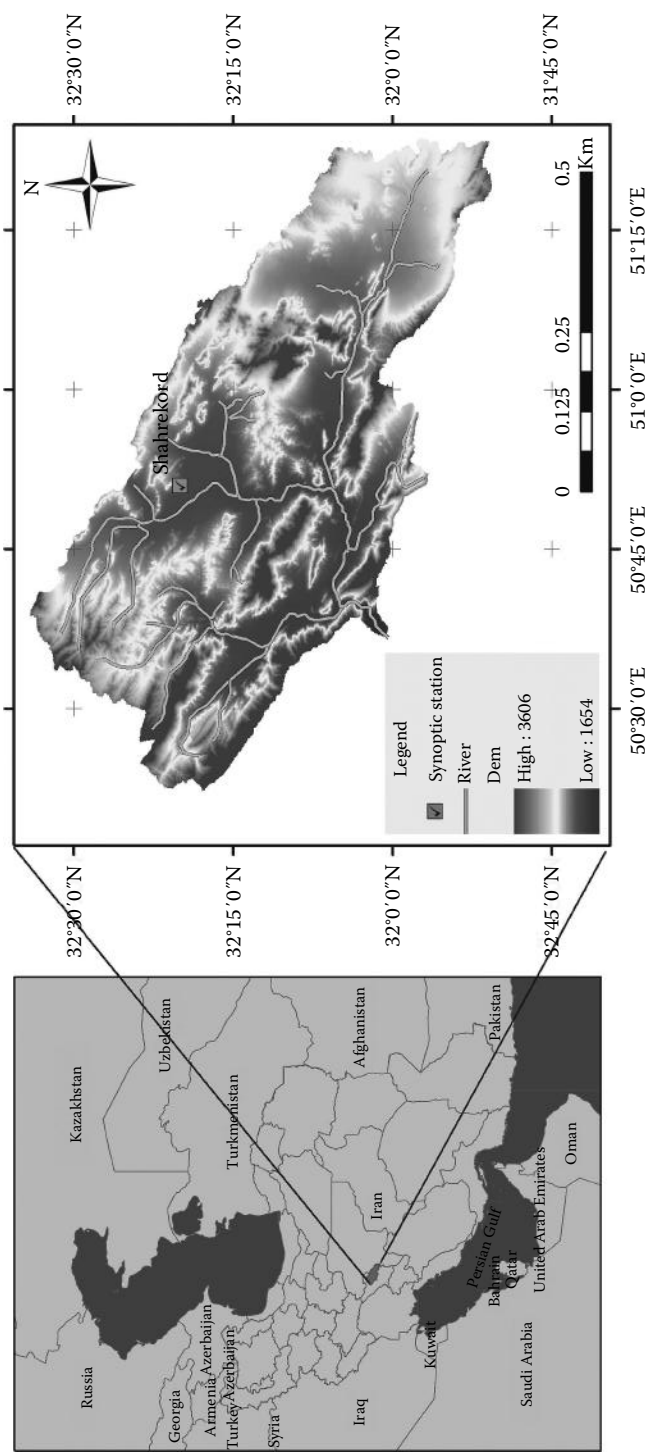

FIGURE 8.3 Study area.

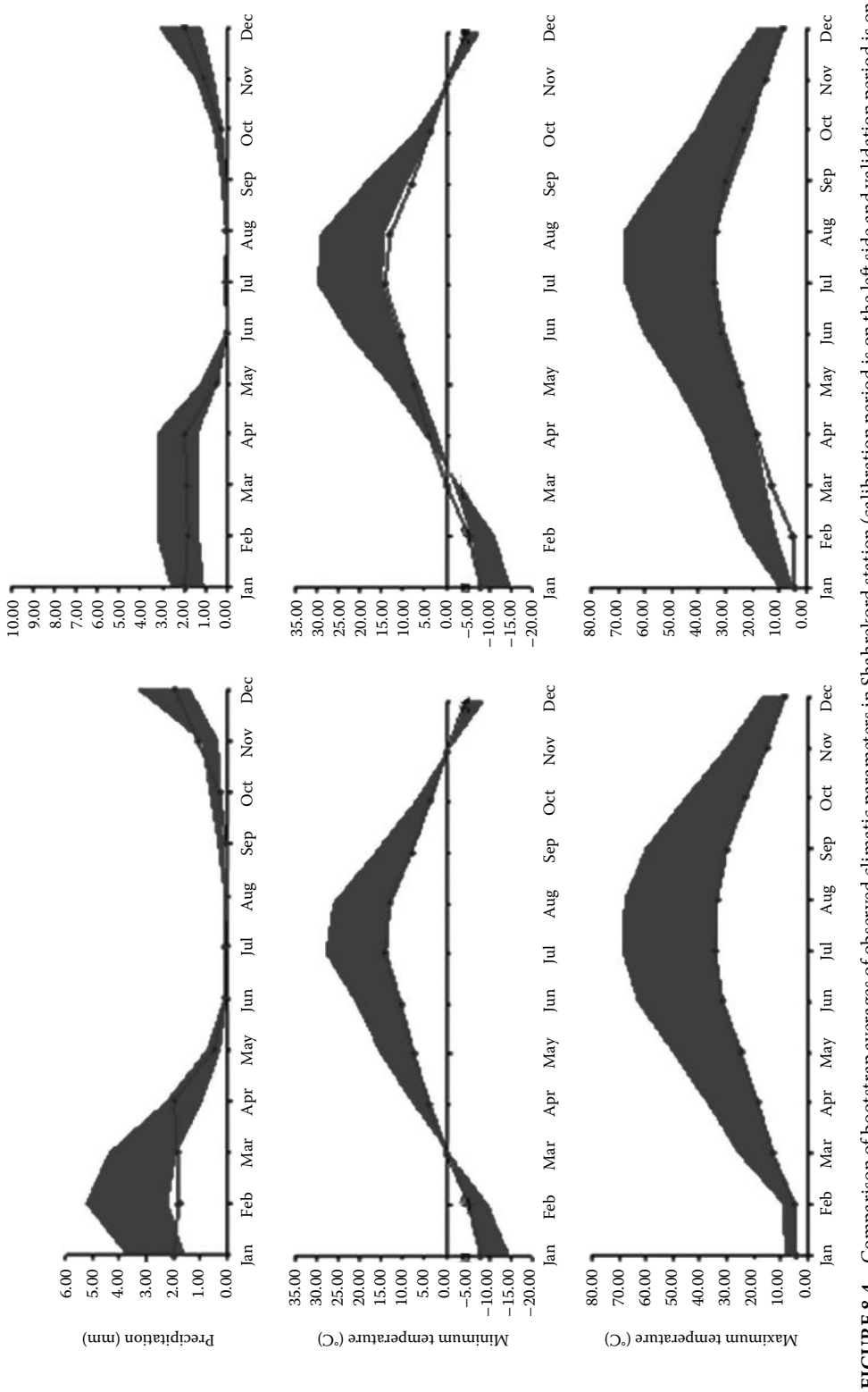

FIGURE 8.4 Comparison of bootstrap averages of observed climatic parameters in Shahrekord station (calibration period is on the left side and validation period is on the right side).

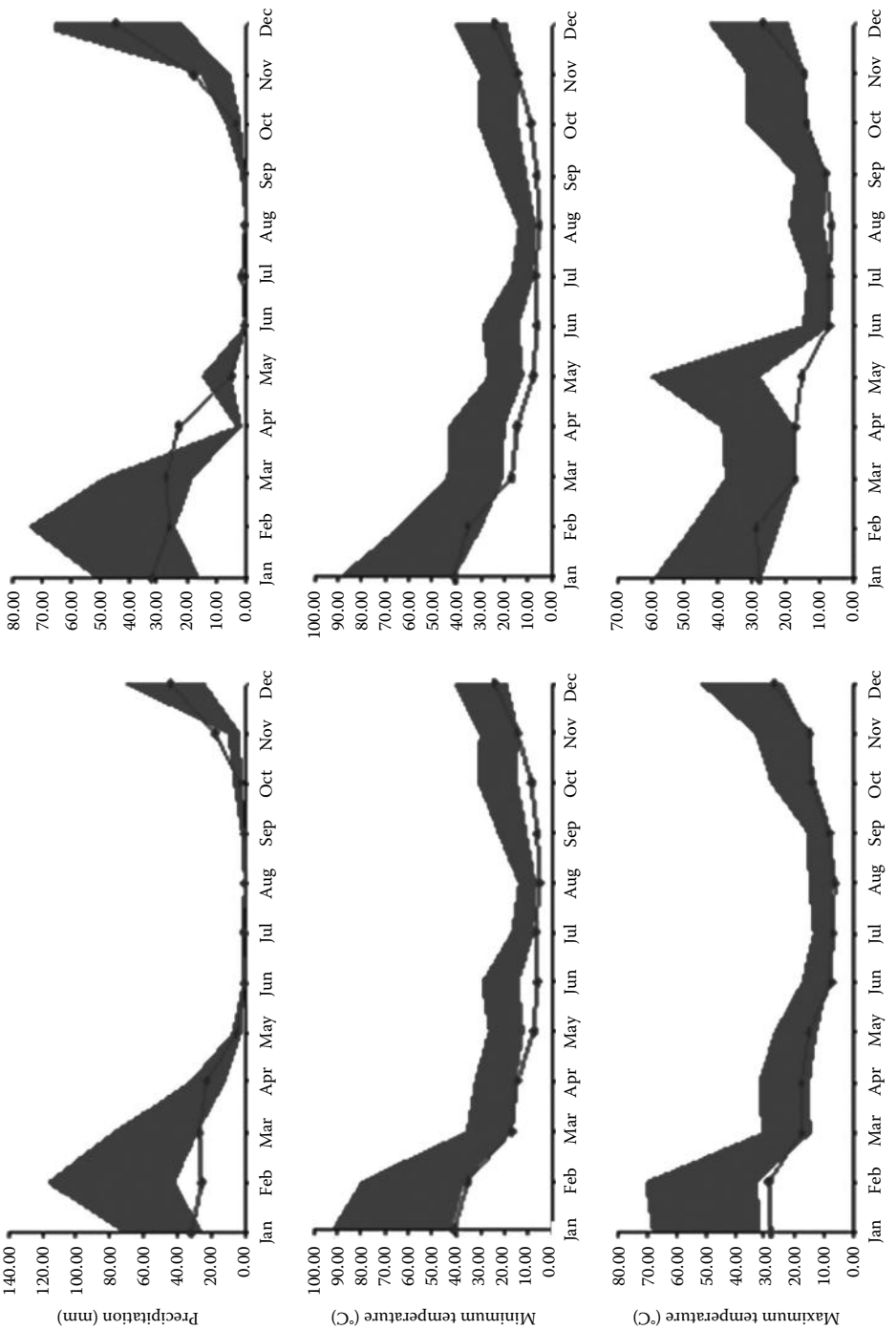

FIGURE 8.5 Comparison of bootstrap variance of observed climatic parameters in Shahrekord station (calibration period is on the left side and validation period is on the right side).

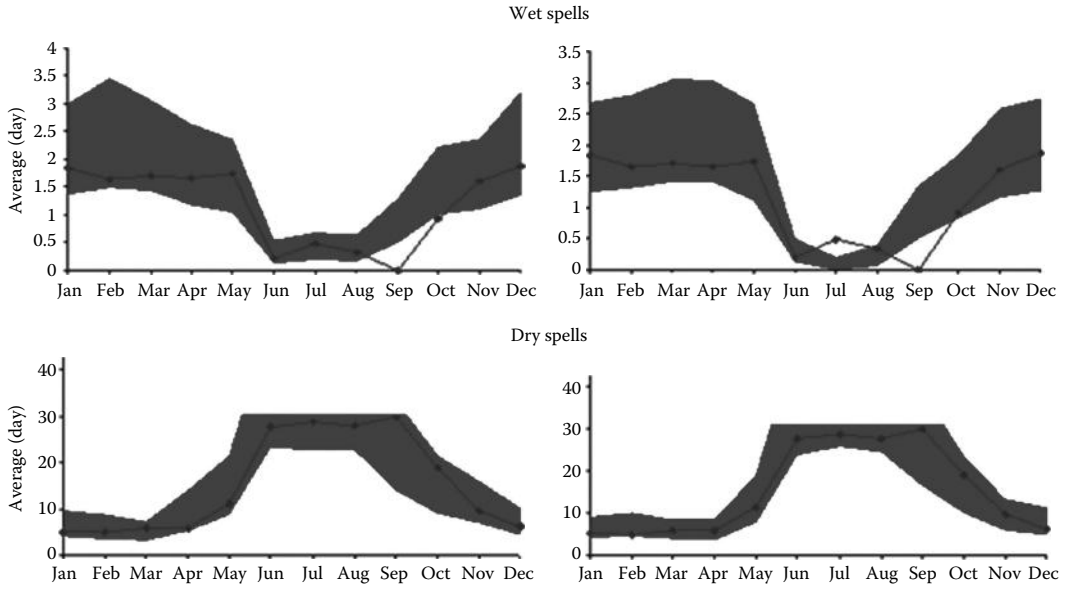

FIGURE 8.6 Comparison of bootstrap dry and wet periods of observed climatic parameters in Shahrekord station (calibration period is on the left side and validation period is on the right side).

Despite partial differences in the estimation of minimum and maximum temperatures and precipitation of some months, generally it could be concluded that the model has a good capability in the estimation of these parameters and their properties, and, on the other hand, a comparison between setup and assessment periods demonstrates a high capability of the model in the estimation of these parameters in the future periods. Therefore, downscaled data produced from SDSM could be used in the estimation of runoff. After assessment of the uncertainty of the whole process (producing temperature and precipitation parameters), now the impact of climate change on the variation of these parameters in future periods can be assessed, which is depicted thematically in Figures 8.7 through 8.9.

As shown in Figure 8.7, except for April (which is accompanied with a 35% reduction of minimum temperature), for the rest, minimum temperature is increased, in a way that 30% increase is obvious for the total period, and consequently snow melting and evaporation has increased and affected directly the water resources of the region.

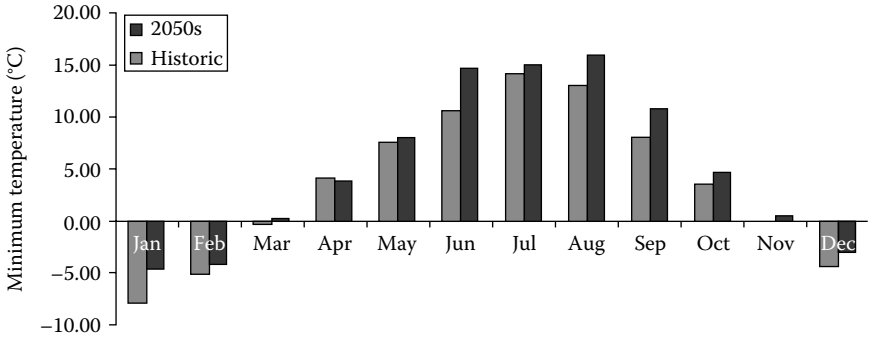

FIGURE 8.7 Monthly average variation of minimum temperature of future periods in comparison with the past periods.

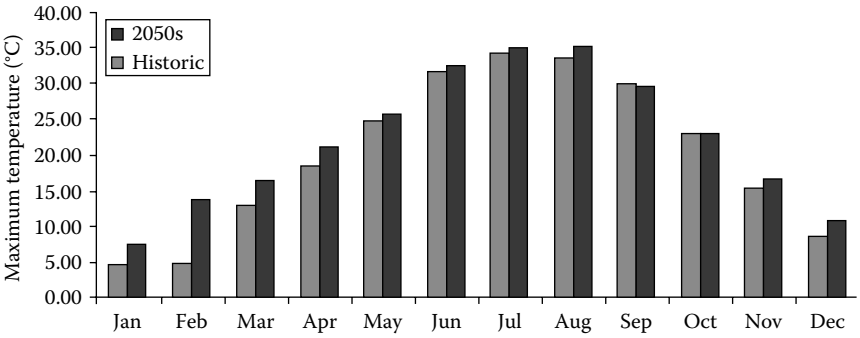

FIGURE 8.8 Monthly average variation of maximum temperature of future periods in comparison with the past periods.

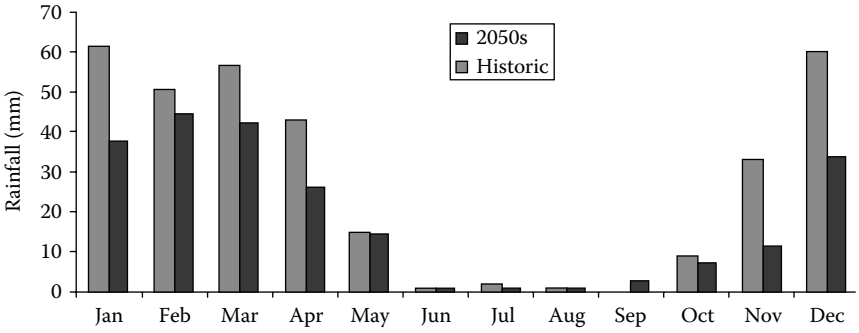

FIGURE 8.9 Monthly variation of precipitation of future periods in comparison with the past periods.

Maximum temperature will increase at the rate of 10% in the future period and, on the other hand, increasing trend of maximum temperature in most of the months demonstrates drought intensity in future. The greatest increase in value is found in February, which results in more snow melting and a higher probability of flood occurrence.

As shown in Figure 8.10, in all months precipitation will reduce and lead to more intensified droughts in the region.

The output of the downscaling process will be used as a hydrologic model input to assess the impacts of climate change in the region. For this, SWAT (Soil and Water Assessment Tools) is chosen as the hydrologic model. At first, using observation data of the base period, and soil, land use and the DEM maps, the model run was executed. Then, using SUFI2 algorithm in SWAT-Cup software, validation and verification of the model was completed and the optimum parameters of the model were selected. In Figures 8.10 and 8.11, the uncertainty band of the hydrologic model is depicted.

Given observation data of the station, the validation of the model was accomplished for the period 1998–2002, and the results are shown in Table 8.2.

The optimal values of the aforementioned indices are one, one, zero, and one, respectively. But because of the uncertainties affecting the model output, these values are never reached. One of the objectives of SUFI-2 algorithm is to reduce uncertainty, in a way that most of observation data would be placed in the 95% band. Rostamian et al. [18] proved that NS (Nash & Sutcliffe) and p-factor values of higher than 0.5 and also d-factor value of lower than 1.35 could be defined as desirable levels. The result demonstrates high accuracy of the model in runoff estimation (Table 8.2).

As shown in Figure 8.10, in all months observation values are located in the 95% confidence of the modeled data and considering the narrow band of the uncertainty, model accuracy is evaluated to be

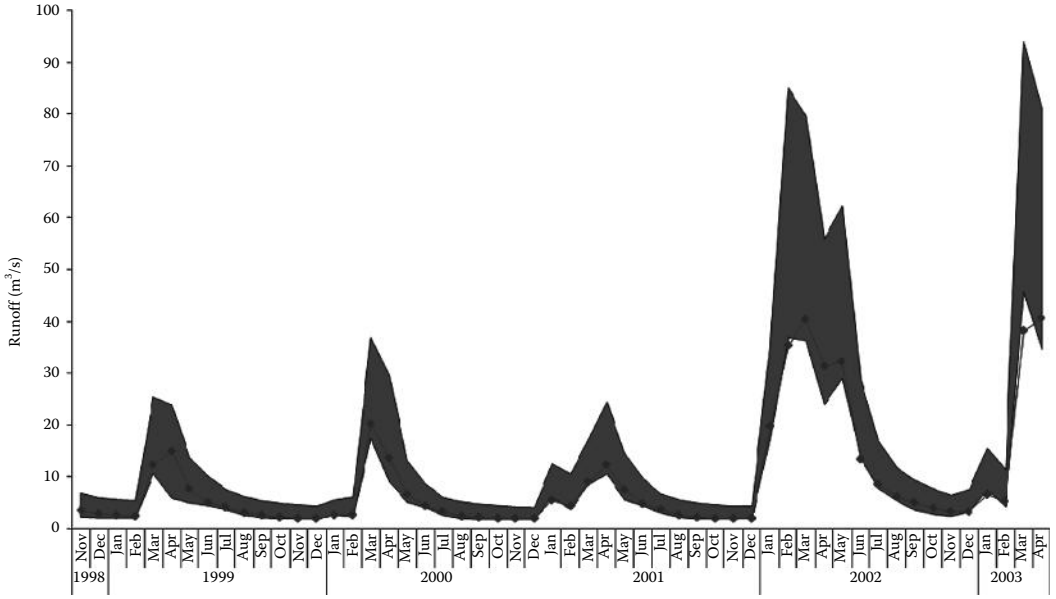

FIGURE 8.10 Uncertainty of the modeled values in validation period of the model with 95% confidence.

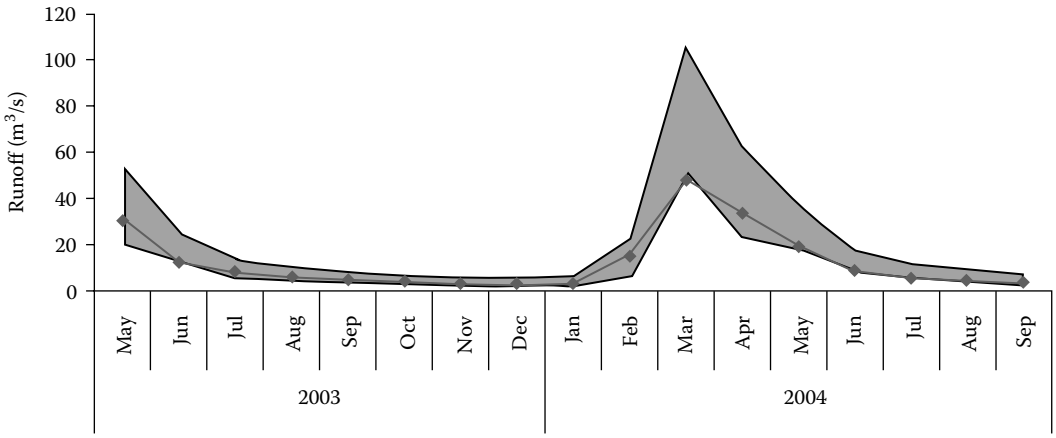

FIGURE 8.11 Uncertainty of modeled values in verification period of the model with 95% confidence.

TABLE 8.2 Performance Indices of the SWAT Model Validation

	P-Factor	D-Factor	R^2	NS
Evaluated values	0.54	0.49	0.85	0.76

good in validation process. In order to achieve more confidence of the resulted outputs, it is necessary to accomplish verification of the model.

For verification of the model, observation data of the period 2002–2004 were used. The results of verification are shown in Table 8.3 in the form of performance indices. This was obviously predictable that the values of these indices would be lower in comparison with the results of validation process, but despite these new ranges, all estimated parameters are placed in an acceptable range.

TABLE 8.3 Performance Indices of the SWAT Model Verification

	P-Factor	D-Factor	R^2	NS
Evaluated values	0.65	1.05	0.54	0.53

Figure 8.11 shows the uncertainty range of the modeled parameters and facilitates their comparison with the observation data. All observation data are placed in 95% confidence of the modeled values and considering the narrow band of the uncertainty, accuracy of the model in verification process would also be concluded and it demonstrates high capability of the model in runoff estimation for future periods.

After this step, by setting calculated parameters as constant parameters of the SWAT model, time series of minimum and maximum temperature and precipitation are introduced to the model in downscaled form, therefore, by rerunning the model, hydrologic components of the past and also near, middle, and distant future would be extracted from the model. In this study, the focus is on, assessment of climate change impact on the runoff values. Figures 8.12 and 8.13 depict the impacts of climate change on, future values of runoff in Behest-abad region.

The results show an increase in temperature and a decrease in precipitation and runoff in the future period of the case study region. Based on these results, the SDSM multiple linear algorithm in downscaling of the temperature and precipitation has been successful. To achieve better results, uncertainty should be considered in all of the downscaling processes. Finally, climate change has a decreasing trend

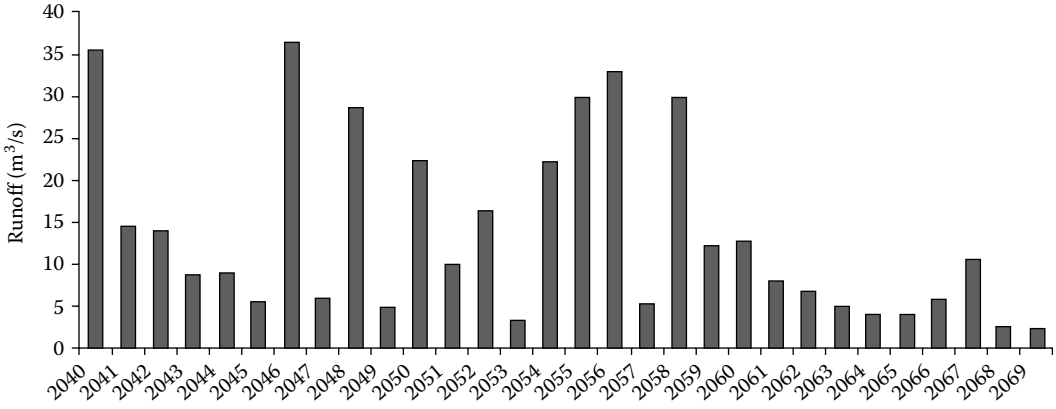

FIGURE 8.12 Runoff peak values in a 30-year period of middle future.

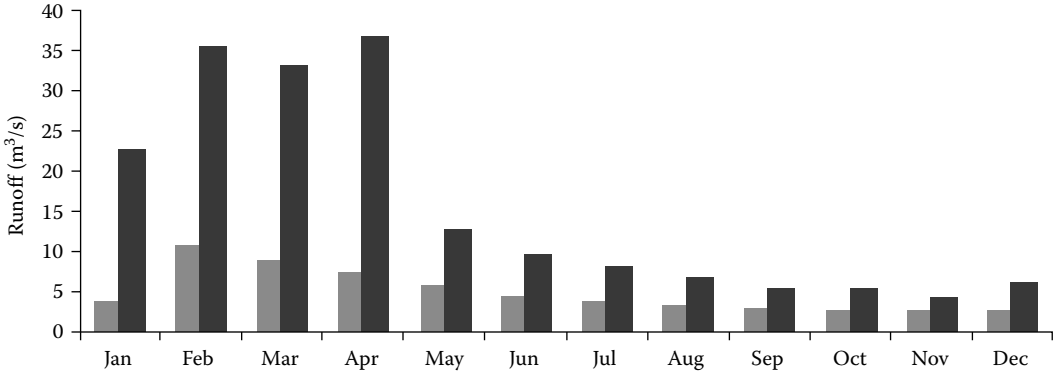

FIGURE 8.13 Maximum and average discharge in future period.

impact on the basin runoff; of course, in some years, the river flow has meaningfully been increased but through a more accurate study of the simulations, the impact of climate change on extreme occurrences like floods would become much clearer. Thus, an assessment of various approaches of climate change adaptation is necessary and useful for this region.

8.11 Summary and Conclusions

In this chapter, a methodology is presented to assess the impacts of climate change and devise some methods to adapt to climate change. The main concepts of climate change, climatic scenarios, and nonclimatic scenarios and usage of these scenarios in the AOGCM simulation models are explained respectively and consequently output data of these models are shortly presented. Some of the well-known databases for receiving output data of these models are also introduced here. After receiving the required data, based on needed computational cell size, downscaling should be executed because the AOGCM model outputs are regularly presented in large cell sizes. Finally, three important issues impact assessment, adaptation, and uncertainty, are described. An interesting finding about uncertainty in climate change studies is that the major portion of total uncertainty is the AOGCM models simulation; even this is true after downscaling.

Adaptation has two dimensions (social and environmental) that should be considered carefully. Adaptation is done in a social and environmental context, and the socioeconomic aspects of each adaptation approach must be predefined and assessed completely. Thus, it is critical to study the social aspects and communicate with the realities in the case study. Also, accounting water and finance resources is of great importance because any action in order to reduce climate change negative effects may cause significant ruining results and vice versa. So through a more specific assessment of a climate change case and its situation and realities, hopefully a better adaptation measure could be done and more positive results would be achieved.

References

1. Aerts, J.C.J.H. and Droogers, P. 2004. *Climate Change in Constrasting River Basins Adaptation Strategies for Water, Food and Environment*. Wallingford, UK: CABI. IX, 264 p.
2. Arthur, N.S., Shaowu, W., and Wei-Chyung, W. 1995. A comparison between observed and GCM-simulated summer monsoon characteristics over China. *Journal of Climate* 8(6): 1690–1696.
3. Baede, A.P.M., Ahlonsou, E., Ding, Y., and Schimel, D. 2001. The climate system: An overview. In *Climate Change 2001: The Scientific Basis.* Contribution of Working Group I to the Third Assessment Report of the Intergovernmental Panel on Climate Change. eds. J.T. Houghton, Y. Ding, D.J. Griggs, M. Noguer, P.J. van der Linden, X. Dai, K. Maskell, and C.A. Johnson, Cambridge University Press, Cambridge, U.K., pp. 525–582.
4. Brohan, P., Kennedy, J.J., Harris, I., Tett, S.F., and Jones, P.D. 2006. Uncertainty estimates in regional and global observed temperature changes: A new data set from 1850. *Journal of Geophysical Research* 111: D12106.
5. Burton, I., Smith, J.B., and Lenhart, S. 1998. Adaptation to climate change: Theory and assessment. In *Handbook on Methods for Climate Change Impact Assessment and Adaptation Strategies*. eds. J.F. Feenstra, I. Burton, J.B. Smith, and R.S.J. Tol, United Nations Environment Programme and Institute for Environmental Studies, Free University of Amsterdam, Amsterdam, the Netherlands.
6. Feenstra, J.R., Burton, I., Smith, J.B., and Tol, R. 1998. *Methods for Climate Change Impacts Assessment and Adaptation Strategies*. Published by United Nations Environmental Program, Nairobi, Kenya.
7. Fowler, H.J., Blenkinsop, S., and Tebaldi, C. 2007. Linking climate change modelling to impacts studies: Recent advances in downscaling techniques for hydrological modelling. *International Journal of Climatology* 27(12): 1547–1578.
8. Hulme, M. and Brown, O. 1998. Portraying climate scenario uncertainties in relation to tolerable-regional climate change. *Climate Research* 10: 1–14.

9. IPCC. 2007. *General Guidelines on the Use of Scenario Data for Climate Impact and Adaptation Assessment*. Alfsen, K., Barrow, Bass, E. B, Dai, Desanker, X.P., Gaffin, Giorgi, S.R.F., Hulme, M.M. et al. (eds), Cambridge University Press, Cambridge, U.K.
10. IPCC-TGCIA. 1999. *Guidelines on the Use of Scenario Data for Climate Impact and Adaptation Assessment*. eds. T.R. Carter, M. Hulme, and M. Lal, Version 1, 69pp. Intergovernmental Panel on Climate Change, Task Group on Scenarios for Climate Impact Assessment.
11. Klein Tank, A.M.G. and Peterson, T.C. 2005. Changes in daily temperature and precipitations extremes in central and south Asia. *Journal of Geophysical Research Atmosphere* 111: D16105.
12. Lambert, F.H., Gillett, N.P., Stone, D.A., and Huntingford, C. 2005. Attribution studies of observed land precipitation changes with nine coupled models. *Journal of Geophysical Research Letter* 32: L18704.
13. Lane, M.E., Kirshen, P.H., and Vogel, R.M. 1999. Indicators of impact of global climate change on U.S. water resources. *ASCE Journal of Water Resources Planning and Management* 125(4): 194–204.
14. Leander, R. and Bouishand, T.A. 2006. Resampling of regional climate model output for the simulation of extreme river flows. *Journal of Hydrology* 332:487–496.
15. Mathews, J. 2007. Seven steps to curb global warming. *Energy Policy* 35: 4247–4259.
16. Mitchell, T.D. 2003. Pattern scaling: An examination of the accuracy of the technique for describing future climates. *Climatic Change* 60: 217–242.
17. Nakicenovic, N., Alcamo, J., Davis, G., de Vries, B., Fenhann, J., Gaffin, S., Gregory, K. et al. 2000. *Emissions Scenarios.* A Special Report of Working Group III of the Intergovernmental Panel on Climate Change. Cambridge University Press, Cambridge, U.K., 599pp.
18. Rostamian, R., Jaleh, A., Afyuni, M., Mousavi, S., Heidarpour, M., Jalalian, A., and Abbaspour, K.C. 2008. Application of a SWAT model for estimating runoff and sediment in two mountainous basins in central Iran. *Hydrology Science Journal* 53(5): 977–988.
19. Oldenborgh, G.J., Philip, S.Y., and Collins, M. 2005. El Niño in a changing climate: A multi-model study. *Ocean Science* 1: 81–95.
20. Pittok, A.B. and Jones, R.N. 2000. Adaption to what and why? *Environmental Monitoring and Assessment* 61: 9–35.
21. Semenov, M.A. and Porter, J.R. 1995. Climatic variability and the modelling of crop yields. *Agricultural and Forest Meteorology* 73: 265–283.
22. Stakhiv, E.Z. 1996. Managing water resources for climate change adaptation. In *Adapting to Climate Change: An International Perspective*. eds. J. Smith, N. Bhatti, G. Menzhulin, R. Benioff, M.I. Budyko, M. Campos, B. Jallow, and F. Rijsberman, Springer, New York, pp. 243–264.
23. Stott, P.A., Tett, S.F.B., Jones, G.S., Allen, M.R., Mitchell, J.F.B., and Jenkins, G.J. 2000. External control of twentieth century temperature variations by natural and anthropogenic forcings. *Science* 15: 2133–2137.
24. Wilby, R.L. and Harris, I. 2006. A framework for assessing uncertainties in climate change impacts: Low flow scenarios for the River Thames, UK. *Water Resources Research*, 42: W02419.
25. Williams, G.D.V., Fautley, R.A., Jones, K.H., Stewart, R.B., and Wheaton, E.E. 1988. Estimating effects of climatic change on agriculture in Saskatchewan, Canada. In *The Impact of Climatic Variations on Agriculture*, Vol. 1, *Assessments in Cool Temperate and Cold Regions*. eds. M.L. Parry, T.R. Carter, and N.T. Konijn, Kluwer, Dordrecht, the Netherlands, pp. 219–379.
26. Yu, P.S., Yang, T.C., and Wu, C.K. 2002. Impact of climate change on water resources in southern Taiwan. *Journal of Hydrology* 260: 161–175.
27. Zhang, S. and Foufoula-Georgiou, E. 1997. Subgrid-scale rainfall variability and its effects on atmospheric and surface variable predictions. *Journal of Geophysical Research* 102: 19559–19573.
28. www.cccsn.ec.gc.ca (accessed October 30, 2012).

9

Dam Risk and Uncertainty

Ehsan Goodarzi
Georgia Institute of Technology

Saeid Eslamian
Isfahan University of Technology

AUTHORS

Ehsan Goodarzi is currently a postdoctoral student in the School of Civil and Environmental Engineering at the Georgia Institute of Technology. He received his PhD from Universiti Putra Malaysia (UPM) in water resource engineering with a focus on overtopping risk and uncertainty analyses of embankment dams based on stochastic concepts. His research interests cover various fields of water engineering including surface water hydrology, watershed management, optimization and stochastic simulation, and risk and uncertainty analyses in hydrosystem engineering.

Saeid Eslamian received his PhD from the University of New South Wales, Australia, with Prof. David Pilgrim. He was a visiting professor in Princeton University, USA, and ETH Zurich, Switzerland. He is currently an associate professor of hydrology in Isfahan University of Technology. He is the founder and chief editor of *Journal of Flood Engineering* and *International Journal of Hydrology Science and Technology*. He has published for more than 200 publications mainly in statistical and environmental hydrology and hydrometeorology.

PREFACE

The increase in population and socioeconomic activities has escalated the water demand for various purposes and put stress on existing water resources across the world, particularly in arid and semiarid countries. An efficient way to manage water resources is dam construction, which creates reservoir to store water and distributes it at the right time into downstream districts. Reservoirs have significant roles in water resource engineering in which their proper design, construction, and maintenance contribute considerably toward fulfilling water supply requirements and minimizing the risk of water shortages. In the past few decades, many risk and uncertainty methods have been developed by water resources engineers for the purpose of finding the optimal way to design safe dams, which can affect the safety of hydrosystem infrastructures. For instance, the proper design of a dam's spillway and the flood control capacity of a reservoir can ensure the safety of a dam and prevent any undesirable problems such as overtopping. In this chapter, the application of risk and uncertainty analyses to dam overtopping is presented for Doroudzan Reservoir located at the south part of Iran. The Monte Carlo simulation (MCS) and Latin hypercube sampling (LHS), as two effective sampling approaches, are applied to perform the uncertainty analysis by considering spillway discharge coefficient, quantiles of peak flows, and initial water surface level as uncertain variables. The inclusion uncertainty of key variables can be resulted in an expanded range of overtopping risks and provides significant information for decision makers to detect the events that indicate a developing failure mode.

9.1 Introduction

The risk concept has a long history and has been a main aspect of life since the beginnings of human experience. About 2400 years ago, Athenians were among the earliest people to use risk theory and risk assessment prior to making decisions. Applications of risk and safety analyses have been developed simultaneously by expanding various facets of technology in all branches of science, such as engineering and environment. The main intentions of risk and safety analyses are to identify existing system threats and predict possible outcomes in the future to provide clearer ideas for making the best possible decisions. In other words, risk analysis not only provides quantitative support for decision makers, but also helps to find the most effective options for decision-making. For instance, engineers could never have designed systems such as great bridges, dams, sewer systems, and so on, without some form of risk assessment. On the other hand, increasing water demands, higher standards of living, growing population, climate variability, and water resource limitations have caused conflicting issues among water consumers and put stress on existing water resources across the world, particularly in arid and semiarid countries [9]. Therefore, the proper management of water resources and risk assessment can provide an opportunity to manage available water resources using a framework. An efficient way to manage water resources is dam construction, which creates reservoir to store water and distributes it at the right time into downstream districts. Reservoirs have significant roles in water resource engineering in which their proper design, construction, and maintenance contribute considerably toward fulfilling water supply requirements and minimizing the risk of water shortages.

9.2 Risk, Reliability, and Uncertainty Analysis

The importance of risk and reliability analyses of hydrosystems has been increasing in recent years due to concern for citizens and government safety, and health and environmental problems. Simply put, risk can be defined as the probability of an undesired event that results in losses or damage. Risk is the probability of an unfavorable event that happens during a certain period of time. In other words,

risk can be defined as the probability that the actual result will differ from the expected outcome. Reliability is the complement of risk and is defined as the probability of nonfailure. Reliability and risk have an inverse relation, as increasing failure probability results in decreasing desired system reliability. In engineering, reliability signifies the ability of a set of components to carry out its required functions under some desired conditions over a specific time interval. Hence, the main objective of risk and reliability in engineering is to calculate a system's probability of failure or nonfailure regarding possible loads and resistance. Load and resistance can be defined differently depending on the analyst's viewpoint, type of system, purpose of analysis, and determined hydrosystem objectives. For example, the load and resistance in overtopping analysis of an embankment dam can be defined as water height in the reservoir and dam height, respectively, while for a culvert, the maximum inflow (based on rational formula) and the culvert's capacity to pass this flood can be defined as load and resistance, respectively. Some of the most applicable methods in the risk and reliability analyses of hydrosystem engineering can be named as performance function and reliability index, direct integration method, mean-value first-order second-moment (MFOSM) technique, and advanced first-order second-moment (AFOSM) method [24].

Another important concept that usually comes up with risk and reliability is uncertainty. Uncertainty refers to the condition that is not exactly quantifiable and can be ascribed as deficient in perfect information regarding phenomena, data, models, and processes. More simply, uncertainty comprises the incidence of events beyond human management capabilities. Any uncertain variable has random characteristics of which randomization yields a particular level of error. Recently, various approaches for measuring error and uncertainty have expanded, and the application of these techniques has shown a steady growth in the uncertainty analysis of hydrosystem engineering. There are different classifications with regard to the types and sources of uncertainty. Tung et al. [24] categorized the main sources of uncertainty in hydrosystem engineering as natural variability and knowledge deficiency. In their classification, the natural variability includes natural events such as climatic, hydrologic, and seismic forces, while knowledge deficiency involves data, model, and operational uncertainties. From another point of view, the sources of uncertainty in water resource engineering can be considered as hydrologic, hydraulic, structural, and economic sources. As uncertainties are a result of lack of perfect knowledge on the phenomena, decisions with some uncertainties are still frequently being made in all engineering processes. Thus, safety of any engineering projects is relative to the level of uncertainty involved. In the probability assessment and random event analysis, statistical procedures would be of great assistance, and applying statistical tools can be very useful for risk and reliability analyses.

Different approaches have been applied to measure uncertainty in hydrosystem engineering. One way to measure the degree of uncertainty is to apply statistical moments in various orders. Useful statistical moments in this case are mean and variance of desired variables. Mean (μ_x) is the first central moment that illustrates the expected variable value, while variance (σ_x^2) is the second-order moment of a variable and presents the scatter of a random variable. Coefficient of variation, defined as ratio of the standard deviation of variable (σ_x) to the mean of variable ($\Omega_x = \sigma_x/\mu_x$), can be applied to explain uncertainty level. This coefficient is used as a normalized measure of uncertainty to be compared in various conditions, and it is also useful for combining uncertainties of different variables [24]. However, the most complete approach is applying the probability density function (PDF) of desired uncertain variables. Generally, the uncertainty techniques can be categorized into analytical, approximation, and sampling of which the most important of them are presented in Table 9.1.

9.3 Sampling Methods

In water resource engineering, making a decision about system operation and capacity is strongly dependent on the system's reaction under some predictable conditions. However, it is not possible to assess the system's reaction with distinct certainty, as the various system components are subject to

TABLE 9.1 Uncertainty Analysis Methods

Analytic Methods	Approximation Methods	Sampling Methods
Derived distribution	First-order variance estimation	Monte Carlo simulation
Fourier, Laplace, and exponential transforms	Rosenblueth's probabilistic point estimation	Latin hypercube sampling
Mellin transforms	Harr's probabilistic point estimation	Correlated sampling
Estimations of probability and quantile using moments	Li's probabilistic point estimation	Antithetic variates

Source: Tung, Y.K. et al., *Hydrosystems Engineering Reliability Assessment and Risk Analysis*, McGraw-Hill Professional, New York, 2005.

different kinds of uncertainty. One problem regarding the different uncertain variables in complex and nonlinear models is deriving the PDF of uncertain variables and determining the appropriate statistical moments or probability distribution of model outputs. Furthermore, any analysis in the real world is based on historical recorded data, while usually historical records are not long enough and the data includes all sorts of errors. Sampling is potentially an applicable method to compound several random input values and get results with appropriate accuracy. Sampling can be defined as the procedure of selecting an individual from a specific statistical population to evaluate characteristics of the entire population. In other words, it is the extrapolation from sample to the population and helps engineers to improve quality of data and saving in time and cost. Hence, the MCS and LHS, as two significant sampling techniques, will be briefly explained in the following sections.

9.3.1 Monte Carlo Simulation

Simulation is a process of recreating a real situation, usually based on a set of hypotheses and mathematical formula. Simulation is a useful tool for evaluating system performance in different conditions and also to test new theories in the form of a computer program. The MC process is a numerical simulation that replicates stochastic variables according to a certain statistical distribution. In other words, MC uses random numbers to model a desired process. To generate continuous random numbers based on the MCS, consider X as a random variable and $F_x(X)$ as its cumulative distribution function (CDF); the inverse function for any value of $u \sim u(0,1)$ can be written as

$$X = F_x^{-1}(u) \tag{9.1}$$

where
$F_x^{-1}(u)$ is the inverse function
u has a uniform distribution on (0,1)

It should be noted that the continuous probability distributions in hydrosystem engineering are strictly uptrend for all random variables X, and thus, there is a unique relationship between $F_x(x)$ and u as $u = F_x(X)$. To generate m random variables using the CDF-inverse method, the following steps should be repeated m times:

1. Draw a uniform random variate as $u \sim u(0,1)$ (random number generator).
2. Find x such that $x = F_x^{-1}(u)$.

There are two major concerns about the MCS. First, it needs large computations to generate random values, and second, its result accuracy strongly depends on the number of iterations and simulations. In this method, increasing sample size is a prerequisite to achieving higher precision results, while the achieved results will lead to sampling errors related to the number of selected random variates with an

inverse relation to the sample size number. On the other hand, increasing sample size entails an increase in computer time needed for generating random variates and the simulation process.

9.3.2 Latin Hypercube Sampling

As stated earlier, increasing sample size in sampling-based methods can reduce sampling errors, but simulation process and computer time for generating random variates will be increased. On this basis, there are some reduction variance techniques to increase the precision of MCS outcomes without the need to increase sample size [24]. Some of the most important methods of variance reduction are antithetic-variate technique, control variates, importance sampling technique, LHS, correlated sampling, and stratified sampling technique. LHS is one of the main variance reduction techniques that can increase the efficiency of the output statistics parameters. This method is frequently used to decrease the number of necessary runs of MCS to achieve a reasonably accurate random distribution. In this method, the range of each variable is divided into m nonoverlapping intervals with the equal probability $1/m$. Then, a random variate is selected from each range with regard to the desire probability distribution [22]. A simple and primary algorithm for applying the LHS method is

1. Divide the range of input variables into the number of m.
2. Generate M uniform random number from $U(0,1/M)$.
3. Perform random permutation.
4. Determine random variates ($x_{i,j}$) by applying the following equation:

$$x_{i,j} = F_j^{-1}\left(\frac{1}{m}\left[P_{i,j} - r_{i,j}\right]\right) \tag{9.2}$$

where $r_{i,j}$ and $P_{i,j}$ are random number and random permutation, respectively [17].

Based on the LHS method, each generated random variate is placed in a separate interval with the equal probability of $1/m$. For example, Figure 9.1 shows the range of each variable for $m = 5$ nonoverlapping intervals with an equal probability of $1/5 = 0.2$.

On the other hand, the generated random variates from the MC technique are randomly distributed, and there may be more than one random variate, or no random variate placed in an equal probability area. Figure 9.2 illustrates the main differences between the MCS and LHS techniques.

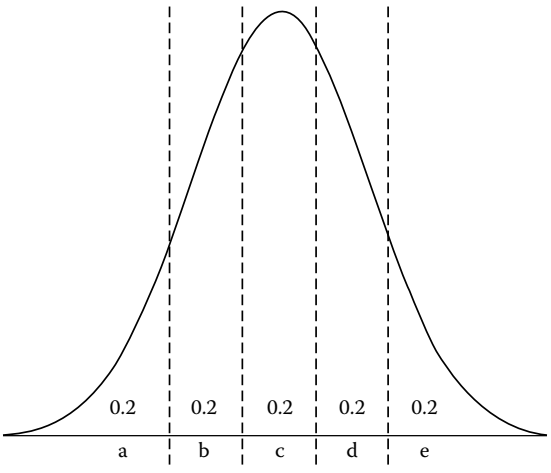

FIGURE 9.1 Nonoverlapping probability area for $m = 5$.

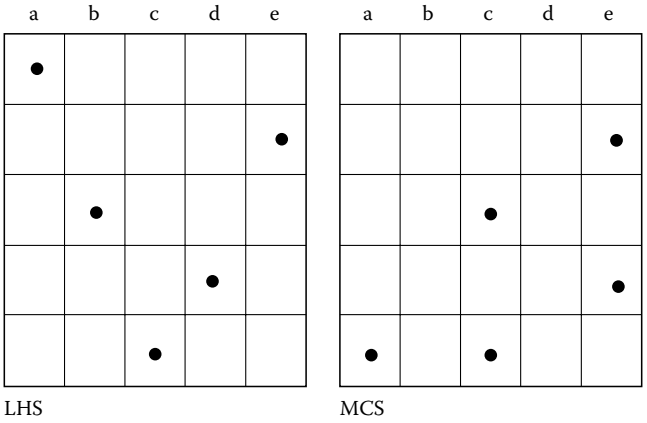

FIGURE 9.2 Generating random variates based on MCS and LHS.

As it can be seen from this figure, with the LHS sampling strategy, each row and each column is filled by a black circle, which represents a generated random variate. Whereas based on MCS method, some rows and columns do not contain any black circle and some rows and columns have been filled with more than one random variate.

9.4 Frequency Analysis

Frequency analysis is an applicable statistical method for analyzing hydrologic phenomena based on the past records and historical data. This analysis is the concept of the probable frequency of occurrence of a certain event in the future within a given time period. Frequency information is commonly applied in different fields of water engineering, and it has been the main concern of hydrologists in particular when they are designing various water resources systems. In other words, reliable estimates of the magnitude and frequency of extreme hydrologic events could be useful to provide the basic and necessary information in the design of hydrosystems, considering the current condition of systems and finding the most sensitive factors that increase the risk of failure. Based on Chow et al. [4], the principal objective of hydrologic frequency analysis is to create a relationship between the magnitudes of extreme events and their frequency of occurrence and predict how often an event (e.g., floods, droughts, wind speeds, and rainfalls) is likely to recur. Therefore, we need to fit a probability distribution to available data and, then, establish a relationship between the event magnitude and its exceedance probability. As frequency analyses are based upon the principle of statistical analyses, it needs a deep understanding of statistical and probability theories.

In addition to that, the number of sample size and observations also are an important feature of frequency studies, in which larger sample sizes generally lead to increasing the accuracy of results. Hydrological data show the quantitative values of each process in water cycle, and so, the importance of this sort of data in forecasting and managing different events cannot be underestimated. Hence, the first key step of any hydrological study like frequency analysis is data collection. Based on Tung et al. [24], there are three basic types of data series extractable from hydrological records: a *complete series*, an *extreme value series*, and a *partial duration series*. The complete series data cover all available values on the magnitude of an event and usually includes a large number of sample sizes containing all the data between the minimum and maximum values. In practice, this type of data series is not applicable for some of the hydrological events that only their largest or smallest values are required. In this case, using extreme value series of data in the form of *annual maximum series* for the largest and *annual minimum series* for the smallest data value could be more relevant. However, there are still specific limitations regarding this class of data in which using annual maximum or minimum series

may contain loss of some information. For example, the second maximum or minimum value of wind speed within a year may be greater or smaller than the largest or smallest value of speed in other years, while it is ignored in annual maximum or minimum series. This problem could be solved by applying the third category of data series as partial duration. This category is a subgroup of complete data series, and it is conducted on values that are above or below a preselected base value. According to this method, a base value is chosen, and all data above or below that certain base will be considered in frequency analysis. For example, the partial duration series may consider all inflows above 500 m^3/s or wind speeds less than 10 m/s.

As stated earlier, the probability distribution also is another input requirement for frequency analysis to describe the frequency of occurrence of an event. However, deciding whether given data come from a particular class of probability distributions still is one of the basic problems of statistics. Two traditional ways to test how a particular distribution sufficiently fits a set of observations are (1) using probability paper and (2) comparing the observed relative frequency with the theoretical relative frequency. Based on the first method, data series is ranked, and exceedance probability or return period is computed using the proper plotting-position formula. Afterward, the probability paper for the desire distribution is obtained, a graph of magnitude of desire random variable versus its probability is plotted, and finally a distribution fitted graphically [26]. For the second method, some statistical goodness-of-fit tests should be applied to compare observed and expected relative frequencies and see how well a probability distribution fits a set of observations. In this case, three of the most applicable tests are Kolmogorov–Smirnov (KS), the Anderson–Darling (AD), and chi-square test. The KS test is a nonparametric test that makes no assumption about the distribution of data, and it does not rely on the probability distribution function being tested. The second one, AD test, is a modification of the KS test and assumes that there are no parameters to be estimated for desire distribution, and so it is distribution-free. The last one, chi-square goodness-of-fit test, is the most used member of the nonparametric family of statistical tests, and it can be applied to any univariate distribution to calculate the CDF. This test is an alternative to the KS and AD tests, and it can be used for discrete distributions, while two other tests are limited to the continuous distributions [5]. Although goodness-of-fit tests are popular yet, and they have been used in many hydrologic design projects, there are kinds of questions and some limitations on using them in hydrological frequency analysis particularly for extreme events. The most important restrictions can be written as insensitivity in the tail regions of the distributions, dependency of quantile function on the method of fit, problems with small samples, and inherent arbitrary rules [28]. Hence, developing methods (e.g., L-moments) are always interesting for both hydrologists and statisticians, and they can increase the accuracy of results and also give a more proper prediction of hydrologic events [7]. The applications of L-moments for conducting goodness-of-fit tests to identify appropriate probability distributions began in the late 1970s and have been increased in the recent years. The name of this method is obtained from their construction as linear combinations of order statistics. L-moments are known as robust model for characterizing the shape of a probability distribution and estimating the distribution parameters, principally for environmental data with small sample sizes [12]. More information on various frequency methods and their application to different hydrologic events are presented by Tung et al. [24] and McCuen [20].

In the case of various hydrologic events, flood and wind speeds both play a significant role in designing hydrosystems, in which the extreme value of these natural events can be resulted in unexpected damaging effects like loss of human life and economic losses. Henceforth, estimating extreme values of flood and wind speeds is an essential task in many fields of environmental and engineering risk analysis. For example, in dam overtopping study, overtopping happens when the flood outlet cannot release water fast enough and water rises above the dam and spills over, or, wind can start waves, raise the height of water in a reservoir, and consequently increase the probability of the occurrence of overtopping. In other words, when the water elevation is very near the crest, the generated waves might wash over, resulting in dam failure. Therefore, flood and wind frequency analyses are used to establish a relationship between flood and wind speed magnitude and frequency of occurrence. Once the

historical data are available, it is possible to use the past data as a representation of future and establish the relationship to predict their extreme values in different return periods. In general, the process of any hydrologic frequency analysis, including flood and wind frequency analyses, briefly includes the following steps:

1. Data collection for interested hydrological event (e.g., rainfall, wind speeds, and reservoir inflows).
2. Find the best fit probability distribution for the available data series (e.g., Gumbel max, general extreme value (GEV), gamma, log-gamma, log-logistic, normal, log-normal, Pearson, log-Pearson Rayleigh, and Weibull).
3. Determine the magnitude and frequency of desire hydrologic events based on the given probability distribution.

In the following sections, the flood and wind frequency analyses for a real case study are presented.

9.5 Dam Overtopping

The proper design of a dam's spillway and the flood control capacity of a reservoir can ensure the safety of a dam and prevent any undesirable problems such as overtopping. The design flood of reservoirs is usually computed based on the univariate flood frequency analysis of peak discharges in which the hydrograph of design flood is routed through the reservoir to determine the spillway design discharge and flood control capacity. However, dams still suffer overtopping, which comprises about one-third of all uncontrolled breach failures [15]. The standard design of dams has not been absolutely solved because of the uncertainty in the variables and applied models, and until now, it is a difficult issue in hydrosystem engineering.

Deterministic approaches, such as the probable maximum flood technique, which assumes that the risk of dam failure is zero, are well established and still used in dam design engineering [23]. However, by improving the mathematical and statistical models through the increasing ability of computer programs, and with the accessibility to data records for longer periods, it is time to move from the deterministic approaches in engineering design to probabilistic methods that consider higher-order uncertainty in the variables and models. In the past, some studies were carried out to consider the risk and reliability analyses in dam safety. Wood [28] evaluated the overtopping risk for an embankment dam by applying the integral transformation approach. Cheng et al. [3] evaluated the risk of overtopping by applying various approaches including direct integration method, MCS, MFOSM, and AFOSM and, then, compared the results of different methods with each other. The Committee on the Safety of Existing Dams [6] offered a risk index for overtopping and structural failures and also discussed the concept of risk-based design for hydrosystems. Singh and Snorrason [21] analyzed some historical earth-filled dam failure events due to overtopping. One finding of this analysis was the identification of a strong correlation between the breach width and dam height. Cheng et al. [2] offered a new approach to estimate the risk of overtopping due to wind. Bowles [1] studied the tolerable risk concept in hydrosystem engineering and presented some examples for tolerable risk criteria in dam safety. Yanmaz and Gunind [29] applied bivariate flood frequency analysis to estimate the overtopping risk of a detention dam. Wang and Bowles [27] studied different breach locations of an earthen dam due to wave overtopping, and based on their results, wind direction, as well as the wind speed, has an important effect on the location of the breach. Kwon and Moon [17] introduced three major innovations to improve overtopping risk elevations using probabilistic concepts for existing dams. The first innovation was the use of nonparametric probability density estimation methods for selected variables, the second was applying LHS to improve the efficiency of MCS, and the third was the use of bootstrap resampling to determine initial water surface level. Marengo [19] studied the probability of overtopping during dam construction by focusing on the upstream water surface elevation during the flood. Kuo et al. [16] conducted a risk analysis for Feitsui Reservoir by considering five uncertainty analysis

methods (MFOSM, RPEM, HPEM, LHS, and MCS) and four initial water levels in five return periods. Li and Zhao [18] introduced a time-dependent reliability method to predict the risk of failures due to the increased wave overtopping and reduced structural capacity in conjunction with some basic applications of its method. In addition, a stochastic process was proposed to model the time variant and random nature of severe waves. Hughes and Mantel [13] studied the application of a hydrological modeling approach to investigate the uncertainty associated with simulating the impacts of farm dams in several South African catchments. The focus of the study was on sensitivity analysis and the limitations of the data that would be typically available for water resources assessments. Fakhri et al. [8] studied the uncertainty assessment of downscaled rainfall and impact of climate change on the probability of flood. Goodarzi et al. [10] present the application of risk and uncertainty analyses to dam overtopping due to various inflows and wind speeds based on univariate frequency analysis for the Meijaran Dam in the north of Iran. The results revealed that rising water level in the reservoir is the most important factor in overtopping risk analysis, and wind speed also has a considerable impact on reservoirs that are placed in windy areas. In another study, Goodarzi et al. [11] presented the application of risk and uncertainty analyses to dam overtopping based on univariate and bivariate flood frequency analyses by applying Gumbel logistic distribution.

The process and application of risk and uncertainty analyses to dam overtopping and application of a probability-based methodology to evaluate the probability of dam overtopping are presented in the following sections. A flood frequency analysis of 33 years of annual maximum discharge is carried out by applying GEV distribution for the Doroudzan Reservoir in the south of Iran. Afterward, the risk of overtopping is calculated for five extreme floods considering inflow hydrographs, initial water levels, and the discharge coefficient of the spillway as uncertain variables. The highest water levels were computed by the reservoir routing technique while the MC and Latin hypercube techniques were applied for uncertainty analysis. It is important to note that when derivation of the PDF of uncertain variables is difficult, the sampling technique is an applicable method that tries to compound several random input values to obtain the best result. These results can be analyzed statistically to predict the behavior of the system. The accuracy of the sampling methods strongly depends on the sample size, and so, a large number of samples (20,000 for MC and 10,000 for LHS) were considered in this study to increase the precision of the calculations. As the LHS can converge with smaller sampling, its sample size is half of the MCS technique.

9.5.1 Case Study: The Doroudzan Dam, Iran

Doroudzan Dam is one of the most important dams in the south part of Iran. The preliminary studies and investigations of the dam were carried out in the years 1963–1966, and dam construction was started and complicated in 1970 and 1974, respectively. The basin of this multipurpose earth-fill dam is situated near northwest Shiraz on the Kor River and in the Bakhtegan lake catchment area. The Kor river watershed is between the longitude 51° 43′ and 52° 54′ East and latitude 30° 08′ and 31° 00′. The elevation of the highest watershed point is 3749 m from the mean sea level and is located northwest of the watershed. The total volume and dead storage of the reservoir are 993 and 133 (10^6 m^3), respectively. Basic technical information concerning Doroudzan Dam, the schematic view of dam, and its basin are shown in Table 9.2, Figures 9.3 and 9.4, respectively.

This dam is a major source of water, supplying for 112,000 ha of agricultural land and domestic–industrials and power plants requirements of Shiraz, the capital of Fars province, and Marvdasht and Zarghan as two other main cities. It is important to note that, two of the most important artifacts, the Pasargadae and Persepolis monuments, which date back to 515 BC, are located downstream of the Doroudzan.

These structures are among the most famous monuments in the world and are visited annually by people from all over the world. Therefore, any problems with the Doroudzan dam will undoubtedly immerse these two ancient and valuable heritage sites.

TABLE 9.2 Physical Characteristics of Doroudzan Reservoir

Type	Earth-Fill
Height	57 (m)
Crest length	710 (m)
Crest width	10 (m)
Fill volume	4.8 (10^6 m^3)
Volume	993 (10^6 m^3)
Dead storage	133 (10^6 m^3)
Spillway type	Ogee spillway

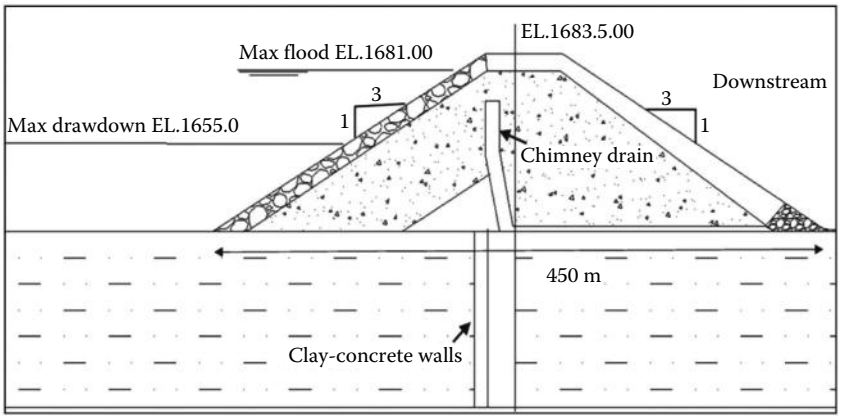

FIGURE 9.3 A schematic view of Doroudzan Dam.

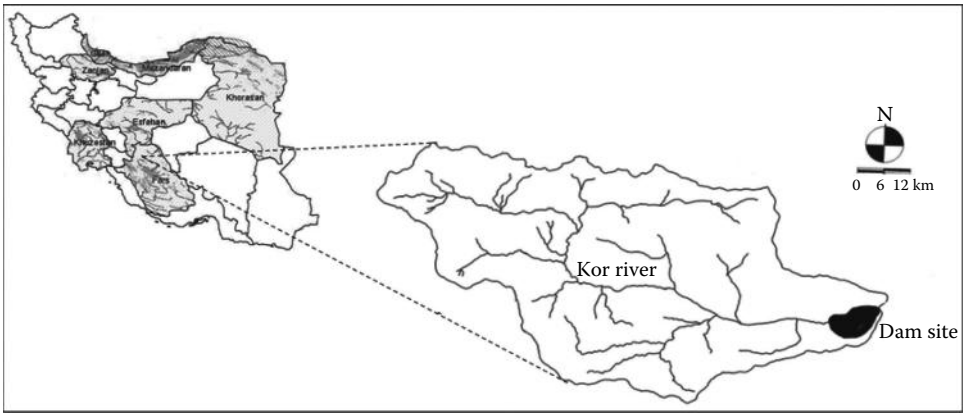

FIGURE 9.4 A schematic view of Doroudzan's basin.

All inflows, reservoir storage, evaporation, and releases from 1975 to 2008 have been collected by the Fars Ministry of Energy Data Center land-based/surface data collection. Team members collected all available meteorological data including inflows, water elevation, rainfall, temperature, etc., for each station along the Kor River, and the recorded data were ported in Microsoft Excel workbooks for data quality assurance and quality control.

9.6 Methodology

9.6.1 Dam Risk Model

If a system is unable to perform expected tasks, the system will fail, and, accordingly, undesirable consequences will occur. Failure can be defined as the load (L) exceeding system resistance or capacity (R). Identifying load and resistance is a fundamental issue in risk analysis, and it noticeably depends on the type of hydraulic structure and problem physics. Tung et al. [24] defined the probability of failure as

$$\text{Probability of failure} = P\left(L > R\right) \tag{9.3}$$

where $P([.])$ is the probability of failure. Risk also can be represented as [22]

$$\alpha = \text{Risk} = P\left(Z < 0\right) \tag{9.4}$$

where Z is the performance function, and it can be defined as $Z = R - L$, $Z = (R/L) - 1$, and $Z = \ln(R/L)$.

It is important to note that the performance function of an engineering system can be described in several forms in which the selection of each form depends on the distribution type of desire performance function. In this study, the system outcomes have been compared with the log-normal and normal distributions, and the goodness-of-fit test was applied to choose the appropriate distribution based on the KS and AD tests (Table 9.3).

The results of the test revealed that log-normal distribution fits the available data better than normal distribution, and thus, the log form of the performance function was selected. Hence, the performance function (Z) can be considered as follows:

$$Z = \ln\left(\frac{R}{L}\right) \tag{9.5}$$

More information on various performance function forms and their application to hydraulic engineering systems is presented by Yen [30].

9.6.2 Overtopping Risk Model

Overtopping happens when the flood outlet cannot release water fast enough and water rises above the dam and spills over. In overtopping analysis, the maximum water height in the reservoir (H_{max}) and dam

TABLE 9.3 Goodness-of-Fit Tests for the System Outcomes

	Goodness-of-Fit Test	Kolmogorov–Smirnov		Anderson–Darling	
T-Year	Probability Distribution	Statistic Value	Table Value	Statistic Value	Table Value
2	Log-normal	0.008	0.030	0.177	2.501
2	Normal	0.014	0.030	0.811	2.501
10	Log-normal	0.008	0.030	0.177	2.501
10	Normal	0.014	0.030	0.811	2.501
20	Log-normal	0.013	0.030	0.206	2.501
20	Normal	0.019	0.030	0.878	2.501
50	Log-normal	0.013	0.030	0.212	2.501
50	Normal	0.019	0.030	0.893	2.501
100	Log-normal	0.013	0.030	0.211	2.501
100	Normal	0.019	0.030	0.879	2.501

height (H_R) can be considered as the load and resistance of the system, respectively. Therefore, the overtopping probability with respect to the performance function due to different inflows and wind speeds can be expressed as follows [22]:

$$Z_f = \ln\left(\frac{H_R}{H_{max}}\right) \tag{9.6}$$

and

$$Z_{fw} = \ln\left(\frac{H_R}{H_{max} + H_w}\right) \tag{9.7}$$

where

Z_f is the performance function of flood
Z_{fw} is the performance function of flood and wind
H_R is the dam crest height
H_w is the total wave height
H_{max} is the highest water level during a flood event that can be calculated from reservoir routing

Finally, the overtopping probability will be computed as

$$\text{Risk} = 1 - \varnothing\left(\frac{\mu_z}{\sigma_z}\right) = 1 - \varnothing(\beta) \tag{9.8}$$

in which β is the reliability index indicator and is defined as the mean ratio of the performance function (μ_z) to its standard deviation (σ_z).

9.6.3 Flood Model (Reservoir Routing)

The main objective of overtopping analysis of an earth-filled dam is estimating the water height in the reservoir under various inflows and wind speeds, and comparing the result with the dam crest elevation. The known and frequently used flood model is the continuity equation with the following basic form:

$$I - Q = \frac{ds}{dt} \tag{9.9}$$

where

I and Q are reservoir inflow and outflow (m^3/s)
S is the storage (m^3)
t is the time (s)

The implementation form of reservoir routing can be written as

$$\frac{I_t + I_{t+1}}{2} - \frac{Q_t + Q_{t+1}}{2} = \frac{S_{t+1} - S_t}{\Delta t} \tag{9.10}$$

where

I_t and I_{t+1} are inflow into the reservoir (m^3/s)
Q_t and Q_{t+1} are outflow from the reservoir (m^3/s)
S_t and S_{t+1} are reservoir storage (m^3) at t and $t+1$, respectively
Δt is the time interval (s)

The maximum water height in the reservoir could be estimated by solving Equation 9.10 step by step. Time interval Δt determines the length of each step in the reservoir routing, and output precision will be increased with decreasing Δt. In this study, a time interval of 30 min was selected to reduce uncertainty due to the highest water level possibility, which may occur between the t and $t+1$. The fourth-order Runge–Kutta is applied to solve reservoir routing throughout this investigation.

9.6.4 Wind Model

Wind can be defined as the horizontal movement of air, which is created if the thermal temperature balance changes because of unequal energy. Wind can start waves, raise the height of water in a reservoir, and, consequently, increase the probability of the occurrence of overtopping. In other words, if the water elevation is very near the crest, the generated waves might wash over and result in dam failure. Wind setup and wave run-up are applicable factors in evaluating the effect of wind speed on the water surface elevation in reservoirs. Hence, there is a requirement to make a relationship between the wind return period (T_w) and wind speed in the desired return period (V_{T_w}) to calculate wind setup, wave run-up, and the total height of water elevation. USBR [25] provided a method to estimate wind-generated waves in reservoirs, which is commonly accepted in the dam engineering community. Based on USBR [25], the minimum duration to reach a maximum wave height, t_{min} in hours, is calculated by the following equation:

$$t_{min} = 1.544 \frac{F^{0.66}}{V^{0.41}} \tag{9.11}$$

where

V is the wind speed over water in km/h
F is the fetch length in km

The significant wave height H_s (m), which is the average of the highest one-third of the waves of a given group or spectrum, can be calculated by the following equation [25]:

$$H_s = 0.00237 V^{1.23} F^{0.5} \tag{9.12}$$

When wind hits the beach, a setup is created and the water level rises higher than the normal water level in the reservoir. This event is called wind setup, and it can be calculated based on the following equation [25]:

$$Y_s = \frac{V^2 F}{62772 D} \tag{9.13}$$

where

Y_s(m) is the wind setup
F is the fetch length (km)
V is the wind speed over the water surface (km/h)
D (m) is the mean water depth along the fetch length

The next effective factor in wind overtopping analysis is wave run-up. If a wave approaches or hits a structure, such as a dam, part of the energy is destroyed because of turbulence, and the rest of the energy is used to run-up the dam embankment. Therefore, wave run-up is defined as the vertical difference

between the highest water level caused by the run-up on the dam and the water level at the slope foot. According to the height of the run-up, it can be determined whether overtopping occurs or not. This parameter is a function of the measured wave characteristics including significant wave height, wavelength, slope of dam body roughness, and dam permeability. Hughes [14] presented an equation to compute the maximum wave run-up based on the wave moment flux as follows:

$$\frac{Y_R}{H_0} = 3.84 \tan\theta \cdot \left(\frac{M_F}{\rho \cdot g \cdot H_0^2} \right)^{1/2} \tag{9.14}$$

where

Y_R is the maximum run-up of regular waves (m)
H_0 is the water depth from the bed to the current water elevation (m)
M_F is the depth integrated wave moment flux per unit width
ρ is the density of water (kg/m^3)
θ is the embankment slope

Hughes [14] also presented an empirical relationship for estimating momentum flux as follows:

$$\left(\frac{M_F}{\rho \cdot g \cdot H_0^2} \right)_{max} = A_0 \left(\frac{H_0}{gT^2} \right)^{-A_1} \tag{9.15}$$

where

$A_0 = 0.6392\left(H/H_0\right)^{2.0256}$

$A_1 = 0.1804\left(H/H_0\right)^{-0.391}$

H (m) is the wave height, which can equal significant weight height [27]

Finally, the total wave height, that is, an integration of the wind setup and wave run-up in the reservoir, could be calculated as follows:

$$H_w = Y_R + Y_S \tag{9.16}$$

9.6.5 Outlier Test

In the first step of this study, an outlier test is applied for 34 year (1975–2008) annual maximum discharges to determine the data that are departed from the trend line. Without the outlier test, the data point will not follow the trend of the assumed population regardless of the probability distribution. Data that are departed from the trend line occur in either upper and lower tails and are called high and low outliers, respectively. In this study, outlier analysis (high and low outliers) was implemented using the Bulletin 17B approach [20]. The steps of the test are as follows:

1. Determining k (Equation 9.17) based on the number of sample size.
2. Calculating mean and standard deviation of annual maximum discharges.
3. Computing Q_{oh} parameter for high outlier as follows:

$$Q_{oh} = \bar{Q} + k \cdot S_Q \tag{9.17}$$

and for low outlier

$$Q_{ol} = \bar{Q} - k \cdot S_Q \tag{9.18}$$

where $\bar{Q}$ and S_Q are mean and standard deviation of inflows.

4. If $Q > Q_{oh}$, Q can be considered as high outlier, and if $Q < Q_{ol}$, Q can be considered as a low outlier.

Table 9.4 shows the results of outlier test for 34 year (1975–2008) annual maximum discharges of Doroudzan Reservoir. According to the outcomes of this test, there is a low event datum, and it should be omitted from the annual maximum flood series. Therefore, the number of recorded data was reduced to 33.

9.6.6 Flood Frequency Analysis

Different statistical distributions are fitted to the annual maximum floods in order to estimate the peak flows in various return periods. The used distributions are Gumbel max, GEV, gamma, log-gamma, log-logistic, gen-gamma (4P), normal, and Pearson 5 (3P). Afterward, a goodness-of-fit test is applied for choosing the best distribution based on the KS test (Table 9.5).

Although the result of test demonstrated that all considered distributions could be selected for recorded flood data, the GEV distribution fits better than others, and it is used in this study. From frequency analysis, the values of mean and standard deviation of estimated peak discharge are obtained at a given return period, and the results are presented in Table 9.6.

9.6.7 Wind Frequency Analysis

There are two main directions for the wind speed in the Doroudzan dam basin, which are southwest and west directions. As the speed of west wind is higher than southwest and its direction is along with the

TABLE 9.4 Outlier Test Results

Sample size = n	34
K	2.61
$\boldsymbol{Q_{oh}}$	3.42
$\boldsymbol{Q_{ol}}$	1.50
Mean	2.46
Standard deviation	0.36

TABLE 9.5 Goodness-of-Fit Test of Maximum Annual Flood

Probability Distribution	Kolmogorov–Smirnov		
	Statistic Value	Table Value	Remark
Gumbel max	0.099	0.230	Ok
GEV	0.085	0.230	Ok
Gamma	0.086	0.230	Ok
Log-gamma	0.110	0.230	Ok
Log-logistic	0.091	0.230	Ok
Gen-gamma (4P)	0.195	0.230	Ok
Normal	0.119	0.230	Ok
Pearson 5 (3P)	0.089	0.236	Ok

TABLE 9.6 Mean and Standard Deviation of Peak Discharges in Various Return Periods

T-Year	2 Years	10 Years	20 Years	50 Years	100 Years
μ_I	524.191	755.388	871.876	1048.4	1201.14
σ_I	21.56	52.74	78.83	126.30	173.85

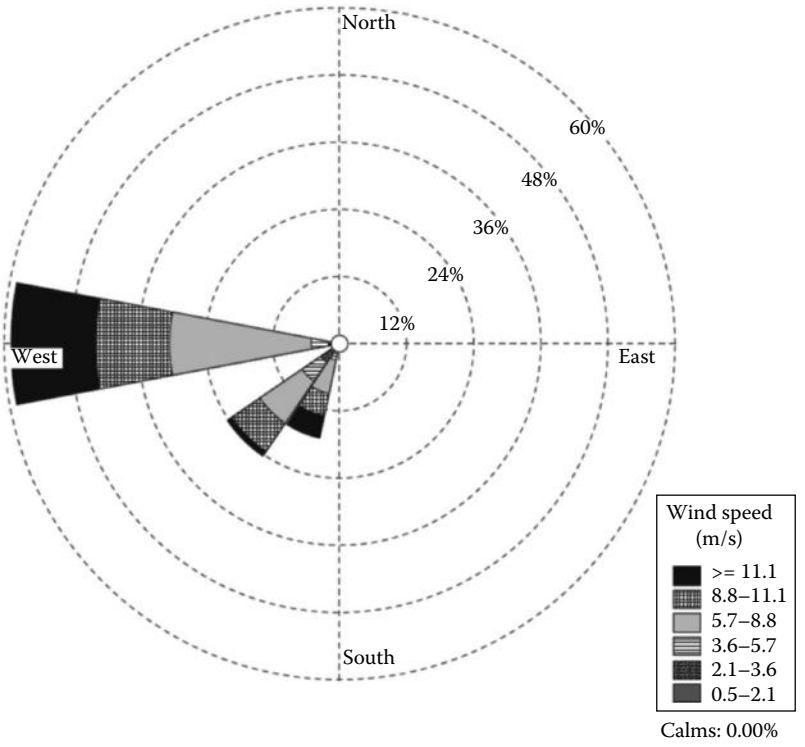

FIGURE 9.5 The wind rows of Doroudzan basin.

fetch length (Figure 9.5), the west wind data have been used to evaluate the wind setup and wave run-up for Doroudzan Reservoir.

Different statistical distributions are fitted to the 34-year (1975–2008) annual maximum wind speed in order to estimate the maximum speeds in various return periods. The used distributions are Gumbel max, GEV, Rayleigh, gamma, log-gamma, gamma (3P), Weibull, Weibull (3P), log-normal 3P, normal, Pearson 5 (3P), log-Pearson 3. A goodness-of-fit test is applied to find the best distribution by using the same statistical tests in flood frequency analysis, and the results are shown in Table 9.7.

Based on the goodness-of-fit test, the GEV, Gumbel max, log-Pearson, and other used distributions can be considered for hydrologic dam risk analysis. In this study, the GEV distribution is selected, and the wind speeds are computed in 2-, 10-, 20-, 50-, and 100-year return periods (Table 9.8).

9.6.8 Statistical Characteristics of Uncertainty Factors

The considered uncertainty parameters in this study are as follows:

1. Quantile of flood peak discharge in different return periods (I): the main reasons for considering peak floods as uncertain variables are error in data recording, lack of data, and lateral inflow into the reservoir. The values for the mean and standard deviation of Doroudzan Reservoir are

TABLE 9.7 Goodness-of-Fit Test for Maximum Annual Wind Speed

Probability Distribution	Kolmogorov–Smirnov		
	Statistic Value	Table Value	Remark
GEV	0.204	0.327	Ok
Rayleigh	0.371	0.327	Not ok
Gamma	0.243	0.327	Ok
Log-gamma	0.228	0.327	Ok
Gamma (3P)	0.240	0.327	Ok
Weibull	0.234	0.327	Ok
Weibull (3P)	0.247	0.327	Ok
Log-normal (3P)	0.237	0.327	Ok
Normal	0.266	0.327	Ok
Pearson 5 (3P)	0.235	0.327	Ok
Log-Pearson 3	0.240	0.327	Ok

TABLE 9.8 Value of Wind Speed and Minimum Duration to Reach Maximum Wave Height

T-Year	*CDF*	*V* (km/h)	t_{min} (h)
2	0.500	53.05	0.24
10	0.900	66.66	0.22
20	0.950	71.61	0.21
50	0.980	77.83	0.20
100	0.990	82.35	0.20

presented in Table 9.6. The estimated peak discharges based on GEV distribution have been used to generate inflow hydrographs, and then, the generated hydrographs were routed into the reservoir to compute the maximum water height.

2. The initial water level (H_0): the average depth of water in the reservoir was computed based on the observed and recorded water elevation over 33 years (1975–2008). The mean and standard deviation of water depth were 43.16 (m) and 1.63 (m), respectively. In addition, six other depths (with 1.5 m increments) have been assumed as initial depths in order to consider the effect of changing initial water depth on the probability of overtopping. The considered depths are 43.16, 44.66, 46.16, 47.66, 49.16, 50.66, and 52.16 m.
3. Spillway discharge coefficient (*C*): Its mean and standard deviation are assumed to be 2.05 and 0.069, respectively.

The overall process of risk and uncertainty analyses can be summarized as data collection, flood and wind frequency analyses, identification of uncertainty factors in the overtopping analysis, reservoir routing, and finally estimating overtopping (Figure 9.6).

9.7 Results and Discussions

9.7.1 Overtopping Probability Due to Different Floods

Based on the equations presented in the previous sections, the probability of overtopping is calculated for various floods of 2-, 10-, 20-, 50-, and 100-year return periods with a consideration of three uncertain variables peak floods, initial water level, and discharge coefficient. All uncertain variables are assumed

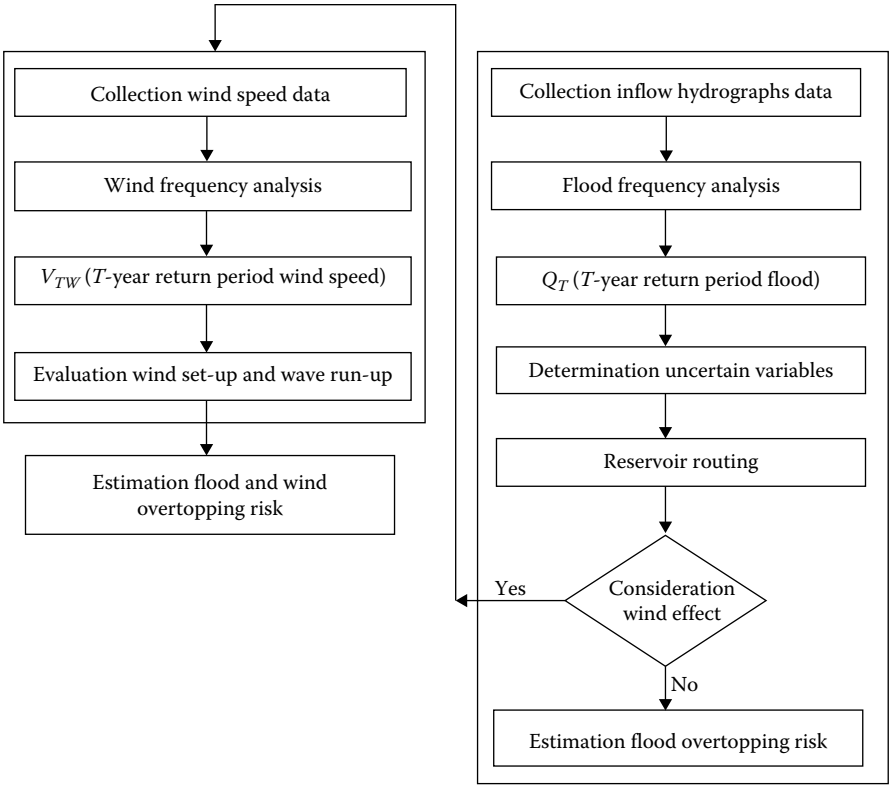

FIGURE 9.6 The process of overtopping risk and uncertainty analyses.

to be independent variables, while the MCS (with a sample size of 20,000) and LHS (with a sample size of 10,000) are applied for uncertainty analysis. The probability of overtopping due to floods in different return periods and initial levels is presented in Tables 9.9 and 9.10.

Based on these tables, by increasing the initial water level in each step, the probability of overtopping (in a constant return period) was raised for both uncertainty approaches adopted in this study.

The trends of computed risks indicated that the calculated probabilities with LHS are slightly higher than the outcomes of MC technique. Figures 9.7 and 9.8 show the results of overtopping risks for two initial water levels: 44.66 (m) and 49.16 (m) based on both MCS and LHS methods.

TABLE 9.9 Overtopping Risk Using Monte Carlo Method Due to Different Inflows

	T				
H_0 (m)	2 Years	10 Years	20 Years	50 Years	100 Years
43.16	1.13E−11	1.67E−10	4.36E−10	2.60E−08	5.30E−07
44.66	3.60E−10	2.91E−09	4.99E−09	1.88E−07	2.53E−06
46.16	3.47E−09	7.95E−08	1.69E−07	2.28E−06	2.99E−05
47.66	2.95E−07	2.88E−06	5.96E−06	2.46E−05	3.13E−05
49.16	2.31E−06	1.46E−05	2.45E−05	4.02E−05	9.52E−05
50.66	4.58E−05	1.16E−04	2.59E−04	3.30E−04	3.89E−04
52.16	8.78E−04	2.75E−03	3.21E−03	3.73E−03	5.23E−03

TABLE 9.10 Overtopping Risk Using LHS Method Due to Different Inflows

	T				
H_0 (m)	2 Years	10 Years	20 Years	50 Years	100 Years
43.16	5.66E–11	4.56E–10	7.83E–10	3.08E–08	8.06E–07
44.66	5.95E–10	3.35E–09	6.78E–09	3.94E–07	4.60E–06
46.16	4.04E–09	1.54E–07	2.69E–07	5.63E–06	4.40E–05
47.66	7.80E–07	5.32E–06	9.80E–06	3.61E–05	8.73E–05
49.16	5.70E–06	3.79E–05	4.25E–05	9.63E–05	1.77E–04
50.66	6.33E–05	1.76E–04	3.78E–04	4.09E–04	7.76E–04
52.16	9.95E–04	3.04E–03	4.43E–03	4.90E–03	6.12E–03

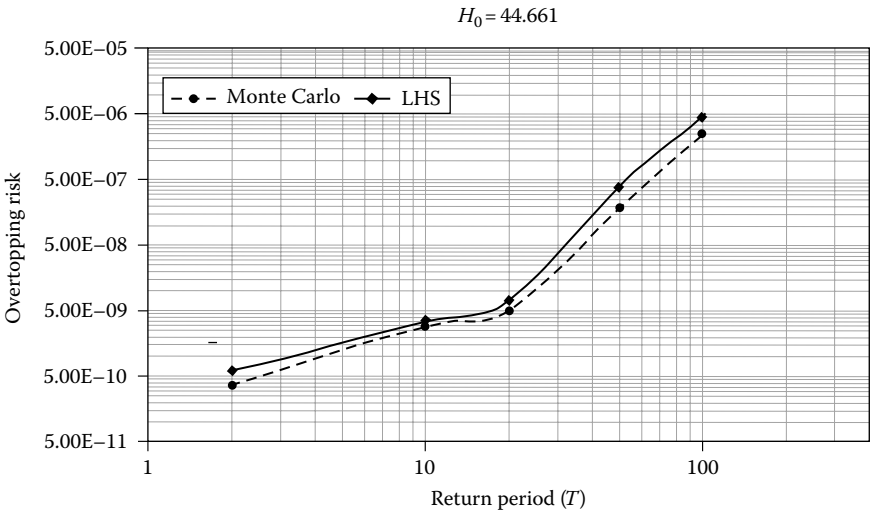

FIGURE 9.7 Variation of overtopping risk versus return period for H_0 = 44.66 (m).

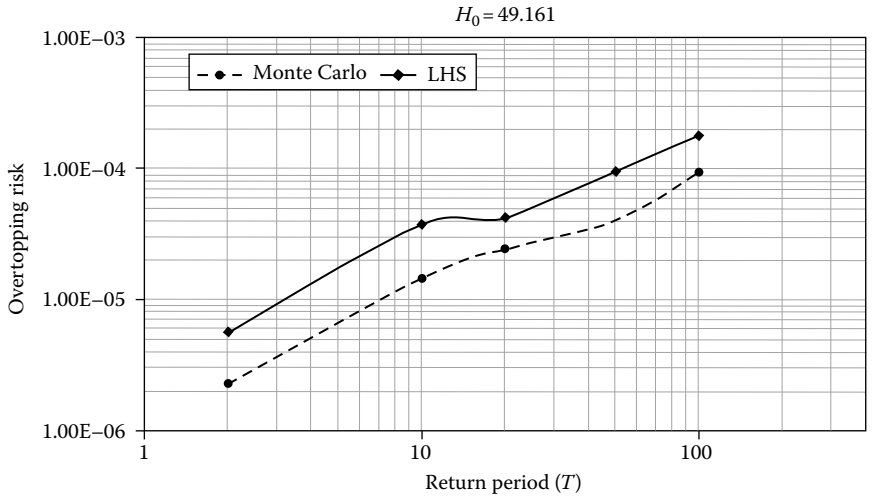

FIGURE 9.8 Variation of overtopping risk versus return period for H_0 = 49.16 (m).

9.7.2 Overtopping Risk Due to Floods and Wind

After obtaining wind speeds in different return periods, the wind setup and wave run-up are calculated using the equations provided by USBR. The wind setup and wave run-up are functions of the initial water level in the reservoir, and hence, they are also subject to uncertainty. It is important to note that there was no strong correlation between the wind speed and inflows ($Corr = 0.152$), and, thus, the wind speeds and flood values are generated separately. In other words, the highest water level in the reservoir and total wave height are calculated individually; after that, the total water elevation, which is the sum of these two factors, is assigned as final water elevation in the risk analysis. However, many combinations of inflows, wind speeds, and water elevations have been considered to cover the most likely conditions that will probably happen in the reservoir. The overtopping risks due to different floods and wind speeds in five return periods and four initial water levels were evaluated by MCS and LHS uncertainty approaches, and the results are presented in Tables 9.11 and 9.12.

The risk of overtopping, based on the MCS method versus different return periods in various wind speeds and constant initial water level (49.16 m), is presented in Figure 9.9.

9.8 Summary and Conclusions

The overall procedure in this study involved frequency analysis of floods and wind speeds, reservoir routing, and integration of wind setup and run-up to calculate the final reservoir water level. The probability of overtopping was assessed by applying two of the most used sampling methods (MCS and LHS) and considering the quantile of flood peak discharge, initial depth of water in the reservoir, and spillway discharge coefficient as uncertain variables. Considering the uncertain input variables can be resulted in an expanded range of overtopping risks in different return periods compared with deterministic analyses, which use only the best estimate value as input and provide a single point as output.

TABLE 9.11 Risk of Overtopping Due to Flood and Wind Using MCS

		T				
T_w	H_0 (m)	2 Years	10 Years	20 Years	50 Years	100 Years
2 Years	47.66	3.45E–07	3.03E–06	6.46E–06	2.56E–05	3.25E–05
	49.16	3.63E–06	1.78E–05	3.81E–05	9.18E–05	2.09E–04
	50.66	5.86E–05	1.51E–04	3.82E–04	5.60E–04	9.34E–04
	52.16	1.19E–03	3.32E–03	4.70E–03	6.91E–03	8.74E–03
10 Years	47.66	5.81E–07	3.83E–06	1.48E–05	4.44E–05	7.67E–05
	49.16	3.92E–06	1.92E–05	4.12E–05	9.94E–05	2.25E–04
	50.66	6.31E–05	1.63E–04	4.12E–04	6.05E–04	1.00E–03
	52.16	9.83E–04	3.58E–03	5.08E–03	7.49E–03	9.01E–03
20 Years	47.66	6.36E–07	4.19E–06	1.62E–05	4.87E–05	8.34E–05
	49.16	4.22E–06	2.06E–05	4.43E–05	1.07E–04	2.42E–04
	50.66	6.66E–05	1.72E–04	4.35E–04	6.39E–04	1.06E–03
	52.16	1.33E–03	3.71E–03	5.27E–03	7.78E–03	9.61E–03
50 Years	47.66	7.99E–07	5.24E–06	2.04E–05	6.11E–05	1.03E–04
	49.16	5.29E–06	2.57E–05	5.56E–05	1.35E–04	3.01E–04
	50.66	8.34E–05	2.15E–04	5.45E–04	8.02E–04	1.30E–03
	52.16	1.67E–03	4.64E–03	6.60E–03	9.77E–03	1.62E–02
100 Years	47.66	1.07E–06	7.00E–06	2.73E–05	8.18E–05	1.36E–04
	49.16	7.08E–06	3.44E–05	7.44E–05	1.81E–04	4.01E–04
	50.66	1.11E–04	2.87E–04	7.29E–04	1.07E–03	1.71E–03
	52.16	2.23E–03	6.19E–03	8.83E–03	1.31E–02	2.17E–02

TABLE 9.12 Risk of Overtopping Due to Flood and Wind Using LHS

		T				
T_w	H_0 (m)	2 Years	10 Years	20 Years	50 Years	100 Years
2 Years	47.66	7.95E–07	5.93E–06	1.07E–05	5.22E–05	9.35E–05
	49.16	6.85E–06	4.39E–05	5.04E–05	1.22E–04	2.70E–04
	50.66	7.02E–05	1.98E–04	3.97E–04	6.00E–04	1.01E–03
	52.16	1.21E–03	3.34E–03	4.74E–03	7.00E–03	8.92E–03
10 Years	47.66	8.78E–07	5.93E–06	1.90E–05	5.49E–05	9.77E–05
	49.16	6.14E–06	4.23E–05	5.34E–05	1.30E–04	2.86E–04
	50.66	6.47E–05	2.01E–04	4.27E–04	6.44E–04	1.08E–03
	52.16	1.00E–03	3.68E–03	5.27E–03	7.98E–03	1.00E–02
20 Years	47.66	9.34E–07	6.28E–06	2.04E–05	5.92E–05	1.04E–04
	49.16	6.44E–06	4.07E–05	5.65E–05	1.38E–04	3.03E–04
	50.66	6.81E–05	1.79E–04	4.50E–04	6.79E–04	1.14E–03
	52.16	1.35E–03	3.80E–03	5.46E–03	8.27E–03	1.06E–02
50 Years	47.66	1.10E–06	7.34E–06	2.45E–05	7.16E–05	1.24E–04
	49.16	6.51E–06	4.18E–05	6.78E–05	1.65E–04	3.62E–04
	50.66	8.49E–05	2.23E–04	5.61E–04	8.42E–04	1.38E–03
	52.16	1.69E–03	4.74E–03	6.80E–03	1.03E–02	1.72E–02
100 Years	47.66	1.37E–06	9.10E–06	3.15E–05	9.23E–05	1.57E–04
	49.16	8.30E–06	4.05E–05	8.66E–05	2.11E–04	4.62E–04
	50.66	1.13E–04	2.95E–04	7.44E–04	1.11E–03	1.79E–03
	52.16	2.25E–03	6.29E–03	9.02E–03	1.36E–02	2.27E–02

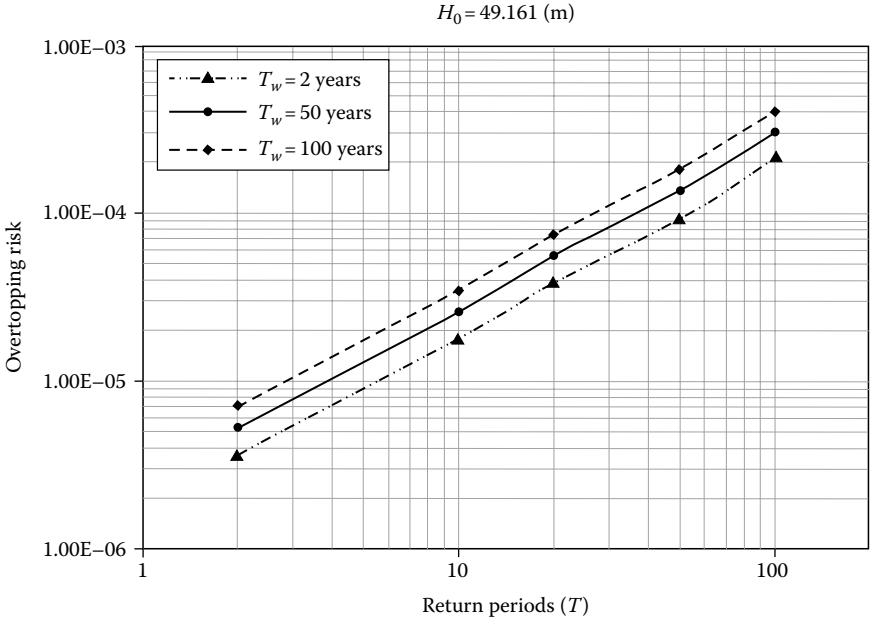

FIGURE 9.9 Variation of flood-wind overtopping risk versus return period in H_0 = 49.16 (m).

TABLE 9.13 Percentage of Increasing Overtopping Risk by Considering Wind Speed in $H_0 = 47.66$ m

	$T = 50$		$T = 100$	
T_w	LHS (%)	MCS (%)	LHS (%)	MCS (%)
2	44.60	4.07	7.10	3.83
10	52.08	80.49	11.91	145.05
20	63.99	97.97	19.13	166.45
50	98.34	148.37	42.04	229.07

Based on the results, by increasing the initial water level in each step, the probability of overtopping (in a constant return period) was raised for both uncertainty approaches adopted in this study. As the LHS stratifies cumulative distribution function (CDF) into several subregions and forces the input variables to be better than that for simple random sampling, the achieved results are different from MCS method. On the other hand, the results revealed that wind speed could have a great impact on reservoirs situated in windy areas, and the probability of overtopping has been increased in different return periods. To show the effect of wind speed on the overtopping risk, the percentage of increasing risk due to various wind speeds for both LHS and MCS methods in $H_0 = 47.66$ m and two flood and four wind speed return periods is presented in Table 9.13.

To sum up, risk analysis in conjunction with uncertainty provides significant information for decision makers to identify the events that indicate a developing failure mode, understand the critical parameters needed to effectively monitor, and determine how to use a warning system for evacuating the downstream community.

Symbols

cms	cubic meter per second
C	coefficient of variation
D	mean water depth along the fetch length (m)
F	fetch length (km)
F_x^{-1}	inverse function
H_0	mean of elevation from bottom (m)
H	wave height (m)
H_1	height difference between the crest of spillway and initial water level (m)
H_2	height difference between the crest of dam and initial water level (m)
H_s	significance wave height (m)
H_{max}	height of water in the reservoir (m)
H_R	height of dam (m)
h_t	wind setup (m)
h_r	wave run-up (m)
h_w	total weight height (m)
h	depth of water from the bed to the current water elevation (m)
I	inflow (cms)

k	number of uniform random numbers
km	kilometer
L	wavelength (m)
L_f	load
m	meter
MCM	million cubic meters
M_F	depth integrated wave moment flux per unit width
$P[.]$	probability of
$P_{i,j}$	random permutation
Q	outflow (cms)
R	resistance
$r_{i,j}$	random number
S	storage (MCM)
t	time (s)
T	flood return period
T_w	wind return period
u_i	uniform random number
V	wind speed over the surface of water (km/h)
V_{T_w}	wind speed in desired return period (km/h)
$x_{i,j}$	random variates
Z	performance function
Δt	time interval (s)
a'	risk
a	reliability
ρ	density of water (kg/m^3)
β	reliability index indicator
μ	mean of variable
σ	standard deviation
Θ	slope of the dam body

References

1. Bowles, D.S. 2001. *Evaluation and Use of Risk Estimates in Dam Safety Decision Making. 20-Year Retrospective and Prospective of Risk-Based Decision-Making*. ASCE, Santa Barbara, CA, pp. 17–32.
2. Cheng, S.T., Yen, B.C., and Tang, W.H. 1986. Wind-induced overtopping risk of dams. In B.C. Yen, ed., *Stochastic and Risk Analysis in Hydraulic Engineering*. Water Resources Publications, Littleton, CO.
3. Cheng, S.T., Yen, B.C., and Tang, W.H. 1982. Overtopping risk for an existing dam. Civil engineering studies, Hydraulic Engineering Series No. 37 University of Illinois, Urbana, IL.
4. Chow, V.T. and Maidment, D.R. 1988. *Applied Hydrology*. McGraw-Hill, New York.
5. Collick, A.S., Easton, Z.M., Adgo, E., Awulachew, S.B., Gete, Z., and Steenhuis, T.S. 2009. Application of a physically based water balance model on four watersheds throughout the upper Nile basin in Ethiopia. *Hydrological Processes* 23, 3718–3372.
6. Committee on the Safety of Existing Dams. 1983. Water Science and Technology Board. Commission on Engineering and Technical Systems and National Research Council. *Safety of Existing Dams' Evaluation and Improvement*. National Academy Press, Washington, DC.

7. Eslamian, S.S. and Feizi, H. 2007. Maximum monthly rainfall analysis using L-moments for an Arid Region in Isfahan Province, Iran. *Journal of Applied Meteorology and Climatology* 46(4), 494–503.
8. Fakhri, M., Farzaneh, M.R., Eslamian, S., and Khordadi, M.J. 2012. Uncertainty assessment of downscaled rainfall: Impact of climate change on the probability of flood. *Journal of Flood Engineering* 3(1), 19–28.
9. Ganji, A., Khalili, D., and Karamouz, M. 2007. Development of stochastic dynamic Nash game model for reservoir operation I. The symmetric stochastic model with perfect information. *Journal of Advances in Water Resources* 30(3), 528–542.
10. Goodarzi, E., Shui, L.T, and Ziaei. M. 2013. Dam overtopping risk using probabilistic concepts—Case study: The Meijaran Dam, Iran. *Ain Shams Engineering Journal*, (4): 185–197.
11. Goodarzi, E., Mirzaei. M., and Ziaei, M. 2012. Evaluation of dam overtopping risk based on univariate and bivariate flood frequency analyses. *Canadian Journal of Civil Engineering*, 39(4), 374–387.
12. Hosking, J.R.M. and Wallis, J.R. 1991. Regional frequency analysis using L-moments. Research Rep., Watson Research Center, IBM Research Division, Yorktown Heights, NY.
13. Hughes, D.A. and Mantel, S.K. 2010. Estimating the uncertainty in simulating the impacts of small farm dams on stream flow regimes in South Africa. *Hydrological Sciences Journal—Journal des Sciences Hydrologiques* 55(4), 578–592.
14. Hughes, S.A. 2004. Estimation of wave run-up on smooth impermeable slopes using the wave momentum flux parameter. *Coast Engineering* 51, 1085–1104.
15. International Commission on Large Dams. 1973. *Lessons from Dam Incidents* (reduced edition). ICOLD, Paris, France.
16. Kuo, J.T., Yen, B.C., Hsu, Y.C., and Lin, H.F. 2008. Risk analysis for dam overtopping-Feitsui Reservoir as a case study. *Journal of Hydraulic Engineering* 133, 955–963.
17. Kwon, H. and Moon, Y. 2006. Improvement of overtopping risk evaluations using probabilistic concepts for existing dams. *Springer* 20, 223–237.
18. Li, C.Q. and Zhao, J.M. 2010. Time-dependent risk assessment of combined overtopping and structural failure for reinforced concrete coastal structures. *Journal of Waterway, Port, Coastal, and Ocean Engineering* 136, 97.
19. Marengo, H. 2006. Case study: Dam safety during construction, lessons of the overtopping diversion works at Agumilpa Dam. *Journal of Hydraulic Engineering* 132, 1121–1127.
20. McCuen, R. 2005. *Hydrologic Analysis and Design*. Pearson Prentice Hall, Upper Saddle River, NJ.
21. Singh, K.P. and Snorrason, A. 1984. Sensitivity of outflow peaks and flood stages to the selection of dam breach parameters and simulation models. *Journal of Hydrology* 68, 295–310.
22. Singh, V.P., Jain, S.K., and Tyagi, A. 2007. *Risk and Reliability Analysis*. American Society of Civil Engineers. Reston, Virginia: ASCE Press.
23. Stedinger, J.R., Heath, D.C., and Thompson, K. 1996. *Risk Analysis for Dam Safety Evaluation: Hydrologic Risk*. U.S. Army Corps of Engineers Institute for Water Resources, Cornell University, Ithaca, NY.
24. Tung, Y.K., Yen, B.C., and Melching, C.S. 2005. *Hydrosystems Engineering Reliability Assessment and Risk Analysis*. McGraw-Hill Professional, New York.
25. USBR. 1992. *Freeboard Criteria and Guidelines for Computing Freeboard Allowance for Storage Dams*. US Department of the Interior, Bureau of Reclamation, Denver, CO.
26. Wallis, J.R. 1988. Catastrophes, computing and containment: Living with our restless habitat. *Speculations in Science and Technology* 11, 295–324.
27. Wang, Z. and Bowles, D.S. 2005. Dam breach simulations with multiple breach locations under wind and wave actions. *Advances in Water Resources* 29, 1222–1237.

28. Wood, E.F. 1977. An analysis of flood levee reliability. *Water Resources Research* 13, 665–671.
29. Yanmaz, A.M. and Beser, M.R. 2004. On the reliability based-safety analysis of the Porsuk Dam. *Turkish Journal of Engineering and Environmental Science* 29, 309–320.
30. Yen, B.C. 1979. *Safety Factor in Hydrologic and Hydraulic Engineering Design. Reliability in Water Resources Management*. Water Resources Publications, Highlands Ranch, CO, pp. 389–407.

10

Design Rainfall Estimation and Changes

Khaled Haddad
University of Western Sydney

Ataur Rahman
University of Western Sydney

AUTHORS

Khaled Haddad is a researcher in water engineering at the University of Western Sydney and has 10 years' experience in this field. His research is focused on regional flood frequency analysis with a particular emphasis on uncertainty in regional flood estimation. He has published over 50 refereed papers and research reports in various aspects of statistical hydrology. Khaled is also heavily involved in the current revision of the "Australian Rainfall and Runoff: A Guide to Flow Estimation."

Ataur Rahman is a senior lecturer in water engineering at the University of Western Sydney, Australia. He has over 20 years' experience in water research. His research interest includes flood hydrology, urban hydrology, and environmental risk assessment. He received "the G. N. Alexander Medal" from the

Institution of Engineers Australia in 2002. He has published over 200 research papers, book chapters, and technical reports in water and environmental engineering field. He is heavily involved in the preparation of the forthcoming revised version of the *Australian Rainfall and Runoff: A Guide to Flow Estimation*.

PREFACE

Design rainfall estimation is frequently needed in practice. Most nations develop their own design rainfall atlas for nationwide application. This chapter intends to provide insights of design rainfall estimation issues to researchers and practitioner to enable them to understand some of the fundamental statistical concepts behind the development of design rainfalls in the form of intensity–duration–frequency (IDF) data.

We have attempted to cover essential aspects of design rainfall estimation, which include (1) at-site and regional perspectives, (2) regional homogeneity and spatial dependence, (3) parametric and nonparametric approaches to fit probability distributions and model selection using different goodness-of-fit tests, (4) data collation, (5) gauged and ungauged site estimation, (6) uncertainty analysis, (7) IDF smoothing, (8) presentation of IDF data for practical application, and (9) impact of climate change on design rainfall estimation.

We would like to acknowledge the supports of the editor-in-chief associate professor Saeid Eslamian and the anonymous reviewers for making constructive comments and suggestions, which have improved the materials presented in this chapter. We would also like to acknowledge the members of our family for supporting us in writing this chapter.

10.1 Introduction

Design rainfall is a primary input to many models used to estimate runoff, pollutants load, and erosion. Many hydrological and hydraulic design applications need to be based on reliable estimates of rainfall quantile/design rainfall, which is the expected rainfall depth corresponding to a given duration and average recurrence interval (ARI). The generalized design rainfall data in the form of intensity–duration–frequency (IDF) curves are generally estimated from a regional rainfall frequency analysis (RRFA) approach using recorded rainfall data from a large number of stations within a country, for example, United Kingdom [60], United States [33], and Australia [40].

A review of rainfall frequency estimation methods was undertaken by Svensson and Jones [82]. They outlined the nationwide approaches adopted for design rainfall estimation in nine countries. The difficulties in the derivation of topographically, spatially, and temporally consistent IDF information arise from the fact that many of the rainfall stations have relatively shorter record lengths and the continuous pluviometers often have poor spatial density. In fact, many countries have very little data availability on continuous rainfall records; however, daily recorded data are often widely available. This allows estimating 24 h design rainfalls; but in many urban applications, much shorter durations are needed. Another difficulty is that rainfall characteristics can vary sharply with distance, in particular, in mountainous terrain, which makes the spatial interpolation of design rainfall characteristics a more difficult task. Design rainfall estimation is generally made using a regional frequency analysis rather than at-site analysis, which is the fundamental difference between design rainfall and flood estimation problems; in flood estimation, at-site analysis is preferred provided there is enough data.

Design rainfall estimation involves a number of steps, which are described in the following sections of this chapter. Various steps are illustrated in Figure 10.1 to provide an overview of the principal steps.

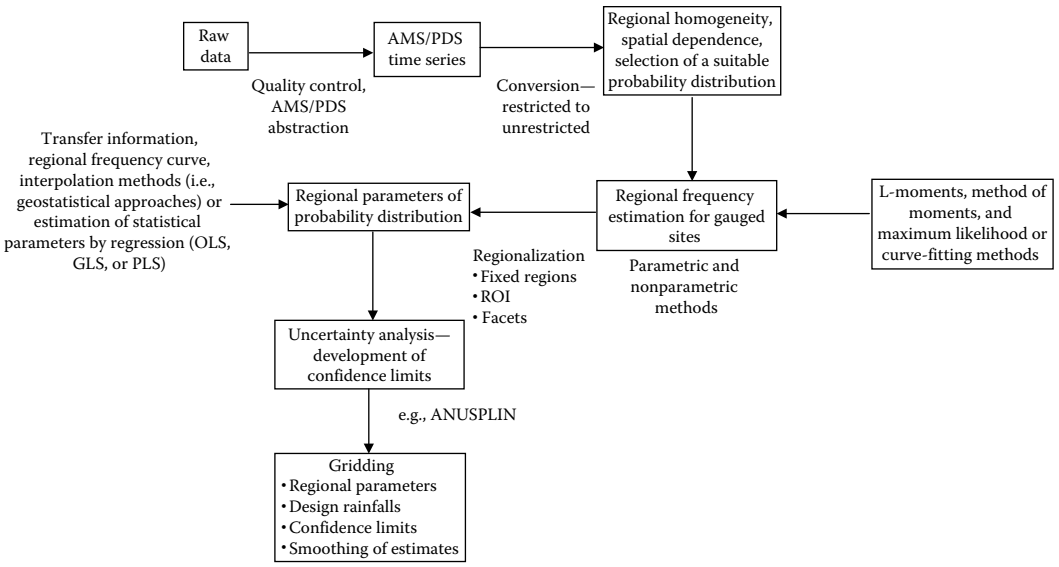

FIGURE 10.1 Approach to design rainfall estimation.

10.2 Design Rainfall Estimation Methods: At-Site and Regional Perspective

To estimate design rainfalls, regional frequency analysis methods are generally used to facilitate the estimation of rainfall quantiles for any site in a region by pooling data from several surrounding sites, which may also include data from the site being analyzed. When sufficient data are available for a particular site, the regional methods exploit the information from nearby sites or sites that are compatible in some capacity to increase the accuracy of design rainfall estimates at the site of interest. From another perspective, for an ungauged site, these methods estimate design rainfalls using regional relationships between the parameters of a probability distribution (e.g., log-Pearson type 3 and generalized extreme value [GEV]) and climatic or physiographic site characteristics (e.g., mean annual rainfall, distance from sea, and aspect).

10.3 Influencing Factors and Regional Frequency Methods

Regional frequency analysis used in design rainfall estimation aims to extract the best and most useful information from data at all the gauged sites within a region. In essence, it attempts to exploit the regional data to derive design rainfall estimates at any point within the region. In pooling the data, the useful information is gathered by excluding the noise by adopting a statistical test for homogeneity, which often identifies discordant sites and excludes them from the region, for example, Hosking and Wallis [35] and Lu and Stedinger [52]. In this, the contribution or the effectiveness of the additional data needs to be assessed, for example, by accounting for the effects of inter-site dependence of the data [54,59,66,75–77]. These issues are briefly discussed in the following sections.

10.3.1 Regional Homogeneity

The regional frequency estimation approaches attempt to combine data from other sites in the region to estimate the at-site quantiles or frequency curves. The similarity of the data is measured by some

measure of regional homogeneity. For the optimal situation, data from a homogeneous region are considered to be coming from a single population (same parent distribution) and are assumed to be identically distributed. For real-world data, this assumption does not always hold, and hence data from different sites exhibit small to large degrees of heterogeneity. The definition of regional homogeneity is essentially dependent on the frequency analysis being considered. In most cases, it is assumed that any differences occurring in at-site frequency curves in a homogeneous region can be attributed to sampling variability. A classic example of this is the index frequency method, which assumes a regional homogeneity after standardizing the at-site data by the at-site mean (or some other measure of central tendency of the data), for example, at-site median [5,18,35,36,44,46,54]. A homogeneous region or group can also be found by selecting a subsample of sites from the region. The selection can be based on geographical contiguity (see IH-FORGE method [59,66,70], region of influence approach [9,10,20,26]). Alternatively, homogeneous regions may be based on site characteristics. For example, Smithers and Schulze [72,74] presented a methodology for the estimation of short-duration design rainfalls in South Africa using a regional approach based on L-moments. The regionalization was performed using only site characteristics (e.g., mean annual precipitation [MAP], rainfall seasonality, and altitude) and minimum subjectivity to relocate stations in order to achieve relatively homogeneous clusters. In contrast to the previous, Schaefer [71] and Alila [2] formed homogeneous datasets by choosing sites with similar L-coefficient of variation (L_{CV}) and L-coefficient of skewness (L_{SK}) values. A similar approach was also investigated by Bates et al. [3] and Rahman et al. [64] for regional flood frequency analysis using data from eastern Australia.

10.3.2 Statistical Test for Homogeneity

In the literature, a large number of statistical tests for assessing regional homogeneity are proposed [6,13,23,35,36,52,84,85,91]. The purpose of these tests is to check whether the inter-site variability of a frequency curve or a distributional parameter (e.g., 1 in 50-year rainfall quantile estimate or L_{SK}) can be attributed to sampling variability.

10.3.3 Spatial Dependence

In design rainfall estimation, more often a dense network of sites is usually encountered. The annual maxima data in this dense network of observations generally show some spatial dependence, which can be attributed to the different meteorological influences; this can be categorized as large and small. The larger-scale meteorological influences stem from such phenomena such as El Niño conditions. The smaller-scale influences are by far more responsible for the high degree of dependency (correlation) between data from the closer stations. Other influences that contribute to spatial dependence include topography and site location.

Spatial dependence leads to increased uncertainty in growth curve estimation (see Hosking and Wallis [30]). Spatial dependence reduces the worth of a given number of station years of pooled data [7,8,16,90]. The use of a spatial dependence correcting model allows attribution of a much higher return period to an observation than implied by the length of the individual site record as noted by Svensson and Jones [82].

10.4 Regional Frequency Estimation for Design Rainfall for Gauged Sites

Regional frequency estimation approaches for gauged sites can be broadly classified into two main groups: (1) methods that use regional average values [24,35–37,71,79] and (2) methods that pool or regionalize recorded data from many sites (e.g., station year method and regional regression approaches) [6,7,29,33,40,41,43,44,46,53,54,56,57,59,60,92]. In the first category, it is common to use some form of

averaging of at-site parameters to derive the regional frequency curve [35], whereas the second category aims to substitute space for time, which essentially jointly analyzes data from the entire region. In any one of the broad groups identified previously, the derivation of design rainfalls in the form frequency curves can be based on two approaches, parametric and nonparametric.

10.4.1 Parametric Approach

The parametric approaches include in particular the assumption of a theoretical probability distribution for the data being analyzed and the estimation of the parameters of the distribution using an appropriate statistical method. The parameters of a statistical distribution can be estimated using a number of alternative methods: (1) method of product moments, (2) method of L-moments, and (3) method of maximum likelihood. Method of product moments may not be suitable for estimation of higher moments of the data such as the standard deviation and skewness as these are highly sensitive to the outliers in the data. In contrast, method of L-moments is generally considered to be more robust [78]. The L-moments method developed by Hosking [37] are linear functions of probability-weighted moments (PWMs) and thus do not involve squaring or cubing the observed values as do product moments. The L-moment ratios are standardized L-moments and are analogous to product moment ratios (e.g., coefficient of variation, skewness, and kurtosis). In addition, sample estimates of L-moments are virtually unbiased and have a relatively small sampling variance. Bobee and Rasmussen [4] show that L-moment estimators may also be problematic as they tend to give too little weight to large sample values that may contain important information on the tail of the parent distribution.

Hosking [37] presented L-moment ratio diagrams for some common distributions. These are quite useful in identifying a suitable distribution for a given set of observed data. Wang [89] developed direct estimators of L-moments, which eliminate the need for calculating the PWMs as an intermediate step. An extension to L-moments is the LH-moments, which are linear combinations of higher PWMs. The LH-moments provide greater weights to the higher observations in the observed data than the L-moments do, in which it is believed that these would lead to improved quantile estimates at higher ARIs [66]. The LH-moments appear to be well suited to regional frequency estimation of design rainfalls. Jakob et al. [44] applied LH-moments in design rainfall estimation in Australia and found that LH-moments utilizing a GEV distribution with a shift of 2 provided estimates that were 10% different than the estimates derived based on L-moments.

Maximum likelihood estimators do not appear to be in common use in rainfall analysis. This may be attributed to the fact that poor fitting data may cause numerical difficulties, which is often time consuming to solve and causes convergence issues.

10.4.2 Nonparametric Approach

In applying the nonparametric approaches to frequency estimation, it is first necessary to assign a plotting position to the observed data and secondly fit an empirical curve (linear or polynomial) to the points on the probability plot. Here, the assumption is made that continuity and differentiability hold in some order in the local fitting. This really is in contrast to the assumption that a particular global form of a distribution function can explain the variability in the observed data. In a single-site analysis, frequency curves derived from a nonparametric approach usually face issues with extrapolation, which is a remnant of the local fitting procedures used. However, in pooling data together from several sites (i.e., in the case of regionalization), an empirical frequency curve may become better defined especially for the larger events. This is advantageous as it eliminates the need for strict extrapolation. The nonparametric approach in the case of regional design rainfall estimation may be useful in the determination of the larger events, where the parametric approaches would prove very useful in the estimation of low to mid events as most of the information is being inferred from the body of the data. It should be kept in mind that nonparametric approaches have number of pitfalls especially when dealing with the

larger observations since larger observations are often associated with a greater degree of error. Data preparation and screening should be carried out initially to look for any anomalies or suspect data.

10.5 Regional Frequency Estimation for Design Rainfall for Ungauged Sites

Estimating design rainfalls using regional frequency analysis for ungauged sites involves the transfer of the best information from the gauged sites to the ungauged site of interest. Homogeneity based on a relevant methodology (see Section 10.3.2, e.g., statistical criteria and physiographic characteristics) is an important basis for securing the transfer of the best information. Inter-site dependence then quantifies the value of the best information in the final estimation at the site of interest. In transferring the information from gauged sites to an ungauged one, two steps are involved: (1) identification of a homogeneous region to which the ungauged site belongs and (2) utilizing the best information possible from the homogeneous region, using adjustments if necessary, to provide an estimate of the quantity required at the ungauged site.

Identifying homogeneous regions or groups can be determined as explained in Sections 10.3.1 and 10.3.2. The information from the homogeneous region can be transferred to the ungauged site in three ways: (1) Regional frequency curve calculated for the homogeneous region may be used directly for the ungauged site of interest [1,35]. (2) Estimation of the desired quantiles at gauged sites and then using interpolation to transfer the information to ungauged sites. This can be achieved using geo-statistical methods [22,58] or other spatial interpolation methods [38,39,80,87]. (3) Estimation of statistical parameters such as L_{CV} and L_{SK} for the ungauged site, using regression (e.g., generalized, partial, or ordinary least squares) or other empirical relationships with climatic and physiographic characteristics obtained from gauged sites and estimate quantiles [5,12,17,18,26,27,29,31,46,53–55,62,71–74].

10.6 Data Collation

Data collation is an important step in RRFA as this is essentially a data-based empirical approach. The quality and quantity of the data affect the accuracy of the final quantile estimates to a great extent. The individual site should have enough record length to generate at-site rainfall statistics with an acceptable level of accuracy. A shorter record length produces at-site rainfall statistics being affected by a high degree of sampling variability. Furthermore, a region should have enough number of sites so that it can deliver statistically meaningful prediction equations as well as an ample opportunity to carry out independent validation of the developed regionalization method. Hence, the selection of a cutoff record length is an important step in any rainfall regionalization study; the record length should be as long as possible while retaining enough sites in the region.

The data collation involves a number of steps: (1) select the data type needed (e.g., daily read data, pluviograph/continuous data, and historical data); (2) select whether annual maximum or partial duration series (PDS) will be used in the modeling; (3) consult the database of the relevant authorities to check how much data is there, its cost, and accessibility; (4) make request of the data to the authority; (5) check the data for accuracy and consistency as rainfall data may be subject to number of errors such as failure of gauges, accumulated data, and manual error in entering the data; (6) infill the gaps in the data where applicable possible; (7) conduct outlier and trend analysis; and (8) extract the events for various rainfall durations.

10.7 Model Selection: Partial Duration and Annual Maximum Series

Most of the literature dealing with the use of annual maximum series (AMS) in comparison to PDS is in the flood frequency analysis domain. There are only a modest number of papers that consider PDS.

Svensson and Jones [82] surveyed nine countries with regard to their design rainfall estimation procedures. All of these nine countries use AMS data as they are more readily available and easy to extract. However, there is some evidence that quantile estimates given by the PDS approach have greater precision than estimates given by the AMS approach [15,56]. Wang [88] extended the work of Cunnane [15] and found that there is no theoretical reason to use the AMS in preference to the PDS approach.

One of the limitations of the AMS method is that it always contains one value per year. As such the very large events that are not the largest in a particular year will not be included in the data series. Another consideration is that the largest event in a particularly dry year may be considerably smaller than events from other years, which may contribute to greater bias in the analysis. Another means of retrieving extra information for the frequency analysis is to use block maxima from blocks that are smaller than a year, like a month or a season, and subsequently derive the design rainfall distribution from these seasonal distributions [19]. In any case, the AMS continues to be the most popular approach given that PDS has two main drawbacks. Firstly, with PDS it is necessary to ensure that the chosen events are independent, that is, the assumption with PDS is that the abstracted peaks are mutually independent [68]. In practice, it is common to adopt some simpler approach or rule to achieve this. Secondly, the use of PDS data requires the selection of a minimum threshold value, which defines the events included in the PDS [54]. The choice of a threshold really becomes a balancing act. If the threshold is set low, many events are identified for the analysis, and some of these may be very small therefore being irrelevant especially for the higher quantile estimation. A more standardized procedure is needed for selecting the threshold value when using the PDS method at a regional level as noted by Madsen et al. [56].

10.8 At-Site Quantile Estimation: Selection of Probability Distribution

Finding a probability distribution that provides a satisfactory fit to design rainfalls (rainfall depth or intensity) has always been a topic of debate and interest in the fields of hydrology, meteorology, and others. The investigations into the design rainfall distributions are primarily spread over three main research areas, namely, (1) stochastic rainfall models, (2) frequency analysis of design rainfalls, and (3) rainfall trends related to global climate change. In this section, we mainly focus on the second group of literature. A key step in frequency analysis of design rainfalls involves selection of a suitable distribution for representing rainfall depth extremes. These analyses can be conducted for multiple rainfall durations.

10.8.1 Different Methodologies

This section describes the different methodologies of analysis used in distributional hypothesis evaluations, namely, L-moment diagram, probability plot correlation coefficient (PPCC) analysis, and model selection based on the Akaike information criterion (AIC) and Bayesian information criterion (BIC) and the modified Anderson–Darling statistic (ADC).

10.8.2 L-Moment Diagrams

The L-moment analysis is a commonly accepted procedure for evaluating the goodness of fit of alternative distributions to a given set of data. The theory and application of L-moments introduced by Hosking [37] are now widely available in literature [21,34,78], and hence it is not reproduced here. The L-moment ratios are approximately unbiased in comparison to conventional moment ratios, which can exhibit enormous bias, even for very large samples as reported by Vogel and Fennessey [86]. Higher-order conventional moment ratios such as skewness and kurtosis are very sensitive to extreme values and can exhibit notable bias even for large sample sizes [86]. The L-moment ratio diagrams provide a convenient

TABLE 10.1 Most Commonly Used Theoretical Probability Distributions Presented on the L-Kurtosis versus L-Skewness L-Moments Diagram

Distribution	Abbreviation and Data	Parameters	L-Moment Diagram	AIC, BIC, and ADC
Log-Pearson type III	LP3–AMS/PDS	3	—	Yes
Pearson type III	P3–AMS	3	(τ_4) vs. (τ_3)	Yes
Lognormal	LN3–AMS	3	(τ_4) vs. (τ_3)	Yes
GEV type III	GEV–AMS	3	(τ_4) vs. (τ_3)	Yes
Generalized logistic	GLO–AMS	3	(τ_4) vs. (τ_3)	Yes
Generalized Pareto	GPA–AMS	3	(τ_4) vs. (τ_3)	Yes
Gamma	GAM–AMS	2	(τ_4) vs. (τ_3)	Yes
Generalized Pareto	GP2–PDS	2	(τ_4) vs. (τ_3)	Yes
Lognormal	LN–AMS	2	(τ_4) vs. (τ_3)	Yes
Weibull	WEI–AMS	2	(τ_4) vs. (τ_3)	Yes
Gumbel	EV1–AMS	2	(τ_4) vs. (τ_3)	Yes
Normal	NORM–AMS	2	(τ_4) vs. (τ_3)	Yes
Logistic	LOGIS–AMS	2	(τ_4) vs. (τ_3)	Yes
Uniform	UNIF–AMS	2	(τ_4) vs. (τ_3)	Yes
Exponential	EXP–AMS/PDS	2	(τ_4) vs. (τ_3)	Yes

visual way to view the characteristics of sample data compared to theoretical statistical distributions. The L-moment diagrams, L-kurtosis (τ_4) versus L_{SK} (τ_3) and L_{CV} (τ_2) versus L_{SK} (τ_3), enable one to compare the goodness of fit of a range of three-parameter, two-parameter, and one-parameter distributions. Table 10.1 displays the different distributions that can be analyzed by means of the τ_4 versus τ_3 L-moment ratio diagrams. The L-moment ratio diagrams have been used extensively before to examine the distribution of annual maximum data series [12,17,18,32,51,63] and PDS [55,56]. Figures 10.2 and 10.3 show the application of the L-moment ratio diagram for use with at-site and regional distribution testing with some of the distributions shown in Table 10.1. Figure 10.4 shows a plot of some typical distributions used for fitting the 12 h duration rainfall for an arbitrary site in New South Wales, Australia.

10.8.3 Probability Plot Correlation Coefficient Goodness-of-Fit Test

The PPCC test introduced by Filliben [25] measures the linearity of a probability plot and is given by

$$\text{PPCC} = \frac{\sum_{i=1}^{n}(x_{(i)} - \bar{x})(M_i - \bar{M})}{\left[\sum_{i=1}^{n}(x_{(i)} - \bar{x})^2 \sum_{i=1}^{n}(M_i - \bar{M})\right]^{1/2}} \tag{10.1}$$

where

$x(i)$ is an ordered observation
M_i is the expected value from the selected distribution for an observation of order i
n is the number of observations
$\bar{x}$ and $\bar{M}$ are the means of x and M, respectively

The PPCC is near unity when the sample is drawn from the selected distribution; the plot of ordered observations versus corresponding expected values M_i for the selected distribution is expected to be nearly linear. The PPCC has been shown to be a powerful statistic for evaluating alternative distributional hypotheses as reported by Stedinger et al. [78].

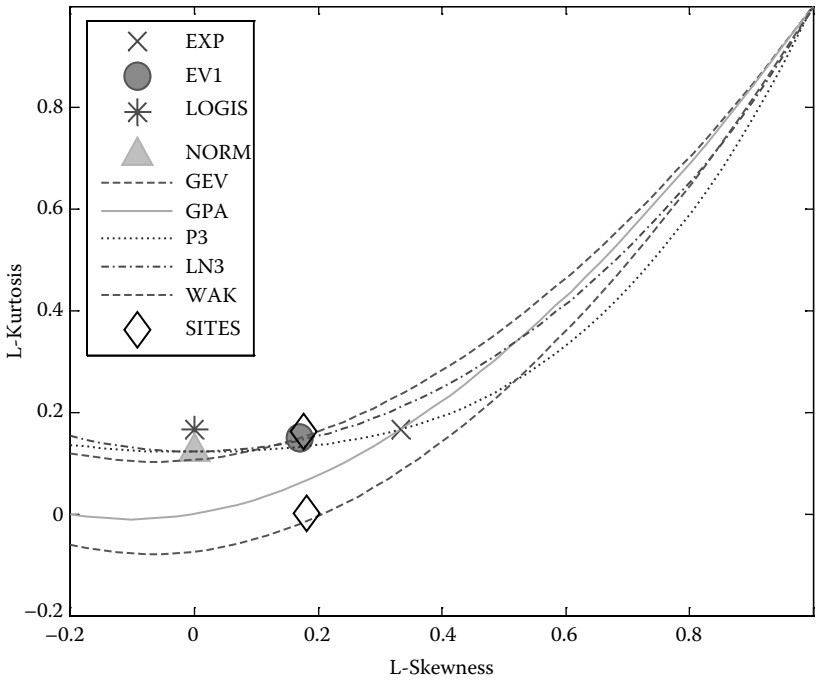

FIGURE 10.2 L-moments diagram at-site analysis for goodness-of-fit (12 h duration rainfall data for two sites in NSW, Australia).

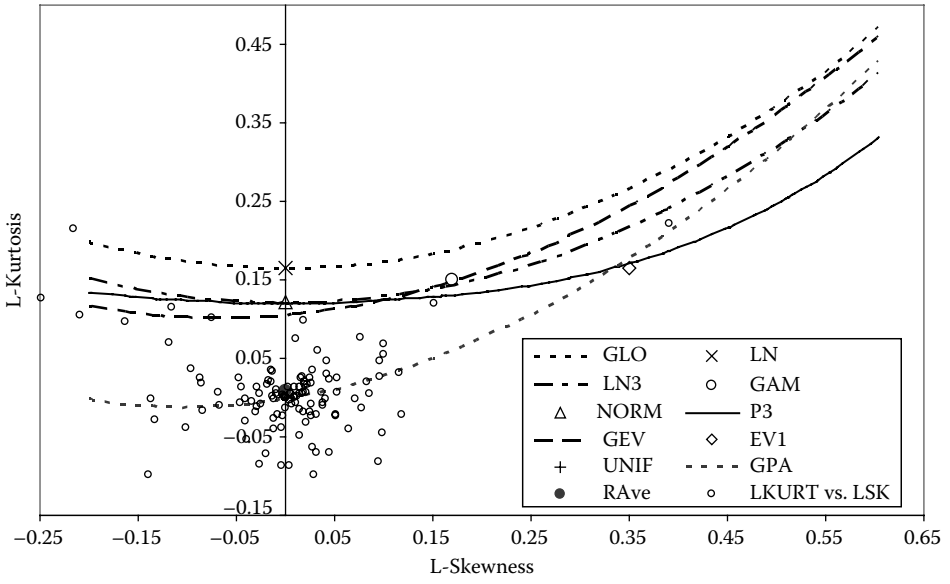

FIGURE 10.3 L-moments diagram regional analysis for goodness-of-fit (12 h duration rainfall data for 134 sites in NSW, Australia).

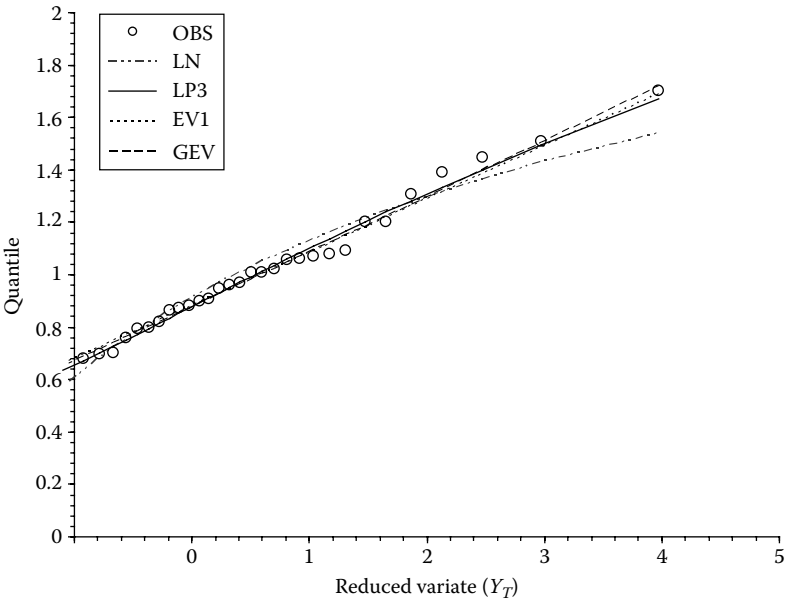

FIGURE 10.4 Types of distributions used for fitting annual maximum rainfall series data for a site in NSW, Australia.

10.8.4 Model Selection Criteria: AIC, BIC, and ADC

The AIC, based on the principle of maximum entropy, has been used in hydrological applications to select the flood frequency model in several previous studies [11,28,49,50,81]. The AIC is given by

$$\mathrm{AIC} = -2\Pi(\theta) + 2p \tag{10.2}$$

where

$\Pi(\theta)$ is the log-likelihood maximized function

p is the number of the model parameters fitted to the available sample

The first term on the right-hand side of Equation 10.2 measures essentially the true lack of fit, while the second term measures the estimation uncertainty, which is due to the number of parameters. In practice, after the computation of the AIC, for all of the operating models, one selects the model with the minimum AIC value, $\mathrm{AIC}_{\min}$. In some situations where the sample size n is small with respect to the number of estimated parameters p, the AIC may perform inadequately. In cases such as these, a second-order variant of AIC, called AIC_c, should be used and is given by Equation 10.3. As reported, AIC_c should be used when $n/p < 40$ to reduce bias as reported by Calenda et al. [11]:

$$\mathrm{AIC}_c = -2\Pi(\theta) + 2p\frac{n}{(n-p-1)} \tag{10.3}$$

The BIC is very similar to the AIC but is developed in a Bayesian framework:

$$\mathrm{BIC} = -2\Pi(\theta) + \ln(n)p \tag{10.4}$$

The BIC penalizes heavier for small sample sizes and models with high values of p. Since $\Pi(\theta)$ depends on the sample, the candidate models can be compared using AIC and BIC only if fitted on the same sample.

The Anderson–Darling statistic has shown good skills for small sample size and heavy-tailed distributions often encountered in flood frequency analysis [50,61]. The ADC can be applied to a set of distributions commonly used for frequency analysis. This criterion accounts for uncertainty through the values of ξ_j, β_j, and η_j (distribution-dependent coefficients that are tabled by Laio [50]), which depend implicitly on the number of parameters of the model. The ADC gives similar results to the AIC and BIC for small samples especially for asymmetrical distributions. After calculation of the ADC_j values for all of the operating models, one selects the model with the minimum ADC value (ADC_{min}).

10.9 Uncertainty Estimation in Regional Design Rainfall Estimation

10.9.1 Uncertainty Sources

It is generally agreed upon that uncertainty in hydrological modeling can be divided into two main categories: (1) data and sampling errors and (2) modeling or structural errors. The first category contains the data and sampling errors that remain within the data despite quality control and that is caused by sparse station density such that significant rainfall events are poorly sampled in space and time. The second category of error, that is, the modeling and structural errors, is attributed to the choice of the adopted models, the assumptions made during modeling to predict the quantile of interest. Rosbjerg and Madsen [69] noted that methods with the most restrictive assumptions lead to smaller uncertainties in the resulting predictions. However, model assumptions are often violated and as such the estimated uncertainties may be misleading. The sophistication of methods applied in assessing uncertainties varies considerably, from standard methods [84] to more complex methods addressing interrelationship between errors in estimating the index rainfall and regional growth curves [47] and methods taking into account the effects of selecting the distribution.

10.9.2 Model Errors

A number of steps are required to produce final design rainfall estimates usually either as a graph or gridded IDF estimates. The different steps and the associated models with the relevant assumptions are briefly discussed in the following.

10.9.3 Parameter Estimation

The L-moments are the most widely used method to summarize the statistical characteristics of the AMS and PDS data. As discussed in Sections 10.4.1 and 10.8.2, L-moments, though reduce the effects of sampling variability, are still subject to uncertainty, which of course transfers on to the parameters of the distribution being fitted to the at-site data. To reduce uncertainty in the parameter estimates, station records with a relatively longer length should be used.

10.9.4 Regional Regression: Bayesian Generalized Least Squares Regression

Generalized least squares (GLSs) as proposed by Stedinger and Tasker [75–77] and Bayesian GLS (BGLS) as adopted by Reis et al. [67] and Haddad and Rahman [30] can be adopted to infer regional L-moments (as a function of climatic and physiographic characteristics) for sites where little or no rainfall data are available [27,29,31,56]. The advantage of the BGLS is that it allows for the partitioning of the total error into sampling and model errors. As observed by Haddad and Rahman [27], Haddad et al. [29], and Haddad and Rahman [31], the sampling errors often dominate the total error in the model especially for the higher-order moments. Reis et al. [67] also found a similar result for the shape parameter of the log-Pearson type 3 distribution.

The BGLS provides estimates of the standard error in (1) the regression coefficients β, (2) the predictions at gauged sites used in deriving the regression equations, and (3) the predictions at ungauged sites, that is, sites not used in deriving the regression equation. The other advantage of using the BGLS is that it provides the associated posterior error variance of each parameter of a specified distribution [67]. The posterior error variance reflects the uncertainty related to the residual regional heterogeneity (model error variance) as well as sampling variability corrected for inter-site correlation, while also reflecting the prior used [56]. From these regional values, one may quantify the uncertainty in the new design rainfall estimates by deriving the 90% or 95% posterior confidence limits.

10.9.5 Gridding

The transformation from point to gridded design rainfall estimates can be carried out by thin-plate smoothing splines, which can be implemented using specific software packages (e.g., ANUSPLIN) [39]. The appropriate level of smoothing for the thin-plate smoothing spline can be chosen through generalized cross-validation by minimizing prediction error of the fitted surface [39]. Distribution point parameters or point rainfall depths can be gridded using commercial software such as ANUSPLIN.

10.9.6 Presentation of IDF Data for Practical Application

IDF data are generally provided in the form of a table or a set of curves as shown in Figure 10.5 in Rahman et al. [65]. The preparation of such data generally involves the smoothing of the initially derived quantiles by polynomial curve fitting. Smoothing IDF curves revolve around a few main aspects: should the curve be smoothed, what methodology should be adopted in smoothing, and what is the optimum order of the polynomial required for sufficient smoothing. The main objective of smoothing is to achieve

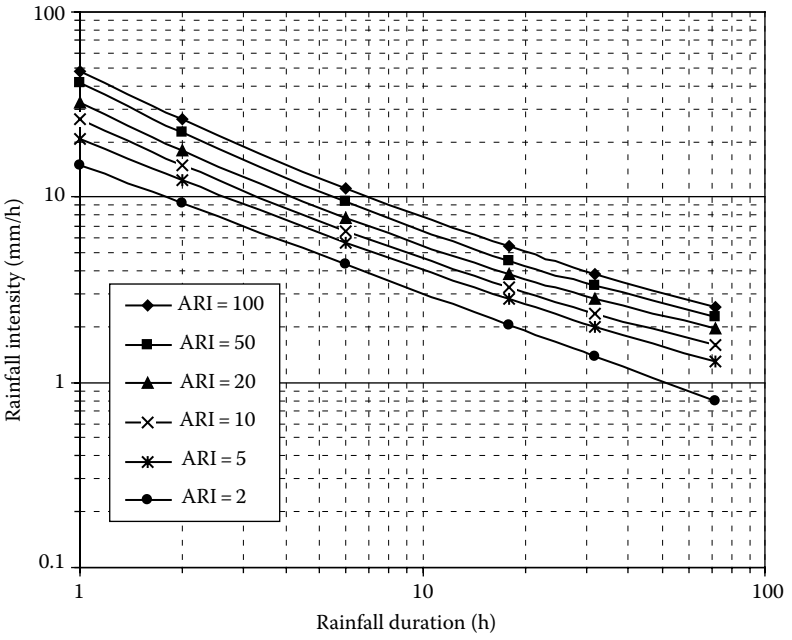

FIGURE 10.5 Typical presentation of IDF data for application. (From Rahman, A. et al., *Monte Carlo simulation of flood frequency curves from rainfall*. Technical Report 01/4. Cooperative Research Centre for Catchment Hydrology, Department of Civil Engineering, Monash University, Melbourne, Australia, 2001, 63pp.)

consistency in design rainfall intensities across the durations. The smoothing can also reduce residual noise in the estimates and unevenly spaced differences in design rainfall estimates at neighboring durations of interest.

10.10 Impacts of Climate Change on Design Rainfall Estimates

All the regional frequency analysis techniques are largely data-based and empirical in nature. The regional design rainfall estimates are derived using the recorded rainfall data. If the climate changes, the at-site and regional rainfall characteristics would also change, which will undermine the use of the past data to make prediction, which are valid for the future. For example, the rainfall data statistics such as the mean or median may change due to climate change and hence the distributional parameters or the parent distribution itself would change. The climate change poses a serious problem where the stationarity assumption may no longer be valid, which is the fundamental assumption in any frequency analysis of hydrological data.

The Intergovernmental Panel on Climate Change (IPCC) fourth assessment report acknowledged that the global surface temperature is expected to continue to warm up over the twenty-first century, affecting all aspects of the hydrological cycle [42]. Many studies have found trends in rainfall data at different parts of the world. For example, Taschetto and England [83] investigated the post-1970 Australian rainfall trends, and they found an increasing trend to the west (except coastlines) and a decreasing trend on the northeast coast of Australia. Chowdhury and Beecham [14] investigated the monthly rainfall trends and their relation to the southern oscillation index (SOI) at ten rainfall stations across Australia covering all the state capital cities. The outcomes of their assessment revealed decreasing trends of rainfall depth at two stations (Perth Airport and Sydney Observatory Hill); no significant trends were found in Melbourne, Alice Springs, and Townsville rainfall data, while the remaining five stations showed increasing trends of monthly rainfall depth. Furthermore, they found that SOI accounted for the increasing trends for the Adelaide and Cairns rainfall data and the decreasing trends for Sydney rainfall. Kunkel et al. [48] found that the overall trend in 1–7 days precipitation covering the period 1931–1996 is upward at a highly statistically significant rate over the southwest United States and in a broad region from the central Great Plains across the middle Mississippi River and southern Great Lakes basins. However, the annual trend for Canada is upward for the period 1951–1993, which is not statistically significant.

10.11 Summary and Conclusions

Many hydrological and hydraulic design tasks need to be based on reliable estimates of rainfall quantiles, generally expressed in the form of IDF data/curves. Design rainfall estimation involves application of a regional frequency analysis since at-site estimation is not preferred in rainfall estimation. The chapter has covered the principal steps in the derivation of design rainfall estimates including data preparation, formation of regions, assessment of homogeneity, building the regional estimation equations, uncertainty estimation, and the impact of climate change on design rainfall estimation.

References

1. Acreman, M.C. and Sinclair, C.D. 1986. Classification of drainage basins according to their physical characteristics: An application for flood frequency analysis in Scotland, *Journal of Hydrology*, 84, 365–380.
2. Alila, Y. 2000. Regional rainfall depth-duration-frequency equations for Canada, *Water Resources Research*, 36(7), 1767–1778.
3. Bates, B.C., Rahman, A., Mein, R.G., and Weinmann, P.E. 1998. Climatic and physical factors that influence the homogeneity of regional floods in south-eastern Australia, *Water Resources Research*, 34(12), 3369–3381.

4. Bobee, B. and Rasmussen, P.F. 1995. Recent advances in flood frequency analysis, *Reviews of Geophysics*, 33, 1111–1116.
5. Brath, A., Castellarin, A., and Montanari, A. 2003. Assessing the reliability of regional depth-duration-frequency equations for gauged and ungauged sites, *Water Resources Research*, 39(12), 1367, doi: 10.1029/2003WR002399.
6. Buishand, T.A. 1982. Some methods for testing the homogeneity of rainfall records, *Journal of Hydrology*, 58, 11–27.
7. Buishand, T.A. 1984. Bivariate extreme-value data and the station-year method, *Journal of Hydrology*, 69, 77–95.
8. Buishand, T.A. 1991. Extreme rainfall estimation by combining data from several sites, *Hydrological Sciences Journal*, 36(4), 345–365.
9. Burn, D.H. 1990. An appraisal of region of influence approach to flood frequency analysis, *Hydrological Sciences Journal*, 35(2), 149–165.
10. Burn, D.H. 1990. Evaluation of regional flood frequency analysis with a region of influence approach, *Water Resources Research*, 26(10), 2257–2265.
11. Calenda, G., Mancini, C.P., and Volpi, E. 2009. Selection of the probabilistic model of extreme floods: The case of the River Tiber in Rome, *Journal of Hydrology*, 27, 1–11.
12. Castellerin, A., Merz, R., and Blöschl, G. 2009. Probabilistic envelope curves for extreme rainfall events, *Journal of Hydrology*, 378, 263–271.
13. Chebana, F. and Ouarda, T.B.M.J. 2007. Multivariate L-moment homogeneity test, *Water Resources Research*, 43, W08406, doi: 10-1029/2006WR005639.
14. Chowdhury, R.K. and Beecham, S. 2009. Australian rainfall trends and their relation to the southern oscillation index, *Hydrological Processes*, 24(4), 504–514, doi: 10.1002/hyp.7504.
15. Cunnane, C. 1973. A particular comparison of annual maxima and partial duration series methods of flood frequency prediction, *Journal of Hydrology*, 18(3–4), 257–271.
16. Dales, M.Y. and Reed, D.W. 1989. Regional flood and storm hazard assessment. Report No. 2, Institute of Hydrology, Wallingford, Oxon, U.K.
17. Di Baldassarre, G., Brath, A., and Montanari, A. 2006. Reliability of different depth-duration-frequency equations for estimating short-duration storms, *Water Resources Research*, 42, W12501, doi: 10.1029/2006WR004911.
18. Di Baldassarre, G., Castellarin, A., and Brath A. 2006. Relationships between statistics of rainfall extremes and mean annual precipitation: An application for design-storm estimation in northern Italy, *Hydrology and Earth System Sciences*, 10, 589–601.
19. Dickinson, T. 1977. Rainfall intensity–frequency relationships from monthly extremes, *Journal of Hydrology*, 35, 137–145.
20. Eslamian, S.S. 1995. Regional flood frequency analysis using a new region of influence approach, PhD thesis, Department of Water Engineering, School of Civil Engineering, The University of New South Wales, Sydney, New South Wales, Australia, 1995, 380 pp.
21. Eslamian, S.S. and Feizi, H. 2007. Maximum monthly rainfall analysis using L-moments for an arid region in Isfahan province, Iran, *Journal of Applied Meteorology and Climatology*, 46, 494–503.
22. Faulkner, D. 1999. *Rainfall Frequency Estimation. Flood Estimation Handbook*, Vol. 2, Institute of Hydrology, Wallingford, U.K.
23. Fill, H.D. and Stedinger, J.R. 1995. Homogeneity tests based upon Gumbel distribution and a critical appraisal of Dalrymple's test, *Journal of Hydrology*, 166, 81–105.
24. Fill, H.D. and Stedinger, J.R. 1998. Using regional regression within IF procedures and an empirical Bayesian estimator, *Journal of Hydrology*, 210, 128–145.
25. Filliben, J.J. 1975. The probability plot correlation coefficient test for normality, *Technometrics*, 17(1), 111–117.
26. Gaál, L., Kyselý, J., and Szolgay, J. 2008. Region-of-influence approach to a frequency analysis of heavy precipitation in Slovakia, *Hydrology and Earth System Sciences*, 12, 825–839.

27. Haddad, K. and Rahman, A. 2009. A pilot study on design rainfall estimation using generalized least squares regression. Research Report prepared for Australian Bureau of Meteorology, School of Engineering, University of Western Sydney, Sydney, Australia.
28. Haddad, K. and Rahman, A. 2011. Selection of the best fit flood frequency distribution and parameter estimation procedure—A case study for Tasmania in Australia, *Stochastic Environmental Research and Risk Assessment*, 25, 415–428.
29. Haddad, K. and Rahman, A. 2011. A pilot study on design rainfall estimation in Australia using L-moments and Bayesian generalized least squares regression: Comparison of Fixed Region, Facets and Region of Influence Approaches. Research Report prepared for Australian Bureau of Meteorology.
30. Haddad, K. and Rahman, A. 2012. Regional flood frequency analysis in eastern Australia: Bayesian GLS regression-based methods within fixed region and ROI framework—Quantile regression vs. parameter regression technique, *Journal of Hydrology*, 430–431, 142–161.
31. Haddad, K., Rahman, A. and Green, J. 2011. Design rainfall estimation in Australia: A case study using L moments and generalized least squares regression, *Stochastic Environmental Research and Risk Assessment*, 25(6), 815–825, doi: 10.1007/s00477-010-0443-7.
32. Hanson, L. and Vogel, R.M. 2008. The probability distribution of daily rainfall in the United States, *ASCE-EWRI, World Water & Environmental Resources Congress 2008*, Honolulu, HI, 2008.
33. Hershfield, D.M. 1961. Rainfall frequency atlas of the United States for durations from 30 minutes to 24 hours and return periods from 1 to 100 years. Tech. Pap. 40, US Weather Bureau, Washington, DC.
34. Hosking, J.R.M. and Wallis, J.R. 1988. The effect of intersite dependence on regional frequency analysis, *Water Resources Research*, 24(1), 8–600.
35. Hosking, J.R.M. and Wallis, J.R. 1993. Some statistics useful in regional frequency analysis, *Water Resources Research*, 29(2), 271–281.
36. Hosking, J.R.M. and Wallis J.R. 1997. Regional frequency analysis—An approach based on L-moments, Cambridge University Press, New York, 224pp.
37. Hosking, J.R.M. 1990. L-moments: Analysis and estimation of distributions using linear combinations of order statistics, *Journal of the Royal Statistical Society Series B*, 52(1), 105–124.
38. Hutchinson, M.F. 1996. ANUSPLINE version 3.0, Centre for Resource and Environmental Studies, The Australian National University, Canberra, Australia.
39. Hutchinson, M.F. 2007. ANUSPLINE version 4.37 user guide, Centre for Resource and Environmental Studies, The Australian National University, Canberra, Australia.
40. Institution of Engineers Australia (I.E. Aust.). 1987. *Australian Rainfall and Runoff: A Guide to Flood Estimation*, D.H. Pilgrim (ed.), Vol. 1, I.E. Aust., Canberra, Australia.
41. Interagency Advisory Committee on Water Data (IAWCD). 1982. *Guidelines for Determining Flood Flow Frequency: Bulletin17-B*, Hydrol. Subcomm., Washington, DC, March 1982, p. 28.
42. IPCC. 2007. The physical science basis. Contribution of Working Group I to the Fourth Assessment Report of the Intergovernmental Panel on Climate Change (IPCC).
43. Jakob, D., Meighen, J., Taylor, B., and Xuereb, K. 2008. Methods for deriving design rainfall estimates at sub-daily durations, *Proceedings of the 31st Hydrology and Water Resources Symposium*, The Institution of Engineers, Canberra, Australia, April 14–17, 2008.
44. Jakob, D., Taylor, B., and Xuereb, K. 2005. A pilot study to explore methods for deriving design rainfalls for Australia—Part 1, Hydrology Report Series, HRS Report No. 10.
45. Jakob, D., Taylor, B., Meighen, J., and Xuereb, K. 2009. A pilot study to explore methods for deriving design rainfalls for Australia—Part 2, Hydrology Report Series, HRS Report No. 11.
46. Jakob, D., Xuereb, K., and Taylor, B. 2007. Revision of design rainfalls over Australia: A pilot study, *Australian Journal of Water Resources*, 11(2), 153–159.
47. Kjeldsen, T.R. and Jones, D.A. 2004. Sampling variance of flood quantiles from the generalized logistic distribution estimated using the method of L-moments, *Hydrology and Earth System Sciences*, 8(2), 183–190.

48. Kunkel, K.E., Karen, A., and David R.E. 1999. Long-term trends in extreme precipitation events over the conterminous United States and Canada, *Journal of Climate*, 12, 2515–2527.
49. Laio, F., Di Baldassarre, G., and Montanari, A. 2009. Model selection techniques for the frequency analysis of hydrological extremes, *Water Resources Research*, 45, 1–11, W07416, doi:10.1029/2007/WR006666.
50. Laio, F. 2004. Cramer-von Mises and Anderson-Darling goodness of fit tests for extreme value distributions with unknown parameters, *Water Resources Research*, 40, 1–10, W09308, doi: 10.1029/2004WR003204.
51. Lee, S.H. and Maeng, S.J. 2003. Frequency analysis of extreme rainfall using L-moment, *Irrigation and Drainage*, 52, 219–230.
52. Lu, L.H. and Stedinger, J.R. 1992. Sampling variance of normalised GEV/PWM quantile estimators and a regional homogeneity test, *Journal of Hydrology*, 138, 223–245.
53. Madsen, H., Rosbjerg, D., and Harremoes, P. 1995. Application of the Bayesian approach in regional analysis of extreme rainfalls, *Stochastic Hydrology and Hydraulics*, 9, 77–88.
54. Madsen, H., Pearson, C.P., and Rosbjerg, D. 1997. Comparison of annual maximum series and partial duration series for modeling extreme hydrologic events, 2. Regional modeling, *Water Resources Research*, 33(4), 759–769.
55. Madsen, H., Mikkelsen, P.S., Rosbjerg, D., and Harremoës, P. 1998. Estimation of regional intensity-duration-frequency curves for extreme precipitation, *Water Science and Technology*, 37(11), 29–36.
56. Madsen, H., Mikkelsen, P.S., Rosbjerg, D., and Harremoes, P. 2002. Regional estimation of rainfall intensity duration curves using generalized least squares regression of partial duration series statistics, *Water Resources Research*, 38(11), 1–11.
57. Madsen, H., Arnbjerg-Neilsen, K., and Mikkelsen, P.S. 2009. Update of regional intensity-duration-frequency curves in Denmark: Tendency towards increased storm intensities, *Atmospheric Research*, 92, 343–349.
58. Merz, R. and Bloschl, G. 2005. Flood frequency regionalization—Spatial proximity vs. catchment attributes, *Journal of Hydrology*, 302(1–4), 283–306.
59. Nandakumar, N., Weinmann, P.E., Mein, R.G., and Nathan, R.J. 1997. Estimation of extreme rainfalls for Victoria using the CRC-FORGE Method, Report 97/4, Monash University, Melbourne, Australia.
60. Natural Environment Research Council (NERC). 1975. Flood studies report, NERC, London.
61. Onoz, B. and Bayazit, M. 1995. Best-fit distribution of largest available flood samples, *Journal of Hydrology*, 167, 195–204, doi: 10.1016/0022-1694(94)02633-M.
62. Overeem, A., Buishand, A., and Holleman, I. 2008. Rainfall depth-duration frequency curves and their uncertainties, *Journal of Hydrology*, 348, 124–134.
63. Pilon, P.J., Adamowski, K., and Alila, Y. 1991. Regional analysis of annual maxima precipitation using L-moments, *Atmospheric Research*, 27, 81–92.
64. Rahman, A., Bates, B.C., Mein, R.G., and Weinmann, P.E. 1999. Regional flood frequency analysis for ungauged basins in south-eastern Australia, *Australian Journal of Water Resources*, 3(2), 199–207.
65. Rahman, A., Weinmann, P.E., Hoang, T., Laurenson, E.M., and Nathan, R.J. 2001. Monte Carlo simulation of flood frequency curves from rainfall. Technical Report 01/4. Cooperative Research Centre for Catchment Hydrology, Department of Civil Engineering, Monash University, Melbourne, Australia, 63pp.
66. Reed, D.W. and Stewart, E.J. 1989. Focus on rainfall growth estimation, *Proceedings of the 2nd National Hydrology Symposium*, British Hydrological Society, Wallingford, U.K.
67. Reis Jr., D.S., Stedinger, J.R., and Martins, E.S. 2005. Bayesian GLS regression with application to LP3 regional skew estimation, *Water Resources Research*, 41, W10419, doi: 10.1029/2004WR00344.

68. Rosbjerg, D. 1985. Estimation in partial duration series with independent and dependent peak values, *Journal of Hydrology*, 76, 183–195.
69. Rosbjerg, D. and Madsen, H. 1995. Uncertainty measures of regional flood frequency estimators, *Journal of Hydrology*, 167(1–4), 209–224.
70. Reed, D.W. 1994. Rainfall frequency analysis for flood design. In chap. 5. *Coping with Floods*, Ed. Rossi, G., Harmoncioglu, N., and Xevjevich, V. NATO ASI Series E Vol. 257, Kluwer Academic, Dordrecht, The Netherlands.
71. Schaefer, M.G. 1990. Regional analyses of precipitation annual maxima in Washington State, *Water Resources Research*, 26(1), 119–131.
72. Smithers, J.C. and Schulze, R.E. 2003. Design rainfall and flood estimation in South Africa, WRC Report No. 1060/01/03, Water Research Commission, Pretoria, South Africa, 155pp.
73. Smithers, J.C. and Schulze, R.E. 2004. The estimation of design rainfall for South Africa using a regional scale invariant approach, *Water SA*, 30(4), 435–444.
74. Smithers, J.C. and Schulze, R.E. 2001. A methodology for the estimation of short duration design storms in South Africa using a regional approach based on L-moments, *Journal of Hydrology*, 241, 42–52.
75. Stedinger, J.R. and Tasker, G.D. 1985. Regional hydrologic analysis, 1. Ordinary, weighted and generalized least squares compared, *Water Resources Research*, 21(9), 1421–1432.
76. Stedinger, J.R. and Tasker, G.D. 1986. Correction to Regional hydrologic analysis, 1. Ordinary, weighted, and generalized least squares compared, *Water Resources Research*, 22, 5, 844.
77. Stedinger, J.R. and Tasker, G.D. 1986. Regional hydrologic analysis, 2. Model error estimators, estimation of sigma and log—Pearson type 3 distributions, *Water Resources Research*, 22(10), 1487–1499.
78. Stedinger, J.R., Vogel, R.M., and Foufoula-Georgiou, E. 1993. Chapter 18: Frequency analysis of extreme events, in D.R. Maidment (ed.) *Handbook of Hydrology*, McGraw Hill Book Co., NY, pp. 18.1–18.66.
79. Stedinger, J.R. and Lu, L. 1995. Appraisal of regional and index flood quantile estimators, *Stochastic Hydrology and Hydraulics*, 9(1), 49–75.
80. Stewart, E.J., Faulkner, D.S., and Reynard, N.S. 1995. Rainfall frequency estimation in England and Wales Phase 1b: Pilot Study, Institute of Hydrology, Wallingford, U.K., R&D note 478, 122pp.
81. Strupczewski, W.G., Singh, V.P., and Weglarczyk, S. 2002. Asymptotic bias of estimation methods caused by the assumption of false probability distributions, *Journal of Hydrology*, 258, 122–148, doi: 10.1016/S0022-1694(01)00563-7.
82. Svensson, C. and Jones, D.A. 2010. Review of rainfall frequency estimation methods, *Journal of Flood Risk Management*, 3, 296–313, doi: 10.1111/j.1753-318X.2010.01079.x
83. Taschetto, A.S. and England, M.H. 2008. An analysis of late twentieth century trends in Australian rainfall, *International Journal of Climatology*, 29, 791–807.
84. Thompson, C.S. 2002. The high intensity rainfall design system: HIRDS, *Proceedings of the International Conference on Flood Estimation*, Bern, Switzerland, March 6–8, 2002.
85. Viglione, A., Laio, F., and Claps, P. 2007. A comparison of homogeneity tests for regional frequency analysis, *Water Resources Research*, 43, 3, doi: 10.1029/2006WR005095.
86. Vogel, R.M. and Fennessey, N.M. 1994. Flow duration curves I: A new interpretation and confidence intervals, ASCE, *Journal of Water Resources Planning and Management*, 120, 4.
87. Wallis, J.R., Schaefer, M.F., Barker, B.L., and Taylor, G.H. 2007. Regional precipitation-frequency analysis and spatial mapping for 24-hour and 2-hour durations for Washington State, *Hydrology and Earth System Sciences*, 11(10), 415–442.
88. Wang, Q.J. 1991. The POT model described by the generalized Pareto distribution with Poisson arrival rate, *Journal of Hydrology*, 129, 263–280.
89. Wang, Q.J. 1996. LH-moments for analyzing hydrological extremes, *Proceedings of the 23rd Hydrology and Water Resources Symposium*, Hobart, Australia, Institute of Engineers, National Conference published, 96/05(2), 601–607.

90. Weinmann, P.E., Nandakumar, N., Siriwardena, L., Mein, R.G., and Nathan, R.J. 1999. Estimation of rare design rainfalls for Victoria using the CRC-FORGE methodology, *Proceedings of the Water 99, Joint Congress,* Brisbane, July 6–8, 1999, Institution of Engineers, Canberra, Australia, pp. 284–289.
91. Wiltshire, S.E. 1986. Regional flood frequency analysis I: Homogeneity statistics, *Hydrological Sciences Journal*, 31(3), 321–333.
92. WMO, 1994. Guide to hydrological practices: Data acquisition and processing, analysis, forecasting and other applications, WMO-No. 168, Geneva, Switzerland, 1994.

11

Discretization in Urban Watersheds

Iván Rivas Acosta
Mexican Institute of Water Technology

AUTHOR

Iván Rivas Acosta is a civil engineer specialized in water resources. Iván attended the University of San Luis Potosi in Mexico, where he graduated in 1995 with a degree in civil engineering (with honors). Rivas holds a master of science degree in water resources from Colorado State University (CSU), and in 2009, Iván also earned a PhD degree from CSU with the dissertation: "Design and Implementation of Hydrologic Unit Watersheds for Stormwater Modeling in Urban Areas." After completing his graduate studies, Rivas developed several drainage studies for land development for Bulloch Brothers Engineering, Inc. in Nevada, and later, Iván worked for PBSJ in Maryland, performing GIS floodplain mapping for Federal Emergency Management Agency (FEMA) inside of the National Flood Insurance Program (NFIP). Currently, Iván works as a senior hydrologist in the Mexican Institute of Water Technology, where his research is focused on assessing the climate change impacts on surface hydrology, developing long-term water resources planning strategies and preparing environmental impact assessments.

PREFACE

Rainfall–runoff modeling in urban watersheds represents one of the most challenging issues in water resources. Two case studies in North Carolina (Pigeon and SW Prong Basins) were used for illustrating an innovative proposed methodology. Such procedure simplifies the drainage network where the entire urban watershed is divided into hydrologic unit watersheds (HUWs). A HUW represents a subcatchment in the watershed in which routing length is obtained by optimization. Irregular subcatchment shapes were converted to regular shapes using a kinematic wave (KW) cascading plane approach. A discretization analysis was performed where a set of hydrologic experiments using different levels of discretization were used, and a threshold discretization value in urban hydrology was investigated.

The representative element area (REA) concept was explored using the Storm Water Management Model (SWMM), and it was found that subcatchment sizes of 3% of the total basin size were appropriate. This magnitude represents the needed level of discretization in urban watersheds after which the improvement in performance becomes asymptotic. Coarser resolution levels underestimated peak flow rates and total runoff volumes.

11.1 Introduction

11.1.1 Urban Drainage Models

The complex hydrology and hydraulics of rainfall–runoff models in urban watersheds represents one of the most challenging problems in water resources engineering, even when it has been an important level of advancement by the scientific community. Geographic information systems (GIS) technology has been applied successfully to represent the complexity of the variables, and optimization methods have been applied to improve calibration as well. Unlike undeveloped watersheds, urban basins present an additional component to be modeled: the drainage network.

The simulation of rainfall–runoff relationships has been a prime focus of hydrologic research for several decades and has resulted in an abundance of models having been proposed [20]. Accurate and reliable modeling of stormwater runoff and associated phenomena has been in the past and continues today to be a challenge [37].

11.1.2 Distributed Parameter Hydrologic Models

Basin discretization is the first process to be done when a rainfall–runoff model is set up. However, there is no clear procedure to perform this task in urban basins. Neither it is fully obvious to what extent these models can provide reliable simulations over a wide range of spatial scales [25]. Many hydrologic models are available, varying in nature, complexity, and purpose [33].

The SWMM was developed by the US Environmental Protection Agency (EPA), and it is one of the most successful models produced by the EPA for the water environment [32]. SWMM is a dynamic rainfall–runoff simulation model, used for single-event or long-term (continuous) simulation of runoff quantity and quality from primarily urban areas [19]. SWMM is widely used worldwide, and it was the model used in this study. SWMM5 [13] was used as the main modeling tool since it was developed especially for urban hydrology, even when SWMM has been applied successfully to nonurban basins [31].

The runoff component of SWMM operates on a collection of subcatchment areas that receive precipitation and generate runoff and pollutant loads. Urbonas [37] pointed out that for distributed

rainfall–runoff models such as SWMM, research and studies are needed to develop guidance on how to discretize a study catchment properly, at least from the end user's perspective. Urbonas [37] specifies that an issue not solved yet is how to reduce an irregular-shaped catchment with an array of street and development patterns into regular shapes called for in models such as SWMM to get consistent and accurate results.

Selecting a higher resolution in distributed hydrologic modeling implies a subsequent set of activities: data acquisition, defining the model parameter values, building the model, simulation, calibration, and maintenance; all the cost of these tasks are increased when selecting a higher resolution. On the other hand, selecting a lower resolution greatly reduces the workload, but there is the risk of losing the advantage of the distributed modeling approach, leading to poor results due to lack of consideration of important spatial features. Clearly, there is a tradeoff between both approaches.

11.1.3 Discretization Issues in Urban Hydrology

Distributed hydrologic models subdivide an entire watershed into smaller units to represent heterogeneity within the watershed. Distributed parameter hydrologic models are being increasingly used in investigations of spatial scale and catchment heterogeneity as well as general rainfall–runoff applications. Sivapalan and Kalma [34] recognized that spatial and temporal scales generally lead to predictive uncertainty in distributed hydrologic modeling. Heterogeneity in urban watersheds presents a great complexity and so far has virtually challenged detailed description and/or measurement given the imposed human cover.

11.1.4 Imperviousness in Urban Hydrology

For modeling purposes, two types of impervious areas have been identified in urban hydrology. The first type, effective impervious area, comprises those impervious surfaces that are hydraulically connected to the channel drainage system. Streets with curb and gutter and paved parking lots that drain onto streets are examples of effective impervious surfaces. This area is known as directly connected impervious area (DCIA). The second type, noneffective impervious area, comprises those impervious surfaces that drain into pervious ground such as roof that drains onto a lawn. The sum of both is known as total impervious area (TIA).

Alley and Veenhuis [2] developed the following empirical relationship between TIA and DCIA from a highly urbanized portion of Denver, using 14 basins:

$$\mathrm{DCIA} = \mathrm{K1}(\mathrm{TIA})^{\mathrm{K2}} \tag{11.1}$$

in which K1 and K2 are dimensionless parameters to be calibrated. K1 and K2 were equal to 0.15 and 1.41 in Denver, whereas the coefficient of determination (r2) was 0.98 and the standard error of estimate was 7.5%. Alley and Veenhuis [2] also suggested to calibrate DCIA using the smaller storms for which runoff is largely from the effective impervious area of the watershed and to calibrate infiltration parameters using the larger storms. Usually, impervious surface maps come in a GIS raster format showing TIA; therefore, it is necessarily a correction through Equation 11.1.

11.1.5 Measurements of Performance

Measurements of performance allow to assess how reliable are the modeling results and, therefore, the predictive power of hydrologic models. The agreement between the observed and simulated volume and peak flow may be expressed in terms of a bias or departure. The bias indicates systematic over- or

underprediction. The departure serves as a measure of the prediction accuracy [39]. Next, there is a description of the measurements of performance used in this chapter.

1. Root Mean Square Error: This measure takes the distance vertically for all the given points (the error) and squares the value. The squaring is done so negative values do not cancel out positive values. Then all values are added and divided by the number of points. Finally, the square root is taken to have the same original units. Hence, the root mean square error (RMSE) is the vertical distance, on average, between the modeled and the observed flows.

$$\mathrm{RMSE} = \sqrt{\frac{1}{N}\sum_{i=1}^{N}\left(O_i - S_i\right)^2} \tag{11.2}$$

2. Pearson's Moment Correlation Coefficients (PMCC): Pearson's correlation reflects the degree of linear relationship between two variables. It ranges from +1 to −1. A correlation of +1 means that there is a perfect positive linear relationship between variables. A correlation of −1 means that there is a perfect negative linear relationship between variables. A correlation of 0 means that there is no linear relationship between the two variables. Correlations are rarely if ever 0, 1, or −1. The statistic is defined as the sum of the products of the standard scores of the two measures divided by the degrees of freedom.

$$\mathrm{PMCC} = \frac{\sum_{i=1}^{N}\left(O_i - \bar{O}\right)\cdot\left(S_i\bar{S}\right)\cdot\left(S_i\bar{S}\right)}{\sqrt{\left[\sum_{i=1}^{N}\left(O_i - \bar{O}\right)^2\right]}\sqrt{\left[\sum_{i=1}^{N}\left(S_i - \bar{S}\right)^2\right]}} \tag{11.3}$$

3. Nash–Sutcliffe Coefficient [26]: This calibration performance equation was suggested by the ASCE [6].

$$\mathrm{NSC} = 1 - \frac{\sum_{i=1}^{N}\left(O_i - S_i\right)^2}{\sum_{i=1}^{N}\left(O_i - \bar{O}\right)^2} \tag{11.4}$$

4. Index of Agreement [41]: The IOA is a standardized RMSE. It can vary from 0 (total disagreement) to 1 (total agreement).

$$\mathrm{IOA} = 1 - \frac{\sum_{i=1}^{N}\left(O_i - S_i\right)^2}{\sum_{i=1}^{N}\left(\left|S_i - \bar{O}\right| + \left|O_i - \bar{O}\right|\right)^2} \tag{11.5}$$

where in Equations 11.2 through 11.5,
O_i is the observed value at the ith time
S_i is the simulated value at the ith time
N is the total number of observations
$\bar{O}$ and $\bar{S}$ are mean values of O_i and S_i

In summary, the best condition is when Pearson's moment correlation coefficient (PMCC), NSC, and IOA yield a value of unity and RMSE to zero.

11.2 Modeling Approach

11.2.1 Methodology

Discretization scenarios were obtained with Arc Hydro [22]. As a computer aid, a GIS toolbox was developed to obtain the needed GIS data to build the SWMM5 models. Several rainfall–runoff experiments were performed in each watershed, where a different level of discretization was modeled in each scenario. Then, from the hydrologic simulations with various watershed configurations, the corresponding measurement of performance was computed.

11.2.2 Case Studies

The proposed methodology was tested on two urban watersheds. Both basins are located in the Wake County, North Carolina, as shown in Figure 11.1.

The land use and main properties of these watersheds are shown in Tables 11.1 and 11.2, respectively. Pigeon presents a higher urbanization level than SW Prong; the much higher TIA value in Pigeon is because it has highly developed and commercial areas. Both basins are located in the Raleigh metropolitan area. These watersheds served as examples of the methodology described herein.

The Urban Infrastructure Index (UII) is a multimetric parameter that represents the degree of development in the watershed and includes census, socioeconomic, infrastructure, land use, and land cover metrics that correlated with population density [24]. However, in this case, UII represents a specific index developed for a set of 30 watersheds in North Carolina, ranging from 0 to 100 [16].

11.2.3 HUW Modeling Principles

The entire urban watersheds were divided into HUWs. A HUW represents a subcatchment in the watershed in which routing length is obtained by optimization. Since drainage network was not modeled, a simplified and equivalent routing channel was obtained to represent the entire drainage network in each subwatershed. Because the only point in the watershed with recorded flows is the outlet, there are no observed flows for any of the subwatersheds; therefore, a synthetic hydrograph method was used to develop a proper size for the routing channel length in each subwatershed.

Unlike undeveloped watersheds, urban watersheds present an additional component to be modeled, the drainage network. Modeling an entire drainage system requires extensive field work just to obtain

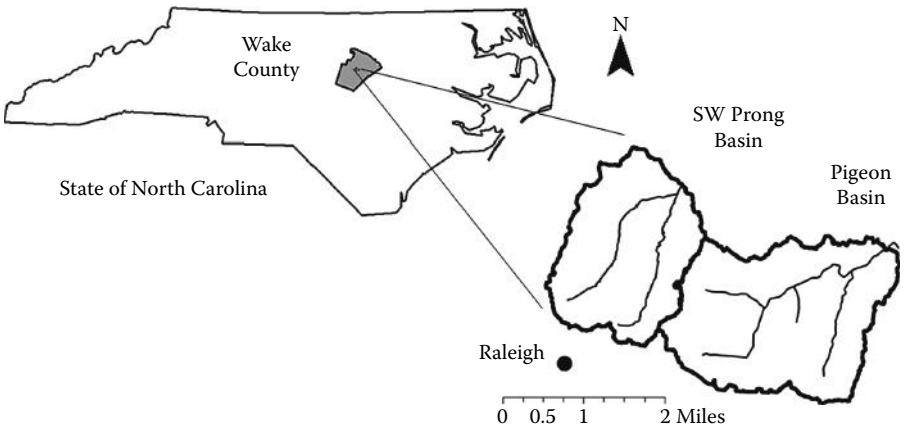

FIGURE 11.1 Location of the basins.

TABLE 11.1 Watershed's Land Use (Year 2000)

	Land Use Breakdown (%)				
Watershed Name	Developed High Intensity	Developed Medium Intensity	Developed Low Intensity	Developed Open Space	Forest or Rural
Pigeon	6	20	28	45	1
SW Prong	1	3	16	75	5

TABLE 11.2 Watershed's Properties (Year 2000)

Watershed Name	Area (mi^2)	TIA[a] (%)	Population Density (hab/mi^2)	Housing Density ($homes/mi^2$)	UII[b]
Pigeon	4.45	30.35	3204	239	100.00
SW Prong	3.02	11.45	3093	198	90.80

[a] TIA, total impervious area.
[b] UII, urban infrastructure index.

the data. However, even if there is an existing GIS shapefile with all links and their corresponding geometric features, such as cross sections and node elevations, modeling the complete network is not feasible in large watersheds. In other words, this task would represent a big engineering effort to model every single storm drainage structure, for instance, gutter flow toward a drop inlet and then to a storm drain. Therefore, realistic simplifications should be made to obtain reliable results and to meet budget and time restrictions.

11.2.3.1 Internal Routing

For the cases studies to be modeled, drainage network data were available. The City of Raleigh [12] located important drainage structures (inlets, pipes, and open channels) using global positioning system (GPS). For Pigeon Basin, the database was composed of more than 5000 link elements. However, the procedure described in the next section was applied to obtain an equivalent drainage network.

Since drainage network was not modeled, a simplified and equivalent routing channel was obtained to represent the entire drainage network in each subwatershed. Some attempts have been made to obtain a comparable drainage network. Brink [8] suggested creating a routing channel with the objective of accounting for in-system storage and attenuation that would occur within a given subarea by developing empirical relationships for length and width of this routing channel as a function of the subcatchment area (A):

$$L = \sqrt{A} \tag{11.6}$$

$$W = \frac{\sqrt{A}}{2} \tag{11.7}$$

where

L is the length of routing channel
W is the width of routing channel

On the other hand, Espey et al. [14] developed a set of generalized equations for the construction of unit hydrographs using a study of 41 watersheds ranging in size from 0.014 to 15 mi^2 and impervious

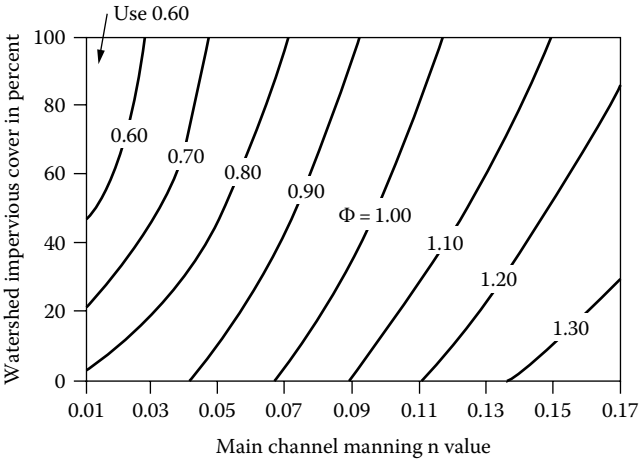

FIGURE 11.2 Dimensionless watershed conveyance factor (Φ).

percentage from 2% to 100%; 9 of the watersheds were located in North Carolina. Espey et al. [14] found the following relationships to estimate the time to peak (T_p, minutes) and the peak flow rate (Q_p, cfs/in.) as follows:

$$T_p = \frac{3.1L^{0.23}\Phi^{1.57}}{S^{0.25}I^{0.18}} \tag{11.8}$$

$$Q_p = \frac{31.62 \times 10^3 A^{0.96}}{T_p^{1.07}} \tag{11.9}$$

where

L is the length of the routing channel (ft)
Φ is the dimensionless watershed conveyance factor, which is a function of the channel roughness and watershed impervious cover or TIA (Figure 11.2)
S is the main channel slope (feet/foot)
I is the imperviousness level (%)

Design storms are developed using long-term runoff simulation and typically are used to design storm sewers, detention ponds, and other flood control facilities. Nevertheless, Urbonas [36] pointed out that it is possible to develop design storms that reasonably duplicate the peak flows from small urban basins at various recurrence intervals. In this study, a 24 h precipitation depth with a return interval of 1 year was estimated to be 2.87 in. [27] at Raleigh State University. Then, using an SCS Type II storm distribution, peak discharges and excess rainfall depths were computed in SWMM for eight experimental subwatersheds ranging from 5 to 140 acre. Using the proposed methodology by Espey et al. [14] for these subwatersheds, the length of the main channel (L) was optimized to minimize the RMSE between the peak runoff of both methods (SWMM and the unit hydrograph). The relationships that minimized the RMSE were found to be $L = A^{0.5967}$ in Pigeon and $L = A^{0.5436}$ in SW Prong.

The lower exponent in SW Prong is due to its lower development level than Pigeon; in other words, in a given subcatchment, the flow paths to reach the outlet are shorter. The latter results are congruent with the relationship provided by Brink and Broek [9]. In both watersheds, channel slopes were used based on a 3 m digital elevation model (DEM), and DCIA imperviousness levels were applied. Table 11.3 shows the used parameters.

TABLE 11.3 Experimental Subcatchment Data

Parameter	Pigeon Basin	SW Basin
Channel slope (S)	0.018	0.024
Manning's roughness (n)	0.035	0.035
Imperviousness level (DCIA, %)	13.57	5.36
Conveyance factor (Φ)	0.85	0.87

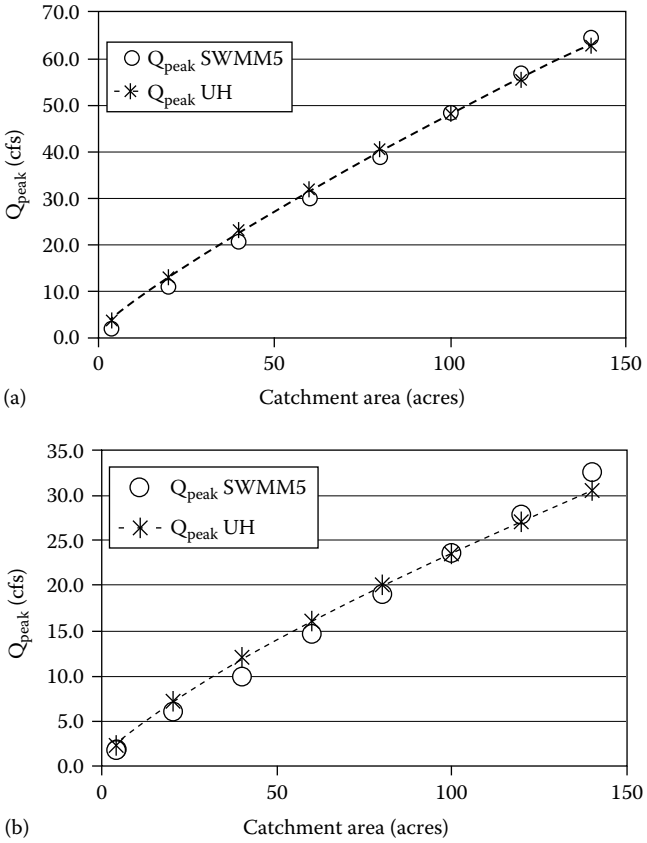

FIGURE 11.3 Peak flow rates in (a) Pigeon Basin and (b) SW Prong Basin.

Figure 11.3 shows a comparison between flows. The RMSE in Pigeon was 1.72 and 1.31 cfs in SW Prong.

11.2.3.2 Conversion of Irregular Watersheds

SWMM5 model requires the width in every subwatershed; the model assumes hypothetically that all subwatersheds have a rectangular shape. However, the subwatersheds defined with Arc Hydro resulted in irregular shapes, and a conversion was needed. As recommended [13], an irregular urban catchment can be converted to its equivalent rectangular shape. As illustrated in Figure 11.4, the uniform rainfall distribution is applied to the rectangular watershed that has a central channel collecting the overland flows from both sloping planes.

The SWMM5 user's manual suggests that the width parameter can be used to account for internal routing and attenuation, enabling delineation for larger subareas with less detail needed in defining the conveyance

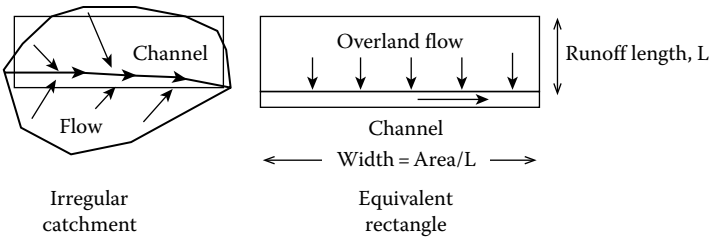

FIGURE 11.4 Conversion of irregular catchments. (From Guo and Urbonas, 2009.)

network. Huber and Dickinson [19] suggested combining many subcatchments into a single lumped or equivalent and calibrating the subcatchment width. Reducing the width increases the flow length and storage within a subarea, resulting in an effective way to attenuate the runoff hydrograph without modeling in-system storage and pipe networks [10]; for this reason, the width parameter is often the primary parameter adjusted to obtain desired peak flow rates and hydrograph shapes. Since travel time is larger, this results in more time for infiltration to occur and, therefore, infiltration volume might be overestimated [9].

However, it is easily observed that a reduction in the width increases overland flow length and overland flow travel time; therefore, there is more allowed time for infiltration to occur. This results in an effective attenuation of the runoff hydrograph without modeling in-system storage and pipe networks [9]. Brink and Broek [9] also pointed out that a solution to this problem would be to avoid large subareas and developed a more detailed conveyance system network. This idea may or may not be feasible, depending on whether the required information is available, project time and budget.

Another approach could be to estimate the runoff length (L_0), that is, the actual distance that flow typically could be expected to travel before reaching a directly connected impervious surface or a natural channel in an urban environment (usually from 100 to 300 ft). After traveling this distance, flow will either reach an impervious surface or become shallow concentrated flow. Then, compute the subcatchment Width (W) as

$$W = \frac{A}{L_0} \tag{11.10}$$

where A is the total area of the subcatchment. Rivas and Roesner [29] used the latter procedure successfully in large urban watersheds. With this approach, for each subwatershed, three to five runoff lengths need to be measured in typical lot sizes (from the back of the lot until the street center line), and then, the arithmetic average is computed. Estimating the runoff length and then computing the width yield more accurate results than taking a direct measurement of the width. This assumption is valid as long as the homogeneity of the watershed remains constant; nonhomogeneous watersheds require further discretization until homogeneous subwatersheds result. However, this task requires the visual estimation of runoff lengths through aerial images in subcatchments. Even when the last procedure is realistic, it might be time consuming and possibly infeasible in large watersheds.

For example, a schematic in Figure 11.5 shows three subwatersheds with three different runoff lengths (L1, L2, and L3). The runoff in each subwatershed drains to the junctions (J1, J2, and J3) and, then, through the drainage network to the outlet.

A more general approach is given by Guo and Urbonas [17] defining a KW cascading plane specified by the plane's area, width, and slope. Traditionally, the current state of practice recommends that the KW plane width be twice the length of the central channel in a symmetric watershed or equal to the length of the side channel along the watershed boundary [19].

Guo and Urbonas [17] developed a methodology to convert an irregular watershed to its equivalent rectangular watershed, where the continuity and energy principles were interpreted to preserve the watershed area and vertical fall over the receiving waterway's length. Figure 11.6 shows how a natural

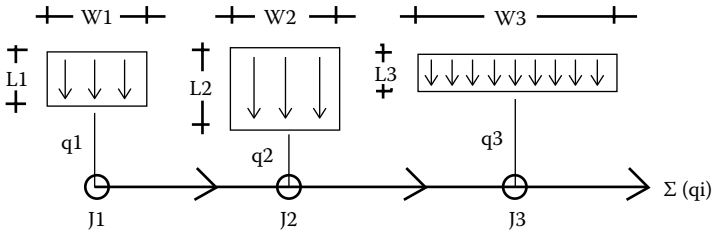

FIGURE 11.5 Width determination.

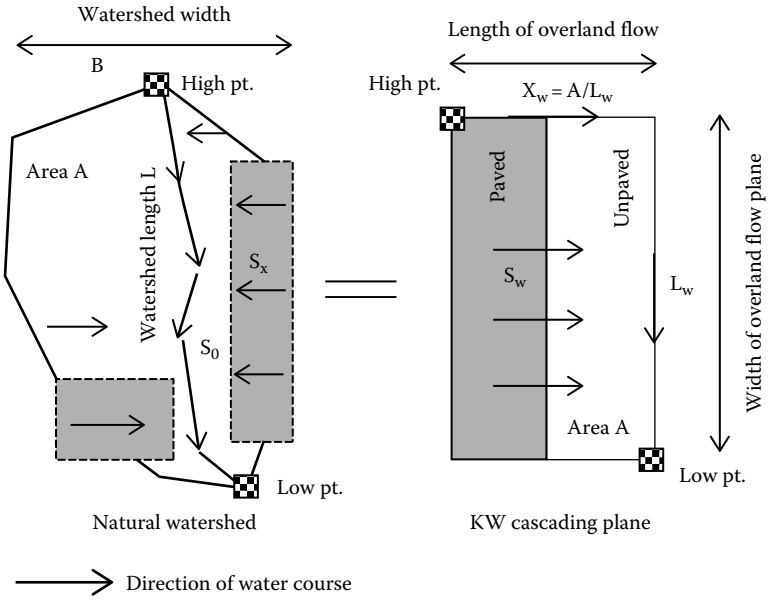

FIGURE 11.6 Natural watershed and KW plane. (From Guo and Urbonas, 2009.)

watershed with irregular shape may be converted to a rectangular watershed. The longitudinal slope (S_0) is defined by the vertical fall along the receiving waterway for the natural watershed. The KW plane slope (S_w) is virtual and used only in computation. After numerous tests, Guo and Urbonas [17] confirmed that the watershed and KW shape factors provide a consistent and stable basis for watershed geometric conversion.

The set of equations to perform the conversion are presented [17]:

1. Natural watershed shape factor (X)

$$X = \frac{A}{L^2} \cong \frac{B}{L} \le K_s \tag{11.11}$$

   K_s is the upper limit of shape factor. The Colorado Urban Hydrograph Procedure suggests $K = 4$ [35] to avoid subareas too wide in shape.

2. KW shape factor (Y)

$$Y = \frac{L_w}{L} = (1.50 - Z)\left[\frac{2}{1-2K_s}X^2 - \frac{4K_s}{1-2K_s}X\right] \tag{11.12}$$

In which $Z = A_m/A$ (area skewness coefficient between 0.5 and 1.0). A_m is the dominating area that is the larger one between the two subareas separated by the collector channel. For a symmetric watershed, $Z = 0.5$. For a side channel along the watershed boundary, $Z = 1$. From visual inspection, all subwatersheds in Pigeon and SW Prong Basins were identified to have a central channel.

3. Finally, the potential energy along the water course is preserved by

$$\frac{S_0}{S_w} = \frac{X}{Y} + Y; \quad X \le K_s \tag{11.13}$$

In summary, in a HUW, the routing channel length (L) was estimated through an optimization algorithm as a function of the subwatershed size (A), and then, it was used as a parameter for the conversion from irregular to regular subcatchments. An advantage of the latter method is that the only parameter needed in each subcatchment is its routing channel length. This proposed procedure showed to be effective and simple to implement, and results were still accurate.

11.2.4 Main Channels

Rainfall in each subcatchment becomes overland surface runoff after the soil is saturated, and then, it is routed through the main channels. However, runoff from the DCIA occurs rapidly and comprises the bulk of the runoff from urbanized areas [21].

Arc Hydro [5] is a GIS extension to obtain drainage patterns in catchments from the DEM. Raster analysis was performed to generate data on flow direction, flow accumulation, stream definition, stream segmentation, and watershed delineation. These data are then used to develop a vector representation of catchments and drainage lines from selected points. It was found that the stream patterns defined with Arc Hydro [5] follow the drainage network.

Natural streams are an integral part of the drainage system. Preliminary site investigations were performed to identify conveyance features of the main streams. Field work was done during November 2005 to obtain the cross sections in main channels using level and rod methods as described by Harrelson et al. [18]. Streams cross sections were taken at approximately 2500 ft intervals along main channels [28].

Channel Manning's roughness was estimated during the field work by following the guidelines provided by Chow [11], and Arcement and Schneider [4]. GPS coordinates of the cross sections were mapped with a unit eTrex Legend [15].

11.2.5 Hydrologic Parameters

Table 11.4 shows the needed watershed model input data, divided by type.

A DEM was obtained through the USGS National Map Seamless Server [38]. The website provides the National Elevation Dataset with a 1/9 as resolution (approximately 3 m). One arc second is the 1/3600th of a degree (1 s) of latitude or longitude. The length of arc subtended is approximately 30 m. Arc Hydro [5] processes the DEM raster to discretize the watershed, that is, the watersheds are discretized into subareas using the Arc Hydro extension of ArcGIS; impervious areas and slopes were estimated for each subarea.

Initial estimates of a watershed's soil infiltration were obtained through soil conservation service (SCS) maps. These maps classify soils into four hydrologic soil groups (A, B, C, and D) based on textures and runoff potentials. It is possible to link these hydrologic soil groups with initial (f_0) and ultimate (f_c)

TABLE 11.4 Watershed Model Input Data

Watershed Model Input Data		
Subcatchment Characteristics	Channel Conveyance	Calibration Data
Drainage area	Cross sections	Rainfall depth
Width	Bottom slope	Streamflow records
Overland ground slope	Length	
Overland flow slope	Roughness	
Soil infiltration rates		
DCIA coefficients		
Depression storage		
Overland flow roughness		
Groundwater parameters		

Horton infiltration values and obtain a weighted initial estimation of watershed infiltrations. Horton method (Equation 11.14) was used to model infiltration as a function of time f_p (t):

$$f_p(t) = f_c + \frac{f_0 - f_c}{e^{Kt}} \tag{11.14}$$

where

f_c is the minimum (final) infiltration rate ([L]/[T])
f_0 is the maximum (initial) infiltration rate ([L]/[T])
K is the decay coefficient (1/[T])
t is the time ([T])

The decay coefficient (K) determines the time elapsed in which the soil becomes saturated, and it reaches its final infiltration rate (f_c). Typical values of infiltration decay coefficients are shown in Table 11.5.

Horton infiltration rates are reported by Natural Resources Conservation Service divided by hydraulic soil groups (Table 11.6).

In SWMM5, another parameter of infiltration is the drying time (T_w, days). T_w represents the time it takes the soil to recover its initial infiltration capacity (return to the initial condition). In other words, it is the time it takes for the soil to dry out. The decay coefficient (K) and drying time (T_w) are especially important for long continuous simulations, since a successive set of storms are applied.

Impervious surface maps come in a GIS raster format, which allows an assessment of the percentage of impervious cover in a watershed. Since imperviousness changes over time, the most recent maps are preferred. In any case, they should be corrected to take into account only the DCIA through Equation 11.1; this is especially necessary in urban areas. DCIA is important to quantify

TABLE 11.5 K and f_c Relationship

Decay Coefficient (1/h)	% Decline of Infiltration Capacity toward Limiting Value f_c after 1 h
2	76
3	95
4	98
5	99

TABLE 11.6 Soil Textures and Hydrologic Soil Groups

Hydraulic Soil Group	f_c (in./h)			f_0 (in./h)
	High	Low	Average	
A	0.45	0.30	0.38	7.50
B	0.30	0.15	0.23	4.50
C	0.15	0.05	0.10	3.00
C/D	0.10	0.03	0.06	2.25
D	0.05	0.00	0.03	1.50

accurately in modeling because it affects not only the large and medium discharge runoff events but also the frequent 2 year or more frequent events that have been shown to produce 90% of the total runoff [30].

If the gross impervious area is taken to be zero (TIA = 0), the original land surface is assumed and any kind of human development is ignored. Raster GIS imperviousness maps were obtained with a resolution of 30 × 30 m. To obtain the overall imperviousness of a particular subwatershed, a weighted average from the individual values of each raster is obtained, that is,

$$\text{Imperviousness} = \frac{\sum_{i=1}^{n} \left(\text{Value}_i \cdot \text{Count}_i\right)}{\sum_{i=1}^{n} \left(\text{Value}_i\right)} \tag{11.15}$$

The necessary adjustments for the correction factors K1 and K2 for imperviousness raster maps showed in Equation 11.1 were found to be minimum. In Pigeon Basin, K1 = 0.13 and K2 = 1.35, and in SW Prong Basin, no modification from the original coefficients proposed by Alley and Veenhuis [2] was needed. The depression storage represents all losses before runoff begins and includes water retained in surface depressions and water taken up by vegetation interception. In urban watersheds, any rainfall less than about 0.05 in. will not produce runoff due to depression storage.

Watershed models have three types of Manning's roughness parameters:

1. Roughness of the pervious ground surface. Typical values range from 0.26 (dense grass) to 0.40 (light underbrush).
2. Roughness of the impervious ground surface, for example, 0.015 for smooth asphalt.
3. Roughness of the channels and/or conduit links, for instance, 0.012 for concrete storm drains.

Even though aerial images do not provide a direct input to the watershed models, they do help in the visual recognition of features in the watershed, such as ponds and commercial/residential/industrial zones. Aerial images may be downloaded through the USGS website (http://seamless.usgs.gov/). Aerial images are especially useful to estimate runoff lengths [29].

11.2.6 Groundwater Simulation

Interflow is the residual groundwater flow that occurs after each storm event. The interflow is not as deep as the baseflow of a watershed, and it feeds into stream channels at a slower rate than the flow of surface runoff produced by the same event. In both basins, the baseflow was estimated on a monthly basis and removed from the USGS monitored record (Figure 11.7). Then, groundwater component in SWMM5 was added to meet the medium and small event discharges due to the presence of interflow in the USGS discharge record.

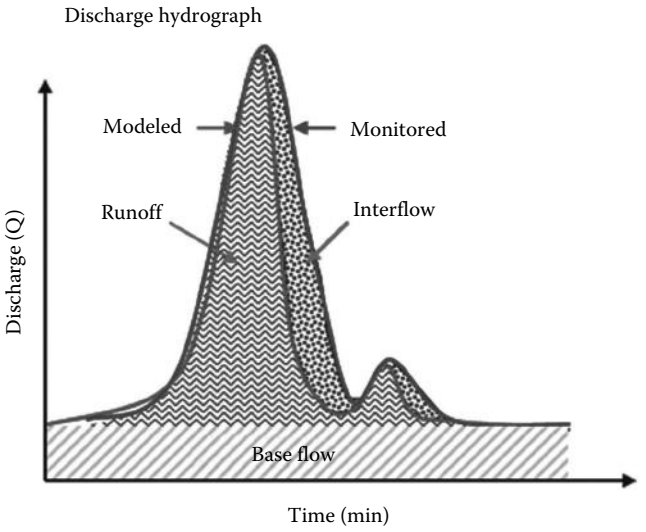

FIGURE 11.7 Runoff, base flow, and interflow volumes.

While baseflow can be estimated on a monthly basis and subtracted from the discharge record, interflow, which occurs on a storm-by-storm basis, cannot be easily removed from the record and must be simulated to improve modeling results. A single aquifer was assumed in both watersheds. According to the USGS, groundwater in the Piedmont Region is likely to flow near the surface as interflow. Because of this, groundwater component was added to the models to account this phenomenon and to properly model the low flows.

11.2.7 Rainfall and Runoff Data

Precipitation data constitute the main input to the model. It comes in a spatial distribution of precipitation over time. Rainfall data should be as close as possible to the watershed being modeled. In some regions, spatial variability plays an important role. However, the use of radar-generated rainfall data overestimates runoff in some cases [37]. USGS rain gage (site no. 0208732885) located at Marsh Creek, New Hope, NC, provided 15 min rainfall data. Refer to Table 11.7 for a complete description.

The streamflow gages were located at the watershed outlets of both basins. Stream depth data were collected by the USGS. Water-level data were collected at 15 min increments for the monitoring period. The water-level data were converted to discharge values by USGS staff using stage–discharge curves established using HEC-RAS models [28]. Streamflow records identified in Table 11.8 provided data for calibration.

TABLE 11.7 Rain Gage Data

Data	Value
ID	317079
In service	May 31, 1954 to present
Elevation	121.9 m (400 ft) above s/l
Lat/Lon	35°48′N/78°42′W
County	Wake

TABLE 11.8 General Data for Stream Flow Gages

Variable	Pigeon Basin	SW Prong
USGS site number:	0208732610	02087304
Geographic location (NAD83)	Latitude 35°48′25″ (N) Longitude 78°36′50″ (W)	Latitude 35°49′04″ (N) Longitude 78°39′35″ (W)
Hydrologic unit:	03020201	
Drainage area (mi^2):	4.45	3.02
Range of 15 min data	July 4, 2002 October 28, 2003	July 4, 2002 July 28, 2003
Number of years	1.32	1.07
Datum of gage, NGVD29 (feet above sea level)	200	240

11.2.8 Model Calibration

Traditionally, stormwater model calibration is performed on six or more individual storms of varying size [1]; it is considered complete for the single storm event when the peak discharge and volume of runoff are accurately reflected by the model.

In general, calibration can be done at a number of temporal scales [28]:

1. Single event: one storm
2. Multiple events: several storms
3. Continuous simulation: long records (months to several years)

Calibration to a single storm is not appropriate for continuous simulation modeling because adjustments of variables to match runoff from one event may over- or underadjust variables and inhibit matching of other events. Pomeroy [28] pointed out that it is important that rainfall–runoff models be able to accurately simulate the full spectrum of flows to evaluate biologic integrity in streams. Therefore, the models were calibrated across the full spectrum of flows during the 2002–2003 (temporal scale (2)) period of level-flow monitoring by the USGS personnel, where model outputs and observed flows were compared.

Large events for flow duration are those equal to or less frequent than 0.2% of time exceeded. Medium events are those falling between 0.2% and 10% of time exceeded and small events are those less than 10% of time exceeded. Small storms are generated mainly by DCIA; however, peak floods also play an important role in urban watershed modeling. Hence, a unique feature of this study is to consider all types of events in the calibration procedure.

The flow duration curve is a graph of all the discharges during a continuous record, and their cumulative exceedances, or the percent of time each discharge occurs during the period of record. These curves were developed from the partial duration series of peak flows. This approach, which is in contrast to the examination of the annual maximum series, was used because it allowed for the analysis of high-frequency, low runoff–producing storms.

The percentage of time for each flow magnitude is equaled or exceeded can be computed by arranging the flow rates in the order of descending magnitude [23]. The return period (T_r) is computed for each event using the Cunnane method:

$$T_r = \frac{n + 1 - 2 \cdot a}{m - a} \tag{11.16}$$

where

n is the length of record, years
a is the plotting position, usually taken as 0.40
m is the rank, 1 for the highest

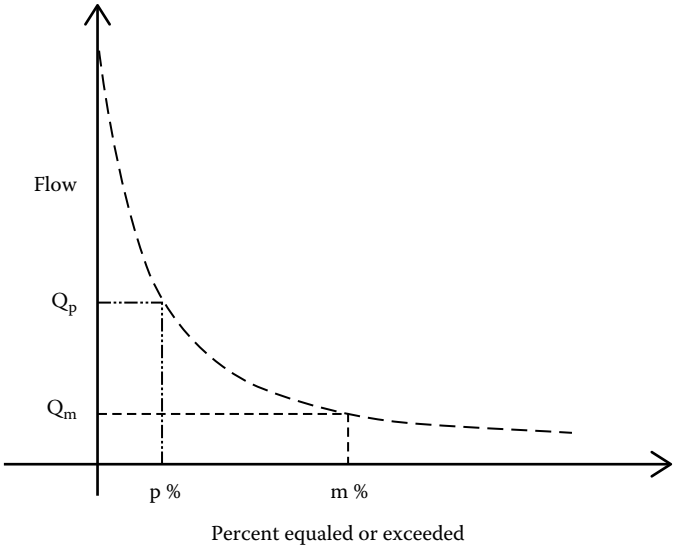

FIGURE 11.8 Flow duration curve.

The return interval was computed to exceedances per year (E) using $1/T_r$. Then, this percentage of time of exceedance is plotted against the flow magnitude. Let Q(A) be a random variable denoting the annual peak floods from a watershed of drainage area A. Then, the pth quantile $Q_p(A)$ is defined with Equation 11.17 and shown in Figure 11.8.

$$P\left(Q(A) > Q_p(A)\right) = p \tag{11.17}$$

11.2.9 Advantages of Continuous Calibration

Continuous calibration involves calibrating to a long duration of multiple events ranging from months to years. The main advantage of continuous calibration is that it makes maximum use of available data over a variable spectrum of hydrologic–hydraulic events [40]. Continuous calibration eliminates the need to select specific storms with various antecedent conditions because all or a large portion of the events of the calibration record are being simulated. Continuous calibration eliminates the time required to select discrete events to calibrate and ensures that a wide range of conditions are assessed in a shorter period of calibration time. Continuous simulation allows modeling the complex interactions between the precipitation patterns. Return periods for storms can be defined on the basis of the simulated record; critical events chosen for study may be substituted for synthetic design storms.

Finally, SWMM simulation errors were verified after simulations. Mass continuity simulation errors for runoff and flow routing represent the percent difference between initial storage + total inflow and final storage + total outflow for the entire drainage system. All simulation errors were verified to be less than 1%. The most common reasons for an excessive continuity error are computational time steps that are too long or conduits that are too short.

11.3 Model Discretization

11.3.1 Modeling Experiment Setup

Several rainfall–runoff models were built in each basin, ranging from a high resolution down to the lowest possible resolution (a single watershed). Then, measurements of performance (PMCC, NSC, IOA,

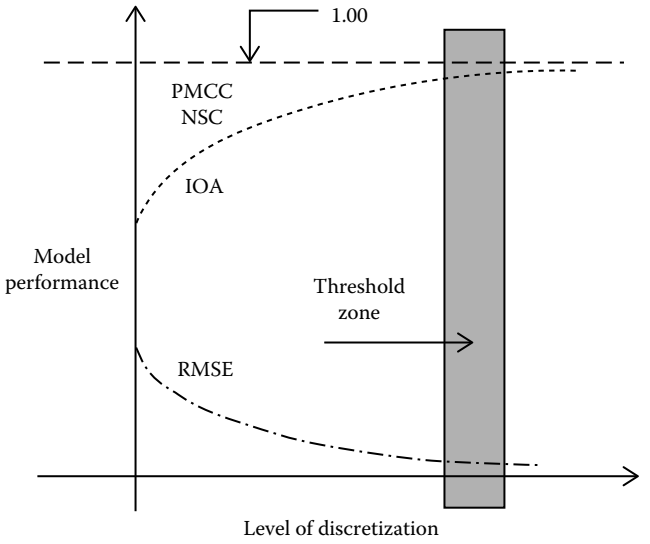

FIGURE 11.9 Threshold zone to be identified.

and RMSE) were computed and compared to identify the existence of a threshold value in which modeling results are acceptable and a finer discretization is no longer needed to obtain satisfactory results. The initial or base scenario was chosen to have an average subbasin size of 43 acre in Pigeon and 55 acre in SW Prong. This size represents a reasonable value in which the homogeneity is kept. From this initial level of discretization, successive scenarios representing a coarser resolution with larger average sizes were built, until get the last scenario, where the total watershed does not have any subdivision level, that is, the entire watershed was lumped as a single unit.

This analysis allowed the determination of a scale-related threshold value to discretize urban basins (see Figure 11.9). Also through the performed simulation analysis, the effects of subbasin scale on peak flow rate and total runoff volume were investigated.

Resulting Arc Hydro subbasins were successively disaggregated in larger sizes until a single unit for the entire watershed was obtained (Scenario 1 in both basins). Scenario 1 represents a model with a single unit, in other words, without any discretization, see Figures 11.10a,b and 11.11a,b.

11.3.2 Peak Flow Rate Estimation

Long-term simulations were performed based on the dates shown in Table 11.8. In terms of peak flow rates, coarser resolution showed larger errors and an underestimation of peak flows in both basins, as it is shown in Figure 11.12a and b. Scenario 5 showed a reasonable estimation of peak flow rate in both basins, considering that the estimation of peak flow rate was not solely indented during calibration. However, the runoff peak rate is the most important hydrologic variable for drainage system design and flooding analysis. Notice that Pigeon had larger errors for coarser scenarios than SW Prong, which could be explained by its higher level of urban development.

11.3.3 Representative Element Area

The REA represents a spatial case over which the hydrologic processes can remain simple in terms of distributed catchment behavior [7]. Therefore, this concept was further investigated to find out an appropriate scale level in urban hydrology. Theoretically, this element size is able to represent the complex

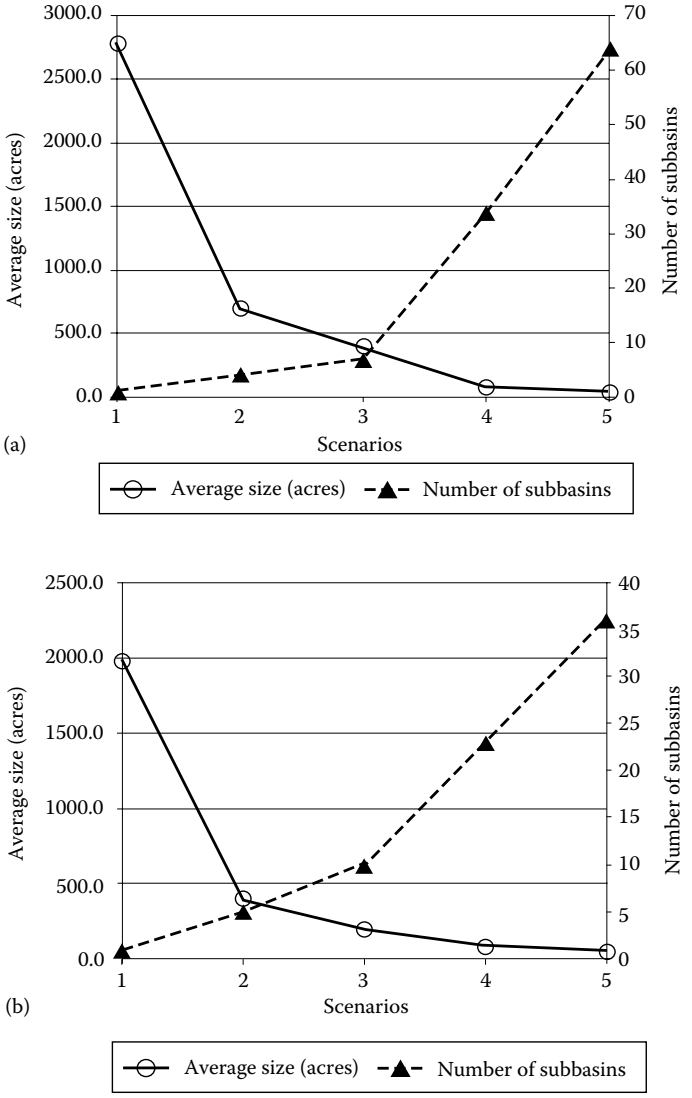

FIGURE 11.10 Discretization levels in (a) Pigeon Basin and (b) SW Prong Basin.

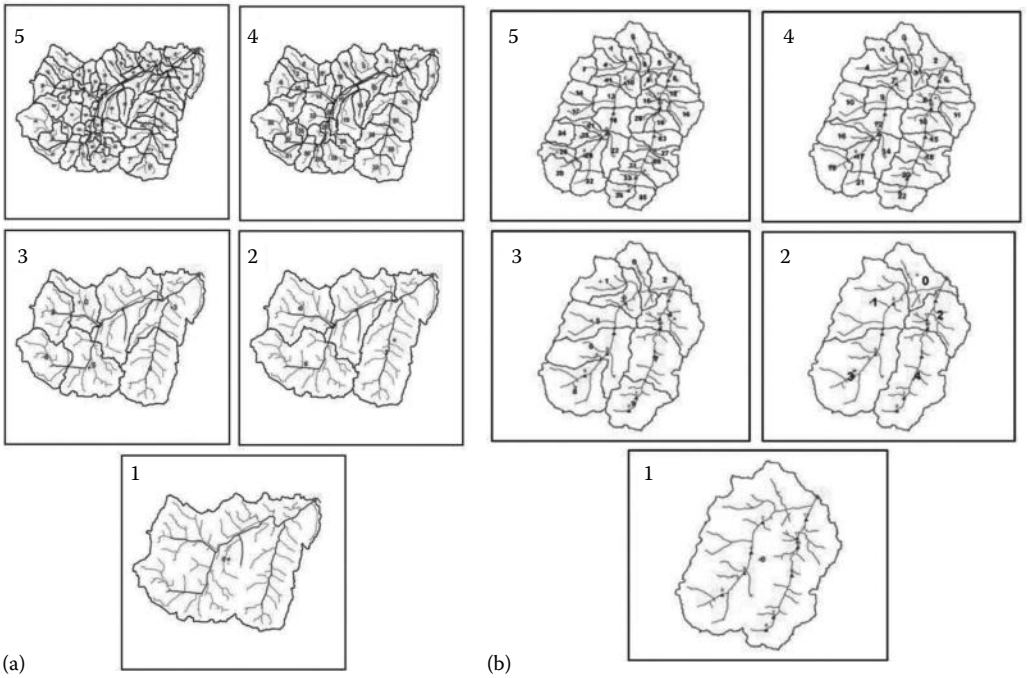

FIGURE 11.11 Discretization scenario map in (a) Pigeon Basin and (b) SW Prong Basin.

heterogeneity in the basin, and this relates directly to an ideal element size for distributed catchment modeling.

Wood et al. [42] determined the runoff volume from 148 subcatchments. These runoff volumes were ranked on the basis of subcatchment size, irrespective of their relative position in the basin. The average of a 15-element filter, moving in steps of 5, was plotted versus area. These plots were then used to determine the REA, defined as the area where the curve is flattened out. In other words, the REA is described as the scale where |dq/da| becomes small, with "q" being the peak volume and "a" the subcatchment area. Based on the concept proposed by Wood et al. [42], the REA was estimated using Scenario 5 in both basins. Figure 11.13a and b shows the effect of averaging.

From the results in Pigeon, it is clear to see than an average area subcatchment of 50 acre might be appropriate (2% of the total basin size). In SW Prong, despite the lower runoff volumes, the runoff showed to be stabilized after a subcatchment area of 60 acre (3% of the total size). We conclude that an average subbasin size of 3% of the total basin may be an appropriate threshold scale in the context of urban hydrology. Arabi et al. [3], using the soil and water assessment model, found appropriate to use subcatchment sizes of approximately 4% of total basin area; in that study, two mostly undeveloped basins were analyzed: Dreisbach and Smith Fry, both basin sizes of about 2.5 mi^2.

11.3.4 Measurements of Performance

The model with a higher resolution level was taken as base model. In both basins, the IOA showed higher values than the PMCC and NSC as it shown in Figure 11.14a and b. In Pigeon, the metrics showed a poor performance for Scenarios 3, 2, and 1, as it was expected. However, surprisingly, Scenarios 3 and 2 showed reasonable values in SW Prong. This behavior means that the imperviousness level might be a factor to estimate the REA. This idea should be further investigated, but it is out of the time framework in this research.

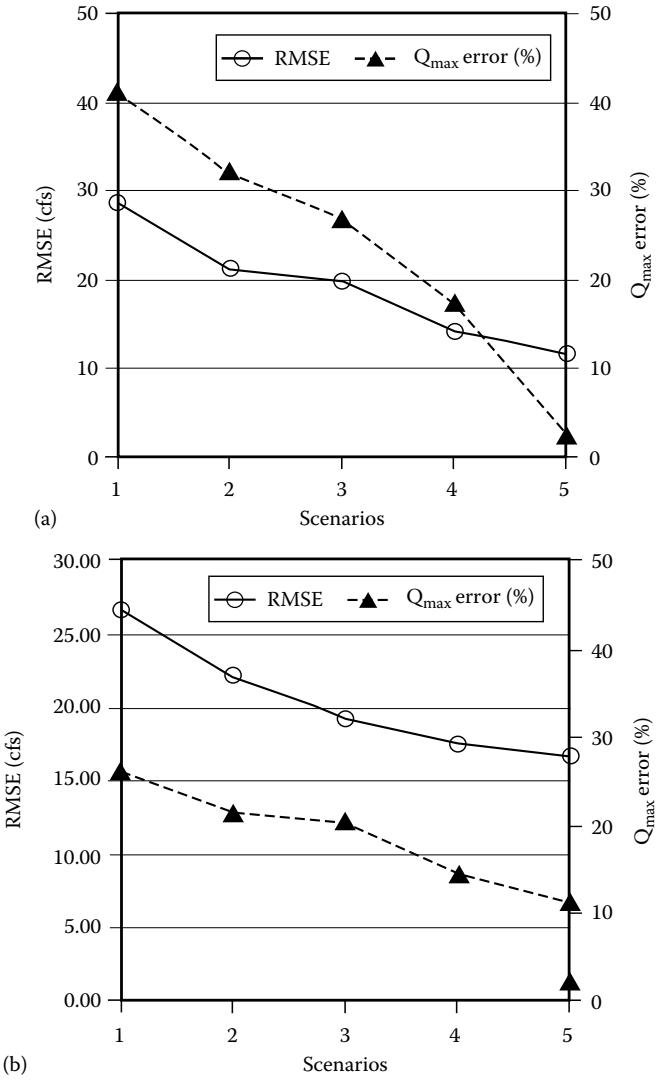

FIGURE 11.12 RMSE and Q_{max} errors in (a) Pigeon Basin and (b) SW Prong Basin.

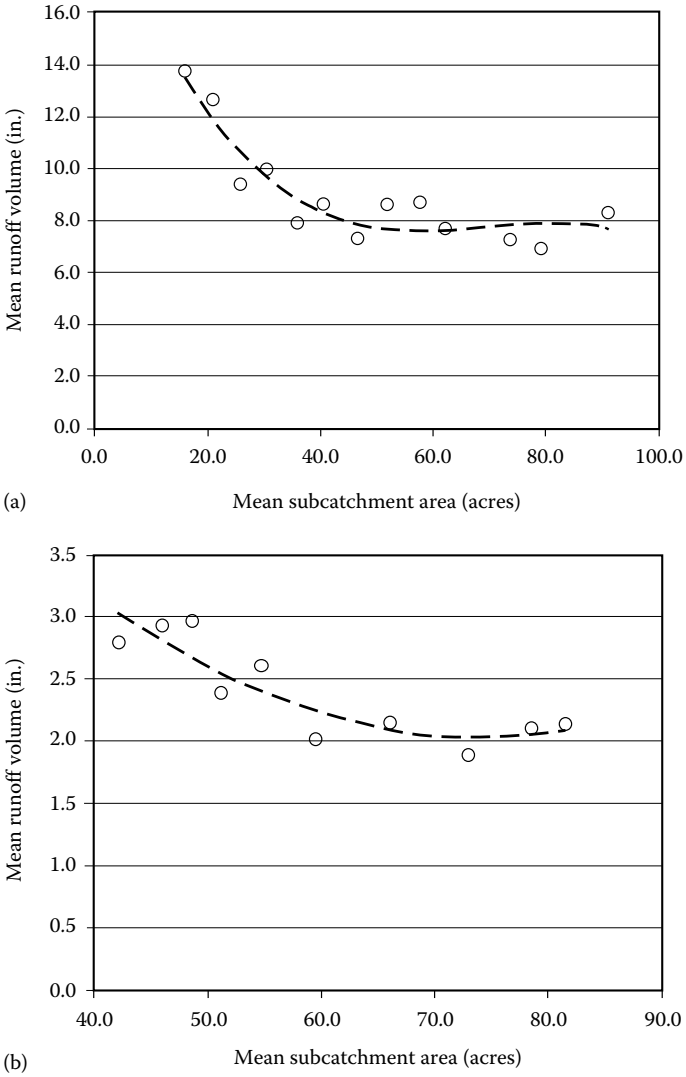

FIGURE 11.13 REA in (a) Pigeon Basin and (b) SW Prong Basin.

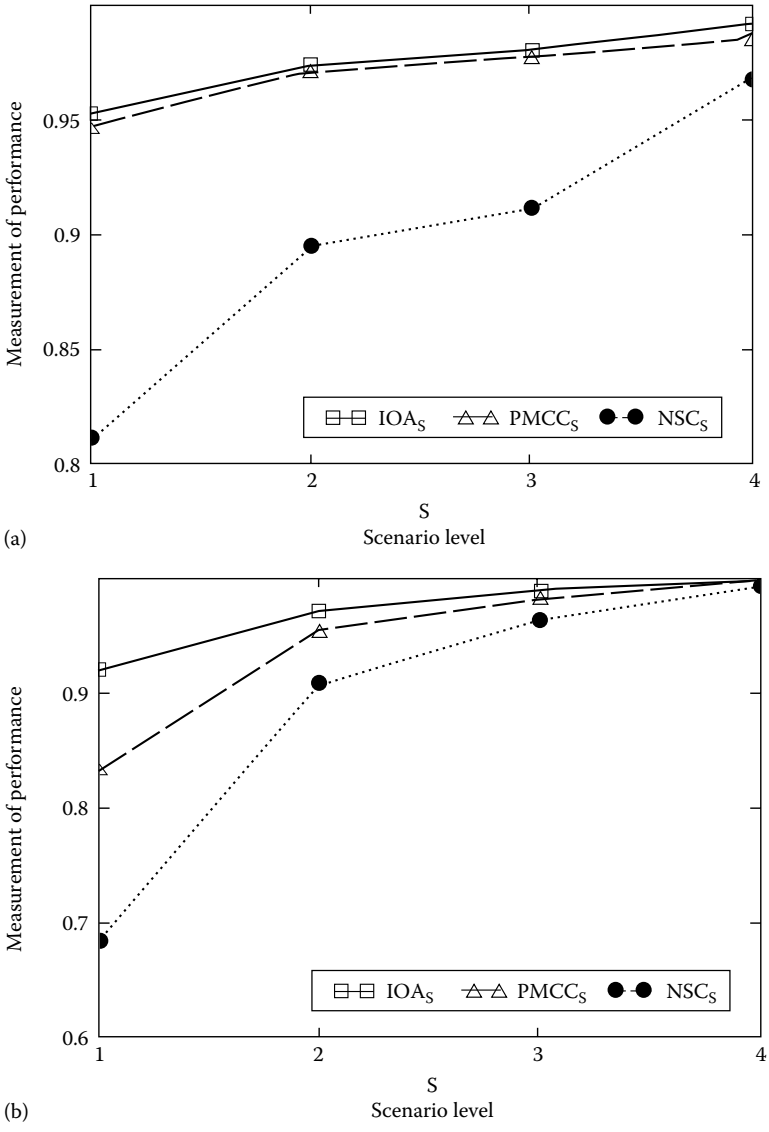

FIGURE 11.14 Measurement of performance in (a) Pigeon Basin and (b) SW Prong Basin.

11.4 Summary and Conclusions

This chapter involved a discretization analysis. A set of hydrologic experiments were performed in each watershed, where different levels of discretization were used in each scenario. Discretization scenarios were obtained with Arc Hydro [22]. Needed GIS data were extracted through a toolbox that was developed, and SWMM5 simulations were performed with the watershed configurations. The main objective was to investigate a threshold value in urban hydrology. This value represents the needed level of discretization in urban watersheds after which the improvement in performance becomes asymptotic either to 1.00 (PMCC, NSC, and IOA) or to 0 (RMSE) and, thus, is not significant to improve the spatial resolution. The REA concept was explored using SWMM, and it was found that subcatchment sizes of 3% of the total basin size were appropriate. Coarser resolution levels underestimated peak flow rates and total runoff volumes.

The practice of urban stormwater hydrology is not an exact science. While the hydrologic processes are well understood, the necessary equations and boundary conditions required to solve them are often quite complex. However, this research work constitutes a step forward since some guidelines were found. A 3% of total basin size is suggested to disaggregate watersheds since REA values of 50 and 60 acre in Pigeon and SW Prong respectively were found. However, this result is by no means a universal concept to apply in all models.

This study arose some issues that should be further researched. For instance, differences between runoff outputs using different DEM resolutions were not addressed; however, as DEM rasters become available with higher resolution, it may be worth it to investigate the effects of the runoff response with different resolution grids. The REA size found here was appropriate for the case studies, but its value may be different for another range of basin sizes, for example, smaller than 1 mi^2 or larger than 10 mi^2. Thus, caution must be taken when using the presented results to other basins with different range sizes.

Acknowledgment

The author expresses his sincere gratitude to Mexico's National Council of Science and Technology (CONACyT, by its name in Spanish) for its continuous financial support to foster research activities.

References

1. Akan, A.O. and Houghtalen, R.J. (2003). *Urban Hydrology, Hydraulics and Stormwater Quality: Engineering, Applications and Computer Modeling*. John Wiley & Sons, Inc., Hoboken, NJ.
2. Alley, W.M. and Veenhuis, J.E. (1983). Effective impervious area in urban runoff modeling. *Journal of Hydraulic Engineering*, 109(2): 313–319.
3. Arabi, M., Govindaraju, R.S., Hantush, M.M., and Engel, B.A. (2006). Role of watershed subdivision on modeling the effectiveness of best management practices with SWAT. *Journal American Water Resources Association*, 42(2): 513–528.
4. Arcement, G.J. and Schneider, V.R. (1989). Guide for selecting Manning's roughness coefficients for natural channels and floodplains. United States Geological Survey Water-Supply Paper 2339. Metric Version.
5. Arc Hydro Tools. (2003). Tutorial, Version 1.1 Beta 2, Redlands, CA.
6. ASCE Task Committee on Definition of Criteria for Evaluation of Watershed Models of the Watershed Management Committee, Irrigation and Drainage Division. (1993). Criteria for evaluation of watershed models. *Journal of Irrigation and Drainage Engineering*, 199(3): 429–442.
7. Blöschl, G., Grayson, R.B., and Sivapalan, M. (1995). On the representative elementary area (REA) concept and its utility for distributed rainfall–runoff modeling. Centre for Resource and Environmental Studies, Australian National University, Canberra City, Australia. *Hydrological Processes*, 9(4): 313–330.

8. Brink, P. (2004). Wayne County Rouge Program Office (RPO). Memorandum. March 26, 2004.
9. Brink, P. and Broek, T. (1988). Characteristic width and infiltration for continuous SWMM, Chapter 17. In *Advances in Modeling the Management of Stormwater Impacts*, Vol. 6, W. James, ed., CHI Publications, Guelph, Ontario, Canada, 504 pp.
10. Brink, P., Regnemorter, L., and TenBroek, M. (1996). Evaluating the city of Detroit's combined sewer overflow storage/treatment facilities through continuous modeling. *Proceedings of the Urban Wet Weather Pollution: Controlling Sewer Overflows and Stormwater Runoff, Specialty Conference of the Water Environment Federation*, Quebec City, Quebec, Canada, pp. 2–61.
11. Chow, V.T. (1959). *Open Channel Hydraulics*. McGraw-Hill, New York, 680pp.
12. City of Raleigh. (2008). Central Engineering Department. Stormwater Division. http://www.raleighnc.gov (accessed on October 20, 2008).
13. Environmental Protection Agency, EPA. (2008). http://www.epa.gov/ednnrmrl/models/swmm/index.htm (accessed on November 04, 2008).
14. Espey, W.H., Altman, D.G., and Graves, C.B. (1997). Nomograph for 10 minutes unit hydrographs for urban watersheds. Technical Memorandum 32. ASCE, New York.
15. Garmin. (2008). eTrex Legend®. http://www8.garmin.com/aboutGarmin/ (accessed on November 05, 2008).
16. Giddings, E.M., Moorman, M., Cuffney, T.F., McMahon, G., and Harned, D.A. (2007). Selected physical, chemical, and biological data for 30 urbanizing streams in the North Carolina Piedmont ecoregion, 2002–2003. US Geological Survey Data Series 279, 14pp.
17. Guo, J. and Urbonas, B. (2009). Conversion of natural watershed to kinematic wave cascading plane. *Journal of Hydrologic Engineering*, *ASCE*, 14(8): 839–846.
18. Harrelson, C.C., Rawlins, C.L., and Potyondy, J.P. (1994). Stream channel reference sites: An illustrated guide to field technique. General Technical Report RM-245. Department of Agriculture, Forest Service, Rocky Mountain Forest and Range Experimental Station, Fort Collins, CO, 61pp.
19. Huber, W.C. and Dickinson, R.E. (1988). *Storm Water Management Model (SWMM) User's Manual*, Version 4.0. United States Environmental Protection Agency, Athens, GA, 595pp.
20. Kokkonen, T. and Jakeman, A. (2001). A comparison of metric and conceptual approaches in rainfall–runoff modeling and its implications. Laboratory of Water Resources, Helsinki University of Technology, Helsinki, Finland. Centre for Resource and Environmental Studies, Australian National University, Canberra, ACT, Australia. *Water Resources Research*, 37(9): 2345–2352.
21. Lee, J.G. and Heaney, J.P. (2002). Directly connected impervious areas as major sources of urban stormwater quality problems, evidence from South Florida. *Proceedings of the 7th Biennial Conference on Stormwater Research and Water Quality Management*, Southwest Florida Water Management District, Brooksville, FL.
22. Maidment, D. (2002). *Arc Hydro: GIS for Water Resources*. ESRI Press, Redlands, CA, 220pp.
23. Mays, L. (2010). *Water Resources Engineering*, 2nd edn. John Wiley & Sons, Inc., New York, 920pp.
24. McMahon, G. and Cuffney, T.F. (2000). Quantifying urban intensity in drainage basins for assessing stream ecological conditions. *Journal of the American Water Resources Association (JAWRA)*, 36: 1247–1261.
25. Moretti, G. and Montanari, A. (2008). Inferring the flood frequency distribution for an ungauged basin using a spatially distributed rainfall–runoff model. *Hydrology and Earth System Sciences*, 5: 1–26.
26. Nash, J.E. and Sutcliffe, J.V. (1970). River flow forecasting through conceptual models. Part 1. A discussion of principles. *Journal of Hydrology*, 10: 282–290.
27. National Climatic Data Center, NCDC. (2008). http://www.ncdc.noaa.gov/oa/climate/climateinventories.html (accessed on December 15, 2008).
28. Pomeroy, Ch. (2007). Evaluating the impacts of urbanization and stormwater management practices on stream response. PhD thesis. Department of Civil and Environmental Engineering, Colorado State University, Fort Collins, CO.

29. Rivas, I. and Roesner, L. (2007). Spatial discretization of large urban watersheds for rainfall–runoff modeling. *World Environmental and Water Resources Congress 2007: Restoring Our Natural Habitat*, Tampa, FL.
30. Roesner, L.A., Bledsoe, B.P., and Brashear, R.W. (2001). Are best management-practice criteria really environmentally friendly? *Journal of Water Resources Planning and Management*, *ASCE*, 127(3): 150–154.
31. Romero-Davis, J. (2008). Guidance for rural watershed calibration with EPA-SWMM. Master's thesis. Department of Civil and Environmental Engineering, Colorado State University, Fort Collins, CO.
32. Rossman, L.A. (2005). *Stormwater Management Model User's Manual*, Version 5.0. United States Environmental Protection Agency, National Risk Management Research Laboratory, Office of Research and Development Report EPA/600/R-05-040, Cincinnati, OH.
33. Shoemaker, L. and Brady, D. (1997). Compendium of tools for watershed assessment and TMDL development. Watershed Branch, Assessment and Watershed Protection Division, Office of Wetlands, Oceans and Watersheds, US Environmental Protection Agency, Washington, DC.
34. Sivapalan, M. and Kalma, J.D. (1995). Scale problems in hydrology: Contributions of the Robertson workshop. In *Scale Issues in Hydrological Modeling*, Kalma, J.D. and Sivapalan, M., eds., John Wiley & Sons Ltd., Chichester, U.K., pp. 141–158.
35. Urban Drainage and Flood Control District, UDFCD. (2008). User manual, Colorado Urban Hydrograph Procedure—CUHP2005. http://www.udfcd.org/downloads/down_software.htm (accessed on September 20, 2008).
36. Urbonas, B. (1979). Reliability of design storms in modelling. *International Symposium on Urban Storm Runoff*, University of Kentucky, Lexington, KY, July 23–26, 1979.
37. Urbonas, B. (2007). Stormwater runoff modeling: Is it as accurate as we think?. *Engineering Conferences, International Conference on Urban Runoff Modeling: Intelligent Modeling to Improve Stormwater Management*, Humboldt State University, Arcata, CA.
38. United States Geological Survey, USGS. (2008). http://waterdata.usgs.gov/nwis/ (accessed on December 16, 2008).
39. Vieux, B.E. (2004). *Distributed Hydrologic Modeling Using GIS*. Water Science and Technology Library, Vol. 48. Kluwer Academic Publishers, Dordrecht, the Netherlands.
40. Walsh, C.J., Roy, A.H., Feminella, J.W., Cottingham, P.D., Groffman, P.M., and Morgan II, R.P. (2005). The urban stream syndrome: Current knowledge and the search for a cure. *Journal of the North American Benthological Society* 24:706–723.
41. Willmott, C.J. (1981). On the validation of models. *Physical Geography* 2: 184–194.
42. Wood, E.F., Sivapalan, M., Beven, K., and Band, L. (1988). Effects of spatial variability and scale with implications to hydrologic modeling. *Journal of Hydrology*, 102: 29–47.

12

Drought Indices for Drought Risk Assessment in a Changing Climate

Brian A. Fuchs
University of Nebraska-Lincoln

Mark D. Svoboda
University of Nebraska-Lincoln

Donald A. Wilhite
University of Nebraska-Lincoln

Michael J. Hayes
University of Nebraska-Lincoln

AUTHORS

Brian A. Fuchs joined the National Drought Mitigation Center (NDMC) in 2005. Before coming to the NDMC, he worked for 5 years for the High Plains Regional Climate Center as a regional climatologist. Brian's responsibilities with the NDMC include working as a climatologist for the center, with various research and service duties related to his position. Brian participates with other NDMC staff in the production of the US Drought Monitor (USDM) as one of the coauthors, and he serves as a media contact for climate- and drought-related topics.

Mark D. Svoboda has been with the NDMC since it was formed in 1995. As the NDMC's Monitoring Program Area Leader, his duties include overseeing the center's operational national drought monitoring activities. Mark cofounded the development of the USDM in 1999 and serves as one of the principal authors of both the weekly USDM and monthly North American Drought Monitor products. Mark is heavily involved with drought monitoring, assessment, and prediction committees at state, regional, and national levels. In addition, he has extensive experience working with the international drought, water, and climate community via project collaboration and consultation and through various training and outreach opportunities with over 50 countries and international organizations to date. Mark earned both his bachelor's degree in geography specializing in climatology and a master's degree in geography with a specialization in remote sensing, climatology, and GIS from the University of Nebraska–Lincoln.

Donald A. Wilhite is a professor of applied climate science at the University of Nebraska–Lincoln, United States. Prior to August 2012, Dr. Wilhite served as director of the School of Natural Resources, a position he held from 2007 to 2012. Previously, Dr. Wilhite was the founding director of the NDMC in 1995

and the International Drought Information Center in 1989 at the University of Nebraska–Lincoln. His research and outreach activities have focused on issues of drought monitoring, planning, mitigation, and policy and the use of climate information in decision making. He has authored or coauthored more than 140 journal articles, monographs, book chapters, and technical reports. Dr. Wilhite is editor or coeditor of numerous books on drought and drought management, including *Coping with Drought Risk in Agriculture and Water Supply Systems: Drought Management and Policy Development in the Mediterranean* (Springer, 2009); *Drought and Water Crises* (CRC Press, 2005); *From Disaster Response to Risk Management: Australia's National Drought Policy* (Springer, 2005); and *Drought: A Global Assessment* (Routledge, 2000). Dr. Wilhite is also the editor of a book series on *Drought and Water Crises* that is being published by CRC Press, a subsidiary of Taylor & Francis Publishers.

Michael J. Hayes is currently the director for the NDMC located within the School of Natural Resources at the University of Nebraska–Lincoln. He became the NDMC's director in August 2007 and has worked at the NDMC since 1995. The NDMC now has 15 faculty and staff working on local, tribal, state, national, and international drought-, climate-, and water-related issues. Dr. Hayes' main interests deal with drought monitoring, planning, and mitigation strategies. Dr. Hayes received a bachelor's degree in meteorology from the University of Wisconsin–Madison and his master's and doctoral degrees in atmospheric sciences from the University of Missouri–Columbia.

PREFACE

There are many drought indicators being used around the world. Some have been developed with a specific needs being addressed, while others have tried to identify drought in all circumstances and scenarios. Over time, the risks associated with drought have become more visible and discussions about how to cope with drought are ongoing. At this time, there is not a single drought index that accomplishes everything that users want it to do, even with the consolidated approaches that are being used. The challenges of a changing climate amplify the need to continue working toward the development of better indicators and methods to monitor drought as part of greater drought early warning system (DEWS). As climate regimes change or seasonal shifts occur, the drought indicators used in the past may not adequately address drought moving forward. This chapter hopes to identify some of the drought indices that are being used and how they were developed. With a better understanding of the various indices available, a better sense of how drought is being monitored can be realized, and also a better understanding of a changing climate may impact the use of these indicators. I would like to acknowledge Mark Svoboda, Don Wilhite, and Michael Hayes for their contributions to this work.

12.1 Introduction

As common as drought occurrences are around the world, a standard definition for drought isn't recognized. Even among the experts who study droughts, a single standard definition is not easy to agree upon. In the simplest of meanings, drought can be identified as a deficit of precipitation from an expected average over an established time frame. To better define drought, one needs to establish the context in which the phenomenon and its associated impacts are being described. Wilhite and Glantz (1985) identified more than 150 published definitions of drought; from these, drought was classified into 4 types: meteorological, agricultural, hydrological, and socioeconomic. As their names imply, these diverse drought types impact different sectors, but in most instances the impacts related to each overlap both temporally and spatially (Figure 12.1).

All droughts begin with a deficiency of precipitation over some time frame. These early stages of accumulating precipitation deficiencies are commonly referred to as meteorological drought.

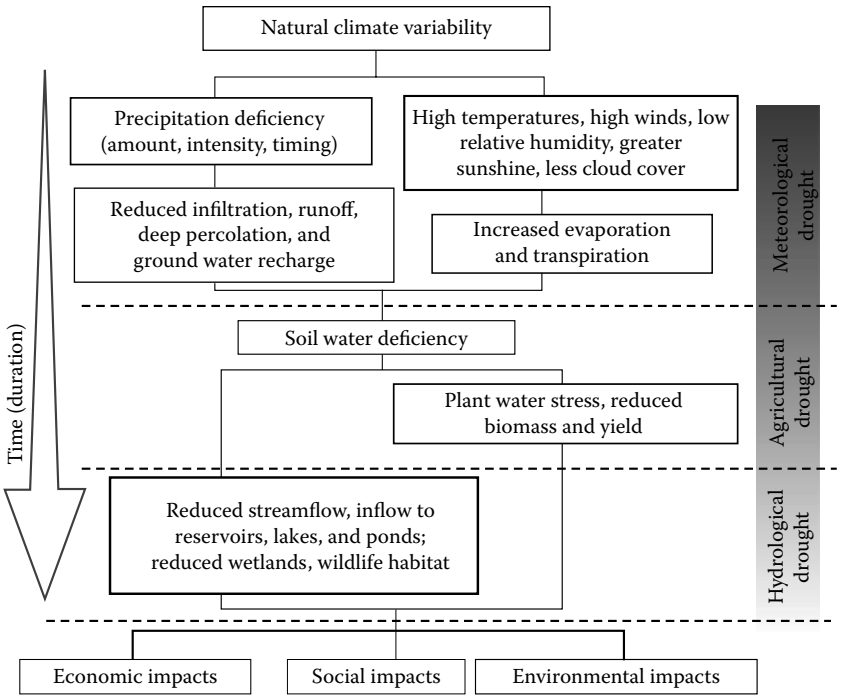

FIGURE 12.1 Four types of drought. (From National Drought Mitigation Center, http://drought.unl.edu/, accessed August 1, 2012.)

A continuation of these dry conditions over a longer period of time, sometimes in association with above-normal temperatures, high winds, and low relative humidity, quickly results in impacts in agricultural and hydrological sectors. Meteorological droughts are driven by a change in the local meteorological conditions, such as dominance by a high pressure ridge as occurred over a large portion of the United States in 2012. The geography and climatology of a region plays an important role in what defines meteorological drought since regions have very different precipitation regimes. Meteorological droughts can develop quickly, but they can also end just as quickly if the precipitation deficits are relatively small. However, these types of drought may also linger on into a multi-seasonal event and develop into the one of the other types of drought.

Agricultural droughts can be characterized as an extended meteorological drought in which there is a deficiency of precipitation during the growing season such that crop growth and development is suppressed. Agricultural drought can also be associated with a dry period prior to the growing season in which soils were not fully recharged with moisture, which carries over to a growing season with inadequate precipitation, especially during critical crop growth stages. It may also include periods where available water for irrigation is lacking. Agricultural droughts are events that become the next phase of meteorological drought. As the name implies, a drought of this nature will extend in duration to the point at which the agricultural concerns of a region are being impacted by dryness and lack of adequate soil moisture. Agricultural drought may extend into portions of more than one growing season, but the natural break between seasons is identified as a period where drought did not worsen or improve, because no agricultural production was taking place (such as in the winter season). Agricultural drought can also precede the actual start of the growing season in which conditions are not favorable for planting because of dryness and the lack of soil moisture, or not enough moisture available for pasture and rangelands to green up.

Hydrological drought, as the name implies, refers to drought events that curtail the amount of water available in rivers, streams, lakes, reservoirs, and groundwater. As meteorological droughts are prolonged,

the lack of runoff from precipitation events due to dry soils will begin to impact the hydrology of a region. There is typically a lag involved that will be unique to each region and for a particular time of the year as the impacts to hydrology will not be immediate after the start of the drought. With an extended dry period, soil moisture diminishes, surface runoff and subsurface recharge are reduced, and the amount of water in the hydrologic system of a region declines. During winter months, frozen precipitation is accumulated for future runoff, so a dry winter can induce hydrological drought months later. Even with precipitation, the dry soils can inhibit substantial runoff, as they will capture excess moisture before it is able to reach rivers, streams, and reservoirs. Dryness and heat (via evaporation) will work together to reduce the amount of water available in hydrologic systems. As some hydrologic systems are managed, water managers can choose to withhold water if hydrological drought is of concern to try to lessen future impacts. Without proper recharge, a long-term drought will impact the hydrology of the region even after precipitation returns to more normal levels. It typically takes the longest time period for a hydrological drought to develop, and, in turn, the recovery time can also take months or even years.

Socioeconomic definitions of drought associate the supply and demand of some economic good with elements of meteorological, agricultural, and hydrological drought. It differs from the aforementioned types of drought because its occurrence depends on the time and space processes of supply and demand to identify or classify droughts (Wilhite and Glantz, 1985). Other weather or climate factors can play into why certain goods are not available, but for socioeconomic drought, the demand for these goods exceeds supply because of drought. Socioeconomic drought impacts can develop immediately once drought advances into a region and may linger for quite some time depending on the severity of the impact and the importance of the goods being impacted in the region.

12.2 How to Monitor Drought

Given the complexity of trying to define drought, we need to know how droughts develop and what indicators are available to determine that this phenomenon is taking place. Gathering information about the primary weather and climate characteristics of a region is an important first step needed to monitor droughts. One must understand both the climate and drought climatology of the region. What may be a regular climatic occurrence in one region may constitute the beginning of a drought in another region or season. We must first understand the climate to determine if the current weather pattern is truly developing into a drought or is expected to do so in the future. Knowing if a particular pattern of dry weather is unique and the possible start of a drought is important in knowing how to properly plan for and mitigate the impacts of drought. Drought early warning systems (DEWSs) focused on monitoring drought conditions are an important part of being adequately prepared for drought (Wilhite, 2005, 2009; WMO, 2011). Without adequate planning and preparedness, the impacts resulting from drought may be worse and may lead to even more severe consequences for many sectors. When the impacts are severe, the recovery process may be delayed considerably.

With the basic characteristics of drought involving a lack, or deficit, of precipitation, it is critical to have reliable and long-term records of precipitation. Most drought monitoring actions, as part of a DEWS, are established with the knowledge of comparing recent weather events to the known climatic values such as long-term averages or normals. Even though precipitation is the basis of many drought indicators, many other indicators are also important in the assessment of drought severity. Ideally, one should try to also monitor rivers and streams, snowpack, water storage and availability, the health of the ecology of the area, soil moisture, evaporation, crop production, and other indicators that might be relevant for understanding water availability and use in that region. For many regions, it may not be possible to look at every single indicator when determining if an area is in drought, particularly because for many regions the data may not be readily available. However, it is best to look at multiple indicators to verify the existence and severity of drought. In determining the historical context of current information, the period of record of indicators used to monitor drought is important. Regardless of the indicator being used, having the longest and most complete (serially complete) record available will help

in establishing the context of current conditions to known historical conditions. One must realize that a drought is a feature categorized on the dry side of a region's precipitation distribution. Those events that are on the statistical tails (extremes) of a distribution will be better understood if more of them fall within the sample size. Guttman (1993, 1999) recommended that at least 50 years of precipitation data is the minimum needed for drought periods of 12 months or less, and more is needed for droughts that cover multiple years (when using the Standardized Precipitation Index [SPI]).

What is problematic is that some indicators may not have a long enough period of record, and this is especially true of remotely sensed data. Monitoring drought properly requires taking some time to construct historical data records or develop data sets for as many data points as possible. Once this work is completed, monitoring current conditions not only adds to the period of record but also allows researchers to learn about the climate of a region intimately and what is expected (or not expected) and when. This is important to understand as it may be more meaningful if while monitoring current conditions it is known how much precipitation is expected over the period being monitored. If the precipitation distribution for a region is typically seasonal, then a shortage of precipitation during this time would not necessarily signal the beginning of a drought. Thus, it is possible to determine the "crucial" period(s) of precipitation for any region.

12.3 Drought Indicators and Indices

An *indicator* is a measure of a meteorological, hydrological, agricultural, or socioeconomic variable that provides an indication of potential drought-related stress or deficiency. An *index* is a method of deriving "value-added" information related to drought by comparing current conditions to historical information based upon statistical calculations or formulas. Indices are an attempt to quantify drought and its magnitude. It is also important to note that indices are indicators as well. For some, the quickest and easiest way to determine drought is by comparing actual precipitation to a long-term average or mean. The percent of normal method allows for a calculation that can be computed over any defined period and gives meaning to the value. This method does have some drawbacks. One such drawback is the difference between the mean and median. These can be significantly different for shorter periods of time (i.e., month to seasonal time periods). Thus, comparing departures of precipitation to the mean or normal amount may be misleading. With that in mind, the simplest method is not always best, and scientists require a better way of determining the precipitation statistics while giving some historical context to the frequency of an event. To do this, drought indices were developed as a way of expressing drought information in a manner that also gives the user more information than just how the current situation compares to a historical average and to identify the degree of water shortage associated with the dry event (duration and intensity).

12.4 History of Drought Indicators and Indices

Heim (2002) showed the evolution of drought indices from the early 1900s to what has become the standard for the United States with the development of the US Drought Monitor (USDM) in 1999. It should be noted that the progression of the development of indices is aimed at trying to derive a number or value that has meaning in the expression of drought severity. Some drought indices looked strictly at agricultural issues, while others focused on water supply or availability. When Wayne Palmer (1965) developed the Palmer Drought Severity Index (PDSI), it was an attempt to put the full water balance into a regional perspective while identifying meteorological and agricultural drought episodes. As other drought indices were developed, it was determined that not all indices worked in all locations because many were developed to address a particular problem in a certain climate. With some indices needing a great deal of data and becoming more complex, the World Meteorological Organization (WMO) wanted to put forward a recommendation for a single meteorological drought index to be the minimum standard and starting point for every country to calculate in the assessment of drought in order to provide more comparability between regions. At a meeting in 2009, the "Lincoln Declaration on Drought

Indices" recommended the SPI as the drought index to be computed and used globally by meteorological and hydrological services as the common meteorological drought index (WMO, 2011). As work toward developing drought indices continues, knowing which indices work best for a region and how to apply them becomes critical in establishing a functional DEWS.

In evaluating and selecting various drought indices, it is best to look at the various applications in which they are likely to be used. Many drought indices have the potential to be used in multiple applications or can be applied to various sectors. The drought indices described in the following are by no means complete, but we will discuss some of those that are most commonly applied globally and how they can be used for meteorological, agricultural, and hydrological analyses.

12.4.1 Standardized Precipitation Index

Even before the WMO recommendation in 2009 the SPI received a great deal of attention throughout the world as countries wanted to calculate and use it operationally to track drought conditions. The SPI was developed by McKee et al. (1993). It uses the historical precipitation record for any location, and a probability of precipitation is developed for various time scales. The intensity scale for SPI has both a positive and negative metric, where the positive values are correlated to wet events and the negative values are used to identify drought events. McKee et al. (1993) also characterized drought events as beginning when the SPI value fell below –1.0 for a particular time period. The duration of the drought event lasted until the SPI became positive. This is where the SPI has a great amount of utility. The SPI is flexible and can be calculated for both short-term and long-term periods by choosing various time steps. Another reason for the SPI's appeal is that the index can be calculated with missing data. In the way that the SPI is calculated (by using a historical precipitation distribution when data are missing), the distribution can still be developed and used. If too many data are missing, the results will be "null" and the program will calculate the next SPI value when enough data are again available. Initially, the SPI was calculated for periods from 1 to 72 months, but it is mostly used for periods of 24 months or less. Having this flexibility has allowed the SPI to be very useful in monitoring meteorological, agricultural, and hydrological droughts in which time scales and impacts are variable (Table 12.1).

Many countries that are trying to develop drought monitoring activities typically have data issues since consistent and quality long-term reporting precipitation stations may be hard to find. Even though there may be a break in the SPI results being calculated, the data can be utilized and knowledge gained from them. Users of the SPI will begin to know which SPI time intervals will make the most sense for their region in helping identify the different types of drought and associated impacts. Since the SPI is a precipitation-only index, it tends to be used more often to identify periods of meteorological and hydrological drought since it does not have a water balance component that is important for monitoring agricultural droughts. There are agricultural drought applications where the SPI is useful, especially when identifying a developing drought situation, because the SPI, with a short time scale, will respond quickly

TABLE 12.1 SPI Classification Scale

SPI Value	Moisture Level
+2.0 and greater	Extremely wet
+1.5 to 1.99	Very wet
+1.0 to 1.49	Moderately wet
−0.99 to 0.99	Near normal
−1.0 to −1.49	Moderately dry
−1.5 to −1.99	Severely dry
−2.0 and less	Extremely dry

Source: Guttman, N.B., *J. Am. Water Resour. Assoc.*, 35(2), 311, 1999.

to a situation where conditions are drying out rapidly. With that being said, the flexibility of the SPI is that it can be calculated for any time period, and this feature makes it possible to calculate a SPI that would be useful for application during a region's particular growing season or off-season moisture recharge periods.

12.4.2 Standardized Precipitation Evapotranspiration Index

One of the more recently developed drought indices is the Standardized Precipitation Evapotranspiration Index (SPEI), which took the basic premise of the SPI and added a temperature component to capture a simplified water balance (Vicente-Serrano et al., 2010). The SPEI, like the PDSI, uses a simple water balance calculation that is based on the Thornthwaite (1948) model for calculating potential evapotranspiration (PET). Several studies have shown that good estimates of PET can be obtained with various meteorological parameters, but for the purpose of a drought index, they are not needed because only a general estimation of the water balance is required. This also keeps the calculations simple and usable given the additional data requirements needed for determining actual evapotranspiration values. Having the same flexibility that the SPI has in being able to be updated weekly using a moving window for each time step, the SPEI uses the difference between the basic calculations for PET and precipitation to determine a wet or dry period. Given the flexible nature of the SPEI, it has the capacity to be utilized in monitoring the various types of droughts because of the included water balance calculations. As such, it has the potential to better track agricultural drought.

12.4.3 Palmer Drought Severity Index

One of the most widely used indices, especially in the United States, has been the PDSI, developed by Wayne Palmer for the US Department of Agriculture in the 1960s (Palmer, 1965). The index was intended to be used as an agricultural drought index, as it measures the availability of moisture in the region being monitored using a water balance equation. Unlike the SPI, in which the only variable needed is precipitation, the PDSI also incorporates temperature and soil moisture as well as a previous PDSI value. The temperature data are used to estimate PET utilizing a Thornthwaite approach, and the default soil moisture information comes from data that have been extrapolated from the soil information collected by the US Geological Survey (Palmer, 1965). The complexity of the variables needed to compute the PDSI makes it more challenging to use as the needed soil information is typically not readily available for all locations.

Like the SPI, the PDSI has both a wet and dry categorization scheme, with most values falling into the range of +4 to −4. Having both scales allows users to become familiar with how the PDSI responds to precipitation events in order to have a better understanding of how the index functions for any particular area. Over time, the agricultural applications of the PDSI have been widely used. Several inherent drawbacks are associated with using the PDSI, and these have been well documented (Steila, 1972; Karl, 1983, 1986; Alley, 1984, 1985; Hayes et al., 1999). For one, the index has a time scale of approximately 9 months, which leads to a lag in identifying drought conditions based upon the simplification of the soil moisture component within the calculations. This lag may be up to several months, which is a drawback when trying to identify a rapidly emerging drought situation. There are also seasonal issues to the PDSI as it does not account for frozen precipitation and frozen soils very well and all precipitation events are treated as if they were liquid precipitation events. Some of the drawbacks to using the PDSI are that this particular index was developed to be used in the Midwest of the United States as a trigger to identify agricultural droughts. Several other papers have discussed the limitations of the PDSI (Alley, 1984; Karl and Knight, 1985; Willeke, 1994; McKee et al., 1995; Guttman, 1997), and they were summarized by Kangas and Brown (2007), which presented applications of using the PDSI for various drought episodes. Kangas and Brown (2007) also described the positive attributes of using the PDSI where the longevity of the index is accounted for. The index has been tested in many situations and illustrates the benefits of using precipitation, temperature, and soil characteristics in characterizing drought (Table 12.2).

TABLE 12.2 PDSI Classification Scale

4.0 or more	Extremely wet
3.0–3.99	Very wet
2.0–2.99	Moderately wet
1.0–1.99	Slightly wet
0.5–0.99	Incipient wet spell
0.49 to −0.49	Near normal
−0.5 to −0.99	Incipient dry spell
−1.0 to −1.99	Mild drought
−2.0 to −2.99	Moderate drought
−3.0 to −3.99	Severe drought
−4.0 or less	Extreme drought

Source: Palmer, W.C., Meteorological drought, U.S. Weather Bureau Research Paper 45, 1965, 58pp.

12.4.4 Crop Moisture Index

As the drawbacks to the original PDSI became apparent, Wayne Palmer responded to some of these issues with his Crop Moisture Index (CMI), which was released 3 years after the original PDSI (Palmer, 1968). The CMI was intended to be an agriculture-only drought index that responded well to rapidly changing climatic situations during the growing season. As with work previously done by Palmer, the CMI was developed for those areas of interest in the grain-producing regions of the United States. The calculations needed are total weekly precipitation and mean temperature along with the previous week's CMI value. The output is weighted for each location, which allows for the comparison of different climate regimes to one another. To respond rapidly to changing agricultural conditions, a simple difference between PET and moisture is calculated to determine if the moisture was sufficient to offset what was lost to PET and, in turn, made it into the soil moisture profile. Because of the targeted nature of what the CMI is monitoring, it is not a very good index for longer-term drought events. The CMI will respond rapidly to precipitation events, but can also provide a false sense of recovery from long-term drought, as improvements in the short term may not necessarily mean that the long-term situation improved.

12.4.5 Self-Calibrated Palmer Drought Severity Index

One of the inherent problems associated with the PDSI was that comparisons were being made from results of different regions, especially those with very different climate regimes, and in many cases this was not appropriate. The self-calibrated Palmer Drought Severity Index (scPDSI) is based upon the original PDSI work, but takes all the constants and replaces them with values that are calibrated based upon the data for each individual location (Wells et al., 2004). With the calculations for the scPDSI accounting for each individual location, the index becomes more reflective of what is happening at each site and allows for comparisons between regions to be more accurate. With these new calculations, the data can be computed at different time steps (weekly, biweekly, and monthly), and the extreme events being calculated by the scPDSI are indeed rare because they are based on calculations at that location and are not a constant.

12.4.6 Deciles

Deciles of precipitation, another approach to characterizing the departure of precipitation from a long-term normal or average, were developed to identify and classify drought. Gibbs and Maher (1967) wanted to try to eliminate the drawbacks of using the percent of normal calculations in classifying

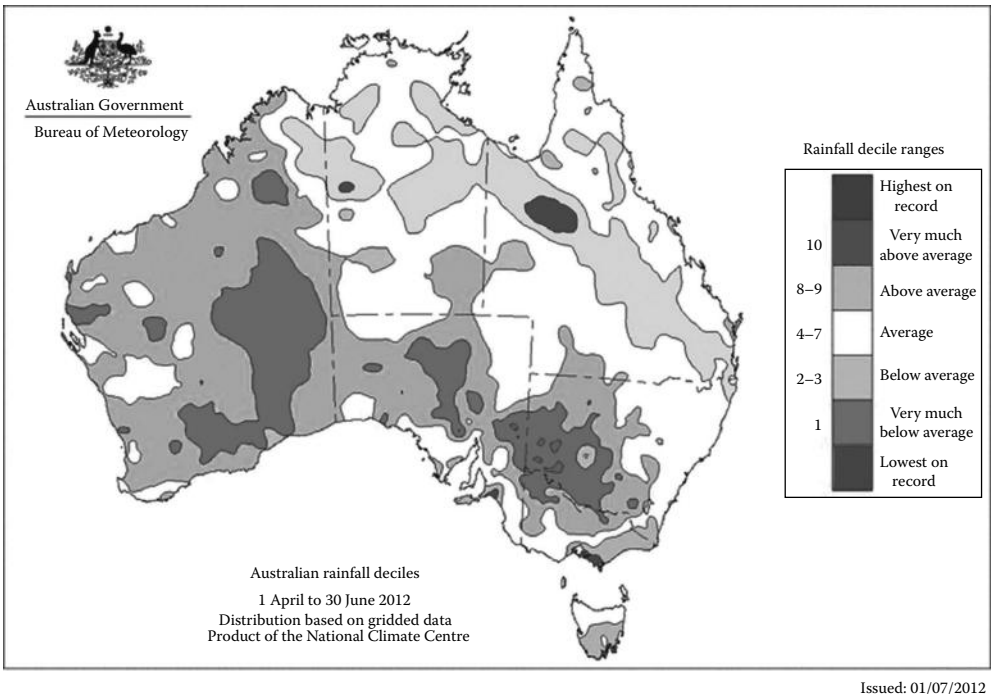

FIGURE 12.2 Deciles are commonly used in Australia to identify drought conditions. (From Australian Bureau of Meteorology, http://www.bom.gov.au/climate/drought/drought.shtml, accessed August 1, 2012.)

droughts in Australia. Using deciles, current precipitation is ranked against the historical record, breaking the record into partitions that are 10% of the record (a decile). The first decile would be precipitation falling in the driest 10% of the record, and the 5th decile would be the median (Figure 12.2).

This method is simple, but needs a long-term period of record to have the most utility. The straightforward nature automatically determines the status of the dryness for a location or region, allowing researchers to know exactly where the current precipitation regime compares historically. Those implementing this method will have certain deciles that are thresholds that trigger some type of response. Having the decile method as part of a DEWS establishes when a drought begins and ends, according to the data and characteristics of drought in the region, by defining the thresholds being used. With the flexibility of establishing thresholds based on the climate of the region, the decile method can be used to monitor all types of drought, as it has been applied to monitor both agricultural and hydrological droughts (Table 12.3).

TABLE 12.3 Deciles Classification Table

Decile Level	Moisture Level
Deciles 1–2: lowest 20% of data	Much below normal
Deciles 3–4: next lowest 20% of data	Below normal
Deciles 5–6: middle 20% of data	Near normal
Deciles 7–8: next highest 20% of data	Above normal
Deciles 9–10: highest 20% of data	Much above normal

Source: Kinninmonth, W.R. et al., Australian climate services for drought management, in Wilhite, D.A., ed., *Drought: A Global Assessment*, Routledge, New York, pp. 210–222, 2000.

12.4.7 Surface Water Supply Index

One of the drawbacks of the PDSI mentioned previously was the lack of consideration of frozen precipitation in the calculations. This problem was addressed with the Surface Water Supply Index (SWSI) in the early 1980s by Shafer and Desman (1982). The SWSI is used primarily as a hydrological drought index, and it addresses what the PDSI lacks by taking into account snowpack in mountainous regions along with the subsequent runoff from the melting snow into a river basin. Four inputs are required for the calculations: precipitation, reservoir storage, snowpack, and streamflow. The inputs are given a weighted value based on the total contributions to the water balance in the basin. The scale is similar to the PDSI with a range of +4.2 to −4.2. Even with the advantages that the SWSI presents over using the PDSI alone, some issues limit its widespread application. As with the PDSI, many inputs are not readily available for many locations or need to be calculated for each data point, in most river basins. As data points are added or subtracted from the basin, the weights assigned to all the points need to be readjusted. Since the calculations are unique to each river basin they are being calculated for, it is hard to make comparisons between basins. The SWSI also doesn't account for management decisions in which water is being withheld due to diversion or other management practices within a basin.

12.4.8 US Drought Monitor

As many drought indicators and indices have been developed, finding one that could handle all the various drought situations well has been futile. The concept of a composite approach was developed in 1999 that would signal the start of the USDM (Svoboda et al., 2002). The theory behind the USDM is that all indicators that are available to be monitored can be used and combined by applying a ranking percentile methodology. Using a composite of multiple indicators covering various short- and long-term time frames, an analysis of all drought conditions can be produced and depicted on a single product. The USDM also has the flexibility to integrate new tools and data as they come online and to add additional information where it may be available to enhance the level of accuracy (i.e., mesonet data) compared to other areas that may not be covered by that particular data. The USDM also identifies areas on the map that are in short-term drought (S), long-term drought (L), or a combination of short- and long-term drought (SL), along with the expected impacts associated with each. The (S) and (L) indicators were recently changed from the A (agricultural) and H (hydrological) labels that were used initially by the USDM. These identifiers give the users an idea of the duration of drought to go along with the color-coded intensity levels from D0 (abnormally dry) to D4 (exceptional drought) (Table 12.4).

When a composite of indicators is being monitored using this methodology, there is usually a mix between where percentile indicators will fall for the various drought intensities. To help form a consensus of what level of drought should be depicted for an area, a network of local experts contributes to the making of the weekly map. At this time, more than 350 people participate in the weekly process of making the USDM, contributing local knowledge, data, and products. This group of experts also provides feedback by critiquing the multiple drafts of the map that come out prior to the official release.

TABLE 12.4 USDM Classification Scheme

USDM Classification	Intensity Level	Percentile Ranking
D0	Abnormally dry	30th
D1	Moderate drought	20th
D2	Severe drought	10th
D3	Extreme drought	5th
D4	Exceptional drought	2nd

Source: Svoboda, M. et al., *Bull. Am. Meteorol. Soc.*, 83(8), 1181, 2002.

In addition, the local experts also relay information on drought-related impacts that are occurring during a drought event (Figure 12.3).

12.4.9 Other Indices

Over the years, many drought indices have been developed. Some were developed for a very specific area and others were targeted to address a particular type of drought. Within the many options available, there have been new types of data and platforms that have augmented and added to drought monitoring efforts. One of the newer platforms being utilized for monitoring and detecting drought has been via the integration of remotely sensed data. Indices, such as the SPI, can be calculated using data for various satellite platforms to determine the degree of dryness being observed from space. The advantage to using remotely sensed data is that they allow for a high-resolution spatial coverage that can help to fill in the gaps of in situ data and are updated frequently to allow for near real-time analyses. The main drawbacks are the short period of record associated with remotely sensed data and how platforms and products have changed, or become obsolete, over time. There are also hybrid types of indices where satellite data are being merged with surface data to determine if the stress being observed in the vegetation could be due to drought conditions instead of disease, pests, etc. One such example is the Vegetation Drought Response Index (VegDRI), which takes into account climate-based drought indices as well as satellite-derived data and other biophysical parameters in order to determine drought-related stress upon vegetation through the utilization of data mining techniques (Brown et al., 2008). Depending on the data availability and quality of data for any particular area, it may be possible to utilize many of the drought indices that are available today and determine which ones work best for any particular area or season. With enough communication and coordination, it may also be possible to replicate a composite approach such as what is being done with the USDM (Figure 12.4).

12.5 Drought Indices in a Changing Climate

The idea of what a changing climate could mean and how to address it has been a very active discussion topic recently in the literature and among scientists engaged in drought early warning. Using not only the written climate record but also paleoclimatic data, it is possible to understand the characteristics of past droughts, even back thousands of years. What is known is that drought has been a constant phenomenon with episodes taking place regularly throughout time. Some events have been short, while others have lasted multiple decades. In the context of a changing climate, it should be noted and expected that droughts will continue to occur, as they are a natural part of the climate cycle. With increasing temperatures for most regions and the uncertainty of precipitation amounts and distribution in the future, the intensity, duration, and frequency of droughts is likely to increase for many locations (Easterling et al., 2000; IPCC, 2007; Meehl et al., 2007). With this knowledge in hand, it is important to recognize the value of those drought indices that include a temperature component, as the water balance for an area will not be dependent upon precipitation alone. Drought indices that also account for temperatures can help put into the proper perspective how temperatures are impacting the water balance of a region. Using an approach such as the USDM that is looking at all available indicators would also allow for the flexibility to implement more temperature-based indicators. We may need to continue working toward newer and potentially better drought indices that can do what is needed to account for a changing climate in which there may be a shift in both temperature and precipitation regimes.

Over time, there have been many approaches to identify, classify, and monitor droughts. As the world's climatic conditions change, some of these approaches may not work as well under new climate regimes, and the science community needs to continue to examine new approaches to capture these observed changes. By doing so, indicators and indices will remain a vitally important component of any DEWS.

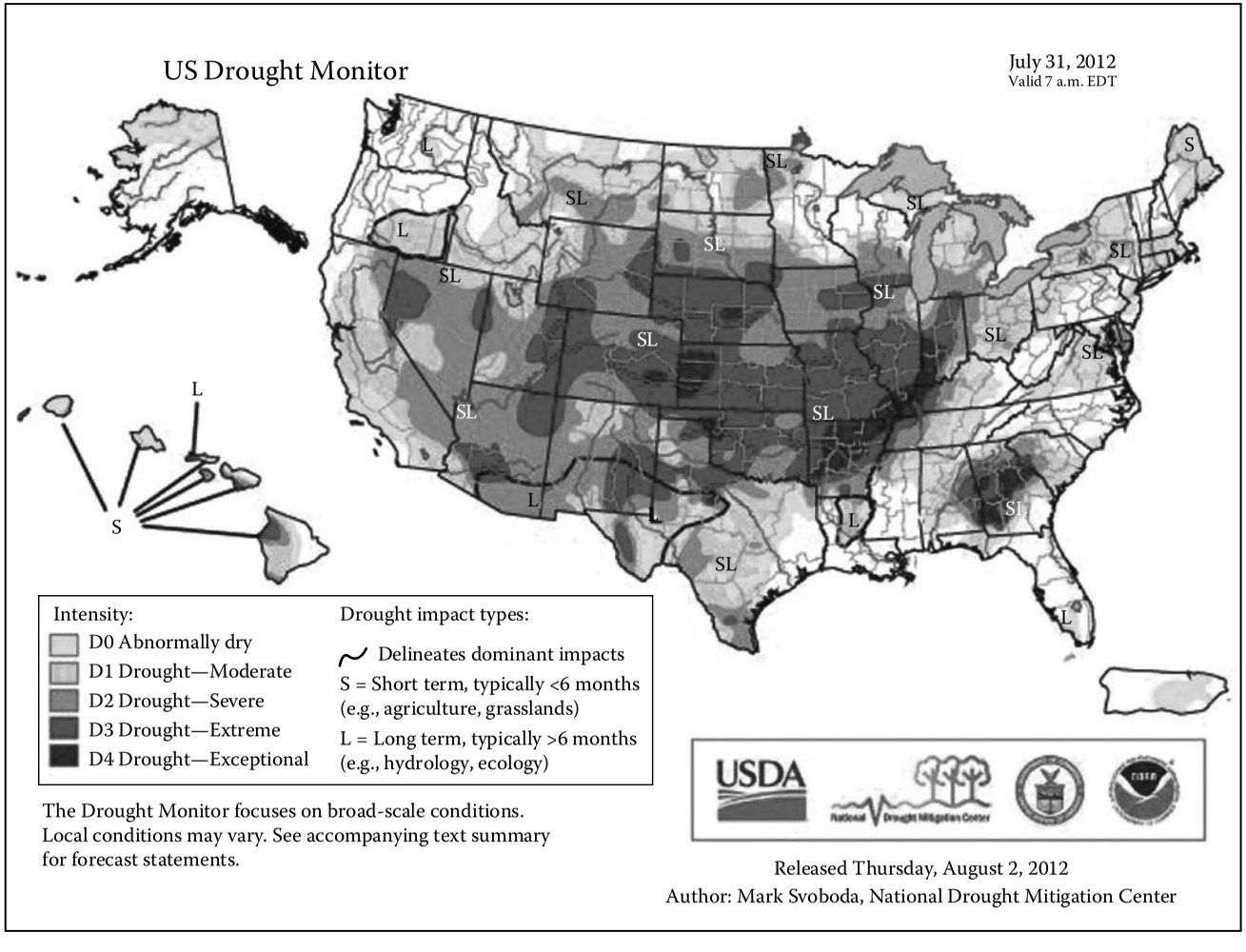

FIGURE 12.3 July 31, 2012, USDM. (From National Drought Mitigation Center, http://drought.unl.edu/, accessed August 1, 2012.)

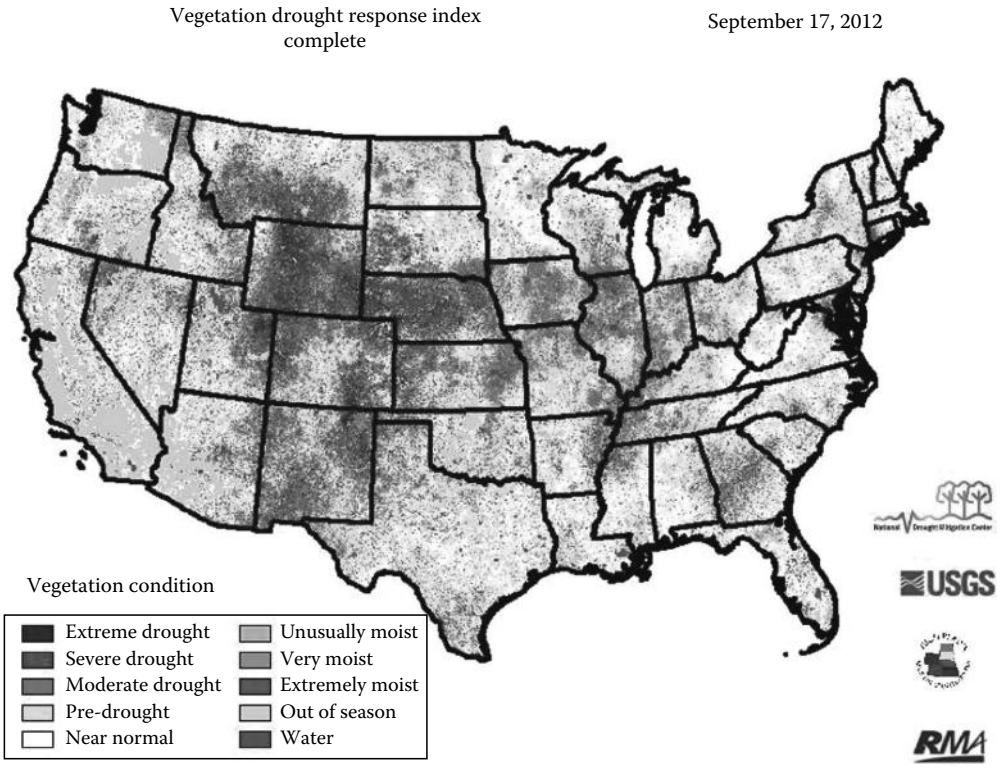

FIGURE 12.4 VegDRI. (From National Drought Mitigation Center, http://drought.unl.edu/, accessed August 1, 2012.)

12.6 Summary and Conclusions

There are many ways to identify drought episodes using a variety of indicators and indices. A universally accepted definition of drought has not been agreed upon. With the variety of ways to explain drought, the simplest is to describe it as a deficiency of precipitation over a defined time period. Scientists have also explained drought by the impacts being experienced. Over time, scientists have tried to better clarify drought by developing various indices in which the duration and intensity of drought could be identified based upon historical occurrences. With the advent of various drought indices, it has also become evident that some indices will work better in certain situations than others. Numerous indices are available, and just a few of the most used indices were discussed in this chapter. With all the indices available, new indices are being developed that help address an unmet need. In the case of the SPEI, this index was developed to directly address how an increase in temperature would impact drought in a changing climate by including a temperature component to the calculations. It is unknown exactly how droughts will evolve in the future, and some of the techniques we use to monitor and assess droughts today may not be adequate. More research may be needed to provide a solution to an unmet need.

References

Alley, W.M. 1984. The Palmer Drought Severity Index: Limitations and assumptions. *Journal of Applied Meteorology*, 23: 1100–1109.

Alley, W.M. 1985. The Palmer Drought Severity Index as a measure of hydrologic drought. *Water Resources Bulletin*, 21: 104–114.

Australian Bureau of Meteorology. 2012. http://www.bom.gov.au/climate/drought/drought.shtml, Accessed August 1, 2012.

Brown, J.F., B.D. Wardlow, T. Tadesse, J.J. Hayes, and B.C. Reed. 2008. The Vegetation Drought Response Index (VegDRI): An integrated approach for monitoring drought stress in vegetation. *GIScience and Remote Sensing*, 45(1): 16–46.

Easterling, D.R., G.A. Meehl, C. Parmesan, S.A. Changnon, T.R. Karl, and L.O. Mearns. 2000. Climate extremes: Observations, modeling, and impacts. *Science*, 289: 2068–2074.

Gibbs, W.J. and J.V. Maher. 1967. *Rainfall Deciles as Drought Indicators*. Bulletin No. 48, Bureau of Meteorology, Melbourne, Victoria, Australia.

Guttman, N.B. 1993. The use of L-moments in the determination of regional precipitation climates. *Journal of Climate*, 6: 2309–2325.

Guttman, N.B. 1997. Comparing the palmer drought index and the standardized precipitation index. *Journal of the American Water Resources Association*, 34: 113–121.

Guttman, N.B. 1999. Accepting the Standardized Precipitation Index: A calculation algorithm. *Journal of American Water Resources Association*, 35(2): 311–322.

Hayes, M.J., M.D. Svoboda, D.A. Wilhite, and O.V. Vanyarkho. 1999. Monitoring the 1996 drought using the Standardized Precipitation Index. *Bulletin of the American Meteorological Society*, 80: 429–438.

Heim, R.R. Jr. 2002. A review of twentieth-century drought indices used in the United States. *Bulletin American Meteorological Society*, 83: 1149–1165.

IPCC. 2007. *Climate Change 2007: The Physical Science Basis*. Contribution of Working Group I to the Fourth Assessment Report of the Intergovernmental Panel on Climate Change, Solomon, S., D. Qin, M. Manning, Z. Chen, M. Marquis, K.B. Averyt, M. Tignor, and H.L. Miller, eds., Cambridge University Press, Cambridge, U.K.

Kangas, R.S. and T.J. Brown. 2007. Characteristics of US drought and pluvials from a high-resolution spatial dataset. *International Journal of Climatology*, 27: 1303–1325.

Karl, T.R. 1983. Some spatial characteristics of drought duration in the United States. *Journal of Climate and Applied Meteorology*, 22: 1356–1366.

Karl, T.R. 1986. The sensitivity of the Palmer Drought Severity Index and Palmer's Z-index to their calibration coefficients including potential evapotranspiration. *Journal of Applied Meteorology*, 25(1): 77–86.

Karl, T.R. and R.W. Knight. 1985. Atlas of Monthly palmer hydrological drought indices (1931–1983) for the Contiguous United States. National Climatic Data Center Historical Climatology Series 3–7, Ashville, NC, p. 319.

Kinninmonth, W.R., M.E. Voice, G.S. Beard, G.C. de Hoedt, and C.E. Mullen. 2000. Australian climate services for drought management, in Wilhite, D.A., ed., *Drought. A Global Assessment*, Routledge, New York, pp. 210–222.

McKee, T.B., N.J. Doesken, and J. Kleist. 1993. The relationship of drought frequency and duration to timescales. Preprints, *Eighth Conference on Applied Climatology*, American Meteorological Society, Anaheim, CA, pp. 179–184.

McKee, T.B., N.J. Doesken, and J. Kleist. 1995. Drought monitoring with multiple-time scales. *Preprints Ninth Conference on Applied Climatology*, American Meteorological Society, Boston, MA, pp. 233–236.

Meehl, G.A., T.F. Stocker, W.D. Collins, P. Friedlingstein, A.T. Gaye, J.M. Gregory, A. Kitoh et al. 2007. Global climate projections, in Solomon, S., D. Qin, M. Manning, Z. Chen, M. Marquis, K.B. Averyt, M. Tignor, and H.L. Miller, eds., *Climate Change 2007: The Physical Science Basis.* Contribution of Working Group I to the Fourth Assessment Report of the Intergovernmental Panel on Climate Change, Cambridge University Press, Cambridge, U.K.

National Drought Mitigation Center. 2012. http://drought.unl.edu/, Accessed August 1, 2012.

Palmer, W.C. 1965. Meteorological drought. U.S. Weather Bureau Research Paper 45, 58pp.

Palmer, W.C. 1968. Keeping track of crop moisture conditions, nationwide: The new crop moisture index. *Weatherwise*, 21: 156–161.

Shafer, B.A. and L.E. Desman. 1982. Development of a surface water supply index (SWSI) to assess the severity of drought conditions in snow pack runoff areas. *Proceedings of the Western Snow Conference*, Reno, NA, pp. 164–175.

Steila, D. 1972. *Drought in Arizona*. Division of Economic and Business Research, University of Arizona, Tucson, AZ, p. 78.

Svoboda, M., D. LeComte, M. Hayes, R. Heim, K. Gleason, J. Angel, B. Rippey, R. Tinker, M. Palecki, D. Stooksbury, D. Miskus, and S. Stephens. 2002. The drought monitor. *Bulletin of the American Meteorological Society*, 83(8): 1181–1190.

Thornthwaite, C.W. 1948. An approach toward a rational classification of climate. *Geographical Review*, 38: 55–94.

Vicente-Serrano, S.M., S. Begueria, and J.I. Lopez-Moreno. 2010. A multiscalar drought index sensitive to global warming: The standardized precipitation evapotranspiration index. *Journal of Climate*, 23: 1696–1718.

Wells, N., S. Goddard, and M.J. Hayes. 2004. A self-calibrating Palmer Drought Severity Index. *Journal of Climate*, 17: 2335–2351.

Wilhite, D.A. 2005. *Drought and Water Crises: Science, Technology, and Management Issues*. CRC Press, Boca Raton, FL.

Wilhite, D.A. 2009. The role of monitoring as a component of preparedness planning: Delivery of information and decision support tools, in Iglesias, A., A. Cancelliere, F. Cubillo, L. Garrote, and D. Wilhite, eds., *Coping with Drought Risk in Agriculture and Water Supply Systems: Drought Management and Policy Development in the Mediterranean*. Springer, Dordrecht, the Netherlands.

Wilhite, D.A. and M.H. Glantz. 1985. Understanding the drought phenomenon: The role of definitions. *Water International*, 10: 111–120.

Willeke G. 1994. *The National Drought Atlas*. Institute for Water Resources REP. 94-NDS-4, U.S. Army Corps of Engineers: Fort Belvoir, VA; 587.

World Meteorological Organization (WMO). 2011. Agricultural Drought Indices *Proceedings of an Expert Meeting Murcia, Spain,* June 2–4, 2010.

13

Flow and Sediment Transport Modeling in Rivers

Masoomeh Fakhri
Chamran University

Hamze Dokohaki
Isfahan University of Technology

Saeid Eslamian
Isfahan University of Technology

Iman Fazeli Farsani
Shahrekord University

Mohammad Reza Farzaneh
Tarbiat Modares University

AUTHORS

Masoomeh Fakhri was born in Iran. She received her BSc degree in water engineering at the University of Razi, Iran. Then, she continued her studies in water structures engineering, Faculty of Water Sciences Engineering, Shahid Chamran University of Ahvaz as an MSc graduate. She teaches at Razi University and is the author of 2 chapters in an international handbook, with more than 10 articles under review and published in conferences and journals such as ASCE; she collaborates in national projects.

Hamze Dokohaki is a former MSc student in the water engineering department at Isfahan University of Technology (IUT), Isfahan, Iran. His research interests include fields related to modeling, basic scientific concepts and computer programming. His academic experiences include being a contributing author in different national or international journals or conference publications. He is also currently working as a research team member in IUT.

Saeid Eslamian received his PhD from the University of New South Wales, Australia, under Professor David Pilgrim. He was a visiting professor in Princeton University, the United States and ETH Zurich, Switzerland. He is currently an associate professor of hydrology in Isfahan University of Technology. He is founder and chief editor of the *Journal of Flood Engineering* and the *International Journal of Hydrology Science and Technology*. He has to his credit more than 200 publications mainly in statistical and environmental hydrology and hydrometeorology.

Iman Fazeli Farsani is currently an MSc student of soil science in Shahrekord University, Shahrekord, Iran. He has been a coauthor for an international handbook; he also has more than five research papers under review and he has published articles in conferences and journals; he has also been a collaborator in two projects.

Mohammad Reza Farzaneh is currently a PhD student of water resources in Tarbiat Modarres University, Tehran, Iran. He has been invited as main and coauthor for two international handbooks and he is adviser of six Master theses in the field of climate change impacts on water resources; more than 50 of his articles are under review and he has published articles in conferences and journals. He is a collaborator in national and international projects such as the study of climate change impact on African water resources; he teaches GIS, hydrology, and water resources and has registered four inventions.

PREFACE

In this chapter, attempts have been made to present different types of models in the simulation of flow and sediment transport in rivers. These models have been classified into four groups: empirical, conceptual, physical, and computational. After that, the different types of models have been reviewed and finally, instructions for choosing and also using these models have been provided.

13.1 Introduction

River play a very important role in establishing civilization and human settlement since they are the most significant natural resource. Humans have always depended on rivers. Rivers are one of the most important cause of erosion, sediment transportation, and sedimentation processes.

In addition, these processes are a function of hydraulic and hydrologic conditions; they are also related to geological characteristics, morphological characteristics, sediment characteristics, etc. Many variables, including river discharge, longitude slope, sediment volume, shore resistance toward the stream, land cover, and geology, affect the sedimentation of rivers. Many studies, experiments, and in-river investigations have been performed to relate these and other parameters.

Although in recent times many studies have been done on soil erosion, sediment transportation, and sediment deposit, we have a long way to go to completely understand this phenomenon. This can be attributed to complications of effective processes on soil erosion. The role of sediments in the life of humans can be divided into both positive and negative aspects: On the positive side, sediments are deposited beside shores and floodplains and fertilize the lands for agricultural use, for example, the floodplains of Nile River in Egypt and Mississippi River in the United States. On the negative side, sediment transportation affects all aspects of programming, developing, and using and sustaining of water resources. For this reason, in the past decade, several scientists have paid attention to this subject and have presented lots of theories.

Each of the three processes, including erosion, transportation, and deposition, are troublesome for humans. Erosion destroys basin soil and natural resources in the basin, which will have a huge impact on the future as we will not be able to recover them easily. Deposition damages the buildings, bridges, reservoirs, and other structures built along the rivers, causing floods. Unfortunately, many man-made structures cause erosion, transportation, and deposition, including cutting or burning land cover that causes severe erosion with plenty of sediments flowing into the river. Changes in rivers and their activity, construction of reservoirs, for instance dams and bridges, and mines producing sand and gravel are the other causes of erosion.

Sediment is not only the main source of pollution but is also an important factor in the transportation and adsorption of pollutants. To minimize the risks and reach our goals, erosion trend estimation and sediment stream calculations have to be performed to estimate the amount of deposition, sediment transportation, etc.

Many scientists have performed studies in the fields of erosion, transportation, and deposition modeling, and have developed different models for different regions. In this study, attempt has been made to present the important and practical models in this area in spite of many explanations about each model being available. Finally, evaluation methods are presented.

13.2 Erosion Models Grouping

Erosion models can be classified in many ways; each model is different from the other and can be based on function, theoretical base of model introduction, calculative framework of model, and data processing. In this study, the classification is based according to the theoretical base of the models.

The models can be based on theory mentally. In other words, there is no clear bound to separate the models from each other, and the models have common bounds. In general, these bounds can be divided into the following groups:

1. Empirical models
2. Conceptual models
3. Physical-based models
4. Computational models

13.2.1 Empirical Models

Empirical models are based on observations and are usually statistical. These models are usually used in average erosion prediction. However, some are utilized to predict sediments. These type of models are simple to use and are beneficial in identifying the source of sediments and nutrition elements.

13.2.2 Conceptual Models

Conceptual models are based on the continuing equations of water and sediment. Disregarding the details, they provide a basin's complete description. These models act as an intermediate between the empirical and physical models.

13.2.3 Physical Models

Physical models are based on physical equations and are developed in order to study the local distribution of runoff and sediment during rainfall and also to predict total runoff and soil loss.

To separate each model from the other, different types of these models are presented.

13.2.4 Computational Models

Computational models have a high variety of empirical, conceptual, and physical models. The authors present a detailed summary of each model (Table 13.1). These types of model include the following.

13.3 Model Description

13.3.1 USLE Model

The first equation to estimate the amount of erosion in a specific slope was the Zing equation (1940) [177], in which only two factors, degree and slope length, were considered. Then, climate and land-covering factors were included in the equation by Musgrave [106] and Smith and Whitt [130], respectively. The best equation to estimate soil erosion was given by Wischmeier and Smith in 1965 to sustain soil and water resources by selecting agricultural management of erosion control in farmlands.

This equation, called the universal equation of soil erosion, has an empirical base and can be achieved from abundant outdoor data and after about 30 years of study on water erosion collected from 46 research stations in 26 different states with different geographical and climate conditions in the United States. We also need to consider the results of other researchers. The following four factors can be used to estimate sheet and rill erosions:

1. Potential erosion of climate
2. Potential erosion of soil
3. Elevation
4. Land use and its management

In this method, the emphasis is on total rainfall energy to calculate erosion severity caused by all kinds of surface and sheet erosions. In the universal equation of soil erosion, the effect of every factor on soil erosion is recognized with a specific number, and finally the erosion amount, as a quantitative value, is calculated by multiplying the numbers. The following is the equation for the USLE model:

$$A = R\ K\ L\ S\ C\ P \tag{13.1}$$

where

A is the erosion amount of soil by sheet and rill erosions (weight/area/time) (In British units, the unit is (ton/ac/year); in metric units, it is (ton/ha/year).)

R is the rainfall factor indicating the potential erosion of rainfall

K is the potential of erosion factor of soil as a number identifying the soil intrinsic sensitivity on erosion

L is the slope length factor calculated by the division of erosion in slope length to erosion in control basin. The control basin is a basin present in the same field and slope. It has no land cover, is fallow, and is plowed in slope aspect. The area, slope, width, and length of the basin are 0.01 ac (40.5 m^2), 9% (5.14°), 6 ft (1.83 m), and 72.6 ft (22.13 m), respectively

TABLE 13.1 Empirical, Physical, and Conceptual Models Description

Model Acronym	Type	Reference/Website	Model Name Description
USLE	Empirical	Wischmeier and Smith [164]	Universal Soil Loss Equation
MUSLE	Empirical	Williams and Berndt [161]	Modified Universal Soil Loss Equation
RUSLE	Empirical	Renard et al. [116]	Revised Universal Soil Loss Equation
AGNPS	Conceptual	Young et al. [173]	Agricultural Non-Point Source Model
ANSWERS	Physical	Beasley et al. [11]	Areal Nonpoint Source Watershed Environment Response Simulation
CREAMS	Physical	Knisel [74]	Chemical Runoff and Erosion from Agricultural Management Systems
EMSS	Conceptual	Vertessey et al. [151], Watson et al. [155]	Environmental Management Support System
GUEST	Physical	Yu et al. [175], Rose et al. [118]	Griffith University Erosion System Template
HSPF	Conceptual	Johanson et al. [65]	Hydrologic Simulation Program, Fortran
IHACRES-WQ	Empirical/ Conceptual	Jakeman et al. [61–63]	Identification of unit hydrographs and component flows from Rainfall, Evaporation and Streamflow Data—Water Quality
IQQM	Conceptual	DLWC [33]	Integrated Water Quantity and Quality Model
LASCAM	Conceptual	Viney and Sivalapan [152]	LArge Scale Catchment Model
LISEM	Physical	Takken et al. [141], De Roo and Jetten [36]	Limburg Soil Erosion Model
MIKE-11	Physical	Hanley et al. [53]	MIKE (named partially after the author Michael, Mike Abbott)
PERFECT	Physical	Littleboy et al. [87]	Productivity, Erosion, and Runoff, Functions to Evaluate Conservation Techniques
SEDNET	Empirical/ Conceptual	Prosser et al. [115]	Sediment River Network Model
TOPOG	Physical	CSIRO Land and Water, TOPOG Homepage; Gutteridge [29], Haskins and Davey [50]	TOPOGraphy
WEPP	Physical	Laflen et al. [78]	Watershed Erosion Prediction Project
EUROSEM	Physical	Morgan et al. [105]	EUROpean Soil Erosion Model
KINEROS	Physical	Smith [131], Woolhiser et al. [166]	KINematic EROsion Simulation
SEDD	Empirical	Ferro and Porto [43]	SEdiment Delivery Distributed
RUNOFF	Physical	Borah [17]	No acronym
WESP	Physical	Lopes [89]	Watershed Erosion Simulation Program
CASC2D-SED	Physical	Johnson et al. [66]	CASCade 2-Dimensional SEDimentation
SEM	Physical	Storm et al. [140]	Soil Erosion and Sediment Transport Model
SHESED	Physical	Wicks [157]	SHE–SEDimentation
EGEM	Empirical	USDA [148], Woodward [165]	Ephemeral Gully Erosion Model
EPIC	Empirical	Sharpley and Williams [128]	Erosion Productivity Impact Calculator
EROSION 2D/3D	Physical	Schmidt [123,124], Werner [156]	National Centre for Earth Resources Observation and Science
MOSES	Physical	http://www.weru.ksu.edu/ftp_site/moses/moses_man/index.html	MOdular Soil Erosion System
PESERA (MESALES)	Physical	Kirkby et al. [72]	Pan-European Soil Erosion Risk Assessment
WATEM (SEDEM)	Conceptual	http://www.kuleuven.be/geography/frg/modelling/erosion/watemsedemhome/index.htm	Water and Tillage Erosion Model

(*continued*)

TABLE 13.1 (continued) Empirical, Physical, and Conceptual Models Description

Model Acronym	Type	Reference/Website	Model Name Description
CAESAR	Physical	Coulthard [27]	Cellular Automaton Evolutionary Slope And River Model
G2	Empirical	http://eusoils.jrc.ec.europa.eu/library/themes/erosion/G2/data.html	Geoland 2
SLEMSA	Empirical	Elwell and Stoking [41]	Soil Loss Estimation Model for Southern Africa
BLM	Empirical	http://www.blm.gov	Bureau of Land Management
EPM	Empirical	Nearing et al. [107]	Erosion Potential Method
FAO	Empirical	http://www.fao.org	Food and Agriculture Organization
PSIAC/ MPSIAC	Empirical	Pacific Southwest Interagency Committee [111]	Pacific Southwest Interagency Committee
HEM	Physical	Lane et al. [80]	Hillslope Erosion Model
Fournier	Empirical	Fournier [45]	Fournier Model
Musgrave	Empirical	Musgrave [106]	Musgrave Model
PEPP	Physical	Schramm [125]	Process-Oriented Erosion Prognosis Program
SHE	Physical	Abbott et al. [2,3]	Système Hydrologique Européen (French acronym for 'European Hydrologic System')
MULTSED	Physical	Li et al. [84]	MULTiple-watershed SEDiment-routing
OPUS	Physical	Smith [132]	No acronym
ACRU	Conceptual	Schulze [127]	Agricultural Catchments Research Unit
Hydro Physical Method (HP)	Empirical	Larionov et al. [81]	Hydrophysical Method
Scalogram	Empirical	Cruz [28]	Scalogram Model
Carson and Kirkby	Empirical	Carson and Kirkby [20]	Carson and Kirkby Model
AL-Kadhimi	Empirical	Al Kadhimi [4]	AL-Kadhimi Model
Stehlik	Empirical	Stehlik [138]	Stehlik Model
Douglas	Empirical	Douglas [38]	Douglas Model
MMMF	Empirical/ Conceptual	Morgan et al. [104], De Jong et al. [35]	Modified Morgan, Morgan and Finney
SHETRAN	Physical	Bathurst et al. [9]	European Distributed Basin Flow and Transport Modelling System
AGWA	Conceptual/ Physical	Burns et al. [19]	Automated Geospatial Watershed Assessment
USPED	Empirical/ Conceptual	Mitasova [97]	Unit Stream Power Erosion Deposition model
THORNES	Conceptual/ Empirical	Thornes [145]	Thornes model
SPL	Empirical/ Conceptual	Barnes and Pelletier [8]	Stream Power Law Model
SWRRB/SWAT	Conceptual	USEPA [149], Arnold et al. [6]	Simulator for Water Resources in Rural Basins/Soil and Water Assessment Tool
SEAGIS	Empirical/ conceptual	DHI [37]	Erosion Assessment Tool of MIKE BASIN & MILW
MATSALU	Conceptual	Krysanova et al. [76]	No acronym
SWIM	Conceptual	Krysanova et al. [77]	Soil and Water Integrated Model
CHILD	Physical	Tucker et al. [147]	Channel-Hillslope Integrated Landscape Development
TOPMODEL	Conceptual	Beven and Kirkby [14]	TOPographic MODEL
SIMWE	Physical	Mitasova et al. [98]	SIMulation of Water Erosion

TABLE 13.1 (continued) Empirical, Physical, and Conceptual Models Description

Model Acronym	Type	Reference/Website	Model Name Description
SEMMED	Physical	De Jong et al. [35]	Soil Erosion Model for Mediterranean Areas
ARMSED	Physical	Riggins et al. [117]	Army Multiple Watershed Storm Water and Sediment Runoff
CSEP	Physical	Kirkby and Cox	Climatic Index for Soil Erosion Potential
MEDRUSH (MEDALUS)	Physical	Kirkby [71]	MEdalus Desertification Response Unit SHe
Dendy and Bolton	Empirical	Dendy and Bolton [32]	Dendy and Bolton Model
CORINE	Physical	EEA [39]	COoRdinate INformation on the Environment

S is the slope factor calculated from the proportion of erosion in the existing slope to the one present in the control basin (9% slope)

C is the factor of land cover estimated from the proportion of erosion in specific land cover to erosion value in the control basin that does not have any cover and is plowed in slope aspect

P is the soil conservation factor calculated from the proportion of erosion in conserved land to the erosion in the same land when no conservation is performed (planting is in the slope path)

13.3.2 MUSLE Model

The universal equation of soil erosion (USLE) to estimate soil loss from a piece of land or in a specific slope is presented, but with its use, the sediment delivery amount of basins could not be estimated. To calculate the sediment amount according to this equation, Williams and Berndt [161] introduced the sediment delivery ratio (SDR) coefficient. The SDR depends on drainage and physiographical characteristics of basins, climatic events, and also land use.

The investigations have shown that the relationship between erosion causes and sediment yield amount is not linear and strong. Therefore, due to changes in the estimated SDR and no linear relationship between *R* and the sediment yield amount, the rainfall factor of the USLE model is replaced with the runoff factor and the model has been named MUSLE.

By replacing the rainfall factor by the runoff factor, it is not necessary to use SDR in the universal equation any more. In MUSLE model, the role of runoff is important and is practical in calculating the annual sediment. This equation, instead of estimation of soil erosion, is presented to estimate the sediment delivery in the outlet of a basin and is based on a single thunderstorm. The model formula is as follows:

$$A = 95\left(Q \cdot q_p\right)^{0.56} KLSCP \tag{13.2}$$

where

A is the sediment delivery amount of an event (kg)

Q is the runoff volume (m^3)

q_p is the severity or maximum discharge of runoff (m^3/s)

13.3.3 RUSLE Model

The RUSLE model has been used increasingly from the 1970s. In 1985, in a meeting, with the presence of some researchers of the agriculture ministry of the United States and other researchers of soil erosion, it was decided that according to the necessity, the universal equation of soil erosion would be developed and after compilations and recommendations, the related dissertation would be revised in 1978.

The revision was begun in late 1987 and from early 1990s. The USLE model was revised and its data were updated and then used to present the erosion estimation model under the name of RUSLE. Although the principal form of the universal equation is maintained, the numerical values used in calculating unique indices in the RUSLE equation are changed significantly.

In the following years, some revisions in the model were made; RUSLE 1.05 (1993), RUSLE 1.06 (1998), and finally RUSLE 2 (2010) were presented; in the latest version, two characteristics have been improved including land covering management and displaying runoff events added to the modeling.

13.3.4 AGNPS Model

The AGNPS model was developed by the US Department of Agriculture, Agricultural Research Service (USDA-ARS), Soil Conservation Service (SCS), and Minnesota Pollution Control Agency in the United States [174]. The model estimates the runoff quality in basins with areas less than 20,000 ha. The input data include basin morphology, land use, and rainfall.

Input parameters for each AGNPS grid cell contain the SCS curve number, land slope, land shape factor, field slope length, slope of channel, slope aspect of channel, channel shape, rough coefficient of Manning, factor of soil erosion potential, management factor, soil texture, soil fertility, fertilization availability factor, gully progress, COD (chemical oxygen demand) factor, and water absorption factor.

The outputs generally include runoff, sediment, nutritious elements, and chemical oxygen demand (COD). The hydrological outputs contain runoff volume and peak runoff ratio. The sediment output includes sediment yield, sediment density, diffusion, and size of sediment particles. The pollution output includes the nitrogen amount in sediment, nitrogen and phosphorus solved in runoff, phosphorus, and organic carbon in sediment.

For simulating erosion and sediment transportation, the universal equation of soil loss is used. In previous versions of AGNPS, the USLE equation was utilized; however, recent versions use the RUSLE one. This model needs much data and its calculations are complicated comparing empirical models defined according to weighting.

13.3.5 ANSWERS Model

The ANSWERS model was developed during middle of the 1980s [102]. The model is a kind of deterministic model and by using distributed factors in a basin and using single-event data, it deals with simulation of hydraulic processes.

The model is easily used for small basins. This model was evaluated in two sub-basins in Black Gulf, basins in Oklahoma, Ohio, North Carolina, Texas, and also in Iran was determined that evaluation verifies the accuracy of the model. ANSWERS is used for a single event of a basin, and it is able to predict maximum flood and the total volume of surface runoff and erosion from rainfall in agricultural basins. This model does most of the calculations of erosion and sedimentation.

One of the input parameters includes landform parameters such as soil data, land use, slope, and slope aspect [11]. Runoff and erosion simulations are the output parameters [44]. This model calculates erosion with empirical equations and uses Yalin's equation [168] to estimate sediment transportation. The limitation is that the model considers erodibility as a constant parameter in time limit.

13.3.6 CREAMS Model

The CREAMS model has been developed as a tool to assess the relative effects of agricultural activities on the pollution of surface runoff and root zone soil water. Input data in the model include precipitation series, monthly air temperature, solar radiation, and soil and crop type data.

The CREAMS model can be operated in both continuous and single-event forms, and it is assumed that land use and soil topography are steady wherever it is used. The process of rain runoff is similar to

the SCS curve number. The erosion factor is based on the USLE model but in this model, the sediment transportation capacity of subsurface flows has also been considered.

In this model, the slope in each unit is hypothetically fixed. With reference to the continuous equation, the sediment transportation flow is assumed a steady-state continuity equation. In addition, the model can calculate sediment yield by gully erosion. This model is usable for basins of about 40 ha area though it could be used for up to 400 ha scale. It shows erosion completely variable as one of the most important aspects of the model. One of the model shortages is that the basin shape has been assumed uniform in topography and land use aspects, which is an unreal assumption.

13.3.7 EMSS Model

The environmental management support system (EMSS) is a software designed for helping in water quality management in the basins located in eastern south Queensland in Australia. This system has been developed in the Cooperative Research Centre for Catchment Hydrology (CRCCH) [156]. Input data include the GIS layer of each subcatchment boundary, land use, rainfall, and daily potential evapotranspiration.

The output contains daily runoff, daily loads of total suspended sediment, and total nitrogen and phosphorous predicted for every subcatchment [151]. This model almost has a low complexity but estimates runoff and pollution transportation well [25]. Considering model structure, its modules can be added or deleted only in-case. However, although it was developed in eastern south Queensland in Australia, it seems inflexible for other regions.

13.3.8 GUEST Model

The GUEST model was introduced in 1983 by Rose, and then Rose and Misra developed it in 1992. GUEST is a physicomathematic model and is profitable for predictions of factors such as potential erosion and its changes, density of sediment, runoff and rainfall, gully and mass erosion in time limit.

GUEST is a single-event model, and its estimation is based on physical characteristics of soil. By measuring these cases, the parameters can be estimated [96].

Input data of the GUEST model include the following:

- Geometry that includes length, width, slope, and compactness of rill.
- Sediment characteristics include sediment density, size distribution of soil particles, and deposition velocity characteristics.
- Rough characteristics contain Manning roughness.
- Erodibility parameter factor.
- Hydrologic characteristics include effective runoff and total runoff sum.

The output includes the following:

Soil erosion value, estimation of soil loss in interval time for the locations where their soil erosion is not measured, and available hydrologic data are the parameters such as runoff severity or rainfall severity.

13.3.9 HSPF Model

This model has been developed based on the 1960s Stanford Watershed Model for the simulation of watershed hydrology and water quality (nitrogen, phosphorous, suspended sediment, and other toxic organic or inorganic pollutants) [154]. The model is practical in catchment scale and the basins are divided into homogenous sections. The model calculates quality and quantity of water for each land use.

The model inputs include rainfall, evaporation, air and water temperature, solar radiation, sediment grain size distribution, point source discharge volume, and water quality data, which should be

calibrated [24]. These data are necessary for all of the subcatchments. The model is able to simulate great limitations of water elements. The output includes runoff, flow rate, sediment load, and nutrient concentrations in a time limit. One of the limitations of the model is that its parameters depend on calibration too much [154].

13.3.10 IHACRES-WQ Model

The IHACRES-WQ model contains the rainfall runoff model of the IHACRES and STARS model. The input data include time series data for streamflow, rainfall and depending on IHACRES versions, also include temperature or evapotranspiration. The model predicts daily streamflow, while the STARS model can be used to predict downstream suspended sediment concentration. The IHACRES-WQ model needs a little input data approximately and local distribution of input data does not need calibration. However, the parameter values should be calibrated with observed data or inferred from regionalization of similar catchments.

13.3.11 IQQM

The Integrated Water Quantity and Quality Model (IQQM) is a largely conceptual model developed by the NSW Department of Land and Water Conservation in Australia. This model is designed for use in water resources management in river scale [34]. Minimum necessary input data to run IQQM include catchment areas and slope, river system configuration, daily rainfall, daily evaporation, daily streamflow, storage characteristics, diversion points, and design of water use. The applied rainfall–runoff module in the IQQM is the Sacramento model, which was developed by the US National Weather Service and the California Department of Water Resources. The model uses many parameters and each of the IQQM modules need many parameters, which should be calibrated, and this is one of the difficulties. For example, QUAL2E needs more than 100 input data.

13.3.12 LASCAM Model

LASCAM is a salt and water balance model including sediment generation and hydrology modeling algorithms at a catchment scale [190]. Hydrologic model input data contain daily rainfall distribution, evaporation pan, and land use information. Topographic data for defining subcatchment and stream networks are needed, and to calibrate sediment components, sediment load records in catchment are necessary.

Nutrient components include 29 parameters, of which respectively 11 and 18 parameters are related to phosphorous and nitrogen; most of them are observed values. The output for hydrology model contains surface and subsurface runoff, actual evaporation, recharge to the permanent groundwater table, baseflow, and measuring soil moisture and salt outflows. The LASCAM model considers water quantity, salt mobilization, and transport and also uses USLE to predict sediment generation.

13.3.13 LISEM Model

This model has been adapted with Geographic Information System (GIS) by Dorsen and Koach. ANSWERS [10] and SWATRER [13] models are the base of the LISEM model. During 1998–2000, as a common project between China and the Netherlands, erosion in loss conservational programs of China was measured based on this model and Hessel [55] published the conclusions. At the same time (1998–1999 duration), other regions of the world evaluated this model.

LISEM is one of the first physical models of soil erosion that has been adapted with the geographic system. It means the input and output of the model are usable in the geographic information system

format. The studied processes in the model include rainfall, interception, pothole, infiltration, surface flows, channel flow, erosion due to rain, erosion due to surface flows, and flow transportation capacity.

Input maps in the LISEM model contain maps of basin, covering, soil surface, soil permeability, and maps of channel and climatic information. The model outputs are total rainfall information, total discharge, maximum discharge, and total soil loss, a map with "asc" format with hydrograph curves and maps of soil erosion and sediment in each rainfall with the PCRaster format.

13.3.14 MIKE-11 Model

MIKE-11 is a software system used in water quality modeling developed by the Danish Hydrology Institute (DHI) [37]. Main modules of this model include rainfall–runoff component, hydrologic module, water quality module, and sediment transportation module. This model simulates unsteady flow in one dimension.

13.3.15 PERFECT Model

The PERFECT model was developed by the Queensland Department of Primary Industries (Land Management Branch and Queensland Wheat Research Institute) and the QDPI/CSIRO Agricultural Production System Research Unit [87]. This model was made to solve such problems as soil management analysis like tillage or fallow management strategies.

The model is designed to predict runoff, erosion, and crop yield for some management components such as planting succession, harvesting, and stubble management in fallow duration of dry farming in Australia [88]. Model inputs include daily climatic data, soil parameters, cropping sequence criteria (i.e., crop type and length of fallow), growth parameters, and fallow management.

The necessary climatic parameters contain daily rainfall, pan evaporation, temperature, and evaporation. This model predicts water balance, erosion, and crop growth on a daily time step. The simulated erosion in the model is with the use of the MUSLE model. However, losses of nitrogen in the surface of soil are simulated by the CREAMS model.

Littleboy et al. [87] showed that the PERFECT model is more reliable than CREAMS according to 77%–89% changes in the daily runoff volume. The authors indicated considering crop covering, surface runoff, and soil evaporation impacts, the PERFECT model is a suitable model to analyze runoff compared with the CREAMS model. Littleboy et al. [86] pointed out that this model is not designed for using beyond the north east of Australia, and it is recommended that the model should be calibrated before using the it for another region.

13.3.16 SedNet Model

SedNet is a steady-state model utilized to estimate sediment yield generation and deposition from hillslopes, gullies, and riverbanks in a river network [114]. It needs the digital elevation model (DEM) for defining river network for input data and the model calculates topography of the basin by using it. The hillslope model requires a grid of mean annual rainfall, soil erodibility, crop management factors, slope, slope length, and management practices.

The gulley erosion model needs a network of gulley density and characteristics explanation. SedNet links to GIS and sediment local pattern in stream is the output. This model has been developed specially on continental scale for the Australian continent. The model needs many parameters and it is difficult to gain most of them for a basin. Compared with other grid-based models such as LISEM and AGNPS, this is an easier tool in showing processes.

13.3.17 TOPOG Model

This model is used to simulate water, carbon, solutes, and sediment balance of catchments [110]. Input data include topography, climate, and soil and plant information [49]. Output of the model includes water fluxes, conservative solutes, and sediment.

TOPOG contains two rainfall–runoff modules: steady-state water balance model (TOPOG-Simuli) and dynamic water balance modeling program (Topog-dynamic), which are able to simulate in every daily and subdaily time step. The TOPOG model is used to predict local distribution of erosion hazard, earthquake risk indices, and dynamic balance between soil, plant, and atmosphere systems in a catchment.

13.3.18 WEPP Model

WEPP is a physical-based model and is designed by USDA-NSCS, USDA-FS, USDA-BLM, and other organizations in environmental planning and water and soil conservation in United States [78]. The model parameters are changed with time and locality and simulate erosion and sediment in each time and locality unit in a catchment, including slopes of hill, channel, and catchment.

These channels can be from simple and uniform to very complicated. The WEPP model has the capability of erosion in a widespread region and it is possible that this region has no financial reason for erosion estimation. WEPP is a continuous model that could be utilized for single events.

Because this model is designed to estimate erosion in a continuous time, it needs much information comparing single-event studies. For example, if soil management changes would be investigated, at least 100 input data for this model are required. This model is created to recognize and study mechanisms of erosion control made by water. The model does not calculate erosion, transportation, and sediment processes in steady channels such as gullies and perennial streams.

In this model, rill and interill erosions are studied. The WEPP model input data include information on climate, soil freezing, snow aggregation and melting, hydraulic infiltration of surface flow, water level, plant growth, decomposition of the residual plant left over, stability, erosion, and sediment. The model output includes pure erosion or sediment, erosion or sediment in rills, erosion and sediment in interill, and sediment density.

The main output indicates runoff and a summary from erosion on daily or monthly scale. One of the WEPP difficulties is that many parameters of the model should be calibrated with observed data, and gulley erosion is not considered as another problem.

Generally, the abilities of the WEPP model can be summarized in the following cases:

1. This model divides total basin rill and interill erosions.
2. The model considers rainfall more than other models since runoff map is important in soil erosion.
3. This model can be used in agriculture basins with 1–2000 ac area.
4. This model cannot be used for regions with a channel or river, because the model cannot simulate the processes that happen there.

13.3.19 EUROSEM Model

EUROSEM [105] is a comprehensive single-event model for prediction of runoff and water erosion of farmland soil or small hydrological catchment. This model is a result of 25 scientists' attempts from 10 European countries. The model can be used for assessment of erosion danger and the methods of water and soil conservation. EUROSEM is a physicomathematical model based on erosion process.

The role of the erosion process in creating this model is in division of raindrops by land covering two sections. The first one passes the plant and reaches bare ground (throughfall). The latter one reaches the plant and creates interception storage, which finally reaches ground level in two ways including

interception storage and leaf drainage. Kinematic energy of interception storage drops and throughfall makes soil particles separated.

A section of rain reaches surface ground, infiltrates soil, and the left over fills surface holes. After that, runoff flows on surface soil, subsequently soil erosion follows. Soil particles can be changed to sediment and the equilibrium between these two-autonomy processes estimates erosion load. This model is designed to correct some problems of the universal model.

The first problem of the universal model is erosion estimation during 1 year, which should be changed to single event in this model. To investigate a single event, the erosion models need a series of equations and physical models. This model uses 1 min time steps to simulate and investigate. The studied basin is divided into a series of homogenous sheets and the data are gained from them.

The main problem of this model is the large numbers of input parameters. The EUROSEM model is not completely a distributional model and has a problem in studying big gullies. This model is designed for simulation of erosion, sediment transportation, and deposition made by rill and interill processes. Application scale of the model includes small farmlands and basins. EUROSEM simulates total runoff volume, total soil loss, hydrograph, and sediment graph of each event.

13.3.20 KINEROS Model

The kinematic wave theory has been used for estimation of runoff in channels and basins from 1970. Although this method needs simple assumptions in theoretical aspects, its hydraulic characteristics are introduced and confirmed well. This model has been studied many times in various regions. The kinematic wave theory was used by Rovey et al. [119] as a network of channels and flat levels in a computer model named KINGEN, and then some corrections were done on infiltration section, regarding basin element, erosion, and sediment transportation estimation and finally the model was named KINEROS.

This model can show basin function in each event and can be used for different types of small basins, such as agricultural, natural, and municipal basins. In this model, utilizing Horton mechanism that rain intensity is more than infiltration capacity, runoff could be made. Therefore, it is not suitable for basins with a high flow.

In this model, differential equations indicating flow into the channel, erosion, and sediment transportation are solved by finite movement. KINEROS is a physical model and is based on physics principles such as conservation of mass and kinematic energy. In addition, KINEROS is a distributed model, which means that the model shows basin and channel network in a collection. Also, this model is stochastic; in the other words, in wet and rainy situations, it calculates surface runoff and erosion due to a thunderstorm.

The KINEROS model components include infiltration, infiltration at the end of rain, surface flow of Horton, flow in channels, flow in the storage, erosion and sediment transportation, channel erosion, sediment transportation, and sedimentation in basins.

13.3.21 SEDD Model

SEDD is an empirical model, based on the USLE model, suggested by Ferro and Porto [43]. The Monte Carlo technique was used to test uncertainty in parameters of sediment yield model. Biesemans et al. [15] did the same study on RUSLE.

13.3.22 RUNOFF Model

Sediment transportation component of RUNOFF [17] computes soil erosion and sediment routes in downstream. The model has two parameters: flow detachment coefficient, which should be calibrated by observed data, and raindrop detachment coefficient, which is fixed. Though the model simulates sediment discharge reasonably, some parameters should be considered fixed in time scale.

13.3.23 WESP Model

The WESP model calculates sediment transportation by a one-dimensional continuity equation as the physical base and is usable for small watersheds [108].

In this model, erosion and sediment happen simultaneously. Santos et al. [122] corrected the WESP model for large watersheds. In this correction, instead of the simultaneous concept of erosion and sediment in the original WESP model, it calculates sediment transportation using overland flow and considering the difference between amounts of erosion and deposition.

13.3.24 CASC2D-SED Model

The model has a physical base and has been introduced by Johnson et al. [65]. This model investigates runoff flow using two-dimensional continuous equations. In a section of upland erosion, transportation capacity was corrected utilizing regression equations by Kilinc and Richardson [67]. Despite runoff hydrographs computed reasonably well, sedigraphs cannot simulate appropriately. The sediment yield was found within a range of 50%–200%.

13.3.25 SEM Model

SEM is a mixture of the SHE modeling system [2,3]. This model simulates spatial and temporal changes of soil erosion. The splash detached soil particles are transported by overland flow. The overland flow has a detachment potential called flow entrainment equivalent to flow transportation capacity.

The net erosion or deposition is calculated by the difference between the sediment load entering and leaving each grid in the catchment. Two parameters including soil erodibility and flow entrainment should be calibrated in this model.

13.3.26 SHESED Model

SHESED is a hydrologic and sediment transportation model of SHE [2]. SHESED considers erosion as the sum of erosion by raindrop and leaf drip impacts. Storm et al. [140] presented the erosion due to raindrops in a theoretical equation. In SHESED, overland flow and sediment transportation are based on the equation of conservation of mass in two dimensions. In this model, gulley erosion, mass movement, channel bank erosion, and erosion in frozen soil are not considered.

13.3.27 EGEM Model

There are a few models to estimate gulley erosion (e.g., WEPP and CREAMS). The EGEM model is created specially to estimate soil loss by gulley erosion. EGEM has a suitable potential for estimation of gulley erosion. Considering the importance of gulley erosion, only some physical models are developed for its estimation.

EGEM contains two components: hydrology and erosion. The model calculates gulley erosion in annual average or single storm. Using EGEM, the length and width of gulley can be measured. Some input parameters include drainage area, slope percentage of basin, curve number, soil class, erosion potential factor, critical shearstress, maximum depth of gulley, bulk density, particle diameter, rainfall distribution, 24-year rain depth, and plow practices [165].

13.3.28 EPIC Model

EPIC is a simulative model studying long period effects of various components of soil erosion on crop yield [162].

EPIC is a general model and soil erosion impact on yield in 66 different countries in Asia, South America, and Europe is investigated by using this model. This model has several components such as soil erosion, economic component, hydrologic component, climate, nutrition, growth, and crop management.

This model needs GIS layer of GRASS including information for series of soil and climate. This information should be in a text file. Recently, there have been many management files for EPIC. The model provides output on crop yields, economics of fertilizer use, and crop values.

13.3.29 EROSION 2D/3D Model

The EROSION 2D/3D is a model calculating runoff due to soil erosion and sediment in one slope (2D) and small watersheds (3D).

The model is developed to predict soil erosion and also to program of conservation and evaluation. Considering the user need, the model calculates runoff production, the amount of particles separated due to rain and runoff, transportation of separated particles by runoff, and the direction of runoff and sediment using basin and sediment process.

Input data of the model could be divided to three main groups: parameters of topography, surface soil, and rainfall including

- Topography parameters: Digital Elevation Model (DEM)
- Parameters of surface soil: texture, bulk density, organic matter content, initial moisture of soil, manning's roughness coefficient, resistance to erosion, canopy cover, infiltration correction factor
- Precipitation parameters: rainfall intensity and duration

Output data contains

- Runoff, sediment discharge, grain size distribution of the transported sediment, net erosion

13.3.30 MOSES Model

MOSES is a tool for estimating wind and water erosion and was designed by the NRCS personnel of the United States in October 2000. MOSES progressively utilizes universal revision equation of soil loss (RUSLE 2) and wind erosion prediction system (WEPS) and estimates wind and water erosions.

13.3.31 PESERA Model

The PESERA model has a physical base [89], and using a model with a spatial distributed base, it predicts quantifying soil erosion throughout Europe. Also using this model, tillage and wind erosion could be predicted. This model as a diagnostic tool is a replacement for existing methods such as the universal equation of soil erosion (USLE), which was hardly suitable for Europe situations.

Input data of the model includes topography, climate, soil, and land covering data.

13.3.32 WATEM Model

WATEM is a spatially distributed model presented to estimate erosion and sediment due to water and tillage practices in two dimensions. In spite of many dynamic complicated models (such as WEPP or EUROSEM), the WATEM model concentrates on local variables and barely on time variables. To avoid the main difficulties related to values and the spatial values and uncertainty in parameters estimation, WATEM is an easy topography-based model.

Water components in this model are achieved from the universal revision equation (RUSLE). Tillage components use an emission equation to describe tillage processes (tillage p coefficient or *ktil*-value).

WATEM could be used in prediction of water erosion, soil erosion due to tillage, and determining agricultural regions having erosion potential.

13.3.33 CAESAR Model

CAESAR is a two-dimensional sediment transportation model. This model can simulate morphological changes in basins during a multithousand year period. CAESAR is one of the Cellular Fluvial models named for reduced complexity too.

Cellar characteristics of CAESAR model include elevation, water discharge depth, land covering, depth of bedrock, and particles size. CAESAR uses hourly rainfall data as hydrological model input [14].

13.3.34 G2 Model

G2 is a new empirical model in erosion estimation and is designed with the cooperation of JRC/IES and Aristotle University in Europe. G2 predicts soil loss (ton/ha) utilizing monthly calculation of rill and interill erosions in landscape scale.

G2 uses standardized input data, universal and European databases such as Europe Soil Database (ESDB), topsoil organic carbon (TOC), and satellite images of SPOT and ASTER as DEM. This makes 1:500,000 scale (MMU = 10 ha) usable throughout Europe. G2 uses the USLE model and needs calibration for erosion potential due to rain. This model calculates rill and interill erosion. The advantages of this model are its simplicity and needing less data.

13.3.35 SLEMSA Model

This model was presented for the southern regions of Africa by Elwell and Stoking in 1982 [41]. In fact, it is a correction on the USLE model to adjust it for agro-climatic conditions of southern Africa. This model is proposed for countries having a severe need for conservational actions but do not have financial and research facilities.

This model is used for prediction of annual average erosion of surface soil on the lands with agriculture potential between two contour lines. The SLEMSA model, in addition to combining main and simple data together, emphasizes some environment relationships specially land covering, rainfall, and erodibility.

13.3.36 BLM Model

This method was designed by the land management office of the United States and is based on evaluation of seven factors:

1. Soil movement (by wind, water, gravity force, etc.)
2. Existence of crop residue cover in soil surface
3. Conditions of stones (mainly in distribution aspect)
4. Firm stone particles
5. Existence of rill erosion
6. Channel form
7. Existence of gulley erosion

Although the evaluation is quantitative in this method, final results are presented qualitatively. Therefore, the BLM model is a qualitative way to assess soil erosion conditions.

13.3.37 EPM Model

This method by using erosion plats information and sediment measurement during 40 years of experiment in Yugoslavia was designed and as the first time, was presented by Gavrilovic [47] through an

international conference of river regime (1988). Utilizing this model, in addition of erosion severity estimation, sediment transportation in rivers could be estimated and also has appropriate application in rivers not having hydrometrics and sedimentary data.

Generally, the EPM method is used for the prediction of three parameters:

1. Erosion severity and net erosion
2. Sediment potential coefficient
3. Net sediment discharge and total sediment discharge

13.3.38 FAO Model

In this model, soil erosion estimation is based on investigation and evaluation of six effective factors on soil erosion and sediment yield in basin. The relationship between soil erosion and effective factors is as follows:

$$S = f\left(A,B,C,D,E,F\right) \tag{13.3}$$

where

S is the soil erosion severity
E is the superficial geology
B is the soil
C is the relief and slope
D is the soil covering
A is the land use manner
F is the current condition of erosion in basin

The presented factors in the FAO model are very similar to the PSIAC model. In fact, A is the surface geology, B the soil, C topography, D soil covering, E land-use manner, and F is the current condition of erosion in the PSIAC method.

Finally, each of these factors is scored according to severity and its effect on soil erosion. The score of each factor is shown in Table 13.2.

After scoring all of the factors in hydrologic units or land units, soil erosion severity is identified using the score's sum and is categorized in six classes. The classification is presented in Table 13.3.

The FAO model is approximately similar to the PSIAC model but PSIAC is more practical and complicated, since it considers nine factors in soil erosion (FAO considers six factors) and it can present quantitative and qualitative descriptions (FAO method presents only quantitative description).

TABLE 13.2 Quality Evaluation of FAO Soil Erosion Model

Factor	Erosion Severity Score
Geology	1–18
Soil	1–16
Relief and slope	1–16
Soil covering	1–20
Land use	0–15
Current condition of erosion	0–15
Total	4–100

TABLE 13.3 Soil Erosion Class and Soil Conservation in the FAO Model

Erosion Class	Score	Modification Practice
I	0–8	Current activities are acceptable.
II	9–20	Reconsideration in land management way with some modification practices.
III	21–40	Reconsideration in land management way should be added to modification practices.
IV	41–65	Widespread and comprehensive changes in land management, general application of modification practices, and construction.
V	66–85	Comprehensive activities in land limitation field, ownership estimation, widespread construction activities.
VI	+86	Restriction in land ownership and maximum modification practices.

13.3.39 PSIAC and MPSIAC Models

This model was presented to predict soil erosion in the basins without stations of sediment measurement in arid and semiarid regions in 1968. In this model, nine different factors are considered for sediment calculation. The factors include the following:

1. Surface geology
2. Soil
3. Climate
4. Runoff
5. Relief
6. Soil covering
7. Land use
8. Upland erosion
9. River bank erosion

Each of these factors has a specific limit of impact score. Finally, the number achieved from adding the nine factors identifies sediment yield degree for that sub-basin. Net sediment and net erosion could be calculated according to the degree. For this reason, in 1982, the model was reconsidered and one formula was regarded for each of the nine factors so that the calculated values would be close to real ones.

13.3.40 HEM Model

HEM is a limitative and distributional model in thunderstorm scale in arid and semiarid pastures presented in the US basin research center by Lane et al. [80]. The model is applied based on the mathematical relationship among sediment and runoff volume, slope characteristics, and soil erosion potential factor. This model estimates erosion and sediment yield in a specific slope and in the scale of a thunderstorm.

HEM is based on a solution of kinematic wave equations for continuous equations of surface flow and runoff in a slope profile and for one runoff event. The model evaluates rill erosion, interill erosion, and sediment transportation and deposition processes. Input information includes runoff volume in area unit (mm), soil texture, and basin characteristics, including slope in percentage, slope length in meter, land covering percentage, and ground covering percentage.

HEM application studies are limited in the world and need specific conditions to use. Cogle et al. [26] evaluated HEM efficiency in India, Australia, and New Zealand. Conclusion of studies showed that this model does not need calibration in New Zealand region and presents suitable estimation in 15.6% slope with the model proposed amount for soil erosion potential. However, the erodibility volume in India and Australia was calibrated to improve model estimations.

Sadeghi et al. [121] in Iran evaluated HEM model efficiency only in pasturage plats with 9% slope in the Khasbian region, Arak province. For this reason, data related to 11 thunderstorm events was used.

The researchers indicated that there is a significant difference between observed and predicted values without calibration, and these two values are close when soil erosion potential factor is calibrated.

They also studied different kinds of regression in normal situations and changed data, and introduced significant relationship between observed and predicted values with calibrated soil erosion potential factor (equivalent 1.1) using fourth-degree polynomial relationship.

13.3.41 Fournier Model

Fournier presented two different methods to predict sediment in a basin:

The first Fournier's method for estimation of sediment in a basin is as follows:

$$\log Q_S = 2.65 \log\left(\frac{P_w^2}{P_a}\right) + 0.46 \log h\left(\tan S\right) - 1.56 \tag{13.4}$$

where

Q_S is the net sediment (ton/km^2/year)
P_w is the average rainfall in a month of a year having the most rain depth (mm)
P_a is the annual average rainfall (mm)
h is the average elevation of basin (m)
S is the average slope (degree) (average slope percentage of basin could be used instead of tan S)

The second Fournier's method to predict sediment in a basin is as follows:

$$\log Q_S = 2.65 \log\left(\frac{P_w}{P_a}\right) + 0.46 \log\left(\frac{H^2}{S}\right) - 1.56 \tag{13.5}$$

All these factors are the same in the previous formula except S, which indicates basin area in km^2.

The Fournier method does not consider the erosion potential of a basin. Therefore, if two regions have similar factors in the formula but are different in conditions of geology, soil science, and land covering, sediment amounts will be evaluated similarly.

Fournier and Douglas models approximately predict erosion in the same way, and both of them make a relationship between some parameters and erosion amount to estimate erosion. Using these models however facilitates estimation; because of the simplicity and low numbers of parameters, the results are severely narrow and could be used in specific regions, because the selective parameters do not have high importance, variation, and impact.

13.3.42 Musgrave Model

Musgrave [106], studying and measuring erosion due to 40,000 thunderstorms in the United States, presented a formula to estimate sheet erosion severity as follows:

$$E = I \cdot R \cdot S^{1.35} \cdot L^{0.35} \cdot P_{30}^{1.73} \tag{13.6}$$

where

E is the soil erosion (in./ac)
I is the soil erosion potential (in.)
R is the soil covering factor
S is the slope (%)
L is the slope length of basin (ft)
P_{30} is the maximum 30 min rain in 2 years (in.)

13.3.43 PEPP Model

PEPP was developed by Schramm [125] and Gerlinger [48]. In this model, runoff, erosion, and sediment for rill and sheet erosions are calculated. This model can also predict Phosphorous loss amounts. For surface runoff modeling, moving wave method is considered in unsteady flow processes. To solve movement equation, Particle loss energy is calculated by Manning–Strickler formula. Input data include slope, climate, and soil data.

13.3.44 SHE Model

SHE is a spatial hydrologic model developed by Britain Hydrology Institute, Denmark Hydrologic Institute, and France SOGREAH [2,3]. Using basins of orthogonal network, the spatial distribution is achieved.

13.3.45 MULTSED Model

MULTSED was developed in Colorado University in the late 1970s [84]. From that time, some changes have been made [129]. Sediment transportation capacity for bed load and suspended load was calculated, respectively, by Meyer-Peter and Müller [93] and Einstein [40].

13.3.46 OPUS Model

OPUS [132,133] by using CREAMS [74] was developed to simulate single-event and multievent runoff and the processes of water flow and nutrition movement. All hydraulic processes of soil are calculated in one dimension and vertically. In surface soil, such processes as runoff and surface erosion are calculated in one dimension and the slope direction. As a result, the soil surface is divided into several sections and erosion rate is calculated for each of them.

OPUS is a computer model for materials transportation in surface soil and water in a small basin. This model is a simulative tool for pollution studies. OPUS simulates water movement using rainfall, crop, topography data, and other management activities of water use. The model contains such models as plant growth; water use; nutrition; cycle of nitrogen, phosphorous, and carbon in soil; and transportation of absorbed pesticides, runoff, and erosion.

13.3.47 ACRU Model

Initial studies of the ACRU model were done in 1970 by using hydrological basins relying on evapotranspiration in Natal Drakensberg [126]. Input data of this model include daily rainfall, daily or monthly evaporation, and soils and land-use parameters. The output includes simulated streamflows, sediment and crop yield, and reservoir yield analysis.

13.3.48 Hydro-Physical Model

Hydro-physical model is utilized to recognize relative sediment yield of hydrological units or different sub-basins of a basin. The base of this method is comparing hydrophysical conditions of hydrological units or various sub-basins of a basin and its relationship with sediment yield potential in basin regions.

In this model, first of all comparative sediment yield (CSY) is calculated for all hydrological units or sub-basins. Then using the results, sediment yield percentage of each hydrologic unit in proportion to sediment yield potential of total basin is calculated. Relative coefficient of sediment yield is also calculated as follows:

$$\mathrm{CSY} = a\left(R \cdot E \cdot V \cdot P\right) \tag{13.7}$$

where
- a is the area factor
- R is the topography or slope factor
- E is the erosion potential factor
- P is the annual average rainfall (mm)

After CSY calculation in each hydrologic unit or sub-basin, the sum or total CSY of basin is achieved. Therefore, sediment yield percentage of each hydrologic unit in proportion to sediment yield potential of total basin could be calculated as Equation 13.8:

$$\mathrm{SY} = \frac{\mathrm{CSY\,hydrologic\,unit}}{\mathrm{Total\,basins\,CSY}} \times 100 \tag{13.8}$$

In general, use of the hydro-physical model just estimates the sediment yield percentage of each hydrologic unit in proportion to the sediment yield potential of the total basin. So the sediment amount cannot be estimated.

13.3.49 Scalogram Model

This model is designed for basins that do not have data and necessary parameters to predict basin erosion situations including land slope, bed stone kind, texture and structure of soil, land covering (plant, residual plant cover, and stone), human management, and existing erosion.

Using this model, erosion potential could be evaluated as a number related to erosion factors. The impacts of different factors of erosion potential in each region could also be evaluated with the use of the scalogram model.

13.3.50 Carson and Kirkby Model

Empirical and simple method to estimate basin sediment uses annual runoff and slope conditions of the basin and Equation 13.9:

$$Q_S = 0.017 Q_w^z \tan\theta \tag{13.9}$$

where
- Q_S is the annual net sediment (kg/m^2)
- Q_w is the annual runoff depth (m)
- θ the slope degree
- z the region coefficient

13.3.51 AL-Kadhimi Model

The AL-kadhimi model connects soil erosion index with the sediment yield in a basin. This index is identified by five factors of rainfall erosion (R) (Fournier factor), soil erosion potential (St), slope (Sl), covering type (C), and soil disassembling due to plow and furrow (D).

Each of the factors has five classes and a limit of scores. Soil erosion potential index is calculated by multiplying the five factors, and if this index were increased, soil erosion would be increased too.

13.3.52 Stehlik Model

Stehlik [138] was investigated in Czechoslovakia and is used for prediction of annual soil erosion:

$$X = D{\cdot}G{\cdot}P\ S\ L\ O \tag{13.10}$$

where
- X is the annual average of soil loss (mm/year)
- D is the climate coefficient
- G is the soil texture and permeability coefficient
- P is the soil erodibility coefficient
- S is the slope coefficient
- L is the slope length coefficient
- O is the land covering coefficient

The Stehlik model is sensitive on land slope degree, and rainfall coefficient and soil erosion potential are respectively more and less important for it. Therefore, this method is mostly useful for agricultural regions with a finite area.

13.3.53 Douglas Model

The Douglas model [38] was designed in Queensland, Australia. In this model, such factors as soil moisture, basin morphology, petrology, and ground surface roughness are considered. Equation 13.11 explains the Douglas model:

$$\log SS = -0.873 + 3.81\log Q_w - 1.54\log\left(\frac{R}{L}\right) + 4.821\log dd \tag{13.11}$$

where
- SS is the sediment yield (ton/km^2/year)
- Q_w is the annual runoff depth (m)
- R/L is the height to length of basin (ft/mile)
- dd is the drainage network density (ft/mile^2)

The second equation is as follows:

$$\log E = -0.841 - 2.704\log\left(\frac{q^2}{P}\right) + 5.6R_n + 2.967\log D_n \tag{13.12}$$

where
- E is the specific sediment amount (ton/km^2/year)
- q is the average rainfall in the most humid month of year (mm)
- R_n is the junction coefficient (junction ratio) in each sub-basin
- D_n is the channel density of each sub-basin (km/km^2)
- P is the annual rainfall (mm)

13.3.54 Morgan, Morgan, and Finney Model

Morgan et al. [104] proposed a model that could be used for prediction of soil loss in the slopes or farmlands. In this manner, in addition of soil erosion universal equation simplicity, new concepts are used achieved from the model.

In this model, results of geomorphology and agriculture engineering studies are utilized, and the erosion process is divided into two phases, water phase and sediment phase. To use it, 15 parameters and 6 equations are necessary. The sediment phase is the same simple scheme of Meyer and Wischmeier [94] in which soil particle separation due to raindrops or water movement is disregarded.

Therefore, two equations in sediment phase are used including particles separation because of rain and the other equation, transportation capacity of surface flow. The required data in these equations, including rain energy and runoff volume, form water phase as the first phase.

13.3.55 SHETRAN Model

SHETRAN [9,158] is a physically based model with spatial distribution. Erosion and sediment yield of the existing European distributed hydrological modeling system (SHE) is usable for catchment scale. For hill slopes represented spatially by the SHE grid square network, SHETRAN models soil erosion by effects of raindrop, leaf drip, and sheet overland flow (disregarding rilling) and also models transported materials by overland flow. In the channels, it is assumed that the flow can carry any load of fine sediments (the diameter less than 0.062 mm) but will happen for coarser load sediments (limitation) [7].

13.3.56 AGWA Model

AGWA is a versatile hydrologic analysis model that it has been used in watershed, water resource, land use, and biological resource management for the studies in watershed and basin scales. AGWA is in relation with GIS, which is jointly developed by the US Environmental Protection Agency, USDA, and the University of Arizona, and it takes advantage of SWAT and KINEROS2 to estimate runoff, sediment yield, and additional nitrogen and phosphorus in different temporal and spatial scales. The minimum data requirement in AGWA is digital elevation models (DEMs), land cover grids, soil data, and precipitation. AGWA is has been developed to be as an extension of the ESRI Institute's software including ArcView versions 3.x and the software package of geographic information system (GIS).

13.3.57 USPED Model

USPED [99] is a simple model that estimates rates of spatial distribution of erosion and deposition for a steady-state overland flow. The model works based on the concept proposed by Moore and Burch [101] with lots of improvements. The USPED model is an empirical model to identify erosion and deposition areas in catchment scale. Recent estimations have showed that the USPED model with the new high-resolution DEM (2 m grid) can successfully identify erosion-prone hotspots in catchments. These locations were similar to those spots that farmers observed.

13.3.58 THORNES Model

Erosion models must organize energy (overland flow and slope), resistance (soil erodibility), and protection (plant covering) together in a physical and simple way. After checking the competition between vegetation growth and soil erosion capability, Thornes [144,145] presented a conceptual erosion model by combining sediment transportation and soil cover. This model includes hydrological parts based on a storage type analogy, sediment transportation component, and plant growth component [146]. When Kirkby et al. modeled the competitive behavior of plant covering and erosion, they indicated that by increasing plant covering, erosion will be decreased exponentially [71].

13.3.59 SPL Model

SPL has been designed for fluvial erosion while erosion is in proportion to the river slope and discharge. From a geological perspective, a change in discharge rate leads to a change in river slope to achieve

equilibrium between uplift and erosion. The model predicts the erosion rate of river bed by using empirical equations.

This model combines equations describing conservation of water mass and momentum in streams with relations for channel hydraulic geometry (width-discharge scaling) and basin hydrology (discharge-area scaling) and an assumed dependency of erosion rate on either unit stream power or shear stress on the bed to produce a simplified description of erosion rate as a function of power laws of upstream drainage area (A), and channel slope (S):

$$E = K \cdot A^m \cdot S^n \tag{13.13}$$

where

E is the erosion rate

K, m, and n are positive [159]

The value of these parameters depends on the assumptions made, but all forms of the law can be expressed in this basic form.

The parameters K, m, and n are not necessarily constant, but rather they may vary as functions of the assumed scaling laws, erosion process, bedrock erodibility, climate, sediment flux and/or erosion threshold. However, observations of the hydraulic scaling of real rivers believed to be in erosional steady state indicate that the ratio m/n should be around 0.5, which provides a basic test of the applicability of each formulation [160].

Although consisting of the product of two power laws, note that the term *stream power law* refers to the derivation of the early forms of the equation from assumptions of erosion dependency on stream power, rather than to the presence of power laws in the equation. Note also that this relation is not a true scientific law, but rather a heuristic description of erosion processes based on previously observed scaling relations that may or may not be applicable in any given natural setting.

13.3.60 SWRRB and SWAT Models

SWRRB was developed by Williams et al. [163]. The aim of this model is to estimate the impact of various management manners on runoff and sediment productions in rural basins without measuring stations. The main process in this model includes surface runoff, deep-seated flow, sub-surface flow, evapotranspiration, surface storage, deposition, and agricultural covering. This model contains three sections of hydrology, climate, and sediment.

The SWRRB model was only applicable for the basins with hundreds of square kilometers of area and could divided only to 10 sub-basins. This limitation causes that a model namely ROTO is developed. ROTO maintains the output from several runs of SWRRB and then finds the flow trend in canals and reservoirs. By connecting ROTO and SWRRB in each run, the dividing difficulty of the SWRRB model is solved.

Though this continuity was effective, input and output files of the SWRRB model were massive. All SWRRB runs are run individually and then input files for ROTO model should be prepared. To solve this problem, in the early 1990s SWRRB and ROTO models were united in a model named SWAT. SWAT models were studied and developed regularly. Different versions of this model up to now include SWAT94.2, SWAT96.2, SWAT98.1, SWAT99.2, SWAT2000, SWAT2005, and SWAT2009.

SWAT is a comprehensive model in basin scale presented by the Agricultural Research Service of the United States to predict impacts of different management methods on flow, sediment, nutrients, and chemical materials balance in the basins with various soil, land uses, and management conditions for long time periods. The characteristics of this model are as follows:

SWAT is a continuous model with high calculative efficiency.

The model is sensitive to changes of management, climate, and plant covering and is able to predict effects of these changes on parameters such as water movement, sediment, and nutrients transportation.

The model is an effective calculator used to simulate big basins without the need for time and high investment.

Long period data are modeled and are not designed for single-event simulation in detail.

Since SWAT is a continuous model and also contains different processes including climate, hydrology, nutrients, pesticides, erosion, plant covering, management manners, and finding flow trend, it seems an appropriate tool in basin scale.

13.4 Computational Models

Evolution of the river bed in alluvial channels has been studied by many researchers using analytical and numerical approaches. Using just the analytical approach is insufficient for solving natural river engineering problems. Some of the simplified assumptions are based on idealized laboratory conditions that may not be suitable for the much more complicated natural river systems. With the rapid growth in computer technology, numerical models have become popular tools for the study of mobile bed hydraulics. The major part of this section derived from the international hydrological program of UNESCO also provides a basic description of different types and also theoretical concepts used in the development of sediment transport computer models.

Sediment transport computer models differ greatly in their characteristics based on their basic concepts. The computational models are divided into many different categories based on their dimension, width, and many other factors that have been considered. Sediment routing models can also be classified as steady or unsteady, coupled or uncoupled, equilibrium or nonequilibrium, and uniform or nonuniform sediment models. Concise descriptions of some model categories are presented in Table 13.4.

13.4.1 Three-Dimensional Model

Flow process in rivers is three dimensional in reality, especially those at or near a meander bend local expansion and contraction, or a hydraulic structure. Many different numerical schemes have been developed to solve accurately three-dimensional flow phenomena. Three-dimensional models need three-dimensional experimental data for testing and calibration. The collection of such data is not only costly but also time consuming. Certain assumptions need to be made before a sediment transport formula developed for one-dimensional flows can be applied to a truly three-dimensional model. With the exception of detailed simulation of flow in an estuary area, secondary current, or flow near a hydraulic structure, three-dimensional models are seldom used, and particularly not for long-term simulations. GSTARS and HEC2SR are two examples of semi-3D simulation models.

13.4.2 Two-Dimensional Model

Two-dimensional models can be categorized into two-dimensional vertically averaged and two-dimensional horizontally averaged models. The former scheme is used where depth-averaged velocity or other hydraulic parameters can adequately describe the variation of hydraulic conditions across a channel. The latter scheme is used where width- or length-averaged hydraulic parameters can adequately describe the variation of hydraulic conditions in the vertical direction. Most two-dimensional sediment transport models are depth-averaged models. The width- or length-averaged two-dimensional models are usually used for modeling helically flows.

TABLE 13.4 Descriptions of Some Computational Model Categories

Model Acronym	Type	Reference	Model Name Description
HEC6	Computational 1D	Thomas and Prashum [143]	Hydraulic Engineering Center
MOBED	Computational 1D	Krishnappan [75]	MObile BED
IALLUVIAL	Computational 1D	Karim and Kennedy [67]	Iowa ALLUVIAL
FULUVIAL 11	Computational 1D	Chang [21]	No acronym
GSTARS	Computational 1D	Molinas and Yang [100]	Generalized sediment transport models for alluvial River simulation
CHARIMA	Computational 1D	Holly et al. [59]	Acronym of the word CHARiage, which means bedload in French
SEDICOUP	Computational 1D	Holly and Rahuel [57]	SEDIment COUPled
OTIS	Computational 1D	Runkel and Broshears [120]	One-dimensional transport with inflow and storage
EFDCID	Computational 1D	Hamrick [52]	Environmental fluid dynamics code
3STD1	Computational 1D	Papanicolaou et al. [112]	Steep stream sediment Transport 1D model
SERATRA	Computational 2D	Onishi and Wise [109]	SEdiment and RAdionuclide TRAnsport
SUTRENCH- 2D	Computational 2D	van Rijn and Tan [150]	Suspended sediment transport in TRENCHes
TABS-2	Computational 2D	Thomas and McAnally [142]	No acronym
MOBED2	Computational 2D	Spasojevic and Holly [136]	MObile BED
ADCIRC	Computational 2D	Luettich et al. [91]	ADvanced CIRCulation
MIKE 21	Computational 2D	Danish Hydraulic Institute [30]	Danish acronym of the word microcomputer
UNIBEST-TC	Computational 2D	Bosboom et al. [18]	UNIform Beach Sediment Transport–Transport Cross-shore
USTARS	Computational 2D	Lee et al. [82]	Unsteady Sediment Transport models for Alluvial Rivers Simulations
FAST2D	Computational 2D	Minh Duc et al. [95]	Flow Analysis Simulation Tool
FLUVIAL 12	Computational 2D	Chang [2]	No acronym
Delft 2D	Computational 2D	Walstra et al. [153]	No acronym
CCHE2D	Computational 2D	Jia and Wang [64]	The National Center for Computational Hydroscience and Engineering
ECOMSED	Computational 3D	Blumberg and Mellor [1]	Estuarine, Coastal, and Ocean Model-SEDiment transport
RMA-10	Computational 3D	King [69]	Resource Management Associates
GBTOXe	Computational 3D	Bierman et al. [1]	Green Bay TOXic enhancement
EFDC3D	Computational 3D	Hamrick [51]	Environmental Fluid Dynamics code
ROMS	Computational 3D	Song and Haidvogel [135]	Regional Ocean Modeling System
CH3D-SED	Computational 3D	Spasojevic and Holly [137]	Computational Hydraulics 3D-SEDiment
SSIIM	Computational 3D	Olsen [108]	Sediment Simulation In Intakes with Multiblock options
MIKE 3	Computational 3D	Jacobsen and Rasmussen [60]	Danish acronym of the word Microcomputer
FAST3D	Computational 3D	Landsberg et al. [79]	Flow Analysis Simulation Tool
DELFT-3D	Computational 3D	Delft Hydraulics [31]	No acronym
TELEMAC	Computational 3D	Hervouet and Bates [5], Zeng et al. [176]	No acronym

13.4.3 One-Dimensional Model

Most sediment transport models are one-dimensional, especially those models used for long-term simulation of a long river reach. One-dimensional models require the minimum amount of field data for calibration and validation. The numerical solutions are more stable and require the least amount of

computer time and capacity. However, one-dimensional models are not suitable for simulating truly two- or three-dimensional local phenomena.

13.4.4 Semi-Two-Dimensional Model

The one-dimensional models cannot simulate the lateral variation of hydraulic and sediment conditions at a given river station. Engineers often take advantage of the nonuniform hydraulic and sediment conditions across a channel in their hydraulic design. There are three types of semi-two-dimensional models. For instance STARS [139], GSTARS [209], FLUVIAL-12 [22,23], and HEC2SR [83] are the models that use the semi-two-dimensional concept in their simulation.

13.4.5 Composite Model

A composite model adds lateral movement of water and sediment on a one-dimensional model. The knowledge of variation of shear stress, or other parameters, is often required in the development of a composite model. For example, Song et al. [134] superimposed the lateral sediment transport across GSTARS [100] stream tubes due to secondary current and lateral shear stress. This composite model enabled them to more accurately simulate sediment transport near a meandering bend.

13.4.6 Strip Model

A strip model divides a channel into longitudinal strips of equal width or nonuniform width. Many modelers consider the main channel as the center strip and represent the flood plain as the left and right strips. There is no lateral variation of hydraulic and sediment parameters within each strip. Diffusion equations govern the movement of water and sediment between strips. Many modelers assume that the diffusion coefficient is a constant in a diffusion equation. In reality, the diffusion coefficient varies with changing channel geometry, which is part of the unknown a computer model is trying to predict. Consequently, from a theoretical point of view, predicting the variation of the diffusion coefficient is difficult and may be impossible.

13.4.7 Stream Tube Model

Stream tubes are conceptual tubes whose walls are defined by streamlines. A streamline is a conceptual line to which the velocity vector of the fluid is tangent at each and every point, at each instant in time. A study reach is divided into stream tubes of equal discharge based on equal conveyance. Water and sediment cannot cross the boundary of stream tubes.

Consequently, there is no need for solving diffusion equations, and the difficulties of determining diffusion coefficients can be avoided. The velocity and sediment concentration distributions in a stream tube are assumed to be uniform across the tube. However, because the stream tube width and location can change with respect to time across a given station, water and sediment can move with stream tubes implicitly across a channel. Yotsukura and Sayre [172] combined the stream function with transverse diffusivity to explain the movement of tracer in a natural channel.

13.4.8 Fixed- and Variable-Width Model

13.4.8.1 Fixed-Width Model

Open-channel hydraulic problems can be solved only if the channel width is fixed or can be assumed. With the exception of empirical relationships, conventional open-channel hydraulics cannot provide theoretical solutions for the determination of channel width. Consequently, most sediment transport

models assume that the channel width is given and would not adjust with changing flow and sediment conditions. This assumption can cause significant errors in the prediction of variation of channel geometry and profile, especially for alluvial rivers, where the width change may be more significant than the depth change during a flood.

13.4.8.2 Variable-Width Model

The concept of threshold tractive force on channel perimeter and the theory of minimum energy dissipation rate [170] or its simplified minimum stream power theory [171] can be used as a theoretical basis for the determination of optimum channel geometry and width.

13.4.9 Computer Model Classification

Sediment routing models can be classified as steady or unsteady, coupled or uncoupled, equilibrium or nonequilibrium, and uniform or nonuniform sediment models.

13.4.10 Steady or Unsteady Model

If the flow and sediment conditions in a model vary over time, it is an unsteady model. Otherwise, it is a steady model. Strictly speaking, flow and sediment conditions in most natural rivers are unsteady due to the changing hydrologic conditions over time. However, a hydrograph may be approximated by a series of constant discharge bursts, and the steady flow techniques can be used for these quasi-steady-flow computations. The basic governing equations for a one-dimensional unsteady flow are as follows:

Water continuity equation

$$\frac{\partial A}{\partial t}+\frac{\partial Q}{\partial x}+p_s\frac{\partial A_s}{\partial t}-q_l=0 \tag{13.14}$$

Water momentum equation

$$\frac{\partial\left(\rho Q^2\right)}{\partial t}+\frac{\partial}{\partial x}\left(\rho\frac{Q^2}{A}\right)+g\rho A\frac{\partial z}{\partial x}-\rho gAS_f=0 \tag{13.15}$$

Sediment continuity equation

$$\frac{\partial\left(C_vA\right)}{\partial t}+\left(1-p_s\right)\frac{\partial A_s}{\partial t}+\frac{\partial Q_s}{\partial x}+C_lq_l=0 \tag{13.16}$$

where

A is the cross-sectional area of flow
A_s is the cross-sectional area of river bed
C_v is the suspended load concentration by volume
C_l is the concentration of lateral flow by volume
g is the gravitational acceleration
p_s is the bed sediment porosity
Q is the water discharge
Q_s is the volumetric total sediment discharge
q_l is the lateral inflow per unit length x
S_f is the energy or friction slope

t is the time
x is the distance along the channel
z is the water surface elevation
ρ is the density of water

For steady flow, Equations 13.16 through 13.18 can be reduced to

$$\frac{\partial Q}{\partial x} - q_l = 0 \tag{13.17}$$

$$\frac{\partial}{\partial x}\left(\frac{Q^2}{A}\right) + gA\frac{\partial z}{\partial x} + gAS_f = 0 \tag{13.18}$$

$$\left(1 - p_s\right)\frac{\partial A_s}{\partial t} + \frac{\partial Q_s}{\partial x} + C_l q_l = 0 \tag{13.19}$$

The friction or energy slope S_f is related to sediment particle size, flow discharge, sediment load or concentration, bed forms, channel geometry and pattern, growth of vegetation, and so on. Strictly speaking, S_f should be treated as an unknown variable. In practice, S_f is treated as a constant and is computed from a resistance function such as the Manning, Chezy, or the Darcy–Weisbach's formula, that is,

$$S_f = \frac{Q|Q|}{K^2} \tag{13.20}$$

$$K = \sum_{j=1}^{m} K_j \tag{13.21}$$

$$K_j = \frac{1}{n_j} A_j R_j^{2/3} \tag{13.22}$$

where
K is the total conveyance
K_j is the conveyance of subsection j
A_j is the cross sectional area of subsection j
R_j is the hydraulic radius of subsection j
n_j is the Manning's roughness coefficient of subsection j
m is the total number of sections

If the English unit is used, 1 should be replaced by 1.486 in Equation 13.24. CHARIMA [58], SEDICOUP [56], and FLUVIAL-12 can be presented as nonsteady models.

13.4.11 Coupled or Uncoupled Model

A coupled model solves the water continuity equation, water momentum equation, and sediment continuity equation simultaneously. If the change of A_s in Equations 13.14 and 13.16 within a short period of time is much smaller than the change of cross-sectional area A, the solution can be uncoupled by

solving the water continuity and momentum equations first. The solutions thus obtained are then used to solve the sediment continuity equation. Uncoupled models solve the water and sediment routings separately to simplify the numerical solution. Generally speaking, a coupled model is more stable than an uncoupled model. The stability of uncoupled and coupled models can be improved by using a smaller time step of computation. SEDICOUP also can be presented as a coupled model.

13.4.12 Equilibrium or Nonequilibrium Model

If we assume that there is an instant exchange of sediments in transportation and those on an alluvial channel bed when and where there is a difference between sediment supply and a river's sediment transport capacity, the model is an equilibrium model. This assumption is valid if sediments are transported mainly as bed load or if the sediments are coarse. The assumption of instantaneous exchange may not be valid for fine sediments, and there is a lag between the time when the imbalance occurs and the time sediments are actually deposited or scoured from the bed. A model that takes this phenomenon into consideration is a nonequilibrium model. Usually, a decay function is used in a nonequilibrium model to reflect the noninstantaneous exchange of sediments.

13.4.13 Uniform or Nonuniform Model

A uniform model applies a representative particle size for sediment routing. A nonuniform model routes sediment by size fraction to more realistically reflect the phenomenon of sediment sorting and the formation and destruction of an armor layer on a river bed.

13.4.14 Numerical Solution

13.4.14.1 Finite-Element and Finite-Difference Methods

Most of the sediment-transport models use the finite-difference method for solving partial differential equations. Martin and McCutcheon [92] and Abbott and Basco [1] presented detailed descriptions of numerical methods commonly used in hydrodynamic computer models. Wu and Molinas [167] described a comprehensive presentation of different techniques, which can be used for solving Equations 13.14 through 13.16. As a general approach the partial derivatives in Equations 13.14, 13.15, and 13.18 should be replaced with quotients of finite differences by using explicit or implicit finite-difference methods. The choice of numerical scheme for a particular situation should be based on its accuracy, stability, and convenience to use. Amein and Fang [5], among others, found that the implicit method is unconditionally stable. This method is also more robust and more accurate than other finite-difference methods when applied to open channel flood routing. The finite-difference method presented by Amein and Fang solves nonlinear algebraic equations by iteration, which is time consuming.

Preissman [113] developed a more efficient implicit finite-difference scheme to approximate a function $f(x, t)$ and its derivatives of Mf/Mx and Mf/Mt at point P by using the following equations:

$$f_p(x,t) \cong \lambda \frac{f_i^{j+1} + f_{i+1}^{j+1}}{2} + (1-\lambda)\frac{f_i^{j} + f_{i+1}^{j}}{2} \tag{13.23}$$

$$\frac{\partial f}{\partial x}\Big|_p \cong \lambda \frac{f_{i+1}^{j+1} - f_i^{j+1}}{\Delta x} + (1-\lambda)\frac{f_{i+1}^{j} - f_i^{j}}{\Delta x} \tag{13.24}$$

$$\frac{\partial f}{\partial x}\Big|_p \cong \frac{1}{2}\left(\frac{f_i^{j+1} - f_i^{j}}{\Delta t} + \frac{f_{i+1}^{j+1} - f_{i+1}^{j}}{\Delta t}\right) \tag{13.25}$$

where

$f_i^j = f(x_i, t^j)$

λ is the $\delta t/\Delta t$

δt is the distance of point P on the time axis for the old time line t^j

Δt is the distance of the time axis between t^j and t^{j+1}

If λ is the 2, the scheme is called center implicit.

If $\lambda = 1$, the scheme is called fully implicit and, on the other hand, if $\lambda = 0$, the scheme is called fully explicit. The scheme that has been proposed by Preissman's finite difference is shown in Figure 13.1. Four commonly used methods of solution are the complete solution, the uncoupled unsteady solution, the known discharge solution, and the uncoupled steady solution. These methods can be categorized into the coupled method of complete solution with known discharge and the uncoupled method of unsteady and steady solutions. The following comments on the advantages and disadvantages of different methods are presented by Wu and Molinas [167]:

1. The coupled method can better account for the continuous interaction between the hydraulic and sediment transport phases.
2. The coupled method can be used with a longer time increment.
3. The formulation of the complete solution of a coupled method is the most elaborate among the four methods.
4. The known-discharge solution is developed solely for sediment routing.
5. The uncoupled method is simpler to formulate than the coupled method.
6. The length of time increment of an uncoupled solution is restricted in that the bed elevation change over one time increment must be small.
7. For a stable channel with mild changes, the uncoupled method should be used for water and sediment routing.
8. Under constant flow conditions, the uncoupled steady method should be used for sediment routing.
9. If the channel is very active, the coupled method is most suitable.
10. The coupled method is desirable for routing both water and sediment.
11. The known discharge solution can be utilized to simulate sediment transients.

13.4.15 Stability and Accuracy

If small numerical truncation and other errors produced at a given time in the numerical procedure do not increase during successive applications of the procedure, the finite-difference procedure would be

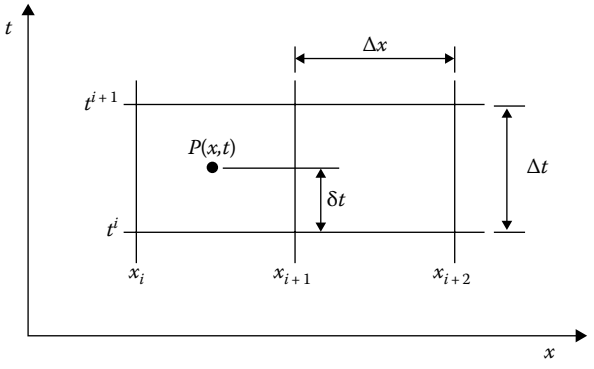

FIGURE 13.1 Representation of Preissman's finite-difference scheme.

stable. Reducing the size of the space and time intervals can improve the stability of a numerical solution. Implicit methods of finite differences are generally unconditionally stable for linear problems. The maximum permitted time step is limited by the required accuracy [46,85]. The stability of an explicit method is governed by the Courant condition $\Delta t \leq \Delta x/C$, where Δx is the distance between x_i and x_1+t; Δt is the time difference between t^j and t^{j+1}; C is the wave celerity $= \sqrt{gy} + V$; y is the water depth; and V is the mean flow velocity. For explicit schemes, the Courant Number should not exceed 1; that is, $C\Delta t/\Delta x$ #1 for stability reasons.

Accuracy is a measure of the disagreement between the computed results and observed values.

The following reasons for possible discrepancies between a mathematical model and the prototype have been presented by Liggett and Cunge [85]:

1. Inaccurate simplification and approximation of the basic equations to simulate a complex prototype.
2. Inaccurate measuring techniques, such as survey errors and badly located gauging stations.
3. Insufficient field data, such as unknown tributary discharges, seepage flow, and so on.
4. Phenomena such as the variations of roughness coefficient with varying bed forms and channel geometry and pattern are not fully understood and their impacts on computed results are ignored.
5. Inaccurate or inadequate schematization of topographic features.

Within the section, it is shown that there exists a variety of different numerical sediment transport models that differ especially concerning steady or unsteady, coupled or uncoupled modeling procedures, side erosion, and automatic width adjustment and especially transport formulae.

13.5 Results and Discussions

As shown in the previous section, the models have a great diversity, which makes it crucial to use the models correctly. At the end of this chapter, attempts have been made to present some of the essential points to answer these two questions: how the models should be used and how the results should be interpreted.

13.5.1 Choosing the Model for Use in Studies

The model's competency for using in studies relies on how the model will be used, the watershed characteristics, required data (such as the count and type of inputs and outputs of the model and their spatial and temporal variability), the and model's validity. Typically, by increasing the accuracy and validity of the models, complexities and requirements of hardware and software would be increased. Meanwhile, the experimental models, because of their simplicity, accuracy, acceptable validity and low-input information, are still considered.

In general, the following should be considered in selecting a model:

1. Model assumptions should be considered.
   For instance if in the model's assumptions, suitable mulch is being into consideration, this assumption should also be considered in the empirical practices.
2. The circumstances in which the model is presented.
   For example, if a model is presented for a humid weather condition, it should not be used in non-wetting weather conditions. Another example, if a model is introduced for small watersheds it shouldn't be used in large watersheds (or vice versa).
3. The requirements of the model must be considered.
   For better understanding, if there is limited input data, a model that fits with these input data should be selected; however, the selected model is less accurate than other models. However, if a

complex model can run with incomplete inputs, the results would be useful. As another example, the model must be selected based on the evaluation, feasibility, cost, and time.

4. The purpose of using the model.
   In particular, if the purpose of study is to estimate the amount of erosion, a model that has been developed for this purpose should be selected; it is wrong to use a model that is not to evaluate the erosion process.

13.5.2 Development and Application of an Erosion Model

The best model of erosion is the model in which the user's feedback is implemented during construction and development. Implementation of a small research model differs with the applications that are used for huge one. But they have a series of cases in common. In general, the following steps should be taken to apply a model.

13.5.2.1 Selecting the Type of the Model

In addition to the model's features, considering the user's needs is one of the most important factors in the creation, development, and application of models. User's needs are important in the creation of the model's output. Most users prefer to use a simple model, with low input requirement, fast and easy to understood, and also accurate enough. The most important decision in using the models is selecting the type and structure of the model. The structure of the models is representative of the equations, inputs, and outputs. Every single model has its own advantageous. A model that is successful in the research field is not useful in huge management practices.

13.5.2.2 Assessment of the Model's Verification

The verification process assures the accuracy of the calculations. Verification ensures users that the equations, parameters, and logics of the model are according to what has been planned. Verification process is carried out through the implementation of the data that the model used.

13.5.2.3 Model Validation

In the validation process, the model ensures that its requirements and targets are maintained with regard to the circumstances and needs of different users. Generally, soil erosion models have an uncertainty of 25%, for average erosion rates 6–60 tons/ha/year. This uncertainty increases 50%, when erosion rates reach more than 100 tons/ac/year. As the main goal of the validation process, the experimental and predicted data should reach the minimum of the error, as far as it is possible. Most of the information that comes from a model has been under research but does not match the conditions of the watershed. The soil erosion models that are being used in the design of large conservation projects often have good accuracy around 1–40 tons/ha/year.

13.5.2.4 Model Assessment

As the first step, before the user wants to apply a model for an area, it should be assessed. The real circumstance is very different from the case studies in which the model is developed. It should be noted that this does not mean that major changes should occur in the model because the new major changes cause new problems, complexity, and additional costs.

13.5.2.5 Sensitivity Analysis

The sensitivity of a model is based on the degree of the output of the model such as soil or sediment loss and how a single unit change of input changes the model's output. The independent variables (a change in one of them will cause drastic changes in the dependent variables or outcomes) are known as sensitive variables. If these critical variables measure accurately, the accuracy of the output will be increased. The model may not be sensitive to a variable in an area, but in another study in a different area the model

may be sensitive to this variable. The loss of soil along a slope would be an example of this relationship. In a region with low slope gradient, the slope may have little effect on erosion, while in the regions with higher slope gradient, this factor can be considered as a sensitive variable.

13.5.3 Evaluation of Erosion Models

For evaluating the performance of the erosion and sedimentation models and assess the degree of validity of each model for a particular region, it is necessary to perform the following three operations on the model's input data:

1. Parameterization
2. Calibration
3. Validation

Parameterization indicates the collecting, measuring, calculating, and correcting of the input data. Calibration process is the basic adjusting of the input parameters. This will be done in order to create the best fit between the model output and the observed value. Since soil characteristics are dynamic and they have time and spatial variations, always the models should be calibrated.

Validation is called evaluation of the models through the factors that have been modified in calibration. In other words, validation is the endpoints of model's assessment process. During this operation, the simulation of future events is determined by the model. In other words, if in the validation stage, simulation is done well by the model, this can be used for future events.

In general, attention should be given to using the model before applying it to an area. After the previously mentioned operations, and achieving satisfying results, the models can be used for the same area or similar areas. The use of the models, mainly associated with the management objectives, means that once a regional model, calibrated and validated, and with satisfying results, in future studies if changes are to be applied in this region (e.g., the dry prairie land into pasture), the model can simulate the effects of these changes and as a consequence, the results would be available to managers and planners.

13.5.4 Selecting the Appropriate Scope of Training and Validation in Simulation

One of the main and disputable issues in the modeling data set is selecting the appropriate range for the model production and intervals for validation of the provided model. Most of the theoretical comments suggest that 70% of data set must be dedicated to the training (model calibration), and 30% may be used for model validation. But there is a knowledge-based approach to make separation between these two series to be used easily to define these ranges. M-test is a test that can be used, to accomplish this separation. M-test by calculating the values of variable Gamma for a given set of observations data provides a chart of Gamma changes. The user can use a descriptive analysis to identify the range of the training and validation. In the presented output graphs of this test, where the Gamma variables get constant, it means that it is the end of the training period and the beginning of the validation period. This test can be performed by using winGamma software.

13.5.5 Simple Performance Models of More Complex Forms of Erosion

One of the problems that the erosion models face is the uncertainty of input parameters. An input parameter might have different values due to a wide range of spatial and time variation in the system. Uncertainty in input parameters can bring these questions into mind, that in the outputs of complex models, which used many input parameters, how much can be trusted. In simple terms, in comparison, what is the efficiency of simplified models with complex types in estimation of soil erosion?

Many efforts have been made in this study area, including the studies by Favis-Mortlock et al. [42]. The study was conducted in a region of the United States, and the output results of different simple models such as CSEP for soil erosion model USLE, EPIC, and GLEAMS and complex process models such as WEPP were compared. The results did not show any significant differences in the efficiency of models for estimating soil erosion. In another study conducted by Morgan and Nearing [103], the performance of USLE, RUSLE, and WEPP models in 1700 natural runoff plots and 208 plots was analyzed. The results suggested that a more sophisticated WEPP model does not provide better results than those of other models that are empirical.

References

1. Abbott, M. and Basco, D. 1989. *Computational Fluid Dynamics: An Introduction for Engineers*. Longman Scientific & Technical, Essex, U.K.
2. Abbott, M.B., Bathurst, J.C., Cunge, J.A., O'Connell, P.E., and Rasmussen, J. 1986. An introduction to the European Hydrological System—Système Hydrologique Européen, "SHE", 1: History and philosophy of a physically-based, distributed modelling system. *Journal of Hydrology* 87:45–59.
3. Abbott, M.B., Bathurst, J.C., Cunge, J.A., O'Connell, P.E., and Rasmussen, J. 1986. An introduction to the European Hydrological System—Système Hydrologique Européen, "SHE", 2: Structure of a physically-based, distributed modelling system. *Journal of Hydrology* 87:61–77.
4. Al Kadhimi, A. 1982. Land use, water yield and soil erosion: Simulation of cause and effect. PhD thesis, Department of Civil Engineering, University of Strathclyde, Glasgow, U.K.
5. Amein, M. and Fang, C.S. 1970. Implicit flood routing in natural channels. *American Society of Civil Engineers Journal of the Hydraulics Division* 96(12):2481–2500.
6. Arnold, J.G., Srinivasan, R., Muttiah, R.S., and Williams, J.R. 1998. Large area hydrologic modeling and assessment Part I: Model development. *Journal of the American Water Resources Association* 34(1):73–89.
7. Banis, Y.N., Bathurst, J.C., and Walling, D.E. 2004. Use of caesium-137 data to evaluate SHETRAN simulated long-term erosion patterns in arable lands. *Hydrological Processes* 18(10):1795–1809.
8. Barnes, J. and Pelletier, J. 2001. *Erosion Mapping of the Bolivian Central Andes Using the Stream Power Law and a Digital Elevation Model*. Department of GeoSciences, University of Arizona, Tucson, AZ.
9. Bathurst, J.C., Wicks, J.M., and O'Connell, J.A. 1995. The SHE/SHESED basin scale water flow and sediment transport modelling system. In *Computer Models of Watershed Hydrology*, V.P. Singh (ed.), pp. 63–94. Water Resource Publication, Highlands Ranch, CO.
10. Beasley, D.B. 1977. ANSWERS: A mathematical model for simulating the effects of land use and management on water quality. PhD thesis, Purdue University, West Lafayette, IN.
11. Beasley, D.B., Huggins, L.F., and Monke, E.J. 1980. ANSWERS: A model for watershed planning. *Transactions of the American Society of Agricultural Engineers* 23:938–944.
12. Bierman, V.J. Jr., DePinto, J.V., Young, T.C., Rodgers, P.W., and Martin, S.C. 1992. Development and validation of an integrated exposure model for toxic chemicals in Green Bay, Lake Michigan. Report for USEPA Large Lakes and Rivers Research Branch, Environmental Research Laboratory, Duluth, MN.
13. Belmans, C., Wesseling, J.G., and Feddes, R.A. 1983. Simulation model of the water balance of a cropped soil: SWATRE. *Journal of Hydrology* 63:271–286.
14. Beven, K.J. and Kirkby, M.J. 1979. A physically based variable contributingarea model of catchment hydrology. *Hydrological Science Bulletin* 24(1):43–69.
15. Biesemans, J., Van Meirvenne, M., and Gabriels, D. 2000. Extending the RUSLE with the Monte Carlo error propagation technique to predict long term average off-site sediment accumulation. *Journal of Soil and Water Conservation* 55(1):35–42.
16. Blumberg, A.F. and Mellor, G.L. 1987. A description of a three-dimensional coastal ocean circulation model. In *Three-Dimensional Coastal Ocean Models*, N. Heaps (ed.), vol. 4, pp. 1–16. Coastal and Estuarine Sciences, American Geophysics Union, Washington, DC.

17. Borah, D.K. 1989. Sediment discharge model for small watersheds. *Transactions of the American Society of Agricultural Engineers* 32(3):874–880.
18. Bosboom, J., Aarninkhof, S.G., Reniers, J.M., Roelvink, J.A., and Walstra, D.J. 1997. UNIBEST TC-2.0 model: Overview of formulations. Report No. H2305-42, Delft Hydraulics, Delft, the Netherlands.
19. Burns, I.S., Scott, S., Levick, L., Hernandez, M., Goodrich, D.C., Miller, S.N., Semmens, D.J., and Kepner, W.G. 2004. Automated Geospatial Watershed Assessment (AGWA)—A GIS-based hydrologic modeling tool: Documentation and user manual version 1.4.
20. Carson, M.A. and Kirkby, M.J. 1972. *Hillslope Form and Process*. Cambridge University Press, Cambridge, U.K., 475pp.
21. Chang, H.H. 1984. Modeling of river channel changes. *Journal of Hydraulic Engineering* 110(2): 157–172.
22. Chang, H.H. 1988. Introduction to Fluvial-12 mathematical model for erodible channels. In: *Twelve Selected Computer Stream Sedimentation Models Developed in the United States,* F. Shou-shan (ed.), 353–412. Interagency Advisory Committee on Water Data, Federal Energy Regulatory Commission, Washington, DC.
23. Chang, H.H. 1993. *FLUVIAL-12 Mathematical Model for Erodible Channels: User's Manual*. San Diego State University, San Diego, CA.
24. Cheung, A.S. and Fisher, I.H. 1995. The use of HSPF program in total catchment management. In *Proceedings of the 16th Federal Convention*, *AWWA*, Sydney, New South Wales, Australia, vol. 2, pp. 747–753.
25. Chiew, F.H.S., Peel, M.C., and Western, A.W. 2002. Application and testing of the simple rainfall-runoff model SIMHYD. In *Mathematical Models of Small Watershed Hydrology and Applications*, P. Singh and D.K. Frevert (eds.), pp. 335–367. Water Resources Publication, Littleton, CO.
26. Cogle, A.L., Lane, L.J., and Basher, L. 2003. Testing the hill slope erosion model for application in India, New Zealand and Australia. *Environmental Modeling and Software* 18:825–830.
27. Coulthard, T.J. 2001. Landscape evolution models: A software review. *Hydrological Processes* 15:165–173.
28. Cruz, R.A.D. 1992. The determination of suitable upland agricultural areas using GIS technology. *Asian Pacific Remote Sensing Journal* 5:123–132.
29. CSIRO TOPOG http://www.clw.csiro.au/topog/intro/intro.html (accessed October 30, 2012).
30. Danish Hydraulic Institute. 1993. *MIKE 21 Short Description*. Danish Hydraulic Institute, Hørsholm, Denmark.
31. Delft Hydraulics. 1999. *Delft3D User's Manual*. Delft Hydraulics, Delft, the Netherlands.
32. Dendy, F.E. and Bolton, G.C. 1976. Sediment yield runoff drainage area relationships in the United States. *Journal of Soil and Water Conservation* 31:264–266.
33. Department of Land and Water Conservation. 1995. IQQM-integrated water quality and quantity model, Catchment Processes and Modelling Branch, TS95.019.
34. Department of Land and Water Conservation. 1999. Integrated water quantity and quality model (IQQM) user manual. Department of Land and Water Conservation.
35. De Jong, S.M., Paracchini, M.L., Bertolo, F., Folving, S., Megier, J., and De Roo, A.P.J. 1999. Regional assessment of soil erosion using the distributed model SEMMED and remotely sensed data. *Catena* 37:291–308.
36. De Roo, A.P.J. and Jetten, V.G. 1999. Calibrating and validating the LISEM model for two data sets from the Netherlands and South Africa. *Catena* 37(3–4):477–493.
37. DHI. 2003. MIKE BASIN 2003. *A Versatile Decision Support Tool for Integrated Water Resources Management Planning*. DHI, Horsholm, Denmark.
38. Douglas, I. 1999. Hydrological investigations of forest disturbance and land cover impacts in South-East Asia: A review. *Philosophical Transactions of the Royal Society of London. Series B, Biological Sciences* 354:1725–1738.

39. EEA. 1995. Corinne soil erosion risk and important land resources. http://reports.eea.europa.eu/COR0-soil/en (accessed October 30, 2012).
40. Einstein, H.A. 1950. *The Bed Load Function for Sediment Transportation in Open Channel Flows*. Technical Bulletin 1026. USDA, Soil Conservation Service, Washington, DC.
41. Elwell, H.A. and Stocking, M.A. 1982. Developing a simple yet practical method of soil loss estimation. *Tropical Agriculture* 59:43–48.
42. Favis-Mortlock, D.T., Boardman, J., and Bell, M. 1997. Modelling long-term anthropogenic erosion of a loess cover: South Downs, UK. *The Holocene* 7(1):79–89.
43. Ferro, V. and Porto, P. 2000. Sediment delivery distributed (SEDD) model. *American Society of Civil Engineers Journal of the Hydraulics Engineering* 5(4):411–422.
44. Fisher, P., Abrahart, R., and Herbinger, W. 1997. The sensitivity of two distributed non-point source pollution models to the spatial arrangement of the landscape. *Hydrological Processes* 11:241–252.
45. Fournier, F. 1972. Rational use and conservation of soil. *Geoforum* 10:35–47.
46. Fread, D.L. 1974. Numerical properties of implicit four-point finite difference equations of unsteady flow. NOAA Technical Memorandum NWS HYDRO18, 38pp.
47. Gavrilovic, Z. 1988. The use of an empirical method (Erosion Potential Method) for calculating sediment production and transportation in unstudied or torrential streams. *International Conference on River Regime*, May 18–20,1988, Wallingford, U.K. John Wiley & Sons, Chichester, U.K., pp. 411–422.
48. Gerlinger, K. 1997. Erosionsprozesse auf LôISbôden: Expérimente und Modellierung. Mitt. Inst. f. Wasserbau und Kulturtechnik, Univ. Karlsruhe, Karlsruhe, Germany, p. 194.
49. Grayson, R., Argent, R., and Western, A. 1999. Scoping study for the implementation of water quality management frameworks. Final report, CEAH report 2/99, May 1999, University of Melbourne, Melbourne, Victoria, Australia.
50. Gutteridge Haskins and Davey. 1991. *Integrated Quantity and Quality Modelling. Stage 3*. Gutteridge Haskins and Davey for Department of Water Resources, Sydney, New South Wales, Australia, 102pp.
51. Hadley, R.F., Lal, R., Onstad, C.A., Walling, D.E., and Yair, A. 1985. *Recent Development in Erosion and Sediment Yield Studies*. UNESCO, Paris, France, 127pp.
52. Hamrick, J.H. 1992. A three-dimensional environmental fluid dynamics computer code: Theoretical and computational aspects. Special Report No. 317, Applied Marine Science and Ocean Engineering, Virginia Institute of Marine Science, Gloucester Point, VA.
53. Hamrick, J.M. 2001. EFDC1D: A one dimensional hydrodynamic and sediment transport model for river and stream networks, model theory, and user's guide. Technical Report, U.S. EPA National Exposure Research Laboratory, Athens, GA and U.S. EPA Office of Science and Technology, Washington, DC.
54. Hanley, N., Faichney, R., Munro, A., and Shortle, J.S. 1998. Economic and environmental modelling for pollution control in an estuary. *Journal of Environmental Management* 52:211–225.
55. Hervouet, J.M. and Bates, P. 2000. The TELEMAC modelling system. Special issue. *Hydrological Processes* 14(13):2207–2208.
56. Hessel, R. 2002. Modelling soil erosion in a small catchment on the Chinese Loess Plateau. PhD thesis, Utrecht University, Netherlands Geographical Studies, Utrecht, the Netherlands, p. 307, 317pp.
57. Holly, F. M. Jr. 1988. Charima and sedicoup codes for riverine mobile-bed simulation. In: *Twelve Selected Computer Stream Sedimentation Models Developed in the United States*, F. Shou-shan (ed.), 263–352. Interagency Advisory Committee on Water Data, Federal Energy Regulatory Commission, Washington, DC.
58. Holly, F.M. and Rahuel, J.L. 1990. New numerical/physical framework for mobile-bed modeling. Part 1: Numerical and physical principles. *Journal of Hydraulic Research* 28(4):401–416.
59. Holly, F.M. and Usseglio-Polatera, J.M. 1984. Dispersion simulation in two-dimensional tidal flow. *Journal of Hydraulic Engineering* 110(7):905–926.
60. Holly, F.M., Yang, J.C., Schovarz, P., Scheefer, J., Hsu, S.H., and Einhellig, R. 1990. CHARIMA: Numerical simulation of unsteady water and sediment movements in multiply connected networks of mobile-bed channels. Report No. 343, Iowa Institute of Hydraulic Research, University of Iowa, Iowa City, IA.

61. Jacobsen, F. and Rasmussen, E.B. 1997. MIKE 3 MT: A three-dimensional mud transport model. Technical Report DG-12 to the Commission of the European Communities, Brussels, Belgium.
62. Jakeman, A., Littlewood, I., and Whitehead, P. 1990. Computation of the instantaneous unit hydrograph and identifiable component flows with application to two small upland catchments. *Journal of Hydrology* 117:275–300.
63. Jakeman, A., Post, D., and Beck, M. 1994. From data and theory to environmental model: The case of rainfall runoff. *Environmetrics* 5:297–314.
64. Jakeman, A., Post, D., Schreider, S., and Yu, Y.W. 1994. Modelling environmental systems: Partitioning the water balance at different catchment scales. In *Computer Techniques in Environmental Studies V*, P. Zannetti (ed.), pp. 157–170. Computational Mechanics Publications, Southampton, U.K.
65. Jia, Y. and Wang, S.S. 1999. Numerical model for channel flow and morphological change studies. *Journal of Hydraulic Engineering* 125(9):924–933.
66. Johanson, R.C., Imhoff, J.C., and Davis, H.H. 1980. User's manual for the Hydrologic Simulation Program-Fortran (HSPF) version No. 5.0, EPA-600/9-80-105. U.S. EPA Environmental Research Laboratory, Athens, GA.
67. Johnson, B.E., Julien, P.Y., Molnar, D.K., and Watson, C.C. 2000. The two-dimensional upland erosion model CASC2D-SED. *Journal of the American Water Resources Association* 36(1):31–42.
68. Karim, M.F. and Kennedy, J.F. 1982. IALLUVIAL: A commuter based flow and sediment routing for alluvial streams and its application to the Missouri River Report No. 250, Iowa Institute of Hydraulic Research, University of Iowa, Iowa City, IA.
69. Kilinc, M. and Richardson, E.V. 1973. Mechanics of soil erosion from overland flow generated by simulated rainfall. Hydrology Papers, vol. 63. Colorado State University, Fort Collins, CO.
70. King, I. 1988. A finite element model for three dimensional hydrodynamic systems. Report to Waterways Experiment Station, U.S. Army Corps of Engineers, Vicksburg, MS.
71. Kirkby, M.J. 1971. Hillslope process-response models based on the continuity equation. In *Slopes Form and Process*, D. Brunsden (ed.), vol. 3, pp. 15–30. Institute of British Geographers, Special Publication.
72. Kirkby, M.J., Abrahart, R.J., McMahon, M.D., Shao, J., and Thornes, J.B. 1998. MEDALUS soil erosion models for global change. *Geomorphology* 24:35–49.
73. Kirkby, M.J. et al. 2004. European Soil Bureau Research Report No.16, EUR 21176, 18pp.
74. Kirkby, M.J., Le Bissonais, Y., Coulthard, T.J., Daroussin, J., and McMahon, M.D. 2000. The development of land quality indicators for soil degradation by water erosion. *Agriculture, Ecosystems and Environment* 81:125–136.
75. Knisel, W.G. 1980. CREAMS: *A Field Scale Model for Chemicals, Runoff and Erosion from Agricultural Management Systems*. USDA, Washington, DC.
76. Krishnappan, B.G. 1981. *User's Manual: Unsteady, Non-Uniform, Mobile Boundary Flow Model-MOBED*. Hydraulic Division, National Water Research Institute, CCIW, Burlington, Ontario, Canada.
77. Krysanova, V., Meiner, A., Roosaare, J., and Vasilyev, A. 1989. Simulation modelling of the coastal waters pollution from agricultural watershed. *Ecological Modelling* 49:7–29.
78. Krysanova, V., Mùïler-Wohlfeil, D.I., and Becker, A. 1996. Integrated modelling of hydrology and water quality in mesoscale watersheds. PIK Report No. 18, Potsdam Institute for Climate Impact Research, Potsdam, Germany.
79. Laflen, J.M., Lane, L.J., and Foster, G.R. 1991. WEPP: A new generation of erosion prediction technology. *Journal of Soil and Water Conservation* 46:34–38.
80. Landsberg, A., Chtchelkanova, A., Lind, C., Boris, J., and Young, T. 1998. Fast3D user and programmer reference manual.
81. Lane, L.J., Renard, K.G., Foster, G.R., and Laflen, J.M. 1992. Development and application of modern soil erosion prediction technology the USDA experience. *Australian Journal of Soil Research* 30:893–912.

82. Larionov, G.A., Dobrovolskaya, N.G., Kiryukhina, Z.P., Krasnov, S.F., and Litvin, L.F. 2004. Hydrophysical model of soil erosion: A basic equation and influence of bed load and suspended sediment on soil detachment by shallow water flow. *IAHS Publication* 288:361–369.
83. Lee, H.Y., Hsieh, H.M., Yang, J.C., and Yang, C.T. 1997. Quasi two-dimensional simulation of scour and deposition in alluvial channels. *Journal of Hydraulic Engineering* 123(7):600–609.
84. Li, R. M., Mussetter, R. A., and Grindeland, T. R. 1988. Sediment-Routing Model, HEC2SR. In: *Twelve Selected Computer Stream Sedimentation Models Developed in the United States*, F. Shoushan (ed.), 413–462. Interagency Advisory Committee on Water Data, Federal Energy Regulatory Commission, Washington, DC.
85. Li, R.M., Simons, D.B., Fullerton, W.T., Eggert, K.G., and Spronk, B.E. 1979. Simulation of water runoff and sediment yield from a system of multiple watersheds. In *Proceedings of the 18th Congress IAHR*, Cagliari, Italy, vol. 5, pp. 219–226.
86. Liggett, J.A. and Cunge, J.A. 1975. Numerical methods of solution of the unsteady flow equations. In *Unsteady Flow in Open Channels*, K. Mahmood and V. Yevjevich (eds.), Chapter 4, vol. 1. Water Resources Publications, Fort Collins, CO.
87. Littleboy, M., Freebairn, D.M., Hammer, G.L., and Silburn, D.M. 1992. Impact of soil erosion on production and erosion risks for a wheat cropping system. *Australian Journal of Soil Research* 30:775–788.
88. Littleboy, M., Silburn, M.D., Freebairn, D.M., Woodruff, D.R., Hammer, G.L., and Leslie, J.K. 1992. Impact of soil erosion on production in cropping systems. I. Development and validation of a simulation model. *Australian Journal of Soil Research* 30:757–774.
89. Littleboy, M., Cogle, A., Smith, G., Yule, D., and Rao, K. 1996. Soil management and production of Alfisols in the semi-arid tropics, I. Modelling the effects of soil management on runoff and soil erosion. *Australian Journal of Soil Research* 34:91–102.
90. Lopes, V.L. 1987. A numerical model of watershed erosion and sediment yield. PhD thesis, The University of Arizona, Tucson, AZ.
91. Lopes, V.L. and Lane, L.J. 1988. Modeling sedimentation processes in small watersheds. *IAHS Publications* 174:497–508.
92. Luettich, R.A., Westerink, J.J., and Scheffner, N.W. 1992. ADCIRC: An advanced three-dimensional circulation model for shelves, coasts, and estuaries: Report 1, theory and methodology of ADCIRC-2DDI and ADCIRC-3DL. Technical Report DRP-92-6, U.S. Army Engineer Waterways Experiment Station, Vicksburg, MS.
93. Martin, J.L. and Mccutcheon, S.C. 1999. *Hydrodynamics and Transport for Water Quality Modeling*. Lewis Publishers, New York.
94. Meyer-Peter, E. and Müller, R. 1948. Formulas for bed-load transport. In *Proceedings of the 2nd Meeting of the International Association for Hydraulic Structures Research*, International Association for Hydraulic Research, Delft, the Netherlands, pp. 39–64.
95. Meyer, L.D. and Wischmeier, W.H. 1969. Mathematical simulation of the process of soil erosion by water. *Transactions American Society Agricultural Engineers* 12:756–762.
96. Minh Duc, B., Wenka, T., and Rodi, W. 1998. Depth-average numerical modeling of flow and sediment transport in the Elbe River. In *Proceedings of the 3rd International Conference on Hydroscience and Engineering*, Berlin, Germany.
97. Misra, R.K. and Rose, C.W. 1996. Application and sensitivity analysis of process-based erosion model GUEST. *European Journal of Soil Science* 47:593–604.
98. Mitasova, H. 1999. *Terrain Modelling and Soil Erosion Simulation*. Geographic Modelling and Systems Laboratory, University of Illinois, Urbana, IL.
99. Mitasova, H., Mitas, L., Brown, W.M., and Johnston, D. 1996. *Multidimensional Soil Erosion/Deposition Modeling. Part III: Process Based Erosion Simulation*. Geographic Modeling and Systems Laboratory, University of Illinois, Urbana, IL.

100. Mitasova, H., Mitas, L., and Brown, W.M. 2001. Multiscale simulation of land use impact on soil erosion and deposition patterns. *In Sustaining the Global Farm, D.E. Stott, R.H. Mohtar, and G.C. Steinhardt (eds.)*, pp. 1163–1169. Selected papers from the 10th International Soil Conservation Meeting held May 24–29, 1999 at Purdue University and USDA-ARS National Soil Erosion Research Laboratory.
101. Molinas, A. and Yang, C.T. 1986. *Computer Program User's Manual for GSTARS Generalized Stream Tube Model for Alluvial River Simulation*. U.S. Bureau of Reclamation Engineering and Research Center, Denver, CO.
102. Moore, I. and Burch, G. 1986. Physical basis of the length-slope factor in the Universal Soil Loss Equation. *Soil Society of America Journal* 50:1294–1298.
103. Moore, I. and Gallant, J. 1991. Overview of hydrologic and water quality modelling. In *Modelling the Fate of Chemicals in the Environment*, I. Moore (ed.), pp. 1–8. Centre for Resource and Environmental Studies, Australian National University, Canberra, Australian Capital Territory, Australia.
104. Morgan, R.P.C. and Nearing, M. 2000. Soil erosion models: Present and future. In *Proceedings of III International ESSC Congress*, Valencia, Spain, pp. 145–148.
105. Morgan, R.P.C., Morgan, D.D.V., and Finney, H.J. 1984. A predictive model for the assessment of soil erosion risk. *Agricultural Engineering Research* 30:245–253.
106. Morgan, R.P.C., Quinton, J.N., Smith, R.E., Govers, G., Poesen, J.W.A., Auerswald, K., Chisci, G., Torri, D., and Styczen, M.E. 1998. The European soil erosion model (EUROSEM): A process-based approach for predicting sediment transport from fields and small catchments. *Earth Surface Processes and Landforms* 23:527–544.
107. Musgrave, G.W. 1947. The quantitative evaluation of factors in water erosion: A first approximation. *Journal of Soil and Water Conservation* 2(3):133–138.
108. Nearing, M.A., Govers, G., and Norton, L.D. 1999. Variability in soil erosion data from replicated plots. *Soil Science Society of America Journal* 63(6):1829–1835.
109. Olsen, N.R. 1994. SSIIM: A three-dimensional numerical model for simulation of water and sediment flow. In *HYDROSOFT 94*, Porto Carras, Greece.
110. Onishi, Y. and Wise, S.E. 1982. SERATRA: User's manual for the instream sediment-contaminant transport model. Technical Report No. PB-83-122739, Pacific Northwest Laboratory, Battelle-Northwest, Richland, WA.
111. O'Loughlin, E.M. 1986. Prediction of surface saturation zones in natural catchments by topographic analysis. *Water Resources Research* 22(5):794–804.
112. Pacific Southwest Interagency Committee (PSIAC). 1968. Report of the management committee, factors affecting sediment yield and measures for reduction of erosion and sediment yield.
113. Papanicolaou, A., Bdour, A., and Wicklein, E. 2004. A numerical model for the study of sediment transport in steep mountain streams. *Journal of Hydraulic Research* 42(4):357–366.
114. Preissman, A. 1960. Propagation des intumescences dans les cannaux et riviers. In *1st congres de l'acesoc*, Francaise de calcul, Grenoble, France, pp. 433–442.
115. Prosser, I.P., Rustomji, P., Young, B., Moran, C., and Hughes, A. 2001. Constructing river basin sediment budgets for the National Land and Water Resources Audit. Technical Report 15/01. CSIRO Land and Water, Canberra, Australian Capital Territory, Australia.
116. Prosser, I.P., Young, B., Rustomji, P., Hughes, A., and Moran, C. 2001. A model of river sediment budgets as an element of river health assessment. In *Proceedings of the International Congress on Modelling and Simulation (MODSIM&rlenis;2001)*, Canberra, Australian Capital Territory, Australia, December 10–13, 2001, pp. 861–866.
117. Renard, K.G., Foster, G.R., Weesies, G.A., McCool, D.K., and Yoder, D.C. 1996. Predicting soil erosion by water: A guide to conservation planning with the revised Universal Soil Loss Equation. Agriculture Handbook No. 703, U.S. Department of Agriculture, Washington, DC.
118. Riggins, R.E., Ward, T.J., and Hodge, W. 1989. ARMSED: A runoff and sediment yield model for army training land watershed management, Vol. I: Parameter estimation and Vol. II: Program documentation. USACERL TR N-89/12, January.

119. Rose, C.W., Coughlan, K.J., Ciesiolka, L.A.A., and Fentie, B. 1997. Program GUEST (Griffith University Erosion System Template), a new soil conservation methodology and application to cropping systems in tropical steeplands. ACIAR Technical Reports, vol. 40, pp. 34–58.
120. Rovey, E.W., Woolhiser, D.A., and Smith, R.E. 1977. A distributed kinematic model for upland watersheds. Hydrology Paper No. 93, Colorado State University, Fort Collins, CO, 52pp.
121. Runkel, R.L. and Broshears, R.E. 1991. OTIS: One-dimensional transport with inflow and storage: A solute transport model for small streams. CADSWES Technical Report 91-01, University of Colorado, Boulder, CO.
122. Sadeghi, S.H.R., Azari, M., and GhaderiVangah, B. 2008. Field evaluation of the hill slope Erosion Model (HEM) in Iran. *Biosystems Engineering* 99:304–311.
123. Santos, C.A.G., Watanabe, M., and Suzuki, K. 2000. Application of a physically-based erosion model for a large river basin in Japan. In Paper presented in the *Symposium on Integrated Water Resources management*, Davis, CA, April 2000.
124. Schmidt, J. 1991. A mathematical model to simulate rainfall erosion. In *Erosion, Transport and Deposition Processes Theories and Models*, H.R. Bork, J. De Ploey, and A.P. Schick (eds.); *Catena* 19:101–109.
125. Schmidt, J. 1992. Modelling long-term soil loss and landform change. In *Overland Flow Hydraulics and Erosion Mechanics*, A.J. Abrahams and A.D. Parsons (eds.). University College London Press, London, U.K.
126. Schramm, M. 1994. Ein Erosionsmodell mit zeitlich und ràumlich veränderlicher Rillengeometrie. Mitt. Inst. f. Wasserbau und Kulturtechnik, University of Karlsruhe 190, Karlsruhe, Germany.
127. Schulze, R.E. 1975. Catchment evapotranspiration in the Natal Drakensberg. PhD thesis, Department of Geography, University of Natal, Pietermaritzburg, South Africa, 244pp.
128. Schulze, R.E. 1995. Hydrology and agrohydrology: A text to accompany the ACRU 3.00 agrohydrological modelling system. Water Research Commission, Pretoria, Technology Transfer Report TT 69/95, 543pp.
129. Sharpley, A.N. and Williams, J.R. 1990. EPIC: Erosion/productivity impact calculator 1. Model documentation. Technical Bulletin 1768. U.S. Department of Agriculture, Washington, DC.
130. Simons, D.B., Li, R.M., Fullerton, W.T., and Wolf, C.G. 1981. User's manual multiple watershed model for water and sediment routing considering cohesive soils. Prepared for New Mexico State University by Simons, Li & Associates, Inc., Fort Collins, CO.
131. Smith, D.D. and Whitt, D.M. 1948. Estimating soil losses from field areas. *Agriculture Engineering* 29:394–396.
132. Smith, R.E. 1981. A kinematic model for surface mine sediment yield. *Transactions of the American Society of Agricultural Engineers* 24:1508–1514.
133. Smith, R.E. 1992. Opus: An integrated simulation model for transport of non-point source pollutants at the field scale, Vol. I. Documentation. USDA. Agriculture Research Service, ARS-98, 120pp.
134. Smith, R.E. 1995. Simulation of crop water balance with Opus. In *Crop Water Simulation Models in Practice*, L.S. Pereira, B.J. van den Broek, P. Kabat, and R.G. Allen (eds.). Wageningen Pers, Wageningen, the Netherlands, pp. 215–227.
135. Song, C.C.S., Zheng, Y., and Yang, C.T. 1995. Modeling of river morphologic changes. *International Journal of Sediment Research* 10(2):1–20.
136. Song, Y.T. and Haidvogel, D. 1994. A semi-implicit primitive equation ocean circulation model using a generalized topography following coordinate system. *Journal of Computational Physics* 115:228–244.
137. Spasojevic, M. and Holly, F.M. 1990. MOBED2: Numerical simulation of two-dimensional mobile-bed processes. Technical Report No. 344, Iowa Institute of Hydraulic Research, University of Iowa, Iowa City, IA.
138. Spasojevic, M. and Holly, F.M. 1994. Three-dimensional numerical simulation of mobile-bed hydrodynamics. Contract Report HL-94-2, U.S. Army Engineer Waterways Experiment Station, Vicksburg, MS.

139. Stehlik, O. 1975. Potential soil erosion by running water on territory of the Czech Socialist Republic. Ceskoslovenska akademie ved, Geograficky Ustav, Brno, Czech Republic, 147pp.
140. Strand, R.I., Orvis, C.J., and Randle, T.J. 1988. Sediment transport and river simulation model. In: *Twelve Selected Computer Stream Sedimentation Models Developed in the United States*, F. Shoushan (ed.), 95–148. Interagency Advisory Committee on Water Data, Federal Energy Regulatory Commission, Washington, DC.
141. Storm, B., Jorgensen, G.H., and Styczen, M. 1987. Simulation of water flow and soil erosion processes with a distributed physically-based modeling system. *IAHS Publications* 167:595–608.
142. Takken, I., Beuselinck, L., Nachtergaele, J., Govers, G., Poesen, J., and Degraer, G. 1999. Spatial evaluation of a physically-based distributed erosion model (LISEM). *Catena* 37(3–4):431–447.
143. Thomas, W.A. and McAnally, W.H. 1985. User's manual for the generalized computer program system open-channel flow and sedimentation-TABS-2. Main Text, Instruction Report HL-85-1, Waterways Experiment Station, U.S. Army Corps of Engineers, Vicksburg, MS.
144. Thomas, W.A. and Prashum, A.I. 1977. Mathematical model of scour and deposition. *Journal of Hydraulic Division* 110(11):1613–1641.
145. Thornes, J.B. 1985. The ecology of erosion. *Geography* 70:222–234.
146. Thornes, J.B. 1990. The interaction of erosional and vegetation dynamics in land degradation: Spatial outcomes. In *Vegetation and Erosion*, J.B Thornes (ed.), pp. 41–53. John Wiley & Sons, Chichester, U.K.
147. Thornes, J.B., Shao, J.X., Diaz, E., Roldan, A., McMahon, M., and Hawkes, J.C. 1996. Testing the MEDALUS hillslope model. *Catena* 26:137–160.
148. Tucker, G., Gasparini, N., Lancaster, S., and Bras, R. 1997. An integrated hillslope and channel evolution model as an investigation and prediction tool. Annual Report. Department of Civil and Environmental Engineering, Massachusetts Institute of Technology 60, Cambridge, MA.
149. USDA. 1995. USDA-watershed erosion prediction project (WEPP). Technical Documentation. National Soil Erosion Research Laboratory, NSERL Report No. 10, Lafayette, IN
150. USEPA. 1994. *SWRRBWQ Window's Interface User's Guide*. U.S. Environmental Protection Agency, Washington, DC.
151. van Rijn, L.C. and Tan, G.L. 1985. SUTRENCH model: Two-dimensional vertical mathematical model for sedimentation in dredged channels and trenches by currents and waves. Rijkswaterstaat communications No. 41, Rijkswaterstaat, the Hague, the Netherlands.
152. Vertessey, R.A., Watson, F.G.R., Rahman, J.M., Cuddy, S.D., Seaton, S.P., Chiew, F.H., Scanlon, P.J., Marston, F.M., Lymbuner, L., Jeanelle, S., and Verbunt, M. 2001. New software to aid water quality management in the catchments and waterways of the south-east Queensland region. In *Proceedings of the Third Australian Stream Management Conference*, Brisbane, Queensland, Australia, August 27–29, 2001, pp. 611–616.
153. Viney, N.R. and Sivapalan, M. 1999. A conceptual model of sediment transport: Application to the Avon River Basin in Western Australia. *Hydrological Processes* 13:727–743.
154. Walstra, D.J., van Rijn, L.C., and Aarninkhof, S.G. 1998. Sand transport at the lower shoreface of the Dutch coast. Technical Report Z2378, Delft Institute of Hydraulics, Delft, the Netherlands.
155. Walton, R. and Hunter, H. 1996. Modelling water quality and nutrient fluxes in the Johnstone River Catchment, North Queensland. In *23rd Hydrology and Resources Symposium*, Sydney, New South Wales, Australia.
156. Watson, F., Rahman, J., and Seaton, S. 2001. Deploying environmental software using the Tarsier modelling framework. In *Proceedings of the Third Australian Stream Management Conference*, Brisbane, Queensland, Australia, August 27–29, 2001, pp. 631–638.
157. Werner, M.V. 1995. GIS-orientierte Methoden der digitalen Reliefanalyse zur Modellierung von Bodenerosion in kleinen Einzugsgebieten. Dissertation, Freie Universitat Berlin, Berlin, Germany.
158. Wicks, J.M. 1988. Physically-based mathematical modelling of catchment sediment yield. PhD thesis, Department of Civil Engineering, University of Newcastle upon Tyne, Newcastle upon Tyne, U.K.

159. Wicks, J.M. and Bathurst, J.C. 1996. SHESED: A physically based, distributed erosion and sediment yield component for the SHE hydrological modelling system. *Journal of Hydrology* 175:213–238.
160. Whipple, K.X. and Tucker, G.E. 1999. Dynamics of the stream-power incision model: Implications for height limits of mountain ranges, landscape response timescales, and research needs. *Journal of Geophysical Research* 104(B8):17661–17674.
161. Whipple, K.X. 2004. Bedrock rivers and the geomorphology of active orogens. *Annual Review of Earth and Planetary Sciences* 32:151–185.
162. Williams, J.R. and Berndt, H.D. 1977. Sediment yield prediction based on watershed hydrology. *Transactions of the American Society of Agricultural Engineers* 20:1100–1104.
163. Williams, J.R., Dyke, P.T., and Jones, C.A. 1983. EPIC: A model for assessing the effects of erosion on soil productivity. In *Analysis of Ecological Systems: State of the Art in Ecological Modeling*. W.K. Laurenroth et al. (eds.). Elsevier, Amsterdam, the Netherlands, pp. 553–572.
164. Williams, J.R., Nicks, A.D., and Arnold, J.G. 1985. SWRRB: A simulator for water resources in rural basins. *American Society of Civil Engineers Hydrology Journal* 111(6):970–986.
165. Wischmeier, W.H. and Smith, D.D. 1978. *Predicting Soil Erosion Losses: A Guide to Conservation Planning. USDA Agricultural Handbook No*. 537, U.S. Department of Agriculture, Washington, DC, 58pp.
166. Woodward, D.E. 1999. Method to predict cropland ephemeral gully erosion. *Catena* 37:393–399.
167. Woolhiser, D.A., Smith, R.E., and Goodrich, D.C. 1990. KINEROS: A kinematic runoff and erosion model. Documentation and User Manual, USDA, Agricultural Research Service, ARS-77, 130pp.
168. Wu, B.S. and Molinas, A. 1996. Modeling of alluvial river sediment transport. In *Proceedings of the International Conference on Reservoir Sedimentation*, M.L. Albertson, A. Molinas, and R. Hotchkiss (eds.), vol. I. Colorado State University, Fort Collins, CO, pp. 281–325.
169. Yalin, M.S. 1963. An expression for bed load transportation. *Journal of Hydraulics Division, American Society of Civil Engineers* 89:221–250.
170. Yang, C.T. and Simões, F.J. 2000. Users' manual for GSTARS 2.1 (Generalized stream tube model for alluvial river simulation version 2.1). Technical Service Center, U.S. Bureau of Reclamation, Denver, CO.
171. Yang, C.T. and Song, C.C.S. 1986. Theory of minimum energy and energy dissipation rate. In *Encyclopaedia of Fluid Mechanics*, ND. Cheremisinoff (ed.). Gulf Publishing Company, Houston, TX, 353–399.
172. Yang, C.T. 1992. Force, energy, entropy, and energy dissipation rate. In *Entropy and Energy Dissipation in Water Resources*, V.P. Sing and M. Fiorentin (eds.), pp. 63–89. Kluwer Academic Publishers, London, U.K.
173. Yotsukura, N. and Sayre, W.W. 1976. Transverse mixing in national channels. *Water Resources Research* 12:695–704.
174. Young, R.A., Onstad, C.A., Bosch, D.D., and Anderson, W.P. 1987. AGNPS: Agricultural non-point source pollution. A watershed analysis tool. Conservation Research Report 35. U.S. Department of Agriculture, Washington, DC.
175. Young, R.A., Onstad, C.A., Bosch, D.D., and Anderson, W.P. 1989. AGNPS: A non-point source pollution model for evaluating agricultural watersheds. *Journal of Soil and Water Conservation* 44(2):4522–4561.
176. Yu, B., Rose, C.W., Cielsiolka, C.A.A., Coughlan, K.J., and Fentie, B. 1997. Towards a framework for runoff and soil loss prediction using GUEST technology. *Australian Journal of Soil Research* 35:1191–1212.
177. Zeng, J., Constantinescu, G., and Weber, L. 2005. A fully 3D nonhydrostatic model for prediction of flow, sediment transport and bed morphology in open channels. In *31st International Association Hydraulic Research Congress*, Seoul, Korea.
178. Zingg, A.W. 1940. Degree and length of land slope as it affects soil loss in runoff. *Agriculture Engineering* 21:59–64.

14

Geostatistics Applications in Hydrology

Pejman Tahmasebi
Stanford University

Gregoire Mariethoz
University of New South Wales

AUTHORS

Pejman Tahmasebi is a research assistant in Stanford University, Department of Energy Resources Engineering in Stanford Center for Reservoir Forecasting (SCRF). His research interests widely span on reservoir modeling, stochastic geostatistical simulation, advance computational methods, and porous media characterization. He obtained his PhD from Tehran Polytechnic on stochastic reservoir simulation in 2012.

Gregoire Mariethoz obtained a PhD in stochastic hydrogeology in the University of Neuchâtel (Switzerland) in 2009 and then moved to Stanford University as a postdoctoral researcher. He is currently senior lecturer at the University of New South Wales, Australia, and has a research focused on water resources modeling. He has extensive experiences in geostatistical characterization of surface and subsurface processes, including the development and application of novel algorithms, optimization methods, data analysis in the earth sciences, and hydrological models.

14.1 Introduction

In more than half a century, geostatistics has become a useful tool for spatial modeling and interpolation [29]. Applications are not limited to just spatial modeling, and one can deal with temporal and spatiotemporal problems as well. One of the most widespread geostatistical tools, kriging, was named after Daniel Krige. After Krige, Matheron developed the main principles of geostatistics [36,37] and developed a suite of methods to accurately estimate spatial attributes, which are broadly known as kriging-based methods. These methods call for a prior model of variability and correlation between the variables, known as the variogram. Kriging is one of the most popular interpolation methods.

However, it has been shown that kriging tends to produce overly smooth results [20,27] and therefore can fail to accurately represent nonsmooth processes. One consequence is the underestimation and

overestimation for low and high values, respectively. Hence, kriging estimation is not very suitable for representing highly structured phenomena such as heterogeneous rain fields, aquifers, or catchment properties. This spans beyond the field of hydrology, with important consequences for applications in fluid flow prediction through modeling subsurface structures. For example, this problem becomes obvious when one tries to predict the water breakthrough and reservoir response to different flow regimes. In the kriging model, the subsurface connectivity and variability cannot be reproduced finely.

The concept of stochastic simulation has been introduced to overcome the limitations of kriging [7,26,36]. Different variogram-based stochastic simulation methods have been proposed [20]. Methods such as sequential Gaussian simulation (SGSIM) and sequential indicator simulation (SISIM) have become popular among different fields of earth sciences. The main difference with kriging is that stochastic simulation reproduces the spatial texture or roughness embodied in a variogram, while kriging only aims at finding a unique estimate minimizing the error variance, which is smooth. A corollary is that sequential simulation cannot provide a unique interpolation, but instead gives a number of "realizations" or interpolation scenarios. Multiple realizations allow to assess the uncertainty and quantify it more accurately [1].

One of the main shortcomings of kriging-based geostatistical simulations is their inability to reproduce complex patterns. The main reason is that they only consider two-point statistics, which is the spatial dependence of locations taken two by two, therefore limiting the order of complexity that can be represented if higher orders were considered. In the last two decades, the need for using methods that can use more than two points simultaneously has been emphasized. This new category of methods is called multiple-point geostatistics (MPS).

In MPS, the spatial statistics are not represented with a variogram, but thorough a conceptual tool named training image (TI), which is an example of the spatial structure to be reproduced. During the recent years, several MPS methods have been developed to address issues related to CPU time and improved graphical representation of the models produced. In this chapter, we first try to present the main two-point-based stochastic simulation methods. Then, the basic terminologies and concepts of MPS are demonstrated. Next, different MPS methods are explained and the advantages and disadvantages associated with each method are demonstrated. Finally, a comparison between some of these methods is carried on.

14.2 Two-Point-Based Stochastic Simulation

Sequential simulation is often considered in order to circumvent the smoothing effect of kriging and to make a tool for accurate quantification of uncertainty. Consider a set of N random variables $Z(\boldsymbol{u}_\alpha)$, $\alpha = 1, \ldots, N$ defined at locations $\boldsymbol{u}_\alpha$. The aim of sequential simulation is to produce realizations $\{z(\boldsymbol{u}_\alpha), \alpha = 1, \ldots, N\}$, conditioned to n available data, and reproduce a given multivariate distribution. For this aim, the multivariate distribution is decomposed into a set of N univariate conditional cumulative distribution functions (ccdfs):

$$F(\boldsymbol{u}_1,\ldots,\boldsymbol{u}_N; z_1,\ldots,z_N \mid (n)) = F(\boldsymbol{u}_1;\ z_1 \mid (n)) \times F(\boldsymbol{u}_2;\ z_2 \mid (n+1)) \times \cdots$$
$$\times F(\boldsymbol{u}_{N-1};\ z_{N-1} \mid (n+N-2)) \times F(\boldsymbol{u}_N;\ z_N \mid (n+N-1)) \tag{14.1}$$

where $F(\boldsymbol{u}_N; z_N|(n+N-1)) = Prob\{Z(\boldsymbol{u}_N) \leq z_N|(n+N-1)\}$ is the conditional ccdf of $Z(\boldsymbol{u}_N)$ conditioned to a set of n original data and $(N-1)$ previously simulated values.

14.2.1 Sequential Gaussian Simulation (SGSIM)

In this method, the lower statistical order such as histogram and variogram is used to determine the multivariate distribution, and the higher order will be expressed by using a multi-Gaussian distribution.

In other words, a Gaussian function can be fully characterized by its mean and covariance matrix [7,13]. Therefore, along a random path, the mean and variance of the Gaussian distribution can be estimated via kriging and kriging variance. Then a random value is drawn from that distribution and can be thereafter considered as conditioning data. The overall algorithm of SGSIM can be summarized as follows: First, a random path is defined that visits all nodes. Then, at each node, the hard data and previously simulated data are considered for estimation of the ccdf by kriging. Then, a random value from the obtained Gaussian ccdf is drawn and added to the simulation grid. Next, another node is simulated, chosen according to the predefined random path. Finally, another random path is used for obtaining another realization.

It is worth noting that the conditioning data should be normally distributed. If it is not the case, it entails transforming them into a Gaussian distribution in order to be useable for SGSIM, and at the end of the simulation the results should be back transformed. Such transformations can be accomplished using normal-score transforms or histogram anamorphosis through Hermite polynomials.

14.2.2 Sequential Indicator Simulation

Indicator simulation is based on the same principle as SGSIM, but is suited for categorical data that do not have an order relationship. Typical examples in surface hydrology are soil type, presence or absence of rainfall, or specific types of lithology in subsurface models. The similar sequential procedure is based on the estimation of the ccdf conditional to neighboring data. This algorithm is based on two-point indicator variograms [8], which represent the spatial variability of each category. An indicator variable is defined for each variable, equal to 1 if at location u a particular category is found and zero otherwise. Also, $E\{I(\boldsymbol{u})\} = p$ is the stationary proportion of a given category. The indicator variogram can be expressed as

$$Prob\{I(\boldsymbol{u}) = 1,\ I(\boldsymbol{u}+h) = 1\} = E\{I(\boldsymbol{u})\ I(\boldsymbol{u}+h)\} = Prob\ \{I(\boldsymbol{u}) = 1 \,|\, I(\boldsymbol{u}+h) = 1\} p \tag{14.2}$$

Usually, the categorical variables are expressed as a set of K discrete categories that $z(\boldsymbol{u}) \in \{0, \ldots, k-1\}$. Therefore, the indicator value for each of the defined classes can be expressed as

$$I(u,k) = \begin{cases} 1 & Z(u) = k \\ 0 & \text{otherwise} \end{cases} \tag{14.3}$$

The aim of the indicator formulation is to estimate the probability of $Z(\boldsymbol{u})$ to be less than the predefined threshold for a category conditional to the data (n) retained:

$$I^*(u,z_k) = E^*(I(u,z_k) \,|\, (n)) = Prob^*(Z(u) < z_k \,|\, (n)). \tag{14.4}$$

We can rewrite the previous equation for categorical variables by using simple kriging as

$$I^*(u,k) - E\{I(u,k)\} = \sum_{\alpha=1}^{n} \lambda_\alpha(u)(I(u_\alpha,k) - E\{I(u_\alpha,k)\})$$

$$\sum_{k=1}^{K} I^*(u,k) = 1 \tag{14.5}$$

where $E\{I(u, k)\}$ is the marginal probability for category k.

The previous formulation can be applied within the sequential scheme that is known as SISIM. In this case, the probability of each category is estimated by indicator kriging (IK). This algorithm can be described as follows: Similarly as SGSIM, a random path is defined by which all of the nodes are visited. Then, for each node on the random path, the neighboring data are selected, and then by using simple kriging, the indicator random variable for each category is estimated. Next, the conditional probability density function (cpdf) is obtained, and a value is randomly drawn from that cpdf and assigned to the simulated node. This procedure is repeated sequentially for all unknown nodes. By choosing another random path, one can generate another realization. More information on this method can be found in Goovaerts [20].

14.3 Multiple-Point Geostatistics

A problem that is general among all of the two-point-based geostatistical simulations is their inability to capture high variability and complex spatial structures. In particular, these methods cannot convey the connectivity and variability when the phenomenon considered contains definite patterns or structures. For example, SGSIM maximizes the entropy of the random function and therefore prevents the realizations to be structured [22]. Using several points at a time is necessary in order to capture the connectivity, variability, and correlations between more than two locations.

An alternative for constructing structured categorical models is the object-based (or Boolean) method. In these algorithms, the simulation grid is filled with proper shapes and objects that can satisfy the hard data [11,21–23,30,32,58]. Since the shape parameters such as size, direction, and sinuosity are all random, they lead the algorithm to be stochastic. Then, an iterative algorithm is incorporated in order to remove, change, add, or in addition modify the objects.

The object-based simulation methods are well fitted for TI construction and can condition to a limited amount of data, but when one simulates a grid with dense data, finding and adjusting the objects can be problematic. On the other hand, pixel-based simulation methods are better able to condition to hard data, but they can fail to reproduce connectivity and complex patterns.

The initial idea of MPS is based on a paper by Guardiano and Srivastava [21]. The idea was to scan the TI with a template of n-points and to find the replicates within the TI. It should be added that generally the TI is a conceptual model or image that tries to convey the subsurface features and heterogeneity. This image is not conditioned to any local data but it represents the structures of interest. The TI is able to quantify some qualitative information and integrate it with the available quantitative data such as well and seismic data. The main problem of this method was that it had to rescan the TI for the simulation of each location and therefore needed a tremendous amount of time and was therefore impractical. After that, several methods have been proposed, which can be classified into three main categories: (a) iterative algorithms, (b) probabilistic algorithms, and (c) pattern-based simulations. In the following discussion, the main features of these algorithms and their limitations are described.

14.3.1 Iterative Algorithms

There are a number of methods in optimization that are based on an iterative loop trying to find the global minimum/maximum in an objective function. In the following discussion, we briefly explain the algorithm used in an iterative framework that allows obtaining MPS realizations.

14.3.1.1 Artificial Neural Networks

Artificial neural networks (ANNs) are a branch of artificial intelligence that tries to fit a linear/nonlinear function on a set of data. This dataset can be pattern, hydraulic conductivity values, rainfall, etc., depending on the problem considered. More details about the ANNs and its applications can be found in Tahmasebi and Hezarkhani [49–53] and Asadisaghandi and Tahmasebi [3]. The first application of ANNs was proposed by Caers and Journel [5] in which multiple-point statistics are

inferred from a TI, and then an ANN is set to simulate values conditionally to these statistics. The results of this method are good, but it is very CPU demanding and has some problems related to network convergence. Also, in another study Caers and Ma [6] used ANNs for data integration. But, as indicated in Tahmasebi and Hezarkhani [52,53], ANNs need to be optimized with respect to its structural elements. In addition, the architecture should be optimized in order to prevent the network to be trapped in local minima.

14.3.1.2 Simulated Annealing

Simulated annealing is a powerful stochastic optimization method that has the ability, in theory, to find the global minima, and it is used in different fields of application. Deutsch [12] and Farmer [17] used this algorithm to reproduce some MPS properties. In their study, they consider an objective function that satisfies some constrains such as histogram and variogram. Furthermore, some researchers applied simulated annealing for simulation of categorical [27] and continuous [16] variables. However, simulated annealing has drawbacks, a major one being CPU time. Therefore, one can only consider a limited number of statistics as constrains, because increasing the number of constrains has a strong effect on CPU time. Also, this algorithm has a lot of parameters that should be tuned and therefore need a large amount of trial and error to achieve optimal values. Peredo and Ortiz [43] use speculative parallel computing to accelerate the simulated annealing; however, the computation times are still far from what is obtained with sequential simulation methods.

14.3.1.3 Gibbs Sampler

The Gibbs sampler [18] is a special case of the Metropolis algorithm. It is also based on drawing samples from a given distribution and having a rule for accepting or rejecting the new value. Lyster and Deutsch [31] used this method for modeling geological features. The method is similar to Markov approaches and realizations are obtained by resampling the values at each node in an iterative fashion until convergence. It is therefore extremely CPU demanding.

14.3.1.4 Markov Random Field

These models incorporate constraints by formulating high-order spatial statistics and enforcing them on the simulated domain using a Metropolis–Hastings algorithm [4,57]. In this case, the computational problem of the previous methods remains because the Metropolis–Hastings algorithm, although always converging in theory, may not converge in a reasonable time. Also, Tjelmeland and Eidsvik [56] used a sampling algorithm that incorporates an auxiliary random variable. All of these methods suffer from extensive CPU demand and instability in convergence. Also, the large structures cannot be reproduced finely, a series of factors that make them difficult to use for 3D applications.

14.3.2 Sequential Algorithms

14.3.2.1 Single Normal Equation Simulation

The main problem of the initial MPS idea of by Guardiano and Srivastava [21] was the need to scan the entire TI for each simulated node. Strebelle [48] proposed an innovative concept where the TI is scanned once and all the conditional probabilities for a given pixel configuration (template) are stored in a dynamic search tree data structure. Then, for the simulation of a new node, there is no need to rescan the TI and one can directly refer to this tree structure and retrieve the conditional probability. The single normal equation simulation (SNESIM) algorithm follows the framework of the traditional sequential algorithms based on a random path and uses the original data and previously simulated values. The main difference is that it uses statistics inferred from the TI instead of a variogram.

One of the problems of SNESIM is that the TI has to be categorical. However, one can divide a continuous TI into categories [47]. However, the method becomes very RAM demanding in the case of a high number of categories.

14.3.2.2 Integrated Methods

These methods combine different approaches. For example, Ortiz and Deutsch [41], under an assumption of independence of the different data sources, integrate the indicator method with MPS. Hence, instead of using a TI, the MPS properties are obtained directly from the available hard data (variogram) and integrated with the results of IK. Finally, a value is drawn from this new distribution. These methods were further investigated by Ortiz and Emery [40] and Hong et al. [25]. However, in most cases, final realization is highly influenced by the initial results of IK.

14.3.2.3 Improved Parallel Multiple-Point Algorithm Using a List Approach (Impala)

This method is the same algorithm as SNESIM, except that a list structure is used for storing the data events instead of the search tree [46]. The advantages are mainly computational, a list being much less computationally demanding than a tree. This is especially useful when dealing with large TIs containing a large number of categories. It was shown that the size of a tree grows exponentially with the TI complexity, whereas the size of a list grows linearly. Another advantage is that it is possible to efficiently parallelize a list, whereas it is very difficult with a tree structure.

14.3.2.4 Direct Sampling

This algorithm was proposed by Mariethoz et al. [35] and Mariethoz and Renard [34]. In this method, there is no need for pattern database. The basic principle is inspired from Shannon [45] and consists in a sampling of the TI conditional to a given pattern or data event. This data event does not need to have the same shape or the same number of neighbors for each simulated node. Since the TI is sampled directly, there is no need to construct a ccdf and also no need to store multiple-point statistics. The sampling of the TI is accomplished by defining a distance between the data event searched for and the one sampled. Using different types of distance allows dealing with categorical, continuous, or multivariate cases.

A first advantage is the very low RAM requirement of the method and also a relatively high computational efficiency. Other advantages are the result of the flexibility of the method in terms of the different data types that can be incorporated.

The algorithm can be summarized as follows: At each simulated node, a neighborhood is selected and a data event defined. Then, the TI is searched according to this data event and a similarity distance is calculated. As soon as the first occurrence of a matching data event in the TI is found (corresponding to a distance under a given threshold acceptance), the value of the central node of the data event in the TI is accepted and pasted in the simulation. If the algorithm finds a pattern that is similar up to a given threshold, the search is stopped. Otherwise, the most similar pattern found is selected and its central node is pasted.

A variation of the method using specific measures of distance between data events (transform-invariant distances) has been proposed [33], which allows using and combining elementary TIs to define the desired spatial patterns.

14.3.2.5 Cumulants

The cumulant approach is an extension of the variograms to account for higher-order statistics, beyond the two-point statistics. The advantage is that the cumulants can be directly inferred from the data rather than from TI. Dimitrakopoulos et al. [14] first used this method to simulate geological structures. As a result, they concluded that the choice of the cumulant appears to depend on the geological process, anisotropy, and pattern redundancy. Mustapha and Dimitrakopoulos [38] developed computer codes that calculate the higher-order cumulants and use them to model the complex spatially distributed natural phenomena [39]. The algorithm first computes the high-order statistics from the data, and only if not enough replicates could not be found, then a TI is used to find the conditional probabilities. One of the shortcomings is related to selecting the spatial cumulants and is different for each type of geological structures, and there is no general strategy for it.

14.3.2.6 Markov Mesh Model

Daly [9,10] used this model in a raster path. The idea is borrowed from texture synthesis. First, a casual template is put on a simulation node, and then the conditional probability is computed for each of the sequential nodes, progressing in a linear (or unilateral) order. Parra and Ortiz [42] used a similar methodology and obtained encouraging results. However, conditioning to hard and soft data still has issues due to the use of a raster path, making it difficult to reproduce the continuity near the hard data. Kjønsberg and Kolbjørnsen [28] used the probability from IK to modify the Markov mesh model (MMM), and they used an iterative algorithm in their method.

14.3.3 Pattern-Based Algorithms

Pixel-based algorithms can have problems to preserve the continuity of the geological structures. To palliate this, some pattern-based methods have been developed that are briefly introduced in the following text. Their commonality is that they do not simulate one pixel at a time, but paste an entire "patch" in the simulation. One of the main aims of using pattern-based simulation methods is their ability to preserve the continuity and overall structure.

14.3.3.1 Simulation of Pattern

This algorithm was introduced by Arpat and Caers [2] to address some of the limitations of SNESIM. This method uses the TI for finding the conditional probabilities and therefore the final pattern that should be pasted on at a data event location. The algorithm can be summarized as follows: First, the TI is scanned with a given template T and stored in a pattern database. Then, the locations to simulate are selected according to a random path. At each node, the data event is found. If the data event is empty and contains no hard data, then a patch from the TI is selected randomly. Otherwise, according to available known nodes and their distance to all of the patterns in pattern database, the most similar pattern is pasted on the data event. Then, the next node in the random path is simulated. This process continues until all nodes are visited. The results are very promising, but due to a high computational burden, this algorithm is not applicable for 3D applications.

14.3.3.2 Filter-Based Pattern Simulation

One of the main drawbacks of simulation of pattern (SIMPAT) is its CPU cost because for each node, one needs to compare a data event with all of the patterns in the pattern database. One possible solution is to use a redundancy algorithm to reduce both data event and comparison for finding the similar pattern. Zhang et al. [59] used a set of 6 and 9 filters in 2D and 3D simulation, respectively, which are used to summarize the basic spatial properties of the patterns contained in the TI. This allows to significantly reduce the dimensionality of the patterns. Therefore, filter-based pattern simulation (FILTERSIM) provides good reduction of CPU time. The patterns are first summarized using the predefined linear filters and, according to similarity criteria, grouped in distinct clusters. Then, for each cluster, a prototype pattern is computed that is the average of all the patterns in that cluster. The rest of the algorithm proceeds, at each node, by selecting the most similar prototype and randomly drawing a pattern from that cluster. This procedure is repeated for all locations to simulate. Therefore, due to the use of a limited number of filters, the CPU cost of this algorithm is reduced compared to SIMPAT.

The major issues related to FILTERSIM are that it uses a limited set of linear filters that cannot always convey all of the information and variability. Also, selecting the appropriate filters and several user-dependent parameters for each TI is another issue that is shared with many MPS methods.

14.3.3.3 Growthsim

Eskandari and Srinivasan [15] proposed a new TI-based algorithm mainly developed for dynamic data integration. The main feature of the method is that it starts the simulation from the data and

the simulated values "grow" from these initial seed locations. The method incorporates an optimal template definition. It is especially suited for the integration of transient flow and transport data in aquifer simulations.

14.3.3.4 Wavelet-Based Simulation

Gloaguen and Dimitrakopoulos [19] used wavelet analysis to simulate both categorical and continuous variables based on TIs. The dimensionality of the TI is reduced, in a similar fashion as with FILTERSIM. The wavelet bands can capture the spatial variability contained in the TI with a limited number of coefficients that correspond to different scales of variability. Then, these coefficients are used to classify the patterns. Whereas FILTERSIM bases the similarity on filter scores, this algorithm is based on wavelet coefficients. The algorithm can incorporate both hard and soft data.

The drawbacks of the method are that a lot of parameters have effect on both quality and CPU time and the modeler has to tune them in order to achieve good results in a reasonable time. This includes finding the wavelet decomposition level.

14.3.3.5 Distance-Based Pattern Simulation

This algorithm is a modification of SIMPAT that was introduced by Honarkhah and Caers [24]. It also incorporates some features of FILTERSIM such as pattern classification and inner patch. In this algorithm, the patterns in the database are represented as points in a Cartesian space using multidimensional scaling. Next, in a kernel space, the dimensionality of the patterns is reduced significantly, which leads to a better classification. Another advantage is that it is possible to expand the pattern's database by creating new patterns similar to the ones existing in the database. The rest of this algorithm is similar to FILTERSIM. This method produces acceptable results with good computation time, but is limited in terms of memory requirements when it comes to very large TIs.

14.3.3.6 Cross-Correlation-Based Simulation

The previous patch-based algorithms were based on a distance calculation. Tahmasebi et al. [55] proposed a methodology based on the cross-correlation function along a raster path. This algorithm can be summarized as follows: First, the algorithm selects a pattern randomly. Then, in a raster path, the data event is shifted and has an overlap with the previous one(s). At this point, the algorithm does not use the entire current data even for comparison, and the overlap regions(s) will only be used for finding the next similar pattern.

In this algorithm, there is no need to make a large pattern database and the selected pattern is directly pasted. Therefore, cross-correlation-based simulation (CCSIM) decreases the RAM demand significantly. Also, since CCSIM uses the overlap concept, it simulates the patterns very quickly. Moreover, it uses an adaptive template splitting that makes it more flexible than most other pattern-based simulation methods for conditioning. In this case, the algorithm first tries to find a pattern that can satisfy both continuity and hard data. If no such pattern can be found, the data event is divided and each of its parts is simulated simultaneously. This solution leads CCSIM to be highly adapted with inconsistent TIs with hard data. It can also select at the beginning of the simulation a large template size to capture the large-scale features in the TI. The comparative results of CCSIM with the previous MPS methods show an improvement in terms of both CPU time and quality. Furthermore, for more acceleration, it is possible to use this method in the Fourier domain [54].

14.4 Examples

14.4.1 First Example

The first example is devoted to a 3D simulation. The used TI is shown in Figure 14.1 and represents complex and continuous channels. The challenge is to reproduce channel connectivity and

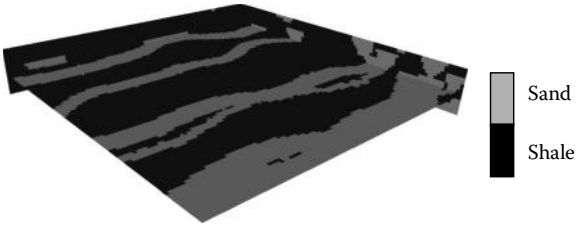

FIGURE 14.1 The used 3D TI for MPS simulation.

distribution. To this end, SNESIM, FILTERSIM, and CCSIM algorithms were are tested and the results are shown in Figure 14.2.

The results are presented in Figure 14.2. One of the primary aims of using the MPS methods is in this case to integrate the geological and morphological data as very important sources of information. It can be seen that CCSIM is better able to capture the connectivities and major aspects of the channels than the other two methods considered. These characteristics are essential for flow and transport models, and their reproduction constrains the uncertainty of quantities such as contaminant estimates.

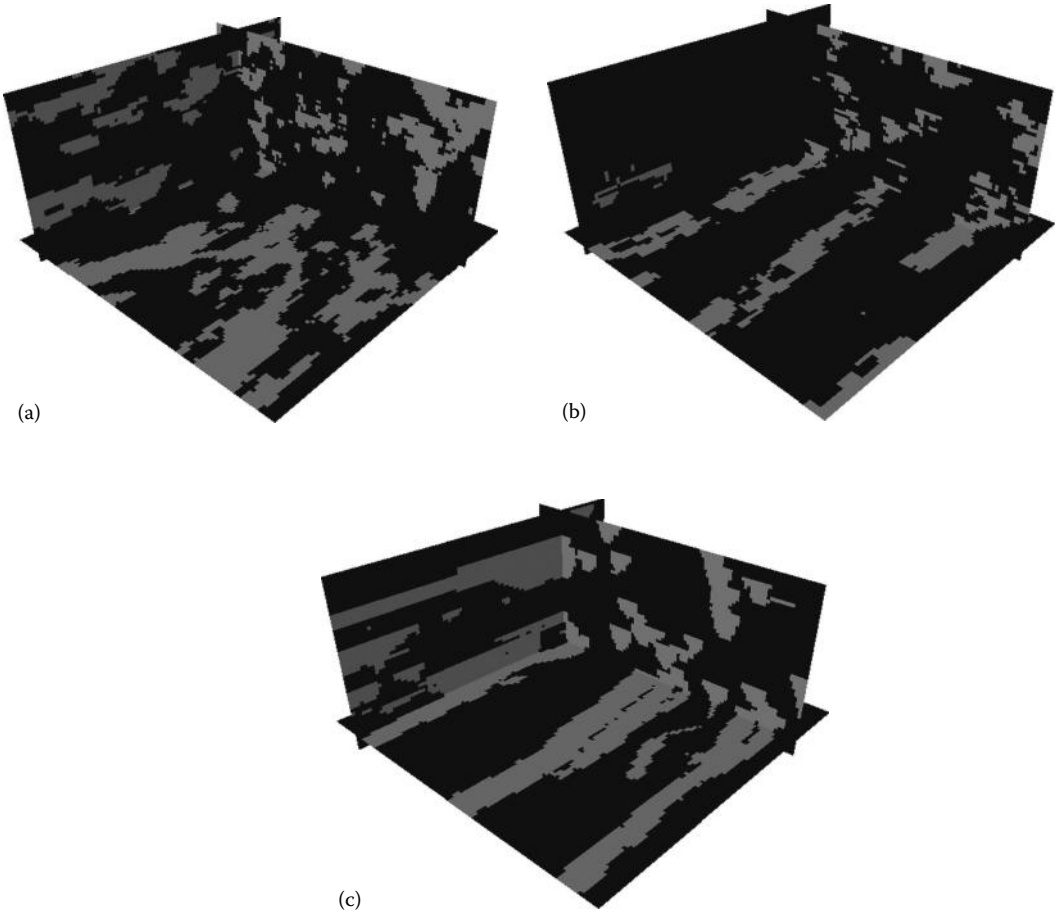

FIGURE 14.2 Results of application of (a) SNESIM, (b) FILTERSIM, and (c) CCSIM for unconditional simulation of the proposed TI in Figure 14.1.

14.4.2 Second Example

In this next example, we test the ability using two-point statistical criterion, uncertainty quantification, hard data conditioning, and flow modeling. The used TI is shown in Figure 14.3. This TI represents a complex hydrological setting with specific channeling characteristics. Two-point geostatistical simulation will be tested and compared.

The results of different simulation methods are shown in Figure 14.4. The methods used in this example are SGSIM, FILTERSIM, and CCSIM. Since the given example is continuous, the SNESIM algorithm is not applicable. The simulation is performed in both unconditional and conditional modes.

Since SGSIM assumes a Gaussian distribution in grids and different nodes, connected channels and structures do not appear with in this algorithm because several points would be needed to represent them. The results using FILTERSIM show a better result than SGSIM. However, these results could be improved by using a lot of clusters and prototypes. This would however be a cumbersome task, and the current choice of filters yields results that do not capture the full variability and connectivity of the TI. Also, it is worth noting that the CPU cost of this method is very high compared to previous methods. Finally, the result of CCSIM represents a better realization where the channels are better connected.

The variogram reproduction of realizations obtained with FILTERSIM and CCSIM is shown in Figure 14.5. Both methods show a similar variogram, with a slightly worse fit for FILTERSIM. This figure shows that low-order statistics are not sufficient to differentiate between models. Therefore, it can be concluded that the results also need to be checked visually. Another verification method can be flow simulation by which one is able to find a model that can show a better flow behavior. This simulation is used in the next example.

The next step is the conditional simulation in which some point of the grid is known and should be preserved during the simulation. Usually, it is a good idea to consider a scenario as a reference image (RI) by which the simulation results can be compared. In synthetic studies, this image is used during the simulation from which the hard data are extracted. The final simulation can be compared with the RI. The RI is generated using CCSIM and shown in Figure 14.6. According to this figure, it is clear that the RI is rich and complex enough to be used in conditional simulation. We picked 110 points randomly form the RI and considered them as hard data. The extracted hard data that should be preserved and reproduced are shown in Figure 14.7. Furthermore, Figure 14.8 shows the conditional simulations. Different methods produced different results that one can easily compare it with the RI in Figure 14.6. One effect of using hard data is to constrain the simulation and decrease the uncertainty. This is represented by the E-type of 50 realizations for different methods shown in Figure 14.9.

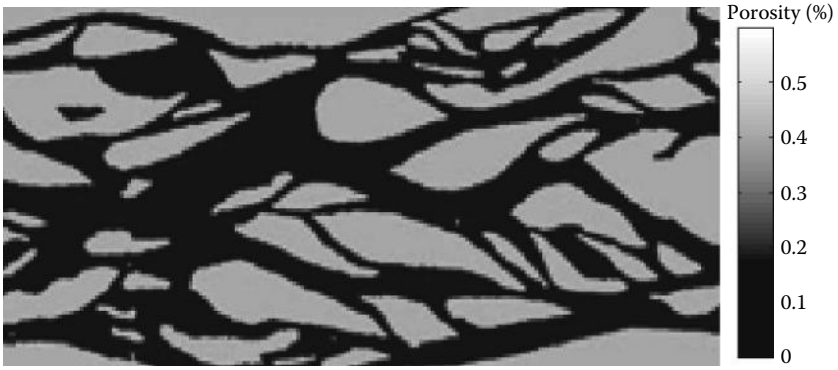

FIGURE 14.3 The used TI for MPS simulation. [44]

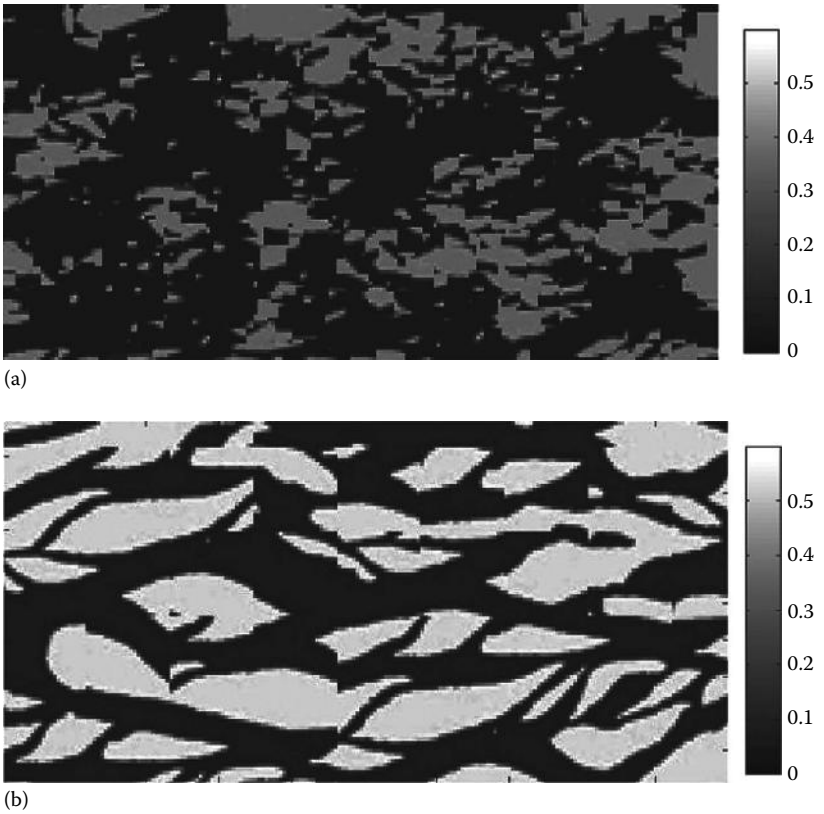

FIGURE 14.4 Results of application of (a) FILTERSIM and (b) CCSIM for unconditional simulation of the proposed channels in Figure 14.3.

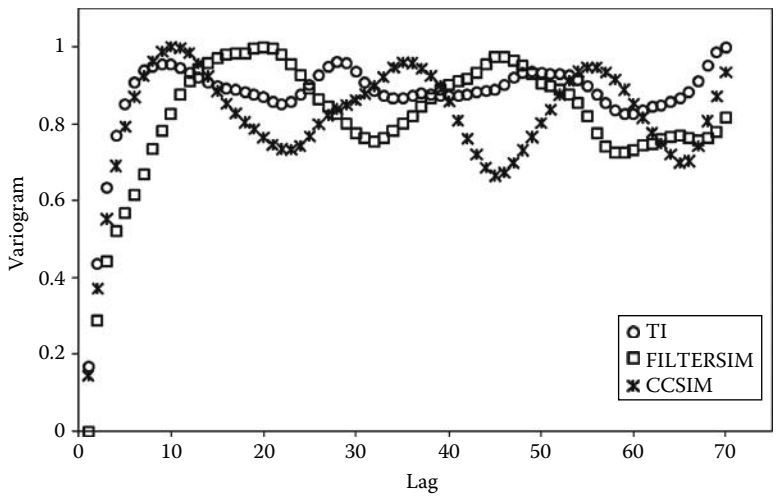

FIGURE 14.5 Comparison of the obtained realizations for variogram reproduction.

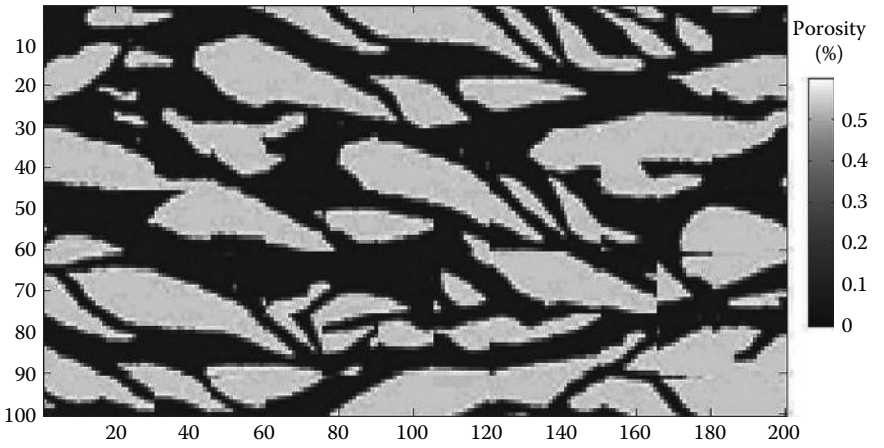

FIGURE 14.6 The RI, which is used for conditional simulation and is obtained by unconditional CCSIM.

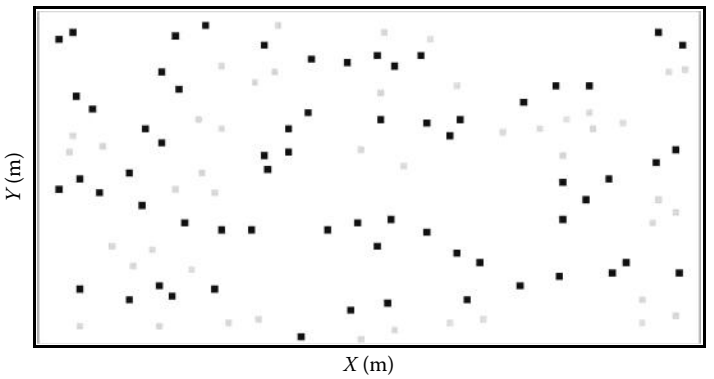

FIGURE 14.7 The location of hard data, which is used for conditional simulation.

The presented E-type maps in Figure 14.9 show that the SGSIM and FILTERSIM methods produce large uncertainty rather than the CCSIM. One reason can be due to large differences between the produced realizations that let them to be very different, and therefore the final E-type map will be different with the RI. With a bit attention to the presented E-type map of CCSIM, it is clear that this method seems to produce close and/or the target RI that lead the E-type map to be close to RI.

According to the presented E-type maps in Figure 14.9, one can see that due to poor ability of SGSIM and FILTERSIM algorithms in pattern reproduction, the hard data seem to be similar to dark or white points that they just have been reproduced and are not associate with a specific patterns, while because of using an adaptive recursive pattern splitting algorithm in CCSIM, it is able to find the appropriate patterns and make the final realizations to be close to the RI. All of these abilities will let the algorithm to quantify and subsequently decrease the uncertainty.

The final test that we will use is the flow modeling by which one is able to see another difference between the produced realizations between different methods.

Most of the previous comparisons show that the realizations can reproduce the lower-order statistical descriptors. But the spatial flow simulation offers a better test for quality checking, because in this test the spatial connectivities can affect in fluid behavior. Therefore, we did a two-phase flow simulation on a high-resolution-obtained 2D grid consisting of 100×200 grid cells, respectively. The size of each grid cell is assumed to be $100 \times 100 \times 50$ (m) long X, Y, and Z directions. Also, the porosity are varied from

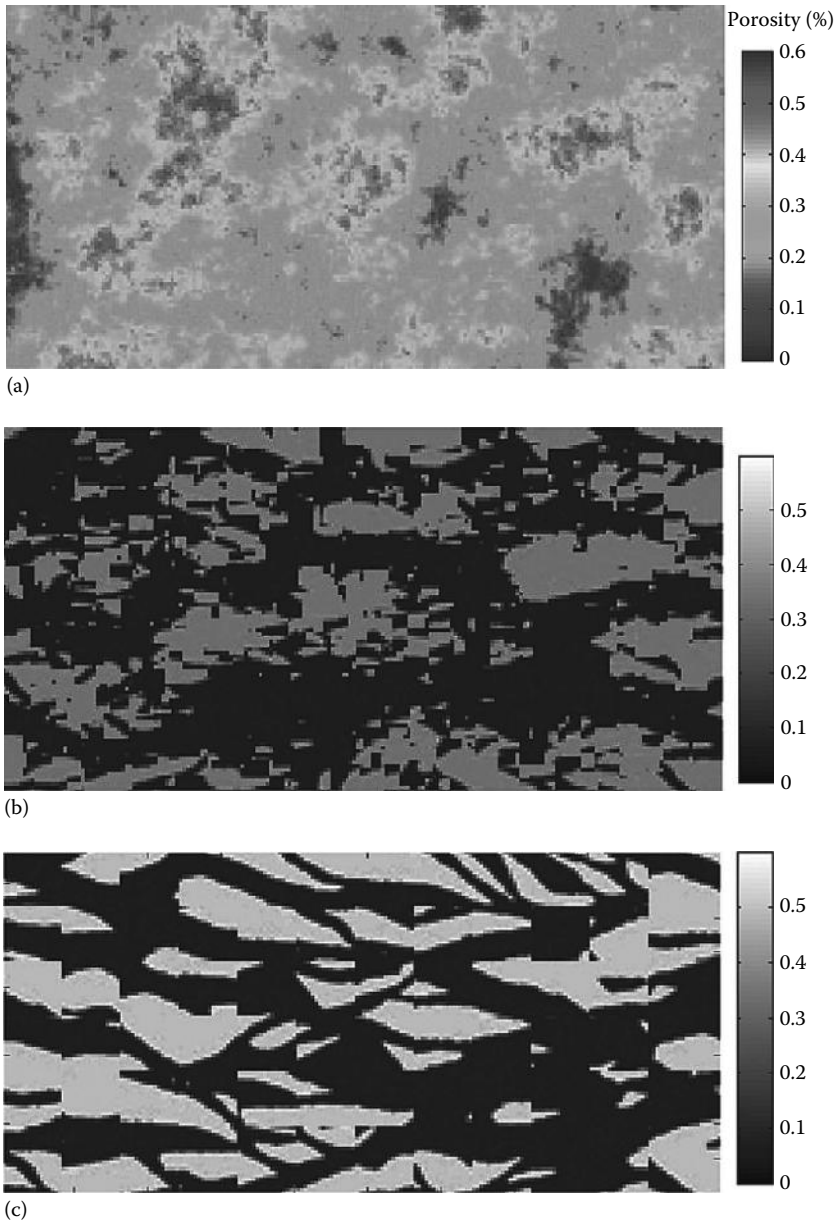

FIGURE 14.8 Results of application of (a) SGSIM, (b) FILTERSIM, and (c) CCSIM for conditional simulation with the shown hard data in Figure 14.7.

0 to 0.6 (%) and the permeability varied from 5 to 1150. Also, no flow conditions were used at boundaries. Injection and production start at the beginning of reservoir.

The results for different algorithms are presented in Figure 14.10. As mentioned earlier, evaluating different algorithms for two-phase flow prediction can be used as a reliable test to discriminate the performance of MPS algorithms. According to the obtained results, any mistake in flow properties can make some serious problems for forecasting, management, appraisal, and even any possible location that a well can be drilled. For example, a wrong prediction of reservoir water cut can lead us to predict the first water production at the production wells mistakenly. Therefore, one of the results

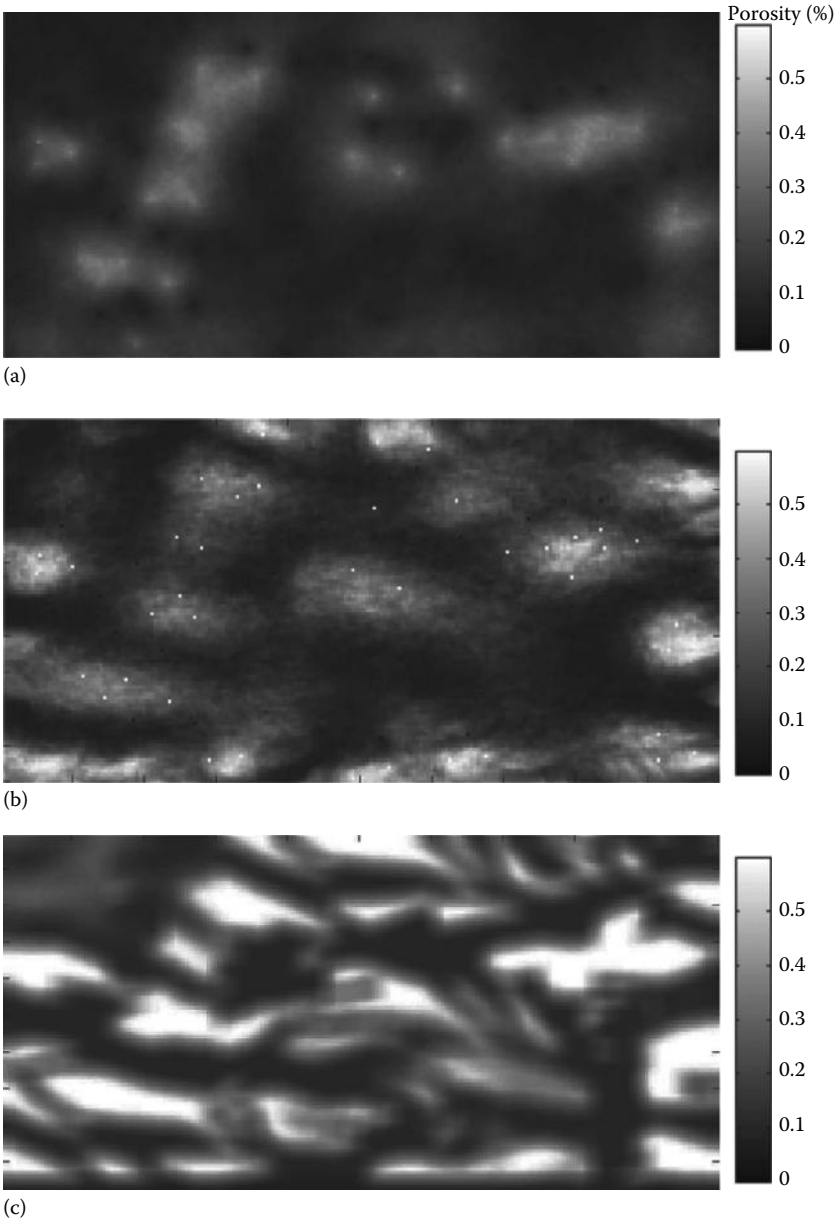

FIGURE 14.9 E-type maps of (a) SGSIM, (b) FILTERSIM, and (c) CCSIM for 50 realizations of conditional simulation.

of this study is decreasing the uncertainty. Also, the results of water cut are presented in Figure 14.11, which approve the previous results.

14.5 Summary and Conclusions

Due to necessity of modeling complex and more realistic structures and more accurate uncertainty quantification, advanced modeling methods are increasingly used. Most of the traditional geostatistical simulations are based on two-point statistics such as variogram. However, these methods are not able to

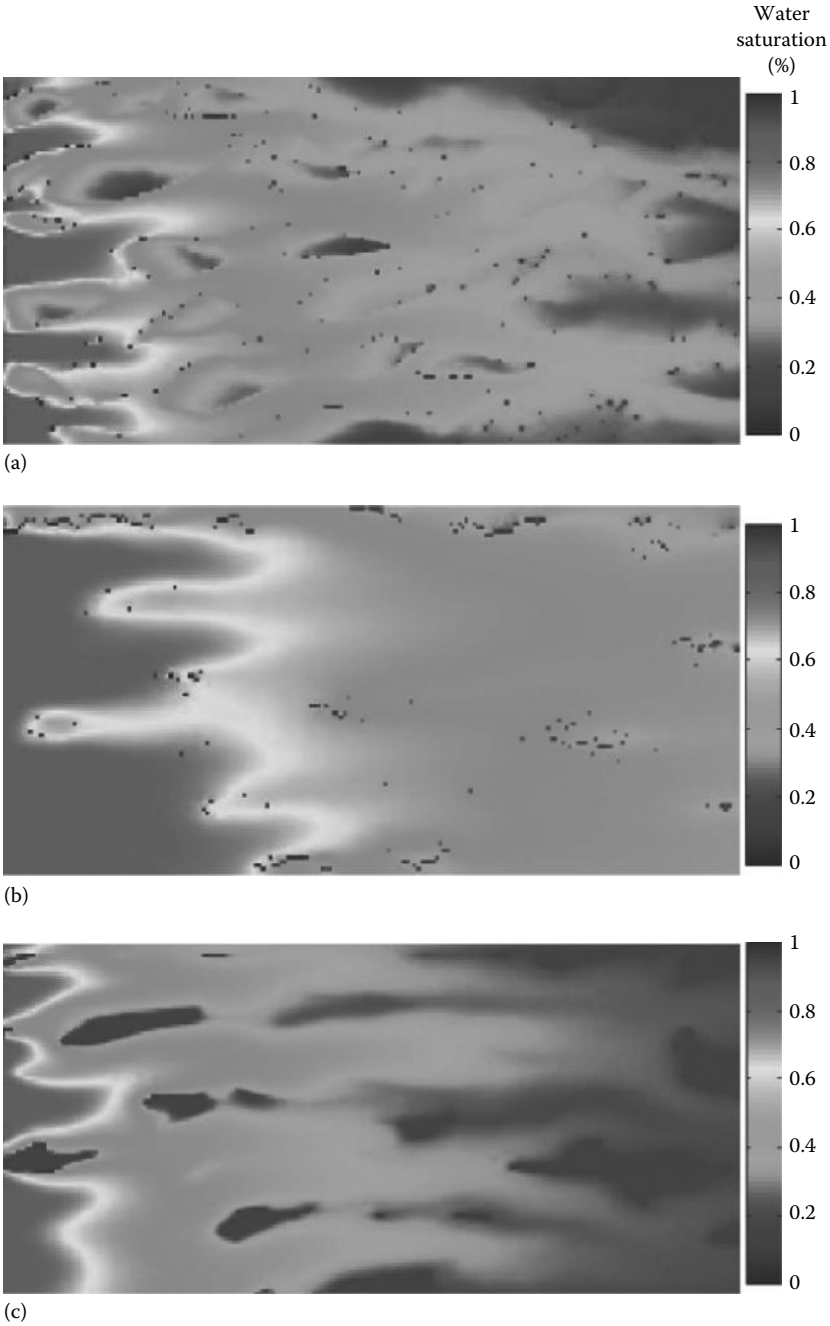

FIGURE 14.10 The graphical results of flow simulation (water saturation) for (a) RI, (b) FILTERSIM, and (c) CCSIM.

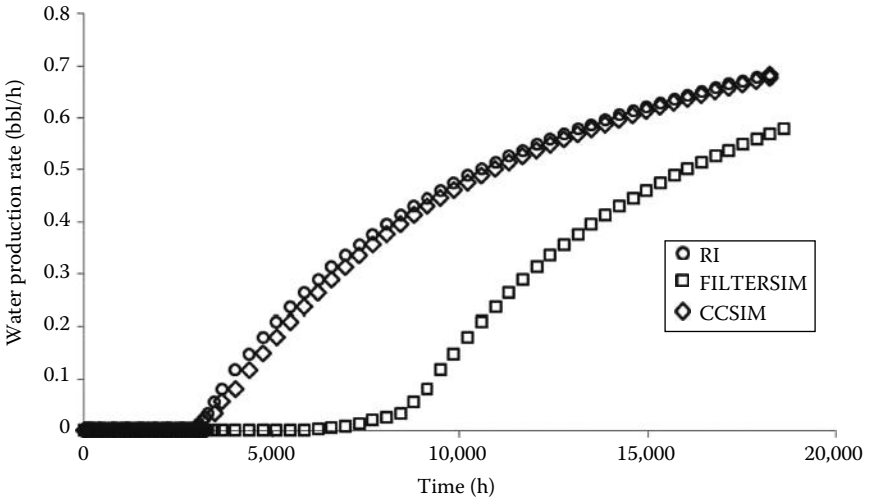

FIGURE 14.11 Comparison of water production rate of RI, FILTERSIM, and CCSIM.

reproduce enough the complex structures and subsequently lead the final model to be less accurate. The idea of using a TI is simple and appealing. Instead of direct inference of conditional probabilities from the available data, one can use the replicates or event in the TI. In essence, the probability scheme was replaced by patterns and several algorithms were proposed.

In this chapter, we reviewed several methods that use MP in their algorithm and tried to compare their performance in two examples. Different MPS algorithms have their individual advantages. For example, the SNESIM algorithm is fast and performs well to model categorical images, while this algorithm has RAM limitation when using large TIs with more than four facies. Also, this algorithm is not able to model the continuous images and geological phenomena such as continuous satellite images or rock thin sections. The SIMPAT algorithm can model both categorical and continuous images finely while it needs tremendous amount of time. To this end, the FILTERSIM algorithm uses a set of linear filters to reduce the dimensionality of the patterns, resulting in a significant acceleration. The distance-based pattern simulation (DisPat) algorithm modifies the FILTERSIM with a multidimensional scaling framework to first transfer the patterns into that dimension and next uses a kernel framework to cluster the pattern similar to FILTERSIM. In this chapter, the results were not compared with this method. Finally, due to lack of connectivity and CPU time, the CCSIM algorithm that uses the advantage of low computational cost of cross-correlation can accelerate the current algorithms and increase the quality of the final realizations. It also benefits from an adaptive recursive template splitting which can improve the conditional simulation.

There are shortcomings and issues that should be addressed in the future works. Most of the current MPS methods are designed for stationary TIs, and they should use some extra features such as considering different regions for simulation or an auxiliary variable to guide the simulation. Through the multigrid approach, one can consider large structures in the simulation grid, but it seems that this method transfers the upper nodes as a conditional point to its lower grids and makes some problems. Also, most of the current MPS methods are limited to the patterns available in the TI. Finally, due to a large uncertainty in TI, it is necessary to design methods able to determine which TI to use in a given context.

References

1. Anderson J.A. 1974. Diagnosis by logistic discriminate function: Further practical problems and results. *J. R. Stat. Soc. C Appl. Stat*. 23: 397–404.

2. Arpat B. and J. Caers. 2007. Stochastic simulation with patterns. *Math. Geol*. 39: 177–203.
3. Asadisaghandi J. and P. Tahmasebi. 2011. Comparative evaluation of back-propagation neural network learning algorithms and empirical correlations for prediction of oil PVT properties in Iran oilfields. *J. Petrol. Sci. Eng*. 78: 464–475.
4. Besag J. 1974. Spatial interaction and the statistical analysis of lattice systems. *J. R. Stat. Soc. B Methodol*. 36: 192–236.
5. Caers J. and A. Journel. 1998. Stochastic reservoir simulation using neural networks trained on outcrop data. In *SPE ATCE Proceedings*, New Orleans, LA, Number SPE 49026, Society of Petroleum Engineers, September.
6. Caers J. and X. Ma. 2002. Modeling conditional distributions of facies from seismic using neural nets. *Math. Geol*. 34: 143–167.
7. Caers J. 2005. *Petroleum Geostatistics*. Society of Petroleum Engineers, Richardson, TX.
8. Chilès J.P. and P. Delfiner. 1999. *Geostatistics: Modeling Spatial Uncertainty*. Wiley, New York.
9. Daly C. and C. Knudby. 2007. Multipoint statistics in reservoir modeling and in computer vision. In *Petroleum Geostatistics*. European Association of Geoscientists and Engineers, Cascais, Portugal.
10. Daly C. 2004. Higher order models using entropy, Markov random fields and sequential simulation. In Leuangthong, O. and Deutsch, C.V. (eds.), *Geostatistics Banff 2004*. Springer, Dordrecht, the Netherlands, pp. 215–224.
11. Deutsch C.V. and L. Wang. 1996. Hierarchical object-based geostatistical modeling of fluvial reservoirs. Paper SPE 36514 presented at the *1996 SPE Annual Technical Conference and Exhibition*, Denver, CO, October 6–9.
12. Deutsch C. 1992. Annealing techniques applied to reservoir modeling and the integration of geological and engineering (well test) data. PhD thesis, Stanford University, Stanford, CA, p. 306.
13. Deutsch C.V. and A.G. Journel. 1998. *GSLIB*: *Geostatistical Software Library and User's Guide*, 2nd edn. Oxford University Press, New York.
14. Dimitrakopoulos R., H. Mustapha, and E. Gloaguen. 2010. High-order statistics of spatial random fields: Exploring spatial cumulants for modeling complex, non-Gaussian and non-linear phenomena. *Math. Geosci*. 42: 65–100.
15. Eskandari K. and S. Srinivasan. 2010. Reservoir modeling of complex geological systems—A multiple-point perspective. *J. Can. Petrol. Tech*. 49: 59–68.
16. Fang J.H. and P.P. Wang. 1997. Random field generation using simulated annealing vs. fractal-based stochastic interpolation. *Math. Geol*. 29: 849–858.
17. Farmer C.L. 1990. Numerical rocks. In King, P.R. (ed.), *The Mathematical Generation of Reservoir Geology*. Clarendon Press, Oxford, U.K., pp. 22–33.
18. Geman S. and D. Geman. 1984. Stochastic relaxation, Gibbs distributions and the Bayesian restoration of images. *IEEE Trans. Patt. Anal. Mach. Intell*. 6: 721–741.
19. Gloaguen R. and R. Dimitrakopoulos. 2009. Two-dimensional conditional simulations based on the wavelet decomposition of training images. *Math. Geosci*. 41: 679–701.
20. Goovaerts P. 1997. *Geostatistics for Natural Resources Evaluation*. Oxford University Press, New York, p. 483.
21. Guardiano F. and M. Srivastava. 1993. Multivariate geostatistics: Beyond bivariate moments. In Soares, A. (ed.), *Geostatistics-Troia*. Kluwer Academic, Dordrecht, the Netherlands, pp. 133–144.
22. Haldorsen H.H. and E. Damsleth. 1990. Stochastic modeling. *J. Petrol. Tech*. 42: 404–412.
23. Holden L., R. Hauge, O. Skare, and A. Skorstad. 1998. Modeling of fluvial reservoirs with object models. *Math. Geol*. 30: 473–496.
24. Honarkhah M. and J. Caers. 2010. Stochastic simulation of patterns using distance-based. *Math. Geosci*. 42: 487–517.
25. Hong S., J. Ortiz, and C. Deutsch. 2008. Multivariate density estimation as an alternative to probabilistic combination schemes for data integration. In Ortiz, J.M. and Emery, X. (eds.), *Geostats 2008 Proceedings of the Eighth International Geostatistics Congress*, Vol. 1. Gecamin Ltda., Santiago, Chile, pp. 197–206.

26. Journel A.G. and C.J. Huijbregts. 1978. *Mining Geostatistics*. Academic Press, London, U.K.
27. Journel A.G. 1974. Geostatistics for conditional simulation of ore bodies. *Econ. Geol*. 69: 673–687.
28. Kjønsberg H. and O. Kolbjørnsen. 2008. Markov mesh simulations with data conditioning through indicator kriging. *Proceedings of the Eighth International Geostatistics Congress*, Santiago, Chile.
29. Krige D.G. 1951. A statistical approach to some basic mine valuation problems on the Witwatersrand. *J. Chem. Metall. Mineral. Soc. South Africa* 52: 119–139.
30. Lantuéjoul C. 2002. *Geostatistical Simulation: Models and Algorithms*. Springer, Berlin, Germany, p. 232.
31. Lyster S. and C. Deutsch. 2007. Artifacts near conditioning data in MPS Gibbs sampling. In: *Centre for Computational Geostatistics* September, Alberta University, Canada.
32. Mallet J.L. 2002. *Geomodeling*. Oxford University Press, New York, p. 624.
33. Mariethoz G. and B.F.J. Kelly. 2011. Modeling complex geological structures with elementary training images and transform-invariant distances. *Water Resour. Res*. 47: W07527.
34. Mariethoz G. and P. Renard. 2010. Reconstruction of incomplete data sets or images using direct sampling. *Math. Geosci*. 42: 245–268.
35. Mariethoz G., P. Renard, and J. Straubhaar. 2010. The direct sampling method to perform multiple-point simulations. *Water Resour. Res*. 46: W11536.
36. Matheron G. 1971. The theory of regionalized variables and its applications. No. 5 in Les cahiers du Centre de morphologie mathe matique de Fontainebleau. *Ecole Nationale Superieure des Mines*, Paris, France.
37. Matheron G. 1973. The intrinsic random functions and their applications. *Adv. Appl. Prob*. 5: 439–468.
38. Mustapha H. and R. Dimitrakopoulos. 2010a. High-order stochastic simulation of complex spatially distributed natural phenomena. *Math. Geosci*. 42: 457–485.
39. Mustapha H. and R. Dimitrakopoulos. 2010b. A new approach for geological pattern recognition using high-order spatial cumulates. *Comput. Geosci*. 36: 313–334.
40. Ortiz J.M. and X. Emery. 2005. Integrating multiple point statistics into sequential simulation algorithms. In Leuangthong, O. and Deutsch, C.V. (eds.), *Geostatistics Banff 2004*. Springer, Dordrecht, the Netherlands, pp. 969–978.
41. Ortiz J.M. and C.V. Deutsch. 2004. Indicator simulation accounting for multiple-point statistics. *Math. Geol*. 36: 545–565.
42. Parra A.J.M. and J.M. Ortiz. 2011. Adapting a texture synthesis algorithm for conditional multiple point geostatistical simulation. *Stoch. Environ. Res. Risk Assess*. 13: 1–11.
43. Peredo O. and J. Ortiz. 2010. Parallel implementation of simulated annealing to reproduce multiple-point statistics. *Comput. Geosci*. 37: 1110–1121.
44. Renard P. 2007. Stochastic hydrogeology: What professionals really need? *Ground Water* 45: 531–541.
45. Shannon C.E. 1948. A mathematical theory of communication. *Bell Syst. Tech. J*. 27: 379–423.
46. Straubhaar J., P. Renard, G. Mariethoz, R. Froidevaux, and O. Besson. 2011. An improved parallel multiple-point algorithm using a list approach. *Math. Geosci*. 43: 305–328.
47. Strebelle S. and T. Zhang. 2005. Non-stationary multiple-point geostatistical models. In Leuangthong, O. and Deutsch, C.V. (eds.), *Geostatistics Banaff 2004*, Vol. 14 of *Quantitative Geology and Geostatistics*. Springer, Dordrecht, the Netherlands, pp. 235–244.
48. Strebelle S. 2002. Conditional simulation of complex geological structures using multiple-point geostatistics. *Math. Geol*. 34(1): 1–22.
49. Tahmasebi P. and A. Hezarkhani. 2009. Application of optimized neural network by genetic algorithm. *IAMG'09*, Stanford University, Stanford, CA.
50. Tahmasebi P. and A. Hezarkhani. 2010a. Comparison of optimized neural network with fuzzy logic for ore grade estimation. *Aust. J. Basic Appl. Sci*. 4: 764–772.

51. Tahmasebi P. and A. Hezarkhani. 2010b. Application of adaptive neuro-fuzzy inference system for grade estimation; case study, Sarcheshmeh porphyry copper deposit, Kerman, Iran. *Aust. J. Basic Appl. Sci*. 4: 408–420.
52. Tahmasebi P. and A. Hezarkhani. 2011a. Application of a modular feedforward neural network for grade estimation. *Nat. Resour. Res*. 20: 25–32.
53. Tahmasebi P. and A. Hezarkhani. 2012b. A hybrid neural networks-fuzzy logic-genetic algorithm for grade estimation. *Comput. Geosci*. 42: 18–27.
54. Tahmasebi P. Caers, J. and M. Sahimi. 2013. Fast pattern simulation based on accelerated multi-scale cross-correlation. *Computers and Geosciences*.
55. Tahmasebi P., A. Hezarkhani, and M. Sahimi. 2012. Multiple-point geostatistical modeling based on the cross correlation functions. *Comput. Geosci*. 16: 779–797.
56. Tjelmeland H. and J. Eidsvik. 2004. Directional metropolis-Hastings updates for posteriors with non linear likelihood. In Leuangthong, O. and Deutsch, C.V. (eds.), *Geostatistics Banff 2004*. Springer, Dordrecht, the Netherlands, pp. 95–104.
57. Tjelmeland H. 1996. Stochastic Models in reservoir characterization and Markov random fields for compact objects. PhD dissertation, Norwegian University of Science and Technology, Trondheim, Norway.
58. Viseur S. 1999. Stochastic Boolean simulation of fluvial deposits: A new approach combining accuracy with efficiency. In *SPE ATCE Proceedings*, Houston, TX, October, Society of Petroleum Engineers
59. Zhang T., P. Switzer, and A. Journel. 2006. Filter-based classification of training image patterns for spatial simulation. *Math. Geol*. 38: 63–80.

15

GIS Applications in a Changing Climate

Mohammed Matouq
Al-Balqa Applied University

Hussam Al-Bilbisi
University of Jordan

Tayel El-Hasan
Mutah University

Saeid Eslamian
Isfahan University of Technology

AUTHORS

Mohammed Matouq is a professor of chemical engineering at Al-Balqa Applied University. Now Matouq is in sabbatical leave at the University of Jordan and published two research reports in ISO 14001, and more than 50 articles in the field of chemical reaction engineering, water resources management, environmental management systems, and climate change in Jordan. He has participated in several international conferences and workshops conducted by NATO, UN, and ECO-ASIA, APEC.

Hussam Al-Bilbisi is an associate professor who received his PhD in remote sensing and GIS from the Center for Environmental Remote Sensing, Chiba University, Japan. He has more than 30 publications in the field of GIS, and is the coauthor of some books. He is a member in Japan Society of Photogrammetry Remote Sensing, Remote Sensing Society of Japan, and Jordanian Geologists Association. He is a referee for the following Journals: *International Journal of Remote Sensing*, *International Journal of Digital Earth* and *Asian Journal of Geoinformatics*.

Tayel El-Hasan is a professor in geology at Mutah University, Jordan. He has participated in more than 30 international conferences and is a reviewer for many scientific journals and had supervised many graduate students.

Saeid Eslamian received his PhD from the University of New South Wales, Australia with Professor David Pilgrim. He was a visiting professor in Princeton University, USA, and ETH Zurich, Switzerland. He is currently an associate professor of hydrology in Isfahan University of Technology. He is the founder and chief editor of *Journal of Flood Engineering* and *International Journal of Hydrology Science and Technology*. He has published more than 200 publications mainly in statistical and environmental hydrology and hydrometeorology.

PREFACE

This chapter will deal with applying the GIS technique in the field of climate change in practical ways. Figures will be used to demonstrate the GIS application in weather data analysis meanly rainfall or temperatures for a certain location to build up geographic maps indicating the changes in weather condition in a certain period of time. The chapter will demonstrate a country case study like Jordan to build up the model for investigating the climate change in a region like the Middle East. All features of Arc View, Arc Map, and Arc Catalogue will be demonstrated in this chapter.

15.1 Introduction

15.1.1 Definition of GIS

Geographical Information System (GIS) is a particular kind of software program that runs on personal computers. In many ways, it resembles a database program as it analyzes and relates information stored as records, but with one crucial difference: each record in a GIS database contains information used to draw a geometric shape. GIS applications allow users to query, analyze, and edit spatial information and to create maps that present the results of these operations [1].

GIS is a frontier branch of science, which integrates space science, survey and mapping science, geography, information science, computer science, environmental science, and management science. The GIS is not only capable of managing data, text information and graph but also of integrating and analyzing spatial data from different sources, with diverse formats, structures, projections, or resolution levels with the aid of a computer. Thus, it is a new and effective technical system in complex processing and analysis of spatial data [5,12].

One of the great insights of GIS is that there is a vast difference between seeing data in a table of rows and columns and seeing it presented in the form of a map. The difference is not simply esthetic; it is conceptual—it turns out that the way you see your data has a profound effect on the connections you make and the conclusions you draw from it. A GIS visually represents the data in any field of a map file, as differing shades of color, as symbols of different sizes, as data pattern of varying density, or in other ways.

The GIS performs various functions, namely, data capture, data management, data manipulation and analysis, and the presentation of results in both graphic and report form, with a particular emphasis on preserving and utilizing inherent characteristics of spatial data. The GIS stores two types of data found on a map: the geographical definitions and the attributes or qualities of those features. There are two broad methods used to store such data in a GIS: raster and vector [5].

15.1.1.1 Raster

A raster is a grid-based representation of data where spatial features and attributes are merged into a unified data file. Each cell (pixel) describes the condition of space at that location; each cell has a numeric value:

- Feature identifier
- Qualitative attribute code (categories differ in kind rather than quantity)
- Quantitative attribute

The quality of a raster image is determined by the total number of pixels (resolution) and the amount of information in each pixel (often called color depth).

15.1.1.2 Vector

Vector layers are composed of points, which are linked to form the lines and areal boundaries of polygons. The points are encoded with latitude and longitude (X, Y) coordinates. Vector representation is feature orientated as they describe features, spatially referenced entities with distinct boundaries.

15.1.2 Brief History of GIS

Two-dimensional GIS began in the computer aided mapmaking in the 1960s, and now it has gone deep into every application field. It is essentially based on an abstract symbolic system, so it cannot provide the original feeling of nature to people, and it is difficult to overcome the shortcoming [4]. However, three-dimensional GIS can solve the problem. With the development of Virtual Reality technology, the concept of "digital earth" has been put forward and three-dimensional GIS become a new technology to promote spatial analysis and expand information representation in GIS. By processing elevation data, three-dimensional GIS can display the landform and objects in three dimensions to create an obvious scene. This display usage can also meet the demand for management, analysis, estimation, decision, and visualization.

The 1960s saw many new forms of geographic data and mapping software. Within computer cartography, the first basic GIS concepts were developed during the late 1950s and 1960s. Linked software modules, rather than standalone programs, preceded GISs. Early influential data sets were the World Data Bank files. The vector topological arc/node data started at the Harvard University GIS was significantly altered by both the PCs and the WSs. During the 1980s, new GIS S/W could better exploit more advanced H/W. User interface developments led to GISs vastly improved during the 1990s [7].

15.2 Components of GIS

The GIS is a computer system for collecting, storing, manipulating, and displaying geographic information. There are many definitions for GIS. However, the major characteristics are the geographic (spatial) analysis functions that provide means for deriving new information based on locations. The GIS integrates hardware, software, and data for capturing, managing, analyzing, and displaying all forms of geographically referenced information. It stores information about the world as a collection of thematic layers that can be linked together geographically. The GIS allows viewing, interpreting, and visualizing data in many ways that reveal relationships, patterns, and trends in the form of maps [9].

The GIS performs various functions, namely, data capture, data management, data manipulation and analysis, and the presentation of results in both graphic and report form, with a particular emphasis on preserving and utilizing inherent characteristics of spatial data:

- The computer system (hardware and operating system).
- The software (Learning the concepts, capabilities, limitations, and interface of GIS software have educational value in itself). The GIS is a tool that is increasingly being used in diverse fields of work, from local government to global scientific research.
- Spatial analysis is the most important function of the GIS, which makes it distinct from other computer-based graphics software. The spatial analysis provides the functions such as spatial interpolation, buffering and overlay operations, and network analysis.
- Data management and analysis procedures: After data are collected and integrated, the GIS provides facilities for effective data management, which include data integrity, storage and retrieval, maintenance and updating abilities.
- The people to operate the GIS.
- The methods or the process for getting data into the computer. This is one of the most important step and we can say: *GIS without data as Car without fuel*

15.3 Geospatial Tools for Climate Change

The GIS has been applied in climate change related studies such as land cover and land use change, glacier and snow cover mapping and modeling, air quality mapping, and modeling relationships between climate change and increasing natural hazards and the influence of extreme weather events on

livelihoods. GIS enables to visualize the changes and its interlinkages in the form of maps so that gaps and priority areas can be easily identified. The GIS is extensively used for making inventories and mapping and monitoring vegetation, glaciers, and snow cover across landscapes, in order to better understand the impact of climate change. The geospatial technology provides powerful tools for decision making related to climate change adaptation, allowing us to measure, model, and monitor, manage, and mitigate its impacts. To avoid a dramatic disruption of society due to climate change, it is imperative that geospatial technology is in place to manage and minimize the many inevitable impacts.

Recently, Geographical Information Systems (GIS) have been used to understand the impacts of global change at the global, regional, and local scales by utilizing a broad range of social, economic, and climate data and by combing this data with up-to-date information from earth observation satellites [2,3,8]. There are a lot of applications of GIS; one of them is using it in the development of weather processing system by integrating weather data into GIS [4,6,10,11]. Display of meteorological data: The first goal in GIS Meteorology is to convert meteorological data and information to "GIS negotiable" formats. The following table summarizes the relationships of weather data to GIS formats (or shape), but it is not intended to be exhaustive.

15.3.1 Spatial and Attribute Data in GIS for Climate Change

ARC GIS is in general used here to predict the impact of global warming and climate change on a certain country, and we chose here for simplicity the Hashemite Kingdom of Jordan (here we call it Jordan).

Arc GIS consist of the following:

- Arc catalog
- Arc map
- Arc tool box
- Arc scene
- Arc global
- Work station
- Desktop administration
- Arc reader

15.4 Arc Catalog

15.4.1 Arc Catalog and Its Application for Climate Change

An arc catalog is used to prepare the coordinate system and entering the spatial data, and an arc map is used to make layers, editing and doing the treatment on the produced map. Here are the steps you need to take to prepare for maps related to climate change taking into consideration that all weather parameters such as temperatures, rainfalls, and humidity are ready and tabulated in the form of an excel file. Another important step is to have the digital map for the study area where the impact of climate change is to be studied. Here, Jordan is selected as an example to apply climate change impact.

In this chapter and in order to give the reader a better idea for GIS application in climate change and step by step, certain regions will be introduced here as sample of study for this application. The Hashemite Kingdom of Jordan (Jordan) is a typical example for this study. Jordan has Geographic coordinates of 31°00′N36°00′E/31.000°N36.000°E/31.000;36.000 and it is situated geographically in Southwest Asia, south of Syria, west of Iraq northwest of Saudi Arabia. The major characteristic of the climate is the contrast between a relatively rainy season from November to April and very dry weather for the rest of the year. With hot, dry, uniform summers and cool, variable winters during which practically all of the precipitation occurs, the country has a Mediterranean-style climate.

15.4.1.1 Steps in Preparing Maps for Climate Change Using GIS

1. The first step to start with GIS is to open Arc catalog to create a geodatabase. Create a file in your hard disk in a certain location, that is, drive C, D, E … etc., and this will be the starting point to your project in climate change (Table 15.1).
2. Start to create a new personal geodatabase (Figure 15.1).
3. Begin to create layers or feature class (geodata set) (Figure 15.2). At this stage, you may choose a suitable geometric shape for your project depending on your data, line, point, and polygon, for example four layers created here such as temperature, rainfall, wind, and humidity (Figures 15.3 and 15.4).
4. Change the precision and scale to be consistent with the data you have (Figure 15.5).
5. After saving your data then, you may close the Arc catalog, and open the Arc map, to start data input after simply importing layers for the location or area you are supposed to study from the arc catalog and then you need to save it into a new file of data in your computer (see Figures 15.6 and 15.7).
6. Insert the digital map that you have here; we chose Jordan digital map (see Figure 15.8) on arc map. Locate the stations that related information to your study target, that is, all other weather information like temperature, rainfall, humidity, wind speed, pressure, and so on, to match with weather stations that you have to locate on your specified map in the form of digital type. In this step by knowing the altitude and elevation for each weather station, it can be located as point in the map and all other weather information will be loaded on this point.

15.4.1.2 Steps Involved in Creating GIS Maps from Available Weather Data

The data should be inserted on the map according to the following steps:

- By right clicking on the layer where data need to be inserted, choose the button (open attribute table) (Figure 15.9).
- The table with the field that is added in arc catalog can now be seen. The data entry will be very easy even if your raw data were saved in the form of Microsoft excel. (see Figure 15.10.)

After the data are entered, right click on the tool bar and choose the button 3D (Figure 15.11),

Then choose from 3D, *create/modify tin*, then *create tin from feature* (Figure 15.12),

After that choose the layer that you started to work on, as it is demonstrated next, for example humidity, and then select the year you started to work in (Figures 15.13 and 15.14).

After data are entered, the software will start to simulate all data saved for that specified year and the final shape can be seen as in Figure 15.15.

The contour line can be changed from tin lines by clicking on *3D* and choosing *surface analysis* and then *contour* (Figure 15.16).

TABLE 15.1 Steps Needed to Change Weather Data to GIS Formats

Shape	Weather Data Type
Point	Surface observation, rain gage, river gage, pilot reports, model grid point data, lightning, tropical cyclone position
Line	Contours, fronts, rivers and river stage, roads and road conditions, air parcel trajectories
Polygon	Radar, watch/warning boxes, area/zone forecasts, plumes (air parcels)
Image	Satellite images, charts
Grid object	Intermediate objects for all data on a surface. Surfaces include constant height (e.g., MSL), constant pressure (isobaric), and constant potential temperature (isentropic).

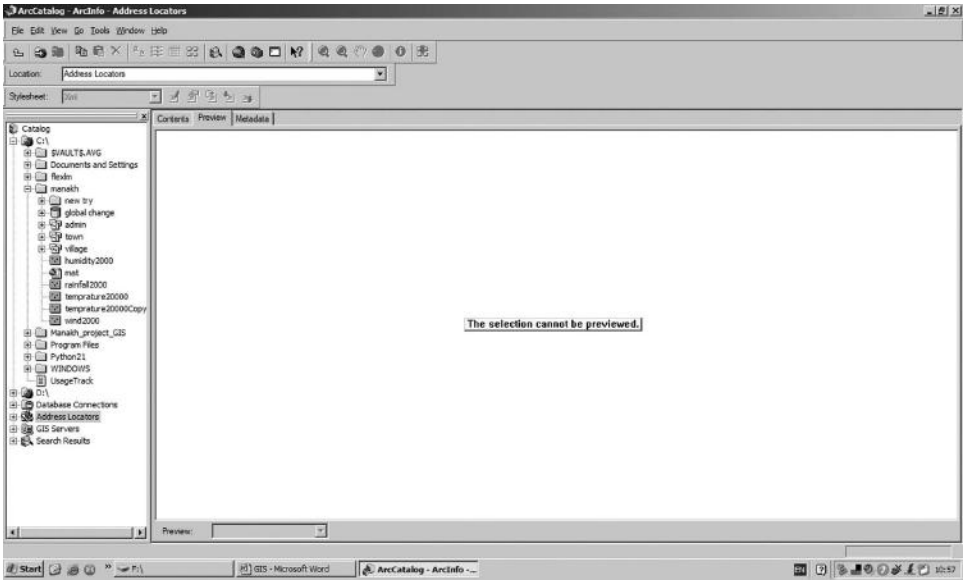

FIGURE 15.1 Arc catalog outlook.

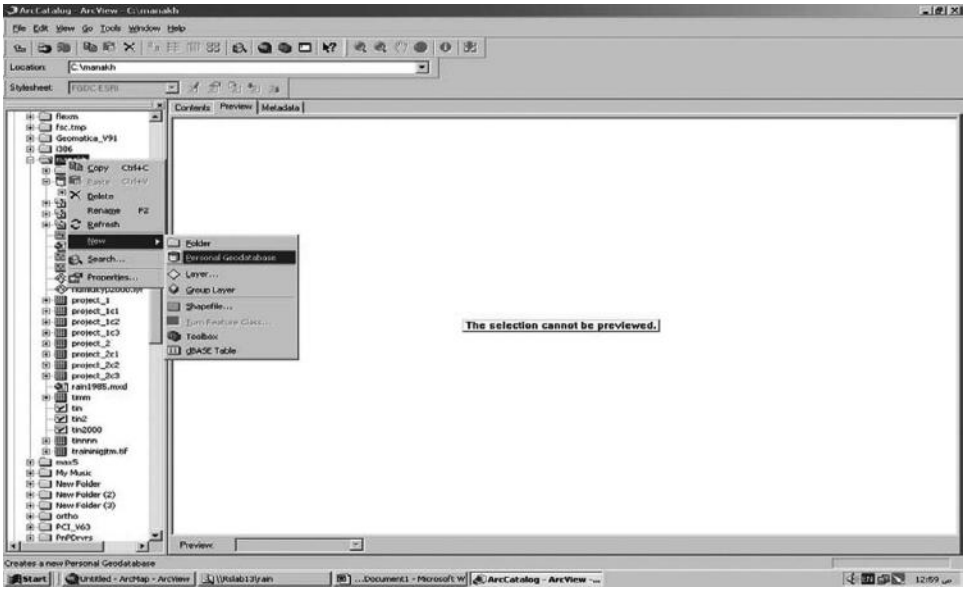

FIGURE 15.2 Geodatabase.

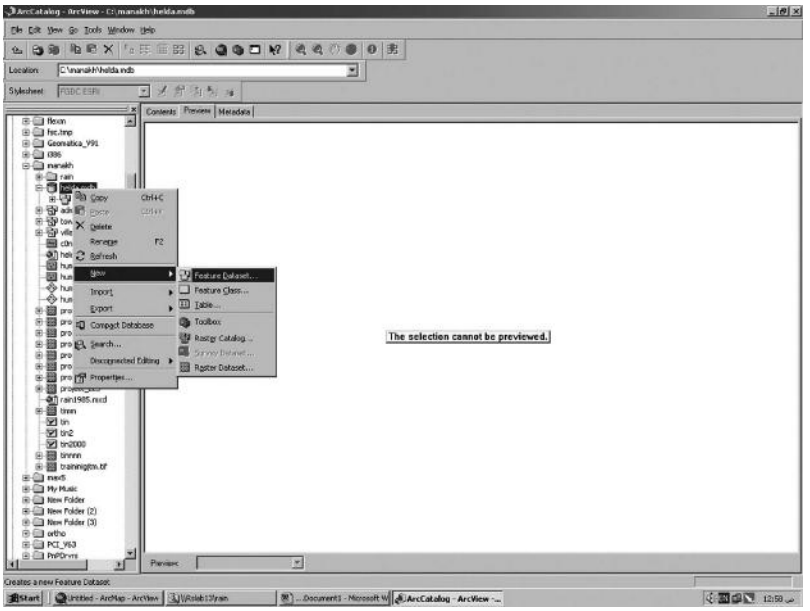

FIGURE 15.3 Create layers or feature class in geodata set.

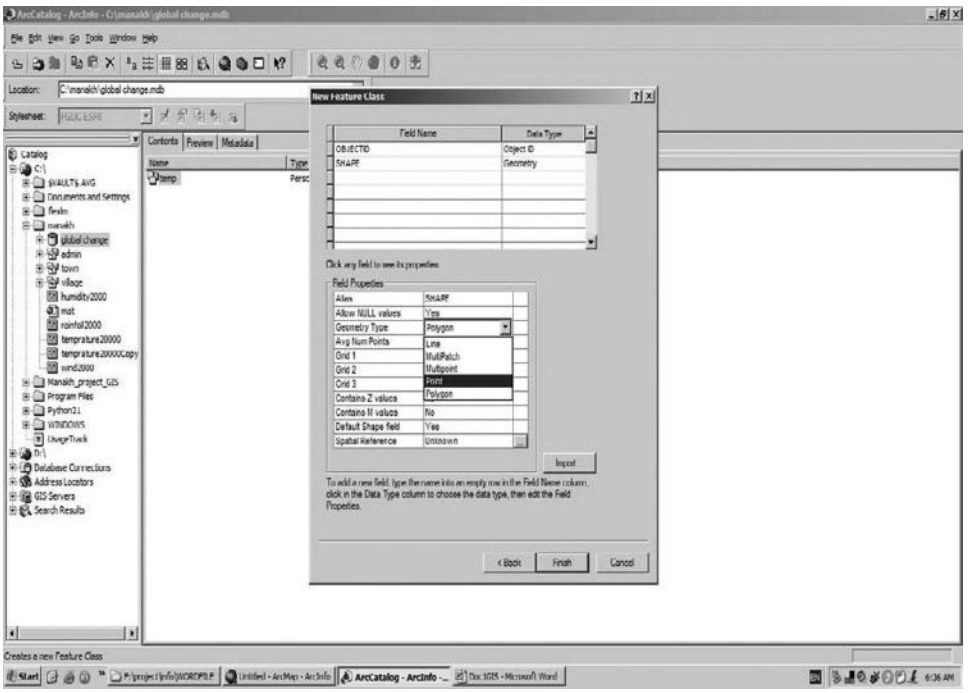

FIGURE 15.4 Establishing a suitable geometry shape for the weather project.

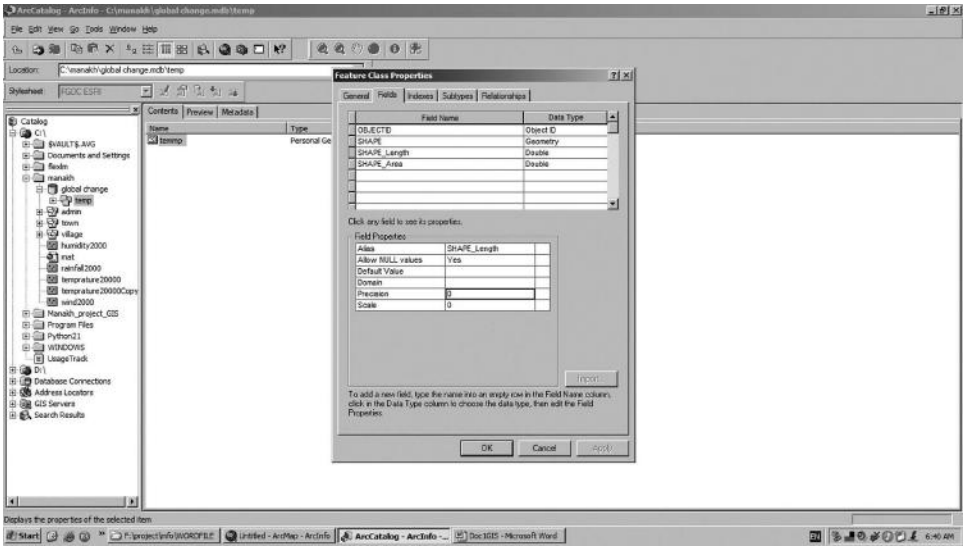

FIGURE 15.5 Starting the precision and scale with the data.

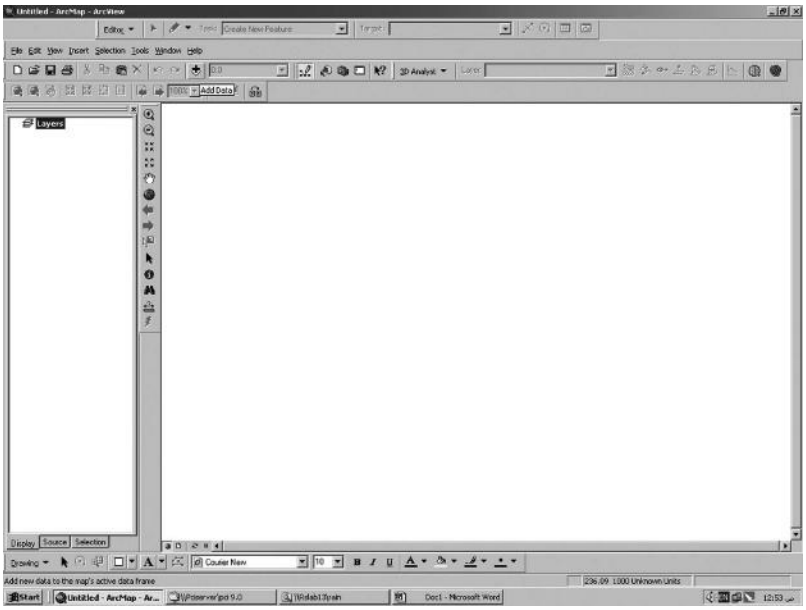

FIGURE 15.6 Arc map outlook and start weather data input.

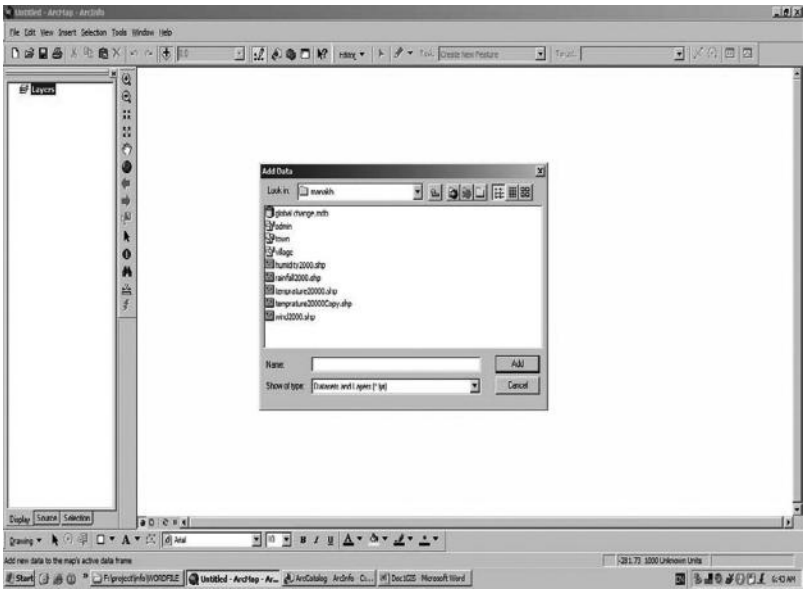

FIGURE 15.7 Weather data input.

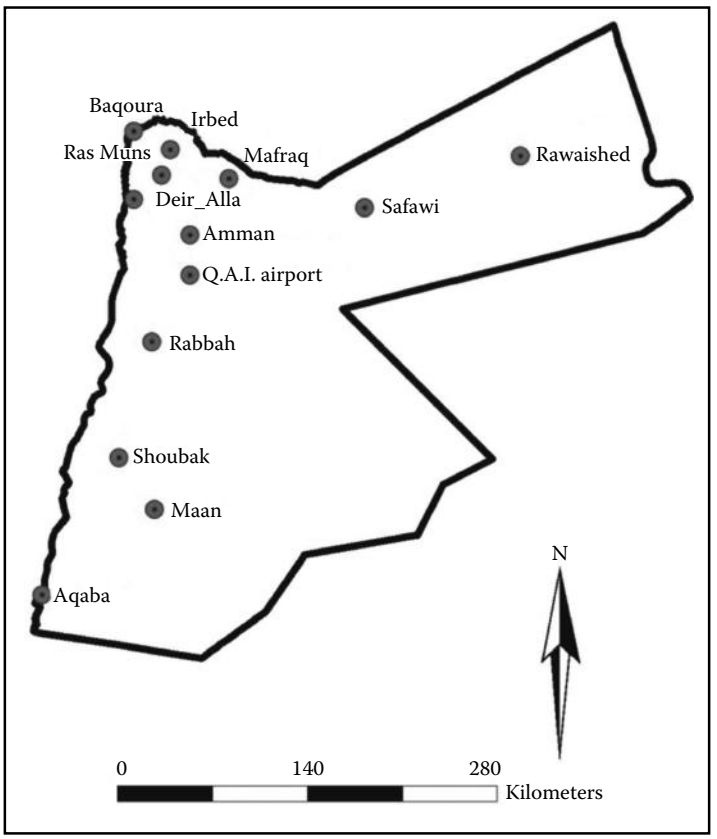

FIGURE 15.8 Jordan digital map. (Courtesy of Royal Jordan Geography Center, Amman, Jordan.)

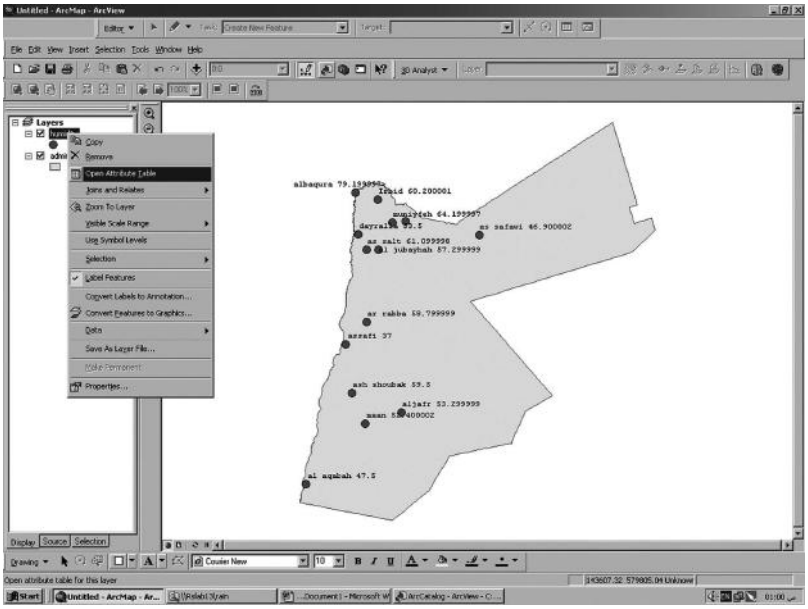

FIGURE 15.9 Insert digital map and layers on the map.

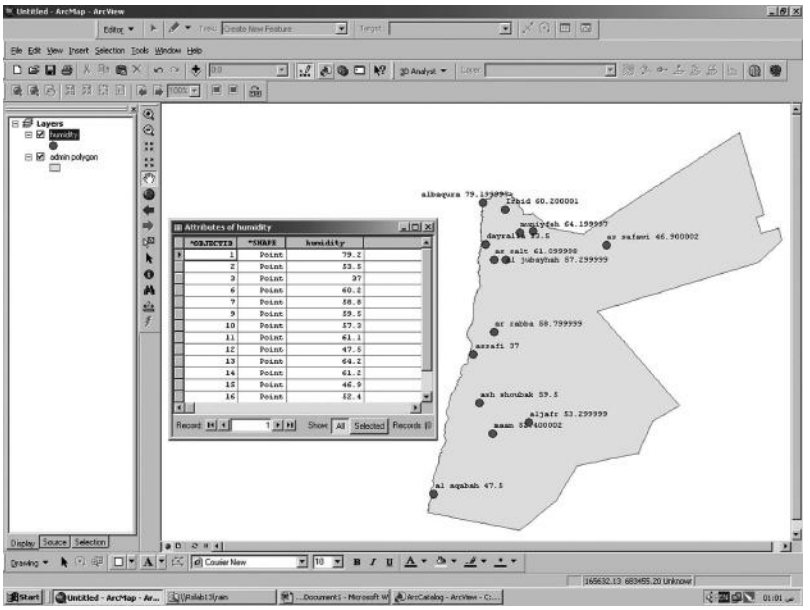

FIGURE 15.10 Weather data input, for example, humidity.

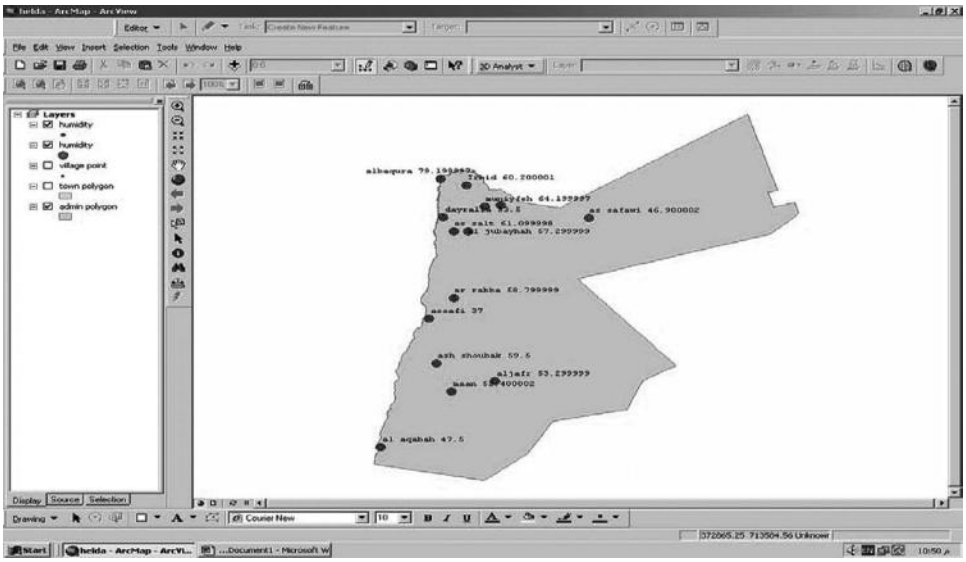

FIGURE 15.11 Data outlook after input on arc map.

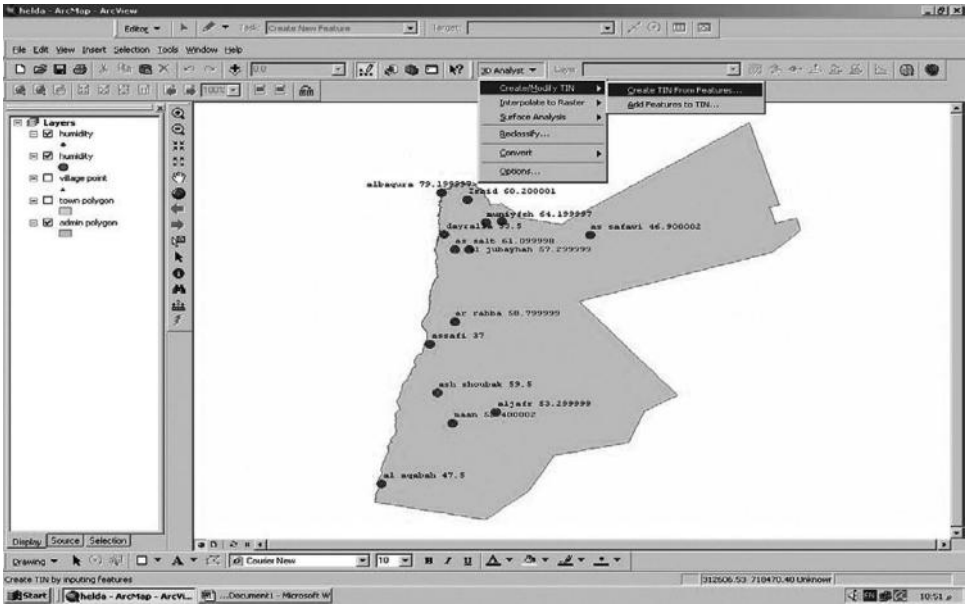

FIGURE 15.12 Introducing the concept of 3D form.

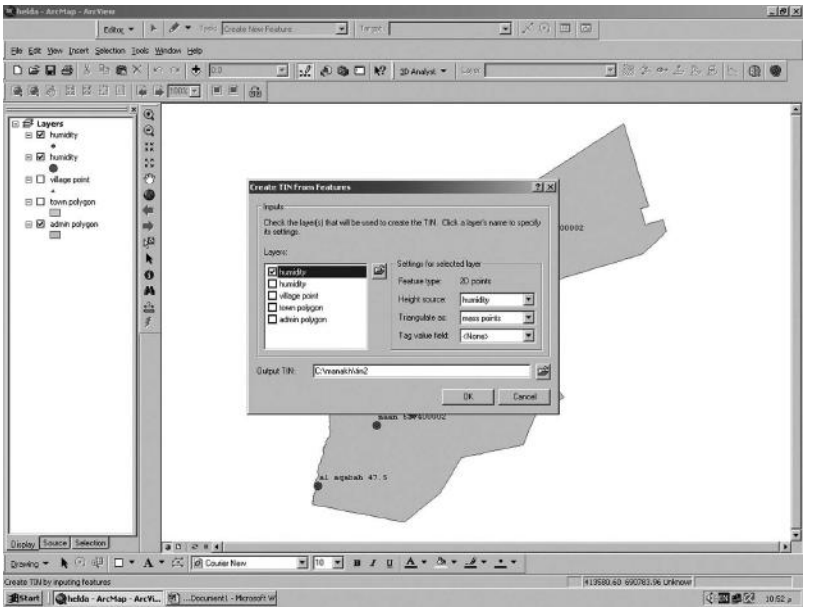

FIGURE 15.13 Choosing the layer to start work on, for example, humidity.

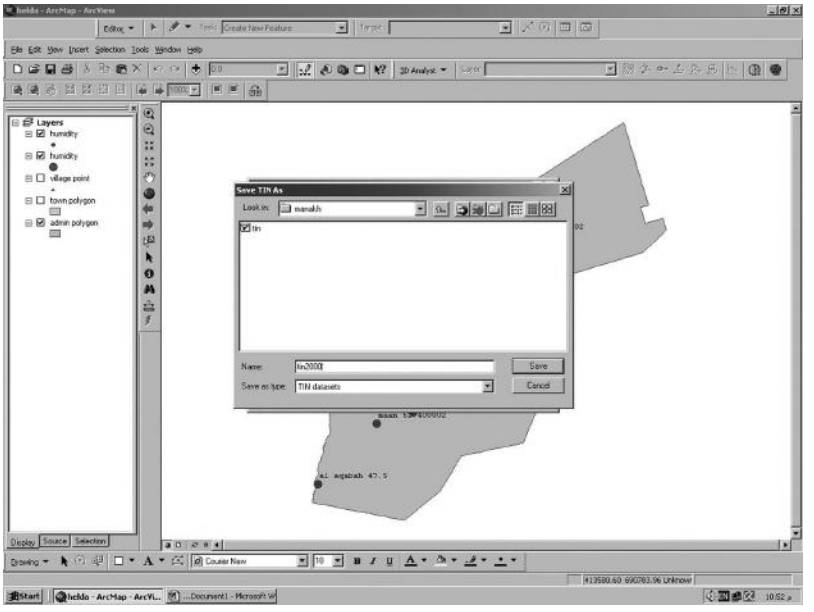

FIGURE 15.14 Year selection to work on to specify the time period.

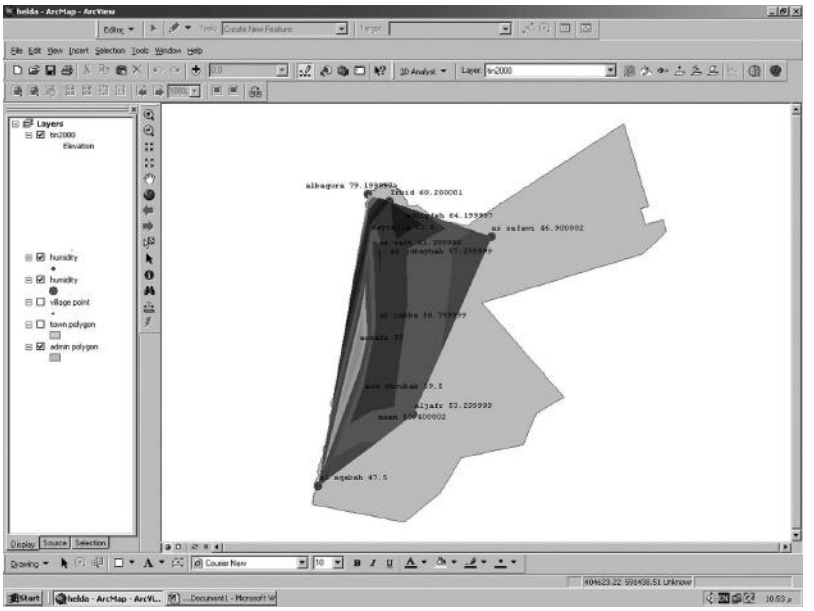

FIGURE 15.15 The final shape after data were entered.

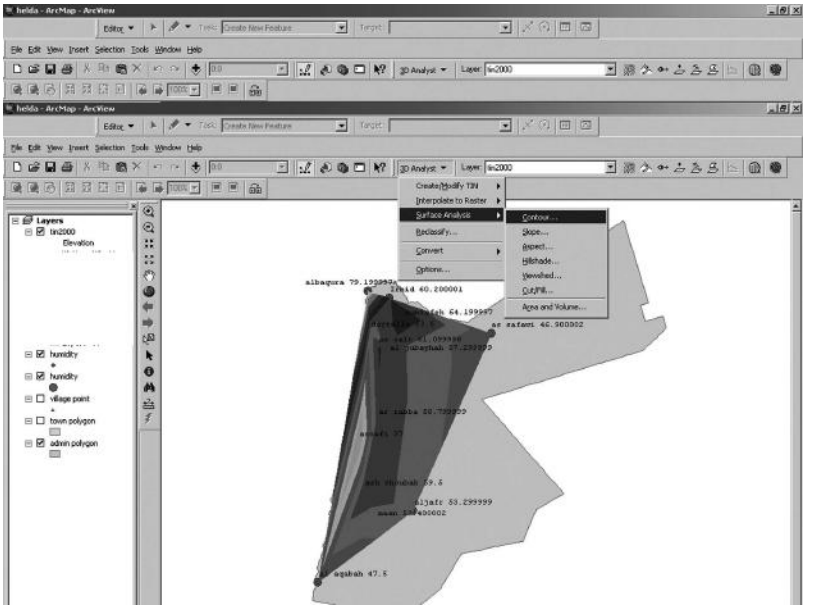

FIGURE 15.16 GIS software will start to simulate and analyze by choosing *surface analysis* and then *contour*.

Choose suitable interval for contour lines, say for example 50, and save the data (Figure 15.17).

The contour map will look like the map in Figure 15.18.

Then all lines need to be treated by GIS, to get the final shape as seen in Figure 15.19.

Then these lines will be analyzed and connected according to the contour lines for the same value; for ease each contour line can be assign a certain color to generate different zones or regions (Figure 15.20).

This will be the same procedure for other weather parameters; you need to change only data from humidity to temperature or rainfall, for example. From these maps, now it is easy to study the effect of

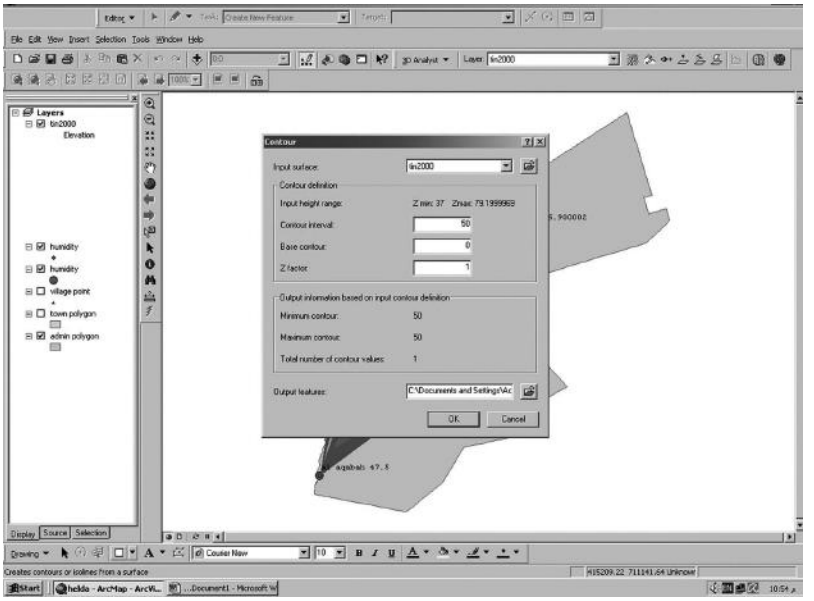

FIGURE 15.17 Choosing suitable interval for contour lines.

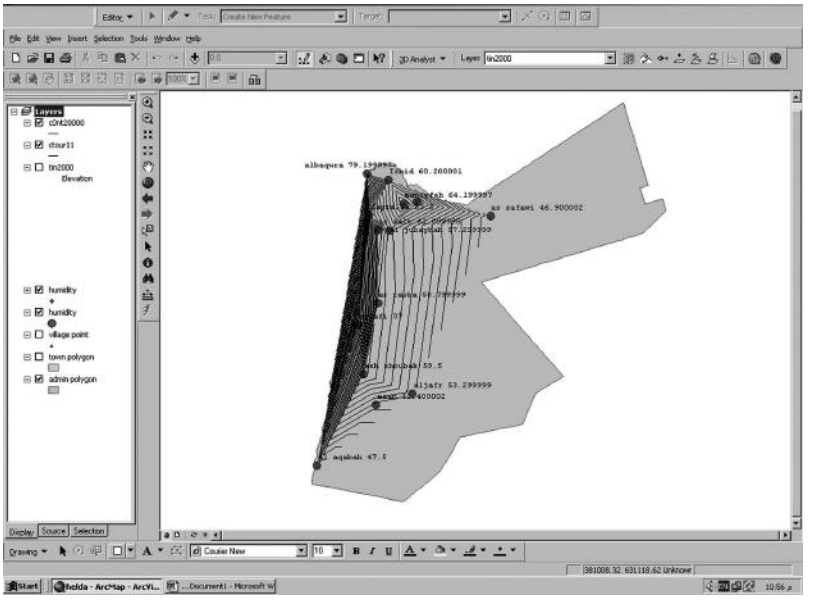

FIGURE 15.18 Final shape for contour map.

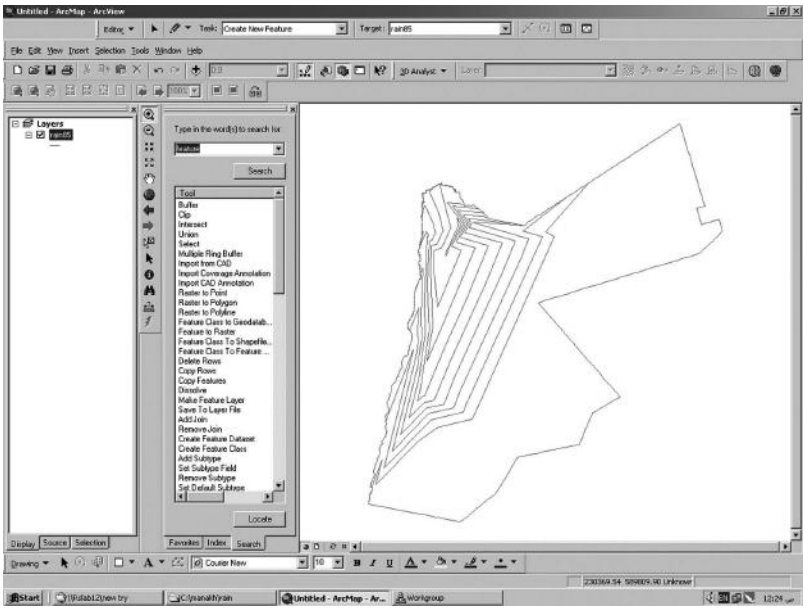

FIGURE 15.19 Final shape for contour lines after treating with GIS software.

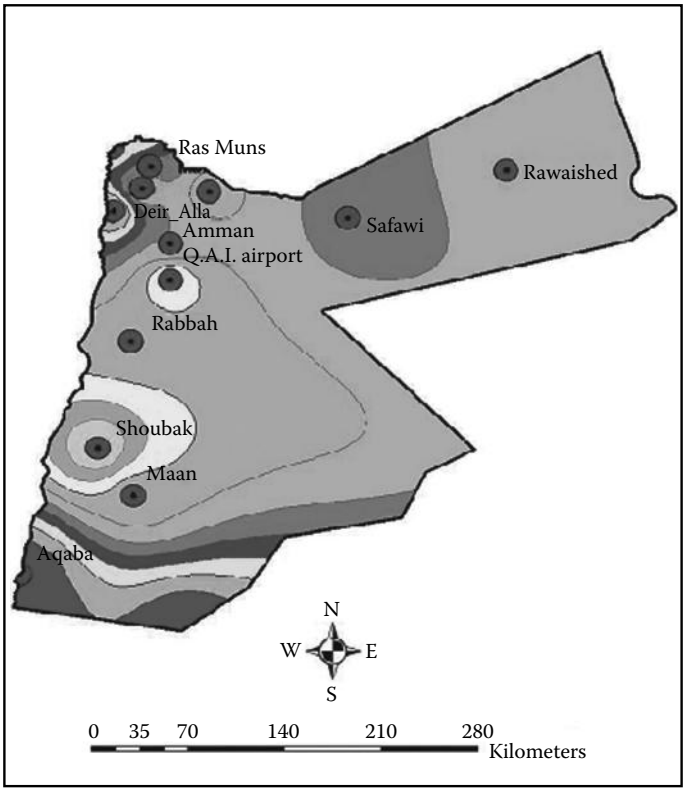

FIGURE 15.20 The final shape for the treated map for certain weather parameters by GIS, indicating zones and lines (gray shadings) of weather parameters distributed in the region.

climate change on the rainfall pattern by investigating the zone generated by the GIS. If the zone area has decreased or increased, we can conclude there is a change in that region. By applying GIS techniques, we can predict if there will be a serious change in rainfall pattern or temperature higher or lower than previous data. The GIS can also give the users a better calculation for each area in each zone; this calculated area will be a great help to scientists to compare more data at different time domains. This time domain can even in some cases be around 100 years to give the right conclusion whether there are any changes in weather parameters during the specified time period resulting in any changes on the weather for that region.

15.5 Summary and Conclusions

The application of GIS in climate change has been investigated in this chapter. The obtained data for weather parameters such as rainfall and temperature have been used here to create maps that demonstrate the changes in weather conditions with different zones and areas inside the maps. These maps and technical data for all weather stations in a certain location or region will be a great help to study the changes that have taken place in the weather over a certain period of time. The maps produced in the GIS will give a good indication of all weather parameters showing clearly whether the region has undergone any changes during the past and current decade of time by calculating and exactly measuring these zones of temperature and rainfall to determine whether any shrinkage or expansion had occurred. These measurements can be easily conducted using the GIS.

References

1. Chrisman, N., 2002, *Exploring Geographic Information Systems*. Wiley, New York.
2. Danermond, J. and Artz, M., 2010, *Climatic Change is a Geographic Problem*. ESRI ebooks, Redlands, CA, USA.
3. Dangermond, J., 2010, The geographic approach to climate change, *GeoSpatial Today*, April.
4. Fagan, B., 2008, *The Great Warming: Climate Change and the Rise and Fall of Civilizations*. Bloomsbury Press, New York.
5. Fotheringham, A. and Wegener, M., 2000, *Spatial Models and GIS: New Potential and New Models*. Taylor & Francis, London, U.K.
6. Liu, D.L., Mo, J., Fairweather, H., and Timbal, B., 2009, A GIS tool to evaluate climate change impact: Functionality and case study, in *18th World IMACS/MODSIM Congress*, Cairns, Queensland, Australia, July 13–17, 2009, pp. 1936–1942.
7. Longley, P., Goodchild, M., Magnire, D., and Rhind, D., 2010, *Geographic Information Systems Sciences*, John Wiley & Sons, Inc, Hoboken, NJ, USA.
8. Kaab, A., Huggel, C., and Fischer, L., 2006, Remote sensing technologies for monitoring climate change impacts on glacier- and permafrost-related hazards, in F. Nadim, R. Pöttler, H. Einstein, H. Klapperich, and S. Kramer, eds., *2006 ECI Conference on Geohazards*, Lillehammer, Norway.
9. Kaiser, W.L. and Wood, D., 2001, *Seeing through Maps: The Power of Images to Shape Our World View*, ODT, Inc., Amherst, MA.
10. Matouq, M., 2008, Predicting the impact of global warming on the middle east region: Case study on Hashemite Kingdom of Jordan using the application of geographical information system, *Journal of Applied Sciences*, 8(3), 462–470.
11. Matouq, M., Elhasan, T., Bilbissi, H., and Abylhadi, M., 2011, The impact of global warming on the middle east region: Case study on Hashemite Kingdom of Jordan during the period of 1978–2008, in *EcoForum Conference & Exhibition*, Sydney, New South Wales, Australia, Poster No. e24.
12. Schuurman, N., 2004, *GIS: A Short Introduction*, Blackwell Publishing, Malden, MA.

16

GIS-Based Upland Erosion Mapping

Soo Huey Teh
United Nations University

Lariyah M. Sidek
Universiti Tenaga Nasional

Pierre Y. Julien
Colorado State University

Jansen Luis
Tenaga Nasional Berhad

AUTHORS

Soo Huey Teh is a program associate for the University Network for Climate and Ecosystem Change Adaptation Research (UN-CECAR) Program of United Nations University, Institute for Sustainability and Peace (UNU-ISP). She received a master's in renewable energy science at the University of Iceland. She was working with Colorado State University and Tenaga Nasional Berhad, which is Malaysia's largest electric utility company for her master's thesis on soil erosion modeling for hydropower development. She received a BS in global environmental science and a minor in geology and geophysics at the University of Hawaii at Manoa.

Lariyah M. Sidek is an associate professor at the Universiti Tenaga Nasional. She completed her PhD in civil engineering at Kyoto University in the field of urban drainage. She is the head of unit of strategic planning and the program coordinator of the Water and Environmental Engineering Unit.

Pierre Y. Julien completed his PhD in civil engineering at Laval University in the field of hydraulics. He pursued postdoctoral studies in sedimentation at Colorado State University in 1983. He became faculty affiliate (1983–1985), assistant professor (1985–1989), tenured associate professor (1989–1994), and tenured full professor (1995–). Since 1997, he is the leader of the hydraulics program and coordinator of the Hydraulics and Wind Engineering Division. He authored more than 300 scientific publications including two textbooks, 50 refereed papers in scientific journals, 100 professional presentations, and 75 technical reports. Under his guidance, 27 PhD and 27 MS students completed their graduate degrees in civil engineering.

Jansen Luis holds a senior engineer (hydro structure) position in Tenaga Nasional Berhad and is also appointed as the civil engineer (engineering) for the construction of 250 MW Hulu Terengganu Project. He has a first-class (honors) bachelor's degree in civil engineering from Universiti Tenaga Nasional and is presently in the final year of his doctorate in engineering.

PREFACE

The main source of sediments in reservoirs is from upland areas. Very high upland erosion rates have been observed in tropical countries around the world. For instance, Malaysia receives 2500 mm of rainfall precipitation per year and the steep mountain areas are subjected to deforestation. The corresponding erosion rates have exceeded 10,000 tons/km^2/year. The example of Cameron (C.) Highlands in Malaysia illustrates how geographic information system (GIS) can be used to examine soil erosion mapping. From this study using the Revised Universal Soil Loss Equation (RUSLE) model, the average annual soil loss rate at C. Highlands was estimated at 282,500 m^3/year in 1997 and increased to 335,000 m^3/year in 2006. The comparison of erosion rates between 1997 and 2006 shows a soil loss increase of 18.5% in less than a decade. These rapid increases in reservoir sedimentation rates are attributed to changes in land use that can be easily monitored with GIS.

16.1 Introduction

16.1.1 Upland Erosion Processes and Models

The main source of sediments in reservoirs is from upland erosion. Morgan and Davidson [22] and Julien [15,16] describe soil erosion processes and dynamics that have been studied for decades. The main factors contributing to upland erosion losses include rainfall erosivity, soil erodibility, land topography, land use, and land conservation practices [9]. Specific degradation rates in reservoirs of the United States are typically less than 2000 tons/km^2/year [18] and are primarily linked to upland erosion rates. Upland erosion losses have been estimated using well-known methods like the Universal Soil Loss Equation (USLE) from Wischmeier and Smith [34]. The USLE includes all the factors affecting upland erosion from sheet and rill erosion. Renard et al. [25] provided a modified version named the Revised Universal Soil Loss Equation (RUSLE).

The advances in geographic information system (GIS) have allowed applications of raster-based formats for the determination of the various parameters of the USLE and RUSLE. Some detailed applications at the watershed scale include Mitasova et al. [20], Molnar and Julien [21], and Kim and Julien [19]. The applicability in tropical areas represents a challenge because of the reduced availability in GIS-gridded information for topography, soil type, and land use, as well as for the evaluation of the rainfall erosivity parameter R.

In tropical regions, the early and widely accepted soil erosion models consist of relatively simple response functions to predict mean annual erosion losses. Forest Research Institute Malaysia (FRIM) [11] provided a guide for soil erosion losses on Malaysian forestland using MUSLE. Schoorl et al. [28] state that the current trend is towards replacing these by far more elaborated process-based models. Among these models include water prediction program (WEPP) of the USDA; the erosion productivity impact calculator (EPIC); chemical, runoff, and erosion from agricultural management systems (CREAMS); and European soil erosion model (EUROSEM). These models are usually event based and are more applicable to agricultural areas than mountainous watersheds. Other models can be useful in the analysis of watershed hydrology (e.g., HEC-HMS, SHETRAN, and MIKE SHE). Other programs combine hydrology and hydraulics such as InfoWork RS, SWMM, SED2D, XP-STORM, and BASINS. Ekhwan et al. [7] studied the use of InfoWork RS to determine the sediment loads and riverbed profiles at Cameron (C.) Highlands. Hartcher and Post [12] studied the mean annual conceptualization of transport and deposition processes of sediments in Thailand using SedNet. Fortuin [10] under the REACH study created Early Warning and Risk Navigation Systems (EWARNS) in order to resolve and minimize the serious soil erosion problems in C. Highlands, Malaysia. TNBR [30] studied the use of DHI's SEAGIS

(Soil Assessment Model) to estimate the sediment entering into the river systems coupled with MIKE 11 and MIKE 12 model for the rainfall and hydrological conditions. Dynamic GIS-based watershed erosion modeling studies showing the processes of upland erosion, sediment transport, and deposition include applications of CASC2D-SED [8,13,17,26]. More recent developments of dynamic simulations of sediment transport and contaminant transport and fate were reported by Velleux et al. [31,32], Caruso et al. [4], and Johnson et al. [14].

C. Highlands in Malaysia is located in the mountains of a tropical region subjected to about 2500 mm of rain every year. The area formerly developed for hydropower development has been plagued with sedimentation problems. C. Highlands has been rapidly deforested and substituted with agriculture, urbanization, and infrastructure development contributing to severe soil erosion. The increase in soil erosion is primarily attributed to agricultural expansion, while the urbanization may also contribute, but to a lesser extent [28]. Changes in land use are therefore considered to have a major effect on the soil erosion losses.

This site provides a unique example for the demonstration of the applicability of GIS techniques for the analysis of upland erosion losses in a mountain tropical watershed. The site requires an evaluation of all the upland erosion parameters using RUSLE. The analysis also demonstrates how temporal changes in land use affect the upland erosion rates. This field site of C. Highlands in Malaysia has been selected because it is one of the most highly erodible areas in the world. The changes in land use between 1997 and 2006 are highlighted in terms of impact of soil erosion.

16.1.2 Field Site Description

The C. Highlands catchment area shown in Figure 16.1 in Peninsular Malaysia is relatively high with mountains ranging from 1524 m to Gunung Brinchang standing at 2032 m. Under the C. Highlands hydroelectric scheme—stage I construction, the high head scheme supplemented by the combined flow from two major rivers, Sg. Telom and Sg. Bertam, is being conveyed to the power house through a closed tunnel. The gross head estimated between Sg. Bertam and Sg. Batang Padang was 568 m.

The application of GIS facilitates the calculations of soil erosion by enabling the integration of hardware and software for the analysis of data capturing the spatial and temporal variability of watershed characteristics of geographically referenced information. GIS allows us to view, understand, question, interpret, and visualize data in many ways that reveal relationships, patterns, and trends in the form of maps, globes, reports, and charts. For this study, ArcGIS version 9.3 was utilized. A raster-based approach is used here because it has proven to be more convenient and very well suited for the analysis of soil erosion at the watershed scale. Overall the simulation models are the most effective way to predict soil erosion processes and their effect by using GIS [1]. GIS provides a great advantage to analyze multilayer of data spatially and quantitatively within the basin. The estimation of soil loss in the basin using GIS is also in the ranges of other studies. GIS not only provides accurate results but also provides cost- and time-effective ways of analysis.

The boundary shape files of C. Highlands were obtained from the Department of Agriculture (DOA), Malaysia, shown in Figure 16.2. These shape files were added as data into ArcGIS. The total drainage area of C. Highlands scheme is 183 km^2 comprising of 111 km^2 for Telom and 72 km^2 for Bertam.

16.2 Upland Erosion Parameters

The well-known and widely used model used to estimate soil erosion losses from the upland areas is the USLE developed by the USDA Wischmeier and Smith [33,34]. The model was later modified and

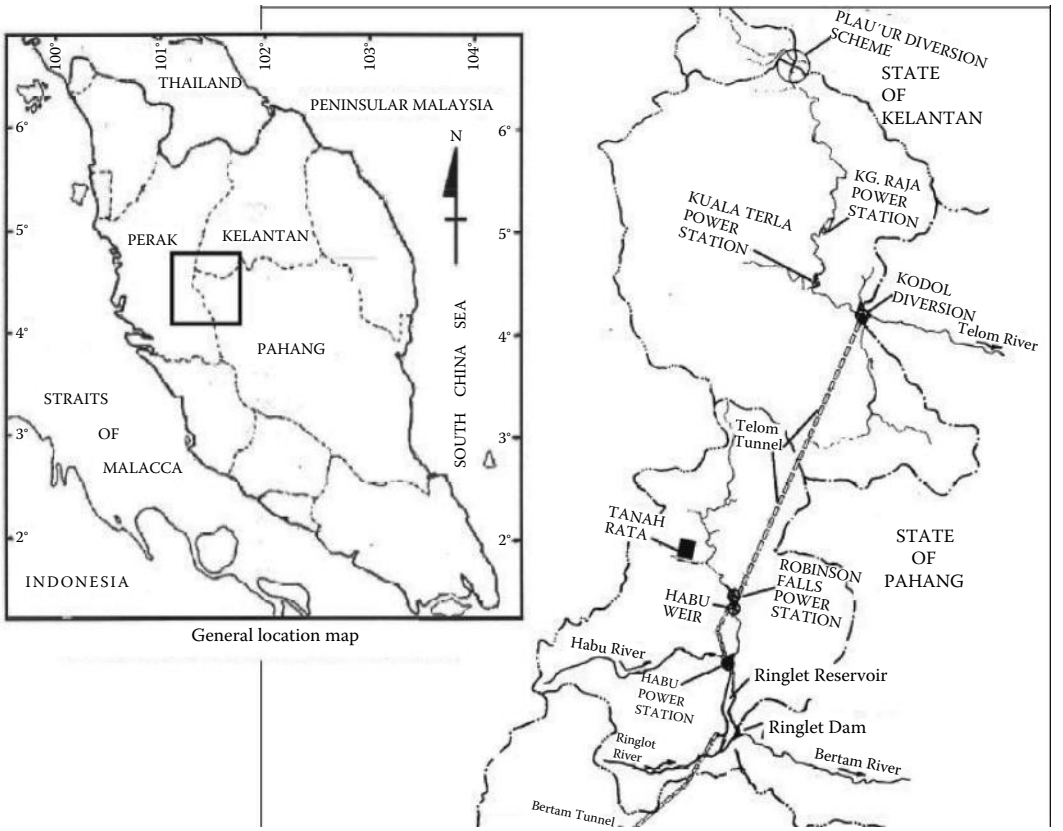

FIGURE 16.1 C. Highlands area.

renamed RUSLE by Renard et al. [25]. More details can be found in Pitt et al. [24] and Blaszczynski [2]. The USLE equation combines six parameters as described in Equation 16.1:

$$\mathbf{A = RKLSCP} \tag{16.1}$$

where

A is the upland erosion loss in tons per acre per year
R is the rainfall erosivity factor
K is the soil erodibility factor
L is the slope length factor
S is the slope steepness factor
C is the cropping and management factor
P is the conservation practice factor

A flow chart for the calculation of soil erosion losses is presented in Figure 16.3. The calculation details for this study can be found in Teh [28].

16.2.1 Rainfall Erosivity

In earlier studies at C. Highlands, the mean annual rainfall precipitation was observed to be approximately 2620 mm fairly evenly distributed over the year with somewhat heavier rainfall periods in April and November. This estimate decreased slightly in recent years where the mean annual rainfall reached

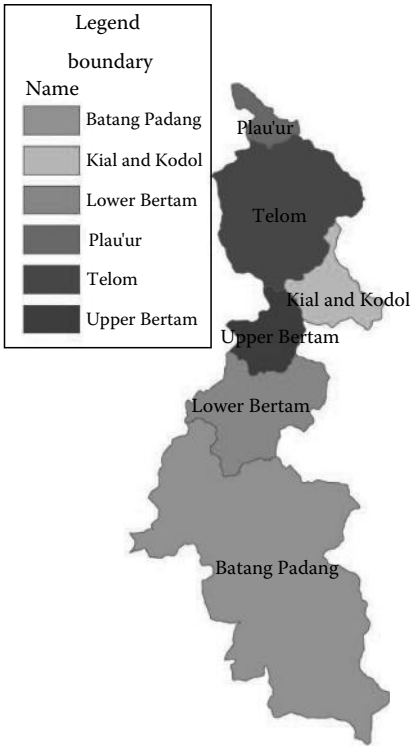

FIGURE 16.2 Boundary map, Department of Agriculture, Malaysia.

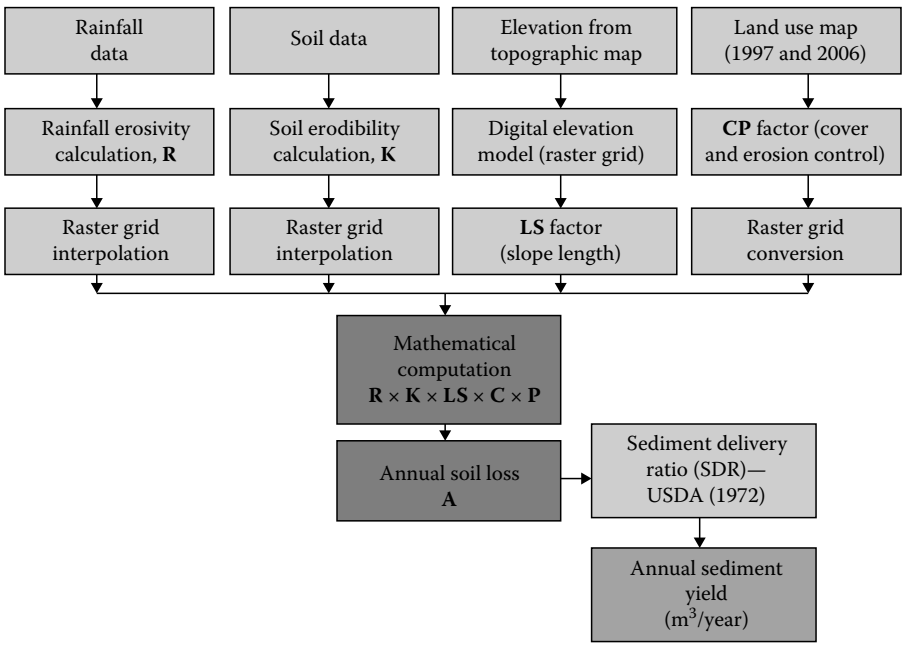

FIGURE 16.3 GIS-based upland erosion flow chart.

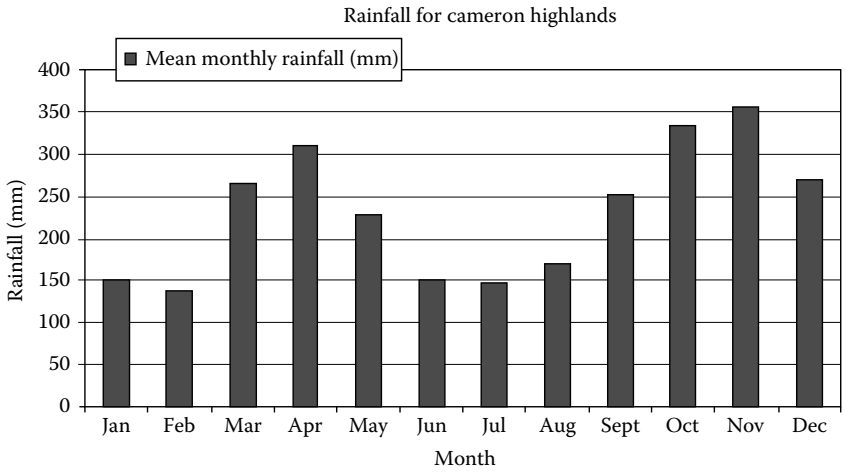

FIGURE 16.4 Mean annual rainfall measured at C. Highlands.

2550 mm. Higher rainfall precipitation occurs twice in a year, as shown in Figure 16.4, during the months of April through May and October through November.

The rainfall erosivity factor **R** describes that the rainstorm energy of the rainfall, which varies with climate and location within a certain region. In Malaysia, the Department of Irrigation and Drainage provided a Design Guides Report (DID) [6] to compute the annual EI_{30} and averaged **R** factor equal to 9068 for Pahang State at Gunung Brinchang. This value is excessively high and had to be discarded. Other studies in Southeast Asia have also suggested relationships for the factor **R**. In Indonesia, Bols [3] provided an equation for the calculation of the **R** value based on an empirical study of the mean annual precipitation **P** in mm:

$$\mathbf{R} = \frac{2.5\mathbf{P}^2}{100(0.073\mathbf{P} + 0.73)} \tag{16.2}$$

In Thailand, Hartcher and Post [12] investigated hillslope erosion. The rainfall erosivity factor was determined using the following Hartcher equation [12]:

$$\mathbf{R} = 38.5 + 0.35\mathbf{P} \tag{16.3}$$

Therefore, the values of the factor **R** at C. Highlands could be estimated from the rainfall precipitation from the 1999 to 2006 rainfall record. Several equations were compared in Table 16.1. Both the methods of Hartcher and Bols [3,12] provided comparable values of **R** factor with 993 and 941, respectively.

Based on isohyets, a map of the rainfall erosivity factor **R** was developed from the equation of Bols [3]. The GIS map in Figure 16.5 shows the distribution in factor **R** for the RUSLE model.

16.2.2 Soil Erodibility

The soil erodibility factor **K** describes the ability of a soil to erode under rainfall. The **K** factor is defined as a unit of mass per area per unit time. It quantifies the amount of soil erosion as a function of soil type, soil texture, and composition. The **K** factor values can be estimated using the soil erodibility

TABLE 16.1 Computed Rainfall Erosivity **R** at C. Highlands

ID	Stn_Name	Lat	Long	Unit	P_99-06	R_99-06[a]	R_99-06[b]	R_99-06[c]	R_99-06[d]
9001	Blue Valley Tea Estate at C. Highlands, Pahang	4.5861	101.4194	mm	2216.300	804.205	814.205	1108.150	755.598
9002	Kg. Raja at C. Highlands, Pahang	4.5514	101.4167	mm	2604.814	940.185	950.185	1302.407	888.648
9003	Telom Intake at C. Highlands, Pahang	4.5422	101.4250	mm	2067.800	752.230	762.230	1033.900	704.743
9004	Sg. Palas Tea Estate at C. Highlands, Pahang	4.5167	101.4167	mm	3146.700	1129.845	1139.845	1573.350	1074.223
9006	Sg. Ruil at C. Highlands, Pahang	4.4944	101.4250	mm	2937.786	1056.725	1066.725	1468.893	1002.678
9007	Kajiklim T. Rata at C. Highlands, Pahang	4.4667	101.3833	mm	2960.486	1064.670	1074.670	1480.243	1010.452
9008	Mardi C. Highlands at Pahang	4.3833	101.3833	mm	2989.229	1074.730	1084.730	1494.614	1020.295
9009	Kajiklim Habu at C. Highlands, Pahang	4.4181	101.3833	mm	2746.957	989.935	999.935	1373.479	937.327
9010	Boh Tea Estate(factory), C. Highlands, Pahang	4.4514	101.4250	mm	2574.700	929.645	939.645	1287.350	878.335
9111	C. Highlands at (Tanah Rata), Pahang	4.4667	101.3667	mm	3339.343	1197.270	1207.270	1669.671	1140.196
				Total Average	2758.411	993.944	1003.944	1379.206	941.249

[a] Harper, 1987, Thailand.
[b] Hartcher, 2005, Thailand.
[c] Morgan, 1974, Malaysia.
[d] Bols, 1978, Indonesia.

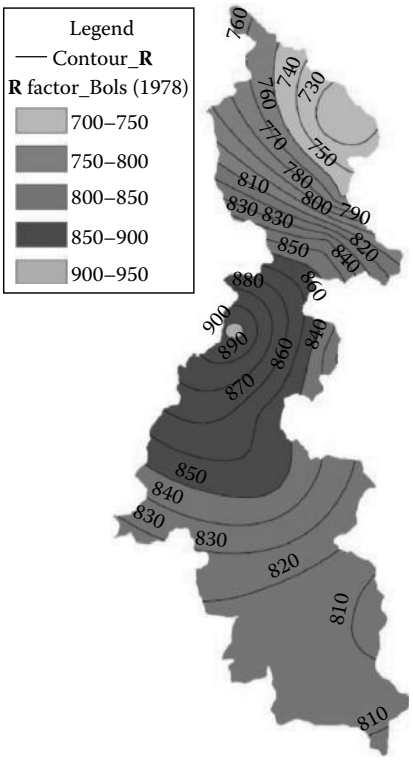

FIGURE 16.5 Rainfall erosivity map, **R**, ranging from 700 to 950 using Bols (1978) method.

nomograph method that depends on soil properties such as the percentage of silt, clay, and fine sand, percentage of organic matter (OM), soil structure code, and permeability class. The Wischmeier et al. [35] equation is

$$\mathbf{K} = \frac{2.1\times10^{-4}\left(12-\mathbf{OM}\right)\mathbf{M}^{1.14}+3.25\left(\mathbf{S}_1-2\right)+2.5(\mathbf{P}_1-3)}{100} \tag{16.4}$$

where

M = (%silt + %very fine sand) × (100 − %clay)
%silt is 0.002–0.05 mm
%very fine sand is 0.05–0.1 mm
%sand is 0.1–2 mm
%clay is <0.002 mm
OM is the % of **OM**
$\mathbf{S}_1$ is the structure index
$\mathbf{P}_1$ is the permeability

From laboratory sampling conducted in 2010, the particle size distribution for sediments at C. Highlands consists of an average composition of 13% sand, 60% silt, 25% clay, and 2% **OM**. For applications in Malaysia, Tew [29] proposed the following slight modification to the following method:

$$\mathbf{K} = \frac{\left[1.0\times10^{-4}\left(12-\mathbf{OM}\right)\mathbf{M}^{1.14}+4.5\left(\mathbf{s}-3\right)+8.0\left(\mathbf{p}-2\right)\right]}{100} \tag{16.5}$$

where

K is the soil erodibility factor (tons/ha)(ha hr/MJ mm)
M = (%silt + %very fine sand) × (100 − %clay)
OM is the % of **OM**
s is the soil structure code
p is the permeability code

Using the Wischmeier et al. [35] formula, the **K** value for C. Highlands was determined to be 0.052, while Tew [29] provided 0.033. Meanwhile, the soil erodibility map for **K** factor developed using the GIS method obtained a higher value of 0.0659. On the other hand, findings from the NREM [23] by the Ministry of Natural Resources and Environment, Department of Environment, Malaysia, for C. Highlands reveal that the soil erodibility factors in the study area range from 0.1 to 0.2. For this study, the values of **K** are assumed to be uniform and are adopted from the DOA. Therefore, the **K** factor used for steep, urban, and mined land was 0.066.

16.2.3 Slope Length and Steepness Factors

The two factors **L** and **S** describe the slope length and steepness factors, respectively. They can be determined from the topography of the area under study. In most studies, both factors are combined together to form the slope steepness factor **LS**. For the C. Highlands area, the topographic factors **L** and **S** were obtained from the topographic information provided by the digital elevation model (DEM) derived from the NASA Shuttle Radar Topographic Mission (thereafter SRTM) dataset. A DEM of scale 1:50,000 was obtained for this study whereby the slope length and slope steepness can be used in a single index, which expresses the ratio of soil loss as defined mathematically by Wischmeier and Smith [34]. Using the raster calculator function under spatial analyst, the **LS** factors were obtained. The slope of the DEM in percentage and the flow accumulation were calculated at a cell size of 20 m. Using the available data from ArcGIS, the slope map is shown in Figure 16.6 and the slope length and steepness for **LS** factor was calculated, and the **LS** map is shown in Figure 16.7.

16.2.4 Cropping Management and Conservation Practice

The cropping management factor represents the ratio of soil loss under a given crop to that of a bare soil freshly tilled in the drainage direction [33]. The cover factor **C** relates to land use characteristics. Based on the previous studies and available land use maps, the values on Table 16.2 from the Ministry of Natural Resources and Environment, Department of Environment, for the **C** factor were used for this study.

As expected, the land use changes have been quite significant since the year 1946. Figure 16.8 shows the forested area reduction is almost all sub-catchment. The average percentage of reduction in forested area is 35% from 1946 to 1997. The Lower Bertam sub-catchment recorded the lowest percentage in 1997 at 30% for the forested area.

The terrain within the study area can be classified according to the slope category as defined by the DOA, Malaysia. The terrain and topography classification is then used in the erosion practice factor, **P** as in Table 16.3, where it considers the best practices to reduce source erosion such as contouring and terracing. The values proposed are dependent on the terrain slope.

Two sets of land use maps from the DOA were available for this study, as shown in Figure 16.9a and b for years 1997 and 2006, respectively. The **C** and **P** factors were generated the same way as the **K** factor

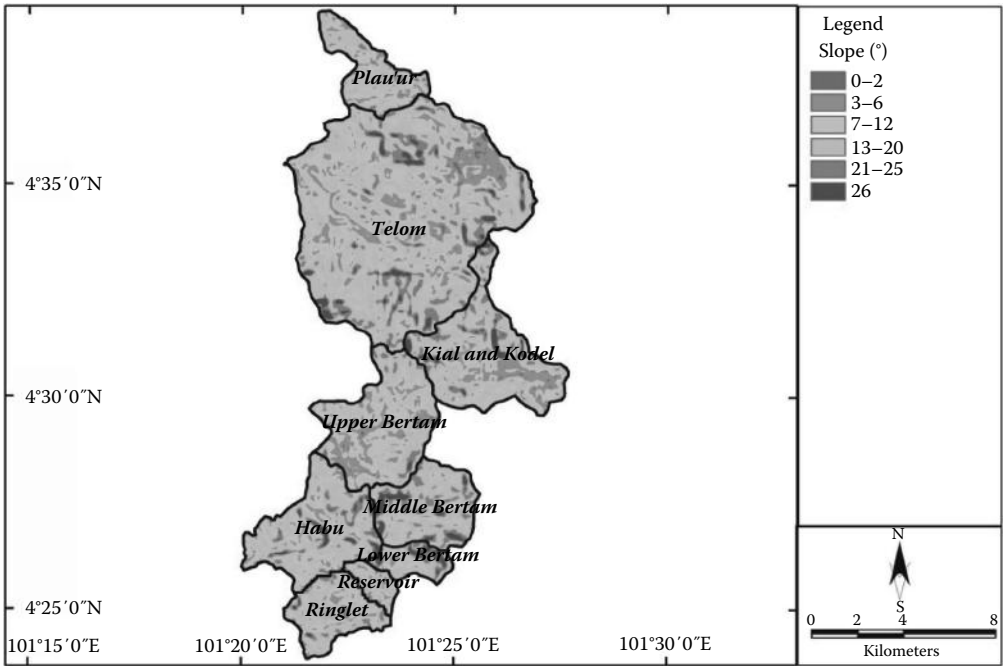

FIGURE 16.6 Slope map derived from DEM.

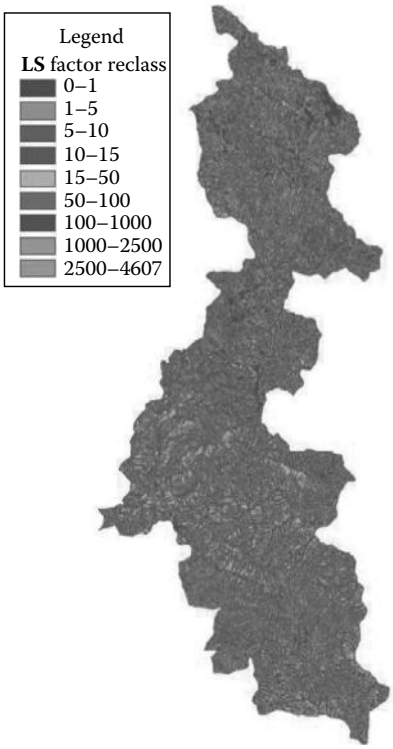

FIGURE 16.7 **LS** factor for C. Highlands.

TABLE 16.2 Land Use Cover Factor, **C** (DOA)

Land Use Type	C Factor
Agriculture experimental stn.	0.600
Associated areas	0.350
Bare land	1.000
Forest	0.010
Grassland	0.015
Market gardening	0.350
Mine	1.000
Mixed agriculture	0.350
Orchard	0.250
Residential area	0.003
Scrub forest	0.010
Shifting cultivation	0.250
Sundry nontree cultivation	0.250
Tea	0.350
Urban	0.500
Water body	0

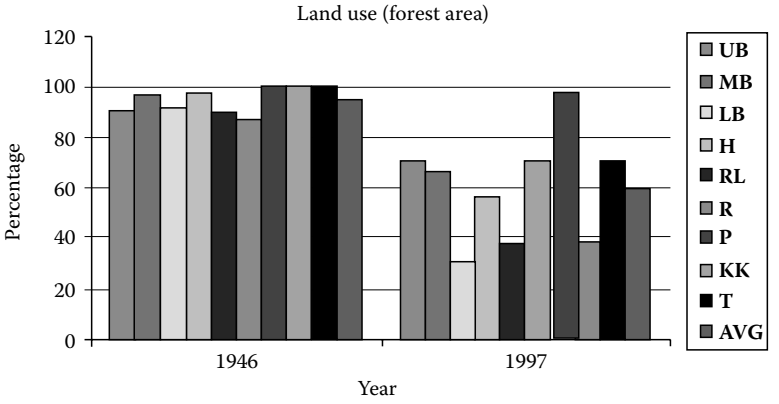

FIGURE 16.8 Comparison of forested areas by subwatersheds between years 1946 and 1997.

TABLE 16.3 Erosion Control Factor, **P** (DOA)

Category	Topography	Slope Range (°)
1	Flat	0–2
2	Undulating	2–6
3	Moderate hilly	6–12
4	Hilly	12–20
5	Moderate steep	20–25
6	Steep	>25

Slope (%)	P Factor
1.1–2.0	0.60
2.1–7.0	0.50
7.1–12.0	0.60
12.1–18.0	0.80
18.1–24.0	0.90

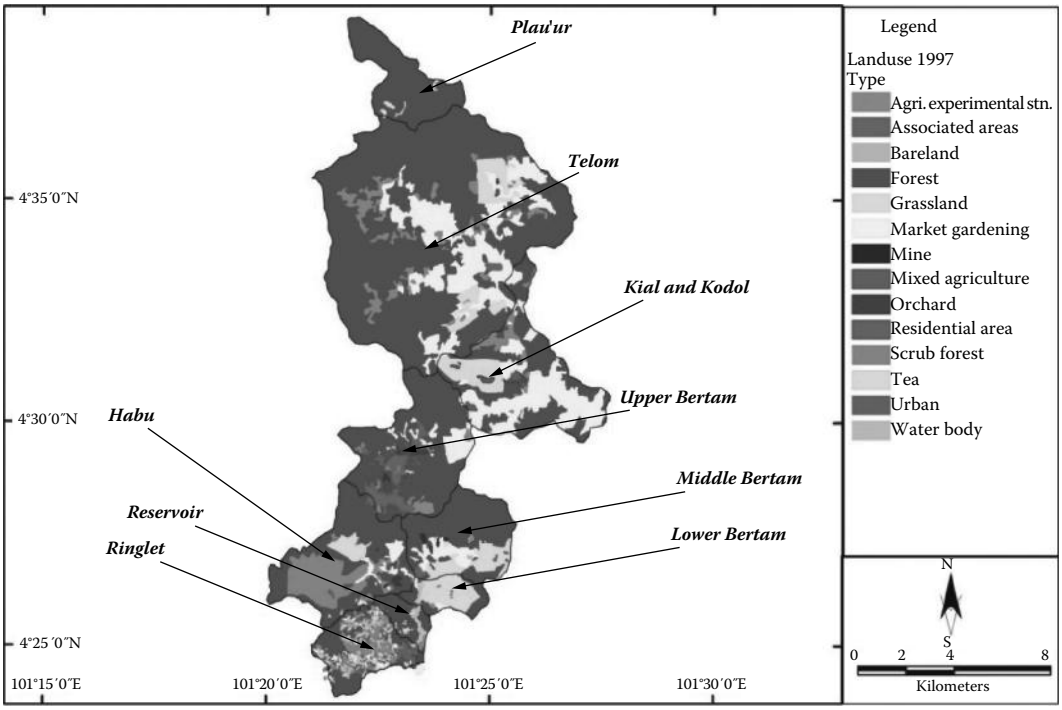

(a)

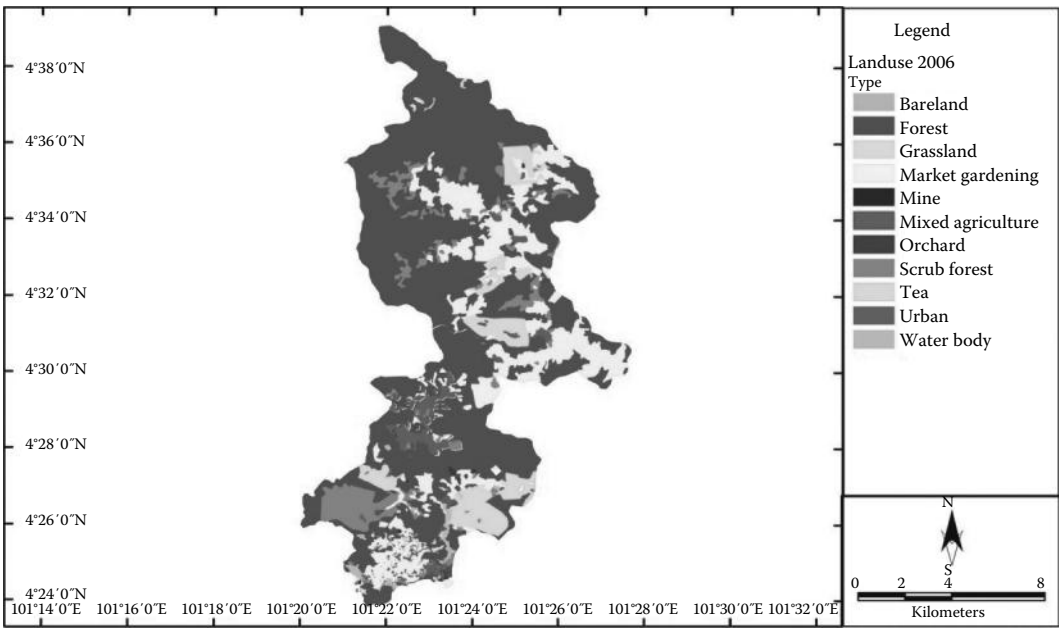

(b)

FIGURE 16.9 Land use maps for (a) year 1997 and (b) year 2006 (DOA).

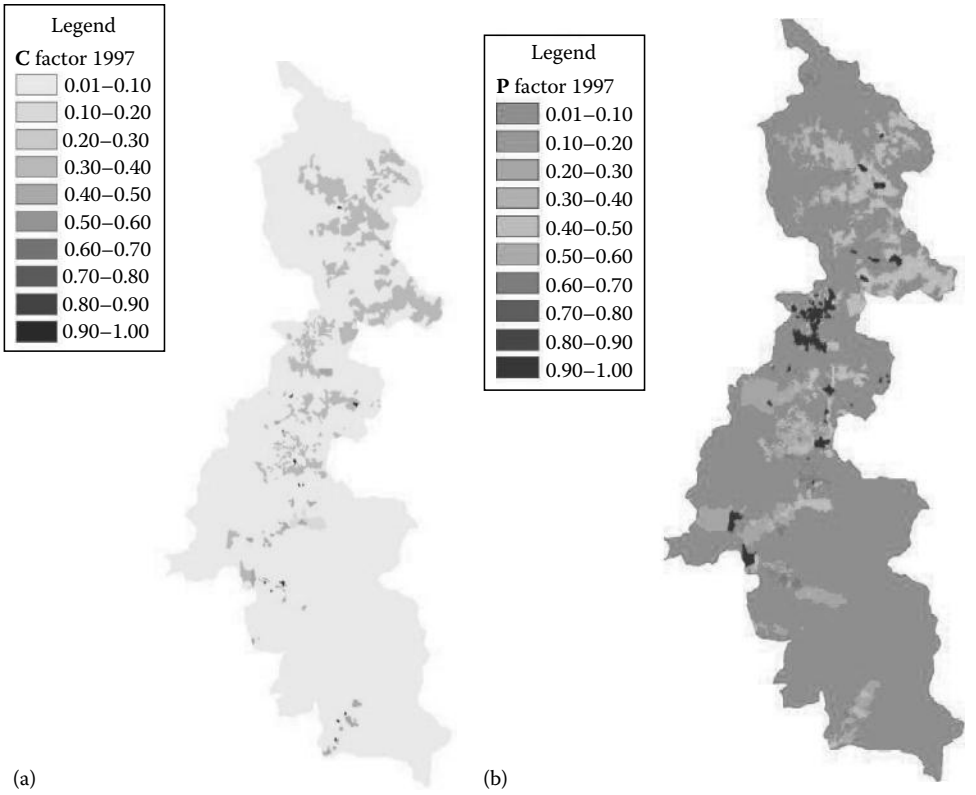

FIGURE 16.10 Computed (a) **C** factor and (b) **P** factor for 1997 using ArcGIS.

by cross-referencing the attribute table to ArcGIS. For this study, **P** values were chosen based on the land use instead of management practice. The GIS converted the information from a vector-based format to a raster-based format at a cell size of 20 m.

Using the ArcGIS, the cover management factor **C** and erosion control factor **P** were developed using the method described previously for 1997 in Figure 16.10 and 2006 in Figure 16.11. The maps produced for 2006 exclude the sub-watershed of Plau'ur due to unavailability of data. The comparison of these maps reflects the impact of the change in land use that has been taking place on the watershed within less than 10 years.

16.3 Upland Erosion Mapping

The maps obtained from RUSLE for C. Highlands are obtained from the product of the six parameters of Equation 16.1. The values of erosion potential were divided into seven classes as shown in Table 16.4. Figure 16.12 shows the upland erosion maps for 1997 and 2006, respectively.

Two separate sub-watersheds Habu and Ringlet were further investigated to examine the rate of increase in soil loss. Using the soil maps for Habu on Figure 16.13, the RUSLE model showed an increase in soil loss from 32,000 m^3/year in 1997 to 50,600 m^3/year in year 2006, which corresponds to a 58.1% increase. Meanwhile the Ringlet area shown in Figure 16.14 also showed a 100% increase in soil loss from 25,600 m^3/year in 1997 to 50,900 m^3/year in year 2006.

These increases in upland erosion losses reflect directly on the increased sedimentation rates measured in these reservoirs. The C. Highlands hydroelectric scheme was planned and constructed from 1959 to 1964. The main feature of the scheme was to harness the Ringlet Falls with Sultan Abu Bakar

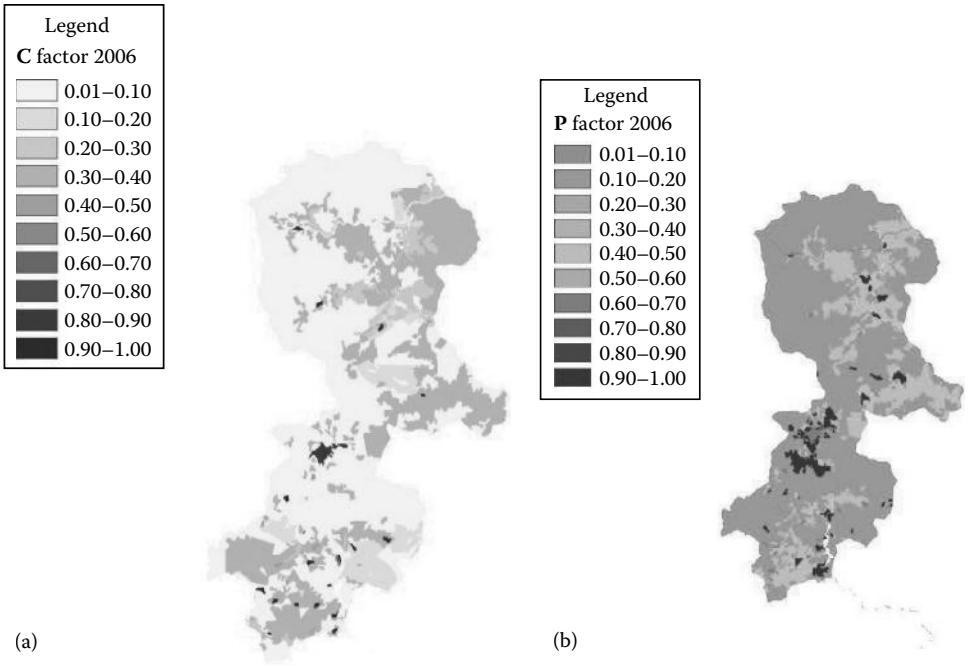

FIGURE 16.11 Computed (a) **C** factor and (b) **P** factor for 2006 using ArcGIS.

TABLE 16.4 Derivation of the Ordinal Categories of Soil Erosion Potential

Erosion Class	Numeric Range (tons/ha/year)	Erosion Potential
1	0–1	Very low
2	1–5	Low
3	5–10	Moderate
4	10–20	High
5	20–50	Severe
6	50–100	Extreme
7	>100	Exceptional

Dam that stands at 40 m height with concrete buttresses fitted to four (4) gated spillways. The reservoir elevation at full supply level is 1070.7 m and has a surface area of 60 ha. The reservoir receives water from three rivers (Sg. Habu, Sg. Bertam, and Sg. Ringlet) and other minor tributaries. Ringlet Reservoir was designed for a gross storage of 6.7 million m^3, of which 4.7 million m^3 is the active/live storage and 2.0 million m^3 is inactive/dead storage. The dead storage was designed for a useful lifespan of approximately 80 years that translates to a design sediment inflow of 20,000 m^3/year [5]. From the bathymetric survey data the sediment rate of 40,000 m^3/year was recorded immediately after construction. The data showed an increase of almost 100% from the designed storage requirement, which means that the dead storage would be filled up after 40 years of operation and not meeting the design life expectancy. Since these earlier studies, the rate of sedimentation increase is directly related to the increase in the upstream activities such as deforestation, uncontrolled farming, residential, and other rapid changes in land use on the contributing watershed areas. The main difference with earlier studies is that GIS has now become a very important tool in the analysis of the prospective changes in reservoir sedimentation rates based on changes in land use.

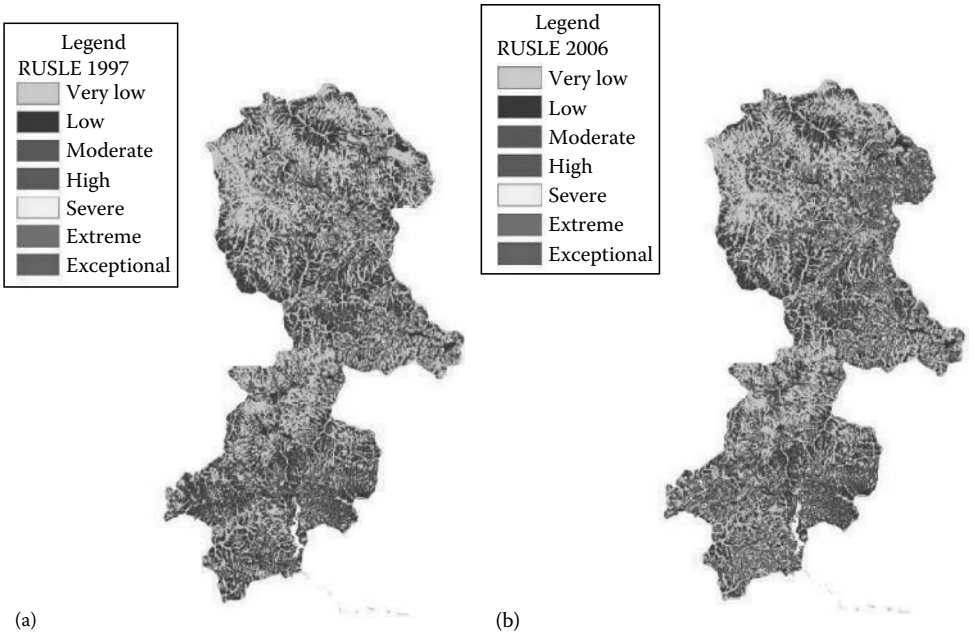

FIGURE 16.12 Computed soil erosion map for (a) 1997 and (b) 2006 using ArcGIS.

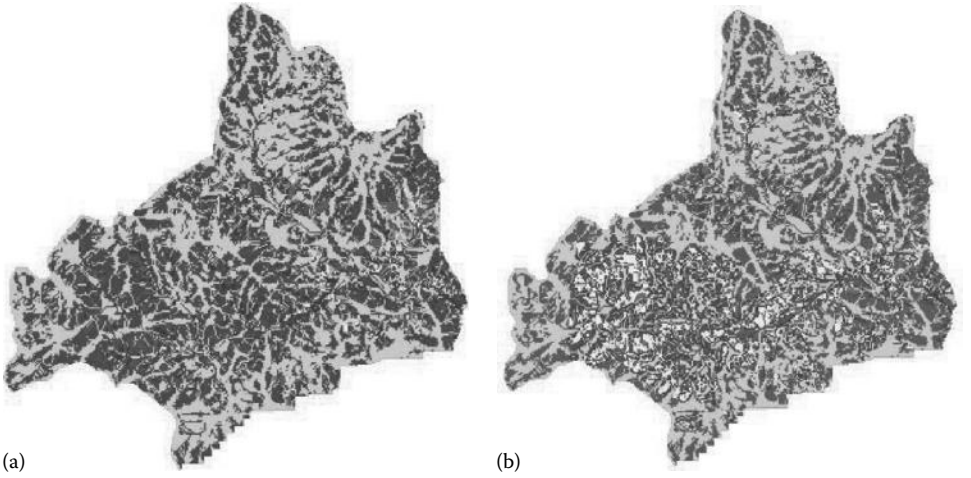

FIGURE 16.13 Soil erosion map for Habu (a) in 1997 and (b) in 2006.

16.4 Summary and Conclusions

Very high upland erosion rates have been observed in tropical countries around the world as a result of deforestation. GIS technology can be used to assess the changes in upland erosion rates from updated monitoring of land use. The USLE and RUSLE are well suited for upland erosion mapping. The methods include the effects of rainfall erosivity from rainfall records, soil erodibility from soil maps, slope length and steepness from surface topography and DEM, cropping management, and conservation practice from land use maps. This example of C. Highlands in Malaysia illustrates how GIS can be used to generate soil erosion maps at different times. Malaysia receives 2,500 mm of rainfall precipitation per year

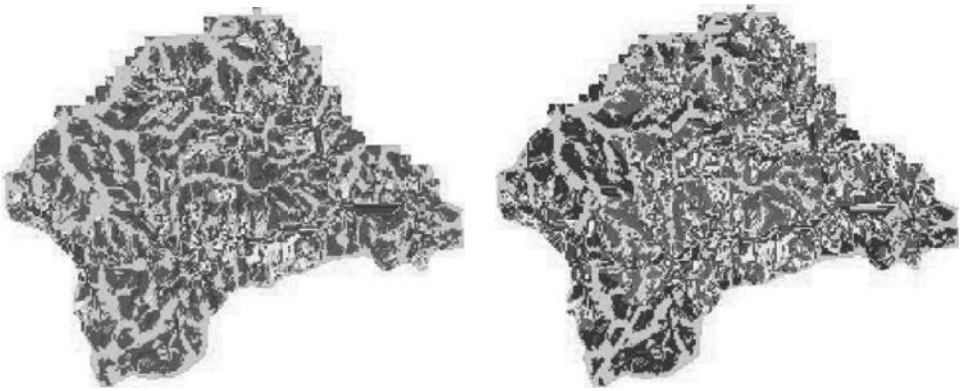

(a) (b)

FIGURE 16.14 Soil erosion map for Ringlet (a) in 1997 and (b) in 2006.

and the steep mountain areas are subjected to erosion rates in excess of 10,000 tons/km^2/year. From this study using the RUSLE model, the average annual soil loss rate at C. Highlands was estimated at 282,500 m^3/year in 1997 and increased to 335,000 m^3/year in 2006. The comparison of erosion rates between 1997 and 2006 shows a soil loss increase of 18.5% in less than a decade. These rapid increases in upland erosion rates result in similar increases in reservoir sedimentation rates. These can be attributed to changes in land use that can be easily monitored with GIS.

References

1. Bizuwerk, A., Taddese, G., and Getahun, Y. 2003. *Application of GIS for Modeling Soil Loss Rate in Awash River Basin, Ethiopia*, International Livestock Research Institute (ILRI), Addis Ababa, Ethiopia.
2. Blaszczynski, J. 2001. Regional sheet and rill soil erosion prediction with the Revised Universal Soil Loss Equation (RUSLE)–GIS Interface. Resource Notes No. 46.
3. Bols, P.L. 1978. The iso-erodent map of Java and Madura. Report of the Belgian Technical Assistance Project ATA 105, Soil Research Institute, Bogor, Indonesia, 39pp.
4. Caruso, B.S., Cox, T.J., Runkel, R.L., Velleux, M.L., Bencala, K.E., Nordstrom, D.K., Julien, P.Y., Butler, B.A., Alpers, C.N., Marion, A., and Smith, K.S. 2008. Metals fate and transport modelling in streams and watersheds: State-of-the-science and US-EPA workshop review. *Journal of Hydrologic Processes*, 22, 4011–4021.
5. Choy, F.K. 1991. Cameron Highlands hydroelectric scheme—Effects of development of the Telom and Upper Bertam catchments on water yield and energy generation. *IEM January Bulletin*, 15–19.
6. DID. 2001. Design rainfall, Chapter 13. In *Urban Stormwater Management Manual*, Manual Saliran Mesra Alam, Department of Irrigation and Drainage, Kuala Lumpur, Malaysia, pp. 1–17.
7. Ekhwan, M.T., Othman A.K., Mazlin, M., Barzani, M.G., and Pauzi, M.A. 2010. Use of InfoWork RS in modeling the impact of urbanisation on sediment yield in Cameron Highlands, Malaysia. *Journal of Nature and Science*, 8(2), 67–73.
8. England Jr., J.F., Velleux, M.L., and Julien, P.Y. 2007. Two-dimensional simulations of extreme floods on a large watershed. *Journal of Hydrology*, 347(1–2), 229–241.
9. Frenette, M. and Julien, P.Y. 1986. Advances in predicting reservoir sedimentation, General Lecture, *Third International Symposium on River Sedimentation, ISRS-III*, Jackson, MS, March 31–April 4, 1986, pp. 26–46.

10. Fortuin, R. 2006. Soil erosion in Cameron Highlands: An erosion rate study in a highland area. Saxion University, Deventer, the Netherlands, Regional Environmental Awareness Cameron Highlands, pp. 1–83.
11. FRIM. 1999. *A Guide for Estimating Surface Soil Loss Using the Modified Universal Soil Loss Equation (MUSLE) on Forest Land*. FRIM Technical Information Handbook No. 25. Forest Research Institute Malaysia, Kuala Lumpur, Malaysia.
12. Hartcher, M.G. and Post, D.A. 2005. Reducing uncertainty in sediment yield through improved representation of land cover: Application to two sub-catchments of the Mae Chaem, Thailand. *SIMMOD Conference*, Bangkok, Thailand, 2005, pp. 1147–1153.
13. Johnson, B.E., Julien, P.Y., Molnar, D.K., and Watson, C.C. 2000. The two-dimensional upland erosion model CASC2D-SED. *Journal of the American Water Resources Association, AWRA*, 36(1), 31–42.
14. Johnson, B., Zhang, Z., Velleux, M.L., and Julien, P.Y. 2011. Development of a distributed watershed contaminant transport, transformation and fate (CTT&F) sub-model. *Soil and Sediment Contamination: An International Journal*, 20(6), 702–721.
15. Julien, P.Y. 2002. *River Mechanics*. Cambridge University Press, New York, 434pp.
16. Julien, P.Y. 2010. *Erosion and Sedimentation*, 2nd edn. Cambridge University Press, Cambridge, U.K., 371pp.
17. Julien, P.Y. and Rojas, R. 2002. Upland erosion modeling with CASC2D-SED. *International Journal of Sediment Research*, 17(4), 265–274.
18. Kane, B. and Julien, P.Y. 2007. Specific degradation of watersheds. *International Journal of Sedimentation Research*, 22(2), 114–119.
19. Kim, H.S. and Julien, P.Y. 2006. Soil erosion modeling using RUSLE and GIS on the Imha Watershed, South Korea, Water Engineering Research. *Journal of the Korean Water Resources Association*, 7(1), 29–41.
20. Mitasova, H., Hofierka, J., Zlocha, M., and Iverson, R. 1996. Modeling topographic potential for erosion and deposition using GIS. *International Journal of Geographical Information Science*, 10(5), 629–641.
21. Molnar, D.K. and Julien, P.Y. 1998. Estimation of upland erosion using GIS. *Journal of Computers and Geosciences*, 24(2), 183–192.
22. Morgan, R.P.C. and Davidson, D.A. 1986. *Soil Erosion and Conservation*. Longman Scientific and Technical, Longman Group UK Ltd., Essex, U.K.
23. NREM. 2010. Preparation of design guides for erosion and sediment control in Malaysia. Department of Irrigation and Drainage (DID), Kuala Lumpur, Malaysia.
24. Pitt, R., Clark, S.E., and Lake, D. 2007. Erosion mechanisms, the revised universal soil loss equation (RUSLE) and vegetation erosion controls, Chapter 4. In: *Construction Site Erosion and Sediment Controls: Planning, Design and Performance*, DEStech Publications, Inc., Lancaster, PA.
25. Renard, K.G., Foster, G.R., Weesies, G.A., McCool, D.K., and Yoder, D.C. 1997. *Predicting Soil Erosion by Water: A Guide to Conservation Planning with the Revised Universal Soil Loss Equation (RUSLE)*. Agriculture Handbook No. 703. U.S. Department of Agriculture, Washington, DC, pp. 14–18.
26. Rojas, R., Julien, P.Y., Velleux, M.L., and Johnson, B.E. 2008. Grid-size effect on watershed soil erosion models. *Journal of Hydrologic Engineering, ASCE*, 134(9), 793–802.
27. Schoorl, J.M., Sonneveld, M.P.W., and Veldkamp, A. 2000. Three-dimensional landscape process modelling: The effect of DEM resolution. *Earth Surface Processes and Landforms*, 25(9), 1025–1034.
28. Teh, S.H. 2011. Soil erosion modeling using RUSLE and GIS on Cameron Highlands, Malaysia for hydropower development, MS thesis, School of Renewable Energy Science, University of Iceland, Akureyri, 76pp.
29. Tew, K.H. 1999. *Production of Malaysian Soil Erodibility Monograph in Relation to Soil Erosion Issues*. VT Soil Erosion Research and Consultancy, Selangor, Malaysia.

30. TNBR. 2010. A Study on the Effectiveness of Check Dams to Reduce River Sedimentation in Cameron Highlands.
31. Velleux, M., Julien, P.Y., Rojas-Sanchez, R., Clements, W., and England, J.F. 2006. Simulation of metals transport and toxicity at a mine-impacted watershed. *Environmental Science and Technology*, 40(22), 6996–7004.
32. Velleux, M.L., England Jr., J.F., and Julien, P.Y. 2008. TREX: Spatially distributed model to assess watershed contaminant transport and fate. *Journal of Science in the Total Environment*, 404, 113–128.
33. Wischmeier, W.H. and Smith, D.D. 1965. *Predicting Rainfall Erosion Losses from Cropland East of the Rocky Mountains*. U.S. Department of Agriculture Handbook 282. Washington, DC, 48pp.
34. Wischmeier, W.H. and Smith, D.D. 1978. *Predicting Rainfall Erosion Losses—A Guide to Conservation Planning*. U.S. Department of Agriculture Handbook 537. Washington, DC.
35. Wischmeier, W.H., Johnson, C.B., and Cross, B.V. 1971. A soil erodibility nomograph for farm land and construction sites. *Journal of Soil and Water Conservation*, 26(5), 189–193.

17

Hybrid Hydrologic Modeling

Pierre Y. Julien
Colorado State University

James S. Halgren
Riverside Technology Inc.

AUTHORS

Pierre Y. Julien is a professor of civil and environmental engineering at Colorado State University. He formerly served as an associate dean for International Research and Development. His research interest includes river mechanics, sediment transport, hydraulics, and hydrologic modeling. Dr. Julien has published extensively in water resources literature including two books and 20 lecture manuals and book chapters. He was an editor of the *ASCE Journal of Hydraulic Engineering* and received several awards including the H. A. Einstein Award for his contributions to sediment transport.

James S. Halgren is a water resources engineer with Riverside Technology, inc., consulting in areas of engineering modeling and programming. Dr. Halgren earned BS and MS degrees in civil engineering from Brigham Young University and received a PhD in civil engineering from Colorado State University in 2012. Dr. Halgren has presented lectures, conferences talks, and webinars on a number of his research and consulting projects, and he is an expert in geographic information systems (GIS), data analysis, and visualization.

PREFACE

This chapter explores a new hybrid approach to hydrologic modeling. Hybrid modeling combines distributed surface runoff modeling with a lumped-parameter rendering of infiltration and subsurface flow. The hybrid model TREX-SMA combines the Sacramento Soil Moisture Accounting (SAC-SMA) model with the TREX surface hydrology model. The capabilities of hybrid modeling are demonstrated with an application to the 30 km^2 California Gulch watershed, near Leadville, Colorado. The results of a 50-day simulation are presented for comparisons with and without the hybrid model component SMA. Surface runoff parameters were obtained from a prior calibration of TREX, and the SMA soil moisture parameters were determined from a priori estimates used by the Arkansas Basin River Forecast Center (ABRFC) of the National Weather Service (NWS). The hybrid simulation results from TREX-SMA show improvement relative to results from the unmodified TREX model. Model results such as surface and channel water depth are processed with Geographic Resources Analysis Support System (GRASS) GIS and Keyhole Markup Language (KML) scripts to create 2.5-D, browsable animations overlaid on a Google Earth™ terrain.

17.1 Introduction to Hybrid Modeling

Systems of classification for different watershed models arise from differences in the way the hydrologic processes are represented [22].

17.1.1 Lumped vs. Distributed

One of the most common systems of hydrologic model classification is lumped vs. distributed. According to Abbot and Refsgaard [1], a *lumped model* is a model where the watershed is regarded as one unit and variables and parameters in the model represent average or effective values for the entire drainage area. On the other hand, a *distributed model* takes into account the spatial differences in all variables and parameters.

17.1.2 Empirical, Conceptual, or Physical

Physically based models represent flow using equations derived from the equations of conservation of mass, momentum, and energy. They internally use variables and parameters that directly represent physically measurable quantities in the field [11,12,23,45,47].

Conceptual models, by comparison, operate on parameters that represent a conceptualization of hydrologic processes. Aral and Gunduz [5] suggest that all lumped models are conceptual and non-physical, asserting that they contain no connection to physical processes except through a black-box empirical function.

17.1.3 Hybrid Modeling Concept

Hybrid models can overcome the problems caused by dissimilarities in temporal and spatial scales of flow processes in the channel, overland plane, and subsurface. Aral and Gunduz [4] introduced the idea of a "hybrid modeling concept" in order to "resolve some of the problems associated with the fully physics-based representation of all subsystem processes of a watershed while providing a much better and sophisticated interpretation that can be provided by an empirically based lumped parameter model." For watershed modeling, "the small-scale requirements of overland and unsaturated zone flow domains

exhibit severe limitations on efforts of fully integrating the system. *Consequently, a hybrid modeling approach is more suitable in which distributed- and lumped-parameter models are essentially linked and blended to obtain a semi-distributed watershed model*" [5].

"Semi-distributed" as used here indicates that a portion of the spatial or temporal domain is distributed while the rest is lumped, hence "semi-distributed." Kirchner [24] uses a similar line of reasoning to propose hybrid "gray box" models to allow some latitude for unexpected physical processes.

TREX and SAC-SMA differ in nearly all of the systems of classification: one is lumped and the other distributed; one is empirical and conceptual and the other is physically based. With these differences, the combination of these models can create a powerful hybrid.

This chapter illustrates the capabilities of hybrid hydrologic models. The example of TREX-SMA applications at California Gulch, Colorado, demonstrates the hybrid modeling capabilities.

17.2 Modeling with TREX and SMA

The main concept of hybrid modeling stems from the possible combination of the distributed surface-water modeling capabilities of TREX with the SAC-SMA techniques for soil moisture volumes and return flow from the subsurface.

The TREX surface runoff model was developed at Colorado State University, and the Sacramento Soil Moisture Accounting (SAC-SMA) model is well known from the National Weather Service (NWS). Each model has strengths that contribute to the hybrid, and each also has limitations, some of which are overcome with the hybrid approach.

17.2.1 TREX

The TREX model is based on the distributed surface hydrology model CASC2D developed at CSU [21,42]. Johnson [18] and Rojas-Sánchez [39] added a sediment transport algorithm, and the code was renamed CASC2D-SED [19,40,41]. Velleux [49] developed a contaminant transport algorithm with capability to model multiphase transport and fate of metals. The new code, now called TREX, was fully tested for the transport of Zn, Cu, and Cd from mining areas at California Gulch, Colorado [50,51]. The current TREX code is available on the web at www.engr.colostate.edu/trex.

17.2.2 SAC-SMA

The SAC-SMA model is part of the National Weather Service River Forecast System (NWSRFS), which is considered the standard in flood forecasting models for the United States [6,45]. SAC-SMA, together with simple routing models, provides a primary method for channel flow forecasting in the NWSRFS. The SAC-SMA model conceptualizes the watershed as an abstracted soil column divided vertically into two storage zones that are filled and emptied to simulate infiltration, percolation, baseflow, and interflow through the watershed. The upper and lower zones represent the infiltration capacity of shallow soils and the underlying aquifer, respectively.

Runoff is computed as the net excess volume remaining from precipitation after interception, and infiltration have been satisfied. Rates of infiltration and water holding capacities of the zones are represented with conceptual parameters that, while not directly physical, correspond closely to physical values such as void space ratio and saturated hydraulic conductivities [6].

The conceptualization of finite volumes filling, draining, and spilling like a collection of interconnected buckets gives rise to the SAC-SMA model's designation as a "bucket" model. Although not physically based, the Sacramento model parameters can be estimated a priori using the assumption that plant extractable soil moisture is related to tension water and that free water storages relate to gravitational soil water [27]. Using soil properties defined in the Soil Survey Geographic (SSURGO) database and

based on calibration experience, Anderson et al. [3] developed a range of acceptable values for 11 of the SAC-SMA parameters. Research by the NWS during recent years has focused on producing estimates of the SAC-SMA parameter values from known soil properties and remotely sensed data. These a priori estimates of the model parameters allow for uncalibrated simulation of watershed scale rainfall–runoff response with distributed versions of the SAC-SMA model [3,25,26,46].

17.3 TREX-SMA: Model Processes and Algorithms

The TREX-SMA hybrid model has three primary layers: the TREX surface, the SAC-SMA upper zone, and the SAC-SMA lower zone. The hybrid model essentially preserves the raster-based distributed nature of the TREX model for the simulation of surface processes as well as the lumped and conceptual nature of soil moisture accounting with SMA. The links between the two models are provided from the following: (1) the infiltration from TREX is input to the SMA upper zone and (2) the SMA returns subsurface flow as point sources to the TREX surface flow algorithm.

More specifically, precipitation excess is calculated at each pixel and routed as 2-D surface runoff across the surface until it is conveyed as 1-D channel flow. The infiltration rates are removed from the surface domain and collectively lumped as input to the soil moisture accounting procedure of the SMA upper zone. Within the soil moisture accounting procedure, the volume (or depth) of water in the soil column is divided into two components: bound water and free-flowing water in both the upper zone and the lower zone. The free-flowing water replenishes the bound water zones when the latter is depleted. Evapotranspiration (ET) is extracted from both the upper zone and the deep bound water to be returned to the atmosphere. The free-flowing water in the upper zone flows into the lower zone according to a percolation function. The capabilities of TREX-SMA are summarized in Table 17.1.

The detailed algorithms for surface hydrology and flow-routing processes of the TREX-SMA hybrid are described in this section.

17.3.1 Rainfall and Interception

Rainfall precipitation starts the hydrologic simulation. TREX-SMA creates a linearly interpolated precipitation function for each gage by reading a user-entered table of intensity-time pairs. If multiple gages are available, an inverse distance-weighted function is applied to compute rainfall intensities at points

TABLE 17.1 Algorithms for Hydrologic Processes in TREX-SMA

Process/Model Component	TREX
Precipitation distribution	Thiessen, inverse distance square weighted, stochastic storms, gridded radar
Snowfall accumulation and melting	Degree-day method
Precipitation interception	User-defined
Overland water retention	Idem
Infiltration	Green and Ampt
Overland flow routing	2-D diffusive wave: Saint Venant equations
Channel routing	1-D diffusive wave: upstream explicit
New components	*In TREX-SMA*
ET	User-entered PET
Soil moisture in vadose zone	Bucket
Lateral groundwater flow	Conceptual
Stream/groundwater interaction	1-way return from SMA zones
Exfiltration	N/A

between the gages. Capabilities to use gridded radar rainfall precipitation from the NEXRAD/WSR88D were also developed by Jorgeson and Julien [20]. Uniform rainfall intensity is used when only one gage is present.

Interception depending on the land use and vegetation type is removed from the rainfall precipitation. In TREX-SMA, the net precipitation volume is expressed as a unit flow rate by multiplying by cell area and dividing by the time step length.

17.3.2 Soil Infiltration

The Green and Ampt [15] equation models infiltration as a step or "piston" wetting front that penetrates downward into an infinite soil horizon according to soil moisture deficit, capillary suction head, and saturated hydraulic conductivity. The Green and Ampt equation determines the maximum rate of water entering the subsurface domain and gives a depth of new infiltration in each cell for each time step. Infiltration depths are summed across the cells belonging to a particular upper zone, and an average is computed as the primary input for the soil moisture code:

$$f = K_h \cdot \left(1 + \frac{H_c \cdot M_d}{F}\right) \tag{17.1}$$

where

f is the infiltration rate [L/T]
K_h is the saturated hydraulic conductivity [L/T]
H_c is the capillary pressure head at the wetting front [L]
M_d is the soil moisture deficit [dimensionless]
F is the total infiltrated depth [L]

$$M_d = (\theta_e - \theta_i)$$
$$\theta_e = (\phi - \theta_r) \tag{17.2a and b}$$

where

θ_i, θ_r are the initial and residual saturation, respectively [dimensionless]
θ_e, ϕ are the effective and total soil porosity, respectively [dimensionless]

$$M_d = (1 - S_e) \cdot \theta_e$$
$$S_e = \frac{\theta_i}{\theta_e} \tag{17.3a and b}$$

$$f = \frac{p_1 + \sqrt{p_1^2 + 8 \cdot p_2 \cdot \Delta t}}{2.0 \cdot \Delta t} \tag{17.4}$$

where p_1 and p_2 are solution parameters as given by Velleux [49]

$$p_1 = K_h \cdot \Delta t - 2.0 \cdot F$$
$$p_2 = K_h \cdot \left(F + H_c \cdot M_d\right) \tag{17.5}$$

with F, K_h, Δt, M_d, and H_c defined from the previous equations:

$$t_l = K_h \cdot \left(1 + \frac{H_w + H_c \cdot M_d}{T}\right) \tag{17.6}$$

where

t_l is the transmission loss rate [L/T]
H_w is the hydrostatic pressure head of water [L]
T is the total depth of transmission losses [L]

17.3.3 Depression Storage

As runoff begins to occur, some of the precipitation excess will be retained in small discontinuous depressions in the land surface. The retained water volume is referred to as depression storage on the land surface and dead storage when it occurs in channels. Dead and depression storage are always subject to infiltration and evaporation. Depression storage acts functionally as a simple abstraction from the volume of water running off of the land surface. For multiple events, dead and depression storage remaining from previous events will contribute to more rapid runoff response in the watershed.

17.3.4 Overland and Channel Flow Routing

TREX-SMA describes conservation of mass and momentum. The diffusive wave approximation of the Saint Venant equation is formulated to estimate the energy grade line or friction slope S_f for both overland and channel flow. The diffusive wave approximation considers flow generated by differences in head due to depth, as well as bed slope. This allows for flow calculations on horizontal and adverse slopes. Manning roughness derived from land cover and soil type defines flow resistance in energy slope calculations.

The diffusive wave approximation neglects the local and convective acceleration terms of the Saint Venant equations. Richardson and Julien [38] investigated the relative magnitude of all the terms of the Saint Venant equation for overland flow. Their analysis confirms that the neglected terms of the Saint Venant equation are insignificant and that the diffusive approximation is appropriate for most cases of overland flow. In channel flows, Lettenmaier and Wood [28] also showed that the neglected terms of the diffusive wave approximation can become significant when the slope is very small. At California Gulch, with the average slope of 12.5%, the diffusive wave approximation is sufficiently accurate.

Ogden and Julien [32] and Molnár and Julien [30] pointed out that spatial and temporal distributions of rainfall and grid scale may be expected to affect the hydrograph calculations far more than the diffusive wave approximation. However, based on their conclusions, the 30 m grid spacing used at California Gulch is adequate to prevent grid-scale effects from influencing the results from this research.

The solution scheme for overland and channel water depth in TREX is the second-order modified Euler scheme (equivalent to the midpoint method of Cheney and Kincaid [8, p. 407]) which uses the current depth plus an approximate first derivative of the state derived from the prior time step to predict the next time step state. The method uses the unit flow computed from the Manning formulation to predict the depth of water in a model cell in the next time step as detailed in Julien et al. [21] and is known to be unconditionally stable as long as the forward step size satisfies the Courant–Friedrichs–Lewy (CFL) condition [2,9].

In TREX-SMA, surface runoff is calculated with a 2-D formulation of the Saint Venant equation with friction slope in each of x- and y-directions defined using the Manning formulation. Channel flow is computed using 1-D formulations for both continuity and momentum with the diffusive wave

approximation. Point inflows or extractions from other sources, such as water treatment plant discharges, springs, or irrigation diversions, can be added or subtracted as source terms:

$$\frac{\partial h}{\partial t} + \frac{\partial q_x}{\partial x} + \frac{\partial q_y}{\partial y} = i_e \tag{17.7}$$

where

i_e is the net rainfall excess [L/T]
$\partial h/\partial t$ is the change in depth with respect to time [L/T]
$\partial q_y/\partial y$, $\partial q_x/\partial x$ are the partial derivatives of planar components of the unit flow (volumetric flow divided by width) with respect to their corresponding flow directions [L/T]

$$h^{t+\Delta t}(j,k) = h^t(j,k) + \Delta t \cdot i_e - \left[\frac{q_x^t(k \to k+1) - q_x^t(k-1 \to k)}{W} + \frac{q_y^t(j \to j+1) - q_y^t(j-1 \to j)}{W} \right] \cdot \Delta t \tag{17.8}$$

where

$h^{t+\Delta t}(j,k)$ is the flow depth in cell (j,k) in next time step
$h^t(j,k)$ is the flow depth at the current time
Δt is the time step
i_e is the net rate of infiltration excess runoff production
$q_x^t(k \to k+1)$; $q_x^t(k-1 \to k)$ are the unit outflow and inflow in x-direction
$q_y^t(j \to j+1)$; $q_y^t(j-1 \to j)$ are the unit outflow and inflow in y-direction
W is the cell width

$$\Delta t < \frac{\Delta x}{V} \tag{17.9}$$

where

Δt is the time step
Δx is the grid cell size
V is the mean flow velocity

$$S_{fx} = S_{0x} - \frac{\partial h}{\partial x} \tag{17.10}$$

$$S_{fy} = S_{0y} - \frac{\partial h}{\partial y} \tag{17.11}$$

where

S_{fx}, S_{fy} is the friction slope in each of x- and y-directions [dimensionless]
S_{0x}, S_{0y} is the change in depth with respect to time [dimensionless]
$\partial h/\partial x$, $\partial h/\partial y$ are the partial derivatives of depth with respect to their corresponding flow directions [L/L]

$$q_x = \alpha_x h^\beta \tag{17.12}$$

$$q_y = \alpha_y h^\beta \tag{17.13}$$

$$\alpha_x = \frac{S_{fx}^{1/2}}{n} \tag{17.14}$$

$$\alpha_y = \frac{S_{fy}^{1/2}}{n} \tag{17.15}$$

where

α_x, α_y is the resistance coefficient in the x- or y-direction [$L^{1/3}/T$]
β is the resistance exponent = 5/3 [dimensionless]
n is the Manning roughness coefficient [$T/L^{1/3}$]

$$\frac{\partial A_c}{\partial t} + \frac{\partial Q}{\partial x} = q_l \tag{17.16}$$

where

A_c is the cross-sectional area of flow [L^2]
Q is the total discharge [L^3/T]
q_l is the unit lateral inflow [L^2/T]

17.3.5 Soil Moisture Accounting in the Upper Zone

In TREX-SMA, the infiltrated water enters the subsurface domain via the upper soil moisture zone. Water is distributed between two portions in the upper zone: the bound water portion (tension water) and the free-flowing portion (free water). Abstractions from the upper zone include evaporation and transpiration, percolation losses to the lower zone, water redistribution, and return flow releases to the surface as interflow.

17.3.5.1 Evaporation and Transpiration

Evaporation and transpiration are central to the mass balance in the inter-storm periods. The ET abstraction is removed first from the bound pore water volumes in the model. TREX-SMA currently uses a single constant ET demand for the entire simulation and uniform across the model domain. Any distribution of ET computed from any model could theoretically be used as input since the model aggregates the demand from all cells to compute a total ET for each upper zone. ET is first removed from the upper zone tension water based on the ET demand computed from the user-entered potential ET scaled by the available water in the upper zone. If the scaled demand is greater than the amount available in the upper zone tension water storage volume, the additional demand is subtracted from the lower zone tension water storage and the upper zone free water storage. In the present formulation, a simple constant potential ET rate is applied across the model. The free water from the lower zone is not consumed by ET:

$$ET_{actual,uz} = ET_{demand} \cdot \frac{Fw_{c,uz}}{Fw_{m,uz}} \tag{17.17}$$

where

ET_{demand} is the accumulated ET demand for the upper zone for the time step [L]
$ET_{actual,uz}$ is the amount of demand removed from the upper zone [L]
$Fw_{c,uz}$ is the upper zone free water current storage [L]
$Fw_{m,uz}$ is the upper zone free water capacity [L]

In addition to gravity-driven percolation, water in the physical soil column is influenced by capillary forces that drive water movement toward dry soils with a high capillary potential. The tension water

zone represents this capillary soil storage. Following the subtraction of ET losses, a balancing equation transfers excess free water to the tension volume. The transfer occurs when the storage ratio of the tension water is less than the storage ratio of free water. Redistribution exchanges water between the free water and tension water storage until the free and tension water ratios (the current volume divided by maximum storage) are equal.

A similar computation balances the water in the lower zone when the evaporation demand is sufficiently high. For the lower zone, the redistribution occurs if the tension water storage ratio is less that the total lower zone storage ratio:

$$\frac{Tw_{c,uz}}{Tw_{m,uz}} < \frac{Fw_{c,uz}}{Fw_{m,uz}} \tag{17.18}$$

$$\frac{Tw_{c,lz}}{Tw_{m,lz}} < \frac{Fw_{c,lz} + Tw_{c,lz}}{Fw_{m,lz} + Tw_{m,lz}} \tag{17.19}$$

The assumption is that if for any reason, the free water storage contains significantly more volume than the tension water than the free water will resupply the tension water. This could happen if the tension water capacity is small relative to the free water capacity and the evaporation is high. This assumption is consistent with the overarching assumption in the Sacramento model that tension water volumes are always satisfied first before any other volumes.

17.3.5.2 Interflow

At each time step, the upper zone free water storage releases water to the surface as interflow. Interflow is computed based on a simple rate equation. An effective depletion coefficient is obtained by multiplying the standard depletion coefficient by the time step.

The upper zone storage depletion coefficient defines the flow released per volume of stored water in the zone, normalized by the area of the model contributing to the given zone. The internal units of the soil moisture accounting procedure are 1-D length (e.g., millimeters) so the outgoing flow is scaled by the upper zone area. As used in the Sacramento model implemented in NWSRFS, the standard upper zone depletion coefficient is calibrated in units of millimeters released per millimeters stored per day. More specifically, the TREX-SMA model uses a conversion factor to account for different time steps:

$$V_{intf} = k_{uz,eff} \cdot Fw_{c,uz} \tag{17.20}$$

where

V_{intf} is the baseflow unit volume for the time step [L]
$Fw_{c,uz}$ is the current unit volume of upper zone free water [L]
$k_{uz,eff}$ is the effective upper zone free water storage depletion coefficient [dimensionless]

$$k_{uz,eff} = k_{uz} \cdot \Delta t \tag{17.21}$$

where

k_{uz} is the standard upper zone free water storage depletion coefficient [L/(L · T)]
Δt is the current model time step [T]

$$V_{intf} = k_{uz} \cdot \Delta t \cdot Fw_{c,uz} \cdot \text{Area} \cdot \text{Conversion factors} \tag{17.22}$$

or written to emphasize the units as

$$V_{intf} = k_{uz,eff} \cdot \Delta t \cdot Fw_{c,uz} \cdot \text{Area} \cdot \text{Conversion factors}$$
$$\left[\text{m}^3\right] = \left[\frac{\text{mm}}{\text{mm} \cdot \text{day}}\right] \cdot [\text{s}] \cdot [\text{mm}] \cdot \left[\text{m}^2\right] \cdot \frac{\text{meter}}{1{,}000\,\text{mm}} \cdot \left[\frac{1\,\text{day}}{86{,}400\,\text{s}}\right] \tag{17.23}$$

Similar scaling is required to obtain an effective storage depletion coefficient for the lower zone free water storage depletion coefficients, taking into consideration the time step and also scaling from the NWSRFS parameter range that is used in TREX-SMA.

17.3.6 Soil Moisture Accounting in the Lower Zone

Water drains into the lower zone via percolation. Losses from the lower zone include ET and baseflow.

17.3.6.1 Percolation

Water is transferred from the upper zones to the lower zones via the percolation computation. The percolation demand is computed as a demand in millimeters per day. A conversion is applied to determine the effective demand for the relatively small time steps occurring in the TREX-SMA model. The lower zone percolation demand (demand for water from the upper zone to fill lower zone free water storages) is computed from a base percolation rate parameter and a two-parameter percolation curve that multiplies the percolation rate based on the current free water state. The actual percolation is reduced from the percolation demand based on the availability of upper zone free water. The total volume removed is limited by the amount in the upper zone free water current storage volume, to prevent mass balance errors. More specifically,

$$Perc_{demand} = Perc_{base} \cdot \left[1 + zperc \cdot \frac{a}{b}^{rexp}\right] \tag{17.24}$$

where

$Perc_{demand}$ is the percolation demand [L/T]
$Perc_{base}$ is the base percolation rate [L/T]
zperc is the percolation multiplier
rexp is the wet vs. dry percolation differentiation exponent
factors *a* and *b* define the aggregate lower zone deficiency ratio:

$$\frac{a}{b} = \frac{Tw_{m,lz} + \Sigma Fw_{m,lz} - Tw_{c,lz} + \Sigma Fw_{c,lz}}{Tw_{m,lz} + \Sigma Fw_{m,lz}} \tag{17.25}$$

$$Perc_{actual} = Perc_{demand,eff} \cdot \frac{Fw_{c,uz}}{Fw_{m,uz}} \le Fw_{c,uz} \tag{17.26}$$

17.3.6.2 Baseflow

In TREX-SMA, the baseflow is returned to surface runoff as a point source as calculated from

$$V_{basf} = k_{lz,eff} \cdot Fw_{c,lz} \tag{17.27}$$

where

V_{basf} is the baseflow volume [L]
$k_{lz,eff} = k_{lz}$[L/(L · T)] · Δt[T] is the effective lower zone free water storage depletion coefficient [dimensionless]

In order to allow multi-event simulation with TREX-SMA, the saturation condition of the soil moisture is used to re-initialize the parameters of the Green and Ampt infiltration equation:

$$\text{SMA summary state} = \frac{\sum Tw_{c,uz}, Fw_{c,uz}, Tw_{c,lz}}{\sum Tw_{m,uz}, Fw_{m,uz}, Tw_{m,lz}} \tag{17.28}$$

Infiltration parameters remain fixed for the duration of each storm and are allowed to recover soil moisture deficit between storms due to ET and drainage. In SMA, a storm ends at cessation of rainfall, when the precipitated water falls below a user-entered threshold value. The model does not change the infiltration parameters immediately upon cessation of rainfall, but continues to allow infiltration to occur using the Green and Ampt parameters set at the beginning of each storm.

17.4 Hybrid Modeling Application at California Gulch

The TREX-SMA model will be demonstrated using data from the California Gulch watershed near Leadville, Colorado, shown in Figure 17.1.

17.4.1 Location and Site Description

A general description of the California Gulch watershed is given by Velleux et al. [51]:

> California Gulch is part of a historical mining district located near Leadville, CO. The site is in the headwaters of the Arkansas River basin and covers an area of 30 km^2. The watershed includes upper and lower reaches of California Gulch (CG), Stray Horse Gulch, Starr Ditch (SD), and several smaller drainages.

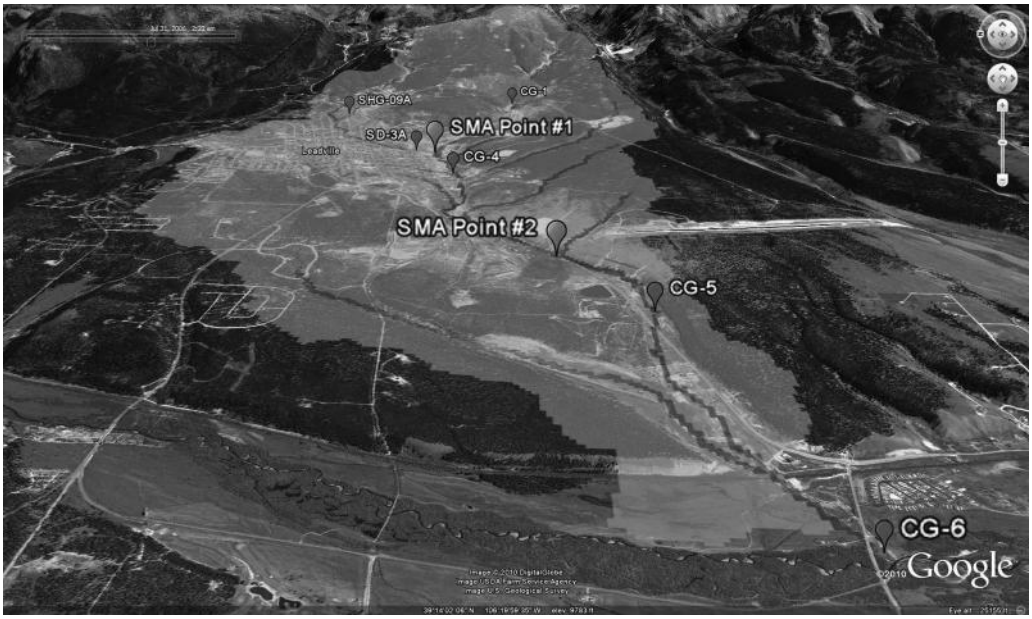

FIGURE 17.1 Oblique view of the California Gulch watershed looking east. The light shading indicates the watershed delineation from the USGS NED at 30 m resolution. CG-4 is located near the city of Leadville. SMA outlets are located above CG-4 and CG-5.

Due to the history of surface mine waste accumulation, the area of California Gulch was added to the US EPA National Priority List in 1983 [16,48]. The national priority list sites are designated as part of the Comprehensive Environmental Response, Compensation, and Liability Act (CERCLA) commonly known as Superfund [48].

17.4.2 Elevation and Topography

Elevations in the watershed range from 2,900 m (9,600 ft) at the Arkansas River to 3,650 m (12,000 ft) on top of Ball Mountain at the eastern boundary of the watershed. The average slope is 12.6% [51]. The city of Leadville, roughly in the center of the watershed, contains a small watershed divide between California Gulch and Malta Gulch with the majority of runoff from the city draining into California Gulch. The deep channel of California Gulch dominates the general topography of the valley as it runs from the bedrock formations of the upper watershed down through the alluvium and glacial deposits in the lower watershed.

The USGS 1/3rd arc second digital elevation model (DEM) from the National Elevation Dataset (NED) provides the basis for all topographic computations in the model. The site was simulated on a 30 m × 30 m grid based on the nominal dimensions of the NED, and the watershed area was delineated with 34,002 cells for the overland plane. All other distributed inputs were converted to the same spacing for purposes of calculation. The model setup from Velleux et al. [51] was replicated for use with the TREX-SMA simulations.

17.4.3 Land Use

In the TREX-SMA model, land use classification is used to determine overland flow roughness and interception depth. The NLCD 2001 land use dataset from NASA and USGS distinguishes 13 different land use classes in the California Gulch watershed. Evergreen forest dominates the majority of the watershed except for the urban area of Leadville, and mining or otherwise industrially impacted lands that are classified as either "commercial" or "bare rock."

17.4.4 Soil Type

Within the watershed, the USDA identifies 14 different soil associations. These were used along with a separate class for soils within the city of Leadville urbanized (subdivided by land use) to create a total of 17 soil classes for the model.

The characteristics (K_h, H_c, K, porosity, grain size distribution, etc.) of each soil class were defined based on values reported in the NRCS SSURGO database as well as texture.

The method of Rawls et al. [34,35] was used to generate initial values for the Green and Ampt parameters (saturated hydraulic conductivity and capillary suction head) for use in the model. K_h values were calibrated by Velleux et al. [51] to achieve agreement between measured and simulated runoff.

17.4.5 Temperature

Hourly air temperature data were obtained for the modeling period from the Western Regional Climate Center (WRCC) for the weather station at the Leadville airport 5 km (3.2 mile) south of Leadville. The Leadville airport gage is at 9,938 ft above mean sea level. A normal adiabatic lapse rate of 3.6°F per 1,000 ft would predict temperatures approximately 8°F cooler at the top of Ball Mountain (elevation 12,300 ft) and 1°F warmer at the watershed outlet (elevation 9,530 ft) into the Arkansas River. The climate record shows that daily extremes stayed well above freezing for nearly all the simulated period eliminating concern about frozen ground effects.

17.4.6 Evapotranspiration

The inter-event recovery of infiltration capacity in the soil moisture zones of TREX-SMA is driven by the release of water to the channel and by ET [43]. Pan evaporation has been measured at the Sugarloaf Reservoir weather station operated by the Bureau of Reclamation since 1948. The pan is located southeast of the dam at 39°15′ north and 106°22′ west at an elevation of 2968 m (9738 ft), approximately 7 km (4.4 mile) west of the City of Leadville and 125 m (410 ft) lower in elevation. During summer months, when snow cover is largely absent, the values from the Sugarloaf Pan should be indicative of conditions in California Gulch [17].

Monthly evaporation values from the WRCC data show that for the months of July and August 2006, evaporation was less than the corresponding cumulative monthly averages for 1948 through 2005 [31]. The reduced evaporation is related to the occurrence of more precipitation that usual, one reason why this summer period was chosen for simulation.

Daily records from the pan show fluctuations between nearly 0 and 0.32 in. per day for July and August 2006. For purposes of simulation, the 2006 monthly averages from the WRCC were used to compute an average potential ET rate of 5.6 in. per month. This value was applied as a constant demand during all simulations.

17.4.7 Precipitation

As part of the CERCLA/Superfund efforts in California Gulch, a program to monitor the impact of mine waste transport on Arkansas River ecology, a network of automated pluviographic and fluvial gaging stations was established by the EPA. Automated sampling stations were installed each summer from 2003 through 2008 approximately from June through September. The automated sampling program 2009 and 2010 only included the peak runoff season. Gage locations and descriptions are given in Table 17.2. Precipitation and channel flow are recorded at 10 min intervals for stations labeled as CG-1, SHG-09, CG-4, and CG-6, and measurements are also made at locations CG-5, SD-3A, OG-1, AR-1, and AR-3A.

The summer of 2006 included at least eight significant convective storms with measurable precipitation recorded at all four automated pluvial gaging stations. A series of nine storms from summer 2006 were used as input to test the multi-event simulation capabilities of the TREX-SMA model. The first and most intense storm in the series occurred on July 19 (the same used for the baseflow modeling simulation). The subsequent storms occurred on a roughly weekly basis following the first storm on July 25/26, July 30/31, August 5/6, and August 10/11. All of these storms occurred when snowmelt influences on streamflow in California Gulch had largely subsided for the summer.

TABLE 17.2 Automated Gage Locations and Available Data

Gage	Description	Available Data
SHG-09	300 ft below Emmett retention pond	1, 2, 3, 4, 5, 6
SD-3A	Flume in Starr Ditch downstream of Monroe St. and upstream of drop structure	1, 2, 3, 4, 5
CG-1	California Gulch immediately upstream of the Yak Tunnel portal	1, 2, 3, 4, 5, 6
OG-1	Oregon Gulch immediately upstream of confluence with California Gulch	1, 2, 3, 4, 5
CG-4	California Gulch downstream of confluence with Oregon Gulch	1, 2, 3, 4, 5, 6
CG-5	California Gulch upstream of the Leadville Wastewater Treatment Plant	1, 2, 3, 4, 5
CG-6	California Gulch immediately upstream of confluence with Arkansas River	1, 2, 3, 4, 5, 6
AR-1	Arkansas River upstream of confluence with California Gulch, approximately 0.25 miles downstream of the confluence with Tennessee Creek	1, 2, 3, 4, 5
AR-3A	Arkansas River approximately 0.5 mile downstream of confluence with California Gulch	1, 2, 3, 4, 5

1, Stage; 2, discharge; 3, temperature; 4, conductivity; 5, pH; 6, precipitation.

During the July 19th storm, the most intense precipitation was measured in SHG at the SHG-09A gage, registering 0.4 in. in 10 min, equivalent to an intensity of 2.4 in./h. For comparison, a 100-year, 2 h storm for the watershed would reach 0.87 in./h, distributed over the watershed [44].

The observations at the four different precipitation gages show that the storms vary in geographic distribution. Throughout the summer, storms were recorded in which not all gages received precipitation. Many of these were biased toward the upper watershed (near CG-1 and SHG-09A). For instance, the August 6th storm was an upper watershed storm that generated significant flow at CG-1 but at no other gage. A simple weighting scheme placing the centroid of the total precipitation along the East–West axis of the watershed classified each storm as primarily upper or lower watershed.

17.4.8 Stream Flow

Data from 2003 through 2007 were evaluated to find a suitable modeling period. The precipitation and streamflow hydrographs from the automatic gaging stations during a nonsnowmelt period at the end of the summer of 2006 were selected for testing TREX-SMA. Several large precipitation peaks and correspondingly significant runoff signatures allow examining simulation quality during both high and low flows.

17.4.9 Hybrid Model Parameters

All surface model parameters for the multi-event simulation were drawn from the model calibration and validation by Velleux [49]. These calibrated parameters have been used for several event-based simulations of contaminant transport as seen in two papers by Velleux et al. [50–52] and further discussed by Caruso et al. [7]. Related work in the same basin has also been published by Rojas-Sánchez et al. [41] and for the simulation of extreme events including the PMP–PMF by England et al. [14].

For the multi-event simulation reported in this chapter, parameters for the SMA zones were drawn from the a priori dataset described by Koren et al. [26]. The parameter values are determined a priori using soils and land use data and are used by scientists at the NWS Arkansas Basin River Forecast Center (ABRFC) for regional hydrologic forecasting using the NWS distributed hydrologic model (DHM) [25]. For this research, the parameters from the three 4 km × 4 km grid cells aligned east and west nearest to Leadville (those most nearly corresponding to the California Gulch watershed area) were averaged to provide values for use in modeling, which are shown in Table 17.3.

17.5 TREX-SMA Results and Discussion

17.5.1 Multi-Event Simulation Hydrographs

We applied the TREX-SMA model to a real case at California Gulch in which 50 days of precipitation inputs were used to drive a model simulation. The multi-event simulation was carried out twice: once with the SMA submodel active, resetting the infiltration parameters at appropriate times, and once again with no infiltration resetting. The simulations and their respective results are distinguished in this discussion as “SMA” for the hybrid TREX-SMA simulations and “no-SMA” for TREX simulations without SMA.

The basin hydrologic response is captured most succinctly in the hydrographs showing the flow as a function of time through the simulated period. As expected, the TREX-SMA simulation reduces the simulated hydrograph peaks, especially for storms later in the series as the SMA zones dry out toward the end of summer. Figure 17.2 shows the aggregate basin response at CG-4 near Leadville for simulations with and without the SMA submodel. Observed flows are also shown on the plot, for comparison to the simulated flow. The graphical evidence of the reduced peaks shown in these figures is the most

TABLE 17.3 Soil Moisture Accounting Parameters for Multi-Event Simulations with Re-Initialization as Given by Anderson et al.

No.	Parameter	Description	Used for Multi-Event Model	Acceptable Ranges
1	UZTWM	The upper layer tension water capacity, mm	52	10–300
2	UZFWM	The upper layer free water capacity, mm	43	5–150
3	UZK	Interflow depletion rate from the upper layer free water storage, day^{-1}	0.51	0.10–0.75
4	ZPERC	Ratio of maximum and minimum percolation rates	45	5–350
5	REXP	Shape parameter of the percolation curve	1.54	1–5
6	LZTWM	The lower layer tension water capacity, mm	240	10–500
7	LZFSM	The lower layer supplemental free water capacity, mm	17.3	5–400
8	LZFPM	The lower layer primary free water capacity, mm	219	10–1000
9	LZSK	Depletion rate of the lower layer supplemental free water storage, day^{-1}	0.180	0.01–0.35
10	LZPK	Depletion rate of the lower layer primary free water storage, day^{-1}	0.0473	0.001–0.05
11	PFREE	Percolation fraction that goes directly to the lower layer free water storages	0.080	0.0–0.8
12	PCTIM	Permanent impervious area fraction	Not used	Not estimated
13	ADIMP	Maximum fraction of an additional impervious area due to saturation	Not used	Not estimated
14	RIVA	Riparian vegetarian area fraction	Not used	Not estimated
15	SIDE	Ratio of deep percolation from lower layer free water storages	0.99	Not estimated
16	RSERV	Fraction of lower layer free water not transferable to lower layer tension water	Not used	Not estimated

Source: Anderson, R.M. et al., *J. Hydrol.*, 320(1–2), 103, 2006.

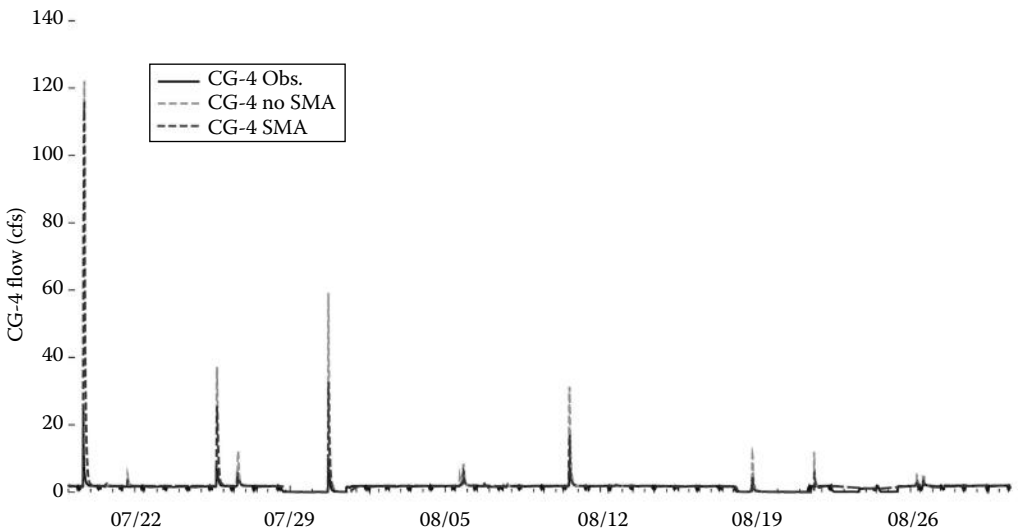

FIGURE 17.2 Simulated TREX-SMA (dark-dashed line), TREX without SMA (light-dashed line), and observed hydrographs (solid line) for California Gulch at CG-4 (just below Leadville) during the multi-event simulation period, July 19 through August 31, 2006.

convincing measure of the improvement brought with the SMA re-initialization procedure. For most storms, the no-SMA case overpredicts the basin response, while the reduced SMA peak corresponds more closely to the observed flow.

Generally speaking, the hydrographs show that the TREX-SMA model has reduced the overprediction of peaks. Only the SHG-09A hydrograph seems unmodified—the soil types in that portion of the watershed have such low infiltration rates that the differences in soil moisture do little to increase or decrease the infiltration. The inter-event periods show apparently very good fit to observed data for both SMA and no-SMA cases.

17.5.2 Overall Statistical Performance

For this research, the statistical performance is an indication of the level of model improvement that can be achieved with a hybrid model. Table 17.4 shows the comparisons of various statistical parameters for the TREX model with and without the SMA hybrid component. Overall, a modest improvement of the simulation results could be achieved by adding the hybrid component to the TREX model. Table 17.4 lists various parameters including the Nash–Sutcliffe coefficient, the percent bias, the absolute percent bias, the root-mean-square error (RMSE) ratio, and other descriptive statistics.

17.5.3 Sources of Uncertainty

A number of sources contribute to the uncertainty in the model. These are not failings in the model—uncertainty is part of engineering modeling [33].

Clearly, the assumptions used to create the individual model components contribute to the modeling uncertainty, for example, the numerical solution of the governing equations. Specific assumptions in this implementation of the model also produce uncertainty, like the very small volume of water not recovered by evaporation from the soil moisture zones. Grid scales provide additional uncertainty since the calibrated parameters are really "effective" parameters for the given grid size and averaging the properties across each cell. It has to be recognized that averaging the properties over each cell is a better approximation than averaging properties over the entire watershed as assumed in lumped-parameter models.

Measurement errors may also be present in some data sources used for the precipitation inputs and for comparison of output. The rainfall input data from the limited number of rain gages are also among the most significant possible sources of error. Rainfall measurements at the four rain gages characterize the precipitation distribution in the basin, and the most elevated of these, SHG-09A and CG-1 (10,450 and 10,331 ft, respectively) were still more than 1,500 ft below the summit of the watershed. Significant orographic precipitation may be found at the greater elevations. The large variation in elevation makes it very difficult to capture all the spatial and temporal variability of rainfall precipitation on

TABLE 17.4 Statistical Analysis Showing Improvement with the SMA Algorithm

Statistic Name	Statistic (Optimal Value)	CG-4		CG-6	
		W/o SMA	With SMA	W/o SMA	With SMA
Nash–Sutcliffe efficiency index	NS (1.0)	0.17	0.19	0.44	0.46
Pearson correlation coefficient	corr (1.0)	0.60	0.56	0.67	0.70
Modified correlation coefficient	modcorr (1.0)	0.48	0.46	0.49	0.52
Percent bias	pb (0.0)	0.31	0.25	−0.03	0.00
Absolute percent bias	apb (0.0)	0.37	0.31	0.15	0.13
RMSE	rmse (0.0)	4.16	3.33	0.78	0.57
Percent RMSE	prmse (0.0)	2.79	2.24	0.36	0.26
RMSE ratio	rrmse (0.0)	4.93	3.96	1.14	0.83

this watershed. This is especially critical because about 95% of the water infiltrates in these simulations, so infiltration location will play a large role in the timing of flood peak arrival.

17.5.4 Advances in Model Visualization

A hydrologic model consists of a hydrologic core and a separate technological shell that is "the programming, user interface, pre- and postprocessing facilities, etc." [37]. GIS in modeling serves to assist where "the hydrologist needs to cooperate intensively with experts in the field of ecology, agriculture, urban planning, and economics" [13]. This is because "the pure numerical results of a simulation are no longer the final products delivered by the hydrologist. The results have to be translated systematically into hydrological effects and subsequently into socially relevant quantities … [so that] the hydrologist can no longer depend on tabular representations of his data … [and] graphical tools [are] a necessity" [10]. Johnson et al. [19] state that the spatial capabilities of the model combined with GIS data for input parameters are the *raison d'être* for CASC2D-SED: "The strength of the model CASC2D-SED lies in its tremendous potential and visual output…."

Viewing the model output in the context of the geography and other imagery is useful for at least two reasons. First, the visual comparison of topography and other geographic and spatial features allows for a rapid evaluation of the success of the simulation. Model output is visually compared to expectation similar to the visual comparison on observed and simulated hydrographs on a plot. Second, the primary consumers of the information from a hydrologic model will have questions with specific respect to location of effects such as overbank flow, points of maximum velocity, and scour problem areas. All of these effects may be evaluated with the TREX-SMA model.

The Google Earth™ viewer allows browsing of the series of overlays in both time and space. Any area may be highlighted for close viewing and the entire series may be animated or a particular time chosen using a time selector in the Google Earth™ interface. Other data such as gage locations may be inserted for additional context.

17.5.5 Results Displayed with KML

In order to further evaluate the simulation results, a 3-D interactive results display was implemented using Google Earth™ and the Keyhole Markup Language (KML). Google Earth™ is a web-based "virtual globe" that shows a 3-D view of the earth's surface in varying resolutions based on various sources of aerial imagery and digital terrain models. The KML is an xml-based scripting language designed to allow display of text and graphics on a virtual globe such as Google Earth™ [36,53].

To use Google Earth™ to display TREX-SMA results, grid cell values of the land surface and channel water depth were exported from the model simulation at given time intervals as raster images, and these images were ingested into a GRASS GIS database [29]. The maps were colorized according to the data values for each cell and then exported as a flat graphic that is referenced as a ground overlay in a simple KML file. The KML file specifies the spatial and temporal extent of the overlay (e.g., an overlay may represent the average model states from 12:00 am to 12:10 am of July 30, 2006, and have a north, south, east, and west maximum extent). The KML time points were specified along with an offset from GMT and positions using latitude and longitude. The appropriate KML tags were inserted to specify the transparency of each overlay to allow partial viewing of the standard Google Earth™ aerial image underneath the overlay showing the modeled value. The ground overlays were produced to show depth of flow (on the land surface and in channels) but could show any other distributed variable from the TREX-SMA output. The Google Earth™ interface also allows for the series of individual frames to be animated showing evolution of model processes over time.

A demonstration of these graphical methods was performed using an application of TREX by Velleux [49] at California Gulch near Leadville, Colorado. The 100-year storm was simulated as 1.73 in. of uniformly distributed rain falling in 2 h over the entire watershed. The 100-year analysis was used to

demonstrate the effect of applying the improved graphical techniques. To produce the animation, the same process described previously was used to create flat frames showing the depth of water on the land surface at various times through the simulation. The color maps were produced according to the data values for each cell and then draped on a DEM, also contained in the GIS.

Figure 17.3 shows the 100-year inundation extent on a background of an aerial image of Leadville and California Gulch, providing valuable information in an integrated view to better visualize surface processes including (1) an extent of inundation and flow interaction between the main channel and the floodplain, (2) runoff from urban and forested hillslopes, and (3) flow convergence and divergence from surface runoff and detention storage. In the sequence of frames from the figure, the progression of flooding mechanism is visible between the Malta Gulch channel and the main California Gulch channel. In the initial frame (Fig. 17.3a) at the cessation of rainfall shows overland flow conditions over the entire watershed. The second frame (Fig. 17.3b) 2 hours after the cessation of rainfall shows minimal overland flow in the light-shaded upland areas while the channels in the upper part of the watershed are flooded. The third frame (Fig. 17.3c), taken 4 hours after the cessation of rainfall, shows that the flood wave has propagated to the lower areas of the watershed. The flood waters from the main channel caused overbank flows. The floodplain waters will thereafter either return to the main channel or infiltrate in the floodplain areas.

Figure 17.3 displays a series of frames from such an animation generated from the simulation output of a 100-year flood. The animation shows movement of the different flood waves and can help in analyzing the watershed flood generation mechanism. For instance, the lower permeability of the bare upland soils is evident in that ponded water is still present well into the simulation when only the impervious surfaces in Leadville city are still producing runoff.

(a)

FIGURE 17.3 Selected frames from a loop showing the depth of water on a land surface using Google Earth 3-D terrain and imagery for a 100-year return period event (1.73 in. in 2 h) at California Gulch. The first frame 17.3a) shows overland flow conditions at cessation of rainfall.

(b)

(c)

FIGURE 17.3 (continued) Selected frames from a loop showing the depth of water on a land surface using Google Earth 3-D terrain and imagery for a 100-year return period event (1.73 in. in 2 h) at California Gulch. The second frame 17.3b) shows minimal overland flow conditions and channel flooding in the upper part of the watershed 2 hours after cessation of rainfall. The third frame 17.3b) shows that the floodwave propagated to the lower areas of the watershed and caused significant overbank flows.

17.6 Summary and Conclusions

A new hybrid approach to hydrologic modeling combines distributed surface runoff modeling with a lumped-parameter rendering of infiltration and subsurface flow. The hybrid model TREX-SMA combines the SAC-SMA model with the TREX surface hydrology model. The capabilities of hybrid modeling are demonstrated with an application to the 30 km^2 California Gulch watershed, near Leadville, Colorado. The results of a 50-day simulation are presented for comparisons with and without the hybrid model component SMA. Surface runoff parameters were obtained from a prior calibration of TREX, and the SMA soil moisture parameters were determined from a priori estimates used by the ABRFC of the NWS. The hybrid simulation results with TREX-SMA improved relative to results from the unmodified TREX model. Model results such as surface and channel water depth are processed with GRASS GIS and KML scripts to create 2.5-D, browsable animations overlaid on a Google Earth™ terrain.

References

1. Abbott, M.B. and Refsgaard, J.C. 1996. *Distributed Hydrological Modelling*. Springer, Heidelberg, Germany.
2. Alexiades, V., Amiez, G., and Gremaud, P.A. 1996. Super-time-stepping acceleration of explicit schemes for parabolic problems. *Communications in Numerical Methods in Engineering*, 12(1), 31–42.
3. Anderson, R.M., Koren, V.I., and Reed, S.M. 2006. Using SSURGO data to improve Sacramento Model a priori parameter estimates. *Journal of Hydrology*, 320(1–2), 103–116.
4. Aral, M.M. and Gunduz, O. 2003. Scale effects in large scale watershed modeling. In *Advances in Hydrology*, V.P. Singh and R.N. Yadava, eds., Allied Publishers, New Delhi, India, pp. 37–51.
5. Aral, M.M. and Gunduz, O. 2006. Large-scale hybrid watershed modeling. In *Watershed Models*, V.P. Singh and D.K. Frevert, eds., CRC/Taylor & Francis Group, Boca Raton, FL, pp. 75–95.
6. Burnash, R. and Ferral, L. 2002. Conceptualization of the Sacramento soil moisture accounting model. NWSRFS User Manual Documentation, National Weather Service, NOAA, Silver Spring, MD.
7. Caruso, B.S., Cox, T.J., Runkel, R.L., Velleux, M.L., Bencala, K.E., Nordstrom, D.K., Julien, P.Y., Butler, B.A., Alpers, C.N., Marion, A., and Smith, K.S. 2008. Metals fate and transport modelling in streams and watersheds: State of the science and USEPA workshop review. *Hydrological Processes*, 22(19), 4011–4021.
8. Cheney, W. and Kincaid, D. 1999. *Numerical Mathematics and Computing*. Brooks/Cole Pub Co., Pacific Grove, CA.
9. Courant, R., Friedrichs, K., and Lewy, H. 1928. Über die partiellen Differenzengleichungen der mathematischen Physik. *Mathematische Annalen*, 100(1), 32–74.
10. Deckers, F. and Te Stroet, C.B.M. 1996. Use of GIS and database with distributed modelling. In *Distributed Hydrological Modelling*, M.B. Abbott and J.C. Refsgaard, eds., Springer, Heidelberg, Germany pp. 215–216.
11. Dunne, T. and Black, R.D. 1970. An experimental investigation of runoff production in permeable soils. *Water Resources Research*, 6(2), 478–490.
12. Dunne, T. and Black, R.D. 1970. Partial area contributions to storm runoff in a small New England watershed. *Water Resources Research*, 6(5), 1296–1311.
13. Engelen, G.B. and Kloosterman, F.H. 1996. *Hydrological Systems Analysis: Methods and Applications*. Water Science and Technology Library, Kluwer, Dordrecht, the Netherlands.
14. England, J.F., Velleux, M.L., and Julien, P.Y. 2007. Two-dimensional simulations of extreme floods on a large watershed. *Journal of Hydrology*, 347(1–2), 229–241.
15. Green, W.H. and Ampt, G.A. 1911. Studies on soil physics. Part I—The flow of air and water through soils. *Journal of Agricultural Science*, 4, 1–24.

16. HDR. 2002. Final focused feasibility study for operable unit 6, California Gulch NPL Site, Leadville Colorado, HDR Engineering, Omaha, NE.
17. Henning, I. and Henning, D. 1981. Potential evapotranspiration in mountain geoecosystems of different altitudes and latitudes. *Mountain Research and Development*, 1(3/4), 267–274.
18. Johnson, B.E. 1997. Development of a storm event based two-dimensional upland erosion model. PhD dissertation, Department of Civil Engineering, Colorado State University, Fort Collins, CA.
19. Johnson, B.E., Julien, P.Y., Molnár, D.K., and Watson, C.C. 2000. The two-dimensional upland erosion model CASC2D-SED. *Journal of the American Water Resources Association*, 36(1), 31–42.
20. Jorgeson, J. and Julien, P.Y. 2005. Peak flow forecasting with CASC2D and radar data. Special Issue, *Water International*, *International Water Resources Association, IWRA*, 30(1), 40–49.
21. Julien, P.Y., Saghafian, B., and Ogden, F.L. 1995. Raster-based hydrologic modeling of spatially-varied surface runoff. *Water Resources Bulletin*, 31(3), 523–536.
22. Kampf, S.K. and Burges, S.J. 2007. A framework for classifying and comparing distributed hillslope and catchment hydrologic models. *Water Resources Research*, 43, 24.
23. Kavvas, M.L., Chen, Z.Q., Dogrul, C., Yoon, J.Y., Ohara, N., Liang, L., Aksoy, H., Anderson, M.L., Yoshitani, J., Fukami, K., and Matsuura, T. 2004. Watershed Environmental Hydrology (WEHY) model based on upscaled conservation equations: Hydrologic module. *Journal of Hydrologic Engineering*, 9(6), 450–464.
24. Kirchner, J.W. 2003. A double paradox in catchment hydrology and geochemistry. *Hydrological Processes*, 17(4), 871–874.
25. Koren, V.I., Reed, S.M., Smith, M.B., Zhang, Z., and Seo, D.-J. 2004. Hydrology laboratory research modeling system (HL-RMS) of the US national weather service. *Journal of Hydrology*, 291(3–4), 297–318.
26. Koren, V.I., Smith, M.B., and Duan, Q. 2003. Use of a priori parameter estimates in the derivation of spatially consistent parameter sets of rainfall–runoff models. In *Calibration of Watershed Models (Water Science and Application)*, Q. Duan, H.V. Gupta, S. Sorooshian, A.N. Rousseau, and R. Turcotte, eds., American Geophysical Union, Washington, DC, pp. 239–254.
27. Koren, V.I., Smith, M.B., Wang, D., and Zhang, Z. 2000. Use of soil property data in the derivation of conceptual rainfall–runoff model parameters. *15th Conference on Hydrology*, American Meteorological Society, Long Beach, CA, 403pp.
28. Lettenmaier, D.P. and Wood, E.F. 1993. Hydrologic forecasting. In *Handbook of Hydrology*, D.R. Maidment, ed., McGraw-Hill, New York, pp. 26.1–26.30.
29. Neteler, M. and Mitrasova, H. 2008. *Open Source GIS: A Grass GIS Approach*. Springer Verlag, New York.
30. Molnár, D.K. and Julien, P.Y. 2000. Grid-size effects on surface runoff modeling. *Journal of Hydrologic Engineering*, 5(1), 8–16.
31. National Climatic Data Center. 2010. NCDC: Weather station. http://www4.ncdc.noaa.gov/cgi-win/wwcgi.dll?wwDI%7EStnSrch%7EStnID%7E20003674 (June 4, 2010).
32. Ogden, F.L. and Julien, P.Y. 1993. Runoff sensitivity to temporal and spatial rainfall variability at runoff plane and small basin scales. *Water Resources Research*, 29(8), 2589–2597.
33. Pappenberger, F., Beven, K.J., Hunter, N.M., Bates, P.D., Gouweleeuw, B.T., Thielen, J., and De Roo, A.P.J. 2005. Cascading model uncertainty from medium range weather forecasts (10 days) through a rainfall–runoff model to flood inundation predictions within the European Flood Forecasting System (EFFS). *Hydrology and Earth System Sciences*, 9(4), 381–393.
34. Rawls, W.J., Brakensiek, D.L., and Saxton, K.E. 1982. Estimation of soil water properties. *Transactions of the ASAE*, 25(5), 1328–1320.
35. Rawls, W.J., Brakensiek, D.L., and Miller, N. 1983. Green-Ampt infiltration parameters from soils data. *Journal of Hydraulic Engineering*, 109(1), 62–70.
36. Reed, S.M. and Halgren, J.S. 2011. Validation of a new GIS tool to rapidly develop simplified dam break models. *Dam Safety 2011*, Association of State Dam Safety Officials, Washington, DC.

37. Refsgaard, J.C. 1996. The role of distributed hydrological modelling in water resources management. In *Distributed Hydrological Modelling*, M.B. Abbott and J.C. Refsgaard, eds., Springer, Heidelberg, Germany p. 17.
38. Richardson, J.R. and Julien, P.Y. 1994. Suitability of simplified overland flow equations. *Water Resources Research*, 30(3), 665–672.
39. Rojas-Sánchez, R. 2002. GIS-based upland erosion modeling, geovisualization and grid size effects on erosion simulations with CASC2D-SED. PhD dissertation, Department of Civil Engineering, Colorado State University, Fort Collins, CO.
40. Rojas-Sánchez, R., Julien, P.Y. and Johnson, B.E. 2003. *CASC2D-SED v 1.0 Reference Manual: A 2-Dimensional Rainfall-Runoff and Sediment Model*. Colorado State University, Fort Collins, CO.
41. Rojas-Sánchez, R., Velleux, M.L., Julien, P.Y., and Johnson, B.E. 2008. Grid scale effects on watershed soil erosion models. *Journal of Hydrologic Engineering*, 13(9), 793–802.
42. Saghafian, B. and Julien, P.Y. 1991. *CASC2D User's Manual: A Two-Dimensional Watershed Rainfall–Runoff Model*. Center for Geosciences, Hydrologic Modeling Group, Colorado State University, Fort Collins, CO.
43. Senarath, S.U.S., Ogden, F.L., Downer, C.W., and Sharif, H.O. 2000. On the calibration and verification of two-dimensional, distributed, Hortonian, continuous watershed models. *Water Resources Research*, 36(6), 1495–1510.
44. Simons and Associates, Inc. 1997. *Hydrologic Analysis of the California Gulch Watershed*. Simons and Assoc., Fort Collins, CO.
45. Singh, V.P. and Woolhiser, D.A. 2002. Mathematical modeling of watershed hydrology. *Journal of Hydrologic Engineering*, 7(4), 270–292.
46. Smith, M.B., Seo, D.-J., Koren, V.I., Reed, S.M., Zhang, Z., Duan, Q., Moreda, F., and Cong, S. 2004. The distributed model intercomparison project (DMIP): Motivation and experiment design. *Journal of Hydrology*, 298(1–4), 4–26.
47. Smith, R.E. and Hebbert, R.H.B. 1983. Mathematical simulation of interdependent surface and subsurface hydrologic processes. *Water Resources Research*, 19(4), 987–1001.
48. US EPA Region 8. 2010. US EPA Region 8 Superfund Colorado Cleanup Sites. California Gulch, Leadville., CO. http://www.epa.gov/region8/superfund/co/calgulch/#2 (September 21, 2010).
49. Velleux, M.L. 2005. Spatially distributed model to assess watershed contaminant transport and fate. PhD dissertation, Colorado State University, Fort Collins, CO.
50. Velleux, M.L., Julien, P.Y., Rojas-Sánchez, R., Clements, W.H., and England, J.F. 2006. Simulation of metals transport and toxicity at a mine-impacted watershed:? California Gulch, Colorado. *Environmental Science & Technology*, 40(22), 6996–7004.
51. Velleux, M.L., England, J.F., and Julien, P.Y. 2008. TREX: Spatially distributed model to assess watershed contaminant transport and fate. *Science of the Total Environment*, 404(1), 113–128.
52. Velleux, M.L., Julien, P.Y., and England, J.F. 2008. *TREX Watershed Modeling Framework User's Manual: Model Theory and Description*. Department of Civil Engineering, Colorado State University, Fort Collins, CO.
53. Whitmeyer, S., Nicoletti, J., and De Paor, D. 2010. The digital revolution in geologic mapping. *GSA Today*, 20, 4–10.

18

Hydrological Changes in Mangrove Ecosystems

Shafi Noor Islam
Brandenburg University of Technology at Cottbus

Albrecht Gnauck
Brandenburg University of Technology at Cottbus

Hans-Jürgen Voigt
Brandenburg University of Technology at Cottbus

Saeid Eslamian
Isfahan University of Technology

AUTHORS

Shafi Noor Islam (PhD in Environmental Sciences) is a lecturer in euro-aquae hydro-informatics and water management, at the Brandenburg University of Technology at Cottbus, Germany. He was also working as a guest lecturer in the master's programme of urban management at the Technische Universität Berlin, Germany. He has postdoctoral research experience in food security issues, and presently he is the candidate of Habilitation (Dr.rer.nat.habil.) research degree on the topic "Ecosystem services and Food Security under Threat in the Mega Deltas of Asian Coastal Regions: An analysis on the Ganges-Brahmaputra-Meghna Delta," in the chair of ecosystems and environmental informatics, Brandenburg University of Technology at Cottbus, Germany. His main activities are in the interdisciplinary water resources research on water salinity and mangrove ecosystem analysis. Wetlands and coastal resource management, and climate change impacts on food security and ecosystem services are the focus research fields. Transboundary water and char-land management strategy, encompassing groundwater quality and urban water supply and ecology management issues, are more subjective interests. He has published 42 articles in international journals and books. He has research experiences in China, Malaysia, Indonesia, Germany, Poland, Denmark, Italy, Spain, France, Netherlands, Sweden, and Mexico.

Albrecht Gnauck (Dr. rer. nat. habil.) is a prominent professor of ecosystems and environmental informatics at Brandenburg University of Technology at Cottbus, Germany. He is one of the prominent experts on system analysis, modeling, and simulation of freshwater ecosystems and wetlands. He has several popular books on modeling and simulation. He has published more than 300 articles in journals and books. His research focuses on water quality, ecosystem simulation and modeling, eutrophication models of lakes

and rivers including sediment/water interactions, monitoring and modeling of point and nonpoint river pollution, time series analysis of water quality data, informatics tools for ecological modeling and ecosystem management including decision support systems for river basin management as well as new mathematical approaches to ecosystem theory. He has international research experiences in European countries (Czech Republic, Hungary, Italy, Poland, Russia, and United Kingdom) and Asian countries like in Bangladesh and Vietnam. He is a member of the board of directors of the International Society for Environmental Protection, Vienna, and a member of the editorial board of the journal *Ecological Indicators*.

Hans-Jürgen Voigt (Dr. rer. nat. habil.) is a professor of environmental geology at Brandenburg University of Technology at Cottbus, Germany. He is an expert on groundwater and geohydrological fields. He has carried out some potential international projects related to groundwater quality assessment and management issues in Asia, Africa, and Europe. He has good quantities of publications in journals and books.

Saeid Eslamian received his PhD from the University of New South Wales, Australia, with Prof. David Pilgrim. He was a visiting professor in Princeton University, USA, and ETH Zurich, Switzerland. He is currently an associate professor of hydrology in Isfahan University of Technology. He is the founder and chief editor of *Journal of Flood Engineering* and *International Journal of Hydrology Science and Technology*. He has published more than 200 publications mainly in statistical and environmental hydrology and hydrometeorology.

PREFACE

In the contemporary world, there has been growing worldwide public concern about a wide range of issues relating to water resources management in the coastal regions. Water resources are most potential to social and economic improvement processes and achieving the millennium development goal to alleviate poverty and hunger for sustainable coastal environment. In Bangladesh, a large mass of the population is almost annually faced with the devastating damage, since records began, that flood water can cause. On the other hand, the coastal regions of the world are using for social, industrial, and settlements and agricultural land use activities. Almost 60% of Asian population is living within 100 km range of the coastal offshore line. In Bangladesh, there are 36.8 million people living in the coastal region and fighting against the natural calamities every year. The majority of the poor population is mostly settled down in the coastal region, and they are directly dependent on the mangrove ecosystem services (ES) and coastal natural resources. Therefore, hydrological changes of the coastal region are an important factor toward protecting and managing the coastal water cycle and mangrove ecosystems. In recent years, the dwellers are using huge ground and surface water for household, irrigation, and industrial purposes. Through this process the mangrove region are losing its hydrological cycle and changing mangrove ecosystem. The mangrove of Bangladesh is under threat due to hydrological imbalance in the coastal region as well as in the Sundarbans region. Therefore, mangrove wetland hydrology is also suffering from different types of disturbances and among the most endangered ecosystems of the world. The management of mangrove wetlands and the regional hydrology is not considered properly worldwide as well as in the mangrove region in Bangladesh.

18.1 Introduction

The hydrology and surface water supply and management are dependent on anthropogenic activities and transboundary water supply condition (Wahid, 1995; Islam et al., 2011). The regional and local hydrological cycle is playing a potential role to make a balance of mangrove wetland ecosystems and its services in different parts of the world (Islam, 2006). Therefore, mangrove conservation and restoration

has become an important topic in recent decades. Wetlands not only support specific plant and animal communities but also provide other important services for humanity, such as water quality improvement, carbon sinks, and community livelihood sustainability (Smolders et al., 2002; Margozczi et al., 2007). The world mangrove refers to both wetlands and the salt-tolerant trees that dominate those wetlands. The world mangroves dominating countries are Indonesia 24%, Brazil 7%, Australia 6%, Nigeria 6%, Cuba 4%, India 4%, Malaysia 4%, Bangladesh 4%, Papua New Guinea 3%, Mexico 3%, and the rest of the world represents 35% only (Mitsch and Gosselink, 1986; Islam and Gnauck, 2008). The mangroves are found along tropical and subtropical coastlines throughout the world, usually between 25°N and 25°S latitude (Sarkar, 1993). The tidal salt marsh is replaced by the mangrove swamp in subtropical and tropical regions of the world. Approximately 14 million of mangrove wetlands are generally dominated by the red mangrove species (*Rhizophora*) and black mangrove species (*Avicennia*) (Mitsch and Gosselink, 1986). The present-world mangrove vegetation cover has been estimated with an average of about 17 million ha, of which half are in the Asia-Pacific region. The remaining 50% is equally distributed in Africa (25%) and America (25%) (Lacerda, 2001; IPCC, 2007).

The scale of mangrove depletion and its causes vary from country to country. Coastal habitats and human stress are the vital reasons for exploitation of terrestrial aquatic and mangrove resources. Some main factors that are responsible for the decline of mangrove resources have been identified (Siddiqi, 1994; Islam and Gnauck, 2008). Mangroves in the South Asian countries especially in Thailand, the Philippines, Vietnam, Indonesia, Malaysia, and Sri Lanka have been converted to shrimp ponds and farms (Islam and Gnauck, 2008, 2009b). Approximately 1000 km^2 of land now utilized for shrimp culture in Bangladesh was originally mangrove forest (Miah, 2003; Islam and Gnauck, 2008). In many countries and regions, withdrawal of freshwater from the upstream rivers for irrigation and other purposes has serious impacts on hydrological cycle, which is extending negative impacts on the mangrove ecosystems (Goodbred and Kuehl, 1999; Ahmed and Falk, 2008). The extensive mangroves in Bangladesh and India, Pakistan, Gambia, Nigeria, Thailand, and Vietnam are facing the problem of upstream freshwater crisis and transboundary water distribution conflicts between two neighboring countries. The Sundarbans mangrove forest is a good example of transboundary Ganges River freshwater conflict between India and Bangladesh and hydrological degradation in the mangrove region in the coastal region of the Ganges delta (Adel, 2001; Ahmed and Falk, 2008; Ahmed et al., 2008).

The Sundarbans mangrove forest is situated in the Ganges delta, and it is part of Ganges–Brahmaputra–Meghna (GBM) River systems. It covers an area 10,000 km^2 in southwest Bangladesh and West Bengal of India. A total area of 62% lies in Khulna region of the south western part of Bangladesh, while the remaining 38% in India (Lacerda, 2001; Siddiqi, 2001; Islam et al., 2011), and it is one of the largest mangrove wetlands and unique ecosystems in the world, which is dependent on hydrological regime (Wahid, 1995). It is a natural shield that protects the coastal landscapes and its ecosystems from storm surges and cyclones in pre- and postmonsoon periods. It is playing a potential role in regional economy and balance ecosystems in the coastal zone of Bangladesh. The Sundarbans landscapes consist of an almost all high tide during the rainy season. The Sundarbans landscapes consist of a large number of fluvial and tidal lands, features created by the three mighty rivers, the Ganges, the Brahmaputra, and the Meghna (Siddiqi, 2001; Islam et al., 2011). Since the diversion of Ganges River water flows at Farakka Barrage in India from early 1975, the water and soil salinity has been penetrated due to capillary upward movement processes. Consequently, both siltation and intrusion of salinity have degraded water quality of Sundarbans Rivers, and it is the root cause of salinity intrusion and threats for coastal mangrove ecosystems (Miah, 2003; Sarker, 2008). The similar condition has been seen in Thailand, Vietnam, Indonesia, Sri Lanka, India, and Pakistan, where the mangrove wetland forest has been destroyed due to anthropogenic influences on upstream surface water and shrimp cultivation. The mangrove wetlands ecosystems are under threat because of hydrological changes in the mangrove wetlands regions in the Asian coast and other parts of the mangrove world (IWM, 2003; Islam and Gnauck, 2011).

A large number of channels and creeks flow into larger rivers in the Sundarbans. The largest of these rivers are the remains of the Ganges, which have shifted eastward. The Gorai River is the main distributary of the Ganges River, which is connected to the Passur River and indirectly with the Sibsa River and playing a potential role to protect the Sundarbans mangrove ecosystems (Islam et al., 2011). The Baleswar River is connected to the Ganges River in the eastern part of the forest and as a result receives huge volume of freshwater from it. It is reported that 2×10^{11} m^3/year of groundwater flows directly into the Bay of Bengal, an outflow equivalent to 19% of the discharge from the Ganges–Brahmaputra river system (Islam et al., 2011). Every year, the groundwater is sinking by at least 0.5 m. The quality of groundwater has been degraded due to salinity (NaCl) and arsenic (As) contamination, which is influencing the mangrove ecosystems in the Sundarbans regions (Sarkar, 1993; Hidayati, 2000). In addition, saltwater intrusion already extends in every mega delta area in many Asian countries and in Bangladesh; it has penetrated 210 km inland, which could increase with higher sea levels (Whyte, 1995). The objective of this chapter is to investigate the water salinity of Sundarbans Rivers, which will be considered as a tool for decision making. Water salinity modeling will support to make a comprehensive management and conservation plan by the decision makers and ensure upstream freshwater supply to protect the coastal ecosystems and mangrove biodiversity in the Sundarbans of Bangladesh.

18.2 Geography and Geological History of the Case Area

The major portion of the Bengal Basins and Ganges delta is floored with quaternary sediments eroded from the high lands on three sides and deposited by the Ganges, Brahmaputra, and Meghna rivers and their tributaries and distributaries. The Ganges River originated in Gangotri Glacier in the southern slopes of the Himalayas and carries discharge from a catchment of about 865,000 km^2 in India to Bangladesh (Figure 18.1) (Joseph, 2006; Islam and Gnauck, 2008). The location of Bangladesh is in South Asia between 20°34′ to 26°38′ north latitude and 88°01′ to 92°42′ east longitude, with an area of 147,570 km^2. The other neighboring countries are India and Myanmar (Burma), sharing mountainous border in the southeast (Figure 18.1).

The Bay of Bengal lies to the south of Bangladesh. The coastal zone consists of about 710 km coastline. Three major types of landscapes are found in Bangladesh: floodplains (80%), terraces (8%), and hills (12%). Excepting the eastern hilly region, almost all of the country lies in the active delta of three of the world's major rivers like the Brahmaputra, the Ganges, and the Meghna (Figure 18.1) (Ahmed and Falk, 2008; Islam et al., 2011).

The Sundarbans region is located in the southwestern corner of Bangladesh and south east of West Bengal of India. The potential estuaries Hooghly Estuary, Saptaganga Estuary, Matla Estuary, Raimangal Estuary, Malancha Estuary, Kunga Estuary, Bangra Estuary, and Baleswar Estuary are located in the Sundarbans region (Figure 18.1) (Islam and Gnauck, 2008, 2009a). Geographically, the Sundarbans lies between latitudes 21°43′30″N and 24°5′20″N and between longitudes 87°47′17″E and 91°21′01″E (Katebi, 2001). The Sundarbans region enjoys a humid tropical monsoon climate with proximity to sea as an added advantage. Temperature varies from 20°C in December–January to 36°C in June–July with an annual range of about 8°C. The Sundarbans mangrove forest spreads over the Ganges delta with an average elevation of 0.9–2.1 m above mean sea level (Bird, 1969; Islam and Gnauck, 2007).

18.3 Data and Methodology

The present applied research has been carried out based on primary and secondary data sources. The time series water salinity data from 2000 to 2003 were collected from the Institute of Water Modelling (IWM), Dhaka. The collected 4 years' time series data were reconstructed by EXCEL interpolation.

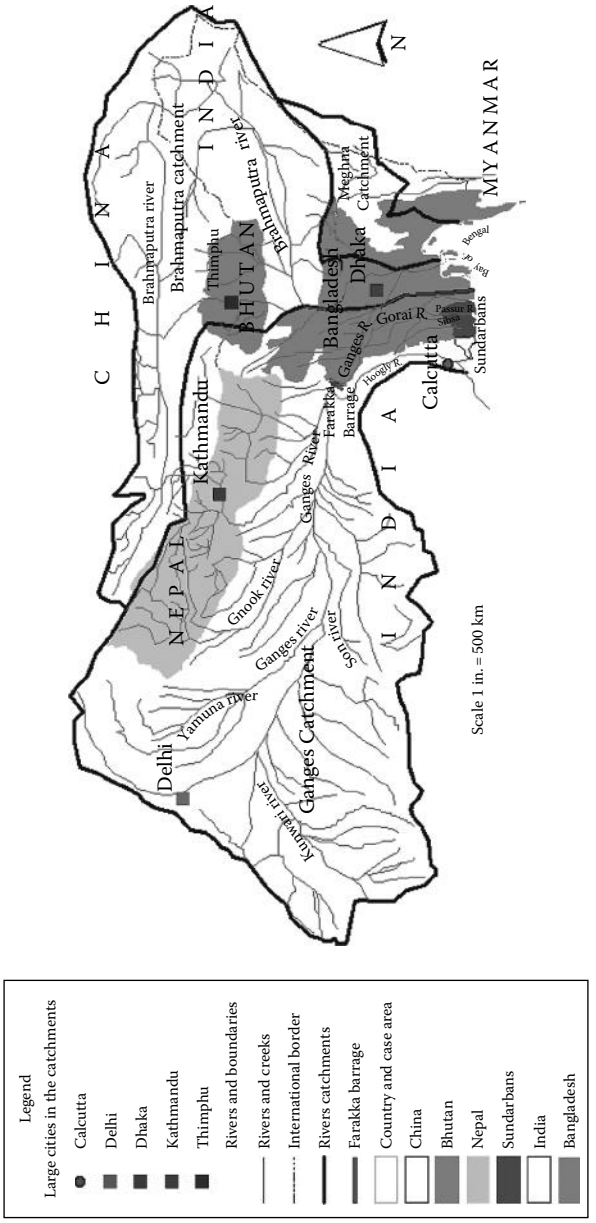

FIGURE 18.1 The geographical location of the Sundarbans region. (From Islam, S.N. and Gnauck, A., *Frontier Earth Sci. China*, 2(4), 439, 2008.)

Field investigation has been conducted in 2003 and 2008. Some potential field-related information was collected from local people and stakeholders' discussions around the Sundarbans mangrove wetland region and the catchment areas.

18.3.1 Data

The study was conducted at the field level, and saline water and soil samples were collected for the laboratory analysis of the salinity situation of ecological and ecosystem degradation in the case area. The study also involved discussions and interviews with the stakeholders, tourists and tour operators, shrimp cultivators, farmers, fishermen, shrimp collectors, business groups, local people, NGO leaders, and decision makers and planners in the Sundarbans region. More than 6 months were spent in the Sundarbans in different sensitive areas where the ecosystems are under pressure and threatened due to human influences on surface water. Areas and important locations including Munchiganj, Mirgang, Koira, Kasiabad, Mongla, Kathka, Kochikhali, Hironpoint, Dublar Char, Mundarbaria, Burigoalini, and Saronkhola, were covered during the survey and data collection in the Sundarbans. Primary data for surface water salinity (four years' time series data) were obtained from 13 rivers including Passur, Sibsa, Chunnar, Kholpetua, Bal-Jhalia, Baleswar, Betmargang, Notabaki, Passakhali, Arpongasia, Kathka, Nilkamol, and Malancha rivers of the Sundarbans by the IWM (2003) and Bangladesh Inland Water Transportation Authority. The collected data were used for water salinity modeling of the rivers in the Sundarbans. Water salinity–related data were obtained from IWM of Bangladesh. The survey was done between February and July, 2003, at different intervals and took into consideration the wet and dry seasons. The tested results from SRDI-Dhaka were used in water salinity modeling. The secondary data as well as published materials and relevant books on the Sundarbans were collected from book markets, university libraries, and research organizations in Dhaka, Khulna, and Chittagong. Soil-related secondary data were collected from SRDI–Dhaka (SRDI, 2001). After completion of data collection, relevant data were processed and analyzed both manually and by employing. The following software like MS Excel and ESRI Geographical Information System (GIS) version ArcGIS 10 have been used for data visualization and mapping specially used for case area map preparation (Figure 18.1). MATLAB® software version 7.1 has been used for Fourier polynomial approximation of water salinity modeling, which has been shown in Figures 18.4 and 18.6 and analyzed in detail.

18.3.2 Methods

In analogy to the "polynomials of best fit," it is possible to write down a model that consists of a sum of sine and cosine functions that best fit the given data. The usage of Fourier polynomials to analyze periodic signals is well known in engineering and serves as an algorithm explaining data variations caused by internal and external driving forces. It is a method for expressing a function by superposition of sine and cosine functions (Smith, 1997). According to the theory development by Fourier, any periodic function $F(X)$, with period T, can be represented by an infinite series of the form. The Fourier Polynomial general equation has been used for water salinity modeling of 13 rivers in the Sundarbans Mangrove wetlands, where the coefficients ∂o, ∂n, and bn for a given periodic function $F(X)$ are calculated by the formulas

$$\omega = \frac{2\pi}{T} \tag{18.1}$$

$$a_0 = \frac{2}{T}\int_{o}^{T} F(X)\,dt \tag{18.2}$$

$$an = \frac{2}{T}\int_{o}^{T} F(X)\cos nw_T X\,dt \quad n = 1,2,\ldots m \tag{18.3}$$

$$bn = \frac{2}{T}\int_{o}^{T} F(X)\sin nw_T X\,dt \quad n = 1,2,\ldots m \tag{18.4}$$

Considering the data that were recorded over some interval of time, it will be necessary to choose a model that is periodic (Figure 18.2). The model that consists of trigonometric functions is called Fourier polynomials. These models are widely used in engineering, physics, and applied sciences to approximate processes that are periodic. According to the theory development by Fourier, any periodic function $F(X)$, with period T, may be represented by an infinite series of the form

$$F(X) = \frac{\partial o}{2} + \sum_{n=1}^{m} (\partial n\cos nw_T X + bn\sin nw_T X) \tag{18.5}$$

where the coefficients ∂o, ∂n, and bn for a given periodic function $F(X)$ are calculated by the formulas given earlier. The periodic function has been measured through equation numbers (18.1), (18.2), (18.3), (18.4), and (18.5). The general Fourier polynomial approximation of order 1–8 models was considered to generate results for the water salinity models of the Sundarbans Rivers. In the study, the Fourier polynomial approximation is carried out based on data and different Fourier polynomial approximation orders. The Fourier polynomial approximation eighth order is given by the following equation, considering coefficients (with 95% confidence bounds):

$$\begin{aligned} f(x) = {} & a_0 + a_1{*}\cos(x{*}\,\omega) + b_1{*}\sin(x{*}\,\omega) \\ & + a_2{*}\cos(2{*}x{*}\,\omega) + b_2{*}\sin(2{*}x{*}\,\omega) + a_3{*}\cos(3{*}x{*}\,\omega) + b_3{*}\sin(3{*}x{*}\,\omega) \\ & + a_4{*}\cos(4{*}x{*}\,\omega) + b_4{*}\sin(4{*}x{*}\,\omega) + a_5{*}\cos(5{*}x{*}\,\omega) + b_5{*}\sin(5{*}x{*}\,\omega) \\ & + a_6{*}\cos(6{*}x{*}\,\omega) + b_6{*}\sin(6{*}x{*}\,\omega) + a_7{*}\cos(7{*}x{*}\,\omega) + b_7{*}\sin(7{*}x{*}\,\omega) \\ & + a_8{*}\cos(8{*}x{*}\,\omega) + b_8{*}\sin(8{*}x{*}\,\omega) \end{aligned} \tag{18.6}$$

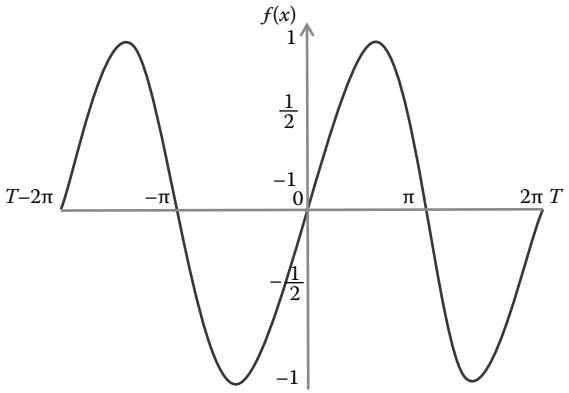

FIGURE 18.2 The concept of periodic function of polynomial.

As a whole, the equation numbers such as (18.1), (18.2), (18.3), (18.4), and (18.5) show the concept of periodic functions which are given the mathematical equation and in addition the number (18.6) is given the general formula of Fourier polynomial approximation concept. To understand of the polynomial behavior of water salinity, the general formula (Equation 18.6) has been used for the investigation of seasonal water salinity intrusion pattern in the Sundarbans Rivers in Bangladesh.

The water salinity modeling results of the Sundarbans Rivers have been discussed in the following section, and the scenarios have been discussed in the results and discussion of the chapter.

18.4 Hydrological Changes in the Sundarbans Mangrove Region

Water is valuable natural resources to man and other living beings (Rahman and Ahsan, 2001). Under the natural conditions, freshwater flow toward the sea limits the landward encroachment of seawater. The surface water disturbs the dynamic balance between freshwater and seawater, which, in turn, allows seawater to intrude to the usable parts of aquifers (Rahman, 1988). Water quality is dominated by both natural and an anthropogenic influences, where the former includes local climate, geology, etc., and the latter covers the construction of dams and embankments, irrigation practices, indiscriminate disposal of industrial effluents, etc. (Rahman and Ahsan, 2001). The amount of the Ganges water flow into Bangladesh is remarkably affected by the amount of water drawn at the Farakka Barrage in India. The Ganges flow in 1962 was 3700 m^3/s, whereas it was 364 m^3/s in 2006 and 370 m^3/s in 2010 (Islam and Gnauck, 2011). The reduction in flow rate has resulted in increase in high saline seawater in the upstream areas. Such diversion of upstream waters resulted in falling water tables and greater salinity downstream for Bangladesh especially in the Sundarbans region. The Gorai River then passes through Kushtia and Faridpur districts and divides at Bardia in the Jessore District. Some portion, almost 16% of the flow of Gorai River, meets the Haringhata–Baleswar estuary system at Madhumati River and the other 85% flow through to join the Passur Basin at Nabaganga River. The last part of the Gorai River joins at sea as Baleswar River (Islam et al., 2011). The Chunar-Munchiganj and Passur are two potential rivers in the Sundarbans region, and they carry freshwater from upstream region and from the regional catchment areas. Water salinity intrusion of these two rivers are dependent on hydrological condition and its changing behavior. Water level inside the Sundarbans is highly fresh and dependent on the upstream river water inflows and on the tidal oscillation at the coast (Siddiqi, 1994). Tides in the Bay of Bengal are semidiurnal exhibiting two high water and two low water levels per day. The variations in water level and tidal amplitude experienced at the coast are also propagated inland during each tidal cycle. It has been observed that the tidal range in the northern fringe of the Sundarbans mangrove forest is higher than that in the southern bay. The lowest record of tidal range was 2.74 m and the highest range was 5.12 m (Duke, 1992; Islam and Gnauck, 2009a; Islam et al., 2011). The maximum inundation period during the spring tide is around 3–4 h. The average velocity of micro-current varies from 10 to 20 cm/s. Both siltation and erosion occur at the end of monsoon. The maximum net siltation and erosion at the end of monsoon were found to be around 50 and 19 mm, respectively (Islam et al., 2011). The hydrological changes in the Sundarbans region will pose a new threat for the mangrove ecosystem, its goods and services. There is close correlation with hydrological cycle and the mangrove ecosystem in any region of the mangrove world.

18.4.1 Relationship between Surface Water Supply and Salinity Intrusion in the Sundarbans

The salinity content of the tidally active delta in the Sundarbans region shows the special variation (Figure 18.3). The water salinity approximation shows both seasonal and special variations. During premonsoon (March–April), the conductivity of river water is high and ranges from 7 to 52 μS/cm. In the postmonsoon season (August–September), the conductivity of river water decreases from 0 to 21.5 μS/cm. Water salinity level in the rivers of the eastern region both in premonsoon and in

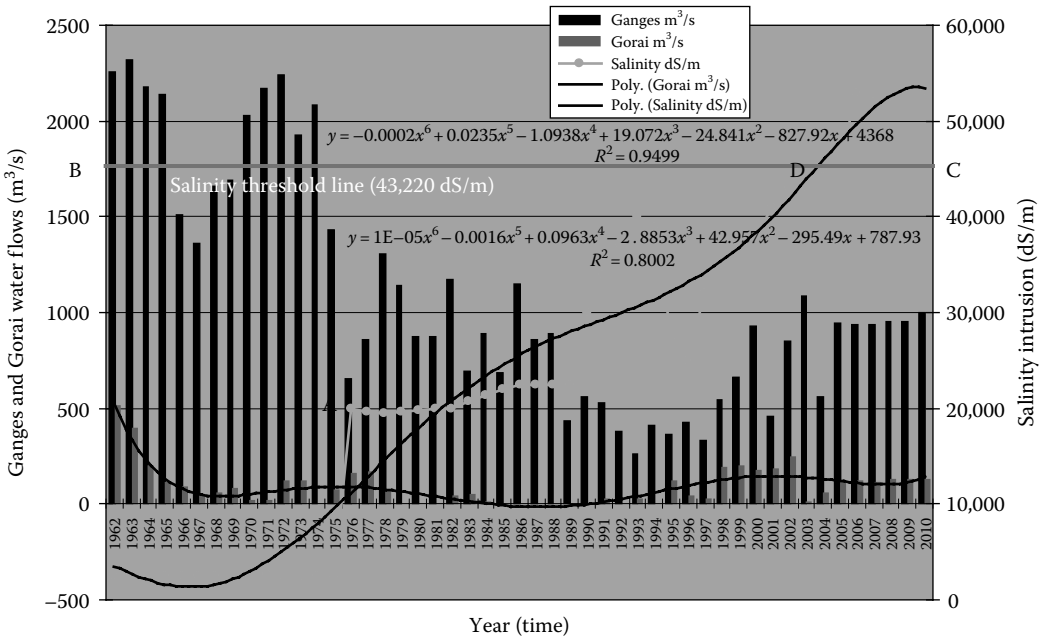

FIGURE 18.3 The Ganges River and Gorai River water flows in the dry season and salinity intrusion at Passur River at Mongla point (1962–2010).

postmonsoon seasons is low (0–7 μS/cm) in comparison to western rivers (Islam and Gnauck, 2007, 2008). Figure 18.3 shows the Ganges water flows at Hardinge Bridge point, the Gorai River flows at the Railway Bridge point in the dry season, and water salinity intrusion at Mongla Point in the Sibsa River. There is a close interlinkage between the Ganges supply to the Sundarbans mangrove forest area and salinity intrusion and penetration in the upstream area. In Figure 18.3, the Ganges water supply level line and salinity intrusion curve have crossed at point A in 1976 just after the construction (1975) of Farakka Barrage on the Ganges River in India (1975). After 1975, the water flow of the Gorai River has also decreased.

In Figure 18.3, BC line has been treated as water salinity threshold line (43,220 dS/m) for mangrove wetland ecosystem in the Sundarbans. The salinity curve has crossed the BC line on point D in 2004 when the Ganges water and the Gorai river water flows were 550 and 35 m^3/s respectively. The point D is the optimal point for mangrove ecosystem for the Sundarbans mangrove wetlands. Therefore, it can be stated that there is a strong relationship between Ganges water supply and salinity intrusion at the Mongla Port point (Sibsa River). Figure 18.3 illustrates the salinity intrusion trends in the Sibsa River, which is a very normal trend where regression value $R^2 = 0.9433$ and it is an acceptable value according to the statistical analysis.

18.5 Results and Discussions

The abnormal hydrological changes in the Sundarbans mangrove wetland regions are a new threat for mangrove ecosystem and its services in the coastal region of Bangladesh. The Farakka Barrage and other dams constructed have resulted in the reduction of freshwater flows to the Sundarbans. Therefore, the results of intrusion of water salinity and alkalinity have damaged vegetation and agricultural cropping system, changing the landscapes in the Sundarbans mangrove wetland region (Bird, 1969; Islam et al., 2011). The impact of soil starts with the destruction of surface organic matter and soil fertility for mangrove germination and plant production. The changes of basic soil characteristics related to

aerations, temperature, moisture, and the organisms that live in the soil. The five core elements of ecosystem such as soil, water, vegetation, wildlife, and temperature are natural resources and have a strong a correlation between freshwater and human activities (Islam et al., 2011).

18.5.1 Water Salinity Approximation of Chunar-Munchiganj River

The Chunar-Munchiganj River is one of the smaller but important rivers in the southwestern part of Bangladesh especially in the northern boundary of the Sundarbans. The Chunar-Munchiganj River is serving as a boundary between the Sundarbans mangrove wetlands and the northern settlement areas of the Indian border toward Munchiganj town. The river is important for local communication and a fertile water shade for shrimp prawn collection. The river is connected with Kanksially River and Kalindi River, which is one of the transboundary rivers in the Sundarbans forest area. After the Chunar-Munchiganj River enters the Sundarbans, it is renamed as Malancha and joins with Ichamati River. The upstream freshwater from the local catchments is flowing into the Chunar-Munchiganj River channel. But recently the situation has changed, and there is not enough freshwater from the upstream, whereas the Chunar-Munchiganj River's water is used in the shrimp field, in the northern boundary of the Sundarbans mangrove wetlands. For various reasons, water and soil salinity have been drastically increased in the Chunar-Munchiganj Basin area. The salinity rate is increasing gradually. The Fourier polynomial model 8 (order 8) has been fit for the Chunar-Munchiganj River as appropriate model considering the best approximation. In the model development process, MATLAB software has been used frequently, which is displaying the possible Fourier polynomial models 1, 2, 3, 4, 5, 6, 7, and 8 (Table 18.1). The Fourier model 8 (Figure 18.4) is considered the appropriate model for this Chunar-Munchiganj River:

$$\begin{aligned} f(t) = {} & 13.59 + 2.099\cos(0.01985\,t) + 0.82\sin(0.01985\,t) - 0.7342\cos(0.0397\,t) \\ & -0.2323\sin(0.0397\,t) - 2.657\cos(0.05955\,t) + 6.032\sin(0.05955\,t) \\ & - 1.318\cos(0.0794\,t) + 1.013\sin(0.0794\,t) + 0.732\cos(0.09925\,t) - 0.4589\sin(0.09925\,t) \\ & -0.4179\cos(0.1191\,t) - 1.682\sin(0.1191\,t) + 0.8124\cos(0.13895\,t) \\ & - 0.2593\sin(0.13895\,t) - 0.09655\cos(0.1588\,t) + 0.5521\sin(0.1588\,t) \end{aligned} \tag{18.7}$$

After the data reconstruction and rearrangement of the Chunar-Munchiganj River, it was used to develop the Fourier polynomial models using Equation 18.7. The Fourier model 8 (Table 18.1, Table 18.2, and Figure 18.4) was considered as appropriate model for this river. In the model, the highest $R^2 = 0.955$,

TABLE 18.1 Water Salinity Model Results of Chunar-Munchiganj River

Models	R^2	Error
Model 1	0.152	5.237
Model 2	0.1584	5.232
Model 3	0.8309	2.352
Model 4	0.8837	1.956
Model 5	0.8952	1.862
Model 6	0.9389	1.426
Model 7	0.9505	1.287
Model 8	0.955	1.231

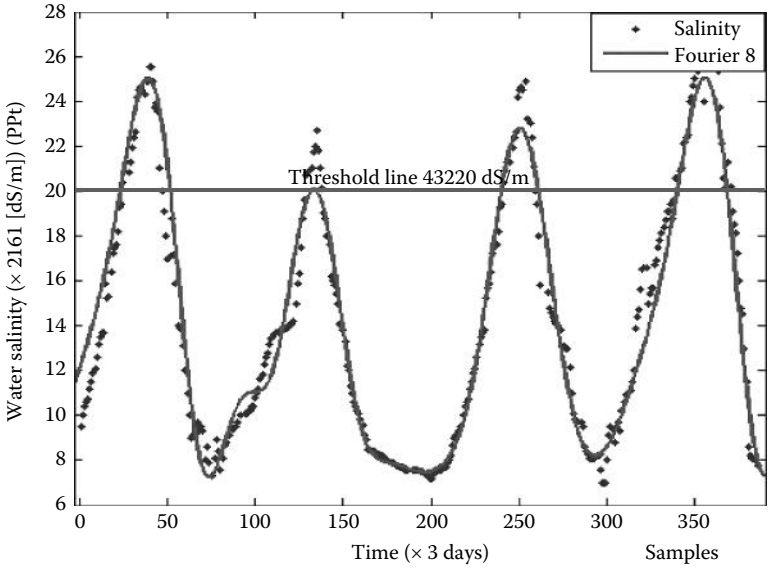

FIGURE 18.4 Fourier approximation of water salinity of Chunar-Munchiganj River in the Sundarbans.

TABLE 18.2 Fourier Polynomial Approximation (Eighth Order) Is Considering Coefficients with 95% Confidence Bounds

Coefficients	Value	95% Confidence Lower	Value Upper	Coefficients	Value	95% Confidence Lower	Value Upper
a0	13.59	13.45	13.72	b1	0.82	0.6246	1.015
a1	2.099	1.912	2.286	b2	−0.2323	−0.4225	−0.04211
a2	−0.7342	−0.9258	−0.5426	b3	6.032	5.818	6.245
a3	−2.657	−2.929	−2.385	b4	1.013	0.821	1.205
a4	−1.318	−1.522	−1.114	b5	−0.4589	−0.6567	−0.2611
a5	0.732	0.542	0.9219	b6	−1.682	−1.87	−1.493
a6	0.4179	−0.6371	−0.1986	b7	−0.2593	−0.456	−0.06266
a7	0.8124	0.6259	0.9989	b8	0.5521	0.3654	0.0199
a8	−0.09655	−0.2853	0.09226	ω	0.01985	0.0198	0.0199

adjusted $R^2 = 0.9528$, the lowest value of RMSE = 1.231, and $\omega = 0.01985$, which have made the model the best approximation. The highest regression value (R^2) and lowest error (RMSE) are given the best approximation.

Figure 18.4 shows the Fourier polynomial model order 8, where the water salinity cyclic behavior has been seen. In this model, the graph shows the dry season (February–June) with average highest salinity value, which is 54,025 dS/m in 2000, 49,703 dS/m in 2001, 54,025 dS/m in 2002, and 56,186 dS/m in 2003. The time series consideration of the water salinity intrusion of Chunar-Munchiganj River is a cyclic increasing behavior. This indicates the future increasing trend of water salinity in this river in the Munchiganj region. The Fourier polynomial model graph shows the increasing behavior of salinity yearly: after 2000, the salinity rate was 54,025 dS/m; suddenly in the following year, the rate decreased at 49,703 dS/m; and again 54,025 dS/m in 2002. The reason was that in March–April 2001, there was early monsoon rainfall, and some water flows have added in channels from the local catchments.

18.5.2 Water and Soil Salinity Intrusion versus Mangrove Ecosystem Services

The mangrove wetland ecosystems are dependent on the water and soil salinity. Almost all of the mangrove forest need freshwater supply from the upstream. In the Sundarbans region, the two potential rivers such as the Passur-Mongla and Chunar-Munchiganj are carrying the high rate of salinity intrusion. The salinity rate was 42,000 dS/m in 2003, whereas in 2010 the salinity rate is 53,000 dS/m in the Passur–Mongla River point. On the other hand, the Chunar-Munchiganj River is showing the highest rate of water salinity in 2010, which is over 53,000 dS/m. In the Sundarbans mangrove forest, 66 mangrove species have been recognized, where 36 are mangrove species and 30 are mangrove-obligate plant species. In Indo-West Pacific region, this is typically 20–40 species (Islam et al., 2011). In this sense, Sundarbans is very rich in mangrove biodiversity considering the other parts of the world. Duke (1992) has listed 71 species of mangroves, while other authors have given variant figures. Table 18.3 shows the distribution of mangrove species in the world. The domination portion of mangroves is located in the Asia-Pacific regions.

The mangrove ecosystem is getting more attention to the environmental community for conservation of nature and natural resources. It has been recognized as potential agenda; the ecosystems are socially valuable in ways that may not be immediately intuited (Daily, 2006). ES are benefits of nature to households, communities, and economics. The sophisticated definition of ecosystem can be structured in different ways: the meaning of the ecosystem is the functions of biotic and abiotic characters. On the other hand, the meaning of ES is the benefits that society receives from soil, water, air, organism, and the processes that govern the interactions. Nursing food and clean water in sufficient quantities are two examples of human needs that would not be met without cycling and regulating the earth's climate. Other services include meeting recreational, aesthetic, and cultural amenities that are essential for human well-being (Fongwa et al., 2009). ES issue exists in the literatures but in-depth information is not being used for value creation and profit from ES. Conversely, even the damages to ecosystems continuously reduced ES have potential for resource development and creation. This could be used for human development and alternative for services by anthropogenic activities leading to the reduction of ES (Fongwa et al., 2009). Value creation from ES could mean how additional value could be added to ES. This could be achieved through the transformation of evaluation results of ES into knowledge and then to business development. It could be fostered if the benefits from ES and underestimated. Therefore, the reduction of ES could be mainly attributed to the action of man in his environment. The UN report stated that almost 50% of land has been highly degraded by anthropogenic influences (Vitousek, 1997; Versfeld and Wassen, 2005).

The agricultural ecosystems produce food, fiber, and nonmarked ES. Agro-ecosystem which is simultaneously producing food, fodder, and bioenergy. The Sundarbans are public goods, ecosystem services they are affecting due to climate change impacts and anthropogenic influences on upstream fresh water flow. ES are components of nature, directly enjoyed, consumed, or used for human well-being.

TABLE 18.3 Estimate of Mangrove Species and Areas

Regions	Number of Species	Mangrove Area (ha) in 2005
Africa	20	3,160,000 (20.8%)
Asia	37	5,858,000 (38.5%)
North and Central America	11	2,263,000 (14.8%)
Oceania	49	1,972,000 (12.9%)
South America	10	1,978,000 (12.0%)
World the total	71	15,231,000 (100%)

Source: FAO (Food and Agricultural Organization), The world's mangroves 1980–2005, FAO forestry paper no. 153, Rome, Italy, 2007.

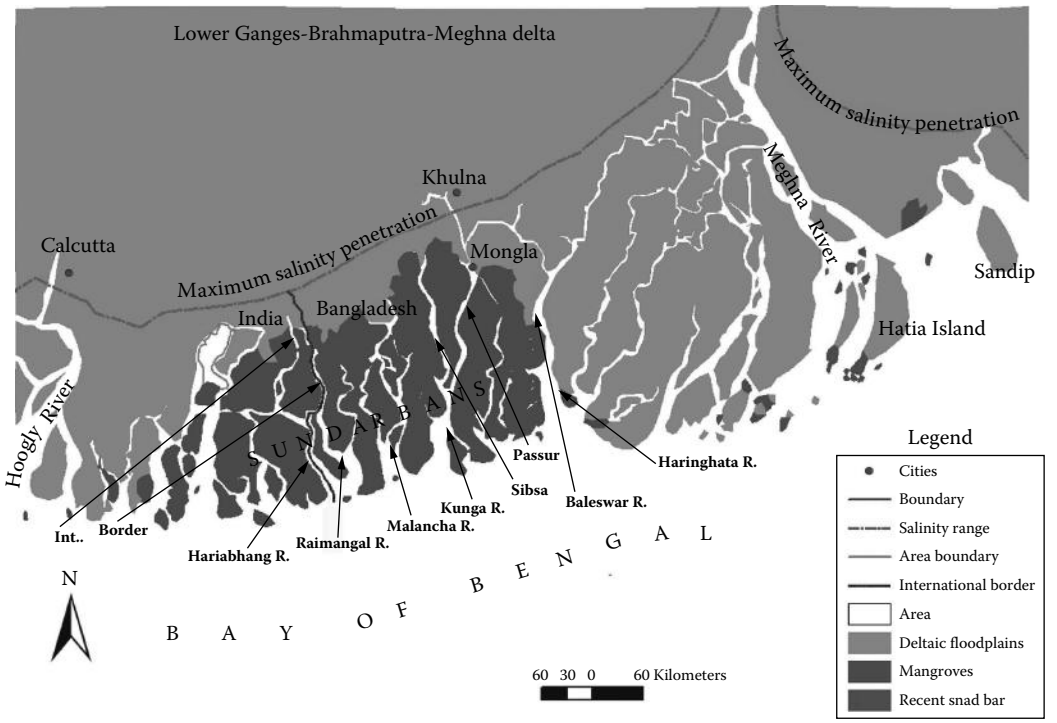

FIGURE 18.5 Saline water intrusion in the upstream area of the Sundarbans regions (Bangladesh and India).

Ecosystem components include resources such as surface water, oceans, vegetation types, and species. Ecosystem processes and functions are the biological, chemical, and physical interactions between ecosystem components (Joseph, 2006). The four types of mangrove ES are functioning in the lower tidally active delta of the GBM River delta in the Sundarbans coastal region.

Figure 18.5 illustrates the largest mangrove wetlands between Bangladesh and India. Due to high salinity intrusion and climate change impacts, the vulnerability of mangrove ES are gradually getting higher. Figure 18.5 shows the high salinity line, which has been demarked at the north site of the Sundarbans mangrove wetlands in Bangladesh and India. Therefore, it can be estimated that the present situation is more vulnerable than before. The climate change impacts, sea-level rise, and shortage of upstream freshwater are global crisis for mangrove ecosystem. The damage and abandon scenarios have been seen in many countries in Asia-Pacific, Latin America, and African countries. The river water has abstracted and using for irrigation purposes in many countries; therefore, hydrological cycle process is facing barrier in many mangrove regions of the world. The salinity investigation results have been analyzed in Figure 18.6 through geostatistical analyses.

18.5.3 Degraded Mangrove Wetland Ecosystems

The time series data of water salinity have been collected from 32 river basins in the Sundarbans mangrove wetland areas in Bangladesh. The approximation of water salinity intrusion has been illustrated in Figure 18.6. The result shows that almost all of the rivers show the high rate of salinity intrusion. The northern rivers in the Sundarbans are carrying the low rate of salinity, the middle rivers are carrying the moderate rate of salinity, and the southern river basins are carrying the high rate of salinity, which has crossed the water salinity threshold value for the mangrove ecosystem and its services (Figure 18.6) (Islam and Gnauck, 2008, 2009a,b).

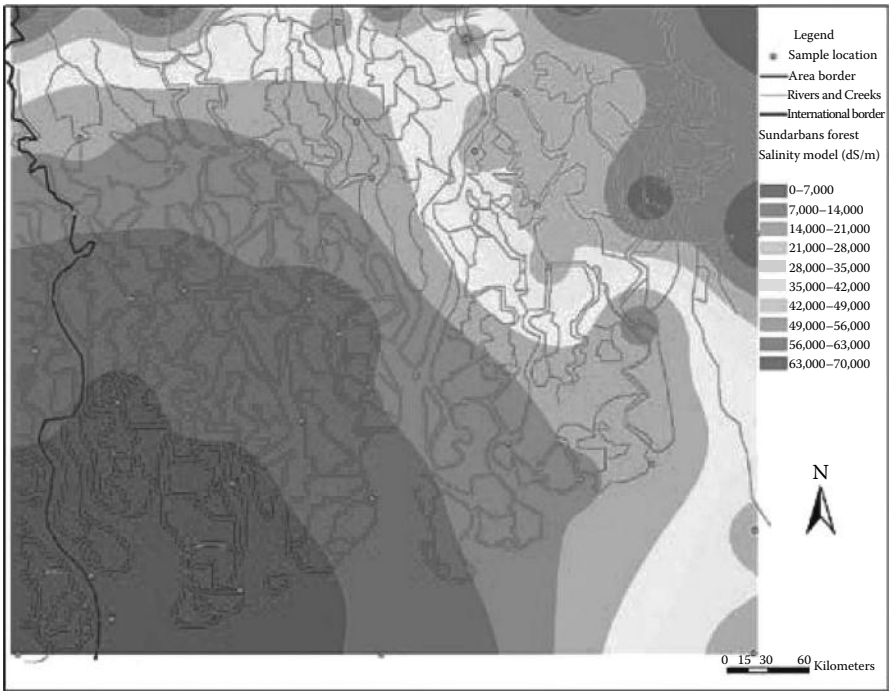

(a)

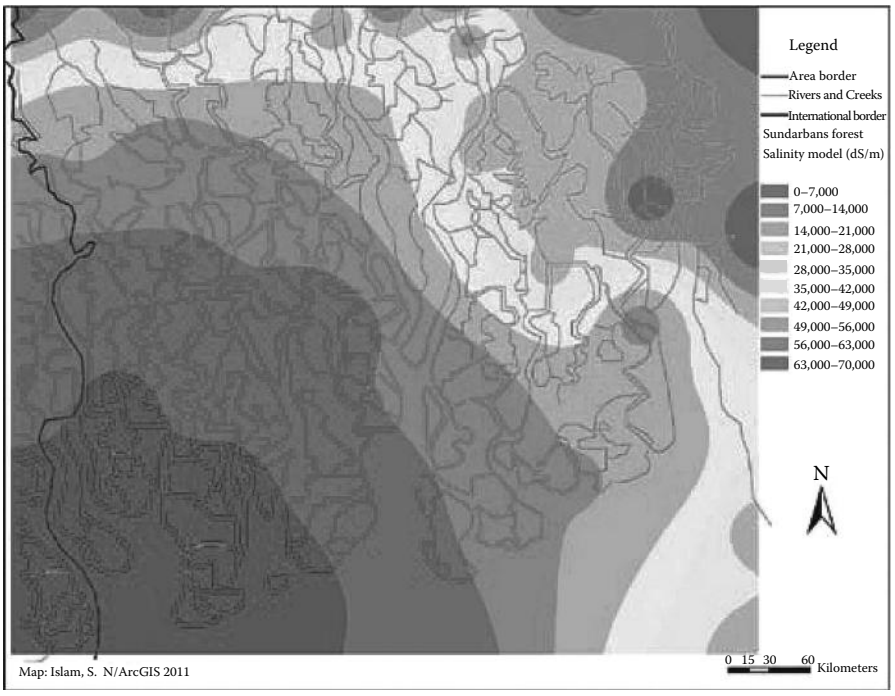

(b)

FIGURE 18.6 Water salinity modeling (a–d) in the Sundarbans mangrove region in 2003.

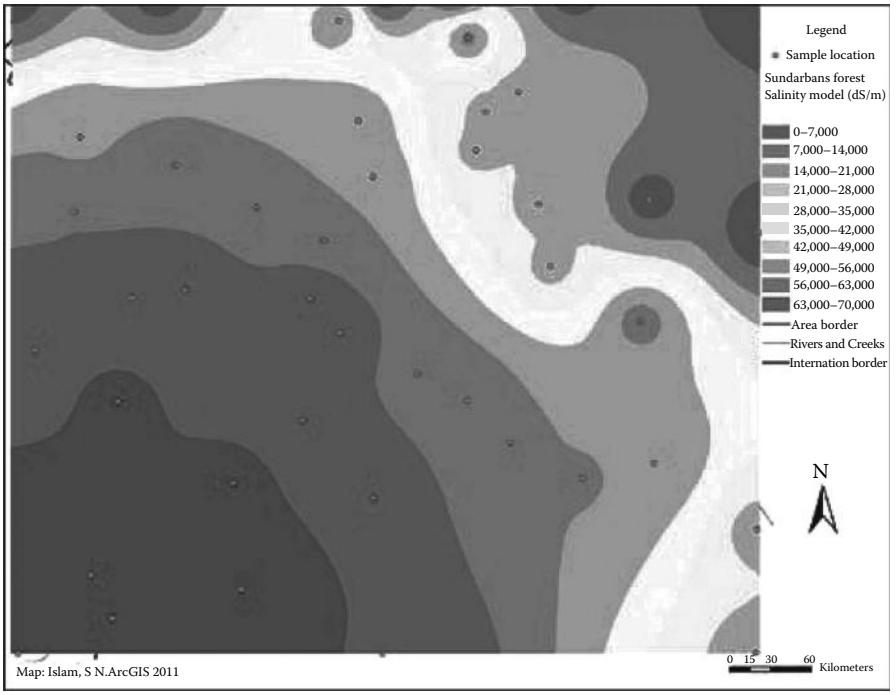

(c)

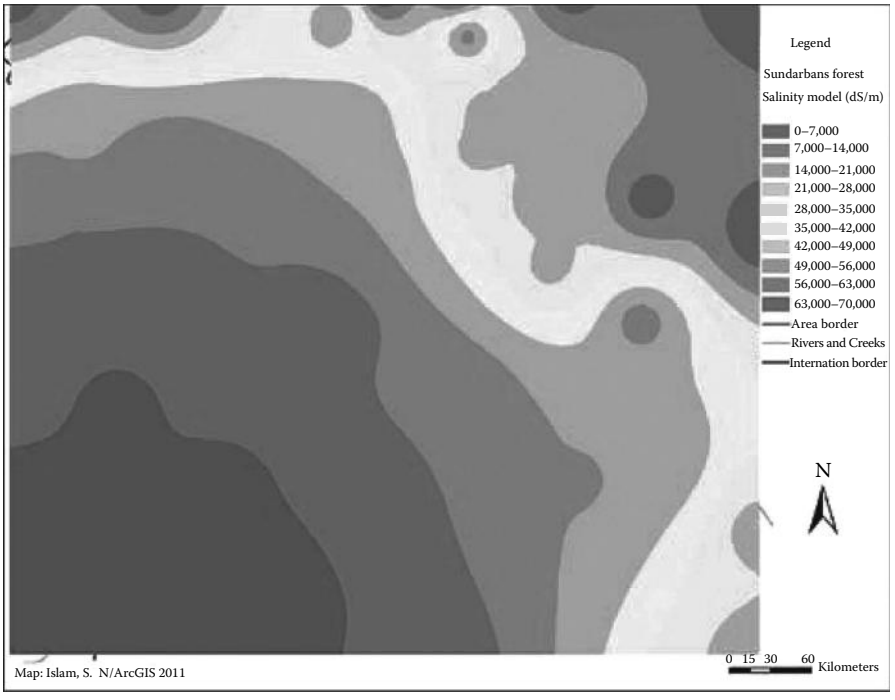

(d)

FIGURE 18.6 (continued) Water salinity modeling (a–d) in the Sundarbans mangrove region in 2003.

Figure 18.6 shows the model (a–b) of the mangrove forest and water salinity intrusion pattern (water and forest landscape layer) based on the time series data analysis on the Sundarbans of Bangladesh area. The model (c–d) shows the sample distribution and water salinity intrusion (water layer). The time series water salinity data on 13 potential rivers in the Sundarbans forest areas have been diagnosed through geostatistical analysis using ArcGIS 10; the models show the present scenarios of water salinity. In water salinity modeling, the 10 different salinity ranges used are illustrated in Figure 18.6. The 1st range, which is located in the northeast corner of the Sundarbans, carries the low salinity. Since the Baleswar and Kocha rivers basins are carrying freshwater from the upstream area this is why the high salinity intrusion rate is low in the eastern part of Sundarbans region.

The second range carries the lowest salinity range of 7,000–14,000 dS/m; third range carries the rate 14,000–21,000 dS/m; fourth range carries the rate 21,000–28,000 dS/m; fifth range carries 28,000–35,000 dS/m; sixth range carries 35,000–42,000 dS/m; seventh range carries 42,000–49,000 dS/m; eigth range carries 49,000–56,000 dS/m; ninth range carries 56,000–63,000 dS/m; and tenth range carries the highest rate, 63,000–70,000 dS/m (Figure 18.6), which is very high for germination, growth, and development.

The salinity investigation results show that the southwest corner of the Sundarbans is carrying the highest rate of water salinity, which is harmful for balancing the mangrove ecosystem management in the coastal region (Islam, 2001; Akter et al., 2010). According to salinity approximation, this high rate is harmful for mangrove ecosystems. The 1st range area is safe for the mangrove ES, where the salinity rate is very low, because the Baleswar–Kocha River is carrying freshwater from the upstream (Akter et al., 2010; Islam et al., 2011). Accordingly, the 8th, 9th, and 10th ranges of the Sundarbans areas are under threat because the water salinity rate in these areas are very high, which has crossed the water salinity threshold line for the mangrove ecosystem and ES. Therefore, the result of salinity modeling in the Sundarbans region shows increasing trend, and it can be stated that almost half of the Sundarbans mangrove wetland areas are under threat for mangrove ecosystems and services.

18.5.4 Threats to Mangrove Biodiversity

The coastal mangrove biodiversity loss is a common scenario in Bangladesh and India. The mangrove reduction rate is 45% in both countries. Deforestation of mangroves due to shrimp farming, salt farming, agricultural land extension, and settlement development adversely affects marine fish production and leads to a loss of biodiversity and livelihood to over 3.5 million people who are dependent on mangrove resources in the coastal region in Bangladesh (Anon, 1995). The estimated mangrove forest in Bangladesh was 685,000 ha (1963–1978), and the present area is about 587,000 ha, which covers 86%, it means that 14% of mangrove already lost or disappeared within 33 years. The degradation of mangroves is caused by anthropogenic influences and natural changes. Tropical storms and tsunami are common in the Bay of Bengal. The damaged forests take a very long time to recover. A cyclone has destroyed about 8.5 million trees in Bangladesh Sundarbans in 2007, which is equivalent to 66.3 million m^3 of sawed timber in the year 1988. The *Heritiera fomes* (Sundari) plant is the dominating one in Sundarbans, which represents 21% of the mangrove diversity. The top-dying disease has damaged about 45 million *Heritiera fomes* (Sundari) trees. This is about 20% of the entire forests in Bangladesh (Hussain and Acharya, 1994). The top-dying disease is believed to be caused by an array of factors: increased soil and water salinity due to reduced upstream river water flow, reduction in periodic inundation, excessive flooding, sedimentation and erosion, nutrient imbalances, pathogenic gall cankers, and cyclone-induced stress (Anon, 1995; Hussain and Acharya, 1994). Approximately 150,000 ha mangroves were destroyed during the past 100 years between Bangladesh and India due to agricultural reclamation. A number of species like Javan rhinoceros (*Rhinoceros Sondaicus*), water buffalo (*Bubalus bubalis*), Swamp deer (*Cervus duvauceli*), Guar (*Bos gaurus*), hog deer (*Axis porcinus*), and marsh crocodile (*Crocodylus palustris*) became extinct during the last 100 years in the Sundarbans (Hussain and Acharya, 1994; Islam and Gnauck, 2008). Oil spill and industrial waste are also creating threat and could cause immense damage, especially to aquatic fauna and seabirds and probably also to the mangrove forest biodiversity. The annual natural calamity,

global warming, and its impacts are new challenging threats for coastal food security and mangrove biodiversity (Rahman, 1988; Hussain, 1995). The siltation in the Sundarbans has increased, and sediment trapping has been aided by pneumatophores and dense roots of mangroves. The dominant species of Sundari (*Heritiera fomes*) and Goran (*Cariops decandra*) are affected by top-dying disease. The finding shows that 285 km^2 areas of *Heritiera*-type forest are moderately affected and 275 km^2 areas are severely affected by this disease, which is one of the main threats for the sustainable mangrove wetland management and the protection of its ecosystems (IWM, 2003).

18.5.5 Approach of Hydrological Balance for Mangrove Ecosystems

Considering the present investigation results in the Sundarbans region in Bangladesh, it has been observed that there is a close correlation between hydrological cycle and the mangrove ecosystems in the Sundarbans region. The similar scenarios have been observed in other parts of the world like the Indus delta mangrove ecosystem, Mekong delta mangrove ecosystem, Red River delta mangrove ecosystem, and Chao Phraya River delta mangrove ecosystems, which are dependent on the upstream freshwater supply and hydrological changes. The changing behavior of hydrological systems is a global common scenario in the mangrove regions especially in Asia-Pacific, Latin America, and African countries. Upstream freshwater is essential for mangrove ecosystem, and in the contemporary world, most of the important river's waters in Asia-Pacific and African countries are used for irrigation, hydropower generation, and industrial purposes (Versfeld and Wassen, 2005). Therefore, limited quantities of freshwater can enter in the mangrove wetland areas. As a result, almost 45% of mangrove forest has been destroyed due to anthropogenic activities and shrimp cultivation. Most of the mangrove regions are now affected due to shortage of freshwater supply, which is the root cause of hydrological change (Ahsan and Rahman, 2001; Miah, 2003; Nishat, 2006). In order to conserve the balance of mangrove ecosystems, it is necessary to balance the hydrological cycle in any mangrove region of the world. In the Sundarbans mangrove wetland areas, the Ganges freshwater supply could make the balance of regional hydrological systems in the Sundarbans region. The present study suggests that water storages in Nepal should be establised within the multilateral agreement (Adel, 2001; Nair, 2004). In Nepal, the major seven rivers are carrying 71% freshwater annually at the Farakka Barrage in the dry season (Elahi et al., 1998; Nishat, 2006; Islam et al., 2011). It has been estimated that through construction of water storage in the upstream areas in Nepal, Bangladesh can achieve extra 45,000 m^3/s water from upstream in the dry season, which could make the hydrological balance in the Sundarbans region and could protect the mangrove ecosystems in the coastal region in Bangladesh (Islam and Gnauck, 2009a,b; Islam et al., 2011). The similar approach could be used in other parts of the mangrove world.

18.6 Summary and Conclusions

The Sundarbans mangrove forest is located in the Ganges delta, and it is the part of GBM River systems. The Sundarbans is one of the largest mangrove wetlands and a unique ecosystem in the world, which is dependent upon the hydrological regime. It is a natural shield that protects the coastal landscapes and its ecosystems from storm surges and cyclones in pre- and postmonsoon periods. The study results show that it is playing a potential role in regional socioeconomic improvement and in balancing ecosystems in the coastal zone of Bangladesh. Since the diversion of Ganges water at Farakka Barrage in India from early 1975, the water and soil salinity has penetrated due to capillary upward movement processes and sea-level rise impacts. Consequently, both siltation and intrusion of salinity have degraded water quality of Sundarbans Rivers, and it is the root cause of salinity intrusion and threats for coastal mangrove ecosystems. The peak salinity rate was found to be about 56,186 dS/m in 2001 and 2002, and it was found to be 58,347 dS/m in 2008 just after the Cyclone Sidr affected in 2007. The study findings show that the river water (13 rivers) salinity rate has increased rapidly, which is damaging the mangrove wetland ecosystem and its services. It has a polynomial behavior, and most of the river water has crossed the water salinity threshold value, which is unsafe for coastal mangrove ecosystems.

The study has investigated the hydrological changes and the water salinity intrusion of the Sundarbans Rivers, which could be considered as a tool for decision making. Water salinity model will support to prepare a mangrove ecosystem management plan by the decision makers, to balance the hydrological cycle in the regional and local bases, and to protect the mangrove ecosystems and its unique biodiversity in the Sundarbans region (Islam and Gnauck, 2009a,b; Islam et al., 2011).

Hydrological changes in different parts of the mangrove wetlands region are the cause of damaging ecosystem and its services. The present study investigated the salinity intrusion pattern in the Sundarbans mangrove region, which is dependent on the freshwater supply and hydrological changing behavior in the region. The sedimentation and salinity intrusion in the Sundarbans are also the reasons of vulnerable environmental degradation and threat to mangrove ES in the coastal region. The coastal landscapes and the Sundarbans mangrove of the deltaic region encompassed strong aesthetic, cultural, biological, and geological values. Therefore, conversation of mangrove biodiversity and maintenance of ecosystems is a global environmental issue. The mangrove ES are potential to ensure its natural services to the coastal communities. Based on the results of this study, it can be stated that the awareness education, applied training, and research should be initiated in order to change the attitude of the people and the government toward protecting water quality and mangrove ecosystem. The transboundary Ganges water flow is patronizing the mangrove ES in the Sundarbans region; therefore to ensure upstream freshwater supply to the Sundarbans region is essential for its ecosystem maintenance. Beside this adaptation and migration strategies should be incorporated in the national development plan for coastal resources management and ecosystems protection. The proposed recommendations should be implemented for the future development of mangrove ES and should ensure food security of the coastal communities in the Sundarbans region in Bangladesh.

- The hydrological condition in the mangrove region must be considered as one of the most impending issues of local and regional developmental agenda and ensure the balance of future maintenance of mangrove ecosystem and its services.
- The Ganges freshwater supply through the Gorai River basin to the coastal region of the mangrove wetland areas is necessary, which could protect the mangrove wetland ecosystem and ES for the coastal community livelihood sustainability in the Sundarbans region in Bangladesh.
- To arrange climate change awarness training activities for capacity building of local stakeholders through participation. Besides, more applied research is needed to find out alternative solutions for the Sundarbans mangrove wetland ecosystem and biodiversity protection.
- Mangrove wetlands and environmental data banks are required, and it is necessary for the future applied research, education, training, and development of the wetland ecosystem and to ensure their goods and services. GIS should be introduced within the mangrove and other wetland data collection, analysis, visualization, mapping, planning, monitoring, and management system.
- Rise in sea level, tidal inundation, and coastal estuaries' wetlands ecosystem are factors that have to be considered within the long-term management strategy for dealing with coastal mangrove ecosystem issues. The coastal ecosystem management plan should be formulated based on the results of the present study of water salinity modeling in the Sundarbans mangrove wetlands.
- The proper regional water resources management plan could ensure the balance of hydrological ecosystem in the Sundarbans coastal region.
- All the aspects of mangrove ecosystem studies and research should ensure future development and sustainable management of coastal natural resources. In such situation, a Mangrove Wetlands Research Institute should be established in a public university in Bangladesh for graduate studies and short training courses could be offered for the professionals for capacity building and good governance to ensure coastal resource management and mangrove biodiversity protection for the sustainability of mangrove ES in the Sundarbans region and other parts of the mangrove world.

References

Adel, M.M. 2001. Effect of water resources from upstream water diversion in the Ganges basin. *Journal of Environmental Quality*, (Environmental Issue), 30(2): 356–368.

Ahmed, I., Deaton, B.J., Sarker, R., and Virai, T. 2008. Wetland ownership and management in a common property resource setting: A case study of Hakaluki Haor in Bangladesh. *Ecological Economics*, 68(1–2): 4294–4236.

Ahmed, R. and Falk, G.C. 2008. Bangladesh: Environment under pressure. *Geographische Rundschau International Edition*, 4(1): 13–19.

Ahsan, M. and Rahman, M. 2001. Salinity constraints and agricultural productivity in coastal saline area of Bangladesh. In: *Proceedings of the Annual Workshop on Soil Resources*, February 14–15, 2001. Soil Resource Development Institute (SRDI), Dhaka, Bangladesh, pp. 1–14.

Akter, J., Islam, S.N., and Gnauck, A. 2010. Water resources management in the coastal region of Bangladesh. In: *Modelling and Simulation of Ecosystems, Workshop Kölpinsee 2009*, Shaker Verlag, Aachen, Germany, pp. 167–185.

Anon, 1995. Integrated resource management plan of the Sundarbans Reserved forest, Vol. 1, Draft final Report of FAO/UNDP project BGD/84/056, Integrated Resource Management of the Sundarbans Reserve Forest, Khulna, Bangladesh.

Bird, E.C.F. 1969. *An Introduction to Systematic Geomorphology: Coasts*. MIT Press, Massachusetts Institute of Technology, Cambridge, MA.

Daily, G. 2006. Conservation planning for ecosystem services. *PLoS Biology*, 4: 2138–2152.

Duke, N.C. 1992. Mangrove floristics and biogeography. In: Robertson, A.I. and Alongi, D.M. (eds.), *Tropical Mangrove Ecosystems, Coastal and Estuarine Studies No. 41*. American Geophysical Union, Washington, DC, pp. 63–100.

Elahi, K.M., Das, S.C., and Sultana, S. 1998. Geography of coastal environment: A study of selected issues. In: Bayes, A. and Mahammad, A. (eds.), *Bangladesh at 25, an Analytical Discourse on Development*. University Press Limited, Dhaka, Bangladesh, pp. 336–368.

FAO (Food and Agricultural Organization). 2007. The world's mangroves 1980–2005. FAO forestry paper no. 153, Rome, Italy.

Fongwa, E., Gnauck, A., and Müller, F. 2009. A hybrid model for sustainable development of ecosystem services. In: *Modellierung und simulation von ökosystemen, workshop Kölpinsee 2009*. Shaker Verlag, Aachen, Germany, pp. 204–223.

Goodbred, S.L. and Kuehl, S.A. 1999. Holocene and modern sediment budgets for the Ganges-Brahmaputra river system: Evidence for highstand dispersal to floodplain, shelf, and deep sea depocentres. *Geology*, 27(6): 559–562.

Hidayati, D. 2000. Coastal management in ASEAN countries. In: *The Struggle to Achieve Sustainable Coastal Development*. UN University Press, Tokyo, Japan, pp. 1–74.

Hussain, Z. and Acharya, G.1994. *Mangrove of the Sundarbans, Volume Two: Bangladesh*. IUCN, Dyna Print, Bangkok, Thailand.

Hussain, Z.K. 1995. The Farakka catastrophe reflections. In: Moudud, H.J. (ed.), *Women for Sharing Water*. Academic Publishers, Dhaka, Bangladesh, pp. 71–72.

IPCC (Intergovernmental Panel on Climate Change). 2007. Summary for policymakers. In: Parry, M.L., Canziani, O.F., Palutikot, P.J. et al. (eds.), *Climate Change 2007: Impact Adaptation and Vulnerability*. Contribution of working group II to the 4th assessment report of the IPCC, Cambridge University Press, Cambridge, U.K., 1000pp.

Islam, M.S. 2001. *Sea-Level Changes in Bangladesh: The Last Ten Thousand Years*. Asiatic Society of Bangladesh, Asiatic Civil Military Press, Dhaka, Bangladesh, pp. 1–185.

Islam, S. (ed.). 2006. *Encyclopedia of Bengal*. Asiatic Society of Bangladesh, Asiatic Civil Military Press, Dhaka, Bangladesh.

Islam, S.N. and Gnauck, A. 2007. Increased salinity in the Ganges delta and impacts on coastal environment in Bangladesh. In: *Proceeding of Logistics and Economic of Resource and Energy-Saving in Industries*, September 12–15. ISPC, Saratov State Technical University, Saratov, Russia, pp. 244–248.

Islam, S.N. and Gnauck, A. 2008. Mangrove wetland ecosystems in Ganges-Brahmaputra delta in Bangladesh. *Frontier Earth Science China*, 2(4): 439–448.

Islam, S.N. and Gnauck, A. 2009a. The coastal mangrove wetland ecosystems in the Ganges Delta: A case Study on the Sundarbans in Bangladesh. In: *Proceeding of American Association of Petroleum Geologist—AAPG Hedberg Conference on Variations in Fluvial-Deltaic and Coastal Reservoirs Deposited in Tropical Environments*, April 29–May 2, 2009, Jakarta, Indonesia, pp. 26–29.

Islam, S.N. and Gnauck, A. 2009b. Threats to the Sundarbans mangrove wetland ecosystems from transboundary water allocation in the Ganges basin: A preliminary problem analysis. In: Eslamian, S. (ed.). *International Journal of Ecological Economics and Statistics (IJEES)*, 13(09): 64–78.

Islam, S.N. and Gnauck, A. 2011. Water salinity investigation in the Sundarbans rivers in Bangladesh. *International Journal of Water*, 6(1–2): 74–91.

Islam, S.N., Gnauck, A., and Voigt, J.H. 2011. Fourier polynomial approximation of estuaries water salinity in the Sundarbans region of Bangladesh. *International Journal of Hydrology Science and Technology*, 1(3–4): 207–223.

IWM (Institute of Water Modeling). 2003. Sundarbans biodiversity project—Surface water modeling TA No. 3158 BAN, Final report, Vol. 1, IWM, Dhaka, Bangladesh.

Joseph, P.S. 2006. The environmental management the better supply of fresh water in transboundary River: The Ganges could run dry. In: Perez, J.G. (ed.), *Proceedings of III International Symposium on Transboundary Waters Management-Overcoming Water Management Boundaries*, May 30–June 2. Universidad de Castilla-La Mancha, Ciudad Real, Spain.

Katebi, M.N.A. 2001. Sundarbans and forestry. In: Haider, R. (ed.), *Cyclone'91—An Environmental and Perceptional Study*. BCAS, Dhaka, Bangladesh, pp. 79–100.

Lacerda, D.D.L. (ed.). 2001. *Mangrove Ecosystems Functions and Management*. Springer-Verlag, Berlin, Germany.

Margozczi, K., Aradi, E., Takacs, G., and Botori, Z. 2007. Small scale and large scale monitoring of vegetation changes in a restored wetland. In: Okruszko, T. Maltby, E., Szatylowicz, J., Swiatek, D., and Kotowski, W. (eds.), *Wetlands—Monitoring, Modelling and Management,* Taylor & Francis, Leiden, the Netherlands, pp. 55–60.

Miah, M. 2003. Hydro-politics of the Farakka Barrage, www.sdnpbd.org/river-basin/bangla. (Accessed on 10 March 2010).

Mitsch, W.I. and Gosselink, I.G. 1986. *Wetlands*. Van Nostand Reinhold, New York, pp. 1–220.

Nair, K.S. 2004. Wetlands management to meet the food and water crisis-example from a tropical region. In: *Proceedings of 7th INTECOL International Conference on Wetlands 2004*. Universiteit Utrecht Press, Utrecht, the Netherlands, p. 217.

Nishat, A. 2006. Water at Farakka Barrage in 2006. www.ajkerkagoj.com/2006/April 08/. (Accessed on 11 March 2010).

Rahman, A.A. 1988. Bangladesh coastal environment and management. In: Hasna, M.J., Rashid, H.E., and Rahman, A.A. (eds.), *National Workshop on Coastal Area Resource Development and Management (CARDMA)*. Academic Publishers, Dhaka, Bangladesh, pp. 1–22.

Rahman, M. and Ahsan, A. 2001. Salinity constraints and agricultural productivity in coastal saline area of Bangladesh. In: Rahman, M. (ed.), *Soil Resources in Bangladesh: Assessment and Utilization (SRDI)*. Prokash Mudrayan, Dhaka, Bangladesh, pp. 2–14.

Sarker, M.H. 2008. Morphological response of the Brahmaputra-Padma-lower Meghna River system to the Assam Earthquake of 1950. Unpublished PhD thesis, School of Geography, University of Nottingham, Nottingham, U.K., pp. 1–296.

Sarkar, S.U. 1993. Faunal diversity and their conservation in freshwater wetlands. In: Nishat, A., Hossain, Z., Roy, M.K., and Karim, A. (eds.), *Freshwater Wetlands in Bangladesh: Issues and Approaches for Management*. IUCN, Gland, Switzerland, pp. 1–364.

Siddiqi, N.A. (ed.). 1994. The importance of mangroves to the people in the coastal areas of Bangladesh. In: *Proceedings of VII Pacific Science International Congress*. International Society of Mangrove Ecosystems (ISME), Tokyo, Japan.

Siddiqi, N.A. 2001. *Mangrove Forestry in Bangladesh*. Institute of Forestry and Environmental Sciences, University of Chittagong, Nibedon Press Limited, Chittagong, Bangladesh, p. 201.

Smith, W.S. 1997. *Scientists and Engineer's Guide to Digital Processing*. California Technical Publishing, San Diego, CA.

Smolders, A.J.P., Tomassen, H.B.M., Lamers, L.P.M., Lomans, B.P., and Roelofs, J.G.M. 2002. Peat tog restoration by floating raft formation: The effects of ground water and peat quality. *Journal of Applied Ecology*, 39(3): 391–401.

SRDI (Soil Resource Development Institute). 2001. *Soil Resources in Bangladesh*. Government of the People's Republic of Bangladesh, Soil Resource Development Institute, Dhaka, Prokash Mudrayan, Dhaka, Bangladesh, pp. 1–107.

Versfeld, N.G. and Wassen, M.J. 2005. Wetland management for nature, what Canada, The Netherlands and Poland can learn from each other. In: Kotowski, W. (ed.), *Anthropogenic Influences on Wetlands Biodiversity and Sustainable Management of Wetlands*. Warsaw Agricultural University Press, Warsaw, Poland.

Vitousek, P. 1997. Human domination of earth's ecosystems. *Science*, 277: 494–499.

Wahid, S.M. 1995. Hydrological study of the Sundarbans. UNDP/FAO Project BGD/84/056, Department of forest, Dhaka, Bangladesh.

Whyte, I.D. 1995. *Climatic Change and Human Society*. Arnold, London, U.K., pp. 141–171.

19

Hydrologic Modeling: Stochastic Processes

Rina Schumer
Desert Research Institute

AUTHOR

Rina Schumer is an associate research professor in the division of hydrologic sciences at the Desert Research Institute in Reno, NV, United States. After completing her undergraduate studies in earth and environmental sciences at Wesleyan University in Middletown, Connecticut, Rina worked in environmental consulting in New England, primarily focused on groundwater remediation. She has graduate degrees in both applied mathematics and hydrogeology. Her doctoral research focused on models for anomalous transport in porous media. Dr. Schumer's current research includes development and application of stochastic models in a broad range of earth and environmental sciences. She is principal investigator with the National Center for Earth Surface Dynamics and the associate director for the University of Nevada Graduate Program of Hydrologic Sciences.

PREFACE

This chapter describes a variety of analytical models that permit incorporation of variability in simulation of hydrologic processes. Emphasis is put on the probabilistic building blocks and assumptions underlying each model. Each class of problems to be solved (e.g., recurrence of extreme events, distance travelled, or time until a threshold is achieved) has a set of useful stochastic models. Statistical characteristics of the data and the scale at which predictions are required can guide the user to specific model selection.

19.1 Introduction

All hydrologic processes in the water cycle are deterministic, governed by physical laws we could use for prediction if we had complete knowledge of the atmosphere, boundary layer, earth surface, and subsurface. More often than not, we must use simplifications of reality for hydrologic prediction, including models that can treat the inherent variation in timing of hydrologic forcing and the spatial distribution of physical properties. Thus, hydrologic models need to account for variability in both space and time. The flow of water, solutes, and sediment over and through heterogeneous media complicates deterministic prediction of hydrologic transport phenomena. Likewise, uncertainty in the timing and intensity of precipitation events and temperature fluctuations affects our ability to forecast snowmelt, recharge, evaporation, overland flow, streamflow, reservoir levels, etc. Stochastic models use probability theory to account for uncertainty in hydrologic prediction and can be used to reproduce the statistical regularity that often appears in physical phenomena after a sufficient amount of time has passed or a sufficiently large space is sampled. As with deterministic modeling, the goal of stochastic modeling is to find an equation that sufficiently describes the important properties of a process with the smallest number of explanatory variables.

One approach to stochastic modeling, known as Monte Carlo analysis, incorporates variability in environmental models by having the user define a domain of possible parameters and run a series of deterministic computations on inputs drawn from one or more probability densities. The aggregated result of a large number of simulations describes a range of possible outcomes and their likelihood. In this chapter, however, we describe stochastic models that have descriptions of variability built into analytical equations.

19.2 Probability Theory

The building blocks of probabilistic models are stochastic processes. A stochastic process is a collection of random variables $\vec{X} = \{X(t), t \in T\} = \{X_1, X_2, \ldots, X_t\}$, where $X(t)$ is the state of the process at time t and T is the set of all possible time. X varies through time and that variation may contain both deterministic and random components. For example, streamflow may follow predictable seasonal cycles but daily discharge may have considerable variability and may not be easily predictable. Instead the bulk behavior of discharge can be described by a probability density function (pdf) that characterizes the mean and spread around it. Notation such as $\vec{K} = \{K(x), x \in X\} = \{K_1, K_2, \ldots, K_x\}$ denotes spatial variability of, for example, hydraulic conductivity at each point x in the spatial domain X.

Probability distributions assign the likelihood of events associated with a random variable. If random variables are *discrete* such that their sample space consists of a discrete set of values $\Omega = \{0,1,2,\ldots\}$, then the distribution is determined by a probability mass function $f(x) = P(X = x)$, where $P(\cdot)$ denotes probability. The number of days between storms is a discrete random variable. If random variables are *continuous,* then their sample space can vary continuously and they are described by a probability distribution function or cumulative distribution function (cdf) $F(x) = P\{X \leq x\}$ or its derivative, the pdf $f(x) = dF/dx$ [8]. It is common, but incorrect, for scientists to mix the terms density function and distribution function. A density function describes the relative frequency of each value in a sample space, while the distribution function describes the likelihood of all outcomes below a given value. Also commonly used in hydrology is the exceedance distribution of a random variable $1 - F(x) = P(X > x)$, which shows the likelihood of all values above a given value. The exceedance distribution function is frequently used to distinguish between thin- and heavy-tailed data. There are many textbooks and numerical codes that execute both distribution fitting and parameter estimation for sample data.

The most commonly used stochastic models in hydrology are those that describe random *increments*, *maxima*, or *sums* of random events. For example, in time series analysis, we may be interested in the distribution of the random event sizes themselves. In flood frequency analysis and other areas of extreme value (EV) theory (see Chapter 22 in this volume), we are interested in the overall distribution

of event sizes and recurrence of the largest events in a given period of time and might track the maxima $M_n = \max\{Y_1, Y_2, \ldots, Y_n\}$ for a collection of random events $\{Y_1, Y_2, \ldots\}$ that occur during the nth year. In studying transport, on the other hand, we represent the location of a particle at time t as the sum of discrete jump lengths that occur with each Δt, $X(t) = \sum_{i=1}^{t/\Delta t} Y(i)$. In all cases, the statistical character of the increments determines the long-term behavior of the maxima or sum. These rules are embodied by the limit theorems discussed in Section 19.4.1. In the case of both maxima and sums, the following properties affect the character of the appropriate stochastic model:

1. Independent versus dependent increments
2. Stationary versus non-stationary increments
3. Thin- versus heavy-tailed distribution of increments

Independence of increments means that the size of each random event is unrelated to previous or future events, while *stationarity* indicates that event size is not related to the time the event occurs. The distinction between thin- and heavy-tailed distributions refers to the rate of upper tail decay, most easily seen in the end of the exceedance distribution. The upper tail represents the probability of events with extreme deviation from the mean or mode. The character of the tail decay determines the limiting distribution to which sums or maxima will converge in the scaling limit. Sums of independent and identically distributed (iid) random variables with thin tails converge in distribution to Gaussian densities. Heavy-tailed refers to distributions the tails of which decay slowly enough that EVs are relatively likely, such that random sums never converge in distribution to a Gaussian density. While heavy-tailed distributions are always power law, distributions with power-law tails are not always heavy-tailed.

The effect of independence, stationarity, and tail characteristics will be described in the following sections on stochastic models for time series analysis, EV theory, and hydrologic transport.

19.3 Discrete Stochastic Models

19.3.1 Increments and Sums: Classical Time Series Analysis

After identifying and subtracting deterministic components (trends, cycles, etc.) of a time series, discrete stochastic models are used to describe the "random" characteristics of data. For example, to determine how streamflow at one site varies from day to day in a given season, we might consider the entire flow series or difference the daily discharge data. If our interest is a model for streamflow to use for forecasting, we could analyze the statistical characteristics of the differenced or incremental data.

The fundamental discrete stochastic process is the white noise process, generally referring to as a collection of iid random variables of arbitrary distribution with zero mean and finite variance. Variations on this definition are also in use. For example, "iid" is often replaced with "uncorrelated" and "finite variance" is often replaced with "unit variance." Gaussian white noise, in which random increments are described by a Gaussian distribution, is the most commonly used model for iid increments with thin tails. Lévy or α-stable noise is used when "iid" increments are heavy-tailed. Importantly, no trends or clusters are associated with white noise processes.

19.3.1.1 Autoregressive Processes

Many hydrologic processes are not uncorrelated in time, and more flexible models must be used to represent randomness. Autoregressive models–such as the autoregressive process of order 1 (AR1): $X(t) = c + aX(t-1) + \sigma\varepsilon(t)$, where c is a constant, σ is a scale parameter, and ε is a white noise process–are named because of their similarity to univariate regression models. Trends appear in the sample paths of an AR(1) because of the dependence of each increment on the prior increment. The mean and variance of AR(1) increments are a function not only of the noise term but also of a and/or c: $E(X(t)) = c/(1-a)$ and $Var(X(t)) = \sigma^2/(1-a^2)$ [5]. When the correlation structure of a time series goes farther back than a

single increment, an AR(p) model may be invoked: $X(t) = c + \sum_{i=1}^{p} a(i)x(t-i) + \sigma\varepsilon(t), t = 0,1,2,\ldots$. One way to estimate how far back in a series dependence runs is to compute the autocorrelation function (ACF) $\rho(h)$ of a time series: $\rho(h) = Cov[X(t), X(t+h)] \Big/ \left(\sqrt{Var[X(t)]}\sqrt{Var[X(t+h)]}\right)$. For an AR(1) process, this reduces to $\rho_{AR(1)}(h) = a^h$ implying geometric decay of autocorrelation well past one lag. This occurs because $X(t)$ is a function of $X(t-1)$ that is a function of $X(t-2)$ and so on. In practice, the ACF of an AR(1) decays so quickly past lag 1 that only lag 1 is significant. It does suggest use of the more intuitive *partial autocorrelation function* (PACF), which for an AR(1) is $\xi(h) = \begin{cases} a & h = 1 \\ 1 & h = 0 \\ 0 & \text{otherwise} \end{cases}$, and for a more general AR(p)-process, we obtain nonzero PACF for the first p lags and zero PACF otherwise.

19.3.1.2 Moving Average Processes, ARMA, and Beyond

Moving average (MA) models are used when observations take the form of a weighted average of one or more previous observations of the noise process. An MA(q) process is given by $X(t) = c + \sum_{i=1}^{q} b(i)\varepsilon(t-i) + \sigma\varepsilon(t)$, $t = 0,1,2,\ldots$. Coefficients can be chosen so that an MA model is stationary, so the conditional mean and variance do not depend on the time for which they are computed; however, the conditional mean does change through time. MA models are typically not used alone in hydrology.

Numerous generalizations of the basic autoregressive and MA models exist. Autoregressive and MA models can be combined to form the *general linear time series model*, the ARMA(p,q)-process. While PARMA(p,q) models incorporate periodicity, GAR models are appropriate for skewed hydrologic processes, ARCH models incorporate time-varying conditional variance, and ARIMA models apply when ARMA models are fit to differenced data.

19.3.2 Increments and Sums: Pre-Asymptotic Continuous Stochastic Models for Time Series and Transport

In some hydrologic applications, it is useful to model stochastic phenomena on a continuous timescale. This may occur because the random variable of interest is naturally measured on a continuous timescale. However, it is also common for discrete stochastic phenomena to be simulated with continuous models because of their analytical tractability. The pre-asymptotic (meaning before a limit theorem can be invoked) models are useful when the exact distribution of random variables can be quantified.

19.3.2.1 Markov Chains and Random Walks

The AR(1) model discussed earlier is an example of a discrete Markov chain, a stochastic process in which the next state of a system only depends on the current state and not on previous states. For a Markov chain $\{X_n, n = 0,1,2,\ldots\}$ where $X_n = i$ signifies that the process is in state i at time n and there is a probability P_{ij} that it will next be in state j, P_{ij} is only a function of X_n and not of X_{n-1}, X_{n-2}, or any previous states. The classic example of a Markov chain in hydrology describes the chance of rain tomorrow or a subsequent day depending on current weather conditions. A two-state chain (state 1 = wet day and state 2 = dry day) might be described by the transition probability matrix $P = \begin{bmatrix} P_{11} & P_{12} \\ P_{21} & P_{22} \end{bmatrix} = \begin{bmatrix} 0.9 & 0.1 \\ 0.5 & 0.5 \end{bmatrix}$ as in Haan [13], where the sum of each row must be one. In this case, the probability of a wet day today followed by a dry day tomorrow is 0.1. To calculate the probability of a wet day today followed by a dry day two days from now or three days from now, we use P^2 or P^3, respectively. Since $P^3 = \begin{bmatrix} 0.8440 & 0.1560 \\ 0.7800 & 0.2200 \end{bmatrix}$, we can conclude that the probability of a wet day today followed by a dry day 3 days from now is 0.1560, or 15.6%. As successive powers of the transition probability matrix P are calculated, the elements converge

to the longtime probability of any day being wet or dry. In our example, after $P^{11} = \begin{bmatrix} 0.8333 & 0.1667 \\ 0.8333 & 0.1667 \end{bmatrix}$, the elements no longer change and are equal in columns, indicating that the long-term probability of a wet day is approximately 83% and the probability of a rainy day is approximately 17%. While the probability of wet or dry days a few days from now is related to today's weather, the long-term forecast is unrelated to the present state. This is an excellent introduction to the concept of asymptotics in probability theory and stochastic processes, in which long-term outcomes may emerge as a result of general statistical properties, but not the initial condition.

While exact transition probabilities as in the preceding example may be difficult to calculate in practice, use of a Markov chain known as a *random walk* is ubiquitous in hydrology, particularly in association with transport processes. Let $\{Y_1, Y_2, \ldots, Y_n\}$ be a sequence of iid random "jump" sizes. A random walk is a stochastic process that gives the running sum of the increments through time $X(t) = \sum_{i=1}^{t/\Delta t} Y_i$. In modeling transport processes, jumps may represent actual distance that a particle (of water, solute, sediment) moves in a single time step, so that the sum represents total distance traveled through time. If the jumps represent daily changes in river flow, then a random walk can be used to model total change in flow through time. Similarly, if jumps represent elevation changes in a reservoir, a random walk can be used to model elevation change through time. The cdf F of jump size can be discrete or continuous (the notation $x \sim F$ means that the random variables x_i have distribution F). In either case, if $n = t/\Delta t$ is the number of steps by time t, the evolution of $X(t)$ can be computed by taking the convolution of F n times, where the convolution operation is defined $(f * g)(x) = \int_{-\infty}^{\infty} f(\tau)g(t-\tau)d\tau$. This is because the cdf of the sum of independent random variables is the convolution of their respective cdfs. In practice, when a random walk fits the conceptual model for a hydrologic process, an asymptotic model, described in Section 19.4.2, is usually invoked.

19.3.2.2 Renewal Processes

The random number of events up to a given time $\{N(t), t \geq 0\}$, say the number of rainstorms at or prior to a 30-day period, is known as a counting process. A counting process is known as a *renewal process* if the length of time between events, known as the inter-arrival times, is iid random variables with arbitrary distribution. The well-known Poisson process is a renewal process with exponentially distributed ($f(t) = \lambda e^{-\lambda t}$) inter-arrivals, with rate parameter λ. Its name derives from the fact that the number of events in any interval of length t is Poisson distributed with mean λt: $P\{N(t) = n\} = (e^{-\lambda t})((\lambda t)^n/n!)$, $n = 0,1,2,\ldots$ Poisson-type processes have long been used to model recurrence of seasonal rainfall and drought timing [7,23].

19.3.2.3 Renewal Reward Process or Continuous Time Random Walk

Classical random walk models represent distance travelled as the sum of discrete random jumps that are assumed to be equally spaced in time (although strictly speaking, a random walk with thin-tailed inter-arrivals will converge in distribution to the same limiting stochastic process as a random walk with equally spaced inter-arrivals). Renewal reward processes, also known as continuous time random walks (CTRWs), combine random walk and renewal counting processes by defining distance traveled as the sum of random jumps that occur randomly in time:

$$X(t) = \sum_{i=1}^{N(t)} Y_i, \quad t \geq 0 \tag{19.1}$$

where

the total distance traveled $X(t)$ is the sum of iid random jump sizes

$\{N(t), t \geq 0\}$ is a renewal process

Use of CTRW is now common in modeling of transport processes that consist of an on- and an off-period for motion. Applications include subsurface transport in porous and fractured media, stream transport with transient storage, and sediment transport in rivers and on hillslopes [2–4,21]. The key is that the distribution governing particle in space and time can be written as a function of the jump length distribution and the inter-arrival time distributions. The master equation in Fourier–Laplace (with transform pairs $x \leftrightarrow k$ and $t \leftrightarrow s$) is expressed as

$$\hat{\tilde{C}}(k,s) = \frac{1-\tilde{\psi}(s)}{s}\frac{1}{1-\hat{f}(k)\tilde{\psi}(s)} \tag{19.2}$$

where

$\hat{\tilde{C}}(k,s)$ is the Fourier–Laplace transform of particle density
$\tilde{\psi}(s)$ is the Laplace transform of the inter-arrival time density
$\hat{f}(k)$ is the Fourier transform of the jump length density

The inverse transform of $\hat{\tilde{C}}(k,s)$ is commonly computed numerically to display the likelihood of single-particle travel distance through time and is interpreted as the form a spreading plume of many particles would take.

19.3.3 Maxima: Extreme Value Theory

EV theory is concerned with the recurrence of large events and plays a significant role in analysis of hazardous events such as floods, large waves, landslides, mudflows, and droughts [18]. When sufficient data do not exist to compute the empirical 10-, 500-, or 10,000-year events, stochastic models are used to estimate recurrence levels based on the distribution of event sizes and event inter-arrivals. As with random walk models, we let $\{Y_1, Y_2, \ldots, Y_n\}$ be a sequence of iid random "jump" or "event" sizes describing peak discharge in a flash flood, the height of a wave, or severity of a drought. Extreme events do not occur at randomly spaced intervals, and so inter-arrivals between events always play an important role. The distribution of the maxima of iid extreme events with distribution F separated by iid inter-arrivals with pdf ψ can be described by the master equation for a continuous time random maxima (CTRM) (in Laplace space) [1]:

$$L\left[P\left(M_{N_t} \le x\right)\right] = \frac{1-\tilde{\psi}(s)}{s}\frac{1}{1-F(x)\tilde{\psi}(s)} \tag{19.3}$$

where

$L[\cdot]$ denotes a Laplace transform
$F(x)$ is the distribution of the event sizes
$\tilde{\psi}(s)$ is the Laplace transform of the inter-arrival density

As with the CTRW, the master equation for the distribution of maxima (19.3) can be used with any event size and jump length distributions. In hydrologic applications, it is most commonly assumed that inter-arrivals are exponentially distributed in which case the CTRM describes the maxima of a Poisson process and can be reduced and transformed into real space such that $P(M_{N_t} \le x) = e^{-\lambda t(1-F(x))}$, where λ is the rate parameter for the exponential inter-arrival times [22].

19.4 Asymptotic Stochastic Models

Although random variables in the stochastic models described in the previous section could be described using continuous probability densities, they may converge in distribution to another set of stochastic processes in the longtime scaling limit. Asymptotic stochastic models describe longtime

emergent properties of pre-asymptotic models and provide a macroscopic view of unmeasurable microscopic properties.

19.4.1 Limit Theorems

Limit theorems exist for both sums and maxima. The generalized central limit theorem (CLT) for sums of random variables specifies that the rescaled sum of stationary iid random variables $\{Y_i\}$ with even infinite variance (heavy tails) converges in distribution to an α-stable density, denoted S_α, with shift μ, spread σ, tail parameter α, and skewness β [10,12]. Restated, we can find the form of the distribution of a sum of random variables:

$$Y_1 + \cdots + Y_n \approx n\mu + \sigma n^{1/\alpha} S_\alpha(0,1,\alpha,\beta) \tag{19.4}$$

This general CLT includes the classical CLT thin-tailed subset that states that the rescaled sum of stationary iid random variables with thin tails converges in distribution to an α-stable density with $\alpha = 2$, which is equivalent to Gaussian density:

$$Y_1 + \cdots + Y_n \approx n\mu + \sigma n^{1/\alpha} N(0,1) \tag{19.5}$$

where

- μ is the mean
- σ is the variance
- $N(0,1)$ represents the standard normal (Gaussian)
- skewness β does not exist for an $\alpha = 2$ stable density

For maxima, the EV theorem states that the rescaled maximum of a sequence of stationary, iid random variables converges in distribution to one of the EV distributions. If a sequence of pairs of real numbers (a_n, b_n) exists such that each $a_n > 0$ and

$$P\left(\frac{\max\{Y_1,\ldots,Y_n\} - b_n}{a_n} \le x\right) \approx F \sim GEV(\mu,\sigma,\xi) \tag{19.6}$$

where $GEV(\mu,\sigma,\xi)$ denotes the generalized EV distributions with location μ, scale σ, and shape ξ parameters. When random variables have thin tails, the Gumbel or type I EV distribution emerges, while heavy-tailed random variables lead to the Frechet, or type II EV distribution. As a result, the EV distributions are commonly used in estimating recurrence of extreme events because they arise naturally for describing the distribution of annual maxima and can be used without knowledge of the exact distribution of the population.

The CLT and EV theorems can be further generalized to account for non-stationarity or long-range correlation in increments, but each must be tailored to the specific type of non-stationarity or correlation. In hydrology, non-stationarity is frequently treated by using stationary models over small areas and varying model parameters in time or space as necessary. Effects of short-term correlation may disappear over the long term, and the CLT and EV theorems can be used. Stochastic models that incorporate the effects of long-range correlation are included in the following section.

19.4.2 Limiting (Asymptotic) Stochastic Processes

Just as CLTs exist for sums or maxima of random variables, analogous limit theorems exist for stochastic processes. The appropriate limiting stochastic processes can be identified with traits such as the tail character or degree of correlation of the increments.

The components that lead to the asymptotic stochastic process are the building blocks for a CTRW: (1) the distribution governing the time between events and (2) the distribution governing the event sizes.

19.4.2.1 Brownian Motion

In the scaling limit, any stationary CTRW with thin-tailed inter-event periods and jumps that do not exhibit any long-range dependence converges in distribution to a Brownian motion. A standard Brownian motion is defined by the following properties [20]:

1. $B(0) = 0$, the Brownian motion starts at zero.
2. $B(t)$, $t \geq 0$ has stationary and independent increments.
3. All increments of the Brownian motion $B(t+h) - B(t)$ are normally distributed with mean zero and variance h.
4. The paths of a Brownian motion are continuous.

As a result of the CLT, a Brownian motion $B(t)$ at time t is normally distributed with mean zero and variance t. It is well known that the diffusion equation (advection–dispersion equation [ADE]) governs the evolution of particles undergoing Brownian motion. It is no coincidence that the spatial solutions to diffusion equations are Gaussian densities.

The diffusion equation and variations on ADEs described in this section are deterministic partial differential equations. They arise as a result of long time/space transport in a random medium because the CLT specifies a deterministic outcome for sums of random variables. Asymptotic distributions and stochastic processes show deterministic macroscopic properties that emerge as a result of microscopic variability. Diffusion-type equations are used to describe infiltration, solute transport, and heat transport, among other phenomena. These equations are frequently derived by inserting the constitutive relation for Fickian flux into a continuity equation. It is within the Fickian flux term that microscopic particle motion governed by iid, stationary, finite variance jumps is hidden.

Having thin-tailed inter-arrivals and event sizes, the largest jump (event) that a particle undergoing Brownian motion can be expected to take in an epoch has an EV1 distribution. In one application, we sum random size jumps (motion) with random inter-arrivals (immobile periods) and think of a physical transport process; in a second type of application, we track the largest jumps (flood sizes) with random inter-arrivals (non-flood periods) using the same underlying conceptual model.

19.4.2.2 Fractional Brownian Motion

A CTRW with deterministic or thin-tailed inter-event times and thin-tailed jumps with long-range correlation converges in distribution to a fractional Brownian motion (fBm) [17]. An fBm is defined by the following properties (REF):

1. $B_H(0) = 0$, the fBm starts at zero.
2. $B_H(t)$, $t \geq 0$ has stationary increments.
3. All increments of the fBm $B_H(t+s) - B_H(t)$ are bivariate normally distributed with mean zero and covariance $1/2(s^{2H} + t^{2H} - |t-s|^{2H})$, where $0 < H < 1$ is known as the Hurst coefficient.
4. The paths of an fBm are continuous.

For Hurst coefficient $H = 0.5$, the fBm reduces to an ordinary Brownian motion with uncorrelated increments. When $H > 0.5$, the covariance of the increments is positive—upward paths tend to continue moving upward and vice versa. For $H < 0.5$, the increments are negatively correlated, and paths tend to exhibit frequent reversals in direction. fBm models primarily have been applied in hydrology in one of two ways. The first is to describe long-term persistence in time series. In fact, the application for which Hurst [14] first observed the phenomenon was in a design study for reservoir capacity. It since has been observed in many streamflow time series [15]. fBm also is used in the design of random fields for simulation of heterogeneous porous media. Hydraulic conductivity fields with long-range dependence, having both preferential pathways and low permeability zones, may be one origin of anomalous dispersion of

particles that travel through aquifers [16]. Recurrence intervals for correlated random processes have not been posed in the CTRM framework, but their characteristics for recurrence of climate statistics have been described [6,9].

19.4.2.3 Lévy Motion

CTRW deterministic or thin-tailed inter-event times and heavy-tailed jumps converge in distribution to a Lévy motion. An α-stable Lévy motion has the following characteristics:

1. $L(0) = 0$, the Lévy motion starts at zero.
2. $L(t)$, $t \geq 0$ has stationary and independent increments.
3. All increments of the Lévy motion $L(t+h) - L(t)$ are α-stable distributed with zero shift, spread $h^{1/\alpha}$, and skewness β.
4. The paths of a Lévy motion exhibit jumps; they are not continuous.

Particles undergoing Lévy motion are governed by fractional-in-space ADEs with non-integer order derivatives, usually of order between one and two on the spatial derivative of the dispersion term. The use of "fractional derivatives" simply generalizes the classical ADE by permitting nonlocal dispersion, characterized by heavy-tailed jump size distributions around a mean value. As a result of the generalized CLT, the solutions to space-fractional ADEs governing particles undergoing Lévy motion are α-stable pdfs. The size of the largest jumps is governed by an EVII distribution. Recurrence times for various size extreme events can be computed with knowledge of this distribution.

19.4.2.4 Subordinated Motions

Heavy-tailed inter-event times change the time evolution of a transport process. In the scaling limit, CTRW with heavy-tailed inter-arrivals is governed by subordinated motions. For example, particles undergoing subordinated Brownian motion spread diffusively during motion (known as "operational time"), but spread anomalously during overall clock time because of heavy-tailed waiting times. For example, a subordinated Brownian motion is obtained from Brownian motion $B(t)$ by replacing its time parameter t by an independent Lévy process $S_{N(t)}$ starting from zero so that Brownian motion only occurs after random (heavy-tailed) time intervals have elapsed. Subordinated motions are typically used to model sub-diffusive spreading, but, in the case of forward only jumps, also can lead to super-diffusive spreading [24]. Particles undergoing subordinated Brownian motion are governed by time-fractional ADEs, while particles undergoing subordinated Lévy motion are governed by space–time-fractional ADEs. The solutions to equations governing subordinated motions can be computed by performing a transform on the solution to the unsubordinated solution, as in [21]. Similarly, the density governing the largest size jump in a time period can be calculated by subordinating the appropriate EV density for thin-tailed inter-arrivals. Subordinated stochastic processes are finding application in the many environmental transport processes thought to be dominated by intermittency.

19.4.3 Use of Pre-Asymptotic, Asymptotic, Tempered, or Truncated Models and Associated Embedded Stochastic Processes

The pre-asymptotic master equation forms of the CTRW (19.2) or CTRM (19.3) offer a detailed picture of statistical evolution of sums or maxima when the distributions of inter-arrivals and event sizes can be fully characterized. Like Markov chains, pre-asymptotic transport and EV models describe transient evolution of solutions from early conditions to the long-term, limiting state. Asymptotic models, on the other hand, do not require full distribution characterization (heavy- versus thin-tailed or correlated versus uncorrelated increments are frequently sufficient) and have well-known solutions related to the outcome of limit theorems.

Application of heavy-tailed stochastic models has grown as hydrologists increasingly see the need for stochastic models with different scaling properties than the classical diffusive model. Reproduction

of "anomalous" scaling behavior is the strength of heavy-tailed stochastic models. However, in many instances, the maximum event size or inter-arrival time is a key characteristic of hydrologic evolution, and standard Lévy models will be physically unrealistic. In these cases, tempered or truncated models–in which a maximum is invoked by imposing either an exponential tail or a cutoff on a power-law density– can be used. Appropriate identification of the cutoff on power-law behavior can elucidate physical controls on threshold or bounded behavior [11].

As a time series fluctuates, it may not be the random sum or maximum event size that is of interest, but of a related quantity. For example, in fluctuations of soil moisture, it may be a threshold value that defines the wilting point. In this case, the return time distribution or crossing time (return from above or below) distributions of the time series can be estimated and used to drive stochastic ecohydrologic models [19]. Finally, in modeling the passage of a solute plume past a monitoring well at a single x–y location, the first-passage time distribution (directly related to the breakthrough curve) of particles is of interest rather than the spatial plume evolution described by a sum. The relationship between random sums and these and many other embedded stochastic processes are described in the mathematics literature and can be transferred for specific applications.

19.5 Summary and Conclusions

Stochastic processes are appropriate model choices when effects of temporal variability or heterogeneity below the scale of measurement are dominant characteristics of hydrologic processes at the observation scale. The type of problem to be solved (recurrence of extreme events, distance traveled, time until a threshold is achieved) drives specific model selection. Disciplinary expertise and data analysis can then be used to identify the probabilistic conceptual model that best represents the relevant characteristics of temporal and spatial evolution of hydrologic processes. Are increments of a random process correlated? independent? thin- or heavy-tailed? stationary? These characteristics drive selection of the appropriate probabilistic models whether they are for time series analysis, EV analysis, or prediction of motion. The discrete-time, continuous, and asymptotic models described in this chapter are commonly used in hydrology. If none is appropriate for a new hydrologic application, generalizations and modifications of these models—with well-understood results—exist in the mathematics, physics, and economics literature.

References

1. Benson, D.A., R. Schumer, and M.M. Meerschaert, 2007. Recurrence of extreme events with power-law interarrival times. *Geophysical Research Letters*, **34**(L16404): DOI:10.1029/2007GL030767.
2. Berkowitz, B. and H. Scher, 1997. Anomalous transport in random fracture networks. *Physical Review Letters*, **79**(20): 4038–4041.
3. Boano, F., A.I. Packman, A. Cortis, R. Revelli, and L. Ridolfi, 2007. A continuous time random walk approach to the stream transport of solutes. *Water Resources Research*, **43**(10): W10415.
4. Bradley, D.N., G.E. Tucker, and D.A. Benson, 2010. Anomalous dispersion in a sand-bed river. *Journal of Geophysical Research—Earth Surface*, **115**: F00A09.
5. Brockwell, P.J. and R.A. Davis, 1991. *Time Series: Series and Methods*, 2nd edn. New York: Springer.
6. Bunde, A., J.F. Eichner, S. Havlin, and J.W. Kantelhardt, 2003. The effect of long-term correlations on the return periods of rare events. *Physica A-Statistical Mechanics and Its Applications*, **330**(1–2): 1–7.
7. Cebrian, A.C. and J. Abaurrea, 2006. Drought analysis based on a marked cluster Poisson model. *Journal of Hydrometeorology*, **7**(4): 713–723.
8. Coles, S., 2001. *An Introduction to Statistical Modeling of Extreme Values*. London, U.K.: Springer-Verlag, 208pp.
9. Eichner, J.F., J.W. Kantelhardt, A. Bunde, and S. Havlin, 2006. Extreme value statistics in records with long-term persistence. *Physical Review E*, **73**(1): 016130-1–016130-10.

10. Feller, W., 1971. *An Introduction to Probability Theory and Its Applications*, 2nd edn. Wiley Series in Probability and Mathematical Statistics, Vol. II. New York: John Wiley & Sons, 669pp.
11. Ganti, V., K.M. Straub, E. Foufoula-Georgiou, and C. Paola, 2011. Space-time dynamics of depositional systems: Experimental evidence and theoretical modeling of heavy-tailed statistics. *Journal of Geophysical Research—Earth Surface*, **116**: F02011-1–F02011-17.
12. Gnedenko, B. and A.N. Kolmogorov, 1968. *Limit Distributions for Sums of Independent Random Variables* (edited and translated from the Russian, and revised by K.L. Chung. With appendices by J.L. Doob and P.L. Hsu), revised edition. Reading, MA: Addison-Wesley.
13. Haan, C.T., 1977. *Statistical Methods in Hydrology*. Ames, IA: Iowa State University Press, 378pp.
14. Hurst, H.E., 1951. Long-term storage capacity of reservoirs. *Transactions of the American Society of Civil Engineers*, **116**: 770–808.
15. Koutsoyiannis, D., 2002. The Hurst phenomenon and fractional Gaussian noise made easy. *Hydrological Sciences Journal-Journal Des Sciences Hydrologiques*, **47**(4): 573–595.
16. Liu, H.H. and F.J. Molz, 1996. Discrimination of fractional Brownian motion and fractional Gaussian noise structures in permeability and related property distributions with range analyses. *Water Resources Research*, **32**(8): 2601–2605.
17. Meerschaert, M.M., E. Nane, and Y.M. Xiao, 2009. Correlated continuous time random walks. *Statistics & Probability Letters*, **79**(9): 1194–1202.
18. Reiss, R.-D. and M. Thomas, 2001. *Statistical Analysis of Extreme Values: With Applications to Insurance, Finance, Hydrology and Other Fields*, 2nd edn. Basel, Switzerland: Birkhauser, 443pp.
19. Rodriguez-Iturbe, I. and A. Porporato, 2004. *Ecohydrology of Water-Controlled Ecosystems: Soil Moisture and Plant Dynamics*. Cambridge, U.K.: Cambridge University Press, 442pp.
20. Ross, S.M., 1997. *Introduction to Probability Models*. San Diego, CA: Academic Press, 669pp.
21. Schumer, R., D.A. Benson, M.M. Meerschaert, and B. Baeumer, 2003. Fractal mobile/immobile solute transport. *Water Resources Research*, **39**(10): 1296–1308.
22. Smith, J.A., 1987. Estimating the upper tail of flood frequency distributions. *Water Resources Research*, **23**(8): 1657–1666.
23. Smith, J.A. and A.F. Karr, 1983. A point process model of summer season rainfall occurrences. *Water Resources Research*, **19**(1): 95–103.
24. Weeks, E.R., J.S. Urbach, and H.L. Swinney, 1996. Anomalous diffusion in asymmetric random walks with a quasi-geostrophic flow example. *Physica D*, **97**: 291–310.

20

Hydrologic Prediction and Uncertainty Quantification

Caleb M. DeChant
Portland State University

Hamid Moradkhani
Portland State University

AUTHORS

Caleb M. DeChant received his BS degree from the University of Portland and his MS degree from Portland State University (PSU). He is currently a PhD candidate at PSU. He has published several papers on various implications of hydrologic data assimilation and ensemble forecasting. In 2011, he won the Maseeh College of Engineering Scholarship at PSU.

Hamid Moradkhani received his BS and MS degrees in water resources engineering and hydraulic structures from Iran, in 1991 and 1994, respectively. In late 2004, he received his PhD in hydrology and water resources from the University of California, Irvine (UCI), and continued as postdoctoral scholar at UCI. He is currently an associate professor in the Department of Civil and Environmental Engineering at PSU and sustainability scholar at the Institute for Sustainable Solution at PSU. He has pioneered and developed the concept of combined state–parameter estimation and uncertainty quantification using data assimilation used in variety of disciplines. He is on the editorial board of *Water Recourses Research* and the *Journal of Hydrologic Engineering* as well as the advisory board of *Science and Technology Journal*. He has over 20 years of professional engineering experience in analysis, design, and management of large-scale water resources systems. He has chaired several technical committees and conference sessions on theoretical and operational implications of data assimilation and uncertainty quantification. Due to his extensive contribution in various aspects of

hydrology and water resources engineering, he earned the distinction of diplomat, water resources engineer (D.WRE) designated by the American Academy of Water Resources Engineers.

20.1 Introduction

20.1.1 Hydrologic Modeling and Forecasting

Nearly all hydrologic forecasting systems incorporate model estimates of land surface states and fluxes into operational forecasts, to provide reliable information to end users. Hydrologic models are a class of computer simulation models that estimate at least some aspects of the hydrologic cycle (Moradkhani and Sorooshian, 2008). Within hydrologic models, climatic and land surface conditions, typically in the form of water and energy fluxes/storages, provide a basis for mass and energy balance approximation (Moradkhani, 2008). These models vary considerably in assumptions, accuracy, complexity, applicability, and computational demand. Differences in the model structure and required forcing data between hydrologic models reflect the differing perceptualizations of hydrologic processes (Beven and Freer, 2001) and the intended use of the model. For example, highly simplified or complex models are often used for research purposes, but these may not be appropriate for use by an operational forecasting agency. Similarly, a hydrologic model may be designed with a specific purpose, such as snow accumulation and ablation models, which do not directly estimate the entire hydrologic cycle. Another common distinction between models is the level of physical basis of model equations, ranging from purely conceptual (no physical basis) to land surface models (minimizing the nonphysically based processes). All models have some conceptual variables that cannot be physically measured, but there is a trend toward developing and using increasingly physics-based models in hydrologic sciences. With such a variety of models, it is essential to find a model that fits a forecasters needs for effective hydrologic forecasting.

Hydrologic forecasting serves the purpose of early warning for flood events and water supply forecasts for water resources management. Flood and water supply forecasting are distinguished by not only their intended purpose but also lead time. Forecasting for flood events at operational agencies is performed with short-lead times, on the scale of hours to weeks (Cloke and Pappenberger, 2009). Short-lead forecasts may aid in evacuation of floodplains or mitigation measures to limit the harm caused by flooding. Alternatively, water supply forecasts require a much longer lead time of forecasts. Long-term forecasts range from seasonal to interannual timescales and may aid in allocating water for irrigation, power generation, or drinking water supply, among other uses (Moradkhani and Meier, 2010; Wood and Werner, 2011). Though the forecast lead time of flood and water supply forecasts is different, both require similar information to be effective. Accurate estimation of the hydrologic state of the land surface prior to forecasting, referred to as the initial conditions, and the future climate factors is essential for hydrologic forecasting at any lead time.

Short-lead forecasts are most often regarded as a modeling problem. Operational forecasts within the National Weather Service (NWS) will use some form of modeled information and forecaster judgment for providing public warnings prior to flood events. Due to errors in the hydrologic modeling process, a model will likely need to be adjusted between simulations to ensure accurate forecasts. Manual or automatic methods may be used to shift modeled states to accurate estimates, and short-term weather forecasts will be used to estimate the forcing inputs to a watershed of interest. Integrating both improved states and accurate forcing data provides a basis for reliable flood forecasts. This contrasts with long-lead forecasting, largely due to the diminished accuracy of meteorological variables at longer timescales. With the contrasting accuracy in meteorological data, a larger range of techniques are applicable to seasonal forecasts than short-lead forecasts.

Some purely statistical methods have found use in streamflow forecasting because of the relationship between seasonal streamflow on land surface states and seasonal climate indicators. Principal component analysis (PCA) (Garen, 1992), independent component analysis (ICA) (Gotelli and Ellison, 2004; Hyvärinen et al., 2001; Moradkhani and Meier, 2010; Najafi et al., 2011a; Westra et al., 2007), and

artificial neural networks (ANNs) (Hsu et al., 1997; Moradkhani et al., 2004) have all found success in forecasting seasonal runoff volumes. Though these methods have been shown to be effective predictors of seasonal streamflow, all assume a stationary climate, leading many hydrologists to question the reliability of such methods in light of global climate change and local land use change (Jung et al., 2011; Moradkhani et al., 2010). This issue has led many forecasters to perform more physically based modeling, which is theoretically more robust in a changing climate/landscape. From a modeling perspective, ensemble forecasting frameworks are becoming popular. In the NWS, ensemble forecasting is performed with ensemble streamflow prediction (ESP) (Day, 1985; Najafi et al., 2012; Twedt et al., 1977; Wood and Lettenmaier, 2008). ESP uses a combination of model spin-up, to estimate the initial conditions, and resampling of historical forcing to create a range of potential runoff quantities. This range is assumed to provide insight about the uncertainty in seasonal predictions. Similar methods utilize seasonal ensemble meteorological forecasts from numerical weather prediction (NWP) models to force seasonal hydrologic modeling. A recent study by Najafi et al. (2012) showed how the ESP for seasonal forecasting can be improved when the historical forcings, for generation of ESP traces, are weighted according to their similarities with the current year forcing data. This leads to a similar framework to flood forecasting.

20.1.2 State-Space Models

In general, viewing hydrologic models as state-space models is beneficial for hydrologic forecast updating and uncertainty quantification. This framework assumes the model produces some states that satisfy the Markovian criteria. That is, the states of a hydrologic model at some time contain all of the information necessary from previous times to propagate the model forward. This allows for analysis of model states at any given time, without the need for examining past model states. Within hydrologic models, states may be physically based (e.g., soil moisture or snow water equivalent) or conceptual (i.e., conceptual reservoir water content). Via the state-space framework, a hydrologic model may be viewed according to the following equation:

$$x_t = f\left(x_{t-1}, u_t, \theta\right) + \omega_t \tag{20.1}$$

In Equation 20.1, x_t represents the true state vector at time t, which is the sum of the model ($f(\cdot)$) estimate and the model error ω_t. This model requires the true states at the previous time (x_{t-1}), the true forcing data at time t (u_t), and model parameters (θ) to characterize the land surface condition. It is often the case in hydrology that a subsequent model must be used to translate these model states into the observation space. A typical example is applying a hydrologic routing model to translate land surface water fluxes to flow at a watershed outlet, allowing for simple comparison of simulated and observed runoff. This model is referred to as an observational operator and is represented in the following equation:

$$y_t = h\left(x_t, \Psi\right) + \nu_t \tag{20.2}$$

where y_t represents the true observation value (note that this differs from the actual observation due to errors in the observation process), which is the sum of the observational operator ($h(\cdot)$) estimate and the observational operator error ν_t. The observational operator requires the true state value and true parameters (Ψ). Though θ and Ψ are identified as independent values/vectors in the previous notation, in hydrologic model analysis, these may be examined in a combined vector, which can be represented as θ for simplicity. Analyzing model operations from the state-space framework simplifies a number of tasks including inverse modeling, calibration, sensitivity analysis, uncertainty analysis, and data assimilation. Application of the state-space model framework to these tasks is expanded on in following sections.

20.1.3 Inverse Modeling and Calibration

Modeling of the land surface is often viewed as an inverse problem. Since a modeler typically has some observations about the water balance of the land surface (i.e., precipitation and runoff), but cannot completely characterize the land surface interactions, these observations are used to make an inference about the land surface (Moradkhani and Sorooshian, 2008). Since a model is only developed for execution forward in time, the inverse model is not available. This situation necessitates iterative methods to search the feasible values of each variable being estimated. It is important to note that this is a one-to-many operation (as opposed to a many-to-one estimation in forward modeling) that typically makes the problem ill-posed. A visual comparison of forward and inverse modeling is presented in Figure 20.1.

Practically, a modeler will focus on estimating some or all of the time-invariant parameters (θ, Ψ), which represent land surface characteristics, based on some land surface observations. Parameter estimation, also referred to as model calibration, is necessary for characterizing the parameters that cannot be observed such as mean hydraulic conductivity, termed process parameters (Gupta et al., 1998), but may also be used for observable, yet unavailable, parameters. Calibration can be performed through a variety of methods. Some modelers simply perform manual adjustments of each parameter and examine the improvements in model performance with respect to the observation. Though manual calibration has the potential to improve hydrologic model simulation, it has become much more common to perform some automated calibration, due to the complexity of the parameter space. A range of techniques are used for automatic calibration of models including optimization and probabilistic methods.

Optimization techniques attempt to estimate the parameter values that provide the most accurate simulation from the model. This accuracy is determined based on some mathematical objective function, represented by Equation 20.4, which examines the model residuals at each time step Equation 20.3. The model residual (ε_t) is calculated as the difference between the model simulation ($\hat{y}_t$) and the observation ($\tilde{y}_t$). The value of the objective function (E) is estimated error residuals from t' to the final simulation time (T). Analysis starts at some t', which could be larger than 1, to allow for the model to reach reasonable state estimates, with respect to the parameters (referred to as a burn-in period). Commonly used objective functions in hydrology are root-mean-square error (RMSE), Nash–Sutcliffe efficiency (NSE) (Nash and Sutcliffe, 1970), heteroscedastic maximum likelihood error (HMLE) (Sorooshian and Dracup, 1980), and bias. In addition to single-objective function optimization, multi-objective function optimization has become popular (Vrugt et al., 2003; Yapo et al., 1998). Multi-objective functions utilize some method for normalizing the output from each objective function, to balance the weight of

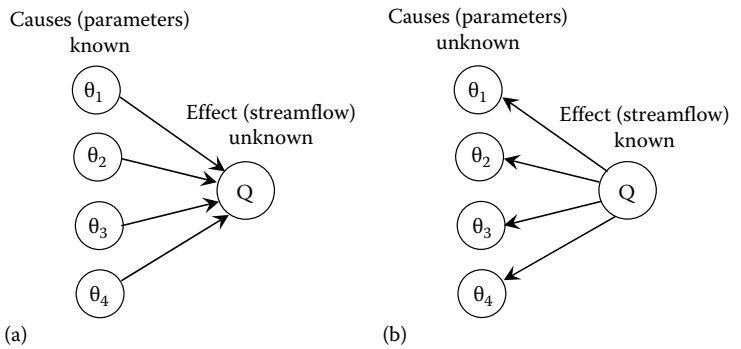

FIGURE 20.1 Comparison of forward and inverse problems. (a) Forward problem well-posed and (b) inverse problem ill-posed. (After Moradkhani, H. and Sorooshian, S., *Hydrologic. Model. Water Cycle Water Sci. Technol. Library*, 63, 1–24, 2008.)

each objective function value. Though objective functions provide information about the accuracy of parameters, these functions alone do not tell the modeler the location of the best parameters. Global optimization algorithms are thus necessary to locate the best parameters, in relation to the objective function:

$$\varepsilon_t = \hat{y}_t - \tilde{y}_t \tag{20.3}$$

$$E = Obj\left(\varepsilon_{t':T}\right) \tag{20.4}$$

Generally, hydrologic models tend to be multidimensional, leading to complex parameter spaces with multiple local optima. A 2-D parameter space is visualized in Figure 20.2, which was created by sampling two parameters from the 5-D HyMod (Boyle et al., 2000) model. Note that this figure suggests several local optima, which may create difficulties when attempting to find the global optimum (at ~[0.63, 0.09]). In order to find the optimum parameter values, many different techniques have been developed that utilize combinations of exploration (random search of the parameter space) and exploitation (gradient approximation). Some optimization is performed entirely with gradient-based methods to maximize the speed of the algorithm, but these tend to be local optimization methods and often become stuck in a local optimum, which may be quite far from the global optimum (see [0.6, 0.0] in Figure 20.2). With a sufficient amount of exploration of the parameter space, the global optimum for the parameters may be located. Several methods have been used to estimate the global optimum of hydrologic models including the shuffle complex evolution method (SCE-UA) (Duan et al., 1992) and genetic algorithms (Shoemaker et al., 2007; Zhang et al., 2009). Though many effective methods for

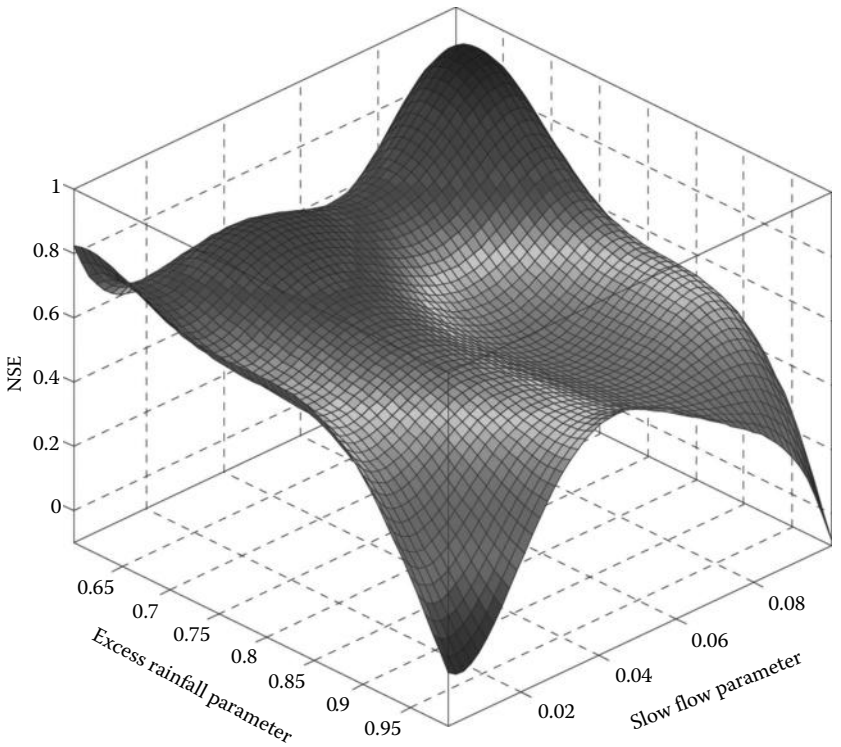

FIGURE 20.2 Plot of the NSE values over a 2-D parameter space, based on two parameters from the HyMod model. (From Boyle, D.P. et al., *Water Resour. Res.*, 36(12), 3663, 2000.)

optimizing model parameters have been developed, hydrologic modelers have begun questioning the value of optimization, because these models ignore the presence of equifinal parameter sets and uncertainty within the modeling framework.

The size of this parameter matrix for hydrologic models tends to be larger than the number of available observation, leading to an ill-posed problem. In the event that a problem is ill-posed, the target quantities will likely have nonunique (equifinal) solutions (Beven and Freer, 2001). Given that a solution is nonunique, a modeler may find it advantageous to determine the uncertainty associated with each parameter, because an optimized parameter is not necessarily correct in this scenario. Several efforts have been made to estimate parameter uncertainty through probabilistic methods, including the generalized likelihood uncertainty estimation (GLUE) (Freer et al., 1996), Markov chain Monte Carlo (MCMC) techniques (Bates and Campbell, 2001; Kuczera and Parent, 1998; Marshall et al., 2004; Vrugt et al., 2008), Bayesian hierarchical methods (Renard et al., 2011), and data assimilation (DeChant and Moradkhani, 2011a,b, 2012; Leisenring and Moradkhani, 2011; Liu et al., 2012; Montzka et al., 2011; Moradkhani 2005a,b; Salamon and Feyen, 2009). Though all of these techniques show potential for accurately quantifying parameter uncertainty in hydrologic models, a deeper understanding of statistical uncertainty is required than for basic inverse modeling. The following sections provide information about the theoretical basis for the aforementioned methods.

20.1.4 Monte Carlo Simulation

Modeling in the presence of significant uncertainty requires creative techniques to estimate the information content of model estimates. Given that model processes are nonlinear, as is the case with nearly all hydrologic models, Monte Carlo experiments are commonly implemented to quantify modeling uncertainty. A Monte Carlo experiment takes advantage of computing power to perform repeated model executions and create a large number of potentially correct, but different, estimates. This group of estimates is referred to as an ensemble. From this ensemble, we can infer the probability of certain outcomes, based on the quantile in which they fall within the ensemble. In order to create this ensemble, a probability distribution of each uncertainty source must be assumed; then estimates are randomly sampled according to that distribution.

Performing Monte Carlo experiments on a hydrologic model will take a form similar to Equations 20.5 through 20.8. In these equations, the forcing and observation data are perturbed based on some function E, and the model and observational operator have additive error terms. The function E may follow any distribution, but is commonly lognormal for precipitation inputs and normal for other variables. The additive error terms for the model operator and observational operator are often normally distributed but heteroscedastic:

$$u_{t,i} = Err_{input}\left(\tilde{u}_t\right) \tag{20.5}$$

$$\hat{x}_{t,i} = f\left(\hat{x}_{t-1,i}, u_{t,i}, \theta_i\right) + \omega_{t,i} \tag{20.6}$$

$$\hat{y}_{t,i} = h\left(\hat{x}_{t,i}, \Psi_i\right) + \nu_{t,i} \tag{20.7}$$

$$y_{t,i} = Err_{observation}\left(\tilde{y}_t\right) \tag{20.8}$$

where

$Err(\cdot)$ represents error models

values with a "$\sim$" represent observed values

each value with an index i represents an individual value sampled from the distribution of that variable

The previous equations expand on the state-space framework to account for uncertainty in different portions of the model. By accounting for each source of uncertainty, the total uncertainty within the modeling framework can be estimated, leading to some observation value $y_{t,i}$ that is equal to a simulation $\hat{y}_{t,i}$. Though Monte Carlo experiments have the potential to estimate the full uncertainty of hydrologic variables, this analysis will provide relatively large uncertainty in many hydrologic prediction scenarios. Fortunately, many observations are available to hydrologists to reduce the spread of the uncertainty prediction, improving the precision of a forecast without compromising its reliability. A general method for incorporating these observations is through Bayes' theorem.

20.1.5 Frequentist Approach vs. Bayes' Theorem

In statistical analysis, a problem is based on either a frequentist or Bayesian approach. Frequentist analysis estimates the probability of a given outcome based on the historical frequency of observations, providing a basic framework for analysis that is entirely reproducible. Though the frequentist approach follows fundamental statistical theory, it can often ignore potentially informative data. Given that an observation of the phenomena of interest is available, as is common in hydrologic sciences, this observation can provide information to the model, thereby improving model estimates. Bayes' theorem extends the frequentist approach by allowing for the inclusion of observations as conditional information. Through Bayes' theorem, a forecaster has the freedom to include any data that may contain information about the target quantity in a forecast. Though this brings some subjectivity into the analysis, Bayesian inference allows for more reliable and precise forecasts, assuming that conditional information is properly utilized. Bayesian analysis is a useful framework within hydrologic forecasting, due to the large quantity of observations with incomplete information content.

Bayes' law estimates the probability of model parameters conditioned on observed information (($p(\theta|y)$), which is referred to as the posterior. In this section, the parameter θ may refer to any variable of interest in the hydrologic model, whereas in other sections, it refers only to the model calibration parameters. Given that some prior probability is available ($p(\theta)$) and the likelihood can be calculated based on the observed information ($p(y|\theta)$), the posterior may be calculated according to the following equation:

$$p(\theta \mid y) = \frac{p(y \mid \theta)p(\theta)}{p(y)} \tag{20.9}$$

In the event that information from prior data and observations are not conflicting, this application of Bayes' law effectively reduces the uncertainty about the parameters.

20.2 Hydrologic Modeling Uncertainty

Uncertainty is persistent in all aspects of hydrologic modeling due to a lack of complete knowledge about land surface properties and fluxes. Though many observations about the land surface are available for model development and evaluation, these observations can never perfectly explain hydrologic processes, due to the relevant spatiotemporal scale at which these processes take place. Within a hydrologic modeling framework, uncertainties can stem from imperfect characterization of model inputs, erroneous model structure, incorrect parameter estimates, and errors in observing the model output. These uncertainties accumulate through the modeling system, reducing the skill of model predictions. In order to accurately quantify the uncertainty in model estimates, all sources of uncertainty must be taken into account. Both the magnitude and form of errors must be effectively estimated to provide a reliable estimate of the uncertainty in hydrologic forecasts. Full accounting of hydrologic prediction uncertainty therefore requires a closer examination of each of the different sources of uncertainty.

20.2.1 Input and Validation Data Uncertainty

Model inputs and validation data both require observations/estimates of land surface or atmospheric conditions. Input and observation data may be observed through either in situ or remote sensors, or this data may be estimated with a separate model (i.e., atmospheric models are often used to estimate hydrologic model input when observations are unavailable) (Clark and Slater, 2006; Hong et al., 2006; Kavetski et al., 2006; Moradkhani and Meskele, 2009; Moradkhani et al., 2006; Renard et al., 2010; Vrugt et al., 2008). Each of these methods for obtaining data for hydrologic modeling is subject to large uncertainties. Data uncertainty can affect the modeling framework by improperly characterizing the mass balance of the basin, incorrectly displaying the timing of water fluxes in a basin, or inaccurately explaining the spatial distribution of water fluxes in a basin, leading to ineffective hydrologic prediction in the basin. Since data uncertainty can lead to significant errors in the model, this uncertainty must be understood for an estimation of predictive uncertainty. By understanding the uncertainties in input and validation data, a hydrologic forecaster can effectively account for data uncertainties within the modeling framework, leading to reliable probabilistic predictions.

20.2.1.1 Sources of Input and Observation Data Uncertainty

Modeling data are subject to three sources of uncertainty: sensor errors, scale/interpolation, and translation errors. Sensor error refers to errors related to the mechanical observation of some value. A straightforward example is errors in rain gauge measurements due to wind, evaporation, or obstructions (Moulin et al., 2009). Sensor errors act at the point of observation and therefore cannot be improved by the modeler, but may be effectively estimated. Scale/interpolation errors result from the spatial averaging or distribution of a given variable for use with a model (Villarini et al., 2008). With a number of techniques for spatial interpolation/averaging of hydrologic values, this uncertainty may be partially addressed with different methods of interpolation. Though scale/interpolation errors may be improved, these will still have some contribution to the total uncertainty in any practical situation. Translation error is the error associated with the need to translate an observation to a different space, for example, the use of a rating curve to estimate discharge from a river stage (Di Baldassarre and Montanari, 2009). Similar to scale/interpolation errors, translation errors may be reduced with improved estimation algorithms, but are impossible to remove completely from a forecasting environment. In some scenarios, it may be possible to reduce this uncertainty by using a subsequent model to translate the simulation into the observation space. Using a hydraulic model to translate flow simulations into hydraulic stage is one example of such a case. This forward translation of the simulated variables is potentially beneficial, but will be situation specific. In all cases, it is necessary to understand the uncertainty in input and validation data to reliably produce probabilistic predictions.

20.2.1.2 Accounting for Input and Validation Data Uncertainty

Accounting for input and validation data uncertainty requires the application of an error model prior to performing any hydrologic modeling. Such a model typically generates an ensemble of data values by perturbing the original data based on some statistical distribution (Equations 20.6 and 20.9). It is up to the forecaster to determine the correct magnitude and form of these errors prior to modeling. Though a number of scientific studies have been performed to quantify these errors, estimation of this uncertainty is still a difficult task as the problem is situation specific and often ill-posed (Kavetski et al., 2002, 2006; Renard et al., 2010, 2011). In estimating these errors, forecasters often assume that precipitation follows a heteroscedastic lognormal distribution, due to the skewed nature of precipitation data and the higher probability of large errors during large events, but this assumption has been questioned in recent research (McMillan et al., 2011). In addition, the magnitude of precipitation error may be assumed to be storm dependent (Kavetski et al., 2006), leading to added complexity in the error model. Streamflow is often assumed to have heteroscedastic errors with a normal distribution, but is overly simplified due to the existence of unsteady flow conditions, seasonal fluctuations in channel roughness,

and the extrapolation of flow estimates beyond the observed data (Di Baldassarre and Montanari, 2009). Alternatively, it is often assumed that temperature inputs are homoscedastic normal because temperature errors are likely independent of magnitude.

20.2.2 Model Structural and Parameter Uncertainty

20.2.2.1 Model Structural Uncertainty

Model structural errors result from the various assumptions and simplifications that a model developer makes to create a computationally tractable model. These assumptions may be rooted in the simplifications of the land surface physical processes to develop representative differential equations or the spatiotemporal discretization of these processes for application of these representative differential equations. Spatial representation of hydrologic processes is a particularly challenging issue, due to the difficulty of examining the physics at relevant scales to develop a mathematical model of a watershed. Typically models assume that equations fit for small scales are representative of the average at watershed scales, which is questionable due to the nonlinearities in hydrologic models (Bulygina and Gupta, 2009). In addition to assumptions in the model development process, imperfect knowledge about hydrologic processes can also lead to errors in model structure. All hydrologic models are limited by these errors in some form, the extent of which is typically not apparent (Liu et al., 2012).

Though model structure is known to be imperfect, the noise that results from model errors is poorly defined (Bulygina and Gupta, 2011; Doherty and Welter, 2010). A loose definition of model structural error is the difference between model simulation and observation (Doherty and Welter, 2010). This definition provides an estimation of model structural uncertainty, but this is incomplete due to errors in input and observation data within the modeling framework. Since these errors are not easily understood, separating them from other errors (e.g., parameter uncertainty as explained in the next section) and quantifying them is quite difficult. A number of strategies for estimating structural uncertainty have been proposed, but the methods vary greatly in strategy and implementation (Beven et al., 2011; Bulygina and Gupta, 2011; Clark et al., 2008; Doherty and Welter, 2010; Gupta et al., 2008; Liu et al., 2012; Moradkhani et al., 2012; Parrish et al., 2012; Thiemann et al., 2001; Wagener, 2003).

20.2.2.2 Parameter Identifiability

Model structural error and parameter uncertainty are distinguished because model structural error stems from model simplifications and discretization, whereas parameter uncertainty results from incomplete information content in the calibration data. The ill-posed nature of hydrologic model calibration leads to uncertainties embedded within estimated hydrologic parameters. Since parameters cannot be perfectly identified, total uncertainty estimation will involve quantifying the uncertainty associated with the parameter values (Beven and Freer, 2001). Beyond the inversion problem being ill-posed, further difficulty in parameter identification stems from the persistence of other sources of uncertainty in the modeling framework. Not only do data and model errors reduce the information content for parameter estimation, leading to reduced identifiability in model parameters, these errors compound the complexity in parameter estimation techniques. In the presence of these additional uncertainties, quantifying parameter uncertainty can become increasingly inaccurate, especially in the case of improperly quantified model structural uncertainty. Since model structural and parameter uncertainty are closely related, innovative methods must be used to account for both sources of error.

20.2.2.3 Representing Model Uncertainty

Four methods are currently used to represent hydrologic model uncertainty. First, model parameter distributions may be estimated probabilistically (Beven and Binley, 1992; Vrugt et al., 2003), thus using the parameters to estimate model structural uncertainty. Probability distributions of each parameter may be estimated through this framework to characterize model uncertainty, thus providing streamflow

prediction distributions. While this method has some potential to estimate model uncertainty, it lumps parameter and model error, which are distinct uncertainty sources, potentially leading to erroneous parameter estimates (Thyer et al., 2009), and ignores model uncertainty that arises from imperfect conceptual structure of the model, because the model parameters will always be bound by the conceptual basis of the model.

Second, the model may be evaluated stochastically through perturbation of model states/forecast. This involves assuming the statistical form of model errors and applying these errors to create a predictive distribution. Early applications of this technique ignored parameter uncertainty (Reichle et al., 2002; Vrugt et al., 2006), thus only adding model noise to state and forecast values, lumping parameter error into model error. Since parameter error is known to exist along with model error, this method likely requires inflated model error estimates to provide reliable forecasts. In light of this issue, a third method for analyzing model error through simultaneous estimation of parameter and state/forecast error was developed. It has become accepted that the stochastic evaluation of the model requires probabilistic parameter estimation, in addition to applying model error to the states/forecast, leading to direct accounting of both model and parameter uncertainty (Kavetski et al., 2006; Moradkhani et al., 2005a,b, 2012). Assuming that a hydrologist knows the statistical form of model errors, stochastic evaluation of the model is likely the most reliable method for probabilistic prediction from hydrologic models. Though this method has potential for reliable uncertainty quantification, estimating the form and magnitude of model errors is a major challenge in hydrologic modeling, leading to model error values that are difficult to validate. This has led to a fourth method for estimating model uncertainty, using multiple independent models indirectly quantifying model uncertainty (Georgakakos et al., 2004).

Multi-modeling may be performed with completely independent model structures (Duan et al., 2007; Najafi et al., 2011b; Parrish et al., 2012) or with different combinations of model components (Clark et al., 2008). Through the use of multiple different models, the model error is implied in the variability of multiple different model predictions. This assumes that there is enough variability in model structures to account for the uncertainties in the general model framework. If this assumption is not violated, the modeler may simplify the model error estimation process, leading to a reliable prediction of model uncertainty without estimating the uncertainty in an individual model. Though multi-modeling simplifies the quantification of model errors, it complicates the modeling application, creating additional work for the forecaster and necessitating additional computational resources. Both stochastic evaluation of hydrologic models and multi-model combinations are of high interest to hydrologists, which will be discussed further in Section 20.3.

20.3 Uncertainty Estimation Techniques

A number of different techniques are available for quantification of hydrologic uncertainty. Though most are rooted in Bayes' theorem, there are significant differences in the application and assumptions of these techniques. Uncertainty quantification may fall into one of the two categories: batch and sequential. Batch and sequential methods are separated by the way Bayes' theorem is applied. In a batch framework, Bayes' law is applied in its simplest form. Thus, batch methods allow for the most straightforward methods of uncertainty estimation. Alternatively, sequential methods require the use of sequential Bayes' law, which can be derived for models satisfying the Markovian criteria. Both methods can theoretically produce the same result, provided the same information, but practically this has not been proven to be the case.

20.3.1 Batch Methods

20.3.1.1 Markov Chain Monte Carlo

MCMC techniques apply Bayes' theorem to a batch of simulation and observations to estimate the posterior parameter distribution of some model. In order to estimate the posterior, a large number of

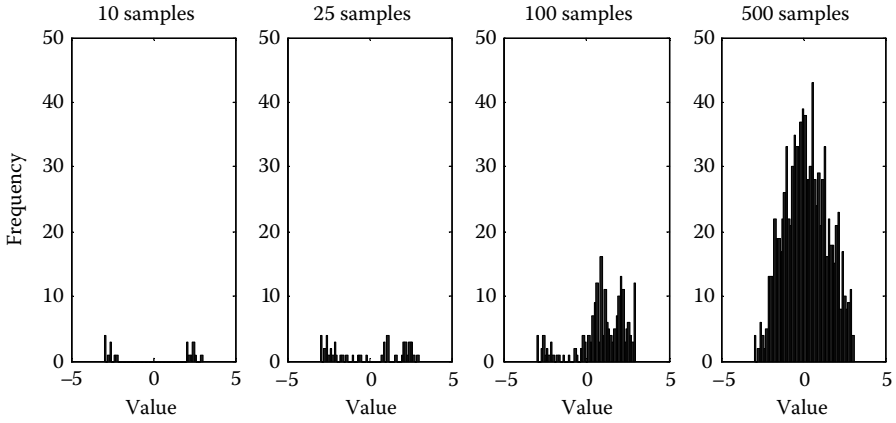

FIGURE 20.3 This figure represents the estimation of a standard normal distribution with two separate chains, initialized at 1 and –1. The first 10, 25, 100, and 500 samples from each chain are presented.

model simulations are performed in sequences. Convergence to the posterior distribution is achieved by creating multiple ergodic chains (see Figure 20.3), all of which will explore the full posterior distribution. Through a sequence of parameter moves and acceptance/rejection criteria, each chain visits locations within the posterior distribution with a frequency equal to the probability of that location. After a sufficient number of simulations, referred to as a burn-in period, the previous locations of each chain provide samples from the posterior distribution. Development of such a chain may be created with the Metropolis or Metropolis–Hastings (MH) algorithm. MCMC techniques have found wide-ranging use in the hydrologic modeling community due to their accuracy and increasing efficiency (Bates and Campbell, 2001; Jeremiah et al., 2011; Kuczera and Parent, 1998; Smith and Marshall, 2008; Vrugt et al., 2003, 2008).

The MH algorithm provides a general framework for Bayesian inference. Performing MH begins by drawing a set of initial parameters θ_i, where $i = 0$. A proposed value $\theta^\star$ is then sampled from some proposal density $q(\theta^\star|\theta_i)$. After evaluation of the model with the proposed parameters, the proposal likelihood is calculated according to Equation 20.10. The MH acceptance criteria are calculated from Bayes' law as the minimum of the ratio of the proposal parameter probability to the initial parameter probability and 1, as shown in Equation 20.11. In Equation 20.11, the probability of the parameters, conditioned on the observation from t' to T, is estimated for both the proposed and current parameters. With a probability of α (evaluated through the comparison with a uniformly drawn random number, $U[0, 1]$), parameters are accepted as the new location within the parameter space (θ_{i+1}) or rejected according to Equation 20.12:

$$p\left(\tilde{y}_{t':T} \mid \theta^\star\right) = L\left(\tilde{y}_{t':T} \mid \theta^\star\right) \tag{20.10}$$

$$\alpha = \min\left[1, \frac{p\left(\tilde{y}_{t':T} \mid \theta^\star\right) p\left(\theta^\star\right) q\left(\theta_i \mid \theta^\star\right)}{p\left(\tilde{y}_{t':T} \mid \theta_i\right) p\left(\theta_i\right) q\left(\theta^\star \mid \theta_i\right)}\right] \tag{20.11}$$

$$\theta_{i+1} = \begin{cases} \theta^\star, & \alpha \geq U[0,1] \\ \theta_i, & \alpha < U[0,1] \end{cases} \tag{20.12}$$

The MH algorithm can be simplified to the Metropolis algorithm if the proposal distribution is symmetric. In this scenario, the acceptance probability simplifies to the ratio of the posterior proposal

parameter probability to the posterior probability of the current parameters. If the proposal distribution is skewed, the MH algorithm must be used to correct for nonequivalent proposal densities ($q(\theta^*|\theta_i) \neq q(\theta_i|\theta^*)$).

20.3.1.2 Hierarchical Bayesian Estimation

Hierarchical Bayesian methods expand on the basic implementation of MCMC to include all sources of uncertainty possible. By accounting for all sources of uncertainty in the analysis, model parameter may be more accurately estimated. In hydrology, much work has been performed on uncertainty analysis using hierarchical methods with the Bayesian total error analysis (BATEA) technique (Kuczera et al., 2006). The general posterior developed in BATEA is presented in Equation 20.13. In this equation, ϕ represents the vector of storm multipliers (a strategy for handling input uncertainty), β_x is the input uncertainty parameter, and β_y is the output uncertainty parameter (Kavetski et al., 2006). Equation 20.13 can be simplified by assuming that the prior error parameters are independent of the forcing data ($p(\theta,\phi,\beta_x,\beta_y \mid \hat{\mu}) = p(\theta,\phi,\beta_x,\beta_y)$) the output likelihood is independent of the input error ($p(\hat{y} \mid \theta,\hat{\mu},\phi,\beta_x,\beta_y) = p(\hat{y} \mid \theta,\hat{\mu},\phi,\beta_y)$), and all of the errors can be evaluated separately, leading to a final form in Equation 20.14:

$$p\left(\theta,\phi,\beta_x,\beta_y \mid \hat{\mu},\hat{y}\right) = \frac{p\left(\hat{y} \mid \theta,\hat{\mu},\phi,\beta_x,\beta_y\right)p\left(\theta,\phi,\beta_x,\beta_y \mid \hat{\mu}\right)}{p(\hat{y} \mid \hat{\mu})} \tag{20.13}$$

$$p\left(\theta,\phi,\beta_x,\beta_y \mid \hat{\mu},\hat{y}\right) = \frac{p\left(\hat{y} \mid \theta,\hat{\mu},\phi,\beta_y\right)p(\theta)p(\phi \mid \beta_x)p(\beta_x)p(\beta_y)}{p(\hat{y} \mid \hat{\mu})} \tag{20.14}$$

With this formulation of the posterior, all sources of error may be accounted for directly, and even estimated empirically. Though this framework can theoretically estimate the magnitude of errors conditioned on the observations, lack of prior information often leads to ill-posedness in the analysis, leading to unreliable error estimates. A detailed discussion of this case is provided by Renard et al. (2011). This generalized framework allows for complete analysis of hydrologic uncertainty. Though this is the most straightforward method of total uncertainty quantification, the case may arise where a hydrologist wants to estimate the uncertainty sequentially. Sequential methods for uncertainty estimation are discussed in the following section.

20.3.2 Sequential Methods

Sequential estimation of the uncertainty in computer simulation models is referred to as sequential Monte Carlo filtering or ensemble data assimilation. Ensemble data assimilation techniques utilize Monte Carlo methods at each model evaluation time step to estimate the uncertainty in some hydrologic value. Of the techniques that can be applied sequentially to estimate the uncertainty in hydrologic quantities, the particle filter (PF) and the ensemble Kalman filter (EnKF) are the most commonly used (Moradkhani et al., 2005a,b). Both techniques are based on Bayes' theorem, but the EnKF extends the PF to the case of Gaussian probability distributions. The underlying theory of these methods is explained through sequential Bayes' law.

Bayes' law can be extended to sequential form as shown in Equation 20.15, for estimating model states and parameters:

$$p\left(\hat{x}_t,\theta_t \mid \tilde{y}_{1:t}\right) = \frac{p\left(\tilde{y}_t \mid \hat{x}_t,\theta_t\right)p\left(\hat{x}_t,\theta_t \mid \tilde{y}_{1:t-1}\right)}{p\left(\tilde{y}_t \mid \tilde{y}_{1:t-1}\right)} \tag{20.15}$$

In Equation 20.16, $p(\hat{x}_t, \theta_t \mid \tilde{y}_{1:t-1})$ represents the prior information, $p(\tilde{y}_t \mid \hat{x}_t, \theta_t)$ represents the likelihood, and $p(\tilde{y}_t \mid \tilde{y}_{1:t-1})$ is the normalizing constant. Since the model of interest is Markovian, the

Chapman–Kolmogorov Equation 20.16 is applied to estimate the prior distribution as the product of the transition probability and the posterior distribution at the previous time step. Estimation of the posterior then requires an estimation of the likelihood. Filtering applications within hydrology most often assume a normal likelihood function is valid. Lastly, the normalizing factor must be estimated. Though this value is not readily available, it may be expanded to the integral of the numerator (total probability), according to Equation 20.17, using the states and parameters as intermediate variables. By substituting (20.16) and (20.17) into Equation 20.15, recursive Bayes' law can be developed to compute the posterior distribution sequentially in time (20.18):

$$p\left(\hat{x}_t,\theta_t \mid \tilde{y}_{1:t-1}\right) = \int p\left(\hat{x}_t,\theta_t \mid \hat{x}_{t-1},\theta_{t-1}\right) p\left(\hat{x}_{t-1},\theta_{t-1} \mid \tilde{y}_{1:t-1}\right) d\hat{x}_{t-1} d\theta_{t-1} \tag{20.16}$$

$$p\left(\tilde{y}_t \mid \tilde{y}_{1:t-1}\right) = \int p\left(\tilde{y}_t \mid \hat{x}_t, \theta_t\right) p\left(\hat{x}_t, \theta_t \mid \tilde{y}_{1:t-1}\right) d\hat{x}_t d\theta_{t-1} \tag{20.17}$$

$$p\left(\hat{x}_t,\theta_t \mid \tilde{y}_{1:t}\right) = p\left(\hat{x}_t,\theta_t \mid \tilde{y}_t,\tilde{y}_{1:t-1}\right) = \frac{p\left(\tilde{y}_t \mid \hat{x}_t,\theta_t\right) p\left(\hat{x}_t,\theta_t \mid \tilde{y}_{1:t-1}\right)}{\int p\left(\tilde{y}_t \mid \hat{x}_t,\theta_t\right) p\left(\hat{x}_t,\theta_t \mid \tilde{y}_{1:t-1}\right) d\hat{x}_t d\theta_{t-1}} \tag{20.18}$$

The flow of data through sequential methods can be seen in Figure 20.4. In this figure, the posterior density at time $t-1$ is used to generate some forecast density at time t. At this point, an observation may become available. This observation is used to estimate the likelihood, which is then compared to the forecast density. The posterior at time t is then developed as the product of the forecast density and the likelihood. After estimation of the posterior, the method can move to the next time step.

20.3.2.1 Particle Filtering

The PF is the most generalized form of applying Bayes' theorem sequentially. This is achieved through developing a posterior weight of each ensemble member after each observation becomes available. Weighting and reweighting samples leads to an estimation that is theoretically equivalent to batch

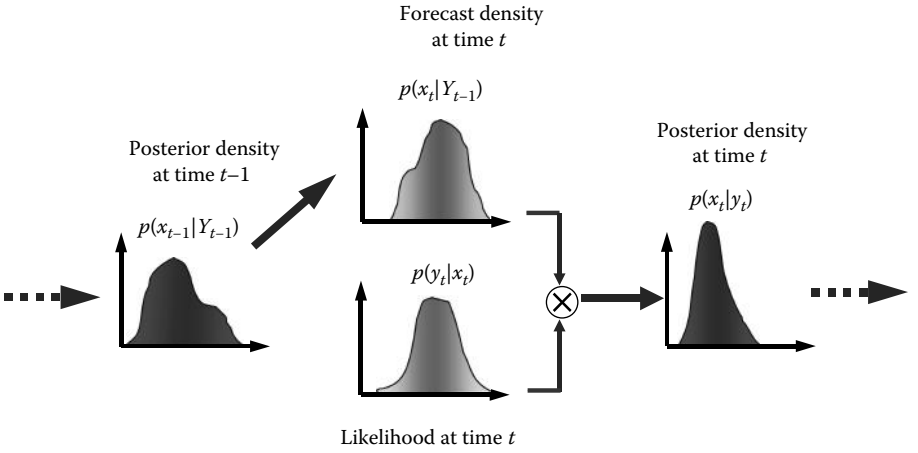

FIGURE 20.4 Sequential Bayesian scheme for evolution of the conditional probability density of the state variables by assimilating observations from time $t-1$ to time t. (After Moradkhani, H. and Sorooshian, S., *Hydrologic. Model. Water Cycle Water Sci. Technol. Library*, 63, 1–24, 2008.)

application of Bayes' law, assuming large enough sample size to represent the full posterior distribution. In its most basic form, a PF performs sequential importance sampling (SIS) (Arulampalam et al., 2002). SIS propagates a Monte Carlo sample of potential states and parameters over a number of time steps. The posterior at each time step is represented by SIS through Equation 20.19. At each time that an observation is available, the weight of each point in the sample is updated. In accordance with sequential Bayes' law, this posterior weight is the normalized product of the likelihood (20.20) and the prior probability, as shown in Equation 20.21:

$$p\left(x_t, \theta_t \mid \hat{y}_t\right) \approx \sum_{i=1}^{N_{ens}} w_{t,i}^{+} \delta\left(x_t - \hat{x}_{t,i}^{-}, \theta_t - \theta_{t,i}^{-}\right) \tag{20.19}$$

$$p\left(y_{t,i} \mid \hat{x}_{t.i}^{-}, \theta_{t,i}^{-}\right) = \frac{L\left(y_{t,i} \mid \hat{x}_{t,i}^{-}, \theta_{t,i}^{-}\right)}{\sum_{i=1}^{N_{ens}} L\left(y_{t,i} \mid \hat{x}_{t,i}^{-}, \theta_{t,i}^{-}\right)} = p\left(y_{t,i} - \hat{y}_{t.i} \mid R_k\right) \tag{20.20}$$

$$w_{t,i}^{+} = \frac{w_{t,i}^{-} \cdot p\left(y_{t,i} \mid \hat{x}_{t,i}^{-}, \theta_{t,i}^{-}\right)}{\sum_{i=1}^{N_{ens}} w_{t,i}^{-} \cdot p\left(y_{t,i} \mid \hat{x}_{t,i}^{-}, \theta_{t,i}^{-}\right)} \tag{20.21}$$

Though SIS can theoretically estimate the posterior distribution at each time step in a hydrologic model, practically the sample will develop a few highly weighted particles with many low-weighted particles. This is referred to as weight degeneracy and leads to a poorly representative sample. In order to avoid this scenario, resampling is typically performed, which replicates particles of high weights and discards particles of low weights. Through sampling importance resampling (SIR) (Moradkhani et al., 2005b), all particles are kept within meaningful portions of the posterior, which leads to a more accurate representation of predictive uncertainty. Recently, Moradkhani et al. (2012) presented a more effective data assimilation approach in particle filtering by combining PF and MCMC leading to less uncertain and more accurate estimation of states and parameters in hydrologic modeling.

20.3.2.2 Ensemble Kalman Filtering

The EnKF is a special case of sequential Monte Carlo filtering in which the states/parameters and predictions have a multivariate Gaussian distribution and model residuals are normally distributed. By making these assumptions, optimal parameter updates can be calculated to develop the posterior. Original implementations of the EnKF were performed with state-only estimation for atmospheric data assimilation (Evensen, 1994), but was extended to hydrologic applications for state (Reichle et al., 2002) and combined state–parameter estimation (Moradkhani et al., 2005a). State/parameter updates within the EnKF are performed with the Kalman gain matrix, as shown in the following equations:

$$\hat{x}_{t,i}^{+} = \hat{x}_{t,i}^{-} + K_x\left[y_{t,i} - \hat{y}_{t,i}\right] \tag{20.22}$$

$$\theta_{t,i}^{+} = \theta_{t,i}^{-} + K_\theta\left[y_{t,i} - \hat{y}_{t,i}\right] \tag{20.23}$$

where

y_t is the observed flow

K_x and K_θ are the Kalman gains for states and parameters, respectively

The Kalman Gain is calculated as follows:

$$K_t = P_t^- H^T \left(H P_t^- H^T + R_t \right)^{-1} = C_{xy} \left(C_{yy} + R_t \right)^{-1} \tag{20.24}$$

where

$P_t^- H^T = C_{xy}$ is the covariance of the states/parameter ensemble with the forecast
$H P_t^- H^T = C_{yy}$ is the variance of the forecast
R_t is the of the observation error variance
H is the linearized observation operator ($H = \partial h / \partial x$)

The model state error covariance P_t^- can now be computed directly from the following ensemble deviations (e_t^-):

$$P_t^- = \frac{1}{N_{ens}} e_t^- e_t^{-T} \tag{20.25}$$

$$e_t^{i-} = \hat{x}_{t,i}^- - \frac{1}{N_{ens}} \sum_{i=1}^{N_{ens}} \hat{x}_{t,i}^- \tag{20.26}$$

$$K = C_{xy} \left(C_{yy} + C_v \right)^{-1} \tag{20.27}$$

where N_{ens} is the total number of ensemble members.

20.3.3 Multi-Modeling to Account for Model Structural Uncertainty

Multi-modeling provides a simplified, from the forecaster's viewpoint, method for handling model structural uncertainties. With the use of multiple independent models, one may be capable of characterizing the model uncertainty with the variability of each of these models. This is often counterintuitive from the traditional standpoint of determining the optimal model for a given situation, but practically, multi-modeling is valuable because it is a rare case that one model can definitively be proven best for a given situation. Even a model that appears to be performing poorly may provide information about a watershed (Parrish et al., 2012).

A variety of methods for multi-modeling within hydrologic forecasting have been developed. The earliest application of multi-model averaging was performed with simple linear–deterministic combinations of competing models (Bates and Granger, 1969). Though linear–deterministic combinations of model observed some success, researchers have recently suggested that a more elegant framework is necessary to preserve all of the information content provided by each model (Hoeting et al., 1999; Raftery et al., 2005). Similar to other uncertainty estimation techniques, the most recently developed techniques are rooted in Bayes' law. Not only does this lead to logical method for weighting the models, combinations provide a probabilistic forecast, thus quantifying the uncertainty in the model estimates. Since Bayes' law provides a robust framework for combining multiple model predictions for uncertainty quantification, methods based on Bayes' law will be the focus of this section.

20.3.3.1 Statistical Postprocessing

Bayesian model combinations rely on the assumption that the model is an unbiased estimator, due to the basic assumptions in model weighting. With respect to hydrologic models, raw forecasts are rarely

unbiased. Due to the tendency toward bias in hydrologic predictions, a forecaster must bias correct the model predictions prior to model averaging. A number of techniques are available to forecasters for performing bias correction.

Linear regressions may be used to correct the bias of each individual model within the multimodel ensemble. Adjusted forecasts are created according to Equation 20.28. This equation represents a linear function with coefficients a_i and b_i. Both coefficients are fit to each individual model to create a function for correcting bias at each forecast step. The forecast with bias removed is represented by $y^u_{t,i}$:

$$y^u_{t,i} = a_i E\left[\hat{y}_{t,i}\right] + b_i \tag{20.28}$$

Another method for correcting model bias is the quantile-mapping (QM) approach. QM corrects bias by comparing the cumulative density of the model prediction with the cumulative density of the observation. Through this comparison, the forecast quantile associated with each forecast value ($F_{y_i'}(\hat{y}_{t,i})$) is replaced with the observed value associated with that quantile. In Equation 20.29, $F_{y'}$ is the cumulative density function associated with the model simulation, and F_y^{-1} represents the inverse cumulative density function of the observed flows:

$$y^u_{t,i} = F_y^{-1}\left(F_{y'}\left(\hat{y}_{t,i}\right)\right) \tag{20.29}$$

Recently, problems with QM have been suggested in certain distributional combinations of simulations and observations. These errors have motivated the examination of copula functions as a potential for bias correction (Madadgar et al., 2012). Copulas may be employed to estimate the joint distribution of model forecasts and observations. Since these two variables are assumed to be correlated, a joint distribution is beneficial for unbiasing the forecast with respect to the observation. The underlying theory behind copulas is Sklar's theorem. This theorem states that for any group of marginal cdfs ($[F_{X_1}(x_1), F_{X_2}(x_2), \ldots, F_{X_n}(x_n)]$), there exists a joint cdf ($H(x_1, x_2, \ldots, x_n)$) that can be estimated by the function C (copula function), as shown in Equation 20.31. In this equation, U_i is the ith uniformly randomly distributed variable transformed from its original distribution (X_i) with the F operator. This then creates a multivariate joint probability of random variables as shown in Equation 20.27:

$$H\left(x_1, x_2, \ldots, x_n\right) = C\left[F_{X_1}\left(x_1\right), F_{X_2}\left(x_2\right), \ldots, F_{X_n}\left(x_n\right)\right] = C\left(u_1, u_2, \ldots, u_n\right) \tag{20.30}$$

$$C\left(u_1, \ldots, u_n\right) = \Pr\left\{U_1 \le u_1, \ldots, U_n \le u_n\right\} \tag{20.31}$$

Through the use of copulas, a joint distribution of forecast and observation values may be developed, leading to accurate debiasing of model forecasts. For a complete explanation of bias correction with copula functions, see Madadgar et al. (2012).

20.3.3.2 Bayesian Model Averaging

Bayesian model averaging (BMA) was the first implementation of Bayesian model combinations (Hoeting et al., 1999). Several years after the method was introduced, it was applied to ensemble forecasts for meteorological applications (Raftery et al., 2005) and later applied to hydrologic modeling applications (Duan et al., 2007). Several subsequent studies have examined this technique (Ajami et al., 2007; Parrish et al., 2012; Rojas et al., 2008; Vrugt and Robinson, 2007). BMA extends the application of Bayes' law to the case of multiple possible models.

The application of Bayes' law for multiple models is shown in the following equation:

$$P\left(\tilde{y}_t \mid M_1, M_2, \ldots, M_k, Y\right) = \sum_{i=1}^{k} P\left(\tilde{y}_t \mid M_i, Y\right) P\left(M_i \mid Y\right) \tag{20.32}$$

where

M_i represents the ith model
Y is the training data
$P(M_i \mid Y)$ is the prior model probability, conditioned on the training data
$P(\tilde{y}_t \mid M_i, Y)$ is the likelihood of the model at time t

Basic applications of BMA assume that a deterministic model is used. Since each model is evaluated deterministically, the uncertainty about each model must be estimated. Typically a normally distributed model errors are assumed, and some error variance (σ_i^2) is estimated for each model. Given some variance associated with each model, probabilities for each model can then take the form of the following equation:

$$P\left(\tilde{y}_t \mid M_1, M_2, \ldots, M_k, Y\right) = \sum_{i=1}^{k} g(\hat{y}_t \mid \hat{y}_{t,i}, \sigma_i^2) * w_i \tag{20.33}$$

where

$g(\cdot)$ assigns weights based on the model forecast ($\hat{y}_{t,i}$)
the variance assumed to represent the error in that model

Note that the index i indicates the ith model, as opposed to the ith ensemble member as presented in the ensemble data assimilation section. The problem now requires estimation of the variance and weight of each model, as suggested by the training data.

Estimation of the variance and weights for each model requires maximization of Equation 20.33, as represented in the following equation:

$$MAX \sum_{t=1}^{T} P\left(\tilde{y}_t \mid M_1, M_2, \ldots, M_k, Y\right) = MAX \sum_{t=1}^{T} \sum_{i=1}^{k} g\left(\tilde{y}_t \mid \hat{y}_{t,i}, \sigma_i^2\right) * w_i \tag{20.34}$$

Since this function cannot be solved analytically, it must be solved iteratively. Early applications of BMA utilized the expectation–maximization method to solve Equation 20.35 (Raftery et al., 2005). Though expectation–maximization has been applied to estimate these weights, it is only a local optimization procedure, which suggests that improved results can be found with newer global optimization techniques (Duan et al., 2007).

20.3.3.3 Sequential Bayesian Combination

In addition to estimating model weights and variance in a batch methodology, it is possible to use the recursive Bayes' law (see Section 20.3.2) to estimate model weights sequentially (Hsu et al., 2009). Though the variance estimates are still required to remain constant in this analysis, weights are allowed to become dynamic. Updating the weights temporally allows for changing accuracy in each model to be examined, reducing the reliance on a stationary hydrologic system. Dynamic probabilities are calculated according to the following:

$$p\left(M_i \mid \tilde{y}_{1:t}\right) = p\left(M_i \mid \tilde{y}_t, \tilde{y}_{1:t-1}\right) = \frac{p\left(\tilde{y}_t \mid M_i\right) p\left(M_i \mid \tilde{y}_{1:t-1}\right)}{\int p\left(\tilde{y}_t \mid M_i\right) p\left(M_i \mid \tilde{y}_{1:t-1}\right) dM_i} \tag{20.35}$$

Similar to Section 20.3.2, this can be evaluated as a series of weights, as shown in Equation 20.36, with a normalized likelihood according to Equation 20.37:

$$w_{t,i}^{+} = \frac{w_{t,i}^{-} \cdot p\left(\tilde{y}_t \mid M_i\right)}{\sum_{i=1}^{N_{ens}} w_{t,i}^{-} \cdot p\left(\tilde{y}_t \mid M_i\right)} \tag{20.36}$$

$$p\left(\tilde{y}_t \mid M_i\right) = \frac{L\left(\tilde{y}_t \mid M_i\right)}{\sum_{i=1}^{N_{ens}} L\left(\tilde{y}_t \mid M_i\right)} = p\left(\tilde{y}_t - \hat{y}_{t,i} \mid R_k\right) \tag{20.37}$$

These equations are similar to equations in Section 20.3.2.2, but weights are calculated for each individual model and applied sequentially.

20.3.3.4 Combination of Data Assimilation with Multi-Modeling

Both the batch and sequential estimation of model weights in the previous sections require assumptions about the distribution of model errors. Typically a modeler will assume that model errors follow a homoscedastic Gaussian distribution. In the previous sections, it was highlighted that assumptions of homoscedastic normal model errors are violated in most hydrologic applications. With knowledge of this problem, it is advantageous to generalize the techniques with the combination of PF techniques and BMA (Parrish et al., 2012). This method utilizes the PF to develop a predictive distribution for each model, as opposed to an estimated variance. This leaves model prediction uncertainty highly flexible and can even handle multimodality or skew in the prediction. At a given time step, assume that the PF has developed a posterior distribution for the *i*th model ($p(\hat{x}_t, \theta_t \mid \tilde{y}_{1:t})_i$). The posterior probability ($p(M_i \mid \tilde{y}_{1:t})$) may then be calculated for each model. This probability has previously been estimated by using kernel density smoothing (Parrish et al., 2012) to create a probability density function. Through this combination of the PF and BMA, the need to estimate the model variance directly has been eliminated, and the weights can be estimated dynamically with minimal assumptions about the form the predictive distribution.

20.4 Deterministic Verification

A hydrologic modeler will often be interested in the errors associated with a single-valued forecast from a given model. This is evaluated with deterministic verification methods. Quantifying the errors associated with a single-value model forecast provides the modeler with a basic understanding of how the model is reproducing some hydrologic phenomenon. Different verification techniques are utilized to compare different aspects of model simulation and observations. A popular measure in hydrology is NSE, as discussed in Section 20.1.4. NSE provides similar information to the least square error, which is a more common verification measure in other fields, because NSE is the mean square error normalized by the observation variance. Since this measure is maximized with the least square estimate and the least square method assumed homoscedastic Gaussian errors, it is a suboptimal solution with homoscedastic errors. In the case that errors are dynamic, a modeler may choose to use a modified error measure, such as the HMLE. The HMLE assumes heteroscedastic errors and thus does not equally weight the error magnitudes with each observation. Further, a modeler may be interested in minimizing the bias of the model over a simulation time period. Measures of model bias provide information about the accuracy of long-term simulations with respect to volumetric flow. All of these measures may be applicable to a given situation, but it is up to the forecaster to determine the measure that maximizes the benefits of their model for a given application.

20.5 Probabilistic Verification

Verifying probabilistic predictions requires the examination of the reliability and sharpness of the probabilistic prediction. Reliability refers to the accuracy of the predictive distribution, showing that the predictive distribution accurately estimates the uncertainty in the system. Sharpness refers to the spread of the predictive distribution, which is the magnitude of uncertainty in the system. An optimal probabilistic forecast will provide a reliable predictive distribution, while minimizing the spread of that distribution, leading to a trustworthy forecast with low uncertainty. Though both reliability and sharpness are important qualities in a forecast, reliability of a forecast is paramount, and a forecast should not be made sharper if it sacrifices reliability.

20.5.1 Quantifying Reliability

Many quantitative measures may be used to quantify the reliability of a predictive distribution. All verification scores of reliability utilize a large number of observations to verify the predictive distribution. This assumes that if a sufficient number of observations are available, the observations will effectively populate the predictive distribution. For example, interquartile range of the predictive distribution will contain 50% of the true flow values, but the 95% predictive interval will contain 95% of the true flow values, over a long enough simulation. In the event of low reliability, there may be two contributing factors: bias and over-/underconfidence. Bias is the case where a disproportionate number of observations fall either above or below the expected value of the predictive distribution, indicating that the predictive distribution is typically shifted either above or below the observation. Over-/underconfidence refers to the case that a predictive distribution is too narrow/wide to accurately characterize the uncertainty in the prediction.

20.5.1.1 Rank Probability Skill Score

Ranked probability score (RPS) is a widely used measure for evaluating the reliability of probabilistic predictions. By definition, RPS is the sum of squared error of the cumulative probability forecasts, averaged over multiple events. In streamflow prediction, the probability forecast is usually expressed using a nonexceedance probability forecast within prespecified categories (i.e., 5%, 10%, 25%, 50%, 75%, 90%, 95%, and 99% nonexceedance). The observed value for a given threshold (forecast category) takes on the value of 1 if the observed flow value is less than the threshold for that category. Otherwise, the observed value is 0. The discrete expression of RPS is given as

$$\mathrm{RPS}_t = \sum_{i=1}^{J} \left[F_i^t - O_i^t \right]^2 \tag{20.38}$$

where

F_i^t is the forecast probability at time t, given by $P(forecast_i < thresh_i)$
O_i^t is the observed probability, given by $P(observed < thresh_i)$
i is the probability category

The rank probability skill score (RPSS) then is computed as the percentage improvement over a reference score (e.g., climatology):

$$\mathrm{RPSS} = \left(1 - \frac{\overline{\mathrm{RPS}}}{\mathrm{RPS}_{ref}} \right) \times 100 = \left(1 - \frac{\overline{\mathrm{RPS}}}{\mathrm{RPS}_{climatology}} \right) \times 100 \tag{20.39}$$

Thus, the RPSS normalizes the RPS in relation to the climatology, which provides a measure in relation to a forecast with minimal information.

20.5.1.2 Predictive Quantile–Quantile Plot and Rank Histogram

Probabilistic verification is often most effective when using graphical techniques, such as the predictive quantile–quantile (QQ) plot or the rank histogram (RH). These diagrams have the benefit of showing the behavior of the probabilistic model. Instead of simply quantifying the reliability of the predictive distribution, model bias and over-/underconfidence can be effectively diagnosed, guiding the forecaster to potential improvements in the model. Both the predictive QQ plot and the RH have a similar mathematical basis. The observation quantile is calculated according to the following equation:

$$z_t = \frac{\sum_{i=1}^{N} \chi_i}{n} \qquad \chi_i = \begin{cases} 1 & y_t > \hat{y}_{t,i} \\ 0 & y_t < \hat{y}_{t,i} \end{cases} \tag{20.40}$$

where

$\hat{y}_{t,i}$ is the predicted value associated with index i and time t
y_t is the true value at time t
n is the total number of values sampled from the predictive distribution

Since the true value is unavailable, the observation is used for comparison, which requires the assumption that the observation error distribution is symmetric and narrower than the forecast error. This provides an estimate of the quantile from the predictive distribution in which the observation falls. Given that the predictive distribution is reliable, the distribution of z should approach uniformity with enough observations. In the predictive QQ plot, the cumulative distribution of z is plotted against the cumulative uniform distribution as calculated in Equation 20.41. This is shown in Figure 20.5, which has been adapted from Laio and Tamea (2007). In this figure, the interpretation of different forecast behaviors in the predictive QQ plot is explained. Note that a completely reliable forecast will follow the uniform line,

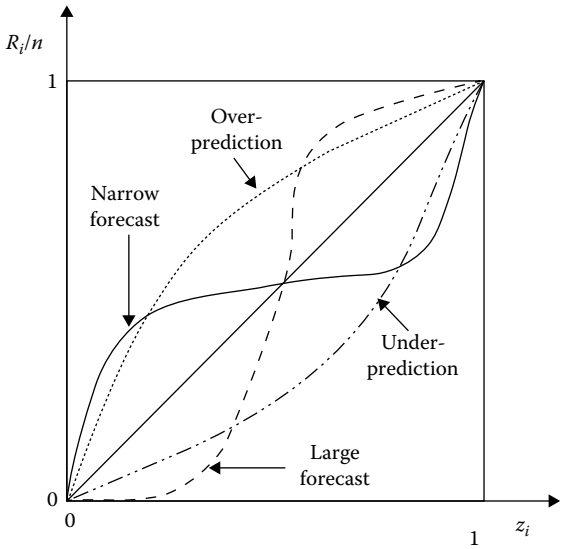

FIGURE 20.5 Interpretation of the predictive QQ plot. Narrow/large forecast is synonymous with over-/underconfidence, respectively, and over-/underprediction is synonymous with high/low bias, respectively. (After Laio, F. and Tamea, S., *Hydrol. Earth Syst. Sci.*, 11, 1267, 2007.) R_i in this figure is equal to U_i in Equation 20.41.

biased predictions will fall above or below the uniform line, and over-/underconfident predictions will cross the uniform line:

$$U = \left(\left(\frac{1}{T}\right), 2\left(\frac{1}{T}\right), 3\left(\frac{1}{T}\right), \ldots (T-1)\left(\frac{1}{T}\right), T\left(\frac{1}{T}\right) \right) \tag{20.41}$$

Similar to the predictive QQ plot, the RH compares z to the uniform distribution, but this is performed with a histogram. Though theoretically equivalent to the predictive QQ plot, the RH provides another method for visualizing reliability, which some forecasters may find easier to interpret. A diagram of RH behavior under different distributional cases is provided in Figure 20.6. Figure 20.3 was adapted from information in Hamill (2001). This figure shows how the RH validates the predictive distribution with different levels of accuracy in estimating a normally distributed random variable with mean of 0 and standard deviation of 1. From left to right, the expected value of the predictive distribution is offset by 0, 0.2, 0.4, 0.8, and 1.6, showing different levels of bias, and from top to bottom, the standard deviation of the predictive distribution is set to 0.25, 0.5, 1, 2, and 4, showing different levels of spread. Note that the middle left plot is the most reliable predictive distribution, as indicated by the uniform RH. The upper subplots indicate that the forecast is too narrow (overconfident) and the lower subplots indicate the forecast is too wide (underconfident). The left subplots indicate no bias and the right subplots indicate a very large bias.

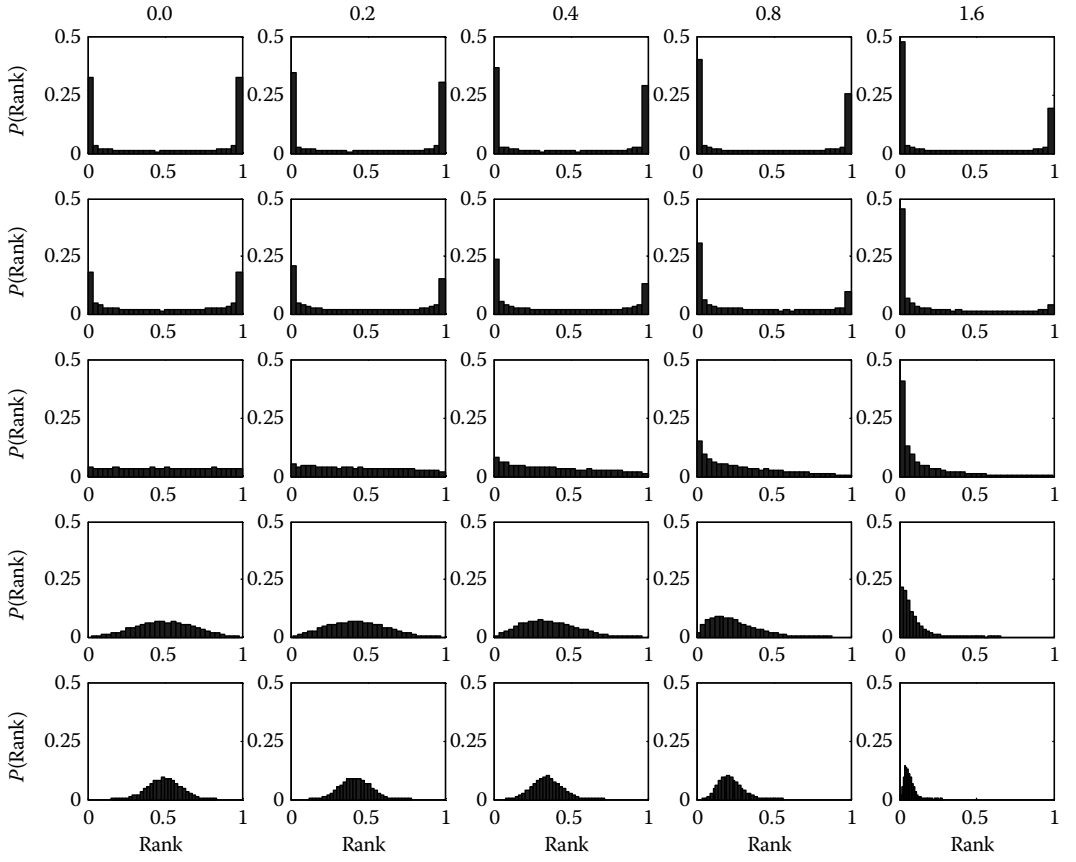

FIGURE 20.6 RHs for a predictive distribution with mean value ranging from 0 to 1.6 (left to right) and standard deviation from 0.25 to 4 (top to bottom), as compared to a standard normal distribution (mean of 0 and standard deviation of 1).

20.5.1.3 Normalized Root-Mean-Square Error Ratio

The normalized root-mean-square error ratio (NRR) is a measure that estimates if the level of spread in the predictive distribution is fitting for the amount of error in the model (Anderson, 2001). NRR is useful in verification of forecast uncertainty by communicating to the forecaster whether the level of uncertainty has been quantified correctly. In the event that the magnitude of uncertainty in model prediction is incorrect, a forecaster may attempt to identify the reason why the model is incorrectly estimating the uncertainty. In addition, NRR may be used as a tool to calibrate uncertainty hyper-parameters in the event that accurate a priori estimates are unavailable (Moradkhani et al., 2005a).

Optimally estimated ensemble spread can be analyzed by comparing the mean square error of the forecast expected value (Equation 20.42) to the mean square error of each ensemble member within the forecast (Equation 20.43). As explained by Murphy (1988), the ratio of R_1 and R_2 is optimal when equal to E[Ra] from Equation 20.44. Overall, the NRR metric may be calculated according to Equation 20.45. When NRR < 1, the ensemble spread is too large, but in the case that NRR > 1, the ensemble spread is too small:

$$R_1 = \sqrt{\frac{1}{T}\sum_{t=1}^{T}\left(y_t - \overline{y'_t}\right)^2} \tag{20.42}$$

$$R_2 = \frac{1}{N}\left\{\sum_{i=1}^{N}\sqrt{\frac{1}{T}\left[\sum_{t=1}^{T} y_t - y'^{\,2}_{t,i}\right]}\right\} \tag{20.43}$$

$$E\left[\mathrm{Ra}\right] = \sqrt{\frac{N+1}{2N}} \tag{20.44}$$

$$\mathrm{NRR} = \frac{\sqrt{(1/T)\sum_{t=1}^{T}\left(y_t - \overline{y'_t}\right)^2}}{(1/N)\left\{\sum_{i=1}^{N}\sqrt{(1/T)\left[\sum_{t=1}^{T} y_t - y'^{\,2}_{t,i}\right]}\right\}\sqrt{(N+1)/2N}} \tag{20.45}$$

20.5.2 Quantifying Sharpness

Quantifying the sharpness of a forecast is necessary for determining the value of a given forecast. Sharpness of a forecast determines the precision at which the forecast is being created and thus the usefulness of the forecast. The goal of a hydrologic forecaster will be to create the sharpest possible forecast possible, without compromising reliability. Current methods for quantifying the sharpness of a forecast include the coefficient of variation (CV) and uncertainty ratios (URs). CV is a commonly used statistic, which analyzes the mean and variance of forecast distributions. With respect to the notation used previously, the CV at time t is calculated according to the following equations:

$$\mathrm{CV}_t = \frac{\sigma_t}{\mu_t} \tag{20.46}$$

$$\mu_t = \frac{1}{N_{ens}}\sum_{i=1}^{N_{ens}} \hat{y}_{t,i} \tag{20.47}$$

$$\sigma_t = \sqrt{\frac{1}{N_{ens}} \sum_{i=1}^{N_{ens}} \left(\mu_t - \hat{y}_{t,i}\right)^2} \tag{20.48}$$

Analysis of the CV from the previous equations will typically be performed with the mean CV over some length of time. This provides a simple analysis of the relative sharpness of the forecast, with respect to the magnitude of the forecast. CV values approaching 0 indicate an increasingly sharper forecasts, and CV values approaching ∞ indicates increasingly wide forecasts. UR provides a similar metric, but can be applied to the width of any quantiles without assuming a Gaussian distribution, leading to a less restrictive measure than the CV. Based on a set quantile bound, the UR for that bound can be calculated according to the following:

$$\mathrm{UR}_t = \frac{\left(50 + (ub/2)\right) - \left(50 - (ub/2)\right)}{\mu_t} \times 100 \tag{20.49}$$

In the previous equation, *ub* is some defined uncertainty bound satisfying $0 < ub \leq 100$. Similar to the CV, the UR will typically be analyzed as the average value over some determined number of time step, and UR values approaching 0 indicate increasingly sharper forecasts, while UR values approaching ∞ indicate increasingly wider forecasts. In addition, any number of desired *ub* values may be chosen and then averaged before analysis. Using multiple *ub* values typically provides more insight into the sharpness of the forecast. Given that either a *ub* value of 50 or multiple values chosen symmetrically about 50 are chosen, $\mathrm{UR} > 100$ indicates a noninformative level of spread and $\mathrm{UR} < 100$ indicates an informative level of spread.

20.6 Summary and Conclusions

Hydrologic forecasting relies on accurate model simulations for prediction of flooding and estimation of water supply. Such models generally require information about land surface energy/water fluxes to characterize land surface processes, but there is much variability in the structure and parameterization of different hydrologic models, due to differing perceptualizations of the land surface. Since the models available to forecasters vary significantly in structure, identification of the proper model for a given application is important. Choice of hydrologic model may be viewed as a first step toward developing a hydrologic forecast. This choice may be based on the specific quantities a hydrologic model predicts, the data available to run the model, or the level of physical basis of the model (among many others). Such a choice is often subjective, which makes the model identification process imperfect, highlighting the fact that there is no one correct model. This lack of a perfect model is evidence of the inherent errors in the modeling process.

In the hydrologic modeling process, errors may be introduced by the model structure, the forcing data, observed data, and model parameters. This large number of uncertainty sources complicates the hydrologic forecasting process, introducing the need to manage these errors. Though it is intuitive to focus on reducing these errors, it is equally as valuable to quantify these errors. Accurate quantification of the uncertainty in hydrologic predictions conveys the certainty that forecasters can place on model predictions. After model selection, uncertainty quantification becomes a valuable step in hydrologic forecasting for the management of risk in hydrologic systems, but requires accounting for all sources of uncertainty and sophisticated techniques to manage that uncertainty. In most probabilistic hydrologic forecasting systems, Bayes' law provides an effective framework for managing and reducing these errors, leading to reliable forecasts. Use of Bayes' law provides flexibility over the frequentist approach by allowing the forecaster to utilize any additional data, which the prediction may be dependent on, to estimate the posterior probability. This makes the Bayesian approach valuable for hydrologic prediction because of the large quantity of informative observations.

Bayes' law may be applied through a variety of strategies to manage uncertainties in the modeling framework. The most basic difference is whether to apply Bayes' law within a batch or sequential framework. Given that the sources of error are accurately quantified, both batch and sequential techniques are appealing, but have different practical advantages. Batch techniques are the simplest to apply because they implement Bayes' law in its most basic form and typically utilize MCMC techniques to estimate the posterior through simulation with ergodic chains. Expanding on batch methodologies, sequential methods rely on sequential Bayes' law. Sequential methods are better able to learn from the temporal organization of the data and structure of information, resulting in more conformity of the model output with observations. Additionally, sequential methods have the advantage of continuously examining data and the potential to manage nonstationary processes. These have made the sequential methods more attractive both theoretically and operationally. This requires an ensemble filtering technique, typically the PF or EnKF for hydrologic applications, which requires a large Monte Carlo sample to effectively estimate the posterior. After applying Bayes' law through either batch or sequential techniques, a probabilistic prediction is produced. At this point, it is necessary to perform some validation of the prediction, which is the final step in hydrologic prediction.

In order to probabilistically validate a prediction, certain verification measures must be utilized, which are referred to as probabilistic verification techniques. These techniques seek to quantify the reliability and sharpness of a forecast. Reliability refers to the accuracy of the forecast distribution, whereas the sharpness refers to the precision of a forecast. Optimally, a forecast will be as sharp as possible while still providing a reliable distribution. In general, reliability metrics compare the observation distribution to the forecast distribution. Methods for quantifying reliability include RPSS, predictive QQ plot, and RH. Measures of sharpness include CV and UR (Moradkhani et al., 2006). With both the reliability and sharpness of a probabilistic forecast, different forecasts can be effectively compared. After validation of a forecast, it may be necessary to revise the methods used in creating the forecast to develop a new forecast. Once a reasonable forecast is developed, the hydrologic modeling process is complete.

The hydrologic forecasting process remains an area of much debate and research interest. This chapter has provided an overview of the techniques and the general process involved in providing a forecast of hydrologic variables. With this general framework, a forecaster has the basis for development and analysis of a hydrologic modeling system. Though a general framework has been provided, there are many opinions about each technique presented and further specific variations of each technique, in the scientific literature. For further details about these techniques, the reader is directed toward the cited works, which will provide further perspective on the application of each method.

References

Ajami, N.K., Q. Duan, and S. Sorooshian (2007), An integrated hydrologic Bayesian multimodel combination framework: Confronting input, parameter, and model structural uncertainty in hydrologic prediction, *Water Resources Research*, 43(1), W01403.

Anderson, J.L. (2001), An ensemble adjustment Kalman filter for data assimilation, *Monthly Weather Review*, 129(12), 2884–2903.

Arulampalam, M.S., S. Maskell, N. Gordon, and T. Clapp (2002), A tutorial on particle filters for online nonlinear/non-Gaussian Bayesian tracking, *IEEE Transactions on Signal Processing*, 50(2), 174–188.

Bates, B.C. and E.P. Campbell (2001), A Markov chain Monte Carlo scheme for parameter estimation and inference in conceptual rainfall–runoff modeling, *Water Resources Research*, 37(4), 937–947.

Bates, J.M. and C.W.J. Granger (1969), The combination of forecasts, *OR*, 20(4), 451–468.

Beven, K. and A. Binley (1992), The future of distributed models: Model calibration and uncertainty prediction, *Hydrological Processes*, 6(3), 279–298.

Beven, K. and J. Freer (2001), Equifinality, data assimilation, and uncertainty estimation in mechanistic modelling of complex environmental systems using the GLUE methodology, *Journal of Hydrology*, 249(1), 11–29.

Beven, K., P.J. Smith, and A. Wood (2011), On the colour and spin of epistemic error (and what we might do about it), *Hydrology and Earth System Sciences*, 15, 3123–3133.

Boyle, D.P., H.V. Gupta, and S. Sorooshian (2000), Toward improved calibration of hydrologic models: Combining the strengths of manual and automatic methods, *Water Resources Research*, 36(12), 3663–3674.

Bulygina, N. and H. Gupta (2009), Estimating the uncertain mathematical structure of a water balance model via Bayesian data assimilation, *Water Resources Research*, 45(12), W00B13.

Bulygina, N. and H. Gupta (2011), Correcting the mathematical structure of a hydrological model via Bayesian data assimilation, *Water Resources Research*, 47(5), W05514.

Clark, M.P. and A.G. Slater (2006), Probabilistic quantitative precipitation estimation in complex terrain, *Journal of Hydrometeorology*, 7(1), 3–22.

Clark, M.P., A.G. Slater, D.E. Rupp, R.A. Woods, J.A. Vrugt, H.V. Gupta, T. Wagener, and L.E. Hay (2008), Framework for Understanding Structural Errors (FUSE): A modular framework to diagnose differences between hydrological models, *Water Resources Research*, 44, W00B02.

Cloke, H.L. and F. Pappenberger (2009), Ensemble flood forecasting: A review, *Journal of Hydrology*, 375(3), 613–626.

Day, G.N. (1985), Extended streamflow forecasting using NWSRFS, *Journal of Water Resources Planning and Management*, 111(2), 157–170.

DeChant, C. and H. Moradkhani (2011a), Radiance data assimilation for operational snow and streamflow forecasting, *Advances in Water Resources*, 34(3), 351–364.

DeChant, C. and H. Moradkhani (2011b), Improving the characterization of initial condition for ensemble streamflow prediction using data assimilation, *Hydrology and Earth Systems Sciences*, 15, 3399–3410, DOI: 10.5194/hess-15-3399.

DeChant, C.M. and H. Moradkhani (2012), Examining the effectiveness and robustness of sequential data assimilation methods for quantification of uncertainty in hydrologic forecasting, *Water Resources Research*, 48(4), W04518.

Di Baldassarre, G. and A. Montanari (2009), Uncertainty in river discharge observations: A quantitative analysis, *Hydrology and Earth System Sciences*, 13, 913–921.

Doherty, J. and D. Welter (2010), A short exploration of structural noise, *Water Resources Research*, 46(5), W05525.

Duan, Q., N.K. Ajami, X. Gao, and S. Sorooshian (2007), Multi-model ensemble hydrologic prediction using Bayesian model averaging, *Advances in Water Resources*, 30(5), 1371–1386.

Duan, Q., S. Sorooshian, and V. Gupta (1992), Effective and efficient global optimization for conceptual rainfall–runoff models, *Water Resources Research*, 28(4), 1015–1031.

Evensen, G. (1994), Sequential data assimilation with a nonlinear quasi-geostrophic model using Monte Carlo methods to forecast error statistics, *Journal of Geophysical Research*, 99(C5), 10143–10162.

Freer, J., K. Beven, and B. Ambroise (1996), Bayesian estimation of uncertainty in runoff prediction and the value of data: An application of the GLUE approach, *Water Resources Research*, 32(7), 2161–2173.

Garen, D.C. (1992), Improved techniques in regression-based streamflow volume forecasting. *Journal of Water Resources Planning and Mangement*, 118(6), 654–670.

Georgakakos, K.P., D.-J. Seo, H. Gupta, J. Schaake, and M.B. Butts (2004), Towards the characterization of streamflow simulation uncertainty through multimodel ensembles, *Journal of Hydrology*, 298(1–4), 222–241.

Gotelli, N.J. and A.M. Ellison (2004), *A Primer of Ecological Statistics*, Sinauer Associates Publishers, Sunderland, MA.

Gupta, H.V., S. Sorooshian, and P.O. Yapo (1998), Toward improved calibration of hydrologic models: Multiple and noncommensurable measures of information, *Water Resources Research*, 34(4), 751–763.

Gupta, H.V., T. Wagener, and Y. Liu (2008), Reconciling theory with observations: Elements of a diagnostic approach to model evaluation, *Hydrological Processes*, 22(18), 3802–3813.

Hamill, T.M. (2001), Interpretation of rank histograms for verifying ensemble forecasts, *Monthly Weather Review*, 129(3), 550–560.

Hoeting, J.A., D. Madigan, A.E. Raftery, and C.T. Volinsky (1999), Bayesian model averaging: A tutorial, *Statistical Science*, 14(4), 382–401.

Hong, Y., K.-l. Hsu, H. Moradkhani, and S. Sorooshian (2006), Uncertainty quantification of satellite precipitation estimation and Monte Carlo assessment of the error propagation into hydrologic response, *Water Resources Research*, 42(8), W08421.

Hsu, K., X. Gao, S. Sorooshian, and H.V. Gupta (1997), Precipitation estimation from remotely sensed information using artificial neural networks, *Journal of Applied Meteorology*, 36(9), 1176–1190.

Hsu, K., H. Moradkhani, and S. Sorooshian (2009), A sequential Bayesian approach for hydrologic model selection and prediction, *Water Resources Research*, 45(12), W00B12.

Hyvärinen, A., J. Karhunen, and E. Oja (2001), *Independent Component Analysis*, Wiley-Interscience, New York.

Jeremiah, E., S. Sisson, L. Marshall, R. Mehrotra, and A. Sharma (2011), Bayesian calibration and uncertainty analysis of hydrological models: A comparison of adaptive Metropolis and sequential Monte Carlo samplers, *Water Resources Research*, 47(7), W07547.

Jung, I., H. Chang, and H. Moradkhani (2011), Quantifying uncertainty in urban flooding analysis by combined effect of climate and land use change scenarios, *Hydrology and Earth System Science*, 15, 617–633.

Kavetski, D., S.W. Franks, G. Kuczera, Q. Duan, H.V. Gupta, S. Sorooshian, A.N. Rousseau, and R. Turcotte (2002), Confronting input uncertainty in environmental modelling, in *Calibration of Watershed Models*, pp. 49–68.

Kavetski, D., G. Kuczera, and S.W. Franks (2006), Bayesian analysis of input uncertainty in hydrological modeling: 2. Application, *Water Resources Research*, 42(3), W03408.

Kuczera, G., D. Kavetski, S. Franks, and M. Thyer (2006), Towards a Bayesian total error analysis of conceptual rainfall–runoff models: Characterizing model error using storm-dependent parameters, *Journal of Hydrology*, 331(1), 161–177.

Kuczera, G. and E. Parent (1998), Monte Carlo assessment of parameter uncertainty in conceptual catchment models: The Metropolis algorithm, *Journal of Hydrology*, 211(1), 69–85.

Laio, F. and S. Tamea (2007), Verification tools for probabilistic forecasts of continuous hydrological variables, *Hydrology and Earth System Sciences*, 11, 1267–1277.

Leisenring, M. and H. Moradkhani (2011), Snow water equivalent prediction using Bayesian data assimilation methods, *Stochastic Environmental Research and Risk Assessment*, 25(2), 253–270.

Liu, Y., A.H. Weerts, M. Clark, H.J. Hendricks Franssen, S. Kumar, H. Moradkhani, D.J. Seo et al. (2012), Toward advancing data assimilation in operational hydrologic forecasting and water resources management: Current status, challenges, and emerging opportunities, *Hydrology and Earth System Sciences*, 16, 3863–3887.

Madadgar, S., H. Moradkhani, and D. Garen (2012), Towards improved reliability and reduced uncertainty of hydrologic ensemble forecasts using multivariate post-processing, *Hydrological Processes*, 15, 1133–1155, DOI: 10.1002/hyp.9562.

Marshall, L., D. Nott, and A. Sharma (2004), A comparative study of Markov chain Monte Carlo methods for conceptual rainfall–runoff modeling, *Water Resources Research*, 40(2), W02501.

McMillan, H., B. Jackson, M. Clark, D. Kavetski, and R. Woods (2011), Rainfall uncertainty in hydrological modelling: An evaluation of multiplicative error models, *Journal of Hydrology*, 400(1–2), 83–94.

Montzka, C., H. Moradkhani, L. Weihermüller, H.-J.H. Franssen, M. Canty, and H. Vereecken (2011), Hydraulic parameter estimation by remotely-sensed top soil moisture observations with the particle filter, *Journal of Hydrology*, 399(3–4), 410–421.

Moradkhani, H. (2008), Hydrologic remote sensing and land surface data assimilation, *Sensors*, 8, 2986–3004, DOI: 10.3390/s8052986.

Moradkhani, H., R.G. Baird, and S. Wherry (2010), Impact of climate change on floodplain mapping and hydrologic ecotones, *Journal of Hydrology*, 395, 264–278.

Moradkhani, H., C.M. DeChant, and S. Sorooshian (2012), Evolution of ensemble data assimilation for uncertainty quantification using the particle filter-Markov Chain Monte Carlo Method, *Water Resources Research*, 48, W12520, DOI: 10.1029/2012WR012144.

Moradkhani, H., K.L. Hsu, H.V. Gupta, and S. Sorooshian (2004), Improved streamflow forecasting using self-organizing radial basis function artificial neural networks, *Journal of Hydrology*, 295(1), 246–262.

Moradkhani, H., K.L. Hsu, H.V. Gupta, and S. Sorooshian (2005b), Uncertainty assessment of hydrologic model states and parameters: Sequential data assimilation using the particle filter, *Water Resources Research*, 41(5), W05012.

Moradkhani, H., K.L. Hsu, Y. Hong, and S. Sorooshian (2006), Investigating the impact of remotely sensed precipitation and hydrologic model uncertainties on the ensemble streamflow forecasting, *Geophysical Research Letters*, 33(12), L12401.

Moradkhani, H. and M. Meier (2010), Long-lead water supply forecast using large-scale climate predictors and independent component analysis, *Journal of Hydrologic Engineering*, 15, 744–762.

Moradkhani, H. and T. Meskele (2009), Probabilistic assessment of the satellite rainfall retrieval error translation to hydrologic response, in *Satellite Applications for Surface Hydrology*, Water Science and Technology Library, Springer, New York, DOI: 10.1007/978-90-481-2915-7, pp. 229–242.

Moradkhani, H. and S. Sorooshian (2008), General review of rainfall–runoff modeling: Model calibration, data assimilation, and uncertainty analysis, *Hydrological Modelling and the Water Cycle*, *Water Science and Technology Library*, 63, 1–24.

Moradkhani, H., S. Sorooshian, H.V. Gupta, and P.R. Houser (2005a), Dual state and parameter estimation of hydrological models using ensemble Kalman filter, *Advances in Water Resources*, 28(2), 135–147.

Moulin, L., E. Gaume, and C. Obled (2009), Uncertainties on mean areal precipitation: Assessment and impact on streamflow simulations, *Hydrology and Earth System Sciences*, 13, 99–114.

Murphy, J.M. (1988), The impact of ensemble forecasts on predictability, *Quarterly Journal of the Royal Meteorological Society*, 114(480), 463–493.

Najafi, M.R., H. Moradkhani, and I. Jung (2011b), Assessing the uncertainties of hydrologic model selection in climate change impact studies, *Hydrologic Processes*, 25(18), 2814–2826.

Najafi, M.R., H. Moradkhani, and T. Piechota (2012), Ensemble streamflow prediction: Climate signal weighting vs. climate forecast system reanalysis, *Journal of Hydrology*, 442–443, 105–116, http://dx.doi.org/10.1016/j.jhydrol.2012.04.003

Najafi, M.R., H. Moradkhani, and S. Wherry (2011a), Statistical downscaling of precipitation using machine learning with optimal predictor selection, *Journal of Hydrologic Engineering*, 16(8), 650–664.

Nash, J.E. and J.V. Sutcliffe (1970), River flow forecasting through conceptual models part I: A discussion of principles, *Journal of Hydrology*, 10(3), 282–290.

Parrish, M.A., H. Moradkhani, and C.M. DeChant (2012), Toward reduction of model uncertainty: Integration of Bayesian model averaging and data assimilation, *Water Resources Research*, 48(3), W03519, DOI: 10.1029/2011WR011116.

Raftery, A.E., T. Gneiting, F. Balabdaoui, and M. Polakowski (2005), Using Bayesian model averaging to calibrate forecast ensembles, *Monthly Weather Review*, 133(5), 1155–1174.

Reichle, R.H., D.B. McLaughlin, and D. Entekhabi (2002), Hydrologic data assimilation with the ensemble Kalman filter, *Monthly Weather Review*, 130(1), 103–114.

Renard, B., D. Kavetski, G. Kuczera, M. Thyer, and S.W. Franks (2010), Understanding predictive uncertainty in hydrologic modeling: The challenge of identifying input and structural errors, *Water Resources Research*, 46(5), W05521.

Renard, B., D. Kavetski, E. Leblois, M. Thyer, G. Kuczera, and S.W. Franks (2011), Toward a reliable decomposition of predictive uncertainty in hydrological modeling: Characterizing rainfall errors using conditional simulation, *Water Resources Research*, 47(11), W11516.

Rojas, R., L. Feyen, and A. Dassargues (2008), Conceptual model uncertainty in groundwater modeling: Combining generalized likelihood uncertainty estimation and Bayesian model averaging, *Water Resources Research*, 44(12), W12418.

Salamon, P. and L. Feyen (2009), Assessing parameter, precipitation, and predictive uncertainty in a distributed hydrological model using sequential data assimilation with the particle filter, *Journal of Hydrology*, 376(3), 428–442.

Shoemaker, C.A., G.R. Rommel, and R.C. Fleming (2007), Watershed calibration using multistart local optimization and evolutionary optimization with radial basis function approximation, *Hydrological Sciences Journal*, 52(3), 450–465.

Smith, T.J. and L.A. Marshall (2008), Bayesian methods in hydrologic modeling: A study of recent advancements in Markov chain Monte Carlo techniques, *Water Resources Research*, 44, W00B05.

Sorooshian, S. and J.A. Dracup (1980), Stochastic parameter estimation procedures for hydrologic rainfall–runoff models: Correlated and heteroscedastic error cases, *Water Resources Research*, 16(2), 430–442.

Thiemann, M., M. Trosset, H. Gupta, and S. Sorooshian (2001), Bayesian recursive parameter estimation for hydrologic models, *Water Resources Research*, 37(10), 2521–2535.

Thyer, M., B. Renard, D. Kavetski, G. Kuczera, S.W. Franks, and S. Srikanthan (2009), Critical evaluation of parameter consistency and predictive uncertainty in hydrological modeling: A case study using Bayesian total error analysis, *Water Resources Research*, 45(12), W00B14.

Twedt, T.M., J.C. Schaake, and E.L. Peck (1977), National Weather Service extended streamflow prediction, National Report Weather Service, Hydrologic Research Laboratory, Silver Spring, MD.

Villarini, G., P.V. Mandapaka, W.F. Krajewski, and R.J. Moore (2008), Rainfall and sampling uncertainties: A rain gauge perspective, *Journal of Geophysical Research*, 113, D11102.

Vrugt, J.A., H.V. Gupta, L.A. Bastidas, W. Bouten, and S. Sorooshian (2003), Effective and efficient algorithm for multiobjective optimization of hydrologic models, *Water Resources Research*, 39(8), 1214.

Vrugt, J.A., H.V. Gupta, B. Nualláin, and W. Bouten (2006), Real-time data assimilation for operational ensemble streamflow forecasting, *Journal of Hydrometeorology*, 7(3), 548–565.

Vrugt, J.A. and B.A. Robinson (2007), Treatment of uncertainty using ensemble methods: Comparison of sequential data assimilation and Bayesian model averaging, *Water Resources Research*, 43(1), W01411.

Vrugt, J.A., C.J.F. Ter Braak, M.P. Clark, J.M. Hyman, and B.A. Robinson (2008), Treatment of input uncertainty in hydrologic modeling: Doing hydrology backward with Markov chain Monte Carlo simulation, *Water Resources Research*, 44(12), W00B09.

Wagener, T. (2003), Evaluation of catchment models, *Hydrological Processes*, 17(16), 3375–3378.

Westra, S.P., C. Brown, U. Lall, and A. Sharma (2007), Modeling multivariable hydrological series: Principal component analysis or independent component analysis? *Water Resources Research*, 43(6), W06429.

Wood, A.W. and D.P. Lettenmaier (2008), An ensemble approach for attribution of hydrologic prediction uncertainty, *Geophysical Research Letters*, 35, L14401.

Wood, A.W. and K. Werner (2011), Development of a seasonal climate and streamflow forecasting testbed for the Colorado River Basin, *Proceedings of the 36th Climate Diagnostic and Prediction Workshop*, Fort Worth, TX, pp. 101–105.

Yapo, P.O., H.V. Gupta, and S. Sorooshian (1998), Multi-objective global optimization for hydrologic models, *Journal of Hydrology*, 204(1), 83–97.

Zhang, X., R. Srinivasan, K. Zhao, and M.V. Liew (2009), Evaluation of global optimization algorithms for parameter calibration of a computationally intensive hydrologic model, *Hydrological Processes*, 23(3), 430–441.

21

Impact of the Development of Vegetation on Flow Conditions and Flood Hazards

Tomasz Kałuża
Poznan University of Life Sciences

Saeid Eslamian
Isfahan University of Technology

AUTHORS

Tomasz Kałuża received his PhD in 2000 and DSc title in 2011 from the Poznan University of Life Sciences (Poland). He is the head of the section of hydraulic engineering in department of hydraulic and sanitary engineering, Poznan University of Life Sciences. His general research interests are environmental fluid mechanics, hydraulics of open channels and use of remote sensing methods to assessment of roughness of floodplains. He is particularly interested in the interaction between flow and vegetation and the description of bed roughness. He is the author or coauthor of more than 100 publications mainly in environmental engineering and land development and was the head of many research projects.

Saeid Eslamian received his PhD from University of New South Wales, Australia with Professor David Pilgrim. He was a visiting professor in Princeton University, USA and ETH Zurich, Switzerland. He is currently an associate professor of hydrology in Isfahan University of Technology. He is founder and chief editor of the *Journal of Flood Engineering* and *International Journal of Hydrology Science and Technology*. He has published more than 200 publications mainly in statistical and environmental hydrology and hydrometeorology.

PREFACE

Flow condition forecasts depend of many natural specific factors of the given river valley. The most important factor influencing the flow conditions is the development of vegetation. Vegetation: both the water of the riverbed and bank-side and floodplain flora increase current turbulence and therefore stimulate by far the growth of flow resistance. As a result, this correlates with lower riverbed throughput. Hydraulic calculations should also reflect such short and long-term forecasts of changes in flow conditions. Vegetation improves also the soil protection against erosion, which is normally caused by the flowing water. What is equally important, plants play an important sanitary function, acting as a biofilter cleansing the flowing waters. The various aspects of the impact of the development of vegetation on flow conditions and flood hazards are explained.

21.1 Introduction

Natural river systems with a typically natural horizontal structure are a severe challenge in the field of hydraulic calculations. The quality of the flow condition forecasts obtained on the basis of hydraulic modeling research depends in this respect on numerous natural specific factors of the given river valley. Due to the fact that investments in flood protection facilities are mostly distributed in a time horizon ranging from 20 to 100 years, hydraulic calculations should also reflect such long-term forecasts of changes in flow conditions. Thanks to the application of modern calculation methods, such as, for example, 2D models analyzing the dynamics of environmental changes and using such tools as GIS, attempts can be made to perform such simulations [21].

The basic biological process affecting the flow conditions is the plant vegetation, commonly referred to as overgrowing of riverbeds. The limits of riverbed overgrowing cannot be accurately determined, as apart from hydraulic and geometrical parameters of the given riverbed, this process is also influenced by four groups of factors: physical (light, temperature, changes in water levels), chemical, soil, and biotic [53].

Vegetation: both the water of the riverbed and bank-side and floodplain flora increase current turbulence and energy loss, and therefore stimulate by far the growth of flow resistance [17]. As a result, this correlates with lower riverbed throughput [47]. On the other hand, vegetation improves the soil protection against erosion, which is normally caused by the flowing water and abrasion of banks by waves [10]. In this case, the role of vegetation as a flow-reducing factor comes to the fore, together with the dispersion of the wave energy by stalks and leaves, as well as the reinforcement of the ground by the root system, which stabilizes the soil particles. The acceptable maximum water velocity in channels with vegetation is two or even three times smaller than that in bare channels [61]. What is equally important is that plants play an important sanitary function, acting as a biofilter cleansing the flowing waters [55]. Due to the peculiar conditions enabling the development of hydrophytes, oxidization and reduction processes are intensified, and, supported by the sorption, sedimentation, and assimilation processes, eliminate a noticeable part of the polluted matter. This activity involves the participation of lower organisms growing on the immersed parts of hydromacrophytes or root systems of bank vegetation.

21.2 Hydraulic Vegetation Classification

In general, the plants existing within the riverbed area may be divided into water plants (growing within the main riverbed area) as well as bank-side and flood plain vegetation (with regard to a riverbed with high water level). The hydraulic classification of flood plain vegetation is associated with the variety of plants and flow conditions. Due to obvious reasons, such a classification necessitates certain simplifications, mainly such as the exclusive distinguishing of those plant properties, which affect the flow

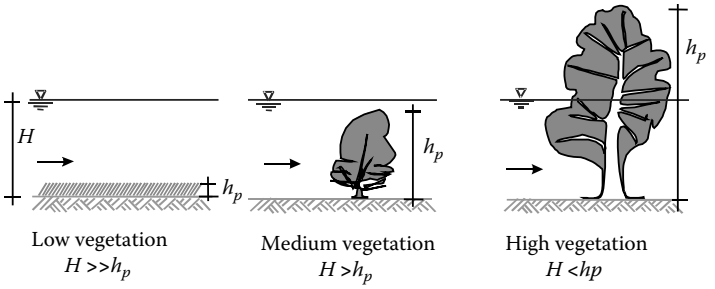

FIGURE 21.1 Hydraulic classification of plants according to Bretschneider and Schultz. (From Bretschneider, H. and Schulz, A., Anwendung von Fließformeln bei naturnahem Gewässerausbau, *DVWK Schriften 72*, Kommissionsvertrieb Verlag Paul Parey, Hamburg und Berlin, Berlin, Germany, 1985.)

conditions, and therefore the distribution of velocity. The comparison of plants with flow depth is the simplest criterion. As proposed by Bretschneider and Schultz [6], river flora has been divided into three basic plant groups (Figure 21.1):

1. Low vegetation: (grass and herbaceous plants) vegetation that, compared to water depth, is small enough to define its impact on flow conditions on the basis of the surface roughness parameter.
2. Medium vegetation: (bushes, small trees) vegetation that is approximately as tall as the water depth.
3. High vegetation: (fully mature trees, certain arborescent bushes), vegetation that is taller or equal to water depth and therefore is not immersed, while the respective flow resistance is principally dependent on the shape of tree trunks, instead of their surface roughness.

While using this simplified classification, one should consider its limits:

The differences between the three described groups are shifting, depending on the riverbed water level, and frequently there may occur problems with the appropriate classification of the specific plants.

As regards the trees, a lack of trunk deformation caused by the current is assumed, which, however, is not so clearly the case of bushes.

While analyzing the impact of vegetation on the riverbed flows during high water levels, it is worth considering the deformation of plants under the influence of the water flow. The schematic classification of flow-related plant deformation may be defined in three categories: stiff (no deformation), elastic (elastic strain), and smooth (collapsing of plants—permanent deformation).

So far, out of these three possible options, only the resistance of stiff and smooth plants has been depicted relatively accurately with mathematical models. At present, the resistance of elastic (intermediate between stiff and smooth) vegetation has not been fully examined. The basic difficulty is that it depends additionally on the biomechanical properties of plants and the impact of the current itself. Out of a series of studies taking into account the elasticity of plants [2,18,28,46] virtually only the Kouwen's method [27] seems to have gained some popularity, although, on the other hand, it did not avoid the reproach of being difficult from the practical point of view.

21.2.1 Submerged and Nonsubmerged Vegetation

In hydraulic calculations of various vegetation groups, one should apply a different water and plant impact model. This naturally correlates with different flow resistance evaluation methods. In the case of trees and bushes of certain height, a model of the stiff plant element not subject to deformation under the flowing current comes into question. On the other hand, low and medium vegetation may become elastically deformed under the impact of water.

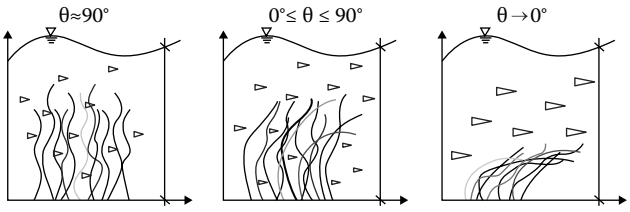

FIGURE 21.2 Deflection of plants depending on the flow velocity. (From Milbradt, P. and Schonert, T., *Ökologische Modellkomponenten in hydrodynamischen Simulationsmodellen, Wasserbaukolloquium. Strömungssimulation im Wasserbau, Dresdener Wasserbauliche Mitteilungen Heft*, Vol. 32, pp. 179–192, 2006.)

With regard to submerged vegetation, the consideration of vegetation elasticity is a source of an additional problem (Figure 21.2). So far, the elastic resistance of vegetation (intermediate between stiff and smooth) has not been fully examined. The basic difficulty is that it depends additionally on the biomechanical properties of plants and the dynamic impact of the current thereon. The relation between the parameters of the current and mechanical and geometrical values defining elastic vegetation has been described by Fenzl and Davies [13]. On basis of the measurements performed, they linked the value of shear strains with the value of bent stalk stiffness, which depends on stalk density per surface unit, plant elasticity module, and the inertia of the stalk cross section. In the course of further research, among others by Kouwen and Li [27], the substitute sandy roughness of submerged vegetation was defined again as a function of plant density, inertia, and elasticity module. Out of a series of studies taking into account the elasticity of plants [27,28], virtually only Kouwen's method [27] has been used in practice. The recent intensive research activities [30,31,57] have featured both the dynamic water pressure models and the specific biomechanical properties (e.g., elasticity module) of different plant species.

Also in the case of flood area vegetation, its deformation is often observed in practice (elastic or permanent) under the influence of the current. This pertains both to elastic vegetation, such as grass, and in many cases also to young trees and bushes (Figure 21.3).

FIGURE 21.3 Bushes after flood in 2010, Warta River, Poznan, Poland.

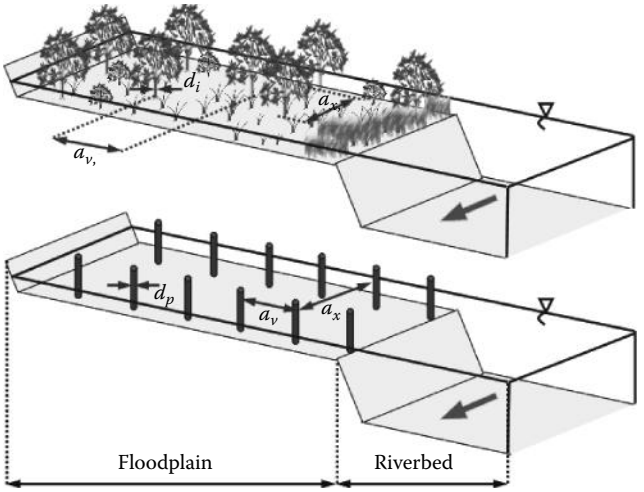

FIGURE 21.4 High vegetation geometric characteristics. (From Szporak, S. et al., *Ann. Warsaw Unive. Life Sci.—SGGW Land Reclamat.*, 40, 45, 2008.)

In the case of nonsubmerged vegetation, as a simplified approach to the parameterization of its structure, it can be regarded as a group of stiff cylindrical elements. The impact analysis of such resistant elements on the conditions of determined flow has been presented by Petryk and Bosmajian [42]. The utilization of their research results has subsequently allowed Lindner [34] and Pasche [43] to derive the relations depicting the resistance coefficient values generated by stiff vegetation. The flow resistance while flowing around high vegetation is calculated on the basis of the substitute average diameter of plants and the substitute distances between the plants along the a_x flow direction and the transverse a_y (Figure 21.4). The flow resistance coefficients calculated in this manner are used for the computation of throughput capacities of riverbeds overgrown with high vegetation. The parameter calculation method for three different structures of medium and high vegetation has been developed, for example, in Germany in the form of design recommendations [11]. Further research dealt with, among others, determination of the value of the dimensionless flow-around resistance coefficient of plant elements.

21.2.2 Assessment of Vegetation Parameters

21.2.2.1 Characteristics of Low Vegetation

In case of low vegetation, there are not many empirical parameters defining its share in the global value of the roughness coefficient. The great discrepancies between the values obtained by different authors are caused by the fluctuation of this element in time (fluctuation within the vegetation period), and they depend on the factors affecting the plants directly (e.g., flooding time and, flow velocity). In practice, low vegetation is most frequently attributed with the appropriate roughness coefficients, values of equivalent sand roughness, and biomechanical parameters.

The value of the Manning's coefficient n may be found, for example, in the Ven Te Chow tables [8]. The practical application of the values specified therein may, however, give rise to several doubts due to the wide n value scope and a descriptive and inexplicit classification of the specific plant groups. In the case of flood plains, the roughness coefficient may be estimated on the basis of the Palmer's nomogram [15]. This method relies on the graphical definition of relations of the roughness coefficient n with the product of the average flow velocity and the vR_h hydraulic radius, as well as with the parameters reflecting the physical properties of grass (length and density). It has been empirically confirmed that a single

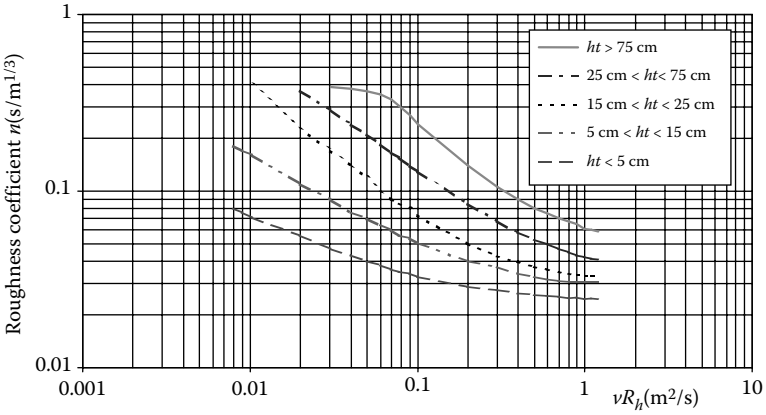

FIGURE 21.5 Dependence of the roughness coefficient on vR_h and grass height. (From USSCS, *Handbook of Channel Design for Soil and Water Conservation*, Publication SCSTP61, US Department of Agriculture, Washington, DC, 1954.)

graphic relation n-vR_h may be defined for the given grass species and length (Figure 21.5). Five curves, referred to as Palmer's curves, corresponding with the vegetation coverage of various heights have been distinguished (Figure 21.5).

Temple [56] on the basis of research results of the n-vR_h developed an empirical formula:

$$n = e^{\left[C_T\left[0{,}0133\ (\ln vR_h)^2 - 0.0322\ (\ln vR_h) + 0.145\right] - 4.16\right]} \tag{21.1}$$

where C_T is the grass category curve index calculated with the formula

$$C_T = 2.5\left(l\sqrt{m}\right)^{1/3} \tag{21.2}$$

where

l is the representative grass stalk length [m]

m is the stalk density [pcs/m^2].

In the literature, table compilations of substitute values of absolute sandy roughness for low vegetation areas can be found extremely rarely. This is why the calculation results of these parameters by Ritterbach [49] for the various vegetation types of the Wupper river flood plains (Table 21.1) are so curious.

Klaassen and Van Urk [26] assessed the value of plant parameters in natural riverbeds in a year view. The changing roughness of grass, determined with the equivalent sand roughness, indicates noticeable differences in flow conditions between the summer and winter time:

$$\text{Winter } 0.18 \text{ m} < k_s < 0.36 \text{ m}$$

$$\text{Summer } 0.72 \text{ m} < k_s < 0.75 \text{ m}$$

Ritterbach [49], based on the results of experiments by Flach and Pieters, calculated the k_s value, depending on the degree of vegetation overgrowth (Figure 21.6).

The consideration of the impact of low vegetation elasticity on flow conditions has been proposed by Kouwen [29]. Based on the measurements of elastic plants, he expressed the equivalent sand roughness as functions of contact shear stress evoked by flow:

TABLE 21.1 List of Equivalent Sand Roughness Values for Low Vegetation

No.	Type of Vegetation	Absolute Sand Roughness k_s [m]
1	Pitch, sod	0.06
2	Lawn	0.10–0.35
3	Meadow	0.13–0.40
4	Bare agricultural field	0.02–0.25
5	Agricultural field with plants	0.25–0.80
6	Forest understory	0.16–0.32
7	Dense forest understory	0.40
8	Herbs, creepers	0.50–0.70
9	Wild vegetation, weak cane vegetation	0.60–1.20
10	Wild vegetation, understory	0.80–1.60
11	Stone surface with grass	0.30
12	Stone surface with herbaceous plants	0.70
13	Stone surface with wild plants	1.00

Source: Ritterbach, E., Wechselwirkungen zwischen Auenökologie und Fließgewässerhydraulik und Möglichkeiten der integrierenden computergestützten Planung, Mitteilungen Institut für Wasserbau und Wasserwirtschaft, RWTH Aachen, Heft 80, 1991.

$$k_s = 0.14 \cdot h_p \cdot \left[\frac{\left(M \cdot E \cdot J / \rho \cdot g \cdot R_h \cdot i \right)^{0.25}}{h_p} \right]^{1.59} \tag{21.3}$$

where

M is the relative plant density: $M = R_h^2 / a_x \cdot a_y$
E is the elasticity module of the plant element
J is the moment of inertia of the cross section of plant element
h_p is the plant height
R_h is the hydraulic radius
i is the hydraulic gradient
ρ is the water density
g is the gravitation

The equivalent roughness in Equation 21.3 depends on the "stiffness" expressed as EJ, where the cross-section moment of inertia J depends on the geometry of plant elements, whereas the elasticity module E is a feature of the elastic properties of plant elements. Kouwen's analyses were verified in flow conditions of riverbeds with natural vegetation. This study has confirmed the need for considering the mechanical features of plants [30].

The cross-sectional obstruction indicator ϖ_p is an important vegetation parameter of riverbeds (both riverbank and water plants), defined as a relation of the plant projection on the cross-sectional surface against the volume of a plant colony. This indicator may be determined among others by measuring the *LAI* value, recalculated thereafter into the *LAD* of the plant cover [16]. The *LAI* leaf density coefficient is defined as a summarized relation of all plant surfaces, including leaves, with the relevant bed surface they are located on [m^2/m^2]. *LAD* is the leaf density indicator expressed as a relation between the summarized surfaces of all plant leaves and its volume [m^3/m^3]. The measurements of the *LAI* coefficient may be performed both with regard to water and low vegetation, as well as bushes and trees [19,33].

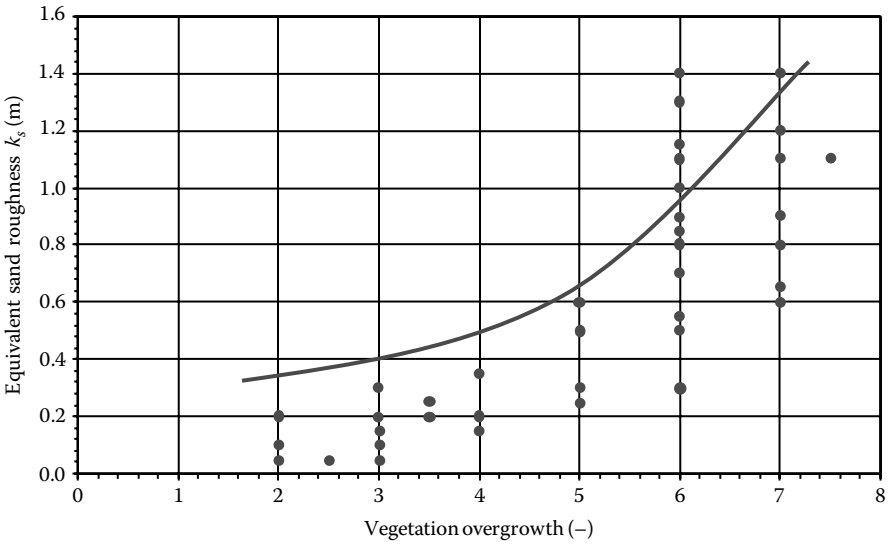

	Cross-Section of Overgrowth Degree	Cross-Section of Overgrowing
1	Perfectly clean	0–1
2	Very clean	1–2
3	Clean or quite clean	2–4
4	Clean to slightly overgrown	4–5
5	Slightly overgrown	5–6
6	Slightly to strongly overgrown	6–7
7	Strongly overgrown	7–8
8	Dense vegetation	8–10

FIGURE 21.6 Equivalent sand roughness depending on the channel cross-section vegetation overgrowth. (From Ritterbach, E., Wechselwirkungen zwischen Auenökologie und Fließgewässerhydraulik und Möglichkeiten der integrierenden computergestützten Planung, Mitteilungen Institut für Wasserbau und Wasserwirtschaft, RWTH Aachen, Heft 80, 1991.)

21.2.2.2 Geometrical Characteristics of Medium and High Vegetation

The throughput of a high water lever riverbed is mainly conditioned by the flow resistance, the most important element of which is the impact of vegetation of the flood plains. In terms of hydraulic calculations, the abundance of growth and plant species acts as a severe challenge for the description and substantial parameterization of the diverse vegetation structure. Having adopted the previously mentioned (21.2) division scheme of flood plain vegetation, Rouvé [50] proposed a hydraulic parameterization of the selected geometrical plant features. It results from the applied description model of movement resistance based on the methods derived from the flow direction power balance analysis, taking into account the various plant structure forms. The resistance of immersed plants is defined with a formula by Colebrook and White [11], whereas the value of equivalent sand roughness k_s acts as an important parameter. While assessing the resistance of nonimmersed plants, the concept of plant shape drag is used. However, in this respect it is referred to as the so-called extreme roughness, that is the impact of shape drag, while the rough element is being "flown around." The hydraulic characteristics of this vegetation are based on the assumption that the impact of an irregular structure may be narrowed down to a substitute model of an arranged group of uniform plant elements. This has been proved among others

by Pasche [43], by confirming the possible use of a regular substitute vegetation model for the assessment of the drag coefficient of natural vegetation.

The essential problem associated with the adopted vegetation division scheme and its impact on the flow is the definition of conditions in which the shift from the hydraulic surface roughness model to the plant shape drag model occurs. The conditions of this shift are undoubtedly of a fluent character and they depend on many factors, which are yet determined mainly by the flow depth. Another equally important question is the manner of defining the substitute geometrical parameters of the natural vegetation clusters within flood plain areas.

While describing the vegetation zone $A_v = b_v \cdot l_v$, it is necessary to present the mutual arrangement of plant elements within the riverbed plain and cross-section. As regards tree trunks, they are reflected on a model of stiff cylindrical elements. High vegetation, and sometimes also medium, is specified with substitute geometrical parameters (Figure 21.7): the average spacing in the flow direction a_x and perpendicularly toward a_y, as well as the average diameter of plant elements d_p. In the case of an irregular vegetation structure, its parameters are presented in the form of average values and standard deflection.

So far, there has been no method that would present, in general, the transition process from nonimmersed to immersed plant form (Figure 21.8). Within the practical calculations, it is thus necessary to divide the vegetation preliminarily (into immersed and nonimmersed) with the consideration of the estimated flooding depth.

The development of suitable hydraulic characteristics in the case of a particularly irregular nonimmersed vegetation structure involves difficulties with choosing the correct method. Therefore, certain facilitations are used in the engineering practice, generally coming down the grouping of plants according to hydraulic criteria. An interesting proposal of plant group classification and description has been presented in Reference 11. Three separate most frequently encountered plant structures have been specified therein (Table 21.2).

Here the summarized specifics of the adopted methods and the detailed solutions of defining the substitute plant parameters are presented:

- Within the macrostructural method (Figure 21.9(1)), it is assumed that the specific bushes n_k or separate tree n_d clusters act as nonpenetrable elements. The average trunk spacing is defined according to Reference 11 as

$$a_x = \sqrt{\frac{A_V}{n_d + n_k}} \tag{21.4}$$

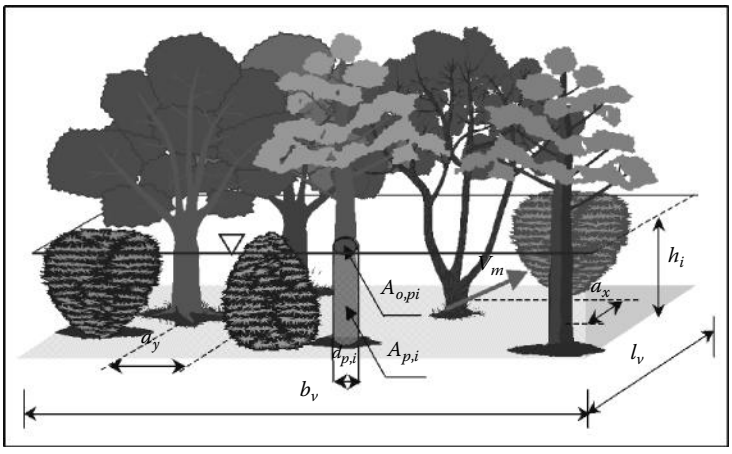

FIGURE 21.7 Parameters adopted in the vegetation zone.

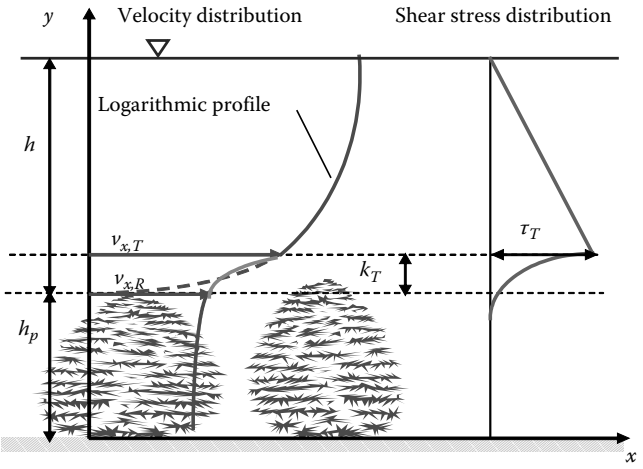

FIGURE 21.8 Parameters adopted in the case of velocity and shear stress distribution above bushes.

TABLE 21.2 Characteristics and Definition Method of the Specific Vegetation Structures

Vegetation Structure	Characteristics	Definition Method
Coherent groups of trees or bushes	The parameter definition method is selected on the basis of water depth in the flooded area. Bushes and trees are subject to microstructural description. In certain conditions, bushes are defined with surface roughness.	Microstructural or equivalent sand roughness
Single trees or bushes	For single bushes and tree clusters, it is recommended to examine the plant macrostructure. Thereupon, the average diameter of a tree or bush cluster and their average spacing is defined.	Macrostructural
Mixed trees and bushes	A combination of trees and bushes is defined first by analyzing the specific parameters of trees and bush branches. Thereafter, the so-called "mixed parameters" of both plant types are calculated.	Microstructural or macrostructural in connection with the sandy roughness model

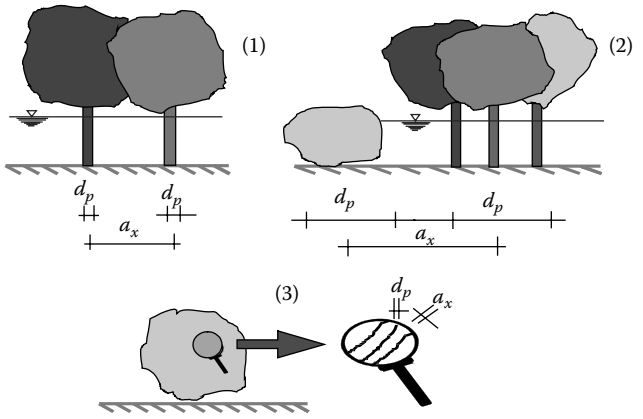

FIGURE 21.9 Schematic presentation of micro- and macrostructure according to Ritterbach. (From Ritterbach, E., Wechselwirkungen zwischen Auenökologie und Fließgewässerhydraulik und Möglichkeiten der integrierenden computergestützten Planung, Mitteilungen Institut für Wasserbau und Wasserwirtschaft, RWTH Aachen, Heft 80, 1991.)

The substitute diameter may be counted with two different formulas:

- Variant I, proposed by Reference 11 for mixed vegetation parameters:

$$d_p = \frac{d_k \cdot n_k + d_d \cdot n_d}{n_k + n_d} \tag{21.5}$$

The substitute bush diameter has been defined according to Rickert [48]:

$$d_k = \sqrt{\frac{\sum A_{pi,k}}{n_k} \cdot 4} \tag{21.6}$$

- Variant II, according to Reference 48, as for inhomogeneous vegetation:

$$d_p = \sqrt{\frac{\sum A_{pi,k} + \sum A_{pi,d}}{n_k + n_d} \cdot 4} \tag{21.7}$$

- Within the microstructural method (Figure 21.9(3)), it is assumed that the flow between the structure of single branches g_k or trunks is of great importance. Within the microstructural method, the average tree structure and trunk spacing or the average bush branch diameter and average bush spacing are defined according to Reference 11:

$$a_x = \sqrt{\frac{A_V}{n_d + n_k}} \tag{21.8}$$

$$d_p = \frac{g_k \cdot m_k + d_d \cdot n_d}{m_k + n_d} \tag{21.9}$$

In the substitute method of sandy roughness, it is assumed that the immersed medium vegetation may be specified with the k_s value. Therefore, the additional consideration of roughness of the very flood plain (low vegetation) has been ignored. Geometrical parameters of trees have been defined according to Reference 11:

$$a_x = \sqrt{\frac{A_V}{n_d}} \tag{21.10}$$

The substitute trunk diameter d_p is adopted as an average value out of a group of trees.

In the case of bushes, instead of using the microstructural method, the assessment of plant structure density with the cross-sectional obstruction indicator ϖ_p is more reasonable, as it expresses the relation of plant surface projected on the cross-sectional surface against plant volume:

$$\varpi_p = \frac{\sum A_{p,i}}{V_v} \tag{21.11}$$

The cross-sectional obstruction indicator is a measurable value, which may also be used in the case of an irregular plant structure (branching, leaves, and free plant arrangement). Due to this reason, it becomes possible to compile the value catalogue ϖ_p according to the species, status, and density of the plant elements.

TABLE 21.3 Elasticity Module of the Examined Plant Samples

	Willow I		Willow II		Reed	Alder	
	Fresh [MPa]	Dry [MPa]	Fresh [MPa]	Dry [MPa]	Fresh [MPa]	Fresh [MPa]	Dry [MPa]
$\bar{x}$	4,077	7,380	4476	8,882	3,328	2523	3762
σ	2,122	3,179	1355	1,634	4,356	852	976
v	0.52	0.43	0.30	0.18	1.31	0.34	0.26
max.	10,171	17,478	7431	12,949	17,279	4597	5666
min.	918	2,568	720	6,913	269	680	1906

Source: Tymiński, T. and Kaluza, T., *Polish J. Environ. Studies*, 21(1), 201, 2012.

Kaiser [20] has defined three groups of the ϖ_p indicator by analyzing the flow conditions:

• Scattered bushes	$\varpi_p = 0.1–0.5$	[1/m]
• Moderately dense bushes	$\varpi_p = 0.5–1.5$	[1/m]
• Dense bushes	$\varpi_p = 1.5–3.0$	[1/m]

Further research by Kaluza et al. [22] specified in greater detail the selection of the ϖ_p indicator values for wicker bushes. In addition, its correlation with the bush height has been proved. As a result of the inhomogeneous form of bushes, the cross-sectional obstruction indicator ϖ_p may change along with the flow depth. The cross-sectional obstruction indicator ϖ_p is also modified due to the accumulation of various biomass on the plant surface (leaves, grass, stray, etc.) carried by the flow. In practice, similarly to low vegetation, the cross-sectional obstruction indicator has been tied to the *LAD* value, which may be defined with instrument-based parameters (*LAI*-2000 device, hemisphere photographs).

In case of completely immersed bushes, frequently their biomechanical parameters have to be considered. In this respect, relation (21.3) may be used. This study was also performed by Tymiński and Kaluza [57]. They have indicated the high natural fluctuation of plant parameters and the impact of moisture on the physical and mechanical properties of vegetation, particularly on elasticity (Table 21.3).

21.3 Quantification of Flow Resistance of Vegetated Channel Bottom, Banks, and Floodplains

The throughput capacity determination methods of open riverbeds, considering three types of vegetation structures, may be divided into three basic groups:

1. Methods based on empirical formulas. In these methods, the analysis of average velocity considers all measured parameters. These methods are developed on the basis of a huge amount of information regarding the geometrical parameters of plants, riverbed geometry, and flow velocity. The application of these methods is narrowed down to the conditions in which they were determined.
2. The definition of resistance coefficients on the basis of model research or field measurements by means of commonly known methods of flow definition in open riverbeds. In order to determine the value of the flow resistance coefficient or roughness, the data of flow value, cross-sectional geometry, or bed slope are necessary. Subsequently, by converting the average flow velocity formula, the flow resistance value is determined. The value, obtained in this manner, cannot be projected on other examined flow conditions.
3. Methods derived from the flow direction power balance analysis, taking into account single plant elements. In the case of a determined continuous movement, it is correct to perform a force balance equation in a cross section where gravity is compensated by resistance forces generated by the roughness of the bed and the presence of plant elements. On this basis, for example,

Petryk and Bosmajian [42], as well as Lindner [34], defined the relations between the roughness coefficient and the density of the vegetation structure. This formed the basis for the development of modern determination methods of the impact of plants on flow conditions, such as the ones by Pasche [43] or Mertens [38].

The indicated methods tie the resistance coefficient value of a surface overgrown with tree and bush vegetation to substitute plant parameters. The definition of plant parameters becomes thus as important as the selection of the appropriate calculation method.

21.3.1 Influence of Submerged Vegetation on the Main Channel Capacity

The correct assessment of the resistance coefficient and the description of phenomena associated with flows in riverbeds of various roughness, caused among others by the presence of vegetation, keeps producing several difficulties. It has been historically assumed that Chezy was the first to derive the dependence on the average water flow velocity in a riverbed [8]:

$$v = C\sqrt{R_h^i} \tag{21.12}$$

where

R_h is the hydraulic radius of the current cross section [m]
i is the hydraulic gradient [–],
C is the velocity coefficient [$m^{1/2}/s$]

Manning defined the velocity coefficient on the basis of the roughness coefficient value n and the hydraulic radius R_h and received the following relation [8]:

$$v = \frac{1}{n} \cdot \sqrt{i} \cdot R_h^{2/3} \tag{21.13}$$

There are a number of sources from which photographic evidence of rivers and their associated hydraulic roughness coefficients can be obtained. Chow [8] is probably the most familiar of these sources and although the channels in Chow are all from America and the photographs are black and white, they cover a wide range of channels and a list of tables is also supplied with the photographs that provide a good initial source of roughness values.

An alternative to Chow's method of estimating Manning's n involves the use of a procedure, as presented by Cowan [9]. This method involves the selection of a basic value of Manning's n for a uniform, straight, and regular natural channel. The basic value is then adjusted for the effects of surface irregularities, shape, and size of channel cross section, obstructions, vegetation, and flow conditions and the meandering of the channel. By this method, the value of n may be calculated by

$$n = (n_0 + n_1 + n_2 + n_3 + n_4)\, m_5 \tag{21.14}$$

where

n_0 is the base value for a straight, uniform channel in natural materials
n_1 is the value added to n_0 to correct for the effect of surface irregularities
n_2 is the value for variations in shape and size of the channel cross section
n_3 is the value for obstructions
n_4 is the value for vegetation and flow conditions
m_5 is the correction factor for meandering of the channel

Another commonly applied equation describing the average water velocity in a riverbed is the formula referred to as the Darcy–Weisbach equation or universal flow equation [8]:

$$v = \sqrt{\frac{8 \cdot g}{f}} \cdot \sqrt{i \cdot R_h} \tag{21.15}$$

where

f is the dimensionless resistance coefficient [–]

g is the gravitational acceleration [m/s^2]

The application of the Darcy–Weisbach equation for the purpose of velocity calculation in open riverbeds also requires the determination of the dimensionless resistance coefficient value f. In the transitory zone, the resistance coefficient f depends both on the viscosity and the relative roughness of walls k_s/d. Due to this, both resistance-related sequences can be presented in the form of an empirical relation, referred to as the equation by Colebrook–White [8]:

$$\frac{1}{\sqrt{f}} = -2.03 \log\left(\frac{2.51}{\mathrm{Re}\sqrt{f}} + \frac{k_s}{14.84\, R_h}\right) \tag{21.16}$$

where

k_s is the absolute roughness of riverbed surface [m]

Re is the Reynold's number [–] calculated out of the following relation:

$$\mathrm{Re} = \frac{vd}{\nu} \tag{21.17}$$

As in open riverbeds, turbulent motion conditions occur most frequently, a simplified form of the equation by Colebrook–White can be applied:

$$f = \left[-2.03 \log\left(\frac{k_s}{14.84\, R_h}\right)\right]^{-2} \tag{21.18}$$

In the literature, there is an abundant collection of C and n coefficient values for various types of riverbed surface and walls, including the presence of vegetation [8].

The most simple correlating relations confirm the impact of water vegetation on flow conditions. The research carried out by Reference 24 confirmed the dependence of the roughness coefficient value on the biomass amount in a cross section (Figure 21.10). On the other hand, Querner [47] presented the impact of cross-sectional obstruction level of overgrown riverbeds on the values of the roughness coefficients (Figure 21.11). The cross-sectional obstruction degree is calculated as a relation of the obstructed cross-section area with the total cross-sectional area.

Blomfeldt [5] summarizes the approach for flexible vegetation with a spectrum ranging from a low flow called "Case 1" to a fully submerged scenario called "Case 3." Case 1 uses cylindrical resistance, and Case 3 is based on Stephan's method [52] (Figure 21.12). Between these two methods, a linear assumption of resistance is used. The limit of $H/h_{p,m} = 0.8$ is an assumption of the upper valid limit of cylindrical resistance.

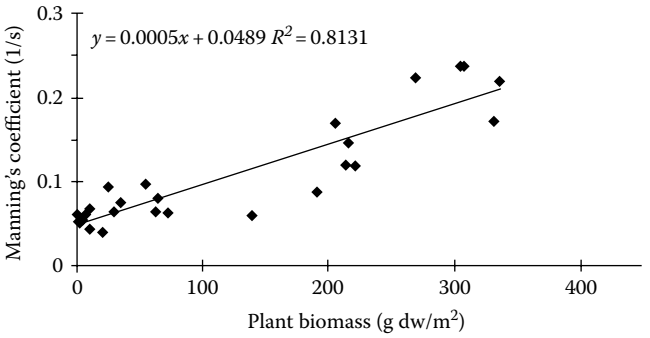

FIGURE 21.10 Dependence between the roughness coefficient value and macrophyte biomass of the Muehlibach river. (From Kenel, B. and Uehlinger, U., *Arch. Hydrobiol.*, 143(3), 257, 1998.)

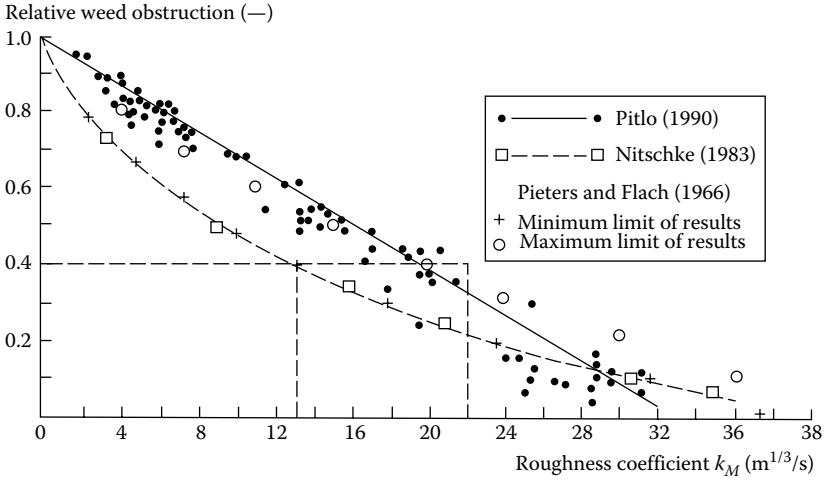

FIGURE 21.11 Dependence between the reversed roughness 1/*n* coefficients and the riverbed cross-sectional obstruction level by water vegetation. (From Querner, E., *Aquatic Weed Control within an Integrated Water Management Framework*, CIP—Gegevens Koninklijke Bibliotheek, Den Haag, the Netherlands, 1993.)

According to Reference 52, Equation 21.19 has its lower boundary at $H/h_{p,}m = 1.8$.

$$f = \frac{8}{\left(\frac{1}{\kappa}\ln\left(\left(H - h_{p,m}\right)/h_{p,m}\right) + 8.5\right)^2} \tag{21.19}$$

where

h is the plant height
$h_{p,m}$ is the deflected plant height
H is the flow depth
C_d is the drag coefficient
k = von Kármán constant (= 0.41);

Subscripts 1, 2, and 3 refer to Cases 1, 2, and 3, respectively, and D is the density parameter:

$$D = \frac{d_p}{a_x a_y} \tag{21.20}$$

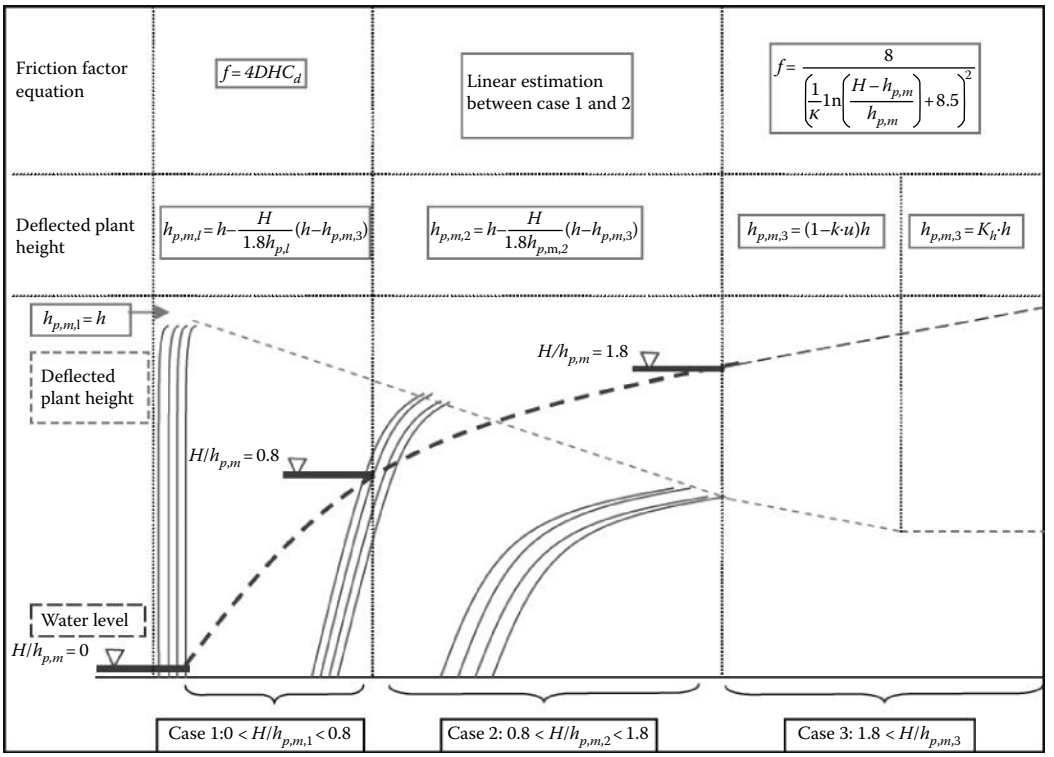

FIGURE 21.12 Division of submerged flexible vegetation resistance equations. (From Blomfeldt, E., Physically based vegetation flow resistance model: Modelling of a semi-urban stream in Nummela, Finland, Master's thesis, Helsinki University of Technology, Department of Civil and Environmental Engineering, Espoo, Finland, 92pp., 2008.)

The deflected plant height presented with linear estimation through Cases 1 and 2 (solved with iteration) and deflection based on velocity or maximum possible deflection in Case 3. Lines represent deflected plant height behavior in relation to a theoretical water level with marked levels of submergence.

Another method involves the *LAI* value of water vegetation. The *LAI* coefficient is defined as a summarized relation of the one-side surface of all leaves to the ground surface equal to 1 m^2. Based on the modified Fathi–Moghadam and Kouwen method, Järvelä [19] proposed the following dependence:

$$f = 4C_{d\chi}LAI\left(\frac{u}{u_\chi}\right)^\chi \frac{H}{h} \quad \text{when} \quad (H \le h) \tag{21.21}$$

where

$C_{d\chi}$ is a species-specific drag coefficient [–]
LAI is the leaf area index [–]
u_χ is used as normalizing velocity when determining χ, which is plant specific [m/s]
H is the water depth [m]
h is the plant height [m]

The parameter *LAI* is widely used in other fields; the difficulty lies in the other plant specific parameters $Cd\chi$ and χ, which are both empirically established. Järvelä [19] established these parameters from their own flume studies, but they also calculated some from other sources. Common discrepancies found

TABLE 21.4 Values of C_{dx} for Different Plants Determined by Järvelä (2004) by Reanalyzing Published Data

C_{dx} [–]	χ [–]	u_χ [m/s]	*LAI* [–]
0.43–0.69	(−0.38) to (−0.57)	0.1	0.1 1.14–3.2

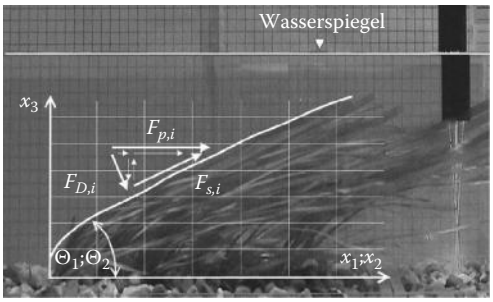

FIGURE 21.13 Flow over flexible vegetation. (From Pasche, E. and Deussfeld, N., *HANSA Int. Maritime J.*, 5, 67, 2003.)

for various leafy woody vegetation are presented in Table 21.4. Despite the lack of precise plant species information provided, the table provides an overview of the possible parameter span.

Another flow resistance value assessment proposal for elastic vegetation has been presented by Pasche and Deussfeld [44]. On the basis of laboratory research results (Figure 21.13), they proposed a determination method of the total flow resistance force as flow resistance through a vegetation structure (F_D force) and rough impact of plant leaf surface (F_S force):

$$F = F_D + F_S \tag{21.22}$$

whereas

$$F_D = \frac{1}{2} \cdot \rho \cdot u^2 \cdot C \cdot LAI \cdot l \cdot d \cdot \sin\theta \tag{21.23}$$

$$F_S = \frac{1}{8} \cdot \rho \cdot u^2 \cdot f_p \cdot LAI \cdot l \cdot d \cdot \cos\theta \tag{21.24}$$

where

f_p is the leaf surface resistance coefficient [–]
C is the flow-around resistance index of a cluster of plants [–]
LAI is the leaf density index [–]
Θ is the plant element inclination angle [°]
ρ is the water density [kg/m^3]

The determination of the flow resistance force on the basis of relations (21.23 and 21.24) necessitates the indication of the *LAI* index. The length l and width d of plant elements (leaves, twigs) are adopted as mean values. The inclination angle of plant elements Θ depends, among others, on the density of plant material ρ_r, length of plant elements l, stiffness EJ, density of vegetation structure *LAI*, flow velocity u, and the Reynolds' number Re [44].

21.3.2 Influence of Vegetated Banks and Floodplains on the Flood-Flow Conditions

Klaassen and van der Zwaard [25] were among the pioneers of the research on the impact of high vegetation on flow resistance, as the floodplains of the Maas River were the main object of their studies. The impact analysis of cylindrical resistance elements on the conditions of determined flow has been presented [42]. Apart from the friction force on the riverbed walls and the bottom surface, they also subdivided the friction force on the plant surface $F_{W,}pi$ by describing it with the Newton's resistance formula:

$$F_{W,pi} = \frac{c_d \cdot \gamma \cdot v_{pi}{}^2 \cdot A_{pi}}{2 \cdot g} \tag{21.25}$$

The shape resistance coefficient c_d depends on the flow impact conditions on the vegetation element i and therefore also on velocity v_{pi}. The value of friction coefficient on the plant surface has been adopted by the authors as equal to one: $c_d = 1$.

The work by Petryk and Bosmajian [42] gave birth to the development of the roughness coefficient determination method for weed-obstructed areas, which is based on the shape resistance method. The results of experiments and measurements performed by researchers [4,12,20,34,43,48] served as a preparation of the river hydraulic calculation guidelines, with the consideration of high vegetation obstruction on flood areas [11]. For the dimensionless computing of the flow resistance of high vegetation, Lindner [34] proposed the following relation:

$$f_V = \frac{4h_p d_p}{a_x a_y} c_d \cos\alpha \tag{21.26}$$

where

h_p is the depth [m]
d_p is the diameter of plant trunks [m]
a_x, a_y are the mean spacing along and across the flow direction [m]
c_d is the plant cluster resistance coefficient [–]
α is the flood plain inclination angle [°]

While presenting the phrases describing the resistances of surface and vegetation structure by means of Equation 21.25, Lindner also provided the dependence for the determination of average velocity as the Darcy–Weisbach equation in the vegetation area:

$$v = \sqrt{\frac{8g}{f_{so} + \left(4A_p c_d / a_x a_y\right)\cos\alpha}} \sqrt{R_h i} \tag{21.27}$$

where

f_{so} is the bed resistance coefficient [–]
$A_{p,i}$ is the plant trunk surface area ($d_p \times h$) [m^2]
R_h is the hydraulic radius [m]

According to Reference 34, the plant cluster flow-around resistance coefficient c_d depends on the shape of a single vegetation element c_d and geometric parameters of plants. The c_d coefficient expresses the resistance of a single element within ideally two-dimensional flow (Figure 21.14). According to Reference 11, c_d adopts the values from 0.6 to 2.4, whereas as an approximate value one can assume $c_d = 1.5$.

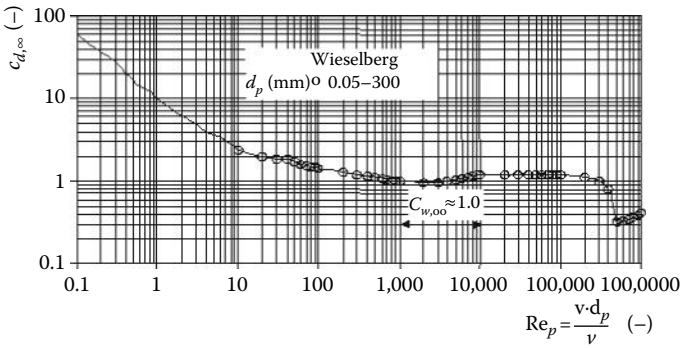

FIGURE 21.14 Dependence of the cylinder resistance coefficient $c_{w,\infty}$ from Reynolds number. (From Pasche, E., *Turbulenzmechanismen in naturnahen Fließgewässern und die Möglichkeiten ihrer mathematischen Erfassung*, Mitteilungen des Instituts für Wasserbau und Wasserwirtschat, Heft 52, Rheinisch-Westfälische Technische Hochschule, Aachen, Germany, 1984.)

The modification of Lindner's method for a dense vegetation structure has been presented by Kaiser [20] who, based on Equation 21.26, modified it, so that it included the cross-sectional obstruction indicator ϖ_p:

$$f_V = 4c_d \varpi_p R_h \tag{21.28}$$

Kaiser [20] assumed (as proved by numerous studies) that the bed resistance coefficient value is much smaller than the vegetation resistance; therefore, the f_{so} coefficient can be ignored. Therefore, in conditions of noticeable vegetation density, appropriately large flow depth, and insignificant bed roughness, the following simplified dependence is obtained:

$$v = \sqrt{\frac{2gi\left(1-\varepsilon_p\right)}{c_d \varpi_p}} \tag{21.29}$$

The $(1 - \varepsilon_p)$ phrase features the reduction of gravity caused by smaller water volume reduced by the volume of submerged vegetation elements.

According to Equation 21.29, in the conditions of high density of plant elements, the average velocity does not depend on the hydraulic radius, but it remains permanent in the plant layer. These solutions for the determination of average velocity in cross section pertain to the special case of nonsubmerged vegetation, provided that $h < h_p$.

21.4 Impact of the Development of Vegetation on Flow Conditions

An additional feature that must be considered in the analysis of the real flow conditions in a riverbed with a complex cross section and vegetation on flood areas is the dynamic character of the main channel capacity fluctuation. A schematic representation of such fluctuation is provided in Figure 21.15.

The transitory changes caused by the current include, for example, elastic deformation of plants, whereas seasonal changes are considered as season-specific variation of plant structures. Permanent vegetation-related changes include the following:

- Changes of plant diameter and structure density
- Macrostructural changes of plants, such as natural dispersion or concentration of plants

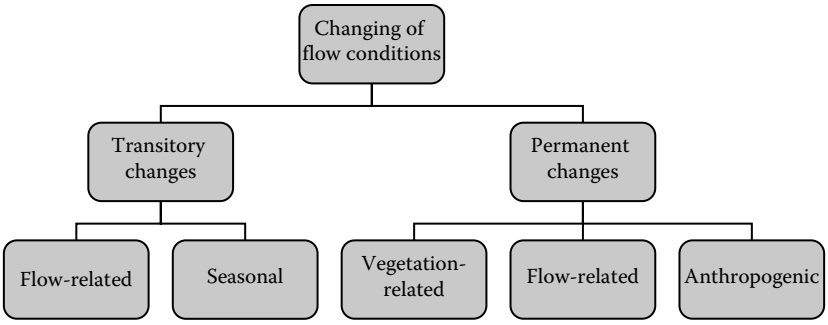

FIGURE 21.15 A schematic representation of factors influencing the flow conditions.

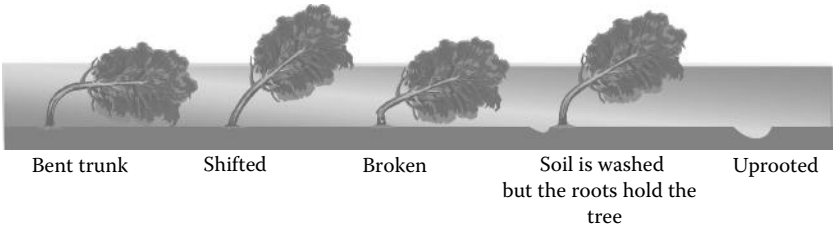

FIGURE 21.16 Observed impact of flow on trees.

The following are regarded as permanent flow-related transformations:

- Damage caused by, for example, washing out of roots
- Structural changes caused by overshadowing or light exposure of plants
- Irreversible changes resulting from among other inclinations of plants

The concept of permanent changes created by anthropogenic factors should be interpreted as transformations of the forest stand by chopping or planting forests within the flood valley area.

Elasticity is a common feature of vegetation (Figure 21.16). In the case of hydraulic calculations, this, however, means an additional dependence of vegetation height on the current flow conditions (water level and velocity) [59]. While rejecting the assumption of fully elastic plant deformation, one should consider the common natural phenomenon of permanent deformation (inclination or fall) or damaging (breaking apart or cracking) of plant elements subject to the flow force. Permanent plant deformations may be estimated only on the basis of information on the pressure of the flowing water and the plant elasticity module.

Flow-related plant deformation is a common feature of vegetation in flood areas. It becomes even more complicated, if the assumption of fully elastic plant deformation is rejected, while taking into account the common natural phenomenon of permanent deformation (inclination or fall) or damaging (breaking apart or cracking) of plant elements subject to the flow force. For analysis purposes of tree damage as a result of flood water flow, they may be divided into five groups (Figure 21.16) [40]. The extreme case of damaging must be noted here, that is the intensive washing out of the bed and creation of craters due to the uprooting of entire trees or bushes from the soil.

21.4.1 Impact of Seasonal Development

Seasonal (phenologic) changes of vegetation pertain to water, riverbank, and onshore plants. Physiological and morphological variations thereof are a response to the seasonal rhythm of climate conditions. They include stages of vegetative development: for example, forming and growth of leaf buds, development of

leaves and underground organs, dropping of leaves and stages of generative development: forming and development of flower buds, flourishing, forming of seeds, spreading of seeds. In the case of onshore plants, various forms may be distinguished, one year plants (one year cycle), perennials (plants with a life-cycle of several years and withering overground elements), as well as trees and bushes which develop and reduce their leaf surfaces on a seasonal basis.

21.4.1.1 Impact of Seasonal Macrophyte Changes on Flow Conditions

The problem of riverbed weed obstruction (overgrowth) is a well-known issue. In hydrology, the development of water plants will cause seasonal changes of the flow curve. The decrease in flow velocity, active flow cross section, changed descending pattern of the water surface altitude, and growth of the flow resistance coefficient observed in connection with water-weed obstruction (immersed, buoyant, and floating) cause the backing up of the water surface in comparison to normal flow conditions (without overgrowth) [51]. Such backing up is often referred to as vegetative.

The reduction of the active flow cross section (Figure 21.18) is associated with the seasonal growth of riverbed obstruction degree (Figure 21.17). This is evident particularly in the comparison of data from naturally weed-obstructed riverbeds and cleared during the vegetation period (Figure 21.17).

The detailed research of the Poelsbeek and Bolscherbeek (Netherlands) have allowed to determine the intensity of main channel weed obstruction [47]. Most of the species existent on the survey locations included nettle, sorrel, glyceria maxima, glyceria fluitans, trinia, and elodea canadensis. Figure 21.18 includes the variation of the vegetation area borders in 1990 within a selected cross section and four chosen dates. As seen in Figure 21.18, vegetation normally exists on the slopes of the riverbed and its growth gradually narrows the free flow cross section.

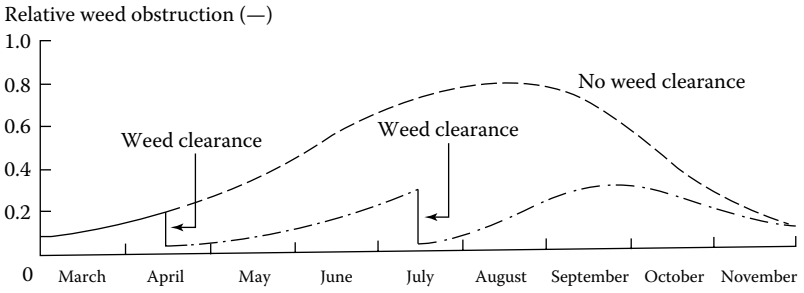

FIGURE 21.17 Change in relative weed obstruction during the summer period. (From Querner, E., *Aquatic Weed Control within an Integrated Water Management Framework*, CIP—Gegevens Koninklijke Bibliotheek, Den Haag, the Netherlands, 1993.)

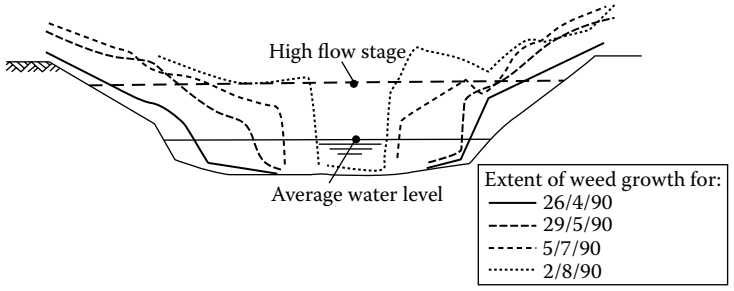

FIGURE 21.18 Fluctuation of vegetation areas at survey location no. 7 during the vegetation period in 1990. (From Querner, E., *Aquatic Weed Control within an Integrated Water Management Framework*, CIP—Gegevens Koninklijke Bibliotheek, Den Haag, the Netherlands, 1993.)

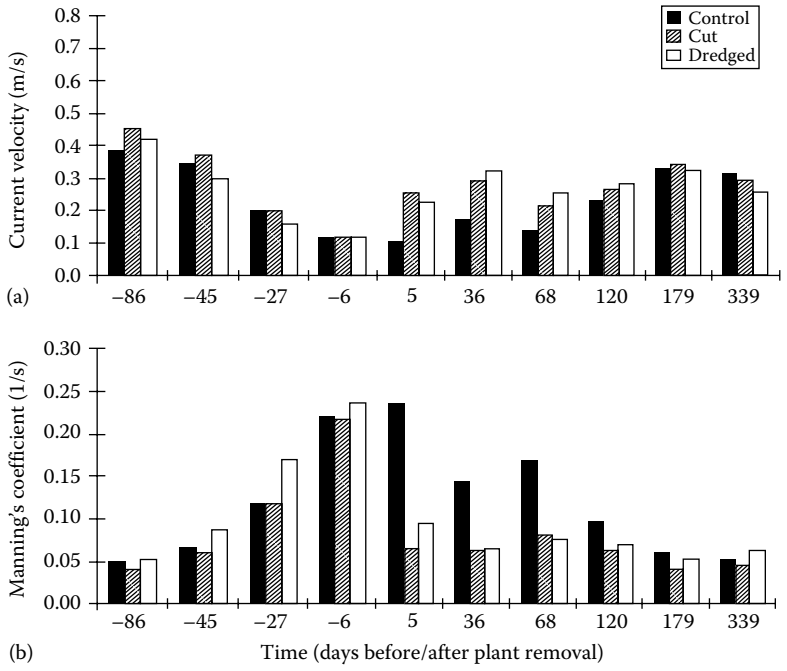

FIGURE 21.19 Mean current velocity and Manning's coefficient in the Muehlibach. (From Kenel, B. and Uehlinger, U., *Arch. Hydrobiol.*, 143(3), 257, 1998.)

Impact of biomass growth within the riverbed on the flow conditions is evident particularly in the comparison of data from naturally weed-obstructed beds and cleared during the vegetation period (Figures 21.17 and 21.19). The research performed by Kenel and Uehlinger [24] on the Muehlibach river allowed for an assessment of the impact of riverbed purification in the vegetation period (by cutting or removing the plants) on the value of mean velocity and the roughness coefficient. The riverbed was cleared in the climax of vegetation. A growth of velocity from approximately 0.1 to 0.28 m/s has been gained, together with the reduction of the roughness coefficient n from 0.024 to 0.07 $m^{-1/3}s$.

In the course of a detailed research, attempts are made to determine the seasonal variation of the substitute sandy roughness value k_s of various vegetation types; Table 21.5 [41]. The research was performed in the Biebrza River valley (Poland).

TABLE 21.5 Roughness k_s Values Adopted for Vegetation in the Biebrza River Valley (Poland) within and outside the Vegetation Period

	Absolute Roughness k_s (m)	
Type of Vegetation	In the Vegetation Period	Outside the Vegetation Period
Meadow vegetation	0.7	0.3
Sedges	1.2	0.4
Sedges (clusters)	1.2	0.5
Glycerietum maximae	1.2	0.5
Phragmitetum australis	1.2	1.2
Understorey (Caltho-Alnetum)	1.6	0.8
Forest understory	0.4	0.4

Source: Kozioł, A. and Miroslaw-Swiatek, D., *Nauka Przyr. Technol.*, 3(3, 88), 1, 2009.

As a result of the overgrowing of rivers with water vegetation, the flow determined with the basic flow curve in connection with vegetative backing up is higher than the real flow. In order to bring the status-flow relation to a real level, the seasonal curves method or the summertime coefficient reduction method can be used.

If changes in the flow curve occur in the considered watermark cross section due to its seasonal overgrowth, the status-flow relation will vary on a continual basis. In this situation, certain periods corresponding with the pace of such variation are defined. For this period, the status-flow relation is determined, by moving from one relation to another. The current intensity curve is obtained in the form of a group of curves valid at a given period of time (Figure 21.20). In practice, frequently only two current curves are defined for the main channel (Figure 21.21): basic curve and vegetation period curve [32]. Riverbed weed obstruction in the river basin of Biebrza (Poland) has brought as much as 10% of flow reduction (Figure 21.21).

The summertime flow reduction coefficient k_L is the quotient of the real flow in the overgrowth period Q_L against the flow read from the current intensity curve Q_0 at the observed water level. This coefficient, enclosed in the $0 < k_L \leq 1$ range, indicates the fluctuation degree of the status-flow relation due to weed obstruction. On the basis of these coefficients, the real flow values are defined:

$$Q_L = k_L Q_0 \tag{21.30}$$

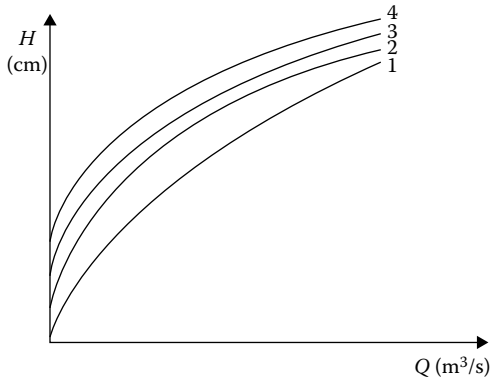

FIGURE 21.20 Seasonal flow curves: 1, basic curve; 2, curve at the beginning and end of the vegetation period; 3, curve of the transitory periods; 4, curve of the vegetation climax.

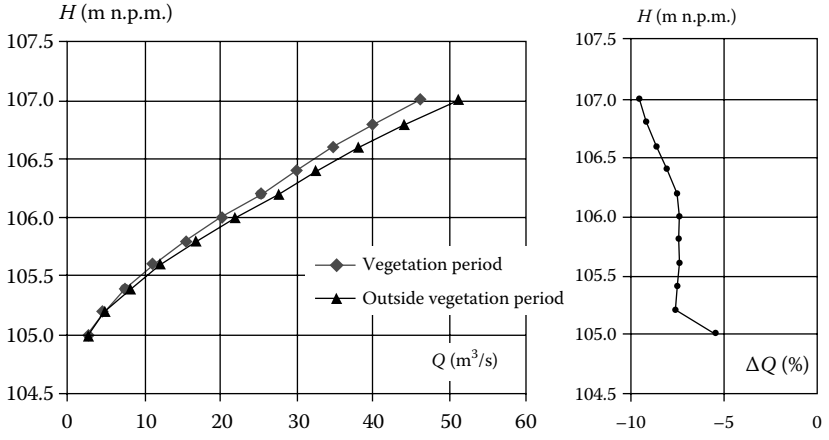

FIGURE 21.21 Rating curves for the Biebrza River main channel and percentage reduction of the discharge within and outside the vegetation period.

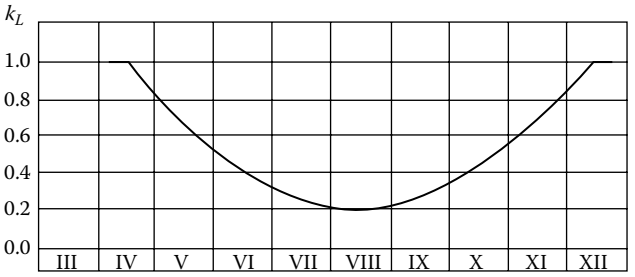

FIGURE 21.22 Summertime reduction coefficient diagram.

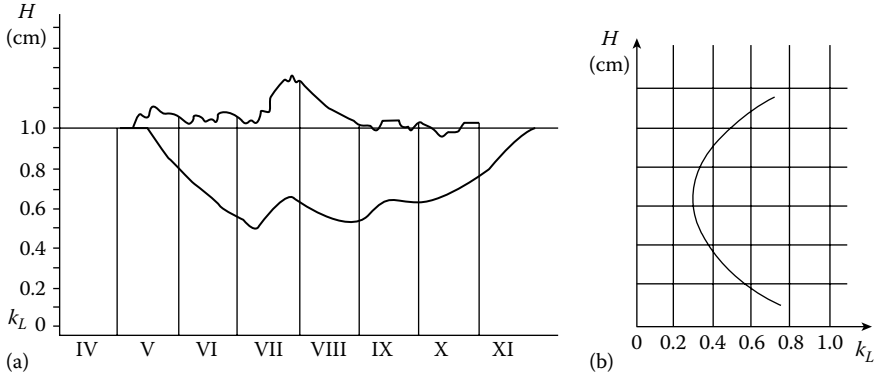

FIGURE 21.23 Summertime reduction coefficient k_L diagram (a) depending on water level H (b) within a single year.

The most frequent determining method of the k_L coefficient is the finding of relations of long-term mean values (Figure 21.22). While using the k_L coefficient, it is necessary to consider the fact that its value depends on the water level (Figure 21.23a). Together with the main channel filling degree, first of all the reduction of the k_L value is observed. Thereafter, along with the further growth of the water level, the value of the k_L coefficient begins to grow (Figure 21.23b).

In the hydrometric practice, this method is frequently used, allowing for the determination of the summertime reduction coefficient on the basis of water level records and water temperature measurements. By incorporating the water or air temperature into this method, the varying vegetation intensity within a given year may be considered, depending on weather conditions.

21.4.1.2 Impact of Seasonal Flood Zone Vegetation Changes on Flow Conditions

The seasonal altering of flow conditions within flood areas, expressed with the *f(T)* coefficient, are a result of the development of low $f_{So}(T)$, as well as medium and high vegetation $f_V(T)$:

$$f(T) = f_V(T) + f_{So}(T) \tag{21.31}$$

Seasonal changes of the low vegetation resistance coefficient $f_{So}(T)$ can be determined from the changes of value in the substitute sandy roughness k_s for different types of vegetation. Another method involves the consideration of the seasonal changing of *LAI* of low vegetation [3]. In the case of trees and bushes, the seasonal fluctuation of flow conditions is mainly a result of altering leaf area (indicated with the *LAI* value). This pertains mainly to bushes, as during floods treetops remain most frequently above water. In the case of bushes, there is a problem with determining the ω_p indicator, whereupon it is easier to use the

automatic leaf area assessment methods enabling the simple and repeatable determination of the *LAD* leaf area density. On the basis of research [22], the linear relation between the ω_p indicator and *LAD* has been found:

$$\omega_p = aLAD \tag{21.32}$$

On the basis of regular field measurements, the function of seasonal leaf density fluctuation may be determined. Figure 21.24 provides an example of the fluctuation of the *LAD* value of a given bush on Warta River flood areas within a single year.

The impact of seasonal vegetation changes is also projected on the status-flow relation of a riverbed affected by a high (flood) water level. The seasonal valley changes observed in the Biebrza River basin (Poland) cause the reduction of the main channel discharge by about 21% (Figure 21.25) [32].

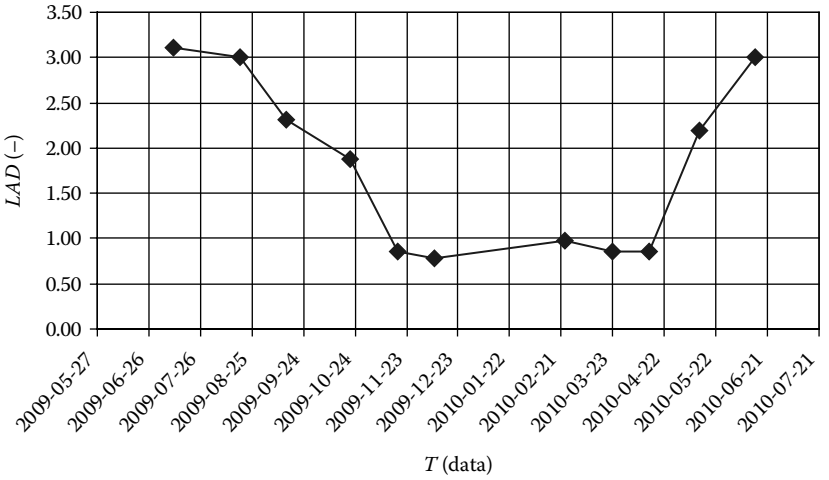

FIGURE 21.24 Fluctuation of the leaf area density *LAD* indicator in time for bush 8 on Warta River flood areas.

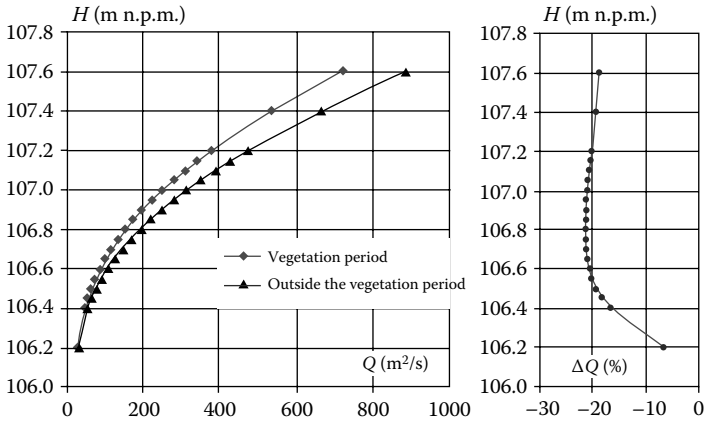

FIGURE 21.25 Rating curves for the Biebrza River valley and percentage reduction of the discharge within and outside the vegetation period.

21.4.2 Impact of Long-Term Development

The analysis of the long-term impact of expanding vegetation on flow conditions is most frequently carried out for riverbank and onshore plants (bushes and trees). Water plants are a difficult object of analysis in all views apart from seasonal. The estimation of flood zone's roughness coefficient caused by development, transformation, and natural succession of vegetation is an important element of the impact of medium and high vegetation on flow conditions [35]. By basing the flow resistance assessment on objectively calculated plant parameters (k_s, d_p, a, LAD), it is possible to forecast changes in a longer run. Such a forecast becomes available only because of the analysis of the possible natural succession of the examined land ecosystems (Figures 21.26 and 21.27) or the application of vegetation development models. The development models provided, for example, on forest tables have been developed to the widest extent for forest stands.

Forest tables describe the dynamic growth of the forest stand according to a certain mean development model prepared on the basis of measurement data of forest stands of the relevant species. Tables are systematized according to habitat valuation class and adopted ageing ranges. The analysis of

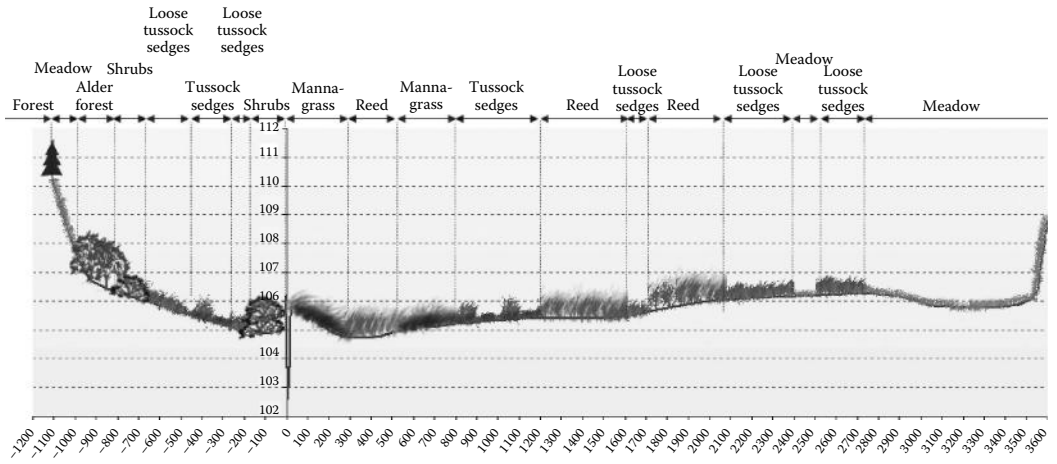

FIGURE 21.26 Cross section in the Lower Biebrza Basin—current status. (From Szporak, S. et al., *Ann. Warsaw Unive. Life Sci.—SGGW Land Reclamat.*, 40, 45, 2008.)

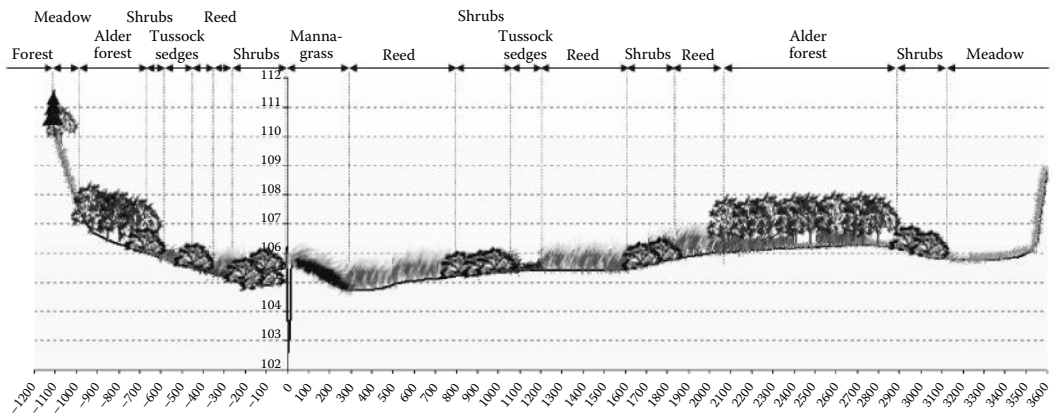

FIGURE 21.27 Cross section in the Lower Biebrza Basin; scenario—natural succession. (From Szporak, S. et al., *Ann. Warsaw Unive. Life Sci.—SGGW Land Reclamat.*, 40, 45, 2008.)

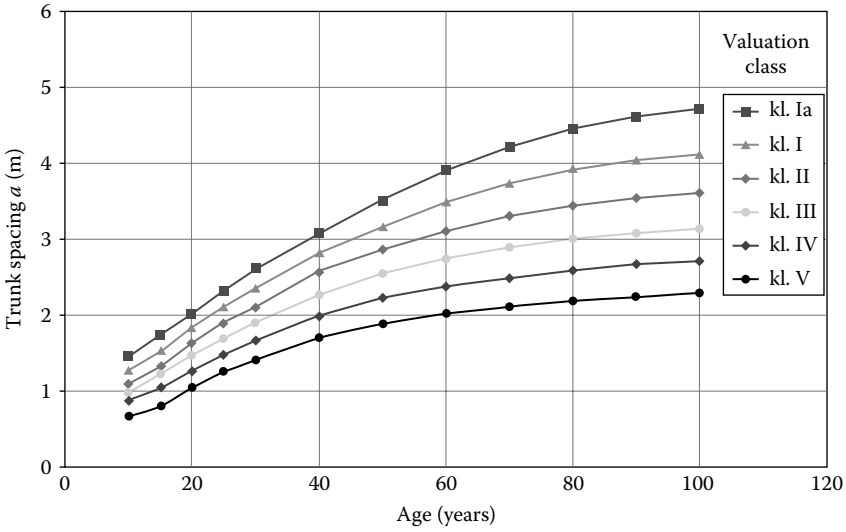

FIGURE 21.28 Change in willow trunk spacing depending on the valuation class.

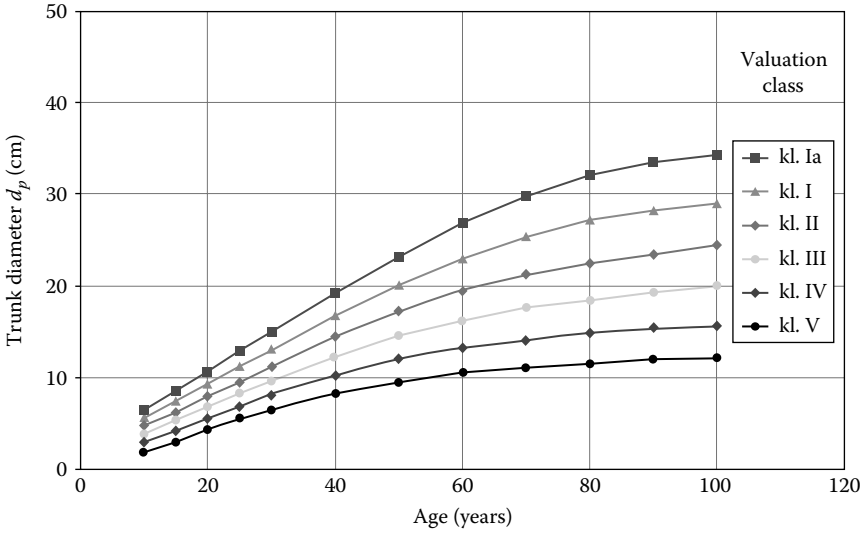

FIGURE 21.29 Change in willow trunk diameter depending on the valuation class.

development-related parameter fluctuation specifically for various plant species has been presented in a study [21]. An exemplary dependence of willow parameter fluctuation on valuation class is presented in Figures 21.28 and 21.29.

The development of forest stands occurs by the change in diameter and trunk spacing. This dependence is additionally associated with a valuation class. Higher trunk spacing and diameter values achieve higher valuation classes (Ia, I, II). This results from a more intensive forest economy and better environmental conditions for plants. On the basis of measurement data provided by Reference 49, it has been proved that for the analysis of flood zone forest stands, classes Ia and I can be adopted. The parameters of the tables are available starting from as late as 10 years of age, so the values of the preceding period have to be assumed on the basis of field measurement results in Reference 48. The fluctuation of plant parameters may be expressed by the change in plant structure density (Figure 21.30).

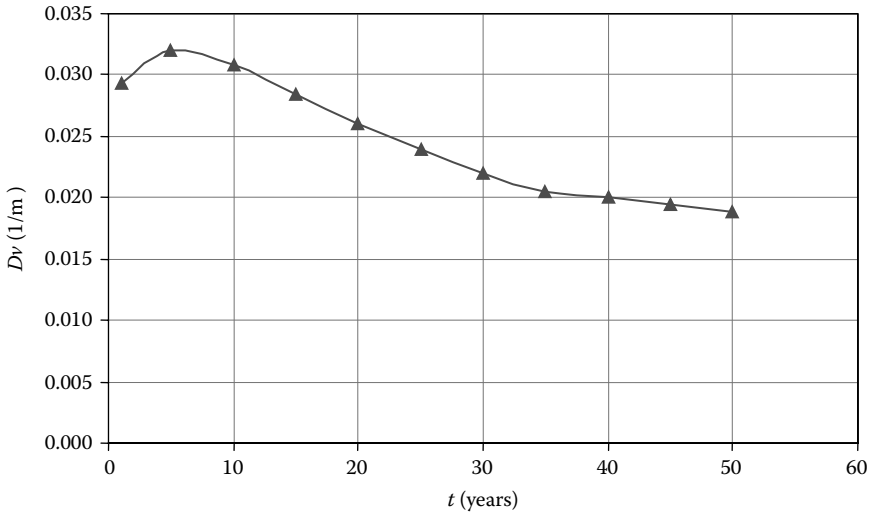

FIGURE 21.30 Willow structure density fluctuation forecast.

By inserting the development model of willow geometric parameters, a long-term forecast of the density structure fluctuation of such forest stands has been obtained (Figure 21.30). As a distinctive feature, a clear maximum density of 0.032 [1/m] of a 5-year willow structure can be observed. The further development of plants implies a fall of density below 0.020 [1/m]. It is also interesting that the highest dynamism occurs within the initial period (up to approximately 30 years), whereas any subsequent changes are insignificant.

By inserting the data on the fluctuation of geometrical growth parameters to the formula (21.26), it is possible to determine the fluctuation of the resistance coefficient value f_V as a function of time. The calculation results of the resistance coefficient caused by the growth of willow trees are presented in Figure 21.29. The age-related decrease of the flow resistance is strongly associated with the valuation class. In the case of willow and birch forest stands, the higher classes (Ia, I, II) correlate with the smaller resistance values (Figure 21.29). Research of other forest stands such as oak, pine, alder, and poplar have indicated that the highest resistance coefficient values are to be expected in the initial phase of forest development (up to 10–30 years), which is associated with the dense structure of a young forest (Figure 21.31).

21.4.3 Hydrological Impacts of River Vegetation, for Example, the Effect on *T*-Year Extreme Flow Events

The impact of plant vegetation on flood areas can be determined on the basis of models of vegetation growth dynamics adopted in Section 21.4.2.

By analyzing the example of the Biebrza River (Figures 21.26 and 21.27) within the hydraulic calculations considering the natural plant succession scenario in flood areas, the impact of vegetation-related weed obstruction has been determined [54]. The water surface ordinates calculated with the one-dimensional hydrodynamic models were used with the GIS and Numeric Terrain Model technologies to determine the range and average flood depth. In terms of maximum flow WQ = 229 m^3/s, a growth of water levels on flood areas has been achieved by approximately 80 cm (from 0.65 to 1.44 m), and in terms of average flow SQ = 70 m^3/s, the growth amounted to about 20 cm (from 0.49 to 0.68 m). The range of flooding on the analyzed river section without embankments grew in terms of the maximum flow by approximately 92% (or 86 km^2) and in terms of average flow by 118% (or 52 km^2).

Another example is the analysis of a section of the Vistula river in its surroundings based on a two-dimensional Rismo modeling system [23]. An important element affecting the high water level riverbed

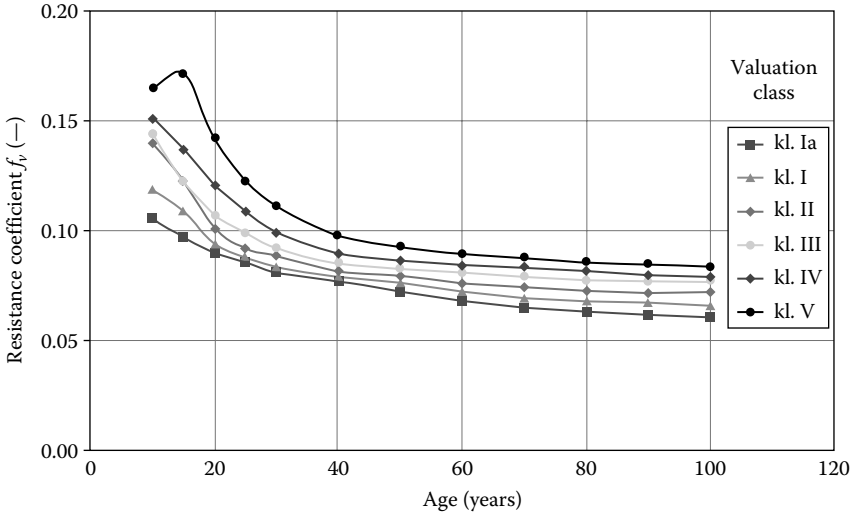

FIGURE 21.31 Fluctuation of the willow's resistance coefficient value.

in this section is the presence of trees on flood areas and dense willow clusters on banks and the isles located within the main channel. The analysis of fluctuation of geometrical growth parameters of wicker is presented in Section 21.4.2 (Figure 21.30). On this basis, the calculation scenarios have been adopted. By means of numeric simulation results of maximum flow $Q = 6120$ m^3/s, a list of results generated by the water surface calculation system of all scenarios has been created for the cross-section at kilometer no. 371 [23]. This allowed for tracing of the temporal fluctuation of the water surface system due to overgrowth and development of wickers on isles (Figure 21.32). The modeled wicker isle overgrowth process has contributed to the backing up of the water surface system by above half a meter. The maximum backing up caused by the vegetation reached 64 cm and it occurred after 10 years. Thereafter, a fall of the water surface ordinate occurs, reaching 11 cm after 20 years (down to 53 cm). The high impact of isle vegetation is quite interesting due to the fact that they cover a surface of a mere 15.7 ha, which is approximately 10% of the entire high water level riverbed area, whereas the main channel occupies 42.5 ha, which is 26.7%. This confirms the important problem of the impact of vegetation, and particularly of its uncontrolled development, on the reduction of throughput capacity of a high water level riverbed.

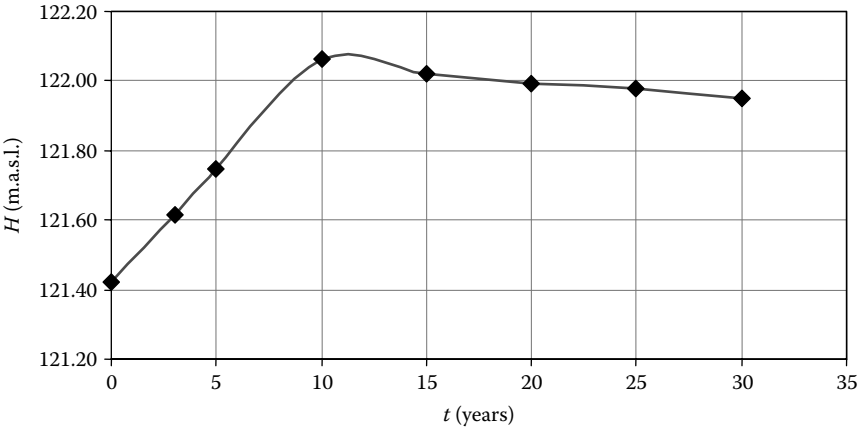

FIGURE 21.32 Forecast of water surface ordinates fluctuation of the Vistula River at the cros ssection at kilometer no. 371 $Q = 6120$ m^3/s due to overgrowing of isles with willow vegetation.

21.4.4 Environmental Impacts of River Vegetation

Water and swamp habitat vegetation create a complex in the transitory zone between water and land ecosystems. Through this complex, the transport and accumulation of allochtonous and autochtonous matter take place. In the course of the performed research, the significance of water, riverbank, and meadow vegetation has been proved. From the perspective of the environmental impacts of river vegetation, bank zone vegetation plays a particular role. The impact of riverbank strip vegetation may be brought down to embankments, riverbed temperature and brightness level adjustments, advantageous impact on water organisms, and the improvement of water quality [37]. As the most important functions of riverbank strips for the water environment and environmental protection, the following should be mentioned:

- Protection of banks and land from erosion and improvement of their stability by ground reinforcement with plant root systems and flow reduction, as well as wave suppression by overground plant elements
- Stabilization of bank collapsing by means of low vegetation, protection against the transporting of collapsed land on banks and flood zones by flood waters
- Increase in flow resistance and backing up of flood waters, and, as a consequence, higher water retention in the river valley
- Overshadowing of the river and thus reduction of its temperature, coupled with the rising of the oxygen saturation limit, its absorption, and content
- Improvement of water quality and self-purification capacity of the river—reduction of light exposure and therefore the suppression of the excessive growth of algae, as well as, on the other hand, the increase in entirely or partially underwater vegetation collecting pollutants from the water and intensifying the sedimentation process [1]
- Differentiating of thermal and light conditions in rivers by the appropriate disposition and interval length in the riverbank strips, creating both light-exposed and warmer, as well as darker and colder, river sections (which enriches the abiotic conditions, and thus the variety of flora and fauna [36])
- Creation of a sequence of biotopes for permanent or periodical fauna and its prey, shelter, lethargy, and hatching locations
- Enabling connection and exchange between biotopes located mainly in the bank areas
- Creation of shelter for species of vertebrates, birds, insects, and other animals and numerous plants threatened by extinction
- Formation of a local microclimate and actions influencing the reduction of evaporation on fields located near to riverbanks, water and land thermal specifics, as well as the intensity of wind
- Creation of a protective zone between the river and agricultural land within the valley, in order to decrease the flow of water into local pollution by retaining land erosion products and chemicals within the vegetation strip, as well as the absorption of pollutants dissolved into water via the rootstock [45]

The functions of riverbank strips are obviously diverse according to the location and plant development conditions. The pollutant purification function is the highest valued one (Figure 21.1). The well-developed rootstock and rhizome system provide a large-surface, the environment of which is inhabited by microorganisms contributing actively to the purifying of water. According to research performed in the United States, it has been proved that riverbank strips are capable of retaining above 80% of sediments reaching the riverbeds from surface erosion [37]. It has also been proved that such vegetation zones may reduce the nitrogen concentration by 78%–98% in surface waters and 68%–100% in ground waters. Tanner [55] carried out a nitrogen elimination efficiency comparison in systems with and without hydrophytes. According to this study, the impact of plants is particularly visible in terms of total nitrogen. Hydrophytes primarily contribute to the process of nitrification and denitrification, effecting the transformation of ammonium nitrogen into gaseous nitrogen (Figure 21.33).

Another research has also proved the impact of the vegetation strip width on the reduction of plant nutrient content [37]. In the case of a riverbank strip of 1.5 m width, the reduction of total phosphorus

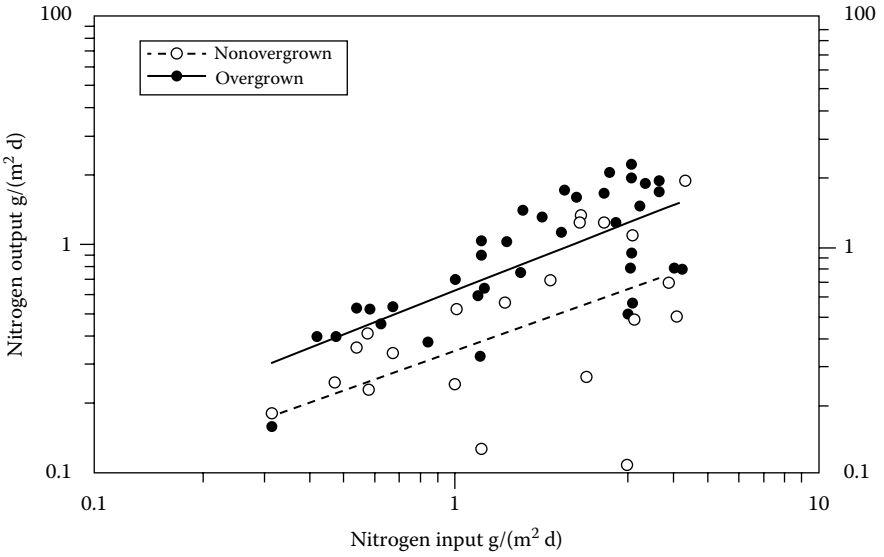

FIGURE 21.33 Comparison of total nitrogen input and output efficiency in systems without and with hydrophytes. (From Tanner, C.C., Plants as ecosystem engineers in subsurface-low treatment wetlands, in *7th International Conference on Wetland Systems for Water Pollution Control*, Lake Buena Vista, FL, Vol. 2, pp. 805–812, 2000.)

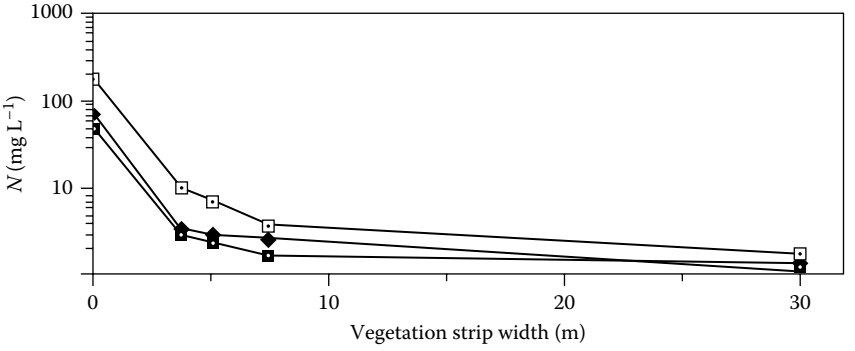

FIGURE 21.34 Impact of the vegetation strip width on the reduction of nitrogen. (From Petersen, R.C. Jr. et al., *Vatten*, 46(4), 244, 1990.)

in surface water amounted on average to approximately 6%, whereas in the case of a 9 m strip, it reached 93%. On the other hand, the research performed in the river basin of the Maryland River, in the case of 19 m wide riverbank strips, has indicated a reduction of 83% and 81% of nitrogen and phosphorus content in water, respectively [37]. According to the research performed by [45], most of the nitrogen reaching the riverbank strips is retained within the first 10 m of their width (Figure 21.34). While selecting the strip width, one should consider the basic rules of operation of a water and land ecosystem, so as to avoid hindering of the downflow of ice and prevent it from increasing the flood risk.

Fischer and Fischenich [14] presented general recommendations for corridor restoration and management:

- Corridors that maintain or restore natural connectivity are better than those that link areas historically unconnected.
- Continuous corridors are better than fragmented corridors.
- Wider corridors are better than narrow corridors.

- Riparian corridors are more valuable than other types of corridors because of habitat heterogeneity and availability of food and water.
- Several corridor connections are better than a single connection.
- Structurally diverse corridors are better than structurally simple corridors.
- Native vegetation in corridors is better than non-native vegetation.
- Practice ecological management of corridors; burn, flood, open canopy, etc., if it mimics naturally occurring historical disturbance processes.
- Manage the matrix with wildlife in mind; apply principles relative to the native plant and animal communities in the area.

While analyzing the impact of macrophytes on the improvement of the environmental status of rivers, one should also remember the possibilities of accumulation of heavy metals by macrophytes. Macrophytes have an advanced mechanism of active (selective) absorption of specific heavy metals. Metals are most commonly collected and used for vegetation purposes (copper and zinc). Passively absorbed metals include lead, cadmium, molybdenum, and nickel [60]. These elements do not participate in the plant metabolism and are thus unnecessary for their development; however, they may be at times strongly concentrated in macrophytes [7]. The absorption of heavy metals by macrophytes depends on numerous local factors (mineral and organic sediment content, pH and environment temperature). Nevertheless, the accumulation of heavy metals in water and riverbank plants is generally higher, compared with their accumulation in onshore vegetation.

21.5 Summary and Conclusions

Natural river floodplains have vital ecological functions in riverine landscapes. Effects of vegetation on flow are significant and cause reduction in the channel capacity. Generally, nonsubmerged and submerged conditions are distinguished, since flow phenomena become more complicated when the flow depth exceeds the height of plants. The correct assessment of the resistance coefficient and the description of phenomena associated with flows in riverbeds of various roughness, caused among others by the presence of vegetation, causes a lot of difficulties.

An additional feature, which must be considered in the analysis of the real flow conditions in a riverbed with vegetation on flood areas, is the dynamic character of the changes of vegetation. The transitory changes caused by the current include, for example, elastic deformation of plants, whereas seasonal changes are considered as season-specific variation of plant structures.

Water vegetation also create a complex in the transitory zone between water and land ecosystems. Through this complex, the transport and accumulation of allochtonous and autochtonous matter take place. In the course of the research performed, the significance of water, riverbank, and meadow vegetation has been proved. From the perspective of the environmental impacts of river vegetation, bank zone vegetation plays a particular role.

This chapter provides an overview of methods for determining the capacity of vegetation troughs. The analysis includes stiff and flexible vegetation. The chapter also presents an assessment of the development of impact of vegetation on flow resistance.

References

1. Anbumozhi, V., Radhakrishnan, J., and Yamaji, E. 2005. Impact of riparian buffer zones on water quality and associated management considerations. *Ecological Engineering* 24(5): 517–523.
2. Aberle, J., Järvelä, J., Schoneboom, T., and Dittrich, A. 2010. Flow resistance of rigid and flexible emergent vegetation revisited. *Proceedings of the 1st European IAHR Congress*, 4–6 May, Edinburgh, U.K.
3. Bavec, F. and Bavec, M. 2002. Effects of plant population on leaf area index, cob characteristics and grain yield on early maturing maize cultivars (FAO 100–400). *European Journal of Agronomy* 16: 151–159.

4. Bertram, H.U. 1985. Über den Abfluß in Trapezgerinnen mit extremer Böschungsrauheit. *Mitteilungen des Leichtweiss-Institut für Wasserbau*, Heft 86, Technische Universität Braunschweig, Brunswick, Germany.
5. Blomfeldt, E. 2008. Physically based vegetation flow resistance model: Modelling of a semi-urban stream in Nummela, Finland. Master's thesis, Department of Civil and Environmental Engineering, Helsinki University of Technology, Espoo, Finland, 92pp.
6. Bretschneider, H. and Schulz, A. 1985. Anwendung von Fließformeln bei naturnahem Gewässerausbau. *DVWK Schriften 72*, Kommissionsvertrieb Verlag Paul Parey, Hamburg und Berlin, Berlin, Germany.
7. Bragato, C., Brix, H., and Malagoli, M. 2006. Accumulation of nutrients and heavy metals in *Phragmites australis* (Cav.) Trin. ex Steudel and *Bolboschoenus maritimus* (L.) Palla in a constructed wetland of the Venice lagoon watershed. *Environmental Pollution* 144: 967–975.
8. Chow, V.T. 1959. *Open Channel Hydraulics*. McGraw-Hill Book Company Inc., New York.
9. Cowan, W.L. 1956. Estimating hydraulic roughness coefficients. *Agricultural Engineering* 37: 473–475.
10. Dittrich, A. and Järvelä, J. 2005. Flow-vegetation-sediment interaction. *Water Engineering Research* 6(3): 123–130.
11. DVWK, 1991. *Hydraulische Berechnung von Fließgewässern*, DK 551.51/54 Fließgewässer, DK 532.543 Hydraulik, DVWK—Merkblätter 220/1991, Kommissionsvertrieb Verlag Paul Parey, Hamburg und Berlin, Berlin, Germany.
12. Evers, P. 1983. *Untersuchung der Strömungsvorgänge in gegliederten Gerinnen mit extremen Rauheitsunterschieden*. Mitteilungen des Instituts für Wasserbau und Wasserwirtschat 45, Rheinisch-Westfälische Technische Hochschule, Aachen, Germany.
13. Fenzl, R.N. and Davies, J.R. 1964. Hydraulic resistance relationships for surface flows in vegetated channels. *Transactions of the American Society of Agricultural Engineers* 7: 46–51.
14. Fischer, R.A. and Fischenich, J.C. 2000. Design recommendations for riparian corridors and vegetated buffer strips. *EMRRP Technical Notes Collection* (ERDC TN-EMRRP-SR-31). U.S. Army Engineer Research and Development Center, Vicksburg, MS.
15. Hewlett, H.W.M., Boorman, L.A., and Bramley, M.E. 1987. Design of reinforced grass waterways. CIRIA Report No. 116, London, U.K.
16. Hicks, S. and Lascano, R. 1995. Estimation of leaf area index for cotton canopies using the LI-COR LAI-2000 plant canopy analyzer. *Agronomy Journal*, 87: 458–464.
17. Järvelä, J. 2002. Flow resistance of flexible and stiff vegetation: A flume study with natural plants. *Journal of Hydrology*, 269(1/2): 44–54.
18. Järvelä, J. 2005a. Effect of submerged flexible vegetation on flow structure and resistance. *Journal of Hydrology* 307(1–4): 233–241.
19. Järvelä, J. 2005b. Flow resistance in vegetated channels: Characteristics of natural woody vegetation. In: Lee, J.H.W. and Lam, K.M. (eds.), *Environmental Hydraulics and Sustainable Water Management*. Taylor & Francis, London, U.K., pp. 1667–1672.
20. Kaiser, W. 1984. Fließwiderstandsverhalten in Gerinnen mit durchströmten Ufergehölzen, *Wasserbau-Mitteilungen der TH Darmstadt,* Darmstadt, Germany, vol. 23.
21. Kaluza, T. 2009. Einfuss der Bewuchsentwicklung auf das Abflusseverhalten in Fließgewassern. *WasserWirtschaft* 4: 29–32.
22. Kaluza, T., Tymkow, P., and Strzelinski, P. 2012. Use of remote sensing for investigation of the structure of riparian shrubs. *Polish Journal of Environmental Studies* 21(1): 115–122.
23. Kaluza, T. 2010. Application of a 2-D flow model to the analysis of forest stability in the Vistula valley. In: Pawłowski, D. and Pawłowski, (eds.), *Environment Eengineering III*. CRC Press (Taylor & Francis Group), Boca Raton, FL, pp. 385–390.
24. Kenel, B. and Uehlinger, U. 1998. Effects of plant cutting and dredging on habitat conditions in streams. *Archives of Hydrobiology* 143(3): 257–273.

25. Klaassen, G.J. and Zwaard, J.J. 1974. Roughness coefficients of vegetated flood plains. *Journal of Hydraulic Research* 12: 43–63.
26. Klaassen, G.J. and Van Urk, A. 1985. Resistance to flow of floodplains with grasses and hedges. *Proceedings of the 21st IAHR Congress*, Vol. 3, Melbourne, Victoria, Australia.
27. Kouwen, N. and Li, R.M. 1980. Biomechanics of vegetative channel linings. *Journal of the Hydraulics Division* 104(HY6): 1085–1103.
28. Kouwen, N. and Unny, T.E. 1973. Flexible roughness in open channels. *Journal of the Hydraulic Division, ASCE* 99(HY5): 713–728.
29. Kouwen, N. 1992. A modern method for the design of grassed channels. *Journal of the Irrigation and Drainage Engineering, ASCE* 118(5): 733–743.
30. Kubrak, E., Kubrak, J., and Rowiński, P.M. 2012. Application of one-dimensional model to calculate water velocity distributions over elastic elements simulating Canadian waterweed plants (*Elodea canadensis*). *Acta Geophysica* 60(4): 1098–1119.
31. Kutja, V. and Hong, H.T. 1996. A numerical model for assessing the additional resistance to flow introduced by flexible vegetation. *Journal of Hydraulic Research* 34(1): 99–114.
32. Kozioł, A. and Miroslaw-Swiatek, D. 2009. Discharge assessment analysis of the Biebrza river in the lower basin. *Nauka Przyroda Technologies* 3(3, 88): 1–10.
33. Lalic, B. and Mihailovic, D.T. 2004. An empirical describing leaf-area density inside the forest for environmental modeling. *Journal of Applied Meteorology* 43: 641–645.
34. Lindner, K. 1982. *Der Strömungswiderstand von Pflanzenbeständen*, Mitteilungen Leichtweiss-Institut für Wasserbau, Technische Universität Braunschweig, Brunswick, Germany.
35. Makaske, B., Maas, G.J., van den Brink, C., and Wolfert, H.P. 2011. The influence of floodplain vegetation succession on hydraulic roughness: Is ecosystem rehabilitation in Dutch embanked floodplains compatible with flood safety standards? *AMBIO: A Journal of the Human Environment* 40(4): 370–376.
36. Mander, U., Hayakawa, Y., and Kuusemets, V. 2005. Purification processes, ecological functions, planning and design of riparian buffer zones in agricultural watersheds. *Ecological Engineering* 24: 421–432.
37. Mascutt, A.D., Harris, G.L., Bailey, S.W., and Davies, D.B. 1993. Buffer zones to improve water quality: A review of their potential use in U.K. agriculture. *Agriculture Ecosystems and Environment* 45(1–2): 59–77.
38. Mertens, W. 1989. Zur Frage hydraulischer Berechnungen naturnaher Fließgewässer, WasserWirtschaft 79. Heft 4.
39. Milbradt, P. and Schonert, T. 2006. *Ökologische Modellkomponenten in hydrodynamischen Simulationsmodellen, Wasserbaukolloquium. Strömungssimulation im Wasserbau, Dresdener Wasserbauliche Mitteilungen Heft* Vol. 32, pp. 179–192.
40. Ministry of Construction (MOC). 1997. *Proposed Guidelines on the Clearing and Planting of Trees in Rivers*. MOC, Sankaido, Tokyo.
41. Miroslaw-Swiatek, D., Kubrak, J., and Chormański, J. 2006. Steady 1 D water surface model of natural rivers with vegetated floodplain: An application to the Lower Biebrza. In: *Proceedings of the Second International Conference on Fluvial Hydraulics—River Flow 2006*, Vol. 1. IAHR, Lisbon, Portugal, pp. 545–553.
42. Petryk, S. and Bosmajian, G. 1975. Analysis of flow through vegetation. *Journal of the Hydraulics Division, ASCE*, 101(HY7): 871–884.
43. Pasche, E. 1984. *Turbulenzmechanismen in naturnahen Fließgewässern und die Möglichkeiten ihrer mathematischen Erfassung*. Mitteilungen des Instituts für Wasserbau und Wasserwirtschat. Heft 52, Rheinisch-Westfälische Technische Hochschule, Aachen, Germany.
44. Pasche, E. and Deussfeld, N. 2003. Hydro- und Morphodynamik in Seegraswiesen. *HANSA International Maritime Journal* 5: 67–73.
45. Petersen, R.C. Jr., Petersen, L.B.M., and Lacoursiere, J.O. 1990. Restoration of lowland streams: The building block model. *Vatten* 46(4): 244–249.

46. Plate, E.J. and Quraishi, A.A. 1965. Modeling of velocity distribution inside and above tall crops. *Journal of Applied Meteorology* 4: 400–408.
47. Querner, E. 1993. *Aquatic Weed Control within an Integrated Water Management Framework*, CIP—Gegevens Koninklijke Bibliotheek, Den Haag, the Netherlands.
48. Rickert, K. 1986. *Der Einfluss von Gehölzen auf die Lichtverhältnisse und das Abflußverhalten in Fliessgewässern*. Der Mitteilungen des Instituts für Wasserwirtschat, Hydrologie und Ladwirtschaften Wasserbau der Universität Hannover. Heft 61.
49. Ritterbach, E. 1991. Wechselwirkungen zwischen Auenökologie und Fließgewässerhydraulik und Möglichkeiten der integrierenden computergestützten Planung. *Mitteilungen Institut für Wasserbau und Wasserwirtschaft*, RWTH Aachen, Heft 80.
50. Rouvé, G. 1987. Hydraulische Probleme beim naturnahen Gewässerausbau, Ergebnisse aus dem Schwerpunktprogramm, Anthropogene Einflüsse auf hydrologische Prozesse, Band 2, Deutsche Forschungsgemeinschaft, Forschungsbericht. VCH, Weinheim, Germany.
51. Schnauder, I. and Sukhodolov, A.N. 2012. Flow in a tightly curving meander bend: Effects of seasonal changes in aquatic macrophyte cover. *Earth Surface Processes and Landforms* 37: 1142–1157.
52. Stephan, U. and Gutknecht, D. 2002. Hydraulic resistance of submerged flexible vegetation. *Journal of Hydrology* 269(1–2): 27–43.
53. Szoszkiewicz, K., Ferreira, T., Korte, A., Baattrup-Pedersen, J., Davy-Bowker, M., and O'Hare. 2006. European river plant communities: The importance of organic pollution and the usefulness of existing macrophyte metrics. *Hydrobiologia* 566: 211–234.
54. Szporak, S., Mirosław-Świątek, D., and Chormański, J. 2008. The flood extent in the lower Biebrza basin calculated by the 1D flow model for different land use scenarios. *Annals of Warsaw University of Life Sciences—SGGW Land Reclamation* 40: 45–54.
55. Tanner, C.C. 2000. Plants as ecosystem engineers in subsurface-low treatment wetlands. In: *7th International Conference on Wetland Systems for Water Pollution Control*, Lake Buena Vista, FL, Vol. 2, pp. 805–812.
56. Temple, D.M. 1987. Closure to velocity distribution coefficients for grass-lined channels. *Journal of Hydraulic Engineering* 113(9): 1221–1226.
57. Tymiński, T. and Kaluza, T. 2012. Investigation of mechanical properties and flow resistance of flexible riverbank vegetation. *Polish Journal of Environmental Studies* 21(1): 201–207.
58. USSCS. 1954. *Handbook of Channel Design for Soil and Water Conservation*. Publication SCSTP61, US Department of Agriculture, Washington, DC.
59. Vischer, D. and Oplatka, M. 1998. Der Strömungswiderstand eines flexiblen Ufer-und Vorlandbewuchses, *WasserWirtschaft* 88, Heft 6.
60. Vymazal, J. 2003. Distribution of iron, cadmium, nickel and lead in constructed wetland receiving municipal sewage. In: Vymazal, J. (ed.), *Wetlands–Nutrients, Metal and Mass Cycling*. Backhuys Publishers, Leiden, the Netherlands, pp. 341–363.
61. Ward, D., Holmes, N., and Jose, P. 1995. *The New Rivers and Wildlife Handbook*. The Royal Society for the Protection of Birds, Bedford, U.K.

22

Regional Flood Frequency Analysis

Ataur Rahman
University of Western Sydney

Khaled Haddad
University of Western Sydney

Saeid Eslamian
Isfahan University of Technology

AUTHORS

Ataur Rahman completed his PhD from Monash University in Australia, supervised by Professor Russell Mein, and master's in hydrology from University College Galway, Ireland. He completed his sabbatical in Cornell University and the University of Newcastle in 2010. He is currently a senior lecturer in water engineering in the University of Western Sydney, Australia. He has over 20 years of experience in water research. His research interests includes flood hydrology, urban hydrology, and environmental risk assessment. He received the G. N. Alexander Medal from the Institution of Engineers Australia in 2002. He has published over 200 research papers, book chapters, and technical reports in water and environmental engineering fields. He has been heavily involved in the preparation of the forthcoming revised version of Australian Rainfall and Runoff—A Guide to Flow Estimation.

Khaled Haddad is a researcher in water engineering in the University of Western Sydney and has 10 years of experience in this field. His research is focused on regional flood frequency analysis with

a particular emphasis on uncertainty in regional flood estimation. He has published over 50 refereed papers and research reports in various aspects of statistical hydrology. Khaled has been heavily involved in the current revision of Australian Rainfall and Runoff—A Guide to Flow Estimation.

Saeid Eslamian received his PhD from University of New South Wales, Australia, with Professor David Pilgrim. He was a visiting professor in Princeton University, United States, and ETH Zurich, Switzerland. He is currently an associate professor of hydrology in Isfahan University of Technology. He is the founder and chief editor of the *Journal of Flood Engineering* and *International Journal of Hydrology Science and Technology*. He has published more than 200 publications mainly in statistical and environmental hydrology and hydrometeorology.

PREFACE

Regional flood frequency analysis (RFFA) is essentially a data-based approach that attempts to substitute space for time to enable design flood estimation at sites with little or no recorded flood data. An RFFA method consists of three principal steps: (1) data preparation, (2) formation of regions, and (3) development of regional estimation models.

This chapter intends to provide a theoretical understanding of various RFFA techniques to researchers and practicing hydrologists. We have attempted to cover essential aspects of RFFA, which include (1) data requirements, (2) selection of probability distributions, (3) formation of regions, (4) various forms of regional estimation equations, (5) validation of RFFA models, (6) RFFA in arid regions, and (7) impact of climate change on RFFA.

We would like to acknowledge the anonymous reviewers for making constructive comments and suggestions, which have improved the materials presented in this chapter. We would also like to acknowledge the members of our family for supporting us in writing this chapter.

22.1 Introduction

Regional flood frequency analysis (RFFA) is widely used to estimate design floods at ungauged or poorly gauged catchments. The success of any RFFA depends on the quantity and quality of gauged streamflow data availability to form homogeneous regions. An RFFA technique is intended for quick design flood estimation where the resolution of a complete streamflow hydrograph is not justified due to time and budgetary constraints. An RFFA method consists of three principal steps (as shown in Figure 22.1): (1) data preparation, selection of a set of gauged catchments, streamflow, climatic and catchment characteristics data preparation, and at-site quantile estimation; (2) formation of regions and formation of homogeneous regions from the available streamflow gauging stations; and (3) development of regional estimation models, and derivation of prediction equations to estimate flood statistics and quantiles.

22.2 Basics of Regional Flood Frequency Analysis

RFFA facilitates extrapolation of flood characteristics information from gauged to ungauged catchments. RFFA attempts to compensate for insufficient temporal characterization of large flood behavior by exploiting the spatial coherence of hydrological variables. RFFA can be used to enhance the reliability of quantile estimates at gauged sites or to obtain quantile estimates at ungauged sites. In an index type of RFFA technique, it is assumed that a region is a set of gauging sites whose flood frequency behavior is homogeneous in some quantifiable manner. A homogeneous region may be defined as a group of sites whose standardized flood frequency curves are similar to within a certain margin of sampling variability.

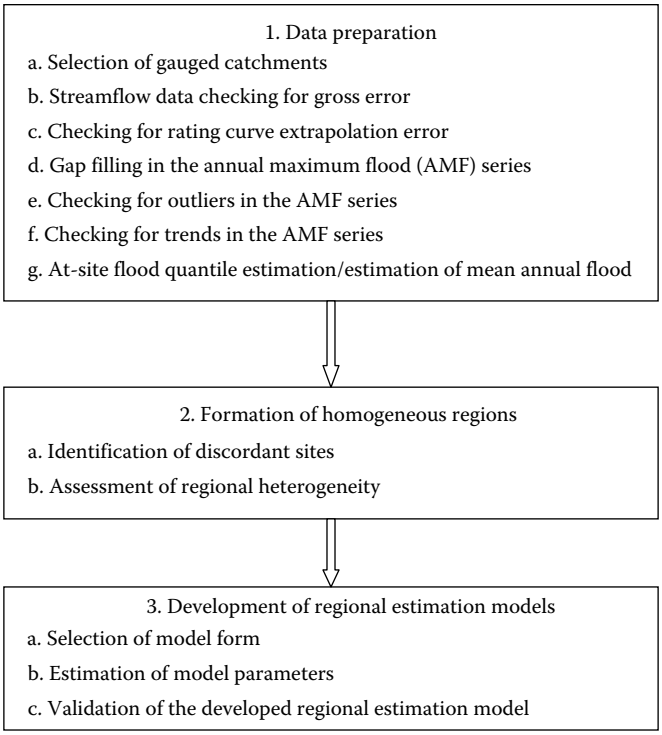

FIGURE 22.1 Steps in the development of an RFFA technique.

Cunnane [16,17] notes that even with RFFA techniques that make no explicit assumptions about homogeneity, it must be expected that the gains in using regional rather than at-site estimation will be greater if the region of interest is homogeneous. In the presence of extreme regional heterogeneity, at-site estimates are preferable to regional estimation [43,50]. This is particularly true for a catchment whose behavior differs most from the average catchment of the region [16]. It has been found that small departures from perfect homogeneity do not appreciably reduce the beneficial aspects of RFFA [50,51].

In defining homogeneous regions, a trade-off needs to be made between including more information from additional catchments and maintaining a high degree of similarity. If more sites are added to a region, more knowledge about flood characteristics is available; however, if the added sites are hydrologically dissimilar, the additional information does not result in more precise flood quantile estimation.

22.3 Data Requirements and Data Preparation

The challenge in preparing a database for developing an RFFA technique lies in maximizing the amount of useful information contained in the flood data, while minimizing the noise in the data, which often are present in varying degrees in streamflow data. In any RFFA study, the preparation of the database demands significant resources, time, and expertise. The development of RFFA technique in any given region largely depends on the quantity and quality of gauged streamflow data on which the RFFA is built on. In relation to quantity, there should be a sufficient number of gauged catchments available in the region to capture the hydrological and catchment variability existing within the region. The selected catchments should represent adequate spatial coverage. In a region with highly variable hydrology, a greater number of gauged catchments should ideally be available to form the region. The selected catchments should not be excessively large sized as RFFA techniques are primarily intended for application to small- to medium-sized ungauged catchments. For example, in Australia an upper limit

of 1000 km^2 has often been recommended [37]. The individual site should have enough record length to generate at-site flood quantiles with an acceptable level of accuracy as at-site flood quantiles are an important element in any RFFA. A shorter record length produces at-site flood quantiles being affected by a high degree of sampling variability. Furthermore, a region should have enough number of sites, so that it can deliver statistically meaningful prediction equations as well as an opportunity to carry out independent validation of the developed RFFA technique. Hence, the selection of a cutoff record length is an important step in any RFFA study; the record length should be as long as possible while retaining enough sites in the region.

The quality of streamflow data is equally important as "noisy" data do not add much useful information, but rather this distorts regional statistics. Streamflow data can suffer from a wide variety of errors. The catchment condition should remain relatively unaltered during the period of streamflow data availability. A catchment condition can change dramatically due to factors such as the clearing of forest, construction of a dam, urbanization, and change of agricultural practice. Another important source of error in streamflow data arises from rating curve extrapolation error [29]. Streamflow gauges being affected by a high degree of rating curve extrapolation error can be identified with some extra efforts such as examination of the rating history of the gauging station. The presence of too many gaps in the recorded streamflow data makes some of the gauged catchments unsuitable for inclusion in the RFFA model data set. An appropriate method such as regression analysis should be adopted to infill the gaps in the streamflow data series where possible. Comparison of daily and monthly maximum flow series often assists in filling some of the existing gaps in the annual maximum flood series data [29]. The streamflow data should be checked for trends. The impact of climate variability can often be minimized by selecting a longer period of data representing an equal number of dry and wet episodes; however, the impact of climate change is more difficult to deal with, for which nonstationary RFFA methods need to be adopted [49].

22.4 Selection of Probability Distribution for At-Site Flood Quantile Estimation

The selection of an appropriate probability distribution and associated parameter estimation procedure is of prime importance in RFFA as this can affect the accuracy of derived at-site flood quantiles. This subject has received notable attention by researchers [6,16,30,54,56,60,77,83]. Cunnane [16] summarized the distributions commonly used in hydrology, mentioning 14 probability distributions.

The selection of an appropriate distribution for a particular application cannot normally be made on a physical basis. Cunnane [16] noted that the distribution can only be supported by empirical data, and thus empirical suitability plays a much larger role in distribution choice than a priori reasoning [16]. WMO [86] reports that in many countries the selection of an annual maximum distribution is actually not made in an objective manner, no particular method of parameter estimation is preferred, and the graphical method is as frequently or even more used as any other method.

In some countries, a common distribution has been chosen to achieve uniformity between different design agencies. The Interagency Advisory Committee on Water Data [38] and the Institution of Engineers Australia [37] recommended the log Pearson type 3 (LP3) distribution for use in United States and Australia, respectively. Other distributions that have received considerable attention include extreme value types 1, 2, and 3; generalized extreme value; Wakeby; generalized Pareto, two-component extreme value, and log-logistic.

The selection of an appropriate method of estimating the parameters of a given probability distribution for a given data set is important. There are various methods for this, including the methods of moments (MOM), maximum likelihood (MLE), *L* moments, *LH* moments, and Bayesian methods. Although the MOM is widely adopted in practice, it has a serious limitation, that is, this gives equal weight to small values that do not constitute floods and to the larger observations. Also, in the MOM, the higher moments (e.g., coefficient of variation and skewness) are much affected by outliers and extremes

in the data series. To overcome the limitations associated with the MOM, method of *L* moments has been proposed that are less affected by extremes in the data series [33,35]. The method of *LH* moments provides more weighting to the larger values in the flood series and hence often provides better fits to the upper tail of the distribution [84].

As an alternative to the traditional MOM and MLE, Bayesian methods have also been proposed where both the likelihood function and the parameters to be estimated are described by probability distributions [30,43–46,48]. One of the limitations of the Bayesian approach is that complex models cannot be processed in a closed form because of the difficulty in computing the normalization factor. In such cases, simulation-based Monte Carlo techniques such as the Markov chain Monte Carlo (MCMC) approach using the Metropolis algorithm is used [47].

22.5 Method of *L* Moments

Hosking [33] defined *L* moments to be linear combinations of the probability-weighted moments (PWMs), introduced by Greenwood et al. [24]. For a random variable *X*, PWMs may be defined as

$$M_{p,r,s} = E\left[X^p \left(F_X(x)\right)^r \left(1 - F_X(x)\right)^s \right] \tag{22.1}$$

where *p, r,* and *s* are real numbers. When $r = s = 0$, Equation 22.1 represents the ordinary product moment about the origin of order *p*. *L* moments are defined by

$$\lambda_r = E\left[XP^*_{r-1} F_X(x) \right] \tag{22.2}$$

where $P^*_r(\cdot)$ is the *r*th shifted Legendre polynomial. *L* moments may be expressed in terms of PWMs:

$$\lambda_{r+1} = \sum_{k=0}^{r} p^*_{r,k} \beta_k \tag{22.3}$$

where $\beta_k = M_{1,k,0}$

and

$$p^*_{r,k} = (-1)^{r-k} \binom{r}{k} \binom{r+k}{k} \tag{22.4}$$

L moment ratios, analogous to product moment ratios, are the following quantities:

$$\tau_r = \frac{\lambda_r}{\lambda_2}, \quad r = 3,4,\ldots \tag{22.5}$$

L moments are more convenient than PWMs in that they are more easily interpretable as measures of distributional shape. For example, λ_1 is the mean of the distribution, a measure of location; λ_2 is the measure of scale; and τ_3 and τ_4 are measures of skewness and kurtosis, respectively. *L* $C_v = \tau = \lambda_2/\lambda_1$ is analogous to the conventional coefficient of variation C_v.

The main advantages of *L* moments (over conventional moments) are that *L* moments, being linear functions of the data, are subject to less bias, suffer less from the effects of sampling variability, and are more robust than conventional moments to extremes in the data. Conventional moment estimators such as the sample variance and sample coefficient of skewness require squaring and cubing the observations, respectively, which cause them to give greater weight to the observations far from the mean, thus introducing a substantial bias and variance [33,77].

The L moments are defined previously for a probability distribution, but in practice, these are generally estimated from a finite sample. Given $x_1 \le x_2 \le x_3 \le \ldots \le x_n$ is a finite ordered sample, the unbiased estimator l_r of λ_r is given by

$$l_{r+1} = \sum_{k=0}^{r} p^{*}_{r,k} b_k \tag{22.6}$$

where

$$b_r = \frac{1}{n} \sum_{j=1}^{n} \frac{(j-1)(j-2)\cdots(j-r)}{(n-1)(n-2)\cdots(n-r)} x_j \tag{22.7}$$

The distributional parameters θ_1, θ_2,…,θ_p are related to λ_1, τ, τ_3,…,τ_p and are estimated by the corresponding sample L moments. From many research studies [56,64], it has been found that index flood procedures, coupled with L moments, yield robust and accurate flood quantile estimation.

Hosking and Wallis [34] proposed three statistics based on L moments to be used in RFFA: (1) a discordancy measure D that identifies the sites that are grossly discordant with the data set as a whole, (2) a heterogeneity measure H that is used to assess the degree of heterogeneity in a proposed region, and (3) a Z statistic that is used to judge the goodness of fit of a candidate probability distribution for a given region. Hosking and Wallis [34] suggested that a region should be considered "acceptably homogeneous" if $H < 1$, "possibly heterogeneous" if $1 \le H < 2$, and "definitely heterogeneous" if $H \ge 2$. The criteria $H = 1$ and $H = 2$, though somewhat arbitrary, were found to be useful by Hosking and Wallis [34] in identifying homogeneous regions. The test is based on the assumption that the data are independent both serially and between sites, an assumption unlikely to be exactly satisfied in practical situations. The amount of serial correlation likely to exist in annual flood series is small and unlikely to affect the reliability of quantile estimates.

22.6 Selection of Predictor Variables in RFFA

In an RFFA study, the initial choice of climatic and physical catchment characteristics (catchment characteristics) is important. There is, however, no entirely objective method for doing this. Many catchment characteristics are highly correlated, and the inclusion of highly correlated variables in prediction equations does not add much new information; it can also cause problems in statistical analysis (e.g., multicollinearity).

Most commonly adopted catchment characteristics used in RFFA studies are listed in Table 22.1. There is no entirely objective method of selecting catchment characteristics for an RFFA study. However, the following guidelines may help in making a reasonable selection [65]:

1. The characteristics should have a plausible role in flood generation.
2. They should be unambiguously defined.
3. Characteristics should be easily obtainable. When a simpler characteristic and a complex one are correlated and have similar effects, the simpler characteristic should be chosen.
4. If a derived/combined characteristic is used, it should have a plausible physical interpretation.
5. The selected characteristics should not be highly correlated because this often results in unstable parameters in regression analysis.
6. The prediction performance of a characteristic in other RFFA studies in similar hydrological regions should be taken into account as this will give some general idea regarding the importance of a characteristic.

From the initially selected predictor variables, a number of statistical criteria can be used to select the final set of predictor variables in the estimation model. These criteria include Bayesian information criterion (BIC), Akaike information criterion (AIC), and Anderson–Darling criterion [32]. Catchment

TABLE 22.1 Most Commonly Used Climatic and Catchment Characteristics Used in RFFA

Category	Name of Predictor Variable
Climatic characteristics	Rainfall intensity with an appropriate duration and ARI
	Mean annual rainfall
	Mean annual snowfall
	Mean annual evaporation
	Mean annual number of rain days
Morphometric characteristics	Catchment area
	Main stream slope
	Stream density
	Main stream length
	Elongation ratio
	Circularity index
	Bifurcation ratio
	Stream order
	Stream junction
	Average land slope
Catchment cover and land use characteristics	Percent forest cover
	Percent urbanization
Geological and soil characteristics	Soil type
	Soil infiltration index
Storage characteristics	Surface storage index
Location characteristics	Latitude
	Longitude
	Distance from coast

area often comes as the principal predictor variable followed by design rainfall intensity of a certain duration and average recurrence interval (ARI). Other predictor variables are often included in the model to enhance the accuracy of model prediction.

22.7 Formation of Regions in RFFA

22.7.1 Fixed Region Based on Administrative Boundary

In RFFA, regions can be formed in geographical or catchment attributes space as illustrated in Figure 22.2. In many previous applications, regions have been defined based on state/political boundaries. In this approach, homogeneous regions are spatially contiguous and are often defined on the basis of administrative, political, or geographical boundaries. For example, Matalas et al. [55] identified 14 homogeneous geographical regions in the United States. Panu et al. [63] divided the island of Newfoundland, Canada, into two geographical regions. In some cases, these regions have been supported by the plot of the regression residuals [39,79]. The problem with this type of fixed regions is that at state/regional boundaries, two different methods can provide quite different flood estimates. Merz and Bloschl [53] and Skoien et al. [74] showed that geographical proximity is a better predictor in RFFA than other catchment attributes.

22.7.2 Regions in Catchment Characteristics Data Space

Regions can be identified in catchment characteristics data space using cluster analysis [1,7,10,26, 57,61,79,80] and many other multivariate statistical techniques such as Andrews curves [59], principal component analysis [65], and canonical correlation analysis [4,61]. One of the limitations with this type

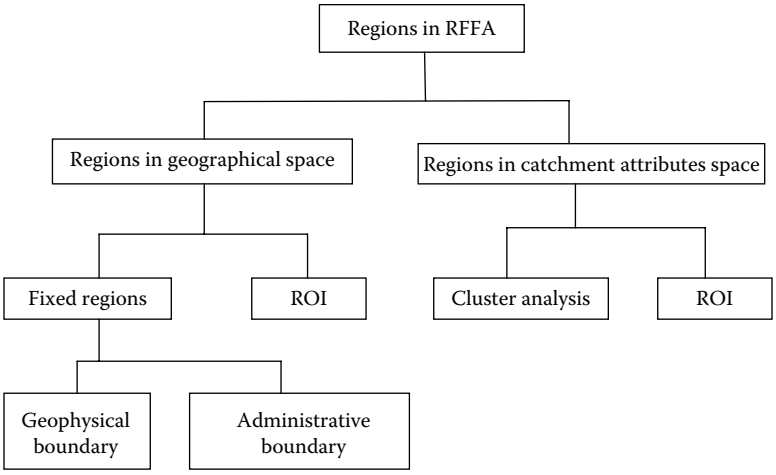

FIGURE 22.2 Methods of forming regions in RFFA.

of region is that a correct method of assigning an ungauged catchment to a "homogeneous" region needs to be formulated, which is often problematic. If the ungauged catchment is assigned to the wrong region/group, the resulting flood estimation is likely to be associated with a high degree of error.

22.7.3 Cluster Analysis

Cluster analysis is often adopted for identifying groups in data. It puts a set of objects into a set of mutually exclusive and exhaustive groups; objects in a group are relatively similar to one another, while objects in different groups are relatively dissimilar.

In cluster analysis, standardization of the data is recommended because differences in the units used for measuring different attributes can arbitrarily affect the similarities among objects. Standardization also makes attributes contributing more equally to the similarities among objects. The following standardization function, which gives zero mean and unit variance, is commonly used in cluster analysis:

$$Z_{ij} = \frac{X_{ij} - \overline{X}_i}{s_i} \tag{22.8}$$

where

Z_{ij} is the standardized value for jth case of the ith variable
X_{ij} is the corresponding original value
$\overline{X}_i$ and s_i are, respectively, the mean and standard deviation of the ith variable

Clustering methods may be divided into two main groups: hierarchical and optimization. Hierarchical methods consist of two classes: (1) the agglomerative method, which proceeds by a series of successive fusions of the n individuals into groups and (2) the divisive method that separates the n individuals successively into finer groupings. The optimization method produces a partition of the individuals for a particular number of groups, by either minimizing or maximizing some numerical criterion. The hierarchical methods represent clusters by a tree called dendrogram. Of all the methods, agglomerative hierarchical methods are most widely used. There are several agglomerative hierarchical techniques:

- Between-groups linkage or unweighted pair-group method using arithmetic averages. This defines the distance between two clusters as the average distance between all pairs of cases, the pairs being formed from cases in each cluster.

- Within-groups linkage. This combines clusters, so that the average distance between all cases in the resulting cluster is as small as possible.
- Nearest neighbor or single linkage. Here, the distance between two clusters is the distance between their two closest points.
- Farthest neighbor or complete linkage. Here, the distance between two clusters is the distance between their two farthest points.
- Ward's method. In this method, the two clusters that are merged are those that result in the smallest increase in the overall sum of the squared within-cluster distance.

The problem in selecting a linkage method for a given application is that different methods, applied to the same data set, often produce significantly different groupings. In order to obtain meaningful results, it seems to be appropriate to use several methods with the expectation that, if any natural groupings exist in the data, most of the methods will result in almost similar groupings.

A resemblance coefficient is used to measure the degree of similarity/dissimilarity between each pair of objects. Several resemblance coefficients have been proposed and use of different coefficients may lead to different groupings with the same data matrix. The difference in results arising from using different resemblance coefficients may be reduced to some extent by using the standardized data matrix. The best possible options seem to be using standardized data matrix and several resemblance coefficients and examine how much difference is found in the obtained groupings. If natural groupings do exist in the data, several methods will give similar results. The squared Euclidean distance and cosine coefficients have been found useful in hydrology by other investigators [59,65].

22.7.4 Region of Influence Approach

Since hydrological characteristics do not change abruptly across state boundaries, it is desirable to avoid fixed boundaries in the formation of region. Regionalization without fixed boundary was performed by Acreman and Wiltshire [2], and based on their research, the region of influence (ROI) approach was introduced by Burn [8,9] where each site of interest (i.e., catchment where flood quantiles are to be estimated) has its own region. This way the defined regions may overlap and gauged sites can be part of more than one ROI for different sites of interest. The great advantage of the ROI approach is that it is not bounded by geographical regions often based on political boundaries such as state lines, and it thus avoids discontinuities at the boundaries of regions. In the ROI approach, a region can be formed based on the proximity in geographical or catchment characteristics space. The ROI approach was enhanced by adding a hierarchical method by Zrinji and Burn [88]. The ROI approach has been adopted in the United Kingdom [36,40,41] and in Australia [21,27,32,67] for RFFA.

22.8 Assessment of the Degree of Homogeneity

Once a region is proposed, it is necessary to check its degree of regional heterogeneity. The degree of heterogeneity of a proposed region is generally judged on the basis of a dimensionless coefficient of the annual maximum flood series, such as the coefficient of variation, coefficient of skewness, or similar measures [1,11,13,18,34,52,85]. The relative power of a number of heterogeneity tests has been investigated by Viglione et al. [82]. The heterogeneity measure by Hosking and Wallis [34], based on the *L* moments, is widely used in RFFA.

22.9 Probabilistic Rational Method

The rational method is often regarded as a deterministic representation of the flood generated from an individual storm and is generally applicable to only small catchments up to about 25 km^2. However, its statistical form known as the probabilistic rational method (PRM) may be regarded as a form of RFFA

method, with catchment area and design rainfall intensity as predictor variables, and is applicable to much larger catchments up to maximum areas used in its derivation. In the PRM, the peak flow for a selected ARI is estimated from an average rainfall intensity of the same ARI. The central component of the PRM is a runoff coefficient; the use of this coefficient involves a simple linear interpolation over the geographic space between the nearest contour lines of the runoff coefficients, which assumes that geographical proximity is a surrogate for hydrological similarity, an assumption that is unlikely to be satisfied in many situations.

The PRM is represented by

$$Q_Y = 0.278 C_Y I_{tc,Y} A \tag{22.9}$$

where

Q_Y is the peak flow rate (m^3/s) for an ARI of Y years
C_Y is the runoff coefficient (dimensionless) for an ARI of Y years
$I_{tc,Y}$ is the average rainfall intensity (mm/h) for a design duration equal to the time of concentration t_c (h) and an ARI of Y years
A is the catchment area (km^2)

The runoff coefficient C_Y is estimated from the frequency analysis of flood peaks of the gauged catchments and design rainfall intensity of selected duration and the same ARI. Runoff coefficients are then plotted for the region for a reference ARI such as C_{10}. An example is shown in Figure 22.3 for eastern New South Wales in Australia. The value of C_Y can then be estimated from $C_Y = FF_Y \times C_{10}$ where FF_Y is frequency factor for a given ARI and C_{10} is the frequency factor for 10-year ARI. The FF_Y values are derived from the results of the flood frequency analysis of the gauged catchments in the region. As an example, the values shown in Table 22.2 were derived from 107 gauged catchments in New South Wales in Australia [68].

The design rainfall intensity $I_{tc,Y}$ is associated with time of concentration t_c. There are several equations available that can be used to estimate t_c. It is important that the same equation be used in the derivation of the runoff coefficients and during its application. The following equation was suggested in Australian Rainfall and Runoff [37], which was also adopted by Rahman et al. [68]:

$$t_c = 0.76 A^{0.38} \tag{22.10}$$

where

t_c is the time of concentration (h)
A is area of catchment (km^2)

Although PRM is widely used in practice due to its simplicity, it has several limitations. The isopleths of the runoff coefficient ignore the existence of watercourses. Rahman et al. [68] found that quantile regression technique (QRT) is preferable to PRM for New South Wales catchments in Australia.

22.10 Index Flood Method

The key assumption in the index flood method [18] is that the distribution of floods at different sites within a homogeneous region is the same except for a site-specific scaling factor, which is called the index flood. In practice, mean or median annual maximum flood is generally taken as the index flood. Homogeneity with regard to the index flood relies on the concept that the standardized flood peaks from individual sites in the region follow a common probability distribution with identical parameter values. The index flood method had been criticized on the grounds that the coefficient of variation of the flood series C_v may vary approximately inversely with catchment area, thus resulting in flatter flood frequency curves for larger catchments. This had particularly been noticed in the case of humid

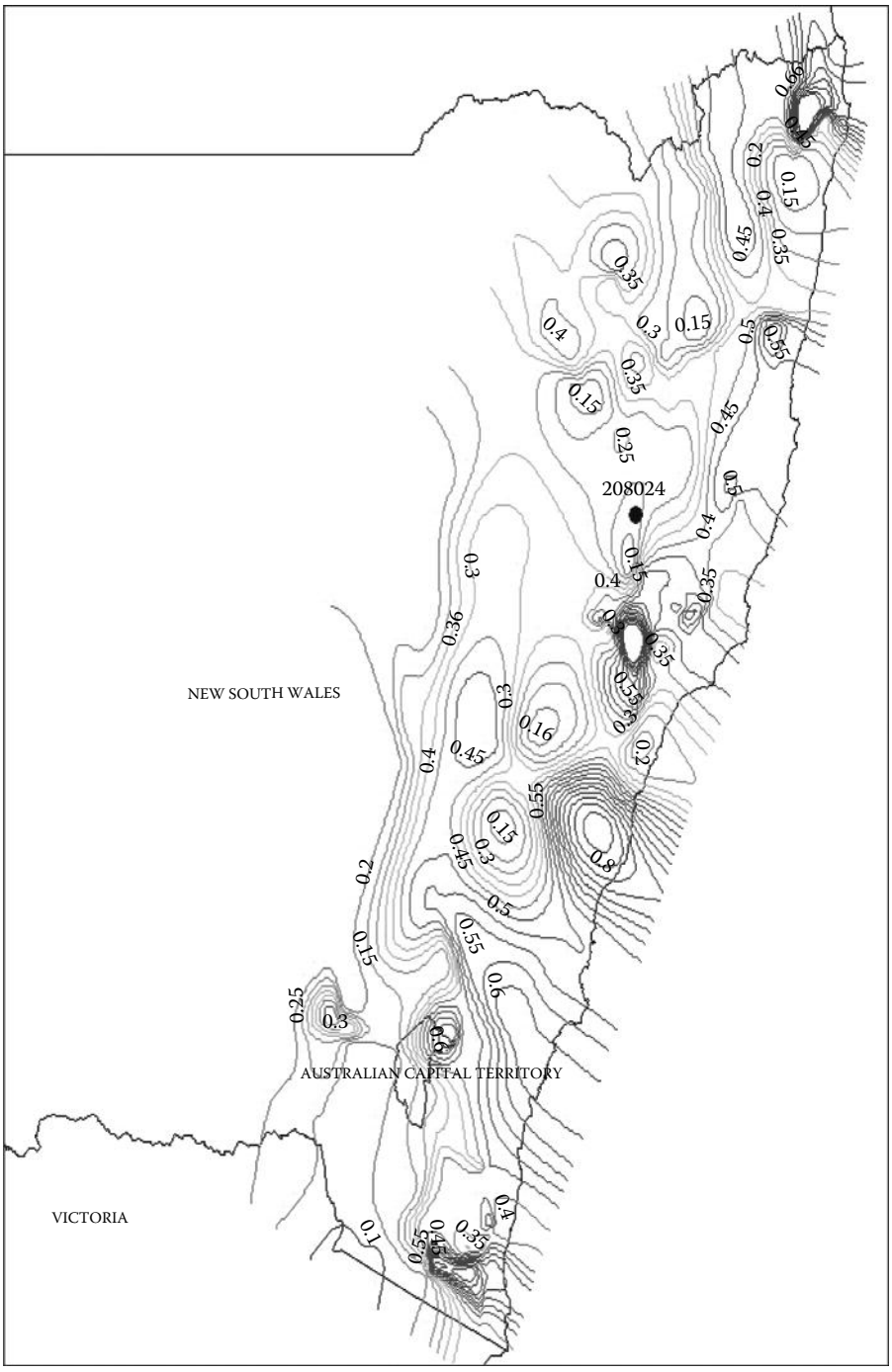

FIGURE 22.3 An example map of runoff coefficients (C_{10}) for the state of New South Wales in Australia. (From Rahman, A. et al., Regional flood methods, Technical Report, Engineers Australia, Canberra, Australian Capital Territory, Australia, 2012.)

TABLE 22.2 Frequency Factor Values (FF_Y) for Eastern New South Wales (Australia)

ARI (years)	2	5	10	20	50	100
FF_Y	0.37	0.73	1.00	1.20	1.45	1.58

Source: Rahman, A. et al., Regional flood methods, Technical Report, Engineers Australia, Canberra, Australian Capital Territory, Australia, 2012.

catchments that differed greatly in size [5,70]. Since the introduction of *L* moments based index flood method [34], this has become a standard RFFA method in many countries. Various aspects of the index flood method have been widely researched [4,11,12,66,78].

In the index flood method, a flood quantile is estimated using the following equation:

$$Q_T = \text{MAF} \times Z_T \tag{22.11}$$

where

Q_T is the *T*-year flood quantile
MAF is the mean annual flood in m^3/s
Z_T is the regional growth factor for *T*-year flood

The MAF is estimated from the prediction equation developed for a given region where MAF is expressed as a function of easily measurable climatic and catchment characteristics such as catchment area, rainfall intensity, and stream density. The regional growth factors for various ARIs are estimated for a homogeneous region and are assumed to be applicable to all the catchments in the homogeneous region.

22.11 Quantile Regression Technique

United States Geological Survey (USGS) proposed a QRT [81] where a large number of gauged catchments are selected from a region and flood quantiles are estimated from recorded streamflow data, which are then regressed against catchment variables that are most likely to govern the flood generation process.

The QRT can be expressed as follows:

$$Q_T = aB^bC^cD^d \ldots \tag{22.12}$$

where

B, C, D, … are catchment characteristics variables
Q_T is the flood magnitude with *T*-year ARI (flood quantile)
a, b, c, … are regression coefficients

In most practical applications of the QRT, Equation 22.12 is linearized through a logarithmic transformation:

$$\log(Q_T) = \log(a) + b\log(B) + c\log(C) + \cdots \tag{22.13}$$

This method is not based on a constant coefficient of variation (C_v) of annual maximum flood series in the region like the index flood method. It has been noted the QRT can give design flood estimates that do not vary smoothly with ARI; however, hydrological judgment can be exercised in situations such as these when flood frequency curves need to be adjusted to increase smoothly with ARI.

The coefficients *a*, *b*, *c*, … of Equation 22.13 are traditionally estimated by ordinary least squares (OLS) regression. But in order for the OLS estimator to be statistically efficient and robust, the annual maximum

flood series in the region must be uncorrelated; all the sites in the region should have equal record length and all estimates of *T*-year events have equal variance. Since the annual maximum flow data in a region do not generally satisfy these criteria, the assumption that the model residual errors in OLS are homoscedastic is violated, and the OLS approach can provide much distorted estimates of the model's predictive precision (model error) and the precision with which the regression coefficients are estimated.

To overcome the previous problems associated with the OLS, Stedinger and Tasker [76] proposed the generalized least squares regression (GLSR), which can result in remarkable improvements in the precision with which the coefficients of regional regression models can be estimated, in particular when the record length varies widely from site to site. In the GLSR, the assumptions of equal variance of the *T*-year events and zero cross-correlation for concurrent flows are relaxed. This has been developed and enhanced by a number of researchers [25,31,32,80]. The GLSR accounts for correlated flood data and different record lengths and also distinguishes between sampling error and model error. Another positive aspect of the GLSR is that it allows for the development of a better uncertainty analysis framework in RFFA.

22.12 Parameter Regression Technique

In the parameter regression technique (PRT), the parameters of a particular probability distribution are regressed against the catchment characteristics similar to the QRT [27,32]. Here, both the OLS and generalized least squares (GLS) methods can be used to develop the prediction equations for the mean, standard deviation, and skewness of the annual maximum flood series [32]. These equations are then used to predict the mean, standard deviation, and skewness of annual maximum flood series for an ungauged catchment to fit a particular probability distribution. This fitted probability distribution can then used to estimate the flood quantiles for the ungauged catchment.

22.13 Validation of an RFFA Method

An RFFA method needs to be independently validated before it can be recommended for practical application for any region. The most commonly used validation methods are as follows: (1) One is split-sample validation where 10% or 20% of the catchments are randomly selected as test catchments; prediction equations are then developed based on the remaining 90% or 80% of the catchments (called model catchments), which are finally applied to the independent test catchments to estimate the most likely uncertainty associated with the regional prediction equation. (2) Another is leave-one-out (LOO) validation where one catchment is selected as a test catchment and the remaining catchments are used as model catchments. The procedure is repeated until all the catchments have been tested independently. (3) Another method is Monte Carlo cross validation (MCCV) where different proportions of catchments are selected as test catchments (e.g., 10%, 20%, 30%, …) and regional prediction equations (developed based on the 90%, 80%, 70%, … model catchments) are tested on them; the procedure is repeated many times in a random fashion to assess the model uncertainty. Further details on MCCV can be found in Song Xu and Zeng Liang [75] and Haddad et al. [28].

22.14 RFFA Methods Based on Artificial Neural Networks

Artificial neural networks (ANNs) are regarded as universal approximators and have been widely applied to a wide range of hydrological problems, such as rainfall–runoff modeling and hydrologic forecasting, but there have been relatively fewer applications of ANNs to RFFA problems. Examples can be found in Muttiah et al. [3,19,58,71–73]. The ANNs can derive the underlying model structure between the inputs and outputs without the prespecification of the model by the user, and hence, ANNs are regarded as model-free techniques. ANNs tend to over fit the data and hence the outputs from ANN-based RFFA models need to be examined in relation to hydrological significance.

22.15 RFFA in Arid Regions

Arid regions are characterized by low rainfall and high evapotranspiration. The ratio of annual precipitation (P) to annual potential evapotranspiration (PET) can be taken as an aridity index resulting in hyperarid region with $P/PET < 0.03$, arid region with $0.03 < P/PET < 0.2$, and semiarid region with $0.2 < P/PET < 0.5$. Due to limited availability of recorded streamflow data, it is rather difficult to derive the RFFA methods for the arid regions. One of the most comprehensive RFFA studies in the arid region was presented by Farquharson et al. [23] that developed an index flood approach using data from 162 catchments from Northwest Africa, Iran, Jordan, Saudi Arabia, Botswana, South Africa, Australia, southwest United States, and Russia. The main finding of this study was that all these arid regions except Iran and Jordan exhibited very similar flood frequency curves. In the case of Iran, floods were largely derived from snowmelt, and for Jordan, it was dominated by groundwater contributions. Thus, it was suggested that all arid areas worldwide could be treated as a single homogeneous region dominated by similar rainfall–runoff process.

The following index flood method can be adopted in the typical arid regions (where region-specific RFFA equations are not available) to estimate approximate flood quantiles [23]:

$$Q_T = \text{MAF} \times Z_T \tag{22.14}$$

where

Q_T is the T-year flood quantile
MAF is the mean annual flood in m^3/s
Z_T is the regional growth factor for T-year flood

According to Farquharson et al. [23], Z_T values may approximately be taken from Table 22.3. The index flood (MAF) should be estimated from the locally available prediction equation. However, in the absence of locally available prediction equation, the MAF flood can approximately be estimated from the suggested equation by Farquharson et al. [23]: $\text{MAF} = 1.87 \times \text{Area}^{0.578}$ where area is in km^2 and MAF is in m^3/s. A recent study for Australian arid regions can be found in Zaman et al. [87].

22.16 Impact of Climate Change on RFFA

RFFA methods are data-based techniques and are generally empirical in nature. An RFFA method is typically based on the following: (1) One is recorded streamflow data in the past; if the climate changes significantly with time, the past data are unable to represent the future, and hence, its use in developing the RFFA methods becomes rather limited. (2) Rainfall and other climate indices such as mean annual rainfall, design rainfall intensity, and mean annual evaporation are likely to be affected by climate change in many regions of the world; thus, the usefulness of these data in regional prediction equations becomes limited. (3) Catchment characteristics such as vegetation cover are likely to be affected by climate change as part of the long-term climate–catchment interaction process. Also, the catchment wetness indices are likely to be affected by climate change. All these factors modify the rainfall–runoff process of a catchment, and hence, the applicability of the regional prediction equations, based on the past data, becomes questionable. To account for the effects of climate change on flood frequency analysis methods, various nonstationary techniques have been investigated [14,15,20,22,42,49,62]. Some of the

TABLE 22.3 Regional Growth Factors for World Arid Regions

Return period, T (years)	2	5	10	20	50	100
Growth factor, Z_T	0.6	1.5	2.1	3.2	4.5	6.2

Source: After Farquharson, F.A.K. et al., *J. Hydrol.*, 138(3–4), 487, 1992.

nonstationary flood frequency analysis techniques assume that due to climate change the distributional parameters are likely to change (e.g., the location and scale parameters become nonstationary), and hence, the use of a nonstationary probability distribution is suggested.

22.17 Summary and Conclusions

The RFFA attempts to transfer flood characteristics information from gauged catchments to ungauged ones on the concept of homogeneous regions. The success of any RFFA method largely depends on the available data in terms of quantity and quality, the adopted regional model estimation method, and independent validation. This chapter has covered principal steps in the RFFA including data preparation, formation of regions, different methods to build the regional estimation equations, adopted validation techniques, and the impact of climate change on RFFA.

References

1. Acreman, M.C. and Sinclair, C.D. 1986. Classification of drainage basins according to their physical characteristics: An application for flood frequency analysis in Scotland, *Journal of Hydrology*, 84, 365–380.
2. Acreman, M.C. and Wiltshire, S.E. 1987. Identification of regions for regional flood frequency analysis, *EOS*, 68(44), 1262.
3. Aziz, K., Rahman, A., Fang, G., Haddad, K., and Shrestha, S. 2010. Design flood estimation for ungauged catchments: Application of artificial neural networks for eastern Australia, *Proceedings of World Environmental and Water Resources Congress*, Providence, RI, pp. 2841–2850, ASCE, Reston, VA.
4. Bates, B.C., Rahman, A., Mein, R.G., and Weinmann, P.E. 1998. Climatic and physical factors that influence the homogeneity of regional floods in south-eastern Australia, *Water Resources Research*, 34(12), 3369–3381.
5. Benson, M.A. 1962. Factors influencing the occurrence of floods in a humid region of diverse terrain, U.S. Geological Survey Water Supply Paper, 1580-B.
6. Bobee, B., Cavidas, G., Ashkar, F., Bernier, J., and Rasmussen, P. 1993. Towards a systematic approach to comparing distributions used in flood frequency analysis, *Journal of Hydrology*, 142, 121–136.
7. Burn, D.H. 1989. Cluster analysis as applied to regional flood frequency, *Journal of Water Resources Planning and Management*, 115(5), 567–582.
8. Burn, D.H. 1990. An appraisal of region of influence approach to flood frequency analysis, *Journal of Hydrology*, 35(2), 149–165.
9. Burn, D.H. 1990. Evaluation of regional flood frequency analysis with a region of influence approach, *Water Resources Research*, 26(10), 2257–2265.
10. Burn, D.H. and Goel, N.K. 2000. The formation of groups for regional flood frequency analysis, *Hydrological Sciences Journal*, 45(1), 97–112.
11. Castellarin, A., Burn, D.H., and Brath, A. 2008. Homogeneity testing: How homogeneous do heterogeneous cross-correlated regions seem? *Journal of Hydrology*, 360, 67–76.
12. Chavoshi Borujeni, S., Sulaiman, W.N.A., and Eslamian, S.S. 2010. Regional flood frequency analysis using L-moments for North Karoon Basin Iran, *Journal of Flood Engineering*, 1(1), 67–76.
13. Chowdhury, J.U., Stedinger, J.R., and Lu, L.H. 1991. Goodness of fit tests for regional flood distributions, *Water Resources Research*, 27(7), 1765–1776.
14. Cunderlik, J.M. and Burn, D.H. 2003. Non-stationary pooled flood frequency analysis, *Journal of Hydrology*, 276(1–4), 210–223.
15. Cunderlik, J.M. and Ouarda, T. 2006. Regional flood-duration-frequency modeling in the changing environment, *Journal of Hydrology*, 318(1–4), 276–291.
16. Cunnane, C. 1988. Methods and merits of regional flood frequency analysis, *Journal of Hydrology*, 100, 269–290.

17. Cunnane, C. 1989. Statistical distributions for flood frequency analysis, Operational Hydrology Report No. 33, WMO, Geneva, Switzerland.
18. Dalrymple, T. 1960. Flood frequency analyses, U.S. Geological Survey Water Supply Paper, 1543-A.
19. Dawson, C.W., Abrahart, R.J., Shamseldin, A.Y., and Wilby, R.L. 2006. Flood estimation at ungauged sites using artificial neural networks, *Journal of Hydrology*, 319, 391–409.
20. El Adlouni, S., Ouarda, T., Zhang, X., Roy, R., and Bobee, B. 2007. Generalized maximum likelihood estimators for the non-stationary generalized extreme value model, *Water Resources Research*, 43, W03410, doi:10.1029/2005WR004545, 13pp.
21. Eslamian, S.S. 1995. Regional flood frequency analysis using a new region of influence approach, PhD thesis, Department of Water Engineering, The University of New South Wales, School of Civil Engineering, Sydney, New South Wales, Australia, 1995, 380pp.
22. Fakhry, M., Farzaneh, M.R., Eslamian, S.S., and Khordadi, M.J. 2012. Uncertainty assessment of downscaled rainfall to investigate impact of climate change on the probability of flood, *Journal of Flood Engineering*, 3(1), 19–28.
23. Farquharson, F.A.K., Meigh, J.R., and Sutcliffe, J.V. 1992. Regional flood frequency analysis in arid and semi-arid areas, *Journal of Hydrology*, 138(3–4), 487–501.
24. Greenwood, J.A., Landwehr, N.C., Matalas, N.C., and Wallis, J.R. 1979. Probability weighted moments: Definition and relation to parameters of several distributions expressible in inverse form, *Water Resources Research*, 15, 1049–1054.
25. Griffis, V.W. and Stedinger, J.R. 2007. The use of GLS regression in regional hydrologic analyses, *Journal of Hydrology*, 204, 82–95.
26. Guse, B., Thieken, A.H., Castellarin, A., and Merz, B. 2010. Deriving probabilistic regional envelope curves with two pooling methods, *Journal of Hydrology*, 380(1–2), 14–26.
27. Hackelbusch, A., Micevski, T., Kuczera, G., Rahman, A., and Haddad, K. 2009. Regional flood frequency analysis for eastern New South Wales: A region of influence approach using GLS log-Pearson 3 parameter regression, *Proceedings of 32nd Hydrology and Water Resources Symposium*, Newcastle, New South Wales, Australia, pp. 603–615.
28. Haddad, K., Rahman, A., Zaman, M., and Shrestha, S. 2010. Applicability of Monte Carlo cross validation technique for model development and validation in hydrologic regression analysis using ordinary and generalized least squares regression, *Journal of Hydrology*, http://dx.doi.org/10.1016/j.jhydrol.2012.12.041, 10pp.
29. Haddad, K., Rahman, A., Weinmann, P.E., Kuczera, G., and Ball, J.E. 2010. Streamflow data preparation for regional flood frequency analysis: Lessons from south-east Australia, *Australian Journal of Water Resources*, 14(1), 17–32.
30. Haddad, K. and Rahman, A. 2011. Selection of the best fit flood frequency distribution and parameter estimation procedure—A case study for Tasmania in Australia, *Stochastic Environmental Research & Risk Assessment*, 25, 415–428.
31. Haddad, K., Rahman, A., and Stedinger, J.R. 2012. Regional flood frequency analysis using Bayesian generalized least squares: A comparison between quantile and parameter regression techniques, *Hydrological Processes*, 25, 1–14.
32. Haddad, K. and Rahman, A. 2012. Regional flood frequency analysis in eastern Australia: Bayesian GLS regression-based methods within fixed region and ROI framework—Quantile regression vs. parameter regression technique, *Journal of Hydrology*, 430–431, 142–161.
33. Hosking, J.R.M. 1990. L moments: Analysis and estimation of distributions using linear combinations of order statistics. *Journal of Royal Statistical Society*, 52(1), 105–124.
34. Hosking, J.R.M. and Wallis, J.R. 1993. Some statistics useful in regional frequency analysis, *Water Resources Research*, 29(2), 271–281.
35. Hosking, J.R.M. and Wallis, J.R. 1997. *Regional Frequency Analysis—An Approach Based on L-Moments*, Cambridge University Press, New York, 224pp.

36. Institute of Hydrology (IH). 1999. *Flood Estimation Handbook*, Institute of Hydrology (IH), Wallingford, U.K.
37. Institution of Engineers Australia (I. E. Aust.) (D.H. Pilgrim, ed.). 1987. *Australian Rainfall and Runoff: A Guide to Flood Estimation*, vol. 1, I. E. Aust., Canberra, Australian Capital Territory, Australia.
38. Interagency Advisory Committee on Water Data (IACWD). 1982. *Guidelines for Determining Flood Flow Frequency: Bulletin17-B*, Hydrology Subcommittee, Washington, DC, March 1982, p. 28.
39. Jingyi, Z. and Hall, M.J. 2004. Regional flood frequency analysis for the Gan-Ming River basin in China, *Journal of Hydrology*, 296, 98–117.
40. Kjeldsen, T.R. and Jones, D.A. 2007. Estimation of an index flood using data transfer in the UK, *Hydrological Sciences Journal*, 52(1), 86–98.
41. Kjeldsen, T.R. and Jones, D.A. 2009. An exploratory analysis of error components in hydrological regression modelling, *Water Resources Research*, 45, W02407, doi:10.1029/2007WR006283.
42. Khaliq, M.N., Ouarda, T.B.M.J., Ondo, J.-C., Gachon, P., and Bobee, B. 2006. Frequency analysis of a sequence of dependent and/or non-stationary hydro- meteorological observations: A review, *Journal of Hydrology*, 329(3–4), 534–552.
43. Kuczera, G. 1982. Robust flood frequency models, *Water Resources Research*, 18(2), 315–324.
44. Kuczera, G. 1982. Combining site-specific and regional information: An empirical Bayes approach, *Water Resources Research*, 18(2), 306–314.
45. Kuczera, G. 1983. A Bayesian surrogate for regional skew in flood frequency analysis, *Water Resources Research*, 1919(3), 821–832.
46. Kuczera, G. 1983. Effect of sampling uncertainty and spatial correlation on an empirical Bayes procedure for combining site and regional information, *Journal of Hydrology*, 65, 373–398.
47. Kuczera, G. and Parent, E. 1998. Monte Carlo assessment of parameter uncertainty in conceptual catchment models: The Metropolis algorithm, *Journal of Hydrology*, 211(1–4), 69–85.
48. Kuczera, G. 1999. Comprehensive at-site flood frequency analysis using Monte Carlo Bayesian inference, *Water Resources Research*, 35(5), 1551–1557.
49. Leclerc, M. and Ouarda, T.B.M.J. 2007. Non-stationary regional flood frequency analysis at ungauged sites, *Journal of Hydrology*, 343, 254–265.
50. Lettenmaier, D.P. and Potter, K.W. 1985. Testing flood frequency estimation methods using a regional flood generation model, *Water Resources Research*, 21(12), 1903–1914.
51. Lettenmair, D.P., Wallis, J.R., and Wood, E.F. 1987. Effects of regional heterogeneity on flood frequency estimation, *Water Resources Research*, 23(2), 313–323.
52. Lu, L.H. and Stedinger, J.R. 1992. Sampling variance of normalized GEV/PWM quantile estimators and a regional homogeneity test, *Journal of Hydrology*, 138, 223–245.
53. Merz, R. and Bloschl, G. 2005. Flood frequency regionalisation—Spatial proximity vs. catchment attributes, *Journal of Hydrology*, 302(1–4), 283–306.
54. Markiewicz, I., Strupczewski, W.G., Kochanek, K., and Singh, V. 2006. Discussion of non-stationary pooled flood frequency analysis, *Journal of Hydrology*, 276, 210–223.
55. Matalas, N.C., Slack, J.R., and Wallis, J.R. 1975. Regional skew in search of a parent, *Water Resources Research*, 11(6), 815–826.
56. Meshgi, A. and Khalili, D. 2009. Comprehensive evaluation of regional flood frequency analysis by L- and LH-moments 1. A re-visit to regional homogeneity, *Stochastic Environmental Research and Risk Assessment*, 23, 119–135.
57. Mosley, M.P. 1981. Delimitation of New Zealand hydrological regions, *Journal of Hydrology*, 49, 173–192.
58. Muttiah, R.S., Srinivasan, R., and Allen, P.M. 1997. Prediction of two year peak stream discharges using neural networks, *Journal of the American Water Resources Association*, 33(3), 625–630.
59. Nathan, R.J. and McMahon, T.A. 1990. Identification of homogeneous regions for the purpose of regionalisation, *Journal of Hydrology*, 121, 217–238.

60. Natural Environment Research Council (NERC). 1975. Flood studies report, NERC, London, U.K.
61. Ouarda, T.B.M.J., Ba, K.M., Diaz-Delgado, C., Carsteanu, C., Chokmani, K., Gingras, H., Quentin, E., Trujillo, E., and Bobee, B. 2008. Intercomparison of regional flood frequency estimation methods at ungauged sites for a Mexican case study, *Journal of Hydrology*, 348, 40–58.
62. Ousmane, S., Ramsay, A., and Nistor, I. 2012. Climate change impacts on extreme floods I: Combining imperfect deterministic simulations and non-stationary frequency analysis, *Natural Hazards*, 61, 647–659.
63. Panu, U.S., Smith, D.A., and Ambler, D.C. 1984. *Regional Flood Frequency Analysis for the Island of Newfoundland*, Environment Canada, Dartmouth, Nova Scotia, Canada.
64. Potter, K.W. and Lettenmaier, D.P. 1990. A comparison of regional flood frequency estimation methods using a resampling method, *Water Resources Research*, 26(3), 415–424.
65. Rahman, A. 1997. Flood estimation for ungauged catchments: A regional approach using flood and catchment characteristics. Unpublished PhD thesis, Department of Civil Engineering, Monash University, Melbourne, Victoria, Australia.
66. Rahman, A., Bates, B.C., Mein, R.G., and Weinmann, P.E. 1999. Regional flood frequency analysis for ungauged basins in south-eastern Australia, *Australian Journal of Water Resources*, 3(2), 199–207.
67. Rahman, A., Haddad, K., Kuczera, G., and Weinmann, P.E. 2009. Regional flood methods for Australia: Data preparation and exploratory analysis. Report No. P5/S1/003, Engineers Australia, Canberra, Australian Capital Territory, Australia.
68. Rahman, A., Haddad, K., Zaman, M., Kuczera, G., and Weinmann, P.E. 2011. Design flood estimation in ungauged catchments: A comparison between the probabilistic rational method and quantile regression technique for NSW, *Australian Journal of Water Resources*, 14(2), 127–137.
69. Rahman, A., Haddad, K., Zaman, M., Ishak, E., Kuczera, G., and Weinmann, P.E. 2012. Regional flood methods, Technical Report, Engineers Australia, Canberra, Australian Capital Territory, Australia.
70. Smith, J.A. 1992. Representation of basin scale in flood peak distributions, *Water Resources Research*, 28(11), 2993–2999.
71. Shu, C. and Burn D.H. 2004. Artificial neural network ensembles and their application in pooled flood frequency analysis, *Water Resources Research*, 40(9), W09301, doi:10.1029/2003WR002816, 10pp.
72. Shu, C. and Ouarda, T.B.M.J. 2007. Flood frequency analysis at ungauged sites using artificial neural networks in canonical correlation analysis physiographic space, *Water Resources Research*, 43, W07438, doi:10.1029/2006WR005142, 12pp.
73. Shu, C. and Ouarda, T.B.M.J. 2008. Regional flood frequency analysis at ungauged sites using the adaptive neuro-fuzzy inference system, *Journal of Hydrology*, 349, 31–43.
74. Skoien, J., Merz, R., and Bloschl, G. 2006. Top-kriging—Geostatistics on stream networks, *Hydrology and Earth System Sciences*, 10, 277–287.
75. Song Xu, Q. and Zeng Liang, Y. 2001. Monte Carlo cross validation, *Chemometrics and Intelligent Laboratory Systems*, 56, 1–11.
76. Stedinger, J.R. and Tasker, G.D. 1985. Regional hydrologic analysis, 1.Ordinary, weighted and generalized least squares compared, *Water Resources Research*, 21(9), 1421–1432.
77. Stedinger, J.R., Vogel, R.M., and Foufoula-Georgiou, E. 1992. Frequency analysis of extreme events. In: D.R. Maidment, ed., *Handbook of Hydrology*, McGraw-Hill, New York. 18.22–18.66.
78. Stedinger, J.R. and Lu, L. 1995. Appraisal of regional and index flood quantile estimators, *Stochastic Hydrology and Hydraulics*, 9(1), 49–75.
79. Tasker, G.D. 1982. Simplified testing of hydrologic regression regions, *Journal of the Hydraulics Division, Proceedings of the American Society of Civil Engineering*, 108(HY10), 1218–1222.
80. Tasker, G.D. and Stedinger, J.R. 1989. An operational GLS model for hydrologic regression, *Journal of Hydrology*, 111, 361–375.

81. Thomas, D.M. and Benson, M.A. 1970. Generalization of streamflow characteristics from drainage-basin characteristics, U.S. Geological Survey Water Supply Paper, 1975.
82. Viglione, A., Laio, F., and Claps, P. 2007. A comparison of homogeneity tests for regional frequency analysis, *Water Resources Research*, 43, W03428, doi:10.1029/2006WR005095, 10pp.
83. Vogel, R.M., McMahon, T.A., and Chiew, F.H.S. 1993. Flood flow frequency model selection in Australia, *Journal of Hydrology*, 146, 421–449.
84. Wang, Q.J. 1997. LH moments for statistical analysis of extreme events, *Water Resources Research*, 33(12), 2841–2848.
85. Wiltshire, S.E. 1986. Regional flood frequency analysis I: Homogeneity statistics, *Hydrological Sciences Journal*, 31(3), 321–333.
86. World Meteorological Organization (WMO). 1984. WMO survey on distribution types currently in use for frequency analysis of extremes of floods by hydrological and other services, Operational Hydrology Report No. 33, WMO, Geneva, Switzerland.
87. Zaman, M., Rahman, A., and Haddad, K. 2012. Regional flood frequency analysis in arid regions: A case study for Australia, *Journal of Hydrology*, 475, 74–83.
88. Zrinji, Z. and Burn, D.H. 1994. Flood frequency analysis for ungauged sites using a region of influence approach, *Journal of Hydrology*, 153(1–4), 1–21.

23

Regionalization of Hydrological Variables

Mehdi Vafakhah
Tarbiat Modares University

Saeid Eslamian
Isfahan University of Technology

AUTHORS

Mehdi Vafakhah received his BSc degree from the department of rangeland and watershed management at Agricultural Sciences & Natural Resources University of Gorgan, Gorgan, Iran, in 1996, and MSc and PhD degrees from the department of watershed management engineering at Tarbiat Modares University and from the department of rehabilitation of arid and mountainous regions at Tehran University in 1999 and 2008, respectively. He has been lecturing in the department of watershed management at Tarbiat Modares University since 1998. His research interests include surface hydrology, snow hydrology, geostatistic and parameter estimation with artificial neural networks, adaptive neuro-fuzzy inference system, and several data-driven techniques. He has published many national and international scientific papers and is also involved in many national watershed management projects.

Saeid Eslamian received his PhD from the University of New South Wales, Australia, with Prof. David Pilgrim. He was a visiting professor in Princeton University, USA, and ETH Zurich, Switzerland. He is currently an associate professor of hydrology in Isfahan University of Technology. He is the founder and chief editor of *Journal of Flood Engineering* and *International Journal of Hydrology Science and Technology*. He has published more than 200 publications mainly in statistical and environmental hydrology and hydrometeorology.

PREFACE

Due to lack and sparse hydrometeorological data in several geographical areas around the world, the formulation and proposal of numerous procedures for regionalization are needed to help reduce the negative consequences of data scarcity. In the context of regionalization, there are various methods. Much of this material is in journals and reports, and usually in a form that is not easily accessible to students and practitioners. The main purpose of this chapter is to present many of these procedures in a unified fashion so that they would be available to students and practitioners. The chapter can be used by hydrologists and water resources managers and planners active in the field of hydrometeorological analysis at the river basin scale. The text is divided into Selection of model inputs, classification, and regionalization approaches topics. Degree and postdegree students, research scholars, and professionals in the fields of civil, water resources, and watershed management engineering find this chapter useful. We would be glad to hear from the readers about the material discussed in this chapter and related matters and will be incorporated in the next edition.

23.1 Introduction

Reliable estimation of hydrological variables, for example, rainfall, peak discharge series, low flow, wind, and evapotranspiration, is needed for a range of purposes in dam construction, reservoir management, environmental flow requirements, water uses, hydropower operation, irrigation schemes, reservoir water losses, water balance computations, and arid and semiarid management. In practice, data are collected only at a limited number of sites, and it therefore frequently happens that no data are available at sites. In cases where no at-site data are available, one may use data from gaged neighboring catchments or, in general, data from catchments with similar hydrologic regimes.

The regionalization is based on the premise that areas of similar geology, vegetation, land use, and topography will respond similarly to similar weather patterns. Regional estimation (or regionalization) methodologies can be used to provide reliable estimates of hydrological variables at locations where hydrological variable records are limited or not available.

23.2 Regionalization Concepts

Regional estimation methodologies involve the pooling of information within a "homogeneous" region into the target site and include two main steps: the identification of groups of hydrologically homogeneous basins (or "homogeneous regions") and the application of a regional estimation method within each delineated homogeneous region. The performance of any regional estimation method strongly depends on the grouping of sites into homogeneous regions [17,18]. Geographically contiguous regions have been used for a long time in hydrology, but have been criticized for being of arbitrary character. In fact, the geographical proximity does not guarantee hydrological similarity.

Regional analysis usually involves three steps: identifying groups of hydrologically homogeneous basins, describing a robust regional probability distribution, and applying a regional estimation method within the identified homogeneous region.

23.3 Hydrological Variables

23.3.1 Rainfall

Rainfall data are collected through a nationwide network of rain gages and, more recently, radar and satellite imagery. These data are archived and readily available on the Internet at a number of websites, the most accessible being the National Climatic Data Center [36]. This site provides free download access for point rainfall data. Data are stored in a database that is accessed through the website allowing the location and extraction of rainfall data that suits a range of selection criteria such as latitude/longitude, state/county/city name, ZIP code, or station identification number.

23.3.2 Flood

Streamflow data are normally obtained at either natural sections. Typically, the water level (stage) is recorded and related to streamflow (discharge) by a stage–discharge relationship called a rating curve. Readings may be taken on an intermittent basis (e.g., weekly readings of a staff gage) or as a continuous record.

Data are usually available on a daily basis, with streamflow values expressed as a total daily volume or an average daily discharge. Instantaneous peak discharges and daily maximum and minimum flows are often provided as well. In the case of the annual maximum series data, the discharge is accompanied by a field that also identifies the date of occurrence of the annual maximum.

23.3.3 Low Flow

The cumulative frequency distribution of daily mean flows shows the percentage of time during which specified discharges are equaled or exceeded during the period of record. The relationship is normally referred to as the flow duration curve. The curve is most conveniently derived from daily discharge data by assigning daily flow values to class intervals and counting the number of days within each class interval. Various indexes can be estimated by flow duration curve. In particular, Q_{95} flow quantile $\left[\Pr(Q > Q_{95}) = 95\right]$, the 95 percentile flow, or rather the flow that has exceeded 95% of the period of record is a key index of low flow. The percentile used as low flow index depends on the type of the river being studied. However, the flows within the range of 70%–99% time exceedance are usually widely used as design low flow.

23.3.4 Wind

Wind speed and direction are measured by anemometer and wind vane respectively. The conventional anemometer is the cup anemometer formed by a circlet of three (sometimes four) cups rotating around a vertical axis. The speed of rotation measures the wind speed, and the total number of revolutions around the axis gives a measure of wind run, the distance a particular parcel of air travels in a specified time. The wind speed is usually 2 m above the surface.

23.3.5 Evapotranspiration

Evaporation is defined as the rate of liquid water transformation to vapor from open water, bar soil, or vegetation with soil beneath. Transpiration is defined as that part of the total evaporation that enters the

atmosphere from soil through the plants. The rate of evaporation has traditionally been estimated using meteorological data from climate stations. The evaporation is usually measured using evaporation pan in climate stations.

23.4 Selection of Model Inputs

23.4.1 Principal Component Analysis

A principal component analysis (PCA) is used to develop a smaller set of components that summarize the correlations among the original variables. The object of PCA is to extract the maximum amount of variance from the data set with each component. The first component extracted is a combination of variables that best separates the individual observations (i.e., spreads them out along an axis). It accounts for as much of the variation in the original data as possible. The second component extracts the maximum amount of remaining variance that is not correlated with the first component (orthogonal to it). Ideally, the interrelationships will be displayed using as few dimensions as will suffice [15].

A problem of PCA is that components are dependent on the scale of the variable, for example, the variable with the highest variance will dominate the first component. It is preferable to first scale variables such that all have a variance near one. Results of a PCA are normally plotted with two axes to represent pairs of components. From these plots, the distance, clustering, and direction of the points relative to the axes can be examined. A large distance away from the origin along an axis indicates a close correlation with that component. Optimally, points should cluster near the end of an axis and near the origin; if clustering is not obvious, a component may not be clearly defined. If clusters do not line up on the axes, it may indicate a need to rotate the axes.

Rotation of axes can improve the usefulness and ease of interpretation of the solution. Varimax (orthogonal) rotation is most commonly employed, which assumes that the underlying processes influencing each component are independent. Spatially, the axes are rotated so that they more closely pass through the variable clusters. This allows each cluster or individual to be more easily ranked by distance along an axis. The resulting components should also be examined in an attempt to understand the underlying unifying principle. This is usually characterized by assigning the component a name, for example, "richness of flavor" or "landscape form." In fact, there is no objective measure for testing how "good" the resulting PCA solution is. The final choice is up to the researcher, based on its interpretability, that is, does it make sense? Useful solutions ideally have a few components that are related by some common processes and are highly unlike the other components.

The Kaiser criterion is the most widely used method to evaluate the maximum number of factors (i.e., linear combinations) to extract from the data set [25]. This criterion requires that factors are retained only if their associated eigenvalues are greater than 1. The variables with the highest factor loadings within each separate factor will likely share a common characteristic or combination of characteristics. These factor loadings are the correlation coefficients between the variables. The efficiency of PCA method was validated using Kaiser–Meyer–Olkin (KMO) and Bartlett tests. In the ideal case, KMO should be 1. High KMO values indicate a PCA with few errors, overall. If KMO is more than 0.5, PCA could be used [39].

Once obtained, principal components can be used as independent variables in regional analysis. Because the components are uncorrelated, the regional analysis results tend to be more stable and reliable than regional analysis made using the original variables [42].

23.4.2 Gamma Test

The gamma test (GT) estimates the minimum mean square error (MSE) that can be achieved when modeling the unseen data using any continuous nonlinear models [32]. Firstly GT is reported by Koncar [27] and Agalbjörn et al. [2] and later enhanced and discussed in detail by Durrant [8] and Tsui et al. [41].

The basic idea is quite distinct from the earlier attempts with nonlinear analysis. Suppose we have a set of data observations of the form

$$\{(x_i, y_i), \leq i_1 \leq M\} \tag{23.1}$$

where the input vectors $x \in R^m$ are m dimensional vectors (with a record length of M) confined to some closed bounded set $C \in R^m$, and without loss of generality, the corresponding outputs $y_i \in R$ are scalars. The vectors x contain predicatively useful factors influencing the output y. The only assumption made is that the underlying relationship of the system is of the form

$$y = f(x_i, x_2, \ldots, x_m) + r \tag{23.2}$$

where

f is a smooth function

r is a random variable that represents noise

Without loss of generality, it can be assumed that the mean of the r's distribution is zero (since any constant bias can be subsumed into the unknown function f) and that the variance of the noise $Var(r)$ is bounded. The domain of a possible model is now restricted to the class of smooth functions that have bounded first partial derivatives. The gamma statistic Γ is an estimate of the model's output variance that cannot be accounted for by a smooth data model.

The GT is based on $N[i,k]$, which are the kth $(1 \leq k \leq p)$ nearest neighbors $x_{N[i,k]}$ $(1 \leq k \leq p)$ for each vector x_i $(1 \leq i \leq M)$. Specifically, the GT is derived from the delta function of the input vectors:

$$\delta_M(k) = \frac{1}{M}\left|X_{M(i,k)} - X_J\right|^2 \quad 1 \leq k \leq p \tag{23.3}$$

where $|...|$ denotes Euclidean distance, and the corresponding gamma function of the output values

$$\gamma_M(k) = \frac{1}{2M}\sum_{i=1}^{M}\left|y_{N(i,k)} - y_i\right|^2 \quad 1 \leq k \leq p \tag{23.4}$$

where $y_{N(i,k)}$ is the corresponding y-value for the kth nearest neighbor of x_i in Equation 23.3. In order to compute Γ, a least-squares regression line is constructed for the p points $(\delta_M(k), \gamma_M(k))$:

$$\gamma = A\delta + \Gamma \tag{23.5}$$

The intercept on the vertical axis $(\delta = 0)$ is the Γ value, as can be shown:

$$\gamma_M(k) \to Var(r) \text{ in probability as } \delta_M(k) \to 0 \tag{23.6}$$

Calculating the regression line gradient can also provide helpful information on the complexity of the system under investigation. A formal mathematical justification of the method can be found in Evans and Jones [12].

The graphical output of this regression line (Equation 23.5) provides very useful information (to be presented later on). First, it is remarkable that the vertical intercept Γ of the y (or Gamma) axis offers an estimate of the best MSE achievable utilizing a modeling technique for unknown smooth functions

of continuous variables [12]. Second, the gradient offers an indication of model's complexity (a steeper gradient indicates a model of greater complexity).

The GT is a nonparametric method, and the results apply regardless of the particular techniques used to subsequently build a model of *f*. We can standardize the result by considering another term V_{ratio}, which returns a scale invariant noise estimate between 0 and 1. The V_{ratio} is defined as

$$V_{ratio} = \frac{\Gamma}{\sigma^2(y)} \tag{23.7}$$

where $\sigma^2(y)$ is the variance of output *y*, which allows a judgment to be formed independent of the output range as to how well the output can be modeled by a smooth function. A V_{ratio} close to 0 indicates that there is a high degree of predictability of the given output *y*. If the standard error value is close to 0, we have more confidence in the value of the gamma statistic as an estimate for the noise variance on the given output. Gradient is actually a rough measure of the complexity of the smooth function that we are seeking to construct. We can also determine the reliability of Γ statistic by running a series of GT for increasing *M*, to establish the size of data set required to produce a stable asymptote. This is known as *M*-test. *M*-test result would help us to avoid the wasteful attempts of fitting the model beyond the stage where the MSE on the training data is smaller than *Var*(*r*), which may lead to overfitting. The *M*-test also helps us to decide how many data points are sufficient for building a model with a mean squared error approximate to the estimated noise variance (when the *M*-test plot becomes flat). In practice, the GT can be achieved through winGamma™ software implementation [41].

23.5 Classification

23.5.1 Cluster Analysis

Cluster analysis (CA) was firstly reported by Tryon [40]. CA is the task of assigning a set of objects into groups (called clusters) so that the objects in the same cluster are more similar (in some sense or another) to each other than to those in other clusters [24,29]. Many algorithms have been proposed for CA divided into two main groups including hierarchical and repeated discriminates.

The catchment characteristics are standardized (Equation 23.8) to ensure that the analysis is independent of measurement units used for these variables:

$$z_{ij} = \frac{x_{ij} - \overline{x}_j}{s_j} \tag{23.8}$$

where

$i = 1, \ldots, n_c$ catchments
$j = 1, \ldots, n_p$ explanatory variables
z_{ij} = standardized variable j at catchment i
x_{ij} = value of variable j at catchment i
$\overline{x}_j$ = mean of variable j for the n_c catchments
s_j = standard deviation of variable j over all the n_c catchments

The clustering technique used is the *K*-means algorithm that can be used to partition *M* objects (catchments) into *K* groups (regions) based on the values of features, or attributes, of the objects. The algorithm starts with an initial centroid, or seed point, for each of the *K* clusters. Each of the objects is then assigned to the "nearest" cluster centroid in terms of a similarity measure. Once all of the objects

have been assigned to a cluster, the centroid for each cluster is recalculated, and the objects may be reassigned to different clusters depending on the distance from the object to the new centroid location. This process is repeated until no object experiences a change in cluster membership. The dissimilarity measure that is used in this work to determine the closeness of each catchment to each cluster centroid is defined as

$$D_{ij}^{d} = \frac{D_{ij} + \left(d_{ij}/d_b\right)w}{1+w} \tag{23.9}$$

where

D_{ij}^{d} is the dissimilarity between catchment i and cluster j
D_{ij} is the weighted Euclidean distance (in attribute space) between catchment i and clustery
d_{ij} is the geographical distance between catchment i and the geographic centroid of cluster j
d_b and w are parameters to be estimated

Since Equation 23.9 defines a dissimilarity measure, lower values for D_{ij}^{d} indicate catchments that are closer to the corresponding cluster centroid.

The weighted Euclidean distance is defined as

$$D_{ij} = \left[\sum_{i=1}^{m} w_k \left(x_{ik} - x_{jk}\right)^2\right]^{1/2} \tag{23.10}$$

where

w_k is the weight applied to attribute k
x_{ik} is the standardized value for attribute k for catchment i where the attribute values are standardized by dividing by the standard deviation for the attribute
x_{jk} is the centroid value for attribute k for clustery
m is the number of attributes used to define similarity

The attributes used in Equation 23.10 are physiographic characteristics of the catchments. The weights in Equation 23.10 are selected to satisfy

$$\sum_{i=1}^{m} w_k = 1 \tag{23.11}$$

The dissimilarity measure defined in Equation 23.9 was originally proposed by Webster and Burough [44] in an attempt to enhance the geographical continuity of clusters. The two parameters, <4 and w, control the relative influence in the composite dissimilarity measure of geographical distance versus the weighted Euclidean distance in attribute space. Within the Euclidean distance measure, the W_k values reflect the relative importance of each attribute in determining catchment dissimilarity. Initial estimates for the weights and the two parameters in the distance function can be selected using judgment and then be refined using either an optimization algorithm or an ad hoc procedure. In this work, the parameters and weights were adjusted using a search technique to enhance the homogeneity of the regions that are formed. Output of hierarchical method is in dendrogramatic form, and the relation between each class of data is displayed by their similarity [40].

23.5.2 Discriminant Analysis

Discriminant analysis (DA) is defined as linear combinations that separate groups of observations, and canonical variates are defined as linear combinations associated with canonical correlations between two sets of variables. Objects that retain similar variances in the analyzed parameters will have similar discriminant scores and, therefore when plotted, will group together. Also relationships between variables can be easily identified by the respective coefficients. Strongly correlated variables will generally have the same magnitude and orientation when plotted, while uncorrelated variables are typically orthogonal to each other [4]. The combination of variables (predictors) that separate from each other called discriminant function. These are much like multiple regression equation but produce a discriminant function "score." This score gives an indication of the group to which a catchment belongs and whether it falls solidly into one class or into gray area between two different classes. Several functions may be needed to reliably separate groups. The total number of possible "dimensions" is either one less than the number of groups or the number of predictor variables, whichever is smaller [15].

23.5.3 Andrews Curves

If only two variables are required for describing the similarity between sites, streams, or catchments, then a simple two-dimensional scatter plot is sufficient for displaying groupings. Displaying these data becomes much more difficult with a larger number of variables. A graphical approach presented by Andrews (1972) provides a good method of viewing patterns of similarity or dissimilarity across multiple dimensions. A point in multidimensional space is represented by a curve described by the function

$$y_t = \frac{x_1}{\sqrt{2}} + x_2 \sin(t) + x_3 \cos(t) + x_4 \sin(2t) + x_5 \cos(3t) + \cdots \tag{23.12}$$

where x_1, x_2, x_3, x_4, x_5, … show each variable used for homogeneous watershed determination. These variables have the most correlation with the dependent variable [33]. The Andrews plot (Fourier curve) is a plot of (t, y_t) in the range of $t\varepsilon[-\pi, \pi]$. Curves representing points that are located near one another in multidimensional space will look similar, whereas points that are distant will produce curves that look different. Results will depend on the order in which the variables are labeled. The first variables will be described by low-frequency components (wider "waves"). These are more readily seen than the higher-frequency components representing the latter variables. Thus, it is more useful to associate the most important variable with x_1, the second with x_2, and so on [35]. This relative importance can be determined from a stepwise multiple regression analysis, PCA, or GT. The values should also be scaled to the same order of magnitude (e.g., by choosing an appropriate unit). One method to standardize is by subtracting the mean and dividing by the standard deviation of all observations of a given variable.

23.6 Regionalization Approaches

23.6.1 Geostatistics

The spatial distribution of hydrological variables such as rainfall, flood, low flow, wind, and evapotranspiration is needed whenever hydrological modeling is undertaken at the watershed scale. These models can be used to simulate hydrological processes at a daily or monthly time steps, and the interpolation of hydrological variables at this time scale poses a particular problem due to its large spatial variation. Geostatistical prediction includes two stages of which the first is the identification and modeling of spatial structure. At this stage, continuity, homogeneity, and spatial structure of a given variable are studied

using variogram. Second stage is geostatistical estimation using kriging technique, which depends on the properties of the fitted variogram that affects all stages of the process.

23.6.1.1 Variogram Analysis

Variogram method is a suitable technique for estimating spatial variability of a variable. Calculation of variogram graph is one of the essential stages in geostatistics, which is defined as follows:

$$\gamma(h) = \frac{2}{2n(h)} \sum_{i=1}^{n(h)} \left[Z(xi) - Z(xi+h) \right]^2 \tag{23.13}$$

where

$\gamma(h)$ is the value of variogram for pair points with distance h
$n(h)$ is the number of pair points with distance h
$Z(xi)$ is the observed value of variable xi
$Z(xi+h)$ is the observed value of the variable with distance h from xi

For variogram plotting, it is necessary to compute $\gamma(h)$ for different values of h and then to plot the values for different distances of h. In other words, variogram is the variance of different points with distance h. The obtained variograph of measured samples is called experimental variogram, which is a vector value that is a dependent on distance and direction.

Once we calculated an experimental variogram, we can fit it using some of the authorized variogram models, such as linear, spherical, exponential, circular, Gaussian, Bessel, power, and similar [14,23]. Figure 23.1 shows the parameters of the variogram model, for example, the nugget (C_0), sill ($C + C_0$), and the range (A) parameter. By knowing these parameters, we can estimate the semivariance at any location in the area of interest.

The variograms are commonly fitted by iterative reweighted least-squares estimation, where the weights are determined based on the number of point pairs or based on the distance. Most commonly, the weights are determined using N_j/h_{2j}, where N_j is the number of pairs at certain lag, and h_j is the distance. Note that this is only a sample variogram—if we would go and collect several point samples, each would lead to a somewhat different variogram plot. The target variable is said to be stationary if several sample variograms are very similar (constant), which is referred to as the covariance stationarity. Otherwise, if the variograms differ much locally and/or globally, then we speak about nonstationary inherent properties. In principle, assumptions of kriging are that the target variable is stationary and that it has a normal distribution, which is probably the biggest limitation of kriging. Once we have

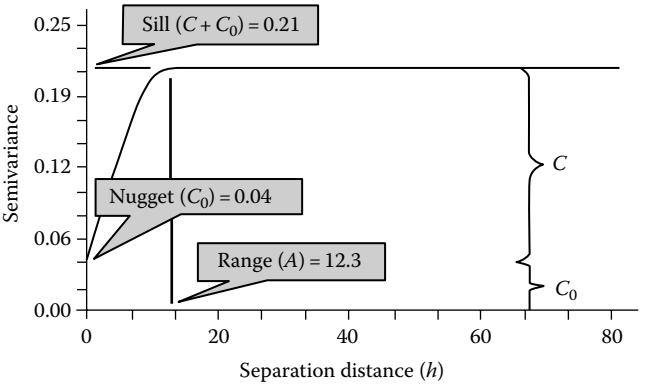

FIGURE 23.1 The parameters of the variogram model.

estimated the variogram model, we can use it to derive semivariances at all locations and solve the kriging weights. The OK weights are solved by multiplying the covariances:

$$\lambda_0 = C^{-1} \cdot c_0; \quad C\left(|h| = 0\right) = C_0 + C_1 \tag{23.14}$$

where

C is the covariance matrix derived for $n \times n$ observations

c_0 is the vector of covariances at new location

Note that C is in fact $(n+1) \times (n+1)$ matrix if it is used to derive kriging weights.

A distinction should be made between isotropic and anisotropic. Isotropic, when

$$h = |x - x'| = \sqrt{(x_1 - x_1')^2 + (x_1 - x_1')^2 + (x_1 - x_1')^2} \tag{23.15}$$

Anisotropic, when h depends not only on the length but also on the orientation of the separation vector. It is common to adapt a model of geometric anisotropy in which anisotropy variability can be turned into isotropic variability through a linear transformation of the coordinates. For example, one can select the x_1,x_2,x_3 direction along the main axes of correlation anisotropy and use

$$h = |x - x'| = \sqrt{\left(\frac{x_1 - x_1'}{c_1}\right)^2 + \left(\frac{x_2 - x_2'}{c_2}\right)^2 + \left(\frac{x_3 - x_3'}{c_3}\right)^2} \tag{23.16}$$

23.6.1.2 Theory of Ordinary Kriging

Kriging has for many decades been used as a synonym for geostatistical interpolation. It originated in the mining industry in the early 1950s as a means of improving ore reserve estimation. The original idea came from the mining engineers D.G. Krige and the statistician H.S. Sichel. The technique was first published in Krige (1951), but it took almost a decade until a French mathematician G. Matheron derived the formulas and basically established the whole field of linear geostatistics [43].

Ordinary kriging is a prediction that considers values of a variable in unsampled points as a linear composition of the values of surrounding points (hydrological variables, e.g., rainfall, flood, low flow, etc.). Considering the values of variable Z in n measured points as follows:

$$Z = \left(Z(x_1),\ Z(x_2),\ \ldots,\ Z(x_n)\right) \tag{23.17}$$

Estimation of Z in point x_0 using kriging estimation is defined as

$$Z^*(x_0) = \sum_{i=1}^{n} \lambda_i Z(x_i) \tag{23.18}$$

The most important part of kriging is statistical weighs assigned to λ_i. To avoid the bias of estimation, the weighted should be determined in a way that summation is equal to one $\left(\sum_{i=1}^{n} \lambda_i = 1\right)$ and the variance of estimates should be minimized as

$$Var\left[Z^*(x_0)\right] = E\left[(Z^*(x_0) - Z(x_0))^2\right] = Min \tag{23.19}$$

23.6.2 Index Flood Method

The index flood method, proposed by Dalrymple [7], is one of the first approaches to regional flood estimation.

The index flood method is carried out by the following steps:

1. Establish a standard record length or base period. This is usually taken as the longest period of record.
2. Estimate annual peak flow for missing years by a regression analysis from other longer-term station.
3. Assign an order to all annual peak flow at each station, compute the plotting position, and plot frequency curves using the best standard distribution fit for each gage.
4. Determine an index flood discharge, usually the mean annual flood, and the ratio of the flood with a 10 year return period (Q_{10}) for each gage. The mean annual flood is commonly assumed to be flood with a return period of 2.33 years (EVI distribution). This can be changed to reflect the chosen probability distribution (e.g., normal distribution has a return period of 2 years).
5. Test the data for homogeneity. This step is carried out in the following steps:
   a. Compute the homogeneity factor by

$$K = \frac{1}{n}\sum_{i=1}^{n}\left(\frac{Q_{10}}{Q_{2.33}}\right) \tag{23.20}$$

   b. For each gage, compute $Q_k = KQ_{2.33}$ and the corresponding return period.
   c. Plot the values of return period obtained in step b. against the effective length of record, L_E, for each gage where L is the actual length of record at a gage and L_B is the length of the base record.
   d. Test for homogeneity by also plotting on this graph envelope curves determined from Table 23.1, taken from Dalrymple [7]. This table gives the upper and lower limits, Tu and TL, as a function of the effective length of record.
6. Using actual flood data, compute the ratio of each flood to the station mean, $Q_{2.33}$, for each record.
7. Compute the median flood ratios of the stations retained in the regional analysis for each rank or order m, and compute the corresponding return period by the Weibull formula, $\mathrm{Tr} = (n+1)/m$. (It is suggested that the median ratio be determined after eliminating the highest and lowest $Q/Q_{2.33}$ values for each ordered series of data).
8. Plot the median flood ratio against the return period on probability paper.
9. Plot the logarithm of the mean annual flood for each gage, $Q_{2.33}$, against the logarithm of the corresponding drainage area. This curve should be nearly a straight line.

TABLE 23.1 Upper and Lower Limit Coordinates of Envelope Curve for Homogeneity Test

Effective Length of Record (Years)	Return Period Limits (Years)	
	Upper Limit	Lower Limit
5	160	1.2
10	70	1.85
20	40	2.8
50	24	4.4
100	18	5.6

10. Determine the flood-frequency curve for any stream site in the watershed as follows:
    a. Determine the drainage area above the site.
    b. From step 9, determine the value of $Q_{2.33}$.
    c. For selected return periods, multiply the median flood ratio in step 9 by the value of $Q_{2.33}$ from step 10b.
    d. Plot the regional frequency curve.

23.6.3 Multiple Regression

Regression can be used to drive equations to predict the value of various hydrologic statistics (including mean, standard deviations, quantile, and normalized regional flood quantile) as a function of the watershed characteristics [38]. The multiple regression model can be expressed in the following form:

$$y_i = \alpha + a\log(A) + b\log(B) + \cdots + \varepsilon \tag{23.21}$$

where

α is regression constant defined by regression analysis
a, b,… are regression coefficients defined by regression analysis
A, B,… are watershed characteristics

This form of the multiple regression model is achieved by linear regression of the logarithms of the variables. The observed ε is a combination of (1) the time-sampling error in sample estimators y_i and (2) underlying model error (lack of fit) due to failure of the model to exactly predict the true value of the y_is at every site [30].

23.6.4 Isoline Mapping

An isoline map is a map with continuous lines joining points of the same value. One regional scheme is described in the UK Flood Studies Report [37], which derived a q_T relationship, where q_T is a regional estimate of $Q_T/\overline{Q}$, which is the mean annual flood), by combining all flood data within a region. U.S. federal agencies recommended procedures for flood-frequency analysis in Bulletin 17B [22]. The skew isoline maps are developed based on the plot of each station skew value at the centroid of its drainage basin and examined the plotted data for any geographic or topographic trend. If a pattern is evident, the isolines are drawn and MSE is computed. If no pattern is evident, then an isoline map cannot be drawn and is, therefore, not further considered.

23.6.5 Hybrid Method

The hybrid method for a regional regression analysis was described in detail by Hjalmarson and Thomas [19]. It is based on the station–year method [13] of a frequency analysis to produce regional flood–frequency relations. The station–year method is based on the assumption that independent records of annual peak discharge from a region can be combined to form one long composite record if the peaks of the individual records can be reduced to a common base. Spatial sampling is assumed to be equivalent to time sampling if the records are reasonably independent. Therefore, for example, a combination of 10 gaging stations, each with 10 years of records, results in a 100 year composite record.

The hybrid method starts with forming a single data set by pooling annual peaks from many gaging stations and historic flood estimates at ungaged sites with the assumption that the annual peaks are reasonably independent. It uses the regression Equation 23.20, which is commonly used in many regional flood–frequency analyses.

Because drainage area is the most significant independent variable that affects flood characteristics, the hybrid method starts the regression between discharge and drainage areas. It involves the following steps:

Step 1: The drainage area for all sites is ranked from the smallest to the largest. The combined single long record is then divided into three or more groups according to the basin drainage area:

$$J \leq \frac{N_f}{100} \tag{23.22}$$

where

J is the maximum number of groups
N_f is the sum composite of the station-year records

Each group has a number of stations. Each station has a number of years with flow or with zero flow. To ensure an unbiased relation in the regression analysis, each group has a nearly equal sample size. The average weighted drainage area in each group is computed by the following formula:

$$\overline{A}_i = \text{antilog}\left[\frac{\sum_{k=1}^{h} \log A_{ijk}}{gh}\right] \tag{23.23}$$

where

$\overline{A}_i$ is the average weighted drainage area in group i
A_{ijk} is the drainage area of station j in group i and station-year k
i is the number of groups ($i = 1, 2, \ldots, f$)
j is the number of stations in group i ($j = 1, 2, \ldots, g$)
k is the number of years in station j and group i

Step 2: Each peak discharge within each group is standardized by dividing by A^b (the exponent b is equal to one for the first iteration):

$$S_{ijk} = \frac{Q_{ijk}}{A_{ijk}^{-b}} \tag{23.24}$$

where

S_{ijk} is the standardized peak discharge k in station j and group i
Q_{ijk} is the annual peak discharge k in station j and group i
A_{ijk} is the drainage area of station j in group i and k station-year

Step 3: In each group, the exceedance probabilities of the standardized peaks can be estimated either by fitting a theoretical flood–frequency curve if appropriate or simply by using a plotting position formula. To avoid extrapolations to the 1% annual chance flood level, each group has at least 100 station-years (peaks) with flow to estimate the 0.01 probability. If an elementary plotting-position formula is used, a theoretical probability distribution is no longer required. This advantage is important because in semi-arid and arid regions, many station flood–frequency relations are typically undefined or unreliable if fitted with a theoretical curve.

Step 4: The frequency flows for each group obtained in Step 3 are destandardized by multiplying by the weighted geometric mean drainage area

$$Q_{t_i} = S_{t_i}(\bar{A}_i)^b \tag{23.25}$$

where

Q_{t_i} is the peak flow discharge with return period t in group i
S_{t_i} is the standardized peak discharge in station i with return period t
$\bar{A}_i$ is the average weighted drainage area

Step 5: For each exceedance probability, a linear regression analysis is conducted between Q and mean drainage area in log space, and a new exponent, b, is computed. To perform a linear regression, the combined data set has to be divided into at least three groups.

Step 6: Using the new exponent, an iterative process that uses a regression and flood–frequency analysis is repeated until the computed exponent converges.

$$b_t = \frac{\sum_{i=1}^{f} \bar{A}_i Q_{t_i} - \left[\left[\sum_{i=1}^{f} \bar{A}_i \sum_{i=1}^{f} Q_{t_i}\right] \Big/ f\right]}{\sum_{i=1}^{f} \bar{A}_i^2 - \left[\left[\sum_{i=1}^{f} \bar{A}_i\right]^2 \Big/ f\right]} \tag{23.26}$$

Each additional parameter can be separately added to the relation with the same iterative technique starting at Step 1. The new parameter (e.g., B or C) is used in place of drainage area. The original peak discharges in Step 2 are replaced with standardized discharges obtained from the last iteration for the previous parameter. The coefficient, a, in Equation 23.20 is determined during the last linear regression (in log space) of the last parameter.

23.6.6 L-Moments

The method of L-moments [20] is now a common and robust method for regional frequency analysis of different hydrologic and climatic variables. For example, Kumar et al. [28], Modarres [31], and Yurekli et al. [45] have used L-moments method for flood, wind speed, and extreme rainfall, respectively. L-moments are linear combinations of order statistics, which is used for summarizing theoretical distribution of an observed sample of a random variable (X). Hosking and Wallis [20] defined L-moments as linear functions of probability weighted moments (PWMs), which are robust to outliers and virtually unbiased for small sample. Greenwood et al. [16] defined PWMs as

$$\beta_r = E\left\{X\left[F_X(x)\right]^r\right\} \tag{23.27}$$

where

β_r is the rth-order PWM
$F(x)$ is the cumulative distribution function of X

Unbiased sample estimators (b_i) of the first four PWMs are calculated as

$$b_0 = \frac{1}{n}\sum_{j=1}^{n} x_{(j)} \tag{23.28}$$

$$b_1 = \sum_{j=1}^{n-1} \left[\frac{(n-j)}{n(n-1)} \right] x_{(j)} \tag{23.29}$$

$$b_2 = \sum_{j=1}^{n-2} \left[\frac{(n-j)(n-j-1)}{n(n-1)(n-2)} \right] x_{(j)} \tag{23.30}$$

$$b_3 = \sum_{j=1}^{n-3} \left[\frac{(n-j)(n-j-1)(n-j-2)}{n(n-1)(n-2)(n-3)} \right] x_{(j)} \tag{23.31}$$

where $x_{(j)}$ represents the ranked annual maximum series with $x_{(1)}$ being the highest value and $x_{(n)}$ the lowest value, respectively. The first four L-moments are given as

$$\lambda_1 = \beta_0 \quad \lambda_2 = 2\beta_1 - \beta_0 \quad \lambda_3 = 6\beta_2 - 6\beta_1 + \beta_0 \quad \lambda_4 = 20\beta_3 - 30\beta_2 + 12\beta_1 - \beta_0 \tag{23.32}$$

In general,

$$\lambda_{r+1} = \sum_{k=0}^{r} p^{\star}_{r,k} \beta_k \tag{23.33}$$

Different L-moment ratios can then be defined [21]. The L-mean, λ_1, is a measure of central tendency and the L-standard deviation, λ_2, is a measure of dispersion. Their ratio $\tau_2 = \lambda_2/\lambda_1$ is termed the L-coefficient of variation (L-CV). The third and fourth moments, λ_3 and λ_4, are analogous to conventional moments. The ratio $\tau_3 = \lambda_3/\lambda_2$ is referred to as L-skewness, whereas the ratio $\tau_4 = \lambda_4/\lambda_2$ is the L-kurtosis.

Once the at-site L-moments are available, they can be used to identify the most suitable (parametric) regional probability distribution using L-moment ratio diagrams. A fundamental assumption of regional flood-frequency analysis is that floods from each site in the region are hydrologically similar, for example, they have similar causes and characteristics. L-moment techniques provide a discordance measure (D) for screening at-site data and a heterogeneity measure (H) to diagnose candidate regions based on simulations. The discordance measure, D, is defined as follows:

$$D = \frac{1}{3} \left(u_i - \frac{1}{N} \sum_{i=1}^{N} u_i \right)^T \left(u_i - \frac{1}{N} \sum_{i=1}^{N} u_i \right) \tag{23.34}$$

where

N is the total number of observations

u is a vector containing the L-moment ratios (i.e., L-CV, L-skew, and L-kurtosis) for the site i: $u_i = \left[\tau_{2i}, \tau_{3i}, \tau_{4i} \right]^T$

The average value of D over all sites is 1. A site with $D > 3$ is considered discordant and should be examined (about 3% of sites should exceed 3 on average).

Heterogeneity, H, is defined as follows [20]:

$$H = \frac{(V_{obs} - \mu_v)}{\sigma_v} \tag{23.35}$$

$$V_1 = \frac{\sum_{i=1}^{N}\left(n_i\left(\tau_{2i} - \overline{\tau}_2\right)^2\right)}{\sum_{i=1}^{N} n_i} \tag{23.36}$$

$$V_2 = \frac{\sum_{i=1}^{N}\left(n_i\sqrt{\left(\tau_{2i} - \overline{\tau}_2\right)^2\left(\tau_{3i} - \overline{\tau}_3\right)^2}\right)}{\sum_{i=1}^{N} n_i} \tag{23.37}$$

where

μ_v and σ_v are the mean and standard deviation of the simulated values of V

V_{obs} is obtained from the regional data [20]

When H is constructed with V_1, it is denoted as H_1 (based on L-CV); H_2 reflects a combination of L-CV and L-skew variability.

The H statistics indicate that the region under consideration is acceptably homogeneous when $H < 1$, possibly heterogeneous when $1 \leq H < 2$, and heterogeneous when $H \geq 2$. A grouping of sites therefore must have $H < 2$ to be considered as a "possibly homogeneous" region. Hosking and Wallis [20] also noted that the assignment of sites to regions must be based on variables other than their L-moments in order for the D and H statistics to have any significance. They also state that H_1 is most closely comparable to a formal statistical test.

23.6.7 Region of Influence

The fundamental of the "region of influence" (ROI) approach is described by Acreman and Wiltshire [1]. This method is applied by Burn [3] in southern Manitoba, Canada, and Eslamian [9] in southeastern New South Wales, Australia.

The basis of the ROI approach is delineation of an "ROI" for each gaging station including the set of sites that are in proximity to the reference station, where proximity is defined in terms of the selected attributes rather than geographical location. Proximity is calculated by the Euclidean distance from Equation 23.10 in a multidimensional attribute space where the attributes are appropriate measures for the identification of stations with a similar extreme flow response.

The attributes can be selected from catchment characteristics for a station or from statistical measures of the data record at each site.

The standardization of the attributes involves dividing the raw data by the standard deviation of data calculated for attribute values from a total number of stations. The standardization process eliminates the units from each attribute and reduces any differences in the range of values among the attributes. This procedure is invoked to avoid the introduction of bias due to scaling differences for the attributes. The distance value from Equation 23.20 will thus provide a measure of how close each station is to every other station (i.e., a symmetric NS by NS matrix of distance measures results).

The next step is the choice of a threshold value of the Euclidean distance that defines a cutoff to exclude gaging sites from the investigation of the region of the reference site. Any surrounding sites having D_{ij} lower than the threshold value is considered for the inclusion in a ROI of the reference site. Remaining sites will be excluded from the ROI of this reference site.

Since all of the stations included in the ROI will not be equally close to the site for which the ROI is being determined, a weighting function is required to reflect the relative importance of each station in the estimation of the at-site extreme flows. The weighting function used was of the form

$$WF_{ij} = 1.0 - \left[\frac{D_{ij}}{THL} \right]^n \tag{23.38}$$

where

WF_{ij} is the weighting for station j in the ROI for site i
THL is a parameter
n is a positive constant

The effect of the parameter *THL* is to dictate the value of the weighting function for stations at the threshold. For this reason, the value of *THL* should logically be greater than or equal to the threshold value. If *THL* is equal to the threshold, then stations at the threshold will have no contribution to the determination of at-site extremes; larger values will increase the weighting of all stations included in the ROI. The value of the constant n will determine the rate of decrease in the weighting values as stations further away from the site (in terms of the distance measure) are considered. Using the procedure outlined earlier, the stations that constitute the ROI for each site may be determined, and the relative importance of each member of the ROI in estimating at-site extreme flow values may be ascertained.

23.6.8 Regional Envelope Curves

To examine flood-producing properties of a catchment and to estimate the maximum expected flood on ungaged streams, envelope curves are a useful tool. Within a given region, the highest observed discharge at all gaging stations is divided by the corresponding catchment area and then plotted against area using log–log axes. A curve that forms an upper bound to the data is called an envelope curve. The graph provides a summary of the flood magnitudes experienced in a region.

23.7 Validation of Regional Models

The jackknife cross-validation procedure is used to assess the model performance. The jackknife cross-validation procedure consisted of the following steps:

1. Remove catchment *i* from the data set
2. Update the catchment classification (if appropriate) for the remaining $n - 1$ catchments
3. Assign catchment *i* to one of the regions obtained in (2)
4. Estimate the coefficients of the regression equation for this region using all catchments in this region apart from catchment *i*
5. Apply the regression equation obtained in (4) to predict the hydrologic variables characteristic at site *i*
6. Repeat steps (1)–(5) for all *n* catchments
7. Calculate the following five indices

The Nash criterion (*NASH*), the root mean squared error (*RMSE*), the relative root mean squared error (*RMSEr*), the mean bias (*BIAS*), and the relative mean bias (*BIASr*). The indices are computed according to the following equations:

$$NASH = 1 - \frac{\sum_{i=1}^{n} \left(Q_i - \hat{Q}_i \right)^2}{\sum_{i=1}^{n} \left(Q_i - \bar{Q}_i \right)^2} \tag{23.39}$$

$$RMSE = \sqrt{\frac{\sum_{i=1}^{n} \left(Q_i - \hat{Q}_i \right)^2}{n}} \tag{23.40}$$

$$RMSEr = \sqrt{\frac{\sum_{i=1}^{n}\left(\frac{Q_i - \hat{Q}_i}{Q_i}\right)^2}{n}} \tag{23.41}$$

$$BIAS = \frac{\sum_{i=1}^{n}\left(Q_i - \hat{Q}_i\right)}{n} \tag{23.42}$$

$$BIASr = \frac{\sum_{i=1}^{n}\left(\frac{Q_i - \hat{Q}_i}{Q_i}\right)}{n} \tag{23.43}$$

where

n is the total number of sites being modeled
Q_i is the at-site estimation for site i
$\hat{Q}_i$ is the estimation obtained from the regional model for site i
$\bar{Q}_i$ is the mean of at-site estimation of the n sites

23.8 Case Study Regionalization

23.8.1 Case Example in Rainfall and Geostatistic

Nabipour [34] applied ordinary kriging, simple cokriging, ordinary cokriging, standardized ordinary kriging, and moving average using inverse distance with powers of 1–5 for spatial analyzing annual, monthly, and 24 h maximum rainfall data in Hajighoshan watershed located in northeast of Iran. The 22 meteorological stations existed in and around the basin with data collection period of 30 years were selected for the analysis. According to the results obtained through the analysis of variogram model, Gaussian models are supposed as the best models for annual, monthly, and 24 h maximum rainfall data. The Gaussian model for annual rainfall data is shown in Figure 23.2.

According to Figure 23.2, nugget (C_0), sill ($C + C_0$), and the range (A) parameters are 100 m, 71.40 km, and 87.17 km, respectively. The results of geostatistic analysis showed that ordinary kriging is the best performed method with MAE = 34.26 and RMSE = 160.67 for annual rainfall, while moving average using inverse distance with power of 5 is the best method for monthly and 24 h maximum rainfall.

23.8.2 Case Example in Flow Duration Curve and Principal Component Analysis, Cluster Analysis, and Discriminant Analysis

Khosrobeigi [26] applied regional flow duration curve analysis in Namak Lake watershed of Iran (watershed no. 41). The 18 physiographical, meteorological, geological, and land use characteristics of existent hydrometric stations are extracted. The independent parameters and homogeneous watersheds were recognized by using PCA (Tables 23.2 and 23.3), CA (Figure 23.3), and DA (Figure 23.4), respectively. The results of Table 23.2 shows that among the 18 variables, first six variables that had eigenvalues more than 1 were selected as independent variables and explained 83.55% of variability. Also, it can be seen from Table 23.3 that since the variable of weighted average height (H_{mean}) in the first factor can explain other factors, it was selected as an independent factor. In other factors, area (A), rangeland area (Pr), drainage density (Dd), permeable formations (PP), and main stream length (SL) were selected as independent parameters respectively. According to Figures 23.4 and 23.5, the watersheds were divided into two homogeneous groups.

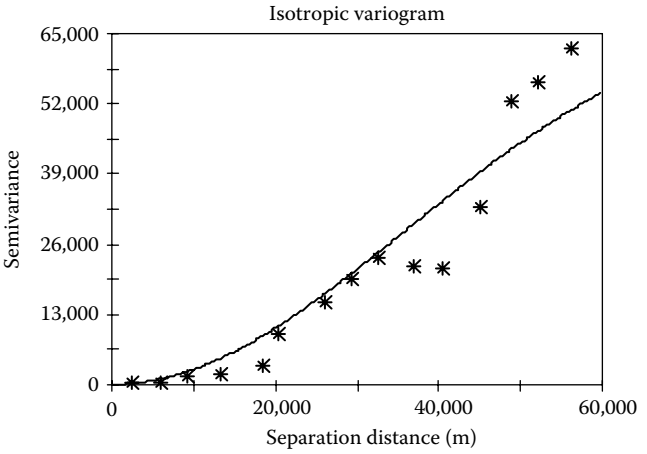

FIGURE 23.2 Variogram for annual rainfall data.

TABLE 23.2 Correlation Matrix of the Factors Selected by PCA

Factor	Eigenvalue	Total Variance (%)	Cumulative Variance (%)
1	5.72	31.80	31.80
2	3.35	18.63	50.44
3	1.79	9.94	60.37
4	1.73	9.61	69.98
5	1.34	7.45	77.43
6	1.10	6.12	83.55
7	0.75	4.17	87.72
8	0.59	3.30	91.02
9	0.58	3.23	94.25
10	0.35	1.97	96.22
11	0.16	0.91	97.13
12	0.15	0.81	97.95
13	0.13	0.70	98.65
14	0.10	0.55	99.19
15	0.08	0.44	99.63
16	0.04	0.22	99.85
17	0.02	0.10	99.96
18	0.01	0.04	100.00

23.8.3 Case Example in Peak Flood Discharge and Hybrid Method

Chavoshi Borujeni and Eslamian [5] applied hybrid method with a total of 311 station-years from 17 gaging stations located Isfahan and Charmahal and Bakhtyari provinces. The regression analysis suggests that the area (A) and average elevation watershed (H) should be included in the hybrid method in the study region because peak flood discharge has reasonable regression relationships with these two parameters. According to Equation 23.21, the data set was divided into three groups:

Group 1: the stations with 12–619 km^2 in area including Marbran, Babahydar, Tong Esferjan, Chehlgerd, Monderjan, Vaneshan, and Godarkabk subwatersheds.

TABLE 23.3 Component Loading Matrix

	Component					
Factor	1	2	3	4	5	6
Area	−0.06	0.96*	−0.08	−0.04	0.014	−0.01
Perimeter	−0.31	0.83*	−0.31	−0.09	−0.09	−0.13
Weighted average slope watershed	0.75*	−0.21	−0.23	0.43	−0.07	−0.07
Maximum height	0.82*	0.13	0.20	0.06	−0.38	−0.01
Minimum height	0.02	−0.11	0.03	−0.00	0.80*	−0.20
Weighted average height	0.89*	−0.13	−0.01	0.21	0.12	−0.07
Average stream slope	−0.10	0.97	−0.08	−0.09	0.05	0.04
Drainage density	0.13	−0.07	0.01	0.96*	−0.06	0.03
Main stream length	0.00	−0.05	−0.05	0.09	−0.02	0.92*
Mean annual rainfall	0.90*	−0.14	−0.01	−0.01	−0.03	0.18
Mean annual temperature	−0.65	−0.05	0.48	−0.24	−0.25	0.11
Mean annual potential evaporation	−0.79*	0.22	0.19	−0.23	0.08	0.14
Permeable formation	−0.17	0.22	−0.01	−0.10	0.70*	0.34
Rangeland area	0.00	0.23	−0.88*	−0.27	−0.15	0.04
Irrigated forming area	−0.03	−0.06	0.77	−0.10	−0.34	−0.05
Dry forming area	−0.34	−0.18	0.71	−0.11	0.32	0.01
Garden area	0.48	−0.30	−0.31	−0.12	−0.08	0.10
Rock area	0.25	−0.07	0.05	0.92*	−0.00	0.07

* >0.7.

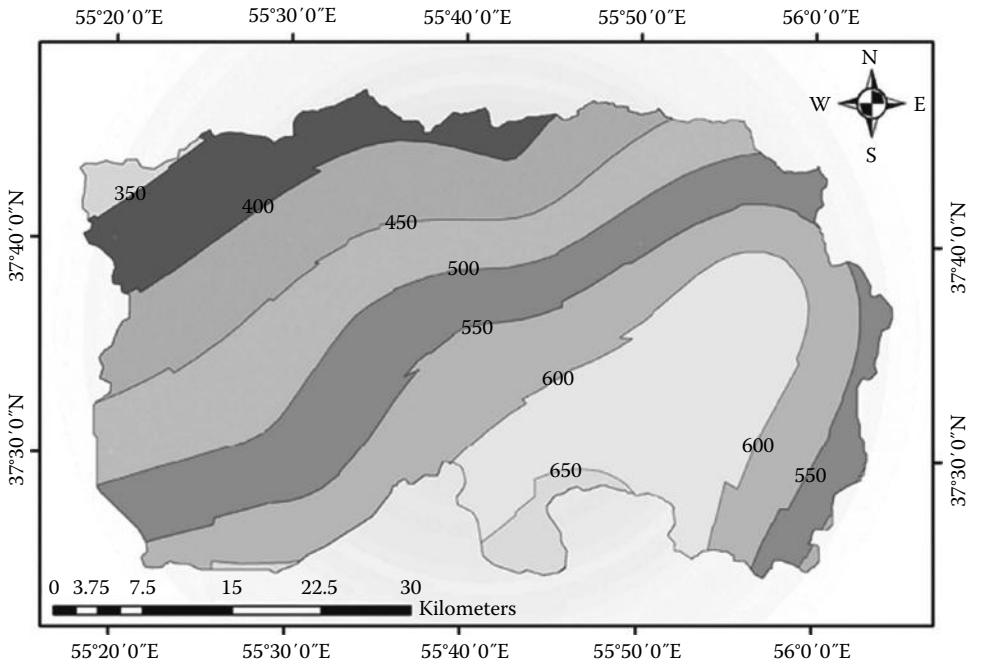

FIGURE 23.3 Annual isohyet map in Hajighoshan watershed.

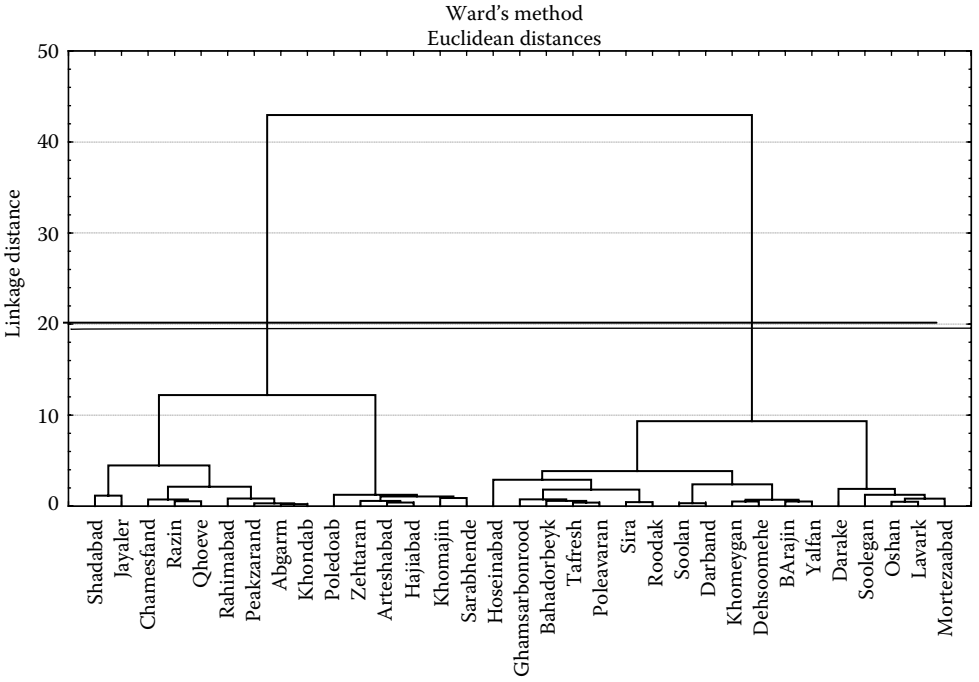

FIGURE 23.4 Dendrogram of the hierarchical clustering on watershed characteristics.

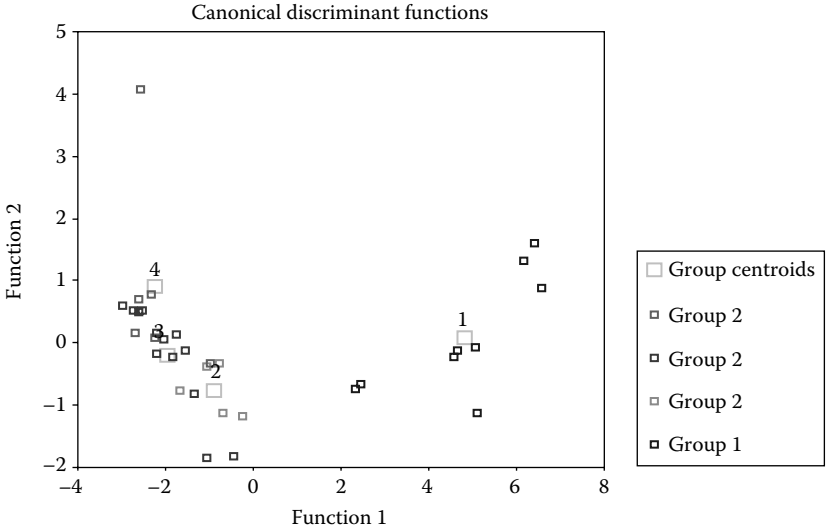

FIGURE 23.5 A plot of the first and second discriminant functions on watershed characteristics using PCA. Variables closely related to the first two functions were weighted average height (H_{mean}) area (A), rangeland area (Pr), drainage density (Dd), permeable formations (PP), and main stream length (SL).

TABLE 23.4 Average Weighted Drainage Area (A) and Average Elevation Watershed (H) in Each Group

Group	Average Weighted Drainage Area (km^2)	Average Weighted Average Elevation Watershed (m)
1	242.42	2588
2	928.16	2447
3	1010.22	2444

TABLE 23.5 S_{ijk} Estimation Values in Repeated One

Return Period → / Group ↓	2	5	10	25	50	100
1	0.07	0.21	0.38	0.69	1.02	1.45
2	0.06	0.14	0.21	0.3	0.36	0.42
3	0.1	0.38	0.78	1.69	2.81	4.44

TABLE 23.6 Q_t (m^3/s) Estimation Values in Repeated One

Return Period → / Group ↓	2	5	10	25	50	100
1	17	51	92	167	247	352
2	56	130	195	279	334	390
3	101	384	788	1707	2839	4485

TABLE 23.7 b_t Estimation Values in Repeated One and Final for Drainage Area (A)

Return Period → / Group ↓	2	5	10	25	50	100
One	0.098	0.264	0.412	0.636	0.825	1.03
Final	0.1	0.266	0.412	0.636	0.83	1.03

Group 2: the stations with 712–1427 km^2 in area including Hna, Savaran, Sarabhedeh, Tang Varkesh, Tang Zardalu, and Ghaleh Shahrokh subwatersheds.

Group 3: the stations with 1642–3820 km^2 in area including Solegan, Eskandari, Kta, and Beheshtabad subwatersheds. Using Equation 23.23, the average weighted drainage area (A) and average elevation watershed (H) in each group were computed (Table 23.4). Also, S_{ijk}, Q_t, and b_t using Equations 23.24 through 23.26 were computed, respectively (Tables 23.5 through 23.7).

As described in Section 23.6.5, each of the regression variables should be determined separately. The second variable, that is, height (H), was analysis in next step and accomplished the hybrid method steps except the instead of peak flood discharge in Equation 23.23 from standardized peak flood discharge in repeat final in last variable (A) are used. The constant model, that is, α coefficient is determined during the final step. Finally, the regional flood analysis equations are estimated as follows:

$$Q_2 = 30A^{0.1}H^{-0.037} \tag{23.44}$$

$$Q_5 = 35A^{0.266}H^{-0.121} \tag{23.45}$$

$$Q_{25} = 20A^{0.636}H^{-0.247} \tag{23.46}$$

$$Q_{50} = 22A^{0.83}H^{-0.266} \tag{23.47}$$

$$Q_{100} = 10A^{1.03}H^{-0.248} \tag{23.48}$$

where

Q_t is the peak flood discharge with t return period
A is the drainage area (km^2)
H is the average elevation watershed (m)

23.8.4 Case Example in Low Flow and Hybrid Method

Eslamian and Biabanaki [9] using the mean daily flow statistics from 41 hydrometric stations in Karkheh Basin, Iran, after checking the region homogeneity by cluster method and Andrew's curves, low flow analysis has performed by several models, namely, multivariate regression for determining the relations between low flow values and hydrologic characteristics of basin (MRLF), index low flow method (ILFM), regionalization model of frequency formula parameters (RFFP, determining regression equation between mean and standard deviation of low flows and hydrologic characteristics of basin), and hybrid low flow model (HLFM). For goodness-of-fit test, the least-squares method (RSS) has been employed, and for determining the best distribution, an arbitrary distinction method has been used. The computed distinctions have been shown that the two parameters gamma distribution is better than the other ones in view of using in this study. Using this distribution, low flows with different return periods have been determined. The results of cluster method and Andrew's curves show that 35 stations are in a homogeneous region. Developed regression models are as follows:

$$Q_5 = 10^{-0.442bf - 5.01\times10^{-4}hm + 1.381\times10^{-4}area + 0.535} \tag{23.49}$$

$$Q_{10} = 10^{-0.460bf - 5.44\times10^{-4}hm + 1405\times10^{-4}area + 0.452} \tag{23.50}$$

$$Q_{20} = 10^{-0.481bf - 5.94\times10^{-4}hm + 1411\times10^{-4}area + 0.386} \tag{23.51}$$

$$Q_{25} = 2.539\times10^{-4}area + 0.124wsa - 1.767 \tag{23.52}$$

$$Q_{50} = 2.211\times10^{-4}area + 0.111wsa - 1.589 \tag{23.53}$$

$$Q_{100} = 1.945\times10^{-4}area + 0.101wsa - 1.438 \tag{23.54}$$

where

area is the area of basin (km^2)
bf is the bifurcation factor
hm is the basin elevation (m)
wsa is the basin slope (%)

In the ILFM, for the stations that are located in the homogeneous region, Q_T/Q_2 should be calculated for different return periods and then their interstation averages should be obtained. For the *ILFM*, the final developed equation is as follows:

$$Q_2 = 10^{-0.409bf - 0.365be + 1.38\times10^{-4} area + 0.634} \tag{23.55}$$

where
area is the area of basin (km²)
bf is the bifurcation factor
be is the basin elevation (m)

For the RFFP method, the relation between averaged (mean) and standard deviation of low flows (Std) and characteristics of basin has been studied, and the obtained models for average and standard deviation are as follows:

$$Mean = 10^{1.435\times10^{-4} area - 2.678 Logbf - 2.8\times10^{-4} be + 0.587} \tag{23.56}$$

$$Std = 10^{6.147\times10^{-4} lms - 0.263 Logbe - 0.203bf + 4.618\times10^{-2}} \tag{23.57}$$

where
area is the area of basin (km²)
bf is the bifurcation factor
be is the basin elevation (m)
lms is the length of main stream (km)

Classifying the area to several regions is the basis of the HLFM. So first, the area will be divided into several regions. In this work, two factors that are the area and mean slope of basin were selected as a criterion for dividing the basin. Reason for using these parameters is that when the hydrologic characteristics of the basin have been used for analysis, only regression coefficients for the area and mean slope of basin were constant. Thus on the basis of these two factors and using the *K* average method (one of the CA methods), the area is divided into five different parts. The regional models for estimating low flows with different return periods according to hybrid method (HLFM) are as follows:

$$Q_5 = 4.86818 area^{-0.15681} \tag{23.58}$$

$$Q_{10} = 14.10158 area^{-0.03121} (bs)^{-0.80828} \tag{23.59}$$

$$Q_{20} = 2.34825 area^{-0.01171} (bs)^{-0.27283} \tag{23.60}$$

$$Q_{25} = 1.76999 area^{-0.00848} (bs)^{-0.19658} \tag{23.61}$$

$$Q_{50} = 1.02680 area^{-0.00279} (bs)^{-0.106444} \tag{23.62}$$

$$Q_{100} = 0.77993 area^{-0.00068} (bs)^{-0.01573} \tag{23.63}$$

where
Q is the low flow (m³/s)
area is the area of basin (km²)
bs is the mean slope of basin (m/m)

After determining the regional model for estimating low flows with four mentioned methods, the model accuracy of four studied methods by relative estimate error and the RMSE has been considered. For this purpose, the stations that have recorded the length of more than 30 years have been used. The results showed that MRLF and ILFM methods are more suitable than HLFM, but the RFFP has less accuracy as compared with HLFM.

23.8.5 Case Example in Low Flow and Principal Component Regression

Eslamian et al. [11] attempted to estimate the low flow index (7Q10), the 7-day, 10-year low flow, using principal component regression (PCR) based on physiographic and hydrologic variables in Karkheh Watershed, Iran. Twelve variables (latitude, longitude, annual average precipitation, watershed area, watershed average slope, distribution ratio, summation of stream lengths, Miller coefficient, main river average slope, length of main channel, watershed average height from sea level, and drainage density) were determined using GIS software. The gamma distribution with two parameters was chosen as the suitable regional distribution using ranking method. Using gamma distribution, 7Q10 was estimated for all of the 35 gaging catchments. PCR was performed in order to eliminate large variances due to multicollinearity. Table 23.8 includes eigenvalues and eigenvectors.

As Table 23.8 shows, the eigenvector loadings for component one are not considerable ($l_{ik} < 0.5$). The variables with high loadings in component number two are the same as those in third component. In other words, components two and three possibly include the same specific data. It is likely that the remaining components, that is, components 4 and 5 are good candidates to be retained in the regression due to the fact that they each are made up of high loading variables (Miller coefficient in component 4 and area in component 5).

To approve the assumptions mentioned earlier regarding which components to retain for use in PCR, factor analysis was performed using varimax rotation.

The data set was analyzed applying two, three, four, five, and six factors. The results indicate that two-factor rotation can better be justified. The results of applying two factors are shown in Table 23.9.

Table 23.9 indicates that the first factor is the size factor because the high loading variables represent size of the catchments in this factor. Factor 2 in which latitude has the highest value can be attributed to precipitation variability, which is represented by geographic position.

23.8.6 Case Example in Peak Flood Discharge and Hybrid Method

Chavoshi Borujeni et al. [6] used L-moment for parameter estimation, homogeneity testing, and selection of the regional distribution in North Karoon catchment, Iran. There are a number of 30 hydrometric sites in the study area, each of them with more than 5-year annual peak flood data. Among them,

TABLE 23.8 Eigenvalues and Eigenvectors of Correlation Matrix

	Component				
Model Variables	1	2	3	4	5
	Eigenvalues				
	3.14	1.3	0.43	0.1	0.01
	Eigenvector				
Latitude (°)	0.25	−0.68	−0.69	−0.06	−0.03
Area (km²)	0.54	0.23	0.03	−0.31	−0.75
Watershed average slope (%)	−0.28	0.63	−0.72	−0.01	−0.04
Stream length summation (m)	0.53	0.24	−0.03	−0.48	0.66
Miller coefficient	0.53	0.19	−0.06	0.82	0.09

TABLE 23.9 Two-Factor Analysis of Data

	1	2	
Factors	Factor	Loadings	Variance
Latitude (°)	0.07	−0.86	0.75
Area (km²)	0.99	−0.01	0.98
Watershed average slope (%)	−0.39	0.70	0.64
Stream length summation (m)	0.98	0.00	0.97
Miller coefficient	0.94	−0.09	0.89
Low flow variance	0.24	0.76	0.64

TABLE 23.10 List of Studied Sites in the Region

Site	River	Area (km²)	Elevation (m)
Zarinderakht	Khan Mirza	397	1770
Koohesookhteh	Kiar	2,909	1980
Dezak	Biregan	630	2152
Tangedarkesh	Jooneghan	899	2000
Godarkabk	Agh Bolagh	716	2150
Marghak	Bazoft	34,221	980
Lordegan	Lordegan	374	1650

TABLE 23.11 L-Moment's Properties and Discordance Measure

Site	*N*	Name	L-CV	L-SKEW	L-KURT	D(1)
1	15	Zarinderakht	0.4671	0.2864	0.1404	0.81
2	14	Koohesookhteh	0.3117	0.2744	0.1091	1.32
3	17	Dezak	0.4617	0.3993	0.2227	0.52
4	15	Tangedarkesh	0.2318	−0.0026	0.0927	1.28
5	21	Godarkabk	0.3226	0.3564	0.2551	1.06
Weighted means			0.3594	0.2728	0.1728	—
Parameters of regional Kappa distribution			0.5539	0.5447	−0.0659	0.3719

sites that are independent, that is, not subjected to upper catchments or any practices, were selected for this study (Table 23.10).

Discordancy measure for each site of the basin has been calculated and found between 0.30 and 2.08. The data range shows no discordancy for the study sites. However, the values of different heterogeneity measures, H_1, H_2, and H_3 are found as 5.93, 2.64, and 0.48, respectively. Since the first two heterogeneity measures, H_1 and H_2, are more than 2, dealing with heterogeneity of the studied sites, two suspected sites were removed and the process repeated. The results for the five remaining sites confirm that the rest of the sites may be considered as homogeneous regions (Table 23.11).

The values of different heterogeneity measures H_1, H_2, and H_3 are found as 1.94, 0.84, and 0.28, respectively. Therefore, the study region demonstrates acceptable homogeneity.

A number of 5 three-parameter distributions, that is, generalized logistic, generalized extreme value, generalized Pareto, general normal (LNIII), and Pearson type III were fitted to the region. The value of ZDIST statistic for the study area for each three-parameter distribution showed that all of the candidates are acceptable; however, LNIII is the most appropriate one. Finally, the regional peak flood estimates for each return period are obtained based on this distribution in the region.

23.8.7 Case Example in Peak Flood Discharge and Region of Influence Method

Eslamian [10] combined the physiographic characteristics of catchments with flood statistics in terms of defining ROI for selected sites in New South Wales, Australia. In this region, 22 catchments are selected for the analysis due to availability of geomorphological and physical characteristics of catchments. Six independent physical attributes including catchment area (A), length of main stream (L), median annual rainfall (MAR), 50-year rainfall intensity with 12-h period (I_{50}), catchment compactness coefficient (K_c), and elevation (E), and three independent statistical attributes including coefficient of variation of flood series in log domain (C_v), the specific 50-year flood (Q_{50}/A), and a new coefficient based on Pearson distribution ($(\mu - m)/(\mu - \gamma)$), for defining the ROI of each site are applied. The relations between C_v, Q_{50}/A, and A, K_c, L, MAR, I_{50}, and E were not found robust because little is generally known regarding some of the factors and processes by which storm runoff occurs.

The physiographic characteristics of catchments were combined with flood statistics at catchment outlet in terms of defining the ROI for each site. When physical attributes were included in the attributes set, sites in the resulting regions were more concentrated around the reference site, and therefore the results were more satisfactory. This was expected since the contiguous sites usually display similar pattern of rainfall and geomorphology.

23.9 Summary and Conclusions

This chapter reviews the estimation methods developed and used in regionalization. It is intended to provide a quick reference guide for such methods used for hydrological prediction in ungaged basins. Having a large number of input variables is one of the main common problems in regionalization. The choice of variable selection plays an important role in regionalization due to collinearity problem. Some different methods have been introduced to reduce regional model inputs. Among them, PCA and GT are useful methods. In the process of regional analysis, the sites must be assigned to homogeneous regions, because approximate homogeneity is required to ensure that regional analysis is more accurate than at-site analysis. Today, there are numerous ways available for detecting homogeneous regions. CA, DA, and AC are suitable for separating homogeneity regions. The information transfer is a fundamental step in regional analysis. In this chapter, index flood method, multiple regression, hybrid method, L-moments, ROI, and regional envelope curves explained for determining the relations between hydrologic variable values and characteristics of basin. Geostatistics was introduced as an approach of mapping hydrological variables. The regional analysis of hydrological variables can be performed by combination of the choice of variable selection, detecting homogeneous regions, and information transfer methods.

References

1. Acreman, M.C. and S.E. Wiltshire. 1987. Identification of regions for regional flood frequency analysis (abstract). *EOS Transactions American Geophysical Union* 68(44): 1262.
2. Agalbjörn, S., N. Koncar, and A.J. Jones. 1997. A note on the gamma test. *Neural Computing and Applications* 5: 131–133.
3. Burn, D.H. 1990. An appraisal of the "region of influence" approach to flood frequency analysis. *Hydrological Science Journal* 35(2): 149–165.
4. Carroll, S.P., L. Dawes, M. Hargreaves, and A. Goonetilleke. 2009. Faecal pollution source identification in an urbanising catchment using antibiotic resistance profiling, discriminant analysis and partial least squares regression. *Water Research* 43(5): 1237–1246.
5. Chavoshi Borujeni, S. and S. Eslamian. 1999. Regional flood frequency analysis in Zayandeh-Roud Watershed using the hybrid method. *Journal of Science and Technology of Agriculture and Natural Resources* 3(3): 1–12.

6. Chavoshi Borujeni, S., W. Nor Azmin Sulaiman, and S. Eslamian. 2010. Regional flood frequency analysis using L-moments for north Karoon basin, Iran. *Journal of Flood Engineering* 1(1): 71–801.
7. Dalrymple, T. 1960. Flood frequency analyses. Water Supply Paper 1543-A. US Geological Survey, Washington, DC, pp. 11–51.
8. Durrant, P.J. 2001. Wingamma: A non-linear data analysis and modeling tool with applications to flood prediction. PhD thesis, Department of Computer Science, Cardiff University, Wales, U.K., 261pp.
9. Eslamian, S. and M. Biabanaki. 2008. Low flow regionalization modeling. *International Journal of Ecological Economics and Statistics* 12(8): 82–97.
10. Eslamian, S. 2010. The physically-statistically based region of influence approach for flood regionalization. *Journal of Flood Engineering* 1(2): 149–158.
11. Eslamian, S., M. Ghasemizadeh, M. Biabanaki, and M. Talebizadeh. 2010. A principal component regression method for estimating low flow index. *Water Resources Management* 24(11): 2553–2566.
12. Evans, D. and A.J. Jones. 2002. A proof of the gamma test. *Proceedings of the Royal Society A* 458: 2759–2799.
13. Fuller, W.E. 1914. Flood flows. *Transactions of the American Society of Civil Engineers* 77(1293): 564–617.
14. Goovaerts, P. 1997. *Geostatistics for Natural Resources Evaluation (Applied Geostatistics)*. Oxford University Press, New York, 496pp.
15. Gordon, N.D., T.A. McMahon, B.L. Finlayson, Ch.J. Gippel, and J.R. Nathan. 2004. *Stream Hydrology: An Introduction for Ecologists*. John Wiley & Sons, New York.
16. Greenwood, J.A., J.M. Landwahr, N.C. Matalas, and J.R. Wallis. 1979. Probability weighted moments: Definition and relation to parameters of several distribution models expressible in inverse form. *Water Resources Research* 15(5): 1049–1054.
17. Groupe de Recherche en Hydrologie Statistique (GREHYS). 1996a. Presentation and review of some methods for regional flood frequency analysis. *Journal of Hydrology* 186(1–4): 63–84.
18. Groupe de Recherche en Hydrologie Statistique (GREHYS). 1996b. Inter-comparison of regional flood frequency procedures for Canadian rivers. *Journal of Hydrology* 186(1–4): 85–103.
19. Hjalmarson, H.W. and B.E. Thomas. 1992. New look at regional flood-frequency relations for arid lands. *Journal of Hydraulic Engineering ASCE* 118(6): 868–886.
20. Hosking, J.R.M. and J.R. Wallis. 1993. Some statistics useful in regional frequency analysis. *Water Resources Research* 29(2): 271–281.
21. Hosking, J.R.M. and J.R. Wallis. 1997. *Regional Frequency Analysis, an Approach Based on L-Moments*. Cambridge University Press, Cambridge, U.K., 224pp.
22. Interagency Advisory Committee on Water Data (IACWD). 1982. *Guidelines for Determining Flood Flow Frequency*, Bulletin 17B, U.S. Department of the Interior, U.S. Geological Survey, Office of Water Data Coordination, Reston, VA.
23. Isaaks, E.H. and R.M. Srivastava. 1989. *An Introduction to Applied Geostatistics*. Oxford University Press, New York, 542pp.
24. Jobson, J.D. 1992. *Applied Multivariate Data Analysis, Vol. II: Categorical and Multivariate Methods*. Springer-Verlag, New York.
25. Kaiser, H.F. 1960. The application of electronic computers to factor analysis. *Educational and Psychological Measurement* 20(1): 141–151.
26. Khosrobeigi, S. 2012. Regional flow duration curve using traditional and intelligence techniques in the Namak Lake Watershed. MSc thesis, Faculty of Natural Resources, Tarbiat Modares University, Tehran, Iran.
27. Koncar, N. 1997. Optimisation methodologies for direct inverse neurocontrol. PhD thesis, Department of Computing, Imperial College of Science, Technology and Medicine, University of London, London, U.K., 191pp.

28. Kumar, R., C. Chatterjee, S. Kumar, A.K. Lohani, and R.D. Singh. 2003. Development of regional flood frequency relationships using L moments for Middle Ganga Plains Subzone 1(f) of India. *Water Resources Management* 17: 243–257.
29. Lin, G.-F. and C.-M. Wang. 2006. Performing cluster analysis and discrimination analysis of hydrological factors in one step. *Advances in Water Resources* 29(11): 1573–1585.
30. Maidment, D.R. 1993. *Handbook of Hydrology*. McGraw-Hill, New York.
31. Modarres, R. 2008. Regional extreme wind speed frequency analysis for arid and semi arid region of Iran. *Journal of Arid Environment* 72: 1329–1342.
32. Moghaddamnia, A., M. Ghafari-Gousheh, J. Piri, S. Amin, and D. Han. 2009. Evaporation estimation using artificial neural networks and adaptive neuro-fuzzy inference system techniques. *Advances in Water Resources* 32: 88–97.
33. Moustafa, R.E. 2011. Andrews curves. *Advanced Review* 3: 373–382.
34. Nabipour, Y. 2011. Evaluation of effect of watershed management measures on flood control in Hajighoshan Watershed. MSc thesis, Faculty of Natural Resources, Tarbiat Modares University, Tehran, Iran.
35. Nathan, R.J. and T.A. McMahon. 1990. Identification of homogeneous regions for the purposes of regionalisation. *Journal of Hydrology* 121: 217–238.
36. National Climatic Data Center (NCDC). 2010. Locate weather observation station record. Available at: http://lwf.ncdc.noaa.gov/oa/climate/stationlocator.html.
37. NERC. 1975. UK flood studies report, Vol. 1. Natural Environment Research Council, London, U.K.
38. Pandey, G.R. and V.T.V. Nguyen. 1999. A comparative study of regression based methods in regional flood frequency analysis. *Journal of Hydrology* 225: 92–101.
39. Shrestha, S. and F. Kazama. 2007. Assessment of surface water quality using multivariate statistical techniques: A case study of the Fuji river basin, Japan. *Environmental Modelling and Software* 22(4): 464–475.
40. Tryon, R.C. 1939. *Cluster Analysis*. McGraw-Hill, New York.
41. Tsui, A.P.M., A.J. Jones, and A.G. De Oliveira. 2002. The construction of smooth models using irregular embeddings determined by a gamma test analysis. *Neural Computing and Applications* 10: 318–329.
42. Wallis, J.R. 1965. Multivariate statistical methods in hydrology—A comparison using data of known functional relationship. *Water Resources Research* 1: 447–461.
43. Webster, R. and M.A. Oliver. 2001. *Geostatistics for Environmental Scientists. Statistics in Practice*. John Wiley & Sons, Chichester, U.K., 265pp.
44. Webster, R. and P.A. Burough. 1972. Computer-based soil mapping of small areas from sample data, 1 smoothing. *Journal of Soil Science* 23(2): 222–234.
45. Yurekli, K., R. Modarres, and F. Ozturk. 2009. Regional maximum rainfall estimation for Cekerec watershed by L-moments. *Meteorological Applications* 16(4): 435–444.

24

Remote Sensing Data and Information for Hydrological Monitoring and Modeling

Reza Khanbilvardi
The City College of New York

Tarendra Lakhankar
The City College of New York

Nir Krakauer
The City College of New York

Rouzbeh Nazari
The City College of New York

Al Powell
Center for Satellite Applications and Research

AUTHORS

Reza Khanbilvardi, a licensed professional engineer, is the director of National Oceanic and Atmospheric Administration—Cooperative Remote Sensing Science and Technology (NOAA-CREST) Center at the City University of New York. Dr. Khanbilvardi obtained his masters (environmental engineering) and doctoral (CE/water resources engineering) degrees and postdoctoral (water resources) award from Pennsylvania State University in 1980, 1983, and 1984 respectively. His research interests include satellite-based remote sensing applications in hydroclimate, hydrology and land processes, surface water hydraulics and hydrology, flash flood monitoring and mapping, climate change impacts on water resources; snow-water equivalent studies.

Tarendra Lakhankar is a researcher working at NOAA-Cooperative Remote Sensing Science and Technology Institute hosted in the department of civil engineering at the City College of New York. Dr. Lakhankar received his BS in civil–water management, MS in environmental engineering, and PhD in civil engineering (water resources) from the Graduate Center of the City University of New York. His research interests range widely from the remote sensing and geographical information system (GIS) application to several research projects including developing satellite-based flash flood warning system, retrieving snowpack properties, and understanding the effect of climate change on human population.

Nir Krakauer is currently an assistant professor of civil engineering at the City College of New York. He received a BSE degree in engineering physics from the University of Michigan, Ann Arbor, and MS and PhD degrees in geochemistry from the California Institute of Technology, Pasadena, CA, with a dissertation titled "Characterizing carbon dioxide fluxes from oceans and terrestrial ecosystems."

He was a National Oceanic and Atmospheric Administration Climate and Global Change Postdoctoral Fellow with Dr. Inez Fung at the department of earth and planetary sciences, University of California, Berkeley.

Rouzbeh Nazari is an assistant professor at the department of construction management and civil engineering technology at New York City College of Technology. He completed his MS and PhD from the City College of the City University of New York. His research interests include application of satellite remote sensing in water resources, environment, and climate studies.

Al Powell served in the US Air Force as a weather officer providing environmental support to various Air Force missions. After his 20-year Air Force career, Dr. Powell worked for Autometric Inc., a remote sensing company that analyzed imagery and developed the tools, visualization, and data fusion applications to support the use of remotely sensed data in an integrated environment. Boeing Inc. purchased Autometric Inc. in 2000. Under Boeing Inc., Al headed the environmental applications division that developed environmental tools and products for the analysis, fusion, and integration of environmental data for government and civil applications. These tools encompassed the atmospheric, oceanic, and space modeling and decision making and included novel ideas about how to track terrorists. Dr. Powell is currently the director for NOAA's Center for Satellite Applications and Research (STAR).

PREFACE

Advances in remote sensing techniques provide capabilities for the estimation of hydrological parameters at different spatial and temporal scales not necessarily possible with traditional field measurement techniques. This chapter provides an overview of how remote sensing techniques have been used over recent decades to estimate hydrological parameters including precipitation, evapotranspiration (ET), soil moisture, snow, lake ice, land use, and land cover. The sensors used are electromagnetic (in the visible [VIS], infrared [IR], or microwave [MW] sections of the spectrum) or gravitational, and may be passive or active. Case studies are presented to illustrate the use of remote sensing–based parameters in distributed hydrological models, for example, for flash flood forecasting, and for environmental studies.

24.1 Introduction

Remote sensing data and information have shown great potential in supplying relevant spatial data and parameters at the appropriate scale for use in distributed hydrological models for water resource applications. In contrast with many conventional data normally given as point measurements, remote sensing–based measurements are spatial averages over pixels, which can be more appropriate for use in distributed hydrological models. Furthermore, remote sensing enables data access from remote areas, where data are typically sparse. Remote sensing technology used electromagnetic spectrum in the range of wavelengths of different radiations reflected or emitted by objects. Although remote sensing spectrum varies from 0.03 nm to 100 cm, VIS, IR, and MW spectra are commonly used in the retrieval of hydrological parameters.

There are two main types of remote sensing: passive remote sensing and active remote sensing. The passive systems are based on the measurement of the natural thermal emission in the form of brightness temperature from the earth surface. On the other hand, the active MW systems generate their own radiation, which is transmitted toward the earth surface, and measure the reflected energy.

The unique characteristics of MW energy compared to the VIS and IR remote sensing systems are the ability to penetrate the atmosphere under various conditions including clouds, light rain, snow,

and smoke, as well as the ability of low frequency to penetrate vegetation up to a certain level. MW radiation is independent of solar radiation and can be used during both nighttime and daytime hours; high-frequency MWs are partially absorbed by vegetation; therefore, emitted signatures contain information on vegetation properties [82]. The MW remote sensing data, which are more suitable to estimate hydrological variables including snow, soil moisture, and precipitation, can be obtained during day- or nighttime.

The two critical characteristics of remote sensing data for advancing the measurement of hydrological parameters are spatial and temporal resolution. Remote sensing obtains spatially distributed information of hydrological variables that is important and helps to understand the spatial variability of watershed properties, to be included in modeling analysis. These data can be obtained at definite time intervals, which vary based on the sensors and type of orbit. The parameters such as precipitation are being monitored at every 15 min interval.

24.2 Monitoring Hydrological Parameters

24.2.1 Precipitation

Precipitation is a crucial parameter that drives the hydrological cycle, thus helps to improve weather and climate predictions. Improving hydrologic forecasting requires accurate quantitative precipitation measurements at higher temporal and spatial scales. The old and usually reliable network of rain gages provides an overview of approximate precipitation. However, spatial densities of these rain gages are the limiting factor to accurately capture the highly varied nature of precipitation. In such cases, remote sensing–based precipitation provides a spatially continuous gridded dataset, using area-averaged remotely sensed information rather than strictly an interpolated point-based rain gage field.

Precipitation retrievals from remote sensing sensors are carried out using VIS, IR, and MW wavelengths on geostationary and polar orbiting satellites. The IR sensor aboard detects radiation within the IR wavelengths that is emitted from the nearest surface beneath the satellite. This radiation is converted to a temperature and may be then correlated to surface-based rainfall based on an assumption such as that colder cloud temperatures indicate clouds of higher vertical extent and thus may be producing more rainfall. The currently operated IR sensors include National Oceanic and Atmospheric Administration (NOAA) Geostationary Operational Environmental Satellite (GOES), European METEOSAT, Russia's Elektro-L, and India's INSAT.

The MW sensors estimate rainfall based on a radiation emitted from sources such as liquid water droplets or suspended ice particles. Surface-based rainfall is thus correlated to the extent and composition of actual water in the atmosphere. The examples of MW-based sensors include NOAA, Defense Meteorological Satellite Program (DMSP), and TRMM satellites. The TRMM precipitation radar (PR) is an active sensor that measures the change between emitted and returned radiation due to atmospheric water particles and relates this to previously determined surface rainfall intensity [51].

The GPM is an international mission by JAXA and NASA as well as other international agencies that aims to unify and advance global precipitation measurements using MW sensors to be expected to be launched in 2014. This mission will provide global uniformly calibrated precipitation observations at every two to four h. The GPM mission will deploy dual-frequency precipitation radar (DPR) and a multichannel GPM Microwave Imager (GMI) with high-frequency capabilities. The GMI will serve as a reference standard for the constellation radiometers by means of an advanced calibration system, and the DPR will provide microphysical measurements such as particle size distribution and vertical structure of precipitating cloud systems. This system will be used in conjunction with cloud-resolving models for the creation of a common cloud-radiation database for precipitation retrievals from both the GMI and the constellation radiometers. The constellation members in GPM will be represented by existing or future satellites of opportunity such as those of the US DMSP, the EUMETSAT Polar System (EPS), the Japanese Global Change Observation Mission, the French–Indian tropical mission Megha-Tropiques,

and several others that are currently being planned. During the last two decades, several algorithms are developed for estimating rainfall from IR and MW satellite observations.

The global precipitation records from point measurements are available through last century (GPCC; http://gpcc.dwd.de). However, these datasets have own inherent adequacies to quantify the distribution of global precipitation to yield acceptable global climatology. The Global Precipitation Climatology Project was established by the World Climate Research Program in 1986 with an approach to merge data and information available from several sources of precipitation including IR and MW remote sensing sensors and rain gages [38].

24.2.2 Evapotranspiration

ET is the largest component in terrestrial water budgets consisting of 60% of land precipitation. It modulates land surface energy budget and constitutes an important source of water vapor to the atmosphere. However, atmospheric water vapor is the most significant greenhouse gas and thus plays a fundamental role in weather and climate [39].

First, the remote sensing approach to estimate ET is based on thermal IR spectrum wavelength, by solving simplified form of surface energy balance model. In this approach, the radiometric surface temperature is used for estimating the sensible heat flux (H) and obtaining ET as a residual of the energy balance. The latent heat flux (LE) representing the ET fraction can be derived from

$$LE = R_n - G - H \tag{24.1}$$

where

LE is the latent heat of evaporation due to ET

R_n is the net radiation absorbed by the land surface, equal to incoming solar radiation (R_s) minus outgoing shortwave and longwave radiations

H is the sensible heat flux to the atmosphere

G is the heat flux to the soil

In this equation, variables are expressed in energy units (W m^{-2}). ET can be calculated from LE by the amount of energy needed to evaporate water at a given temperature and pressure. If heat transfer coefficients are known or can be estimated, H can, in theory, be calculated from the difference between air temperature at reference height and the land surface temperature, measured by thermal IR bands on satellites such as the Landsat series [2,7], GOES [40], the Advanced Very High Resolution Radiometer series [58], the Advanced Spaceborne Thermal Emission and Reflection Radiometer [24,77], and the Moderate Resolution Imaging Spectrometer (MODIS) sensors, both on the Terra satellite [63,64]. Estimates of R_n and G are available from remote sensing or ground data, allowing LE to be calculated as a residual in the earlier equation. This approach has been applied widely to ET measurements with higher accuracy in semiarid regions.

The second approach to estimate ET is based on vegetation indices derived from canopy reflectance data. In this approach, the crop coefficients are estimated, which are further used to convert reference ET to actual crop ET. The crop coefficients are modified for water demands by irrigated crops. The crop coefficients are empirical ratios relating crop ET to a calculated reference-crop ET that is based on atmospheric water demand over a crop cycle or to actual ET measurements [65]. A time series of vegetation indices is correlated with measured ET to develop a curve over the crop cycle. This approach requires local meteorological and soil data to maintain a water balance in the root zone of the crop [28]. Duchemin et al. [18] developed linear relationship between NDVI and crop coefficients with good accuracy to derive maps of leaf area index (LAI) and transpiration requirements using Landsat7-(Enhanced Thematic Mapper) ETM+ images for agricultural area. The vegetation indices–based approach is also tested successfully using AVHRR [21,68] and MODIS [16,32,54,65]. Future earth observation systems

designed with higher spatial and temporal resolutions would make these approaches feasible for the operational monitoring of ET at a regional and global scale.

24.2.3 Soil Moisture

Soil moisture is a very important variable in hydrology because its variations influence the evolution of weather and climate. The soil moisture controls runoff, affects vegetation growth, and plays a significant role in evaporation and transpiration at the land–atmosphere boundary as well as surface energy flux [9]. However, conducting ground-based measurements of soil moisture consistently and regionally is difficult. Remote sensing provides an opportunity without the limitation of time and area. Active and passive remote sensing systems and especially those operating in the MW region of the electromagnetic spectrum have shown the ability to measure the soil moisture content since it is very sensitive to the dielectric properties of the soil. Low-frequency MW spectrum has the advantage of longer penetration and, therefore, less atmospheric effect.

Spaceborne active MW sensors are able to provide high spatial resolution (up to 10 m), but have low temporal resolution and are more sensitive to surface characteristics than passive systems. However, passive MW sensors provide low spatial resolutions (40–50 km) with a higher temporal resolution (12–24 h). Most of the applications of active MW in soil moisture retrieval are based on the hypothesis that the signal backscattered from the observed scene is widely dependent on the dielectric contrast that exists between wet and dry soils. Indeed, under the same land cover condition, the stronger radar backscattering values are observed for high soil moisture. However, soil moisture estimation based on active MW data only may face several challenges since the MW sensors are sensitive to other land cover characteristics such as vegetation density, surface roughness, and soil texture [20,34,83].

The accuracy of satellite-derived soil moisture is usually affected by the presence of vegetation, which significantly modifies and attenuates the outgoing MW radiation of the soil and makes the retrieval of realistic soil moisture from satellite-based sensors difficult and inaccurate. Soil moisture estimation by active remote sensing involves the measurement of backscattering, which may be affected by both vegetation canopy and soil moisture. The vegetation canopy may affect the backscattered energy by contributing to the volume backscatter of the observed scene and by attenuating the soil component of the total backscatter [44,83]. The total amount of attenuation and backscatter depends on several vegetation parameters, such as vegetation height, LAI, and vegetation water content, and on sensor-related characteristics such as angle of incidence, frequency, and polarization.

Two MW satellite missions, the European Space Agency (ESA) Earth Explorer Soil Moisture and Ocean Salinity (SMOS) launched in November 2009 and Soil Moisture Active Passive (SMAP) by NASA, which has been proposed to launch in 2015, take advantages of low frequency in soil moisture retrievals. SMOS mission has been designed to observe soil moisture over the global land with the first-ever polar-orbiting spaceborne radiometer. This novel technique of the SMOS mission will provide operational monitoring of water in soils. SMAP mission will overlap with the SMOS mission in time so that it will enable intercalibration and intercomparison of their respective data. Moreover, the synthetic aperture radar (SAR) in the SMAP will provide higher spatial resolution (1–3 km) soil moisture product. The EPS METOP will be a continuation of ERS scatterometer mission carrying the advanced scatterometer ASCAT. The METOP satellite series, with advanced scatterometer on board, will be the first operational satellite system dedicated to the retrieval of soil moisture information.

24.2.4 Snow

The storage of water in snowpack affects the surface runoff and soil moisture and is therefore important at the regional scale for various applications such as flood prediction and water resource management. The rising in air temperature over land and at most high northern latitudes, where snow cover is projected to contract, widespread melting of snow and ice could lead to rising global average sea level [39].

Satellite observations in the VIS and MW spectral range have been used for the global monitoring of snow cover properties for more than three decades.

Remote sensing sensors in VIS/IR spectrum that are well-appropriate snow cover mapping due to the high albedo of snow present a good contrast with most other natural surfaces except clouds. The two VIS- and IR-based snow products are widely used for large-scale climate research. First, the Interactive Multisensor Snow and Ice Mapping System (IMS) by NOAA provides daily snow cover information for the Northern Hemisphere. The IMS product is based primarily on VIS and near-IR observations, judged and mapped manually, and covers the period from late 1998 to present. It continues to undergo improvements and refinements. The IMS snow cover product is produced every day, regardless of the presence of clouds, which interfere with satellite visible and infrared retrievals. This is possible due to IMS analysts looping through sequential GOES and AVHRR images to evaluate snow cover based on time-integrated information [36,72]. Second, the suite of products derived from the MODIS by NASA provides weekly global snow cover information. The MODIS snow products are provided as a sequence of products beginning with a swath product and progressing, through spatial and temporal transformations, to an 8 day global-gridded product (http://modis-snow-ice.gsfc.nasa.gov/). Snow cover products derived from MODIS are based on a band rationing of MODIS band 4 (green) (0.545–0.565 μm) and band 6 (near-IR) (1.628–1.652 μm). These bands are used to calculate the normalized difference snow index [33].

The passive MW remote sensing sensors, the Scanning Multichannel Microwave Radiometer (SMMR, 1978–1987), Special Sensor Microwave/Imager (SSM/I, 1987–present), and the Advanced Microwave Scanning Radiometer-Earth Observing System (AMSR-E) on board the Aqua satellite (2002–2011), provided opportunity to global snow cover and snow water equivalent (SWE) mapping [6,46]. MW emission from snowpack depends on the snow grain size, density, depth, and SWE [31]. Passive MW sensors have the advantage of penetrating the cloud cover unlike VIS/IR sensors. However, passive MW data suffer from being a low-resolution measurement, on the order of 25 km. Therefore, an effort is being made to develop a combination of the two products to provide a significant improvement of snow cover and SWE product with high spatial resolution from the VIS/IR data and cloud transparency from the MW data [3,23,25,56,86].

24.2.5 River and Lake Ice

An effect of ice in river and lake produces an increased hydraulic resistance by growing ice and storage of frozen winter precipitation that can readily be seen in dramatic short-term changes in flow and water levels [70]. Changes in freeze-up and break-up dates of the ice in rivers and lakes affect the seasonal hydrograph, as significant quantities of water are stored and later released within river channels. Variability and trends in river and lake ice dynamics can serve as indicators of climatic change, as climate influences the timing of lake ice melt and freeze onset, ice duration, and lake thermal dynamics that feedback to the climate system initiating further change [53].

In the past decade, the use of satellite data has gradually developed to the point that today remote sensing–based techniques are the main tool in lake and river ice observation and monitoring. VIS and IR channels on board of polar orbiting satellites are capable of the visualization of the lake and river ice and location under cloud-free condition. Polar orbiting satellites such as MODIS, AVHRR, and Landsat were extensively being used due to their higher spatial resolution. Latifovic and Pouliot [53] proposed a profile feature extraction technique for lake ice phenology from historical satellite records acquired by the series of AVHRR sensors and then compared them with in situ observations successfully with high accuracy.

Active MW SAR data are also used successfully in conjunction with VIS and IR channels in order to monitor the ice extent, growth, and thickness even in the presence of cloud. However, temporal resolution (5–6 days) of current radar sensors and the short period for which measurements are available limit their use for climate change studies and operational monitoring [19]. Using SAR data (ERS-2 and RADARSAT-1), Nolan et al. (2003) were able to determine dates of lake ice formation, snowmelt, and ice melt to within a few days for four winter seasons [67].

24.2.6 Water Storage

Changes in terrestrial surface water storage affect the gravity field, where the added water mass exert a slight additional attraction. Precise measurements of changes in the gravity field sensed by orbiting satellites give information about seasonal and interannual shifts in the surface mass distribution. Over land, the filling and emptying of water pools, including soil and aquifers, is the main contributor to gravity changes, though hydrologically irrelevant contributions such as glacial rebound of the lithosphere exists and must be subtracted from the total gravity signal to estimate the change in water storage. While gravimetric remote sensing cannot distinguish between different surface water pools at a given location, subtracting known changes in pools (such as lakes and snowpack) permits inference of changes in otherwise poorly observed regional pools (such as groundwater).

Gravity Recovery and Climate Experiment (GRACE) is a pair of NASA satellites launched in March 2002, which measure earth's gravity field from orbits at about 500 km height. Small changes in the distances between the satellites, due to gravity field variations, are measured via onboard K-band MW signals and the global positioning system. GRACE generates maps of gravity anomalies at approximately monthly time resolution and ~250 km spatial resolution [79].

Over land, GRACE products show seasonal wet–dry cycles in areas such as the Amazon and Mississippi basins [78]. Interannual variability in water storage can be used to quantify drought and pluvial episodes. Regional decreasing trends in water storage over the observation period have been found, due to ice sheet melting over parts of Greenland and Antarctica and due to unsustainable groundwater withdrawals in regions such as northern India [81] and California's Central Valley.

The constraints provided by GRACE data for hydrological variability have been used in various ways to test and improve hydrological models. For example, Niu et al. (2007) subtracted modeled soil moisture and groundwater variability from total water storage change inferred from GRACE to deduce SWE over boreal river basins [66]. Syed et al. (2008) compared water storage variability inferred from GRACE with that given by the Global Land Data Assimilation System [80]. Assimilation of water storage information from GRACE into regional hydrologic models, combined with other data such as streamflow, has been shown to improve the realism of these models' simulations of river discharge and groundwater levels [57,85]. On the scale of large river basins, GRACE storage changes have been used together with precipitation, evaporation, and streamflow estimated from remote sensing and/or ground observations to test whether these estimates are good enough to close the water budget [76], and the correlation of GRACE water storage with observed streamflow has been used to extend water storage estimates to times where GRACE data are not available [8]. GRACE water storage has also been compared to streamflow in small watersheds (tens of square km) in order to clarify the consistency of the relationship between streamflow and watershed storage [50]. Bloom et al. (2010) correlated GRACE water storage with anomalies in column atmospheric methane, inferring that tropical moisture status is the leading contributor to interannual variability in methane emissions [11].

24.2.7 Water Quality

Water quality is a general descriptor of water properties in terms of physical, chemical, thermal, and/or biological characteristics that are suitable for human consumption. Major factors affecting water quality in water bodies include suspended solids, algae (chlorophylls), chemicals, dissolved organic matter, thermal releases, aquatic vascular plants, pathogens, and oils. Monitoring and assessing the water quality are critical for managing and improving its quality. Polar orbiting, high spatial resolution hyperspectral remote sensing sensors are being used increasingly as a tool for monitoring water quality conditions in inland and near-coastal waters. Remote sensing techniques to estimates these water quality parameters are based on changes in the spectral signature from water bodies and relate these measured changes on-site by empirical or analytical models. The empirical approach is based on using experimental datasets and statistical regression techniques to generate algorithms relating the water reflectance or radiances at the sensor in specific spectral bands or band ratios/combinations to the observed in situ water quality

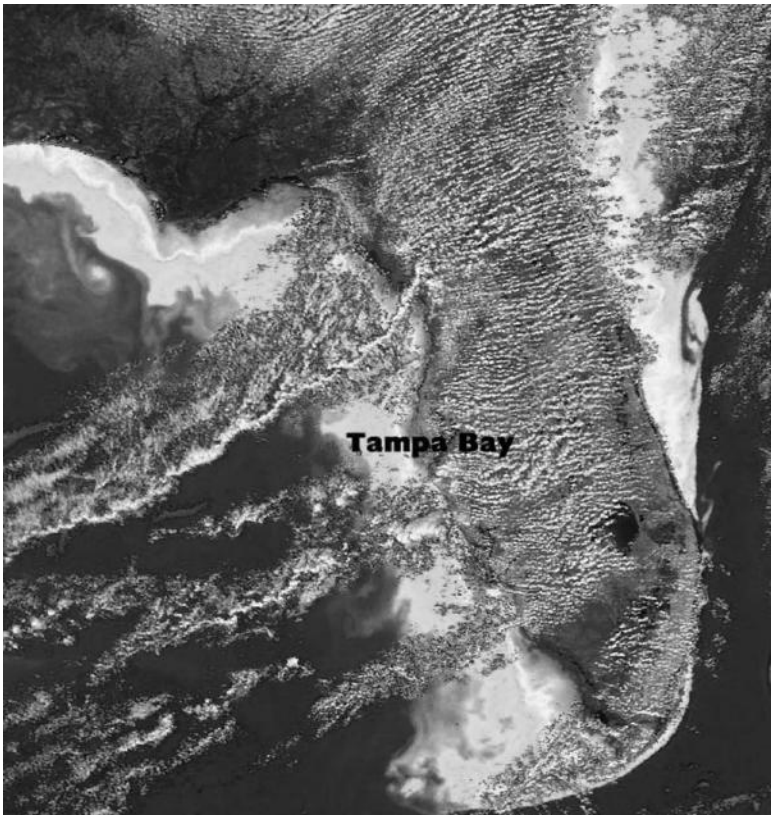

FIGURE 24.1 High concentrations of microscopic plants called phytoplankton (brighter regions) along the Florida coast and in Tampa Bay are an indicator of ocean health and change as seen in this SeaWiFS image from October 2004. (Photo courtesy of NASA, Washington, DC.)

parameters [62]. The selection of spectral channel depends upon the expected type and concentration of water constituents that affect quality (Figures 24.1 and 24.2).

Most of the research for water quality using remote sensing sensors has been carried out for chlorophyll content estimation, which is then used as an estimate for observing algal content and hence water quality. Commonly detected water quality parameters include the concentrations of phytoplankton pigments chlorophyll a (Chl a) [1,12,62], total suspended solids and inorganic suspended solids [26,45,48,55,84], absorption by colored dissolved organic matter [52], and indicators of water clarity such as turbidity [30,69]. High-resolution Landsat ETM was used to estimate chlorophyll a (Chl a) concentrations using band ratios for lakes [1,12] and coastal sewage outfall area [22]. The Medium Resolution Imaging Spectrometer (MERIS) on board ESA's ENVISAT is used successfully to estimate algal bloom and colored dissolved oxygen [15,27,59]. MODIS remote sensing data in conjunction with logarithmic band ratio model have shown its capability to monitor the impact of hurricane impact on chlorophyll-a concentration in Pensacola Bay system [37]. Estimation of water quality parameters from remote sensing has proved to be useful and successful and is being investigated for operational use.

24.2.8 Land Use–Land Cover

The vegetation or land cover plays critical part in hydrological processes including interception and transpiration, which are sink or loss term in water balance model. The runoff curve number uses land

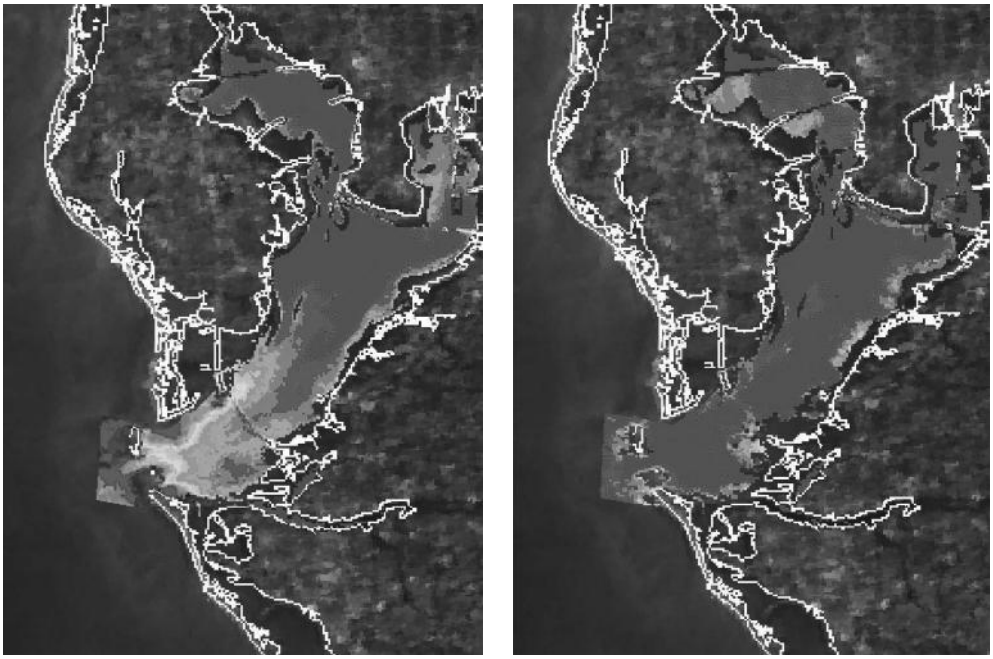

(a) (b)

FIGURE 24.2 MODIS imagery has shown that water quality of Florida's Tampa Bay decreases in winter months compared to summer. More particles suspended in the water, a measure called turbidity, show up as brighter in December (a) than in July (b). Images are composites of turbidity data collected in December and July, respectively, over a span of three years. (Photo courtesy of NASA/USF, Washington, DC.)

use/land cover condition with soil texture to estimate runoff from precipitation. Therefore, accurate information on land cover and land use and their changes over time is necessary for hydrological and environmental modeling and decision making. Remote sensing is a powerful and cost-effective tool for assessing the spatial and temporal dynamics of land use and land cover to evaluate deforestation, biodiversity loss, and climate change [71,74]. Multitemporal images provided by remote sensing sensors for same location are being used in conjunction with geographical information system to effectively determine the land use and land cover changes over time [42]. In addition, retrospective and consistent synoptic coverage over 40 years from remote sensing satellites is greatly benefited to assess the historic or long-term land cover changes for climate studies.

Change detection methods including pre- and postclassification have been used wildly to evaluate land use and land cover changes using remote sensing satellite data [35,41,47] In preclassification approach, procedures such as image differencing [10], band rationing [4], change vector analysis [5], and principal component analysis [14] have been developed and used. These techniques are developed on basic approach to estimate the differences in the pixel reflectance values between the dates of interest. However, while these techniques are effective for identifying change, they cannot identify the nature of change. On the other hand, in postclassification method, the comparison was done over independently classified land cover data. Despite the difficulties associated with postclassification comparisons, this technique is most widely used for identifying land use and land cover changes [17].

24.3 Remote Sensing in Hydrological Modeling

The emergence of distributed hydrological model provides a powerful tool for water resource management under changing environments. Distributed hydrological models are commonly physically based

water balance/water transport model that requires large amounts of high-resolution input data. The constant improvement of remote sensing data availability made it possible to meet data needs in distributed hydrological simulation. Compared with the conventional observation method, remote sensing can periodically obtain grid-based ground observations within a certain period, so as to elevate the temporal–spatial resolution of data.

24.3.1 Land Surface Modeling

Historically, regional and global analyses and reanalyses used for weather forecasting or for diagnosing climate variability and change did not directly use observations of many water fluxes and stores, either due to lack of observations (e.g., soil moisture) or because the assimilation techniques for using these variables were not developed (e.g., precipitation) [43]. This has improved to some extent in recent years, for example, the North American Regional Reanalysis [60] ingested land and sea snow/ice cover products based on remote sensing, and precipitation gage observations over land as well as precipitation information from satellites (CMAP) over oceans. In numerical weather forecasting models, there is a fundamental need to incorporate those physical processes in the analysis that are linked to atmospheric moisture and dynamics. NASA's Land Data Assimilation System project has used observation-based forcing (precipitation, temperature, and radiation) datasets to drive land surface models over recent decades, helping elucidate trends and variability in soil moisture [29,73,88], but still does not use available observations of soil moisture or many other land surface variables.

Several recent pilot studies have showed encouraging results in assimilating remotely sensed soil moisture into land surface models in reanalysis mode, taking into account that soil moisture information based on MW is typical only for a surface layer rather than for the entire soil column [75,89].

Preliminary work has also sought to assimilate both thermal and MW information on moisture status in order to better constrain soil moisture at different depths. Additional data streams to assimilate include observed streamflow, which could in some cases be estimated from remote sensing, and GRACE water storage change [87]. Improvements in analyzed hydrology resulting from making full use of earth observing satellite observations promise to not only result in more accurate retrospective estimates of regional-to-global hydrological variability and change but also improve intermediate-to-seasonal range weather forecasts through better capturing land–atmosphere feedback [13,49,61].

24.3.2 Flash Flood Guidance and Forecasting

Climate change and variability increase the probability of frequency, timing, intensity, and duration of flood events. After precipitation, soil moisture is the most important factor dictating flooding, since rainfall infiltration and runoff are based on the saturation of the soil. Flash flood guidance (FFG) systems provide lead-time for emergency responders to evacuate citizens and deploy resources to assess flood damage. Remote sensing technologies have proved to be valuable tools to support effective early flood warning system for disasters. There are few FFG systems that have the capability to indicate the likelihood of flooding of small streams or rivers over large regions by using bias-corrected remotely sensed precipitation estimates and real-time soil moisture estimates to produce FFG. The FFG systems have the potential to provide advance warning of situations likely to lead to floods and thus provide additional lead-time for emergency managers to monitor the situation and provide improved flood forecasting services. The FFG models are commonly water balance models that portray the grid-based runoff generation process, using grid-based inputs including precipitation, evaporation, soil moisture, soil type, vegetation, and other underlying surface information.

Currently, National Weather Service issues a daily national map of gridded flash flood guidance, which is produced based on surface soil moisture deficit and threshold runoff estimates. Similarly, the Central America Flash Flood Guidance System (a regional FFG system) has been in operation since 2004. These systems use real-time remotely sensed precipitation datasets from NOAA satellites. However,

these systems are limited by real-time observations of soil moisture and hence use model-derived soil moisture information. Improved flash flood forecasting requires accurate and high-resolution soil surface information. Recent development in soil moisture estimation using remote sensing shows potential in flash flood application. The already launched SMOS satellite's mission and future SMAP mission are two potential sources of remotely sensed soil moisture data. SMAP is a directed mission within the NASA Earth Systematic Mission Program and is planned to launch in 2015, while SMOS is a Living Planet Programme from the ESA and launched in November 2009.

24.4 Summary and Conclusions

Advances in remote sensing techniques provided many advantages in the estimation of hydrological parameters at different spatial and temporal scales over traditional field measurement techniques reliably with sufficient accuracy. Over the last 10 years, use of remote sensing techniques in hydrology has advanced greatly with the launch of research platforms such as Terra and Aqua, TRMM, and operational platforms such as GOES and the DMSP series, as well as many other satellite platforms, and with the development of more sophisticated retrieval algorithms.

Currently, remote sensing data are being used operationally for the estimation of hydrological variables including precipitation, soil moisture, snow, and ice at varying spatial and temporal resolutions and accuracy via remote sensing. In the next decade, significant progress is expected in measuring other variables including albedo measurements, ET, sediment loads, erosion, and groundwater, to be operationally available for hydrological models. In some cases, current operational remote sensing–based techniques are used in only limited areas due to restriction from heavy forest or higher elevation mountains, but their use is expected to expand in the future. However, these problems can be solved through additional research and development.

Using passive MW remote sensing for measuring snow, soil moisture, and precipitation has been used operationally; however, one of the limitations in measuring these parameters is lower spatial scale. Much effort is needed to develop a framework to integrate multifrequency remote sensing information to produce high-resolution hydrological products that can be used over a range of spatial scales, from field, farm, and watershed, up to regional scales. In case of precipitation, there are many remote sensing possibilities including ground-based radar, VIS and thermal IR satellite imagery, and MW satellite data. However, the development of hybrid solutions to combine the benefits of satellites and ground observations (e.g., ground radars and gage networks), and advanced multispectral algorithms to improve the accuracy and spatial resolution of satellite precipitation is needed.

References

1. Allan, M.G., D.P. Hamilton, B.J. Hicks, and L. Brabyn. 2011. Landsat remote sensing of chlorophyll a concentrations in central North Island lakes of New Zealand. *International Journal of Remote Sensing*. 32(7):2037–2055.
2. Allen, R.G., M. Tasumi, and R. Trezza. 2007. Satellite-based energy balance for mapping evapotranspiration with internalized calibration (METRIC)—Model. *Journal of Irrigation and Drainage Engineering*. 133(4):380–394.
3. Armstrong, R.L. and M.J. Brodzik. 2003. Multi-sensor approach to mapping snow cover using data from NASA ' s EOS Aqua and Terra Spacecraft (AMSR-E and MODIS), EOS Trans, AGU, 84(46), Fall Meet Suppl., Abstract H 32B-0549, 2003.
4. Bahadur, K.C. 2009. Improving landsat and IRS image classification: Evaluation of unsupervised and supervised classification through band ratios and DEM in a mountainous landscape in Nepal. *Remote Sensing*. 1(4):1257–1272.
5. Baker, C., R.L. Lawrence, C. Montagne, and D. Patten. 2007. Change detection of wetland ecosystems using landsat imagery and change vector analysis. *Wetlands*. 27(3):610–619.

6. Basist, A., N.C. Grody, T.C. Peterson, and C.N. Williams. 1998. Using the special sensor microwave/imager to monitor land surface temperatures, wetness, and snow cover. *Journal of Applied Meteorology*. 37(9):888–911.
7. Bastiaanssen, W.G.M., E.J.M. Noordman, H. Pelgrum, G. Davids, B.P. Thoreson, and R.G. Allen. 2005. SEBAL model with remotely sensed data to improve water-resources management under actual field conditions. *Irrigation and Drainage*. 131(February):85–93.
8. Becker, M., B. Meyssignac, L. Xavier, A. Cazenave, R. Alkama, and B. Decharme. 2011. Past terrestrial water storage (1980–2008) in the Amazon Basin reconstructed from GRACE and in situ river gauging data. *Hydrology and Earth System Sciences*. 15(2):533–546.
9. Betts, A.K., J.H. Ball, A.C.M. Beljaars, M.J. Miller, and P.A. Viterbo. 1996. The land surface-atmosphere interaction: A review based on observational and global modeling perspectives. *Journal of Geophysical Research*. 101(D3):7209–7225.
10. Bindschadler, R.A., T.A. Scambos, H. Choi, and T.M. Haran. 2010. Ice sheet change detection by satellite image differencing. *Remote Sensing of Environment*. 114(7):1353–1362.
11. Bloom, A.A., P.I. Palmer, A. Fraser, D.S. Reay, and C. Frankenberg. 2010. Large-scale controls of methanogenesis inferred from methane and gravity spaceborne data. *Science*. 327(5963):322–325.
12. Brezonik, P., K. Menken, and M. Bauer. 2005. Landsat-based remote sensing of lake water quality characteristics, including chlorophyll and colored dissolved organic matter (CDOM). *Lake and Reservoir Management*. 21(4):373–382.
13. Brunet, G., M. Shapiro, B. Hoskins, M. Moncrieff, R. Dole, G.N. Kiladis, B. Kirtman et al. 2010. Collaboration of the weather and climate communities to advance subseasonal-to-seasonal prediction. *Bulletin of the American Meteorological Society*. 91(10):1397–1406.
14. Cakir, H.I., S. Khorram, and S.A.C. Nelson. 2006. Correspondence analysis for detecting land cover change. *Remote Sensing of Environment*. 102(3–4):306–317.
15. Campbell, G., S.R. Phinn, A.G. Dekker, and V.E. Brando. 2011. Remote sensing of water quality in an Australian tropical freshwater impoundment using matrix inversion and MERIS images. *Remote Sensing of Environment*. 115(9):2402–2414.
16. Cleugh, H.A., R. Leuning, Q. Mu, and S.W. Running. 2007. Regional evaporation estimates from flux tower and MODIS satellite data. *Remote Sensing of Environment*. 106(3):285–304.
17. Dewan, A.M. and Y. Yamaguchi. 2009. Land use and land cover change in Greater Dhaka, Bangladesh: Using remote sensing to promote sustainable urbanization. *Applied Geography*. 29(3):390–401.
18. Duchemin, B., R. Hadria, S. Erraki, G. Boulet, P. Maisongrande, A. Chehbouni, R. Escadafal, J. Ezzahar, J. Hoedjes, and M. Kharrou. 2006. Monitoring wheat phenology and irrigation in Central Morocco: On the use of relationships between evapotranspiration, crops coefficients, leaf area index and remotely-sensed vegetation indices. *Agricultural Water Management*. 79(1):1–27.
19. Duguay, C.R. and P.M. Lafleur. 2003. Determining depth and ice thickness of shallow sub-Arctic lakes using space-borne optical and SAR data. *International Journal of Remote Sensing*. 24(3):475–489.
20. Engman, E.T. 1995. Measuring soil moisture with imaging radars. *IEEE Transactions on Geoscience and Remote Sensing*. 33(4):915–926.
21. Fisher, J.B., K.P. Tu, and D.D. Baldocchi. 2008. Global estimates of the land-atmosphere water flux based on monthly AVHRR and ISLSCP-II data, validated at 16 FLUXNET sites. *Remote Sensing of Environment*. 112(3):901–919.
22. Forster, B., X. Sha, and B. Xu. 1993. Remote-sensing of sea-water quality parameters using landsat-tm. *International Journal of Remote Sensing*. 14(15):2759–2771.
23. Foster, J.L., D.K. Hall, J.B. Eylander, G.A. Riggs, S.V. Nghiem, M. Tedesco, E. Kim, P.M. Montesano, R.E.J. Kelly, K.A. Casey, and B. Choudhury. 2011. A blended global snow product using visible, passive microwave and scatterometer satellite data. *International Journal of Remote Sensing*. 32(5):1371–1395.
24. Galleguillos, M., F. Jacob, L. Prévot, A. French, and P. Lagacherie. 2011. Comparison of two temperature differencing methods to estimate daily evapotranspiration over a Mediterranean vineyard watershed from ASTER data. *Remote Sensing of Environment*. 115(6):1326–1340.

25. Gao, Y., H. Xie, N. Lu, T. Yao, and T. Liang. 2010. Toward advanced daily cloud-free snow cover and snow water equivalent products from Terra–Aqua MODIS and Aqua AMSR-E measurements. *Journal of Hydrology*. 385(1–4):23–35.
26. Giardino, C., A. Oggioni, M. Bresciani, and H. Yan. 2010. Remote sensing of suspended particulate matter in Himalayan Lakes. *Mountain Research and Development*. 30(2):157–168.
27. Gons, H.J., M.T. Auer, and S.W. Effler. 2008. MERIS satellite chlorophyll mapping of oligotrophic and eutrophic waters in the Laurentian Great Lakes. *Remote Sensing of Environment*. 112(11):4098–4106.
28. Gonzalez-Dugo, M.P., C.M.U. Neale, L. Mateos, W.P. Kustas, J.H. Prueger, M.C. Anderson, and F. Li. 2009. A comparison of operational remote sensing-based models for estimating crop evapotranspiration. *Agricultural and Forest Meteorology*. 149(11):1843–1853.
29. Gottschalck, J., J. Meng, M. Rodell, and P. Houser. 2005. Analysis of multiple precipitation products and preliminary assessment of their impact on global land data assimilation system land surface states. *Journal of Hydrometeorology*. 6(5):573–598.
30. Graves, D., J. Kearney, and K. Williams. 2004. Remote sensing of turbidity and water clarity along the North Carolina Coast with the use of SeaWiFS Data. *North*.
31. Grody, N. 2008. Relationship between snow parameters and microwave satellite measurements: Theory compared with Advanced Microwave Sounding Unit observations from 23 to 150 GHz. *Journal of Geophysical Research*. 113(D22):1–17.
32. Guerschman, J.P., A.I.J.M. Van Dijk, G. Mattersdorf, J. Beringer, L.B. Hutley, R. Leuning, R.C. Pipunic, and B.S. Sherman. 2009. Scaling of potential evapotranspiration with MODIS data reproduces flux observations and catchment water balance observations across Australia. *Journal of Hydrology*. 369(1–2):107–119.
33. Hall, D.K. and G.A. Riggs. 2007. Accuracy assessment of the MODIS snow products. *Hydrological Processes*. 21(12):1534–1547.
34. Hall, F.G., J.R. Townshend, and E.T. Engman. 1995. Status of remote sensing algorithms for estimation of land surface state parameters. *Remote Sensing of Environment*. 51(1):138–156.
35. He, C., A. Wei, P. Shi, Q. Zhang, and Y. Zhao. 2011. Detecting land-use/land-cover change in rural–urban fringe areas using extended change-vector analysis. *International Journal of Applied Earth Observation and Geoinformation*. 13(4):572–585.
36. Helfrich, S.R., D. McNamara, B.H. Ramsay, T. Baldwin, and T. Kasheta. 2007. Enhancements to, and forthcoming developments in the interactive multisensor snow and ice mapping system (IMS). *Hydrological*. 1586(12):1576–1586.
37. Huang, W., D. Mukherjee, and S. Chen. 2011. Assessment of Hurricane Ivan impact on chlorophyll-a in Pensacola Bay by MODIS 250 m remote sensing. *Marine Pollution Bulletin*. 62(3):490–498.
38. Huffman, G.J., R.F. Adler, P. Arkin, A. Chang, R. Ferraro, A. Gruber, J. Janowiak, A. McNab, B. Rudolf, and U. Schneider. 1997. The global precipitation climatology project (GPCP) combined precipitation dataset. *Bulletin of the American Meteorological Society*. 78(1):5–20.
39. IPCC. 2007. IPCC fourth assessment report: Climate change 2007. Intergovernmental Panel on Climate Change, IPCC, Valencia, Spain.
40. Jacobs, J.M., M.C. Anderson, L.C. Friess, and G.R. Diak. 2004. Solar radiation, longwave radiation and emergent wetland evapotranspiration estimates from satellite data in Florida, USA. *Hydrological Sciences Journal*. 49(3):461–476.
41. De Jong, B.H.J., S. Ochoa-Gaona, M.A. Castillo-Santiago, N. Ramírez-Marcial, and M.A. Cairns. 2000. Carbon flux and patterns of land-use/land-cover change in the Selva Lacandona, Mexico. *AMBIO A Journal of the Human Environment*. 29(8):504–511.
42. Joshi, P.K., M. Kumar, A. Paliwal, N. Midha, and P.P. Dash. 2009. Assessing impact of industrialization in terms of LULC in a dry tropical region (Chhattisgarh), India using remote sensing data and GIS over a period of 30 years. *Environmental Monitoring and Assessment*. 149(1–4):371–376.
43. Kalnay, E. et al. 1996. NCEP-NCAR 40-year reanalysis project.pdf. *Bulletin of the American Meteorological Society*. 77(3):437–470.

44. Kasischke, E., K. Smith, L. Bourgeau-Chavez, E. Romanowicz, S. Brunzell, and C. Richardson. 2003. Effects of seasonal hydrologic patterns in south Florida wetlands on radar backscatter measured from ERS-2 SAR imagery. *Remote Sensing of Environment*. 88(4):423–441.
45. Katlane, R., B. Nechad, K. Ruddick, and F. Zargouni. 2011. Optical remote sensing of turbidity and total suspended matter in the Gulf of Gabes. *Arabian Journal of Geosciences*, 6(5):1527–1535.
46. Kelly, R.E., A. Chang, L. Tsang, and J.L. Foster. 2003. A prototype AMSR-E global snow area and snow depth algorithm. *IEEE Transactions on Geoscience and Remote Sensing*. 41(2):230–242.
47. Kintz, D.B., K.R. Young, and K.A. Crews-Meyer. 2006. Implications of land use/land cover change in the buffer zone of a national park in the tropical Andes. *Environmental Management*. 38(2):238–252.
48. Kishino, M., A. Tanaka, and J. Ishizaka. 2005. Retrieval of Chlorophyll a, suspended solids, and colored dissolved organic matter in Tokyo Bay using ASTER data. *Remote Sensing of Environment*. 99(1–2):66–74.
49. Koster, R.D., M.J. Suarez, and M. Heiser. 2000. Variance and predictability of precipitation at seasonal-to-interannual timescales. *Journal of Hydrometeorology*. 1(1):26–46.
50. Krakauer, N.Y. and M. Temimi. 2011. Stream recession curves and storage variability in small watersheds. *Hydrology and Earth System Sciences*. 15(7):2377–2389.
51. Kummerow, C., W. Barnes, T. Kozu, J. Shiue, and J. Simpson. 1998. The tropical rainfall measuring mission (TRMM) sensor package. *Journal of Atmospheric and Oceanic Technology*. 15(3):809–817.
52. Kutser, T., D.C. Pierson, K.Y. Kallio, A. Reinart, and S. Sobek. 2005. Mapping lake CDOM by satellite remote sensing. *Remote Sensing of Environment*. 94(4):535–540.
53. Latifovic, R. and D. Pouliot. 2007. Analysis of climate change impacts on lake ice phenology in Canada using the historical satellite data record. *Remote Sensing of Environment*. 106(4):492–507.
54. Leuning, R., Y.Q. Zhang, A. Rajaud, H. Cleugh, and K. Tu. 2008. A simple surface conductance model to estimate regional evaporation using MODIS leaf area index and the Penman-Monteith equation. *Water Resources Research*. 44(10):1–2.
55. Li, R.-R., Y.J. Kaufman, B.-C. Gao, and C.O. Davis. 2003. *Remote Sensing of Suspended Sediments and Shallow Coastal Waters*. Institute of Electrical and Electronics Engineers, Inc., Piscataway, NJ.
56. Liang, T., X. Zhang, H. Xie, C. Wu, Q. Feng, X. Huang, and Q. Chen. 2008. Toward improved daily snow cover mapping with advanced combination of MODIS and AMSR-E measurements. *Remote Sensing of Environment*. 112(10):3750–3761.
57. Lo, M.-H., J.S. Famiglietti, P.J.F. Yeh, and T.H. Syed. 2010. Improving parameter estimation and water table depth simulation in a land surface model using GRACE water storage and estimated base flow data. *Water Resources Research*. 46(5):1–15.
58. Loukas, A., L. Vasiliades, C. Domenikiotis, and N.R. Dalezios. 2005. Basin-wide actual evapotranspiration estimation using NOAA/AVHRR satellite data. *Physics and Chemistry of the Earth Parts ABC*. 30(1–3):69–79.
59. Matthews, M.W., S. Bernard, and K. Winter. 2010. Remote sensing of cyanobacteria-dominant algal blooms and water quality parameters in Zeekoevlei, a small hypertrophic lake, using MERIS. *Remote Sensing of Environment*. 114(9):2070–2087.
60. Mesinger, F. et al. 2006. North American regional reanalysis. *Bulletin of the American Meteorological Society*. 87(3):343–360.
61. Mishra, A.K. and V.P. Singh. 2011. Drought modeling—A review. *Journal of Hydrology*. 403(1–2):157–175.
62. Moses, W.J., A.A. Gitelson, S. Berdnikov, and V. Povazhnyy. 2009. Satellite estimation of chlorophyll-concentration using the red and NIR bands of MERIS—The Azov Sea case study. *IEEE Geoscience and Remote Sensing Letters*. 6(4):845–849.
63. Mu, Q., F.A. Heinsch, M. Zhao, and S.W. Running. 2007. Development of a global evapotranspiration algorithm based on MODIS and global meteorology data. *Remote Sensing of Environment*. 111(4):519–536.

64. Mu, Q., M. Zhao, and S.W. Running. 2011. Improvements to a MODIS global terrestrial evapotranspiration algorithm. *Remote Sensing of Environment*. 115(8):1781–1800.
65. Nagler, P.L., J. Cleverly, E. Glenn, D. Lampkin, A. Huete, and Z. Wan. 2005. Predicting riparian evapotranspiration from MODIS vegetation indices and meteorological data. *Remote Sensing of Environment*. 94(1):17–30.
66. Niu, G.-Y., K.-W. Seo, Z.-L. Yang, C. Wilson, H. Su, J. Chen, and M. Rodell. 2007. Retrieving snow mass from GRACE terrestrial water storage change with a land surface model. *Geophysical Research Letters*. 34(15):1–5.
67. Nolan, M., G. Liston, P. Prokein, J. Brigham-Grette, V.L. Sharpton, and R. Huntzinger. 2003. Analysis of lake ice dynamics and morphology on Lake El' gygytgyn, NE Siberia, using synthetic aperture radar (SAR) and Landsat. *Journal of Geophysical Research*. 108(D2):1–12.
68. Pan, Y., X. Li, P. Gong, C. He, P. Shi, and R. Pu. 2003. An integrative classification of vegetation in China based on NOAA AVHRR and vegetation-climate indices of the Holdridge life zone. *International Journal of Remote Sensing*. 24(5):1009–1027.
69. Potes, M., M.J. Costa, and R. Salgado. 2011. Satellite remote sensing of water turbidity in Alqueva reservoir and implications on lake modelling. *Hydrology and Earth System Sciences Discussions*. 8(6):11357–11385.
70. Prowse, T.D. and M.G. Ferrick. 2002. Preface—Hydrology of ice-covered rivers and lakes: Scoping the subject. *Hydrological Processes*. 16(4):759–762.
71. Pyke, C.R. and S.J. Andelman. 2007. Land use and land cover tools for climate adaptation. *Climatic Change*. 80(3–4):239–251.
72. Ramsay, B.H. 1998. The interactive multisensor snow and ice mapping system. *Hydrological Processes*. 12(10–11):1537–1546.
73. Rodell, M., P.R. Houser, U. Jambor, J. Gottschalck, K. Mitchell, C.J. Meng, K. Arsenault et al. 2004. The global land data assimilation system. *Bulletin of the American Meteorological Society*. 85(3):381–394.
74. Rogan, J. and D. Chen. 2004. Remote sensing technology for mapping and monitoring land-cover and land-use change. *Progress in Planning*. 61(4):301–325.
75. Sabater, J.M., L. Jarlan, J.-C. Calvet, F. Bouyssel, and P. De Rosnay. 2007. From near-surface to root-zone soil moisture using different assimilation techniques. *Journal of Hydrometeorology*. 8(2):194–206.
76. Sahoo, A.K., M. Pan, T.J. Troy, R.K. Vinukollu, J. Sheffield, and E.F. Wood. 2011. Closing the terrestrial water budget from satellite remote sensing. *Remote Sensing of Environment*. 115(8):1850–1865.
77. Sarwar, A. and R. Bill. 2007. Mapping evapotranspiration in the Indus Basin using ASTER data. *International Journal of Remote Sensing*. 28(22):5037–5046.
78. Schmidt, R., P. Schwintzer, F. Flechtner, C. Reigber, A. Güntner, P. Döll, G. Ramillien, A. Cazenave, S. Petrovic, H. Jochmann, and J. Wünsch. 2006. GRACE observations of changes in continental water storage. *Global and Planetary Change*. 50(1–2):112–126.
79. Swenson, S. and J. Wahr. 2006. Post-processing removal of correlated errors in GRACE data. *Geophysical Research Letters*. 33(8):1–4.
80. Syed, T.H., J.S. Famiglietti, M. Rodell, J. Chen, and C.R. Wilson. 2008. Analysis of terrestrial water storage changes from GRACE and GLDAS. *Water Resources Research*. 44(2):1–10.
81. Tiwari, V.M., J. Wahr, and S. Swenson. 2009. Dwindling groundwater resources in northern India, from satellite gravity observations. *Geophysical Research Letters*. 36(18):1–5.
82. Ulaby, F.T., M. Dobson, and G. Bradley. 1981. Radar reflectivity of bare and vegetation covered soil. *Advanced Space Research*. 1:91–104.
83. Ulaby, F.T., R. Moore, and A. Fung. 1986. *Microwave Remote Sensing Active and Passive from Theory to Applications*. Artech House, Norwood, MA.
84. Volpe, V., S. Silvestri, and M. Marani. 2011. Remote sensing retrieval of suspended sediment concentration in shallow waters. *Remote Sensing of Environment*. 115(1):44–54.

85. Werth, S. and A. Güntner. 2010. Calibration analysis for water storage variability of the global hydrological model WGHM. *Hydrology and Earth System Sciences*. 14(1):59–78.
86. Zaitchik, B.F., M. Rodell, and R. Reichle. 2008. Assimilation of GRACE terrestrial water storage data into a land surface model: Results for the Mississippi River Basin. *Journal of Hydrometeorology*. 9(3):535–548.
87. Zhang, H., X., T. Liang, H. Xie, X. Wang, Q. Feng, and Q. Chen. 2012. A new approach of dynamic monitoring of 5-day snow cover extent and snow depth based on MODIS and AMSR-E data from Northern Xinjiang region. *Hydrological Processes*, (26) 3050–3061, doi:10.1002/hyp.8253.
88. Zhang, J., W.-C. Wang, and J. Wei. 2008. Assessing land-atmosphere coupling using soil moisture from the Global Land Data Assimilation System and observational precipitation. *Journal of Geophysical Research*. 113(D17):1–14.
89. Zhang, S.-W., X. Zeng, W. Zhang, and M. Barlage. 2010. Revising the ensemble-based Kalman filter covariance for the retrieval of deep-layer soil moisture. *Journal of Hydrometeorology*. 11(1):219.

25

Significance of Statistical Tests and Persistence in Hydrologic Processes

Khaled H. Hamed
Cairo University

AUTHOR

Khaled H. Hamed holds a BSc and an MSc in civil engineering from Cairo University, Egypt, and a PhD in civil engineering from Purdue University, United States. He has 25 years of practical experience in the fields of surface hydrology, stochastic hydrology, time series analysis, and flood frequency analysis. He has long experience in watershed modeling, stochastic reservoir analysis, time series modeling and forecasting, detection of trends and variations due to climatic changes, and stochastic as well as physical rainfall–runoff modeling. He is also the coauthor of two textbooks on flood frequency analysis and stationarity analysis of hydrologic and environmental time series published in the United States. Professor Hamed is an associate editor of the *IAHS Hydrologic Sciences Journal (HSJ)* and a reviewer for a number of prominent international scientific journals, which include *Water Resources Research*, *Journal of Hydrology*, *Hydrological Sciences Journal*, and *Climate Research*, among others.

PREFACE

Several statistical tests have been performed in the literature on hydrologic and climatological data. The most commonly used tests are those of trend and cross-correlation between data. A basic assumption of many of these statistical tests is that the data in each involved variable are randomly ordered in time. However, while most natural data violate this assumption, many studies simply ignore the effect that persistence in natural data has on the results of statistical tests of significance. Although such effect has been noted and warned against very early in the literature, many past and current studies simply fail to consider taking this effect into account. This chapter sheds some light on the effect of persistence on the distribution of some commonly used statistical tests of significance. Methods to account for the effect of persistence on these statistical tests are also discussed.

25.1 Introduction

Measurement of different types of hydrologic and meteorological variables had been carried out for many past years. In fact, some sort of hydrologic measurements have been made since the dawn of civilization as in the case of the Nile River [3]. The accumulation of various continuous measurements over the past century with reasonable quality and coverage has prompted many researchers to make use of this wealth of data for the benefit of mankind. This has been motivated by the need to assess the impacts of the observed large climatic variability and possible future changes in global and local climates. Two major directions have evolved in recent years that are based on statistical analysis of hydrologic and meteorological data. The first direction is concerned with the detection of the effect of climate change on various hydrologic processes, such as rainfall, runoff, and evapotranspiration, among others. The aim of this type of analysis is mainly to detect significant trends or possible abrupt change points within the observed time series in response to climate change. The second direction, on the other hand, is concerned with the prediction of various hydrologic phenomena, such as river flow or rainfall amounts, based on some global climatic indices that are observed in advance with sufficient lead times. In this case, statistical tests on the significance of the cross-correlation between hydrologic and global climatic indices are often used for the selection of best predictors.

Statistical analysis of hydrologic and meteorological data relies heavily on statistical tests of significance. Originally, these statistical tests had been developed for random data obtained from random experiments, and as such, no correlation is expected between successive values of the measured variable or variables. This is a key fact that has often been overlooked by some researchers when dealing with natural data. Most natural data exhibit some type of "persistence," which means that successive observations are significantly correlated, and are often referred to as "autocorrelated" or "serially correlated" data. The strength and extent of this autocorrelation in time has been typically divided into "short-term" and "long-term" persistence, but with no clear boundary between the two types. Because persistence violates the basic assumption of statistical tests of significance, many results become questionable if persistence is not properly dealt with. This chapter will concentrate on two widely used types of statistical tests of significance, which are trend tests and cross-correlation tests, although the same principles apply to other statistical tests of significance as well.

Typically, statistical tests are grouped into parametric tests, that is, those tests that depend on the statistical distribution of the tested data, and nonparametric (or distribution-free) tests, that is, those that are independent of the statistical distribution of the data. Under Gaussian (normal) distribution conditions, parametric tests are more powerful than nonparametric tests, that is, they are favorably more sensitive to small deviations from the null hypothesis. However, parametric tests have the disadvantage of losing power when the data deviate from the normality assumption, and distribution-free tests become more powerful [43]. Since most hydrologic data are skewed, with various degrees of deviation from normality, distribution-free tests will be considered in this chapter.

In the following sections, a sample of the previously mentioned statistical tests will be reviewed and the effect of persistence on the significance of their results will be discussed. Finally, methods to deal with the effect of persistence on these tests are surveyed.

25.2 Trend Tests

Through the past few decades, the topic of global warming, or climate change in general, has received a great deal of attention from researchers all over the world. In particular, there has been an interest to detect whether the observed changes in climate have significantly affected various hydrologic processes, such as rainfall and runoff. Studies have considered many aspects of change for both the magnitude and frequency of various events. For example, Kundzewicz et al. [29] studied trends in a number of river flow time series in different parts of the world, while Svensson et al. [37] studied trends in flood and

low-flow index series for the same group of rivers. Similarly, Andreadis and Lettenmaier [1] studied trends in the twentieth-century drought over the continental United States, Cunderlik and Ouarda [6] studied trends in the timing and magnitude of floods in Canada, McBean and Motiee [33] studied the impact of climate change on the great lakes of North America, and Estrela et al. [10] studied the impacts of climate change on water resources in Spain. These are but a few samples from a very long list of studies dealing with the subject.

The effect of persistence on the results of trend tests has long been known. For example, Cox and Stuart [5] stated that "Positive serial correlation among the observations would increase the chance of a significant answer even in the absence of a trend." Nevertheless, a large number of earlier studies as well as a considerable number of recent studies fail to account for the effect of persistence on their results. This by itself does not automatically invalidate their results, but the statistical evidence may be weaker than implied, and therefore some of the conclusions may not be properly supported. Methods to deal with persistence in observed data were suggested in the literature since the early 1970s. Lettenmaier [30] considered the detection of trends in water quality data with dependent observations. Hirsch and Slack [22] suggested a nonparametric test for seasonal data with serial dependence. Van Belle and Hughes [38] also suggested a nonparametric test for trends in water quality. El-Shaarawi and Damsleth [11] surveyed a number of parametric and nonparametric tests for dependent data. Zetterqvist [46] discussed statistical estimation and interpretation of trends in water quality data. Von Storch [39] proposed a prewhitening procedure to eliminate the effect of serial dependence on trend results. Hamed and Rao [20] suggested a modified Mann–Kendall trend test for autocorrelated data. More recent literature deals in more detail with the issues of temporal and spatial correlation. Douglas et al. [9] investigated the impact of spatial correlation on trends in floods and low flows in the United States. Yue and Wang [41] discussed regional streamflow trend detection with consideration of both temporal and spatial correlation. Matalas and Sankarasubramanian [32] investigated the effect of persistence on trend detection via regression. Yue et al. [45] discussed the impacts of serial and cross-correlation on Canadian streamflow trend detection. Hamed [19] suggested a procedure for testing trend significance using the Mann–Kendall trend test for data that exhibit long-term dependence.

In this section, we will consider two commonly used distribution-free trend tests. The details of each test are reviewed and the effect of persistence on each test is then investigated.

25.2.1 Mann–Kendall Trend Test

The first test we consider is the Mann–Kendall trend test. The test is based on Kendall's tau rank correlation statistic [24] and was proposed for use as a trend test by Mann [31] through calculating the correlation between the ranks of the observations with their order in time. The null hypothesis of this test is that data are randomly ordered in time. This means that the alternative hypothesis is that data are not randomly ordered, which encompasses both monotonic trends, whether linear or nonlinear, and serial correlation. In fact, the alternative hypothesis also covers abrupt changes (jumps) in the mean of the observations, although more specific tests are available for that specific case.

For a given sequence of observed data $x_1, x_2, \ldots, x_n$, the Mann–Kendall test statistic S is calculated as

$$S = \sum_{i=1}^{n} \sum_{j=i+1}^{n} \operatorname{sgn}(x_j - x_i) \tag{25.1}$$

where $\operatorname{sgn}(x_j - x_i)$ is the signum (or sign) function that evaluates to +1 if $x_j > x_i$, to −1 if $x_j < x_i$, and to zero if $x_j = x_i$. Because of the use of the indicator function sgn(.), the value of the test statistic S depends only on the ranks of the observations and not on their actual distribution, giving the test its distribution-free property.

Under the null hypothesis of random ordering, the statistic S has a zero mean [24] with a variance given by

$$V_0(S) = \frac{n(n-1)(2n+5)}{18} \tag{25.2}$$

where n is the number of observations. The standardized test statistic u can be obtained by dividing S by its standard deviation. Kendall [24] suggests a correction of continuity by subtracting 1 from a positive S and adding 1 to a negative S:

$$u = \begin{cases} \dfrac{(S-1)}{\sqrt{V_o(S)}} & S > 0 \\ 0 & S = 0 \\ \dfrac{(S+1)}{\sqrt{V_o(S)}} & S < 0 \end{cases} \tag{25.3}$$

Kendall [24] shows that the distribution of the standardized variate u tends to a standard normal variate as the number of observations n becomes large and that the normal distribution is a good approximation for n greater than 10 observations. For n less than 10 observations, the full distribution is tabulated by Kendall [24]. Kendall also discusses a correction of the variance for tied ranks. However, since we are dealing mainly with continuous data, the probability of exact ties is theoretically equal to zero. If a few ties do exist, they would be due to rounding effect or lack of precision in measurements, but the effect on the test should not be large in this case. Hamed [19] gives a detailed discussion of the effect of ties on the variance of the Mann–Kendall trend test statistic.

When the data are serially correlated, and under the null hypothesis of no trend, it has been shown by Hamed and Rao [20] and Hamed [19] that the mean of the Mann–Kendall test statistic remains to be zero, while the variance can be calculated as

$$V(S) = \frac{2}{\pi}\sum_{i=1}^{n}\sum_{j=i+1}^{n}\sum_{k=1}^{n}\sum_{l=k+1}^{n}\sin^{-1}\frac{\rho_{jl} - \rho_{il} - \rho_{jk} + \rho_{ik}}{\sqrt{(2-2\rho_{ij})(2-2\rho_{kl})}} \tag{25.4}$$

where ρ_{ij} for any two subscripts i and j is the autocorrelation coefficient between observations i and j of normally distributed data. If the observations are not normally distributed, these autocorrelations can be obtained after using a suitable transformation of the data, such as the well-known Box–Cox transformation. Alternatively, the autocorrelation ρ_{ij}^R between the ranks, which is distribution-free, can be used to obtain the normalized autocorrelations using Kendall's formula [24] as follows:

$$\rho_{ij} = 2\sin\left(\frac{\pi}{6}\rho_{ij}^R\right) \tag{25.5}$$

Inspection of the variance given by Equation 25.4 reveals that the variance increases as the strength of positive autocorrelation among the data increases (variance inflation) and decreases as the negative correlation increases (variance deflation). The program P1 in Appendix 25.A is a simple MATLAB® code for calculating the variance of S for the case of AR(1) data, but the code can be easily modified to accommodate any other dependence model, simply by changing the formula used for calculating the autocorrelation coefficients of the data at different lags and supplying the required inputs.

Figure 25.1 depicts the variance inflation factor $V(S)/V_0(S)$ for data with AR(1) dependence for different values of the first-order autocorrelation coefficient and sample size, while Figure 25.2 depicts the same for fractional Gaussian noise (FGN) data. To appreciate the adverse effect of variance inflation,

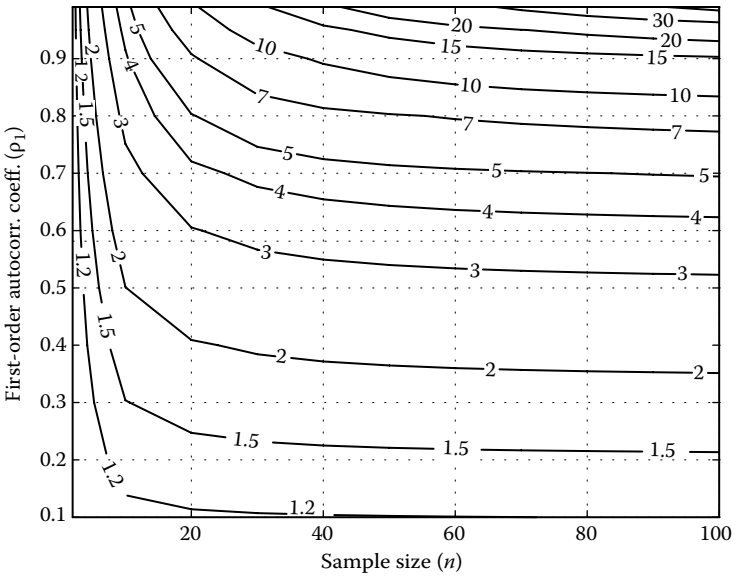

FIGURE 25.1 Variance inflation factors of the Mann–Kendall trend statistic S for AR(1) data as a function of sample size n and first-order autocorrelation coefficient ρ.

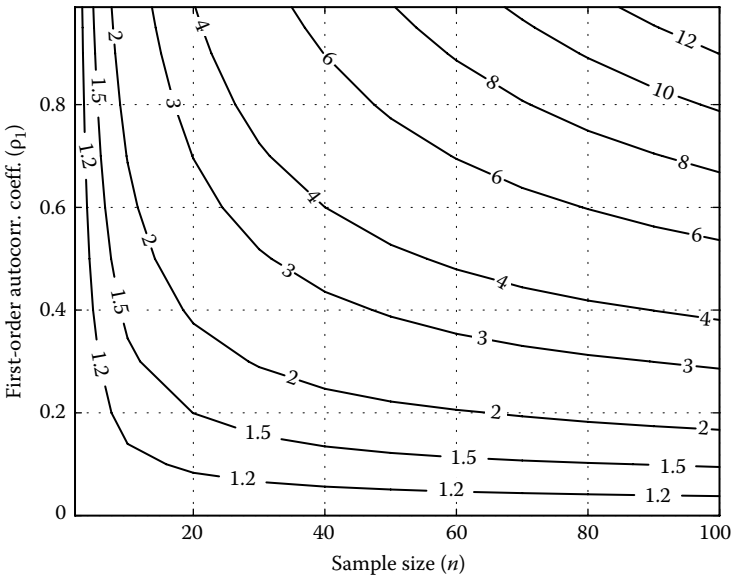

FIGURE 25.2 Variance inflation factors of the Mann–Kendall trend statistic S for FGN data as a function of sample size n and first-order autocorrelation coefficient ρ.

Hamed [16] shows that a variance inflation as low as 1.1 results in the rate of false significant results (type I error) being increased relative to its nominal values by 16%, 24%, and 30% at significance levels 10%, 5%, and 2% (two-sided test), respectively, while an inflation factor as low as 1.2 increases the rate by 34%, 48%, 70%, respectively. The variance inflation factors depicted in Figures 25.1 and 25.2 thus demonstrate how badly persistence can affect the results of trend tests. Hamed [17] discusses the full probability distribution of the Mann–Kendall trend test statistic for persistent data.

25.2.2 Daniels Trend Test

Another distribution-free trend test that is less commonly used is the Daniels trend test [7]. The test is based on Spearman's rho rank correlation coefficient [36] between the observations and their order in time. The null and alternative hypotheses of the Daniels test are the same as those for the Mann–Kendall test. For a given sequence of observed data $x_1, x_2, \ldots, x_n$, the Daniels test statistic r_s is calculated as

$$r_s = 1 - \frac{6\sum d^2}{n^3 - n} \tag{25.6}$$

where n is the number of observations and

$$\sum d^2 = \sum_{i=1}^{n} \left[R(x_i) - i\right]^2 \tag{25.7}$$

where $R(x_i)$ is the rank of observation x_i.

Under the null hypothesis of random ordering, the test statistic r_s has a zero mean with variance given by

$$V_0(r_s) = \frac{1}{n-1} \tag{25.8}$$

Kendall and Gibbons [25] show that the distribution of r_s tends to normal as the sample size n increases, albeit at a lower rate than that of the Mann–Kendall test statistic S and that the standard normal table gives an accurate approximation for $n > 35$. They also give distribution tables for sample sizes less than 17 and selected quantile values of r_s for n up to 35.

For correlated data, the mean of r_s can be shown to remain equal to zero, while the variance is given by

$$\mathrm{var}(r_s) = \frac{72}{\pi n^2 (n^2-1)^2} \sum_{i=1}^{n} \sum_{j=1}^{n, j\neq i} \sum_{k=1}^{n} \sum_{l=1}^{n, l\neq k} (i-1)(k-1) \sin^{-1} \frac{\rho_{jl} - \rho_{il} - \rho_{jk} + \rho_{ik}}{\sqrt{(2-2\rho_{ij})(2-2\rho_{kl})}} \tag{25.9}$$

where ρ_{ij} is as defined before in Equation 25.4. The program P2 in Appendix 25. A is a simple MATLAB code for calculating the variance of r_s for the case of AR(1) data, but the code can be easily modified to accommodate any other dependence model.

Figure 25.3 depicts the variance inflation factor $V(r_s)/V_0(r_s)$ for data with AR(1) dependence for different values of the first-order autocorrelation coefficient and sample size, while Figure 25.4 depicts the same for FGN data. The distribution of the variance inflation factor in Figures 25.3 and 25.4 are very similar to that in Figures 25.1 and 25.2. This is not surprising, as the Mann–Kendall test and Daniels test are equivalent and have similar power [13,43].

25.3 Cross-Correlation Tests

The interest in the cross-correlation between hydrologic data and meteorological data, and between hydrologic and global climatic indices, started earlier than the interest in trends and climate change. In fact, as early as the 1930s (and probably much earlier), the topic of "teleconnection" between measurements in different parts of the world has been tackled [8]. In recent years, a great number of studies tried to establish cross-correlations between different hydrologic and climatic data. In particular, many attempts have been made to connect hydrologic data in different parts of the world to global climatic

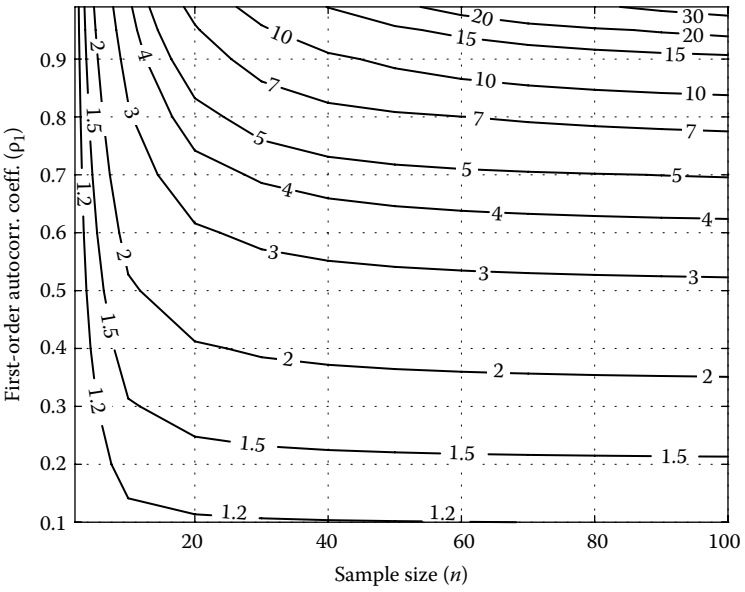

FIGURE 25.3 Variance inflation factors of the Daniels trend statistic r_s for AR(1) data as a function of sample size n and first-order autocorrelation coefficient ρ.

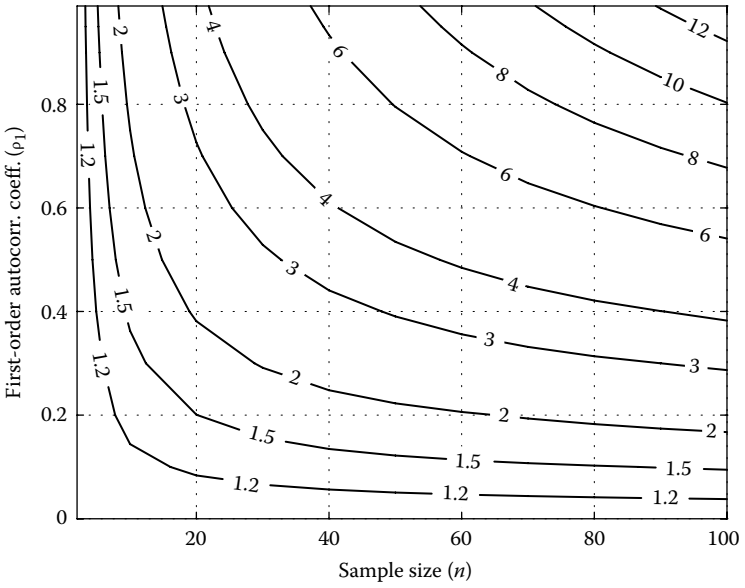

FIGURE 25.4 Variance inflation factors of the Daniels trend statistic r_s for FGN data as a function of sample size n and first-order autocorrelation coefficient ρ.

indices. Such global climatic indices are usually based on sea surface temperature (SST) in various parts of the oceans (e.g., El Niño, EN), variations in atmospheric pressure at different locations (e.g., southern oscillations, SO), zonal wind anomalies (e.g., equatorial Indian Ocean oscillations, EQUINOO), or a combination thereof (e.g., ENSO), in addition to many other types of indices. In some cases, other types of data such as ice core measurements, lake depositions (varves), or tree ring width/density measurements were also investigated as proxy to temperature as well as hydrologic data. For example,

Chiew et al. [4] studied the links between EN/SO and Australian rainfall, streamflow, and drought and the potential for using these links in forecasting. Huang et al. [23] studied the correlation of precipitation to temperature variation in the Huanghe River (Yellow River) basin. Zhang et al. [47] studied flood and drought variability in the Yangtze Delta and association with the climatic changes from the Guliya ice core. Fana et al. [12] attempted annual temperature reconstruction in the central Hengduan Mountains, China, using tree rings. Soukup et al. [35] studied the long lead-time streamflow forecasting of the North Platte River incorporating oceanic–atmospheric climate variability. Ghanbari et al. [14] studied the coherence between lake ice cover, local climate, and teleconnections in Lake Mendota, Wisconsin. Again, these are only a few examples from a very long and diversified list of studies, most of which concentrate on the correlation between observations that are not directly related but are thought to be connected through some type of global climatic system interactions.

It is to be noted again that most of the natural time series involved in cross-correlation studies exhibit some type of persistence. Similar to the case of trend tests, positive autocorrelation between successive values results in a larger chance to identify significant cross-correlations when in fact none exists. This occurs through the same mechanism of inflation of the variance of the test statistic due to the nonrandomness of the tested data. We reiterate that this in itself does not automatically invalidate the results of previous studies, but some type of accounting for the effect of persistence should be made before solid conclusions can be reached. In particular, there should be a sound physical basis for the causality of the relationship between the two studied variables [26] to insure that the identified cross-correlations are not spurious. This is actually very important since research has expanded to cover variables for which causality may be hard to prove. For example, Panarello and Dapeña [34] argued that large-scale meteorological phenomena, ENSO and ITCZ, defined the Paraná River isotope composition. Many other applications appear also in other fields, such as economics, medicine, and natural hazard. For example, Wang et al. [40] studied the correlations between forest fires in British Columbia, Canada, and SST of the Pacific Ocean and Kovats et al. [28] studied the correlation between ENSO and a number of epidemic diseases, to mention a few.

In this section, we will consider two commonly used distribution-free tests of cross-correlation between two variables. These two tests correspond to the two trend tests mentioned earlier. The details of each test are reviewed and the effect of persistence on each test is then investigated.

25.3.1 Kendall's Tau

Kendall's tau [24] is a measure of concordance between two observed random variables. For a given bivariate sequence (x_1, y_1), (x_2, y_2), …, (x_n, y_n) of two observed variables X and Y, Kendall's tau test statistic S can be calculated as

$$S = \sum_{i=1}^{n} \sum_{j=i+1}^{n} \operatorname{sgn}(x_j - x_i) \operatorname{sgn}(y_j - y_i) \tag{25.10}$$

The formula in Equation 25.10 is similar to that in Equation 25.1 but involves the two variables x and y. Under the null hypothesis of X and Y being independent, that is, there is no cross-correlation between X and Y, and that the observations of each of the two series are randomly ordered, the test statistic S has a zero mean and the same variance $V_0(S)$ given by Equation 25.2 for the Mann–Kendall trend test.

When X and Y are each serially correlated, Hamed [16] shows that the mean of S remains to be zero in the null case of independence between X and Y, while the variance is given by

$$V(S) = \frac{4}{\pi^2} \sum_{i=1}^{n} \sum_{j=i+1}^{n} \sum_{k=1}^{n} \sum_{l=k+1}^{n} \sin^{-1} r_x(i,j,k,l) \sin^{-1} r_y(i,j,k,l) \tag{25.11}$$

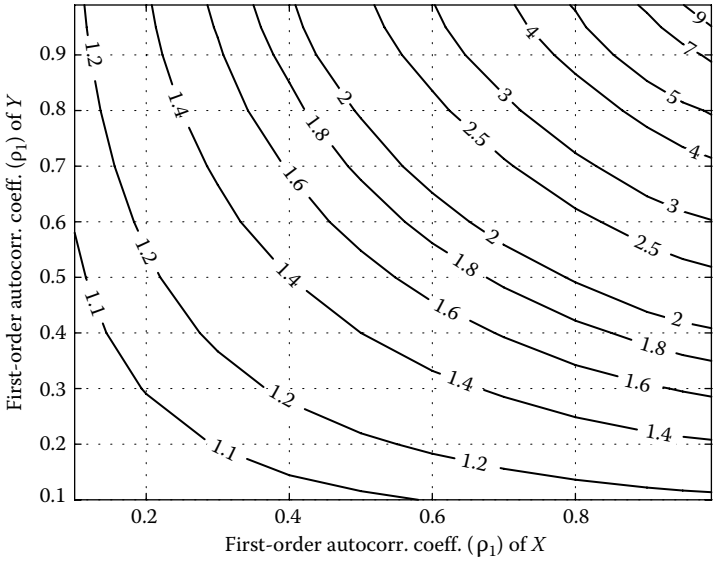

FIGURE 25.5 Variance inflation factors of Kendall's tau statistic S for bivariate AR(1) data as a function of first-order autocorrelation coefficients $\rho_1(X)$ and $\rho_1(Y)$.

where

$$r_x(i,j,k,l) = \frac{\rho_{jl} - \rho_{il} - \rho_{jk} + \rho_{ik}}{\sqrt{(2-2\rho_{ij})(2-2\rho_{kl})}} \tag{25.12}$$

where

ρ_{ij} for any two subscripts i and j is the autocorrelation coefficient between observations i and j of the equivalent normal X data

$r_y(i, j, k, l)$ is defined similarly for the variable Y

The program P3 in Appendix 25.A is a simple MATLAB code for calculating the variance of S for the case of AR(1) data, but the code can be easily modified to accommodate any other dependence model, where the autocorrelation models of X and Y need not be the same.

Figure 25.5 depicts the variance inflation factor $V(S)/V_0(S)$ for data with AR(1) dependence for a sample size $n = 50$ and different values of the first-order autocorrelation coefficients of X and Y as an example, while Figure 25.6 depicts the same for different sample sizes of X and Y for a set of equal correlation coefficients. It should be noted that for variance inflation to vanish, it suffices that one of the two involved variables be randomly ordered (i.e., not autocorrelated).

25.3.2 Spearman's Rho

Similar to Kendall's tau, Spearman's rho [24,36] is a measure of rank correlation between two variables X and Y. For a given bivariate sequence (x_1, y_1), (x_2, y_2), …, (x_n, y_n) of the two observed variables X and Y, Spearman's rho test statistic is given by

$$r_s = 1 - \frac{6\sum d^2}{n^3 - n} \tag{25.13}$$

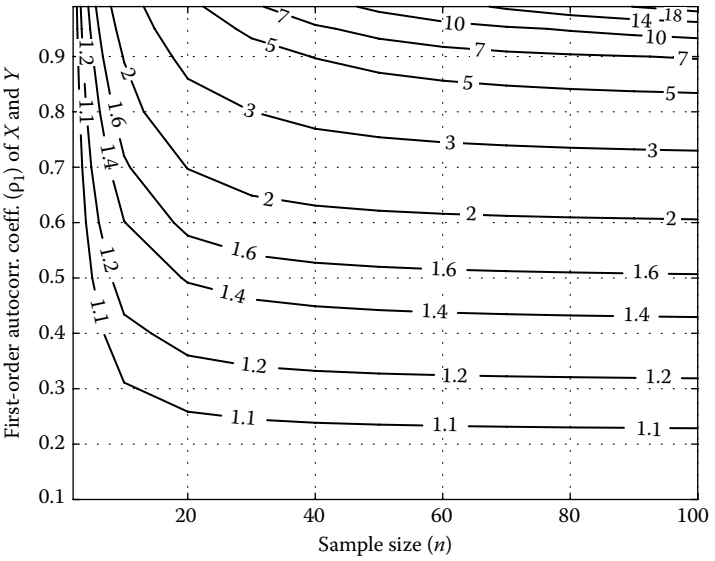

FIGURE 25.6 Variance inflation factors of Kendall's tau statistic S for bivariate AR(1) data as a function of sample size n and equal first-order autocorrelation coefficients $\rho_1(X) = \rho_1(Y)$.

which is the same as in Equation 25.6 in the case of the Daniels test, while now we have

$$\sum d^2 = \sum_{i=1}^{n} \left[R(x_i) - R(y_i) \right]^2 \tag{25.14}$$

where

$R(x_i)$ is the rank of observation x_i

$R(y_i)$ is the rank of observation y_i

Under the null hypothesis of X and Y being independent, the statistic r_s has a zero mean and a variance given by Equation 25.8, the same as in the case of the Daniels trend test.

When the data are serially correlated, it can be shown that the mean remains to be zero, while the variance is given by

$$\mathrm{var}(r_s) = \frac{36}{\pi^2 n^2 (n^2-1)^2} \sum_{i=1}^{n} \sum_{j=1}^{n, j\neq i} \sum_{k=1}^{n, k\neq i} \sum_{l=1}^{n} \sum_{u=1}^{n, u\neq l} \sum_{w=1}^{n, \mathbf{w}\neq l} \sin^{-1} r_x(i,j,u,l) \sin^{-1} r_y(i,k,w,l) \tag{25.15}$$

where $r_x(\cdot)$ and $r_y(\cdot)$ are as defined before. The program P4 in Appendix 25.A is a simple MATLAB code for calculating the variance of r_s for the case of AR(1) data, but the code can be easily modified to accommodate any other dependence model. It should be noted that the formula for the variance of r_s involves six nested summations, making the calculation of the variance more computationally demanding than the three previous test statistics.

Figure 25.7 depicts the variance inflation factor $V(r_s)/V_0(r_s)$ for data with AR(1) dependence for different values of the first-order autocorrelation coefficients of X and Y for sample size $n = 20$ as an example, while Figure 25.8 depicts the same for different sample sizes of X and Y for a set of equal correlation coefficients.

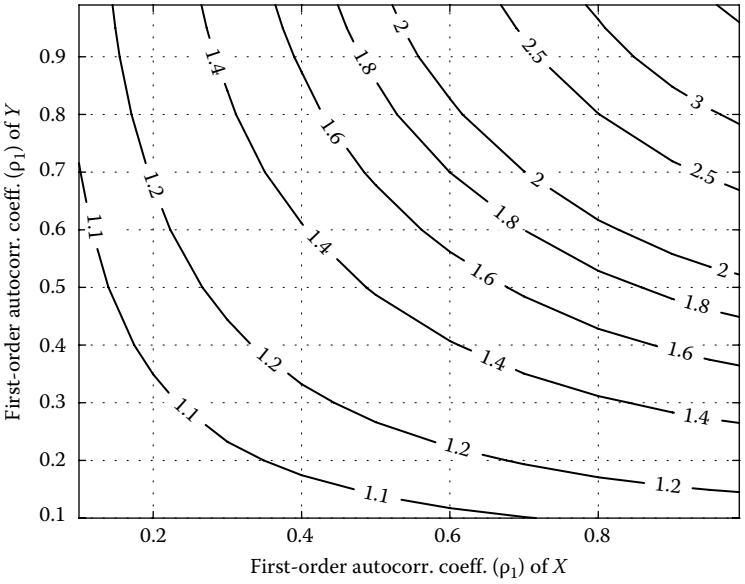

FIGURE 25.7 Variance inflation factors of Spearman's rho statistic r_s for bivariate AR(1) data as a function of first-order autocorrelation coefficients $\rho_1(X)$ and $\rho_1(Y)$.

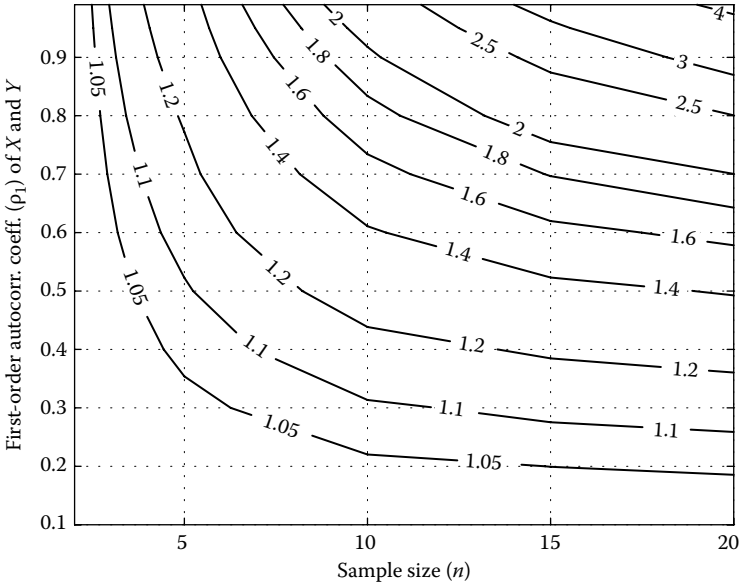

FIGURE 25.8 Variance inflation factors of Spearman's rho statistic r_s for bivariate AR(1) data as a function of sample size n and equal first-order autocorrelation coefficients $\rho_1(X) = \rho_1(Y)$.

25.4 Dealing with Persistence

Several methods have been suggested in the literature to deal with the effect of persistence on the results of statistical tests of significance. These methods can be divided into three categories. The first category involves dealing directly with the statistical tests themselves, making necessary corrections in the

distribution of the test statistics. The second category involves the use of the principle of effective sample size. The third category involves manipulating the data to remove the effect of persistence. Each of these methods has its advantages and disadvantages that are explained in this section, along with examples of their applications.

25.4.1 Modified Statistical Tests

In this method, the distribution of the test statistic under the effect of persistence is derived, and testing is conducted considering the correct distribution of the test statistic. The same test procedure is used, replacing the original variance of the test statistic with the correct inflated variance (e.g., Equations 25.4, 25.9, 25.11, 25.15) based on the autocorrelation information extracted from the data. Hamed [19] used the Mann–Kendall test modified by the inflated variance given in Equation 25.4 to reassess trends in a group of 57 worldwide total annual river flow time series that had been shown in an earlier study to exhibit significant trends. The use of the modified trend test resulted in a considerable reduction in the number of significant trends when the effect of persistence is taken into account. The exact full probability distribution of the Mann–Kendall trend test statistic for persistent data has been addressed by Hamed [17]. Similarly, Hamed [16] used a modified Kendall's tau test to illustrate the role of persistence in the false identification of significant cross-correlation between unrelated segments of the Nile flow and North Hemisphere temperature time series. The exact full probability distribution of Kendall's tau for persistent data has also been addressed by Hamed [15].

This method has the advantage that the original test is modified directly using basic probability theory, without the need to perform any modifications on the tested data, which might interfere with the results of the test. This is done with minimum assumptions about the structure of the data, since the autocorrelation among the ranks of the data is the only needed information to modify the variance. On the other hand, one disadvantage of this method is that each test has to be dealt with individually by deriving the distribution of the test statistic, which may not be a simple task. Also, the calculation of the modified variance becomes computationally demanding, if at all practical, as is the case with the variance of Spearman's rho as given by Equation 25.15.

25.4.2 Effective Sample Size

Since the variance of many statistics is inversely proportional to the sample size n, the inflated variance can be obtained by simply using a smaller value n^* for the sample size to calculate the variance. The idea of using this "effective" sample size to calculate the variances of the sample mean, sample second moment, and sample variance was suggested by Bayley and Hammersley [2]. For example, the effective sample size n^* for the sample mean for data with autocorrelation function $\rho(j)$, $j = 1, 2, \ldots, n$ is given by

$$\frac{1}{n^*} = \frac{1}{n} + \frac{2}{n^2}\sum_{i=1}^{n-1}(n-j)\rho(j) \tag{25.16}$$

Lettenmaier [30] suggested the use of this effective sample size as an approximation to test the significance of trends in autocorrelated time series using nonparametric tests. For the case of AR(1) autocorrelation with first-order autocorrelation coefficient ρ, the formula in Equation 25.16 reduces to

$$\frac{1}{n^*} = \frac{1}{n} + \frac{2}{n^2}\frac{\rho^{n+1} - n\rho^2 + (n-1)\rho}{(\rho-1)^2} \tag{25.17}$$

Hamed and Rao [20] suggested the use of a more accurate formula for the specific case of the Mann–Kendall trend test, which is given by

$$\frac{1}{n^*} = \frac{1}{n} + \frac{2}{n^2(n-1)(n-2)} \sum_{i=1}^{n-1} (n-i)(n-i-1)(n-i-2)\rho_R(i) \tag{25.18}$$

where $\rho_R(.)$ is the autocorrelation function of the ranks of the observations. Yue and Wang [42] give an assessment of the use of effective sample size in detecting trends in serially correlated hydrologic series using the Mann–Kendall trend test.

The advantage of using the effective sample size is that the tested data are not modified. However, it should be noted that the formula for calculating the effective sample size depends not only on the autocorrelation function of the data but also on the distribution of the statistic under consideration. For example, the formula given in Equation 25.16 is only exact for calculating the variance of the sample mean, while its use in other cases may give varying accuracy depending on the type of statistic under consideration. Hamed [16] further discussed this aspect of variation in the effective sample size for different test statistics.

25.4.3 Prewhitening

As mentioned earlier, one basic assumption of statistical tests of significance is that the tested data are random. In the field of signal processing, random signals are commonly known as "white noise," while autocorrelated signals are known as "colored noise." The change of autocorrelated data into uncorrelated data has thus been known as "prewhitening," that is, changing colored noise into white noise prior to performing a statistical test. This prewhitening is performed by applying an inverse transformation of a suitable autocorrelation model for the data. Von Storch [39] suggested that for AR(1) data series X_t, trend tests can be performed on the prewhitened series Y_t that is calculated as

$$y_t = x_t - \rho x_{t-1} \tag{25.19}$$

where ρ is the first-order autocorrelation coefficient of the series X_t. However, he warns that for higher-order AR processes or other autocorrelation models, prewhitening using Equation 25.19 would be insufficient.

Yue and Wang [41], as well as Yue et al. [44], show that the existence of a real trend in the data may lead to overestimation of positive autocorrelation among the data, thus causing "the removal of a portion of the trend" as a result of prewhitening. Hamed [18] further discussed this issue and suggested the simultaneous estimation of trend and first-order autocorrelation coefficient ρ from the data, in which case ρ would be downward biased, followed by a bias correction of ρ using one of the following two suggested formulas:

$$\rho^* = \frac{(n\hat{\rho}+2)}{n-4} \tag{25.20}$$

$$\rho^* = 2\hat{\rho} - \frac{1}{2}(\hat{\rho}_1 + \hat{\rho}_2) \tag{25.21}$$

where $\hat{\rho}$ is the estimate of ρ from the full length n of the time series, while $\hat{\rho}_1$ and $\hat{\rho}_2$ are estimates of ρ from the first and second halves of the time series. In the general case, including the AR(1) model, the following generalized formula for prewhitening can be used [21]:

$$\mathbf{y} = \mathbf{M}^{-1}(\mathbf{x} - \hat{\mu}\mathbf{u}) \tag{25.22}$$

where
- $\mathbf{x}$ is the vector of original time series
- $\mathbf{y}$ is the prewhitened series
- $\mathbf{u}$ is a vector of ones of size n
- $\hat{\mu}$ is the estimated mean of $\mathbf{x}$
- $\mathbf{M}$ is an $n \times n$ lower triangular matrix obtained by the Cholesky decomposition of the autocorrelation matrix $C_n(\mathbf{x})$

Alternative methods of obtaining the matrix $\mathbf{M}$ are discussed by Koutsoyiannis [27].

25.5 Summary and Conclusions

Persistence is a property that is naturally found in many hydrologic as well as other natural data, where observations that are adjacent in time are positively correlated. Using statistical tests that are originally designed for random data violates a basic assumption of such tests and often results in overstating the significance of the calculated test statistics. It has been shown that even moderate values of autocorrelation among the data can result in considerably exaggerated significance. Examples from nonparametric tests of trend and cross-correlation have been given along with detailed effects of persistence on the variance of their test statistics. For the conclusions arising from statistical tests of significance to be properly founded, the effect of persistence has to be accounted for in these tests. A number of methods for achieving this goal have been surveyed. These methods include adjustments of the tests to derive the correct variances of the test statistics, adjustment of the number of observations used to calculate the variances, and removal of autocorrelation by means of prewhitening.

References

1. Andreadis, K.M. and Lettenmaier, D.P., 2006. Trends in 20th century drought over the continental United States, *Geophysical Research Letters*, 33, L10403.
2. Bayley, G.V. and Hammersley, J.M., 1946. The 'effective' number of independent observations in an autocorrelated time series, *Journal of the Royal Statistical Society*, 8(2), 184–197.
3. Breasted, J.H. 1906. *Ancient Records of Egypt*, Vols. I–IV. The University of Chicago Press, Chicago, IL.
4. Chiew, F.H.S., Piechota, T.C., Dracup, J.A., and McMahon, T.A., 1998. E1 Niño/Southern Oscillation and Australian rainfall, streamflow and drought: Links and potential for forecasting, *Journal of Hydrology*, 204, 138–149.
5. Cox, D.R. and Stuart, A., 1955. Some quick sign tests for trend in location and dispersion, *Biometrika*, 42, 80–95.
6. Cunderlik, J.M. and Ouarda, T., 2009. Trends in the timing and magnitude of floods in Canada, *Journal of Hydrology*, 375, 471–480.
7. Daniels, H.E., 1950. Rank correlation and population models, *Journal of Royal Statistical Society Series B*, 12, 171–181.
8. De Geer, G. 1935. Teleconnections contra so-called telecorrelations, *Geologiska Föreningen i Stockholm Förhandlingar*, 57(2), 341–346.
9. Douglas, E.M., Vogel, R.M., and Kroll, C.N., 2000. Trends in flood and low flows in the United States: Impact of spatial correlation, *Journal of Hydrology*, 240, 90–105.
10. Estrela, T., Pérez-Martin, M.A., and Vargas, E., 2012. Impacts of climate change on water resources in Spain, *Hydrological Sciences Journal*, 57(6), 1154–1167.
11. El-Shaarawi, A.H. and Damsleth, E., 1988. Parametric and non-parametric tests for dependent data, *Water Resources Bulletin*, 24(3), 513–519.

12. Fana, Z.X., Bräuning, A., and Caoa, K.F., 2008. Annual temperature reconstruction in the central Hengduan Mountains, China, as deduced from tree rings, *Dendrochronologia*, 26, 97–107.
13. Fredricks, G.A. and Nelsen, R.B., 2007. On the relationship between Spearman's rho and Kendall's tau for pairs of continuous random variables, *Journal of Statistical Planning and Inference*, 137, 2143–2150.
14. Ghanbari, R.N., Bravo, H.R., Magnuson, J.J., Hyzer, W.G., and Benson, B.J., 2009. Coherence between lake ice cover, local climate and teleconnections (Lake Mendota, Wisconsin), *Journal of Hydrology*, 374, 282–293.
15. Hamed, K.H., 2011. The distribution of Kendall's Tau for testing the significance of cross-correlation in persistent data, *Hydrological Sciences Journal*, 56(5), 841–853.
16. Hamed, K.H., 2009. Effect of persistence on the significance of Kendall's tau as a measure of correlation between natural time series, *European Physical Journal Special Topics*, 174, 65–79.
17. Hamed, K.H., 2009. Exact distribution of the Mann-Kendall trend test statistic for persistent data, *Journal of Hydrology*, 365, 86–94.
18. Hamed, K.H., 2009. Enhancing the effectiveness of prewhitening in trend analysis of hydrologic data, *Journal of Hydrology*, 368, 143–155.
19. Hamed, K.H., 2008. Trend detection in hydrologic data: The Mann–Kendall trend test under the scaling hypothesis, *Journal of Hydrology*, 349(3–4), 350–363.
20. Hamed, K.H. and Rao, A.R., 1998. A modified Mann-Kendall trend test for autocorrelated data, *Journal of Hydrology*, 204, 182–196.
21. Hipel, K.W. and McLeod, A.I., 1994. *Time Series Modeling of Water Resources and Environmental Systems*. Elsevier Publishing Company, Amsterdam, the Netherlands, 1013pp.
22. Hirsch, R.M. and Slack, J.R., 1984. Non-parametric trend test for seasonal data with serial dependence, *Water Resources Research*, 20(6), 727–732.
23. Huang, Y., Cai, J., Yin, H., and Cai M., 2009. Correlation of precipitation to temperature variation in the Huanghe River (Yellow River) basin during 1957–2006, *Journal of Hydrology*, 372, 1–8.
24. Kendall, M.G., 1948. *Rank Correlation Methods*. Griffin, London, U.K.
25. Kendall, M.G. and Gibbons, J.D., 1990. *Rank Correlation Methods*, 5th edn. Griffin, London, U.K.
26. Kenny, D.A., 1979. *Correlation and Causality*. Wiley, New York.
27. Koutsoyiannis, D., 2000. A generalized mathematical framework for stochastic simulation and forecast of hydrologic time series, *Water Resources Research*, 36(6), 1519–1533.
28. Kovats, P.S., Bouma, M.J., Hajat, S., Worrall, E., and Haines, A., 2003. El Niño and health, *The Lancet*, 362(1), 1481–1489.
29. Kundzewicz, Z.W., Graczyk, D., Maurer, T., Piñskwar, I., Radziejewski, M., Svensson, C., and Szwed, M., 2005. Trend detection in river flow series: 1. Annual maximum flow, *Hydrological Sciences Journal*, 50(5), 797–809.
30. Lettenmaier, D.P., 1976. Detection of trends in water quality data from records with dependent observations, *Water Resources Research*, 12(5), 1037–1046.
31. Mann, H.B., 1945. Nonparametric tests against trend, *Econometrica*, 13, 245–259.
32. Matalas, N.C. and Sankarasubramanian, A., 2003. Effect of persistence on trend detection via regression, *Water Resources Research*, 39(12), 1342, doi: 10.1029/2003WR002292.
33. McBean, E. and Motiee, H., 2006. Assessment of impacts of climate change on the water resources—Great Lakes of North America, *Hydrology and Earth System Sciences*, 3, 1–27.
34. Panarello, H.O. and Dapeña, C., 2009. Large scale meteorological phenomena, ENSO and ITCZ, define the Paraná River isotope composition, *Journal of Hydrology*, 365(2009), 105–112.
35. Soukup, T.L., Aziz, O.A., Tootle, G.A., Piechota, T.C., and Wulff, S.S., 2009. Long lead-time streamflow forecasting of the North Platte River incorporating oceanic–atmospheric climate variability, *Journal of Hydrology*, 368, 131–142.
36. Spearman, C., 1904. The proof and measurement of association between two things, *American Journal of Psychology*, 15, 72–101.

37. Svensson, C., Kundzewicz, Z.W., and Maurer, T., 2005. Trend detection in river flow series: 2. Flood and low-flow index series, *Hydrological Sciences Journal*, 50(5), 811–824.
38. Van Belle, G. and Hughes, J.P., 1984. Nonparametric tests for trend in water quality, *Water Resources Research*, 20(1), 127–136.
39. Von Storch, V.H., 1995. Misuses of statistical analysis is climate research. In: *Analysis of Climate Variability: Applications of Statistical Techniques*, V.H. von Storch and A. Navarra (Eds.). Springer-Verlag, Berlin, Germany, pp. 11–26.
40. Wang, Y., Flannigan, M., and Anderson, K., 2009. Correlations between forest fires in British Columbia, Canada, and sea surface temperature of the Pacific Ocean, *Journal of Hydrology*, 365, 105–112.
41. Yue, S. and Wang, C.Y., 2002. Applicability of prewhitening to eliminate the influence of serial correlation on the Mann-Kendall test, *Water Resources Research*, 38(6), 1068, doi: 10.1029/2001WR000861.
42. Yue, S. and Wang, C.Y., 2004. The Mann-Kendall test modified by effective sample size to detect trend in serially correlated hydrological series, *Water Resources Management*, 8(3), 201–218.
43. Yue, S., Pilon, P., and Cavadias, G., 2002. Power of the Mann-Kendall and Spearman's rho tests for detecting monotonic trends in hydrological series, *Journal of Hydrology*, 259, 254–271.
44. Yue, S., Pilon, P., Phinney, R., and Cavadias, G., 2002. The influence of autocorrelation on the ability to detect trend in hydrological series, *Hydrological Processes*, 16, 1807–1829, doi: 10.1002/hyp.1095.
45. Yue, S., Pilon, P., and Phinney, R., 2003. Canadian Streamflow trend detection: Impacts of serial and cross-correlation, *Hydrological Sciences Journal*, 48(1), 51–63.
46. Zetterqvist, L., 1991. Statistical estimation and interpretation of trends in water quality time series, *Water Resources Research*, 27(7), 1637–1648.
47. Zhanga, Q., Chena, Y.D., and Chenb, J., 2008. Flood/drought variability in the Yangtze Delta and association with the climatic changes from the Guliya ice core: A wavelet approach, *Quaternary International*, 189, 163–172.

Appendix

The following programs are written in MATLAB language. The text should be saved as a plain text file with the same function name and extension ".m". For example, Program P1 should be saved as "calvarMKS.m."

Program P1: Calculation of the Variance of the Mann–Kendall Test Statistic S

```
function [v v0] = calvarMKS(n,r);
cf = @(t,r) r.^abs(t);
t = -n+1:n-1;
cr = cf(t,r);
ee = 0;
ss = (2-2*cr).^-.5;
for j = 1:n
    for l = 1:n
        a = cr(j-l+n);
        for k = 1:l-1
            c = cr(j-k+n);
            for i = 1:j-1
                b = cr(i-l+n);
                d = cr(i-k+n);
                e = (a-b-c+d)*ss(j-i+n)*ss(l-k+n);
                ee = ee+asin(min(e,1));
```

```
            end;
        end;
    end;
end;
v = ee*2/pi;
v0 = n*(n-1)*(2*n+5)/18;
```

Program P2: Calculation of the Variance of the Daniels Test Statistic r_s

```
function [v v0] = calvarDRS(n,r)
cf = @ (t,r) r.^abs(t);
t = -n:n;
cr = cf(t,r);
cr2 = (2-2*cr).^-0.5;
ee = 0;
on = 1+n;
for i = 1:n
    for l = 1:n
        e1 = cr((i-l)+on);
        for u = 1:n
            if l = =u, continue;end;
            e2 = cr((i-u)+on);
            d1 = cr2((l-u)+on);
            for j = 1:n
                if i = =j, continue;end;
                e3 = cr((j-u)+on);
                e4 = cr((j-l)+on);
                d2 = cr2((j-i)+on);
                e = (e3-e2-e4+e1)*d2*d1;
                if abs(e)>1;e = sign(e);end;
                ee = ee+asin(e)*(i-1)*(l-1);
            end;
        end;
    end;
end;
v = ee/(2*pi)*144/(n*(n^2-1))^2;
v0 = 1/(n-1);
```

Program P3: Calculation of the Variance of the Kendall Test Statistic S

```
function [v v0] = calvarKTS(n,r1,r2);
cf = @ (t,r) r.^abs(t);
t = -n+1:n-1;
cr1 = cf(t,r1);
cr2 = cf(t,r2);
ee = 0;
ss1 = (2-2*cr1).^-.5;
ss2 = (2-2*cr2).^-.5;
for j = 1:n
    for l = 1:n
        a1 = cr1(j-l+n);
        a2 = cr2(j-l+n);
        for k = 1:l-1
            c1 = cr1(j-k+n);
            c2 = cr2(j-k+n);
```

```
            for i = 1:j-1
                b1 = cr1(i-l+n);
                b2 = cr2(i-l+n);
                d1 = cr1(i-k+n);
                d2 = cr2(i-k+n);
                e1 = (a1-b1-c1+d1)*ss1(j-i+n)*ss1(l-k+n);
                e2 = (a2-b2-c2+d2)*ss2(j-i+n)*ss2(l-k+n);
                ee = ee+asin(min(e1,1))*asin(min(e2,1));
            end;
        end;
    end;
end;
v = ee*(2/pi)^2;
v0 = n*(n-1)*(2*n+5)/18;
```

Program P4: Calculation of the Variance of the Spearman Test Statistic r_s

```
function [v v0] = calvarSRS(n,r1,r2)
cf = @ (t,r) (r).^abs(t);
t = -n:n;
cr1 = cf(t,r1);
cr2 = cf(t,r2);
cr15 = (2-2*cr1).^-0.5;
cr25 = (2-2*cr2).^-0.5;
on = 1+n;
ee = 0;
for i = 1:n
    for l = 1:n
        e14 = cr1((i-l)+on);
        e24 = cr2((i-l)+on);
        for j = 1:n
            if i = =j;continue;end;
            e13 = cr1((j-l)+on);
            s11 = cr15((j-i)+on);
                for k = 1:n
                if i = =k;continue;end;
                e23 = cr2((k-l)+on);
                s21 = cr25((k-i)+on);
                for u = 1:n
                    if l = =u;continue;end;
                    e11 = cr1((j-u)+on);
                    e12 = cr1((i-u)+on);
                    s12 = cr15((l-u)+on);
                    for w = 1:n
                        if l = =w;continue;end;
                        e21 = cr2((k-w)+on);
                        e22 = cr2((i-w)+on);
                        s22 = cr25((l-w)+on);
                        e1 = (e11-e12-e13+e14)*s11*s12;
                        e2 = (e21-e22-e23+e24)*s21*s22;
                        if abs(e1)>1;e1 = sign(e1);end;
                        if abs(e2)>1;e2 = sign(e2);end;
                        ee = ee+asin(e1)*asin(e2);
                    end;
                end;
```

```
            end;
        end;
    end;
end;
v = ee/pi^2*36/(n*(n^2-1))^2;
v0 = 1/(n-1);
```

26

Statistical Parameters Used for Assessing Hydrologic Regime

Rezaul K. Chowdhury
United Arab Emirates University

Saeid Eslamian
Isfahan University of Technology

AUTHORS

Rezaul K. Chowdhury has been recognized for his innovative and industry-oriented research activities in water resources management. He is an assistant professor of water resources at the United Arab Emirates University. Previously, Dr. Chowdhury was a research fellow of water engineering at the University of South Australia and was a scientist of integrated water systems planning and management at the Commonwealth Scientific and Industrial Research Organization (CSIRO) in Australia. Dr. Chowdhury started his career as a lecturer of civil and environmental at the ShahJalal University of Science and Technology in Bangladesh. He has published more than 40 research articles in leading international journals and conferences. He is an active reviewer of several high–impact factor journals. Dr. Chowdhury is involved in supervising postgraduate research students.

Saeid Eslamian received his PhD from the University of New South Wales, Australia, with Professor David Pilgrim. He was a visiting professor in Princeton University, United States, and ETH Zurich, Switzerland. He is currently an associate professor of hydrology in Isfahan University of Technology. He is the founder and chief editor of the *Journal of Flood Engineering* and *International Journal of Hydrology Science and Technology*. He has published more than 200 publications mainly in statistical and environmental hydrology and hydrometeorology.

PREFACE

The importance of hydrologic flow regimes and flow metrics is well acknowledged by hydrologists, ecologists, and water resource managers. Human interventions, such as water reservoir, water supply, hydropower generation, flood control, recreation, and navigation, modify the flow regimes and thereby affect their ecosystems. Stream flow characteristics such as magnitude, frequency, duration, timing, and rate of change of flow events are significantly important for developing flow regime and stream regionalization. Each stream possesses their own flow characteristics that support a particular biological community. The interannual variability of flow acts as a dynamic force affecting stream ecosystem functions. Urbanization affects the flow regime by changing their flow frequency, volume, peak, base flow, erosion and sedimentation, and water quality. Urbanization-induced changes in flow regime include increased flow frequency, increased peak flow and total flow, and decreased base flow. Runoff from impervious areas generally flows quickly and carries diverse sources of pollutants. Therefore, proper understanding and quantification of flow regime is critically important. A number of statistical flow parameters are being used for classification of flow regimes. In this chapter, stochastic flow parameters used in flow regime classification and in ecohydrological studies are delineated.

26.1 Introduction

A hydrologic flow regime is a specific combination of stream flow events. The flow regime can be characterized by runoff magnitude, frequency, predictability, duration, flashiness, and sequences of these flow characteristics [35]. Streams possess their own flow characteristics that support a particular biological community [5]. Several previous studies discussed the importance of hydrologic processes in explaining temporal and spatial stream biota distributions [8,20,21]. Urbanization and water infrastructure development are two widely accepted phenomena that significantly affect stream flow regime by changing their flow frequency, volume, peak, base flow, erosion and sedimentation, and water quality [7,17]. In many cases, streams exhibit a distinctive variability in annual flows and peak discharges, characterized by large statistical moments of skewness and kurtosis. The interannual variability of flow acts as a dynamic force affecting stream ecosystem functions [8]. Proper understanding and quantification of flow regime is therefore critically important for sustaining streams.

The physical processes of stream ecosystems consist of water and sediment movements within the stream and between the stream and the floodplain [15,35]. Sediment transport and streambed disturbances are essential components for establishing a relationship between stream hydrology and ecological processes [6,24,25]. For example, macroinvertebrate diversity and density is a significant sign of stream ecological health. Rural streams generally possess an immense diversity of macroinvertebrates, whereas urban streams are dominated by less variety with few disturbance-tolerant species [34]. This distinction is because of changes in flow regime and deterioration of stream water quality from urban pollution [2,43].

Previous studies have indicated six major flow components in natural flow regimes and have delineated their key roles in sustaining stream ecological and geomorphological processes [4,31,35,36,39]. Figure 26.1 shows a conceptual representation of different flow components. These flow components are the following:

1. *Cease to flow* indicates no discernible flow and is generally observed in lowland streams; this flow component is responsible for localized extinction of certain species and increase of diversity and biomass in the long term.
2. *Low flow* is the minimum continuous flow derived from base flow contributions into the stream; low flows are essential for recruitment of native fish species in lowland streams.

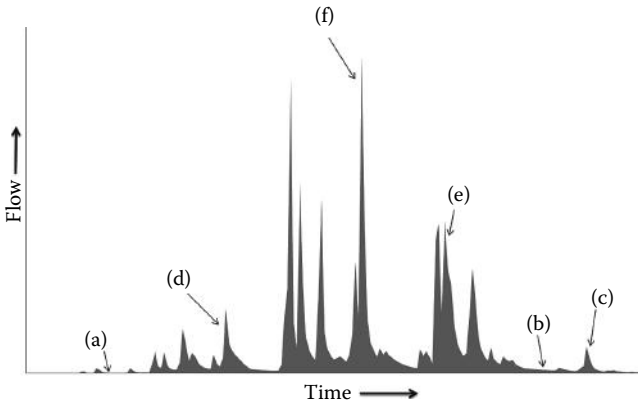

FIGURE 26.1 Conceptual representation of major flow components of a natural flow regime. (a) Cease to flow, (b) low flow, (c) freshes, (d) high flow, (e) bankfull flow, and (f) overbank flow.

3. *Freshes* are small short-duration peak flows, a key contributor to the variability of flow regimes, providing short pulses in flow, and are essential for a range of ecosystem functions.
4. *High flows* involve a persistent seasonal base flow component, and they are necessary for the breeding of some fish species.
5. *Bankfull flow* is the highest flow confined within a stream; they create habitat for macroinvertebrates, plants, and fishes and are important for shaping and maintaining distributaries; bankfull flow has a specific return period depending on climate and other hydrologic factors; bankfull flow is approximately equal to the *dominant flow* (channel-forming flow) at or near the dynamic equilibrium of streams, and for incised streams, bankfull flow is greater than dominant flow [27].
6. *Overbank flows* inundate adjacent floodplains; they are important for floodplain productivity, carbon returns to the river, fish and water bird community diversity, invertebrate colonization, and linkages with the stream channel, wetlands, and lakes.

The stream flow that is responsible for transporting the majority of the sediment and is responsible for creating or maintaining the characteristic size and shape of the channel is known as the channel-forming flow or the *dominant discharge* [27]. The maximum sediment transport usually occurs at relatively moderate flow events rather than large flow events since moderate flows occur much more frequently than larger events. In channels at or near dynamic equilibrium, the dominant discharge is approximately equal to the *bankfull discharge* or the flow that fills the channel from bank to bank before spilling into the floodplain [27]. In streams that have been significantly incised, the dominant discharge is typically less than the bankfull discharge, for example, the Navarro River, at Hendy Woods State Park, in December 2002.

A number of statistical flow parameters are being used for the classification of flow regimes. Kennard et al. [22] developed a methodology for stream classification in Australia based on a range of flow parameters in order to determine environmental flow requirements in streams. Arthington et al. [1] proposed a stream regionalization approach on the basis of natural flow variability as described by Poff et al. [35]. In this chapter, stochastic flow parameters used in flow regime classification and in ecohydrological studies are being described.

26.2 Predevelopment Flow Regime

Urbanization causes changes to predevelopment stream flow characteristics. Predevelopment is generally defined by 0% impervious area. Changes in flow regime include increased frequency, increased peak flow and total flow, and decreased base flow [12]. Figure 26.2 shows the general changes in stream

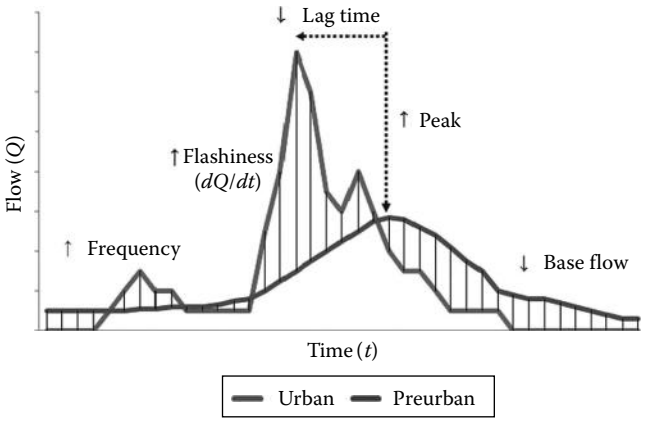

FIGURE 26.2 Schematic diagram showing changes in flow event due to urbanization (increase [↑] and decrease [↓]). (Based on Chowdhury, R. et al., Catchment hydrologic modelling for stormwater harvesting study in SEQ: From instrumentation to simulation, in Begbie, D.K. and Wakem, S.L. (eds.), *Science Forum and Stakeholder Engagement: Building Linkages, Collaboration and Science Quality*, Urban Water Security Research Alliance, Brisbane, Queensland, Australia, September 28–29, 2010, pp. 65–67.)

flow characteristics with urbanization. Runoff from impervious areas generally flows quickly and carries diverse sources of pollutants. Consequently, urbanization changes the quality, flow characteristics, and ecosystem conditions of streams and riparian vegetation [41,42]. Increased imperviousness reduces infiltration and subsequently base flow. Small rainfall events over an impervious surface generate runoff and increased flow frequency in urban streams. Impervious surfaces generally cause increases in the flow velocity and peak discharges. Consequently, the lag time to peak discharge is decreased. In addition, reduced infiltration capacity in the urbanized catchment increases flow volume in urban creeks. A set of ecological consequences in urban streams such as loss of riparian zones, reduced diversity of indigenous flora and fauna, introduction of pests and weeds, and reduced dispersal of biota have been summarized in [7]. Streams behave differently in maintaining their ecological conditions. Rural (country side) streams are generally affected by extraction and storage of water and subsequent loss of natural ecosystems [13,17], whereas urban streams experience hydrologic changes and changes in pollutant loads, channel erosion, and sedimentation [25,26,41]. While environmental flow restoration is essential for rural streams, urban streams generally require a reduction of runoff frequency, peak flow, and volume.

26.3 Stream Ecosystem Health

Stream ecological conditions are influenced by the degree of catchment imperviousness [40]. Stream health indicators are generally categorized into four groups based on changed flow regime, water quality, biodiversity, and stream erosion and sedimentation [34]. Macroinvertebrate diversity and density is a significant sign of urban stream health. Forested or unimpacted streams have an immense diversity of macroinvertebrates, whereas urban streams are dominated by less variety with few disturbance-tolerant species [26,34]. Stream ecosystem health is generally represented by some ecohydrological indicators. These are categorized into (1) species organization (biodiversity, composition, food web structure), (2) vigor (production rates, nutrient cycling), and (3) their resilience to recover from disturbances [37]. Screening a wide range of stream health indicators in Australian streams, Bunn and Smith [9] classified indicators into five categories. These are (1) physicochemical, (2) fish, (3) ecosystem processes, (4) nutrient cycles, and (5) macroinvertebrates. Some studies [32] recommended four categories of indicators: (1) biological (abundance of benthic macroinvertebrates), (2) physical (channel condition and suspended

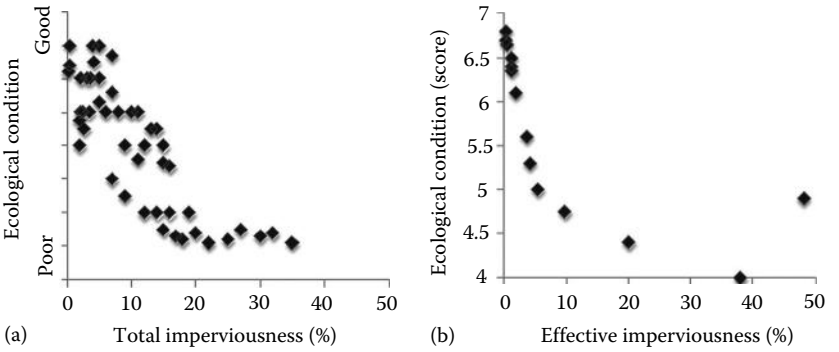

FIGURE 26.3 Relationship between stream ecosystem health and catchment imperviousness. Scattered relationship with TIA (a) and good correlation with DCIA (effective imperviousness) (b). (Based on Walsh, C.J. et al., *J. North Am. Benthol. Soc.*, 24(3), 690, 2005.)

solids), (3) chemical indicators (total phosphorus, total nitrogen, electrical conductivity, and pH), and (4) pathogenic indicators (*Escherichia coli* bacteria).

A scattered relationship between total impervious area (TIA) and stream health score in the United States was observed—with the highest dispersion observed from 3% to 17% of TIA (Figure 26.3) [2]. Based on a review of several previous studies [2], the *ten-percent rule* showed that streams are degraded when catchment TIA approaches 10% and beyond. In Australian catchments, Walsh [40] and Ladson et al. [26] reported that rather than TIA, a stream ecosystem is strongly influenced by directly connected impervious areas (DCIAs), a proportion of TIA that is connected to stormwater drainage inlets. DCIA is also known as the effective imperviousness. Decreased stream ecological conditions (water quality deterioration, algal biomass growth, and diatom and macroinvertebrate assemblage compositions) were observed with increased DCIA (1%–14%) until a threshold value, beyond which no further degradation occurred. Therefore, it was argued that it is possible to go beyond the *ten-percent* limit by means of disconnection of DCIA. This can be achieved through implementation of stormwater best management practice, water-sensitive urban design, sustainable urban drainage, and low-impact development concepts. While DCIA was identified as a good predictor of urban stream ecosystem health, the difficulties in estimating DCIA cause many researchers to instead use a relationship between TIA and ecosystem health.

26.4 Stream Flow and Ecosystem

The interannual variability of flow characteristics has been identified as a significant dynamic force affecting stream ecosystem processes [8]. Therefore, understanding and quantification of pre- and post-development flow regimes is critical for sustaining stream ecosystem health. Stream ecology is more reliant on natural flow variability [1]. Assigning a minimum flow using a *rule of thumb* is not a well-accepted approach for sustaining environmental flows. Their study proposed a stream regionalization approach based on natural flow variability as described in [35]. Their four-step approach of stream regionalization is shown in Figure 26.4.

Several previous studies focused on the importance of natural flow regimes in sustaining native biodiversity and stream integrity [1,4,5,35,38]. Quantity and timing (predictability) of the stream flow are critical for water supply, water quality, and ecological integrity of stream water systems [35]. The temporal variation of flow influences the aquatic and riparian zone community structures, population dynamics, and functional processes in the stream [5]. From subdaily to annual temporal scales, stream flow variability affects stream geomorphology and ecosystems in different ways. In terms of sustaining stream ecosystems, Tables 26.1 and 26.2 summarize the significance of flow magnitude and temporal variability, respectively.

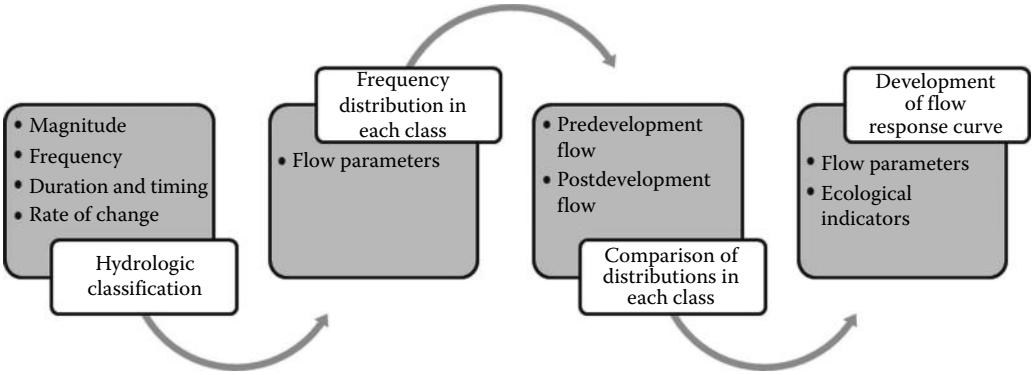

FIGURE 26.4 Stream regionalization process for environmental flow estimation on the basis of natural flow variability. (Based on Arthington, A.H. et al., *Ecol. Appl.*, 16, 1311, 2006; Poff, N.L. et al., *Bioscience*, 47, 769, 1997.)

TABLE 26.1 Significance of Flow Magnitudes in Sustaining Stream Ecosystem Health

Flow Events	Ecological Significance	References
High (>1 year ARI)	• Exerts larger disturbances • Removes and transports sediments from gravel interstitial spaces • Imports woody debris into the stream and creates high-quality habitat	[4,35]
Small	• Maintains habitat quality by flushing away silt and sediments	[4]
Low	• Limits habitat quantity • Provides recruitment opportunities for riparian species • Species have physiological adaptation capability to survive dry spells	[4,31]
Variable	• Flow variability is required by some aquatic and riparian species in their life cycle (e.g., spawning periods or migration upstream or downstream) • Species persistence can be influenced by flashiness of flow	[31,35]

ARI is average recurrence interval; in some countries, return period is used instead of ARI.

TABLE 26.2 Influence of Temporal Scales of Flow Variability on Stream Ecological Processes

Temporal Scale	Influence	References
Subdaily	Channel geomorphology controls the velocity and flow variability in the vicinity of benthic organisms. Channel roughness can increase turbulence (variation of velocity) due to vortices. Some benthic autotrophs change their growth form as a result of turbulence.	[5]
Daily	Stream ecosystem characteristics are influenced by drag disturbance–related processes. Drag disturbance indicates loss of biomass due to high velocities and associated abrasion of bed sediments. A moderate-magnitude flood event (flow velocity > 1.5 m s^{-1}) can remove up to 1% of biomass covering a wide range of species. Usually low-frequency, high-magnitude storm events are destructive to benthic macroinvertebrates.	[5,38]
Monthly	Local topography has a strong effect on rainfall and intraannual flow variability that is linked with stream biota characteristics at the community level through diffusion and sediment crushing and stranding processes.	[5]
Annual	Interannual flow variability is controlled by regional climatic systems that govern the whole ecology. In Australia, a number of natural climatic phenomena (El Niño Southern Oscillation Index, Southern Annular Model, Walker Oscillation, etc.) are responsible for interannual variability of rainfall and runoff.	[3,10,11,12]

The physical processes affecting stream ecosystems include water and sediment movement within the stream and between the stream and the floodplain [15,35]. Conventionally, streams are assessed in terms of changes in flow statistics (such as changes in peak flow, lag to peak or time of concentration, recession rate or event volume, etc.) without considering geomorphic or ecological consequences [25]. In order to establish relationships between hydrologic changes and stream ecosystems, both sediment transport and streambed disturbances should be considered [6,24,25].

26.5 Stream Flow Parameters

Stream flow characteristics such as magnitude, frequency, duration, timing, and rate of change of flow events are significantly important for developing flow regime and stream regionalization. A number of statistical flow parameters have been used in recent ecohydrological studies to regionalize streams and to develop environmental flow rules [22]. All of the parameters listed in this chapter are based on historical daily flow data.

26.5.1 Flow Magnitude

Flow magnitude is the volume of flow events generally expressed in mega liter day^{-1} or $m^3\ day^{-1}$. It is important to measure statistical parameters separately for low-, high-, and average-flow conditions. List of parameters, their definition, and measurement units are provided in Table 26.3. Some commonly used flow statistics are defined below for easy understanding of readers.

- *Mean daily flow* is a measure of central tendency. It is calculated as the average of all flow records considered over the analysis period (sum of flow values/number of days).
- *Median daily flow* is a measure of central tendency. The median flow (Q_{50}) is the "middle" flow for the entire record. That is the median is the flow exceeded 50% of the time. The median is usually much lower than the mean daily flow because the distribution of discharge data is negatively skewed with a lower limit of zero and no upper limit.
- *Minimum daily flow* is the smallest input value for the specific reporting period.
- *Maximum daily flow* is the largest input value for the specific reporting period.
- Q_{10} is the flow exceeded 10% of the time, that is, it is the discharge that indicates the top 10% of the flow for the reporting period.
- Q_{90} is the flow exceeded 90% of the time, that is, it is the discharge that indicates the lower 10% of the flow for the reporting period.
- *The number of zero flow days* for the entire record under analysis is counted. The number of zero flow days does not include days with a missing record unless they are filled with zero values.

26.5.2 Flow Distribution

26.5.2.1 Coefficient of Variation of Daily Flow

The coefficient of variation (CV) is a measure of variability of data. The CV of daily flow is the standard deviation for the daily flow values divided by the mean of all daily flow values. It is dimensionless. In annual scale, it can be used for flow regionalization purposes [16].

26.5.2.2 Standard Deviation of Daily Flow

The standard deviation is a measure of how widely the values are dispersed from the mean value. The standard deviation has the same units as the input data.

TABLE 26.3 Hydrologic Metrics for Low-Flow Condition

Flow Metric	Definition of Metric	Resolution	Unit
Median of annual minimum flows	Median of the lowest annual daily flow divided by the mean annual daily flow (MADF) averaged across all years	Annual	Dimensionless
Base flow index	Ratio of base flow to total flow, averaged across all years, where base flow is calculated using three-way digital filter [19]	Annual	Dimensionless
Coefficient of variation (CV) of base flow index	CV in base flow index	Annual	Dimensionless
Low-flow discharge • 75th percentile • 90th percentile • 99th percentile	75th, 90th, and 99th percentiles, respectively, from the flow duration curve	Annual	ML day^{-1}
Specific mean annual minimum runoff	Mean annual minimum flow divided by catchment area	Annual	ML day^{-1} km^{-2}
Low-flow spell count (less than 75th, 90th, and 99th percentiles)	Mean number of annual occurrences during which the magnitude of flow remains below a lower threshold defined by the 75th, 90th, and 99th percentiles, respectively (from the flow duration curve)	Annual	$Year^{-1}$
CV of low-flow spell count (less than 75th, 90th, and 99th percentiles)	CV in a number of annual occurrences during which the magnitude of flow remains below a lower threshold (75th, 90th, and 99th percentiles, respectively)	Annual	Dimensionless
Low-flow spell duration (less than 75th, 90th, and 99th percentiles)	Mean duration of flows that remains below a lower threshold defined by the 75th, 90th, and 99th percentiles, respectively (from the flow duration curve)	Annual	Days
CV of low-flow spell duration less than 75th, 90th, and 99th percentiles)	CV in duration of annual occurrences during which the magnitude of flow remains below a lower threshold (75th, 90th, and 99th percentiles, respectively)	Annual	Dimensionless
Number of zero-flow days	Mean annual number of days having zero flow	Annual	$Year^{-1}$
CV of number of zero-flow days	CV in annual number of days having zero flow	Annual	Dimensionless
Predictability (P) of minimum daily flow	Colwell's predictability (P) of minimum daily flow	Day	Dimensionless
Seasonality (M/P) of minimum daily flow	Colwell's seasonality (M/P) of minimum daily flow	Day	Dimensionless

26.5.2.3 Skewness of Daily Flow

Skewness is a measure of how different the mean and median flows are. It is a ratio of mean and median flows. For a small catchment, base flow is generally very low. After a big storm event, dramatic changes in discharge happen. Therefore, large discharges are observed during a storm, but most of the days, there exists a low base flow. Hence the median flow is low, and the mean flow is elevated by the much larger event-based discharges. As a result, skewness of a small catchment would be greater than that of a large catchment. Similarly, the skewness of an unregulated stream will tend to be greater than that of a regulated stream.

26.5.2.4 Variability of Daily Flow

The measure of variability is based on the use of the median flow as a measure of central tendency. Variability of flow can be calculated as the range divided by the median. The range of flow is the difference between the Q_{10} and Q_{90} flows. Other quartile values can also be used as a range.

26.5.2.5 Standard Deviation of the Log of Daily Flows

The standard deviation of the log of daily flow (S_Log) is an estimate of the standard deviation of the logarithm (base 10) of the daily flow values. Flow data are often logged to reduce the skew; S_Log is a measure of the distribution of this transformed data.

26.5.2.6 Lane's Variability Index

The Lane's variability index is described as the standard deviation of the logarithms of the Q_5, Q_{15}, Q_{25}, …, Q_{85}, and Q_{95} values. Lane's variability index is unsuitable for data sets with more than 5% zero values ($Q_{95} = 0$) or data sets dominated by zero flows [18].

26.5.3 Flow Duration Curve

Flow duration curve is widely used for representing the range and spread of stream flows in a time domain. To develop a flow duration curve, historical flow data need to be ranked from the largest to the smallest value and then plotted against a percentage value of time duration from 0% to 100%. The percentage time duration value indicates the proportion of time that a flow is exceeded. The first quarter (0%–25%) and the last quarter (75%–100%) of flow duration curve generally represent high-flow and low-flow conditions, respectively. The curve describes the characteristics of stream flow. As an example, flow duration curves for two creeks are shown in Figure 26.5. The Aldgate Creek exhibits a perennial stream flow characteristics (flow exists all the year-round) whereas the Inverbrackie Creek shows an ephemeral flow characteristics (seasonal flow exists, not all the year-round).

26.5.4 Base Flow Index

A long period of relatively consistent groundwater-fed low flow is considered as base flow. The base flow index (BFI) can be defined as the ratio of base flow volume to the total flow volume. Base flow is important for the development of stream macrophyte beds, algae growth, and macroinvertebrate density [28]. A three-way digital filter method [19] is used in the BFI estimation. Digital filters create a relatively smooth transition of the base flow period before and after a storm event. The Lyne and Hollick filter (described in [19]) can be applied to estimate the base flow component during a storm event. The BFI can be estimated using Equations 26.1 and 26.2:

$$q_f(i) = \phi q_f(i-1) + \{q(i) - q(i-1)\}^{(1+\phi)/2} \quad \text{for} \quad q_f(i) \geq 0 \tag{26.1}$$

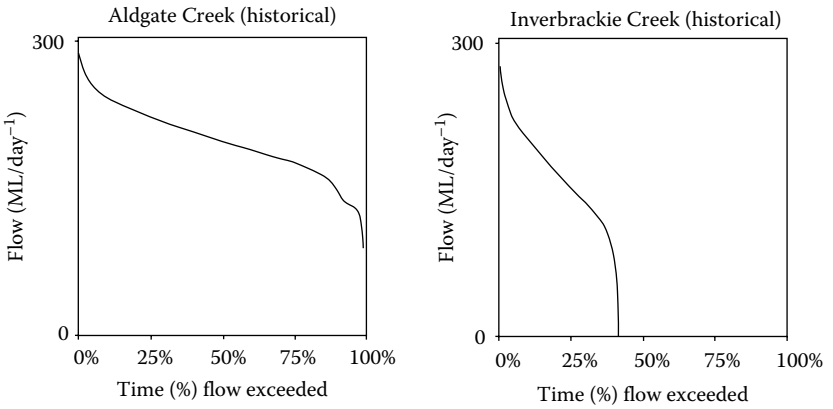

FIGURE 26.5 Flow duration curve for two creeks (Aldgate Creek and Inverbrackie Creek) in the South Australian Mount Lofty Ranges region.

$$\text{BFI} = \frac{q - q_f}{q} \tag{26.2}$$

where

$q_f(i)$ is the filtered quick flow response for the ith observation
$q(i)$ is the original stream flow at the ith observation
ϕ is a filter parameter

Nathan and McMahon [30] recommended $\phi = 0.925$ for daily flow in Australian streams. The filter needs to be applied in three passes: the first and third passes are based on "forward" passes (Equation 26.1) and the second pass is based on "backward" pass using $(i + 1)$ instead of $(i - 1)$ in Equation 26.1. Observed stream flow data are used as $q(i)$ in the first pass. Estimated base flows from the first pass are used as $q(i)$ in the second pass and base flows from the second pass are used in the third pass.

26.5.5 Colwell's Indices

Colwell's indices of predictability, constancy, and contingency describe aspects of periodicity in biological phenomena [14]. These indices provide a measure of seasonal predictability of environmental events such as fish spawning. Colwell's indices can be estimated for average-, maximum-, and minimum-flow conditions. Predictability is a measure of how strongly an event is linked to a season. Predictability is maximized if the same seasonal pattern of events is repeated every year. It is the converse of uncertainty and has two components, constancy and contingency. Constancy is a measure of temporal invariance, and its value is maximized if any event or state is the same for all seasons in all years. For example, an ephemeral stream with many zero flow days will have a high constancy value. Contingency is a measure of periodicity, and its value is maximized if the state is different for each season but the pattern is the same for all years. Contingency is minimal when the probability of occurrence of each state or event is independent of season. For example, if high flows occur every winter, the stream has a high contingency value. To estimate Colwell's indices, flow time series data need to be converted to categorical data by selecting time series value classes. Frequencies of occurrence of values in each class in a time period are recorded. According to Kennard et al. [22], 11 flow classes have been considered with a central class of 20 times mean daily flow. For a frequency matrix with t columns and s rows, let N_{ij} be the number of years for which the phenomenon is in state i at time j. Then column totals (X_j), row totals (Y_i), and grand total (Z) can be estimated as

$$X_j = \sum_{i=1}^{s} N_{ij} \tag{26.3}$$

$$Y_i = \sum_{j=1}^{t} N_{ij} \tag{26.4}$$

$$Z = \sum_i \sum_j N_{ij} = \sum_j X_j = \sum_i Y_i \tag{26.5}$$

Uncertainty with respect to time $(H(X))$, state $(H(Y))$, and interaction of time and state $(H\,(XY))$ can be expressed as

$$H(X) = -\sum_{j=1}^{t} \frac{X_j}{z} \log \frac{X_j}{z} \tag{26.6}$$

$$H(Y) = -\sum_{i=1}^{s} \frac{Y_i}{z} \log \frac{Y_i}{z} \tag{26.7}$$

$$H(XY) = -\sum_{i} \sum_{j} \frac{N_{ij}}{z} \log \frac{N_{ij}}{z} \tag{26.8}$$

The conditional uncertainty ($H_X(Y)$) with respect to state (with time given) can be defined as

$$H_X(Y) = H(XY) - H(X) \tag{26.9}$$

Predictability (P), constancy (C), and contingency (M) can then be estimated within the range (0, 1):

$$P = 1 - \frac{H_X(Y)}{\log(s)} = 1 - \frac{H(XY) - H(X)}{\log(s)} \tag{26.10}$$

$$C = 1 - \frac{H(Y)}{\log(s)} \tag{26.11}$$

$$M = \frac{H(X) + H(Y) - H(XY)}{\log(s)} \tag{26.12}$$

$$P = C + M \tag{26.13}$$

26.6 Hydrologic Matrices

Hydrologic metrics are statistical flow parameters that can be used to describe ecologically relevant components of the hydrologic regime in terms of flow magnitude, frequency, duration, timing of flow events, rate of change in flow, and the temporal variability in these measures [22,33]. Several hydrologic metrics are used in ecohydrological analyses. In the United States, Olden and Poff [33] examined 171 hydrologic metrics and quantified their ability to describe the key ecologically relevant components of hydrologic regimes in 420 stream gages. A number hydrologic metrics can be assessed using the Indicators of Hydrologic Alteration software package [29]. About 120 hydrologic metrics were listed for Australian streams that are ecologically important [22]. The extent of multicollinearity among hydrologic metrics, as evaluated by examining crosscorrelations between all 120 metrics, was found low [23]. Selected hydrologic metrics are listed in Tables 26.3 through 26.5 for low-flow, average-flow and high-flow conditions, respectively.

26.7 Summary and Conclusions

The importance of hydrologic flow regimes and flow metrics is well recognized by hydrologists, ecologists, and water resource managers. Aquatic ecosystems are linked to their hydrologic flow regimes. Anthropogenic activities, such as water reservoir, water supply, hydropower generation, flood control, recreation, and navigation, modify the natural flow regimes and thereby affect their ecosystems. Development of environmental flow rules requires understanding of flow regimes. Changes in flow regimes due to human interventions can be quantified using hydrologic metrics. Hydrologic metrics are

TABLE 26.4 Hydrologic Metrics for Average-Flow Condition

Flow Metric	Definition of Metric	Resolution	Unit
Mean daily runoff	Mean daily flow divided by catchment area	Daily	ML day^{-1} km^{-2}
Median daily runoff	Median daily flow divided by catchment area	Daily	ML day^{-1} km^{-2}
CV of daily flow	CV in daily flows	Daily	Dimensionless
Skewness in daily flow	Skewness in daily flows	Daily	Dimensionless
Mean monthly flows	Mean daily flow for each month averaged across years	Monthly	ML day^{-1}
CV monthly flows	CV in mean daily flows per month	Monthly	Dimensionless
Mean annual runoff	Mean annual flow divided by catchment area	Annual	ML $year^{-1}$ km^{-2}
CV of annual runoff	CV in annual flows	Annual	Dimensionless
Skewness in annual runoff	Skewness in annual flows	Annual	Dimensionless
Kurtosis in annual runoff	Kurtosis in annual flows	Annual	Dimensionless
Median annual runoff	Median annual flow divided by catchment area	Annual	ML $year^{-1}$ km^{-2}
Predictability (P) of mean daily flow	Colwell's predictability (P) of mean daily flow	Day	Dimensionless
Constancy (C) of mean daily flow	Colwell's constancy (C) of mean daily flow	Day	Dimensionless
Seasonality (M/P) of mean daily flow	Colwell's measure of contingency (M), expressed as a proportion of predictability (P)	Day	Dimensionless
Rise rate of flow events	Mean rate of positive changes in flow from one day to the next	Day	ML day^{-1} day^{-1}
CV of rise rate of flow events	CV in the rate of positive changes	Day	Dimensionless
Fall rate of flow events	Mean rate of negative changes in flow from one day to the next	Day	ML day^{-1} day^{-1}
CV of fall rate of flow events	CV in the rate of negative changes	Day	Dimensionless

useful to classify regional streams. Streams and rivers that cluster together based on metrics presumably share certain ecological features.

Importance of natural flow regimes in sustaining native biodiversity and stream integrity is acknowledged. Amount and timing (predictability) of stream discharge are critical for water supply, water quality, and ecological integrity of stream water systems. Temporal variation of stream discharge influences the aquatic and riparian zone community structures, population dynamics, and functional processes in the stream. Urbanization (expressed in terms of the degree of imperviousness) causes changes to stream flow regimes. Changes in flow regime include increased frequency, increased total and peak flow, and decreased base flow, thereby affecting the stream ecosystem conditions and riparian vegetation. Stream ecosystem conditions are generally expressed by stream health indicators that are categorized into four groups based on changed flow regime, water quality, biodiversity, and stream erosion and sedimentation. Macroinvertebrate diversity and density is a significant sign of urban stream health.

The physical processes affecting stream ecosystems include both water and sediment movement within the stream and between the stream and the floodplain. In order to establish relationships between hydrologic changes and stream ecosystems, both sediment transport and streambed disturbances should be considered. Stream flow characteristics are conventionally used to develop flow regime and stream regionalization. Several stochastic flow parameters are applied to develop environmental flow rules. Numerous hydrologic metrics are used to describe ecologically relevant components of the hydrologic regime. These metrics can effectively be applied in ecohydrological studies.

TABLE 26.5 Hydrologic Metrics for High-Flow Condition

Flow Metric	Definition of Metric	Resolution	Unit
Median of annual maximum flows	Median of the highest annual daily flow divided by mean annual daily flow averaged across all years	Annual	Dimensionless
High-flow discharge (equal or greater than 1st, 10th, and 25th percentile values)	1st, 10th, and 25th percentiles, respectively, from the flow duration curve	Annual	ML day^{-1}
Specific mean annual maximum runoff	Mean annual maximum flow divided by catchment area	Annual	ML day^{-1} km^{-2}
Flood magnitude (1-, 2-, 5-, 10-, 15-, and 20-year ARI)	Magnitude of flood events with ARIs of 1, 2, and 5 years, respectively (calculated using partial series) and 10, 15, and 20 years, respectively (calculated using annual series)	Annual	ML day^{-1}
Skewness in maximum annual flows	Skewness in maximum annual flows	Daily	Dimensionless
High-flow spell count (greater than 25th, 10th, and 1st percentiles)	Mean number of annual occurrences during which the magnitude of flow remains above a higher threshold defined by the 25th, 10th, and 1st percentiles, respectively (from the flow duration curve)	Annual	$Year^{-1}$
CV of high-flow spell count (greater than 25th, 10th, and 1st percentiles)	CV in the number of annual occurrences during which the magnitude of flow remains above a higher threshold (25th, 10th, and 1st percentiles, respectively)	Annual	Dimensionless
High-flow spell duration greater than 25th, 10th, and 1st percentiles)	Mean duration of flows that remains above a higher threshold defined by the 25th, 10th, and 1st percentiles, respectively (from the flow duration curve)	Annual	Days
CV of high-flow spell duration (greater than 25th, 10th, and 1st percentiles)	CV in duration of annual occurrences during which the magnitude of flow remains above a higher threshold (25th, 10th, and 1st percentiles, respectively)	Annual	Dimensionless
Predictability (*P*) of maximum daily flow	Colwell's predictability (*P*) of maximum daily flow	Day	Dimensionless
Seasonality (*M/P*) of maximum daily flow	Colwell's seasonality (*M/P*) of maximum daily flow	Day	Dimensionless

References

1. Arthington, A.H., Bunn, S.E., Poff, N.L., and Naiman, R.J., 2006. The challenge of providing environmental flow rules to sustain river ecosystems. *Ecological Applications*, 16: 1311–1318.
2. Beach, D., 2003. *Coastal Sprawl: The Effect of Urban Design on Aquatic Ecosystems in the United States*. Pew Oceans Commission, Arlington, VA.
3. Beecham, S. and Chowdhury, R.K., 2010. Temporal characteristics and variability of point rainfall: A statistical and wavelet analysis. *International Journal of Climatology*, 34(3): 458–473.
4. Biggs, B.J.F., Ibbitt, R.P., and Jowett, I.G., 2008. Determination of flow regimes for protection of in-river values in New Zealand: An overview. *Ecohydrology and Hydrobiology*, 8(1): 17–29.
5. Biggs, B.J.F., Nikora, V.I., and Snelder, T.H., 2005. Linking scales of flow variability to lotic ecosystem structure and function. *River Research and Application,* 21: 283–298.
6. Booth, D.B., Karr, J.R., Schauman, S., Konrad, C.P., Morley, S.A., Larson, M.G., and Burges, S.J., 2004. Reviving urban stream: Land use, hydrology, biology, and human behavior. *Journal of the American Water Resources Association*, 40: 1351–1364.
7. Breen, P. and Lawrence, I., 2005. *Urban Waterways in the Australian Runoff Quality—A Guide to Water Sensitive Urban Design*, T.H.F. Wong (ed.), Engineers Australia, Barton, Australian Capital Territory, Australia, pp. 13–15.

8. Bunn, S.E., Edwards, D.H., and Loneragan, N.R., 1986. Spatial and temporal variation in the macroinvertebrate fauna of streams of the northern jarrah forest, Western Australia: Community structure. *Freshwater Biology*, 16: 67–91.
9. Bunn, S. and Smith, M.J., 2002. Design and implementation of an ecosystem health monitoring program for streams and rivers in Southeast Queensland, Australia: An overview. *50th Annual Meeting of the North American Benthological Society*, Bulletin of the North American Benthological Society, May 26–June 01, Pittsburgh, PA, pp. 1–17.
10. Chowdhury, R.K. and Beecham, S., 2013. Influence of SOI, DMI and Niño3.4 on South Australian Rainfall. Stochastic Environmental Research and Risk Assessment, DOI: 10.1007/s00477-013-0726-x.
11. Chowdhury, R. and Beecham, S., 2010. Australian rainfall trends and their relation to the southern oscillation index. *Hydrological Processes*, 24(4): 504–514.
12. Chowdhury, R., Gardner, T., Gardiner, R., Chong, M., and Tonks, M., 2010. Catchment hydrologic modelling for stormwater harvesting study in SEQ: From instrumentation to simulation. In Begbie, D.K. and Wakem, S.L. (eds.) *Science Forum and Stakeholder Engagement: Building Linkages, Collaboration and Science Quality*. Urban Water Security Research Alliance, September 28–29, Brisbane, Queensland, Australia, pp. 65–67.
13. Close, A., 1990. The impact of man on the natural flow regime. In Mackay, N. and Eastburn, D. (eds.), *The Murray*. Murray Darling Basin Commission, Canberra, Australian Capital Territory, Australia, pp. 61–76.
14. Colwell, R.K., 1974. Predictability, constancy and contingency of periodic phenomenon. *Ecology*, 55: 1148–1153.
15. Dunne, T. and Leopold, L.B., 1978. *Water in Environmental Planning*. W. H. Freeman & Co., San Francisco, CA.
16. Eslamian, S.S., 1995. Regional flood frequency analysis using a new region of influence approach, PhD thesis, University of New South Wales, School of Civil Engineering, Kensington, New South Wales, Australia, 380pp.
17. Fletcher, T.D., Mitchell, V.G., Deletic, A., Ladson, T.R., and Séven, A., 2007. Is stormwater harvesting beneficial to urban waterway environmental flows? *Water Science and Technology*, 55(4): 265–272.
18. Gordon, N.D., McMahon, T.A., and Finlayson, B.L., 1992. *Stream Hydrology: An Introduction for Ecologists*. John Wiley & Sons, Chichester, U.K., 526pp.
19. Grayson, R.B., Argent, R.M., Nathan, R.J., McMahon, T.A., and Mein, R.G., 1996. *Hydrological Recipes—Estimation Techniques in Australian Hydrology*. Cooperative Research Centre for Catchment Hydrology, Canberra, Australian Capital Territory, Australia, 125pp.
20. Hughes, J.M.R. and James, B., 1989. A hydrological regionalization of streams in Victoria, Australia with implications for stream ecology. *Australian Journal of Marine and Freshwater Research*, 40: 303–326.
21. Hughes, J.M.R., 1987. Hydrological characteristics and classification of Tasmanian Rivers. *Australian Geographical Studies*, 25: 61–82.
22. Kennard, M.J., Pusey, B.J., Olden, J.D., Mackay, S.J., Stein, J.L., and Marsh, N., 2010. Classification of natural flow regimes in Australia to support environmental flow management. *Freshwater Biology*, 55: 171–193.
23. Kennard, M.J., Pusey, B.J., Olden, J.D., Mackay, S.J., Stein, J.L., and Marsh, N., 2008. Ecohydrological classification of Australia's flow regimes, Appendix 5. In Pusey, B.J., Kennard, M.J., Stein, J.L., Olden, J.D., Mackay, S.J., Hutchinson, M.F., and Sheldon, F. (eds.), *Ecohydrological Regionalisation of Australia: A Tool for Management and Science* (Innovations Project GRU36, Final Report to Land and Water Australia (http://www.lwa.gov.au). Land & Water Australia, Canberra. Available at: http://lwa.gov.au/files/products/innovation/pn22591/pn22591.pdf. Assessed on: 26 May 2012.
24. Konrad, C.P. and Booth, D.B., 2005. Hydrologic changes in urban streams and their ecological significance. In Brown L.R., Gray, R.H., Hughes, R.M., and Meador, M.R. (eds.), *Effects of Urbanisation on Stream Ecosystems*. American Fisheries Society Symposia, Bethesda, MD, Vol. 47, pp. 317–332.

25. Konrad, C.P., Booth, D.B., and Burges, S.J., 2005. Effects of urban development in the Puget lowland, Washington, on inter annual stream flow patterns: Consequences for channel form and streambed disturbance. *Water Resources Research,* 41(7): 1–15.
26. Ladson, A.R., Walsh, C.J., Fletcher, T.D., Cornish, S., and Horton, P., 2004. Improving stream health by reducing the connection between impervious surfaces and waterways. *Proceedings of the WSUD 2004*, Adelaide, South Australia, Australia, pp. 246–257.
27. Leopold, L.B., Wolman, M.G., and Miller, J.P., 1964. *Fluvial Processes in Geomorphology*. W.H. Freeman & Co., San Francisco, CA.
28. Marsh, N., 2004. *Time Series Analysis Module: River Analysis Package*. Cooperative Research Centre for Catchment Hydrology, Canberra, Australian Capital Territory, Australia.
29. Mathews, R. and Richter B.D., 2007. Application of the indicators of hydrologic alteration software in environmental flow setting. *Journal of the American Water Resources Association*, 43: 1400–1413.
30. Nathan, R.J. and McMahon, T.A., 1990. Evaluation of automated techniques for base flow and recession analyses. *Water Resources Research*, 26(7): 1465–1473.
31. Nilsen, E.T., Sharifi, M.R., and Rundel, P.W., 1984. Comparative water relations of phreatophytes in the Sonoran Desert of California. *Ecology,* 65: 767–778.
32. Nolte, U. and Loose, P., 2004. *The Stream Health Manual*. Environmental Services Department, Pine Rivers Shire Council, Brisbane, Queensland, Australia.
33. Olden, J.D. and Poff, N.L., 2003. Redundancy and the choice of hydrologic indices for characterizing streamflow regimes. *River Research and Applications,* 19: 101–121.
34. Paul, M.J. and Meyer, J.L., 2001. Streams in the urban landscape. *Annual Review of Ecology and Systematics*, 32: 333–365.
35. Poff, N.L., Allan, J.D., Bain, M.B., Karr, J.R., Prestegaard, K.L., Richter, B.D., Sparks, R.E., and Stromberg, J.C., 1997. The natural flow regime: A paradigm for river conservation and restoration. *Bioscience*, 47: 769–784.
36. Puckridge, J.T., Walker, K.F., and Costelloe, J.F., 2000. Hydrological persistence and the ecology of dryland rivers. *Regulated Rivers: Research and Management*, 16: 385–402.
37. Rapport, D.J., Costanza, R., and McMichael, A.J., 1998. Assessing ecosystem health: Challenges at the interface of social, natural, and health sciences. *Trends in Ecology and Evolution*, 13(10): 397–401.
38. Riis, T. and Biggs, B.J.F., 2003. Hydrology and hydraulic control of macrophytes in stream. *Limnology and Oceanography,* 48: 1488–1497.
39. SKM., 2003. Determination of environmental water requirements of the Onkaparinga River catchment. Summary Report, Version 1, Sinclair Knight Merz Pty Limited (SKM), Canberra, Australian Capital Territory, Australia.
40. Walsh, C.J., 2004. Protection of in-stream biota from urban impacts: To minimize catchment imperviousness or to improve drainage design? *Marine and Freshwater Research*, 55: 317–326.
41. Walsh, C.J., Fletcher, T.D., and Ladson, A.R., 2005. Stream restoration in urban catchments through redesigning stormwater systems: Looking to the catchment to save the stream. *Journal of the North American Benthological Society*, 24(3): 690–705.
42. Walsh, C.J., Roy, A.H., Feminella, J.W., Cottingham, P.D., Groffman, P.M., and Morgan, R.P., 2005. The urban stream syndrome: Current knowledge and the search for a cure. *Journal of the North American Benthological Society*, 24(3): 706–723.
43. Walsh, C.J., Leonard, A.W., Ladson, A.R., and Fletcher, T.D., 2004. Urban stormwater and the ecology of streams. Cooperative Research Centre for Freshwater Ecology and Cooperative Research Centre for Catchment Hydrology, Canberra, Australian Capital Territory, Australia.

27

Time Series Analysis of Hydrologic Data

Óli Grétar Blöndal Sveinsson
Landsvirkjun

AUTHOR

Óli Grétar Blöndal Sveinsson is the executive vice president of R&D at Landsvirkjun, the National Power Company of Iceland. He has a degree in physics from the University of Iceland (1995) and MSc (1998) and PhD (2002) degrees in civil engineering specializing in hydrologic processes from Colorado State University. He did postgraduate work (2002–2004) at the International Research Institute for Climate Prediction, Columbia University. Since 2004, he has worked for Landsvirkjun or its subsidiaries first as a department head for engineering research and since end of year 2010 as EVP of R&D.

PREFACE

Time series modeling of hydroclimatic processes is a very powerful tool for planning and management of water resources systems. Time series models are used for generation of long synthetic time series, forecasting, evaluation of operational rules for water resources systems, sizing of reservoirs, detection of trends and shifts, and filling in missing data and extending records. Analysis and modeling of time series of hydrologic data under climate variability and change can be used for evaluation of impacts and risks that can arise from natural variability and anthropogenic climate change in hydrologic time series. While time series models are in general stationary, they can be used to model nonstationary behavior such as trends and shifts. An important feature of time series models is their ability to model a complex dependence structure within a single time series and across multiple time series.

27.1 Introduction

Time series modeling of hydroclimatic processes has been widely used for planning and management of water resources systems [2,16,33,54]. The time series models are used to generate stochastic synthetic series that may occur in the future, and the series are utilized for estimating the probability distribution of key decision parameters such as reservoir storage size. Likewise, the models may be utilized for forecasting water supplies and water demands days, weeks, months, and years in advance with possible links to exogenous hydrometeorological information. The synthetically generated series and forecasts are used for real-time operation, for planning and testing operating rules, in estimating future power output of hydroelectric systems, for evaluating the performance of an irrigation system under uncertain irrigation water deliveries, and in linking future streamflow or hydrological response to measures of atmospheric circulation such as climate indices. For proper application of time series models for any hydroclimatic process, it is important to understand the underlying physical and stochastic mechanisms involved.

A number of time series models have been considered in the literature for synthetic generation and forecasting of hydrologic processes. Parametric models [2,16,51,54] of hydrologic processes such as annual streamflow and precipitation may be well represented by stationary linear models such as autoregressive (AR) and autoregressive–moving-average (ARMA) models. These models are usually capable of preserving the historical annual statistics, such as the mean, variance, skewness, and covariance. Parametric methods differ significantly from their nonparametric alternatives. Parametric methods require assumptions regarding the marginal probability distributions of the variables and the spatial and temporal covariance dependence structure, while nonparametric methods retain the empirical structure of the observed variables. Nonparametric data-driven methods have been gaining popularity in the last decades [28,75]. Nonparametric methods are based on resampling or bootstrapping techniques [8], and they provide flexible and similar ways for modeling different types of data at a single site and multiple sites and for disaggregation of time series. Parametric models usually assume that the process follows the normal distribution that can introduce biases when transforming generated series back into the original domain. Nonparametric models are flexible, but the omission of an assumed parametric form makes it difficult to describe the modeling process mathematically, and in addition, any simulated values beyond the range of the sample observations may be significantly biased.

This chapter focuses on time series models used to model hydroclimatic data that are correlated in time and space but does not include stochastic process models such as Markov chain and point process models that are commonly used for modeling precipitation processes [50,51]. Stochastic processes of hydrologic data are described in Chapter 19. Many of the time series models in this chapter can be

found in common software packages, such as MATLAB®, R, SAS, and SPSS, and in specialized software for time series analysis [4] of hydrological systems, such as SAMS [57,66] and Spigot [15]. The methods presented here have been used for modeling of complex water resources systems such as the Colorado River, the Great Lakes, and St. Lawrence River System [9] and the Nile River.

27.2 Properties of Hydrologic Time Series

Statistical analysis of hydroclimatic time series involves calculation of basic statistic, estimating the autocorrelation function (ACF), partial ACF (PACF), and spectrum, analyzing the seasonal structure, and plotting the time series. Run, storage, drought, and flood statistics [51], the Hurst slope, and other statistics of interest may also be calculated. The time series may be tested for normality, trends, and shifts and transformed to normal if necessary.

27.2.1 Mean, Variance, and Skewness

The descriptive basic sample statistics of a time series y_t of length N are the mean, standard deviation, and skewness $\{\overline{y}; s; g\}$:

$$\overline{y} = \frac{1}{N}\sum_{t=1}^{N} y_t; \quad s = \sqrt{\frac{1}{N}\sum_{t=1}^{N}\left(y_t - \overline{y}\right)^2}; \quad g = \frac{(1/N)\sum_{t=1}^{N}\left(y_t - \overline{y}\right)^3}{s^3} \tag{27.1}$$

where

$\overline{y}$ is a measure of location
s is a measure of spread
g is a measure of shape

The corresponding population statistics are denoted by $\{\mu; \sigma; \gamma\}$. The previous maximum likelihood estimates for s and g are biased for small samples, where for an uncorrelated time series, unbiased estimate for s is given by using a divisor $(N - 1)$ instead of N and for g by using $N/[(N - 1)(N - 2)]$ instead of $1/N$. For an autocorrelated series, the effective sample size is reduced due to the internal dependence structure, and thus complex bias corrections are needed to estimate unbiased statistics [51]. Similarly seasonal time series, such as monthly flows, are characterized by seasonal statistics. Let $y_{\nu,\tau}$ be a seasonal time series, where the year $\nu = 1,\ldots, N$ and the season $\tau = 1,\ldots, w$. The mean, standard deviation, and skewness for season τ $\{\overline{y}_\tau; s_\tau; g_\tau\}$ with corresponding population statistics $\{\mu_\tau; \sigma_\tau; \gamma_\tau\}$ are estimated similarly as in (27.1) as

$$\overline{y}_\tau = \frac{1}{N}\sum_{\nu=1}^{N} y_{\nu,\tau}; \quad s_\tau = \sqrt{\frac{1}{N}\sum_{\nu=1}^{N}\left(y_{\nu,\tau} - \overline{y}_\tau\right)^2}; \quad g_\tau = \frac{(1/N)\sum_{\nu=1}^{N}\left(y_{\nu,\tau} - \overline{y}_\tau\right)^3}{s_\tau^3} \tag{27.2}$$

27.2.2 ACF and PACF

The lag-h ACF(h) $= \rho_h$ with the corresponding sample estimators r_h is simply the cross-correlation between consecutive values of the process at lag-h:

$$r_h = \frac{c_h}{c_0}, \quad \text{with} \quad c_h = \frac{1}{N}\sum_{t=1}^{N-h}\left(y_{t+h} - \overline{y}\right)\left(y_t - \overline{y}\right) \tag{27.3}$$

where c_h is the lag-h sample autocovariance with $c_0 = s^2$. The corresponding population autocovariance function, ACVF(h), is $C_h = E[(y_{t+h} - \mu)(y_t - \mu)]$. Across two sites i and j, the lag-h cross-correlation function is $\rho_h^{ij} = C_h^{ij} / \sqrt{C_0^{ii} C_0^{jj}}$ with the lag-h cross-covariance function $C_h^{ij} = E[(y_{t+h}^{(i)} - \mu^{(i)})(y_t^{(j)} - \mu^{(j)})]$ and the corresponding sample cross-covariance estimator $c_h^{ij} = (1/N) \sum_{t=1}^{N-h} (y_{t+h}^{(i)} - \overline{y}^{(i)})(y_t^{(j)} - \overline{y}^{(j)})$ for $h = \ldots$, $-2, -1, 0, 1, 2, \ldots$. Similarly the sample lag-h ACF of a seasonal time series is $r_{h,\tau}$ representing the season-to-season correlation between season τ and $\tau - h$:

$$r_{h,\tau} = \frac{c_{h,\tau}}{\sqrt{c_{0,\tau} c_{0,\tau-h}}} = \frac{c_{h,\tau}}{s_\tau s_{\tau-h}}, \quad \text{with} \quad c_{h,\tau} = \frac{1}{N} \sum_{\nu=1}^{N} \left(y_{\nu,\tau} - \overline{y}_\tau \right) \left(y_{\nu,\tau-h} - \overline{y}_{\tau-h} \right) \tag{27.4}$$

where $c_{h,\tau}$ is the lag-h sample season-to-season autocovariance with $c_{0,\tau} = s_\tau^2$. The lag-h season-to-season sample cross-correlation function between two sites i and j is similarly $r_{h,\tau}^{ij} = c_{h,\tau}^{ij} / \sqrt{c_{0,\tau}^{ii} c_{0,\tau-h}^{jj}}$ with $c_{h,\tau}^{ij} = (1/N) \sum_{\nu=1}^{N} (y_{\nu,\tau}^{(i)} - \overline{y}_\tau^{(i)})(y_{\nu,\tau-h}^{(j)} - \overline{y}_{\tau-h}^{(j)})$. For example, the lag-1 season-to-season correlation coefficients, $r_{1,\tau}$, represent $r_{1,1}$ as the correlation between season 1 of the current year with season w of the previous year, and the correlation coefficients between season τ and $(\tau - 1)$ of the same year, $\tau = 2, \ldots, w$. Plot of the ACF versus h is referred to as a correlogram, where a quickly decaying correlogram to zero represents short memory of the process, while a slowly decaying correlogram to zero represents a long-memory process often referred to as persistence or storage effect. The PACF is also a measure of serial dependence like the ACF but with all autocorrelations within the specified lag (i.e., 1 to $h - 1$) partialled out [3]. The PACF from a sample time series is estimated by repeatedly fitting AR(p) models to the time series (Section 27.4.1), where the PACF at lag p is equivalent to φ_p in the fitted AR(p) model. Approximate confidence intervals for both the ACF and PACF of a white noise process at the α significance level are $\pm z_{1-\alpha/2} / N^{0.5}$ [4] where z is the quantile of the standard $N(0,1)$ distribution, that is, approximate 95% confidence intervals are estimated by $\pm 1.96 / N^{0.5}$.

27.2.3 Spectral Density

Spectral analysis of the time series is used to detect cyclic components of the time series both with high and low frequency. The power spectrum and the spectral density function are mathematical characteristics of the time series in the frequency domain, while the corresponding functions in the time domain are the autocovariance and ACFs, respectively. The spectral density function can be estimated in various ways by both parametric and nonparametric methods [4,5,24,44], and most software packages today include one or more methods for estimation of the spectrum. A simple estimate of the spectral density function in terms of the ACF is [24,54,80]

$$g(f_j) = 2 \left(1 + 2 \sum_{k=1}^{m} D_k r_k \cos(2\pi f_j k) \right) \quad \text{where} \quad f_j = \frac{j}{2m}, \quad j = 0,1,2,\ldots,m \tag{27.5}$$

where

r_k is the ACF

D_k is a smoothing function [24]

For $D_k = 1$, the raw sample spectrum is estimated. Recommended values for m are between $N/6$ and $N/4$, that is, the number of lags of the ACF used in the estimation. The frequency spacing of 2 m in (27.5) is arbitrary, and the spectrum may be calculated at any frequency between 0 and 0.5. The raw sample spectrum is χ^2 square distributed with approximate 2 N/m degrees of freedom for a white noise process.

The approximate confidence interval at the α significance level is $[2df/x(1-\alpha/2, df), 2df/x(\alpha/2, df)]$ where df are the degrees of freedom, x is the χ^2 quantile, and the value of (27.5) for a white noise process is 2.

27.3 Time Series Modeling

A number of different alternative models are available for modeling of hydroclimatic time series. The choice of model should reflect its ability to reproduce important statistics of the process under consideration. Time series is said to be stationary if the statistical properties of the time series do not change with time, that is, the probability distribution of the process is the same at all times. Conversely if any statistical property depends on time, then the process is nonstationary with regard to that statistical property. Most parametric time series models assume that the process being modeled is normally distributed and stationary in the mean and variance. Typical steps in decomposition of a time series that is non-normal and nonstationary are as follows [4]: (1) test for normality and transform the data to normal, (2) test for trends and shifts and remove them if necessary, and (3) if seasonality is present in the mean or variance, then remove them if a model with nonperiodic parameters is used. The typical steps involved in time series modeling are model identification, parameter estimation, and model testing and validation.

27.3.1 Tests of Normality

Plotting the empirical cumulative distribution function (CDF) on a normal probability paper based on selected plotting position formula provides a nonparametric way of visually checking if the data plots as a straight line and conforms to the normal distribution (Q–Q plot). Commonly used plotting position formulas of nonexceedance probabilities for a time series of length N ordered from the smallest to the largest are Cunnane $(i-0.4)/(N+0.2)$, Hazen $(i-0.5)/N$, and Weibull $i/(N+1)$ for $i=1,\ldots, N$. Probability plot correlation tests of normality are available for different plotting positions [12,25,74] with the Filliben probability plot correlation coefficient test of normality being the most popular one. Other tests include the skewness test of normality [63] for testing the hypothesis of zero skewness. The sample skewness g in (27.1) is asymptotically distributed as $N(0, \sigma^2 = 6/N)$. The null hypothesis H_0: $g=0$ versus H_1: $g \neq 0$ is rejected at the α-significance level if $\mathbf{abs}(g) > z_{1-\alpha/2}\sqrt{6/N}$.

27.3.2 Transformation to Normal

Most time series models assume that the underlying process is normally distributed. Time series failing a normality test can be transformed to normal using variety of parametric transformations [3,16,51,54]. Common transformations include Box–Cox $Y = ((X+a)^b - 1)/b$ for $b \neq 0$, gamma $Y = \text{gamma}(X)$, logarithmic $Y = \ln(X+a)$, and power $Y = (X+a)^b$, where Y is the transformed normal series and X is the original observed series. The variables Y and X can represent either annual or seasonal data, where for seasonal data, the transformation coefficients a and b can be periodic if a periodic model is to be fitted to the data. Hydroclimatic data are often positively skewed and a widely used transformation for hydroclimatic data is the lognormal transformation assuming that the underlying variable X is approximately lognormally distributed with a lower bound a. Transformation is also helpful when a time series shows changing variability with the level of the process. Nonparametric kernel density estimation (KDE) [59,62,70] can also be used where the corresponding estimated CDF is mapped onto the normal distribution function to transform the data quantiles to normal. This may be useful for modeling bimodality and other behavior that may be difficult to describe by a parametric function.

27.3.3 Removal of Trends

A number of parametric (e.g., t-test) and nonparametric (e.g., Mann-Kendall) tests [16,17,51] are available for testing for linear or nonlinear trends and for testing for shifts in the mean. In today's changing

climate, trends may vary over time, for example, historical global temperature has been rising and projections of expected future trends from general climate circulation models exist [22]. Trends can by removed by a nonparametric smoothing filter, but often a parametric form of the trend is wanted so that the trend can be extrapolated for the purposes of prediction and simulation. In this context, a nonlinear trend can be approximated by piecewise linear trends, and the slowly varying time-dependent trend is simply removed by subtracting it from the data. Another form used for trend removal is differencing the time series at lag-1. Such procedures relate to the family of nonstationary autoregressive integrated moving average (ARIMA) models (Section 27.4.5). As for removal of seasonalities in the following discussion, for physically bounded hydroclimatic process, subtraction of a deterministic trend is preferred over differencing, although for time series of accumulated statistics, such as groundwater or aquifer levels, it may be necessary to differentiate these time series to make them stationary.

27.3.4 Removal of Seasonality in the Mean and Variance

Hydroclimatic data are usually affected by the annual cycle, with monthly data showing a 12 month periodic structure and being nonstationary in the mean and the variance. The seasonality in the mean is removed for each season by subtraction of the seasonal sample mean. Similarly the seasonality in the variance is removed by division of the seasonal standard deviation. Seasonal standardization is done by both subtracting the seasonal mean and dividing by the seasonal standard deviation for each season $z_{\nu,\tau} = (y_{\nu,\tau} - \overline{y}_\tau)/s_\tau$, where $z_{\nu,\tau}$ is normally distributed variable with standard deviation one and mean zero for year ν of the seasonal series for season τ. Alternatively, seasonal differencing can be used for removal of seasonalities, that is, differencing monthly hydrologic time series at lag-12 removes the 12-month periodic hydrologic annual cycle from the time series. As explained in Section 27.4.5, it is preferred to use seasonal standardization over seasonal differencing for hydrologic time series that are considered to be physically bounded.

27.3.5 Model Selection

Often several alternative models may be fitted to the data. The ACF and PACF are often used to get an idea of the appropriate model to fit, and the model with the minimum residual variance is often selected as the best model. This does not penalize for number of parameters and a common practice is to use information criteria for selecting the best model penalizing for the number of parameters used in the model. The corrected Akaike information criterion (AICC) [4,19] and the Schwarz information criterion (SIC) [20,61] also referred to as the Bayesian information criterion are defined as

$$\text{AICC} = N \ln \hat{\sigma}^2(\varepsilon) + N + \frac{2(k+1)N}{N-k-2}; \quad \text{SIC} = N \ln \hat{\sigma}^2(\varepsilon) + N + k \ln N \tag{27.6}$$

where

N is the size of the sample used for fitting the model
k is the number of parameters excluding constant terms ($k = p + q$ for the ARMA(p,q) model)
$\hat{\sigma}^2(\varepsilon)$ is the maximum likelihood estimate of the residual variance as in (27.1)

The AICC statistic is efficient but not consistent and is good for small samples but tends to overfit for large samples and large k. The SIC is consistent but not efficient and is good for large samples, but tends to underfit for small samples. Efficiency is usually more important than consistency since the true model order is not known for real-world data. For a multivariate m-dimensional model, the AICC and SIC are given by

$$\text{AICC} = N \ln |\mathbf{G}| + Nm + \frac{2(km^2+1)N}{N-km^2-2}; \quad \text{SIC} = N \ln |\mathbf{G}| + Nm + km^2 \ln N \tag{27.7}$$

where $|\mathbf{G}|$ is the norm of the estimated residual variance–covariance $\mathbf{G}$. The model that minimizes the AICC and/or the SIC is chosen as the best model.

27.3.6 Model Testing

All the sample information on lack of fit is contained in the residuals. In most time series models, the residuals are assumed to be normally distributed with mean zero and variance $\sigma^2(\varepsilon)$. Thus, a plot of the residuals should look like an independent drawing from the normal distribution. The residuals should be uncorrelated with zero ACF and PACF and also independent of the explanatory variables used in the model. Nonnormal residuals may indicate lack of transformation of the data, while correlated residuals with nonzero terms in the ACF and PACF may indicate that a higher-order model is needed. In addition, synthetically simulated series from the model of the same length as the historical series should be capable of approximately reproducing the historical statistical properties of the original time series.

27.4 Univariate Modeling

In the parameterization of the models in this and following sections, the mean of the process is usually not shown. This is to simplify the representation where it is assumed that the mean has been subtracted from the process under consideration unless otherwise stated.

27.4.1 ARMA

Stationary ARMA models [2–4,16,51] have become widely used for modeling of hydroclimatic time series and in particular of precipitation and streamflow, where physical justification of ARMA models of the conceptual rainfall–runoff process has been presented [16,56]. The ARMA models are flexible and can accommodate features of alternative models such as fractional Gaussian noise [37], broken line [40], and shifting mean (SM) [69]. The ARMA(p,q) of AR order p and moving average order q for a hydroclimatic process is defined as

$$Y_t = \sum_{i=1}^{p} \varphi_i Y_{t-i} + \varepsilon_t - \sum_{j=1}^{q} \theta_j \varepsilon_{t-j} \tag{27.8}$$

where

Y_t is normally distributed with mean zero and variance $\sigma^2(Y)$
ε_t is the independent normally distributed noise term with variance $\sigma^2(\varepsilon)$
$\{\varphi_1,\ldots, \varphi_p\}$ and $\{\theta_1,\ldots, \theta_q\}$ are the AR and moving average parameters, respectively

ε_t is uncorrelated with Y_{t-i}, that is, the noise is independent of past observations Estimation methods include method of moments, least squares, and maximum likelihood. For an AR(p) process, the well-known Yule–Walker equations [16] or moment equations are given by $\sigma^2(Y) = \sigma^2(\varepsilon) + \sum_{i=1}^{p} \varphi_i C_i$ and $C_h = \sum_{i=1}^{p} \varphi_i C_{h-i}, h \geq 1$, where C_h is the lag-h population autocovariance $C_h = E[Y_t\ Y_{t-h}] = C_0 \rho_h = \sigma^2(Y)$ ρ_h. Simple models such as AR(1) and ARMA(1,1) may often be adequate, while higher-order AR models are necessary for modeling of time series that show signs of quasiperiodic behavior although the use of higher-order models than AR(2) or AR(3) is rare. The characteristics of the ACF and the PACF of the ARMA(p,q) model for different p and q are given in Table 27.1. The AR(1) model $Y_t = \varphi_1 Y_{t-1} + \varepsilon_t$ has ACF(h) $= \varphi_1^h$ and PACF(1) $= \varphi_1$ with PACF($h > 1$) $= 0$. The parameter estimates based on the method of moments are given by $\hat{\varphi}_1 = r_1$ and $\hat{\sigma}^2(\varepsilon) = s^2(1 - \hat{\varphi}_1^2)$, where r_1 is the sample ACF(1) and s^2 is the sample variance. The least square method minimizes the sum of the squared residuals $F = \sum_{t=1}^{N} \varepsilon_t^2$ where N is the number of years of data and the residuals are estimated from (27.8). For a pure AR(p) model, (27.8)

TABLE 27.1 Properties of the ACF and PACF of ARMA(p,q) Processes

	AR(1)	AR(p)	MA(q)	ARMA(p,q)
ACF	Decays geometrically	Tails off	Zero at lag > q	Tails off
PACF	Zero at lag > 1	Zero at lag > p	Tails off	Tails off

is a traditional regression equation only conditioned on past observations, while for the ARMA(p,q) model with moving average terms, the past residuals in (27.8) are unknown. In that case, a high-order AR(p) model is fitted to the data to get initial estimate of the noise terms ε_t. Then iteratively a regression model is fitted to the data and the parameters φ's and θ's are reestimated and the residuals are recalculated until the sum of the squares of the residuals has converged to a minimum value. For details on parameter estimation, refer to [3,4].

In Figure 27.1, naturalized flows of the Colorado River at Lees Ferry are plotted. The ACF and PACF indicate that a low-order model is appropriate such as AR(1) or ARMA(1,1). The spectral density shows weak indication of a low-frequency component with period around 13 years, which could result from low-frequency atmospheric forcing and should be looked into before fitting a model.

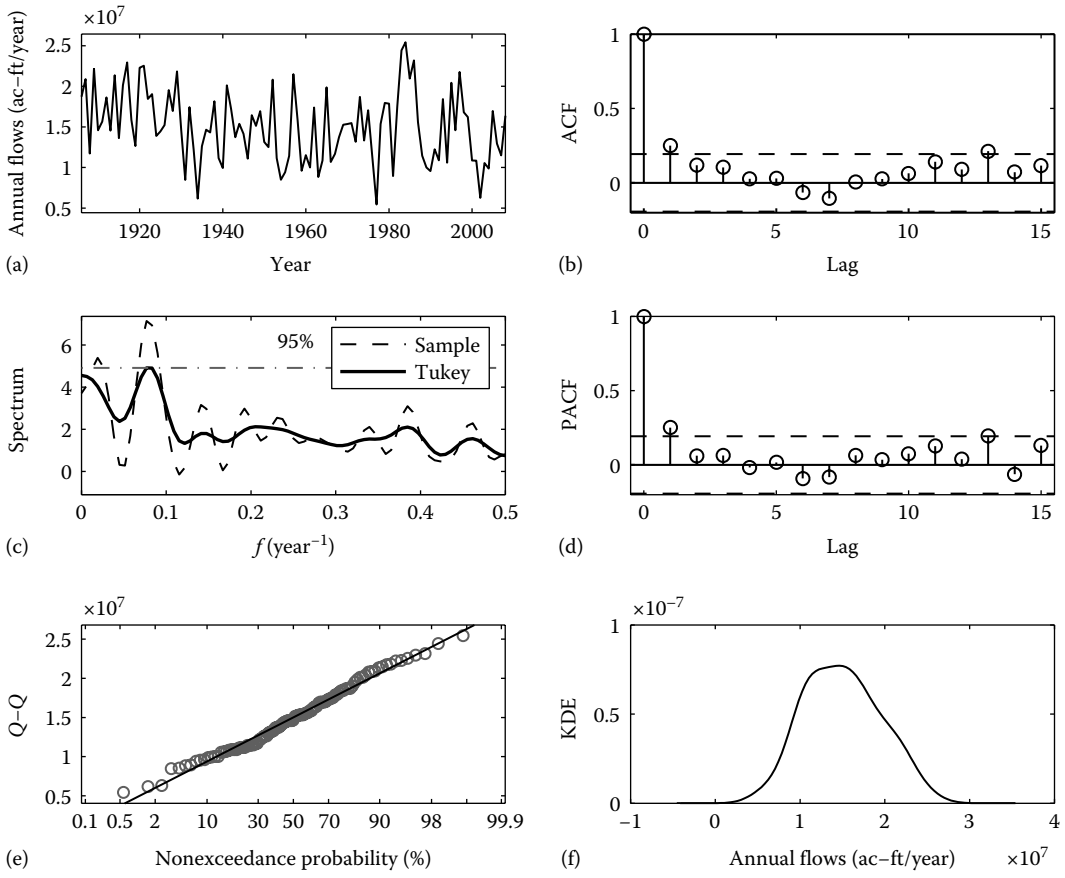

FIGURE 27.1 Naturalized annual flows of the Colorado River at Lees Ferry obtained from http://www.usbr.gov. (a) 1906–2008 annual flows in ac ft/year, (b) ACF, (c) spectral density with 95% one-sided CIE for a white noise process for the Tukey smoother. (d) PACF, (e) normal probability paper plot, (f) KDE with normal kernel. In (b) and (d), 95% CIE for a white noise process is also shown.

The normal probability paper plot and the kernel density estimate indicate that the annual flows are near normally distributed.

27.4.2 PARMA

For seasonal hydrologic time series, such as monthly series, seasonal statistics such as the mean and standard deviation may be reproduced by a stationary ARMA model by means of standardizing the underlying seasonal series by subtracting the seasonal mean and dividing by the seasonal standard deviation. However, this procedure assumes that season-to-season correlations are the same throughout the year for a given lag and thus do not preserve the seasonality in the covariance structure. Hydrologic time series, such as monthly streamflows, are usually characterized by different dependence structure (month-to-month correlations) depending on the season (e.g., spring or fall). Periodic ARMA (PARMA) models have been suggested in the literature for modeling such periodic dependence structure. A PARMA(p,q) model may be expressed as [51,53,54]

$$Y_{\nu,\tau} = \sum_{i=1}^{p} \varphi_{i,\tau} Y_{\nu,\tau-i} + \varepsilon_{\nu,\tau} - \sum_{j=1}^{q} \theta_{j,\tau} \varepsilon_{\nu,\tau-j} \tag{27.9}$$

where

$Y_{\nu,\tau}$ represents the hydrologic process for year ν and season τ
The $\varepsilon_{\nu,\tau}$ is the uncorrelated noise term that for each season is normally distributed with mean zero and variance $\sigma_\tau^2(\varepsilon)$
The $\{\varphi_{1,\tau},\ldots, \varphi_{p,\tau}\}$ are the periodic AR parameters
The $\{\theta_{1,\tau},\ldots, \theta_{q,\tau}\}$ are the periodic moving average parameters

If the number of seasons is ω, then a PARMA(p,q) model consists of ω-number of individual ARMA(p,q) models, where the dependence is across seasons instead of years. In most practical applications, PAR(1), PAR(2), and PARMA(1,1) have been found to be adequate, although residuals should always be tested to ensure adequate model fit. The PAR(1) model $Y_{\nu,\tau} = \varphi_{1,\tau} Y_{\nu,\tau-1} + \varepsilon_{\nu,\tau}$ preserves the lag-1 season-to-season correlation coefficient in addition to the seasonal mean and variance. Parameter estimates based on method of moments are $\hat{\varphi}_{1,\tau} = (s_\tau / s_{\tau-1})\, r_{1,\tau} = c_{1,\tau}/c_{0,\tau-1}$ and $\hat{\sigma}_\tau^2(\varepsilon) = s_\tau^2 - s_{\tau-1}^2 r_{1,\tau}^2$ for $\tau = 1,\ldots, w$. The PARMA model is able to preserve the seasonal historical statistics of the annual cycle. However, since annual observations or statistics are not used in the estimation process, the annual statistics of the process may not be preserved from aggregated simulated samples to the annual scale. Disaggregation models (Section 27.6) modeling jointly the annual and seasonal process can be used as alternatives for joint preservation of annual and seasonal statistics.

In Figure 27.2, naturalized monthly flows of the Colorado River at Lees Ferry are plotted. The seasonal distribution in (b) and the spectral density in (c) show periodicities due to the annual hydrologic cycles. In (e) and (f), the flows have been standardized by removing the seasonal mean and dividing by the seasonal standard deviation. There are two options, either to fit a PARMA model with periodic parameters to the data in (a) and (b) or to fit an ARMA model to the seasonally standardized data. An ARMA model would not be able to reproduce the seasonality in the month-to-month correlation coefficients in graph (d), where the ARMA model would reproduce the month-to-month correlations at different lags as horizontal lines (i.e., all lag-1 values the same, lag-2 values the same). In addition, the ARMA model would not be able to reproduce seasonality in higher-order moments such as skewness and kurtosis. Despite this, an ARMA model could prove sufficient if it is not considered important to reproduce those seasonalities, which the PARMA model is capable of doing. From the boxplots of seasonal distributions, it is clear that the data are positively skewed and need to be transformed to normal before fitting a stationary ARMA or PARMA model.

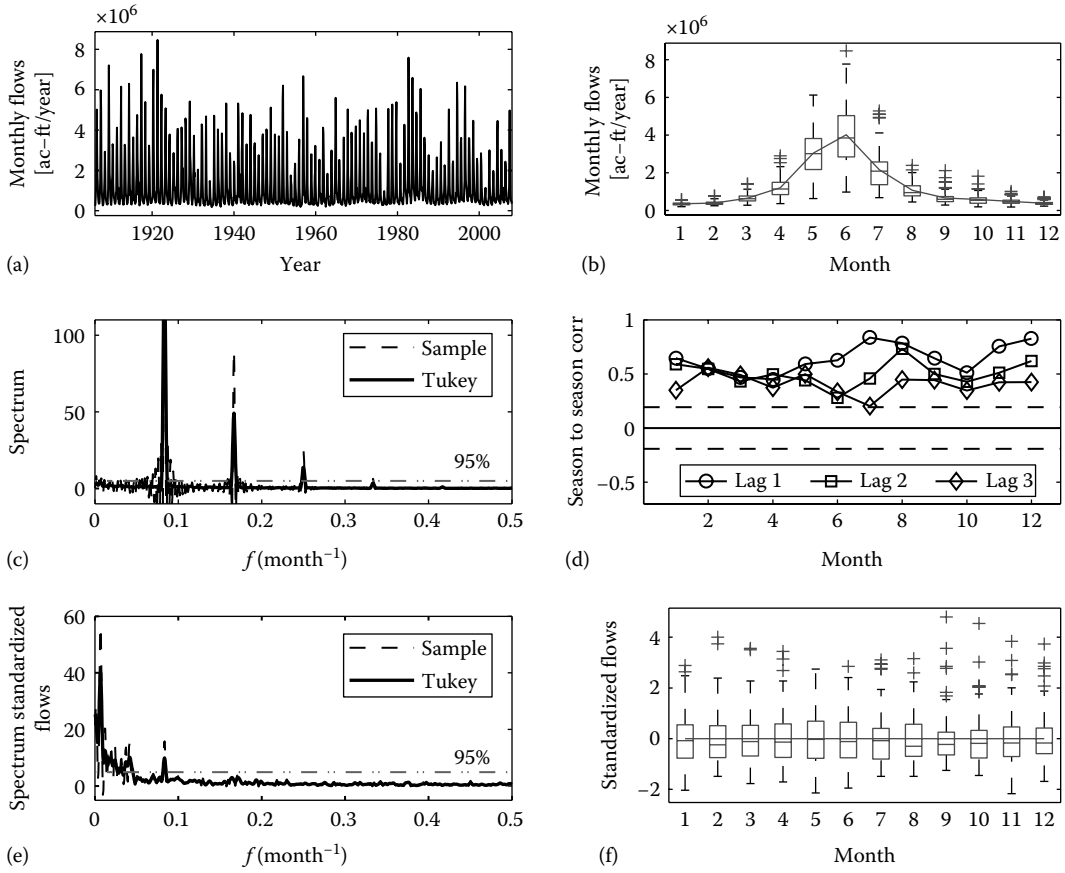

FIGURE 27.2 Naturalized monthly flows of the Colorado River at Lees Ferry obtained from http://www.usbr.gov. (a) 1906–2008 monthly flows in ac ft/year, (b) seasonal distribution, (c) spectral density with 95% one-sided CIE for a white noise process for the Tukey smoother. (d) month-to-month correlation at lags 1, 2, and 3, (e) spectral density of seasonally standardized flows, (f) seasonal distribution of seasonally standardized flows.

27.4.3 GAR, PGAR

Gamma-distributed AR(1) and PAR(1) models have been suggested [10,11,51] for direct modeling of skewed time series from a gamma-distributed process instead of the traditional approach of transforming such time series to normal before applying the selected ARMA or PARMA model. The gamma autoregressive (GAR) model is expressed as $Y_t = \varphi Y_{t-1} + \varepsilon_t$ where Y_t is a three parameter gamma variable, φ is the autoregression coefficient, and ε_t is the independent noise term. Similarly the periodic gamma autoregressive (PGAR) model is expressed as $Y_{\nu,\tau} = \varphi_\tau Y_{\nu,\tau-1} + \varepsilon_\tau$ for season τ.

27.4.4 SM

The SM model [67–69] is characterized by sudden shifts or jumps in the mean and can be used to model high- and low-frequency shifts in the mean of hydroclimatic processes [69]. More precisely, the underlying process is assumed to be characterized by multiple stationary states, which only differ from each other by having different means that vary around the long-term mean of the process. The process is stationary and autocorrelated, where the autocorrelation arises only from the sudden shifting pattern in the mean. A general definition of the SM model [68,69] is $X_t = Y_t + Z_t$ where $\{X_t\}$ is a sequence of

random variables representing the hydrologic process of interest and $\{Y_t\}$ is a sequence of *iid* normal variables and mutually independent of the mean-level sequence $\{Z_t\}$, where the length of each mean-level state is a discrete stationary delayed renewal sequence. Bayesian version of the SM model has also been proposed [13], and it has been shown that the SM models belong to the class of hidden Markov chain models [13,71].

27.4.5 ARIMA, SARIMA, and ARFIMA

ARIMA models, where "I" stands for integrated, are ARMA models applied on differenced time series [3,4] and can be used to model certain types of nonstationary characteristics like trends. The ARIMA models in [3] were extended for modeling of seasonal time series (SARIMA) by using long-term seasonal differencing (representing the annual cycle for hydroclimatic time series) in addition to short-term seasonal differencing for trend elimination. Both of these models are sometimes referred to as multiplicative models. The SARIMA has been applied for modeling of monthly streamflows [2,39], but like the ARMA applied on deseasonalized time series, it is not able to reproduce the seasonality in the covariance structure since it does not have periodic parameters. As for the ARMA, these limitations may be overcome by applying a multiplicative PARMA model with periodic parameters. Care should be taken when using such differencing models to make the time series stationary in the mean and alternative methods of trend removal, and deseasonalization should be considered along with traditional application of ARMA and PARMA models, as the major drawback of ARIMA and SARIMA models is the increasing uncertainty of post-sample forecasts with the length of the forecasting horizon [34–36]. ARIMA models are nonstationary and as such might not always be appropriate for simulation of long time series of hydroclimatic data that usually are bounded by some physical process, although for time series representing accumulated statistics such as groundwater levels or aquifer levels, ARIMA models may perform very well. For short-term forecasting conditioned on past observations, ARIMA models often perform well and sometimes even better than other traditional ARMA models.

Fractional ARIMA (ARFIMA) models [5,16,18], on the other hand, are stationary models where fractional differencing $(1 - B)^d$ for $-0.5 < d < 0.5$ is applied as opposed to d being an integer in the ARIMA model. The fractionally differenced time series is then modeled by an ARMA model. An interesting feature of an ARFIMA process is its long memory, where the ACF converges to zero with increasing lag-h at a much slower rate than for a traditional ARMA process. The ARFIMA model has been used for modeling of monthly and daily flows [42,43], and the ARFIMA($p = 0$, d, $q = 0$) process is similar to fractional Gaussian noise that has been used in studies of the Hurst phenomenon and analyses of long-term dependence in hydroclimatic time series [27].

27.4.6 Intermittent Models

Modeling of intermittent processes, such as short-term rainfall or flow in intermittent or ephemeral streams, can be done by using annual $Y_t = B_t X_t$ or seasonal $Y_{\nu,\tau} = B_{\nu,\tau} X_{\nu,\tau}$ product models [6,7,51]. Here, B_t or $B_{\nu,\tau}$ is a discrete correlated Bernoulli (0,1) variable mutually independent of X that is modeled by any traditional time series model such as ARMA, PARMA, GAR, or GPAR.

27.5 Multivariate Modeling

Multivariate models are used for modeling of complex dependence structure in space and time at multiple lags. Properties of the multivariate ARMA (MARMA) model have been widely studied [3–5,16,61] and of multivariate PARMA [1,4,5]. For modeling of hydroclimatic data at multiple sites, simpler contemporaneous ARMA (CARMA) and PARMA models [16,51,54] are often used. The difference between the full multivariate model and its contemporaneous counterpart is that the parameter matrixes in the contemporaneous models are diagonal. Thus, both models can preserve complex dependence structure

for each site, but only lag-0 cross-correlation coefficients are preserved across sites in the contemporaneous model, while higher lagged cross-correlation coefficients can be preserved in the full multivariate model. For example, for the MAR(2) and the equivalent CARMA(2,0), presented as follows, both models preserve AR(2)-type dependence structure for each site, but the MAR(2) model preserves correlation in space across all sites up to lag-2, while the CARMA model is capable of preserving only the lag-0 cross-correlation in space between different sites, which is usually considered adequate for hydroclimatic series. On the other hand, the CARMA is more parsimonious than MAR, where, for example, the number of parameters for a MAR(2) model compared to a CARMA(2,0) for n sites is $2n^2+0.5(n^2+n)$ versus $2n+0.5(n^2+n)$ or for 5 sites 65 versus 25, respectively.

27.5.1 Multivariate and Contemporaneous ARMA(p,q)

The full MARMA and the CARMA models for n sites are expressed in the same way as

$$\mathbf{Y}_t = \sum_{i=1}^{p} \Phi_i \mathbf{Y}_{t-i} + \boldsymbol{\varepsilon}_t - \sum_{j=1}^{q} \Theta_j \boldsymbol{\varepsilon}_{t-j} \tag{27.10}$$

where $\mathbf{Y}_t$ is a $n \times 1$ column vector of normally distributed zero mean variables. The AR and moving average parameter matrixes Φ_i and Θ_j, respectively, are full $n \times n$ matrixes for the MARMA model but diagonal for the CARMA model, and $\{\boldsymbol{\varepsilon}_t\} \sim iid$ MVN(0,$\mathbf{G}$) is the $n \times 1$ vector of normally distributed noise terms with mean zero and variance–covariance matrix $\mathbf{G}$. In practice, the MAR(1) = MARMA(1,0), MAR(2), and MARMA(1,1) [16,38,52,54] have been used for modeling of streamflow, with MAR(1) being the most used one. The moment equations of the MAR(p) model are $\mathbf{C}_0 = \mathbf{G} + \sum_{i=1}^{p} \Phi_i \mathbf{C}_i^T$ and $\mathbf{C}_h = \sum_{i=1}^{p} \Phi_i \mathbf{C}_{h-i}, h \geq 1$, with $\mathbf{C}_h$ being the lag-h population cross-covariance matrix of $\mathbf{Y}_t$ defined as $\mathbf{C}_h = E[\mathbf{Y}_t \mathbf{Y}_{t-h}^T]$ for mean subtracted series. Thus, the parameters of the MAR(1) models can be estimated as $\hat{\Phi}_1 = \mathbf{c}_1 \mathbf{c}_0^{-1}$ and $\hat{\mathbf{G}} = \mathbf{c}_0 - \mathbf{c}_1 \mathbf{c}_0^{-1} \mathbf{c}_1^T$, where $\mathbf{c}_h$ is the lag-h sample cross-covariance matrix. Since the CARMA models have diagonal parameter matrixes, the multivariate CARMA model can be decoupled into univariate ARMA models, and the parameters are estimated independently for each single site by regular univariate ARMA model estimation procedures. This allows for identification of the best univariate ARMA model for each site. After having estimated the diagonal parameter matrixes, what remains is estimation of the noise variance–covariance matrix $\mathbf{G}$, but the lag-0 cross-correlation coefficients of $\mathbf{Y}_t$ are preserved through $\mathbf{G}$. The procedure requires that the CARMA(p,q) is causal, a common requirement in estimation procedures of ARMA models. Causality implies that $\mathbf{Y}_t$ in (27.10) can be presented by an infinite moving average model [4] $\mathbf{Y}_t = \sum_{j=0}^{\infty} \Psi_j \boldsymbol{\varepsilon}_{t-j}$ with the lag-0 cross-covariance matrix given by $\mathbf{C}_0 = \sum_{j=0}^{\infty} \Psi_j \mathbf{G} \Psi_j^T$, where Ψ_j are matrixes with absolutely summable elements given by $\Psi_0 = \mathbf{I}$ and $\Psi_j = -\Theta_j + \sum_{i=1}^{p} \Phi_i \Psi_{j-i}^T$. Since Ψ_j are diagonal, the ith row and jth column element of the noise variance–covariance matrix $\mathbf{G}$ is estimated from $\hat{G}^{ij} = c_0^{ij} / \sum_{k=0}^{\infty} \psi_k^{ii} \psi_k^{jj}$, where c_0^{ij} is the ith row and jth column element of the lag-0 sample cross-covariance matrix and ψ_k^{ii} is the ith row and ith column diagonal element of Ψ_k.

27.5.2 Multivariate and Contemporaneous PARMA(p,q)

The full periodic multivariate PARMA (MARMA) and the periodic contemporaneous PARMA (CPARMA) models for n sites are expressed in the same way as

$$\mathbf{Y}_{\nu,\tau} = \sum_{i=1}^{p} \Phi_{i,\tau}\mathbf{Y}_{\nu,\tau-i} + \boldsymbol{\varepsilon}_{\nu,\tau} - \sum_{j=1}^{q} \Theta_{j,\tau}\boldsymbol{\varepsilon}_{\nu,\tau-j} \tag{27.11}$$

where $\mathbf{Y}_{\nu,\tau}$ is a $n \times 1$ column vector of normally distributed zero mean variables representing the process for year ν and season τ. The $\Phi_{1,\tau}, \Phi_{2,\tau}, \ldots, \Phi_{p,\tau}$ and $\Theta_{1,\tau}, \Theta_{2,\tau}, \ldots, \Theta_{q,\tau}$ are the AR and moving average parameter matrixes, full $n \times n$ matrixes for the MPARMA model but diagonal for the CARMA. The $\{\boldsymbol{\varepsilon}_{\nu,\tau}\} \sim iid\ \text{MVN}(0, \mathbf{G}_\tau)$ is the $n \times 1$ vector of normally distributed noise terms with mean zero and periodic $n \times n$ variance–covariance matrix $\mathbf{G}_\tau$. The moment equations for the MPAR(p) model are given by $\mathbf{C}_{0,\tau} = \mathbf{G}_\tau + \sum_{i=1}^{p} \Phi_{i,\tau}\mathbf{C}_{i,\tau}^T$ and $\mathbf{C}_{h,\tau} = \sum_{i=1}^{p} \Phi_{i,\tau}\mathbf{C}_{h-i,\tau-i}$ for $h \geq 1$, where $\mathbf{C}_{h,\tau}$ is the lag-h cross-covariance matrix defined as $\mathbf{C}_{h,\tau} = E[\mathbf{Y}_{\nu,\tau}\mathbf{Y}_{\nu,\tau-h}^T] = \{E[\mathbf{Y}_{\nu,\tau-h}\mathbf{Y}_{\nu,\tau}^T]\}^T = \mathbf{C}_{-h,\tau-h}^T$. The parameter estimation follows in a similar way as for the MAR and CARMA with, for example, the parameters of the MPAR(1) model given by $\hat{\Phi}_{1,\tau} = \mathbf{c}_{1,\tau}\mathbf{c}_{0,\tau-1}^{-1}$ and $\hat{\mathbf{G}}_\tau = \mathbf{c}_{0,\tau} - \mathbf{c}_{1,\tau}\mathbf{c}_{0,\tau-1}^{-1}\mathbf{c}_{1,\tau}^T$, where $\mathbf{c}_{h,\tau}$ is the sample season-to-season lag-h cross-covariance matrix.

27.6 Disaggregation Models

Disaggregation models in space and time (downscaling) are an important tool for modeling of complex hydroclimatic processes, whether it is downscaling of precipitation to fine time scales or disaggregating flows and precipitation in a complex stream network both in space and time [2,16,51,54]. Disaggregation model is able to reproduce statistics at different aggregation levels such as annual and seasonal. Valencia and Schaake (VS) [73] with a later extension by Mejia and Rousselle (MR) [30,41] introduced the basic disaggregation model for temporal disaggregation of annual flows into seasonal flow, although both models can also be used for spatial disaggregation. The VS and MR models have full parameter matrixes and require many parameters for temporal disaggregation; thus, alternatively condensed (Lane) [31] and contemporaneous (Spigot) [14,15] models with periodic parameters for temporal disaggregation were suggested reducing the number of parameters required drastically. For comparison, the numbers of parameters in disaggregation of annual flows to monthly (12 seasons) for one site in the VS, MR, Lane, and Spigot models are 156, 168, 36, and 48, respectively. In practice for hydroclimatic data, the VS and MR models are generally used for disaggregation in space and the MR, Lane, or Spigot for temporal disaggregation. Stagewise disaggregation [58] in time has been suggested to reduce the number of parameters in each disaggregation step, for example, going from annual values to sum of four months to monthly to finer scales. The number of parameters in the aforementioned models going from annual to sum of four months (three seasons) is 12, 15, 9, and 12, respectively, thus reducing the differences in number of parameters for different models.

The VS and MR models for spatial disaggregation of annual data from n key sites to m subsites are represented by

$$\mathbf{Y}_\nu = \mathbf{A}\mathbf{X}_\nu + \mathbf{B}\boldsymbol{\varepsilon}_\nu \quad \text{and} \quad \mathbf{Y}_\nu = \mathbf{A}\mathbf{X}_\nu + \mathbf{B}\boldsymbol{\varepsilon}_\nu + \mathbf{C}\mathbf{Y}_{\nu-1} \tag{27.12}$$

respectively, where

- $\mathbf{X}_\nu$ is the $n \times 1$ column vector of annual flows at the key sites modeled by an ARMA, CARMA, or MAR model
- $\mathbf{Y}_\nu$ is the corresponding $m \times 1$ column vector at the subsites
- $\boldsymbol{\varepsilon}_\nu$ is the $m \times 1$ column noise vector uncorrelated in space
- $\mathbf{A}$, $\mathbf{B}$, and $\mathbf{C}$ are full $m \times n$, $m \times m$, and $m \times m$ parameter matrixes, respectively

After applying the models once, they can be applied repeatedly using the subsites as key sites for further spatial disaggregation to new subsites as is common when modeling of complex streamflow networks.

Both models preserve the lag-0 correlation coefficient in space between all subsites through the matrix **B** and the lag-0 correlation in space between all subsites and key sites through the matrix **A**. The MR model additionally preserves the lag-1 correlation coefficient in space between all subsites through the matrix **C**, but hydroclimatic data usually show such type of persistence. The parameters are estimated by method of moments. For example, the parameters of the VS model are given by $\mathbf{A} = \mathbf{C}_0(\mathbf{YX})\mathbf{C}_0^{-1}(\mathbf{X})$ $\mathbf{BB}^T = \mathbf{C}_0(\mathbf{Y}) - \mathbf{AC}_0(\mathbf{X})\mathbf{A}^{-1}$ where $\mathbf{G} = \mathbf{BB}^T$ is the noise variance–covariance matrix (**B** is the Cholesky decomposition of **G**) and $\mathbf{C}_h(\mathbf{Y}) = E[\mathbf{Y}_\nu \mathbf{Y}_{\nu-h}^T]$ and $\mathbf{C}_h(\mathbf{YX}) = E[\mathbf{Y}_\nu \mathbf{X}_{\nu-h}^T]$. The previous models can also be presented in different form, for example, the MR model for spatial disaggregation of seasonal data is represented as $\mathbf{Y}_{\nu,\tau} = \mathbf{A}_\tau \mathbf{X}_{\nu,\tau} + \mathbf{B}_\tau \boldsymbol{\varepsilon}_{\nu,\tau} + \mathbf{C}_\tau \mathbf{Y}_{\nu,\tau-1}$, one model for each season τ, and the same model for temporal disaggregation of annual data to seasonal data at same sites is represented as $\mathbf{Y}_{\nu,\tau} = \mathbf{AY}_\nu + \mathbf{B}\boldsymbol{\varepsilon}_{\nu,\tau} + \mathbf{CY}_{\nu,\tau-1}$ with $\mathbf{Y}_{\nu,\tau}$ being a $n\omega \times 1$ column vector with the first ω-values being the seasonal values for site 1 and the last ω-values being the seasonal values for site n. This model does preserve additivity of the disaggregated level in the normal domain. The model can be repeatedly applied in a stagewise manner down to finer time scales. The aforementioned Lane and Spigot temporal disaggregation models are represented in a similar way as the temporal MR model except that the parameter matrixes are periodic as mentioned previously. The Lane model requires adjustments of seasonal values to ensure additivity up to the aggregated level, while the Spigot model includes a transformation-dependent term ensuring approximate additivity of the model in the original domain.

When using disaggregation models for data generation for data requiring normalizing transformation or when various elements of the parameter matrixes are taken as zero for simplification, then summability may be lost and adjustments may be needed to ensure additivity constraints in the original domain, for instance, in spatial disaggregation, to ensure that the generated flows at subsites add to the total or a fraction of the corresponding generated flow at a key site or in temporal disaggregation, to ensure that the generated seasonal values add exactly to the generated annual value [14,66].

27.7 Nonparametric Models

Nonparametric models are an attractive alternative to parametric models. They do not require the data to be transformed to normal, and they can capture features, such as bimodality and nonlinear dependence structure that is difficult to capture with traditional parametric models [28]. The simplest nonparametric models are pure resampling or bootstrapping models such as the simple bootstrap based on resampling with replacement the historical time series. To account for autocorrelation, block bootstrapping can be used [75]. Nonparametric simulation models based on conditional KDE have been used for monthly streamflow modeling $f_{Y_{\nu,\tau}|Y_{\nu,\tau-1}}(y_{\nu,\tau}|y_{\nu,\tau-1})$ and disaggregation of annual to monthly flows $f_{\mathbf{Y}_{\nu,\tau}|Y_\nu}(y_{\nu,\tau}|y_\nu)$ [60,70]. The *k* nearest neighbor (KNN) resampling models have been used for resampling of monthly streamflows, disaggregation of annual to monthly flows, and simulation of rainfall and other climatic variables [29,32,45–48,55,79].

27.7.1 KDE

Kernel density estimates are closely related to smoothed histograms. A kernel density estimate for a time series y_t of length *N* is defined as

$$\hat{f}(y) = \frac{1}{N}\sum_{i=1}^{N} K_h(y - y_i) = \frac{1}{Nh}\sum_{i=1}^{N} K\left(\frac{y - y_i}{h}\right) \tag{27.13}$$

where

h is the bandwidth or smoothing parameter
K is the kernel function [45,47]

Multivariate kernel densities are obtained by replacing the scalars in (27.13) by vectors and the Mahalanobis distance is used as opposed to Euclidean distance in (27.13) to account for cross-covariances between the variables. Typical kernel functions are uniform, normal, biweight, Epanechnikov, and others. The choice of the kernel function has been viewed as secondary in estimating the density, and the normal kernel of the standard normal distribution is commonly used $K(x) = 1/\text{sqrt}(2\pi)\ \exp(-0.5x^2)$, although it has also been suggested for hydrologic data to log-transform the data prior to the density estimation [49,50] or use skewed gamma kernels [55]. The asymptotic equivalent smoothing factors assuming that the underlying distribution is normal are for the normal kernel [62] $h \approx 1.06 s_y N^{-1/5}$ where s_y is the sample standard deviation as in (27.1).

27.7.2 KNN

The KNN procedures with stationary time series are similar to the KDE procedure except KNN-estimated densities are used as opposed to KDE estimates. The simple KNN density is equivalent to using KDE with a uniform kernel and a location-dependent radius

$$\hat{f}(\mathbf{y}) = \frac{k}{N v_k(\mathbf{y})} \tag{27.14}$$

where $v_k(\mathbf{y})$ is the volume of the ellipsoid bounded by $\mathbf{y}$ to its kth nearest neighbors, with the distance to the kth nearest neighbor being measured by the Mahalanobis distance in the multivariate case and the Euclidean distance in the univariate one. It has been suggested using $k = \sqrt{N}$ [29]. Similarly as in (27.13), a kernel function can also be used representing any probability density function [62].

27.8 Simulation

27.8.1 Approach

Time series models are used to generate equally likely synthetic time series (simulation). Exact generation procedures are available for some simpler models, while for more complex correlated models depending on past observations and residuals, initial assumption can affect the generation process, with, for example, the first generated value always being close to the mean of the process or the first values of a generated time series being correlated with the first values of the other generated time series. A simple way to remove the effects of initial assumptions is to use a short warm-up period of say length L, for example, arbitrarily chosen as 50, but a long-memory process needs longer warm-up period than a short-memory process. For example, for ARMA models, values of Y_t prior to $t = 1$ are assumed to be equal to the mean of the process (which is zero in our presentation). Thus, $Y_1, Y_2, \ldots, Y_{N+L}$ are generated using Equation 27.8 where N is the required length to be generated and L is the warm-up length required to remove the effect of the initial assumptions of Y_t. Simulations can also start from some point or from the end of the historical records, where historical observations are used to initialize the models and no warm-up period is used. In this case, all generated synthetic time series are generated in forecasting mode, where all generators are initialized with the past values of the historical data and all noise processes are initialized to zero.

27.8.2 Random Noise Generation

Random generators of standard normal variables $\{z_t\} \sim iid\ N(0,1)$ are available in most software packages. The white noise process in univariate models $\{\varepsilon_t\} \sim iid\ N\left(0, \sigma^2(\varepsilon)\right)$ is generated by first generating a standard uncorrelated normal random variable z_t and then estimating ε_t as $\varepsilon_t = \hat{\sigma}(\varepsilon) z_t$. Similarly for n-dimensional multivariate models, $\{\boldsymbol{\varepsilon}_t\} \sim iid\ \text{MVN}(0, \mathbf{G})$ is the $n \times 1$ vector of normally distributed noise terms with mean zero and variance–covariance matrix $\mathbf{G}$. The noise vector is independent in time and

correlated in space at lag-0. The following notation is commonly used to simplify the generation process $\boldsymbol{\varepsilon}_t = \mathbf{B}\mathbf{z}_t$ where $\{\mathbf{z}_t\} \sim iid\ \text{MVN}(0,\mathbf{I})$ is a $n \times 1$ vector of independent standard normally distributed variables uncorrelated in both time and space. The $n \times n$ matrix $\mathbf{B}$ is a lower triangular matrix such that $\mathbf{G} = \mathbf{B}\mathbf{B}^T$, where $\mathbf{B}$ is the Cholesky decomposition of $\mathbf{G}$.

27.8.3 Length and Number

How long should the simulated series be? For comparison of model statistics and historical statistics, the length of the simulated series should be the same as the length of the historical record. For operational and planning studies, the length of the simulated series should match the planning horizon. For determination of extreme floods or drought of a certain return period T, the length of the simulated series must coincide with T. Similarly for estimation of a return period of a specific event, the simulations must be carried out until the event is exceeded for floods or deceeded for droughts. For determination of a firm energy capacity of a power system for a predefined reliability close to one, the length of the simulated series needs to correspond to that reliability in a similar way as for return periods. The number of generated series should make it possible to estimate the probability distribution or the uncertainty of the decision parameter. As a rule of thumb, 1000 or more generated series or instances of the decision variable should be adequate, exceeding most statistical criteria used [51]. For estimation of a probability that certain event occurs in the generated time series, much higher number of series may be needed if the event is only occurring in a small fraction of the generated of series.

27.9 Forecasting

Starting simulations from the end of the historical data conditioned on the most recent historical observations can be used for both short-term and long-term forecasting, where all simulated time series can be regarded as equally likely to happen from that point on (refer to Section 27.8).

27.9.1 Method

Forecasting method is said to be "adaptive" if model parameters are updated as soon as new data are available, that is, one-step-ahead forecast for $t+1$ always uses model parameters estimated using data up to time t. The method is "nonadaptive" if model parameters are updated after a block of new data are available, that is, model parameters estimated using data up to time t are used to compute forecasts up to time $t+k$ at which time the model parameters are reestimated.

27.9.2 Performance

The forecast error at time t is denoted by $\hat{e}_t = y_t - \hat{y}_t$ where y_t is the observation at time t and $\hat{y}_t$ is the forecast at time t. To measure performance of different model alternatives for a common forecasting period of length m, the following mean-absolute-forecast error (MAFE) and root-mean-square-forecast error (RMSFE) can be used:

$$\text{MAFE} = \frac{1}{m}\sum_{i=1}^{m}\text{abs}(e_i) \quad \text{and} \quad \text{RMSFE} = \sqrt{\frac{1}{m}\sum_{i=1}^{m}e_i^2} \tag{27.15}$$

27.9.3 Models

All the time series models presented in this chapter can be used for forecasting. In practice, models including exogenous information usually perform better than models based only on past observation of

the process being forecasted. For example, for forecasting of streamflow, the exogenous variable may be basin precipitation, a climate index such as ENSO or the PDO, or other measures of atmospheric circulation influencing the local climate [65]. The transfer function noise (TFN) model [3,4] and the simpler special cases of TFN, the ARMAX and PARMAX models, with X denoting the exogenous variables are commonly used for forecasting. For example, ARMAX(p,q,r) model with one exogenous variable is denoted by

$$Y_t = \sum_{i=1}^{p} \varphi_i Y_{t-i} + \varepsilon_t - \sum_{j=1}^{q} \theta_j \varepsilon_{t-j} + \sum_{i=1}^{r} \alpha_i X_{t-i-k} \tag{27.16}$$

with X being the exogenous variable leading the dependent variable by lag-k. It is not uncommon to have $p=0$ and $q=0$ and thus the only input being the exogenous variable especially when Y_t is weekly correlated. When analyzing the relationship between X_t and Y_t using cross-correlation, then the autocorrelation should be removed from both series (pre-whitening) with appropriate ARMA models, and the resulting residuals from both models should be cross-correlated at different lags. If there are many exogenous variables available, many alternative models could be fitted and the resulting forecasts combined by averaging or weighting [64]. In these circumstances, principal components [76,78] on the exogenous variables could be used to reduce the parameter space. Exact forecast procedures exist for models such as linear regression models and low-order ARMA, where the predictive distribution of the forecast is defined [4,25]. For complex models repeated, one-step-ahead prediction can be used for estimation of the prediction interval. In addition, if non-normality of the residuals is of concern, bootstrapping of the residuals with replacement and reestimating the model parameters can be used as an alternative for estimation of the prediction interval [64]. Other forecasting models exist for forecasting of hydroclimatic processes with many of the approaches and their application, including the previous ones, being described in [16,72].

27.10 Climate Change Implications

The modern climate change is dominated by human influences [26], and to date, there does not appear to be any study attributing the global warming observed over the last 50 years to any known natural causes [77]. Newer analyses of proxy data for the northern hemisphere indicate that the increase in temperature in the twentieth century is likely to have been the largest of any century during the past 1000 years and that 11 of the 12 years during 1995–2006 rank among the 12 warmest years of the instrumental record of global surface temperature since 1850 [21,22]. The historical trend in the global instrumental record from 1906 to 2005 is 0.74°C/century, and from 1956 to 2005 the trend is 1.3°C/century with projected temperature trends ranging from 1.8°C to 4.0°C/century over the next 100 years depending on different emission scenarios of greenhouse gases [22].

Changing climate due to anthropogenic impacts leads to changing distributional properties of the process under consideration calling for sophisticated risk analyses of possible climate change in both near and far future, where different methods must be explored for different situations and tasks. The methods for time series analysis presented in this chapter can be used for modeling changing distributional properties over time, where historical deterministic anthropogenic changes are removed from the process to make it stationary prior to fitting the appropriate stationary model to the process. Synthetic time series can be generated from the fitted model and corrected into original domain by reapplying the historical or projected anthropogenic changes. Common changes in distributional properties include the following [23]:

- The distribution shifts or slides over time. This is equivalent to time-varying trend in the mean μ_t. The process is made stationary by subtracting μ_t.

- Increased or decreased variability with time. This is equivalent to having time-varying trend in the standard deviation σ_t. The process is scaled by σ_t to make it stationary. Alternative the process is standardized by μ_t and σ_t to make it stationary in both the mean and the variance.
- The shape of the distribution is asymmetrically changed with time. This is more complex and calls for a time-varying transformation of the process to normal.

Synthetically simulated series may need to be adjusted for different planning horizons into the future, for example, one year for operations, 10 or 20 years for investment planning, and 100 years or more when safety issues are considered. For estimation of a design event based on appropriate level for risk of failure, the simulated time series need to be adjusted over the expected lifetime of the project.

27.11 Parameter Uncertainty

The foregoing discussion has not dealt with parameter uncertainty. In practice, when modeling complex hydroclimatic systems, model parameters are often treated as being deterministic and the only random components are the model noises or residuals. In a sense when multiple time series are synthetically generated from a parametric model for analysis of the distribution of certain design statistics, it can be argued that parameter uncertainty is being somewhat implicitly embedded in the generation process, since for each synthetic series, the parameters could be reestimated and they certainly would be different than the original parameter set. This type of uncertainty analysis is, for example, common in frequency analysis of extreme events, where the uncertainty distribution of a design quantile is estimated by regenerating (from the initially estimated model) time series of the same length as the historical sample. Then for each time series, the model parameters are reestimated resulting in a new estimate of the design quantile. The classic time series texts [3,4,16,54] include sample distributions of the parameters of the ARMA and PARMA models. Also, since the parametric modeling schemes are usually linear in the parameters and most of them assume that the data are normally distributed, then in theory inclusion of parameter, uncertainty can be achieved by adopting the theory of parameter inferences from the classical univariate and multivariate regression model [25]. In addition, Bayesian modeling [1] offers a framework taking into account the uncertainty in the model parameters.

27.12 Summary and Conclusions

Analysis and modeling of time series of hydrologic data under climate variability and change can be used for evaluation of impacts and risks that can arise from natural variability and anthropogenic climate change in hydrologic time series. Such studies may be used for estimation of design events and generation of long synthetic time series used for adaptation strategies to the natural climate variability and expected future climatic change. While time series models are in general stationary, they can be used to model nonstationary behavior such as trends and shifts. Time series models have been used traditionally for generation of long synthetic time series, for evaluation of operational rules for water resources systems and for sizing of reservoirs, for forecasting, for detection of trends and shifts, and for filling in missing data and extending records. An important feature of time series models is their ability to model the dependence structure within a single time series of sequential observations (autocorrelation) and across multiple time series both in space and time (cross-correlation) and across time scales such as years to seasons to months to finer scales. This feature separates time series models from traditional probabilistic models, which commonly assume that the time series being modeled is independent and identically distributed that is usually not the case since most hydrologic time series show different types of dependence structure due to the annual hydrologic cycle and persistence and cycles in atmospheric circulation patterns.

References

1. Bernardo, J.M. and Smith, M.F.A. 1994. *Bayesian Theory*. Chichester, UK: Wiley.
2. Bras, R.L. and Rodriguez-Iturbe, I. 1985. *Random Functions and Hydrology*. Menlo Park, CA: Addison-Wesley.
3. Box, G.E.P., Jenkins, G.M., and Reinsel, G.C. 1994. *Time Series Analysis: Forecasting and Control*, 3rd edn. Upper Saddle River, NJ: Prentice Hall.
4. Brockwell, P.J. and Davis, R.A. 2002. *Introduction to Time Series and Forecasting*, 2nd edn. Springer Texts in Statistics. New York: Springer-Verlag.
5. Brockwell, P.J. and Davis, R.A. 1991. *Time Series: Theory and Methods*. New York: Springer Verlag.
6. Chang, T.J., Kavvas, M.L., and Delleur, J.W. 1984. Daily precipitation modeling by discrete autoregressive moving average processes. *Water Resources Research*, 20(5):565–580.
7. Chebaane, M., Salas, J.D., and Boes, D.C. 1995. Product periodic autoregressive processes for modeling intermittent monthly streamflows. *Water Resources Research*, 31(6):1513–1518.
8. Efron, B. and Tibshirani, R.J. 1993. *An Introduction to the Bootstrap*. New York: Chapman & Hall.
9. Fagherazzi, L., Guay, R., Sparks, D., Salas, J., and Sveinsson, O.G.B. 2005. Stochastic modeling and simulation of the Great Lakes—St. Lawrence River System. Report prepared for the Lakes Ontario–St. Lawrence River Study of the International Joint Commission, Ottawa, Ontario, Canada and Washington, DC.
10. Fernandez, B. and Salas, J.D. 1986. Periodic gamma autoregressive processes for operational hydrology. *Water Resources Research*, 22(10):1385–1396.
11. Fernandez, B. and Salas, J.D. 1990. Gamma-autoregressive models for streamflow simulation. *Journal of Hydrologic Engineering* (*ASCE*), 116(11):1403–1414.
12. Filliben, J.J. 1975. The probability plot correlation coefficient test for normality. *Technometrics*, 17(1):111–117.
13. Fortin, V., Perreault, L., and Salas, J.D. 2004. Retrospective analysis and forecasting of streamflows using a shifting level model. *Journal of Hydrology*, 296(1–4):135–163.
14. Grygier, J.C. and Stedinger, J.R. 1988. Condensed disaggregation procedures and conservation corrections for stochastic hydrology. *Water Resources Research*, 24(10):1574–1584.
15. Grygier, J.C. and Stedinger, J.R. 1990. SPIGOT: A synthetic streamflow generation software package, technical description, version 2.5, School of Civil and Environmental Engineering, Cornell University, Ithaca, NY.
16. Hipel, K. and McLeod, A.I. 1994. *Time Series Modeling of Water Resources and Environmental Systems*. Amsterdam, the Netherlands: Elsevier.
17. Hirsch, R.M., Helsel, D.R., Cohn, T.A., and Gilroy, E.J. 1993. Statistical analysis of hydrologic data. In: *Handbook of Hydrology* D.R. Maidment, ed., Chapter 17, 17.11–17.37. New York: McGraw-Hill.
18. Hosking, J.R.M. 1981. Fractional differencing. *Biometrika*, 68:165–176.
19. Hurvich, C.M. and Tsai, C.L. 1989. Regression and time series model selection in small samples. *Biometrika*, 76(2):297–307.
20. Hurvich, C.M. and Tsai, C.-L. 1993. A corrected Akaike information criterion for vector autoregressive model selection. *Journal of Time Series Analysis*, 14:271–279.
21. IPCC. 2001. Climate change 2001: The scientific basis. Contribution of Working Group I to the Third Scientific Assessment Report of the Intergovernmental Panel on Climate Change, Cambridge University Press, Cambridge, U.K., 944pp.
22. IPCC. 2007. Climate change 2007: Synthesis report. Contribution of Working Groups I, II and III to the Fourth Assessment Report of the Intergovernmental Panel on Climate Change. Core Writing Team, Pachauri, R.K. and Reisinger, A., eds. IPCC, Geneva, Switzerland, 104pp.

23. IPCC. 2012. Managing the risks of extreme events and disasters to advance climate change adaptation, Field, C.B., Barros, V., Stocker, T.F., Qin, D., Dokken, D., Ebi, K.L., Mastrandrea, M.D., Mach, K.J., Plattner, G.-K., Allen, S.K., Tignor, M., and Midgley, P.M. eds. Cambridge University Press, Cambridge, U.K., 582pp.
24. Jenkins, G.M. and Watts, D.G. 1968. *Spectral Analysis and Its Applications*, 1st edn. New York: Holden-Day.
25. Johnson, R.A. and Wichern, D.W. 2002. *Applied Multivariate Statistical Analysis*, 5th edn. New York: Prentice-Hall.
26. Karl, T.R. and Trenberth, K.E. 2003. Modern global climate change. *Science*, 302:1719–1723.
27. Koutsoyiannis, D. 2002. The Hurst phenomenon and fractional Gaussian noise made easy. *Hydrological Sciences-Journal-des Sciences Hydrologiques*, 47(4):573–595.
28. Lall, U. 1995. Recent advances in nonparametric function estimation: Hydraulic applications. U.S. National Report to International Union of Geodesy and Geophysics 1991–1994. *Reviews of Geophysics*, 33:1093–1102.
29. Lall, U. and Sharma, A. 1996. A nearest neighbor bootstrap for resampling hydrologic time series. *Water Resources Research*, 32(3):679–693.
30. Lane, W.L. 1981. Corrected parameter estimates for disaggregation schemes. *International Symposium on Rainfall Runoff Modeling*, Mississippi State University, Starkville, MS.
31. Lane, W.L. 1979. Applied stochastic techniques (last computer package), User Manual, Division of Planning Technical Services, U.S. Bureau of Reclamation, Denver, CO.
32. Lee, T. and Ouarda, T.B.M.J. 2011. Identification of model order and number of neighbors for *k*-nearest neighbor resampling. *Journal of Hydrology* (Elsevier), 404:136–145.
33. Loucks, D.P., Stedinger, J.R., and Haith, D.A. 1981. *Water Resources Systems Planning and Analysis*. Englewood Cliffs, NJ: Prentice-Hall.
34. Makridakis, S., Andersen, A., and Carbone, R. 1982. The accuracy of extrapolative (time series methods): Results of a forecasting competition. *Journal of Forecasting*, 1(2):111–153.
35. Makridakis, S. and Hibon, M. 1979. Accuracy of forecasting: An empirical investigation (with discussion). *Journal of the Royal Statistical Society*, *Series A*, 142(Part 2):79–145.
36. Makridakis, S., Wheelwright, S., and McGee, V. 1983. *Forecasting Methods and Applications*, 2nd edn. New York: Wiley & Sons.
37. Mandelbrot, B.B. and Wallis, J.R. 1969. Computer experiments with fractional Gaussian noises. Part 1: Averages and variances. *Water Resources Research*, 5(1):228–241.
38. Matalas, N.C. 1967. Mathematical assessment of synthetic hydrology. *Water Resources Research*, 3(4):937–945.
39. McKercher, A.I. and Delleur, J.W. 1974. Application of seasonal parametric linear stochastic models to monthly flow data. *Water Resources Research*, 10:246–255.
40. Mejia, J.M., Rodriguez-Iturbe, I., and Dawdy, D.R. 1972. Streamflow simulation: 2. The broken line process as a potential model for hydrologic simulation. *Water Resources Research*, 8(4):931–941.
41. Mejia, J.M. and Rousselle, J. 1976. Disaggregation models in hydrology revisited. *Water Resources Research*, 12(3):185–186.
42. Montanari, A., Rosso, R., and Taqqu, M.S. 1997. Fractionally differenced ARIMA models applied to hydrologic time series: Identification, estimation and simulation. *Water Resources Research*, 33(5):1035–1044.
43. Montanari, A., Rosso, R., and Taqqu, M.S. 2000. A seasonal fractional ARIMA model applied to the Nile River monthly flows at Aswan. *Water Resources Research*, 36:1249–1259.
44. Percival, D.B. and Walden, A.T. 1993. *Spectral Analysis for Physical Applications: Multitaper and Conventional Univariate Techniques*. Cambridge, U.K.: Cambridge University Press.
45. Prairie, J., Nowak, K., Rajagopalan, B., Lall, U., and Fulp, T. 2008. A stochastic nonparametric approach for streamflow generation combining observational and paleoreconstructed data. *Water Resources Research*, 44(6):W06423, doi: 10.1029/2007WR006684.

46. Prairie, J.R., Rajagopalan, B., Fulp, T.J., and Zagona, E.A. 2006. Modified K-NN model for stochastic streamflow simulation. *Journal of Hydrologic Engineering*, 11(4):371–378.
47. Prairie, J., Rajagopalan, B., Lall, U., and Fulp, T. 2007. A stochastic nonparametric technique for space-time disaggregation of streamflows. *Water Resources Research,* 43(3):W03432, doi:10.1029/2005WR004721.
48. Rajagopalan, B. and Lall, U. 1999. A k-nearest-neighbor simulator for daily precipitation and other weather variables. *Water Resources Research*, 35(10):3089–3101.
49. Rajagopalan, B., Lall, U., and Tarboton, D.G. 1997. Evaluation of Kernel density estimation methods for daily precipitation resampling. *Journal of Stochastic Hydrology and Hydraulics*, 11(6):523–547.
50. Rajagopalan, B., Salas, J.D., and Lall, U. 2010. Stochastic methods for modeling precipitation and streamflow, Chapter 2, p. 17–52. In: *Advances in Data-Based Approaches for Hydrologic Modeling and Forecasting*. B. Sivakumar and R. Berndtsson, eds. Singapore: World Scientific.
51. Salas, J.D. 1993. Analysis and modeling of hydrologic time series. In: *Handbook of Hydrology*, Chapter 19. D.R. Maidment, ed. New York: McGraw-Hill, Inc.
52. Salas, J.D., Boes, D.C., Pegram, G.G.S., and Yevjevich, V. 1979. The hurst phenomenon as a preasymptotic behavior. *Journal of Hydrology*, 44:1–15.
53. Salas, J.D., Boes, D.C., and Smith, R.A. 1982. Estimation of ARMA models with seasonal parameters. *Water Resources Research*, 18(4):1006–1010.
54. Salas, J.D., Delleur, J.W., Yevjevich, V., and Lane, W.L. 1980. *Applied Modeling of Hydrologic Time Series*. Littleton, CO: Water Resources Publications.
55. Salas, J.D. and Lee, T. 2010. Non-parametric simulation of single site seasonal streamflows. *Journal of Hydrologic Engineering*, 15(4):284–296.
56. Salas, J.D. and Smith, R.A. 1981. Physical bases of stochastic models of annual flows. *Water Resources Research*, 17:428–430.
57. Salas, J.D., Sveinsson, Ó.G.B., Lane, W.L., and Frevert, D.K. 2006. Stochastic streamflow simulation using SAMS-2003. *Journal of Irrigation and Drainage Engineering*, 132(2):112–122.
58. Santos, E.G. and Salas, J.D. 1992. Stepwise disaggregation scheme for synthetic hydrology. *Journal of Hydraulic Engineering* (*ASCE*), 118(5):765–784.
59. Scott, D.W. 1992. *Multivariate Density Estimation, Theory, Practice, and Visualization*. New York: John Wiley & Sons.
60. Sharma, A., Tarboton, D.G., and Lall, U. 1997. Streamflow simulation: A nonparametric approach. *Water Resources Research*, 33(2):291–308.
61. Shumway, R.H. and Stoffer, D.S. 2000. *Time Series Analysis and Its Applications*, 1st edn. New York: Springer.
62. Silverman, B.W. 1986. *Density Estimation for Statistics and Data Analysis: Monographs on Statistics and Applied Probability*. London, U.K.: Chapman & Hall.
63. Snedecor, G.W. and Cochran, W.G. 1980. *Statistical Methods*, 7th edn. Ames, IA: Iowa State University Press.
64. Sveinsson, Ó.G.B., Lall, U., Fortin, V., Perrault, L., Gaudet, J., Zebiak, S., and Kushnir, Y. 2008. Forecasting spring reservoir inflows in Churchill falls basin in Québec, Canada. *Journal of Hydrologic Engineering* (*ASCE*), 13(6):426–437.
65. Sveinsson, Ó.G.B., Lall, U., Gaudet, J., Zebiak, S., Kushnir, Y., and Fortin, V. 2008. Analysis of climatic states and atmospheric circulation patterns that influence Quebéc spring streamflows. *Journal of Hydrologic Engineering* (*ASCE*), 13(6):411–425.
66. Sveinsson, O.G.B., Lee, T.S., Salas, JD., Lane, W.L., and Frevert, D.K. 2009. Stochastic analysis, modeling and simulation (SAMS): Version 2009—Users manual, Department of Civil and Environmental Engineering, Colorado State University, Fort Collins, CO.
67. Sveinsson, O.G.B. and Salas, J.D. 2006. Multivariate shifting mean plus persistence model for simulating the Great Lakes net basin supplies. *Proceedings of the 25th AGU Hydrology Days*, Colorado State University, Fort Collins, CO, pp. 173–184.

68. Sveinsson, O.G.B., Salas, J.D., and Boes, D.C. 2005. Prediction of extreme events in hydrologic process that exhibit sudden shifting pattern. *Journal of Hydrologic Engineering* (*ASCE*), 10(4):315–325.
69. Sveinsson, O.G.B., Salas, J.D., Boes, D.C., and Pielke Sr., R.A. 2003. Modeling the dynamics of long term variability of hydroclimatic processes. *Journal of Hydrometeorology*, 4:489–505.
70. Tarboton, D.G., Sharma, A., and Lall, U. 1998. Disaggregation procedures for stochastic hydrology based on nonparametric density estimation. *Water Resources Research*, 34(1):107–119.
71. Thyer, M. and Kuczera, G. 2000. Modeling long term persistence in hydro-climatic time series using a hidden state Markov model. *Water Resources Research*, 36(11):3301–3310.
72. Valdés, J.B., Burlando, P., and Salas, J.D. 2002. Stochastic forecasting of precipitation and streamflow processes, Chapter 34. In: *Handbook of Weather, Climate, and Water*, T.D. Potter and B. Colman, eds. New York: John Wiley & Sons, pp. 642–665.
73. Valencia, D. and Schaake, Jr., J.C. 1973. Disaggregation processes in stochastic hydrology. *Water Resources Research*, 9(3):580–585.
74. Vogel, R.M. 1986. The probability plot correlation coefficient test for the normal, log-normal, and Gumbel distributional hypotheses. *Water Resources Research*, 22(4):587–590.
75. Vogel, R.M. and Shallcross, A.L. 1996. The moving blocks bootstrap versus parametric time series models. *Water Resources Research*, 32(6):1875–1882.
76. von Storch, H. and Zwiers, F.W. 1999. *Statistical Analysis in Climate Research*. Cambridge, U.K.: Cambridge University Press.
77. Weaver, A.J. 2003. The science of climate change. *Geoscience Canada*, 30(3):91–109.
78. Wilks, D.S. 1995. *Statistical Methods in the Atmospheric Sciences: An Introduction*, Vol. 59. New York: Academic.
79. Yakowitz, S. and Karlsson, M. 1987. Nearest-neighbor methods with application to rainfall-runoff prediction. In: *Stochastic Hydrology*, J.B. Mcneil and G.J. Humphries, eds. Hingham, MA: Reidel, pp. 149–160.
80. Yevjevich, V. 1972. *Stochastic Processes in Hydrology*. Littleton, CO: Water Resources Publications.

28

Uncertainty of the PMP and PMF

Jose D. Salas
Colorado State University

Germán Gavilán
University of California, Merced

Fernando R. Salas
The University of Texas at Austin

Pierre Y. Julien
Colorado State University

Jazuri Abdullah
Colorado State University

AUTHORS

Jose D. Salas is a professor emeritus of civil and environmental engineering at Colorado State University (CSU). He received BS and civil engineering degrees from the National University of Engineering of Lima, Perú; MSc degree in hydraulics; and PhD degree in hydrology and water resources from CSU. At CSU, he supervised (main advisor) 42 MSc and 37 PhD students. Dr. Salas has been consultant of national and international organizations and worked in several countries sponsored by UNESCO, FAO, AID, IICA, Hydro-Quebec, and the World Bank. Dr. Salas has been member of the editorial board of several international journals and has published extensively in water resources literature including two books and 12 chapters in books and handbooks. He was awarded the 1996 Arid Lands Hydraulic Engineering Award and the 2010 Ven Te Chow Award both by the American Society of Civil Engineers. He is a corresponding member of the Academy of Engineering of Mexico and the Academy of Engineering of Peru.

Germán Gavilán is an assistant dean of engineering at the University of California at Merced (UC Merced) and chief scientist at the Center for Information Technology Research in the Interest of Society (CITRIS). He received a bachelor degree in civil engineering from Universidad Industrial de Santander (UIS) in Colombia, MSc degree in water resources, and PhD degree in environmental engineering from Purdue University. Prior to joining UC Merced, he was professor at the School of Civil Engineering and Environmental Engineering at UIS, where he was also head of the Civil Engineering School for three years

and chair of the water resources graduate program for two years. He has been a consultant in the areas of water resources, hydrology, and environmental engineering for various private and government agencies for over 25 years. He is the author or coauthor of four books in the fields of hydraulics and hydrology.

Fernando R. Salas is a PhD student in environmental and water resources engineering at the University of Texas at Austin where he received his MSE degree in 2010. Through the Center for Research in Water Resources (CRWR) at the University of Texas, Mr. Salas has focused his research on the development of environmental information systems that improve the knowledge and understanding of the water cycle. Since 2010, Mr. Salas has been an active member of the Greater Austin Chapter of Engineers without Borders where he has worked on projects in Panama and Peru. He is currently the founder and co-project lead of the Climate Adaptation in Mountain Basins in the Andean Region (CAMBIAR) program. Before moving to Texas, Mr. Salas received his BS in civil and environmental engineering from Cornell University in 2008.

Pierre Y. Julien is a professor of civil and environmental engineering at CSU. He received BSc degree in civil engineering, MSc degree in hydraulics, and PhD degree in hydraulics from Laval University, Canada. His research interest includes river mechanics, hydraulics, and hydrologic modeling. At CSU, he supported and guided 58 MSc and 33 PhD students. Dr. Julien has been consultant of national and international organizations and worked in several projects in various countries such as India, Malaysia, Peru, Korea, and Canada. He was editor of the *ASCE Journal of Hydraulic Engineering* during 2002–2005 and received several awards including the H. A. Einstein Award from the American Society of Civil Engineers. Dr. Julien has published extensively in water resources literature including two books and 20 lecture manuals and book chapters.

Jazuri Abdullah is a PhD student in civil and environmental engineering at CSU. He received bachelor of engineering degree from the University of Technology, MARA (UiTM), Malaysia and the MSc degree in water resources engineering and management from the University of Stuttgart, Germany. Mr. Abdullah is also a lecturer of the Faculty of Engineering at UiTM and is a member of the Board of Engineers of Malaysia (BEM) and a graduate member of the Institute of Engineers of Malaysia (IEM).

PREFACE

Probable maximum precipitation (PMP) and probable maximum flood (PMF) have been commonly used in engineering practice for designing major hydraulic structures. However, in recent decades, there has been a growing concern regarding the uncertainties involved in estimating such extreme events. In this chapter, the concepts and methods for estimating the PMP and PMF considering their associated uncertainties are examined. After briefly reviewing the underlying concepts and definitions, an overview of the methods for estimating the PMP is presented, which includes hydrometeorological methods, the statistical method by Hershfield, and some other statistical alternatives. Regardless of the methods applied for obtaining the PMP and PMF, a number of studies have shown that their estimates involve many uncertainties. While hydrometeorological methods likely provide the best estimates of PMP, however, in many regions of the world, hydrometeorological data are lacking, and consequently feasibility studies and designs of flood-related projects are being made based solely on Hershfield's statistical method that provides a single value for the PMP. Thus, a method for quantifying the uncertainty of the PMP if Hershfield's method is to be applied has been included in this chapter. Furthermore, the chapter includes sensitivity analysis, Monte Carlo analysis, and some statistical alternatives for PMF estimation and uncertainty.

28.1 Introduction

Probable maximum precipitation (PMP) and the corresponding probable maximum flood (PMF) have commonly been utilized in engineering practice [81], particularly for designing hydraulic structures such as spillways of large dams whose failure may cause losses of life and catastrophic damage to nuclear power plants. In the United States, many federal and state agencies use the PMP and PMF for evaluating the adequacy and safety of major hydraulic structures. Regardless of the method utilized for obtaining the PMP, the practice of designing and evaluating flood-related structures based on such PMP has been criticized among others because of the many uncertainties involved in determining them, the lack of a standard approach for estimating the PMP, and the perception that such estimated PMP (and the ensuing PMF) is an upper bound that may not be exceeded and as such a zero risk. However, an upper bound with zero risk is not realistic because there have been documented cases where the recorded floods have exceeded the estimated PMFs [4,15,45]. Thus, a risk-based design approach has been advocated by some hydrologists. For instance, Dawdy and Lettenmaier [15] suggested as an alternative "to retain the PMF as a reference event and estimate its exceedance probability." And they added "…there will be uncertainties associated with any risk estimates, especially for flood peaks and volumes with exceedance probabilities as low as those for the PMF. Any rational design approach must recognize this uncertainty."

Therefore, in this chapter, the concepts and methods for estimating the PMP and PMF considering their associated uncertainties are examined. The main purpose is to summarize the alternative methods that are available for determining the uncertainties involved in estimating the PMP and PMF. The second section is a brief review of concepts and definitions of the PMP and PMF. The third section gives an overview of the classical methods for estimating the PMP such as hydrometeorological methods, the statistical method by Hershfield, and some other statistical alternatives. The fourth section discusses the uncertainty of the PMP considering hydrometeorological factors, and Section 28.5 presents in some detail a procedure for estimating the uncertainty of the PMP based on Hershfield's method. Section 28.6 describes PMF estimation and uncertainty, which includes sensitivity analysis and Monte Carlo analysis, as well as some statistical alternatives. The chapter ends with a section of concluding remarks.

28.2 Concepts and Definitions of the PMP and PMF

PMP has its origin in what used to be called maximum possible precipitation (MPP) where it was defined as an upper bound maximum value [4], that is, the concept was to find a maximum value of precipitation for a given storm duration over a basin that physically could occur but would not be exceeded. Unfortunately, it has been reported in literature that in some real cases, such MPP values have been exceeded [4]. This observation as a consequence has led to the renaming of "maximum possible precipitation" to "PMP." Thus, the PMP definition that has been widely accepted in literature is: "theoretically the greatest depth of precipitation for a given storm duration that is physically possible over a given size storm area at a particular geographical location at a certain time of the year" [31,83]. The PMP definition used by the World Meteorological Organization (WMO) [84] has been slightly changed, but the essence remains the same. The referred definition highlights the PMP as a physical upper limit, and often it is perceived to be a quantity that cannot be exceeded. However, WMO [84] acknowledges the fact that the value of the PMP that is calculated for a particular study area is only an approximation "due to the physical complexity of the phenomena and limitations in data and the meteorological and hydrological sciences." Furthermore, as hinted by WMO [83], one must distinguish between the "theoretical PMP," that is, an upper limit that is unknown, and the "operational PMP," which is the PMP obtained by a given method that involves a number of assumptions, steps, and data that are uncertain.

The PMF is a deterministic upper limit flood that is commonly utilized as a design criterion by several organizations in many countries. However, the PMF is not so generally defined as the PMP. Newton [55] cites various definitions used by different US and international agencies. The PMF definition used

by some organizations such as the US Bureau of Reclamation (USBR) is "the maximum runoff condition resulting from the most severe combination of hydrologic and meteorological conditions that are considered reasonably possible for the drainage basin under study" [14]. Other similar definitions of PMF are: "a flood that can be expected from the most severe combination of critical meteorologic and hydrologic conditions that are reasonably possible in a region" [34] and "PMF is the theoretical maximum flood that poses extremely serious threat to the flood control of a given project in a design watershed. Such a flood could plausibly occur in a locality at a particular time of the year under current meteorological conditions" [84]. The PMF is generally viewed as the flood resulting from a PMP, plus snowmelt where appropriate, applied to assumed antecedent basin conditions. However, the assumptions and procedures for selecting antecedent conditions and estimating the flood hydrograph from the PMP vary depending on the country, agency, and hydrologist. For example, there are some aspects of the PMP to PMF conversion that are unique to the USBR [73].

28.3 Overview of Methods for Estimating the PMP

The manual of WMO [84] describes six methods for estimating the PMP: (a) the local method (local storm maximization model), (b) the transposition method (storm transposition model), (c) the combination method (temporal and spatial maximization of storm), (d) the inferential method (theoretical model), (e) the generalized method, and (f) the statistical method. In addition, the manual describes two other methods that may be applicable for very large basins. The previous methods, categorized as hydrometerological (a–e) are generally based on deterministic approaches, that is, based on physical laws and principles, while method (f) is essentially the statistical method proposed by Hershfield [35,36]. The previous methods, categorized as hydrometeorological methods, the statistical method by Hershfield, and some statistical alternatives (that have been proposed in the last three decades), are summarized in the following section.

28.3.1 PMP Based on Hydrometeorological Methods

There are several key references in literature outlining in some detail the various hydrometeorological methods available for estimating the PMP [31,32,84]. Modifications and improvements have evolved over the years. Hansen [32] summarized the developments through the mid-1980s for the various regions of the United States and discussed advances in estimating the PMP for regions where the convergence (nonorographic) and orographic components of the PMP can be determined. Hansen also reexamined the data of estimates of PMPs and observed storms obtained by Riedel and Schreiner [69] and concluded that the PMP estimates were not too high. For example, for the east of the 105th meridian, out of 75 storms considered, 18 storms exceeded 70% of the PMPs and three storms exceeded 90%. Recently England et al. [25] reviewed the various PMP procedures and databases used in estimating the PMP based on hydrometeorological methods particularly those utilized for developing the hydrometeorological reports (HMRs) that provide generalized PMP estimates over large regions of the United States (e.g., HMR 58 for California). They also described the key concepts involved including depth-area duration analysis of large storms, storm maximization, storm transposition, and envelopment. Further technical details of the underlying concepts and procedures may be found in Hansen et al. [33] and WMO [84].

The methods based on storm models use physical parameters such as dew point temperature, storm depth, and inflow and outflow fluxes depending on the storm type [12]. For example, in areas subject to the occurrence of hurricanes, a hurricane model may be applied for estimating the PMP. An advection–diffusion model of clouds for determining the temporal and spatial dynamics of extreme precipitation in a catchment located in the Bernese Alps of Switzerland has been suggested [67]. Atmospheric models such as the Regional Atmospheric Modeling System (RAMS) and the fifth-generation NCAR/Penn State mesoscale model (MM5) are being investigated for modeling extreme rainfall [13,62]. Storm maximization consists of adjusting a large observed storm precipitation to enable the convergence of the

maximum atmospheric moisture, that is, moisture maximization is increasing storm rainfall depth for the location and season, for higher atmospheric moisture than was available in the actual storm [25,37]. Transposition of storms means that the observed storm at a given location is translated to another location (say for an ungauged basin area) with appropriate adjustments such as those for differences in altitude [83]. The method assumes a region of homogeneous meteorology and topography. Using probability concepts for storm transposition has been examined by some researchers [1,30,26,27]. The regionalization methods (also called generalized PMP) are developed for large areas and generally are based on maximization and transposition of several types of storms (e.g., convective or cyclonic storms), depth–area–duration analysis, and envelopment. An example of this method is that developed by the National Weather Service of the United States [59]. Applications and developments in several other countries can be found in WMO [84 and the references therein].

28.3.2 PMP Based on Hershfield's Statistical Method

Hershfield's statistical method [35,36] was developed as an alternative to the traditional methods that are based on physical concepts. Hershfield's method, popularized internationally by WMO [82–84], has been commonly utilized in practice, particularly for basins lacking hydrometeorological data. It has been utilized in several countries worldwide for comparing with other methods for determining the PMP [2] and for preliminary and feasibility hydrologic studies [5]. Hershfield's statistical method is based on an equation similar to that of Chow [9] where a quantile of the underlying distribution is expressed as a function of the sample mean, the sample standard deviation, and a frequency factor K [10]. In the typical procedure for fitting the empirical frequency distribution of the data at hand using a probability distribution function (PDF), the value of K is related to the skewness coefficient and the exceedance probability. But in Hershfield's method, the value of K was established after analyzing a large number of historical data of storm annual daily maximums so that an upper bound of K was determined, which was bigger than all values of K obtained from the historical sample.

Hershfield's method was based on 24 h maximum precipitation data of 2645 stations (90% of which were stations in the United States and the rest for other parts of the world), which gave a total of about 95,000 station-year data. The method uses the equation

$$PMP = \overline{X}_n + K S_n \tag{28.1a}$$

where

$\overline{X}_n$ is the mean annual maximum daily precipitation
S_n is the corresponding standard deviation
K is a frequency factor

Hershfield recognized that because $\overline{X}_n$ and S_n are quantities that are estimated from a limited sample (n), they must be adjusted for sample size and for the effect of outliers. Graphs are available for obtaining the appropriate adjustment factors [35,83,84]. Another correction suggested by Hershfield was to account for the difference that exists between the daily maximum values and the 24 h maximums regardless of the calendar day.

Based on the data analysis of the 2,645 sites, Hershfield [35] found that the value of K in (28.1a) varied in the range 1.00–14.99 and that K ranged between 13.00 and 14.49 for only four stations. Consequently, he suggested utilizing the value of $K = 15$ for estimating the PMP. However, additional studies by Hershfield [36] indicated that K varied with the storm duration and the mean annual maximum precipitation; therefore, he provided additional relations (graphs) that enable one in determining the value of K for practical applications. Furthermore, other studies appeared in literature documenting the most appropriate values of K according to the climatic region of the study area. For example, Mejía and Villegas [50] analyzed 1, 2, and 24 h duration storm data for Colombia and suggested the corresponding envelopes for

determining K as a function of the mean annual maximum precipitation. Similar studies can be found for other locations in the world such as the southern half of the Indian peninsula [17], the Alpine region in Austria [56], the north region of India [66], the Czech Republic [68], the south region of Malaysia [16], and the Cataluña region of Spain [8]. Hershfield [35, pp. 101–102] recognized that K is a random variable and illustrated this point by associating the values of K with the return period (or exceeding probability) using as examples the Gumbel and lognormal distributions. Nevertheless, his rationale and intent was finding a value (actually an envelope function) that could be applicable for a given storm duration and climatic region. Such an envelope was obtained based on a large database of numerous storms that have been observed in historical records at similar locations. Hershfield [36, p. 967] argued that "enveloping K as a function of the mean serves a transposition purpose."

For easy of explanation and subsequent reference, Hershfield's method may be summarized as follows: (a) adjust $\overline{X}_n$ and S_n for effect of outlier; (b) adjust $\overline{X}_n$ and S_n for effect of sample size; (c) select K as a function of $\overline{X}_n$, the storm duration, and the study region; (d) estimate the PMP from (28.1a); and (e) make an additional adjustment to account for the difference between the maximum of a given time period (storm duration) and the maximum of the observation time period (e.g., to account for the difference between the maximum of 1440 min storm duration and the maximum observed daily).

28.3.3 Statistical Alternatives for Estimating Extreme Precipitation (Including PMP)

Koutsoyiannis [45] argued that K used by Hershfield could be fitted using some type of PDF and suggested the general extreme value (GEV) as a logical function since it deals with extreme events. Koutsoyiannis reexamined Hershfield's results and concluded that the $K = 15$ suggested by Hershfield corresponds approximately to a return period of 60,000 years based on the GEV distribution. Koutsoyiannis also illustrated his alternative approach using 136 years of data of annual maximum daily rainfall in Greece. As expected, such a long record offers the alternative of fitting the frequency distribution of the data and finding quantiles for any desired return period. Likewise, Papalexiou and Koutsoyiannis [63] suggested finding design values of maximum precipitation simply using the frequency analysis of the observed data based on the GEV distribution. Douglas and Barros [19] approached the design of maximum precipitation using a completely different method, which is based on applying multifractal concepts for determining what they called the fractal maximum precipitation (FMP), and applied their approach to the eastern United States.

In addition to the proposed methods summarized previously, efforts have been made to extend (extrapolate) the traditional frequency curves (FCs) that may be obtained from historical records at single sites. However, extending the FCs also implies increasing uncertainty of the estimated quantiles. Figure 28.1 illustrates the "credible" limits of extrapolation for events considered as large, rare, and extreme as the annual exceedance probability (AEP) increases [53]. A technique that is often used for extrapolating the FCs is based on regional precipitation frequency analysis (e.g., using the index flood approach). This way one can determine precipitation quantiles for return periods further beyond the usual historical record lengths, which may be of the order of 50–100 years. Table 28.1 summarizes the ranges of "credible extrapolation" for various types of data and methods [53,77]. Also, the tendency has been to assign an AEP to the PMP. While assigning an AEP to the PMP may be inconsistent with the "upper limit" concept of the PMP, it has been argued that given that the PMP is an uncertain quantity, it may conceivably be exceeded [53]. Based on a review conducted by Laurenson and Kuczera [47] on studies made in Australia and elsewhere and considering that at present there is no conceptually sound basis for assigning an AEP to the PMP, a recommendation was made where the AEP of PMP estimates vary solely as a function of catchment area [53]. The recommendation is summarized in Figure 28.2. Note that Nathan and Merz [54] cautions that "there is considerable uncertainty surrounding these recommendations as they are for events beyond the realm of experience and are based on methods whose conceptual foundations are unclear."

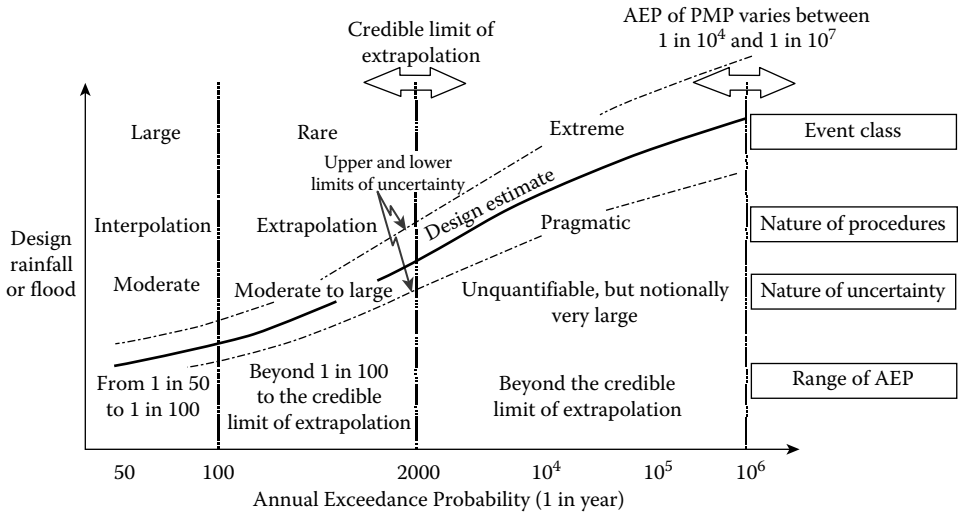

FIGURE 28.1 Increase of design events and corresponding uncertainty as the Annual Exceedance Probability (AEP) increases. (From Nathan, R.J. and Weinmann, P.E., Estimation of large to extreme floods, Book VI, *Australian Rainfall and Runoff: A Guide to Flood Estimation*, National Committee on Water Engineering, Institution of Engineers, Australia, 2001. With permission.)

TABLE 28.1 Data Type and Extrapolation Ranges for Frequency Analysis of Extreme Events

	Range of Credible Extrapolation for AEP	
Type of Data Used for Frequency Analysis	Typical	Most Optimistic
At-site precipitation data	1 in 100	1 in 200
At-site gauged streamflow data[a]	1 in 100	1 in 200
Regional streamflow data[b]	1 in 500	1 in 1,000
At-site streamflow and at-site paleoflood data[c]	1 in 4,000	1 in 10,000
Regional precipitation data	1 in 2,000	1 in 10,000
Regional streamflow and regional paleoflood data	1 in 15,000	1 in 40,000
Combination of regional data sets and extrapolation	1 in 40,000	1 in 100,000
[a]At-site gauged streamflow data (Australia)	1 in 50	1 in 200
[b]At-site/regional gauged streamflow data (Australia)	1 in 200	1 in 500
[c]At-site gauged and paleoflood data (Australia)	1 in 5,000	1 in 10,000

Source: Adapted from Nathan, R.J. and Weinmann, P.E., Estimation of large to extreme floods, Book VI, *Australian Rainfall and Runoff: A Guide to Flood Estimation*, National Committee on Water Engineering, Institution of Engineers, Australia, 2001; US Bureau of Reclamation, A framework for characterizing extreme floods for dam safety risk assessment, prepared by Utah State University and USBR, Denver, CO, 67pp., 1999. With permission.

28.4 Uncertainty of the PMP Considering Hydrometeorological Factors

The most recent manual of the WMO [84] states "Storms, and their associated floods, have physical upper limits, which are referred to as PMP and PMF. It should be noted that due to the physical complexity of the phenomena and limitations in data and the meteorological and hydrological sciences, only approximations

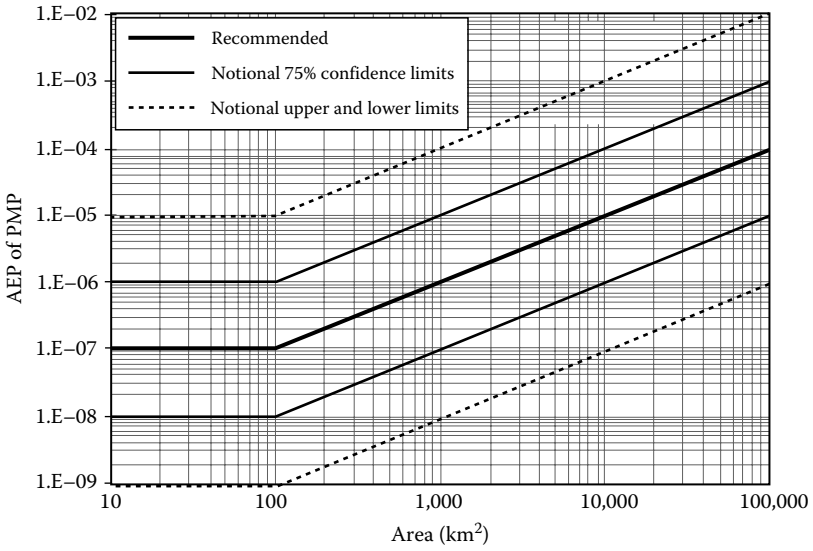

FIGURE 28.2 Values of AEP of PMP as a function of the catchment area. (From Nathan, R.J. and Weinmann, P.E., Estimation of large to extreme floods, Book VI, *Australian Rainfall and Runoff: A Guide to Flood Estimation*, National Committee on Water Engineering, Institution of Engineers, Australia, 2001. With permission.)

are currently available for the upper limits of storms and their associated floods." This concept must be clearly understood by water resources specialists involved in determining the so-called PMP and PMF.

The US National Research Council [58] considers two types of uncertainties that are summarized as follows: (1) Natural uncertainty represents the inherent variability of the physical system; it cannot be reduced. For example, if a given system is represented by a PDF say $f(x,\underline{\theta})$ with known parameter set $\underline{\theta}$, then X is random and as such its variability (uncertainty) is irreducible. (2) Knowledge uncertainty is due to the lack of understanding of the system and insufficient data. Using the same example as previously discussed, suppose we know the PDF but the parameter set $\underline{\theta}$ is unknown, so it must be estimated from data such as $x_1, x_2, \ldots, x_N$ where N is the sample size. Then, the parameter set is now referred to as $\hat{\underline{\theta}}$ and any quantile say $\hat{X}_q$ will be uncertain because of the uncertainty of the parameter set. However, knowledge uncertainty is reducible, for example, as the sample size N increases, the uncertainty of $\hat{\underline{\theta}}$ and consequently the uncertainty of $\hat{X}_q$ will decrease. In fact, as $N \to \infty$, the uncertainty of $\hat{\underline{\theta}}$ (and the uncertainty of $\hat{X}_q$) will become zero. Note that generally the PDF $f(x,\underline{\theta})$ is also unknown. Sometimes knowledge uncertainty has been referred to as "epistemic" [51].

As example of the previous concepts, we illustrate a method for determining the uncertainty of extreme precipitation (approaching the PMP) considering some of the hydrometeorological factors involved in estimating the PMP. Papalexiou and Koutsoyiannis [63] argued that the estimates of the PMP based on maximization of storm moisture do not appear having an upper bound. Based on the analysis of dew point temperature, atmospheric moisture, and maximized precipitation, they concluded that no upper bounds of the PMP estimates were evident. Instead of using the variability of these factors as they affect the estimates of PMP, the concepts proposed by Klemes et al. [43] and Klemes [44] are described. The concepts are simple but have important implications for estimating precipitation FCs for extreme events and near the PMP. Actually two approaches were suggested that are summarized as follows. Let us consider that N years of one-day maximum rainfall data R_t are available for a given site. Based on this data set, one can make frequency analysis following any well-known technique. Let us further assume that it is possible to separate the one-day maximum rainfall R_t into the convergence component C_t and the orographic component O_t. Thus, three sets of data of length N years each would be available. Klemes argued that the occurrence of the

convergence part of the storm is independent of the occurrence of the orographic part since they depend on different physical mechanisms. Then it is possible that in any given year, the maximum one-day rainfall may arise from any combination of the convergence and orographic components. Therefore, the combination of the two sets of data, that is, the convergence and orographic, will produce data of size N^2, which is a significant gain. For example, if $N = 100$, the procedure outlined previously will lead to 10,000 data points.

The second approach suggested by Klemes et al. [43] builds on the same concept as in the previous discussion but brings a third component, that is, moisture maximization of storms and precipitable water (storm efficiency). The assumption is to combine the actual P/M ratio of a given storm (where P and M stand for precipitation and precipitable water, respectively) with the maximum observed precipitable water. Considering the P/M ratios of the orographic and convergence components as independent, the N orographic P/M ratios are combined with the N convergence P/M ratios yielding N^2 total storm P/M ratios that are then combined with the N values of precipitable water. Thus, a total sample of N^3 possible precipitation values are obtained, which can be useful for frequency analysis.

Klemes et al. [43] and Klemes [44] illustrate the previous approaches for estimating the one-day PMP at Coquitlam Lake (CL) basin in Canada. The basin has an area of 193 km^2, is located in the western Coast Mountains (elevations ranging from 153 m to over 2000 m), and is about 30 km NE of Vancouver. The referred authors used 40 years of relevant hydrometeorological variables such as maximum one-day precipitation and precipitable water, that is, $N = 40$. Various estimates of the PMP using the traditional hydrometeorological methods have been made for CL, and the referred papers suggest for comparison a PMP of about 400 mm. Precipitation essentially free of orographic influence is recorded at Vancouver International Airport (the airport is located in the general direction of the southwesterly flows) and has been considered as a good approximation of the convergence component of CL precipitation. Thus, the orographic component was estimated as the difference between the total precipitation recorded at CL and that recorded at the airport. Figure 28.3 shows the precipitation FCs for the total precipitation at CL and those for the two components. Also Figure 28.3 shows with arrows a graphical extrapolation through 100 years (which is about twice the length of record, i.e., $2N$ in general). The resulting FC based on the combined sample of length 1600 (40^2) is shown in Figure 28.4. The figure shows also the original FC based on the original sample of size 40 (square symbol). Figure 28.4 shows a pretty good agreement between the two FCs. Also note the final point (based on the extrapolations in Figure 28.3 as previously indicated), which shows a precipitation of 340 mm corresponding to about 10,000 years of return period. Figure 28.4 also points to about 100,000 years of return period for the estimated PMP of 400 mm. The interested reader may refer to the paper by Klemes et al. [43] for applications using the approach based on storm maximization, which enables one estimating the uncertainty of precipitation further closer to the range of the estimated value of the PMP.

28.5 Uncertainty of the PMP Based on Hershfield's Method

The statistical method developed by Hershfield [35,36] gives a single value of the PMP. A simple method is proposed here to take into account the uncertainty of the PMP estimator arising from the uncertainty of the sample mean and sample standard deviation.

28.5.1 Assumptions and Derivations

Referring to the original equation used by Hershfield [35], we observe that the PMP is a function of the sample mean $\overline{X}_n$, the sample standard deviation S_n, and the coefficient K. Let us denote by $\hat{P}$ the estimator of the PMP such that

$$\hat{P} = \overline{X}_n + K S_n \tag{28.1b}$$

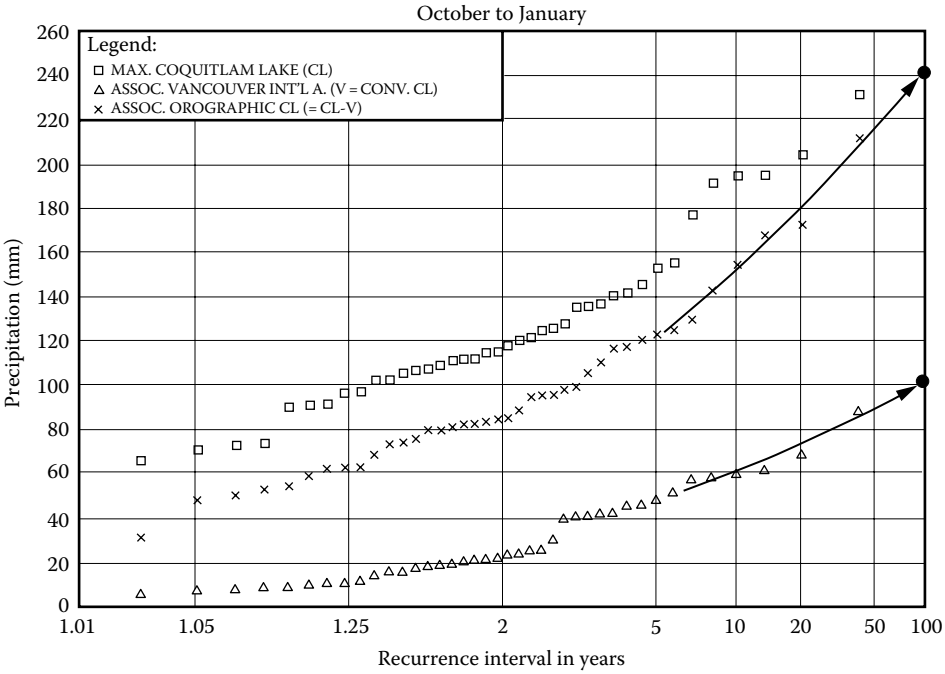

FIGURE 28.3 Empirical frequency distribution of annual maxima of daily precipitation at Coquitlam Lake (CL, square symbol) and their orographic (x symbol) and convergence (triangular symbol) components. (From Klemes, V. et al., *Dam Safety*, 1, 1992. With permission.)

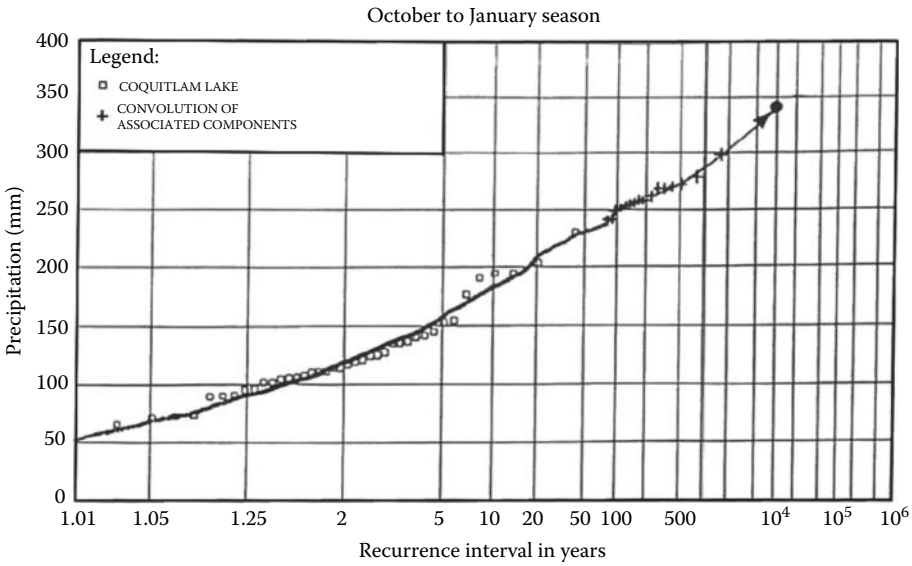

FIGURE 28.4 Empirical frequency distribution of annual maxima of daily precipitation at Coquitlam Lake obtained from the 1600 combinations of the orographic and convergence components. (From Klemes, V. et al., *Dam Safety*, 1, 1992. With permission.)

where n represents the sample size (number of years of data). Also let us recall that

$$\bar{X}_n = \frac{1}{n}\sum_{i=1}^{n} X_i \text{ and } S_n = \sqrt{\left[\frac{1}{(n-1)}\right]\sum_{1}^{n}(X_i - \bar{X}_n)^2}$$

where $X_1, X_2, \ldots, X_n$ is a random sample from an unknown distribution with population mean μ and variance σ^2. Because $\bar{X}_n$ and S_n are uncertain quantities and considering K as a constant (i.e., a maximum value corresponding to the duration of the storm, the value of $\bar{X}_n$, and the region where the basin of interest is located), one can calculate the mean and the variance of the PMP estimator $\hat{P}$. It may be worthwhile mentioning that a constant value of K is considered following Hershfield's approach in which a value of K is established after analyzing many data of historical storms that have occurred in the region under study. Thus, the uncertainty associated with K is accounted for by using an envelope function and as such K is a constant. And the remaining uncertainty is associated with $\bar{X}_n$ and S_n, which is the main subject of the argument herein.

The expected value of the estimator of the PMP, $\hat{P}$, is equal to

$$E(\hat{P}) = E(\bar{X}_n) + KE(S_n) \tag{28.2a}$$

It is clear that $E(\bar{X}_n) = E\left[(1/n)\sum_{1}^{n} X_i\right] = (1/n)\sum_{1}^{n} E(X_i) = \mu$. Likewise, it may be shown that $E(S_n) = \Gamma(n/2)\sigma/\sqrt{(n-1)/2}\,\Gamma[(n-1)/2]$ [42] where μ and σ represent the mean and the standard deviation of the population, respectively, and $\Gamma(a)$ represents the incomplete gamma function with argument a. Then (28.2a) may be written as

$$E(\hat{P}) = \mu + K\frac{\Gamma(n/2)}{\sqrt{(n-1)/2}\,\Gamma[(n-1)/2]}\sigma \tag{28.2b}$$

Note that in estimating $E(\hat{P})$ for an actual case, the population quantities μ and σ are replaced by their corresponding sample estimates (after the appropriate adjustments for outliers as needed as suggested by Hershfield).

The variance of the PMP estimator $\hat{P}$ of (28.1b) can be calculated as [52]

$$Var(\hat{P}) = Var(\bar{X}_n) + K^2 Var(S_n) + 2KCov(\bar{X}_n, S_n) \tag{28.3a}$$

Since $X_1, X_2, \ldots, X_n$ is a random sample, it is clear that $Var(\bar{X}_n) = \sigma^2/n$. Also it may be shown that the normal approximations for determining $Var(S_n)$ and $Cov(\bar{X}_n, S_n)$ are as follows: $Var(S_n) \approx \sigma^2/2(n-1)$ and $Cov(\bar{X}_n, S_n) \cong 0$ [42]. Then (28.3a) may be approximated as follows:

$$Var(\hat{P}) \cong \frac{\sigma^2}{n} + K^2\frac{\sigma^2}{2(n-1)} = \frac{\sigma^2}{n}\left[1 + \frac{nK^2}{2(n-1)}\right] \tag{28.3b}$$

And the standard deviation of the PMP estimator $\hat{P}$ is

$$\sigma(\hat{P}) \cong \frac{\sigma}{\sqrt{n}}\sqrt{1 + \frac{nK^2}{2(n-1)}} \tag{28.4}$$

The referred approximations $Var(S_n) \approx \sigma^2/2(n-1)$ and $Cov(\bar{X}_n, S_n) \cong 0$ are known to be valid where the underlying distribution of the random variable X is normal, that is, $N(\mu,\sigma^2)$ [42]. However, extreme hydrologic events, such as annual maximum precipitation, are generally skewed, and one must check

whether the referred normal approximations for determining $Var(S_n)$ and the covariance $Cov(\overline{X}_n,S_n)$ are still valid for skewed variables. Thus, a limited simulation experiment has been conducted for checking the foregoing approximations and introducing the needed corrections as appropriate. For this purpose, the GEV type 1 or Gumbel distribution was assumed as the underlying distribution of annual maximum precipitation.

Firstly, to verify the approach, 1000 samples of size $n=15$ were generated from the standard normal distribution and determined from each sample $\overline{X}_n(i)$ and $S_n(i)$, $i=1,\ldots,1000$, that is, the sample mean and standard deviations, respectively. Then, based on the pair of 1000 values, the variance $\hat{\sigma}^2(S_n)$ and covariance $\hat{Cov}(\overline{X}_n,S_n)$ were estimated. The results from the simulated samples gave $\hat{\sigma}^2(S_n)=0.035$ and $\hat{Cov}(\overline{X}_n,S_n)=0.00062$, while the theoretical normal approximations give $Var(S_n)=\sigma^2/2(n-1)=0.0357$ and $Cov(\overline{X}_n,S_n)=0$. Hence, the simulation results indicate that even for a short sample, that is, $n=15$, the approximations for obtaining $Var(S_n)$ and $Cov(\overline{X}_n,S_n)$ are correct (as expected).

For the Gumbel distribution, the CDF is given by $F(x;\underline{\theta})=\exp\left\{-\exp\left[-(x-x_0)/\alpha\right]\right\}$ in which $\underline{\theta}=\{x_0,\alpha\}$ is the parameter set where x_0 is the location parameter and $\alpha>0$ is the scale parameter [72]. Thus, Gumbel random numbers were generated by $x=x_0-\alpha\ln(-\ln u)$ in which u is a uniform (0,1) random number. The simulation experiments were made assuming that $\alpha=1$ and $x_0=1.9878$, 0.7053, 0.06405, and –0.256575, which correspond to coefficients of variation $\eta_X=0.5$, 1.0, 2.0, and 4.0, respectively (note that for $\alpha=1$, the population variance of the Gumbel distribution is $\sigma^2=1.645$.) Also in this case, 1000 samples were simulated for sample sizes $n=15$, 50, 100, and 150 and the variance $\hat{\sigma}^2(S_n)$ and correlation coefficient $\hat{\rho}(\overline{X}_n,S_n)$ determined. Table 28.2 summarizes and compares the results obtained for the variance and the correlation coefficient using the formulas that are valid for the normal distribution and using simulation, assuming the Gumbel distribution. In Table 28.2, the rows corresponding to $Var(S_n)=\sigma^2/2(n-1)$ were obtained based on the assumed values of $\sigma^2=1.645$ and n (e.g., for $n=15$, $Var(S_n)=0.05875$). On the other hand, the rows corresponding to simulation were obtained from the

TABLE 28.2 Comparison of the Variances $Var(S_n)$ and Correlation Coefficients $\rho(\overline{X}_n,S_n)$ Obtained Based on the Normal Approximations and from Generated Random Samples Gumbel Distributed with Parameters $\alpha=1$ and $x_0=1.9878$, 0.7053, 0.06405, and –0.256575 (for Coefficients of Variation $\eta_X=0.5$, 1.0, 2.0, and 4.0, respectively)

Sample Size n (1)	Variance and Correlation (2)	Approach[a] (3)	Coefficient of Variation η_X 0.5 (4)	1.0 (5)	2.0 (6)	4.0 (7)	Average (8)	Correction Factor f_n (9)
15	$Var(S_n)$	$\sigma^2/2(n-1)$	0.05875	0.05875	0.05875	0.05875	0.05875	1.752
		Simulation	0.1011	0.1026	0.1006	0.1075	0.10295	
	$\rho(\overline{X}_n,S_n)$	0.0	0.0	0.0	0.0	0.0	0.0	
		Simulation	0.5494	0.5550	0.4942	0.5388	0.5344[b]	
50	$Var(S_n)$	$\sigma^2/2(n-1)$	0.01679	0.01679	0.01679	0.01679	0.01679	1.979
		Simulation	0.0323	0.0342	0.0328	0.0336	0.03322	
	$\rho(\overline{X}_n,S_n)$	0.0	0.0	0.0	0.0	0.0	0.0	
		Simulation	0.5581	0.5097	0.5515	0.5634	0.5457[b]	
100	$Var(S_n)$	$\sigma^2/2(n-1)$	0.00831	0.00831	0.00831	0.00831	0.00831	2.133
		Simulation	0.0163	0.0173	0.0191	0.0182	0.01772	
	$\rho(\overline{X}_n,S_n)$	0.0	0.0	0.0	0.0	0.0	0.0	
		Simulation	0.5541	0.5367	0.5332	0.5516	0.5439[b]	
150	$Var(S_n)$	$\sigma^2/2(n-1)$	0.00552	0.00552	0.00552	0.00552	0.00552	2.120
		Simulation	0.0110	0.0118	0.0120	0.0120	0.0117	
	$\rho(\overline{X}_n,S_n)$	0.0	0.0	0.0	0.0	0.0	0.0	
		Simulation	0.5377	0.5628	0.5279	0.5480	0.5441[b]	

[a] $Var(S_n)=\sigma^2/2(n-1)$ and $\rho(\overline{X}_n,S_n)=0$ are based on the normal approximation.

[b] The average value of $\rho(\overline{X}_n,S_n)$ obtained from the simulated samples is about 0.542.

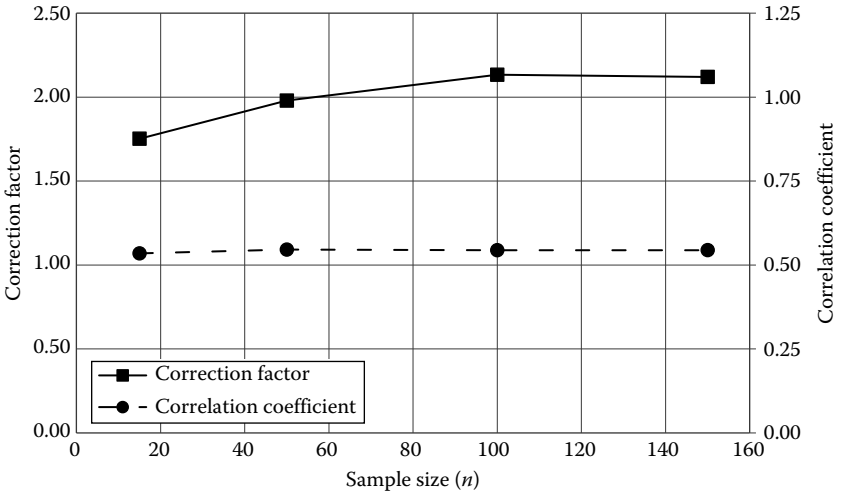

FIGURE 28.5 Variation of the correction factor f_n and the correlation coefficient $\rho(\bar{X}_n,S_n)$ as a function of the sample size n obtained by simulation using Gumbel random numbers (see Table 28.2). The correction factor f_n and the correlation coefficient $\rho(\bar{X}_n,S_n)$ are used in developing $\sigma(\hat{P})$ of (28.5).

1000 values of $S_n(i)$, $i=1,\ldots,1000$. Likewise, for $\rho(\bar{X}_n,S_n)$, the rows of zero's correspond to the result based on the normal approximation, while the values in the rows corresponding to simulation were obtained by correlating $\bar{X}_n(i)$ and $S_n(i)$, $i=1,\ldots,1000$.

First of all, one may observe that the values of $Var(S_n)$ obtained by simulation do not vary that much with the coefficient of variation η_X; thus, one may use the average figures shown in the eighth column of Table 28.2 (e.g., 0.10295 for $n=15$). The ratios of the average values (obtained by simulation) and those from the formula (based on the normal approximation) are 1.752, 1.979, 2.133, and 2.120 for $n=15$, 50, 100, and 150, respectively, as shown in the last column of Table 28.2 (e.g., for $n=15$, $f_n=0.10295/0.05875\approx 1.752$). As expected, $Var(S_n)$ varies with n, but the ratios, denoted correction factors f_n, after an initial increase for small n, seem to converge to a constant value as n increases, as shown in Figure 28.5. Thus, the factor f_n can be used to calculate $Var(S_n)$ for the Gumbel as $Var(S_n)\approx[\sigma^2/2(n-1)]\times f_n$ where f_n, for a particular value of n, can be either interpolated from the values of Table 28.2 or read of from Figure 28.5. Note that for values of $n\geq 100$, one may use $f_n\approx 2.13$, which is an average value for large n. Likewise, Table 28.2 shows that the correlation coefficient $\rho(\bar{X}_n,S_n)$, obtained from simulation, does not vary much with the coefficient of variation η_X nor with the sample size n (Figure 28.5); thus, an average figure such as 0.542 may be a reasonable correlation to use for the Gumbel distribution (Table 28.2).

Therefore, (28.4) was modified so as to consider the corrections pertaining to the variance $Var(S_n)$ and the covariance $Cov(\bar{X}_n,S_n)$ as described previously. The covariance term can be written as

$$Cov(\bar{X}_n,S_n)=\sigma(\bar{X})\sigma(S_n)\rho(\bar{X}_n,S_n)=\frac{\sigma}{\sqrt{n}}\frac{\sigma\sqrt{f_n}}{\sqrt{2(n-1)}}\rho(\bar{X}_n,S_n)$$

and using $\rho(\bar{X}_n,S_n)\approx 0.542$, one can rewrite (28.4) as

$$\sigma(\hat{P})\cong\frac{\sigma}{\sqrt{n}}\sqrt{1+\frac{nK^2f_n}{2(n-1)}+1.084\left[\frac{nK^2f_n}{2(n-1)}\right]^{1/2}} \tag{28.5}$$

which is the standard deviation of the PMP estimator $\hat{P}$ after the corrections as described previously that are applicable for skewed distributions such as the Gumbel distribution (the assumed distribution here).

28.5.2 Design PMP and Risk

Considering the uncertainty of the mean $\overline{X}_n$ and the standard deviation S_n and the ensuing uncertainties of the PMP estimator $\hat{P}$, one can estimate design values of the PMP by

$$\hat{P}_d = E(\hat{P}) \pm c\,\sigma(\hat{P}) \tag{28.6}$$

where
$\hat{P}_d$ represents a design PMP value
$c > 1$

In other words, $\hat{P}_d$ is a quantile of the uncertain quantity $\hat{P}$ of which we do not know its distribution but only the estimate of its mean $E(\hat{P})$ and the estimate of its standard deviation $\sigma(\hat{P})$. Furthermore, in order to have an approximation to the probability that the PMP estimator $\hat{P}$ may be smaller or greater than the said quantile $\hat{P}_d$, one can apply Chebyshev's inequality [52], which can be expressed as

$$P[E(\hat{P}) - c\,\sigma(\hat{P}) < \hat{P} < E(\hat{P}) + c\,\sigma(\hat{P})] \geq 1 - \frac{1}{c^2} \tag{28.7}$$

This inequality gives a bound of the probability that does not depend on the distribution of $\hat{P}$. As expected, the probability bound is conservative since one only knows the mean and the standard deviation of $\hat{P}$ but not its distribution. The applicability of (28.7) is illustrated in the case study presented in the following section.

The proposed method for determining the PMP estimate, the corresponding uncertainty, the design PMP, and associated probability bounds may be summarized as follows: (a) adjust $\overline{X}_n$ and S_n for effect of outlier as in the original method by Hershfield; (b) select K as a function of $\overline{X}_n$, the storm duration, and the study region; (c) estimate the expected value of the PMP estimator $E(\hat{P})$ by using (28.2b) and multiply this value by an adjustment as in step (e) of Hershfield's method as described previously at the end of Section 28.3.2; (d) estimate the standard deviation of the PMP estimator $\sigma(\hat{P})$ by using (28.5) where the correction factor f_n is obtained by interpolating from Table 28.2 or from Figure 28.5; (e) use (28.6) to obtain design values $\hat{P}_d$ of the PMP; and (f) use Chebyshev's inequality (28.7) for obtaining probability bounds of the PMP estimator $\hat{P}$. This modified method is further illustrated in the following case study.

28.5.3 Case Study

The case study refers to the design of the spillway capacity of a high dam that is being constructed at the Tona River north of Bucaramanga, Colombia, near its confluence with the Surata River (the area of the basin at the dam site is 195 km^2 and the mean slope of Tona River is about 7%.) For this purpose, the Metropolitan Aqueduct for Bucaramanga contracted the pertinent hydrologic studies with leading consulting firms in Colombia. The consultants and designers of the dam decided using the PMP and PMF approach for estimating the design flood for the spillway. The hydrologic data and basic studies performed by the consultants considered estimating the PMP for various storm durations, and the methods utilized included storm maximization and transposition and Hershfield's original statistical method. However, in this case study, only the statistical method due to Hershfield's including the proposed modifications to account for the uncertainty (as described previously) is compared and discussed. The statistical estimates were based on 15 years of annual maximum daily precipitation recorded at the Martín Gill station (located within Tona's River basin) where $\overline{X}_n = 66.5$ mm, $S_n = 24.5$ mm, and $n = 15$ (Table 28.3).

The main results of applying the original (statistical) method by Hershfield and those obtained using the proposed method of PMP with uncertainty are included in Table 28.3. The first line of results in Table 28.3 corresponds to the estimates based on the original method of Hershfield as described previously. The adjustments for the mean and the standard deviation to account for the limited sample size

TABLE 28.3 Comparison of the 24 h PMP for Tona River Obtained Based on Hershfield's Original Method and Based on the Proposed Method Considering Uncertainty Assuming the Normal and Gumbel Approximations for Calculating $Var(S_n)$ and $Cov(\overline{X}_n, S_n)$

Mean $\overline{X}_n$ (mm)		Std. Deviation S_n (mm)			Traditional Hershfield's PMP (mm) from (28.1a)	PMP with Uncertainty (mm)		
Original	Adjusted Hershfield	Original	Adjusted Hershfield	K		$E(\hat{P})$ (28.2b)	$\sigma(\hat{P})$ (28.4)	$\hat{P}_d^*$ (28.6)
66.5	68.5	24.5	27.7	8.9	369[a]			
66.5		24.5		8.9		328[b]	41.7	370[c] 411[d] 453[e] 495[f]
							From (28.5)	
							58.2	386[c] 444[d] 503[e] 561[f]

[a] PMP = $(68.5 + 8.9 \times 27.7) \times 1.17 \approx 315 \times 1.17 \approx 369$ mm (using an adjustment factor 1.17).
[b] The $E(\hat{P})$ obtained from (28.2b) is multiplied by the adjustment factor 1.17.
$\hat{P}_d$ of (28.6) considering the upper limit, that is, $\hat{P}_d^* = E(\hat{P}) + c \times \sigma(\hat{P})$ in which
[c] $c = 1$.
[d] $c = 2$.
[e] $c = 3$.
[f] $c = 4$.

(as suggested by Hershfield) were made using the graphs available at WMO [83], (Figure 4.4) that gave adjustment factors equal to 1.03 and 1.13, for the mean and the standard deviation, respectively. Thus, the adjusted values of the sample mean and standard deviation are 68.5 and 27.7 mm, respectively (Table 28.3). In addition, the value of the frequency factor $K = 8.9$ was obtained from the results for Colombia for 24 h duration of precipitation [50]. Then using the foregoing values, one can obtain from Equation 28.1a the value of PMP = 315 mm. Note that Hershfield [35] recommended an additional adjustment of 1.13 on the estimated PMP value to account for the difference between the daily maximums and the 24 h maximums. But other recent studies such as those in Spain [8] and Great Britain [20] gave adjustment factors of 1.16 and 1.17, respectively. Hence, in all subsequent calculations, the factor 1.17 was applied. Therefore, the PMP adjusted value using Hershfield's method becomes 369 mm as shown in Table 28.3 (see the notes at the bottom of table). One must also note that no adjustments for outliers were made because the analysis of the 15 years of data did not show any evidence of outlying observations. In addition, Hershfield's method for adjusting for outliers gave adjustment coefficients for the mean and the standard deviation that were practically equal to one in both cases.

While Hershfield's adjustments for the mean and the standard deviation have been a way of taking into account the limited sample size of the available precipitation records, however. Hershfield's method does not give any information on the uncertainty of the PMP estimates, that is, the standard error of the estimator $\hat{P}$ of (28.1b), which arises from the uncertainties of the estimators $\overline{X}_n$ and S_n. As suggested in Section 28.5.1 previously, those estimates with uncertainties can be obtained approximately by (28.2b), (28.4), and (28.5), depending on the approximations utilized. For example, the second row of results in Table 28.3 shows that $E(\hat{P}) = 328$ mm, which is obtained from (28.2b) based on $\overline{X}_n = 66.5$, $S_n = 24.5$, $n = 15$, and $K = 8.9$ and then multiplying the result from (28.2b) by the adjustment factor 1.17 as described previously. Next (column before the last one) are the results obtained for $\sigma(\hat{P})$ applying (28.4), based on the normal approximation that gave $\sigma(\hat{P}) = 41.7$ mm and (28.5) based on the Gumbel approximation, which gave $\sigma(\hat{P}) = 58.2$ mm. In addition, the last column in Table 28.3 shows results of the design PMP $\hat{P}_d$ of (28.6) considering four values of c, that is, $c = 1$, $c = 2$, $c = 3$, and $c = 4$. First, the concepts based on the results obtained using the normal approximations (for $Var(S_n)$ and $Cov(\overline{X}_n, S_n)$) are illustrated, and subsequently the results

obtained based on the Gumbel approximation are discussed. One may observe that (28.6) with $c = 1$ and the + sign, that is, $\hat{P}_d^* = E(\hat{P}) + \sigma(\hat{P})$, gives $\hat{P}_d^* = 370$ mm, which is the least conservative estimate and is about the same value obtained using Hershfield's original method, that is, PMP = 369 mm. Obviously, the most conservative estimate included in Table 28.3 corresponds to $c = 4$, that is, $\hat{P}_d^* = 495$ mm. The decision for selecting a design value of the PMP based on statistical concepts must consider the fact that the estimates are based on statistics that are computed from a limited sample, and in this case study, the sample is only 15 years long. Thus, the selected design value must be such that the probability of that value being exceeded must be small.

The Inequality 28.7 provides some useful information that may help in selecting the design PMP value. Thus, applying (28.7) and $\sigma(\hat{P})$ based on (28.4) gives the following:

$$\text{For } c = 1, \quad P[286 < \hat{P} < 370] \geq 0.0$$

$$\text{For } c = 2, \quad P[245 < \hat{P} < 411] \geq 0.75$$

$$\text{For } c = 3, \quad P[203 < \hat{P} < 453] \geq 0.89$$

$$\text{For } c = 4, \quad P[161 < \hat{P} < 495] \geq 0.94$$

These results must be interpreted as follows. For example, for $c = 3$, the probability that the PMP estimator $\hat{P}$ is bigger than 453 mm and smaller than 203 mm is less than 11%. For comparison, if the true underlying distribution of $\hat{P}$ were normal, then that probability would be less than 0.3% (instead of 11%). Likewise, if we take instead $c = 4$, then in this case the foregoing probabilities would be less than 6% and 0.01%, respectively. Naturally, one could select even higher values of c and obtain more conservative values of the PMP with smaller risks of exceedances.

The foregoing analysis of the results included in Table 28.3 suggests that the PMP estimates considering the effect of uncertainty and the normal approximations vary in the range of 370–495 mm (the top four values shown in the last column of Table 28.3). The lowest value 370 mm corresponds to the case where the PMP is obtained simply by adding one standard deviation to the estimated mean value $E(\hat{P})$. Without further information beyond the mean $E(\hat{P})$ and the standard deviation $\sigma(\hat{P})$, the probability bound previously suggests that it is very likely (in fact almost certain) that such value of 370 mm will be exceeded because of the uncertainty associated with estimating $\overline{X}_n$ and S_n that are based on only 15 years of records. On the other hand, the value of 495 mm corresponds to a conservative estimate, that is, it is less likely that it will be exceeded because of the uncertainties associated with $\overline{X}_n$ and S_n. Thus, the results show a major difference between the single value of the PMP (equal to 369 mm) that one obtains applying the original method of Hershfield and the range of PMP values obtained by the proposed method that takes into account the effect of uncertainty and their associated probabilities of exceedances.

The calculations and analysis of design PMP and probability bounds of the previous discussion have been made using (28.4) for calculating the standard deviation of the PMP estimator $\sigma(\hat{P})$, which assumes the normal approximations for the variance $Var(S_n)$ and the covariance $Cov(\overline{X}_n, S_n)$ as described previously. However, using $\sigma(\hat{P})$ of (28.5) will give more accurate results if the distribution of the annual maximum daily precipitation is skewed as one may expect. Thus, for comparison, we applied (28.5) where $n = 15$, $\sigma = 24.5$, $K = 8.9$ (Table 28.3), and $f_{15} = 1.752$ (see Section 28.5.1 and Table 28.2), which gives $\sigma(\hat{P}) = 58.2$ mm, an amount that is about 40% higher than that based on (28.4). However, the overall increase in the design value of the PMP of (28.6) is not as high. Thus, we computed four design values of the PMP based on (28.6) for $c = 1$, 2, 3, and 4, and the values obtained are those shown in the lower portion of the last column of Table 28.3. For illustration, for $c = 1$, we get $\hat{P}_d^* = 386$ mm, which compared to the value 370 mm (Table 28.3) represents an increase of about 4%. Likewise, the percent increases for the other cases shown in Table 28.3 are about 8%, 11%, and 13% for $c = 2$, 3, and 4, respectively.

One must note that the previous analysis clearly indicates the striking difference between the PMP value obtained using the traditional Hershfield's method (PMP = 369 mm) and the PMP values that are obtained using the proposed method that accounts for the uncertainties involved, which gives values varying in the range of 386–561 mm (lower portion of the last column in Table 28.3). These values (386, 444, 503, and 561 mm) are, respectively, about 5%, 20%, 36%, and 52% higher than the single value of PMP obtained with the original Hershfield's method. Furthermore, the proposed method, which includes the probability bounds, suggests that using say the smaller value of 386 mm as the design PMP (which is even 5% bigger than the 369 mm PMP obtained from the original Hershfield's method) would not be wise because it is certain that it will be exceeded. Therefore, a bigger value must be selected considering the associated exceedance probabilities (risk) as described previously.

28.6 PMF Estimation and Uncertainty

28.6.1 PMF Estimation from PMP

Several books and manuals have documented the procedures for determining the PMF from the PMP [14,57,65]. The following list is a simplified summary of the procedures followed by USBR and many other agencies in the United States [73]: (1) divide the basin into subbasins as needed and determine the drainage areas; (2) estimate the PMP; (3) arrange the PMP into a storm rainfall pattern; (4) estimate the rainfall losses due to surface detention and infiltration, and determine the rainfall excess for each time interval; (5) route the rainfall excess through each subbasin to estimate the flood hydrograph for each subbasin; (6) add to the flood hydrograph of each subbasin the corresponding base flow, flow from prior storms, as the case may be, to get an estimate of the flood hydrograph for each subbasin; (7) route the flood hydrograph from each subbasin to estimate the PMF at the point of interest (e.g., site of a dam); and (8) route the PMF through the reservoir storage, outlets, and spillway to obtain estimates of maximum storage, elevation, discharges, and durations at the project site. The procedures also include comparisons of applicable envelope curves of flood peaks and volumes if available.

Some of the previous steps (e.g., steps 4 through 7) may be computed using a given rainfall–runoff model. For this purpose, a number of models have been developed for the past several decades. For example, in the United States, the Hydrologic Engineering Center (HEC)-1 [75] and HEC-Hydrologic Modeling System (HEC-HMS) [76] models are widely utilized in practice for flood hydrograph computations. These models are based on the unit hydrograph concept, and also the flood hydrograph and runoff (FHAR) model promoted by the USBR uses the unit hydrograph [73]. The unit hydrograph approach represents the rainfall–runoff process as a linear system. Also, various rainfall–runoff models that consider the underlying nonlinear mechanism of the rainfall–runoff processes have been proposed in literature such as CASC2D [40] and Two-dimensional runoff, erosion, and expert model (TREX) [80].

In addition, the advances in GIS-based computer models in the past decades brought further capabilities for analyzing runoff hydrographs as a function of the watershed characteristics and enhancing the applicability of distributed modeling in watershed hydrology. For example, CASC2D [39,40,41] is a raster-based watershed model that accounts for the spatial variability in the watershed topography, soil type, and land use. The CASC2D model has been extended to TREX by Velleux et al. [80] to simulate the transport and fate of metals in relation to rainfall–runoff and sediment transport at the watershed scale. England et al. [23] applied TREX to simulate extreme storms including the PMP on the Upper Arkansas watershed covering 12,000 km^2 in Colorado.

As one may observe from the previous summarized steps, estimating the PMF for a specific basin (project) involves a wide range of factors such as rainfall depth and duration (PMP), temporal pattern of the PMP, spatial distribution of the PMP, centering of the storm over the basin, lag time and unit hydrograph estimation, loss rates estimation, antecedent flooding before the onset of the PMP (previous storms and snowmelt as the case may be), and flood routing through the basin channels and reaches. Each of the referred factors of the previous discussion and the calculation steps to estimate the PMF involve some

degree of uncertainty. While this issue has been recognized in literature, still the knowledge for quantifying the various uncertainties and their effects on the PMF is lacking. Bondelid et al. [6] indicated that the uncertainty in estimating the lag time may cause errors in estimating the maximum floods of the order of 75%. Useful references on uncertainties of time of concentration and lag time for various types of watersheds and formulas commonly utilized in practice are available [29,48,49,74]. In the following sections, we illustrate the variability of the PMF based on sensitivity analysis and Monte Carlo simulation.

28.6.2 Sensitivity Analysis

The TREX model is applied for sensitivity analysis of some of the model parameters on the PMF. For this purpose, the Semenyih watershed (236 km^2), which is located in the state of Selangor in Malaysia, is utilized. The watershed is partially used for agriculture but urbanization (residential and industrial) development has rapidly transformed the area in recent decades. The topography of the watershed has been discretized with 29,139 cells at a 90 m × 90 m grid scale. The digital elevation model (DEM) data for the study site (Figure 28.6a) were obtained from the Department of Surveying and Mapping of Malaysia. The lowest elevation at the outlet is 40 m above sea level, while the highest point reaches 1100 m at the upstream end of the watershed. The average terrain slope is about 45% and ranges between 4% and 85% with very steep mountains overhanging flat and wide valleys (Figure 28.6a). The DEM also allowed the delineation of the channel network of the watershed where the total stream length reached about 36 km. Four soil types (Figure 28.6b) and six land uses (Figure 28.6c) were included in the raster-based GIS representation of the watershed. The soil types allowed the definition of the effective hydraulic conductivity K_h, and the land use types enabled the definition of the land surface Manning's roughness coefficients n.

The April 13, 2003, storm was used for model calibration where the precipitation and flow records were obtained from the Department of Irrigation and Drainage of Malaysia. The calibration procedure focused on properly simulating peak flow, discharge volume, and time to peak at the outlet. The TREX model has several parameters such as hydraulic conductivity, Manning's roughness coefficient, interception depth, capillary suction head, and soil moisture deficit. These parameters were adjusted during calibration so as to achieve good agreement between the measured and simulated flow. The antecedent moisture condition of the watershed was assumed dry. Table 28.4 gives the values of the calibrated parameters K_h and n for the specified type of soils and land use (the other parameters are omitted).

Several studies have been made to estimate the PMP for Malaysia. For example, Poon and Hwee [64] reviewed earlier studies and Figure 28.7 shows the PMP estimates for various storm durations in the state of Selangor (S-PMP). For comparison, the figure also shows the rainfall depths for the 100-year-return period [18] and the world's greatest precipitation events [38]. For the purpose of this study, the 16 h precipitation depths were utilized as input to the calibrated TREX model. These rainfall events are summarized in Table 28.5. TREX calculates the distribution of flow depth on each calculation cell as a function of time. To illustrate the results, Figure 28.8 shows the calculated distribution of the peak flow depth on the Semenyih watershed at the time of the peak discharge during the S-PMP. The PMF hydrograph at the outlet of the basin is shown in Figure 28.9. For comparison, this figure also shows the flood hydrographs calculated for the 100-year and the world's greatest storm events (Table 28.5). Also for comparison, the figure shows the hydrographs obtained using the HEC-HMS model (dashed lines).

Experience using the TREX model in simulating a wide range of rainfall–runoff events has shown that the most sensitive parameters are the saturated hydraulic conductivity K_h and the overland flow resistance Manning's coefficient n [22,79]. Thus, the sensitivity analysis of the PMF considered here uses the range of values of the parameters K_h and n shown as lower and upper values in Table 28.4. The combination of the upper, lower, and calibrated values of K_h and n gave a range of calculated PMF values that are summarized in Table 28.6. It shows that the PMF values vary in the range of 1245–1866 cm and the mean and standard deviation are about 1527 and 270 cm, respectively. The maximum discharge is obtained for the lowest values of K_h and n. Besides showing the variability of the computed PMF, the results also suggest that the Manning's roughness coefficient is the most important parameter controlling the flow at the outlet of the basin.

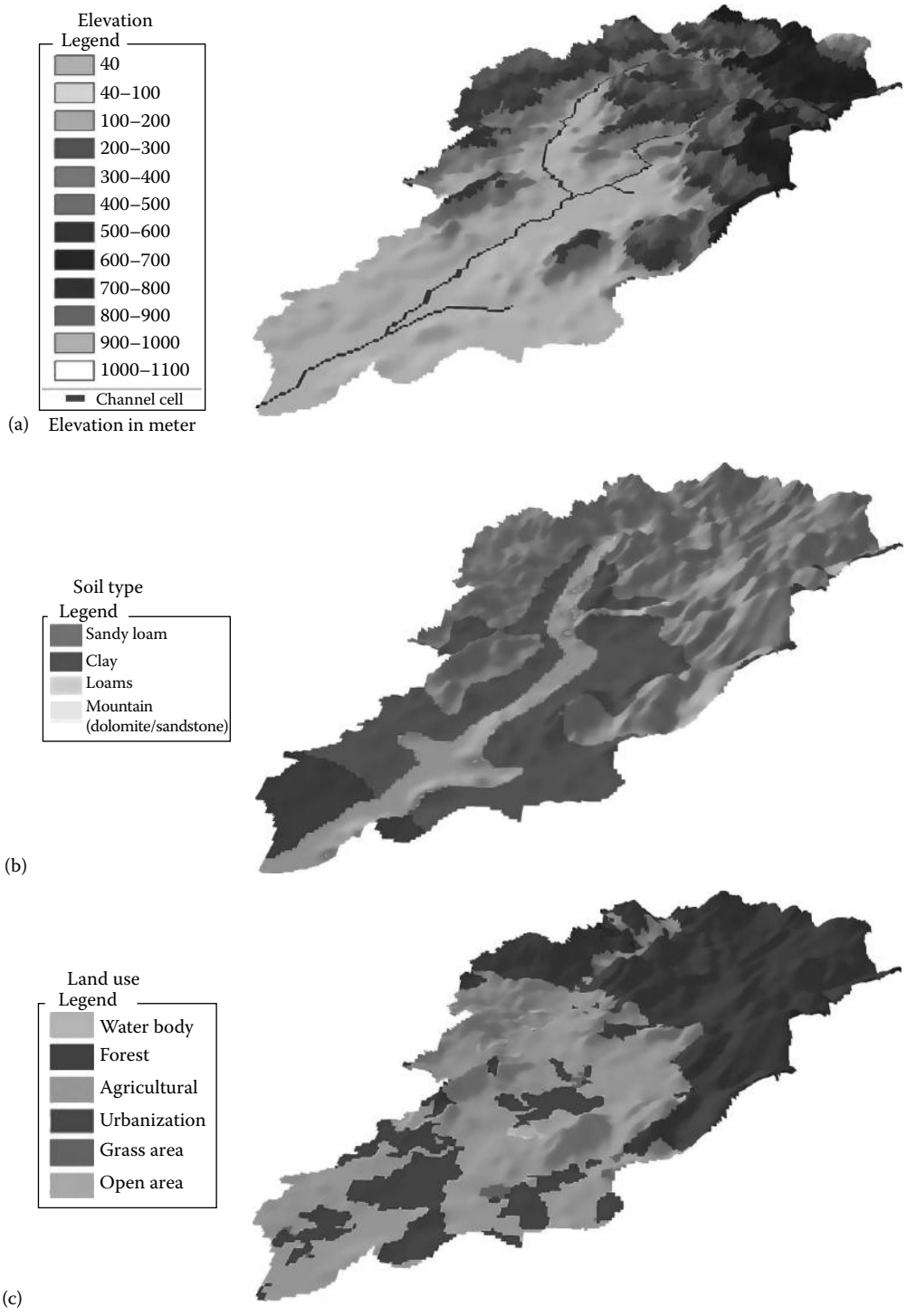

FIGURE 28.6 (a) Elevation, (b) soil type, and (c) land use for the Semenyih watershed in Malaysia.

TABLE 28.4 Hydraulic Conductivity K_h and Manning's n Values Obtained after Calibrating TREX Model for the Semenyih Watershed

Parameter	Lower	Calibrated	Upper	Soil Type/Land Use
Hydraulic conductivity K_h (m/s)	5.60×10^{-9}	1.12×10^{-8}	1.68×10^{-8}	Sandy loams
	6.35×10^{-9}	1.27×10^{-8}	1.91×10^{-8}	Loams
	1.53×10^{-9}	3.06×10^{-9}	4.59×10^{-9}	Clay
	5.90×10^{-11}	1.18×10^{-10}	1.77×10^{-10}	Mountain–limestone
Manning's n	0.050	0.100	0.150	Agriculture
	0.025	0.050	0.075	Urban/commercial
	0.100	0.200	0.300	Forest
	0.050	0.100	0.200	Grass area
	0.050	0.100	0.150	Open area
	0.020	0.040	0.060	Channel bed

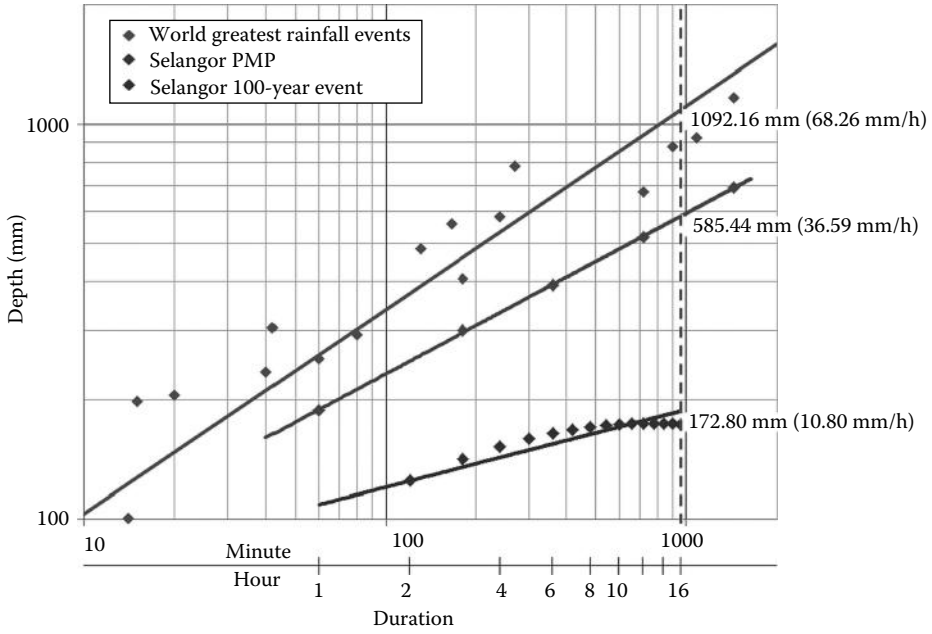

FIGURE 28.7 PMP estimates for the state of Selangor, Malaysia, for various storm durations. For comparison, the 100-year rainfall depths and the world's greatest rainfall depths are also shown.

TABLE 28.5 Precipitation Depth and Intensity and Corresponding Flood Properties Obtained from Model TREX for the 100-year, PMP, and World's Greatest Storms for the Semenyih Basin

	Precipitation		Flood Hydrograph Results	
Events	Depth (mm)	Intensity (mm/h)	Peak Discharge (cm)	Time to Peak (24 h)
100-year	173	11	223	23:36
PMP	585	37	1484	19:06
World's greatest rainfall	1092	68	3686	17:30

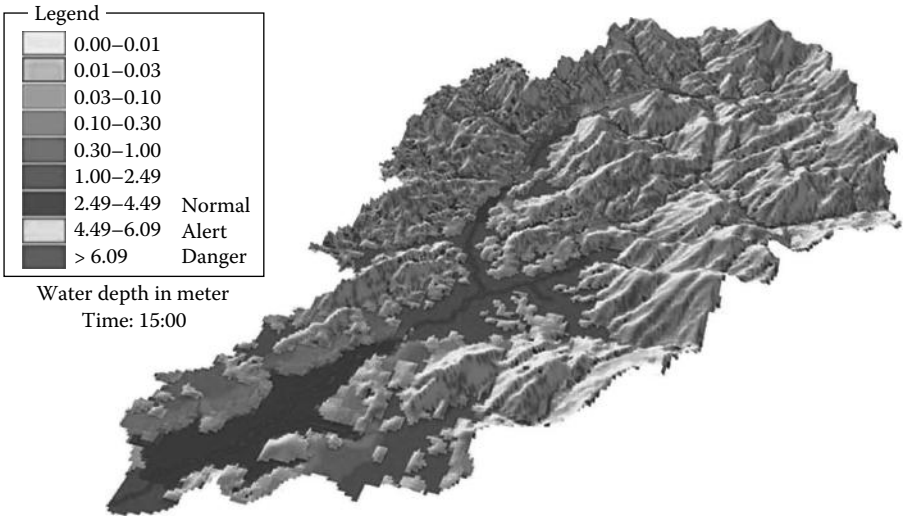

FIGURE 28.8 Spatial distribution of peak flow depth in meters for the PMP event (37 mm/h at 16 h duration).

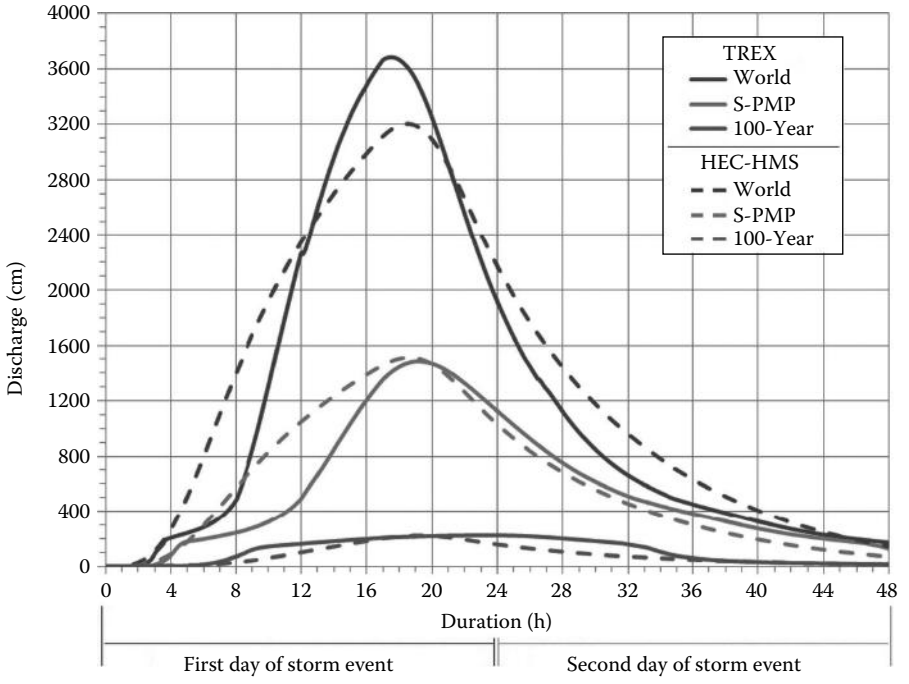

FIGURE 28.9 Flood hydrographs obtained from TREX and HEC-HMS models using the 16 h 100-year, PMP, and world's greatest storms.

28.6.3 Monte Carlo Analysis

A Monte Carlo method has been developed to determine the uncertainty of the PMP in a joint effort by the USBR and Washington state [3]. Since then, a number of articles and applications have been made [70]. In Barker et al. [3], the various factors involved in estimating the PMF including some of

TABLE 28.6 Sensitivity Analysis of the PMF Obtained from the TREX Model for Various Combinations of the Parameters for the Semenyih Watershed

Hydrologic Model Parameters		Flood Peak (cm)
Hydraulic Conductivity K_h	Manning's n	
Calibrated values		1474
Lower limit	Lower limit	1866
Upper limit	Upper limit	1242
Lower limit	Upper limit	1249
Upper limit	Lower limit	1859
Calibrated value	Lower limit	1859
Calibrated value	Upper limit	1245
Upper limit	Calibrated value	1476
Lower limit	Calibrated value	1472
Mean		1527
Standard deviation		270

the hydrologic model input parameters were treated as variables with specified distributions. Values of the various factors and parameters were drawn at random from the corresponding distributions that were then utilized for estimating the PMF. The overall method is summarized in the following steps: (a) select the season of occurrence of the PMP; (b) select all hydrometeorological, hydrologic, and hydraulic parameters that are dependent upon season of occurrence; (c) select all parameters that are independent of other parameters; (d) select all hydrologic and hydraulic parameters that are dependent upon other flood model parameters; (e) estimate the flood; (f) repeat steps (a) through (e) a large number of times, for example, 500 times; and (g) do statistical analysis of the estimated flood values.

The method summarized previously has been applied to the Bumping Lake basin located in the Cascade Mountains in Washington state [3]. The basin area is 67 miles^2, the topography ranges from 3400 ft at the dam site to over 6000 ft at the headwaters near the crest of the mountains, and the mean annual precipitation varies from about 48 in. near the dam to over 70 in. at the headwaters. The PMPs were determined based on the HMR-57 [60] as 10.6 in. for 6 h, 20.6 in. for 24 h, and 32.2 in. for the 72 h. The HEC-1 program was utilized for the flood computations [75], and probability distributions were used for the following input parameters: season of occurrence of the PMP, antecedent precipitation, initial streamflow, antecedent snowpack, antecedent soil moisture, occurrence of frozen ground, minimum infiltration rate, and unit hydrograph time lag. Since the HEC-1 model utilized does not account for subsurface catchment response, appropriate additional steps were added to account for that component. Based on detailed analysis of the hydrometeorological historical data for the study region, appropriate PDFs were selected for the various input parameters as summarized in Table 28.7. The results of 500 Monte Carlo simulations based on the PMPs specified in HMR-57 (as noted previously) are shown in the frequency distribution of the PMFs in Figure 28.10. The simulated PMFs gave the following: mean PMF = 64,000 cfs and standard deviation of PMF = 7,220 cfs and a range of 45,000–84,000 cfs. Note that the PMF computed using the standard USBR approach gave a PMF equal to 71,000 cfs that is about one standard deviation above the mean of the simulated results. The results obtained suggest the uncertainty of the PMF (for the specified PMP) that arises from the uncertainty of the various hydrometeorological factors involved in estimating the PMF.

Two additional Monte Carlo studies were made where the magnitude and temporal characteristics of the precipitation input were assumed to vary in addition to the other parameters described previously [3]. In the first case, the 24 h PMP (20.6 in.) specified by HMR-57 was held constant, and the temporal characteristics were varied by examining the depth-duration curves contained in HMR-57 and the extreme storms observed in the past. The results of 500 simulations gave mean PMF = 42,300

TABLE 28.7 Probability Distributions Utilized in the Monte Carlo Method

Parameter	Probability Model
PMP season of occurrence	Beta distribution
Antecedent precipitation (bimonthly)	Beta distribution
Antecedent temperature (bimonthly)	Normal distribution
Antecedent snowpack (bimonthly)	Regression with antecedent precipitation and temperature plus error term
September 1 soil moisture deficit	Beta distribution
Minimum infiltration rate	Symmetrical beta distribution
Deep percolation rate	Symmetrical beta distribution
Unit hydrograph lag (natural variability)	Normal distribution
Unit hydrograph lag (runoff mechanism)	Linear scaling factor
Initial streamflow	Regression with antecedent precipitation plus error term

Source: Barker, B. et al., A Monte Carlo approach to determine the variability of PMF estimates, Final Report on Bumping Lake Dam for USBR Dam Safety Office, 1997. With permission.

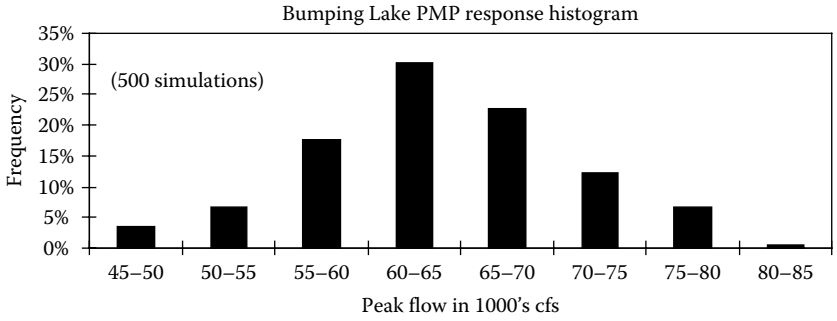

FIGURE 28.10 Relative frequency distribution of the PMFs obtained from the 500 simulations for Bumping Lake using the PMP specified in HMR-57. (From Barker, B. et al., A Monte Carlo approach to determine the variability of PMF estimates, Final Report on Bumping Lake Dam for USBR Dam Safety Office, 1997. With permission.)

cfs and standard deviation of PMF = 10,200 cfs and a range of 14,700–75,100 cfs. Figure 28.11 shows the frequency plot of the PMFs obtained. The results show the sensitivity of the peak flow to the temporal pattern of the storm, the peak precipitation intensity, and the total volume of the storm [3]. In the second case, the 24 h precipitation depth was allowed to vary for each simulation run. For this purpose, the 4-parameter kappa distribution was fitted to the historical 24 h annual maximum precipitation events. Monte Carlo simulations of the 24 h precipitation gave an AEP = $10^{-7.3}$ of the PMP, and the corresponding simulations of the flood peaks gave a frequency distribution as shown in Figure 28.12. The figure shows that the PMF (71,000 cfs) has an AEP of 1.5×10^{-8}, and the mean of the flood conditioned on the occurrence of the 24 h PMP (42,300 cfs, Figure 28.11) has an AEP of 1.8×10^{-6}. This implies that the methods that are used to develop the PMF (standard USBR procedures) give a flood that is about two orders of magnitude more rare than the 24 h PMP that was used to generate the flood [3]. The results of the simulations serve not only for quantifying the uncertainty of the PMF but also for estimating the order of magnitude of the AEP of the PMF that is estimated using the traditional approaches.

28.6.4 Statistical Alternatives for Estimating Extreme Floods (Including PMF)

In the last decades, a tendency worldwide has been towards risk-based approaches for designing flood-related structures such as flood walls and spillways [24]. As for extreme precipitation, studies of high

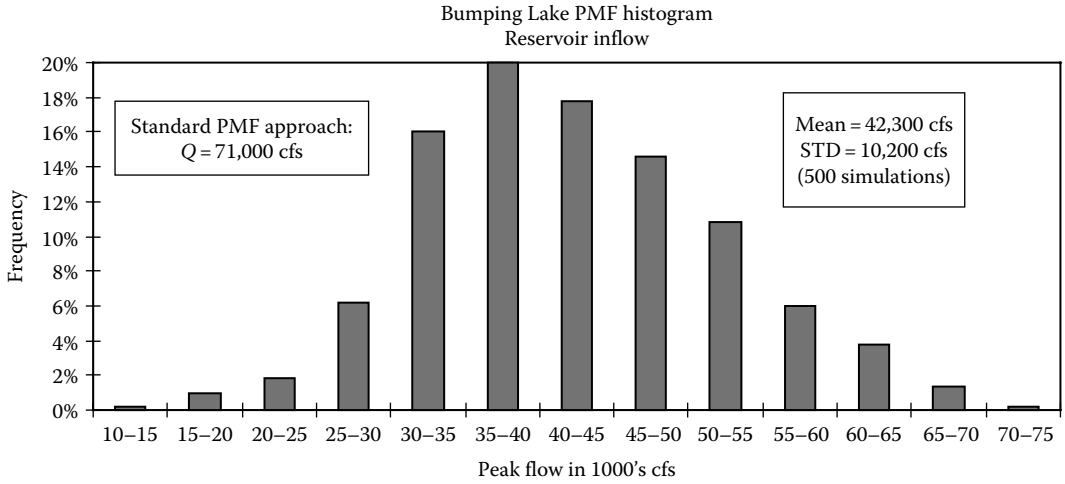

FIGURE 28.11 Relative frequency distribution of the PMFs obtained from the 500 simulations for Bumping Lake where the 24 h precipitation was held constant at the PMP, while the other variables, including the precipitation temporal pattern, varied. (From Barker, B. et al., A Monte Carlo approach to determine the variability of PMF estimates, Final Report on Bumping Lake Dam for USBR Dam Safety Office, 1997. With permission.)

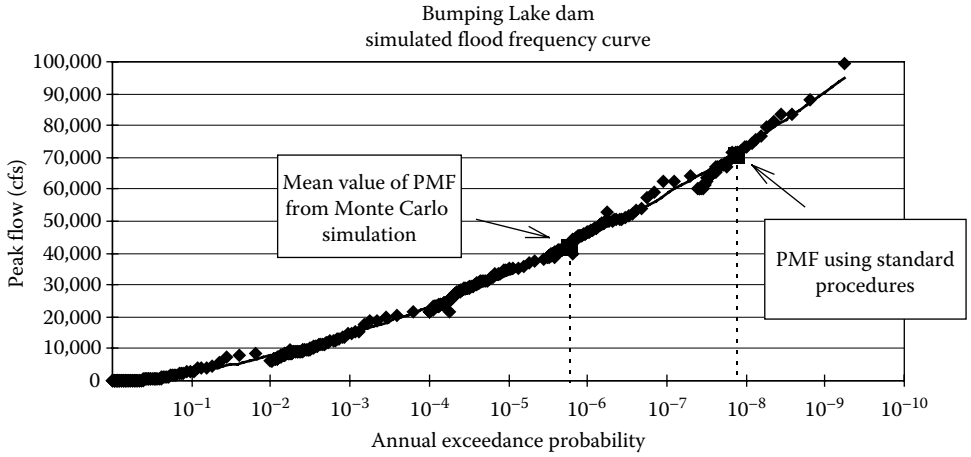

FIGURE 28.12 Frequency distribution of the flood peaks obtained by Monte Carlo simulation considering the uncertainty of the 24 h annual maximum precipitation in addition to the uncertainty of the other driving variables to estimate the flood. (From Barker, B. et al., A Monte Carlo approach to determine the variability of PMF estimates, Final Report on Bumping Lake Dam for USBR Dam Safety Office, 1997. With permission.)

return period floods based on statistical approaches have been proposed. They generally involve extrapolations of the FCs obtained from the systematic flood records including historical and paleoflood data [7,21,28,71]. However, federal and state agencies in the United States and similar organizations in other countries still use the PMF as the standard for assessing flood-related infrastructure. For example, the USBR's current policy is to use the PMF as an upper limit to hydrologic hazard curve extrapolations [78] without directly assigning an AEP to the PMF [24], that is, there is no fixed assumption for AEP of the PMF. Examples of an array of techniques developed by USBR in the last two decades can be found in Swain et al. [73]. They involve using historical and paleoflood data, mixed-population approach, expected moments algorithm (EMA), and Bayesian maximum likelihood [11,21,61].

Likewise, the USACE has been developing methods for extrapolating the flood frequency curves (FFCs) all the way to the AEP of the PMF. For example, the HEC has been developing methods for FFC extension to the level of the PMF and provides simple methods to estimate the AEP of the PMF [34]. For this purpose, the return period for the PMF is assumed to be in the range 10^{-3} to 10^{-6} and provide a simple equation to calculate the AEP of the PMF. In some cases, the extrapolation of FFCs beyond the range of the 100-year flood has been based on assuming (assigning) an AEP to the PMF. For example, the guidelines on extreme flood analysis for the Department of Transportation of Alberta, Canada, specify that the AEP for the PMF be set to 10^{-5} (100,000 years of return period) so that flood estimates for return periods of 1,000 and 10,000 years can be made [2].

28.7 Summary and Conclusions

The topic of uncertainty in estimating the PMP and PMF has been the main trust of this chapter. There are many studies documenting the various developments for estimating the PMP and PMF based on physically based (hydrometeorological) and statistical approaches. And many federal and state organizations worldwide use the PMP and PMF as standards for designing some flood-related hydraulic structures. However, in recent decades, there has been a growing concern (expressed in literature) regarding the uncertainties involved in estimating such extreme events, and the tendency has been to estimate their exceedance probabilities. In this chapter, we included some developments directed to quantify the uncertainty of the PMP and PMF. While hydrometeorological methods likely provide the best estimates of PMP, however, in many regions of the world, hydrometeorological data are lacking, and consequently feasibility studies and actual designs of flood-related projects are being made based solely on the well-known Hershfield's statistical method that provides a single value for the PMP. Thus, a method to quantify the uncertainty of the PMP if Hershfield's method is to be applied has been included in this chapter.

Regardless of the method used for estimating the PMP and PMF, the current concern of climate change brings the issue on how possible changes in hydrometeorological variables such as air temperature, wind, humidity, snow cover, and sea levels may affect the estimates of extreme events in general and PMP and PMF in particular. Many studies have been made documenting possible trends in extreme precipitation and flood events and the possibility of using the so-called global climate model (GCM) outputs and projections for estimating extreme events, but results are still debatable and controversial (e.g., [25,46,65]). A review on efforts made on this issue in the past decades is available [25].

Acknowledgments

We acknowledge the cooperation received from Ings. Alvaro Prada Arciniegas (Metropolitan Aqueduct of Bucaramanga), Jairo Jaramillo Vallejos (Conalvias S. A.), and Juan Luis Cadavid (Integral Consulting Engineers, Colombia), in connection with the study of the Tona River dam at Bucaramanga, Colombia, which was quite useful in writing this chapter. Also acknowledgment is due to Dr. John F. England of the USBR for providing us with useful material for preparing this chapter.

References

1. Alexander, G.N. 1963. Using the probability of storm transposition for estimating the frequency of rare floods. *J. Hydrol.* 1, 46–57.
2. AT (Alberta Transportation). 2004. Guidelines on extreme flood analysis, Transportation & Civil Engineering Division, Civil Projects Branch, 87 pages + Appendices, Alberta, Canada.
3. Barker, B., Schaefer, M.G., Mumford, J., and Swain, R. 1997. A Monte Carlo approach to determine the variability of PMF estimates, Final Report on Bumping Lake Dam for USBR Dam Safety Office.

4. Benson, M.A. 1973. Thoughts on the design of design floods. Floods and droughts, *Proceedings of the 2nd International Symposium in Hydrology*, Fort Collins, CO, Water Resources Publications, pp. 27–33.
5. BIDR-WE (China Water Resources Beifang Investigation Design and Research Co. Ltd. and China International Water & Electric Corporation). 2009. Kohala Hydropower Project, Updating of Feasibility Study, Main Report, Chapter 3, Hydrology.
6. Bondelid, T.R., McCuen, R.H., and Jackson, T.J. 1982. Sensitivity of SCS models to curve number variation. *Water Res. Bull*. 18(1), 111–116.
7. Botero, B.A. and Frances, F. 2010. Estimation of high return period flood quantiles using additional non-systematic information with upper bounded statistical models. *Hydrol. Earth Syst. Sci*. 14, 2617–2628, EGU.
8. Casas, C.M., Rodríguez, R., Nieto, R., and Redaño, A. 2008. The estimation of probable maximum precipitation, the case of Catalonia. *Ann. N. Y. Acad. Sci*. 1146, 291–302.
9. Chow, V.T. 1951. A general formula for hydrologic frequency analysis. *Trans. Am. Geophys. Union* 32, 231–237.
10. Chow, V.T., Maidment, D.R., and Mays, L.W. 1988. *Applied Hydrology*, McGraw Hill Book, Co., New York.
11. Cohn, T.A., Lane, W.L., and Baier, W.G. 1997. An algorithm for computing moments-based flood quantile estimates when historical information is available. *Water Resour. Res*. 33(9), 2089–2096.
12. Collier, C.G. and Hardaker, P.J. 1996. Estimating probable maximum precipitation using a storm model approach. *J. Hydrol*. 183, 277–306.
13. Cotton, W.R., McAnelly, R.A., and Ashby, T. 2003. Development of new methodologies for determining extreme rainfall, Department of Atmospheric Sciences, Colorado State University, Fort Collins, CO.
14. Cudworth, A.G. 1989. *Flood Hydrology Manual*, A Water Resources Technical Publication, Bureau of Reclamation, Denver, CO, 243pp.
15. Dawdy, D.R. and Lettenmaier, D.P. 1987. Initiative for risk-based flood design. *ASCE J. Hydrau. Eng*. 113(8), 1041–1051.
16. Desa, M.N. and Rakhecha, P.R. 2007. Probable maximum precipitation for 24-hr duration over an equatorial region: Part 2-Johor. Malaysia. *Atmos. Res*. 84, 84–90.
17. Dhar, O.N., Kulkarni, A.K., and Rakhecha, P.R. 1980. Probable maximum point rainfall estimation for the southern half of the Indian peninsula. *Proc. Indian Acad. Sci. (Earth Planet. Sci.)* 90(1), 39–46.
18. DID (Department of Irrigation and Drainage). 2000. *Urban Stormwater Management Manual (MSMA Manual)*, Percetakan Nasional Malaysia, Kuala Lumpur, Malaysia, p. 13-3.
19. Douglas, E.M. and Barros, A.P. 2003. Probable maximum precipitation estimation using multifractals: Application in the eastern United States. *J. Hydrometeorol*. 4, 1012–1024.
20. Dwyer, I.J. and Reed, D.W. 1994. Effective fractal dimension and corrections to the mean of annual maxima. *J. Hydrol*. 157, 13–34.
21. England, J.F., Jarrett, R.D., and Salas, J.D. 2003. Comparisons of two moment-based estimators that utilize historical and paleoflood data for the log-Pearson type III distribution. *Water Resour. Res*. 39(9), 1243, doi:10.1029/2002WR001791.
22. England, J.F. 2006. Frequency analysis and two-dimensional simulations of extreme floods on a large watershed. PhD dissertation, Department of Civil and Environmental Engineering, Colorado State University, Fort Collins, CO.
23. England, J.F., Velleux, M.L., and Julien, P.Y. 2007. Two-dimensional simulations of extreme floods on a large watershed. *J. Hydrol*. 347(1–2), 229–241.
24. England, J.F. 2011. Flood frequency and design flood estimation procedures in the United States: Progress and challenges. *Aust. J. Water Resour*. 15(1), 33–46.

25. England, J.F., Sankovich, V.L., and Caldwell, R.J. December 2011. Review of probable maximum precipitation procedures and databases used to develop hydrometeorological reports, U.S.B.R., Report for the Nuclear Regulatory Commission.
26. Fontaine, T.A. and Potter, K.W. 1989. Estimating probabilities of extreme rainfalls, *ASCE J. Hydrau. Eng*. 115(11), 1562–1575.
27. Foufoula-Georgiou, E. 1989. A probabilistic storm transposition approach for estimating exceedance probabilities of extreme precipitation depths, *Water Resour. Res*. 25(5), 799–815.
28. Frances, F., Salas, J.D., and Boes, D.C. (1994). Flood frequency analysis with systematic and historical or paleoflood data based on the two-parameter general extreme value models, *Water Resour. Res*. 30(5), 1653–1664.
29. Grimaldi, S., Petroselli, A., Tauro, F., and Porfiri, M. 2012. Time of concentration: A paradox in modern hydrology, *Hydrol. Sci. J*. 57(2), 217–228.
30. Gupta, V.K. 1972. Transposition of storms for estimating flood probability distributions, Hydrology Papers 59, Colorado State University, Fort Collins, CO.
31. Hansen, E.M., Schreiner, L.C., and Miller, J.F. 1982. Application of probable maximum precipitation estimates—United States East of 105th Meridian, Hydrometeorological Report 52, US Department of Commerce, NOAA, US Weather Bureau, Washington, DC.
32. Hansen, E.M. 1987. Probable maximum precipitation for design floods in the United States, *J. Hydrol*. 96, 267–278.
33. Hansen, E.M., Fenn, D.D., Schreiner, L.C., Stodt, R.W., and Miller, J.F. 1988. Probable maximum precipitation estimates—United States between the Continental Divide and the 103rd Meridian, Hydrometeorological Report 55A, National Weather Service, NOAA, US Department of Commerce, Silver Spring, MD, 168p.
34. Harris, J. and Brunner, G. 2011. Approximating the probability of the probable maximum flood, *Proceedings of the World Environmental and Water Resources Congress*, *ASCE*, Palin Springs, California, pp. 3695–3702.
35. Hershfield, D.M. 1961. Estimating the probable maximum precipitation, *ASCE J. Hydrau. Div*. 87(5), 99–116.
36. Hershfield, D.M. 1965. Method for estimating probable maximum rainfall, *J. AWWA* 57, 965–972.
37. Ho, F.P. and Riedel, J.T. 1980. Seasonal variation of 10-square-mile probable maximum precipitation estimates, United States East of the 105th Meridian, Hydrometeorological Report 53, National Weather Service, NOAA, US Department of Commerce, Silver Spring, MD, 168p.
38. Jennings, A.H. 1950. World's greatest observed point rainfalls. Hydrometeorological Section, US Weather Bureau, Washington, DC, pp. 4–5.
39. Johnson, B.E., Julien, P.Y., Molnár, D.K., and Watson, C.C. 2000. The two-dimensional upland erosion model CASC2D-SED, *J. Am. Water Resour. Assoc*. 36(1), 31–42.
40. Julien, P.Y., Saghafian, B., and Ogden, F.L. 1995. Raster-based hydrologic modeling of spatially-varied surface runoff. *Water Resour. Bull., AWRA* 31(3), 523–536
41. Julien, P.Y. and Rojas, R. 2002. Upland erosion modeling with CASC2D-SED, *Int. J. Sediment Res*. 17(4), 265–274.
42. Kendall, M. and Stuart, A. 1963. *The Advanced Theory of Statistics*, Vol. 1, *Distribution Theory*, 2nd edn., Hafner Publishing Company, Inc., New York.
43. Klemes, V., Nikleva, S., and Chin, W.Q. 1992. Probability of a PMP—A feasibility study. *Dam Safety* 1992, 1–16.
44. Klemes, V. 1993. Probability of extreme hydrometeorological events—A different approach. *Proceedings of the Yokohama Symposium*, July, IAHS Pub. No. 213, pp. 167–176.
45. Koutsoyiannis, D. 1999. A probabilistic view of Hershfield's method for estimating probable maximum precipitation. *Water Resour. Res*. 35(4), 1313–1322.
46. Kundzewicz, Z.W. and Stakhiv, E. 2010. Are climate models "ready for prime time" in water resources management applications, or is more research needed? *Hydrol. Sci. J*. 55(7), 1085–1089.

47. Laurenson, E.M. and Kuczera, G.A. 1999. Annual exceedance probability of probable maximum precipitation. *Aust. J. Water Resour*. 3(2), 167–176.
48. Loukas, A. and Quick, M.C. 1996. Physically-based estimation of lag time for forested mountainous watersheds. *Hydrol. Sci. J*. 41(1), 1–19.
49. McCuen, R.H. 2009. Uncertainty analyses of watershed time parameters. *ASCE J. Hydrol. Eng*. 14(5), 490–498.
50. Mejia, G. and Villegas, F. 1979. Maximum precipitation deviations in Colombia. *Third Conference on Hydrometeorology*, *American Meteorological Society*, Boston, MA, pp. 74–76, August 20–24, Bogota, Colombia.
51. Merz, B. and Thieken, A.H. 2005. Separating natural and epistemic uncertainty in flood frequency analysis, *J. Hydrol*. 309, 114–132.
52. Mood, A., Graybill, F., and Boes, D.C. 1974. *Introduction to the Theory of Statistics*, 3rd edn., McGraw Hill, New York.
53. Nathan, R.J. and Weinmann, P.E. 2001. Estimation of large to extreme floods, Book VI in *Australian Rainfall and Runoff: A Guide to Flood Estimation*, National Committee on Water Engineering, Institution of Engineers, Australia.
54. Nathan, R.J. and Merz, S.K. November 2001. Estimation of extreme hydrologic events in Australia: Current practice and research needs. *Proceedings of the Hydrologic Research Needs for Dam Safety*, Meeting Sponsored by FEMA, Paper 13, pp. 69–77.
55. Newton, D.W. 1983. Realistic assessment of maximum flood potentials. *ASCE J. Hydrau. Eng*. 109(6), 905–918.
56. Nobilis, F., Haiden, T., and Kerschbaum, M. 1991. Statistical considerations concerning probable maximum precipitation (PMP) in the Alpine Country of Austria. *Theor. Appl. Climatol*. 44, 89–94.
57. NRC (National Research Council). 1988. *Estimating Probabilities of Extreme Floods*, National Academy Press, Washington, DC.
58. NRC (National Research Council), 2000. *Risk Analysis and Uncertainty in Flood Damage Reduction Studies*, National Academy Press, Washington, DC, 202 pp.
59. NWS (National Weather Service). 1980. Probable maximum precipitation estimates, United States between the Continental Divide and the 103rd Meridian. Hydrometeorological Report 55A, Silver Spring, MD, 259pp.
60. NWS (National Weather Service). October 1994. Probable maximum precipitation for the Pacific Northwest States—Columbia, Snake River, and Pacific Coastal Drainages, Hydrometeorological Report 57, Silver Spring, MD.
61. O'Connell, D.R.H., Ostenaa, D.A., Levish, D.R., and Klinger, R.E. 2002. Bayesian flood frequency analysis with paleoflood bound data. *Water Resour. Res*. 38(5), 14, DOI 10.1029/2000WR000028.
62. Ohara, N., Kavvas, M.L., Kure, S., Chen, Z.Q., Jang, S., and Tan, E. 2011. Physically based estimation of maximum precipitation over the American River Watershed, California. *ASCE J. Hydrol. Eng*. 16(4), 351–361.
63. Papalexiou, S.M. and Koutsoyiannis, D. 2006. A probabilistic approach to the concept of probable maximum precipitation. *Adv. Geosci*. 7, 51–54.
64. Poon, H.C. and Hwee, H.H. 2010. Probable maximum precipitation derivation in Malaysia: review and comparison. *Int. J. Hydro-Climatic Eng*. 1(ii) 37–72.
65. Prasad, R., Hibler, L.F., Coleman, A.M., and Ward, D.L. 2011. Design-basis flood estimation for site characterization at nuclear power plants in the United States of America, NUREG/CR-7046, PNNL-20091, Office of Nuclear Regulatory Research, Pacific Northwest National Laboratory, Richland, WA.
66. Rakhecha, P.R. and Soman, M.K. 1994. Estimation of probable maximum precipitation for a 2-day duration: Part 2—North Indian region. *Theor. Appl. Climatol*. 49, 77–84.
67. Receanu, R., Hertig, J.A., and Fallot, J.M., 2012. The estimation of PMP and PMF on Alpine basins in Switzerland. *Aerul si Apa: Componente ale Mediului,* Cluj University Press, 212–219.

68. Rezacova, D., Pesice, P., and Sokol, Z. 2005. An estimation of the probable maximum precipitation for river basins in the Czech Republic. *Atmos. Res*. 77, 407–421.
69. Riedel, J.T. and Schreiner, L.C. 1980. Comparison of generalized estimates of probable maximum precipitation with greatest observed rainfalls, Tech. Report NWS No. 25, National Weather Service, US Department of Commerce, Silver Spring, MD, 66pp.
70. Smith, J.B., Barker, B.L., and Pernela, L.M. 2010. Annual exceedance probability of probable maximum flood using a stochastic hydrologic model, *Proceedings of the 30th Annual USSD Conference: Collaborative Management of Integrated Watersheds*, Sacramento, CA, April 12–16, 2010. CD-ROM.
71. Stedinger, J.R. and Cohn, T.A. 1986. Flood frequency analysis with historical and paleoflood information, *Water Resour. Res*. 22(8), 785–793.
72. Stedinger, J.R., Vogel, R.M., and Foufoula-Georgiou, E. 1993. Frequency analysis of extreme events, in *Handbook of Hydrology* (D.R. Maidment, Ed.), Chapter 18, McGraw Hill, New York.
73. Swain, R.E., England, J.F., Bullard, K.L., and Raff, D.A. June 2006. *Guidelines for Evaluating Hydrologic Hazards*, US Department of the Interior, Bureau of Reclamation.
74. Thomas, W.O. Jr., Monde, M.C., and Davis, S.R., 2000. Estimation of time of concentration for Maryland streams, Transportation Research Record 1720, Paper No. CO-1267, pp. 95–99.
75. USACE (US Army Corps of Engineers). 1990. HEC-1 hydrograph package, Hydrologic Engineering Center, Davis, CA.
76. USACE (US Army Corps of Engineers). 2010. *Hydrologic Modeling System HEC-HMS—User's Manual*, August 2010, USACE, Davis, CA.
77. USBR (US Bureau of Reclamation). 1999. A framework for characterizing extreme floods for dam safety risk assessment, prepared by Utah State University and USBR, Denver, CO, 67pp.
78. USBR (US Bureau of Reclamation). 2002. Hydrologic risk analysis and extreme flood considerations, Interim Guidance for Bureau of Reclamation Dam Safety Office, D-6600, July, 3pp.
79. Velleux, M.L. 2005. Spatially distributed model to assess watershed contaminant transport and fate, PhD dissertation, Department of Civil and Environmental Engineering, Colorado State University, Fort Collins, CO.
80. Velleux, M.L., Julien, P.Y., Rojas-Sanchez, R., Clements, W., and England, J.F. 2006. Simulation of metals transport and toxicity at a mine-impacted watershed: California Gulch, Colorado. *Environ. Sci. Technol.* 40(22), 6996–7004
81. Wang, B.H. 1984. Estimation of probable maximum precipitation: Case studies. *ASCE J. Hydrau. Eng*. 110(10), 1457–1472.
82. WMO (World Meteorological Organization). 1973. Manual for estimation of probable maximum precipitation. Operational Hydrology Report 1, 1st edn., Publication 332, WMO, Geneva, Switzerland.
83. WMO (World Meteorological Organization). 1986. Manual for estimation of probable maximum precipitation. Operational Hydrology Report 1, 2nd edn., Publication 332, WMO, Geneva, Switzerland.
84. WMO (World Meteorological Organization). 2009. Manual on estimation of probable maximum precipitation (PMP), WMO-No. 1045, 259 pp.

29

Impact of Urbanization on Runoff Regime

Never Mujere
University of Zimbabwe

Saeid Eslamian
Isfahan University of Technology

AUTHORS

Never Mujere holds a master of philosophy degree in geography from the University of Zimbabwe (UZ). Currently, he is a physical geography lecturer in the UZ's department of geography and environmental science. He is the founder of a local nongovernmental organization, Environmental Management Trust (EMT). His areas of research interests are water resources and environmental issues. He has authored two books, contributed to some chapters of four books, published seven papers in refereed journals, and presented papers at international workshops.

Saeid Eslamian received his PhD from the University of New South Wales, Australia, with Prof. David Pilgrim. He was a visiting professor in Princeton University, United States, and ETH Zurich, Switzerland. He is currently an associate professor of hydrology in Isfahan University of Technology. He is the founder and chief editor of the *Journal of Flood Engineering* and *International Journal of Hydrology Science and Technology*. He has published more than 200 publications mainly in statistical and environmental hydrology and hydrometeorology.

PREFACE

There are four separable but interrelated effects of land-use changes on the hydrology of an area: changes in peak flow characteristics, changes in total runoff, changes in the quality of water, and changes in the hydrologic amenities. Of all land-use changes affecting the hydrology of an area, urbanization is by far the most forceful. This chapter presents a review of literature on the effects of urbanization on runoff regime. The rainfall–runoff response of a catchment can be radically altered as a consequence of urbanization. The introduction of impervious surfaces such as concrete, tarmacs, and tiles inhibits infiltration and reduces surface retention. The proportion of storm rainfall that goes to surface runoff is increased while the proportion that goes to evapotranspiration, groundwater recharge, and baseflow is reduced. Urbanization also causes an increase in the amount of runoff, a more rapid response to produce more runoff in less time, yielding a flood hydrograph that is faster to peak, faster to recede, and of increased peak discharge.

29.1 Introduction

Urbanization involves the removal of natural vegetation and top-soil, recontouring the land, and compacting the subsoil with heavy machinery as human populations concentrate into discrete areas [2]. This process leads to transformation of land for residential, commercial, industrial, and transportation purposes. Urbanized areas include densely populated centers as well as their adjacent suburban fringes. During the last 25 years, rapid urbanization has taken place in most developing countries. Substantial increase in built-up areas has taken place due to the development of residential and commercial areas mostly through private land developers and real estate business.

The urbanization process comprises construction of roads, buildings, driveways, parking surfaces, installation of services such as stormwater drains and water supply systems, replacement of top-soil, and addition of lawns. These activities affect streamflows because the newly created surfaces such as roads and roofs increase the impervious area and hence create obstruction to natural drainage pattern, provide a greater volume of runoff from storms compared to natural areas, and shorten runoff concentration time. Runoff also reaches the streams more quickly through efficient drainage network of gutters and pipes. In addition, the water storage and holding capacity of the topsoil is reduced, further increasing peak runoff from urbanized areas. Thus, the increase in built-up and impervious area with the progression of urbanization within a catchment has corresponding changes to stream's flow regime [4]. This chapter highlights the impact of land use and land cover changes due to urbanization on runoff characteristics.

29.2 Urban Dual Drainage Components and Imperviousness

Urban stormwater drainage systems usually, termed dual drainage in the urban hydrology nomenclature, consist of two elements: (1) surface components such as streets, rooftops, and ditches; and (2) subsurface components such as pipes and other manmade stormwater drainage conduits. These two elements are linked through street curb inlets and manholes. On the other hand, in partially urbanized catchments, these urban drainage components are often mixed with the natural channel drainage in portions of most of the confounding factors that can be controlled.

1. *Impervious cover (IC)*: all hard surfaces that do not allow water to penetrate the soil, such as rooftops, driveways, streets, swimming pools, and patios
2. *Total impervious area (TIA)*: all impervious area in catchment
3. *Effective impervious area (EIA)*: impervious area in catchment that is directly connected to stream channels (i.e., precipitation falling on that area is effectively transported to the stream)

EIA (also known as drainage connection or directly connected impervious area) is a better predictor of ecosystem alteration in urban streams [6]. The strength of EIA relationships suggests that stormwater management techniques aimed at disconnecting impervious areas from stream channels can improve urban water quality.

29.3 Stages of Urban Development Vital to Stream Hydrology

One of the major impacts of urbanization on streams is the effect on stream hydrology. Stream hydrology is defined as the study of the movement or flow of water in streams. Understanding water movement is essential to understanding the impact of the development on urban streams.

There are three stages of urbanization that have repercussions on river channels. These are (1) a stable or equilibrium predevelopment stage; (2) a period of construction during which bare land is exposed to erosion; and (3) a final stage consisting of a new urban landscape dominated by houses, rooftops, gutters, and sewers. Accompanying the construction phase is an initial increase in sediment production because of the erosion of bare surfaces, leading to sedimentation within channels. Central to the last stage is increasing impervious surfaces leading to greater runoff, which, together with decreasing sediment production, is followed by channel erosion and channel widening or enlargement. A conceptual model of urban change is shown in Figure 29.1.

Thus, urban development is characterized by

Riparian/channel alteration: Removal of riparian vegetation reduces stream cover and organic matter inputs; direct modification of channel alters hydrology and physical habitat.

Wastewater inputs: Human, industrial, and other wastewaters enter streams via point (e.g., wastewater treatment plant effluents) and nonpoint (e.g., leaky infrastructure) discharges.

Impervious surfaces: IC increases surface runoff, resulting in increased delivery of stormwater and associated contaminants into streams.

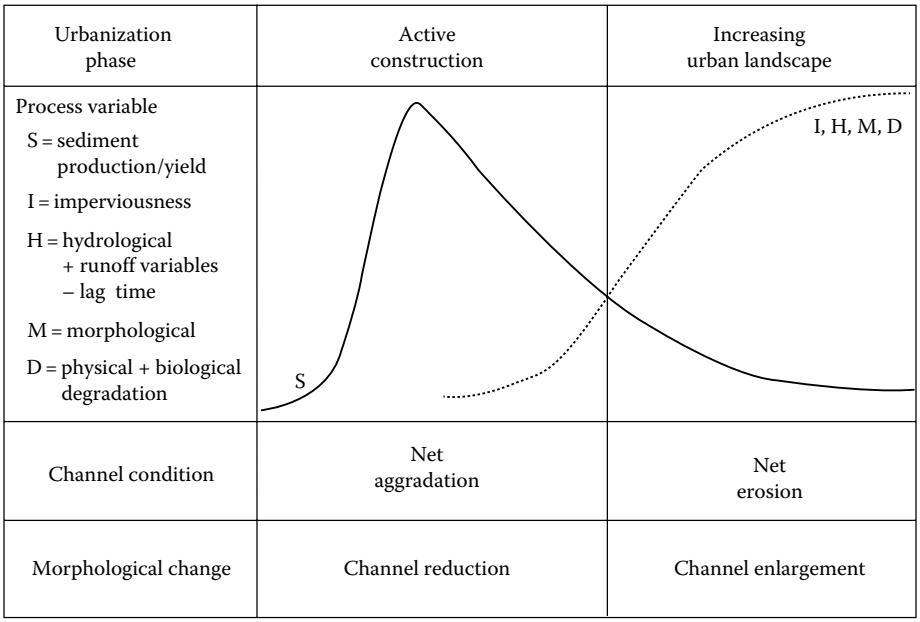

FIGURE 29.1 General phases of urbanization with associated process changes, channel conditions, and morphological adjustments. (From Chin, A., Urban transformation of river landscapes in a global context, Department of Geography, Texas A&M University, College Station, TX, 2006, p. 6.)

29.4 Effects of Urbanization on Water Resources

The water cycle, also known as the hydrological cycle, is the continuous exchange of water between land, water bodies, and the atmosphere. Approximately 97% of the earth's water is stored in the oceans, and only a fraction of the remaining portion is usable freshwater. When precipitation falls over the land, it follows various routes. Some of it evaporates, returning to the atmosphere, some seeps into the ground, and the remainder becomes surface water, traveling to oceans and lakes by way of rivers and streams.

The effects of urbanization on water resources can be organized into four categories: water movement (hydrology), stream channel shape and function (fluvial geomorphology), water quality, and habitat. With regard to urban hydrology, urban development of rural areas generally has a significant impact upon the hydrologic and hydraulic regime of nearby creeks and rivers. Urbanization alters the overland flow paths, reduces the amount of water that is able to seep into groundwater sources, and reduces the time that it takes for the runoff to reach the catchment outlet. This reduction in travel time leads to higher peak flows that reach the catchment outlet much earlier than in the natural state. The increase in runoff observed can be attributed to the increase in average rainfall intensity that results from the decrease in travel time through the catchment. However, the effects of urbanization vary with average recurrence interval [10].

29.5 Flow Alteration in Urban Hydrology

How does urbanization affect stream hydrology? This is an invaluable question in urban hydrology because any change in runoff characteristics induced by urbanization is important for understanding the effects of land use and cover changes on earth surface hydrological processes.

With urban land development, impermeable land surfaces enlarge rapidly, the capability of rainfall detention declines sharply, and runoff coefficient increases. Urbanized land usually leads to a decrease in surface roughness; hard road and drainage system can greatly shorten the time of runoff confluence. Therefore, urbanized area would become more susceptible to flood hazard under conditions of high precipitation intensity.

Urbanization modifies hydrological processes by replacing vegetated land cover with impervious surfaces and by extending the natural drainage network to include artificial ponds, ditches, and conduits laid on the ground and underground. Impervious surfaces reduce infiltration, generally resulting in increased surface runoff and reduced baseflow. Artificial ditches and conduits alter runoff pathways and change stormwater drainage. In urbanizing catchments, surface flow may be diverted to artificial ponds or flood detention ponds built to reduce flood risks or in some cases for irrigation purposes [7].

Hydrological changes associated with urbanization have been extensively studied, and results from these studies have clearly shown that urban development leads to larger and more frequent floods. The main parameters demonstrated to have changed are peak discharge, lag time, flood frequency, and total runoff or water yield.

29.6 Hydrological Changes That Occur with Urban Development

Alteration of natural hydrologic regimes is a consistent and pervasive effect of urbanization on stream ecosystems, as discharge patterns, the amount, and timing of water flow through streams change with urban development [3]. Common aspects of urbanization affecting streamflow regimes are shown in Table 29.1.

With regard to baseflow in urban rivers, urbanization generally results in increased magnitude and frequency of peak flows, but baseflow effects typically are more variable [11]. The effect of urbanization on the average annual flood is shown in Table 29.2, which shows the increase in average annual flood for different degrees of urbanization as measured by the increase in percentages of impervious area and area served by storm sewers.

TABLE 29.1 Hydrological Effects of Urbanization

Flow Characteristic	Effect of Urbanization
Stormflow	• ↑ High flow frequency • ↑ High flow magnitude • ↑ Flashiness or rapidity of flow changes • ↓ High flow duration • ↓ Lag time
Baseflow	• ↓ Low flow magnitude • ↓ Low flow frequency • ↑ Low flow duration • ↓ Infiltration and ↑ surface runoff of precipitation associated with impervious (and effectively impervious) surfaces • ↑ Speed and efficiency of runoff delivery to streams, via stormwater drainage infrastructure • ↓ Evapotranspiration due to vegetation removal • ↑ Direct water discharges, via wastewater and industrial effluents • ↑ Infiltration due to irrigation and leakage from water supply and wastewater infrastructure • ↑ Water withdrawals and interbasin transfers Studies have shown that decreases in baseflow may result from • ↓ Infiltration due to ↑ impervious surfaces • ↑ Water withdrawals (surface or ground) These decreases may be offset, however, by increases in baseflow resulting from • ↑ Imported water supplies (i.e., interbasin transfers) • ↑ Leakage from sewers and septic systems • ↑ Irrigation (lawn watering) • ↑ Discharge of wastewater effluents • ↑ Infiltration due to water collection in recharge areas • ↓ Evapotranspiration due to ↓ vegetative cover
Flooding	• Disrupts natural water balance • Increases flood peaks, stormwater runoff, and bankfull flows • More frequent flooding • Lower baseflow to streams (less water in the stream)

Source: Donaldson, S. and Hefner, M., Impacts of urbanization on waterways, Center for Watershed Protection, University of Nevada Cooperative Extension, Reno, NV, 1999.

TABLE 29.2 Effect of Urbanization on Annual Flood

Percentage of Area Sewered	Percentage of Area Impervious	Ratio to Average Annual Flood
0	0	1
20	20	1.5
40	40	2.3
50	50	2.7
80	60	4.2
100	60	4.4

Source: Leopold, B.L., *Hydrology for Urban Land Planning: A Guidebook on the Hydrologic Effects of Urban Land Use*, Geological Survey Circular 554, US Geological Survey, Washington, DC, 1968, p. 7.

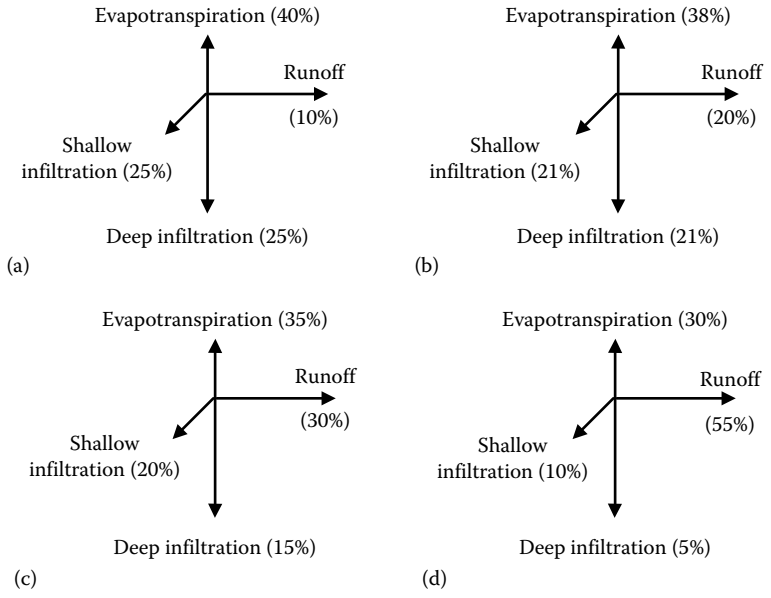

FIGURE 29.2 The shift in relative hydrological flow with increasingly imperviousness of watersheds. Note the large increase in stormwater runoff as imperviousness increases, at the expense of infiltration. (a) Natural groundcover/forested, (b) 10%–20% imperviousness, (c) 35%–50% imperviousness, (d) 75%–100% imperviousness. (From Paul, M.J. and Meyer, J.L., *Annu. Rev. Ecol. Syst.*, 32, 333, 2001.)

The volume of runoff is governed primarily by infiltration characteristics and is related to land slope and soil type as well as to the type of vegetative cover. It is thus directly related to the percentage of the area covered by roofs, streets, and other impervious surfaces (Figure 29.2).

With natural groundcover, 25% of rain infiltrates into the aquifer and only 10% ends up as runoff. As imperviousness increases, less water infiltrates and more runs off. In highly urbanized areas, over one-half of all rain becomes surface runoff, and deep infiltration is only a fraction of what it was naturally. The increased surface runoff requires more infrastructure to minimize flooding. Natural waterways end up being used as drainage channels and are frequently lined with rocks or concrete to move water more quickly and prevent erosion. In addition, as deep infiltration decreases, the water table drops, reducing groundwater for wetlands, riparian vegetation, wells, and other uses.

29.7 Effect of Urbanization on Hydrograph Peak Discharge

Urbanization tends to increase the flood potential from a given basin as river channels receive flows exceeding their storage capacities. Thus excessive runoff volumes lead to flooding. These excessive volumes are caused by both the total amount of IC and the rate at which the runoff is delivered to the stream. Flooding is enhanced because [6]

- Curbs and gutters, storm drains, storm drain pipes, ditches, catch basins, and other drainage systems quickly speed the runoff to a stormwater detention/retention facility or directly into the nearest water body.
- Curbs and gutters are designed to deliver stormwater away from the road surface in an efficient and timely manner.
- Catch basins or inlets collect stormwater and direct it through pipes to a downstream stormwater detention/retention facility or to the nearest water body.

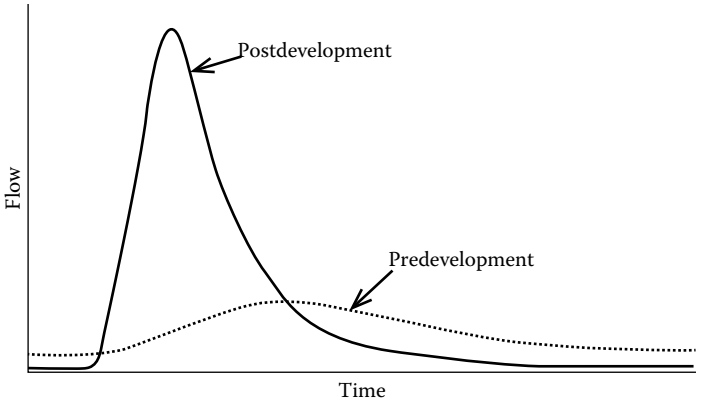

FIGURE 29.3 A typical storm hydrograph showing changes in streamflow before and after a high degree of urbanization. (From Elliott, S. et al., A guide for assessing effects of urbanisation on flow-related stream habitat, *NIWA Science and Technology Series* No. 52, 2004, p. 7.)

Streamflow can be divided into two components: the flow component that appears in the stream soon after rainfall is termed quickflow and a baseflow component infiltrates into the ground and reaches the stream slowly. Urbanization typically increases the quickflow component so that the magnitude and frequency of high flows are increased, and storm peak occurs more quickly after the onset of rain. This often leads to channel widening. At the same time, there are reduced opportunities of infiltration of water into the ground, and so there is reduced baseflow [4]. The changes are shown schematically in Figure 29.3.

A hydrograph is a graph showing the changes in streamflow with respect to time. During storms, in predeveloped or natural conditions (the solid line), the streamflow gradually increases to a relatively flat prolonged peak that is about twice the prestorm flow rate and gradually descends to a low-flow condition or gradual recession.

During storms, in the urbanized condition (dashed line), the flow rapidly increases to a peak that occurs earlier in time due to the rapid delivery of water from storm drains and pavement. It is clear that the peak flows are more than double than that prior to development. As a result, flows in the stream will be higher than that occurred during predevelopment period; hence, flooding may increase. The flow then sharply decreases, often to a low-flow condition that is lower than that occurred prior to development. This means that during dry periods, the flow in streams is decreased, and impacts to water users or aquatic habitat may occur. Urban development is thus characterized by higher, sharper, and reduced baseflows.

Water balance is a measure of the amount of water entering and leaving a system. As rain falls to earth, some of it is infiltrated, absorbed, evaporated, transpired, and some becomes runoff. In a predeveloped setting, much of the rainfall is absorbed by the surrounding vegetation, soil, and ground cover. The diagram (Figure 29.3) shows how development and its corresponding increase in IC disrupt the natural water balance. In the postdevelopment setting, the amount of water running off the site is dramatically increased and the amount of water infiltration is decreased. The changes in the water balance in urban streams are affected by changes in the volume of runoff, increased peak flows and frequency of bankfull flows, floodplain widening, and decreased dry weather flows.

Figure 29.4 illustrates differences in lag times between stormwater peak discharges in an urban catchment (high peak) and a less developed rural catchment (low peak). In an urbanized catchment with large amounts of IC, there is more flooding, larger volume, and faster rate of discharge than that in less developed catchments.

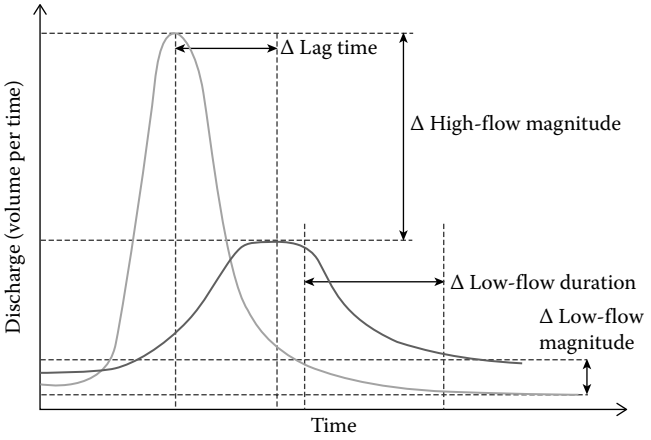

FIGURE 29.4 Hypothetical hydrographs for an urban stream (high peak) and rural stream (low peak) after a storm illustrating some changes in stormflow and baseflow that occur with urban development. (From Paul, M.J. and Meyer, J.L., *Annu. Rev. Ecol. Syst*., 32, 333, 2001.)

29.8 Urbanization and Water Yield

A major effect of urbanization is the introduction of effluent from sewage disposal plants and often the introduction of raw sewage, into channels. In rivers passing through the city of Harare in Zimbabwe, raw sewage constitutes 70% of the total flow. As volume of runoff from a storm increases, the size of flood peak also increases. Runoff volume also affects low flows because in any series of storms, the larger the percentage of direct runoff, the smaller the amount of water available for soil moisture replenishment and for groundwater storage. An increase in total runoff from a given series of storms as a result of imperviousness results in decreased groundwater recharge and decreased low flows. Thus, increased imperviousness has the effect of increasing flood peaks during storm periods and decreasing low flows between storms. A sample of the early work conducted by Rao and Rao [12] indicates that development had an overall effect of increasing runoff volume or water yield on the order of two to four times.

29.9 Decline in Streamflow Due to Diminished Groundwater Recharge

Urbanization not only increases high flows, but can also reduce baseflow, reflecting the reduced groundwater recharge under impervious surface such as roofs and roads. An increase in impervious surface often decreases the amount of rainfall available for infiltration. Without infiltration, the groundwater will not be recharged and the stream will lose this potential source of water. Urbanization not only increases high flows, but it can also reduce baseflow, reflecting the reduced groundwater recharge under impervious surfaces such as roofs and roads. Studies have shown that as the percentage of imperviousness within a catchment increases, the baseflow decreases [4]. Thus low flows tend to be lower in urbanized catchments than in natural watersheds (Figure 29.5). As the percentage of imperviousness within a catchment increases, the baseflow decreases [3].

The hydrological impact of urbanization is not limited to storm events. During dry weather periods, urban streams tend to have less flow because groundwater recharge from stormwater infiltration has been diminished [10]. While streams that have never been developed retain their flow during dry weather conditions, many urban streams lack the baseflow (flow contributed by groundwater) necessary to sustain healthy habitat conditions during extended periods of dry weather.

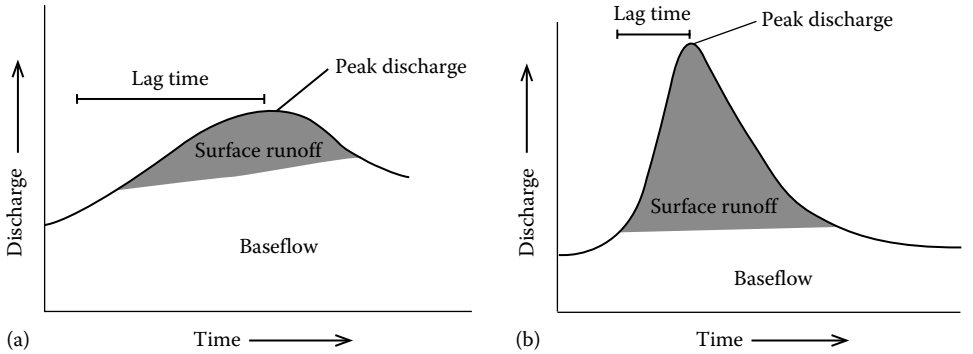

FIGURE 29.5 Decrease in baseflow due to an increase in impervious surface. (a) Natural watershed and (b) urbanized watershed. (From Donaldson, S. and Hefner, M., Impacts of urbanization on waterways, Center for Watershed Protection, University of Nevada Cooperative Extension, Reno, NV, 1999.)

29.10 Urban Rainfall–Runoff Modeling

In urban areas, catchment characteristics such as volume, peak flow, and flood return are generally highly heterogeneous. Hence the application of physically based process models of urban runoff is restricted to hydraulic planning and design of small catchments. Thus, urban catchment runoff and its period can be determined using simple rainfall–runoff models. These models (whether manual or computerized) generally incorporate precipitation, the casual process behind runoff into estimates of discharge. There are over a hundred urban rainfall–runoff models described in the literature [8]. All can be grouped according to the following classification that reflects their design purpose and complexity (Table 29.3).

Simple urban rainfall–runoff models take two forms. The simplest type estimates runoff as a function of rainfall and the runoff coefficient (i.e., ratio of runoff to rainfall) that is used to account for losses due to land-use and land cover characteristics such as interception, infiltration, and storage. The second type estimates runoff as a function of runoff depth and catchment area.

29.11 Managing and Restoring Urban Rivers

The process of urbanization is linked with economic development and makes an increasingly higher contribution to the national economy. However, when the growth of urban population takes place exceptionally at a rapid rate, most cities and towns are unable to cope with changing situations due to their internal resource constraints and management limitations. As population and land values increase, the effect of uncontrolled runoff becomes an economic burden and poses a serious threat to the health and well-being of citizens.

Urbanization is largely an irreversible process that changes earth surfaces; urbanizing stream channels are necessarily changed through the adjustment process, regardless of how well they can adjust [2,5]. Managing urban river channels poses particular challenges because most are undergoing adjustments at one stage or another. Thus, how can changing urban rivers be properly managed and potentially restored? Such understanding can assist in decision making, even if the magnitude of change cannot be predicted precisely.

Management of runoff from even a minor storm is rapidly becoming an engineering requirement to help reducing water logging, flooding, and stream erosion. It is important to realize that very few urban drainage systems are designed and built as a complete system. For the design of an adequate drainage system, it is essential to understand the changes in storm runoff characteristics with land-use changes. Urbanization of the land usually results in the highly accelerated removal of stormwater with

TABLE 29.3 Types and Characteristics of Urban Rainfall–Runoff Models

Type	Characteristics
Simple models	• Simple representation of the urban watershed • Simplistic rainfall–runoff relationship based on runoff coefficient and catchment area e.g., $Q = C \times P$ or $Q_p = C \times I \times A$ where Q is the annual runoff (mm/year) Q_p is the peak flow (m^3/h) C is the dimensionless runoff coefficient P is the mean annual rainfall (mm/year) I is the average rainfall intensity (mm/h) A is the catchment area normally only impervious (km^2) • Minimal data requirements • Cheap and easy to apply • Produces long-term averages • Use empirical and statistical methods such as coefficients and rational methods
Simple routing models	• Routes flow through a rudimentary model of drainage network • Accounts for delaying effect of routing • Used to produce hydrographs over several years • Use statistical and deterministic approaches based on unit hydrograph methods
Complex routing models	• Routes flow through an extensive network of the drainage network • Perform continuous simulation of hydrologic catchment system • Used to produce hydrographs over short term (e.g., hours or days) • Use deterministic methods to the process

Source: Knapp, H.V. et al., A review of rainfall–runoff modeling for stormwater management, Illinois Sate Water Survey Report 516, Champaign, IL, 1991.

corresponding increases in the volume and peak rate of runoff. The principal hydrological effects of land-use and land cover changes have been related to changes in peak flow characteristics and total runoff.

29.12 Summary and Conclusions

Urbanization has been observed to have significant effects on water balance in urban areas. The most dramatic changes occur in surface runoff, which generally increases most significantly due to the increase in paved areas and impervious surfaces. The increased volume and peak flows of stormwater discharges may cause problems of flooding and erosion. In urban areas, there is a variety of storm pollutant sources. Thus, in some cases, urban stormwater is a significant source of water pollution to receiving waters.

Impervious surfaces associated with urbanization alter the natural amount of water. The consequences of this change are a decrease in the volume of water that percolates into the ground and a resulting increase in volume and decrease in the quality of surface water. These hydrological changes have significant implications for the quantity of fresh clean water that is available for use by humans, fish, and wildlife.

Increased IC associated with urbanization also alters the natural cycling of water. Changes in the shape and size of urban streams, followed by decreased water quality, are the most visible effects of increased imperviousness. Greater frequency and severity of flooding, channel erosion, and destruction of aquatic habitat commonly follow catchment urbanization [1,2]. Urbanization increases the hydrograph peak and overland flow volume and decreases the basin concentration time.

References

1. Burns, D. 2005. Effect of suburban development on runoff generation in the Craton River Basin, New York, USA. *Journal of Hydrology*, 311: 266–281.
2. Chin, A. 2006. Urban transformation of river landscapes in a global context. Department of Geography, Texas A&M University, College Station, TX.
3. Donaldson, S. and Hefner, M. 1999. Impacts of urbanization on waterways. Center for Watershed Protection, University of Nevada Cooperative Extension, Reno, NV.
4. Elliott, S., Jowett, I.G., Suren, A.M., and Richardson, J. 2004. A guide for assessing effects of urbanisation on flow-related stream habitat. National Institute of water and Atmospheric Research Science and Technology Series No. 52, 59pp.
5. Graham, T.D. and Jenkins, G.A. 2001. Predicting the impact of urbanisation on peak runoff. *Proceedings of the 6th Conference on Hydraulics in Civil Engineering: The State of Hydraulics*, Institution of Engineers, Barton, Canberra, Australia, 2001, pp. 229–238.
6. Hatt, B. 2004. The influence of urban density and drainage infrastructure on the concentrations and loads of pollutants in small streams. *Environmental Management*, 34(1): 112–124.
7. Herrmann, B. 1999. The effect of urbanization on water runoff in the Big Creek Watershed. Institute of Ecology, University of Georgia, Athens, GA.
8. Knapp, H.V., Durgunoglu, A., and Ortel, T.W. 1991. A review of rainfall–runoff modeling for storm-water management. Illinois Sate Water Survey Report 516, Champaign, IL.
9. Leopold, B.L. 1968. *Hydrology for Urban Land Planning: A Guidebook on the Hydrologic Effects of Urban Land Use*. Geological Survey Circular 554, US Geological Survey, Washington, DC.
10. Mansell, M.G. 2003. *Rural and Urban Hydrology*. Thomas Telford, London, U.K.
11. Paul, M.J. and Meyer, J.L. 2001. The ecology of urban streams. *Annual Review of Ecology and Systematics*, 32: 333–365.
12. Rao, R.G.S. and Rao, A.R. 1976. Analysis of the effects of urbanization on runoff characteristics by nonlinear rainfall–runoff models. IWRRC Technical Reports. Paper 57 (available on: http://docs.lib.purdue.edu/watertech/57). (accessed on October, 01, 2013)

Water Science and Engineering

Handbook of Engineering Hydrology

Modeling, Climate Change, and Variability

While most books examine only the classical aspects of hydrology, this three-volume set covers multiple aspects of hydrology and includes contributions from experts comprising more than 30 countries. It examines new approaches, addresses growing concerns about hydrological and ecological connectivity, and considers the worldwide impact of climate change.

It also provides updated material on hydrological science and engineering, discussing recent developments as well as classic approaches. Published in three books, **Fundamentals and Applications; Modeling, Climate Change, and Variability; and Environmental Hydrology and Water Management,** the entire set consists of 87 chapters and contains 29 chapters in each book.

The chapters in this book contain information on

- Climate change and hydrological hazards, hydrological modeling, and urban water systems, as well as climate change impacts on hydrology and water resources, climate change uncertainty, vulnerability, and adaption
- Rainfall estimation and changes, hydrological changes of mangrove ecosystems, impact of the development of vegetation on flow conditions and flood hazards, urbanization impacts on runoff regime, and discretization in urban watersheds
- Artificial neural network-based modeling of hydrologic processes, flow and sediment transport modeling in rivers, hybrid hydrological modeling, hydrologic modeling: stochastic processes, and time series analysis of hydrologic data
- Dam risk and uncertainty, drought indices for drought risk assessment in a changing climate, hydrologic prediction and uncertainty quantification, uncertainty and risk of the PMP and PMF
- Geostatistics applications in hydrology, GIS applications in a changing climate, GIS-based upland erosion mapping, regional flood frequency analysis, regionalization of hydrological extreme events, remote sensing data and information for hydrological monitoring and modeling
- Application of copulas in hydrology, bankfull frequency of rivers, statistical parameters used for assessing hydrological regime, significance of statistical tests and persistence in hydrologic processes

Students, practitioners, policy makers, consultants, and researchers can benefit from the use of this text.

K15217

CRC Press
Taylor & Francis Group
an informa business
www.crcpress.com

6000 Broken Sound Parkway, NW
Suite 300, Boca Raton, FL 33487
711 Third Avenue
New York, NY 10017
2 Park Square, Milton Park
Abingdon, Oxon OX14 4RN, UK

ISBN: 978-1-4665-5246-3
90000
9 781466 552463